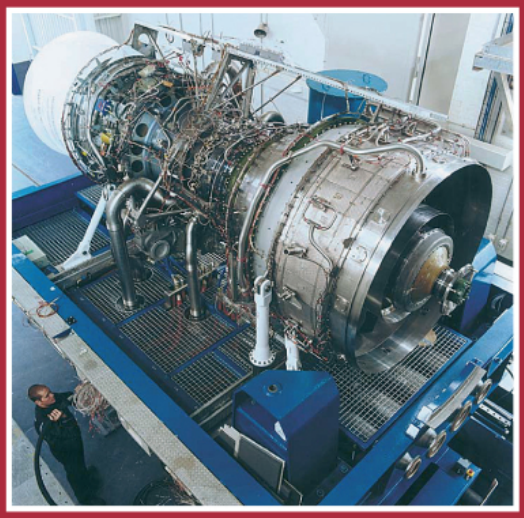
WOODHEAD PUBLISHING SERIES IN ENERGY



Modern gas turbine systems

High efficiency, low emission, fuel flexible power generation

Edited by Peter Jansohn

WP
WOODHEAD PUBLISHING

Modern gas turbine systems

© Woodhead Publishing Limited, 2013

Related titles:

Advanced power plant materials, design and technology
(ISBN 978-1-84569-515-6)

Power plant life management and performance improvement
(ISBN 978-1-84569-726-6)

Combined cycle systems for near-zero emission power generation
(ISBN 978-0-85709-013-3)

Details of these books and a complete list of titles from Woodhead Publishing can be obtained by:

- visiting our web site at www.woodheadpublishing.com
- contacting Customer Services (e-mail: sales@woodheadpublishing.com; fax: +44 (0) 1223 832819; tel.: +44 (0) 1223 499140 ext. 130; address: Woodhead Publishing Limited, 80 High Street, Sawston, Cambridge CB22 3HJ, UK)
- in North America, contacting our US office (e-mail: usmarketing@woodheadpublishing.com; tel.: (215) 928 9112; address: Woodhead Publishing, 1518 Walnut Street, Suite 1100, Philadelphia, PA 19102-3406, USA)

If you would like e-versions of our content, please visit our online platform: www.woodheadpublishingonline.com. Please recommend it to your librarian so that everyone in your institution can benefit from the wealth of content on the site.

We are always happy to receive suggestions for new books from potential editors. To enquire about contributing to our Energy series, please send your name, contact address and details of the topic/s you are interested in to sarah.hughes@woodheadpublishing.com. We look forward to hearing from you.

The team responsible for publishing this book:

Commissioning Editor: Sarah Hughes
Publications Coordinator: Adam Hooper
Project Editor: Sarah Lynch
Editorial and Production Manager: Mary Campbell
Production Editor: Adam Hooper
Project Manager: Newgen Knowledge Works Pvt Ltd
Copyeditor: Newgen Knowledge Works Pvt Ltd
Proofreader: Newgen Knowledge Works Pvt Ltd
Cover Designer: Terry Callanan

© Woodhead Publishing Limited, 2013

Woodhead Publishing Series in Energy: Number 20

Modern gas turbine systems

High efficiency, low emission, fuel flexible power generation

Edited by
Peter Jansohn



Oxford Cambridge Philadelphia New Delhi

© Woodhead Publishing Limited, 2013

Published by Woodhead Publishing Limited,
80 High Street, Sawston, Cambridge CB22 3HJ, UK
www.woodheadpublishing.com
www.woodheadpublishingonline.com

Woodhead Publishing, 1518 Walnut Street, Suite 1100, Philadelphia,
PA 19102-3406, USA

Woodhead Publishing India Private Limited, 303 Vardaan House, 7/28 Ansari Road,
Daryaganj, New Delhi – 110002, India
www.woodheadpublishingindia.com

First published 2013, Woodhead Publishing Limited
© Woodhead Publishing Limited, 2013; chapters 4, 5, 6, 8, 9 and 15
© Alstom Technology Ltd, 2013. The publisher has made every effort to
ensure that permission for copyright material has been obtained by authors wishing to
use such material. The authors and the publisher will be glad to hear from any copyright
holder it has not been possible to contact.
The authors have asserted their moral rights.

This book contains information obtained from authentic and highly regarded
sources. Reprinted material is quoted with permission, and sources are indicated.
Reasonable efforts have been made to publish reliable data and information, but
the authors and the publishers cannot assume responsibility for the validity of all
materials. Neither the authors nor the publishers, nor anyone else associated with
this publication, shall be liable for any loss, damage or liability directly or indirectly
caused or alleged to be caused by this book.

Neither this book nor any part may be reproduced or transmitted in any form or
by any means, electronic or mechanical, including photocopying, microfilming and
recording, or by any information storage or retrieval system, without permission in
writing from Woodhead Publishing Limited.

The consent of Woodhead Publishing Limited does not extend to copying for
general distribution, for promotion, for creating new works, or for resale. Specific
permission must be obtained in writing from Woodhead Publishing Limited for
such copying.

Trademark notice: Product or corporate names may be trademarks or registered
trademarks, and are used only for identification and explanation, without intent to
infringe.

British Library Cataloguing in Publication Data
A catalogue record for this book is available from the British Library.

Library of Congress Control Number: 2013942580

ISBN 978-1-84569-728-0 (print)
ISBN 978-0-85709-606-7 (online)
ISSN 2044-9364 Woodhead Publishing Series in Energy (print)
ISSN 2044-9372 Woodhead Publishing Series in Energy (online)

The publisher's policy is to use permanent paper from mills that operate a
sustainable forestry policy, and which has been manufactured from pulp which is
processed using acid-free and elemental chlorine-free practices. Furthermore, the
publisher ensures that the text paper and cover board used have met acceptable
environmental accreditation standards.

Typeset by Newgen Knowledge Works Pvt Ltd
Printed by Lightning Source

© Woodhead Publishing Limited, 2013

Contents

Contributor contact details *xiii*
Woodhead Publishing Series in Energy *xvii*

Part I Overview of modern gas turbine systems 1

1 Introduction to gas turbines 3
A. J. A. Mom, European Turbine Network ETN, Belgium

1.1 Introduction 3
1.2 The importance of gas turbines for worldwide CO_2 reduction 4
1.3 Importance of gas turbines for the aviation sector 5
1.4 Importance of gas turbines for the power generation sector 7
1.5 Efficiency improvement: impact on other issues 11
1.6 Other trends in gas turbine technology 16
1.7 Market trends 19
1.8 Conclusion 19
1.9 References 20

2 Overview of gas turbine types and applications 21
P. Jansohn, Paul Scherrer Institute, Switzerland

2.1 Introduction 21
2.2 Gas turbine types by application 21
2.3 Power generation 23
2.4 Aero-engines 28
2.5 Industrial turbines 31
2.6 Microturbines 35
2.7 Advantages and limitations 36
2.8 Future trends 38

© Woodhead Publishing Limited, 2013

2.9 Sources of further information and advice 41
2.10 References 41

3 Fundamentals of gas turbine cycles: thermodynamics, efficiency and specific power 44
U. Desideri, Università degli Studi di Perugia, Italy

3.1 Introduction 44
3.2 Thermodynamic properties of gases 46
3.3 The Joule–Brayton cycle 50
3.4 Improvements to the simple cycle 64
3.5 Combined gas–steam cycles 79
3.6 Basics of blade cooling 83
3.7 Conclusion and future trends 84
3.8 References 85

Part II Modern gas turbine systems and major components 87

4 Compressors in gas turbine systems 89
W. Kappis, Alstom (Schweiz) AG, Switzerland

4.1 Introduction: role of the compressor 89
4.2 Types of compressor systems 90
4.3 Stationary gas turbine compressor elements 96
4.4 Compressor characteristic parameters 103
4.5 Operational requirements inside a gas turbine 116
4.6 Compressor design process 135
4.7 Technological trends and special features 141
4.8 Acknowledgement 148
4.9 References 148
4.10 Appendix: variables and indexes 149

5 Combustors in gas turbine systems 151
P. Flohr and P. Stuttaford, Alstom (Schweiz) AG, Switzerland

5.1 Introduction 151
5.2 Design principles 153
5.3 Combustor operation 162
5.4 Fuel flexibility 179
5.5 Future trends 184
5.6 References 186

© Woodhead Publishing Limited, 2013

6 Turbines for industrial gas turbine systems 188
M. Schnieder and T. Sommer, Alstom (Schweiz) AG, Switzerland

6.1 Introduction 188
6.2 Interfaces and integration 192
6.3 Aerodynamics 193
6.4 Cooling 202
6.5 Durability and damage mechanisms 207
6.6 Typical parts and interfaces 212
6.7 Future trends 218
6.8 References 220

7 Heat exchangers and heat recovery processes in gas turbine systems 224
B. Sundén, Lund University, Sweden

7.1 Introduction 224
7.2 Heat exchange processes 225
7.3 Heat transfer equipment 228
7.4 Applications 241
7.5 Future trends 242
7.6 Conclusion 243
7.7 Sources of further information and advice 243
7.8 Acknowledgement 243
7.9 References 243
7.10 Appendix: nomenclature 246

8 Turbogenerators in gas turbine systems 247
B. Gellert, Alstom Power Thermal Products, Switzerland

8.1 Introduction 247
8.2 Generator component design 251
8.3 The history of turbogenerator development 276
8.4 Design concepts of turbogenerators for modern gas turbines 294
8.5 Turbogenerator development for gas turbines 312
8.6 Recent developments 318
8.7 Future trends 322
8.8 Acknowledgement 325
8.9 Standard literature 325
8.10 References 326

© Woodhead Publishing Limited, 2013

9 Materials and coatings developments for gas turbine systems and components 327
M. Konter and H-P. Bossmann, Alstom (Schweiz) AG, Switzerland

9.1 Introduction 327
9.2 Turbine parts 327
9.3 Combustor parts 341
9.4 Coatings for hot gas path parts 342
9.5 Ceramics for hot gas path parts 370
9.6 Rotor parts 372
9.7 References 375
9.8 Appendix: nomenclature 379

Part III Operation and maintenance of modern gas turbine systems 381

10 Gas turbine operation and combustion performance issues 383
B. Prade, Siemens AG Energy, Germany

10.1 Introduction 383
10.2 Flame stabilisation mechanisms 387
10.3 Emissions variations 396
10.4 Combustion dynamics 407
10.5 Future trends 415
10.6 References 420

11 Gas turbine performance modelling, analysis and optimisation 423
A. M. Y. Razak, Gas Path Analysis Ltd, UK

11.1 Introduction 423
11.2 Design-point modelling of gas turbine cycles 424
11.3 Steady flow energy equation 426
11.4 The ideal simple gas turbine cycle 427
11.5 Reversibility and efficiency 431
11.6 Thermophysical properties of air and products of combustion 441
11.7 Thermodynamic modelling of gas turbine components applicable for practical gas turbine cycles 444

© Woodhead Publishing Limited, 2013

11.8 Determining component performance using specific heats 463
11.9 Design-point performance modelling, analysis and performance optimisation of practical (shaft power) gas turbines 464
11.10 Design-point performance modelling of aero gas turbines, analysis and optimisation 474
11.11 Component characteristics 483
11.12 Engine configurations 486
11.13 Off-design performance prediction 491
11.14 Transient performance modelling 496
11.15 Off-design performance behaviour of gas turbine cycles 500
11.16 Adaptive model-based control 504
11.17 Future trends 510
11.18 References 512

12 Advanced gas turbine asset and performance management 515
T. Álvarez Tejedor, Endesa Generación, Spain and R. Singh and P. Pilidis, Cranfield University, UK

12.1 Introduction 515
12.2 Gas turbine degradation 518
12.3 Hot gas path management 523
12.4 Centre for remote monitoring and diagnostics (CMD) 533
12.5 E-maintenance and future trends 559
12.6 Key definitions 561
12.7 Acknowledgement 561
12.8 Sources of further information and advice 562
12.9 References 562

13 Maintenance and repair of gas turbine components 565
T. Álvarez Tejedor, Endesa Generación, Spain and R. Singh and P. Pilidis, Cranfield University, UK

13.1 Introduction 565
13.2 Maintenance factors 566
13.3 Outage cycle 569
13.4 Advanced component repair technology 573
13.5 Compressor cleaning 623
13.6 Future trends 628
13.7 Acknowledgement 630
13.8 Bibliography 630
13.9 References 631

© Woodhead Publishing Limited, 2013

14 Fuel flexibility in gas turbine systems: impact on burner design and performance 635
M. Huth and A. Heilos, Siemens AG Energy, Germany

14.1 Introduction 635
14.2 Primary fuel characterization 636
14.3 Fuels directly introduced into gas turbine burners 637
14.4 Integrated gasification combined cycle (IGCC) technology options with and without air-side integration and carbon capture and storage (CCS) 647
14.5 Characterizing fuel gases 650
14.6 Measures for extending operation range for fuel gases 673
14.7 Characterizing liquid fuels 678
14.8 Future trends 680
14.9 References 682

15 Carbon dioxide (CO_2) capture and storage for gas turbine systems 685
C. D. Soothill, M. T. Bialkowski, G. L. Guidati and A. Zagorskiy, Alstom (Schweiz) AG, Switzerland

15.1 Introduction 685
15.2 CO_2 capture technologies 687
15.3 Impact of carbon capture and storage (CCS) on current gas turbines 694
15.4 Novel approaches 700
15.5 Implementation of carbon capture and storage (CCS) for gas turbines 708
15.6 Conclusion 711
15.7 Acknowledgements 711
15.8 References 712

16 Ultra-low nitrogen oxides (NO_x) emissions combustion in gas turbine systems 715
G. E. Andrews, University of Leeds, UK

16.1 Introduction 715
16.2 The NASA clean combustor programme 718
16.3 Acoustic resonance and catalytic combustion 730
16.4 Thermal NO_x formation 734
16.5 Prompt NO_x 740
16.6 Predictions of thermal NO_x 747
16.7 Influence of mixing on thermal NO_x 758

© Woodhead Publishing Limited, 2013

16.8 Impact of fuel-and-air mixing quality on thermal NO_x emissions 763
16.9 Influence of air inlet temperature 765
16.10 Influence of residence time in premixed combustion: reference velocity and reference Mach number 768
16.11 Conclusions 780
16.12 Acknowledgements 781
16.13 References 781

Index *791*

© Woodhead Publishing Limited, 2013

Contributor contact details

(* = main contact)

Editor and Chapter 2

P. Jansohn
Combustion Research Laboratory
Paul Scherrer Institute
5232 Villigen PSI
Switzerland

E-mail: peter.jansohn@psi.ch

Chapter 1

André J. A. Mom
European Turbine Network ETN
Rue Saint Georges 30
1050 Brussels
Belgium

E-mail: andremom@kpnmail.nl

Chapter 3

U. Desideri
Dipartimento di Ingegneria
Università degli Studi di Perugia
Via Duranti 93
06125 Perugia
Italy

E-mail: umberto.desideri@unipg.it

Chapter 4

W. Kappis
Alstom (Schweiz) AG
Brown-Boveri Strasse 7
CH-5401 Baden
Switzerland

E-mail: wolfgang.kappis@power.alstom.com

Chapter 5

P. Flohr
Alstom (Schweiz) AG
Brown-Boveri Strasse 7
CH-5401 Baden
Switzerland

E-mail: peter.flohr@power.alstom.com

Chapter 6

M. Schnieder* and T. Sommer
Alstom (Schweiz) AG
Brown-Boveri Strasse 7
CH-5401 Baden
Switzerland

E-mail: martin.schnieder@power.alstom.com; thomas.sommer@power.alstom.com

© Woodhead Publishing Limited, 2013

Chapter 7

B. Sundén
Department of Energy Sciences
Lund University
SE-221 00
Lund
Sweden

E-mail: bengt.sunden@energy.lth.se

Chapter 8

B. Gellert
Brown Boveri Strasse 7
CH-5401 Baden
Switzerland

E-mail: bernd.gellert@power.alstom.com

Chapter 9

M. Konter* and H-P. Bossman
Alstom (Schweiz) AG
Brown-Boveri Strasse 7
CH-5401 Baden
Switzerland

E-mail: maxim.konter@power.alstom.com; Hans-Peter.Bossmann@power.alstom.com

Chapter 10

B. Prade
Siemens AG Energy
Postbox 101755
45466 Muelheim
Germany

E-mail: prade.bernd@siemens.com

Chapter 11

A. M. Y. Razak
The Annex
Southcross Farm
Hill Lane
Old Sudbury
Bristol
BS37 6RH
UK

E-mail: zak@gpal.co.uk; zak.razak@btinternet.com

Chapters 12 and 13

T. Álvarez Tejedor*
Endesa Generación
C) Ribera del Loira
28042 Madrid
Spain

E-mail: tomas.alvarez@endesa.es

R. Singh and P. Pilidis
Cranfield University
UK

E-mail: R.Singh@cranfield.ac.uk; p.pilidis@cranfield.ac.uk

Chapter 14

M. Huth* and A. Heilos
Siemens AG Energy
Postbox 101755
45466 Muelheim a.d. Ruhr
Germany

E-mail: michael.huth@siemens.com; andreas.heilos@siemens.com

© Woodhead Publishing Limited, 2013

Chapter 15

C. D. Soothill*, M. T. Bialkowski, G. L. Guidati and A. Zagorskiy
Alstom (Schweiz) AG
Brown-Boveri Strasse 7
CH-5401 Baden
Switzerland

E-mail: charles.soothill@power.alstom.com

Chapter 16

G. E. Andrews
Energy and Resources Research Institute
School of Process, Environment and Materials Engineering
University of Leeds
Leeds
LS2 9JT
UK

E-mail: profgeandrews@hotmail.com

© Woodhead Publishing Limited, 2013

Woodhead Publishing Series in Energy

1 **Generating power at high efficiency: Combined cycle technology for sustainable energy production**
Eric Jeffs

2 **Advanced separation techniques for nuclear fuel reprocessing and radioactive waste treatment**
Edited by Kenneth L. Nash and Gregg J. Lumetta

3 **Bioalcohol production: Biochemical conversion of lignocellulosic biomass**
Edited by K. W. Waldron

4 **Understanding and mitigating ageing in nuclear power plants: Materials and operational aspects of plant life management (PLiM)**
Edited by Philip G. Tipping

5 **Advanced power plant materials, design and technology**
Edited by Dermot Roddy

6 **Stand-alone and hybrid wind energy systems: Technology, energy storage and applications**
Edited by J. K. Kaldellis

7 **Biodiesel science and technology: From soil to oil**
Jan C. J. Bart, Natale Palmeri and Stefano Cavallaro

8 **Developments and innovation in carbon dioxide (CO_2) capture and storage technology Volume 1: Carbon dioxide (CO_2) capture, transport and industrial applications**
Edited by M. Mercedes Maroto-Valer

9 **Geological repository systems for safe disposal of spent nuclear fuels and radioactive waste**
Edited by Joonhong Ahn and Michael J. Apted

10 **Wind energy systems: Optimising design and construction for safe and reliable operation**
Edited by John D. Sørensen and Jens N. Sørensen

11 **Solid oxide fuel cell technology: Principles, performance and operations**
Kevin Huang and John Bannister Goodenough

12 **Handbook of advanced radioactive waste conditioning technologies**
Edited by Michael I. Ojovan

© Woodhead Publishing Limited, 2013

13 **Membranes for clean and renewable power applications**
Edited by Annarosa Gugliuzza and Angelo Basile
14 **Materials for energy efficiency and thermal comfort in buildings**
Edited by Matthew R. Hall
15 **Handbook of biofuels production: Processes and technologies**
Edited by Rafael Luque, Juan Campelo and James Clark
16 **Developments and innovation in carbon dioxide (CO_2) capture and storage technology Volume 2: Carbon dioxide (CO_2) storage and utilisation**
Edited by M. Mercedes Maroto-Valer
17 **Oxy-fuel combustion for power generation and carbon dioxide (CO_2) capture**
Edited by Ligang Zheng
18 **Small and micro combined heat and power (CHP) systems: Advanced design, performance, materials and applications**
Edited by Robert Beith
19 **Advances in clean hydrocarbon fuel processing: Science and technology**
Edited by M. Rashid Khan
20 **Modern gas turbine systems: High efficiency, low emission, fuel flexible power generation**
Edited by Peter Jansohn
21 **Concentrating solar power technology: Principles, developments and applications**
Edited by Keith Lovegrove and Wes Stein
22 **Nuclear corrosion science and engineering**
Edited by Damien Féron
23 **Power plant life management and performance improvement**
Edited by John E. Oakey
24 **Electrical drives for direct drive renewable energy systems**
Edited by Markus Mueller and Henk Polinder
25 **Advanced membrane science and technology for sustainable energy and environmental applications**
Edited by Angelo Basile and Suzana Pereira Nunes
26 **Irradiation embrittlement of reactor pressure vessels (RPVs) in nuclear power plants**
Edited by Naoki Soneda
27 **High temperature superconductors (HTS) for energy applications**
Edited by Ziad Melhem
28 **Infrastructure and methodologies for the justification of nuclear power programmes**
Edited by Agustín Alonso

© Woodhead Publishing Limited, 2013

29 **Waste to energy conversion technology**
Edited by Naomi B. Klinghoffer and Marco J. Castaldi

30 **Polymer electrolyte membrane and direct methanol fuel cell technology Volume 1: Fundamentals and performance of low temperature fuel cells**
Edited by Christoph Hartnig and Christina Roth

31 **Polymer electrolyte membrane and direct methanol fuel cell technology Volume 2: *In situ* characterization techniques for low temperature fuel cells**
Edited by Christoph Hartnig and Christina Roth

32 **Combined cycle systems for near-zero emission power generation**
Edited by Ashok D. Rao

33 **Modern earth buildings: Materials, engineering, construction and applications**
Edited by Matthew R. Hall, Rick Lindsay and Meror Krayenhoff

34 **Metropolitan sustainability: Understanding and improving the urban environment**
Edited by Frank Zeman

35 **Functional materials for sustainable energy applications**
Edited by John A. Kilner, Stephen J. Skinner, Stuart J. C. Irvine and Peter P. Edwards

36 **Nuclear decommissioning: Planning, execution and international experience**
Edited by Michele Laraia

37 **Nuclear fuel cycle science and engineering**
Edited by Ian Crossland

38 **Electricity transmission, distribution and storage systems**
Edited by Ziad Melhem

39 **Advances in biodiesel production: Processes and technologies**
Edited by Rafael Luque and Juan A. Melero

40 **Biomass combustion science, technology and engineering**
Edited by Lasse Rosendahl

41 **Ultra-supercritical coal power plant: Materials, technologies and optimisation**
Edited by Dongke Zhang

42 **Radionuclide behaviour in the natural environment: Science, implications and lessons for the nuclear industry**
Edited by Christophe Poinssot and Horst Geckeis

43 **Calcium and chemical looping technology for power generation and carbon dioxide (CO_2) capture: Solid oxygen- and CO_2-carriers**
P. Fennell and E. J. Anthony

© Woodhead Publishing Limited, 2013

44 **Materials' ageing and degradation in light water reactors: Mechanisms, and management**
Edited by K. L. Murty

45 **Structural alloys for power plants: Operational challenges and high-temperature materials**
Edited by Amir Shirzadi, Rob Wallach and Susan Jackson

46 **Biolubricants: Science and technology**
Jan C. J. Bart, Emanuele Gucciardi and Stefano Cavallaro

47 **Wind turbine blade design and materials: Improving reliability, cost and performance**
Edited by Povl Brøndsted and Rogier Nijssen

48 **Radioactive waste management and contaminated site clean-up: Processes, technologies and international experience**
Edited by William E. Lee, Michael I. Ojovan, Carol M. Jantzen

49 **Probabilistic safety assessment for optimum nuclear power plant life management (PLiM): Theory and application of reliability analysis methods for major power plant components**
Gennadij V. Arkadov, Alexander F. Getman and Andrei N. Rodionov

50 **The coal handbook Volume 1: Towards cleaner production**
Edited by D. G. Osborne

51 **The coal handbook Volume 2: Coal utilisation**
Edited by D. G. Osborne

52 **The biogas handbook: Science, production and applications**
Edited by Arthur Wellinger, Jerry Murphy and David Baxter

53 **Advances in biorefineries: Biomass and waste supply chain exploitation**
Edited by K. W. Waldron

54 **Geoscience of carbon dioxide (CO_2) storage**
Edited by Jon Gluyas and Simon Mathias

55 **Handbook of membrane reactors Volume 1: Fundamental materials science, design and optimisation**
Edited by Angelo Basile

56 **Handbook of membrane reactors Volume 2: Reactor types and industrial applications**
Edited by Angelo Basile

57 **Alternative fuels and advanced vehicle technologies: Towards zero carbon transportation**
Edited by Richard Folkson

58 **Handbook of microalgal bioprocess engineering**
Christopher Lan and Bei Wang

© Woodhead Publishing Limited, 2013

59 **Fluidized bed technologies for near-zero emission combustion and gasification**
Edited by Fabrizio Scala
60 **Managing nuclear projects: A comprehensive management resource**
Edited by Jas Devgun
61 **Handbook of process integration: Minimisation of energy and water use, waste and emissions**
Edited by Jiří Klemeš
62 **Membranes for clean and renewable power production**
Edited by Annarosa Gugliuzza and Angelo Basile

© Woodhead Publishing Limited, 2013

1

Introduction to gas turbines

A. J. A. MOM, European Turbine Network ETN, Belgium,

DOI: 10.1533/9780857096067.1.3

Abstract: This chapter provides an overview of the importance of gas turbines for the power generation and oil and gas sector and – in less detail – the aviation sector. Worldwide trends in power generation and electricity conversion processes and the role of gas turbines to minimise CO_2 emissions are addressed. Gas turbines are essential and crucial to reduce emissions both in aviation and in power production. Technologies for improving gas turbine and system efficiency, through higher turbine inlet temperatures, improved materials, cooling methods and thermal barrier coatings are described. New thermodynamic approaches, including intercooling, water and steam injection and hybrid cycles are addressed. Major issues are also fuel and operational flexibility, reliability and availability, cost reduction and power density, especially for the offshore sector. Market trends have been sketched. In the coming decades, gas turbines will be one of the major technologies for CO_2 emission reductions in the power generation, aviation, oil and gas exploration and transport sectors. This prognosis is based on their high current efficiency and further efficiency improvement potential, both for simple cycle as for combined-cycle applications.

Key words: aircraft propulsion, simple and combined cycle efficiency, NO_x reduction, 450 scenario, global warming, zero carbon emission, IGCC, CO_2 capture, life cycle costs, hybrid cycles, bottoming cycles, fuel flexibility, operational flexibility, carbon capture and storage, hydrogen.

1.1 Introduction

In modern society there is still little appreciation of what a gas turbine is or does. This is in contrast to diesel or gasoline engines, the so-called reciprocating engines, since most people know that these are the motors which drive our cars and trucks. Despite this general lack of recognition, gas turbines are essential to everyday life. Modern air traffic would not exist without gas

© Woodhead Publishing Limited, 2013

turbines, and we would also have serious shortages in electricity production without them.

So what is a gas turbine? It is an internal combustion engine that burns gaseous or liquid fuel. It delivers the energy of this combustion either by means of thrust, in an aircraft jet engine; or – by means of a rotating shaft – it provides (a) electricity via a generator, or (b) mechanical power for driving compressors or ship propulsion.

Most aircraft engines are now gas turbines. In the early part of the twentieth century reciprocating (gasoline) engines were used as the main propulsion units for aircraft, but this changed after the World War II. Nowadays, civil and military airplanes, helicopters and business jets all use gas turbines because of their superior thrust/weight ratio. Only the small general aviation aircraft still use reciprocating engines.

In the power generation sector, gas turbines have also become the main technology for conversion of fossil fuels into electricity. Conventional gas- and oil-fired steam plants have been replaced by very efficient combined-cycle power plants using gas turbines for the combustion of gas or oil. The combined-cycle works as follows. Firstly, the gas turbine drives a generator, delivering two-thirds of the total power output. Secondly, the hot exhaust gas from the turbine passes through a boiler to produce steam that drives a steam turbine and a coupled generator. This secondary system delivers the remaining third of the total power output of the combined-cycle power plant. An important variation is co-generation, or combined heat and power. In this case, the steam produced in the boiler is used for process heat. There are many applications for co-generation, for example, in the paper, process and food and beverage industries.

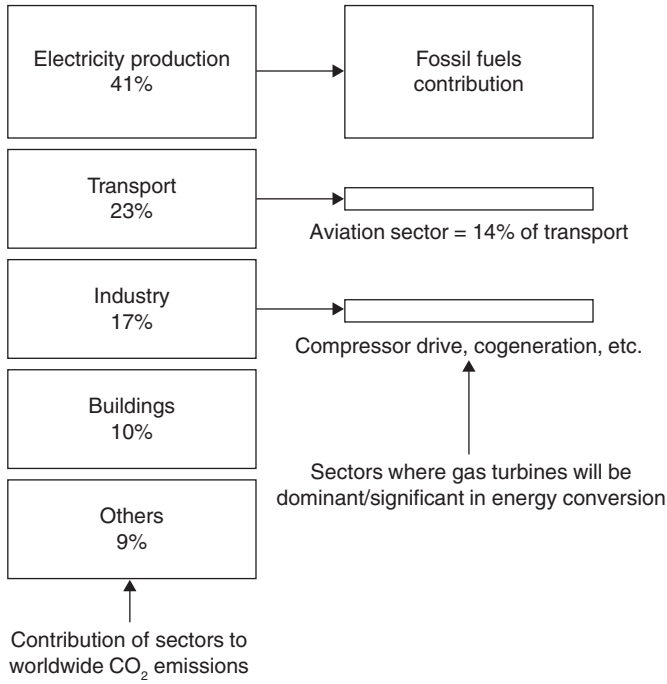
Apart from these major areas, gas turbines are also used in a variety of other applications. In the oil and gas sector, gas turbines drive compressors or pumps for gas- and oil-processing and transport. Furthermore, gas turbines often power fast ferries and military vessels owing to their superior power/weight ratio. There is also a new trend to apply very small gas turbines for pre-firing in central heating systems.

1.2 The importance of gas turbines for worldwide CO_2 reduction

Gas turbine technology is very important in terms of future worldwide reduction of CO_2 emissions. In the power generation sector, which is the greatest contributor to CO_2 emissions, CO_2 reduction is currently the driving factor, see Fig. 1.1. If worldwide CO_2 emissions have to be reduced by 20% in 2020, and by more than 50% in 2050, then gas turbines will surely play a crucial role, owing to their high efficiency and fuel flexibility.

In the aviation sector, propulsion is delivered principally by gas turbines, as mentioned earlier. There is massive political pressure to make air

© Woodhead Publishing Limited, 2013



1.1 Sources of worldwide CO_2 emissions and potential of gas turbines (in 2010).

transport cleaner, both in terms of noise reduction as well as fuel reduction, and hence reduced CO_2 and NO_x emissions. Gas turbine technology improvements will be crucial here too.

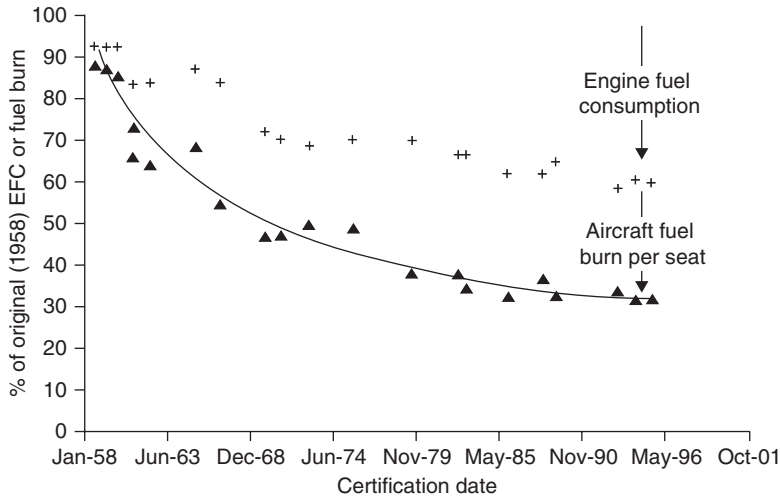
Overall, it can be seen from Fig. 1.1 that gas turbines play, or will play, an important role in the sectors, responsible for about 50% of the total worldwide CO_2 emissions. It is evident that these very ambitious goals for reducing CO_2 emissions cannot be achieved without full exploitation of advanced gas turbine technology.

Although this book addresses the topic of modern gas turbines for the power generation and oil and gas sector, the author considers it important to sometimes make a short excursion to the aviation sector, to highlight the versatility of the technology and the opportunities and potential of gas turbines.

1.3 Importance of gas turbines for the aviation sector

During the last decades the efficiency increases achieved in the aviation sector have been enormous. Figure 1.2[1] shows the engine and aircraft fuel

© Woodhead Publishing Limited, 2013



1.2 Efficiency developments in the aviation sector since 1960.[1]

consumption over a 50-year time period. A more than 70% increase in efficiency (per passenger seat) can be noted, and the gas turbine engine has been responsible for the greatest part of it. For the next decades, additional and large improvements are foreseen.

The ACARE (Advisory Council for Aviation Research and Innovation in Europe) Group of Personalities, which in 2001 produced its Vision 2020 report,[2] and which has now produced a vision beyond 2020 towards 2050, mentioned three main goals for the aviation sector to be realised in 2020:

- 50% reduction in fuel consumption.
- 50% reduction of perceived noise.
- 80% reduction in NO_x emission.

Of course, air transport emissions should be seen in the right perspective. Aviation currently accounts for 2% of global CO_2 emissions. In the worst-case future scenario, this figure would grow to about 5% in the next 30 years. However, even though this is still a relatively small contribution, the political pressure to drastically lower this figure will be enormous.

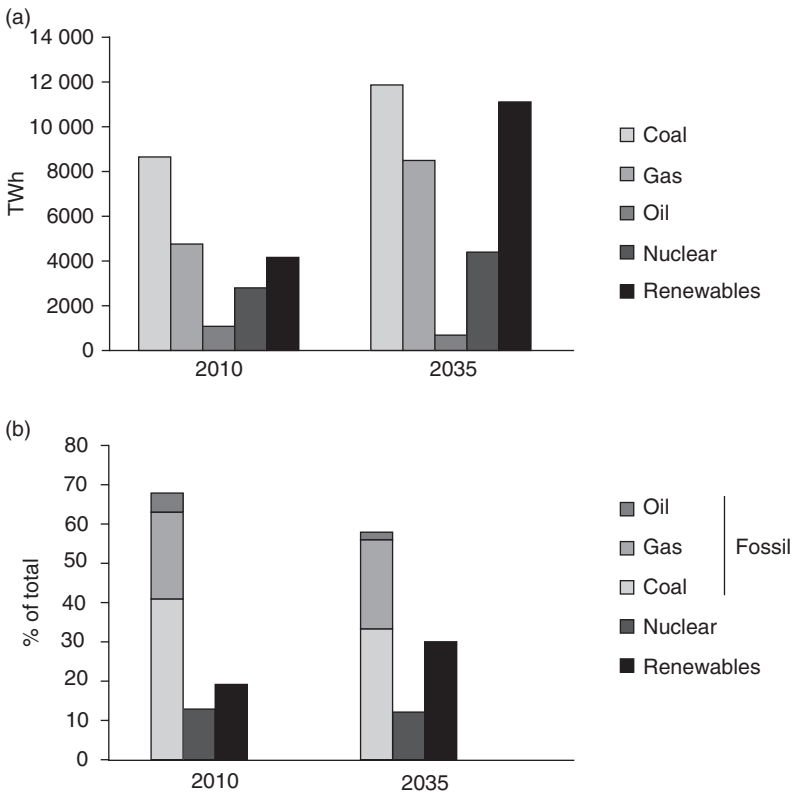
It is evident that the gas turbine engine must be responsible for the biggest share in the achievement of all these ambitious goals. It will not be easy, because some ambitions, for example, increased efficiency and lower NO_x levels, conflict with current technology. Achieving all the above goals is extremely challenging and may need very complex and innovative technical

© Woodhead Publishing Limited, 2013

solutions. Nevertheless, major efforts are underway to address these issues, including trade-offs between conflicting targets.

1.4 Importance of gas turbines for the power generation sector

Gas turbines are not only crucial for developments in the aviation sector, they are essential and critical as well for modern electricity production. This will be illustrated in this and following paragraphs, indicating trends in worldwide electricity production, the various conversion processes for power generation, including their CO_2 emissions, and the role gas turbines can play in reducing these emissions. Figure 1.3 shows the worldwide electricity generation by fuel type in 2010, and the outlook for 2035.



1.3 Electricity production by fuel type in 2010 and 2035 (absolute (a) and relative (b)).

© Woodhead Publishing Limited, 2013

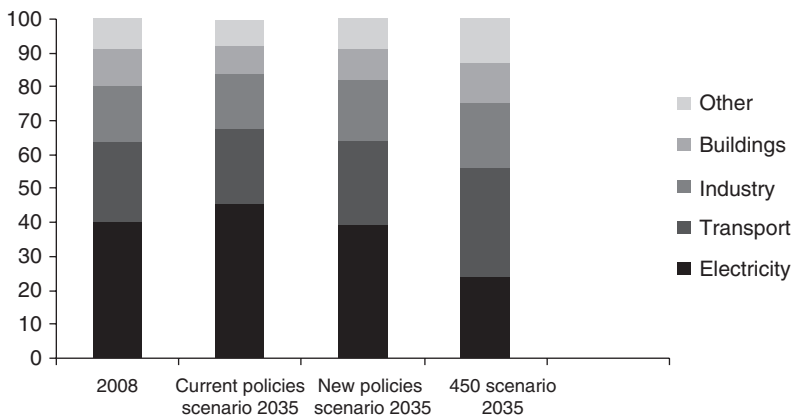
1.4.1 Global power generation

Global electricity power generation rises from 21 400 TWh in 2010 to over 36 000 TWh in 2035 (New Policies Scenario IEA, 2012[3]). It turns out that the coal share in electricity production drops significantly from 41% to 33%; renewables grow from 19% to 30%. The gas share is slowly rising (the absolute amount is strongly increasing); the nuclear share makes an opposite shift. Oil falls to only 2%. Despite the considerable growth of renewables up to 2035, fossil fuels will still account for 58% of worldwide electricity production.

As indicated before, electricity production is the biggest contributor to worldwide CO_2 emissions, compared to transport, industry or residential heating (Fig. 1.4[4]). In 2008, electricity production accounted for 41% of worldwide CO_2 emissions. This percentage will either grow or slightly fall, dependent on the scenario foreseen. However, in the 450 scenario, considered as a plausible pathway for deriving a maximum of 450 ppm CO_2 in the atmosphere, required to limit global warming to 2°C, the power sector emissions have to decrease dramatically. In this context it is important to realise that the European Member States adopted in 2011 a policy which should lead to an essentially carbon emission free power generation sector in 2050. As fossil fuels will still play an important role in the production of electricity at that time, it is clear that the efficiency of the conversion processes is of paramount importance and carbon capture and sequestration (CCS) techniques need to be employed on a large scale.

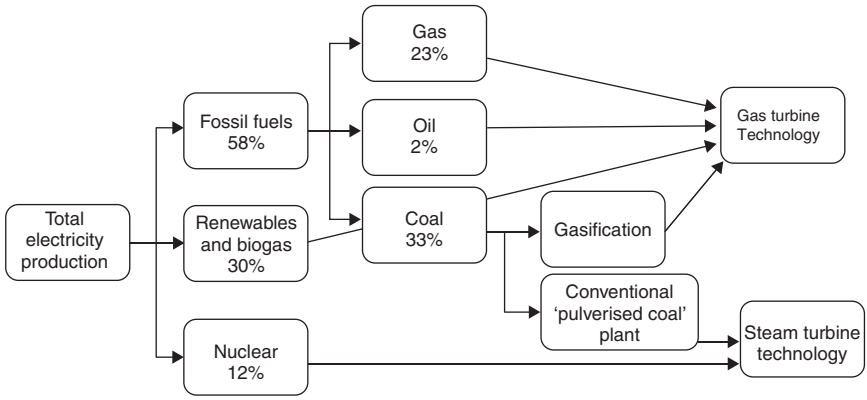
1.4.2 Conversion processes for power generation

Figure 1.5 shows the conversion processes for generating electricity, showing the 58% share of fossil fuels in 2035. For gas and oil there is only one



1.4 Worldwide CO_2 emissions (relative shares) per sector in 2008 and 2035 (various scenarios).[4]

© Woodhead Publishing Limited, 2013



1.5 Conversion processes for electricity production (2035).

conversion route in practice: gas turbines.* Reciprocating engines are sometimes used for electricity production, but this amounts to only a minor portion of the market.

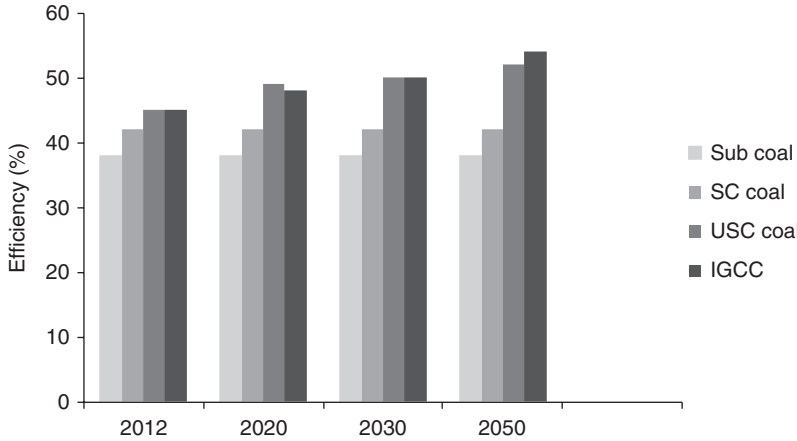
For coal conversion into electricity there are basically two routes: the conventional pulverised coal power plant, and the integrated gasification combined-cycle (IGCC) plant. The first route uses only the conventional steam cycle, whereas the gas turbine and steam turbine cycles are combined in the IGCC plant. Currently IGCC plants are still in the early stages of development and application, and only a few are presently generating power.

However, it is the author's opinion that in the coming decades IGCC plants will be eventually favoured over conventional pulverised coal plants, for environmental and efficiency reasons, see Fig. 1.6.[5] Japanese sources foresee an even much faster introduction and efficiency growth of IGCC than presented here, leading to IGCC efficiencies of 55% before 2025, see Section 1.5.3. Especially when CO_2 capture is, or becomes, mandatory, the available capture systems may well be more easily and efficiently integrated into the IGCC cycle than simply being added at the end of the conventional cycle (end-of-pipe solution).

Hence to conclude: gas turbines are the method of choice for conversion of gas and oil into electricity. For coal, bearing in mind that the IGCC cycle will become more important in the future, gas turbines are also going to play an important role in the conversion process. It is the author's opinion that gas turbines will become the major conversion technology for obtaining electricity from fossil fuels in the decades to come.

* Note: for electricity production gas turbines will normally be combined with steam turbines for efficiency reasons.

© Woodhead Publishing Limited, 2013



1.6 Commercial availability and efficiency improvements of coal conversion technologies (IEA).[5]

1.4.3 CO_2 emission reductions

The need for CO_2 emission reductions is currently the driving force in the power generation sector. Basically there are two routes available:

- Efficiency increase, so less CO_2 is emitted.
- Capture of CO_2, either process-integrated or as an end-of-pipe solution.

Apart from the costs involved in applying the latter method, there is a more valid and negative aspect: the efficiency of the total power plant drops by about 10%-point if a CO_2 capture system is installed. This means, at the current conversion efficiency, that nearly 20% more fuel is needed to produce the same amount of electricity. This is not a very attractive prospect, considering the world's energy resources.

1.4.4 The need for efficiency improvement to reduce CO_2 emissions

The most effective way to reduce CO_2 emissions is to improve the process efficiency. This results in lower CO_2 emissions, and hence less CO_2 to be captured if additional reduction is required. It also implies that scarce resources are not needlessly reduced any further. An example makes this clear: a 1% efficiency increase for a 1000 MW gas fired combined-cycle gas turbine (CCGT) power plant reduces the CO_2 emissions by 50 000 ton/year.

Since gas turbines represent the preferred method of obtaining electricity from fossil fuels, gas turbine efficiency should be the major focus of technology development in the coming decades. We may expect that increases in gas

© Woodhead Publishing Limited, 2013

turbine efficiency and the retrofitting of new technologies in older installations will result in major CO_2 emission reductions. It should also be emphasised that higher plant efficiency greatly mitigates the cost penalty for CO_2 capture.

The vast efficiency increases in modern gas turbine power plants make clear that retrofit of existing plants is of utmost importance. There is an enormous CO_2 reduction potential if older, existing plants are either replaced by new ones or retrofitted with the latest technology. An article in Power Engineering[6] stated that worldwide 1 Gton of CO_2 could be avoided if the older coal-fired power plants were to be brought up to an efficiency level of 35.5%, which is an (easily) achievable target.

Total CO_2 emissions of all power plants worldwide are currently about 12 Gton/year. The emission reduction figure of 1 Gton/year increases if conventional gas and oil plants are also considered. In addition, a further efficiency increase of coal-fired power plants is attainable, both for pulverised coal power plants by using the latest technology (e.g., the supercritical steam cycle) and, surely, by applying IGCC. If all these efficiency measures are applied, a 20–30% reduction in worldwide CO_2 power plant emissions is easily achievable.

Besides the above considerations, it is important to note that gas turbines will be used in the future to convert bio-fuels into electricity or propulsive power for aircraft.

1.5 Efficiency improvement: impact on other issues

So far, this chapter has focused on the importance of gas turbine efficiency in view of greenhouse gas (CO_2) emissions and climate change. However, efficiency has a much broader significance. For stationary gas turbines the following additional factors can be mentioned:

- Fuel cost is the dominating factor in total life cycle costs of gas turbine power plants.
- High plant efficiency strongly increases the incentive to replace older, low efficiency, units.

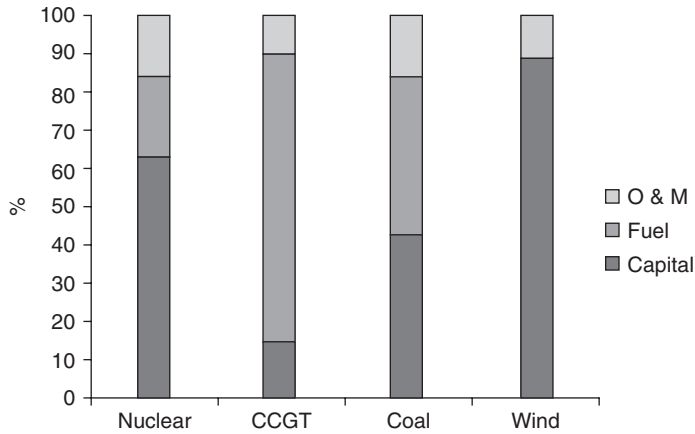
These factors will be discussed in more detail below.

1.5.1 Total life cycle costs: importance of efficiency measures

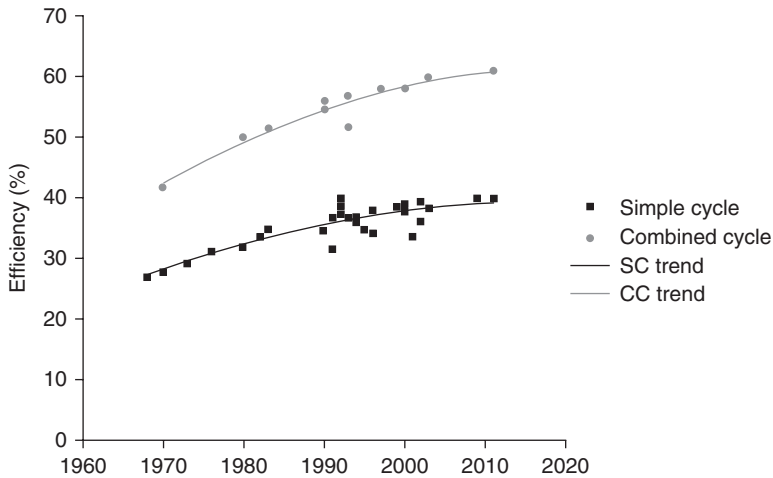
The total life cycle costs of power plants are based on capital costs, fuel costs and operation and maintenance costs. Figure 1.7[7] shows these cost elements for the current electricity generation systems.

Fuel costs turn out to be the most important for CCGT power plants; hence, efficiency increases will have a direct and major effect on the financial

© Woodhead Publishing Limited, 2013



1.7 Factors influencing life cycle costs for various power generation systems.[7]



1.8 Efficiency improvement of gas turbines since 1960.

performance of these plants. In addition, investments in gas turbine efficiency will have a relatively shorter payback time than similar efficiency measures for competing systems. In this regard it is not surprising that the sharp increase in fuel prices since the early 1970s has stimulated much R&D on gas turbine and system efficiency.

Basically there have been two technology routes:

- Efficiency improvement of the gas turbine itself.
- Efficiency improvement of the total system.

© Woodhead Publishing Limited, 2013

The gas turbine efficiency, in particular, has increased enormously over the last decades. This is illustrated by Fig. 1.8.

1.5.2 Technologies for improved gas turbine and system efficiency

The gas turbine efficiency improvements have resulted from a combination of technology efforts:

- Improved materials with better high temperature capability.
- Improved cooling.
- The development of thermal barrier coatings.
- More advanced aerodynamic design for blades.
- Reduction of losses (e.g., by better sealing capability).

The total system efficiency improvements have been realised by:

- Optimised thermodynamic design for the gas turbine and steam turbine cycle.
- Improved performance of the steam cycle (supercritical steam loop).
- The application of bottoming cycles or waste heat recovery units (e.g., for city heating).

In the future these developments will continue, certainly if fuel prices continue to increase. Further advances are foreseen in materials, thermal barrier coatings and, especially, cooling technology. In Japan a superalloy was recently developed with 100°C better temperature capability!

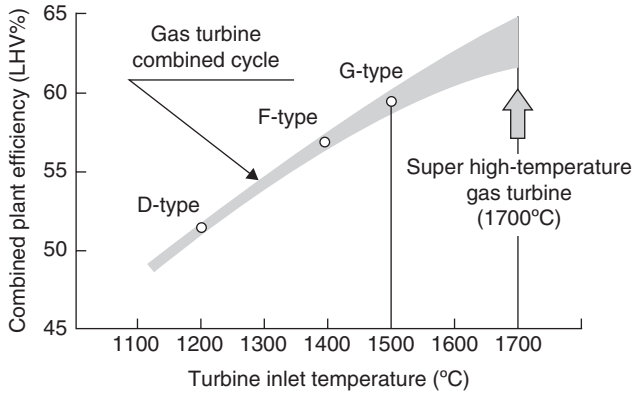
Higher turbine inlet temperatures

Some decades ago much attention was being paid to the development of ceramics for providing a major step in gas turbine efficiency. At the time, the general opinion was that the limits of the 'standard' superalloys for further temperature increases had been reached, and major turbine temperature increases would require the use of ceramics.

However, the expectations about ceramic applications for gas turbine blades have not been fulfilled until now, owing to concerns about manufacturing quality, ductility and operational life. Hence, higher turbine inlet temperature developments still concentrate on Ni-superalloy improvement, in combination with advanced processing (directionally-solidified and single-crystal processing), on new cooling features and on the application of advanced thermal barrier coatings. These have all led to remarkable improvements.

However, future major efficiency improvements may require substitutes for the current Ni-superalloy substrate materials. These might be sought not only

© Woodhead Publishing Limited, 2013



1.9 Turbine inlet temperature and combined-cycle plant efficiency.[8]

in ceramics but also in ceramic matrix composites (CMC), hybrid materials, etc. These topics will be treated in the appropriate sections in this book.

Current advanced stationary gas turbine inlet temperatures are in the 1300–1500°C range. The Mitsubishi J-type machine, entering the market in 2013, will be based on a 1600°C inlet temperature. The national gas turbine R&D programme in Japan is aiming for a 1700°C turbine inlet temperature. This will enable a combined-cycle plant efficiency of 65%, see Fig. 1.9.[8]

Other potential ways to improve efficiency

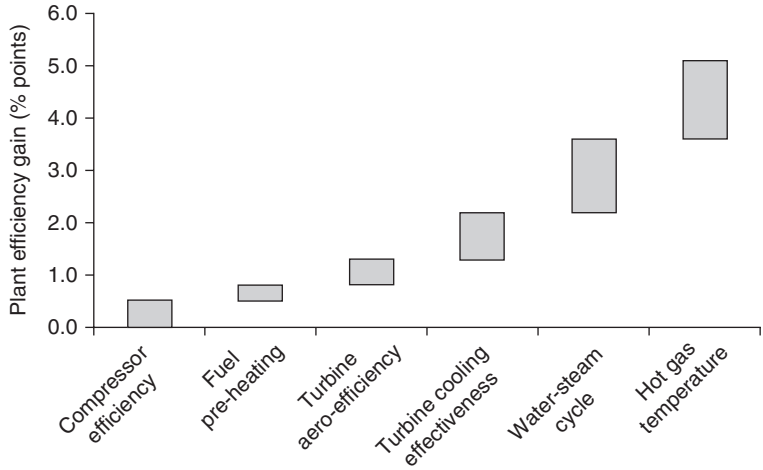
Manufacturers have presented several options for improved efficiency, see Fig. 1.10.[7] These range from the gas turbine itself, for example, compressor and turbine efficiency improvement by more advanced aerodynamic design, to cooling effectiveness, fuel pre-heating and again to turbine inlet temperature increase.

In addition, thermodynamic improvements of the total system provide serious potential. Much research is being done on advanced cycles. Rolls-Royce have presented various aero-derivative cycle options for increased efficiency, see Fig. 1.11.

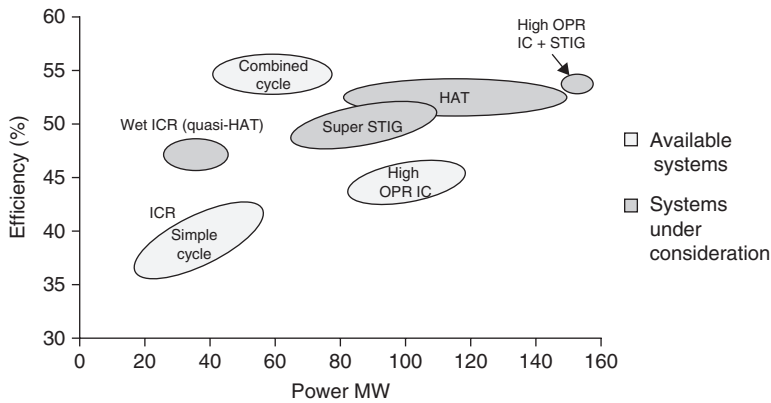
Options which are seriously being addressed and applied are:

- *Intercooling*: the gas turbine compressor consumes about two-thirds of the total energy input. Cooling of the compressed air at one or various stages in the compressor reduces the amount of compressive work. In addition, a lower compressor exit temperature provides colder cooling air for the turbine and allows the turbine inlet temperature to be increased. All these effects result in a higher total efficiency.
- *IC/Overall pressure ratio (OPR)*: intercooling provides an additional opportunity to increase the overall pressure ratio and hence the efficiency.

© Woodhead Publishing Limited, 2013



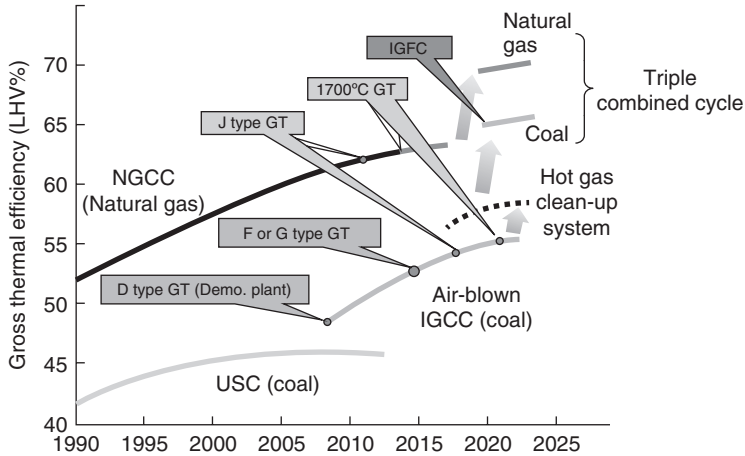
1.10 Future potential pathways to improve heavy duty GTCC plant efficiency (Alstom).[7]



1.11 Cycle options for aero-derivative-based GTCC plants (Rolls-Royce).[7]

- *Water injection in the compressor*: the heat required for evaporation of injected water restricts the temperature increase in the compressor and hence the required compressive work.
- *Steam injection (STIG) in the combustor*: this will result in an increase in mass flow and the specific heat of the working fluid. Apart from efficiency improvements, this results in lower NO_x emissions.
- *Recuperation*: part of the exhaust heat energy of the gas turbine is used to preheat the compressor exit air before it enters the combustor.

© Woodhead Publishing Limited, 2013



1.12 Efficiency improvement of gas fired CC and coal-fired IGCC and their combination with fuel cells (Mitsubishi).[9]

Full implementation of these technological options has yet to be done. The GE LM100 turbine is presently the best example for which some (intercooling, OPR and STIG) have been applied. This partial implementation has already led to a single cycle efficiency of more than 46%, well beyond the limit for simple cycles, see Fig. 1.11.

1.5.3 Hybrid cycles

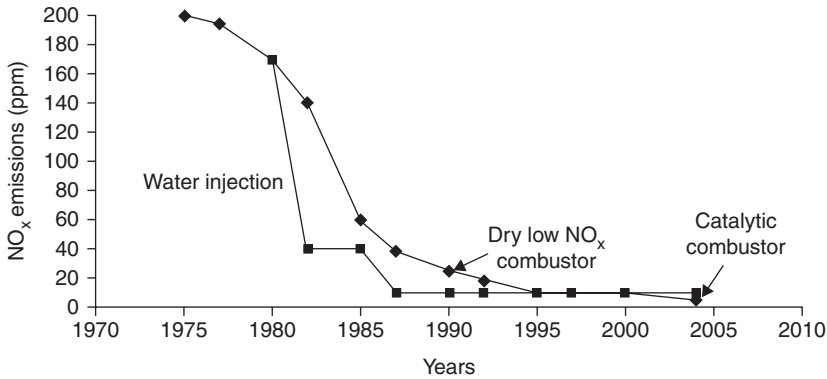
In the near future hybrid cycles combining gas turbines and, for example, fuel cells might become available. If this is feasible, efficiencies above 70% will come within reach. This still requires much work on the commercialisation of the fuel cell, in terms both of technology and cost. Integration of the fuel cell and the gas turbine in a hybrid cycle would then be the next step. Mitsubishi have shown various scenarios for efficiency improvement by combining gas fired combined cycles and coal-fired IGCC with fuel cells leading to efficiencies of 65% for IGCC and more than 70% for gas fired CC, see Fig. 1.12.[9]

Another future option for hybrid cycles is the GT-CSP system. Concentrated solar power (CSP) will then act as an external combustor for a gas turbine. Currently, ideas are being developed for early demonstration of this advanced technology.

1.6 Other trends in gas turbine technology

Besides efficiency, other developments play an important role in gas turbine development. Emission reduction, especially related to NO_x, has been

© Woodhead Publishing Limited, 2013



1.13 Control of gas turbine NO_x emissions over the years.[10]

a major issue for the last 30 years. Fuel and operational flexibility, the reliability and availability of gas turbines, and the lowering of life cycle costs are also main concerns for the gas turbine operators and users.

1.6.1 NO_x reduction

NO_x emission reduction has received much attention since the 1970s, owing to emission regulations in various countries. Until that time, NO_x emissions were far above 100 ppm, because of the use of diffusion-type burners using undiluted fuel with massive amounts of secondary air. The resulting high combustion temperatures caused severe NO_x emissions. In the following years the NO_x emissions gradually decreased, see Fig. 1.13.[10]

Water injection was initially applied for reducing emissions. In the 1990s the DLN (Dry Low NO_x) technique was introduced, resulting in a large reduction of NO_x formation. Nowadays, NO_x emissions of 9 ppm using DLN technology are attainable, although it should be realised that the application of DLN, and the reliable control and operation of the gas turbine over its full operating envelope, is a continuous challenge.

If further reductions in NO_x emissions below the 9 ppm level are required, additional steps will be needed, such as selective catalytic reduction. In this case the SCR end-of-pipe cleaning system converts NO_x into molecular N_2 and O_2.

1.6.2 Fuel flexibility

Fuel flexibility is one of the major and inherent advantages of gas turbines. In principle, any gaseous or liquid fuel can be burnt in a gas turbine. Gaseous fuels might be, for example, natural gas, refinery gas, coke oven gas, low BTU coal gas, syngas or biomass gas. Liquid fuels might vary between the light

© Woodhead Publishing Limited, 2013

distillates, naphtha, kerosene and diesel, up to heavy distillates and even crude oil. Care must be taken to remove trace elements such as vanadium, sodium and potassium, because of their strong influence on hot corrosion. Fuels consisting of heavy distillates and crude oil require pre-heating.

Natural gas is currently the standard fuel for land-based gas turbines. It results in the longest lifetimes for gas turbine components. The use of liquid fuels is decreasing, especially for electricity production, but it is still popular where these fuels are abundantly available, as in offshore locations, the Middle East, or along pipelines.

Although gas turbines are fuel-flexible, there is still a need for increased fuel flexibility, especially when carbon capture and storage (CCS) is applied. CO_2 capture technologies, especially pre-combustion CO_2-capture, will require the combustion of H_2-rich gases in the gas turbine. Some current technologies developed by gas turbine manufacturers allow for a small percentage of syngas to be mixed with natural gas. However, there are no generally available techniques to enable low NO_x operation with undiluted hydrogen-rich syngas.[11] This means that research on combustion of H_2-rich syngas in gas turbines is essential to enable the introduction of coal gasification in combination with pre-combustion CO_2-capture.

Operational flexibility is another major issue in power generation. The increasing share of solar and wind power in electricity production requires a fast-reacting back-up system, to counterbalance their intermittent nature and to prevent an unstable grid. Gas turbines can and will play a key role in ensuring flexibility in the electricity system and in matching the intermittency of the renewable energy sources. However, this new requirement will change the mode of operation of CCGT power plants dramatically in the coming years. For example, from a base load operation of 12 starts per year and 8000 h of operation, operation will become cyclic, load following, with as many as 250 or more starts with only 3000 h (or less) of operation per year, often at part load. This type of operation, including maintaining a spinning reserve to provide back-up during periods of reduced renewable power production, will result in lower efficiency, higher costs and higher emissions of CO_2 and NO_x per produced kWh.

Gas turbine and power plant technology has to change radically in the coming decades to adapt to these operational flexibility requirements. Transient behaviour, fatigue characteristics, part load efficiency and ensured low emission levels will be essential in new development programs.

1.6.3 Reliability and availability

Apart from efficiency and costs, reliability and availability are of great importance to the gas turbine operator. Reliability and availability have been enormously improved over the last decades. Data published in 2011

© Woodhead Publishing Limited, 2013

and 2012[12,13] show that gas turbine reliability, dependent upon plant type and performance cycle, varies between 97% and 99% (median values, average values considerably lower), and availability varies between 92% and 97% (median values) or 89–95% average. The market, however, still requires further significant improvements, with long term reliability and availability goals above 99% and 98% respectively.

1.7 Market trends

From the previous sections of this chapter it should be clear that there is an enormous potential in market growth for gas turbines. Basically there are four reasons for this:

- The absolute growth in power generation.
- Growth in the production and transport of fossil fuels, requiring compressor capacity and new high density power concepts (low weight and volume).
- The growing application of gas turbines for conversion of coal into electricity (IGCC).
- The replacement of conventional steam power plants by modern combined-cycle plants.

Current worldwide power capacity (in 2011) is about 5429 GW.[3] This figure will grow to 9340 GW by 2035, a net increase of 3900 GW (IEA, New Policies Scenario). However, the total capacity addition between 2011 and 2035, including replacements of old plants, will be 5890 GW. Nearly 1400 GW of these gross capacity additions will be gas fired power plants; coal (including IGCC) and wind will take respectively 1100 and 1250 GW. Based on these figures, an average yearly minimum of 58 GW of gas turbine powered plants will be realised up to 2035. Based on an estimate that eventually half of the new coal capacity would be built as IGCC, this figure could easily grow to 80 GW per year. Moreover, these figures reflect only the market potential of gas turbines in the power generation sector. There is an additional high potential for the growing oil and gas exploration and transport sectors.

1.8 Conclusion

The future for gas turbine technology looks bright, with many new developments and potentially new applications. Efficiency, also at part load, flexibility, emission reduction, reduction of operational costs, reliability, availability and power density, that is, compact weight and volume, the latter especially for the oil and gas sector, are major issues to be addressed. New hybrid concepts under development will enable a further step in efficiency improvement.

© Woodhead Publishing Limited, 2013

In the coming decades, gas turbines will become one of the major technologies for CO_2 emission reductions in the power generation, aviation, oil and gas exploration and transport sectors. This prognosis is based on their high current efficiency, and their strong potential for further efficiency improvement, both for simple cycle machines as for combined-cycle applications. In addition, highly efficient gas turbine combined-cycle power plants will provide a strong incentive to replace old and inefficient plant capacity.

In the aviation sector, gas turbines will be the main instrument for realising the ACARE Vision 2020 objectives of 50% fuel reduction, 80% NO_x reduction and 50% noise reduction. New technologies developed in the aviation sector will be adopted in other transport and land-based gas turbines and vice versa. This book will provide the reader with an overview of the current gas turbine technology status and new and exciting developments to come.

1.9 References

1. The IATA Technology Roadmap Report, (June 2009), 3rd Edition.
2. ACARE (Advisory Council for Aviation Research and Innovation in Europe), 'European Aeronautics: A Vision for 2020', (January 2001).
3. 'World Energy Outlook 2012'; International Energy Agency IEA, ISBN 978-92-64-18084-0.
4. 'World Energy Outlook 2010'; International Energy Agency IEA, ISBN 978-92-64-08624-1.
5. IEA, Energy Technology Perspectives, (2012).
6. S. Stallard and P. DiPietro, 'An opportunity to improve coal-fired generation efficiency', *Power Engineering*, 122–125, (2009).
7. P. Holmes and J. Logan, 'Gas Turbine OEMs – What next efficiency', *Presentation at ETN's The Future of Gas Turbine Technology 3rd International Conference*, (October 2006), Brussels.
8. M. Ishikawa, M. Terauchi, T. Komori and J. Yasuraoka, 'Development of high-efficiency gas turbine combined cycle power plant', Mitsubishi Heavy Industries, *Technical Review*, **45**(1), (2008).
9. K. Sakamoto, *Commercialization of Mitsubishi IGCC/Gasification Technology*, Gasification Technologies Conference, San Francisco, (October 2011).
10. M.P. Boyce, *Gas Turbine Engineering Handbook,* Elsevier Inc, Burlington, MA 01803, (2006). ISBN 0-88415-732-6.
11. 'Gas Turbine Fuel Flexibility for Zero Emission Plant', ETN Position Paper, European Turbine Network, Brussels, http://www.etn-gasturbine.eu, (August 2007).
12. S.A. DellaVilla, Updating gas-turbine reliability, availability; *Combined Cycle Journal*, Published by PSI Media Inc, Las Vegas, (1Q/2012).
13. S.A. DellaVilla, RAM statistics: can everyone be above the average? *Combined Cycle Journal*, Published by PSI Media Inc, Las Vegas, (2Q/2011).

© Woodhead Publishing Limited, 2013

2

Overview of gas turbine types and applications

P. JANSOHN, Paul Scherrer Institute, Switzerland

DOI: 10.1533/9780857096067.1.21

Abstract: Various gas turbine types have been introduced into a wide range of commercial applications. In this chapter the key performance characteristics are described for gas turbines in use for power generation, propulsion systems on land, sea and air, as well as for mechanical drives in industrial processes. Characteristic operating parameters are provided for large stationary systems (multi-MW range) down to small size (kW range) mobile systems.

Key words: combined cycle gas turbine plants, aero-derivative gas turbines, mechanical drives, industrial gas turbines, microturbines.

2.1 Introduction

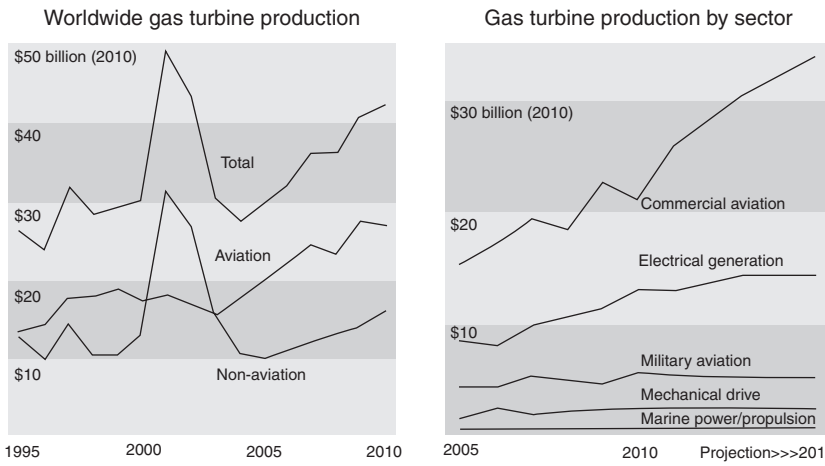
Gas turbines have made their way into quite a number of applications since this type of thermal machine was proposed for the first time in the late eighteenth century (Barber, 1791). After a tough learning period – it was not until 1903 that the first gas turbine with net power output was assembled by Aegidius Elling (Store Norske Leksikon) – gas turbine based technologies are now setting world standards in two major industrial applications in the mobility sector and the electric power generation business: jet engines for the aero industry, and combined cycle power plants for electricity generation (Fig. 2.1).

Besides these two 'lighthouse' applications, gas turbine based systems have conquered a very wide range of further fields of use, be it for reasons of efficiency, emissions characteristics, fuel flexibility, power-to-weight (or footprint), cost (investment, operational), operational flexibility (fast start-up and load changes), or other performance characteristics (noise, vibration, maintenance, …).

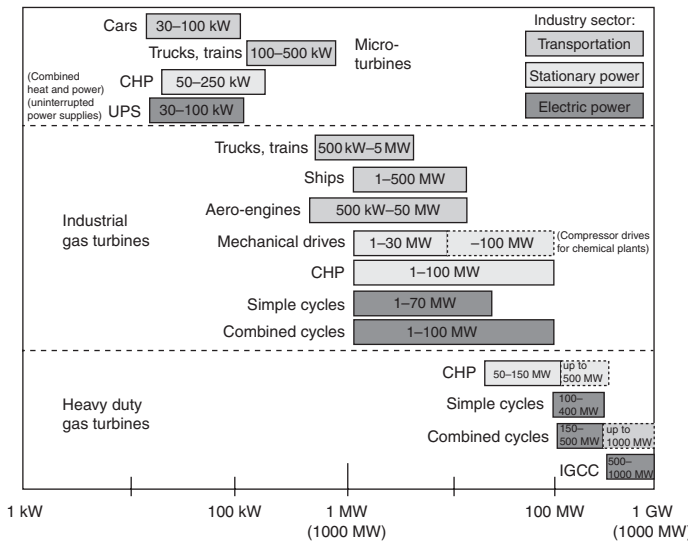
2.2 Gas turbine types by application

Gas turbines are used in the mobility sector for land, sea and air transport applications, not only for commercial but also for military purposes (Fig. 2.2).

© Woodhead Publishing Limited, 2013



2.1 Global gas turbine production (Source: IGTI /Forecast Int'l).



2.2 Gas turbine application *vs* power output.

The mechanical power output for such gas turbine products ranges from a few (10–100) kilowatts (for use in passenger cars (Volvo, 1992) to multiple (10) megawatts (for use in jet engines and ship propulsion) (GE Energy, 2011b; Rolls-Royce, 2011a; Pratt and Whitney).

The products at the low-power range (microturbines) find their use also in stationary applications for combined heat and power (CHP) systems for

© Woodhead Publishing Limited, 2013

apartment houses, community heating networks, hotel resorts, campgrounds and farming/greenhouses (Capstone).

However, CHP systems are most popular in plants in the low $MW_{thermal}$ range (maximum up to about 100 $MW_{thermal}$) for local/regional heating networks and for integrated solutions in industrial processes (paper mills, refineries, chemical industries, …), which require significant amounts of heat (in form of steam and/or hot water) for their operation. Only in extraordinary cases do such networks include large scale gas turbines even in the multiple hundred megawatt range (Power Engineering International, 2007; Brennstoff Wärme Kraft, 2012).

The domain of gas turbine products with 5–50 MW mechanical shaft power output is predominantly so-called aero-derivative turbine systems, which are (slight) modifications of respective aero-engine designs specifically adapted to more rugged stationary operational uses. This industrial gas turbine class is a popular drive for fluid-mechanical machines such as pumps, compressors (along gas/oil pipelines) and large blower/fans in industrial production plants (GE Energy, 2011ab; Siemens, 2011b; Solar, 2011; MAN, 2011). The aero-derivative gas turbine designs lend themselves mostly to modifications of the simple cycle gas turbine configuration towards more sophisticated (higher efficiency) system arrangements, including compressor inter-cooling and/or exhaust heat recuperation (for further details on thermodynamics of advanced cycles, see Chapter 3).

Electric power generation based on gas turbine systems covers the full range of power output, from the kW (single simple cycle machine) to the GW scale (multi-turbine configuration in a combined cycle plant). While the smaller size gas turbine systems (below 10 MW_{el}) are mostly operated in a simple cycle configuration, addition of a bottoming steam cycle, which makes use of the gas turbine exhaust heat for additional electricity generation, is the most widespread set-up for large scale plants (more than 100 MW_{el}). Such combined cycle configurations do provide world record electric efficiencies of (since recently) above 60%. These high efficiencies do also benefit from economy-of-scale effects that come about with single gas turbine unit sizes on the order of 300 MW_{el}.

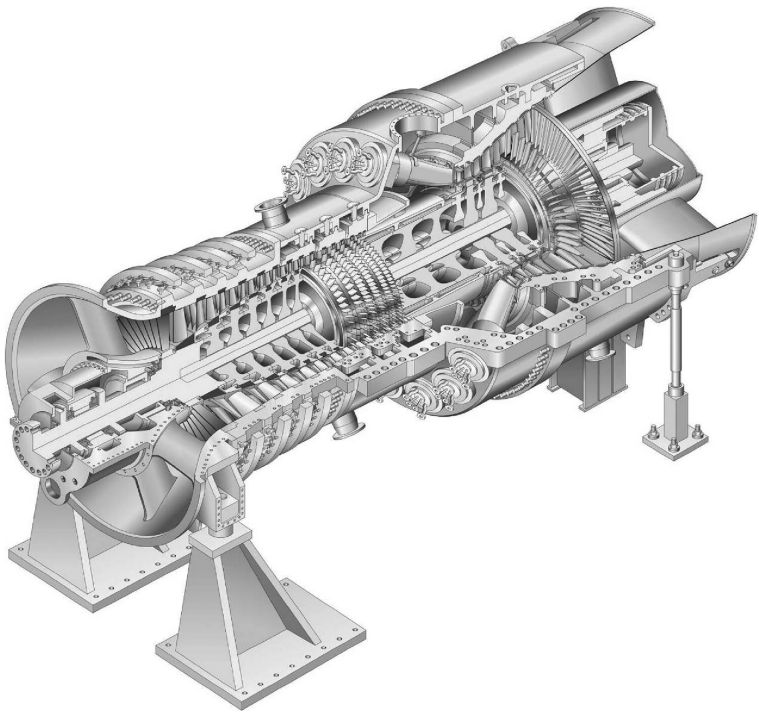
2.3 Power generation

Gas turbine based processes for electric power generation span the whole size range, from a few (10) kilowatts (microturbines OEM's: Capstone; Turbec) to multiple (hundred) megawatts for large combined cycle power plants (large heavy duty gas turbine manufacturers: GE; Siemens, 2011; Mitsubishi, 2010; Alstom, 2011) (Table 2.1). The largest power output for a single unit (gas turbine only) reaches meanwhile close to 400 MW_{el}, which makes a combined cycle plant size well beyond 500 MW_{el}. Due to attractive

© Woodhead Publishing Limited, 2013

Table 2.1 Typical operating parameters vary depending on gas turbine size

Power (MW_e)	<5	5–15	15–50	50–150	>150
Pressure (bar)	6–12	12–15 (20)	12–15 (>20/35)	12–15 (>20)	15–25 (>25/35)
Temperature (°C) (compressor exit)	270–380	350–450 (500)	350–450 (500)	350–450 (500)	400–480 (550)
Temperature (°C) (turbine entry)	700–1100	850–1150	1100–1230	1150–1280	1230–1280 (1400)
Temperature (°C) (turbine exit)	350–550	400–500	450–550	500–600	550–600 (640)



2.3 Large heavy duty gas turbine model (Siemens).

economy-of-scale effects, so-called 2-in-1 plant configurations (the exhaust gas heat from two gas turbines is fed into one bottoming steam cycle/steam turbine) are quite popular and deliver up to almost 1 GW_{el} (Fig. 2.3).

The electric efficiency achieved with such large power plants has now surpassed the 60% mark. All major OEMs (GE; Siemens, 2011; Mitsubishi, 2010; Alstom, 2011) of such large turbine engines have announced 60+% efficiency levels with their latest products (but with only one OEM having

© Woodhead Publishing Limited, 2013

it already proven and certified by an independent agency (Siemens, 2011a)). Depending on the electric grid network these plants serve and are integrated with, the gas turbine design is specifically tailored for grid frequency (50/60 Hz). In order for the electric generator to be synchronous with the grid (and the generator being directly coupled with the turbine shaft due to mechanical reasons) the entire turbomachine rotor (which holds the compressor and turbine blades) needs to be run within a narrow tolerance (e.g., ±0.2 Hz) at a given constant rotational speed – usually 3000 rpm for 50 Hz applications, and 3600 rpm for 60 Hz networks. With the common design criterion that the blade tip speed (circumferential velocity) should not exceed the sonic velocity (speed of sound) of the fluid medium around the blade tip, the maximum diameter is defined (and therefore the length of the blades). This in turn puts an upper limit on the cross-section of the compressor (inlet) section and restricts the maximum air mass flow to the engine. For these reasons, large gas turbine designs for 50 Hz electric networks (e.g., in Europe) are always higher in their electric power rating than equivalent turbine designs for 60 Hz applications (e.g., in North America) (Table 2.2).

Even though rotational speed for gas turbines connected with a generator for electricity production has always to be maintained at a given synchronisation speed, the rounds per minute (RPM) the turbine is designed for can be more freely chosen if the connection between the turbine rotor and the generator can be accomplished by a gear box. Due to mechanical load limitations, a gear box can be applied only for turbine power ratings below about 100 MW_{el}, eliminating the need for separate turbine designs for 50/60 Hz applications and allowing for the turbine shaft to rotate at different (higher) RPM than the generator.

Medium sized gas turbines for electric power generation (30–100 MW_{el}) are often based on multi-shaft (up to three spools) aero-derivative engine designs, which will be covered in the next paragraph (2.4 'aero-engines' and 2.5 'industrial turbines'). These multi-spool arrangements include a power

Table 2.2 Scaling criteria for 50 *vs* 60 Hz designs

Parameter	50 Hz	60 Hz
Frequency (number of revolutions per time)	1.2	1
Tip speed (circumferential velocity)	1	1
Diameter (defines cross sectional area)	1	1.2
Blade length	1	1.2
Flow velocity (e.g., through compressor section)	1	1
Volumetric Flow (cross-section × flow velocity)	1	$(1.2)^2 = 1.44$
Power (corresponding to mass flow)	1	$(1.2)^2 = 1.44$
Torque (corresponding to mechanical load; proportional to power (force) × (blade) length)	1	$(1.2)^3 = 1.73$

© Woodhead Publishing Limited, 2013

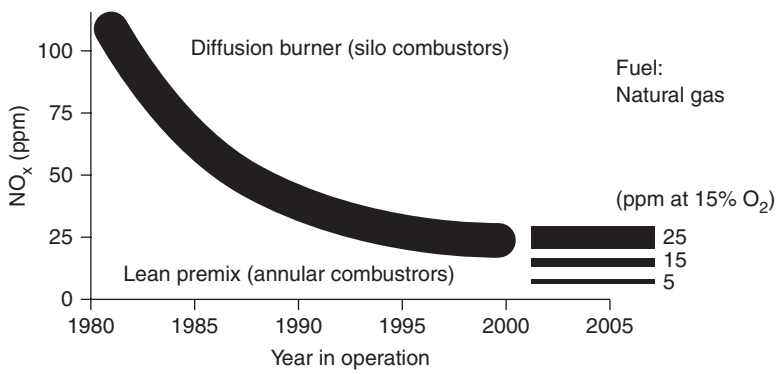
turbine shaft mechanically connected to the electric generator but otherwise driven only by the aerodynamic forces of the hot exhaust gas expelled from upstream (medium pressure) sections of the turbine.

Small size gas turbines (<2 MW_{el}) have a certain efficiency deficit (electric efficiency: <30%) compared to similarly sized reciprocating internal combustion engines, and are thus only applied as niche products where other features are specifically asked for (e.g., low noise and vibration, less maintenance).

In this size class of gas turbines, special design features might be found, such as radial type/centrifugal compressor and turbine wheels (Turbec, 2011; OPRA, 2011) (see more details on radial type compressors in Chapter 4). Due to the limited operating parameters (maximum pressure at 100% load: <10 bar; maximum turbine inlet temperature: <900°C), active cooling of the hot gas path components (see more details on cooling of turbine blades in Chapter 6) can be avoided, which allows for a more simplified design.

Another differentiating design element between certain gas turbine products for stationary power generation is based on the combustion chamber and burner technology applied. Tremendous improvements in terms of emission characteristics (mainly related to NO_x and CO emission) have been achieved over the last few decades with the introduction of lean premix combustion technology (fuel and air are (pre-)mixed before they enter the combustion chamber where the flame is stabilised) (Fig. 2.4).

This combustion technology runs a higher risk of flame instability (lean blow-out), which is the reason why it has (so far) only found widespread use in stationary power generation type gas turbines. With the more compact flame zone (heat release zone) of premixed flames, combustion chamber



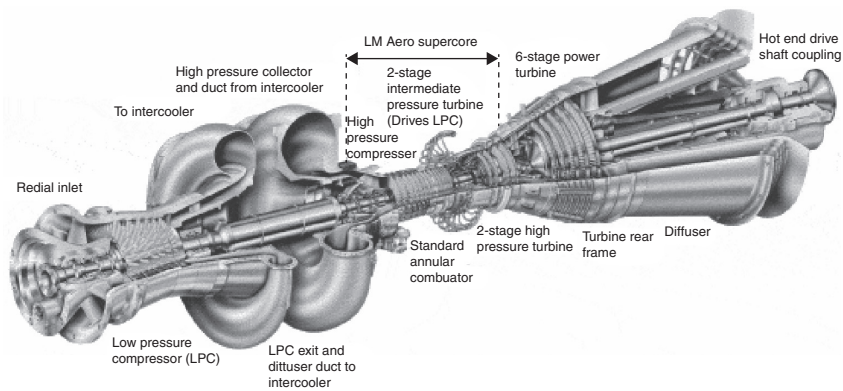
2.4 NO_x emission trend for gas turbine combustors state-of-the-art (2010) – industry standard <25 ppm; best-in-class <15 ppm; ultra-low NO_x option: <10 ppm (catalytic combustion, SCR).

© Woodhead Publishing Limited, 2013

design solutions were also affected, which increased the market share of (can-)annular combustor designs (find more details on combustor designs in Chapter 5). Gas turbines with silo combustor(s) are nowadays niche products applied to 'difficult' fuels, such as heavy fuel oil, crude oil or low heating value type of chemical process (off-)gases. With a wider variety of natural gas qualities introduced to the fuel market (e.g., natural gas with low heating value due to high amounts of inert species (N_2, CO_2) or natural gas with high amounts of higher hydrocarbons (C_{3+})), additional challenges arise with respect to flame stability and emission limits (NO_x, CO) (more details on fuel flexibility can be found in Chapter 16).

Due to a larger footprint and overall size and weight (sophisticated) modifications to the simple cycle gas turbine configuration (for thermodynamics of advanced cycles, see Chapter 3) are most often found only for stationary power generation gas turbine products, where these factors (power-to-weight ratio) do not play such a significant role as in mobile/transport applications (e.g., aero-engines). Examples for such advanced cycle type gas turbines in power generation are:

- ALSTOM's GT24/26 (Alstom, 2011) gas turbine products, which comprise a gas turbine cycle with a reheat step.
- GE's LMS100 (GE Energy, 2011a) gas turbine, which includes inter-cooling between low pressure and high pressure compressor sections.
- Rolls-Royce WR-21 (Rolls-Royce, 2011a), applied as power plant in all-electric ship propulsion systems, incorporating inter-cooling (with sea water) and exhaust gas heat recuperation in the gas turbine set-up.
- the Capstone (Capstone, 2011) micro-gas turbines, which make use of a recuperative (exhaust gas/air) heat exchanger to boost their electric efficiency (Fig. 2.5).



2.5 Example of gas turbine product incorporating an advanced cycle feature (here: inter-cooling) (GE Energy, 2011a).

© Woodhead Publishing Limited, 2013

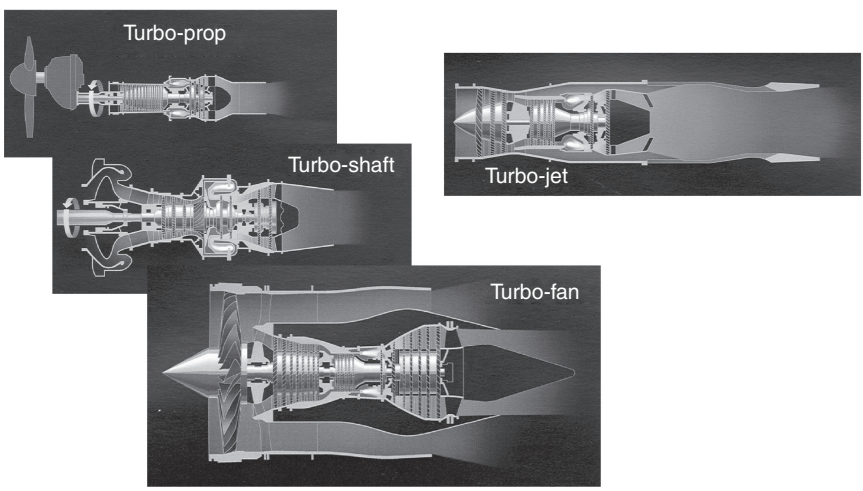
2.4 Aero-engines

Turbofan engines are the most popular use of gas turbines in the transportation sector, and play an enormously important role in moving goods and people around the world in a time- and energy-efficient way.

Gas turbines for air transport applications (aero-engines) come in three different configurations (Rolls-Royce, 2011b), namely:

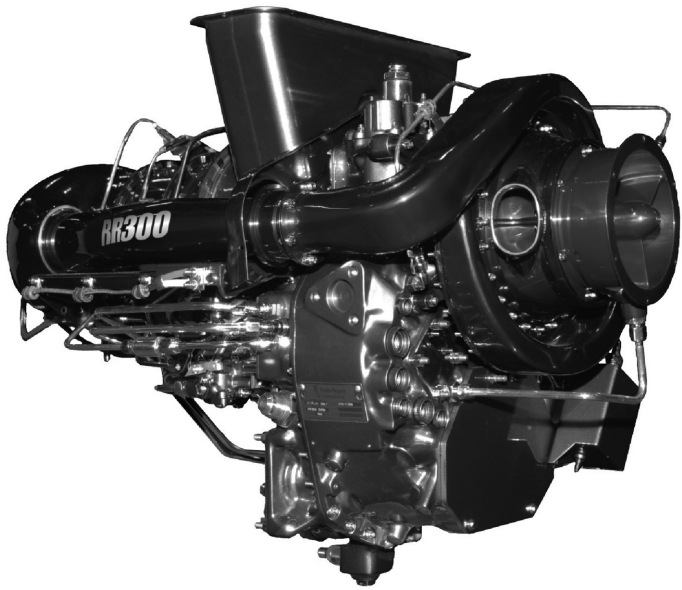
- turbojet/turbofan (generating thrust from the kinetic energy of the hot exhaust gas and additional air – bypass air – forced around the core engine);
- turboprop (driving a propeller as mechanical load), and;
- turboshaft designs (conveying mechanical power to a rotating shaft, for example, helicopter rotor) (Fig. 2.6).

A common feature of all aero-engine designs is the division of the turbine and compressor section in a low pressure and a high pressure part. These sub-systems are configured as separate rotating units (individual shafts), transferring mechanical power from the respective turbine section to the corresponding compressor section via direct coupling (torque forces in the rotor shaft). The surplus energy – deliberated by the combustion of fuel – still contained in the hot exhaust gas after leaving the low pressure turbine section, is either directly converted to thrust via acceleration of the flow in the exit nozzle (turbojet) or is transformed to mechanical shaft power in another turbine section. The shaft of this final turbine section transfers



2.6 Types of aero-engines (Rolls-Royce, 'The jet engine', ed. 2005).

© Woodhead Publishing Limited, 2013



2.7 Turboshaft engine (175–220 kW shaft power) for helicopter and other small aircraft (Rolls-Royce, 2011b).

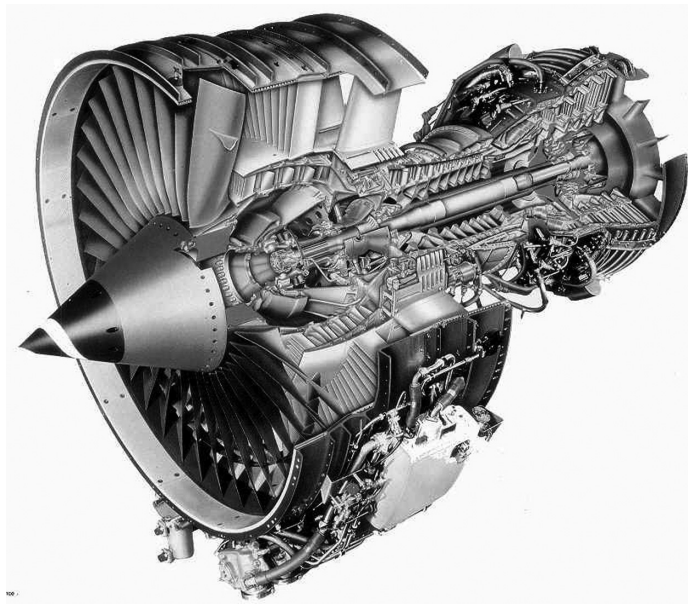
all useful power generated by the engine core either directly to the air bypass fan (turbofan) or via a gear box to a propeller device (turboprop, turboshaft).

The (mechanical) power rating of turboprop/turboshaft engines is in the range of 0.3/2 MW shaft power, which satisfies the propulsion needs for small and medium aircraft (including helicopters) (Fig. 2.7).

The most powerful aero-engines are turbofan designs with a large bypass air ratio (up to more than ten times the air mass flow of the core engine is blown by a large fan through the bypass air duct around the core). The GE90 has long held the world record with 127 900 pounds of thrust (GE Aviation, 2001) achieved on a test stand. Products from the Trent turbine family from Rolls-Royce follow suit (Trent XWB: up to 97 000 pounds of thrust (Rolls-Royce, 2011c)). These powerful engines provide propulsion power for the latest large wide body aircraft from Boeing (B787, B777) and Airbus (A380, A350). The most popular engine type (more than 21 000 engines delivered) is the CFM56 (CFM, 2011), which finds use in the medium size air plane product families B737 and all Airbus classes (Fig. 2.8).

Turbojet engines (or supersonic turbofan designs with low bypass air ratio) find application in high speed military aircraft (flight speed beyond Mach 2) (US Air Force, 2012). For additional thrust, these engines include optional afterburning (reheat of the exhaust gas before the turbine exit nozzle).

© Woodhead Publishing Limited, 2013



2.8 Turbofan engine (CFM56–5A/B product family) (CFM, 2011).

The highly dynamic operational schemes of aircraft engines do pose a challenge for the control of the (transient) flow pattern in the compressor and the turbine sections. Very steep load gradients need to be mastered during take-off coupled with maximum power demand in this (relatively short) operating period. In contrast, cruising at Mach 0.8 (or just above) typically requires only about 50% of take-off thrust. Operation at different altitudes (civil aircraft: up to 10 000 m above sea level) brings about strongly different ambient conditions (intake pressure: 1 atm down to 0.25 atm, intake temperature: +40°C down to –50°C) for aircraft engines to cope with. Short duration (a few minutes) operation at maximum load – which means highest mechanical load due to high pressure and highest thermal load to highest firing temperature – allows for maximising the process parameters to compressor pressure ratios above 40 and peak firing temperatures above 1600°C.

Due to operational safety concerns (related to flame stability) and requirements for relight ability (after flame out) during flight conditions, aero-engines are still equipped with diffusion type burners and combustors designed with a hot primary flame zone with subsequent addition of cooling/dilution air. Associated consequences are higher NO_x (especially at take-off) and CO emission (at idle/taxi) compared to stationary gas turbines based on lean premix combustion technology.

© Woodhead Publishing Limited, 2013

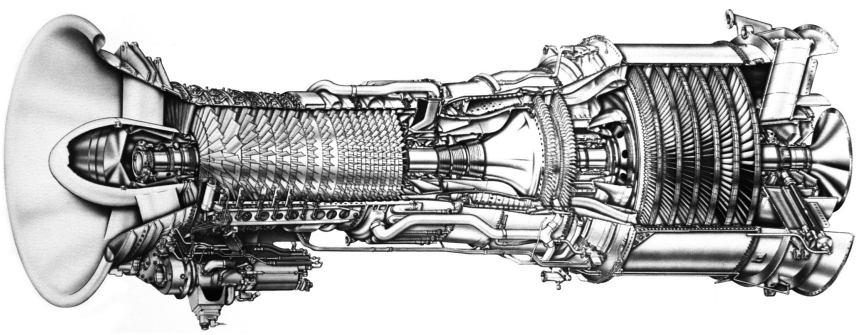
Frequent inspection events and short time intervals between maintenance have favoured aero-engine configurations that are specifically designed for easy maintenance. Vertically split designs allow simple dismantling of compressor and turbine sections for visual inspection and quick replacement of complete engine modules, if required (more information on maintenance, inspection, condition monitoring and repair can be found in chapters 13, 14 and 15).

2.5 Industrial turbines

Industrial turbines are the equivalent of aero-engines for land-based applications. Many of the designs are closely linked to respective aero- engine products, thus called 'aero-derivative' such as, for example, the LM series of engines from GE (GE Energy, 2011b). Multi-spool (2-/3-shaft designs) arrangements are thus very popular with industrial turbines in the power range (mechanical output) from 0.5 to 50 MW. Shaft power is generally extracted from the turbine system via a – free rotating – separate power turbine (extracting power from the hot exhaust gas via aerodynamic forces). This allows for very flexible operation schemes (quick load variation with variable rotational speed) but also bears the risk of overspeed of the power turbine in the event of a sudden (emergency) loss of load (trip) (Fig. 2.9).

The compact design of industrial turbines allows for packaged (container or frame based) solutions with all auxiliaries pre-assembled at the manufacturing/workshop site. In the event of failure of the turbine system, the complete unit can be removed and (quickly) replaced by a spare engine.

The multitude of applications for industrial turbines requires systems that can be operated on a wide range of fuels. Depending on the boundary conditions imposed by the process the turbine is integrated in, liquid and gaseous fuels with a large spectrum of physical (density, viscosity) and chemical properties (reactivity, heating value) are being used to run such



2.9 Industrial turbine (LM 2500; 24 MW) (GE Energy, 2011b).

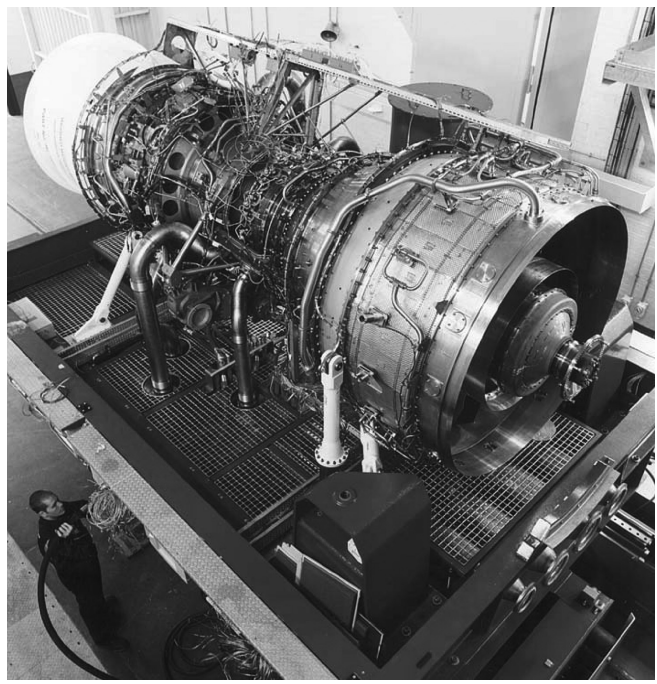
© Woodhead Publishing Limited, 2013

engines (more information on gas turbine operation with different fuels flexibility can be found in Chapter 16).

2.5.1 Surface transport (ships, trains and trucks)

Land and sea based transportation solutions with turbine driven propulsion systems are found in niche applications where specific features of gas turbine products are specifically asked for. The main competing technology is internal combustion (piston) engines, which offer higher efficiency (30–40+%) for small unit sizes (100 kW–5 MW) and very good load change capabilities.

For ship propulsion systems, gas turbines are sought if very compact design (small volume/space requirements; reduced weight) is a valuable asset, such as in some tanker/freight/container ships. If required, the gas turbine driving the propeller or a water jet device can be placed more favourably within the (narrow) hull of some ship designs. Additional benefits important for cruise ships (Koehler, 2000; Jofs, 2004) and some military marine applications (US Navy, 2011; Rolls-Royce, 2011d) are provided by gas turbines, through their low vibration level and (relatively) low noise emission (Fig. 2.10).



2.10 Gas turbine for marine propulsion systems (MT30; 36 MW) (Rolls-Royce Marine gas turbine engines; http://www.rolls-royce.com/marine/products/diesels_gas_turbines/gas_turbines/mt30.jsp).

© Woodhead Publishing Limited, 2013

If high power output is required (10–50 MW) – for instance, for high speed applications as ferries, battle ships and large bulk carriers – the efficiency disadvantage of gas turbines vs diesel engines becomes marginal, especially if advanced cycle type gas turbine products (including inter-cooling and reheat) are used (Rolls-Royce, 2011a) (for more details on advanced cycles, see Chapter 3). A major disadvantage of gas turbine based propulsion systems is their insufficient capability to cover extremely low load (below 20% of full power output) operating conditions. As these load conditions are quite frequently required during ship operation (e.g., manoeuvring in/out of the harbour), if gas turbine based systems are selected they often come in combination with a (lower power output) diesel engine with a (higher power output) gas turbine, dubbed CODAG (Jofs, 2004) or in some cases even in an arrangement involving a small gas turbine with a larger size turbine, COGAG (Net Resources International, 2011a). Recent developments towards (full) electric ships (Net Resources International, 2011b) are based on systems with waste (exhaust) heat recovery via steam generation (COGES, Combined Gas Turbine and Steam Turbine Integrated Electric Drive System) in order to further improve the fuel efficiency.

Land-based transportation devices propelled by gas turbines have only been explored in a few cases, such as a high speed train (Silverberg, 2004), in truck/tram/bus or passenger car applications (Chrysler, 1979; Volvo, 1992), and in battle tanks (Honeywell, 2000). The desire to use gas turbine systems in these cases was again driven by specifically appealing features, such as compactness (volume, weight), and low emission signature (noise, vibration, exhaust pollutants). Unfortunately, in all these applications, the gas turbine based propulsion system suffers from inherent disadvantageous operational characteristics of small (low-power output) turbine units, mainly their mediocre efficiency and inferior part load capabilities.

2.5.2 Mechanical drives

For applications requiring significant mechanical shaft power (above 1 MW), direct drive type arrangements with gas turbine engines are quite popular. Such cases are most often found in the oil and gas business and in the (chemical) process industry, where powerful drives are needed to operate process gas compressors, blowers/fans and pumps (Solar Turbines, 2011; MAN Turbo and Diesel, 2011; Siemens, 2011b). Direct mechanical drives have an advantage for (remote) locations where an equivalent electric power supply is not available or difficult/expensive to install. Especially the compression needs for the transportation of oil and gas in pipelines is generally provided by gas turbines (as the necessary fuel is available right on site). This holds also true for oil and gas production sites that need to be able to operate in

© Woodhead Publishing Limited, 2013



2.11 Gas turbine for mechanical drive applications (7 MW) (MAN, 2011).

an island mode disconnected from electric grids. For offshore production platforms, the small footprint of gas turbine installations is another highly valued feature (Fig. 2.11).

2.5.3 Combined heat and power

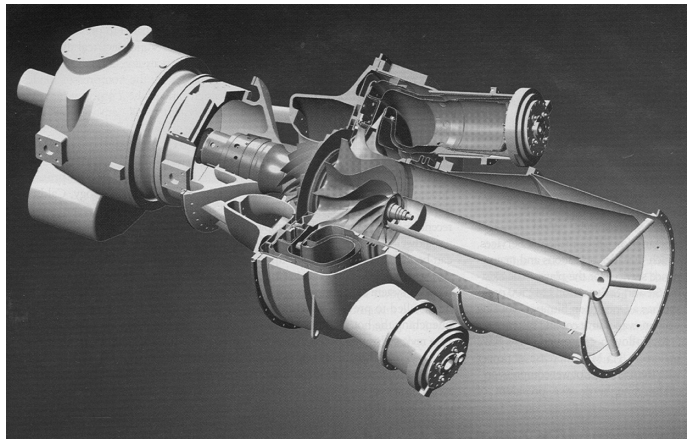
In order to make best use of the primary energy contained in the fuel needed to run a gas turbine, further use of the exhaust heat still available after the expansion step in the turbine section of the engine is mandated. Combined cycles make use of this heat with a bottoming steam cycle to produce additional electricity in a steam turbine. Recuperated gas turbines reintroduce this heat into the gas turbine cycle via preheating of the combustion air between the compressor exit and the combustor inlet (thermodynamics of advanced cycles, see Chapter 3).

The extent of external use of the gas turbine exhaust heat is very much dependent on the temperature requirements of the external process(es) the heat is delivered to. Whereas industrial processes (e.g., paper mills, chemical plants, refineries) usually require significant amounts of heat input (1–50 MW_{th}) as steam at moderately high temperature levels (100–400°C), local heating (network) installations use low-temperature heat below 100°C in the form of hot water. Generally, the capacity of such heating networks is limited to a few (10) MW_{th}, and limited to industrial agglomerations or larger communities (Fig. 2.12).

The gas turbine products serving CHP applications are thus commonly found in a power output range (significantly) below 100 MW_{total} delivering a heat-to-electricity ratio of 3/1 to 1.5/1 and overall efficiencies of 80–85%.

The smaller the size of the gas turbine unit, the more likely a meaningful use of the exhaust heat can be accomplished. Thus, systems at the low-power end (<500 kW) of the gas turbine spectrum are most often used for CHP applications, including microturbines (30–200 kW), which can serve hotels, vacation resorts, agriculture industry (greenhouses, drying plants),

© Woodhead Publishing Limited, 2013



2.12 Gas turbine for CHP applications (2 MW_e; 4 MW_{heat}) (OPRA, 2011).

local communities and large apartment buildings (Capstone, 2011; Turbec, 2011).

2.6 Microturbines

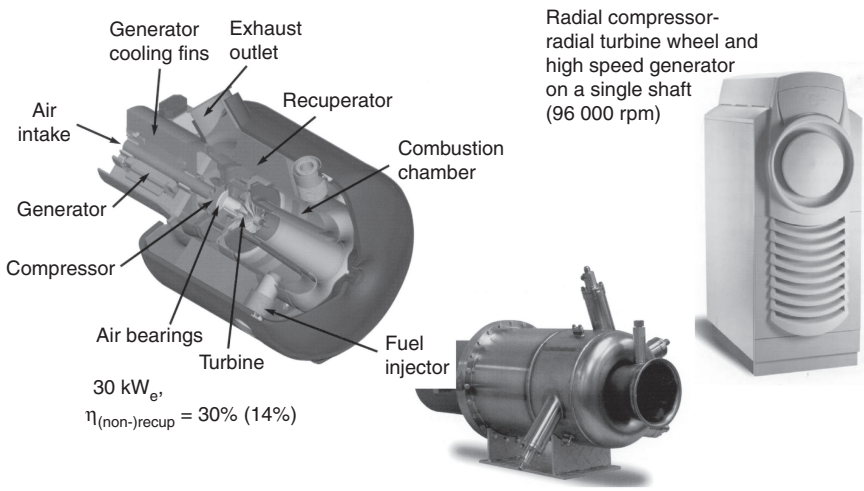
Gas turbines with a power output below 200 kW are commonly classified as 'microturbines'. Due to the low mass flow required for such power ratings (only few hundred g/s of air), single stage radial type turbomachinery components (compressor and turbine wheels) are often being used, which limits the achievable pressure levels to below 6 bar. The small geometrical dimensions of microturbines require (and allow) high rotational speed – on the order of 100 000 rpm – to achieve the required mass flow and compression/expansion characteristics (Fig. 2.13).

Microturbines find use in applications where their low electric (or mechanical) efficiency (15–30%) is still competitive and acceptable. (Sole) electricity generation with microturbines provides solutions where uninterrupted power supply (UPS) on a local scale is required (e.g., offices, banks, computing centres, service providers, manufacturing plants) in emergency situations for a limited time span.

They have also been considered as alternative propulsion systems for road transportation in passenger cars and buses, but have so far not made major inroads into these applications. Maybe as an on-board electricity generation device for hybrid power trains or all-electric vehicles, they might get a second chance in the near future (Capstone, 2010; Green Car Congress, 2010).

For the combined provision of heat and power micro-gas turbines are quite well suited, as they can provide competitive overall efficiencies on the

© Woodhead Publishing Limited, 2013



2.13 Micro-gas turbine (30 kW$_e$) (Capstone, 2011).

order of 85% with an electric share of up to 30% (if equipped with a recuperative heat exchanger). Exhaust heat recuperation (additional heating of the compressed air to the combustor by means of heat exchange with the hot exhaust from the turbine outlet) improves the electrical efficiency of microturbines significantly, as the heat can be effectively transferred for the low pressure conditions (i.e., low compressor outlet temperature) realised in such engines.

In the power range of microturbines, competition with internal combustion engines (piston engines) is most severe, as piston engines suffer less from inherently encountered increased (mechanical, thermal) losses of small-scale power systems. Thus, microturbines cannot compete head on with piston engines in terms of mechanical (and consequently electric) efficiency. Similar to the situation in the industrial turbine sector micro-gas turbines are selected for certain applications due to specific characteristics (maintenance, emission, noise, vibration), which can give them a competitive edge for reciprocating engines.

2.7 Advantages and limitations

Economy-of-scale is a very important aspect of gas turbines in all the applications mentioned above. As some loss mechanisms do not scale with geometrical size but rather are fixed at a minimum absolute dimension (such as the material wall thickness of blades and vanes, or the clearing distance (tip gap) between rotating and stationary parts), maximum turbomachinery component efficiency will only be achieved for (really)

© Woodhead Publishing Limited, 2013

large gas turbine products. These engines achieve their world class electric efficiencies (60+%) also because they are most appropriate to be operated at maximum temperature and pressure levels allowed by the choice of most modern materials and cooling technologies. Along with the efficiency of these large plants, the maximum power output has been pushed to ever higher values, now reaching about 500 MW_{el} for a single gas/steam turbine power train, and up to almost 1 GW_{el} for so-called 2-in-1 plant configurations (the exhaust gas heat from two gas turbines is fed into one bottoming steam cycle/steam turbine) (Mitsubishi, 2010; Siemens, 2011c) (Fig. 2.14).

Part load performance of gas turbines is hampered by the inherent linking of mass flow/pressure/temperature during the compression and expansion steps of the process. Lower power output requires lower mass flow, which in turn reduces the maximum achievable pressure level at the turbine inlet and thus requires lowering the turbine inlet temperature in order not to increase the loss of enthalpy via excessively high exhaust gas temperatures (and to risk overheating of hot gas path components). Only in a reheat process type gas turbine can this effect be mitigated to some extent, as the conditions (pressure, temperature) can be kept at a favourable maximum level in the first section of the engine throughout a certain part of the upper load range (Alstom, 2011).



2.14 Large combined cycle power plant (800 MW_e class, 50 Hz) (Siemens, 2011c).

© Woodhead Publishing Limited, 2013

Despite reduced part load efficiency, gas turbines provide excellent load following characteristics for highly cyclic operational schemes such as for air/sea/land transportation applications. High load gradients can be covered also by stationary gas turbine power plants, which is why they have been important for peak load shaving for so long. In the future this capability of fast load following will gain even more relevance for electricity networks, which will have to cope with significantly higher shares of fluctuating renewable energy sources.

High power density (e.g., expressed as MW power output per mass flow of air) – translated into high power-to-weight ratios – is a major asset of gas turbine engines and makes them the unrivalled propulsion system for air transportation vehicles. Safety concerns (reliability of aero-engines is of utmost importance) put certain limitations on the development of (even) more efficient systems with lower emission of noise and harmful pollutants (NO_x, CO/UHC). On the other hand, this challenge will also trigger new advanced solutions, which land-based/stationary gas turbine engines might profit from subsequently.

Low space requirements/small footprint and low vibration levels allow gas turbines to supersede other energy converters (such as piston engines) in certain applications. Low maintenance (e.g., no oil change, long time intervals between overhaul) is another feature that might make gas turbine engines the preferred technology choice.

Flexible low emission operation on a huge variety of liquid and gaseous fuels is an important factor, which allows the widespread use of gas turbines in all kinds of mobile and stationary applications. Ultra-low emission of nitrogen oxides (NO_x) and products of incomplete combustion (carbon monoxide (CO), unburned hydrocarbons (UHC), soot) – even without additional exhaust gas treatment equipment – makes gas turbine based systems an environmentally friendly power conversion solution and gives them an important competitive edge on alternative technologies.

The main limitations (but thus also main opportunities for improvement) for the performance of gas turbines relate to the properties of materials available for the manufacturing of the engine components. Material properties set the limit for the most important performance parameter, the temperature of the hot gas entering the turbine section, which otherwise can only be pushed higher with more efficient cooling techniques (which inherently introduce aerodynamic and thermodynamic losses). As pressure and temperature are directly coupled in terms of a thermodynamic optimum performance, temperature limitations directly translate into reasonable pressure limits.

2.8 Future trends

Ever increasing temperature and pressure, due to continuing progress in materials development and cooling effectiveness

© Woodhead Publishing Limited, 2013

The ultimate challenge for gas turbine engines will remain, that is, pushing the operational boundary conditions for compressor/combustor/turbine components to ever more demanding limits in order to continuously keep improving the efficiency and the specific power density of the systems. Improvement of component efficiencies will allow exploiting a larger share of the theoretically possible potential (described by the ideal Joule–Brayton cycle).

Fuel spectrum will be widened to accommodate unconventional gas resources and hydrogen-rich fuels to reduce the carbon footprint

Due to the continuous depletion of conventional natural gas resources (with the main fuel constituent being methane CH_4) the fuel spectrum for which gas turbine systems will be designed for (or at least will be able to be operated on with sufficient reliability, efficiency and emissions) will be continuously widened to comprise unconventional gas resources that can contain significant amounts of higher hydrocarbons (C3 and higher) and/or inert diluents (N_2, CO_2). There will be a general shift towards higher hydrogen content fuels (up to almost 100% H_2) as CO_2 emission mitigation grows in importance in the future.

Carbon capture and storage (CCS) concepts will have an effect on the operation of future gas turbines

Even though gas turbines will be predominantly operated on (relatively) low carbon content fuels (such as methane CH_4 which generates less than 200 g CO_2 per MWh of heat released), gas turbine based power plants will also need to adopt CCS concepts, which will have an impact on the operational characteristics of such plants. The consequences will be the need to provide safe operation (against flashback) for hydrogen-rich fuel gases (up to almost 100% H_2 in pre-combustion carbon capture concepts), as well as the need to operate safely (no pressure pulsations or even lean blow-out events) with high amounts of diluents (such as CO_2 and N_2) in exhaust gas recirculation mode (introduced with post-combustion carbon capture concepts to increase the concentration of CO_2 in the flue gas and thus reduce the specific cost per ton of CO_2 captured). The addition of carbon capture equipment to gas turbine based power plants will also have an impact on the operational flexibility concerning load changes, and will require additional means to retain the attractive load response capabilities of today's gas turbine plants.

Grid stabilisation characteristics and load following capabilities are becoming more important

Gas turbine based power generation is gaining increased importance as back-up power resource for fluctuating renewable energies (wind, solar). As electricity generation from such renewable resources takes up a

© Woodhead Publishing Limited, 2013

considerable share in the overall electricity market, significant amounts of dispatchable back-up power, which can follow steep load gradients and have quick response times, will be required to stabilise the electric grid network. As traditional base load capacity will be required less in such future energy systems, operational characteristics (efficiency, emissions) at part load will gain in importance. Increased demand on load following capability, and a reduced number of full load operating hours, will rather support the application of medium to smaller size engine units in the power range from 50 to 200 MW_e, thus the drive for ever larger single unit size gas turbines (currently up to almost 400 MW_e) will probably not continue.

Exploration of more sophisticated cycle options
As the thermodynamic limits of a simple gas turbine cycle (best described by a Joule–Brayton process) are being explored ever more closely, additional benefits will be sought for more frequently by cycle modifications, such as including inter-cooling, reheat combustion and exhaust heat recuperation (thermodynamics of advanced cycles are covered in Chapter 3). These future advanced cycle options might include special variants of exhaust heat recuperation via steam and humidified air (so-called wet cycles) being re-injected into the gas turbine in order to do additional work in the gas turbine expander section. In order for other energy carriers (solid fuels such as biomass/coal; liquid/solid residues from industrial processes) to benefit from the high electric efficiency of gas turbine based power plants, externally heated process options (like GT-SOFC hybrids) as well as integrated gasification concepts (like coal/biomass based IGCC plants) will be further pursued in the future. Even for aero-engines – for which the power-to-weight ratio is a highly sensitive parameter – new concepts (Aviation Week, 2008) beyond the simple cycle gas turbine process are being studied and considered as future products in the quest for increased fuel efficiency.

(All) electric systems for transportation applications might be based on gas turbine power units
Hybrid cars
Use of electric propulsion systems in transport applications (on land and sea) will become more widespread in the future. In such a scenario, microturbines are being considered as electricity generators ('range extenders') in (hybrid) electric cars, but face the challenge of competing with reciprocating engines for this application. Industrial size gas turbines (5–30 MW_e) are being studied for use as electric power plants in future (all-)electric ships in which all on-board services including the propulsion system would be operated based on electric power.

© Woodhead Publishing Limited, 2013

2.9 Sources of further information and advice

http://mysolar.cat.com (Solar Turbines).
www.alstom.com/power.
www.capstoneturbine.com.
www.energy.siemens.com.
www.ge.com/products_services/aviation.html.
www.ge-energy.com.
www.mandieselturbo.com.
www.mpshq.com (Mitsubishi Power Systems).
www.opraturbines.com.
www.rolls-royce.com.
www.turbec.com.
Rolls-Royce, 'The jet engine', edition 2005, ISBN 0 902121 2 35.

2.10 References

Alstom. (2011), 'GT24/26 gas turbine', product brochure http://www.alstom.com/Global/Power/Resources/Documents/Brochures/gt24-and-gt26-gas-turbines.pdf.

Aviation Week and Space Technology. (2008), 'Heart of the matter', 46–51, issue May 12, 2008, http://www.aviationweek.com/AWST.aspx.

Barber, J. (1791), 'Obtaining and applying motive power, and a method of rising inflammable air for the purposes of procuring motion, and facilitating metallurgical operations', UK Patent No. 1833.

Brennstoff Wärme Kraft. (2012), GuD-Kraftwerk Mellach in Betrieb', 29, Nr. 7/8, Bd. 64.

Capstone. (2010), 'Capstone drive solution – range extender', product data sheet http://www.capstoneturbine.com/_docs/CAP1100_Drive%20Solution_Range%20Extender_LR.pdf.

Capstone. (2011), 'C30 microturbine', product specification http://www.capstoneturbine.com/prodsol/products/.

CFM. (2011), 'CFM engine models', http://www.cfmaeroengines.com/engines.

GE Aviation. (2001), 'The GE90 – world record holder', http://www.geaviation.com/engines/commercial/ge90/world_record_holder.html.

GE Energy. (2011a), 'LMS 100 aeroderivative gas turbines', product information http://www.ge-energy.com/products_and_services/products/gas_turbines_aeroderivative/lms100.jsp.

GE Energy. (2011b), 'Gas turbines – aeroderivative', product overview http://www.ge-energy.com/products_and_services/products/gas_turbines_aeroderivative/index.jsp.

Green Car Congress. (2010), 'Jaguar introduces C-X75 gas micro-turbine extended range electric vehicle concept', announcement http://www.greencarcongress.com/2010/09/cx75–20100930.html.

Green Car Journal. (2007), 'Volvo ECC a challenge to the zero-emission concept', originally published February 1993 http://www.greencar.com/articles/volvo-hybrid-environmental-concept-car.php.

© Woodhead Publishing Limited, 2013

Honeywell. (2000), 'AGT1500 turbine technology' http://www51.honeywell.com/aero/common/documents/myaerospacecatalog-documents/SurfaceSystems/AGT1500_Turbine_Technology.pdf.

Jofs, K. (2004), 'Gas turbine technology for advanced cruise ships', TouchBriefings, Business Briefing. Global Cruise, 35–38.

Koehler, H.W. (2000), 'Diesel engines and gas turbines in cruise vessel propulsion', presentation at the Institution of Diesel and Gas Turbine Engineers, London http://www.mandieselturbo.de/files/news/filesof931/0200Gas%20turbines.pdf.

MAN Turbo and Diesel. (2011), 'Industrial gas turbines', product overview http://www.mandieselturbo.com/0001188/Products/Turbomachinery/Industrial-Gas-Turbines.html.

Mitsubishi. (2010), 'MHI begin installation of J-Series gas turbine in combined-cycle power plant for verification testing at Takasago Machinery Works', press release, http://www.mhi.co.jp/en/news/story/1011151386.html.

Net Resources International. (2011a), naval-technology.com http://www.naval-technology.com/projects/garibaldi/.

Net Resources International. (2011b), ship-technology.com http://www.ship-technology.com/projects/millennium/.

OPRA Turbines. (2011), 'Gas turbine power', company brochure http://www.opraturbines.com/upload/Products/9070_Corporate_OPRA07.pdf.

Power Engineering International. (2007), 'CHP goes state-of- the-art', 24–26.

Rolls-Royce. (2011a), 'WR-21 marine gas turbine', product information http://www.rolls-royce.com/marine/products/diesels_gas_turbines/gas_turbines/wr21.jsp.

Rolls-Royce. (2011b), 'Civil aerospace products', product overview http://www.rolls-royce.com/civil/products/.

Rolls-Royce. (2011c), 'Trent XWB', product fact sheet http://www.rolls-royce.com/civil/products/largeaircraft/trent_xwb/index.jsp.

Rolls-Royce. (2011d), 'Rolls-Royce to power ten Littoral Combat Ships for the U.S Navy', press release http://www.rolls-royce.com/marine/news/2011/120116_ten_lcs_order_us_navy.jsp.

Siemens. (2011a), 'Trail-blazing power plant technology in Irsching', press release, 19 May, 2011.

Siemens. (2011b), 'Industrial gas turbines – the comprehensive product range from 5 to 50 megawatts', product brochure http://www.energy.siemens.com/hq/en/power-generation/gas-turbines/#content=Output%20Overview%20.

Siemens. (2011c), 'Power plant SCC5–8000H 1S', product information sheet http://www.energy.siemens.com/hq/en/power-generation/power-plants/gas-fired-power-plants/combined-cycle-power-plant-concept/scc5–8000h-1s.htm.

Silverberg, D. (2004), 'Superman of trains: all aboard Bombardier's JetTrain', http://digitaljournal.com/article/35254.

Solar Turbines. (2011), 'Turbomachinery systems for oil and gas applications', brochure http://mysolar.cat.com/cda/layout?m=35420&x=7.

Store Norske Leksikon: 'Aegidius Elling', http://snl.no/.nbl_biografi/%c3%86gidius_Elling/utdypning.

Turbec. (2011), 'On-site turbine power', datasheet http://www.turbec.com/products/techspecific.htm.

US Air Force. (2012), 'F15 – Eagle', fact sheet http://www.af.mil/information/factsheets/factsheet.asp?id=101.

© Woodhead Publishing Limited, 2013

US Navy, 'Amphibious assault ships', fact sheet http://www.navy.mil/navydata/fact_display.asp?cid=4200&ct=4&tid=400.

Volvo. (1992) (originally published in February 1993; reprinted in *Green Car Journal* 2007), "Volvo ECC – a challenge to the zero-emission concept". http://www.greencar.com/articles/volvo-hybrid-environmental-concept-car.php

© Woodhead Publishing Limited, 2013

3

Fundamentals of gas turbine cycles: thermodynamics, efficiency and specific power

U. DESIDERI, Università degli Studi di Perugia, Italy

DOI: 10.1533/9780857096067.1.44

Abstract: This chapter describes the thermodynamics of gas turbine cycles, starting from the simple cycle and including all the modifications and improvements that have been proposed and developed over the years. This chapter is aimed at understanding the principles on which gas turbines are based and operated. All the different configurations will be described and studied, considering their efficiency and specific power output and the main technological issues with their advantages and drawbacks. The contribution of the main gas turbine parameters to the efficiency and specific power output is discussed, and shown in equations and graphs.

Key words: thermodynamics of gas turbine cycles, gas turbine efficiency, gas turbine specific power.

3.1 Introduction

Gas turbines have had quite a slow development in their early history, when all efforts to build a gas turbine were halted by the impossibility of obtaining a useful power output. In fact, the theoretical assessment of the cycle was already clear and only technological issues, concerning the strength of materials at high temperature and component efficiency, were the cause of those failures.

Most of the critical issues were solved during the Second World War, after which the development of the gas turbine has been steady, and also quite rapid. We can set the starting date of the technological development of gas turbines at the end of the Second World War, and it must be acknowledged that air travel would have never become a mass means of transportation without the gas turbine.[1–5]

As in every technology, several ideas to improve the performance of gas turbines have been proposed and studied over the years. Most modifications of the simple cycle gas turbine have been thoroughly studied and

© Woodhead Publishing Limited, 2013

demonstrated, but only a few of them have been successfully developed commercially.

This is because the gas turbine is a machine that needs highly sophisticated and technologically advanced components, but it requires a very limited number of them, in comparison with other systems that could perform the same task. In fact, only three components are necessary to build a gas turbine: a compressor, a combustor and a turbine. The gas turbine has the additional advantage of using a working fluid that is also free and does not need any pre-treatment: air and, after combustion, the flue gases contain oxygen, nitrogen, carbon dioxide and water.

All the modifications that have been proposed to improve the cycle require additional components or fluids and, therefore, only those that have greatly increased the performance have had a successful commercial outcome.[5]

It must also be noted that the major utilisation of gas turbines is as aircraft engines, where the main specific requirements are the weight and the size of the engine. Any additional component or fluid has been totally excluded in gas turbines employed as aircraft engines. The gas turbine with only the three components listed above is commonly indicated as operating in simple cycle.

In the last three decades, gas turbines have also been used for power generation. They are the so-called heavy duty gas turbines, whose design has other requirements: high efficiency, no weight problems, and high power output to compete with other power generation systems such as steam cycles and reciprocating engines. In the same period, there has also been a significant development of combined heat and power, or cogeneration, systems, and the gas turbine has the desirable feature of delivering large amounts of heat at high temperature in the turbine exhaust without having its performance affected by the collection of this heat, which would be otherwise lost to the atmosphere.

In the field of power generation the real innovation has been the combined gas–steam cycle, where the heat released by the gas turbine is used as the heat source of a steam cycle. The development of this technology, which is not suitable for aircraft utilisation due to the large number of heavy components and the use of water, has also been steady and strong in the last three decades, reaching efficiencies approximately 20% points higher than those of the steam cycle and reciprocating engines.[4, 5]

Combined cycles are the most efficient technology for large-size power generation systems, and gas turbines are the almost sole technology for use as aircraft engines.

This chapter will describe the basic thermodynamic issues of the simple cycle gas turbine, and of all the major modifications including the combined cycles, with the aim of showing the main parameters that affect the performance of gas turbines and the reasons for the technological development that will be described in the following chapters.

© Woodhead Publishing Limited, 2013

3.2 Thermodynamic properties of gases

Gas cycles would not be possible in their current form if gases did not possess a peculiar set of properties, which will shortly be described in this section. The description will start with ideal gases, for which the mathematical equations that allow modelling of their behaviour are simple and can be easily integrated and derived.

The behaviour of an ideal gas can be summarised as follows:

1. the equation of state is $pv = RT$;
2. from (1) it can be demonstrated that the internal energy is a function of temperature only, $u = f(T)$;
3. from (2) and the definition of the specific heat at constant volume $c_v = \partial u/\partial T$, it follows that $c_v = f(T)$ and $\mathrm{d}u = c_v \mathrm{d}T$ for any infinitesimal process;
4. from the definition of enthalpy $h = u + pv$, it follows that enthalpy is also a function of T only, $h = f(T)$;
5. from (4) and the definition of the specific heat at constant pressure $c_p = \partial h/\partial T$ it follows that $c_p = f(T)$, and that $\mathrm{d}h = c_p \mathrm{d}T$, and eventually that $c_p - c_v = R$;
6. from all the above equations, if we also assume that the specific heats at constant volume and pressure are constant, instead of being a function of temperature, we may derive the following expressions for any process joining points 1 and 2:

$$u_2 - u_1 = c_v(T_2 - T_1) \qquad [3.1]$$

$$h_2 - h_1 = c_p(T_2 - T_1) \qquad [3.2]$$

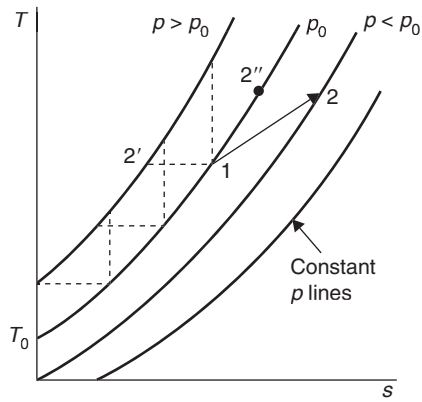
$$s_2 - s_1 = c_v \ln\frac{T_2}{T_1} + R\ln\frac{v_2}{v_1} = c_p \ln\frac{T_2}{T_1} - R\ln\frac{p_2}{p_1} \qquad [3.3]$$

It is now possible to make some interesting considerations by examining the T-s diagram of an ideal gas (Fig. 3.1), where a set of constant pressure lines are shown. If we move along an isothermal process from any point of the p_0 line to any other pressure, either higher or lower, Equation [3.3] reduces to:

$$s_{2'} - s_1 = -R\ln\frac{p_{2'}}{p_1} \qquad [3.4]$$

from which it is clear that the entropy difference is constant at constant temperature, that is, all constant pressure lines can be easily plotted on the

© Woodhead Publishing Limited, 2013



3.1 T-s Diagram for an ideal gas.

diagram by shifting all of them horizontally. Equation [3.4] also shows that the horizontal distance between any pair of constant pressure lines, divided by the same pressure ratio, is the same at any temperature.

Let us now look at the slope of the constant pressure lines. If we move along a constant pressure line, Equation [3.3] can be written as:

$$s_{2''} - s_1 = c_p \ln \frac{T_{2''}}{T_1} \qquad [3.5]$$

Considering the differential form of Equation [3.5]:

$$\mathrm{d}s = c_p \frac{\mathrm{d}T}{T} \qquad [3.6]$$

we may write:

$$\frac{\mathrm{d}T}{\mathrm{d}s} = \frac{T}{c_p} \qquad [3.7]$$

that is, the slope of a constant pressure line is proportional to temperature and increases with temperature.

If Equations [3.4] and [3.7] were not valid, thermal machines based on the Joule–Brayton cycles could not be feasible.

Similarly, if we draw constant volume lines on the T-s diagram, Equation [3.3] shows that any constant volume line can be drawn by shifting another one horizontally, and that the slope is proportional to temperature:

$$\frac{\mathrm{d}T}{\mathrm{d}s} = \frac{T}{c_v} \qquad [3.8]$$

© Woodhead Publishing Limited, 2013

Since $c_v < c_p$, because R is always positive, constant volume lines have a steeper slope on the T-s diagram.

It is interesting to note that if we follow an adiabatic-isentropic process from a given constant pressure line p_0 to a second constant pressure line p_1, the temperature difference increases with the initial temperature (Fig. 3.1). Since the temperature difference along an adiabatic-isentropic process is proportional to the enthalpy difference, and therefore to the work done along the process, the higher the initial temperature of the compression process the higher is the work required by the compressor. Similarly, the higher the initial temperature of the expansion, the higher is the work done by the expander.

This characteristic is the fundamental reason why the Joule–Brayton cycle can work: a compression with the fluid entering at a lower temperature will require less work than that provided by the expansion of the same fluid at a higher temperature.

Even though the real gas behaviour is not wholly represented by the assumptions described above for an ideal gas, the differences are quite small in the range of pressures and temperatures normally encountered in gas cycles.

Several equations of state have been studied and proposed for different gases, but they are normally used to draw the thermodynamic charts and cannot easily be used in calculating thermodynamic properties in engineering applications.

However, the departure of a real gas from an ideal gas is much larger when the real gas is far from the following situations:

1. The molecules are perfectly elastic and perfectly rigid, so that no momentum is lost during collision of the molecules among them and with the wall containing the gas.
2. The volume occupied by the molecules is negligible compared with the total volume.
3. The attractive forces between molecules are negligible.

Most of these assumptions are valid for a real gas when the gas is rarefied, that is, it is in a state where pressure is low and/or temperature is high with respect to critical pressure and temperature.

This can be simply defined as a state far from critical conditions in the direction of lower pressures and higher temperatures.

These assumptions can be better quantified by writing the equation of state for real gases by using the compressibility factor:

$$Z = \frac{pv}{RT} \qquad [3.9]$$

© Woodhead Publishing Limited, 2013

The value of Z depends on the gas, and it is also a function of pressure and temperature. This does not greatly reduce the difficulties in calculating the equation of state, unless we consider this approximation.

Let us consider the so-called reduced properties, defined as the ratio of the property with its critical value:

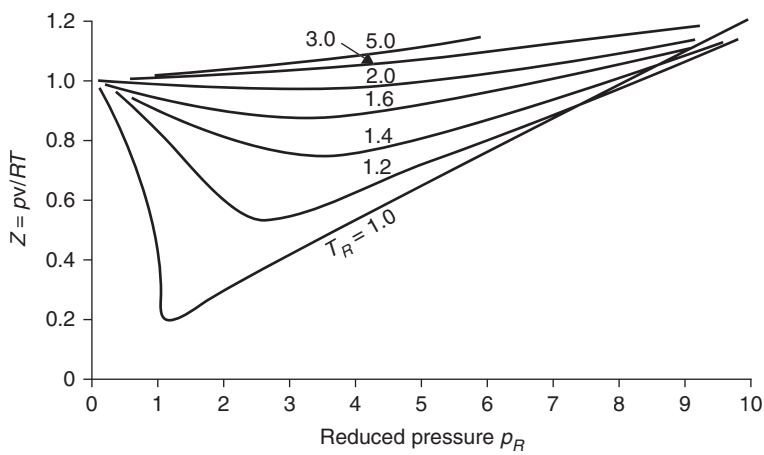
$$P_R = \frac{p}{p_c};\ v_R = \frac{v}{v_c};\ T_R = \frac{T}{T_c} \qquad [3.10]$$

If the reduced properties data for all gases were to lie on the same set of curves, we could deduce that two gases with the same reduced pressure and temperature would have the same reduced volume. If this were true, we could then define a single set of curves providing the variation of Z as a function of the critical value of Z and the reduced properties of the gas:

$$Z = \frac{pv}{RT} = \frac{p_C v_C}{RT_C}\frac{P_R v_R}{T_R} = Z_C \frac{P_R v_R}{T_R} \qquad [3.11]$$

Unfortunately this set of curves does not exist, since $Z \to 1$ when $p_R \to 0$ for all gases, but Z_C is not the same for all gases, and therefore this expression cannot be used as a general equation of state for all gases.

However, all gases follow the same set of constant T_R lines on a Z-p_R diagram (Fig. 3.2) and if we consider the reduced pressure and temperature of engineering interest, and in particular of interest in gas turbines ($T_R > 2$ and $p_R < 5$) the distance of the constant T_R lines from $Z = 1$ is shorter than 10%. This means that the approximation of real gases with the ideal gas equation of state is accurate enough for most technical purposes.



3.2 Compressibility factor vs reduced pressure.[6]

© Woodhead Publishing Limited, 2013

The second characteristic of ideal gases, that is, that the specific heats at constant pressure and volume area function of the temperature only, is valid for most real gases in the same range of reduced pressure and temperature listed above. In general, it is accurate enough for most engineering purposes to express c_p and c_v as a second or third order polynomial functions of the temperature:

$$c_p = a + bT + cT^2 \quad [3.12]$$

$$c_v = a' + bT + cT^2 \quad [3.13]$$

In conclusion we may therefore assume that the equation of state for ideal gases can be used for most engineering calculations in gas cycles. Similarly, polynomial expressions, as a function of temperature only, can be accurately used for calculating the specific heats of real gases and subsequently their enthalpy and internal energy.

3.3 The Joule–Brayton cycle

The Joule–Brayton cycle is a conceptually simple thermodynamic cycle that can be technically made in operation with a very small set of components. The cycle consists of four processes with a gas or a mixture of gases as working fluid. The first process is an adiabatic compression followed by a heat supply at constant pressure, an adiabatic expansion, and a heat release at constant pressure.

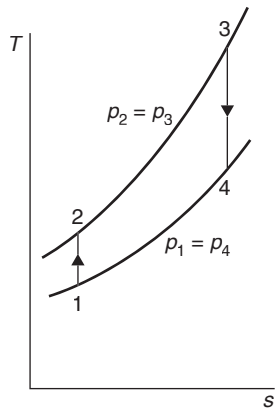
The cycle consists of two adiabatic and two constant pressure processes, which can be easily accomplished in a compressor and a expander and in two heat exchangers working at different pressures.

With reference to Figs 3.3 and 3.4, the starting point for the description of the cycle is point 1, with the lowest pressure and temperature of the whole cycle. The gas is then compressed in a compressor to reach point 2, which is at the maximum pressure of the cycle, and then introduced into a heat exchanger where heat is supplied from an external source, which is commonly provided by the combustion of a fuel. The heat supply in the heat exchanger is at constant pressure to reach the maximum pressure and temperature at point 3. The gas is then expanded in a turbine until it reaches the lowest cycle pressure at point 4, which lies on the same pressure line as point 1.

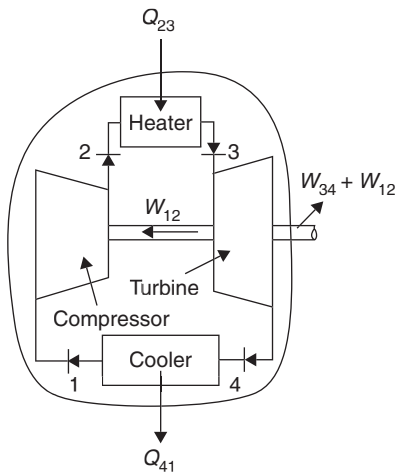
The cycle can be either closed or open. The above description holds true for a closed cycle, where any gas can be used and the heat transfer in the heat exchangers is from and to external sources.

Most of the Joule–Brayton cycles have been built as open cycles, where the fluid entering the cycle is air at ambient pressure and temperature (Fig. 3.5).

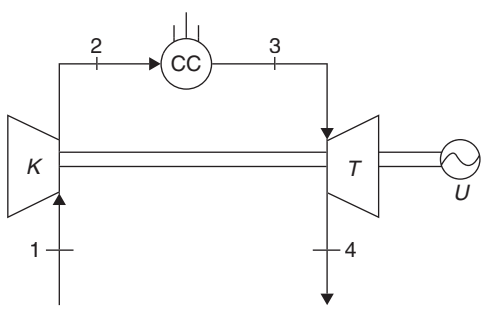
© Woodhead Publishing Limited, 2013



3.3 T-s diagram of the Joule–Brayton cycle.



3.4 Schematic of a closed gas turbine cycle.



3.5 Schematic of an open gas turbine cycle.

© Woodhead Publishing Limited, 2013

Therefore, point 1 represents the ambient conditions. The air pressure is raised in the compressor to reach point 2, before being mixed with a fuel in a combustor where heat is released in a constant pressure combustion process, which ends at point 3. The oxygen in the air is the oxidant in the combustion process. Therefore, between points 2 and 3, the working fluid does not only reach a higher temperature but its composition also changes from air to the combustion products, which then expands in the expander to reach the ambient pressure at outlet.

The cycle can be assumed as a closed cycle by considering that the environment is able to provide an infinite flowrate of air at ambient pressure and temperature to the cycle, and to cool and transform an infinite amount of flue gases, without changing its original composition and thermodynamic conditions. In an open cycle, the 4–1 process is therefore accomplished by the environment.

In both cases the compression process requires a significant fraction of the expander work output.

The cycle consisting of the basic components completing the processes described above is generally called the simple Joule–Brayton cycle, to distinguish it from some of the modifications that have been proposed over the years to improve its performance.

The performance of the cycle will be evaluated by using two parameters: the thermal efficiency and the work output.

As in all the thermodynamic closed cycles, the efficiency can be expressed as:

$$\eta = \frac{W}{Q_1} \qquad [3.14]$$

where Q_1 is the heat supplied to the cycle and W is the work output.

However, considering that in a closed cycle the first principle of thermodynamics states that:

$$W = Q_1 - Q_2 \qquad [3.15]$$

where Q_2 is the heat released from the cycle, the efficiency can also be expressed as:

$$\eta = \frac{W}{Q_1} = \frac{Q_1 - Q_2}{Q_1} = 1 - \frac{Q_2}{Q_1} \qquad [3.16]$$

The work output of the cycle is the difference between the expansion and the compression work. In a closed cycle, the fluid expanding in the expander has the same flowrate and composition of the fluid being compressed in the compressor, thus giving:

© Woodhead Publishing Limited, 2013

$$W = W_T - W_C \quad [3.17]$$

All the considerations about the simple cycles and its modifications and improvements will be assessed in terms of efficiency and work output.

3.3.1 The ideal Joule–Brayton cycle

The Joule–Brayton cycle will be first described as an ideal cycle, where the fluid is assumed to be an ideal gas having a constant flowrate and constant composition throughout all the components, and the thermodynamic processes will be ideal in all the components, that is, without any irreversibility. These assumptions allow us to derive a simple expression of the efficiency and the specific work of the cycle.

Let us start by discussing the work output. Since both the compression and expansion work can be expressed as an enthalpy difference between the outlet and inlet and vice versa respectively, the work output of the ideal cycle can be written as follows:

$$W = W_T - W_C = mc_p(T_3 - T_4) - mc_p(T_2 - T_1) \quad [3.18]$$

Hence, dividing by mc_pT_1 we can write the expression of the specific work of the ideal Joule–Brayton cycle as:

$$\frac{W}{mc_pT_1} = \left(\frac{T_3}{T_1} - \frac{T_4}{T_1}\right) - \left(\frac{T_2}{T_1} - 1\right) \quad [3.19]$$

We may define $\tau = T_3/T_1$ as a characteristic number for the cycle, since it represents the ratio between the highest and the lowest cycle temperatures. The lowest temperature T_1 is defined by the ambient conditions, whereas T_3 represents the turbine inlet temperature, that is, the technological limit that the cycle can reach with the materials, with which it is built.

The ratio T_2/T_1 is the temperature ratio over the compression process, which is both adiabatic and isentropic in the ideal cycle.

In any adiabatic reversible process, pressure and volume are linked by the following expression:

$$pv^k = \text{constant} \quad [3.20]$$

where $k = c_p/c_v$ and is always higher than 1, since c_p is always higher than c_v.

© Woodhead Publishing Limited, 2013

By applying the ideal gas equation of state, we can write:

$$pv^k = p\left(\frac{RT}{p}\right)^k = p^{1-k}T^k = \text{constant} \qquad [3.21]$$

and thus between points 1 and 2:

$$p_1^{1-k}T_1^k = p_2^{1-k}T_2^k \rightarrow p_1^{\frac{1-k}{k}}T_1 = p_2^{\frac{1-k}{k}}T_2 \qquad [3.22]$$

expressing Equation [3.22] in terms of the temperature ratio, we obtain:

$$\left(\frac{p_2}{p_1}\right)^{\frac{1-k}{k}} = \frac{T_1}{T_2} \rightarrow \frac{T_2}{T_1} = \left(\frac{p_2}{p_1}\right)^{\frac{k-1}{k}} = \beta^{\frac{k-1}{k}} = \beta^{\varepsilon} \qquad [3.23]$$

where β is the pressure ratio of the compression process and ε is a characteristic parameter of the fluid. With k always higher than 1, $0 < \varepsilon < 1$.

The T_4/T_1 temperature ratio can be similarly calculated from the following expression:

$$\frac{T_4}{T_1} = \frac{T_4}{T_3}\frac{T_3}{T_1} = \frac{T_4}{T_3}\tau \qquad [3.24]$$

In the adiabatic expansion process:

$$p_3^{\frac{1-k}{k}}T_3 = p_4^{\frac{1-k}{k}}T_4 \qquad [3.25]$$

$$\frac{T_4}{T_3} = \left(\frac{p_3}{p_4}\right)^{\frac{1-k}{k}} = \beta^{\frac{1-k}{k}} = \beta^{-\varepsilon} \qquad [3.26]$$

Therefore:

$$\frac{T_4}{T_1} = \frac{\tau}{\beta^{\varepsilon}} \qquad [3.27]$$

Considering Equations [3.23] and [3.27], Equation [3.19] may be written as:

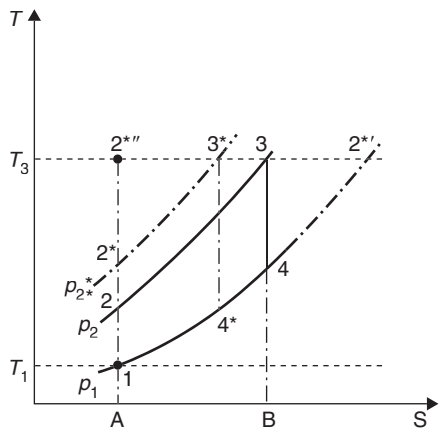
$$\begin{aligned}\frac{W}{mc_pT_1} &= \tau - \frac{\tau}{\beta^{\varepsilon}} - \beta^{\varepsilon} + 1 = \tau - \beta^{\varepsilon} - \left(\frac{\tau}{\beta^{\varepsilon}} - 1\right) = \tau - \beta^{\varepsilon} - \left(\frac{\tau - \beta^{\varepsilon}}{\beta^{\varepsilon}}\right) \\ &= (\tau - \beta^{\varepsilon})\left(1 - \frac{1}{\beta^{\varepsilon}}\right)\end{aligned} \qquad [3.28]$$

© Woodhead Publishing Limited, 2013

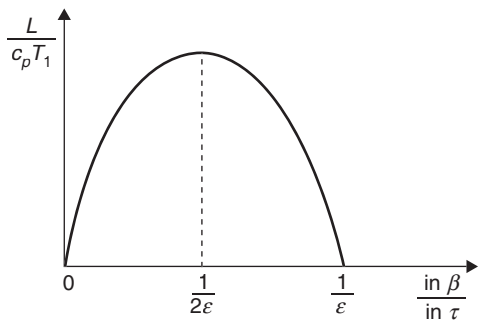
Examining Equation [3.28], we may notice that the specific work is null when $\beta^{\varepsilon} = 1$, which occurs in a cycle where point 1 and 2 and points 3 and 4 coincide, and there is neither compression nor expansion, with the fluid being heated from point 2 to point 3′ and then cooled at the same pressure to point 1 (Fig. 3.6)

The specific work is also null when $\tau = \beta^{\varepsilon}$. This is the case when the final point of the compression reaches the maximum temperature of the cycle and the cycle consists of two processes only: a compression and an expansion, both requiring and providing the same work respectively. The cycle moves from point 1 to point $2^{*\prime\prime}$ and vice versa (Fig. 3.6).

Between these two limiting values of β we can find the maximum value of the specific work (Fig. 3.7). Since at both extremes the Equation [3.28] is null, and for any other value of β the function is positive, by deriving



3.6 The Joule–Brayton cycle with different pressure ratios.



3.7 Specific work vs pressure ratio.

© Woodhead Publishing Limited, 2013

Equation [3.28] and equating the result to zero, we obtain β at which the specific work is maximum:

$$\frac{\partial\left(W/mc_pT_1\right)}{\partial\beta} = \frac{\tau\varepsilon}{\beta^{\varepsilon+1)}} - \varepsilon\beta^{\varepsilon-1)} = 0 \qquad [3.29]$$

$$\tau = \beta^{2\varepsilon} \Rightarrow \beta = \tau^{\frac{1}{2\varepsilon}}$$

The efficiency of the ideal Joule–Brayton cycle given in Equation [3.16] can be modified as follows, by considering an ideal cycle and dividing the upper and lower side of the fraction by T_1:

$$\eta = \frac{W}{Q_1} = 1 - \frac{Q_2}{Q_1} = 1 - \frac{mc_p(T_4 - T_1)}{mc_p(T_3 - T_2)} = 1 - \frac{\frac{T_4}{T_1} - 1}{\frac{T_3}{T_1} - \frac{T_2}{T_1}} \qquad [3.30]$$

Using the same notation defined for the calculation of the specific work, we may write Equation [3.30] as follows:

$$\eta = 1 - \frac{\frac{T_4}{T_1} - 1}{\frac{T_3}{T_1} - \frac{T_2}{T_1}} = 1 - \frac{\frac{\tau}{\beta^{\varepsilon}} - 1}{\tau - \beta^{\varepsilon}} = 1 - \frac{1}{\beta^{\varepsilon}} \qquad [3.31]$$

It can be noted that the efficiency of the ideal Joule–Brayton cycle only depends on the pressure ratio and the characteristics of the fluid (Fig. 3.8).

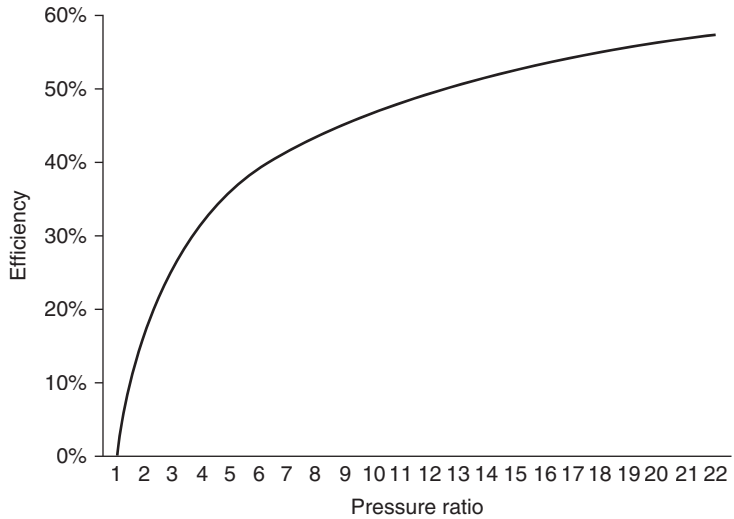
From a purely mathematical point of view, Equation [3.30] states that the efficiency does not depend on the maximum temperature of the cycle. However, this is not true, because β is limited by the fact that the final compression temperature cannot exceed the maximum cycle temperature. Therefore Equation [3.30] reaches a maximum value depending on the T_3 fixed for the cycle and tends to 1 only for infinite values of T_3.

In any case, since ε is positive but less than 1, the efficiency increases with β, has a null value for $\beta = 1$, and reaches its maximum value when $\beta = \tau^{1/\varepsilon}$.

3.3.2 The real Joule–Brayton cycle

The ideal cycle described in Section 3.4 is based on the assumption that the working fluid is an ideal gas, with constant composition, flowrate and specific heat at constant pressure in all the cycle processes, and that all the transformations occur in ideal machines without any irreversible process: heat exchangers do not have any heat loss to the environment or any

© Woodhead Publishing Limited, 2013



3.8 Ideal efficiency of the Joule–Brayton cycle vs pressure ratio.

pressure loss in the fluid flow, and the compression and expansion processes are adiabatic and isentropic.

The real Joule–Brayton cycle can be described by removing all the simplifying assumptions concerning the working fluid and the components.

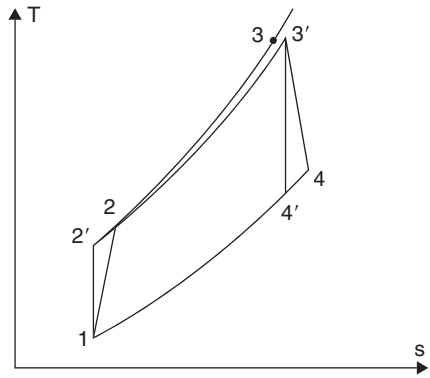
If we consider a closed cycle the following assumptions can be made:

1. The fluid is real and the specific heat at constant pressure is a polynomial function of the temperature.
2. The heat exchangers in the closed cycle or the combustor in the open cycle have heat losses, and the passage of the working fluid in them and in any other duct produces friction losses, thereby reducing the pressure from the inlet to the outlet of each component.
3. The fluid in the compressor and the expander produces friction losses and the compression and expansion processes are adiabatic but they are not isentropic. The non-ideal behaviour of the compressor and the expander can be described by defining an adiabatic compression and an adiabatic expansion efficiency as follows (Fig. 3.9):

$$\eta_C = \frac{h_{2'} - h_1}{h_2 - h_1} \qquad [3.32]$$

$$\eta_T = \frac{h_{3'} - h_4}{h_{3'} - h_{4'}} \qquad [3.33]$$

© Woodhead Publishing Limited, 2013



3.9 T-s diagram of the real Joule–Brayton cycle.

If the cycle is open we have the additional assumption that the fluid flowrate and composition change after point 2 when the fuel is added to the air flow and the combustion process transforms the composition from air to flue gases.

A parameter that is generally used to take account of these changes in flowrate and composition is the air/fuel ratio:

$$\alpha = \frac{m_{\text{air}}}{m_{\text{fuel}}} \qquad [3.34]$$

In gas turbines α affects the turbine inlet temperature T_3 of the cycle. Since the maximum temperature of the cycle is fixed by the maximum temperature that the materials of the expander can withstand, it is necessary to set α in order to reach the desired T_3.

The minimum α is the stoichiometric air/fuel ratio, at which all the oxygen in the air is used as oxidant in the combustion process. If we assume the reaction of a generic hydrocarbon with the oxygen contained in the air, and assuming that air is a mixture of nitrogen and oxygen only with a volume concentration of 79% and 21% respectively, we can write the chemical reaction as follows:

$$C_nH_m + \left(n + \frac{m}{4}\right)O_2 + \frac{79}{21}\left(n + \frac{m}{4}\right)N_2 \rightarrow nCO_2 + \left(n + \frac{m}{4}\right)H_2O + \frac{79}{21}\left(n + \frac{m}{4}\right)N_2 \qquad [3.35]$$

Equation [3.35] shows that for each mole of fuel, $\left(n + (m/4)\right)$ moles of air are necessary to complete the chemical reaction. If we use the molecular weight to calculate the mass balance of the reaction, we can write the stoichiometric air/fuel ratio as:

© Woodhead Publishing Limited, 2013

$$\alpha_{st} = \frac{\left(n + m/4\right) \times 32 + \left(n + m/4\right) \times 105.33}{n \times 12 + m} \quad [3.36]$$

If methane is used as fuel, $n = 1$ and $m = 4$ and $\alpha_{st} = 17.16$.

We can also define the excess air from the air/fuel ratio and the stoichiometric air/fuel ratio:

$$\lambda = \frac{\alpha - \alpha_{st}}{\alpha_{st}} \quad [3.37]$$

The higher the excess air the lower is T_3. Any air in excess of the stoichiometric air acts as a dilutant in the combustion process, because the unreacted oxygen and the corresponding nitrogen amount do not react with the fuel and are heated by the combustion process subtracting heat from the chemical reaction. The heat introduced in the cycle Q_1 can be calculated as:

$$Q_1 = \frac{\text{LHV}}{\alpha + 1} \quad [3.38]$$

where LHV is the lower heating value of the fuel used for the combustion process.

We can calculate the specific heat that is supplied to the cycle as:

$$Q_1 = \int c_p \mathrm{d}T = c_{p23}\left(T_3 - T_2\right) \quad [3.39]$$

Therefore the maximum temperature is a function of the air/fuel ratio by means of Equation [3.38] and [3.39]

$$T_3 = T_2 + \frac{\text{LHV}}{c_{p23}(\alpha + 1)} \quad [3.40]$$

Since the maximum cycle temperature is limited by the resistance of the materials of which the turbine is made, α (or alternatively the excess air λ) is the main parameter to control such temperature. Current values of λ are slightly higher than 2, but at the beginning of the gas turbine era, common values of λ exceeded 4.

Those values have required the combustor to be built with a peculiar set-up to separate the air necessary for combustion from that used to dilute combustion products before entering the turbine. These features will be discussed in next chapters.

In the real cycle, the specific work can be calculated as:

$$W_r = \frac{\alpha + 1}{\alpha} W_{Tr} - W_{Cr} \quad [3.41]$$

© Woodhead Publishing Limited, 2013

With reference to Fig. 3.9 we can calculate the real turbine and compressor specific work by using the efficiency of the turbine and the compressor:

$$W_{\mathrm{Tr}} = \eta_T \int_{3'}^{4'} c_p \mathrm{d}T = \eta_T c_{p3'4'}(T_{3'} - T_{4'}) \quad [3.42]$$

$$W_{\mathrm{Cr}} = \frac{\int_{1}^{2'} c_p \mathrm{d}T}{\eta_C} = \frac{c_{p12'}(T_{2'} - T_1)}{\eta_C} \quad [3.43]$$

The integrals in Equations [3.42] and [3.43] can be easily calculated as shown in Section 3.4 being two adiabatic-isentropic processes, giving:

$$\frac{W_{\mathrm{Tr}}}{c_{p3'4'}T_1} = \eta_T \left(\tau - \frac{\tau}{\beta^{\varepsilon}} \right) \quad [3.44]$$

$$\frac{W_{\mathrm{Cr}}}{c_{p12'}T_1} = \frac{(\beta^{\varepsilon} - 1)}{\eta_C} \quad [3.45]$$

and taking a mean value of the specific heat at constant pressure:

$$\frac{W_r}{\frac{\alpha+1}{\alpha} c_p T_1} = \eta_T \left(\tau - \frac{\tau}{\beta^{\varepsilon}} \right) - \frac{(\beta^{\varepsilon} - 1)}{\eta_C} \quad [3.46]$$

With a similar procedure to that described for the ideal cycle, we may calculate the maximum of the specific work, which is reached when:

$$\beta = (\eta_C \eta_T \tau)^{\frac{1}{2\varepsilon}} \quad [3.47]$$

The efficiency of the real cycle can be expressed as:

$$\eta_r = \frac{W_r}{Q_{1r}} = \frac{W_{\mathrm{Tr}} - W_{\mathrm{Cr}}}{Q_{1r}} \quad [3.48]$$

Let us now define the internal efficiency as the ratio of the real and ideal efficiencies:

$$\eta_i = \frac{\eta_r}{\eta_{id}} \rightarrow \eta_r = \left(1 - \frac{1}{\beta^{\varepsilon}} \right) \eta_i \quad [3.49]$$

If we divide Equation [3.48] by Equation [3.30] we obtain:

© Woodhead Publishing Limited, 2013

$$\eta_i = \frac{Q_1}{Q_{1r}} \frac{W_{Tr} - W_{Cr}}{W_T - W_C} = \vartheta \frac{W_{Tr} - W_{Cr}}{W_T - W_C} \quad [3.50]$$

where ϑ can be calculated as:

$$\vartheta = \frac{c_{p2'3}(T_3 - T_{2'})}{c_{p23'}(T_{3'} - T_2)} \quad [3.51]$$

As a first approximation we can assume that the mean specific heats between 2′ and 3 and between 2 and 3′ (3 and 3′ are at the same temperature) are the same. Then, we can express Equation [3.51] as a function of the compressor efficiency:

$$\eta_C = \frac{W_C}{W_{Cr}} = \frac{c_{p12'}(T_{2'} - T_1)}{c_{p12}(T_2 - T_1)} = T_2 \cong T_1 + \frac{T_{2'} - T_1}{\eta_C} \quad [3.52]$$

We can then write Equation [3.51] as:

$$\vartheta = \frac{c_{p2'3}(T_3 - T_{2'})}{c_{p23'}(T_{3'} - T_2)} \cong \frac{T_3 - T_{2'}}{T_3 - T_1 - \dfrac{T_{2'} - T_1}{\eta_C}} = \frac{\tau - \beta^{\varepsilon}}{\tau - 1 - \dfrac{\beta^{\varepsilon} - 1}{\eta_C}} = \eta_C \frac{\tau - \beta^{\varepsilon}}{\eta_C(\tau - 1) - (\beta^{\varepsilon} - 1)} \quad [3.53]$$

Getting back to Equation [3.50] we can then proceed as follows:

$$\eta_i = \vartheta \frac{W_{Tr} - W_{Cr}}{W_T - W_C} = \vartheta \frac{\eta_T W_T - W_C/\eta_C}{W_T - W_C} = \frac{\vartheta}{\eta_C} \frac{\eta_T \eta_C - W_C/W_T}{1 - W_C/W_T}$$

$$= \frac{\vartheta}{\eta_C} \frac{-1 + \eta_T \eta_C + 1 - W_C/W_T}{1 - W_C/W_T}$$

$$\eta_i = \frac{\vartheta}{\eta_C}\left(1 - \frac{1 - \eta_T \eta_C}{1 - W_C/W_T}\right) = \frac{\vartheta}{\eta_C}\left(1 - \frac{1 - \eta_T \eta_C}{1 - \beta^{\varepsilon}/\tau}\right) \quad [3.54]$$

Replacing the final result of Equation [3.54] in Equation [3.49] we can write the expression of the efficiency of the real Joule–Brayton cycle:

$$\eta_r = \frac{\vartheta}{\eta_C}\left(1 - \frac{1 - \eta_T \eta_C}{1 - \beta^{\varepsilon}/\tau}\right)\left(1 - \frac{1}{\beta^{\varepsilon}}\right) \quad [3.55]$$

© Woodhead Publishing Limited, 2013

The real efficiency is thus the product of a term increasing with pressure ratio and one decreasing with it, showing the trend shown in Fig. 3.10.

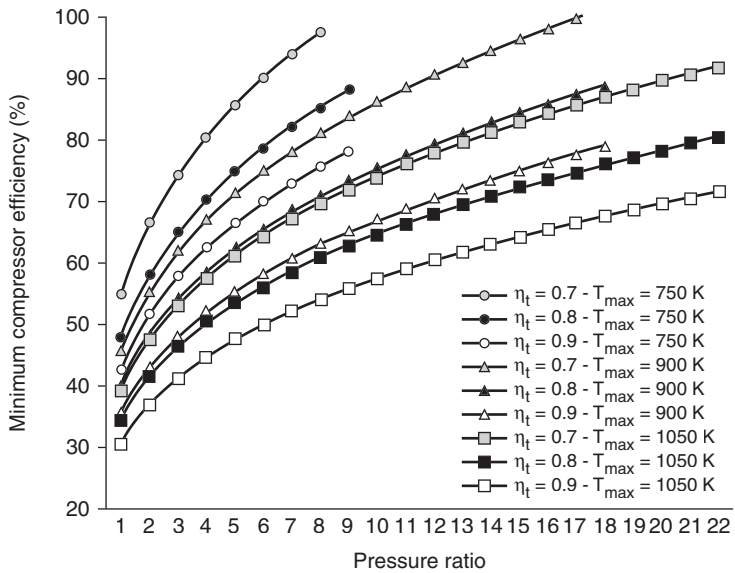
It is also noteworthy that Equation [3.55] provides a positive result if

$$\eta_T \eta_C > \frac{\beta^{\varepsilon}}{\tau} \qquad [3.56]$$

This is the fundamental reason why the gas turbine has had a very slow development. In fact, building compressors with high pressure ratios and high efficiency has been a challenge for decades, which was solved concretely during the Second World War and released to the public after the 1950s, when most of the studies of fluid dynamics of compressors and turbomachinery were published.

The disequation [3.56] could be solved if τ were high enough to make the right-hand side larger than the left-hand side. However, in the early stages of gas turbine development the available materials were not able to withstand temperatures higher than 600°C, giving a very low τ.

Figure 3.10 shows the minimum compressor efficiency that should be attained for a given turbine efficiency and turbine inlet temperature to verify Equation [3.56]. It can be noted that if the turbine efficiency is less than 0.7, the compressor efficiency should not be less than 0.8 for any turbine inlet temperature. Unless the pressure ratio is less than 10, the compressor



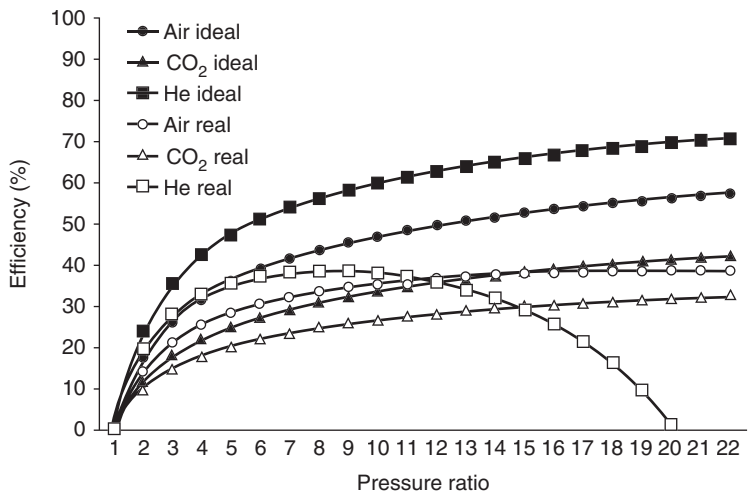
3.10 Minimum compressor efficiency to verify Equation [3.56] vs pressure ratio and for given values of turbine efficiency and TIT.

© Woodhead Publishing Limited, 2013

efficiency is the critical parameter to ensure gas turbine operation at an acceptable efficiency and power output. All curves are limited to a pressure ratio such as $\beta^{\varepsilon} < 0.7^{*}\tau$, which is a reasonable level to avoid too small a power output.

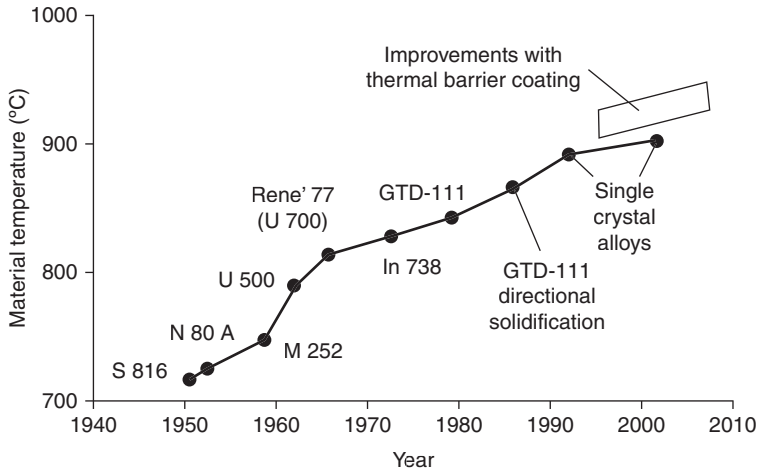
Disequation [3.56] was not verified for many years, slowing down the development of the gas turbine until the last 50 years. If the cycle is closed we may use different fluids from air and combustion products and take advantage of their thermodynamic properties to increase specific work and efficiency. The most suitable fluids to increase specific work are those with a high specific heat at constant pressure. Among the gases which have this property, it is possible to cite carbon dioxide and, in general, triatomic gases. Instead, in order to increase the efficiency, fluids with a higher k value would be preferable, because a higher value of k provides a higher value of ε. Gases with higher k are generally mono atomic gases, such as helium. Eventually, closed cycles have an additional degree of freedom, due to the pressure of point 1. Open cycles are constrained to use air at atmospheric pressure, but in closed cycle it is possible to pressurise point 1, thus increasing the mass of the working fluid with the same volume and size of the gas turbine. The size of the gas turbine may be reduced if the pressure at point 1 is increased from ambient pressure.

Figure 3.11 shows the ideal and real efficiency of gas turbines using different fluids as working fluid. Gas turbines using helium have a higher ideal cycle efficiency than those using air or carbon dioxide. The same holds true for the real cycle at low pressure ratios.



3.11 Ideal and real efficiency of gas turbines using different working fluids.

© Woodhead Publishing Limited, 2013



3.12 Improvements of gas turbine nozzles and blades material temperature during the years.[4]

It is interesting to note that the optimal pressure ratio for maximum power output in the ideal cycle increases with turbine inlet temperature. This is the reason why the pressure ratio has grown during the years following the trend of increasing turbine inlet temperature. The increase in turbine inlet temperature has been the main goal of gas turbine research since the beginning.

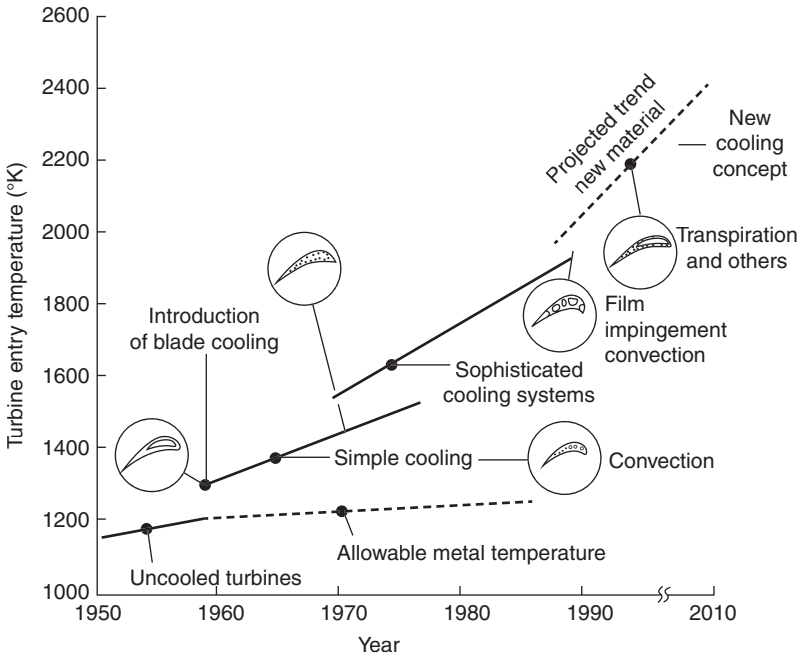
Improvements in metal resistance at high temperature may be seen in Fig. 3.12, where the maximum temperature blade and nozzles that materials can withstand has grown from 700°C to almost 900°C over the last six decades. But nozzle and blade cooling has helped to allow much higher turbine inlet temperatures while keeping the metal temperature at a safe level. Figure 3.13 shows how cooling techniques have enabled reaching turbine inlet temperatures higher than 1900 K over the last decade.

Figure 3.14 shows the increase of pressure ratio during the years. This can be compared with the ideal pressure ratio for maximum specific power as a function of turbine inlet temperature that is shown in Fig. 3.15.

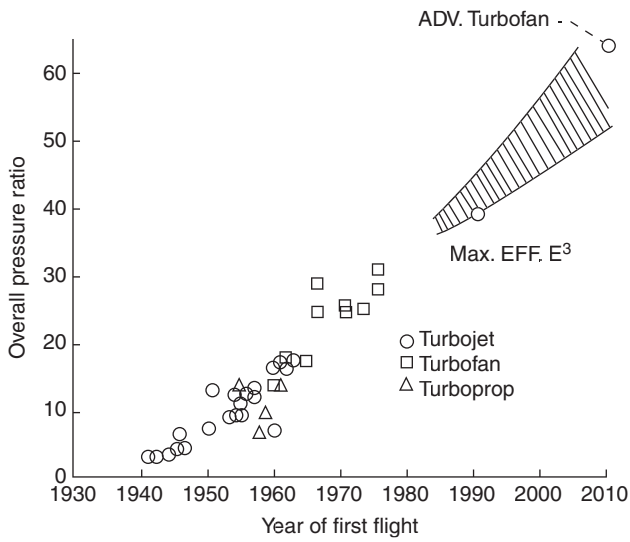
3.4 Improvements to the simple cycle

The development of the gas turbine described previously has followed a steady trend, with a number of significant innovations in the main components but always with a careful attention to maintain a leading role as aircraft engines. The main features of aircraft engines are a high power/weight ratio, small overall volume (length and external diameter of the gas turbine) to fit the aerodynamic casings located under the wings or in

© Woodhead Publishing Limited, 2013

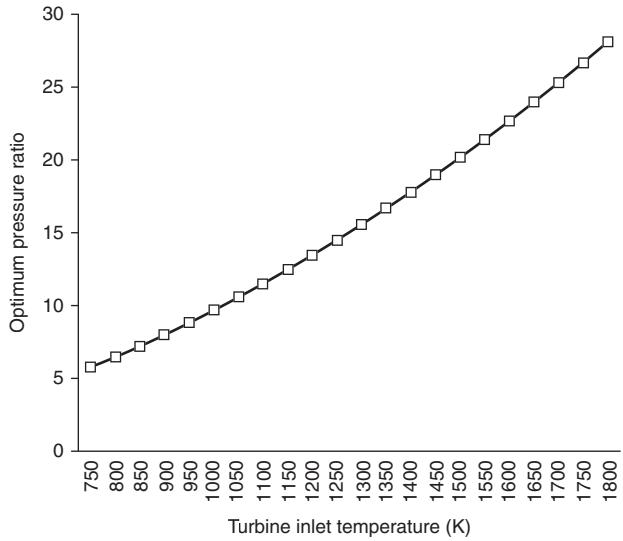


3.13 Evolution of TIT with cooling techniques.[3]



3.14 Increase of compressor pressure ratio during the years.[3]

© Woodhead Publishing Limited, 2013



3.15 Pressure ratio for maximum power output vs TIT.

the tail, and a low specific fuel consumption to increase the load capacity of the aircraft for a given cruise range. All those features have required a significant effort in improving all the components: higher loading of compressors and turbines, more compact combustion chambers, higher pressure ratios, and higher turbine inlet temperatures. Fundamental studies of fluid dynamics of turbomachinery, of combustion, of high temperature materials, and the introduction of nozzles and turbines blade cooling, have made the current technology reach compressor and turbine efficiencies well above 92%, a pressure ratio of axial compressor up to 30, and a turbine inlet temperature of 1700 K. The marginal improvements of those parameters has become smaller and smaller, and even the turbine inlet temperature is reaching its limit, due to environmental regulations that prevent combustion temperatures exceeding 1800 K, in order to keep NO_x emissions under control.

Therefore, the simple Joule–Brayton cycle is approaching its real limits, and only new concepts may further improve the performance of gas cycles. Several improvements to the Joule–Brayton cycles have been proposed over the years, but only few of them have been commercially developed for industrial and ship propulsion utilisation. Modifying the Joule–Brayton cycle means using additional components that are generally either heavy or bulky, or that use mixtures of air and water or steam. Most of the proposed changes improve either the efficiency or the specific work, and only in a few cases both of them. Among the proposed solutions, the following will be described:

© Woodhead Publishing Limited, 2013

1. Recuperated gas turbine.
2. Intercooled compression.
3. Reheat.
4. Wet cycles.

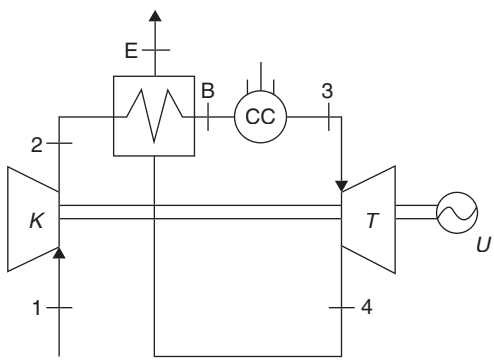
One section will be dedicated to combined gas–steam cycles, which represent the greatest commercial development of gas turbines for heavy duty utilisation but are based on coupling the simple Joule–Brayton cycle with a closed steam cycle. In these cycles the gas turbine is practically unchanged.

3.4.1 The recuperated gas turbine

Gas turbines release the Q_2 heat contained in flue gas at temperatures normally ranging between 700 and 900 K. A source of sensible heat at this temperature may be transferred internally in the cycle to heat compressed air between the compressor and the combustor. The schematic of the gas turbine is conceptually simple and is depicted in Fig. 3.16. The only addition to the simple cycle is the insertion of an air/flue gas heat exchanger whose hot side is located after the turbine exhaust (point 4-E) and the cold side between the compressor and the combustor (points 2-B).

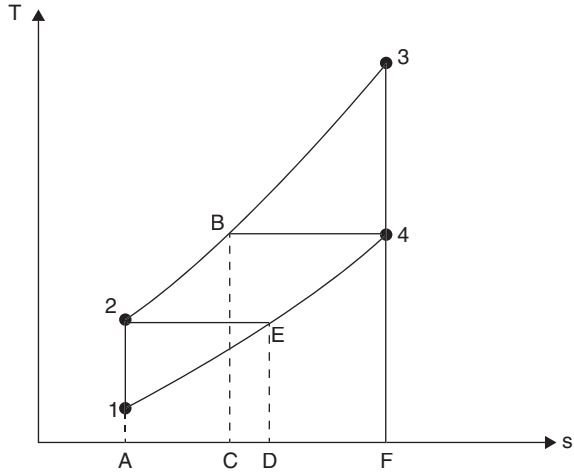
The T-s diagram of the recuperated cycle is shown in Fig. 3.17, for the ideal cycle, where the compression and expansion processes are adiabatic-isentropic, no pressure is lost in ducts and in the heat exchanger, the heat exchanger has no heat losses to the environment, and the heat transfer has a null temperature difference between the hot and the cold fluids. These assumptions are quite limiting in this case, but they allow deriving some interesting expressions for the efficiency to compare with the simple cycle.

With these assumptions the heat released by the cycle between points 4 and E is wholly and internally transferred to the compressed air by heating



3.16 The recuperated gas turbine cycle.

© Woodhead Publishing Limited, 2013



3.17 T-s diagram of the recuperated gas turbine ideal cycle.

it from point 2 to point B. This allows a significant saving of fuel, because the compressed air only needs to be heated by the combustion process from point B to point 3.

However, for this heat to be transferred, the necessary condition is that $T_4 > T_2$.

In the recuperated ideal cycle the specific work is the same as that of a simple cycle with the same pressure ratio and turbine inlet temperature. This can immediately be observed by looking at the T-s diagram. In fact, the area within the cycle, which is proportional to the specific work in the ideal case, is the same as that of a simple cycle with the same pressure ratio and turbine inlet temperature.

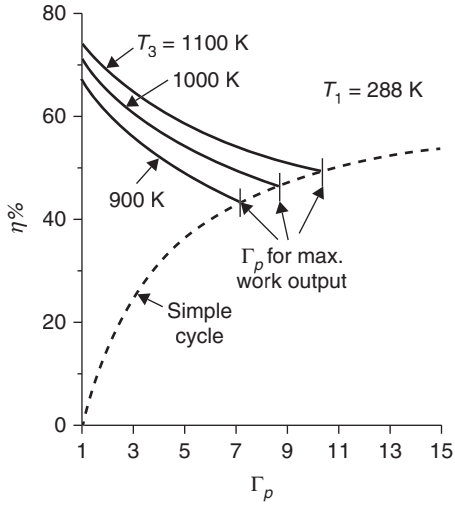
As far as the efficiency is concerned, we may use the same expression as was used for the simple cycle, but replacing T_2 with T_B and T_4 with T_E. Then if $T_B = T_4$ and $T_E = T_2$, we may write:

$$\eta_{rec} = 1 - \frac{Q_{2rec}}{Q_{1rec}} = 1 - \frac{T_E - T_1}{T_3 - T_B} = 1 - \frac{T_2 - T_1}{T_3 - T_4} = 1 - \frac{\beta^{\varepsilon} - 1}{\tau - \frac{\tau}{\beta^{\varepsilon}}} = 1 - \frac{\beta^{\varepsilon} - 1}{\frac{\tau}{\beta^{\varepsilon}}(\beta^{\varepsilon} - 1)} = 1 - \frac{\beta^{\varepsilon}}{\tau} \quad [3.57]$$

The efficiency is thus decreasing with β, differently from the simple cycle where the efficiency is increasing with β.

Figure 3.18 shows the efficiency vs the pressure ratio of the recuperated cycle and the simple cycle. The point where the curve of the recuperated cycle meets that of the simple cycle has a special meaning, which will be

© Woodhead Publishing Limited, 2013



3.18 Efficiency of the recuperated and the simple ideal cycles vs the pressure ratio.

described shortly. The point where the recuperated cycle efficiency crosses the simple cycle efficiency can be found by equating the two expressions of the efficiency [3.31] and [3.57]:

$$1-\frac{1}{\beta^{\varepsilon}}=1-\frac{\beta^{\varepsilon}}{\tau}\rightarrow\tau=\beta^{2\varepsilon}\rightarrow\beta=\tau^{\frac{1}{2\varepsilon}} \qquad [3.58]$$

The same results can be obtained if we calculate the condition by which $T_4 = T_2$:

$$T_4=T_2\rightarrow\frac{T_4}{T_3}\frac{T_3}{T_1}=\frac{T_2}{T_1}\rightarrow\frac{\tau}{\beta^{\varepsilon}}=\beta^{\varepsilon}\rightarrow\beta=\tau^{\frac{1}{2\varepsilon}} \qquad [3.59]$$

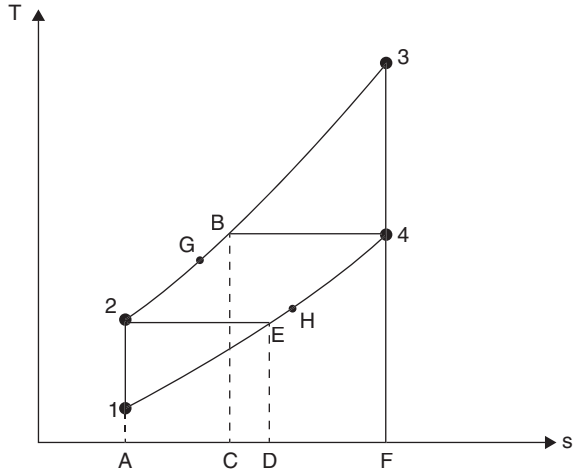
This means that the maximum specific work condition is reached when $T_4 = T_2$, which is also the point of maximum pressure ratio at which we can have a recuperated cycle.

If we eliminate the assumption that the temperature difference between the cold and the hot fluid is not null, the air temperature at the combustor inlet will be lower than T_4.

Looking at Fig. 3.19, we can now define the recuperation ratio as:

$$R=\frac{c_p(T_{\mathrm{G}}-T_2)}{c_p(T_{\mathrm{B}}-T_2)} \qquad [3.60]$$

© Woodhead Publishing Limited, 2013



3.19 T-s diagram of the recuperated cycle with $R < 1$.

R is 0 for the simple cycle and 1 for the ideal recuperated cycle with complete heat recovery described earlier.

For $R < 1$, we can now calculate the heat supplied and released:

$$\begin{aligned} Q_{1\text{rec}R} &= c_p(T_3 - T_4) + (1-R)c_p(T_4 - T_2) \\ Q_{2\text{rec}R} &= c_p(T_2 - T_1) + (1-R)c_p(T_4 - T_2) \end{aligned} \quad [3.61]$$

and calculate the efficiency of the partially recuperated cycle as:

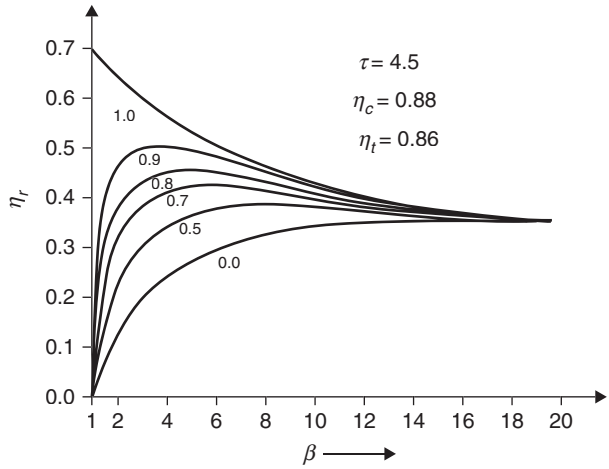
$$\eta_{\text{rec}R} = 1 - \frac{Q_{2\text{rec}R}}{Q_{1\text{rec}R}} = 1 - \frac{T_3 - T_4 + (1-R)(T_4 - T_2)}{T_2 - T_1 + (1-R)(T_4 - T_2)} = 1 - \frac{\tau - \frac{\tau}{\beta^c} + (1-R)\left(\frac{\tau}{\beta^c} - \beta^c\right)}{\beta^c - 1 + (1-R)\left(\frac{\tau}{\beta^c} - \beta^c\right)}$$

$$= 1 - \frac{\tau - \frac{\tau}{\beta^c} + (1-R)\left(\frac{\tau}{\beta^c} - \beta^c\right)}{\beta^c - 1 + (1-R)\left(\frac{\tau}{\beta^c} - \beta^c\right)} \quad [3.62]$$

If Equation [3.62] is plotted for different R, all the curves lie between the $R = 1$ and the $R = 0$ curves as shown in Fig. 3.20.

It can be observed that the optimal value of the pressure ratio for the recuperated cycle with any value of $R > 0$ is always much less than for the simple cycle, and also much smaller than the pressure ratio for maximum

© Woodhead Publishing Limited, 2013



3.20 Efficiency of the recuperated cycle vs pressure ratio for different *R*.

specific work. This means that recuperated cycles are convenient for very small pressure ratios, which are not normally encountered in modern gas turbines.

Today, recuperated cycles are only used in microturbines that have only one centrifugal compressor stage and therefore a very low pressure ratio.

In the real cycle the assumptions listed for the ideal cycle are no longer valid, and those concerning the heat exchanger are those that most affect the performance. The heat exchanger is a gas–gas compact heat exchanger and its size is generally quite large compared to the size of the gas turbine, so that the plant volume is practically doubled by its presence. The large size is mainly due to the small heat transfer coefficient between air and flue gases, and to allow ample ducts to prevent too high pressure losses on both sides.

Nonetheless, in real recuperated gas turbines *R* is always less than 1, because it is impossible to exchange heat with a null temperature difference between the hot and the cold fluids, and pressure losses have to be accounted on both sides.

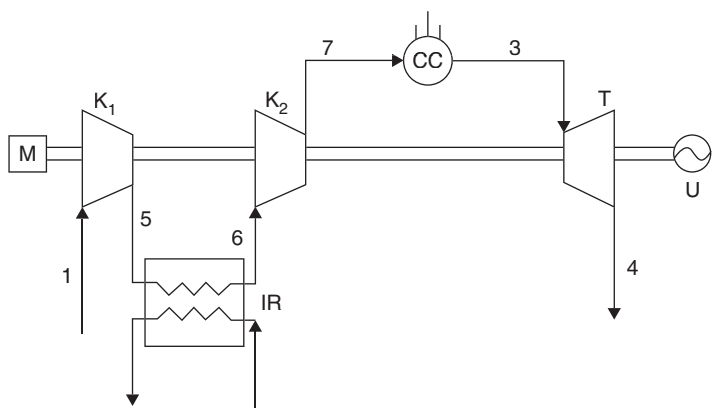
These two factors affect the efficiency of the cycle, as is shown in Fig. 3.15, but they also reduce the specific power. In fact pressure losses on both the cold side, where they are added to the combustor pressure losses, and on the hot side, where they cause the exhaust pressure of the turbine to rise over the ambient pressure, reduce the expansion ratio of the turbine with respect to the compression ratio of the compressor. In addition, it is important to note that compact heat exchangers are subject to fouling, and thus to a reduction of their performance with time, and the insertion of a large

© Woodhead Publishing Limited, 2013

volume after the compressor may produce additional risks of surge if the compressor is not specifically designed for this application. For all those technical reasons, recuperated gas turbines have not had the success that they might deserve for the high efficiency that could be reached.

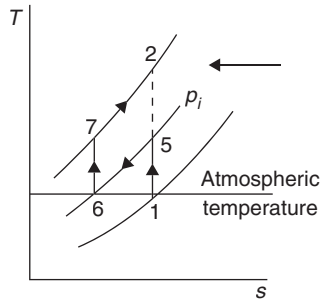
3.4.2 The gas turbine with intercooled compressor

The compressor requires a significant share of the work produced by the turbine. In the early stages of development of the gas turbine, it was very difficult to build a compressor that required less work than that produced by the turbine. This is mainly due to the adiabatic process, which is common in most turbomachinery and requires more work than in a constant temperature compression process. However, it is not easy to conjugate a high fluid dynamic efficiency of compressors with the possibility of extracting heat from the compressed fluid. High fluid dynamic performance is achieved with thin and geometrically complex aerodynamic profiles of the blades, and an efficient heat transfer is instead possible with large heat transfer surfaces and simple geometrical passages. In addition, it is important to mention that heat exchangers are static components, and turbomachinery has parts rotating at high speed. For those reasons, it is technically impossible to build an efficient compressor for a constant temperature process. Therefore, a compromise between an adiabatic and a constant temperature compression may be achieved with a series of adiabatic compressor stages followed by a series of heat exchangers that cool the compressed air (Fig. 3.21). The optimal condition is reached when point 6 is at the same temperature as point 1, that is, ambient temperature.



3.21 Schematic of a gas turbine with an intercooled compression.

© Woodhead Publishing Limited, 2013



3.22 T-s diagram of an intercooled compression.

The compression process on the T-s diagram is shown in Fig. 3.22.

The compression specific work is lower than in the case of an adiabatic compression from point 1 to point 2. As it was described in Section 3.2, by moving along a constant entropy line the distance between two constant pressure lines increases with temperature. Therefore, line 6–7 is shorter than line 2–5 and the overall compression work in the intercooled case is smaller than in the adiabatic case:

$$W_{IC} = c_p(T_5 - T_1 + T_7 - T_6) < c_p(T_2 - T_1) = W_{AD} \qquad [3.63]$$

This is valid for the ideal intercooled compression cycle but this consideration can be easily extended to the real case.

A reduction in the compression work causes an increase in the overall specific work output of the cycle because the expansion work is unchanged.

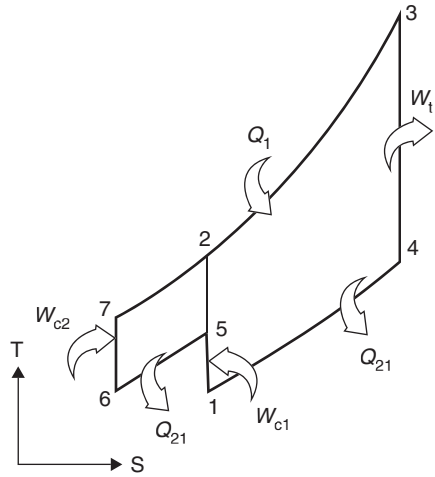
Keeping an eye on the ideal cycle, we can show that the efficiency decreases when we add intercooled compression. With reference to Fig. 3.23, we can divide the cycle in two sub-cycles I and II. Cycle I can be considered the reference simple cycle, which is modified by dividing the compression two stages with intercooling. In this way the cycle with intercooled compression can be compared with a simple cycle with the same pressure ratio and turbine inlet temperature.

The efficiency of the whole cycle can be calculated as follows:

$$\eta_{IC} = \frac{W_I + W_{II}}{Q_{1I} + Q_{1II}} = \frac{\eta_I Q_{1I} + \eta_{II} Q_{1II}}{Q_{1I} + Q_{1II}} \qquad [3.64]$$

Since cycles I and II are two ideal Joule cycles, one with the overall pressure ratio and one with a lower pressure ratio. From Equation [3.31], it is clear that cycle I has a higher efficiency than cycle II and therefore their weighted average in Equation [3.64] is lower. The efficiency of the intercooled ideal cycle is always lower than of a simple cycle with the same pressure ratio

© Woodhead Publishing Limited, 2013

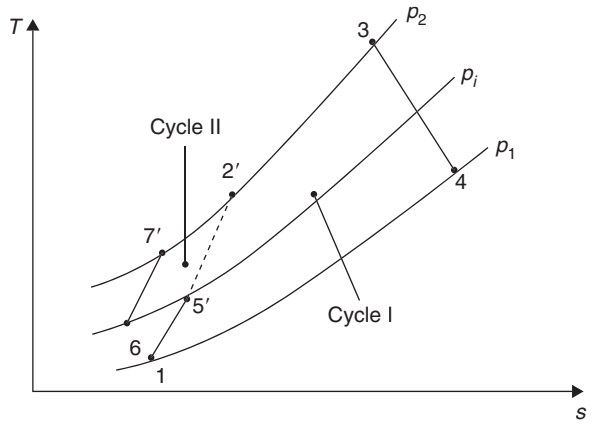


3.23 T-s diagram of an intercooled compression ideal cycle.

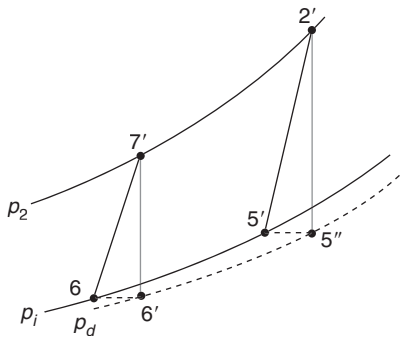
and turbine inlet temperature. The same cannot be said in general for the intercooled real cycle. If we look at Fig. 3.24, which depicts an intercooled real cycle and Fig. 3.25 that is an enlargement of cycle II, we cannot immediately determine if cycle II has a lower efficiency than cycle I because we cannot use Equation [3.31] which is valid only for the ideal cycle. Moreover, point 6 in the real cycle will not be at the same temperature as point 1, since the heat exchanger cannot cool the air at a lower temperature than ambient temperature.

However, if we draw a constant temperature line from 6 to 6′ and from 5′ to 5″ and find the intersection with a constant entropy line from 7′ to 6′ and from 2′ to 5″, from the description of the thermodynamic properties of gases in Section 3.2, we can affirm that points 6′ and 5′ lie on the same constant pressure line p_d. Moreover, cycle 67′2′5′ is energetically equivalent to cycle 6′7′2′5'' because they receive the same amount of heat in the 7′2′ process and release the same amount of heat in the 65′ and 6′5″ processes. Line 6′5″ is perfectly translated from 65' and therefore the heat released is exactly the same. Two cycles with the same heat received and released have the same efficiency, but cycle 6′7′2′5″ is an ideal Joule cycle and its efficiency can be easily calculated from Equation [3.31]. However, it is possible to notice that the cycle 6′7′2′5″ has a higher pressure ratio than the cycle 67′2′5′ and in some peculiar cases its pressure ratio could be high enough to have cycle II efficiency higher than cycle I. Therefore, in the intercooled compression real cycle we cannot state for sure that the efficiency will decrease with respect to the simple cycle with the same pressure ratio and turbine inlet temperature.

© Woodhead Publishing Limited, 2013



3.24 T-s diagram of an intercooled compression real cycle.



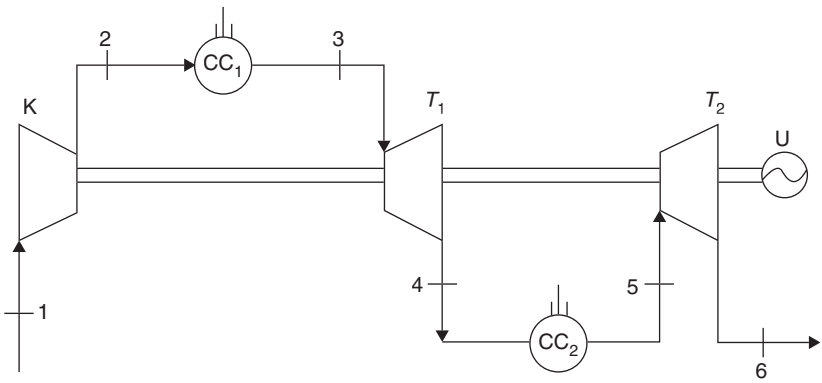
3.25 T-s diagram of cycle II of an intercooled compression real cycle.

3.4.3 The gas turbine with reheat

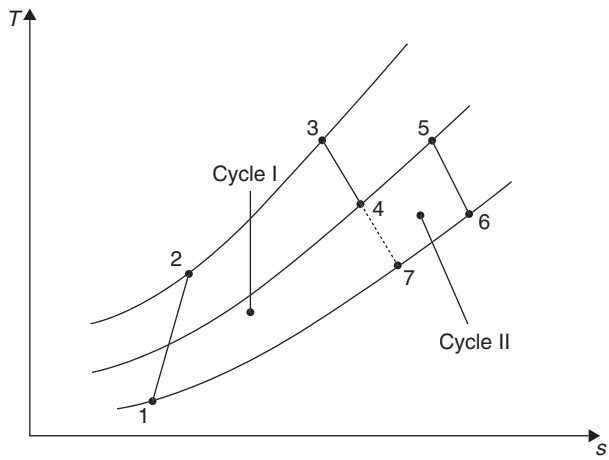
Reheat in gas turbines is a similar modification as intercooled compression. The aim of this improvement is to use the same advantage from the thermodynamic properties of gases by allowing a partial expansion of the gas in the turbine, followed by a reheat and a second expansion to the ambient pressure (Fig. 3.26).

Reheat is made possible by inserting a second combustor between the first turbine and the second. As we have discussed earlier in this chapter, all gas turbines operate with quite large excess air and there is still enough oxygen available after the first combustion process to be able to burn additional fuel in the second combustor. The second combustor will provide heat to reach the same maximum temperature T_5 as the first combustor T_3 (Fig. 3.27).

© Woodhead Publishing Limited, 2013



3.26 Schematic of the reheat gas turbine.



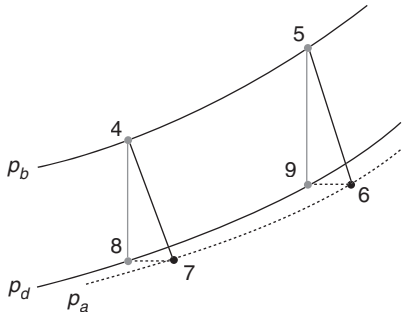
3.27 T-s diagram of the reheat real cycle.

With identical considerations as for the intercooled compression cycle, we can state that in the ideal cycle the specific work is always higher than in the simple cycle with the same pressure ratio and turbine inlet temperature, and the efficiency is always lower than in the simple cycle.

In the real cycle, the specific work is always higher but the efficiency is always lower. We can show this by looking at Fig. 3.28, where cycle 8459 has a pressure ratio that is always smaller than cycle I.

We can eventually state that both intercooled compression and reheated gas turbines have a higher specific work than simple cycle gas turbines with the same pressure ratio and turbine inlet temperature. The efficiency is generally lower in both cases, and for the above reasons these modifications have significance when having a higher specific power is more important than

© Woodhead Publishing Limited, 2013



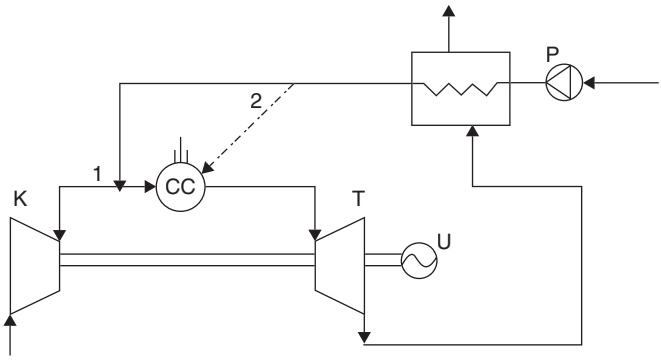
3.28 T-s diagram of cycle II of reheated real cycle.

having a lower fuel consumption. These is the case with marine propulsion in war ships, where the availability of a cooling fluid for intercooling is unlimited (sea water), the size and weight of the gas turbine is not the major constraint, and manoeuvring ability is essential. A few commercial propulsion systems for marine applications include intercooling and heat recuperation in the same gas turbine, thus having the double advantage of an increased power output and higher efficiency. Moreover, intercooling enlarges the temperature difference between the turbine exhaust and the compressor discharge and allows recuperating heat in gas turbines with higher pressure ratios.

3.4.4 Wet cycles

One of the main characteristics of the gas turbine is the possibility of operating with no additional working fluid than air. This is a very important feature, because it makes the cycle operation simple, and requires a limited number of components: just three for the simple cycle and a couple more for the modified cycles described so far. However, the modified gas turbine cycle that has had the greatest commercial success is the steam injected gas turbine. Steam injection consists in introducing a flowrate of steam after the gas turbine compressor, which is generated in a heat recovery steam generator using the gas turbine exhaust gas as heat source. Conceptually, it is a recuperated cycle where the heat, which would otherwise be released to the environment, is internally transferred to the compressed air entering the combustor, but the heat is transferred to a different fluid, which is thus mixed with the compressed air. The advantage is double: not only is heat transferred, but also a mass flowrate. Therefore, the fluid flowrate expanding in the turbine is larger than in the simple cycle, and it increases the specific power, since it has not been compressed as a vapour in the compressor but as a liquid in a pump, requiring a much smaller fraction of work. The schematic of the steam injected gas turbine is shown in Fig. 3.29.

© Woodhead Publishing Limited, 2013



3.29 Schematic of a steam injected gas turbine.

Steam is generated at a slightly higher pressure than that of compressed air, and its temperature is generally higher than compressed air temperature. Steam can be mixed with air before the combustor or inside the combustor, and the heat supplied by the fuel is partially reduced.

The increase in the specific power is due to the increase in the overall flowrate in the turbine and to the very small pump work compared to the compression work necessary to bring steam to the same pressure as compressed air.

The main advantage is the increase in efficiency and specific power output; the main drawbacks are the use of water, which needs to be treated to be used in the steam generator and is lost to the environment after the heat recovery system, the size of the heat recovery equipment, and the possible consequences of the steam injection: the compressor operating point moves towards surge conditions, the blade cooling system is not designed to work with a different fluid the effect of impurities in the water on materials and combustion, the presence of steam in the exhaust gas (visibility of plume from the stack, local changes in microclimate).The maximum steam flowrate is lower than 15–20% of the air flowrate, due to the limits imposed by the heat balance of the heat recovery steam generator.

Steam injected cycles are quite commonly used with small size gas turbines having a power output lower than 40 MW, and in combined heat and power applications.

To limit the complexity of the plant, water could be injected in the liquid state. However, this type of modification is seldom practised because it increases specific work but it considerably decreases the efficiency. The increase in specific work is for the same reasons as described above for the steam injected cycle.

However, adding liquid water after compression will reduce the air temperature because of the heat required for the evaporation of water, and the

© Woodhead Publishing Limited, 2013

gas turbine will require more fuel to reach the same turbine inlet temperature. The increase in power output does not compensate for the additional fuel required, and the efficiency is reduced.

A third category of wet cycles are the so-called humid air cycles (HAT cycles), where the heat recovery steam generator is replaced by an air saturator to improve the heat and mass transfer before the combustor. Humid air cycles, even with more promising performance than steam injected cycles, have not had the same commercial success and have not yet developed further than a few demonstration units worldwide.

3.5 Combined gas–steam cycles

As it was mentioned earlier in this chapter, the gas turbine exhaust gas releases large amounts of heat at high temperature. Exhaust gas temperature ranges between 400°C and 620°C, with flowrates that can be as large as 600 kg/s.

Such a heat source can be used for several purposes, without affecting the gas turbine performance and its safety of operation. Since the temperature exceeds 400°C, exhaust heat can be used in a heat recovery steam generator (HSRG) to generate steam that can be used in a steam cycle. Such an arrangement is actually a development of steam injected cycles, but the steam is not mixed with air in the gas turbine but is used in a separate steam cycle.

There are several advantages in comparison with steam injected cycles:

1. Steam is not mixed with air and is not exhausted to the atmosphere, thus reducing water treatment costs and water consumption.
2. Since steam is not lost, the size of the combined cycle is not a limiting factor.
3. Large-size combined cycles can use more advanced technologies and more complex and efficient steam generators.
4. Since steam is used in a closed cycle, steam pressure can be optimised to recover the maximum amount of heat in the steam generator, and it can be expanded to very low condensing pressures, providing additional work.

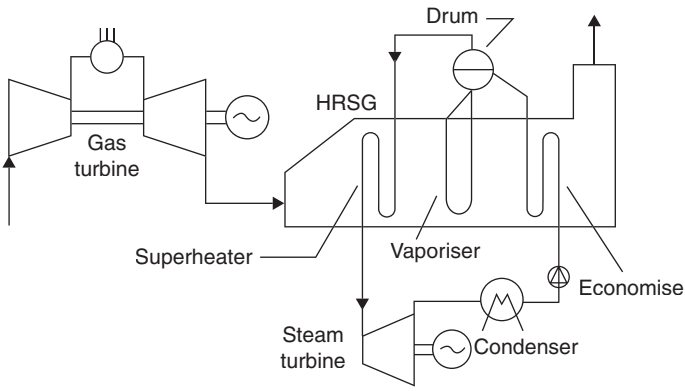
The development of combined cycles in the last three decades has resulted in the most efficient power plant commercially available today, with the highest values over 60% (based on the fuel Lower Heating Value).

The concept of combined cycle can be described with reference to Fig. 3.30.

The gas turbine exhaust gas are introduced in a HRSG consisting of a series of tube bundles, which can be divided into three main sections:

1. The economiser, where steam is preheated from the condenser temperature, close to ambient temperature, to a few degrees of temperature below saturation temperature. This small sub-cooling is to avoid

© Woodhead Publishing Limited, 2013



3.30 Schematic of gas–steam combined cycle.

evaporation of steam in the economiser. The water from the economiser flows into a drum, where liquid and steam are separated.

2. The vaporiser, which receives saturated water from the drum and vaporises it, delivering a water/steam mixture to the drum for separation.
3. The superheater, which receives saturated steam from the drum and where steam temperature is increased to the desired steam turbine inlet temperature.

Superheated steam is then delivered to the steam turbine and then to the condenser, which returns liquid water to a pump to close the cycle.

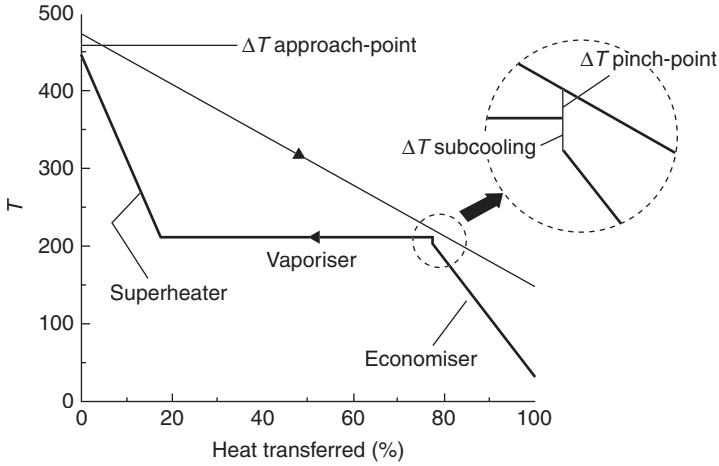
The described combined cycle has a single pressure HSRG. If we draw the heat transferred-temperature diagram for the HRSG (Fig. 3.31), we may notice that the temperature difference along the heat transferred is quite large in the superheater and vaporiser because of the constraint imposed by the pinch point temperature difference, which is the point where the exhaust gas meets the vaporiser's inlet. The pinch point and the constant temperature vaporisation prevent the temperature difference between the hot and the cold gas getting smaller. A high temperature difference in a heat exchanger is correlated with irreversibilities and finally hinders the capacity to convert the heat of our source into useful work.

The specific work of the combined cycle is provided by the sum of the gas turbine work and the steam cycle work, divided by the gas turbine flowrate.

$$\frac{W_{CC}}{m_{TG}} = \frac{W_{TG}}{m_{TG}} + \frac{W_{ST}}{m_{TG}} \qquad [3.65]$$

As a rule of thumb we may say that the combined cycle specific work is between 50% and 70% higher than the specific work of the gas turbine in simple cycle.

© Woodhead Publishing Limited, 2013



3.31 Temperature-heat transferred diagram for a single pressure HRSG.

In defining an expression for the efficiency of the combined cycle, we have to consider that the sole external heat input to the cycle is provided to the gas turbine, and that the HRSG has an efficiency that can be defined by the ratio of the recovered heat to the recoverable heat. This definition of efficiency does not include heat losses to the environment through the HRSG walls, but only the heat lost to the stack, which has not been recovered by the steam.

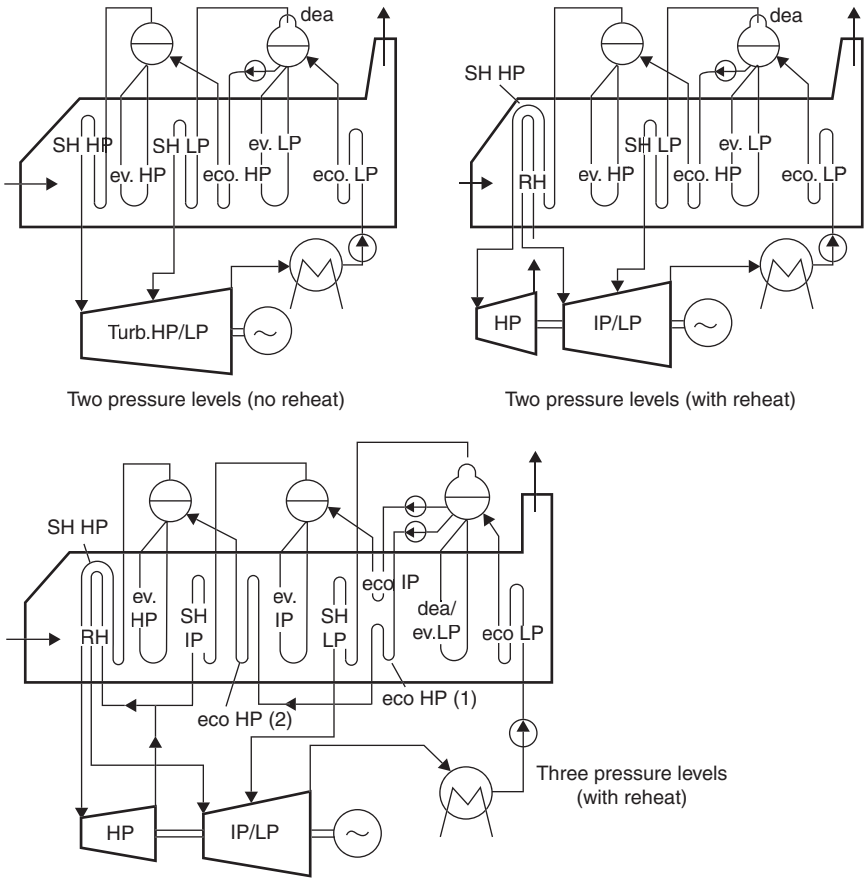
We can therefore write:

$$\begin{aligned}\eta_{CC} &= \frac{W_{GT} + W_{ST}}{Q_{1GT}} = \frac{\eta_{GT} Q_{1GT} + \eta_{ST}\,\eta_{HRSG} Q_{2GT}}{Q_{1GT}} \\ &= \frac{\eta_{GT} Q_{1GT} + \eta_{ST}\,\eta_{HRSG} Q_{1GT} - \eta_{ST}\,\eta_{HRSG}\,\eta_{GT} Q_{1GT}}{Q_{1GT}} \\ \eta_{CC} &= \eta_{GT} + \eta_{ST}\,\eta_{HRSG} - \eta_{ST}\,\eta_{HRSG}\,\eta_{GT}\end{aligned} \quad [3.66]$$

The gas turbine efficiency is only slightly influenced by its integration in a combined cycle. The steam cycle efficiency is dependent on steam turbine inlet temperature and pressure, condensation temperature and steam cycle components efficiencies. When the steam cycle is optimised, we may also consider its efficiency as a fixed parameter in Equation [3.66]. The most important efficiency in Equation [3.66] is the HRSG efficiency.

The HRSG efficiency can be slightly improved by adjusting the steam pressure and temperature, but the only possibility to overcome the limitation imposed by the pinch point, is to push the cold fluid closer to the hot fluid. This is possible by vaporising the water at different pressure levels

© Woodhead Publishing Limited, 2013



3.32 Different configurations of HRSG for combined cycles.[4]

inside the HRSG, creating multiple pinch points and a more complicated arrangement of the heat exchangers in the HRSG, but also greatly improving its efficiency and consequently the combined cycle efficiency.

Figure 3.32 shows the development of the HRSG from the double pressure to the three pressure levels with reheat. The cycle configurations are more complex, but the efficiency of the three pressure level combined cycle is more than ten percentage points higher than that of a single pressure combined cycle.

The development of combined cycles has brought to build HRSGs with two pressure levels in the early 1990s, and with three pressure levels in the late 1990s. The current most optimised commercial technology is a combined cycle with three pressure levels and reheat, with power output of hundreds of MW and efficiency higher than 57–58%. This is the maximum performance that can be achieved by a combined cycle where gas and

© Woodhead Publishing Limited, 2013

steam are completely separated and the only energy transferred between them is through the HRSG.

The latest technology that is fast approaching a commercial level is the combined cycle, where the gas turbine nozzles and blades are cooled by steam in closed circuit that is then used in the steam cycle. With this additional heat exchange, which also affects the gas turbine performance, the overall combined cycle efficiency is higher than 60%.

3.6 Basics of blade cooling

In all the thermodynamic descriptions made in this chapter, the expansion process has been assumed adiabatic. This is quite a limiting assumption, considering the turbine inlet temperature levels currently used in commercial gas turbines, which are several hundred degrees higher than the maximum temperature that metal alloys can stand.

This large gap, between the turbine inlet temperature and the maximum metal temperature, can only be filled by using a cooling technology to prevent the metal of the nozzles and blades exceeding its technological limit.

One of the following chapters will be entirely dedicated to this subject, and the aim of this section is to shortly describe the effect of such technology on the thermodynamic cycle and its performance.

First of all, it is important to understand the meaning of the turbine inlet temperature, which has at least three definitions:

1. Combustor outlet temperature (COT), which is the temperature of the combustion products before the first nozzle of the gas turbine. If the turbine is adiabatic the turbine inlet temperature is the same as the COT, and this is the meaning of turbine inlet temperature throughout this chapter. However, the combustion outlet temperature is never provided on gas turbine data sheets by manufacturers.
2. Turbine inlet temperature (TIT), is the first rotor inlet stagnation temperature, which is important for most cycle calculations and simulations, and is the COT reduced by the mixing of the gases exiting the combustor with the cooling air of the first nozzle.
3. ISO Turbine inlet temperature (TIT_{ISO}) is the temperature obtained after mixing the gases exiting the combustor with the overall nozzle and blade cooling flowrate.

High temperature nozzles and blades are commonly cooled by bleeding air from the compressor at the discharge temperature (generally lower than 350°C) and letting it flow inside the nozzles and blades. After passing through the blades, cooling air is mixed with the hot gases. The thermodynamic

© Woodhead Publishing Limited, 2013

process is quite complex because the non-adiabatic expansion and mixing involves a detailed knowledge of the turbine cascades and the heat transfer characteristics of the blades and nozzles. A simplified calculation can be performed by assuming the cooled turbine as a sequence of adiabatic expansions followed by a mixing of colder air with the hot gases.

Even though a cooled expansion is conceptually worse than an adiabatic one, it is not correct to compare a cooled and an adiabatic turbine with the same inlet temperature, because it would be useless to cool a turbine from temperatures where an adiabatic turbine could be operated safely and, at the same time, it would be impossible to use an adiabatic turbine at temperatures where cooling is necessary.

Therefore, when comparing an adiabatic turbine with a TIT of 900°C with a cooled turbine with an inlet temperature of 1500°C, it is clear that the specific work and efficiency of the cooled turbine will be much higher than that of the adiabatic turbine.

3.7 Conclusion and future trends

Studying the development of the gas turbine, it is clear that the winning innovations have mainly been in the components, and only in one case in the thermodynamic cycle.

The development of the gas turbine has required significant efforts in research, and gas turbine manufacturers have always been quite conservative in accepting proposals involving major redesign of the system. Therefore, the advancements were mainly made in compressor and turbine aerodynamics, combustion efficiency and reduction of pollutant emissions, high temperature materials and nozzles and blades cooling.

Most of these technologies have reached a very detailed level of design and performance, expected improvements are slow, and only unexpected breakthroughs will be able to move from the current development paths and trends that are well known to gas turbine researchers and manufacturers.

Looking at the thermodynamic cycles, there has been a significant interest in the last two decades for wet cycles using air and water, or a mixture of them, as working fluids. This was mainly due to significant improvements in the performance in terms of efficiency and specific power.

Combined cycles of the last generation with steam cooling of the nozzles have represented a major innovation that still requires development and may produce further improvements in the performance.

The real innovation for the future may come from the integration of gas turbines and high temperature fuel cells in the so-called hybrid cycles. However, the major issues to be solved in this technology are on the fuel cell side. The expected efficiencies for this type of plant may reach 70%, which is currently a very distant goal for combined cycles, with the additional

© Woodhead Publishing Limited, 2013

advantage of being able to reach such performance levels even for small size power plants.

3.8 References

1. Saravanamuttoo, H.I.H., Rogers, G.F.C., Cohen, H. and Straznicky, P.V. (2009), *Gas Turbine Theory*, 6th Edition, Pearson Education Ltd., UK, ISBN 9780132224376.
2. Bathie, W.W. (1996), *Fundamentals of Gas Turbines*, 2nd Edition, John Wiley & Sons, USA, ISBN 0471311227.
3. Han, J.C., Dutta, S. and Ekkad, S. (2000), *Gas Turbine Heat Transfer and Cooling Technology*, Taylor & Francis, USA, ISBN 156032841X.
4. Lozza, G. (2006), *Turbine a Gas e cicli Combinati*, Società Editrice Esculapio, Italy, ISBN 8874881231 (in Italian).
5. Horlock, J.H. (2003), *Advanced Gas Turbine Cycles*, Elsevier Science Ltd., UK, ISBN 0080442730.
6. Rogers, G.F.C. and Mayhew, Y.R. (1980), *Engineering Thermodynamics Work and Heat Transfer*, 3rd Edition, Longman Ltd, USA, ISBN 0582305004.

© Woodhead Publishing Limited, 2013

4

Compressors in gas turbine systems

W. KAPPIS, Alstom (Schweiz) AG, Switzerland

DOI: 10.1533/9780857096067.2.89

Abstract: This chapter describes compressors in gas turbines. It describes key components of the compressor, its hardware, the operational requirements and other important issues.

Key words: compressor systems and operation, compressor design, compressor aerodynamics, compressor mechanical integrity, compressor mechanical design and manufacturing.

4.1 Introduction: role of the compressor

Huge volume flows at high pressure are required to support suitable power generation in gas turbines. Delivering high pressurised volume flows is achieved by a compressor: a radial compressor is used for smaller volume flows, while an axial compressor is used for higher volume flows. The technology used is largely based on the development of gas turbines in aircraft. Aero-derivative engines are therefore used for small power requirements (usually below 50 MW). These small engines have the advantage of multiple shafts, which allow a better site-specific/local optimisation. The power requirement from the compressor is more than 60% of the overall generated gas turbine power. Particular attention has to be given to this component to ensure a high overall gas turbine efficiency.

The inlet fogging and high fogging applications involved in new power peaking facilities pose a further mechanical challenge to the compressor, as fine water droplets or mist enters the compressor, and the droplets that develop must be sustained. In standard fogging applications, on the other hand, no droplets (or at least only a small number of droplets) enter the compressor blading. To increase the efficiency of the compressor, cycle applications with intercooling stages can be used, which boost the simple cycle efficiency but still require high additional investment in terms both of cost and space, and have a high level of complexity. Unfortunately, although this approach increases the simple cycle efficiency, it actually reduces the combined cycle efficiency and is therefore only useful in special cases.

Published by Woodhead Publishing Limited, 2013

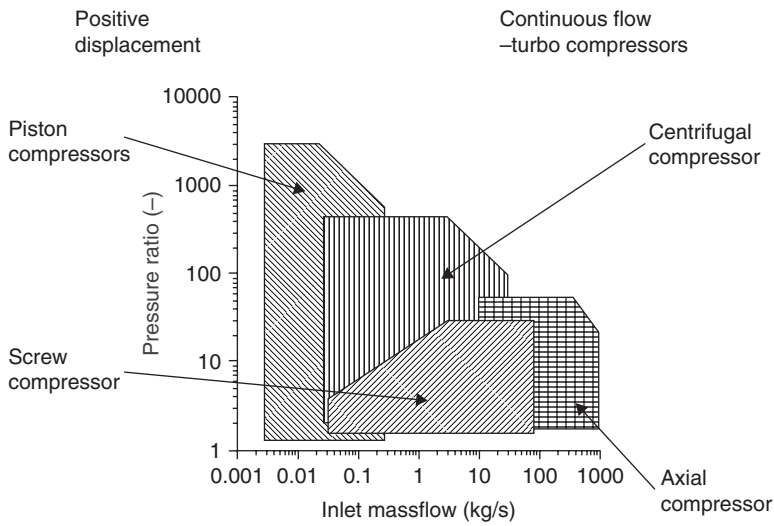
Further challenges are also emerging with respect to CO_2 capture. This can be achieved, for example, through recirculation of the gas in order to condense the local CO_2 content, which facilitates CO_2 capture but can also require wider ranges of mass flows, and so on. An in-depth understanding of the complex elements of the compressor is therefore essential, including its operational behaviour and the limits on its application.

4.2 Types of compressor systems

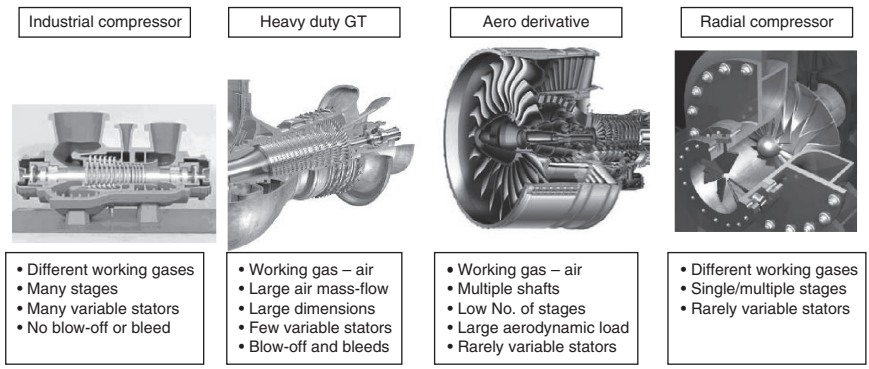
A compressor delivers a determined mass flow at a specific pressure ratio. The most suitable compressor for a given situation varies according to the requirements of the site; several different types have been developed for a variety of scenarios, and are discussed in this section.

4.2.1 Basic compressor types

Several factors must be assessed in the selection of the correct type of compressor, most importantly the mass flow or required volume flow. Larger volumes can only be efficiently supplied by axial compressors, whereas radial compressors are increasingly used when smaller volumes are involved. Mixed compressor types may also be used on some occasions; for example, a system could have three axial compressor stages followed by two radial compressor stages. Typical volume flows for the different compressor types can be found in Fig. 4.1.



4.1 Different compressor types to suit mass flow and pressure ratio requirements.



4.2 Some typical compressor types and drivers. Industrial compressor. (*Source*: Image reproduced with the permission of DAC (website: DACworldwide.com).) Aero derivative. (*Source*: Image reproduced with the permission of MTU Aero Engines GmbH). Radial compressor. (*Source*: Image reproduced with the permission of FIMA Maschinenbau GmbH.)

Another important parameter is the required mass flow variation range, which is principally driven by the specific application of the cycle, and can be achieved by varying the mechanical shaft speed or through the use of variable vanes. The mechanical shaft speed is strongly linked to the required drive for the compressor, and is clearly predefined for a single-shaft gas turbine: for example, if the gas turbine is on the same shaft as the generator, the grid will determine the shaft speed. The use of variable vanes is only suitable in some circumstances, since they require additional hardware, thereby incurring increased cost and complexity, and can affect the peak efficiency.

Some typical applications and their requirements are shown in Fig. 4.2.

4.2.2 Typical stationary gas turbine compressor systems

The varying levels of complexity of the compressor in a gas turbine cycle can be categorised as follows:

- Single-shaft application.
- Multi-shaft application.
- Intercooling application.
- High/inlet fogging application.

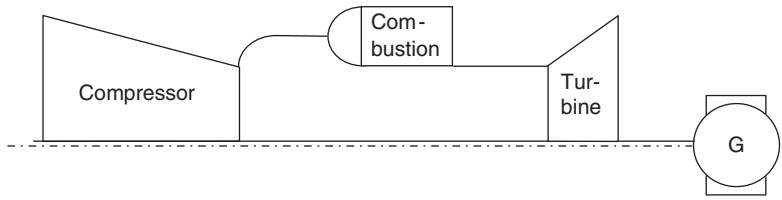
These different applications, which are each suitable for different plants and projects, depending on their specific requirements, are discussed in detail in the following subsections.

Single-shaft application

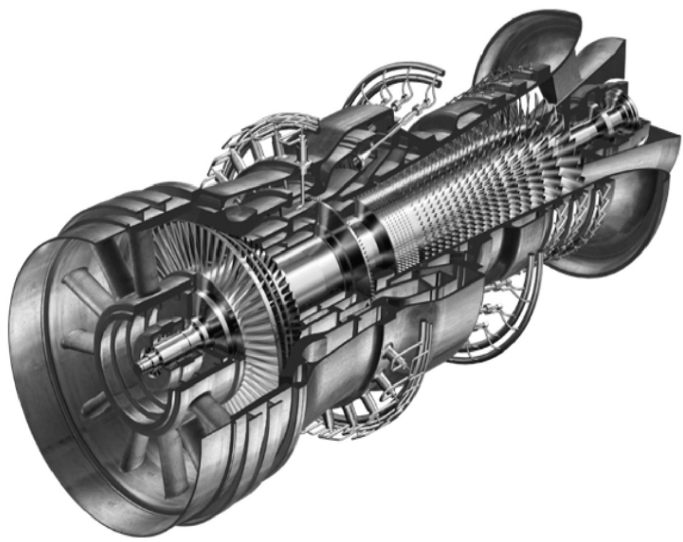
The simplest configuration is the single-shaft application with a single compressor and a single turbine on one shaft, which can also be directly linked to the generator. A diagram of the concept is presented in Fig. 4.3, and a practical real application in Fig. 4.4.

Multi-shaft application

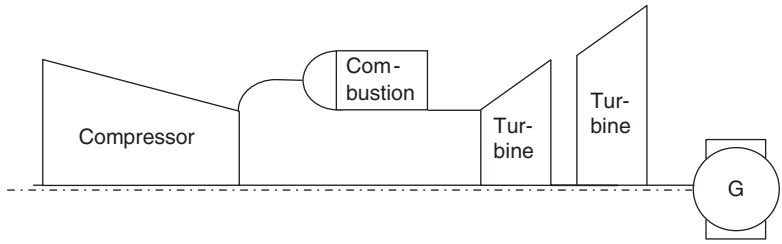
The multi-shaft application is more complex, with a configuration of a compressor and a driving turbine along with an additional power turbine, which can be directly linked to the generator. A diagram of the concept is shown in Fig. 4.5, and a practical real application is shown in Fig. 4.6.



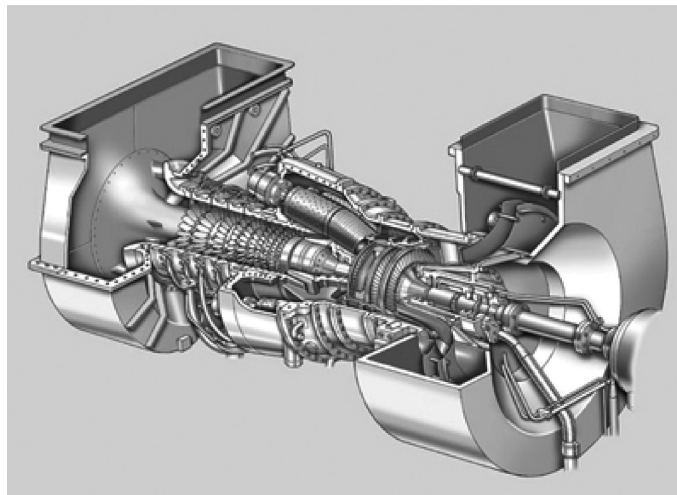
4.3 Process chart of a typical single-shaft application.



4.4 Actual demonstration of a typical single-shaft application.



4.5 Process chart of a typical multi-shaft application.



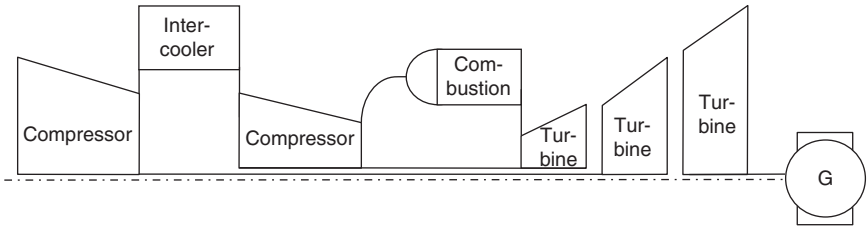
4.6 Actual demonstration of a typical multi-shaft application. Image reproduced with the permission of Siemens AG.

Intercooling application

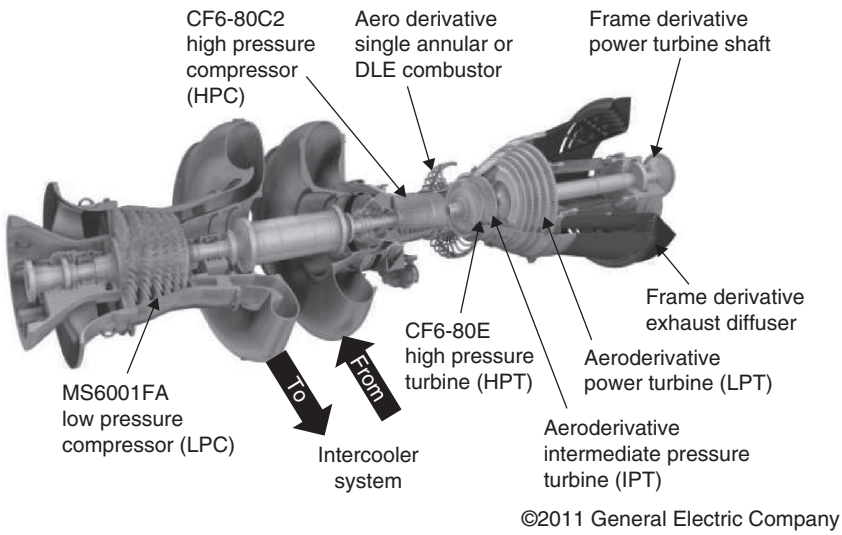
In the intercooling application, a cooler is used inside the low pressure and the high pressure compressors. A typical example of this application is a two-shaft engine, where the cooler is placed between the low pressure and the high pressure compressor. The cooling device is quite large, and the cooling process can cause additional pressure losses; however, it significantly improves the efficiency of the compressor. A diagram of the concept is shown in Fig. 4.7, and a practical real application is shown in Fig. 4.8.

Inlet or high fogging application

There are two basic methods for using water injection to boost power in the compressor. The first is the inlet fogging system, in which water is sprayed into the intake system as far upstream as possible. The amount of water is

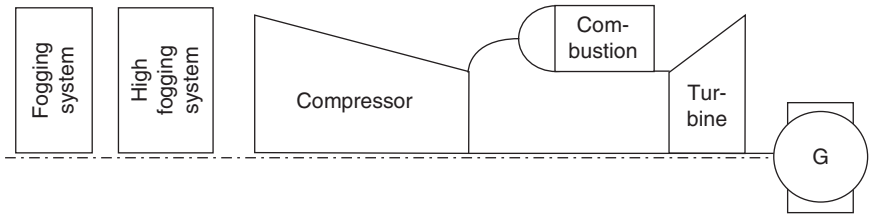


4.7 Process chart of a typical inter cooling multi-shaft application.

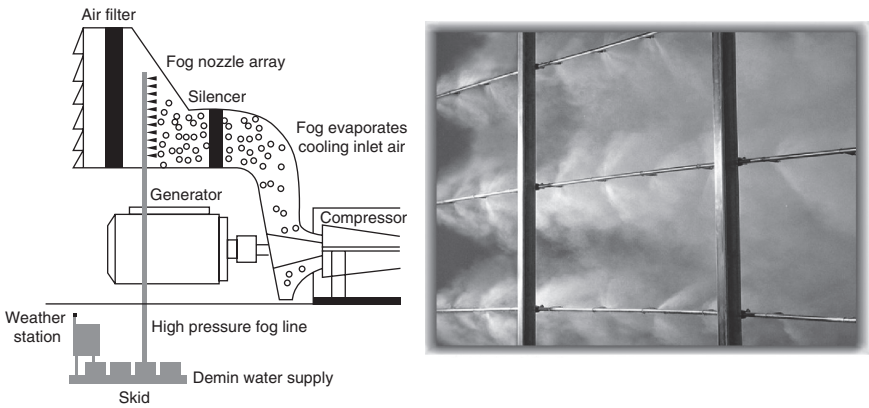


4.8 Actual demonstration of a typical intercooling multi-shaft application. (*Source*: Image reproduced with the permission of GE Energy.)

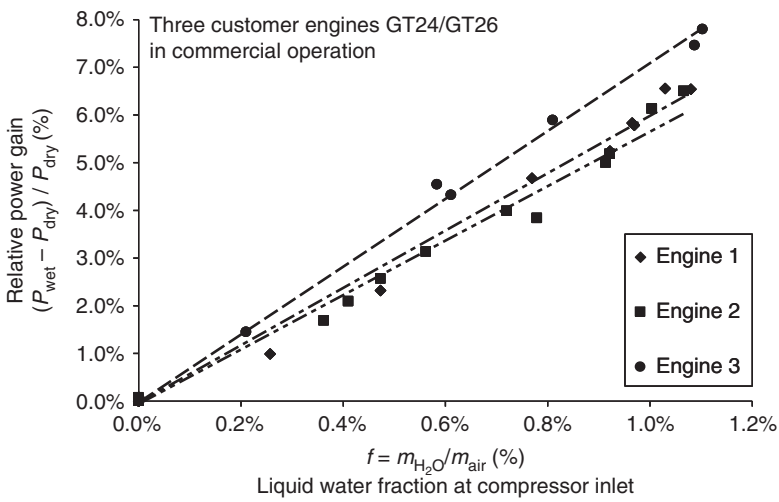
calculated to be aligned with the ambient conditions, so that all the injected water evaporates before entering the compressor blading. Depending on the ambient conditions, this method can only be used in a limited number of cases. The second system is known as the high fogging system, in which water is injected by fine nozzles, and evaporation takes place inside the compressor blading. A major disadvantage of this method is that it significantly reduces the working life of the blading. A diagram of the concept is shown in Fig. 4.9, and a practical real application is shown in Fig. 4.10. Figure 4.11 demonstrates the potential power gain that can be achieved using the inlet/high fogging method. It is important to note, however, that the water must be sprayed in the form of very fine high quality droplets, and is therefore not suitable for all sites, such as those in desert regions where the ambient temperature is high but water is scarce.



4.9 Process chart of a typical inlet and high fogging application.



4.10 Actual demonstration of a typical inlet and high fogging application.



4.11 Gas turbine power gain by application of a fogging rsp. high fogging system.

4.2.3 Typical stationary gas turbine compressor data

This section aims to provide an approximate idea of the typical compressor data that are available, using actual gas turbine data acquired from commercial suppliers relating to 50 and 60 Hz applications sitting directly on the generator shaft. In principle, data scaling with the factor 1.2 can be carried out between the 50 and 60 Hz engines, and it can be demonstrated that the mechanical integrity and aerodynamic values remain constant. The data are therefore recalculated to 50 Hz size, which increases the mass flow by a factor of 1.44 (1.2^2) and the pressure ratios remain the same. The following method is used to calculate the required compressor power:

- Assume ISO inlet conditions
  $p_{amb} = 1.0133$ (bar)
  $T_{amb} = 15$ (°C).
- Assume the compressor inlet mass flow is 97% of the exhaust mass flow.
- Assume a polytropic compressor efficiency of 90.5%, an averaged specific heat of 1020 (J/kg/K) and a gas constant of 288 (J/kg/K).
- Calculate the exit temperature with the polytropic equation
- $$\frac{T_{t,out}}{T_{t,inl}} = \left[\frac{p_{t,out}}{p_{t,inl}}\right]^{\frac{R}{c_p \cdot \eta_{pol}}}$$
- Calculate the power by p = Mass × Specific Heat × Temperature Rise.

All data shown in Table 4.1 are approximate figures, simply to indicate orders of magnitude, and are not suitable for use in detailed competitive analyses

4.3 Stationary gas turbine compressor elements

If all components before the combustion system are defined as part of the compressor, then the major hardware components of the compressor are as follows (also shown in Fig. 4.12):

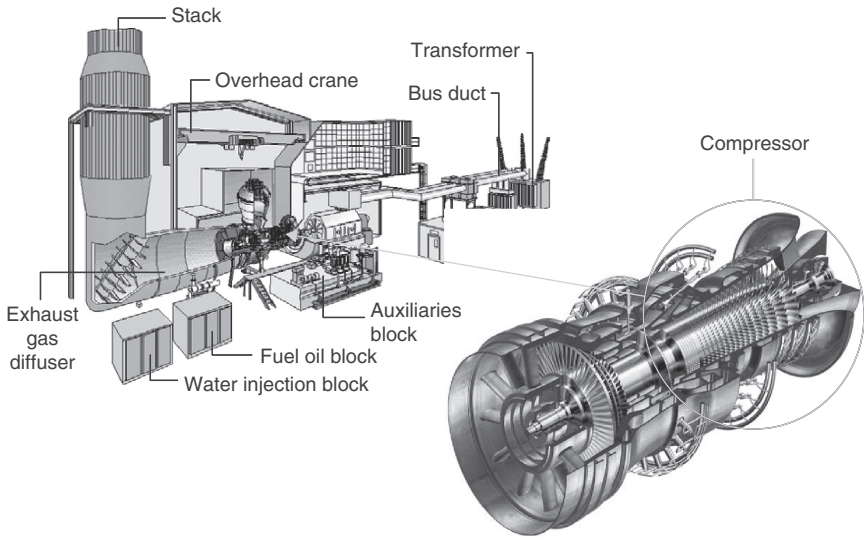
- Filter and intake housing, including fogging and high fogging applications.
- Silencers.
- Intake duct.
- Compressor blading.
- Compressor diffuser.
- Rotor including front bearing.
- Casing structure.
- Extraction channels and blow-off systems.

Published by Woodhead Publishing Limited, 2013

Table 4.1 Some stationary gas turbine compressor data

Supplier name	Gas turbine name	ISO base rating (MW)	Shaft speed (Hz)	Inlet mass flow (kg/s)	Temperature rise (K)	Press. ratio	Equivalent 50 Hz Mass flow (kg/s)	Required 50 Hz comp. power (MW)
Alstom	GT13E2	182.2	50	537	408	16.9	537	223.4
Alstom	GT26	292.8	50	612	579	34.2	612	361.5
GE Energy Heavy Duty	9E	126.1	50	397	347	12.6	397	140.6
GE Energy Heavy Duty	9FB	284.2	50	622	422	18.0	622	267.7
Hitachi	PG9171(E)	125.4	50	397	347	12.6	397	140.5
Hitachi	PG9351(FA)	255.6	50	630	409	17.0	630	263.0
Mitsubishi Heavy Industry	M701DA	144.1	50	419	368	14.0	419	157.3
Mitsubishi Heavy Industry	M701G2	334.0	50	700	457	21.0	700	326.3
Siemens Energy	SGT5–4000F	292.0	50	658	424	18.2	658	284.6
Siemens Energy	SGT5–8000H	375.0	50	779	436	19.2	779	346.7
Siemens Energy	SGT6–8000H/W501F	208.0	60	483	414	17.4	695	293.7

Source: Basic data are taken from Gas Turbine World, 2010 GTW Handbook.



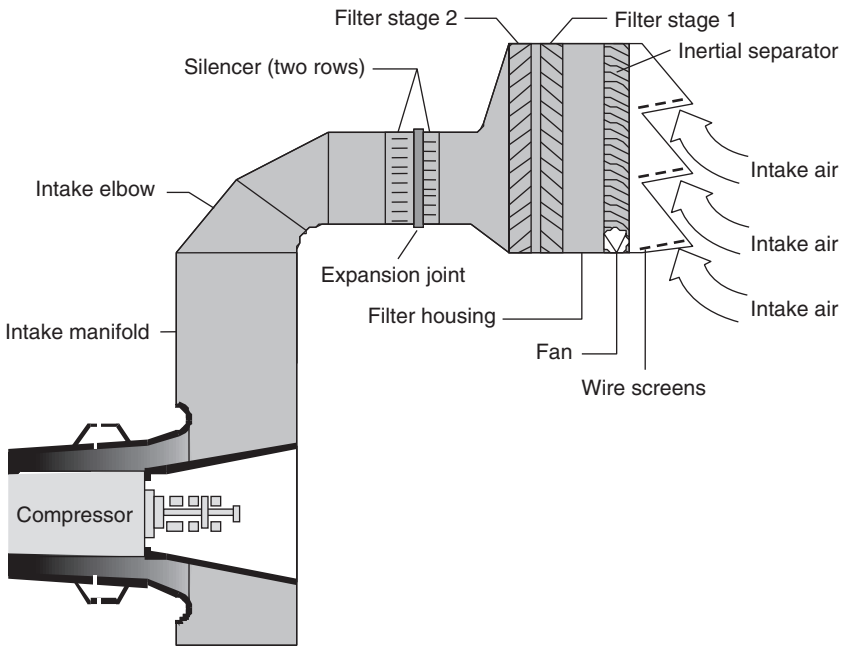
4.12 Overall inlet and compressor components of a gas turbine.

The role of the flow path systems before the compressor blading is to keep the flow medium clean and to control and guide it to the face of the compressor blading with a uniform velocity profile. Keeping the flow medium clean requires filter systems that are able to function in a variety of ambient conditions: for example, the filters must work in both very dusty and very humid environments without clogging, which could cause a significant drop in pressure. Despite the uniform flow conditions, this pressure drop is the most critical part of the system, because any pressure lost in the intake system must be rebuilt by the compressor blading, requiring a significant amount of energy and reducing the overall efficiency of the gas turbine.

The intake system itself is usually developed on a site-specific basis, due to constraints imposed by the local area. However, it is always important to ensure that the filter housing is built up to a certain height, in order to avoid high concentrations of dust from the ground, and to ensure a homogeneous flow over the whole filter face. Noise level is becoming an increasingly important consideration, with ever stricter requirements, particularly if the plant is located inside an industrial environment or close to towns. Figure 4.13 shows the high level of complexity of a typical intake system.

Another feature that must be taken into consideration is the bearing system of the gas turbine rotor shaft. At the front part of the compressor, these bearings have to be able to handle axial thrusts of up to 150 tons in large gas turbines, and therefore have specific requirements. The bearings usually run in an oil bed, and sealing air is supplied principally from the first bleed of

Published by Woodhead Publishing Limited, 2013



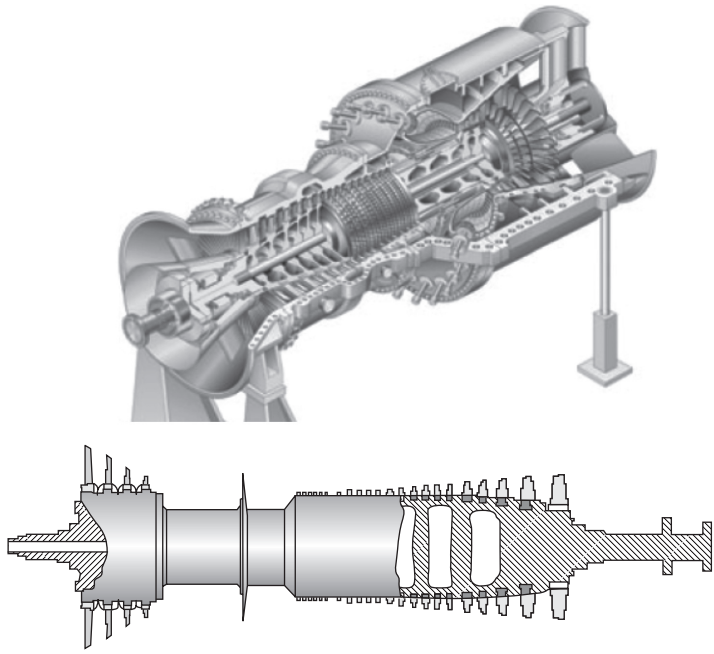
4.13 Intake system example for a stationary gas turbine.

the compressor in order to prevent oil from entering the compressor, which could cause major degradation of the compressor blading and, in the worst case, even fire.

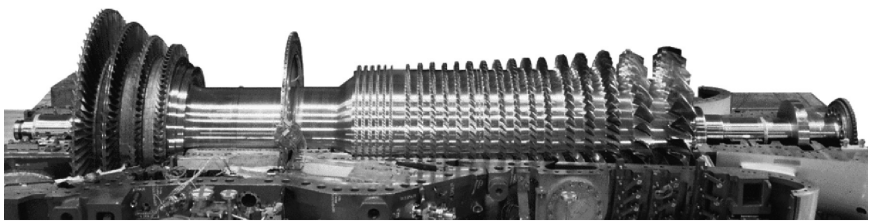
In order to start the engine, energy is required to turn the shaft and bring it up to speed before the gas turbine accelerates. This can be achieved by two different methods: the first uses the existing generator in an inverse mode by taking energy from the grid, while the second uses an additional motor. This second option is often employed as a back-up solution to ensure start-up capability if the whole grid collapses. The required power for huge stationary gas turbines can easily reach a few MW, and must be taken into account in any cost assessments: 1 MW of additional start-up power costs roughly €0.5 million.

The inner flow channel of the blading is determined by the rotor contour. Once again, there are two completely different approaches that can be adopted here (see Fig. 4.14): the first is known as the solid rotor, in which huge blocks are welded together to achieve a very stiff heavy construction; the second approach uses the bolted rotor, whereby different discs are generated and later bolted together into one unit. Both variants have advantages and disadvantages in terms of, for example, transient behaviour, cost, complexity of assembly, and blading time. Operationally, the main functional

Published by Woodhead Publishing Limited, 2013



4.14 Example of a single-shaft bolted and a solid gas turbine rotor. Image reproduced with the permission of Siemens AG.



4.15 Example of a solid compressor rotor and a compressor casing structure.

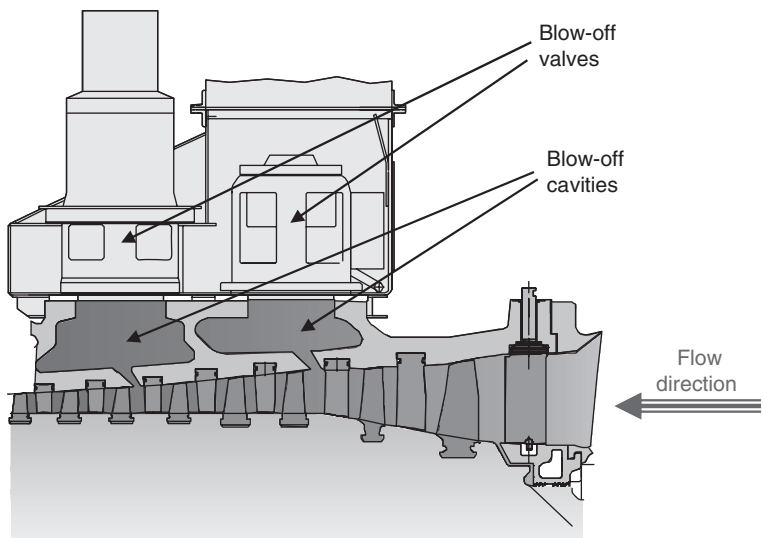
difference is in their thermal transient behaviour, which in turn requires the implementation of different methods to control the clearances, mainly in the rear part of the engine.

The outer flow channel is determined by the casing structure. For small engines and aircraft engines, a round welded structure is often used, while for larger engines fairly solid structures of casing material are usually employed, as shown in Fig. 4.15. The use of casing structures offers improved stiffness and economic benefits; however, their weight is a disadvantage, and they struggle to keep the roundness controlled. Some casing structures even employed

Published by Woodhead Publishing Limited, 2013

virtual flanges at 6 and 12 o'clock to balance the thermal impact on roundness, but due to the heavy weight involved in this method, it has not been continued. Anything that affects roundness has a huge impact on the possible clearances that can be achieved inside the compressor blading, and also therefore a significant impact on the efficiency and surge margin of the compressor.

Additional elements to be considered inside the casing structure are the extraction flows, normally used for the purposes of cooling the combustion system and turbine parts, and the linked blow-off channels and valves, which are required to control the flow inside the blading during the transient start-up and shutdown phases. The main challenge involved with these elements is to ensure sufficient extraction mass flow while keeping costs as low as possible. Blow-off valves can easily cost up to € 50 000–80 000, with the stainless steel piping required incurring additional costs. Moreover, as with the intake system, noise emissions have to be controlled. The extraction flow is quite often directed to the exhaust stack, which again requires a long and expensive section of stainless steel piping. A flow collecting cavity is built around the whole circumference of the engine at a certain axial position in order to uniformly extract the flow. This ensures that the blading does not undergo circumferential distortion in respect to the aerodynamic flow conditions. From these cavities, one or two extractions are usually carried out, either via piping, including a valve to the exhaust, or via a blow-off system consisting of a valve and a silencer connected to the external environment (see Fig. 4.16). Multiple axial extractions are usually used to ensure safe and reliable start-up and shutdown of the engine with minimum power.

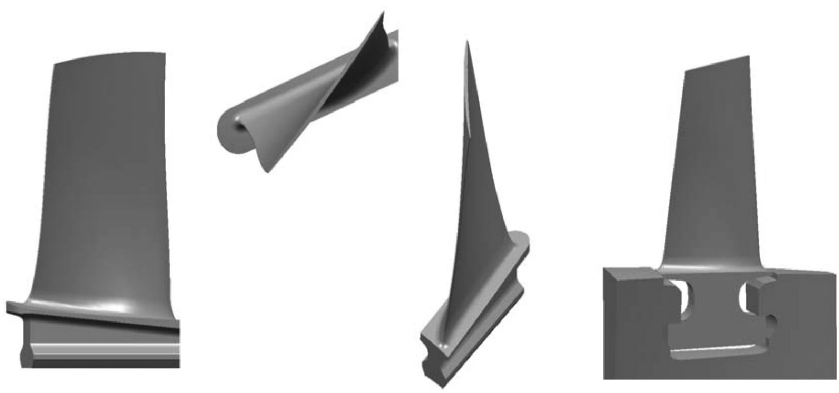


4.16 Example of a typical blow-off system application.

Located inside the outer casing structure are the mechanisms that turn the variable vanes of the compressor blading. A variety of engine types exist in which at least the first vane row, known as inlet guide vane, is turnable and should be considered as a kind of pre-swirler for the flow. It is used to control the inlet mass flow, but additionally helps to increase the stability and part load efficiency of the compressor. New engine types use up to five additional variable vane rows, in order to widen the working range and further increase stability and part load efficiency.

Relatively high velocities are present inside the compressor blading, for example axial velocities of up to 200 m/s, to ensure that the compressor blading operates efficiently, whereas in the combustion system quite small velocities in the order of 15–25 m/s are required. An efficient compressor diffuser must therefore be placed in between the compressor blading and the combustion system: its role is to convert kinetic energy into a static pressure rise with minimal losses of energy and total pressure. All pressure losses generated inside the flow systems must be recovered by the compressor blading, causing a higher overall pressure ratio to required, thereby reducing the overall effectiveness of the gas turbine. The compressor diffuser is therefore evidently a crucial element in a gas turbine.

The last element to be considered is the compressor blading (Fig. 4.17). In very large stationary gas turbines there are usually 15–20 stages, each consisting of a rotating blade with its fixation on the rotor and a non-rotating vane with its fixation inside the casing structure. In aero-derivative engines with multiple shafts, a maximum of eight stages are usually placed on one spool. Different methods can be used to fix the blades in their corresponding grooves. For the disc rotors, axial roots are very often used; these fit directly into a corresponding slot inside the rotor via an axial assembling procedure. The casing sides or solid rotors usually have circumferential grooves; blades



4.17 Example of different compressor blading views/types.

Published by Woodhead Publishing Limited, 2013

with a specific socket are slid into the corresponding grooves in the split plane. The blading is made mainly from stainless steel, but special titanium blades may be used for large front stages. Temperatures are higher in the rear part of the blading, so steel mixtures containing nickel are frequently used.

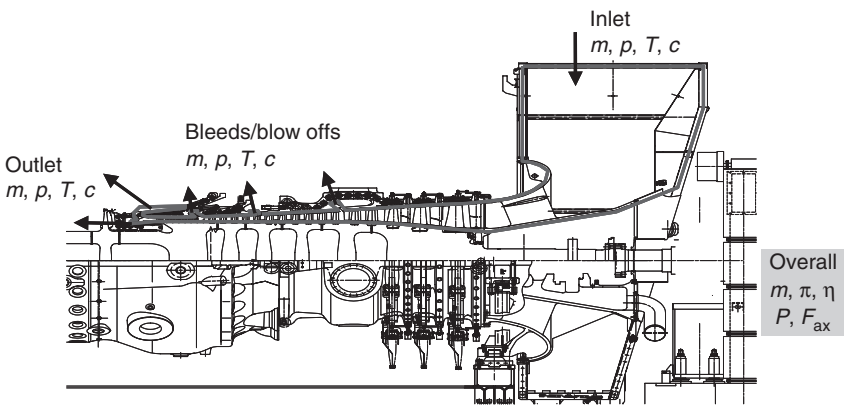
4.4 Compressor characteristic parameters

The main aims of this section are firstly to introduce the reader to some key considerations regarding the compressor blading and its behaviour, and secondly to provide more detailed information for assessing and designing individual blade rows.

4.4.1 General considerations

A variety of aspects of typical parameters relevant to compressors must be taken into account. Taking the thermodynamic parameters as a starting point, and focusing on controlling the volume around the compressor as a whole, the following parameters are key (see also Fig. 4.18).

- Inlet conditions.
  mass/volume flow, pressure, temperature, humidity.
- Extraction/injection conditions.
  mass/volume flow, pressure, temperature.
- Outlet conditions.
  mass/volume flow, pressure, temperature.
- Rotational shaft speed.



4.18 Thermodynamic interfaces of the compressor.

- Shaft power.
- Shaft thrust.

The inlet conditions are determined by the ambient conditions, through the use of the variable vanes discussed above, which are used to regulate the inlet mass flow, and by adapting the pre-swirl of the first blade rows. The compressor exit conditions are principally determined by the turbine, but can also be influenced by the firing conditions (fuel composition, firing temperature, NO_x water injection, etc.), whereas extractions inside the compressor channel usually have little effect.

The overall operational behaviour of the compressor blading under different operating conditions is usually described using a compressor map. This reflection of the component behaviour inside the map is carried out in such a way that the speedlines (lines showing constant mechanical speed but with varying exit pressure) can be drawn up. These speedlines are calculated and drawn for different mechanical speeds and different inlet guide vane positions. The maximum achievable pressure ratio inside the compressor for a certain speedline is defined by the surge pressure ratio.

Although the compressor blading behaviour is dependent on the firing temperature, the fuel composition and the turbine characteristics, it is also strongly influenced by the inlet conditions. The compressor map is therefore usually produced on the basis of similarity parameters, often normalised for the reference conditions (e.g., the design point value), and defined as follows:

Aerodynamic/reduced speed

$$n_{red} = \frac{n_{mech}}{\sqrt{RT_{t,inl}}}$$

Normalised aerodynamic/reduced speed (gas constant reflects humidity)

$$n^* = \frac{n_{mech}}{n_{mech,ref}} \sqrt{\frac{R_{ref}\ T_{t,inl,ref}}{RT_{t,inl}}} \qquad [4.1a]$$

Blading pressure ratio

$$\pi = \frac{p_{t,out}}{p_{t,inl}}$$

Normalised blading pressure ratio

$$\pi^* = \frac{\pi}{\pi_{ref}} \qquad [4.1b]$$

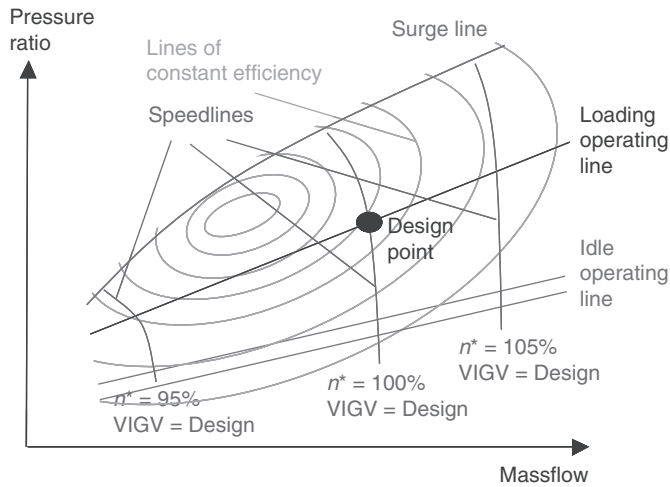
Reduced inlet mass flow

$$m_{red} = m_{inl} \cdot \frac{\sqrt{R \cdot T_{t,inl}}}{p_{t,inl} \cdot A_{inl}}$$

Normalised reduced inlet mass flow (gas constant reflects humidity)

$$m^* = \frac{m_{inl}}{m_{inl,ref}} \cdot \frac{p_{t,inl,ref}}{p_{t,inl}} \cdot \sqrt{\frac{R \cdot T_{t,inl}}{R_{ref} \cdot T_{t,inl,ref}}} \qquad [4.1c]$$

Published by Woodhead Publishing Limited, 2013



4.19 Typical compressor map for a stationary gas turbine (const. VGV angle).

Polytropic blading efficiency

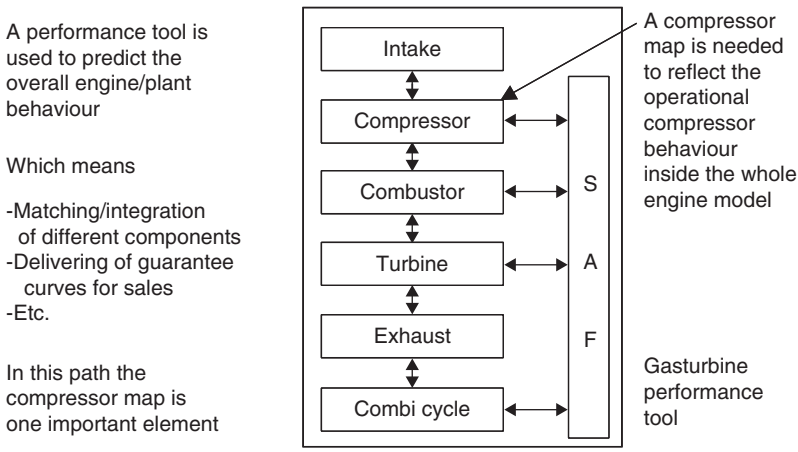
$$\eta_{pol} \approx \frac{R}{c_p} \cdot \frac{\ln\left(p_{t,out} / p_{t,inl}\right)}{\ln\left(T_{t,out} / T_{t,inl}\right)}$$

Normalised polytropic blading efficiency

$$\eta^* = \frac{\eta_{pol}}{\eta_{pol,ref}} \qquad [4.1d]$$

A typical compressor map, reflecting the normalised reduced values given above, is shown in Fig. 4.19 (VIGV defines the position of the variable inlet guide vane).

This map shows 'aerodynamic speedlines'; as mentioned previously, these reflect a relationship between the mechanical shaft speed, ambient temperature and humidity. A compressor can run along a speedline, depending on the pressure ratio set by the combustion system/turbine, with the upper limit determined by the surge pressure ratio, where a reverse flow occurs and the engine is at risk of major damage. Lining up the surge pressure ratios for different aerodynamic speeds produces a 'Surge Line'. Lines of constant efficiency curves are shown on the map, and these vary according to the required design. Maximum efficiency is quite often observed away from the design point as a result of ensuring a sufficient operating range for the compressor. Two additional operating lines are shown, with the lower 'Idle Operating Line' reflecting an operation with no power output to the grid (self-sustaining gas turbine only) and the upper 'Loading Operating



4.20 Overall thermodynamic simulation of a gas turbine by a cycle performance tool.

Line' showing a running engine at fixed combustion conditions but varying mechanical shaft speeds.

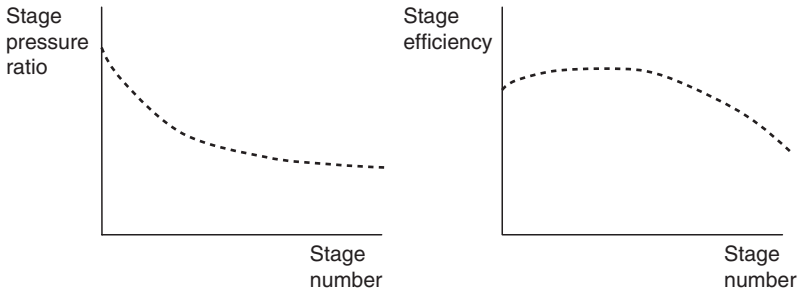
This kind of compressor map is used as part of the overall performance simulation of a gas turbine and is therefore one of the most critical thermodynamic elements with respect to thermal integration. To achieve this performance simulation, cycle performance tools have been developed, in which every major component of a gas turbine is characterised to varying degrees of detail. Figure 4.20 shows the concept of the overall gas turbine simulation.

4.4.2 Compressor blading considerations

The compressor blading must be able to handle certain tasks. Starting with the front part, an 'inlet guide vane' might be used to determine a certain preswirl (tangential velocity), which reduces the inlet velocity to the next blade row. The same vane can also be used for mass flow variation, when this is variable. The compressor stages are the next important element: these consist of one rotating and one non-rotating blade row, known as 'blades' and 'vanes', which build up the pressure ratio and the swirl for the following stage. Finally 'outlet guide vanes' may be added to ensure that all remaining swirl is converted to a static pressure rise before entering the compressor diffuser.

Aerodynamics of compressor stages

As mentioned above, the compressor stages are key in understanding the aerodynamics of the compressor; these are characterised by the stage



4.21 Main thermodynamic stage parameter of a compressor.

pressure ratio and the stage efficiency. Figure 4.21 shows a typical example of the compressor stages. The front stages can handle quite high pressure ratios with reasonable efficiencies by supporting the required operating range. The rear stages experience wide variation in their inlet conditions (pressure, temperature, velocity and swirl) during part load operation and therefore cannot be as heavily loaded as the front stages. A smooth distribution of the pressure ratio is essential to ensure that the stages are operating with reasonable efficiency at part load, and that there is no single stage/row that causes unstable operation. Due to the high thermal impact of the rotor and the structure, the rear stages often suffer in efficiency terms due to the relatively high clearances required. The pressure ratio distribution also has to take into account the pressure requirements for bleed positions, which are often used for sealing air and to cool thermally overloaded parts inside the combustion system and the turbine during operation.

Other integral stage factors which can be used to analyse the complete set of stages for an engine during different operating conditions are the flow factor and the work factor.

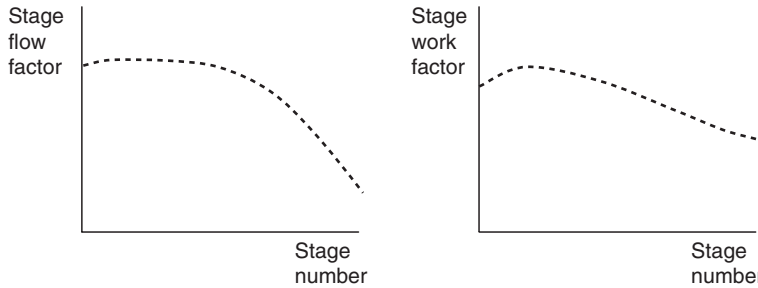
The flow factor describes the ratio of the axial velocity with respect to the whirl velocity (tangential velocity of the shaft at a certain radius)

$$\varphi = \frac{c_{ax}}{u} \qquad [4.2a]$$

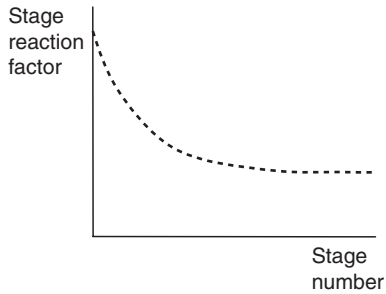
and the work factor describes the enthalpy (thermal energy) rise as a function of the kinetic energy of the whirl velocity, which for axial compressors without significant radial shift of the flow can be interpreted as the ratio of the tangential velocity change over the rotating compressor blade with respect to the whirl velocity

$$\psi = \frac{\Delta h_{ta}}{u^2} \approx \frac{\Delta c_u}{u} \qquad [4.2b]$$

Published by Woodhead Publishing Limited, 2013



4.22 Main aerodynamic stage parameter of a compressor.



4.23 Thermodynamic blade/vane loading balance parameter of a compressor.

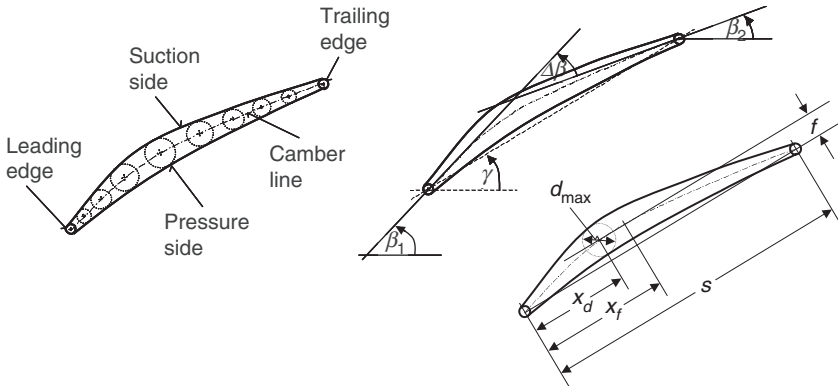
Some typical curves for these parameters are shown in Fig. 4.22.

Another important aerodynamic stage factor is the reaction number. This factor describes the relationship of the static enthalpy rise in between the rotating blades compared to the stage as a whole and is defined as

$$\Re = \frac{\Delta h_{\text{blade}}}{\Delta h_{\text{stage}}} \qquad [4.2c]$$

The selected reaction is strongly dependent on the possible pressure rise of the individual stages. For the front stages with high inlet Mach numbers for the blades (and lower Mach numbers for the vanes), quite high figures (0.8–0.9) are usually used. Moving inside the compressor stages, these numbers decrease rapidly and can fall to around 0.5 in the rear stages for similar stagger angles between blades and vanes, which indicates a similar static pressure rise between the blades and vanes and ensures stable operation at part load conditions. A typical example is shown in Fig. 4.23.

Published by Woodhead Publishing Limited, 2013



4.24 Geometrical blading parameter along flow sections.

Geometry of compressor blading

Next, the details of the individual blading must be considered. Although channel height and clearances are important, the geometry of the blading is primarily determined by the blading parameter along a flow section, for example, chord length, maximum thickness etc. as shown in Fig. 4.24.

The principle geometric parameters are:

- Chord length s.
- Maximum profile thickness d_{max}.
- Point of maximum profile thickness $x_{d.}$
- Maximum camber line deviation f.
- Point of maximum camber line deviation x_f.
- Metal inlet angle β_1.
- Metal outlet angle β_2.
- Metal turning angle $\Delta\beta$.
- Metal stagger angle γ.
- Leading and trailing edge thicknesses.

Classes of compressor airfoils have previously been developed based on the above parameters. Representative models to predict connected exit flow angles and total pressure losses have been made available and are still widely in use.

Aerodynamics of compressor blading

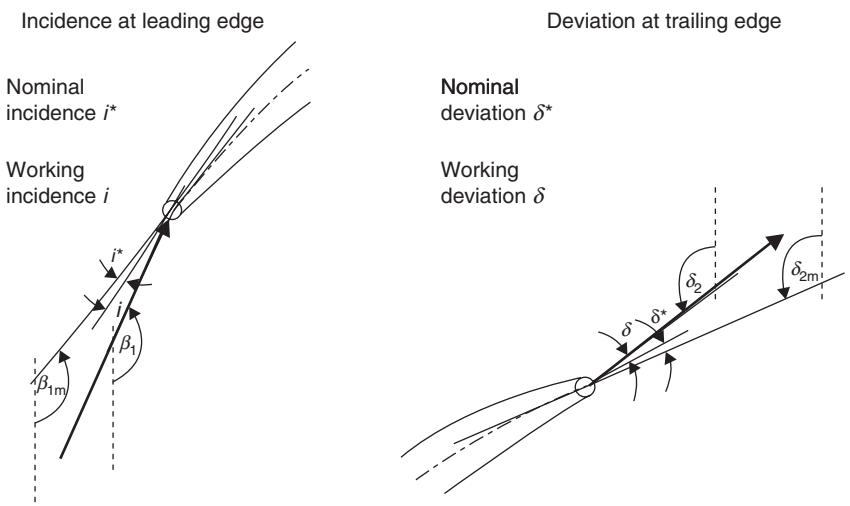
The main aerodynamic parameters that determine a blading profile section are:

- Inlet Mach number.
- Flow turning.
- De Haller number.

The inlet Mach number gives a clear indication of the expected aerodynamic shock, which on the one hand strongly supports a high pressure rise but, on the other, is connected with increased total pressure losses and possible aerodynamic separation. The Mach number is therefore usually kept below 1.3 for stationary gas turbines. Due to operational requirements, these high Mach numbers can only be applied for the front stages of the rotating blading; for later stages, they rapidly decrease, down to values of 0.4–0.5 at the compressor blading exit.

The interaction of the blading geometry with the aerodynamic flow is also important from an aerodynamic perspective, particularly the flow angles for the leading and the trailing edges of the blading. The blading has a certain inlet flow angle, which is linked with a minimum loss. This angle is defined as the nominal inlet flow angle and usually differs from the metal inlet angle due to a lifting effect caused by the blade turning. Deviations to this nominal inlet flow angle are called 'incidence angles' and are widely used to describe the working range of the blading. The second flow angle of interest is the exit flow angle, where the difference between the blading metal exit angle and the exit flow angle is defined as the 'deviation angle'. Figure 4.25 provides a detailed graphical representation as well as showing the exit flow angle for minimum losses (nominal deviation) and the actual exit flow angles.

A further important parameter is the total pressure loss coefficient. This describes the total pressure loss over a blade row as a fraction of the inlet dynamic head, and therefore also indirectly describes the blading efficiency. Due to its application in rotating and non-rotating systems, the coefficient has to take into consideration possible work by radial shift, and can be generally specified as



4.25 Angle definitions for compressor blading.

Published by Woodhead Publishing Limited, 2013

Total pressure loss coefficient for compressor blading

$$\omega = \frac{p_{tr,2,is} - p_{tr,2}}{p_{tr,1} - p_1} \qquad [4.2d]$$

where 'is' stands for an isentropic reference process.

The de Haller number is crucial in understanding the aerodynamic loading of a profile section, which is defined as the ratio of the exit velocity to the inlet velocity. As a rough guide, it can be stated that profile sections with de Haller numbers below 0.7 usually tend towards flow separation.

$$H_{No} = \frac{w_2}{w_1} \qquad [4.2e]$$

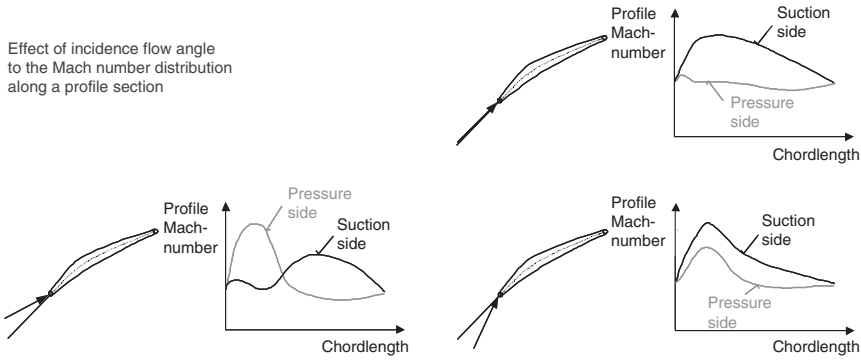
A more precise parameter to estimate the aerodynamic loading along a profile section is the diffusion number, which can be seen as an extension of the de Haller number which also takes into account the blading geometry. It defines the ratio of the maximum deceleration along the suction side as a fraction of the inlet velocity. This approach to estimating the maximum suction side velocity as a fraction of the actual aerodynamic inlet and outlet conditions and the solidity (= chord/pitch) is based on an initial theory. The diffusion number should be considered as a parameter that indicates the boundary layer level/stability of the flow field. A typical limit used for this factor is in the order of 0.4–0.45 for stationary gas turbine compressors. One typical formulation is

$$\frac{w_{\max}}{w_1} = 1 + \frac{r_1 \cdot w_{u,1} - r_2 \cdot w_{u,2}}{2 \cdot \sigma \cdot \frac{r_1 + r_2}{2} \cdot w_1} \quad \text{Max. suction side velocity} \qquad [4.2f]$$

$$D = \frac{w_{\max}}{w_1} - \frac{w_2}{w_1} \quad \text{Diffusion number} \qquad [4.2g]$$

Looking at this in more detail, it is necessary to consider the aerodynamic flow structure around a profile itself. Modern blades are aerodynamically optimised for every individual section and 'controlled diffusion airfoils' (CDA) have been developed as a standard. This kind of blading individually controls the development of the aerodynamic boundary layer along the profile and can be used to optimise the individual sections according to given requirements, such as those connected to the required working range. A typical Mach number distribution and the development of the respective boundary layer parameter along a profile are shown in Plate I (see colour section between pages 346 and 347).

Published by Woodhead Publishing Limited, 2013



4.26 Mach number distributions along a profile section for different inlet flow angles.

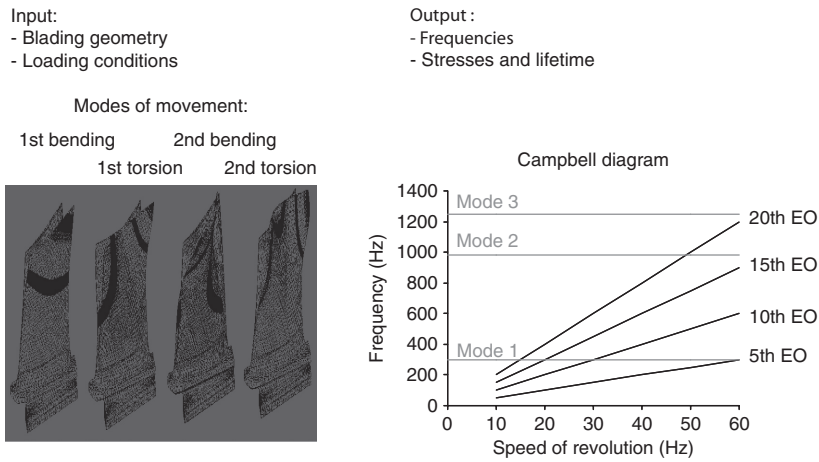
Finally, a full three-dimensional (3D)-aerodynamic assessment is executed in order to observe the three-dimensional flow structures and to understand in detail the interaction of the different blade rows, as also shown in Plate I.

Despite the design point analyses, a significant amount of work is required to assess the 'off-design' conditions, which reflect the compressor during start-up and part load behaviour. As discussed previously, the effects of mechanical shaft speed and ambient temperature variation must also be considered in this respect; the compressor blading is therefore subject to a wide range of operational requirements. Figure 4.26 shows the impact of different inlet conditions on the Mach number distribution along the pressure side and suction side of a typical compressor blade section.

A whole range of aerodynamic tools is used to assess these operating points. Wherever possible, high end 3D-CFD tools are used, as these generally deliver the best results. Nevertheless, in strong part load conditions, for instance during start-up, these tools can experience convergence problems, mainly triggered by local flow phenomena interacting with the core flow (e.g., a corner stall/separation). In these cases more robust, but strongly simplified one-dimensional (1D)- and two-dimensional (2D)-tools are used; the disadvantage of these tools is that they work with empirical correlations, which then need to be modified to meet the requirements of the specific application.

Mechanical integrity of compressor blading

In order to develop a safe and reliable product, Mechanical Integrity Assessment of the blading is of crucial importance. The basic critical items to be considered are frequencies and stresses. The forces acting on the blading are the centrifugal force and the aerodynamic force introduced by turning the flow. As the incoming flow to the individual rows is non-continuous, dynamic change in the blading forces must also be taken into account. The



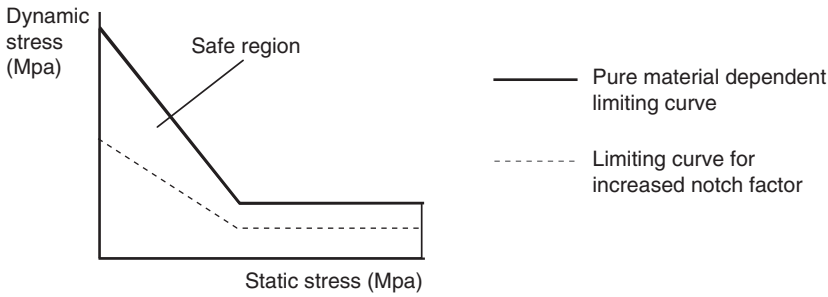
4.27 Mechanical Integrity Assessment examples.

basic principle of the Mechanical Integrity Assessment can be described as shown in Fig. 4.27. As a first step the static stresses are assumed to work at a reasonable level. The frequencies are also tuned by modifying the blade shape without any substantial impact on the aerodynamic requirements. In this context, resonances with multiples of the engine order and with possible excitation frequencies upstream and downstream have to be considered. In addition, careful simulation of the clamping conditions is required, as these can have a significant impact.

The first 2–4 modes are usually basic eigen frequencies, namely:

- first bending mode;
- first torsion mode;
- second bending mode;
- second torsion mode.

Based on the individual blading design with regard to mass and stiffness distribution, mixed modes can already be observed at the third eigen frequency or later. Higher modes, known as 'corner modes', where a tip corner starts to bend, must also be taken into account, because rubbing and/or wake passing frequencies from the up- or down-stream row might generate resonance, which can cause blading damage. Other elements to be considered are the blading root clamping, the frequency range of the engine under standard operation, manufacturing tolerances and to a certain extent even the dynamic behaviour of the rotor disks. Appropriate safety bands must be put in place before releasing a blade row. During the start-up of the engine



4.28 Detailed Mechanical Integrity Assessment including dynamical forces/Haigh diagram.

resonances have to be crossed; it must therefore be ensured that this is carried out in a non-stationary manner to avoid resonance excitation.

As a final step in the analysis of the blading, dynamic stresses driven by wakes from upstream blade rows must be considered, along with possible excitations generated by passing a resonance (dynamic force) in order to understand the conditions required for the safe operation of the engine; this is mainly achieved using the Haigh diagram. Safety measures must be implemented to ensure safe operation even in case of erosion or pitting corrosion, which can become a significant problem over time, as shown in Fig. 4.28. These issues could also be resolved through the use of an erosion coating; these coatings are mainly used for the front part of the compressor.

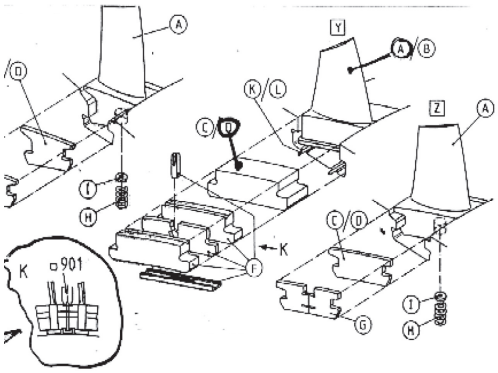
The root sections require particular attention, starting with the positioning of the blade row on the root platform so as to achieve reasonable balance in the hook loading. The hooks must then be checked carefully to avoid overstressed regions. Undercuts are implemented quite frequently inside highly loaded regions of the fir tree roots in order to reduce stress concentrations. All the issues described in this section are part of an interactive and interconnected process involving a number of disciplines, and are hence somewhat challenging.

Mechanical design of compressor blading

In the early stages of a project, the mechanical design element has a supporting role, because those involved in aerodynamic aspects and mechanical integrity issues require significant support in the shape of blading models for use in assessments. Some challenges that arise at this stage are the smoothness of the blading surface in all directions and the intersection between the blading profile and the root platform, where special transition radii distributions might be required to smoothly transfer the stresses caused by the profile into the root sections. On the one hand, the root should be as wide as

Published by Woodhead Publishing Limited, 2013

Example : Row complete
Circumferential root fixation



	X	Y								Z	
	①	②	③	④	⑤	⑥	⑦	⑧	⑨	⑩	⑪	⑫
Ⓐ	200	208	216	225	235	244	253	262	271	280	289	297
Ⓑ	–	–	217	226	236	245	254	263	272	281	–	–
Ⓒ	201	209	218	227	237	246	255	264	273	282	290	298
Ⓓ	202	210	219	228	238	247	256	265	274	283	291	299
Ⓔ	203	211	–	–	–	–	–	–	–	–	–	–
Ⓕ	–	–	220	229	239	248	257	266	275	284	–	–
Ⓖ	–	–	–	–	–	–	–	–	–	–	292	300
Ⓗ	204	212	–	–	–	–	–	–	–	–	293	301
Ⓘ	205	213	–	–	–	–	–	–	–	–	294	302
Ⓚ	–	–	221	230	240	249	258	267	276	285	–	–
Ⓛ	–	–	222	231	241	250	259	268	277	286	–	–

4.29 Mechanical design details to support complete compressor blading row.

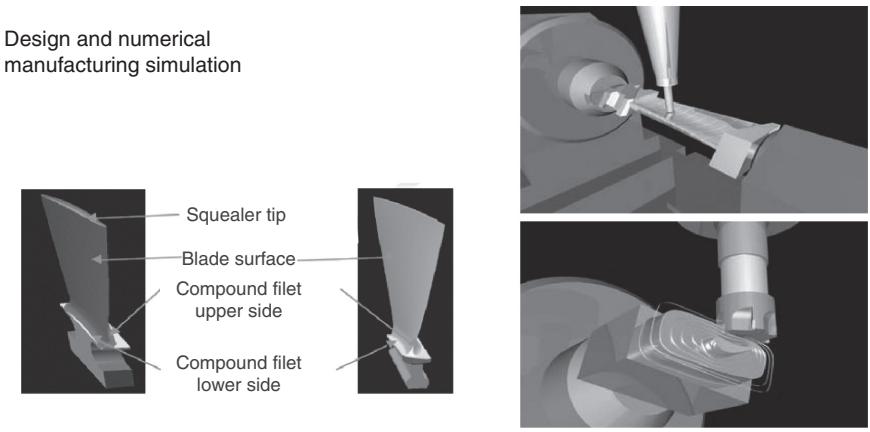
possible to achieve a smooth transition; but on the other, the root should be kept as narrow as possible, as a wider root means more bar material for milling, which makes the blading more expensive. A reasonable compromise between these two requirements must be identified.

Once a satisfactory design has been established, the mechanical design team then has to satisfy all the requirements for manufacture and assembly. In this context, full 3D modelling has been proven to help in significantly reducing errors by, for example, simulating the entire assembly procedure. Figure 4.29 provides an example of the overall complexity of all required blading modelling details.

Manufacturing of compressor blading

For large stationary gas turbine compressors the blading is usually milled from bar material or preforgings. The size of the blading makes electrochemical eroding expensive, and it is thus rarely performed. Using a standard interface between the aero-mechanical and the mechanical design, it is advantageous if the final blading model can be directly linked to the manufacturing process. This is reflected in models known as Computational Added Manufacturing (CAM) models, which combine the model with the manufacturing attributes, such as the required tolerances, by creating a 3D blading shape. For this purpose the blading model has to be split into the different elements that need to be linked with the required attributes. With all this information available, the milling process can be modelled in a virtual environment, which reduces risk and also significantly cuts down the development time on the milling machines. Figure 4.30 illustrates some basic steps in the process.

Published by Woodhead Publishing Limited, 2013



4.30 CAM models for fast and reliable milling processes.

For concurrent engineering purposes, different phases of the development must be clearly defined. Ordering the material for large or preforged blades usually takes several months. If the dimensions of the outer envelopes of the blading can be established within a certain accuracy without the need for aerodynamic and mechanical detailed assessment, the blading material can be ordered instantly, potentially saving up to 6 months of development time.

One final point to note is that casted rows can be used instead of milled blade rows, particularly for small rear stages. Electrochemical erosion from bar material can also be used for these small blades.

4.5 Operational requirements inside a gas turbine

As part of a site-specific gas turbine application, a compressor will handle a number of different challenges, including engine start-up, changes in the ambient conditions, different load commands, fouling and degradation effects and perhaps corrosion and erosion effects on the blading, which is the focus of this section.

4.5.1 Operational behaviour and requirements under load conditions

The compressor map shows that the compressor delivers a specific mass/volume flow depending on the specific aerodynamic speed. The pressure ratio achieved is defined by the combustion process and the turbine, which can be understood as a kind of throttle. The compressor then has to raise the pressure ratio until it fits through the defined throttle of the turbine.

Published by Woodhead Publishing Limited, 2013

Stodola (1982) developed a simple equation that is valid for the major operating range of a given turbine. It only states that the reduced turbine inlet mass flow stays constant, and is principally valid for multistage turbines or highly loaded first stage turbines.

$$m_{Turb,red} = \text{const} \qquad [4.3a]$$

Combined with the relationship for the similarity parameter, this function can be written as

$$m_{Turb,red} = \frac{m_{Turb,in} \cdot \sqrt{R_{Turb,in} \cdot T_{Turb,t,in}}}{p_{Turb,t,in} \cdot A_{Turb,in}} \qquad [4.3b]$$

and with the further assumption that aspects such as firing temperature, fuel composition, relative compressor bleed mass flows and losses do not undergo significant change, this equation can be developed into

$$\frac{\Pi_{Comp}}{\Pi_{Comp,ref}} = \frac{p_{Comp,t,in,\,ref}}{p_{Comp,t,in}} \cdot \frac{(\dot{m}_{Comp,out} + \dot{m}_{Fuel})}{(\dot{m}_{Comp,out,ref} + \dot{m}_{Fuel,ref})} \cdot \frac{\sqrt{R_{Turb,in} \cdot T_{Turb,t,in}}}{\sqrt{R_{Turb,in,ref} \cdot T_{Turb,t,in,ref}}}$$

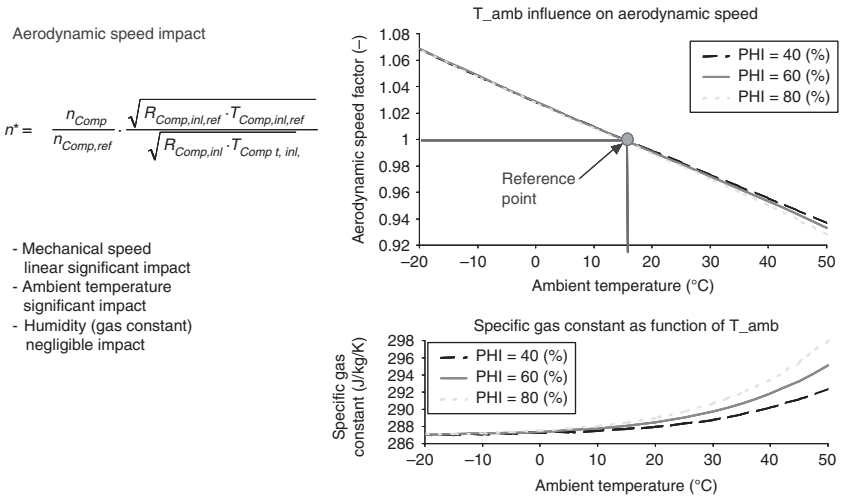
This is known as the 'operating line' equation, and shows that the compressor pressure ratio, and therefore the overall performance of the gas turbine, is mainly determined by two parameters: the compressor inlet mass flow, which can be modified by variable vanes, and the combustion firing temperature.

The aerodynamic speed discussed in a previous section has so far been used inside a compressor map, with no further details provided regarding its relationship to other factors. Figure 4.31 shows the basic dependency of this parameter on mechanical shaft speed, ambient temperature and humidity in absolute terms.

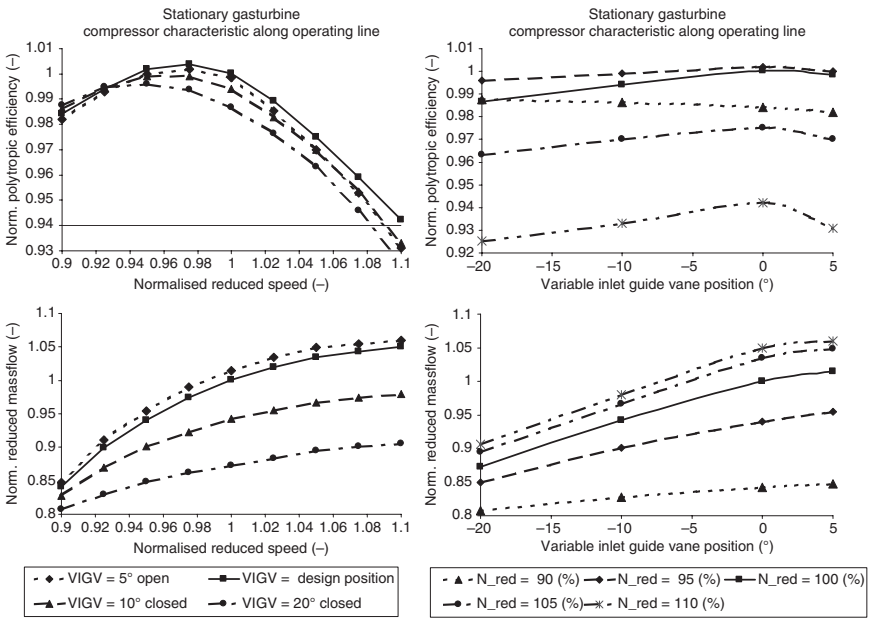
In addition to the mechanical requirements that need to be fulfilled, the main focus is on the effect of aero-thermodynamic factors on operational behaviour, mainly mass flow and efficiency, because this essentially drives the overall power and efficiency of the gas turbine. In the first assessments, the part load characteristics are considered, which describe mass flow and efficiency behaviour along the operating line. A typical example with mass flow and efficiency is shown in Fig. 4.32, based on the normalised similarity parameter.

The reduced mass flow parameter shows that there is a significant mass flow reduction for lower aerodynamic speeds, which appears not only for a mechanical speed reduction but also for increasing ambient temperatures. Some general dependencies are described in Fig. 4.33; it should be noted

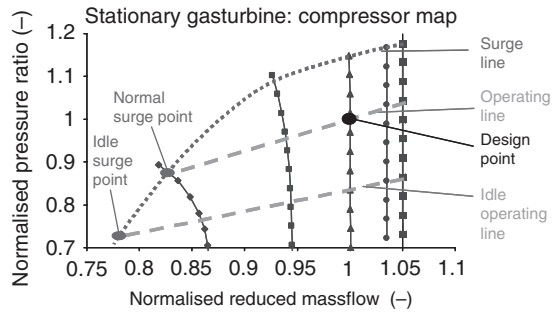
Published by Woodhead Publishing Limited, 2013



4.31 Dependencies of the aerodynamic speed in absolute terms.



4.32 Operational behaviour along quasi operating lines.



- Only the reduced compressor map can be used for changed ambient conditions
- The overall compressor performance strongly depends on ambient conditions

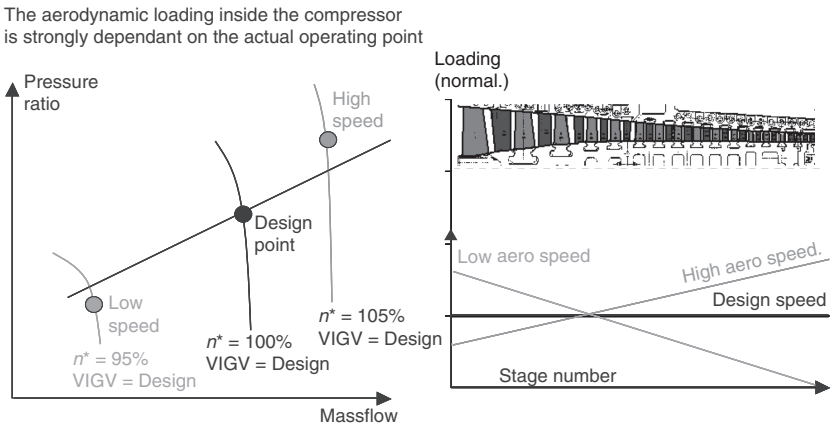
Variation	Engine/Compressor reaction		
p_{amb} ↑	m ↑	n^* = const	Π^* = const
T_{amb} ↑	m ↓	n^* ↓	Π^* ↓
φ_{amb} ↑	m ↓	n^* ↓	Π^* ↓ Minor impact
n_{mech} ↑	m ↑	n^* ↑	Π^* ↑

4.33 Gas turbine interaction with changed ambient conditions.

that a reduced mass flow also causes the pressure ratio to drop, which means it acts twice (via mass flow and pressure ratio) on the overall engine power.

This change in ambient conditions also shifts the loading inside the compressor. Given the different mass flows and densities of the fluid, the turning and channel contractions do not fit as intended in the original design. A mistuning over the compressor length will occur as a result, and is dependent on the ambient conditions. Figure 4.34 illustrates the different effects that can occur and offers an easy way of understanding them.

Starting at the design point, the pressure rise (flow turning angles) and channel contraction are harmonised, ensuring solid compressor operation. If the exit pressure increases, for example due to an increased firing temperature, the inlet mass flow will not change, as shown by the steep speedline on the map. The additional pressure ratio must therefore be built up in the rear of the engine, which decreases the axial velocity; higher pressure results in higher density, and the axial velocity decreases depending on the mass flow. This provides a positive incidence angle for the flow to the blading, thereby increasing the load, while the opposite occurs when the pressure is lower. Decreasing the aerodynamic speed, for example by employing high ambient temperatures, reduces the inlet mass flow and therefore provides positive incidence angle for the flow to the front stages if the channel contraction is



4.34 Internal compressor load shift based on ambient conditions.

higher than planned. The velocity therefore increases to the rear and deloads the rear stages; the opposite is observed if the aerodynamic speed increases.

4.5.2 Operating range requirements

The operating range is also important. Official guidelines exist, known as grid code requirements; these usually vary between countries, but the following requirements are typical:

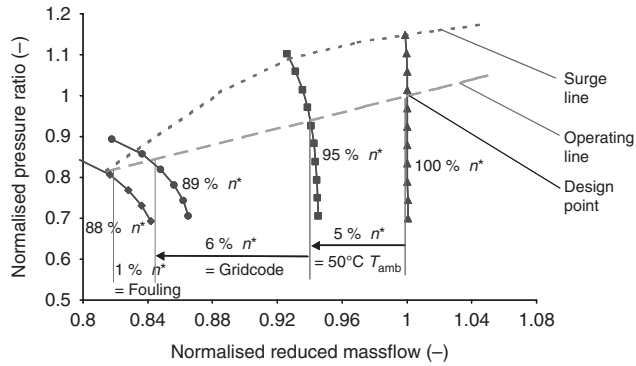
- 6% mechanical underfrequency operation for all ambient temperatures
- 5% mechanical overfrequency operation for all ambient temperatures

If ambient operating temperature ranges are defined as those between +50°C and –20°C, the above requirements mean that the necessary aerodynamic speed ranges are between 89% and 110%. Particular attention must therefore be paid to the surge line, which can clearly be seen in Fig. 4.35.

The compressor map shown above is only valid for a single variable vane setting. If variable vanes are used, the surge margin behaviour of all the operational variable vane settings must be taken into account. As shown in Fig. 4.36 the surge line can show a significant decrease in aerodynamic speed if the variable vanes are opened, shown principally by a reduction in the surge pressure ratio compared to the pressure ratio of higher aerodynamic speeds. At these low aerodynamic speeds the front stages take a greater load, while deloading occurs at the rear stages. The surge drivers in the front stages are thus very important, and tight clearances and/or other stabilising special features may be required. Another alternative is to adapt

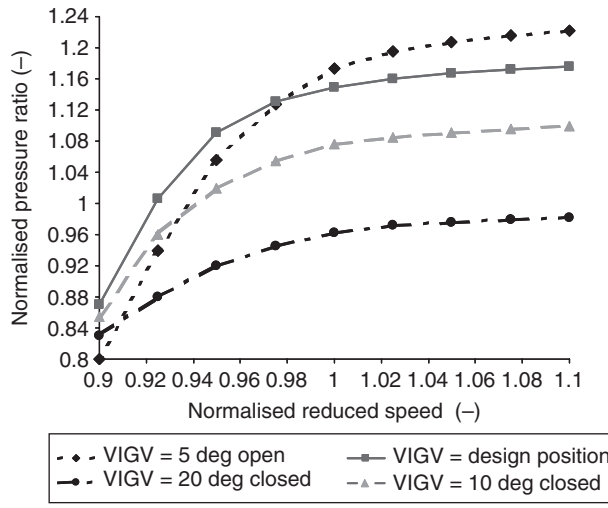
Gridcode requirements for a compressor

- Gridcode requires only speed and temperature variation
- Fouling has to be taken into consideration additionally
- The engine operating concept has to ensure safe operation for all cases



4.35 Requested underfrequency operating ranges of a stationary gas turbine compressor.

Operational behaviour of the surgeline for different reduced speedsand different variable inlet guide vane (VIGV) settings



4.36 Compressor surge lines with respect to variable vane settings.

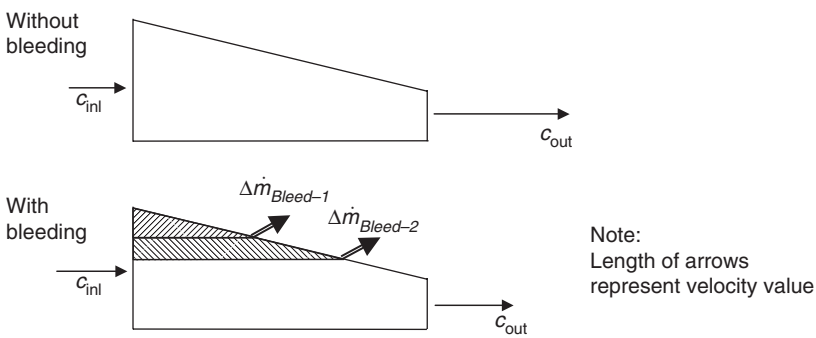
the operating process so that the vane closes quickly in the case of reduced aerodynamic speed. A compressor surge under load conditions can easily destroy the blading and cause severe damage to the engine, making this a critical issue in compressor operation. In this respect fouling/degradation behaviours must also be considered, as these also affect the mass flow, making the engine more sensitive for surge conditions.

4.5.3 Start-up requirements

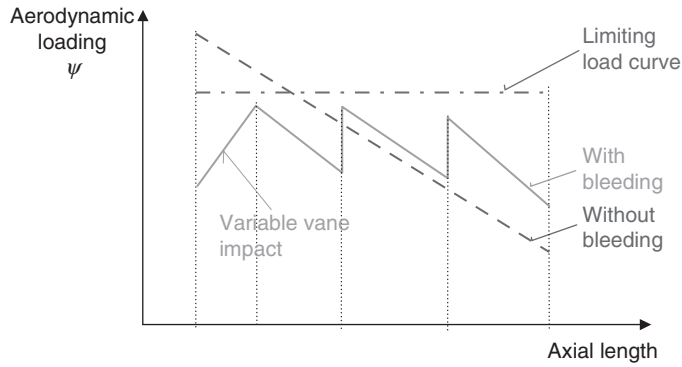
As previously mentioned, a compressor is designed for a specific mass flow and pressure ratio, and the blading design and channel contraction are matched to ensure a high efficiency engine. The required operating range, however, imposes some restrictions on this; the start-up and shutdown behaviour therefore becomes increasingly important. During these transient operations, the pressure rise over the length of the compressor is not compatible with the channel contraction, so blow-off systems are used to ensure that the engine can work properly. Figure 4.37 provides a clear picture of this behaviour, showing the principle of the velocity behaviour for a given inlet mass flow while running a significantly lower pressure ratio.

If the contraction during the start-up phase is higher than was intended when the system was designed, the axial velocity at the outlet of the compressor will significantly increase, as shown in Fig. 4.37. This could easily lead to transonic conditions at the exit, which would in turn lead to a choking effect. Choking means that the mass flow passing a certain area is limited or blocked and therefore that the overall inlet mass flow is reduced. This effect would cause significant incidence angles in the flow at the front of the compressor, which could force a rotating stall or a surge event, where the flow would completely collapse. This is the point at which the blow-off systems are introduced in order to extract flows at certain axial positions that are not compatible with the contraction during transient conditions, as shown in Fig. 4.37.

It is clear, then, that aerodynamic loading can also be tailored for transient conditions. However, the use of blow-offs can be quite expensive, as mentioned earlier, because stainless steel is required for the piping system; moreover, due to the potential size of the extraction required, the valves needed can easily cost up to €20 000–30 000. For health and safety reasons the temperature of the extracted air must be controlled, and limits are also imposed with regard to the noise of the output: both of these issues incur



4.37 Compressor blow-off concept for keeping the axial velocity.



4.38 Compressor loading during start-up.

additional costs in the form of either an extended piping to the exhaust stack or an additional silencer system.

The use of blow-off valves goes some way towards addressing the issue of incompatibility between the channel contraction on the one hand and the airflow contraction or pressure rise on the other, but the problem is still not fully solved, as the channel is still not quite right for the mass flow. To reduce the number of blow-offs required, more air than necessary is extracted for this area, leading to an aerodynamic overload at the stages directly after the bleed positions. Variable vanes are used during these transient operating conditions so that the flow angles are adapted to the front part of the compressor as effectively as possible. A typical loading distribution during this transient behaviour is shown in Fig. 4.38. The required number and position of blow-offs is ultimately determined by a number of factors, between which a reasonable balance must be found, including the cooling air flow requirements (with a certain pressure and temperature), the variation range of the variable inlet guide vanes, the compressor loading distribution and the turbine throttling behaviour.

Up to this point, only the aerodynamic aspects of the compressor blading have been considered. However, the compressor is a part of a gas turbine, meaning that additional restrictions are imposed by the engine as a whole. During start-up a specific acceleration, and therefore also a certain amount of energy, is required: a starting motor or a static frequency converter is used for this purpose. The generator is frequently used in a transverse mode to act as a static frequency converter. The overall power balance of an engine can be formulated as follows:

Start-up power balance:

Start-up is possible if

$$P_{\mathrm{SFC}} + P_{\mathrm{Turb}} + P_{\mathrm{Acc}} + P_{\mathrm{Comp}} > 0$$

Published by Woodhead Publishing Limited, 2013

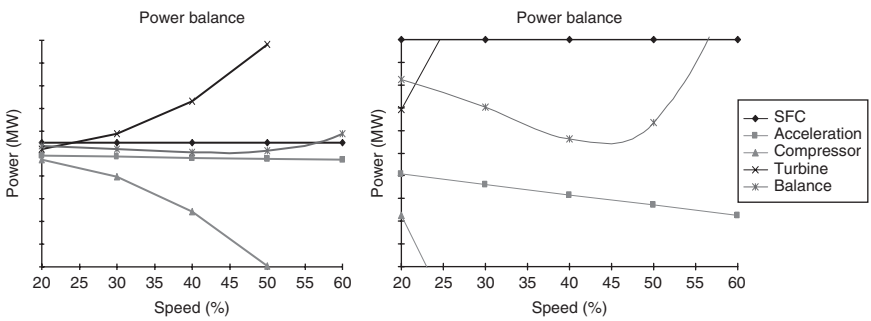
where the following description applies

P_{SFC}: Power delivered by the start-up device (e.g., Static Frequency Converter);
P_{Turb}: Power delivered by the turbine;
P_{Acc}: Power required for defined acceleration;
P_{Comp}: Power required to drive the compressor.

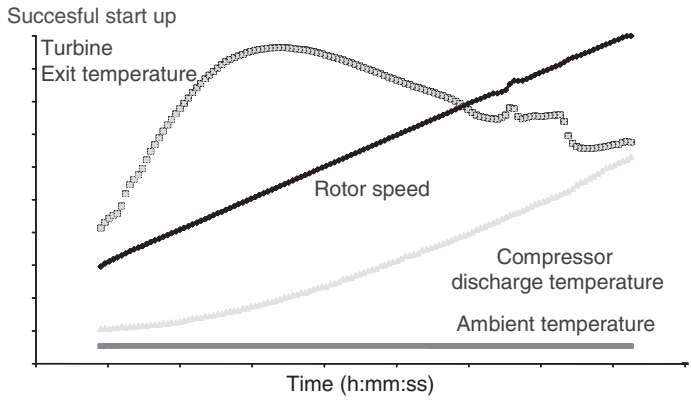
This initially looks reasonable, with no immediately obvious problems. Looking in more detail it becomes clear that the turbine power is correlated to the mass flow and pressure ratio, as discussed before. Mass flow is extracted at the blow-off systems, and therefore a lower mass flow is available at the turbine inlet. Additionally the pressure ratio has to be kept quite low due to the aerodynamic loading of the compressor stages directly after the bleed stations. As a result, only a relatively small amount of power is delivered by the turbine, while the compressor has a high power requirement. One means of addressing this problem would be simply to increase the start-up power; however, the required power can easily be in the megawatt range, which would be a substantial financial investment for the starting device.

Another option would be to reduce the acceleration rate, which would raise two further issues. The first is mechanical: the bladings would need to pass their resonances more slowly, which could excite the blading and even lead to mechanical damage over time. Secondly, acceleration does not actually have a particularly high power requirement; reducing acceleration therefore does not contribute significantly to any power saving. All these effects must be carefully monitored during the design of a compressor and its integration into a gas turbine. A typical power balance over time/speed is shown in Fig. 4.39.

An example of typical successful start-up behaviour can be found in Fig. 4.40. The exit pressure and turbine outlet temperature can be easily



4.39 Gas turbine start-up power contributors and overall balance.



4.40 Typical gas turbine start-up graph.

measured in order to control the start-up behaviour, while rotor vibration control is also strongly recommended for these phases.

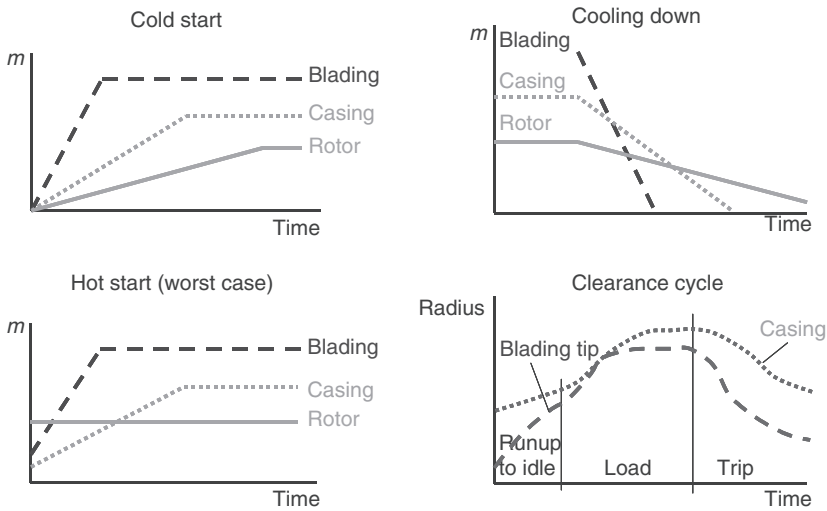
Monitoring of the engine during transient operation is essential. A trip during this phase can cause a delay of an hour in installing the engine on the grid, which would often be unacceptable. Engine trip is the most common problem during start-up, and can be caused by low acceleration, high turbine temperature, or high vibration levels. The root causes of these issues can be different and include:

- Blow-off valves not opening as expected.
- VGV positioning not as expected.
- Fuel rate not as expected.
- Rotating stall during start-up.
- Heavy compressor fouling.
- High engine temperature.

If these problems occur, the start-up controls software must be adapted, or, in the worst case, redesign may be required. Modifications to be considered in the case of start-up problems are:

- Change of VGV settings.
- Change of blow-off schedules.
- Change of fuel rate (as function of speed).
- Increase of firing temperature;
- Higher start-up power.
- Higher blow-off mass flows.
- High solidity blading (i.e., more blades) after bleed stages.
- Redesign of critical stages.

Published by Woodhead Publishing Limited, 2013



4.41 Thermal growth of structural parts during transients.

The warm-up phase is another important part of the compressor system that contributes to the behaviour of the engine as a whole. At this point the rotor and the structural parts take heat out of the system and develop their own thermal growth, which affects the operation of the compressor. The mass flow is determined by the front stages, which experience only a minor thermal change. The mass flow therefore remains as shown on the unchanged standard compressor map. Depending on the chosen rotor design, a significant time delay can occur between the thermal growth of the structure, and the rotor and blading: solid rotors are the most problematic in this respect, with disk rotors offering better performance (i.e., shorter delay). Typical thermal growth figures for different start-up and shutdown conditions are shown in Fig. 4.41.

In a cold engine, contact between the blading and the flow involves a huge surface area and a small volume. The thermal growth of the blading is consequently rapid, resulting in a decrease in clearances. These operating conditions therefore determine the clearances permitted in the first stages without causing rubbing. In the next stage, the casing structure also undergoes thermal growth, which will lead to an increase in clearances. Finally the solid rotor is heated up, which then reduces the clearances once again. The increase and decrease in the clearances has a significant effect on the efficiency of the compressor and therefore also on the performance of the engine as a whole.

From an aerodynamic perspective, there are two main issues connected to the clearance changes: firstly, the average clearance change determines the

efficiency of the compressor efficiency, and secondly, the maximum clearance contributes significantly to the surge margin. The effect of the clearance changes on the surge margin can mainly be seen in very cold ambient conditions or closed variable vanes, because in these cases the rear part is strongly loaded and can trigger surge.

4.5.4 Additional operational requirements

The axial compressors used in stationary gas turbines are required for very high reliability. However, there are some circumstances that can lead to damage to the blading and, on rare occasions, also to the engine. Blading damage can be caused by corrosion or erosion, by increased mechanical loading due to vibration (mainly in surge conditions), or even by foreign objects. In certain cases even strong rubbing can cause damage to the blading. Moreover, if strong fouling or degradation occurs, or if filter systems become blocked, there is a further risk of compressor surge, which can cause high mechanical load to the blading and can give a severe risk to damage the engine.

Compressor icing

If the ambient temperature at the inlet is very low, ice can form on the elements of the intake housing (filter housing, silencers, struts, etc.) and even on the first blading rows. The inlet guide vane and the first rotating blade row are the main elements involved in this problem. The icing formation in this case is driven by strong flow acceleration, which reduces the static temperature. This icing can therefore occur even at ambient temperatures well above 0°C, with temperatures of 6–8°C known to cause icing in standard stationary gas turbines; this is also connected to the restagger or flow turning conditions of the inlet guide vane.

If filter icing occurs, there can be an increased loss of pressure in the filter system, generating severe underpressure after the filter system, which then has to be recovered by the compressor blading. To avoid damage to the intake system caused by severe underpressure, special implosion doors are implemented, which open if conditions become critical.

Pre-heating systems are generally installed in plants with a serious risk of ice formation. These systems often use air either from the compressor exit or from the neighbouring steam cycle, which is injected into the intake system. This injection should preferably be positioned in front of the filter system to avoid or at least reduce possible filter icing or clogging. Furthermore, the flow velocity at this point is very low, ensuring an easy mixing process. An overview of icing mechanisms and possible mitigation measures can be found in Stoff and Kovács (1985).

Published by Woodhead Publishing Limited, 2013

Compressor fouling and cleaning

The intake mass/volume flows utilized by gas turbines are generally very high, meaning that the blading experiences quite significant fouling over time even if a good filtering system is in place. The regular exchange of some intake elements (e.g., filter panels) and cleaning of the compressor blading is therefore essential to maintain plant performance data at reasonable levels. In addition, the contamination of the blading and the channel with aggressive particles can generate aggressive solvents, lye and acids, resulting in standstill corrosion and pitting corrosion, which can significantly reduce blading and root stress and frequency margins. Oil and soot layers are the typical contaminants affecting the front stages, while the rear stages are affected by higher salt concentrations of various types. The type and the rate of these fouling conditions are strongly dependent on site-specific conditions, namely the local environmental and operational conditions.

Today, wet cleaning procedures are usually used to clean the compressor blading: this means cleaning using water, which might be mixed with a solvent (detergent). There are two basic methods of application: off-line cleaning, where the engine is put out of operation to be cleaned; and on-line cleaning, which is carried out during standard operation, sometimes with slightly reduced power generation as a result. Both methods can be used even at low temperatures, as long as a corresponding anti-freezing agent is added into the water solvent.

On-line cleaning uses a special nozzle system to inject the water solvent in front of the blading. The amount of water injected is quite small compared to the airflow, because the procedure is applied during the operation of the engine. An even distribution of the water ensures that the whole front blading undergoes the same wetting/cleaning, thereby minimising possible droplet erosion. Unfortunately, this method can be only used to clean the front stages, which are the most important blade rows in determining the mass flow, since the water solvent will be centrifuged radially and then evaporates further downstream. An additional disadvantage of this method is that deposits taken from the front stages can be transported to the rear stages and can either become trapped or generate increased fouling at the rear stages. The use of this method is therefore somewhat restricted, and off-line cleaning, or even an outage to clean the whole blading, is also occasionally required.

Off-line cleaning also uses a special nozzle system to inject the water solvent in front of the blading. However, in this case more water is used, as the procedure is carried out while the engine is disconnected from the grid. A turning device is used to turn the rotor at a rate of a few hundred rounds per minute while the water solvent is injected. The injection of water solvent can be interspersed with clear water injection to achieve maximum cleaning

Published by Woodhead Publishing Limited, 2013

effects. Before this cleaning procedure is carried out, it is crucial to ensure that the engine is well cooled down, to minimise the risk of an uncontrolled stress concentration due to the fast cooling of parts. Similarly, following the procedure, it is critical to ensure that all water has been drained from the engine, including from inside the blow-off lines, the piping and drainage systems, and cooling lines. Off-line cleaning can allow efficiency and possible mass flow to be regained, and therefore the overall performance of the engine to be improved, thereby partially counteracting the effects of ageing.

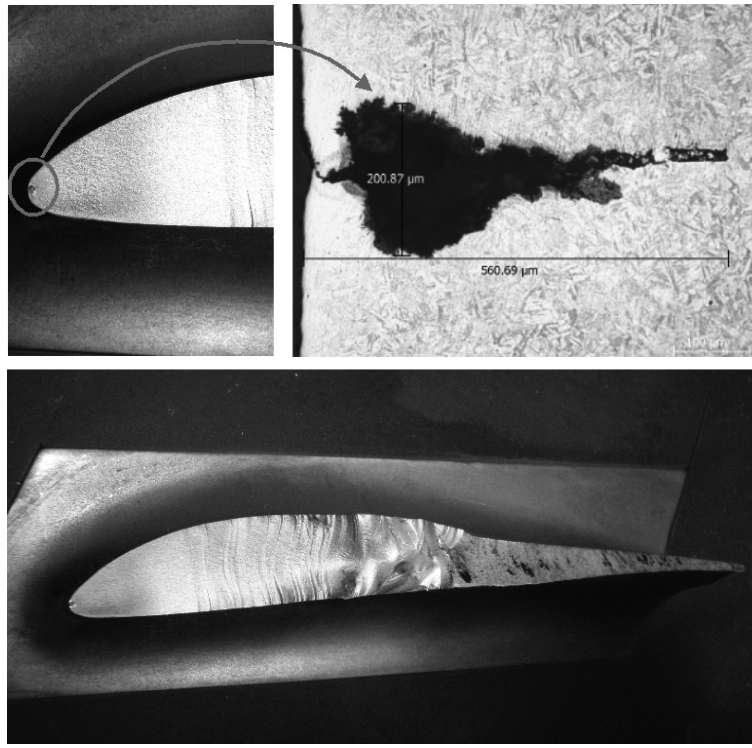
The optimisation of the washing intervals for both on-line and off-line cleaning can have a significant effect on the energy production costs of a plant and is therefore of substantial interest. The basic principle of this optimisation is to understand the site-specific degradation mechanisms, the impact of on-line or off-line cleaning, and the balance between the downtime required for off-line cleaning and its economic benefits. The required fuel consumptions for power generation must be carefully balanced against the expected earnings: Schepers and Hagemann (1999) discuss the basic principles of the procedure and some possible assessment methods.

Compressor ageing

Ageing of gas turbine compressors usually occurs due to a worsening of the surface quality of the blading and the channel, and increases in the radial clearances for the rotating blades and the non-rotating vanes caused by rubbing during start-up, shutdown and operation. Furthermore, for sites operating under very challenging ambient conditions, for example, in coastal environments with a high salt concentration, the blading geometry can be altered by erosion and similar phenomena.

The reduction in the surface quality of the blading is primarily driven by corrosion, principally standstill corrosion in the rear stages of the compressor, because salts that are deposited on the blading during operation under fouling conditions will generate aggressive solvents during long standstill periods. During normal operation, the temperature in the rear stages is high enough that all water evaporates, meaning that aggressive solvents cannot be generated. For the front stages this corrosion attack can also occur during operation, because the blading surfaces here can also be wetted. The front stages are therefore quite often coated; alternatively, more corrosion-resistant steels, such as those with a higher chromium content, may be used. A typical example of corrosion attack on the blading and its possible consequences is given in Fig. 4.42. A small pit has developed at the leading edge of an individual blade, which is difficult to spot even during an inspection. As this small pit grows to a larger size, it begins to affect the mechanical strength. The blade then begins to crack slowly, mostly during the start/stop cycles, as

Published by Woodhead Publishing Limited, 2013



4.42 Pitting corrosion and consequential damage of a compressor blade.

can be seen from the beach marks along the blade surface, before the blade finally cracks over the whole length due to a mechanical overload.

Corrosion on the blading surfaces has two major effects on engine performance: firstly, it decreases the efficiency by increasing the total pressure loss of the individual blade rows; secondly, it slightly reduces the turning behaviour of the blading. If this effect occurs at the front stages the inlet mass flow is usually reduced. The increase in blading clearances due to rubbing has very similar effects and can also be significant in ensuring the operating range and surge margin. For compressors with high pressure ratios, abradable systems are often used to control the clearances as far as possible. If these abradable systems are properly designed they can be easily exchanged during revisions, thereby counteracting some of the effects of engine ageing.

Compressor damage from rubbing and/or foreign objects

A fairly common cause of damage to the compressor blading is foreign objects from a variety of sources interfering with the blading. These foreign

objects are often small parts lost during assembly or engine inspections, such as screws, supporting parts, and assembly tools. In addition, the quality of the assembly must be carefully checked to ensure that no parts of the blading become detached or broken off and lost over time, causing damage. Correct installation and maintenance of the filter and intake systems is also essential in restricting foreign object damage. Finally, some foreign objects can be sucked in from the external environment and cause damage to the blading.

Small foreign objects do not usually damage the blading directly. Nevertheless, they can cause minor 'pre-damage', which, given the constant stress and frequency excitation, is enough to cause blade damage over time. Very small foreign objects can be eliminated by polishing during an outage without the need to disassemble the blading. If more severe damage occurs, or if the damage is at critical locations in respect to high dynamical and/or stationary mechanical stresses, the exchange of the blading is highly recommended.

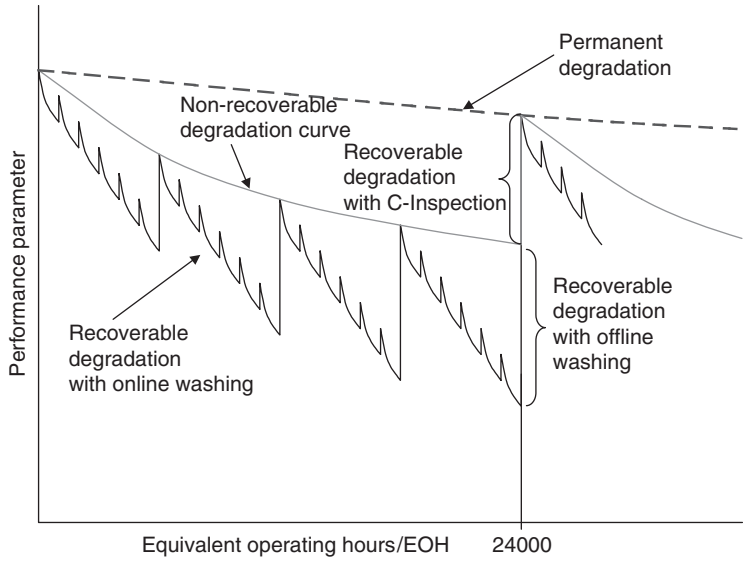
Rubbing of free standing compressor blade rows at high mechanical speeds does not usually generate major blading damage. The blading tip melts away due to the high friction heat generated by the rubbing, thereby reducing the forces acting at the tips. At low mechanical speeds, for example during start-up, the heat has less impact, and therefore a stronger force acts on the blading. Under these circumstances, the worst case scenario is the occurrence of self-excited resonances that can cause partial or even complete blading damage.

Compressor performance degradation

The effects of fouling, ageing, erosion, corrosion and rubbing significantly contribute to the degradation of the engine as a whole, or at least to a reduction in power and efficiency over time. This degradation and its typical impact on performance are shown in Fig. 4.43, in which EOH means equivalent operating hours. Possible performance improvements that can be achieved through on-line and off-line cleaning (washing) and through a 'C-Inspection' or outage are also shown in order to provide a schematic overview.

As a significant level of performance can be regained through on-line cleaning it is clear that this procedure mainly acts on the front stages, thereby contributing substantially to regaining the original inlet mass flow. Mass flow reductions due to fouling of up to 3–5% have been observed. Stronger deposits can only be removed by off-line cleaning, while more severe damage, such as increased clearances, erosion and corrosion effects, can only be remedied by replacing the parts, which is carried out during a C-Inspection if required.

Published by Woodhead Publishing Limited, 2013



4.43 Gas turbine performance degradation versus equivalent operating hours.

Compressor degradation and ageing affect the shape of the blading and thus also its aerodynamics. Erosion effects and/or an increase in the surface roughness, for example due to corrosion, can reduce the working range of the compressor (as a result of earlier flow separation). The additional mass flow reduction due to fouling results in further aerodynamic mistuning. As an overall conclusion, it may therefore be stated that all these effects contribute to reducing the working range of the compressor and therefore make surge events more likely if the parts of the compressor are not properly maintained.

Compressor surge and rotating stall

The aerodynamic operating regime of a compressor is restricted by the upper and lower limits of the most critical blade row, which depends on the local operating conditions, as discussed previously. Two different flow phenomena are observed, as follows:

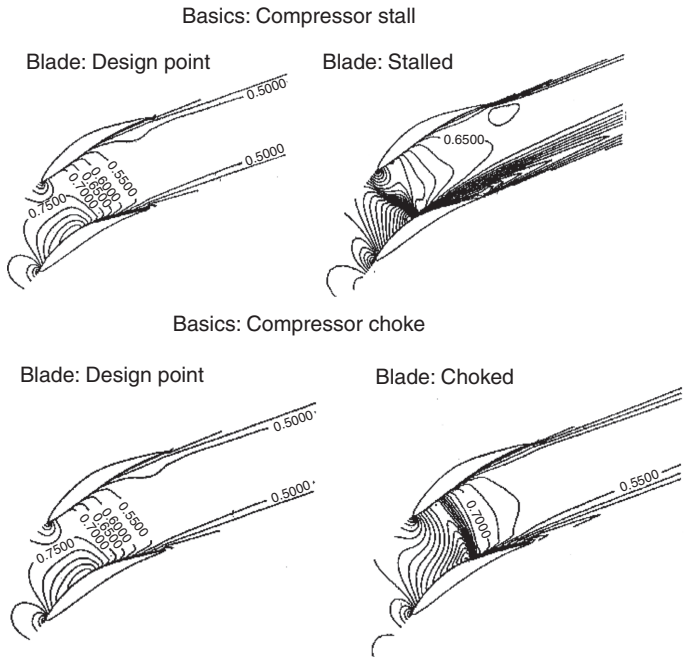
1. 'Choking Conditions', where the maximum possible mass flow passes through a blading passage which is aerodynamically blocked by an aerodynamic shock (usually high negative incidence, with flow to the suction side of the blading).

Published by Woodhead Publishing Limited, 2013

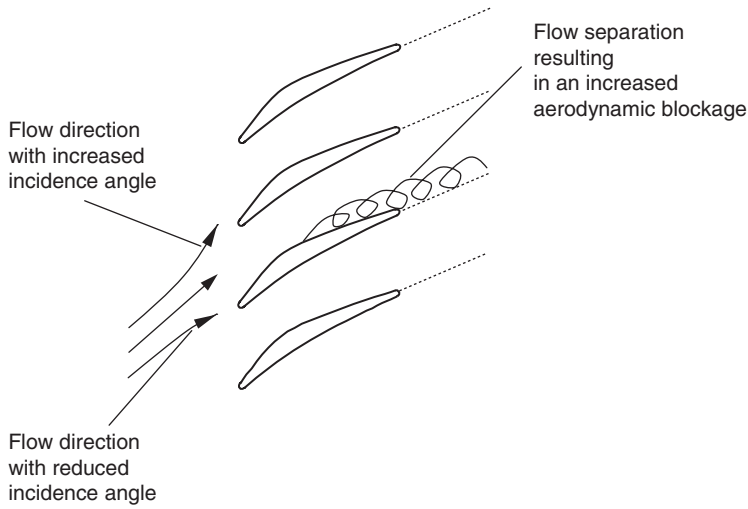
2. 'Stall Conditions', where the minimum possible mass flow passes through a blading passage which is linked with a massive aerodynamic flow separation at the trailing edge suction side (usually high positive incidence, with flow to the pressure side of the blading).

Both effects are driven by interaction with the endwall regions (corner stall) and/or the vortex structures of the secondary flow and/or the clearance flow. A diagram of these choking and stalling effects is provided in Fig. 4.44.

Under stalled conditions, two further flow phenomena can develop. The first one is known as the 'rotating stall' effect, in which a single passage blocks the incoming flow due to massive separation at the trailing edge of the suction side. As a result, slightly more mass flow is transferred to the neighbouring passages, which stabilises the aerodynamic behaviour of the passage in the direction of rotation and weakens that against the direction of rotation, as seen in Fig. 4.45. Due to this weakening/strengthening process the separation proceeds in the direction of the rotation. If this movement of the separation occurs only in one blade passage over the circumference it is known as a 'one cell rotating stall' and travels at about 50% of the circumferential speed. A 'multiple cell rotating stall' can also develop, but is



4.44 Aerodynamic flow limits for a typical compressor blading section.



4.45 Aerodynamic flow structure during rotating stall of a compressor blade row.

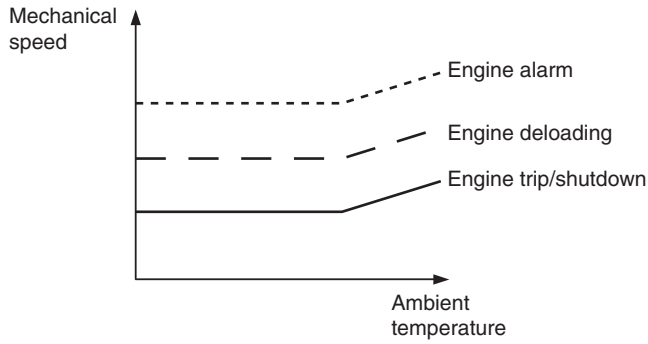
not usually as significant. Rotating stall phenomena mainly occur during the starting phase of a stationary gas turbine.

The second possible flow phenomenon that can develop during stall, in this case when all blading passages of one row are stalled, is the complete blocking of the flow. The turbine, however, continues to suck off the mass flow, leading to underpressure generation after the stalled row. At a certain point, the pressure ratio between the stalling row and the turbine inlet is high enough to initiate reverse flow from the turbine, passing down through the whole compressor. This reverse flow usually causes an extremely loud noise. This aerodynamic effect of surge can happen during standard operation if the system is not properly protected.

As already mentioned above, compressor surge is a flow effect, whereby the flow changes to an inverse mode from the combustion system throughout the compressor blading. This can occur when a compressor operating at high aerodynamic speeds (high mechanical speed and/or low ambient temperatures) is required to deliver a certain pressure ratio. This pressure ratio can be too high for the rear stages if fouling has occurred, causing overloading. The same effect can also occur when a compressor operating at low aerodynamic speeds (low mechanical speed and/or high ambient temperatures) is required to deliver a certain pressure ratio; in this case, it is the front stages that can experience an excessively high pressure ratio and become overloaded if fouling has occurred.

Due to the extreme misalignment of the flow angles with the blading geometry, a full load surge generates a fairly high dynamic force on the

Published by Woodhead Publishing Limited, 2013



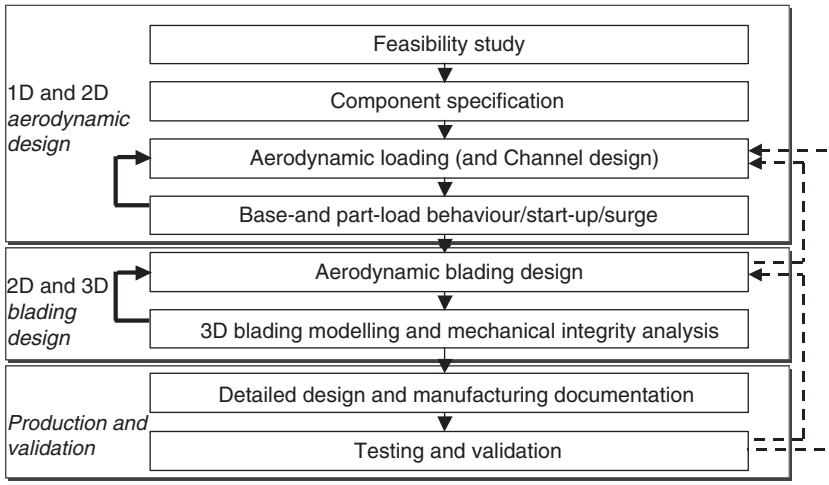
4.46 Underfrequency/surge protection scheme for a stationary gas turbine.

compressor blading. In some rare cases this can lead to continuous deformation or even damage to the blading. Furthermore a significant risk of rubbing and damage to the intake system can be combined with a compressor surge event. Therefore, stationary gas turbines have a surge protection control mechanism, which implements safer operating conditions in the case of a surge event by deloading the engine or even by cutting the connection to the grid and shutting the engine down entirely.

For stationary gas turbines 'Underfrequency Protection' charts are used and implemented inside the control logic of the gas turbine to ensure safe operation. For this kind of gas turbine the firing temperature, and other factors that contribute to the pressure ratio, are checked and controlled separately; consequently, the compressor surge margin can be determined by the mechanical speed and the ambient temperature. A three-step approach is used, beginning with the implementation of an alarm to act as an early warning system for the operator. If the engine speed continues to fall, two further steps can be taken. The first is deloading of the engine, often combined with disconnection from the grid. This keeps the engine running, and reloading and reconnection can be carried out fairly quickly. The second is the complete shutdown of the engine; this is avoided as far as possible, because reconnection and reloading can take some time (for example, for a combined cycle requiring boiler purging this can easily take 0.5 h). Figure 4.46 shows a typical protection graph.

4.6 Compressor design process

Before the compressor design begins, an approximate architecture for the gas turbine has to be drawn up and the corresponding cycle analyses carried out. This leads to certain constraints for the compressor being determined, such as the required inlet mass flow and the overall blading pressure ratio. Once the



4.47 Compressor overall design process.

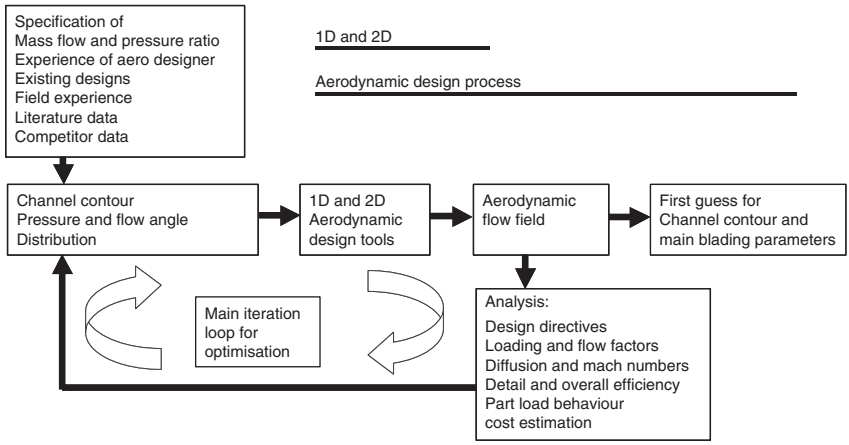
power to be transmitted to the generator has been established, and a first estimation made of the required bearing size, some restrictions can be set on the minimum required rotor diameter. If the generator is placed in front of the gas turbine this restriction is usually quite significant. The outer diameter of the channels is also established to a certain extent for the rear part, in order to ensure that the diameter of the whole gas turbine remains a reasonable size.

Taking these constraints into account, preliminary aerodynamic studies based on a one-dimensional mid streamline approach are carried out to establish a suitable axial length for the compressor and a reasonable number of stages. Some initial very rough mechanical assessments are required to confirm that the selected parameters are feasible for the requirements of the blading profile. A clear project plan must then be developed based on these feasibility studies in order to obtain a complete picture of the schedules and budgets involved, but also to mitigate any risks identified during the feasibility phase. The overall compressor design process can be summarised as shown in Fig. 4.47.

A compressor is mainly driven by the aerodynamics and is only to a lesser extent constrained by mechanical integrity and/or lifetime issues. The following sections therefore concentrate on the aerodynamic aspects of compressor design.

4.6.1 Detailed aerodynamic steps

A great deal of experience, as well as suitable design tools, is required in designing the aerodynamic loading system and channels; major decisions

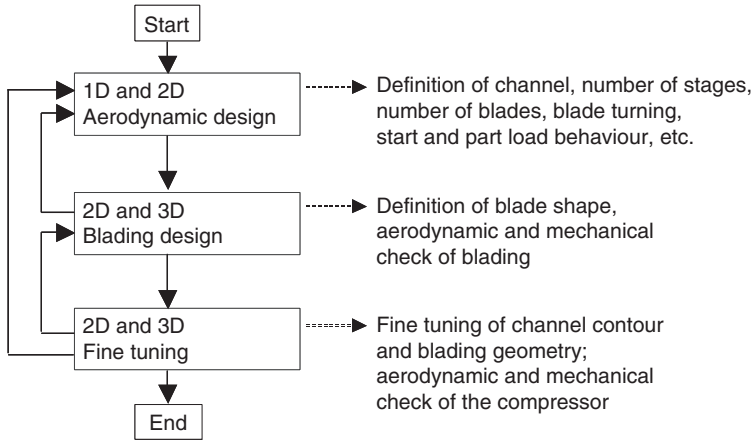


4.48 Compressor design process inside the concept phase.

are made during this phase which, if incorrect, can have serious implications. For example, the loading of the front stages is usually higher than that of the following stages, but if the operating range is estimated incorrectly, possible effects include a reduction in performance if the grid or ambient conditions change, or an insufficient variation range delivered by the mass flow reduction capability for closed variable vanes. Another example is the impact of an incorrectly set channel contour in the rear part of the compressor. This area is strongly influenced by the transient thermal behaviour of the structural parts; consequently, if the thermal growth of the channel and blading are not properly harmonised, significant clearances, which would affect the efficiency of the compressor and also the operating range: the average clearance determines the efficiency, while the maximum clearance determines the surge behaviour. Figure 4.48 shows an approximate diagram of the overall procedure; preliminary checks for mechanical integrity are not shown but should nevertheless be carried out at this stage in the development.

Once this phase is complete, a review of the engine integration must be carried out, and all interfaces have to be cross-checked with the targets of the engine as a whole. For gas turbine development, to continuously review the progress and integration of all components is crucial so as to ensure that the targets for the engine as a whole can still be met. Even these whole engine targets must be continuously cross-checked to ensure, for example, that the market requirements are still achievable and the product suits the market. Engineers may try to avoid this particular issue, but the schedule, costs and targets are essential elements of every project

Published by Woodhead Publishing Limited, 2013



4.49 Overall compressor blading design process.

and must be considered carefully in order to meet customer requirements and be successful.

In the next design phase the blading itself is developed. The main numerical tools required for this task are:

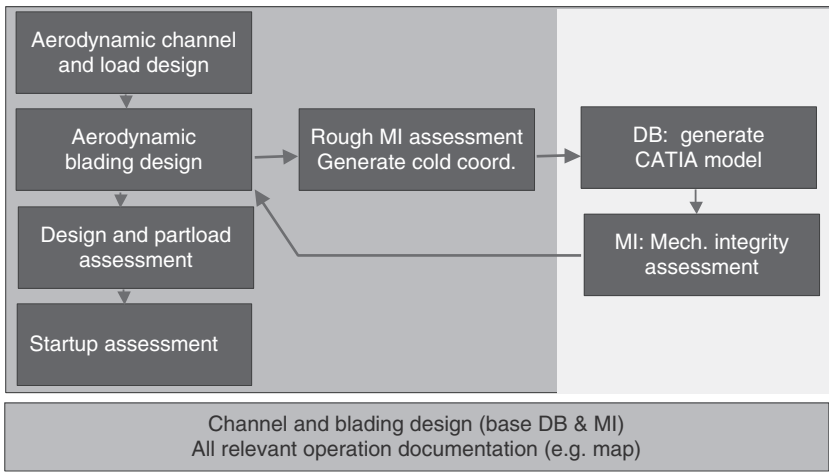
- geometry tools for blade shape generation;
- 2D and 3D aerodynamic assessment tools;
- 2D and 3D mechanical integrity tools;
- (occasionally) 3D unsteady tools.

Figure 4.49 shows the division of the task itself.

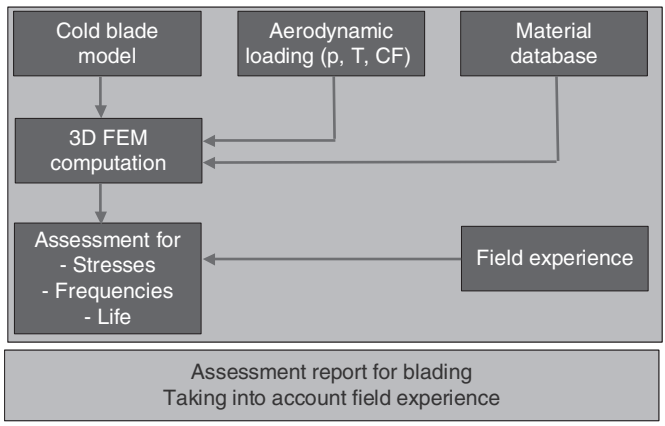
Experience has demonstrated that a stepwise approach from 1D to 2D and then to 3D delivers the best results in the shortest time. This is based on the fact that for compressors the 3D features are essentially add-ons rather than basic elements for pressure and swirl distribution. Furthermore, it has been observed when designs are drawn up in a 3D environment, too much emphasis is given to the 3D aerodynamic impact; at later stages it then emerges that the design struggles to meet the basic component requirements, such as optimised efficiency for design conditions but reduced mass flow throttling capability for closed variable vanes. Finally, Fig. 4.50 shows the overall process for aerodynamic compressor design.

4.6.2 Basic mechanical integrity steps

As mentioned above, aerodynamic considerations are most important for compressor design, whereby mechanical design limits have to be achieved



4.50 Overall aerodynamic compressor blading design process.



4.51 Overall mechanical integrity compressor blading design process.

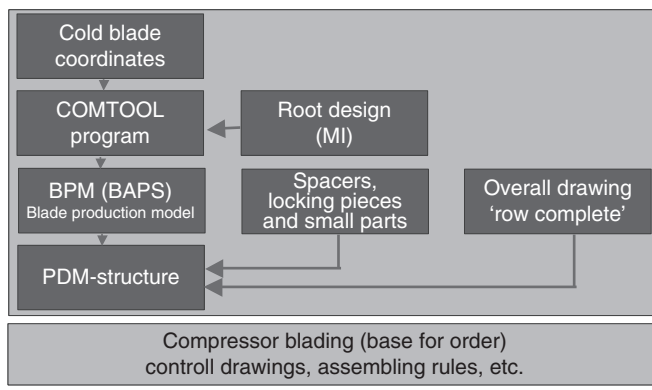
all the time. In terms of mechanical integrity, the key process is the mechanical assessment and release of the blade row, which is illustrated in Fig. 4.51. The main point to be kept in mind in this respect is that roles and responsibilities must be clearly defined; in other terms, it is important to clarify who is responsible for determining the required 'cold' geometry to be manufactured. Meanwhile, the aerodynamic side of the design is concerned with 'hot' geometry, which is involved in the flow during operation: at this point, the centrifugal force can cause some untwist in the blades, and some elongation can occur depending on the temperature. Both of these factors

must be taken into account when considering the mechanical integrity of the design.

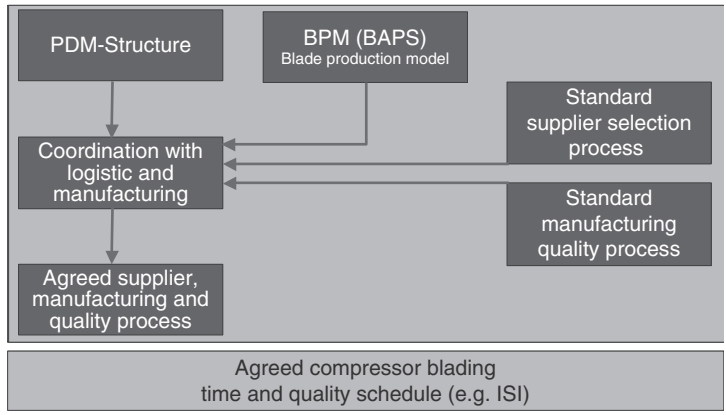
4.6.3 Basic mechanical design steps

In both the concept and the design phases, mechanical designers play largely a supporting role; however, they are essential in the process, because today even CFD can be carried out using the 3D models generated through mechanical design. The major work of the mechanical design team begins when the blading profile and root are aerodynamically and mechanically designed and approved by all parties. One major challenge is the development of 3D models and corresponding drawings for the blading and all the required consumables, as shown in Fig. 4.52.

The mechanical designers also have to support the manufacturing process as shown in Fig. 4.53. This begins with logistical support in developing orders with all the required design input, including acceptance protocols and work instructions for surface treatments and so on. The majority of information is distributed via 3D models, which provide a high level of detail and accuracy, but can be difficult to use in discussion of the finer details. Engineers therefore prefer to use some basic drawings and sketches, which are also useful in discussions with other interested parties, such as suppliers. Moreover, it has emerged that early meetings with suppliers and development engineers can reduce the number of iterations required and can also offer the possibility of a concurrent engineering process, which means that information is transmitted step by step, and not when all work is complete. A simple example of this is the material ordering process, which can be started as soon as the basic blading dimensions are known.



4.52 Model and drawing generation process of discipline mechanical design.



4.53 Manufacturing support process of discipline mechanical design.

4.6.4 Use of a design system

As observed across the whole design process, interaction between several engineering disciplines is required, along with reference to relevant field experience. A design system provides significant improvements in this regard, both in terms of reducing the time required and minimising risk. A good design system should address two major issues:

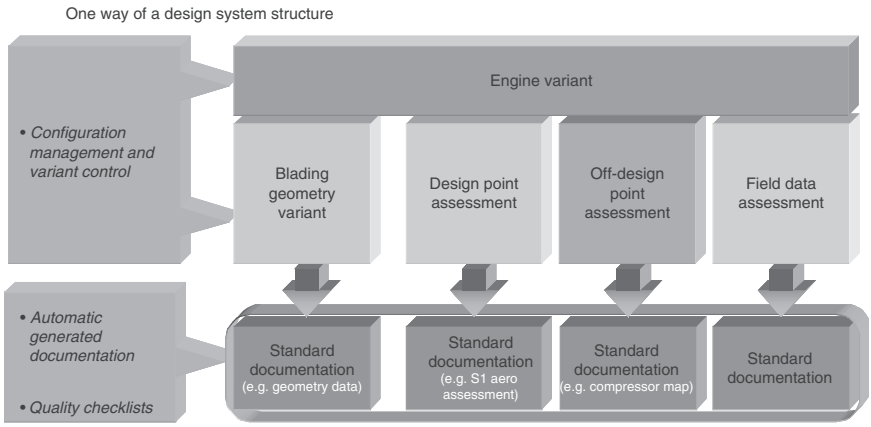
- Automatic generation of links/interfaces between tools and disciplines.
- Quality control through criteria checks and versioning.

One possible setup of this type of design system is shown in Fig. 4.54.

It is also extremely advantageous if this design system can also incorporate automated documentation of results. This is driven by the idea that all development steps should be correct and documented in a comparable way, making comparison between two different variants much easier. A system of this type would have the further benefit of ensuring that all the required documentation is completed and available.

4.7 Technological trends and special features

The basic aims of research in aircraft and power generating gas turbines are usually quite similar: for example, one common focus is efficiency improvement. One general difference does exist, however: in the aircraft industry, gas turbine design is driven by the power/weight ratio and noise conditions; the stationary gas turbine industry, on the other hand, is driven by the need



4.54 Possible design system setup to support development.

to develop designs able to support much higher absolute mass flows, wider operating ranges due to the use of single-shaft applications, and reduced inspection and outage intervals.

Up to the 1990s, fairly repetitive development cycles were carried out, with the focus on understanding and improving the flow around an airfoil, including Reynolds number and secondary flow effects. The resulting technology was known as 'Controlled Diffusion Airfoil' technology, and uses the behaviour of the boundary layer along the airfoil as a design parameter. Furthermore, endwall contouring was tested and introduced, in which the channel contour was modified along the axial length of the blading to compensate for the impact of the airfoil thickness, thereby reducing the peak velocities on the suction side of an airfoil and improving secondary flow interactions. The reduced axial velocity of the channel endwall regions, which is due to the endwall boundary layer, have been addressed by the 'Endbend' designs, in which either the endwall profile section is restaggered and/or the leading edge of the profile is more aligned with the incoming flow angle. A final significant development is the introduction of blading bow and lean technology (bowed staggering of the centre of gravity lines in a tangential and axial direction), which generates additional radial forces, enhancing the control of the flow (see Plate II).

Developments in technology are also addressing aerodynamic, mechanical and commercial issues, mainly driven by the fact that high end computing is increasingly allowing a greater understanding and use of detailed studies, which is in turn removing some previous restrictions. Turbomachinery conferences (such as the ASME conferences) are a useful source of information in this respect and provide details of the different technologies used in vari-

Published by Woodhead Publishing Limited, 2013

ous research programs. The following sections discuss the most outstanding examples of these new technological developments.

4.7.1 Aerodynamically driven technological trends

Various ways of improving the overall compressor aerodynamics are currently under investigation: these focus not only on the design point but also on the improvement or extension of part load operation. Some basic trends are described below.

Efficiency improvement

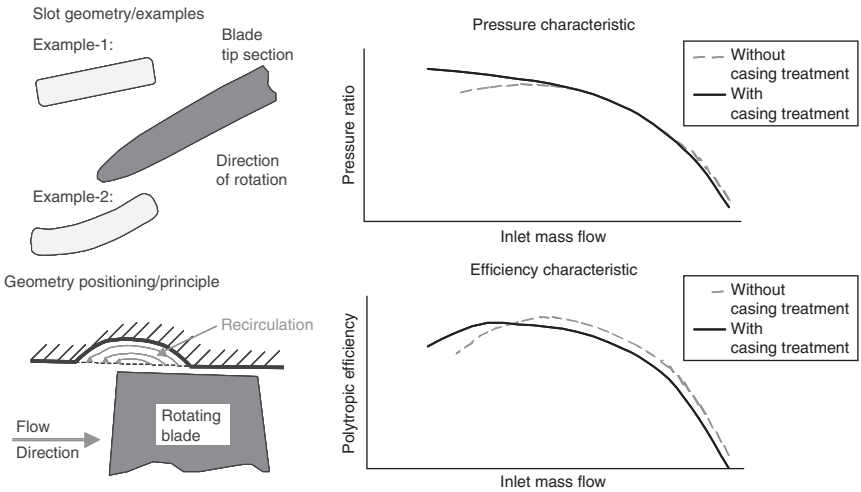
Improvements in efficiency are often directly correlated to the number of blades/stages. In this respect, then, the focus is on achieving higher loadings supplied by the individual blade rows. A limiting factor in flow turning is the boundary layer on the suction side of a profile, due to possible separation in case of overloading. Consequently, one idea is to suck off and/or re-energize the boundary layer flow, at least in this area (Plate III). As a consequence, it is possible to use a reduced number of blades, thereby increasing the efficiency. One research project attempted an extended approach, in which the boundary layer is sucked off and re-energizing is achieved by means of injection inside a closed loop. This would be extremely beneficial in supporting the part load behaviour, but requires complex external hardware.

Both concepts demonstrate potential for improvement; unfortunately, however, the complex hardware and additional control logic required means that detailed risk assessment is required before these can be used in standard industrial applications.

Part load behaviour extension

The 'stand-by' operation of gas turbines has become increasingly important due to the fact that the power grid requests a more dynamic response. This type of engine operation should be considered as a back-up solution in case of a fast peak power demand. It involves the engine running at minimum load, allowing it to transfer to full load within a short time frame. In order to reduce the costs of this stand-by operation, attempts have been made to provide significantly reduced power at a reasonable level of efficiency. Multiple variable vanes have therefore been introduced, which allow the compressor to run with quite small inlet mass flows, sometimes as low as 50% mass flow of the intended original design. However, the efficiency still drops significantly due to the significant misalignment of the aerodynamic loading of the various compressor stages; moreover, this operation

Published by Woodhead Publishing Limited, 2013



4.55 Casing treatment concept to extend compressor surge margin.

can cause surge effects due to the shifting of a high load to the rear stages of the compressor.

In addition to the introduction of multiple variable vanes, different loading concepts for the front stages have also been considered, in order to maintain reasonable efficiencies at strong part loads. In addition, pre-heating systems can be employed to increase the volume flow by keeping the absolute mass flow low; and various recirculation concepts can also be used. These last two improvements have to be implemented on site quite often and are heavily dependent on the available hardware on site.

Surge margin extension

The required aerodynamic speed range and the surge margin constraints often put the optimum efficiency outside the design point of the compressor. To overcome this issue, special features that increase the working range of mainly the front stages have been addressed in a number of research projects. The 'Casing Treatment' is one of these features, and focuses on surge effects triggered by the blade tip flow (see Fig. 4.55). The surge is triggered by two effects: firstly by the strong incidence angle (misaligned incoming flow angle) and secondly by the clearance vortex, which is generated due to the pressure difference at the pressure and suction side, and causes a flow over the tip of the blading. Axial slots in the casing are used to capture and damp this flow inside a cavity above the casing and to re-inject it at a later point, sometimes with a modified flow angle in order to avoid the generation of separation or surge cells. Unfortunately, this procedure often causes

a slight decrease in efficiency and increase in cost and is consequently rarely used in stationary gas turbines.

Noise reduction

Increased power and higher loading figures, mainly for the front stages of the compressor, have been the main focus of research and development for some time. More strict environmental requirements on noise and emission levels have forced this to be reconsidered to a certain extent. Within the aircraft industry, meeting the requirements for noise levels has been particularly challenging, because the fans usually have quite high blading tip section Mach numbers that can generate significant noise levels. Noise is also becoming an increasing concern on the power generation side, as gas turbine plants are often located inside industrial environments with certain legal noise and emission regulations. To overcome this problem and identify potential solutions, a great deal of work was carried out on the development of 3D unsteady CFD codes and on the understanding of corresponding flow phenomena. Today, these codes can be used to predict noise levels and have allowed suitable designs to be drawn up, such as swept blades. The basic concept is to avoid a strong pressure fluctuation line, instead distributing the pressure axially. This allows the same fluctuation energy to be transported but in a more distributed manner, thereby reducing the noise level. Some basic effects of this technology are shown in Plate IV.

4.7.2 Mechanical integrity and manufacturing driven technological trends

Achieving the required lifetime for a compressor by controlling the stress and frequency behaviour of the compressor blading for a reasonable cost is essential. Mechanical integrity and manufacturing considerations are therefore strongly linked: this section describes some basic trends in both fields.

Blade weight reduction

The front stages of a compressor can be quite large and are therefore usually associated with a heavy weight, which the blading root and its corresponding fixation inside the rotor grooves have to take into account. Two basic technologies have been developed to improve this situation: hollow blades and composite blades.

Both blade types are already in industrial operation in the aircraft industry as fan blades; however, the long inspection intervals in stationary power generating gas turbines make their use somewhat limited in this industry.

Published by Woodhead Publishing Limited, 2013



4.56 Application examples of composite material for compressor blading. Image reproduced with the permission of MTU Aero Engines GmbH.

Hollow blades reduce the weight significantly but require intensive development from a mechanical integrity standpoint to ensure reasonable peak stresses and frequency behaviour. Additionally, very detailed risk assessments have to be carried out to take into account the possible effects of foreign objects, including the well-known example in the aircraft industry of a bird entering the blading. Furthermore, the manufacture of these hollow blades is quite challenging; a special technology has been developed for the purpose, to produce separate pressure and suction sides for the airfoil which are later combined.

Composite blades (see Fig. 4.56) have a significantly lower specific weight. By using orientated fibreglass layers, these blades can be trimmed very specifically for stresses and frequencies. Unfortunately, this complex manufacturing process makes the blade quite expensive. In addition, any damage to the fibreglass layer can significantly decrease the allowable stress limits; once a layer is damaged, it can easily react with water and decrease in strength even further. These blades therefore often have a metal coating added, at least around the leading edges.

Leakage reduction by blisk technologies

Compressor blade rows with axial and/or circumferential grooves constantly have to handle some leakages around the root sections, because the pressure at the trailing edge is higher than that of the leading edge and therefore a pressure gradient is available to drive some leakage flow. These small slots

Published by Woodhead Publishing Limited, 2013



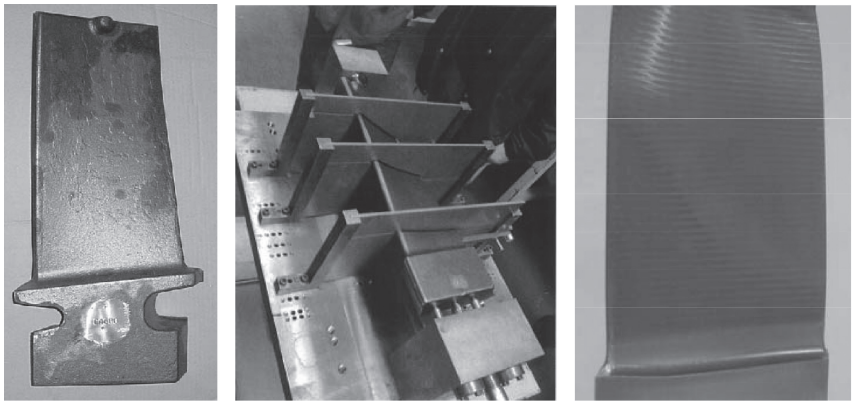
4.57 Application of blisk technologies for compressor front stages. Image reproduced with the permission of MTU Aero Engines GmbH.

between the blade root and the channel contour have some flow devicing impact and must therefore be minimised. Furthermore, the roots at the front stages are quite large and cannot be implemented at low radii, which would allow the radial flow channel shift to be used. All these disadvantages can be overcome with blisk technology. In this case, the rotor shaft contour/disk and the corresponding compressor blading are one (see Fig. 4.57). It is immediately clear that a large block of material is required for manufacturing, and the milling process involved is very time consuming: both of these factors make the application of this technology quite expensive. Another technological development based on the same concept uses a rotor disk and applies friction welding to the individual blade rows on the disk. This involves much lower cost but the welding is a possible failure risk if not carried out correctly. Both technologies offer significant aerodynamic and mechanical advantages but pose some challenges in terms of repair and/or single blade replacement.

Different blading manufacturing processes

Although composite blades have been investigated, the compressor blading is usually produced using some form of steel, or for very highly mechanical loaded profiles, using titanium alloys. These materials are well established and can be used in the three main manufacturing processes of precision forging or preforging, milling and casting.

Forging is generally used for large front stages. Due to the significant improvements in technology in the milling procedures, including in the



Pre-forged blade | Pre-forged blade inside a profile gauge | Milled blade without surface treatment

4.58 Example of a preforged and a milled compressor blade.

corresponding milling machines, less attention is sometimes paid to precision forging, and preforging, a type of rough forging with some material on top, is used instead. Using this approach also allows the forging dyes to be used for a much longer period, because less accurac y is required (example see Fig. 4.58). Casted blades are sometimes used for the rear stages of the compressor, mainly if doubles and/or triples can be implemented to one rack. The casting process is also sometimes used if complex shroud geometries are present. For compressor blades, the milling procedure is most commonly used; today, high surface quality in terms of both accuracy and roughness can be achieved at a reasonable cost. Additional steps are required to treat the final surface: these might include grinding and polishing.

4.8 Acknowledgement

The author wishes to express his highest recognition to all Alstom employees supporting him in developing this comprehensive compressor workbook, but also to the entire compressor community worldwide and to several connected companies for their support, both in terms of figures provided and discussion and feedback offered.

4.9 References

ASME Turbo Expo, yearly conference with papers for turbomachinery technologies and experiences.

Broszat, D., Kennepohl, F., Tapken, U., Enghardt, L., Lengani, D. and Marn, A., Validation of an Acoustically 3d-designed Turbine Exit Guide Vane.

AIAA-2010–3806, 16th AIAA/CEAS Aeroacoustics Conference, Stockholm, Sweden, June 7–9, (2010).
Cumpsty, N. A., *Compressor Aerodynamics*, Verlag Longman Group UK Limited, (1989).
Denton, J. D., 'The Calculation of Three Dimensional Viscous Flow Through Multistage Turbomachines', Trans. ASME, 90-GT-19, (1990).
Horlock, J. H., 'Axialkompressoren', Verlag G. Braun, Karlsruhe, (1975).
Lechner, Ch. and Seume, J. (Hrsg.), *Stationäre Gasturbinen*, Springer Verlag, Berlin Heidelberg, (2002).
Schepers, W. and Hagemann O., Optimierung der On-line- und Off-line-Wäsche an einer 26-MW-Gasturbine unter besonderer Berücksichtigung der Leistungssteigerung. VGB Kraftwerkstechnik 3/99.
Stoff, H. and Kovács P., Vereisung an Gasturbinenverdichtern und Maßnahmen für einen störungsfreien Betrieb. Brown Boveri Technik 4–85.
Traupel, W., *Thermische Turbomaschinen*, Bd. II, Dritte Aufl., Springer, (1982).

4.10 Appendix: variables and indexes

Variables

Pressure	p	(N/m^2)
Blading pressure ratio	Π	(-)
Temperature	T	(K)
Density	ρ	(kg/m^3)
Enthalpy	h	(J/kg)
Entropy	s	(J/kg/K)
Specific gas constant	R	(J/kg/K)
Specific heat	c_p	(J/kg/K)
Efficiency	η	(%)
Flow angle/absolute	α	(deg)
Flow angle/relative	β	(deg)
Flow velocity/absolute	c	(m/s)
Flow velocity/relative	w	(m/s)
Rotational speed	n	(rpm)
Area	A	(m^2)
Mass flow	m	(kg/s)

Indexes

Stagnation value	tot	(-)
Reference value	ref	(-)
Surge value	surge	(-)
Normalised similarity parameter	*	(-)
Mechanical value	mech	(-)
Reduced value	red	(-)

Blading inlet value	inl	(-)
Blading outlet value	out	(-)
Absolute frame of rotation	*a*	(-)
Relative frame of rotation	*r*	(-)
Polytropic	pol	(-)
Isentropic	isen	(-)

Published by Woodhead Publishing Limited, 2013

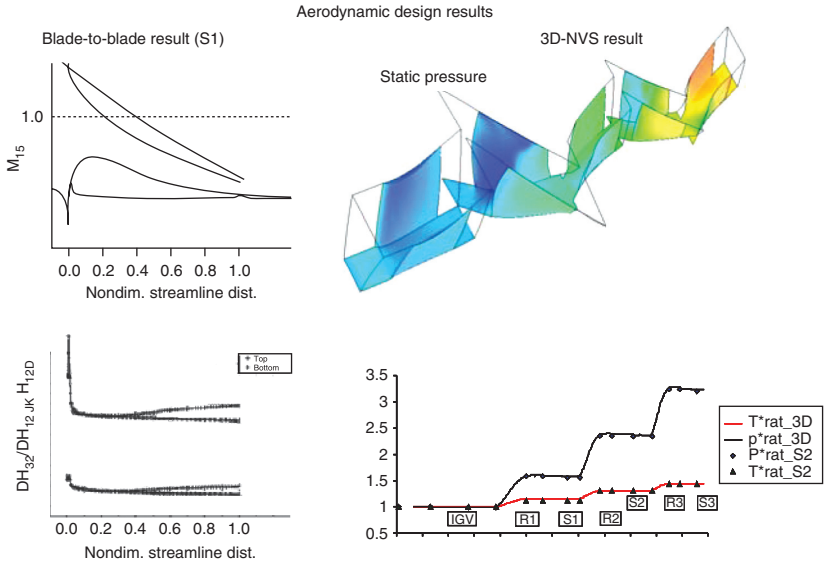


Plate I (Chapter 4) Detailed aerodynamic assessment of sections (S1-surface) and multiple rows.

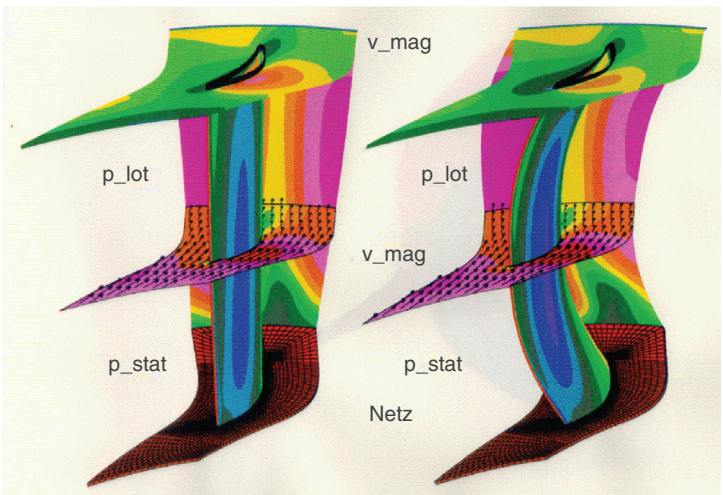


Plate II (Chapter 4) Example of the flow field along a straight and a bowed vane.

© Woodhead Publishing Limited, 2013

Plates.indd 1 9/21/2013 9:21:55 PM

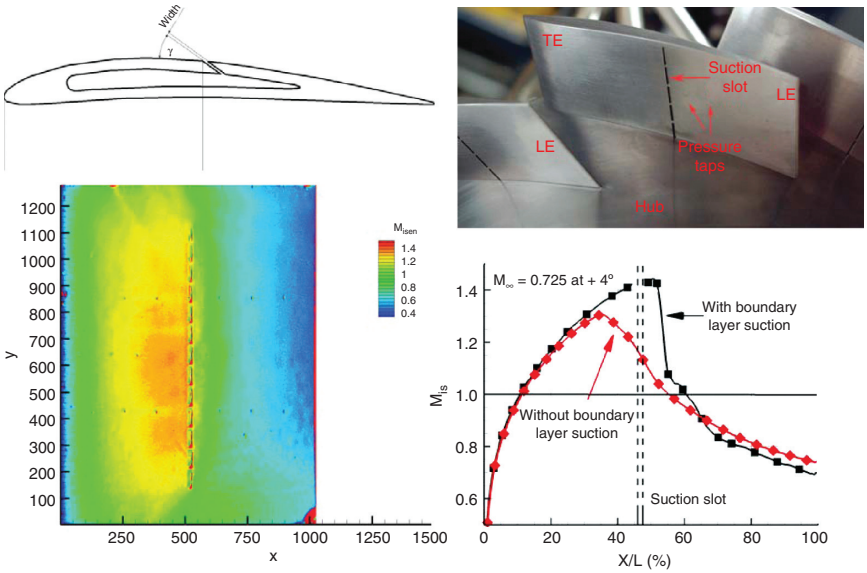


Plate III (Chapter 4) Profile boundary layer flow suction to increase loading range. Image reproduced with the permission of EPFL Lausanne.

© Woodhead Publishing Limited, 2013

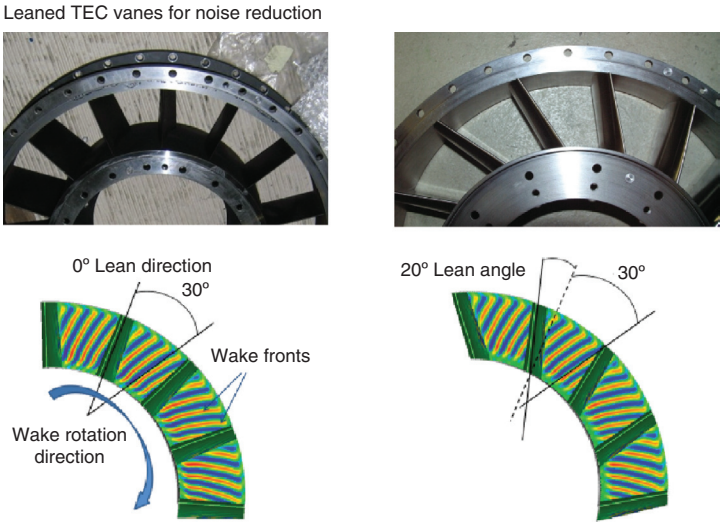


Plate IV (Chapter 4) Noise reduction by leaned vanes. Image reproduced with the permission of MTU Aero Engines GmbH.

© Woodhead Publishing Limited, 2013

5

Combustors in gas turbine systems

P. FLOHR and P. STUTTAFORD,
Alstom (Schweiz) AG, Switzerland

DOI: 10.1533/9780857096067.2.151

Abstract: This chapter discusses combustion systems in gas turbines. It begins by reviewing basic design principles before discussing developments in technology such as advanced fuel staging and reheat combustion systems. The chapter also covers the impact of different natural gas types on combustor operations, including combustor design for low calorific gases and fuel oils.

Key words: combustion systems, combustors, gas turbines, advanced fuel staging, reheat combustion systems.

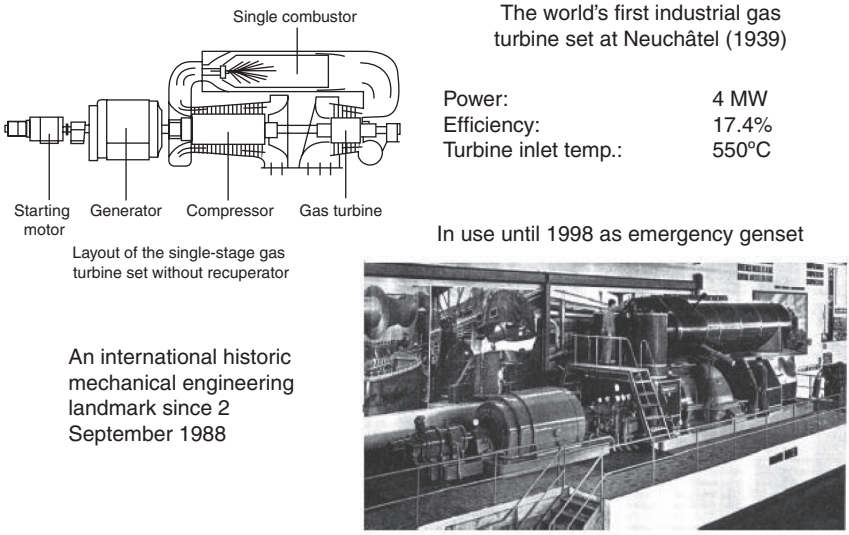
5.1 Introduction

Modern gas turbine combustion chambers have little in common with the combustion system that was used in the first industrial gas turbine at Neuchatel in Switzerland, built in 1939 (Fig. 5.1). The thermal combustion intensity has increased from 10 MW/m^3 up to levels of more than 200 MW/m^3. At the same time, the requirement to meet ever-increasing environmental standards has brought nitric oxide (NO_x) emission levels down from more than 500 vppm to well below 25 vppm. In addition, today's power generation market requires highly reliable and robust combustor components, being able to achieve high flexibility in engine power output, as well as handling a variety of different fuel qualities. Operating efficiency improvement is a key development driver, and the associated higher firing temperatures, while minimizing emissions and parasitic pressure loss, require innovative combustor solutions. This chapter outlines some of the key features that are the building blocks for these requirements of modern gas turbine combustors. While describing the general elements of state-of-the-art combustion technologies, Alstom's combustor systems will be used as examples for best practices applied today.

The chapter is organized as follows:

The first section describes the basic design principles of a modern combustion system for power generation turbines. The first element is the

Published by Woodhead Publishing Limited, 2013



5.1 The first gas turbine for power generation.

choice of a premix burner system with a small pressure drop. The second element is a suitable multi-burner arrangement. The third element is the selection of an appropriate cooling scheme. In the last step, the combustor operation concept, which is the key element for engine integration, is highlighted.

In the next section we address one of the key topics in combustor development from the past decade, namely the development of advanced fuel-staging principles. The fundamental limitation of a premix burner is the lean flame stability limit, that is the amount of excess air which is permitted for stable combustion. During engine start-up and low loads this limit is typically exceeded, and flame stability could be reached only by reverting to simple non-premixed combustion. Non-premixed combustion is very stable, but results in higher emission values. Therefore, the implementation of premix combustion for the widest possible load range by means of fuel-staging principles has been a field of active work for all manufacturers, and such staging concepts will be discussed here.

An alternative way of fuel staging is given by reheat combustion. In a separate section we discuss the basic working principle of this combustion concept, which affects the engine architecture. By explaining the complementary flame stabilization mechanisms of reheat combustion it will become clear why this concept is well suited to operate over an extreme range of load conditions with low emissions. An alternative is to stage the combustor in such a way that the burner is divided within one combustor and separately optimized for operations at minimum load and full load points.

Published by Woodhead Publishing Limited, 2013

A modern combustor must also be able to handle a variety of fuels, ranging from fuel oil to more exotic fuels such as low calorific gases. The full range of fuels is explained in a separate chapter of this book, but we will touch briefly on the implications of different natural gas qualities for combustor operation, and a brief overview of a typical combustor design for low calorific gases, as well as the use of fuel oil as backup fuel.

We conclude with a brief overview of future trends in combustor development.

5.2 Design principles

Gas turbines are designed for increasingly higher turbine inlet temperatures. This increasing temperature requires a step-by-step experience-based development procedure, and validated design principles, on all hot gas path components as far as fulfilling lifetime requirements are concerned. In addition, it becomes increasingly difficult to achieve emissions targets, due to an exponential relationship between combustor flame temperature and NO_x emissions.

This section describes the basic design principles of a modern combustion system for power generation turbines, focusing on applications as implemented in the Alstom gas turbines (Eroglu *et al*., 2009). The first principle is the choice of a premix burner system with a small pressure drop. The second principle is a suitable multi-burner arrangement. The third principle is the selection of an appropriate cooling scheme. In the last step, the combustor operation concept, which is the key element for engine integration, is discussed.

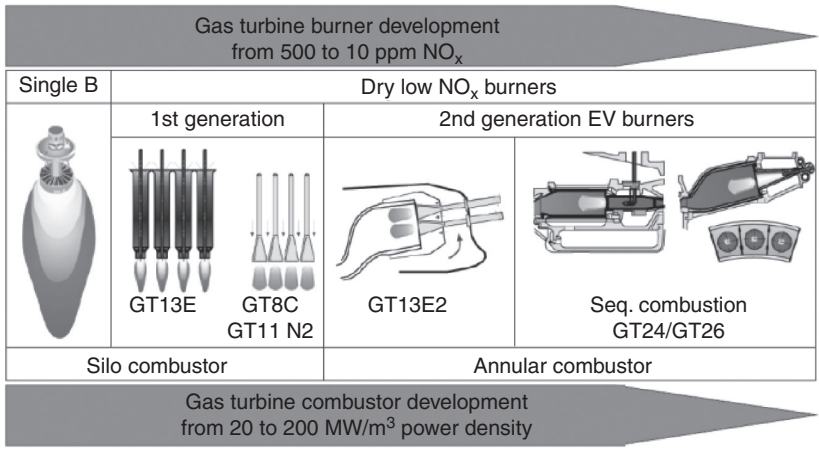
5.2.1 Premix burner

The main component of a gas turbine combustor is the burner itself. The key design requirements for a burner are:

- safe and reliable operation,
- good combustion efficiency, and
- low emissions.

The functional elements for such a burner are typically the fuel injector, a mixing device, and a flame holder.

During the past 30 years, these burners have evolved from large, single diffusion burners, to compact premix burners in multi-burner arrangements, see Fig. 5.2. Detailed descriptions of the development evolution can be found in Döbbeling *et al*. (2005) and references therein. The actual design



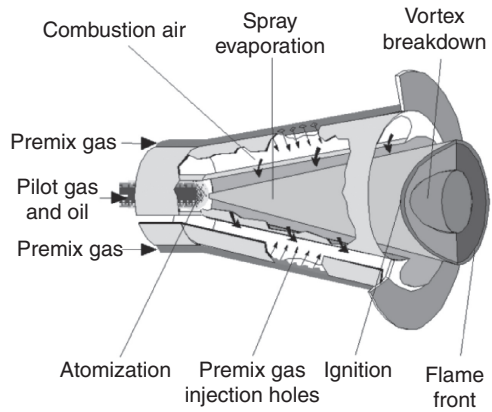
5.2 Important milestones in the burner and combustor development at Alstom.

and shape of modern premix burners has varied significantly, to the present day, between the different manufacturers, but the key design features are common:

- Distributed fuel ports in combination with highly swirling flow are used to achieve good fuel–air mixing for premix combustion.
- Multiple fuel injection systems, that is, two or more independent fuel control lines, are used to achieve stable combustion for the entire load range.
- High flow velocities inside the burner premixers are needed to avoid flame flashback.
- Flame anchoring is ensured by reversed flow, caused by central vortex breakdown in a highly swirling flow, or a reversed flow about a low swirl, robust stagnation point

As a specific design example, we describe the premix burner design from Alstom, the EnVironmental (EV) burner. It has been developed through a number of evolutionary step-by-step modifications.

The basic EV burner operating principle is shown in Fig. 5.3. Air is fed into the slots generated by two radially displaced half cones. Inside the burner cone a swirling flow is generated. As the air passes through the slots, premix gas is evenly distributed in the air before being further mixed inside the cone section of the burner. When the vortex flow expands upon entering the combustion chamber, a central reverse flow field is generated (called vortex breakdown) in which the flame front can stabilize without attaching to the metal surfaces of the burner.



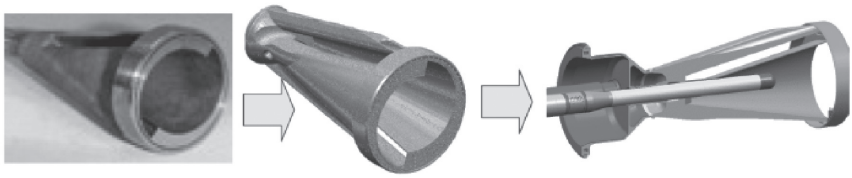
5.3 The EV burner principle.

A second fuel injection point is at the head or apex region of the burner where pilot gas is injected. The pilot gas remains concentrated on the burner axis so that a diffusion flame is formed for low load operation and gas turbine start-up. As the load is increased, premix fuel can be introduced, spreading the fuel in all the supplied air for low emissions and the pilot is deactivated.

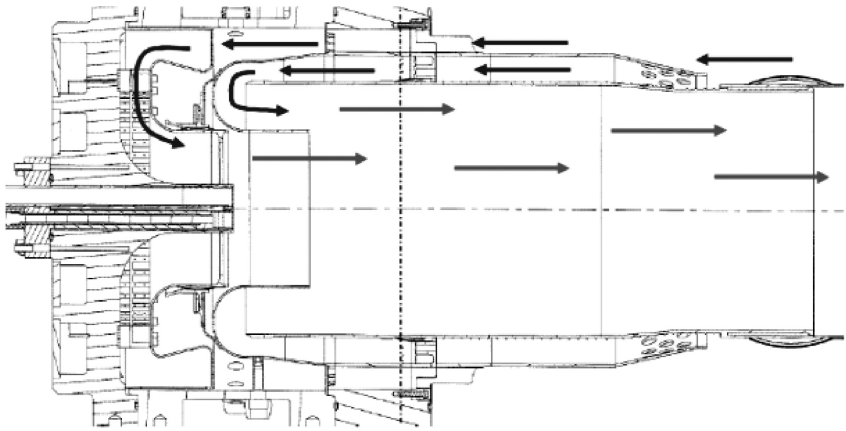
The EV burner was first introduced in GT11N engines with silo combustors in 1991. It has been since then successfully implemented in GT8C, GT13E2, GT11N2, GT24 and GT26 engines. A number of evolutionary step-by-step modifications have been implemented in the EV burner, in order to reduce emissions and to improve overall performance. The design optimizations include improvements of the swirler aerodynamics, optimization of the fuel injector distribution, and an adjustment of the central fuel lance position (Paschereit *et al.*, 2002), as shown in Fig. 5.4. The most recent design variant, currently used in the GT26 engine fleet, has eliminated completely the central diffusion flame (Zajadatz *et al.*, 2007), and this is described in more detail in the next section.

A further design example is that of the Alstom FlameSheet Combustor (Stuttaford *et al.*, 2010). The FlameSheet combustor is a dry lean premixed combustion system, designed specifically for extended turndown and fuel flexible operation. The name derives from the method used for injecting the fuel–air mixture as a continuous uninterrupted sheet into the reaction zone of the combustor, whereupon an aerodynamically generated trapped vortex is utilized to anchor and stabilize the flame.

The combustor consists of two aerodynamic stages and multiple fuel stages. The stages are designed for specific operational issues, such as transient loading and extended turndown operation. The two aerodynamic stages



5.4 The evolution of the EV burner.



5.5 Overall flow design of the FlameSheet system.

consist of a pilot along the axis of the combustor and a main stage surrounding the pilot. Figure 5.5 illustrates the overall structure of the FlameSheet system. The pilot and main stage are fed from a compressor discharge plenum. Pilot air passes in the radially outermost circuit to the head end of the combustor where it enters a radial inflow swirler. Fuel is mixed into the air stream through a row of vanes. The fuel–air mixture enters the combustor, and a flame is swirl stabilized behind a bluff body on the centerline of the combustor. The main stage air flows along the backside of the combustion liner, and then through a main fuel injector. The fuel–air mixture is then turned 180° and flows into the combustor. As the flow enters the combustor it separates and forms a strong recirculation, or aerodynamically trapped vortex, which stabilizes the flame.

5.2.2 Combustor design

The combustor provides the geometrical boundary of the combustion space within the gas turbine. The key design requirements for a combustor include:

- integration of the burner into a multi-burner arrangement;
- stable operation for an entire engine operation envelope;
- homogeneous hot gas temperature profile for the turbine inlet plane;
- minimal losses (pressure drop and heat), and;
- robustness, maintainability and low cost.

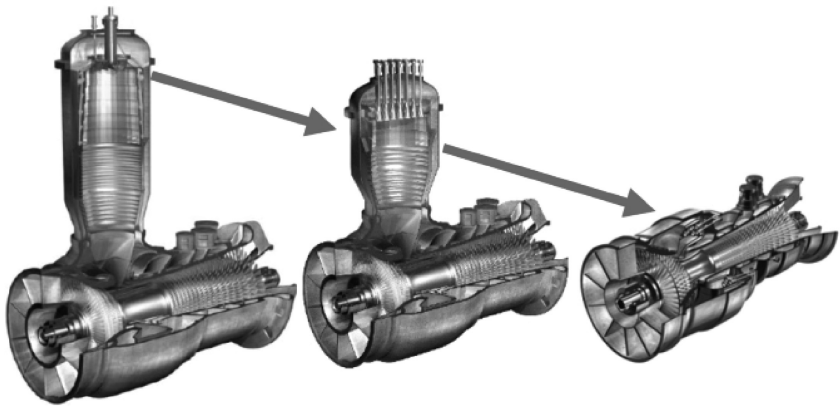
The functional elements for combustors include burners or groups thereof, hot gas liners, cold carrying and casing structures, and fuel distribution systems.

As for the burners themselves, the actual design and shape of modern premix combustors has varied significantly between the different manufacturers until today, but many of the key design features are in fact common:

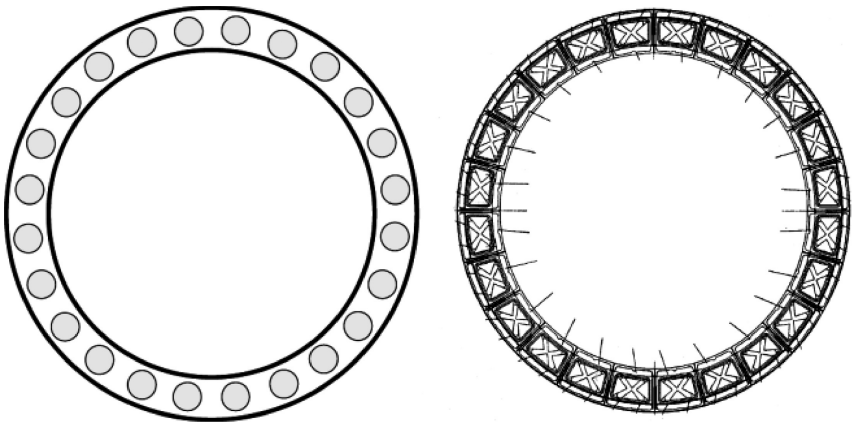
- A compact combustion space is chosen to minimize NO_x emissions, with a minimum volume requirement given by CO burnout times.
- The injection of cooling flow downstream of the heat release zone is avoided, to maintain lowest possible flame temperatures.
- Thermal barrier coatings (TBCs) are applied to the hot gas liners.
- A number of parts of the combustor are retractable from the engine casing (fuel lances, burners, or cans) for ease of maintenance.
- The flame distribution and air management is such that the temperature distribution at the combustor exit is highly homogeneous.

Traditionally, industrial and heavy-duty gas turbine combustors have been of the silo type. This type of design was preferred for robustness and ease of maintenance. However, the cooled surface per unit volume is known to be high for this geometry. Moreover, turbine inlet temperature distribution is highly non-uniform and the cost of the combustor and the space required was high. At Alstom, the combustors have evolved through various steps since the early 1990s. Starting from single diffusion burners in a single silo combustor, multiple premix burners were implemented in a single silo combustor, and finally multiple burners were integrated in compact annular combustors. The development steps are shown in Fig. 5.6. Today's compact combustors require significantly less cooling air and provide a much more uniform turbine inlet temperature distribution (Eroglu *et al.*, 2009), and other manufacturers have since adopted similar design principles.

Today, essentially two types of annular combustors are used at Alstom. The EV and the Sequential EV (SEV) combustor (which will be described in a subsequent section in more detail) of the GT24/GT26 engines are typical examples of single-row combustors, as shown in Fig. 5.7. In the case of the GT26, 24 burners each for the EV and SEV are used. The second type of annular combustor is the EV combustor of the GT13E2, with a multi-row



5.6 Transition from a single-burner combustor via a multi-burner silo to an annular combustor.

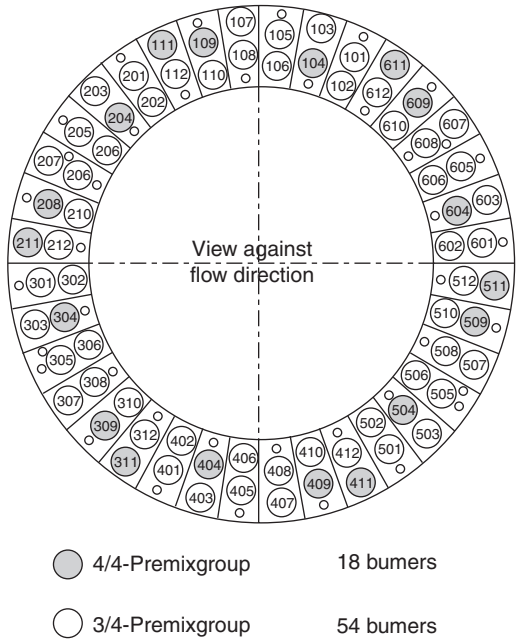


5.7 EV and SEV single-row annular combustors in the GT26 configuration.

arrangement of 72 burners in four rows, similar to the sketch in Fig. 5.8. In this case, two types of burners are mixed with clockwise and counter-clockwise swirl direction. This configuration has been selected during the concept phase, due to optimal mixing properties and most homogeneous flow profile within the annulus. In this multi-row annular combustor it is possible to form several staging patterns within different groups of burners, to cope with a variety of pulsation and extinction topics with very small deterioration of the combustor exit temperature profile.

The introduction of annular combustors with the distribution of multiple burners around the circumference of the engine has brought significant advantages, for example:

Published by Woodhead Publishing Limited, 2013

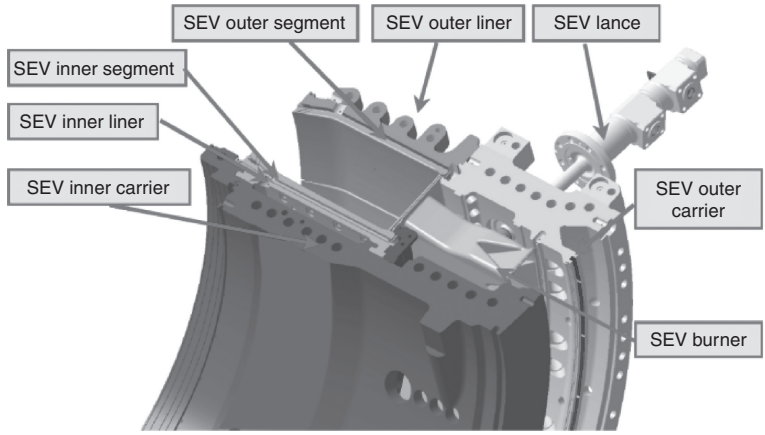


5.8 EV double-row combustor in the GT13E2 configuration.

- The hot combustor surface (which is exposed to the flame) is minimized, and thereby the cooling air consumption required is automatically minimized.
- The annular combustor generates naturally a very homogeneous hot gas temperature distribution, which is key for long turbine lifetime.
- Cross-ignition between individual burners is ensured without the need for cross-fire tubes or multiple ignition torches.
- Operation at part load or full load with burner groups at different flame temperatures is possible. Burners which are running below the extinction point are stabilized by their neighbors, and the shearing flow in the combustor leads to homogenized exit temperature profiles.
- The annular design is compact and cost-effective compared to single or can combustors.

The basic design of the EV and SEV annular combustors consists of a ring-shaped combustion volume between inner and outer combustor liners, as shown in Plate V (see colour section between pages 346 and 347) and Fig. 5.9. A combustor front panel is used to install individual burners which are fired in this volume. At the downstream end of the combustion volume, a contraction accelerates the flow into the first vane of the turbine.

Published by Woodhead Publishing Limited, 2013



5.9 Main components of the GT24/GT26 SEV combustor.

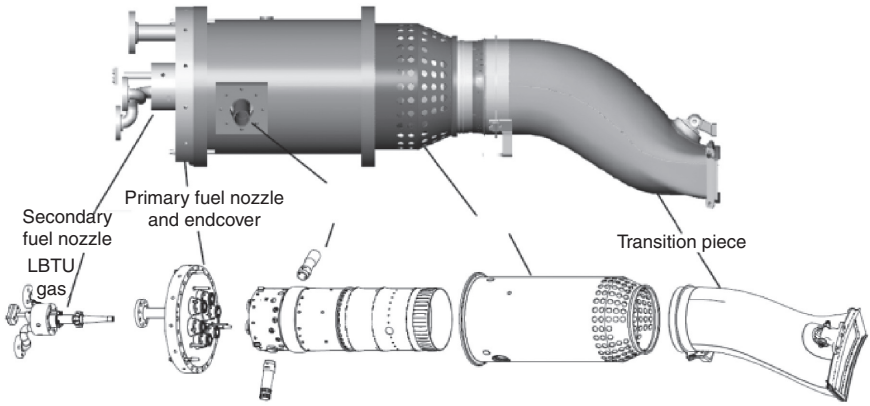
Inner and outer liners are basically cold carrying structures and they are shielded against hot gases with discrete segments, which are cooled by the combustion airflow along the backside. These casted segments can be replaced and reconditioned at regular intervals. In addition to the backside cooling, the segments are protected on the hot side with a TBC. The number of segments is the same as the burner number, which ensures a repeating hot gas loading and cooling pattern for all segments.

Both, burners and lances can be retracted in the EV combustor without opening the engine. In the SEV combustor, the fuel lance can be retracted, thus allowing easy inspection of both combustors.

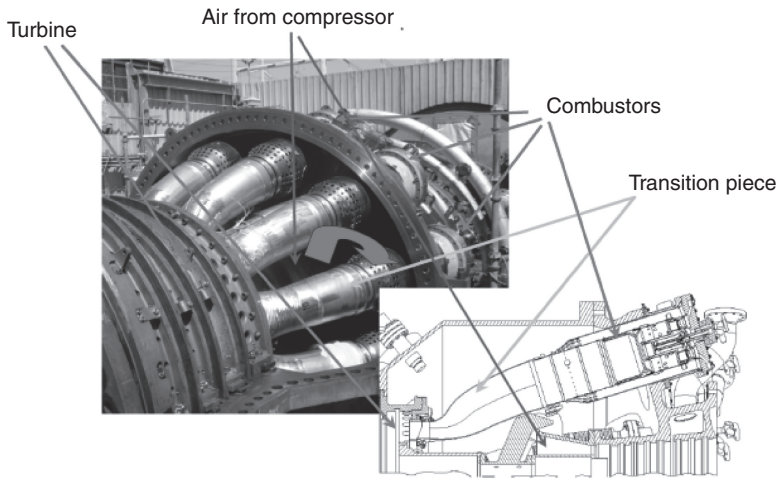
Multiple can combustors have additional advantages in their modularity for installation and removal as simple individual units, while allowing flexible modular upgrades, all without opening the engine. Often, the number of cans required by a specific unit is adjusted depending on whether implementing the system on a 50 or 60 Hz machine while maximizing the use of identical hardware. The Alstom FlameSheet and LEC-III® combustion systems are examples of such systems. In both cases, an array of combustion cans (typically 10–20 cans) is arranged around the engine centerline providing hot air via a transition piece to the turbine. The LEC-III®, which is currently in operation on more than 40 machines, evolved from a 25 ppm NO_x system to a sub-5 ppm guaranteed NO_x system through a number of cooling and mixing development enhancements. An example of the LEC-III® burner arrangement is shown in Fig. 5.10. The engine arrangement of such a combustion system is shown in Fig. 5.11.

5.2.3 Cooling

The combustor liners are cooled with a serial cooling scheme, as shown in Fig. 5.9.

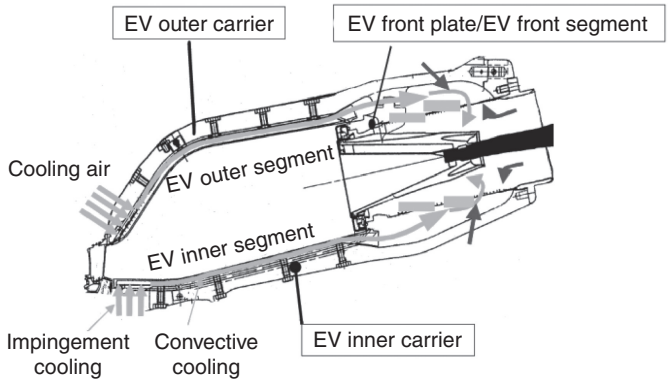


5.10 Components making up the sub-5 ppm NO_x LEC-III® combustion system.



5.11 A typical can combustor layout with the Alstom LEC-III® combustor implemented on a Siemens 501D5 machine upgraded and now operating below 5 ppm NO_x.

The cooling air enters the cooling passage at the downstream end, through a number of impingement holes, ensuring locally high heat transfer rates through impingement cooling in this highly loaded area (Fig. 5.12). The rest of the liner segments are cooled convectively, augmented through various turbulators and rib combinations. The liner segments are installed on rails, with highly compliant seals, which reduce leakages down to only a few percent. Individual gaps between liner segments are purged against hot gas ingestion with precisely designed gap-purging holes. The front segments are cooled with



5.12 Cooling of casted-metal liner segments.

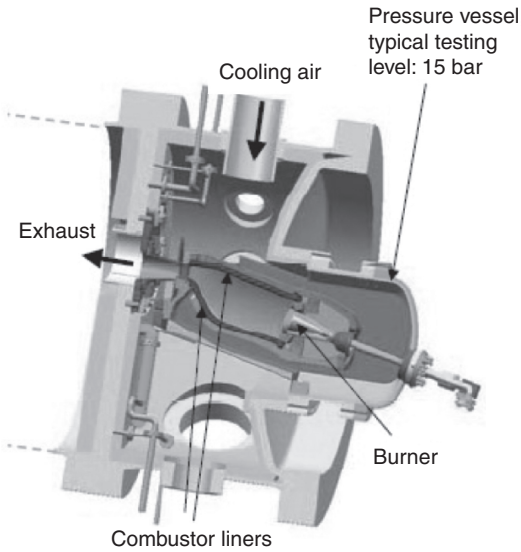
impingement cooling combined with film cooling and a TBC layer on the hot side.

It is emphasized that testing, from feature to full engine tests, is key for successful combustor development. Combustion tests to understand stability and emission behavior of premix combustion are well established. As an example for other advanced testing methods carried out at Alstom, it is reported that a series of full-scale, full-pressure sector tests has been carried out as part of the validation program for the cyclic lifetime of combustor liners with an improved cooling scheme. A schematic of the rig is shown in Fig. 5.13. Thermal loading of the segments can be simulated in this rig with a cyclic pattern as indicated in Fig. 5.14. Results of this type of cyclic test series, in combination with thermal paint test results as shown in Plate VI, were used to validate mechanical integrity calculations of the segments.

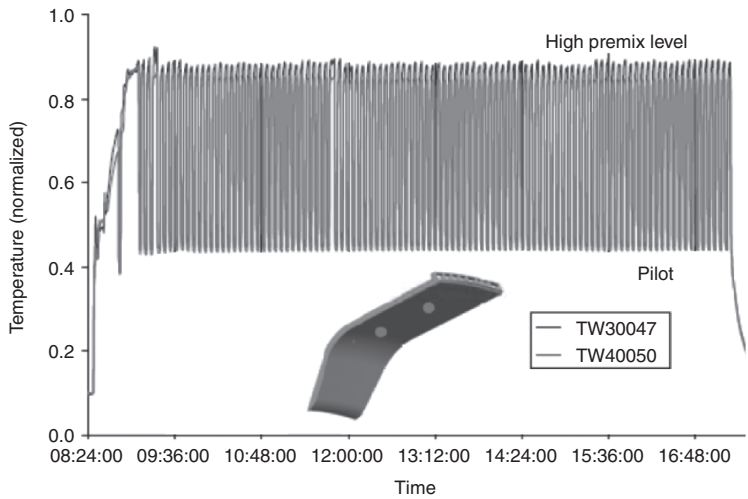
Different sealing geometries are used for the sealing of combustor parts, ranging from rope seals to C- or double-E, or even brush seals. An example is given in Fig. 5.15, showing the sealing of a longitudinal gap between two liner segments with a double-E seal. Several test rigs, such as impact-, fretting-, fatigue- and leakage-rigs, have been utilized to optimize the sealing and lifetime characteristics of different seal concepts. Finally, selected seals have been implemented in the GT26 test power plant in Birr, Switzerland, and validated before field implementation.

5.3 Combustor operation

As an example for a typical combustor operation concept of a standard gas turbine, the GT13E2 operation concept is described here. The discussion includes an upgrade that has been implemented in the existing fleet.

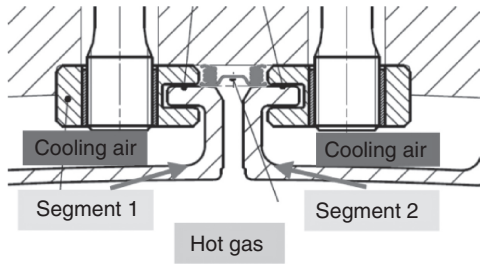


5.13 High pressure rig for liner segments.

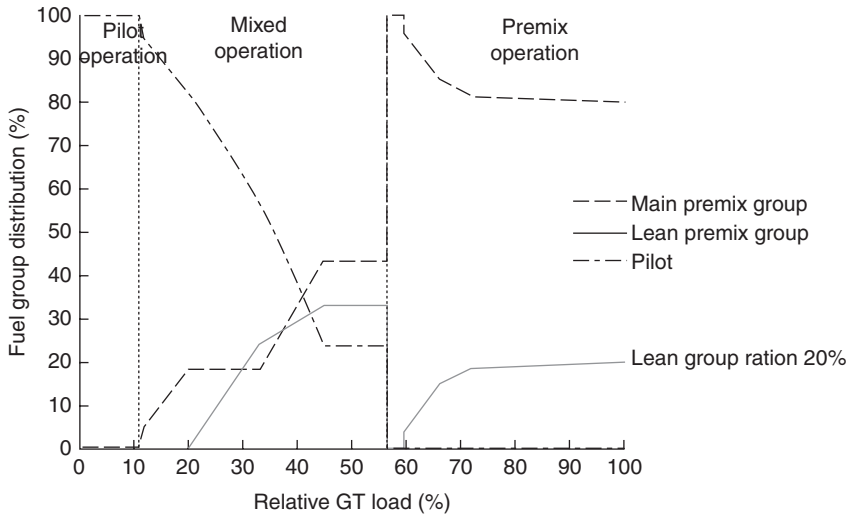


5.14 A typical cyclic thermal loading pattern in sector tests.

Figure 5.16 shows the basic elements of the operation concept. The GT13E2 engine is started with the EV burners in pilot mode (diffusion flame) operation. As soon as combustor stability is sufficient for reliable operation, the main premix groups are taken into operation between 10% and 20% load. From medium load onwards, between 50% and 60% load,



5.15 A typical sealing geometry for liner segments.

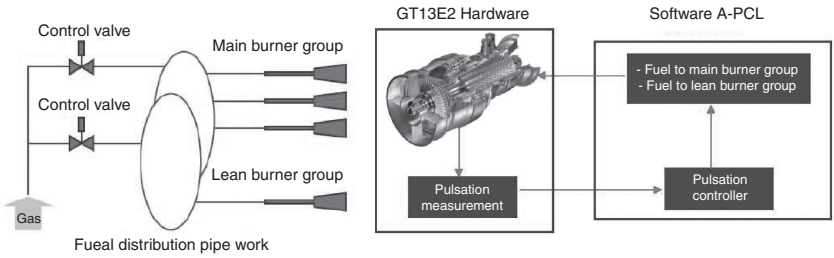


5.16 GT13E2 operation concept.

the pilot mode is switched off completely and the engine is operated with the premix burners only.

For optimal combustion control two premix groups are applied, a 'main' premix group and a 'lean' premix group. The division between the groups is such that three-quarters of the burners are in the main group, and a quarter of the burners are in the lean group, Fig. 5.17. The lean premix group operates at or below the lean stability limit, and its combustion is supported in the annular combustor by the main premix group. This additional degree of freedom allows the combustor to operate stably at all load conditions.

In 2005, an upgrade of the combustor was implemented by introducing a closed-loop (i.e., feedback) controller, which is used to automatically adjust the main and lean premixed groups for constant combustion stability



5.17 GT13E2 APCL.

even if ambient conditions or fuel composition changes (Döbbeling *et al.*, 2008).

From field experience it was found that across the entire range of ambient conditions, gas compositions, and gas turbine loads, the stability limits of the combustor can change, requiring time-consuming, regular local adjustments. To overcome this restriction, the correlation between the lean blow-out limit of the combustor and the occurrence of low frequency pulsations was used to implement an Advanced Pulsation Control Logic (APCL), which constantly monitors the flame stability by pulsation measurements and adjusts the gas distribution according to known characteristics, such that the combustor operates stably but with minimal emissions.

Another example of an automatic tuning system is given in Stuttaford (2011). It has been developed and fielded on multiple GT units, which ensures emissions compliancy in operation while maintaining acceptable levels of frequency pulsations to avoid unit trips and maximize the hardware operating life.

5.3.1 Staged premix combustion

All manufacturers of power generation turbines have pursued the development of advanced fuel-staging principles over the past decade (Lefebvre, 1999). This work was motivated by the lean flame stability limit of premix combustion, that is, the amount of excess air which is permitted for stable combustion. During engine start-up and at low loads, this limit is typically exceeded.

In principle, there are four ways to overcome the limit. First, one reverts to non-premixed combustion mode, accepting the high emissions associated with it. Secondly, air to the combustion zone is restricted in such a way that the excess air in the flame zone is reduced. To some degree this can be achieved by variable guide-vanes in the compressor to limit the mass flow for a given power output; implementation of air staging within a combustor is, however, generally impracticable. Thirdly, one applies fuel staging within

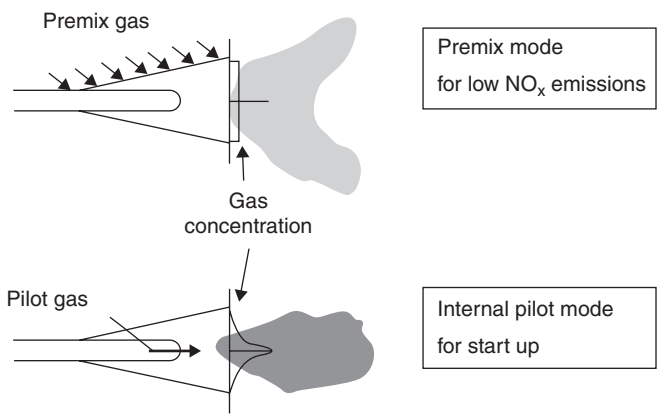
a group of burners circumferentially, or even axially. Effectively, this staging principle creates an 'air by-pass' through a set of burners that are not in operation in the low load operation regime. An example of this configuration is described in the next section. Finally, the burner itself is optimized with fuel staging, such that the use of non-premixed diffusion combustion can be avoided.

A case study is given here as one example where a burner system, in this case the Alstom EV burner, has been improved, such that the need for diffusion combustion could be avoided altogether.

Staging concept

In Fig. 5.18, the operation with the standard EV burner is shown schematically. This burner is operating with pilot fuel gas injection at gas turbine start-up and low part load. The pilot gas injection with the central pilot fuel lance leads to a fuel rich core in the EV burner flow field. Under those conditions, a broad operation range with respect to flame extinction and pulsations can be generated, but emission levels are high when the pilot is in operation. To avoid high emission levels, the burner must be switched over with increasing load to premixed operation to provide an evenly distributed fuel gas concentration at the burner exit. In this case, the fuel injection is accomplished over the premix fuel gas injection system in the air slots of the EV burner, which is a pattern of distributed small gas injection holes. The pilot gas injection is turned off in order to achieve lowest NO_x emissions.

A development project was carried out with the target to eliminate the pilot system, while maintaining good combustion stability over the entire



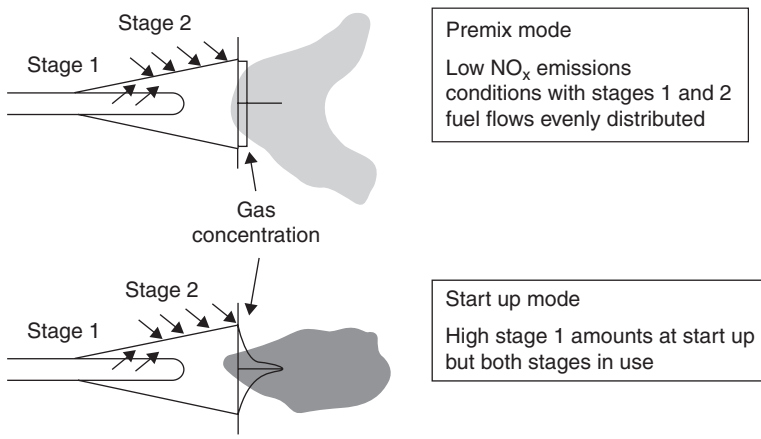
5.18 The operation modes of the standard EV burner with pilot and premix operation.

load range. A number of variants were investigated (reference Martin's paper), and the final design solution with staged-fuel injection is described here.

The EV burner with staged-fuel gas injection is shown in Fig. 5.19. Fuel is injected over two separate gas injection patterns termed as stage 1 and stage 2. The stage 1 fuel is injected upstream of the lance tip in radial direction, while stage 2 is injected at the air slot of the EV burner. Both stages are in use over the complete gas turbine acceleration phase and load range. During start-up and low load, a significantly higher amount of fuel is fed in the stage 1 through the lance. Therefore, similar to the pilot/premix EV, a fuel rich core in the flow field can be generated, which produces a stable flame. At higher load more relative fuel flow through stage 2 downstream in the EV air slot has to be generated to provide (in addition with the remaining stage 1) an even fuel distribution at the burner exit.

The injection of fuel gas is still divided between the burner air slots and the center of the burner cone, but the additional fuel–air mixing in the core flow has multiple advantages. The staging layout allows a closer control of the homogeneity of the premix mixture at the flame front. In addition to the reduced NO_x emissions, the staged concept gives the possibility of adjusting the burner characteristics on-line in response to changes of the operation, and it simplifies the auxiliary systems required by the combustion system because both fuel systems are in continuous operation.

The additional advantage of this staged system is that no redesign of the EV burner itself is required. This staged concept can be simply applied by modifying the gas injection hole pattern at the fuel lance and the EV burner.



5.19 The operation modes of the staged EV burner with premix stages 1 and 2.

The key advantage of an EV burner with a staged premix gas injection is simplified operation concept without premix pilot switchover procedures. This allows a fast and reliable reaction of the gas turbine in transient operation such as frequency response and load rejection. As both fuel stages are kept in operation over the complete load range, the previously required nitrogen-based purge of the fuel lines, on switching from pilot to premix, can be avoided for gas operation.

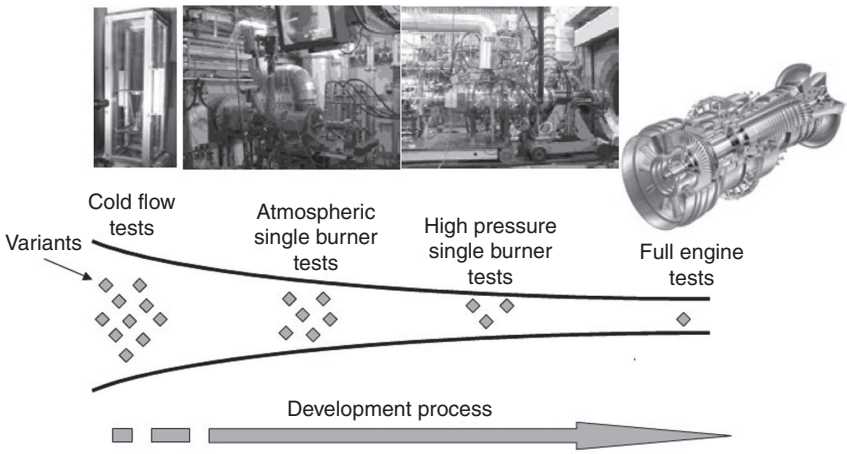
The LEC-III® and FlameSheet can combustors also require fuel staging to ensure robust flame stability over the gas turbine load range. In both cases a centrally located fully premixed pilot is used for initial light-off and low load operation. The main burner is wrapped around the pilot and is fueled as the unit is ramped up in speed and load. The pilot burner fuel–air ratio is maintained at a high enough level to ensure the combustor does not flameout until the main burner flames are fully lit. At this point the pilot burner fuel–air ratio may be reduced to optimize emissions without negatively impacting the stability of the combustor. In the FlameSheet the main burner stage is also circumferentially staged to provide greater flexibility in ensuring the transient stability of the combustor while also allowing a further dimension for optimization of combustion pulsation and emissions.

Mixing properties

To improve the combustion performance of the EV burner, various stage 1 patterns have been designed, to vary penetration depth, mixing length, azimuthal orientation within the cone, etc. In a first step, the mixing and aerodynamic properties of these variants were calculated by CFD. Plate VII shows the EV burner slots with the fuel injection ports, as well as a fuel lance for staged gas injection. The fuel lance has a multi-hole fuel injection pattern, which allows the calculation of the various design parameters. One such parameter was the definition of the appropriate fuel momentum of the injection on the fuel lance, in order to adjust the fuel penetration into the passing air stream. In order to minimize the risks and costs within the development phase, a funneling approach has been applied (see Fig. 5.20), where a large number of variants are tested in the first development steps and only the most promising are promoted to the next steps, with the target of obtaining one single variant for validation in the gas turbine itself. The first step usually consists of cold flow tests for the flow field and mixing investigations, then the burner is tested under atmospheric pressure conditions, and finally under high pressure conditions, before gas turbine validation.

The water channel provides a cost-effective and flexible way to investigate turbulent flow and mixing phenomena within a gas turbine burner, as

Published by Woodhead Publishing Limited, 2013



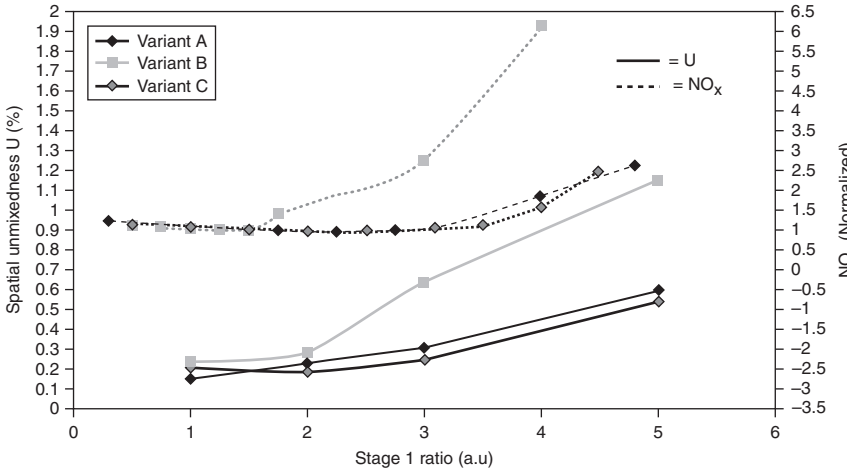
5.20 Experimental burner development process.

several non-invasive laser-based measurement techniques can be applied in water, and its density allows for sufficiently high Reynolds numbers. For mixing studies the laser-induced fluorescence (LIF) technique is used where water containing a small concentration of a fluorescent dye is injected in the burner to simulate fuel injection.

An example of the mixing fields produced by LIF tests during the variants selection step of the staged EV burner development is presented in Plate VIII. It is clear that variant B has a fuel rich core which can possibly lead to high NO_x emissions, while the other two variants, especially variant C, show a more uniform fuel distribution and therefore better potential for low NO_x. To quantify mixing quality, a spatial unmixedness parameter is used, defined by average and root mean square values of pixel concentrations in the LIF. Figure 5.21 shows that the correlation between spatial unmixedness and emissions measured in atmospheric combustion experiments was well established.

It was also instructive to compare the mixing fields of the staged EV burner with the mixing field of the original design. It appeared that with appropriate choice of stage 1, it was possible to achieve a better mixing than in the standard case, that is, a more uniform concentration distribution, see Plate IX. Indeed, the NO_x advantage that became apparent during early development could be later exploited in the final design.

A key mixing design feature of the LEC-III® and FlameSheet can combustors is that the air is mixed into the fuel, rather than the fuel mixed into the air. Since around 96% of the working fluid in an F-class premixer is air, such a strategy provides good mixing with low cycle parasitic pressure loss. A further benefit is that, since the momentum of the fuel exiting the injector



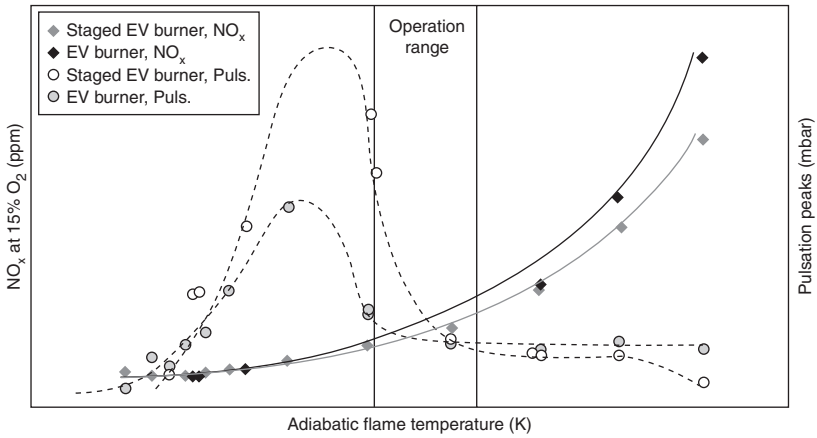
5.21 Correlation between unmixedness of mixing field (waterlab) and NO_x emissions (atmospheric combustion tests).

is dependent on the constituents of the fuel, minimizing the effect of fuel jet momentum minimizes the changes observed in combustor performance as the properties of the fuel vary.

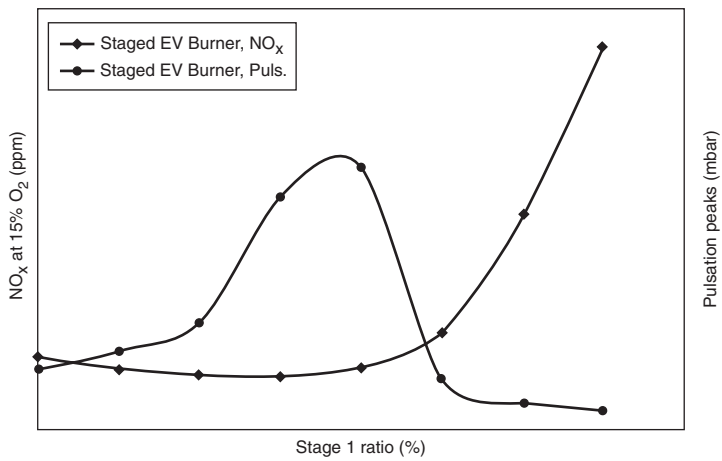
Flame stability

Atmospheric single-burner tests were used to evaluate design variants in terms of pulsations and emissions. For natural gas combustion, the behavior of the flame, regarding shape and position relative to the burner exit, is independent of the operation pressure as long as other parameters like preheat temperature, burner velocity, etc. are kept the same as under engine conditions. The rig length was, however, adjusted such that it matches the pulsation frequency spectrum that is typically observed in the gas turbine itself.

Figure 5.22 shows NO_x emissions and combustion forced pulsations as a function of flame temperature for the standard EV burner and the staged EV burner. For the plot shown here the burner is operated with a constant stage 1 ratio. For high flame temperatures, the staged EV burner shows lower NO_x values; for low flame temperatures, the range of low pulsations is clearly extended. The additional degree of freedom for the staged EV burner is shown in Fig. 5.23. For constant air and flame temperatures the stage 1 ratio is varied. The minimum NO emissions are reached with a stage ratio between 20% and 30%. With the variation of the stage ratio, the mixing of air and fuel can be changed. This means at higher engine load levels where low emissions are favored, the mixing is optimized regarding emissions, and at lower load



5.22 NO_x emissions and pulsations against adiabatic flame temperature.

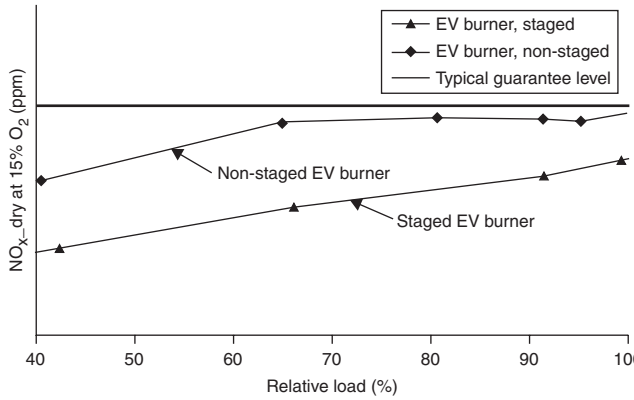


5.23 NO_x emissions and pulsations against stage 1 ratio, for constant flame temperature.

operation modes, the stage ratio is optimized for high flame stability and sufficient blow-out margin.

Emission characteristics

To conclude this section, the emission characteristics of the staged EV burner are compared to the standard EV burner, as implemented in the GT26 engine, in Fig. 5.24. This graph shows two effects: firstly, emission levels



5.24 NO_x emissions of the staged and standard EV burners, measured in the GT26.

are reduced and thus confirm the expected improvement of the staged combustion principle. Secondly, the emission gradient is changed over a wide load range (in this plot between the measured points between 65% and 100% load). This change in gradient is interesting, because it is a direct consequence of the optimization described earlier. The emission levels of the EV combustor are now so low that the total emissions of the engine start to become dominated by the SEV combustor.

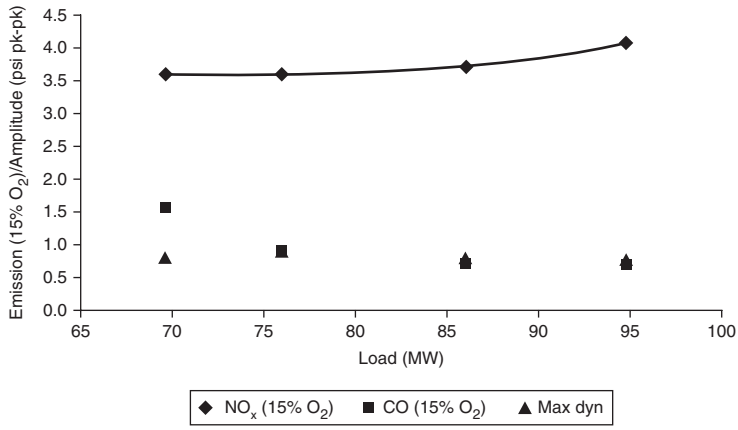
As will be shown in the next section, the fuel input in the SEV is increased with load, and, as a result, now visible in the engine emissions performance even if absolute values are very low.

The low emissions engine operation of the LEC-III® is shown in Fig. 5.25. The ability to operate the combustor in fully premixed mode resulted emissions being reduced from diffusion operation with water injection at 42 ppm NO_x, to premixed dry operation with 4 ppm NO_x on this machine.

5.3.2 Reheat combustion

An alternative route to fuel staging is given by reheat combustion. We start by summarizing the basic working principle of this combustion and, indeed, engine concept (Joos *et al.*, 1996; Eroglu *et al.*, 2001).

Following a short overview of the SEV burner design principle, the generic operational and fuel flexibility of the reheat system is explained. The flexibility is based on the presence of two fundamentally different flame stabilization mechanisms, namely flame propagation in the first combustor stage and auto-ignition in the second combustor stage. Only recently has it become clear that the possibility of operating only one combustor and shutting down the SEV combustor altogether can be attractive to some



5.25 LEC-III® emissions characteristic following successful retrofit of the 501D5 machine (95 MW being the 100% load condition).

engine operators, and we conclude this section with this low load operation concept.

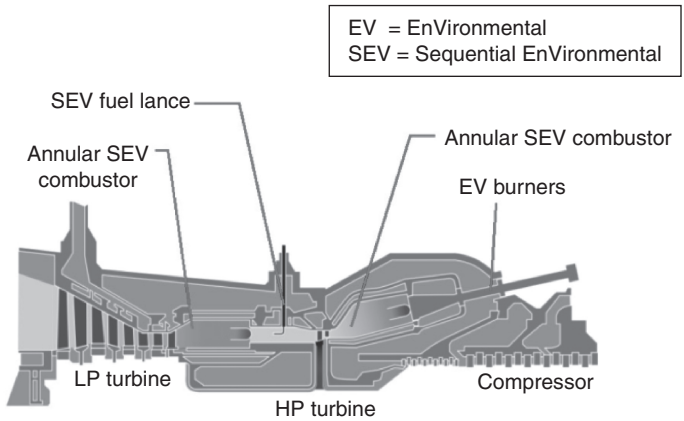
Reheat concept

Sequential combustion was first introduced into the market in 1948 as a way of increasing efficiency at low turbine inlet temperature levels. But only when the development of the sequential or reheat combustion technology for the GT24/GT26 engines started in 1990 did this concept become widely recognized and accepted in the industry (Güthe *et al.*, 2007, and references therein). Using a pressure ratio of 30:1, the compressor delivers nearly double the pressure ratio of a conventional compressor.

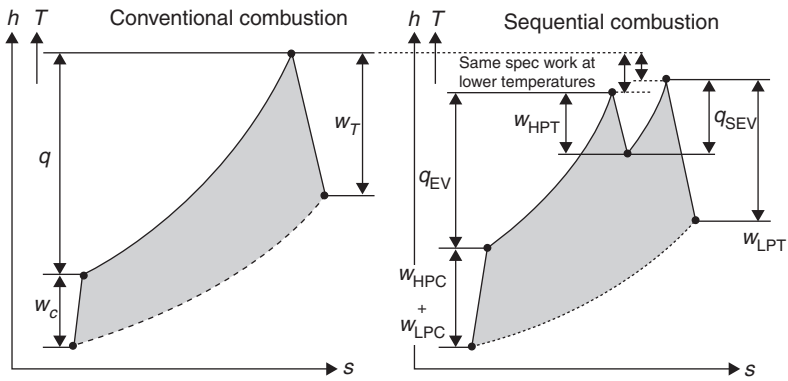
The compressed air is heated in a first, annular EV combustor, based on the well-proven EV burner principle. Approximately 50% of the total fuel (at base-load) is added in this combustor, the combustion gas expands through a single-stage high pressure turbine, which lowers the pressure by approximately a factor of 2. The remaining fuel is added together with some additional cooling air into the second combustion chamber, the SEV combustor. The combustion gas is heated a second time to the maximum turbine inlet temperature and finally expanded in the four-stage low-pressure turbine, Fig. 5.26. Relative to a conventional non-reheat cycle the same specific power output is achieved at lower turbine inlet temperature, and this is illustrated in Fig. 5.27.

Combustor design

The SEV combustor consists of 24 burners, each with four vortex generators, as can be seen in Fig. 5.28. These vortex generators are formed as



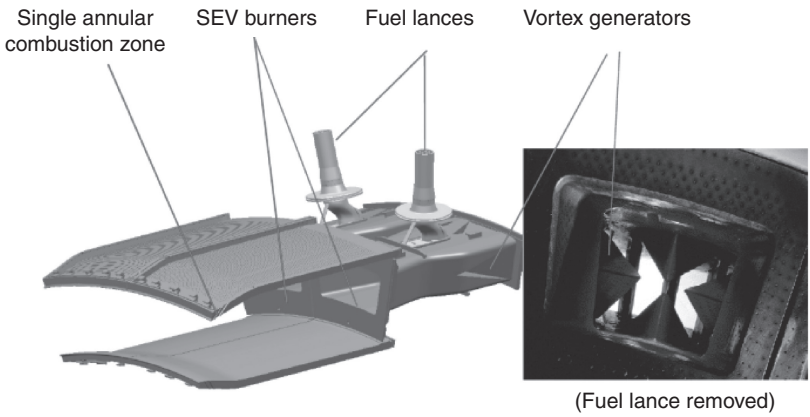
5.26 The sequential combustion gas turbine.



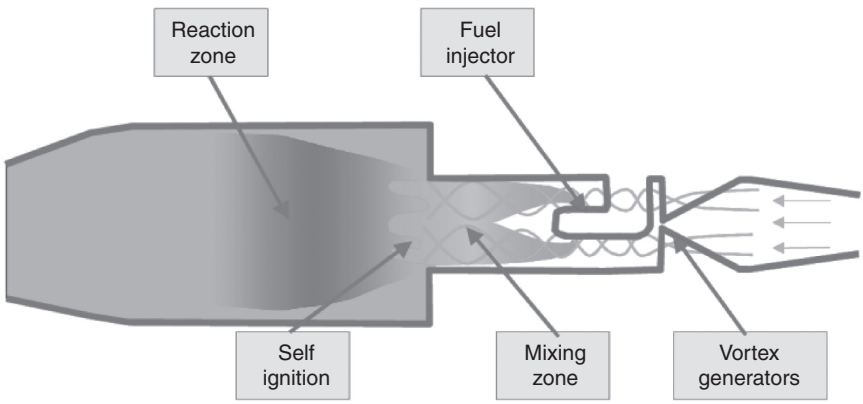
5.27 Principle of the reheat cycle, compared to a standard gas turbine cycle.

delta-wing shaped ramps, which roll up the incoming flow into a pair of streamwise vortices. The burner itself, including the front panel is cooled via laser-drilled effusion holes to cope with the high temperatures within the burner, in excess of 1000°C.

The operation principle of the SEV burner is shown in Fig. 5.29. A central lance is used for the injection of gaseous or liquid fuel directly in the center of four pairs of vortices generated by the vortex generators. Four holes are used for fuel injection, each consisting of a central fuel injector surrounded by a shielding air flow. This coaxial injection scheme allows, first, cooling of the SEV fuel lance itself, and subsequently protection of the fuel against premature ignition on the near field of injection. Additionally, injection momentum is increased, ensuring sufficient penetration even under low



5.28 A side view and an upstream view from the combustor into the SEV burner.



5.29 Operation principle of the SEV burner.

load conditions, where fuel mass flow is only a fraction of the base-load level.

The fuel injection is aligned with the vortex pattern emanating from the vortex generators. Injection parameters, such as hole size and angle, have been carefully optimized in order to place the fuel in the vortices as quickly as possible.

It is very important to achieve sufficient mixing quality prior to auto-ignition, which takes place within a few milliseconds at SEV conditions.

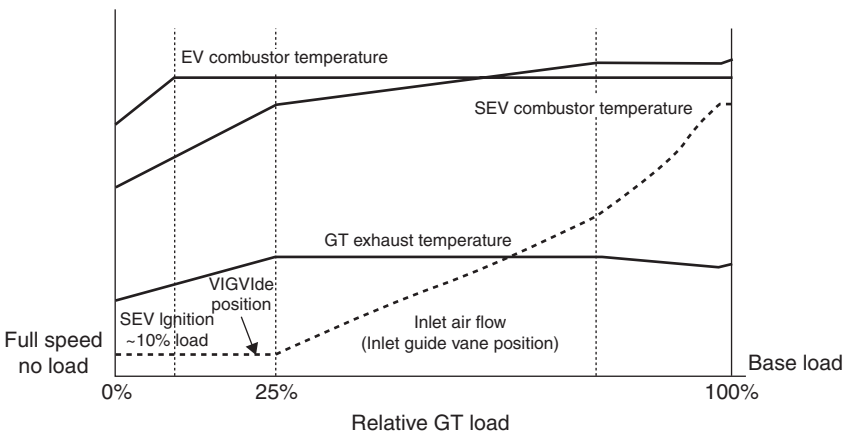
In other words while, in a conventional lean premix combustor, spontaneous or auto-ignition must be avoided at all circumstances, the SEV combustor has been specifically designed to operate at auto-ignition conditions. The mixing system is designed with very high flow velocities to prevent any

premature self-ignition during the process of fine-scale mixing between fuel and the hot EV combustor exhaust gases. The combustion takes place in the combustion space, where stabilization is supported by additional recirculation zones behind the inner and outer backward facing steps at the expansion. This expansion also retards the flow inside the vortex cores of the central flow, and as a result, auto-ignition reaction is simultaneously initiated at the outer recirculation zones and inner vortex cores. There is no need for a flame ignition torch or flame monitor for this robust flame behavior.

Engine operation

The introduction of reheat combustion allowed development of a completely new operation concept in the GT24/GT26 engines. The basic features of this operation concept are explained in Fig. 5.30.

The engine is ignited and operated up to approximately 10% load with the EV combustor alone. At this point the EV combustor is operating at the nominal premixed conditions. The fuel injected in the SEV combustor at these conditions will ignite spontaneously. Due to that, the turndown ratio of the SEV combustor is practically down to zero fuel flow. This ensures intrinsically a smooth transition, from EV only to EV-plus-SEV operation, without reaction and load instabilities. After this point, the gas turbine is further loaded with constant EV combustor temperature, and the loading consists of several phases from the initial ignition of the EV burners, the subsequent ignition of the SEV burners, and then the loading of the gas turbine by opening the variable guide vane to allow a greater air mass flow through the gas turbine. When the guide vane is fully open, the firing temperature of the



5.30 Operation concept of the GT24/GT26 engines with reheat combustion.

SEV combustor is increased further to achieve the base-load value. From the operation concept, two points become apparent. Firstly, the EV combustor temperature is kept high and constant across a wide low range – this promotes low emissions, also at low part load ranges. Secondly, the exhaust gas temperature of the engine exiting to the heat recovery steam generator is kept high and constant, also across a wide load range. This allows the combined-cycle part load efficiency to be maximized.

Emissions

The low emission levels, which can be achieved with a reheat system, are the combined effect of three key mechanisms.

Firstly, a reheat combustor makes more efficient use of the oxygen by burning twice in lean premix mode. At the inlet of the second stage, the oxygen content is at approximately 15% (reduced from 21% by combustion in the EV combustor). The oxygen content at the engine exhaust is then approximately 10%, yielding a beneficial normalization factor against the correction to 15% oxygen that is commonly used. Emissions quantified in the widely used emission index defined as $g(NO_2)/kg(fuel)$ are reduced accordingly.

Secondly, there exists a fundamental chemical advantage of reheat combustion, which can be exploited. This is caused essentially by the combustion at reduced oxygen-levels and increased water content (approximately 5%), as a result of the combustion in the EV combustor. Essentially, this chemical advantage is linked to the internal flue-gas 'recirculation' in the reheat combustor. This allows the SEV combustor to operate at higher firing temperatures and produce less NO_x than an EV combustor would produce at the same temperature.

Thirdly, the flame stabilization by auto-ignition leads to increased flexibility, which allows for operating in low emission mode at a wide load range by avoiding high peak flame temperatures. The higher SEV inlet temperature results in much higher reactivity, and this high reactivity at high combustor inlet temperatures has the consequence that flame stabilization always occurs under premixed conditions by auto-ignition and no piloting is needed to stabilize the SEV flame. The flame temperatures of the two combustors are ideally optimized primarily with respect to performance and turbine lifetime, but also at a given load for equal amounts of NO_x produced deriving an absolute minimum in engine emissions.

The reheat concept enables operating the two combustors at different temperatures, with only a little impact on overall power output. This increases the flexibility of the combustion system allowing burning more or less reactive fuels in the same engine by adjusting the relative load between the two combustors and allows mitigation of ranges where operation would become difficult (see next section for more details).

Published by Woodhead Publishing Limited, 2013

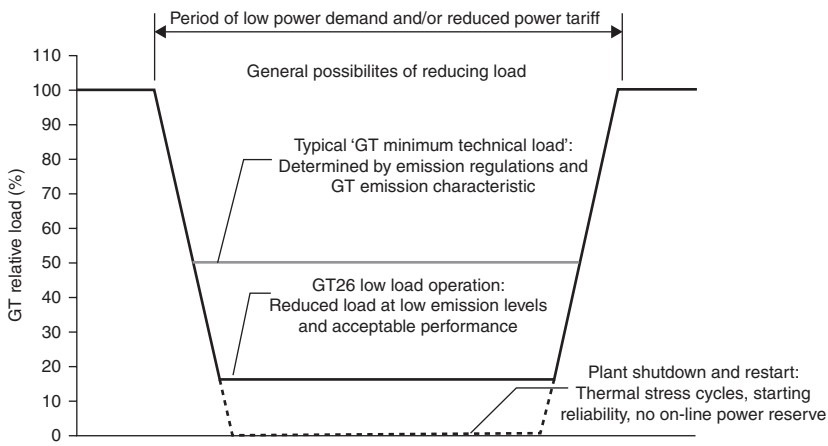
In general, the engines are adjusted so that the first combustor runs at low firing temperatures, keeping the emissions as low as possible for conventional premix combustion, while the second combustor is operated at higher temperatures producing similar emissions (on absolute scale) due to the reasons mentioned above. Note that while the EV is running more or less at the constant conditions keeping low NO_x even at very low loads, the loading is obtained by varying the fuel input in the SEV, starting as low as ~25% GT load (as well as increasing the mass flow of air). The high inlet temperature to the SEV burners allows operation without pilot for the entire operation range, entirely relying on auto-ignition for the SEV flame.

5.3.3 Low load operation concept

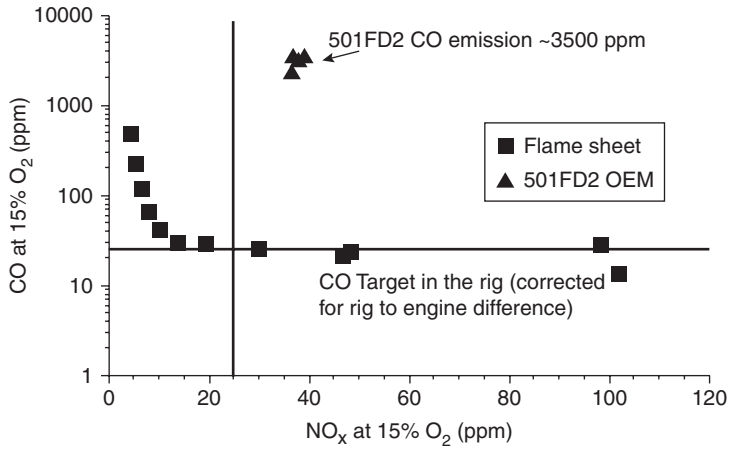
The introduction of the staged EV burner, which was explained in the previous section, in combination with the sequential combustion, enabled a new gas turbine feature altogether.

The gas turbine can be 'parked' at around 15% load of the engine, just before the ignition point of the SEV combustor where the staged EV burner is already operated in full premix mode, resulting in extremely low emissions, both for NO_x and CO which would be difficult to achieve otherwise, Fig. 5.31.

At these conditions, the turbine exit temperature is sufficiently high (despite the SEV combustor being switched off), and the steam cycle of a combined-cycle power plant can be kept in operation. This is attractive to



5.31 The low load operation concept of the GT24/GT26 engines, with a 'parking point' at around 15% gas turbine load. Single-stage combustion turbines need to be shut-down to avoid excessive emission values.



5.32 FlameSheet and conventional 501FD2 emissions measured back-to-back on full-scale test rig at 10–20% load.

operators that need to respond to high fluctuations in power demand, and who will benefit from start-up times within minutes instead of hours (Lilley *et al.*, 2007).

An alternate method for extended low load operation is used by the FlameSheet combustion system. By having radially staged premixers and combustors, which are able to operate independently at very low load and in tandem at high load, emissions can be optimized at both extremes of the operating envelope. Figure 5.32 compares the back-to-back CO emissions at 10–20% load on a conventional SW501F premixed combustor with that of the FlameSheet combustor able to improve the CO emissions by two orders of magnitude. Such a can combustor upgrade retrofit dramatically improves the range of operation over which the gas turbine is able to remain within emissions compliance.

5.4 Fuel flexibility

Today's power generation market requires considerable flexibility in terms of gas turbine fuels. Market forecasts predict a significant shift in these fuels over the next decades. Already today, pipeline gases have a fluctuation in composition, which will increase with the introduction of LNG in the near future. In 20–30 years, other fuels such as syngases, might become more prominent. The full range of fuels is explained in a separate chapter of this book, but we will discuss a few case studies here, with a particular focus on the implication of different natural gas qualities on combustor operation, more details can be found in Pennell *et al.* (2010).

Published by Woodhead Publishing Limited, 2013

5.4.1 Natural gases

The range of natural gases for gas turbine combustion continues to become wider in terms of species composition, Wobbe index and heating value, and thus can be significantly different from pure methane. The gas composition may include large fractions of rich gases, or higher hydrocarbons with more than one carbon atom. Those higher hydrocarbons are summarized as 'C2+', which is the sum of all mole fractions of hydrocarbons with more than one carbon atom. At the same time the inert content of natural gases, mainly CO_2 and N_2, may be large and varying. Thus when talking about fuel flexibility of natural gases, this means that the gas turbine must handle:

- Different fuel gases without hardware changes.
- A large range of C2+ levels (high hydrocarbons).
- A large range of inert contents.
- Fast and wide variations in gas composition.

Fuel flexibility is essentially driven by the discovery of new gas fields with large variations in gas composition (including diluents and higher hydrocarbons, and LNG) and the need to burn such fuels without additional treatment to limit fuel cost. This trend is becoming highly significant to many operators in the near and mid-term future, and puts pressure on the gas turbine manufacturers to develop improvements to combustion systems to ensure maximum flexibility while maintaining extremely low emissions. Operators may encounter sudden changes in fuel composition because, for example, a gas supplier is changing from one well to another, or a different LNG gas source is being used. Gas turbines must be able to handle such changes without interruption of power generation.

The variation of C2+ levels changes the reactivity of the fuel. As the amount of higher hydrocarbons increases, flame propagation speed increases, and auto-ignition temperature decreases. These variations in reactivity lead to altered stability characteristics of flames as well as a shifted flame position.

The variation in inert content is characterized by the Wobbe index of the fuel. It results in greater or smaller penetration of gas through the injector holes into the combustion air and therefore affects the premixing quality of the gaseous fuel. These variations in premixing can lead to altered emission behavior of the combustor.

As an example for typical variations observed, Plate X summarizes the natural gases' qualities for some of today's GT26 fleet engines, in terms of Wobbe index and C2+ content. The majority of units lie in the range of 0–16% C2+, but it is expected that higher C2+ concentrations will be observed in the future. Likewise, it is expected that values even lower than

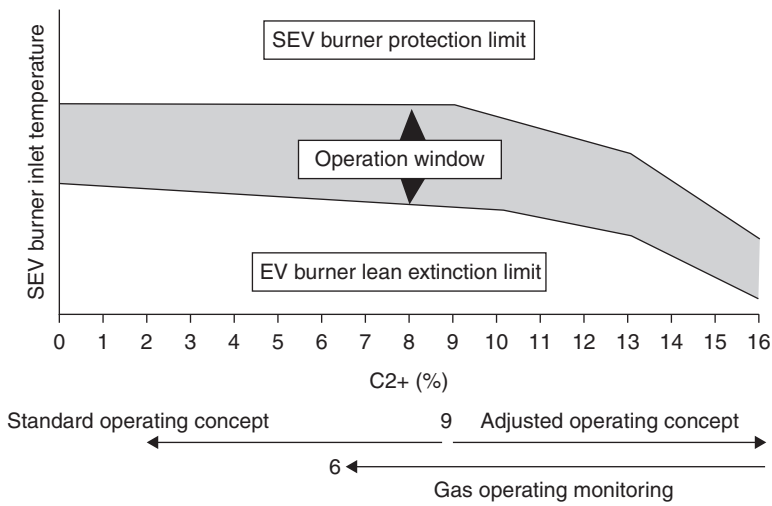
Published by Woodhead Publishing Limited, 2013

a Wobbe index of 30 MJ/m^3 will be reached in pipeline natural gases in future.

To mitigate the effects of changing gas composition on combustion performance, one may strictly limit the allowable range of fuels and modify the combustor hardware for different ranges of gas qualities. However, this implies a severe restriction for the gas turbine operator who is likely to receive various gases during the lifetime of the power plant. It is therefore better to implement sufficiently robust burner hardware, in combination with an appropriate gas turbine control system, to counter-act the changed combustion behavior.

At Alstom, the second strategy has been adopted (Riccius *et al.*, 2005), and it led to the 'C2+ operation concept' for the GT24/GT26 gas turbines. Three key elements form the basis of this operation concept. Firstly, the fundamental design of the EV and SEV combustor is sufficiently robust and insensitive against variations in diluents; this is achieved fundamentally by making the fuel injector insensitive against variations in volumetric fuel flow. Secondly, a rapid fuel composition measurement system is available, which is able to monitor composition changes in C2+ within fractions of a second; this has been achieved by developing a sensor that is much faster than traditional gas chromatographs. Thirdly, the combustor operation concept is linked to the actual fuel composition.

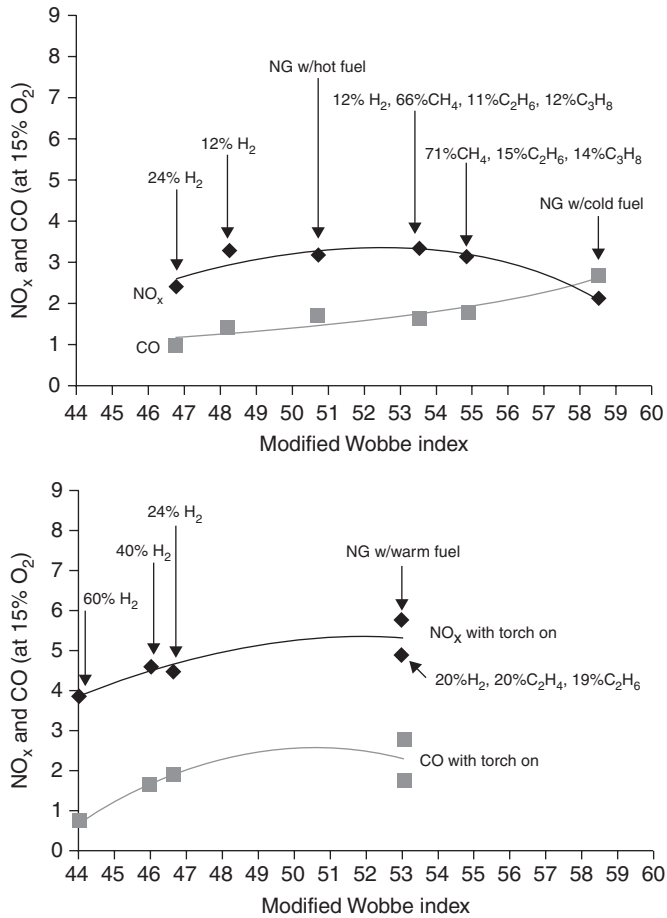
A schematic of the operation concept is shown in Fig. 5.33. In the previous section the relation between EV combustor firing temperature and SEV inlet temperature has been explained. It turns out that with increased C2+ content in the fuel, and therefore increased reactivity, the lean stability



5.33 The C2+ operation concept for reheat engines.

limit of the EV combustor at lowered firing temperatures is improved. This allows the inlet temperature of the SEV combustor to be reduced to stay within the optimum operating window. However, the SEV flame itself is rather insensitive to changes in fuel composition. This implies that the C2+ operation concept has only little loss in overall power due to the reduced temperature in the EV, as more fuel can be added to the SEV. This operation concept is unique to reheat combustion until today.

Also the FlameSheet can combustor system has demonstrated the potential for running on a wide range of fuels through full-scale high pressure rig tests. The nature of the premixers, mixing air into fuel, as well as high premixer exit velocities allowed operation with a range of fuels shown in Fig. 5.34, including fuels containing up to 60% hydrogen.



5.34 FlameSheet full-scale high pressure rig results operations on varying fuels.

5.4.2 Fuel oil

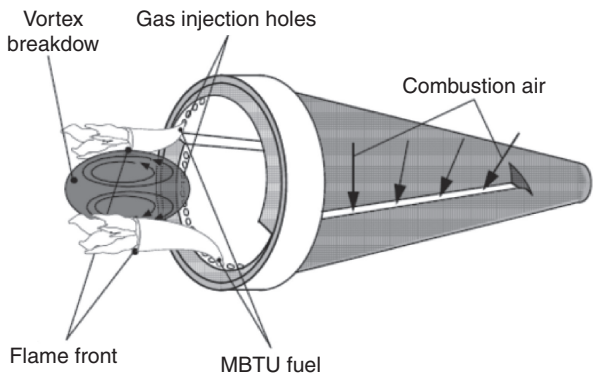
For completeness, it is stressed that most gas turbines are designed such that they are able to burn fuel oil in addition to natural gas, but this fuel is mostly used as backup fuel only.

For the EV burner, shown in Fig. 5.3, the fuel oil is injected via a central plain jet nozzle in the cone head. Water can be added to the fuel for emission control. The liquid plain jet disintegrates into small droplets within the burner cone. The swirling flow distributes the droplets in the whole flow field, and the flame stabilization occurs near to the burner outlet with the help of the central recirculation zone, similar to the combustion with natural gas.

5.4.3 Low calorific gases

All gas turbine manufactures have developed in the past tailored solutions both for medium and highly diluted fuels such as blast furnace gases or syngases. We show here the design examples from Alstom, which are able to burn these highly diluted and/or highly reactive gases.

For syngas fuels the EV burner was further developed in order to burn fuels with hydrogen content of up to 50%, and heating values in the range of 6–15 MJ/kg. In order to account for the high reactivity of hydrogen, the fuel injection location was repositioned closer to the burner exit. The gas channel volume and injector size was increased to minimize the gas pressure requirements from the higher volume flows of the fuel. A sketch of this burner variant is shown in Fig. 5.35. The burner has been installed in a GT13E2 gas turbine (Reiss *et al*., 2002).



5.35 EV burner for combustion of syngas fuels with hydrogen concentrations up to 50%.

For low calorific gases such as blast furnace gases, the heating value can be as low as 2 MJ/kg. In this case, the volumetric flow of the fuel is of the same order as the air flow itself, and the engine (i.e., the matching of compressor and turbine) needs to be adjusted. For the combustor itself, one typically applies a design that is similar to the large silo combustors shown in Fig. 5.6. A detail of the burner design is shown in Plate XI where it can be seen that the main burner swirler is built in a sandwich format with low calorific gas supplied through fins in each of the swirler blades. The gas channel is split into an inner and outer section to be able to control the flammability limits of the fuel with the incoming air, while maintaining optimum emissions. On the central axis of the burner a lance is installed for backup oil operation as well as an injection of more reactive gases containing hydrogen of natural gas.

The vortex breakdown stabilizes the flame in the silo combustor similar to the principle employed for flame stabilization in the EV burner.

5.5 Future trends

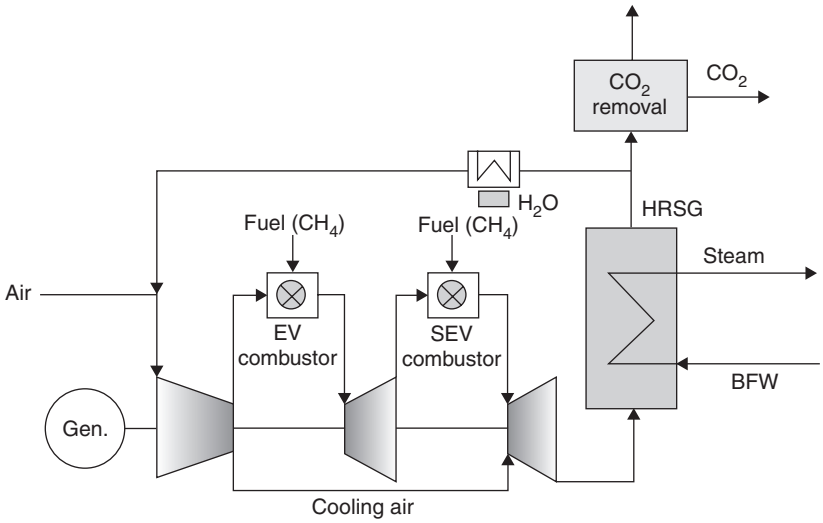
Progress in gas turbine combustion continues to be made not only by step improvements of existing concepts, but also through major innovations with novel combustion concepts. The key drivers for progress continue to be emission reduction, handling an increasing number of fuels or fuel blends, and generally extending the range of operation in low emission mode.

5.5.1 Emission reduction

The need to find new ways for emission reduction is driven by two conflicting targets. Environmental legislation continues to drive allowable emission levels of NO_x further down to single digit values. At the same time, the hot gas temperatures continue to increase to achieve even higher engine efficiencies, leading to increased NO_x emissions for the existing technologies. Perfecting fuel–air mixing within the burner, increasing the complexity of fuel-staging techniques (where cumbersome switchover or purging sequences are to be avoided to maintain reliability), or applying advanced cycles such as reheat combustion is pursued in the industry.

One innovation area that has recently gained interest for various manufacturers is flue-gas recirculation. In the context of the development of CO_2-free gas turbines, it has been identified as an effective technique for post-combustion CO_2 sequestration in natural gas power plants. As an example, Fig. 5.36 shows a sketch of the Alstom GT26 gas turbine, integrated into a flue-gas recirculation cycle. The gas flow is split after the heat recovery steam generator with a certain ratio into a flow entering the CO_2 removal section and a recirculating flow. This appears on the one hand to

Published by Woodhead Publishing Limited, 2013



5.36 Flue-gas recirculation concept.

be an effective means to enrich the CO_2 content in the exhaust, thereby reducing the cost of the CO_2 capture equipment. At the same time, flue-gas recirculation is a promising technique for further NO_x emission reduction. Further reading can be found in Güthe *et al.* (2009, 2011). Another alternative for CO_2 reduction is the removal of carbon from the fuel prior to burning the fuel. The operating efficiency of such systems is optimized by using the already existing gas turbine compressor to drive a fuel partial oxidation system as described in Stuttaford and Oumejjoud (2008).

5.5.2 Engine firing temperature increase

The drive to continuously improve cycle efficiency leads to ever-increasing operating temperatures. This is a challenge for the durability of the hardware, as well as the NO_x emissions. Novel materials will be required to minimize the cooling air on combustor parts while operating those components at higher temperature. Novel techniques as mentioned in the previous paragraph will be required to control and even reduce NO_x emissions even as the reaction zone temperatures are increased.

5.5.3 Fuel flexibility

Properties of natural gases are already varying today and this variation is expected to increase in the future. The degree of variation is difficult to predict but already today fluctuations in Wobbe index can easily exceed 10%

for some power plants. It is clear that gas turbine combustors must be able to cope with such an increased variability of natural gas qualities preferably without change of hardware. Solutions have to be found where on the one hand the fuel–air mixing is inherently insensitive to changes in fuel composition (volumetric flow and reactivity), and on the other hand the control of engine operation is linked to parameters of fuel composition.

It is the view of the author that a stepwise extension of the capability to burn various fuels is also the right way towards co-firing of future fuels like biogases or hydrogen.

5.5.4 Operation flexibility

Through the lifetime of a power plant it is difficult to predict the expected load range where the plant will be operating for most of the time. Many plants will run extensively in the part load regime, due to increased use of fluctuating renewable energy such as wind power. Others will continue to require highly efficient operation at base-load with lowest possible emissions. Future combustors will have to cover both ends of the extreme, using only a single hardware. These requirements are not only key for new systems, but also when retrofitting existing engines (Stuttaford *et al*., 2010).

5.6 References

Döbbeling, K., Hellat, J. and Koch, H. (2005), 25 Years of BBC/ABB/ALSTOM lean premix combustion technologies, ASME Turbo Expo, GT2005-68269.

Döbbeling, K., Meeuwissen, T., Zajadatz, M. and Flohr, P. (2008), Fuel flexibility of the Alstom GT13E2 medium sized gas turbine, ASME Turbo Expo, GT2008-50950.

Eroglu, A., Brunner, P., Hellat, J. and Flohr, P. (2009), Combustor design for low emissions and long lifetime requirements, ASME Turbo Expo, GT2009-59540.

Eroglu, A., Döbbeling, K., Joos, F. and Brunner, P. (2001), Vortex generators in lean-premix combustion, *Transactions of the ASME, Journal of Engineering for Gas Turbines and Power*, **123**, 41–49.

Güthe, F., Hellat, J. and Flohr, P. (2007), The reheat concept: the proven pathway to ultra-low emissions and high efficiency and flexibility, ASME Turbo Expo, GT2007-27846.

Güthe, F., de la Cruz Garcia, M. and Burdet, A. (2009), Flue gas recirculation in gas turbine: investigation of combustion reactivity and NO_x emission, ASME Turbo Expo, GT2009-59221.

Güthe, F., Stankovic, D., Genin, F., Syed, K. and Winkler, D. (2011), Flue gas recirculation of the Alstom sequential gas turbine combustor tested at high pressure, ASME Turbo Expo, GT2011-45379.

Joos, F., Brunner, P., Schulte-Werning, B., Syed, K. and Eroglu, A. (1996), Development of the sequential combustion system for the ABB GT24/GT26 gas turbine family, ASME Turbo Expo, 1996-GT-315.

Lefebvre, A.H. (1999), *Gas Turbine Combustion*, CRC Press (Taylor & Francis Group).

Lilley, D., Ruecker, F., Lachner, R., Lindvall, A. and Rebhan, D. (2007), Low load operation concept for Alstom's GT26 gas turbine, PowerGen Europe.

Paschereit, O., Flohr, P., Knöpfel, H., Geng, W., Steinbach, C., Stuber, P., Bengtsson, K. and Gutmark, E. (2002), Combustion control by extended EV burner fuel lance, ASME, 2002-GT-30462.

Pennell, D., Hiddemann, M. and Flohr, P. (2010), Alstom fuel flexibility for today's and future market requirements, PowerGen Europe.

Reiss, F., Griffin, T. and Reyser, K. (2002), The Alstom GT13E2 medium BTU gas turbine, ASME Turbo Expo, 2002-GT- 30108.

Riccius, O., Smith, R., Güthe, F. and Flohr, P. (2005), The GT24/GT26 combustion technology and high hydrocarbon ("C2+") fuels, ASME Turbo Expo, GT2005-68393.

Stuttaford, P.J. and Oumejjoud, K. (2008), Low CO_2 Combustion System Retrofits for Existing Heavy Duty Gas Turbines, ASME GT2008-50814.

Stuttaford, P.J., Rizkalla, H., Chen, Y., Copely, B. and Faucett, T. (2010), Extended Turndown, Fuel Flexible Gas Turbine Combustion System, ASME GT2010-22585.

Stuttaford, P.J. (2011), Extended Fuel Flexibility for E and F-class Gas. Turbine Combustion Systems, Power Gen Europe, ASME GT2010-22585, Milan, Italy, 2011.

Zajadatz, M., Lachner, R., Bernero, S., Motz, C. and Flohr, P. (2007), Development and design of Alstom's staged fuel gas injection EV burner for NO_x reduction, ASME Turbo Expo, GT2007-2773.

Published by Woodhead Publishing Limited, 2013

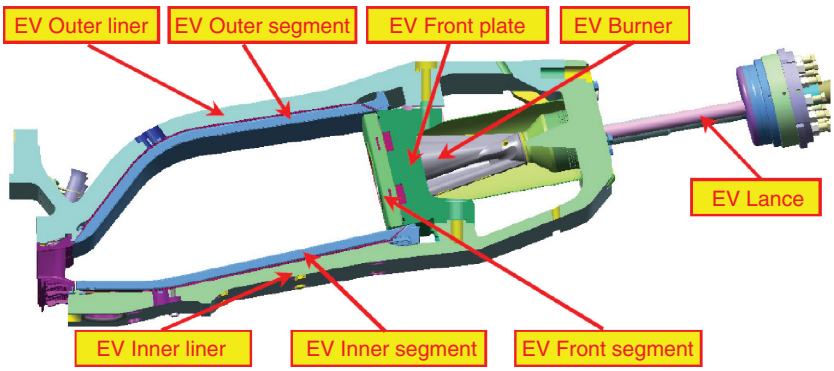


Plate V (Chapter 5) Main components of the GT24/GT26 EV combustor.

© Woodhead Publishing Limited, 2013

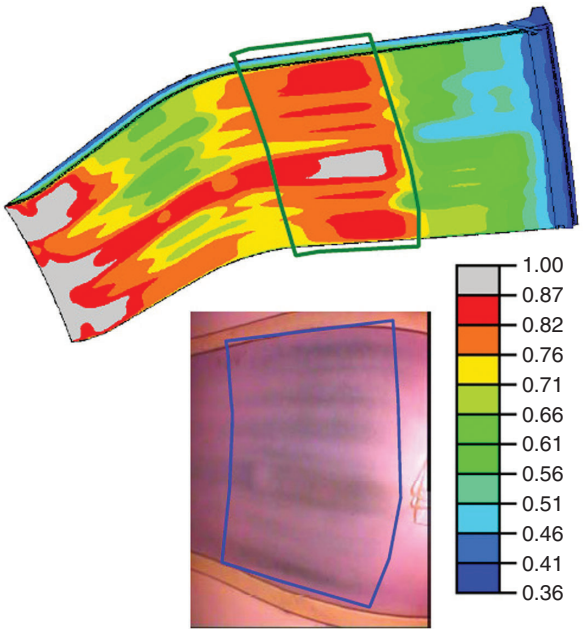


Plate VI (Chapter 5) Calculated temperatures and thermal paint results from a liner segment.

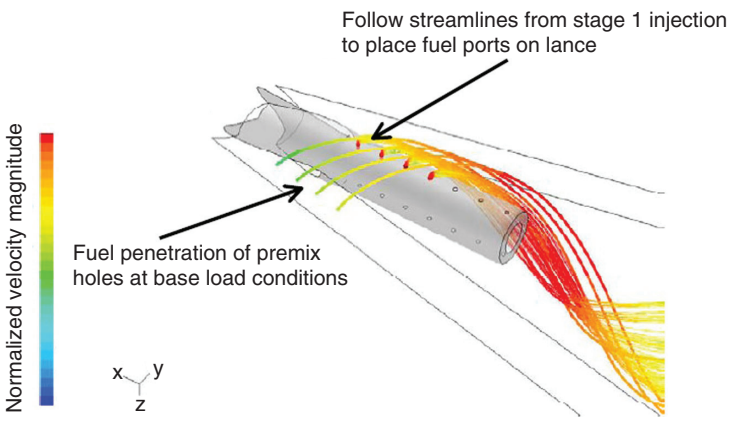


Plate VII (Chapter 5) Comparison of fuel streamlines for premixed and staged fuel gas injection.

© Woodhead Publishing Limited, 2013

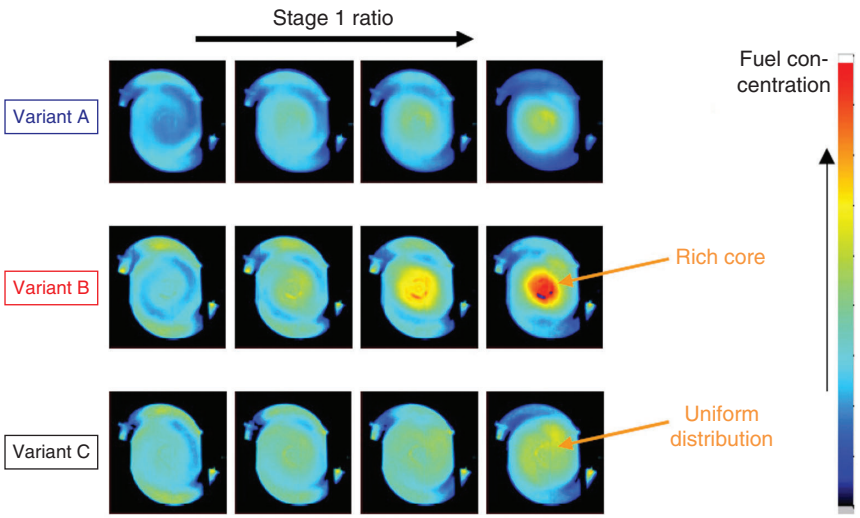


Plate VIII (Chapter 5) Comparison of mixing fields between different staged EV variants.

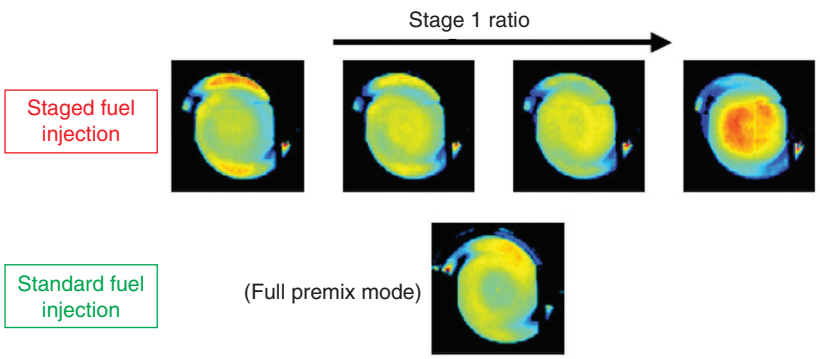


Plate IX (Chapter 5) Comparison of mixing fields of the staged and standard EV burners.

© Woodhead Publishing Limited, 2013

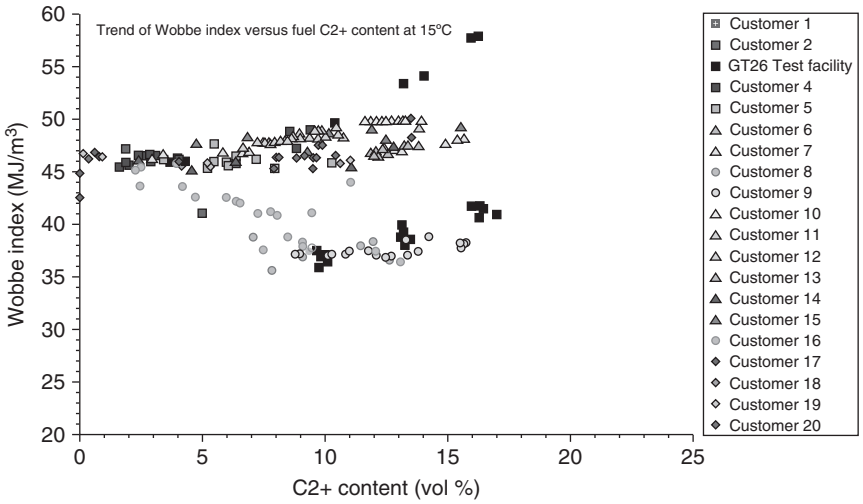


Plate X (Chapter 5) GT26 fleet C2+ concentrations and Wobbe index variantions.

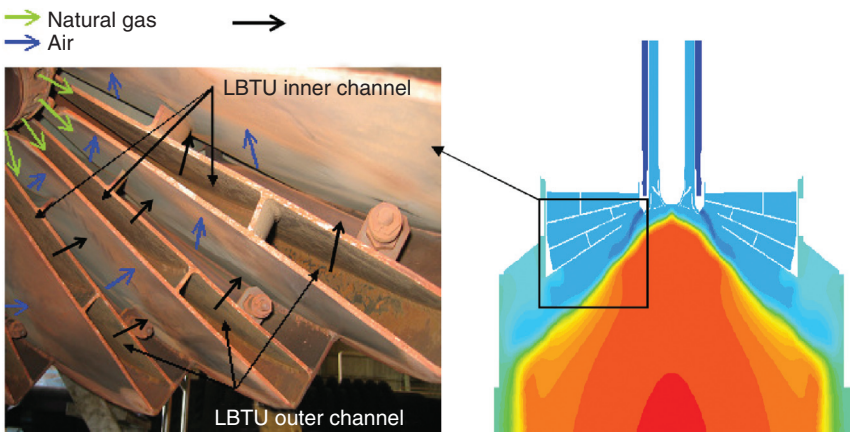


Plate XI (Chapter 5) Single burner design for combustion of low calorific gases and fuels with high hydrogen content.

© Woodhead Publishing Limited, 2013

6

Turbines for industrial gas turbine systems

M. SCHNIEDER and T. SOMMER,
Alstom (Schweiz) AG, Switzerland

DOI: 10.1533/9780857096067.2.188

Abstract: This chapter reviews materials, design and performance issues relating to turbines in power stations. Key performance issues include aerodynamics and cooling as well as durability and damage mechanisms. The chapter the looks at key components and their performance requirements.

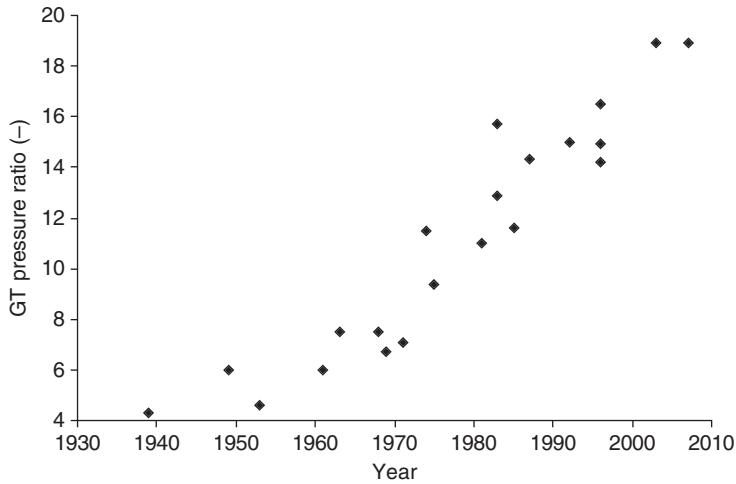
Key words: gas turbines, aerodynamics, interfaces, damage mechanisms.

6.1 Introduction

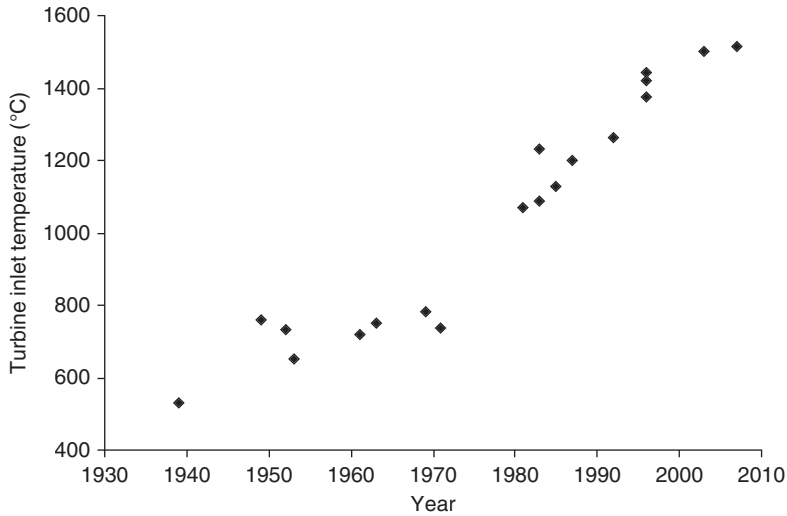
In terms of total engine output, the vast majority of the new orders for gas turbines for power generation in recent years have been for gas turbines with a power output of 120 MW or more. In fact, power generation order surveys (McNeely, 2007; Anon, 2008; Gailloreto, 2009; Haight, 2010) show that this market had contributed about two-thirds or more of total power output of gas turbine orders since 2005. In contrast, gas turbines with a power output below 60 MW have contributed at most up to a quarter of the orders, and often significantly less. The focus of the following chapter will, therefore, be on this segment of the market, and the authors will attempt to give an overview of the key features of the turbines used in this type of engine, and to point out the main differences from aircraft engines.

For a historical perspective, it is interesting to look at the development of the key turbine boundary conditions since the introduction of the first power generation gas turbine in 1939 (Van der Linden, 1988). The gas turbine pressure ratio, and with it the turbine pressure ratio, of single-shaft gas turbines with a conventional gas turbine cycle, has grown five-fold in 70 years of power gas turbine history, and Fig. 6.1 shows that this growth

Published by Woodhead Publishing Limited, 2013



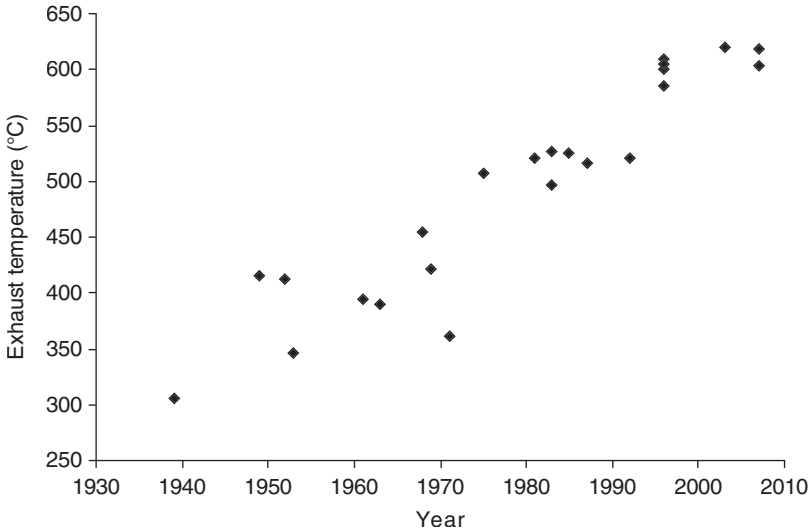
6.1 GT pressure ratio over year.



6.2 Turbine inlet temperature over year.

was nearly linear with time. While the reheat cycle engines, introduced in the 1990s with the Alstom GT24 and GT26 engines, were omitted from this picture, it should be pointed out that, as far as the low pressure turbine is concerned, these engines fit into the general picture represented by Fig. 6.1. The hot gas temperature at the turbine inlet has more than doubled, again following a linear trend (Fig. 6.2), and the turbine exhaust mass flow has grown ten-fold. The development of the turbine exhaust temperature has

Published by Woodhead Publishing Limited, 2013



6.3 Turbine exhaust temperature over year.

been somewhat less linear (Fig. 6.3) with only a low increase of exhaust temperature throughout the 1950s and 1960s, followed by two large jumps in the late 1970s and in the 1990s. These jumps are related to the development of combined-cycle power plants, where an optimisation of the plant efficiency results in higher exhaust temperatures. Live steam temperatures around 500°C were used when combined-cycle plants first became commercially attractive in the 1980s (although the idea of combined-cycle plants had already been discussed much earlier, see e.g. Meyer, 1939; Seippel and Bereuter, 1960). With the advent of the F-class gas turbines in the 1990s, live steam temperatures up to nearly 600°C were achieved, leading to highly efficient combined-cycle plants.

This remarkable evolution of the turbine boundary conditions was made possible by improvements in materials, manufacturing, cooling technology and aerodynamics. Advances in these areas were driven by improvements in the underlying methods, such as finite element methods and computational fluid dynamics, as well as in experimental techniques, such as laboratory testing methods, that were a prerequisite for the development of advanced cooling features.

The development steps in power gas turbines are closely linked to aero-industry turbines. Although the first power gas turbines were introduced nearly simultaneously with the first jet engines, the aircraft engine industry had a leading role in gas turbine development for a long time, with some 5–10 years lag between the technology introduction in commercial

Published by Woodhead Publishing Limited, 2013

aircraft engines and power gas turbines. One example of this lag is the introduction of cooled turbine blades. Since the commercial introduction of the F-class engines, the difference in technology has been significantly reduced and there are now some areas where some of the technology is led today by the heavy-duty gas turbine industry. Again, an example in the field of cooling comes to mind: due to the stricter emissions requirements, power gas turbines generally have more uniform turbine inlet temperature traverses than aircraft engines, and they use more advanced cooling technologies for vane and blade platforms. It is expected that in the future new regulations will lead to similar constraints in aircraft engines, so that low emissions technology will also be required for aircraft engines.

Engine requirements and mission profiles of power generation gas turbines are quite different from those of aircraft engines, leading to different drivers for the turbine development. Engine weight, for example, is a crucial factor in aircraft engines. In heavy-duty power gas turbines, on the other hand, weight in itself is not a key driver and may only be considered in the sense that cost is influenced by the amount of material used. Other major differences that influence turbine design are the differences in lifetime and inspection intervals, as well as in the proportion of time spent at full temperature between overhaul intervals. Finally, the overall engine design and assembly process is also a key factor affecting the turbine.

While multi-shaft arrangements are frequent in the so-called aero-derivative gas turbines used in power generation engines up to about 100 MW, gas turbines with higher power output are exclusively single-shaft arrangements, and the turbines are of the axial flow type. With few exceptions of gas turbines with just above 100 MW output, where gear boxes are used, the rotational speed is synchronous to the electrical grid and the engines run at either 3000 or 3600 rpm, depending on the market the gas turbine is designed for. The generator acts to fix the rotational speed, and only small deviations occur, due to relatively small grid frequency variations about the nominal value. This is, of course, very different from aircraft engines where the speed varies over a wide range with load.

Integration between turbine parts and of the turbine into the engine is clearly a key topic, both for a discussion of turbine design in general and for illustrating the differences between aircraft engines and heavy-duty power gas turbines. The detailed discussion in the remainder of the chapter will, therefore, start with a chapter on integration and interfaces, before going through the individual engineering disciplines involved in turbine design. The focus will then go back into a more integrative view, in an outline of typical turbine parts and operational characteristics. The chapter will close with a discussion of current research trends expected to make their way into future power generation gas turbines.

Published by Woodhead Publishing Limited, 2013

6.2 Interfaces and integration

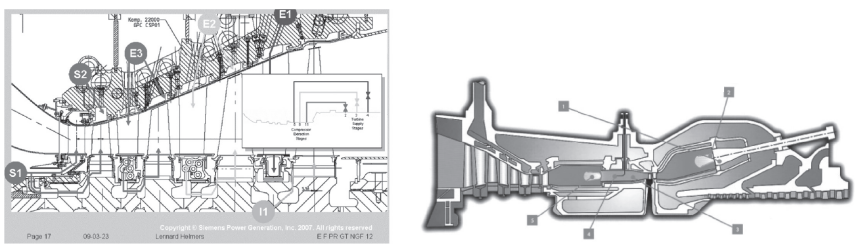
6.2.1 Secondary air systems (SAF)

Secondary air systems (SAF) provide the cooling air from the compressor to the combustor and turbine component (see Fig. 6.4). Besides the cooling air supply, SAFs ensure an outflow into the hot gas path under all operating conditions, that is, positive pressure margins. For failsafe design the pressure must be throttled and sufficient pressure margin kept, which is a constraint on the performance of the engine. To improve engine performance, the modern SAF system may draw from a number of technology features:

- increased number of supply systems into the combustor and turbine component to better match the different pressure requirements;
- use of recooling for improvement of combined-cycle performance, reduced cooling air temperature where required at structural or rotor parts, control of whole engine model clearance, and operating pinch point clearance control;
- use of active control devices for the orifices, to adjust the required pressure and mass flow requirements over load and ambient conditions;
- increased number of variable guide vanes in the compressor to ensure load/pressure redistribution adjustment in relation to the compressor end pressure;
- advanced sealing technology.

6.2.2 Combustor

A key topic for turbine cooling is the hottest area of the turbine, that is, the turbine inlet/combustor outlet. Emission requirements have resulted in premix combustion technology with low turbine inlet turbulent intensity and flat temperature profile to be used. To meet CO emission requirements, high temperature levels can be kept to the low part load regime (Eppler *et al.*, 2008).



6.4 Example of modern sAF turbine systems (left: SGT5–8000H, right: GT26).

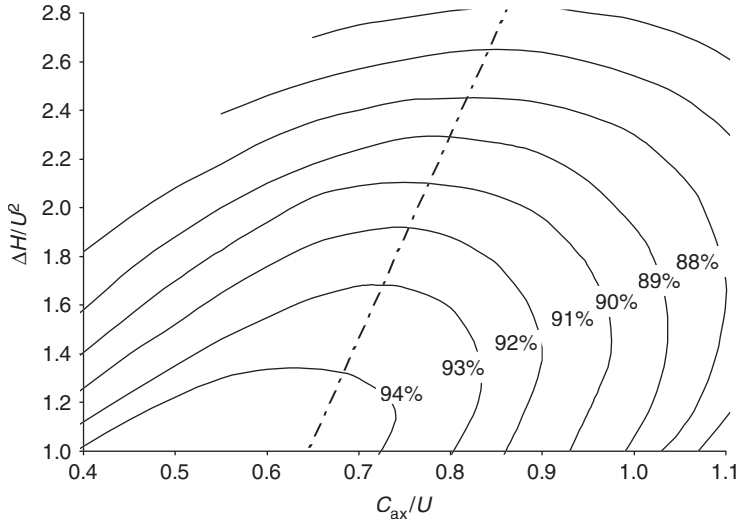
Two principle combustor concepts have evolved over time, the can annular combustor (e.g. General Electric 7FA, Siemens-Westinghouse SGT6–5000) and the ring annular combustor (e.g. Alstom GT26, Siemens SGT5–4000). Reheat technology (Alstom GT26) or staged combustion offers additional emission reduction benefits. Common to all modern GT system interfaces is that, for premix combustion with flat temperature profiles, the turbine endwalls (platforms, blade tips, blade shrouds, heat shields, etc.) need particular attention and differ significantly from aircraft engine turbines.

The combustor provides the hot gas temperature interface into the turbine. Modern gas turbine systems have certain characteristics that significantly impact the combustor turbine interface:

- Premix combustion, reheat and staged combustion in relation to aeroengine combustor technology have small turbulence levels. Ring annular combustors, compared to can annular combustors, also feature reduced leakage introduction into the turbine interface and therefore more homogeneous flow conditions.
- Emission requirements in terms of NO_x (peak temperature driven) and CO (part load and cold ambient driven) drive vs small temperature distortion in radial and circumferential direction. As a consequence, endwalls are thermally highly loaded. Hot streak migration is present to a much smaller extent.
- Combustor pressure drop (compressor exit to turbine inlet flow path) is required to achieve sufficient cooling pressure over the operating range, mainly for the first stage vane, but has a performance penalty. Low pressure drop design technology is required for the front stage turbine parts. Bow wave and trailing edge wave effects of the front stage vane have to be minimised to reduce the SAF purge flow requirements.
- Combustor and turbine components form large structural parts with significant thermal expansion over the operating range setting geometrical constraints to the interface.
- Premix combustion often requires staging to avoid thermo-acoustic pulsations within the combustor. Staging increases the circumferential temperature distortion.

6.3 Aerodynamics

Perhaps the most important factor determining general turbine design is how the overall expansion in the turbine is distributed into individual turbine stages. The first consideration is the choice of the number of stages. The impact of this choice on the aerodynamic design and the turbine efficiency can be understood using the Smith chart (1963), where turbine stage efficiency is presented as a function of the flow coefficient C_{ax}/U and the



6.5 Smith chart.

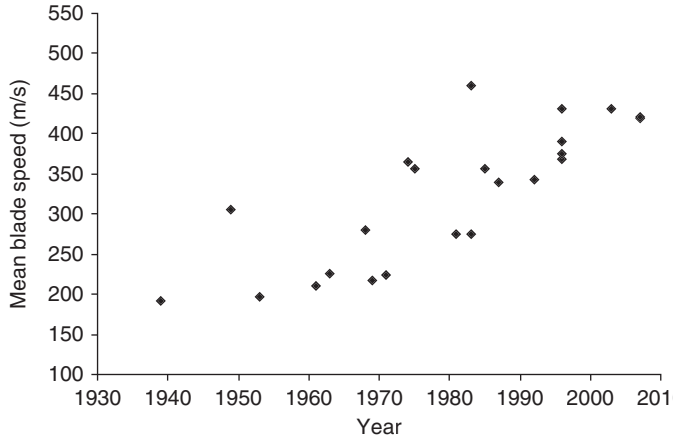
loading coefficient $\Delta H / U^2$ (Fig. 6.5). The highest stage efficiency is achieved for small values of flow and loading coefficients.

Due to the fixed rotational speed in power generation gas turbines, the blade speed U is only a function of the radius. The only other way to influence the stage loading for a given overall enthalpy drop is by the choice of the number of stages. A higher number of stages will result in higher stage efficiencies but, due to the lower stage enthalpy drop, there will be more stages with high gas temperatures. The choice of the stage loading thus becomes a trade between efficiency, blade cooling, and cost, as well as mechanical and structural design considerations. Note that a reduction in the number of stages does not necessarily lead to a proportional reduction in parts count in the turbine, since an increase in stage loading tends to increase the blade count per stage.

Historically, this trade led to vastly different choices in mean stage loading made by different companies. For example, there is a factor of about two between the estimated mean turbine stage loading in the first power generation gas turbines from Brown Boveri and General Electric (Van der Linden, 1988; Somerscales and Henricks, 1984). There continued to be a large spread up into the 1970s and 1980s, but values for stage loading appear to have converged to values typically between 1.3 and 1.5. This is probably driven by a convergence of engine application design towards gas turbines for high efficiency combined-cycle power plants.

In view of the five-fold increase in turbine pressure ratio discussed in the introduction, the turbine mean stage loading has remained remarkably

Published by Woodhead Publishing Limited, 2013



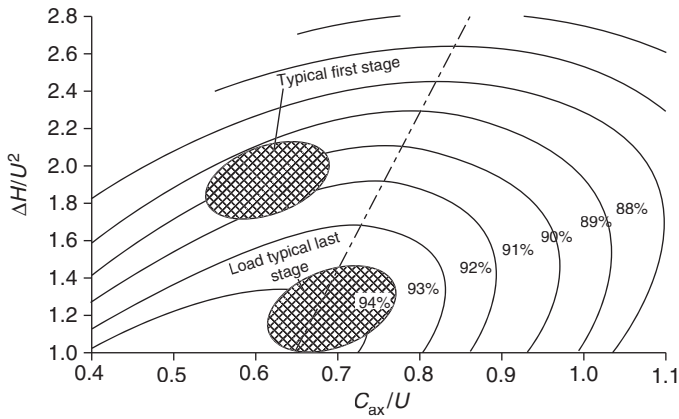
6.6 Mean blade speed over year.

constant in time, particularly since most companies have reduced the number of stages rather than increasing them. This was made possible by a strong increase in mean blade speed, that is, mean radius (Fig. 6.6). This is testament to advances in other areas, such as design, materials, durability and manufacturing of rotors.

The determination of the distribution of the turbine enthalpy drop to the individual stages entails a trade with much the same considerations as the choice of the mean stage loading. On the one hand, aerodynamic efficiency is higher when more work is done in the rear stages, both because their stage loading is lower due to the higher mean radius and less secondary flow and tip leakage losses. On the other hand, more work done on the front stages results in a higher temperature reduction early on in the turbine. The aerodynamic efficiency impact and the cooling and leakage air consumption can be can be stacked up against each other in terms of their impact on the gas turbine cycle efficiency in a quantitative assessment. Risk aspects, such as the relative risk of having higher or lower gas temperatures in a second stage, are more difficult to quantify, but still play an important role in turbine design.

Typical Smith chart locations of the first and last turbine stages in modern power generation gas turbines are shown in Fig. 6.7. Turbines in these engines are all designed with a mean radius that increases from inlet to exit, such that the blade speed is higher in the last stage. Furthermore, the higher temperature in the first stage leads to a higher enthalpy drop in the first stage than in the last one. The first stage loading is close to the numbers reported for HP turbine stages in aircraft engines, typically in the range $\Delta H/U^2 \approx 1.5$ to 2.5 (Cohen *et al.*, 1987), depending on the application.

Published by Woodhead Publishing Limited, 2013



6.7 Typical Smith chart location, first stage, last stage.

The shape of the velocity triangles for a turbine stage is defined by the choices of the flow coefficient, stage loading and stage reaction

$$R_T = \frac{h_2 - h_3}{h_1 - h_3}$$

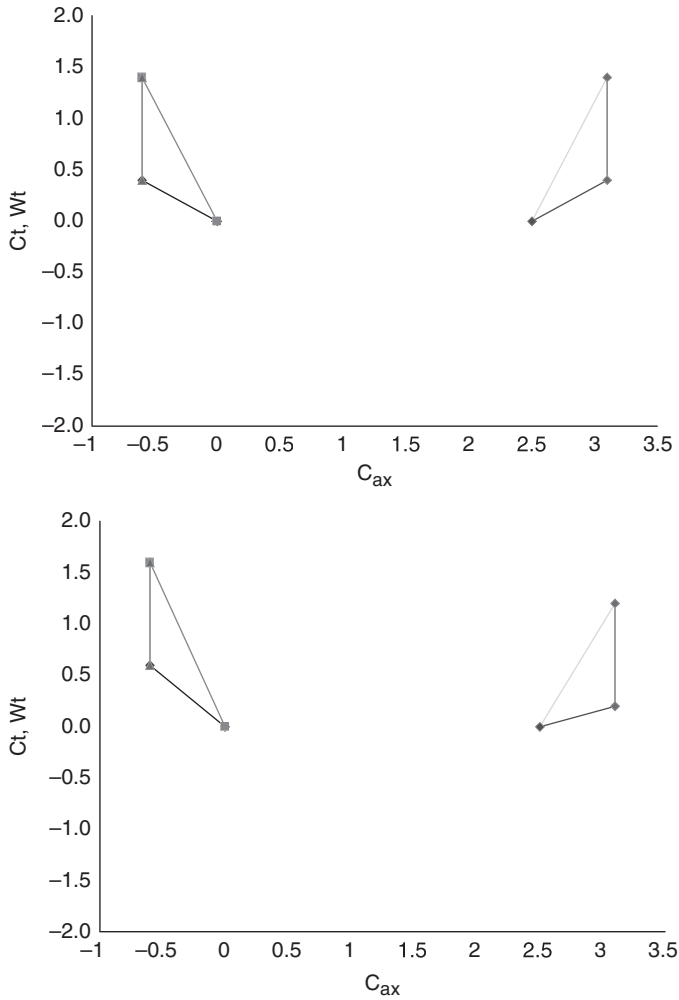
The stage reaction in power generation as well as aircraft engines is usually chosen to be near $R_T = 0.5$. This results in the best stage efficiency, since $R_T = 0.5$ implies equal exit Mach numbers in the vane and the blade. Since the entropy generated in a turbine stage is related to the square of the exit Mach numbers

$$\Delta s / c_p = \frac{\chi - 1}{2}(\zeta_v M_{is,V}^2 + \zeta_B M_{is,B}^2)$$

the optimum efficiency is achieved for equal exit Mach numbers in the two blade rows, at least when the loss coefficients are equal in both rows. For first stages, however, the stage reaction is often chosen to be as low as $R_T = 0.3$, since a lower reaction leads to a lower relative total temperature at the blade inlet.

The velocity triangles for a typical first stage with a stage loading and flow coefficient from Fig. 6.7 for two choices of stage reaction, $R_T = 0.5$ and $R_T = 0.3$, respectively, are shown together with representative blade shapes in Fig. 6.8. In constructing the diagrams, the usual assumptions of constant blade speed and axial velocity as well as equal stage inlet and exit velocities were made. Strictly, the latter assumption is violated in a first stage where there is a strong acceleration of the flow from the combustor interface (or vane inlet) to the stage exit. Nevertheless, the accuracy of the estimates is

Published by Woodhead Publishing Limited, 2013

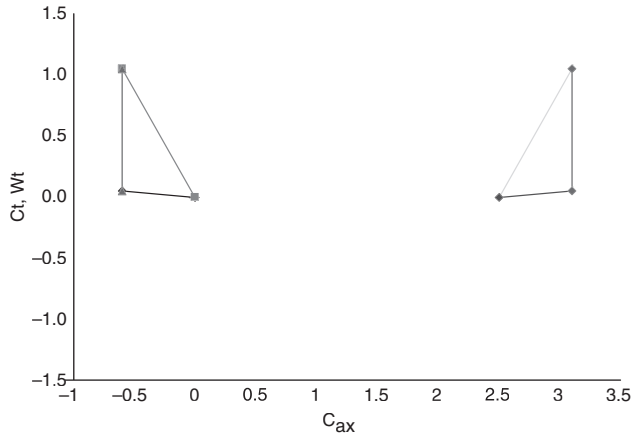


6.8 $R_r = 0.3$ velocity triangles, $R_r = 0.5$ and $R_r = 0.3$.

still good enough for our purpose. The velocity triangle and typical blade shape for a rear stage are shown in Fig. 6.9. Clearly, the resulting velocity triangles are quite different, with much higher flow turning in a first stage than in a last one.

There are very little published data on the profile aerodynamics in power gas turbines. In the field of aircraft engines, significant advances have been made in the last 20 years. Moustapha *et al*. (2003), for example report an increase in blade mean Zweifel coefficient, from about 0.85 around 1980 to values of 1.15 in the case of uncooled blades and 1.05 for cooled blades by

Published by Woodhead Publishing Limited, 2013



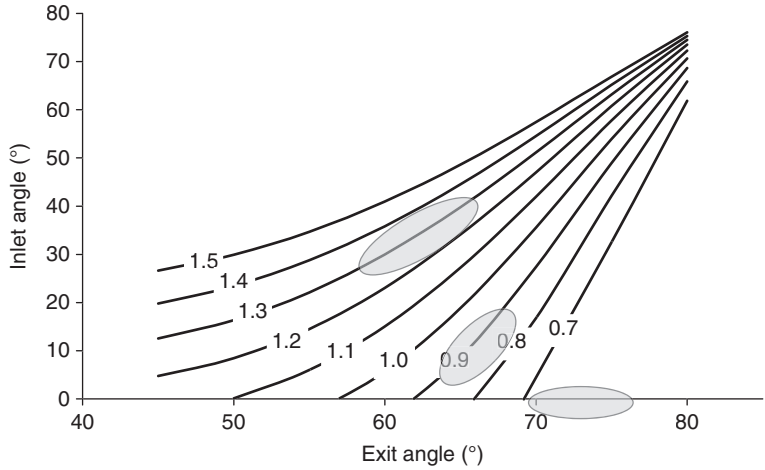
6.9 Last stage blade velocity triangles.

1990. Without giving numbers for the actual lift coefficients, Haselbach *et al*. (2001) report the design and testing of a redesigned low pressure turbine where ultra-high lift blading was applied with an 11% increase in lift coefficient over the previous 'high lift' blades. The profiles feature high suction side diffusion with a ratio of peak to trailing edge Mach number in excess of 1.3. Cascade tests of a high lift profile, with a Zweifel coefficient just below 1.3 and a similar level of diffusion, are reported by Michàlek *et al*. (2010). Much of the work in aircraft engine low pressure turbines is related to better understanding of boundary layer transition, including unsteady effects such as wake passing. Nevertheless, one would expect that, with the high Reynolds numbers present in power gas turbines, at least some sort of 'high lift' profile could be used with high suction side diffusion, even though due to higher airfoil blockage for cooled blades, the achievable lift levels may be somewhat lower than for the thin profiles in aircraft engine low pressure turbines.

Due to the lack of data, a direct comparison of the Zweifel lift coefficient for power gas turbines is not feasible. On the other hand, a reasonably good estimate of the ratio of axial chord to blade pitch l_{as}/s , or axial solidity, is possible. Dyschlevskij, in his 1965 PhD thesis, derived a correlation for the optimum blade spacing accounting for the relative blade thickness $t_{\max}/l$ as well as the blade turning (Abianz, 1979).

$$\frac{s_{opt}}{l} = k\left(\frac{180}{\beta_2 + \beta_3}\frac{\cos\beta_2}{\cos\beta_3}\right)^{1/3}\left(1 - \frac{t_{\max}}{l}\right)$$

Dyschlevski's correlation was translated into the corresponding value for axial solidity using the relations between true chord, axial chord and inlet



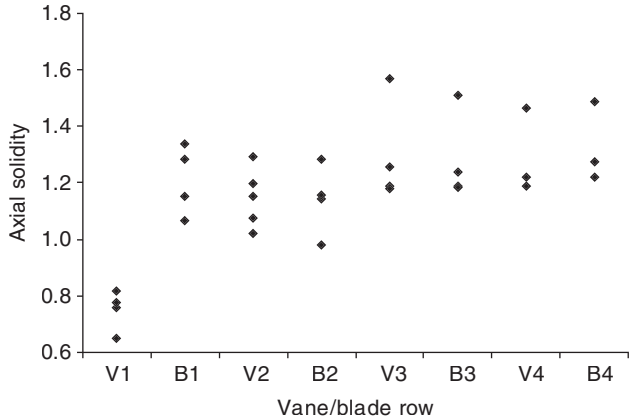
6.10 Optimum axial solidity with typical angles for first stage vane and blade and last stage blade.

and exit angles from Cohen *et al*. (1987). Isolines of optimum axial solidity as a function of inlet and exit angle for a relative thickness of $t_{max}/l = 0.2$ are shown in Fig. 6.10. Referring back to the typical range of first stage blade inlet and exit angles discussed earlier, the optimum axial solidity is roughly $l_{ax}/s = 1.3$ for $t_{max}/l = 0.2$. For a lower blade thickness, less solidity is required, for example, $l_{ax}/s \approx 1.15$ for $t_{max}/l = 0.1$. For first stage vanes, the optimum solidity would be below $l_{as}/s = 0.7$.

The axial solidity for the different blade rows of current F-, G- and H-class turbines is shown in Fig. 6.11. The observed values are close to the optimum values given by the correlation from Dyschlevski, dating back to 1965, indicating that even modern turbines are using quite conservative values of lift coefficients. This is confirmed by the few publications, such as Bahls (2002) discussing profile lift distributions where the suction side diffusion is characterised by a ratio of peak to exit Mach number of below 1.25. It is clear that one driver calling for high lift blading in aircraft engines, that is the impact on engine weight, plays no role in the design of a power gas turbine. Thus, it appears that the turbine designers came to the conclusion that the drawbacks of the higher lift in terms of higher secondary flow losses and the impact on the tip leakage (Moustapha *et al*., 2003) outweigh the benefit of a lower blade count. The axial solidity in the rear stages is also higher than required from Fig. 6.10. Here the blade chord is driven by mechanical and frequency requirements more than by aerodynamics.

A detailed discussion of the different stacking options for three-dimensional (3D) aerodynamic design can be found in Denton and Xu (1999). Haselbach *et al*. (2001) show an application of 3D stacking to an aircraft

Published by Woodhead Publishing Limited, 2013

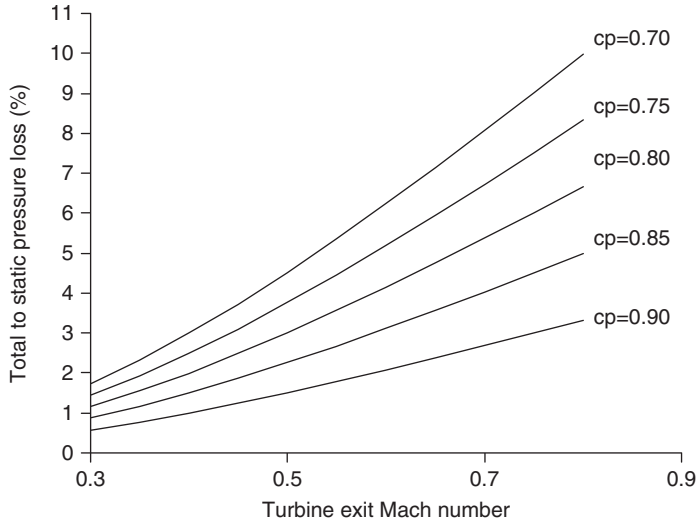


6.11 Axial solidity of vanes and blades in F-, G- and H-class turbines.

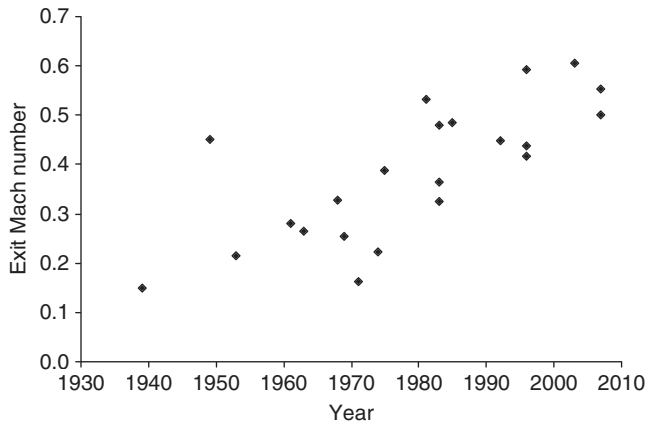
engine low pressure turbine, where compound lean is applied to the vanes. For power gas turbines, only two applications of significant compound lean have been reported (Aoki, 2000), where two generations of 3D stacking were applied to the vanes in the 501F and 501G engines from Mitsubishi, respectively, and their counterparts from the Siemens SGT6–5000 series.

The exhaust diffuser design has a significant impact on turbine performance. With increasing turbine exit Mach number, the total pressure loss in the diffuser for any given recovery factor *cp* increases as shown in Fig. 6.12, thus reducing the turbine pressure ratio. In terms of overall gas turbine performance impact a 1% increase in total pressure loss is equivalent to 0.2–0.3% turbine efficiency reduction. Early on in gas turbine development, the exhaust mass flow was usually small relative to the available area, thus leading to turbine exit Mach numbers well below 0.3 (Fig. 6.13). By the mid- to late 1960s, the exit Mach numbers had risen above 0.3, and diffuser design started to take more importance (Seippel, 1966). For the lower Mach numbers, a rather low area ratio in the exhaust diffuser was acceptable. This then led to simple diffuser designs resembling a sudden expansion. The reason is clear when looking at the pressure recovery plotted against the inlet-to-exit area ratio in Fig. 6.14. The figure gives both the ideal recovery and the actual recovery for a sudden expansion. For ratios of inlet-to-exit area of 0.7 and above, the difference in pressure recovery becomes quite small and there is no real benefit in going to more elaborate designs. However, for ratios in the region of 0.2, as frequently used in modern gas turbines, the difference becomes very large. In terms of aerodynamics, the layouts of current exhaust systems of gas turbines from different companies are quite similar. In a first section, an annular diffuser with a small area increase is located. Here a number of struts are located that contain a support structure for

Published by Woodhead Publishing Limited, 2013



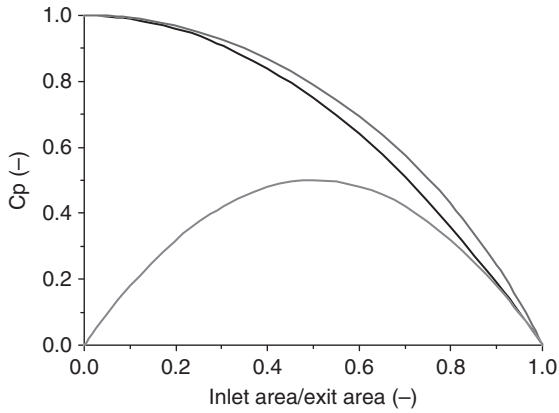
6.12 Diffuser pressure loss as function of turbine exit Mach number.



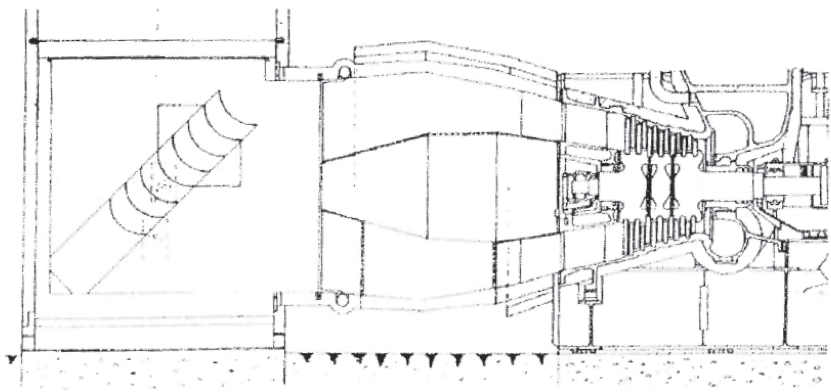
6.13 Turbine exit Mach number over time (year).

the bearing, arranged radially or leaned, and often profiled to reduce the swirl exiting the turbine. Following this so-called exhaust gas housing, an annular diffuser is located, typically making up about half the area ratio. At the end, there are again supporting struts, and a sudden expansion is located immediately downstream, before an equalising section finally either takes the flow to the HRSG or the flow is turned into the stack. The sudden expansion is sometimes made less severe by a cone at the inner diameter,

Published by Woodhead Publishing Limited, 2013



6.14 Diffuser pressure recovery vs are ratio; ideal diffuser and sudden expansion.



6.15 Typical diffuser arrangement 1966 and modern GT.

while at other times the inner diameter at the end of the bearing tunnel ends abruptly (Brummel, 2002). Examples of a diffuser from 1966 and a modern one are shown in Fig. 6.15. Modern diffusers typically have an area ratio of about 0.2 from turbine exit to the equalising section, and reach a pressure recovery in the region of 0.75.

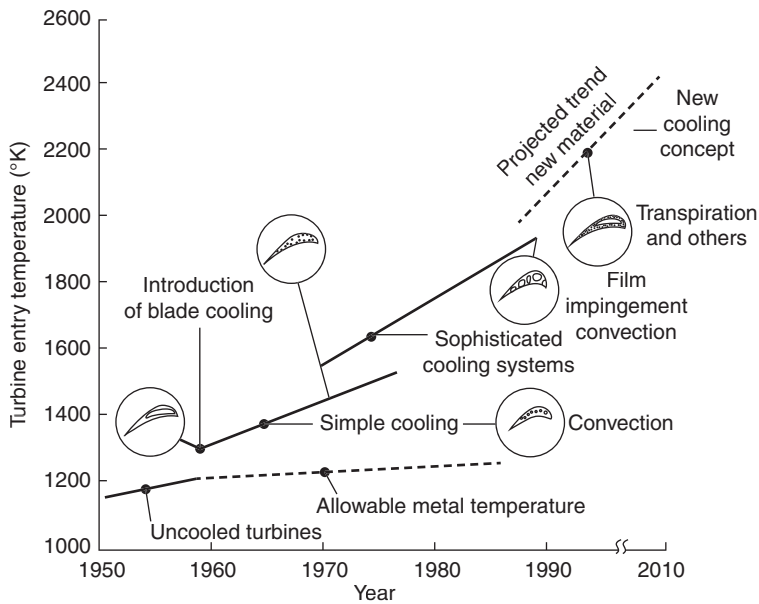
6.4 Cooling

Major development drivers and achievements for GT development have been power output, GT efficiency and reduction in emissions. These performance achievements have been mainly realised through improvements in the detailed component design (Figs 6.1–6.3). For the turbine component,

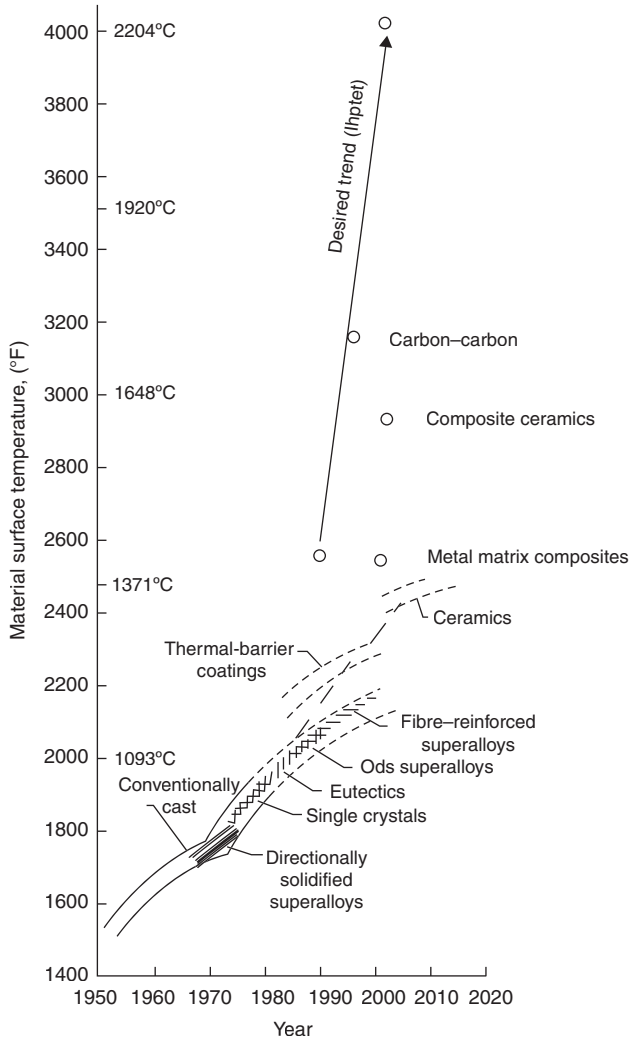
the evolution beyond the performance and aerodynamic evolution can be attributed to:

- Increase in hot gas temperature capability through the introduction of new materials, coatings and cooling technology (Figs 6.16–6.18). This allows the spread in between the driving gas temperature that the part sees and the metal temperature that is achieved through active cooling to be increased. The constraint for the metal temperature is imposed by lifetime requirements to be achieved.
- The allowable metal temperature has been raised through the introduction of new materials, the so-called super alloys.
- Introduction of ceramic coatings that function as thermal barrier coatings, as well as oxidation protection coatings to protect the mechanical load carrying base metal super alloys.
- Manufacturing technology that allows complex geometrical features to be realised mainly through investment castings, thermal sprayed coatings and three-dimensional machining operations.

Simple convective cooling schemes have been introduced during the mid-1960s to the 1970s (Figs 6.16 and 6.18). The manufacturing technology used was mainly based on forging and machining. Aero-engine technology available by then allowed an accelerated introduction of casting



6.16 Aero-engine cooling technology chart.



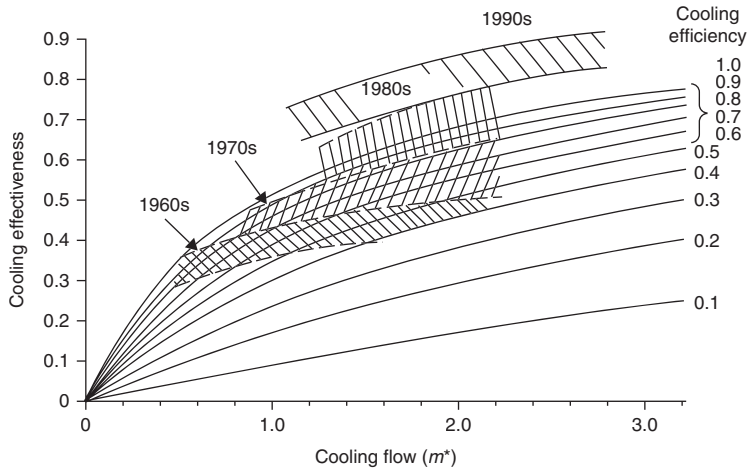
6.17 Aero-engine evolution of material surface temperature over time.

technology. Advanced convective schemes using means of impingement cooling for static parts followed in the late 1970s and the beginning of the 1980s.

Improvements in secondary air systems, such as pre-swirl nozzle systems and advanced sealing technology, allowed having a positive BFM for the front stage static and rotating parts. Subsequently, film cooling technology was introduced, first on the front stage vanes leading edges and later on the rotating blades.

Advancements in manufacturing and materials technology led to the introduction of investment castings (ceramic cores), first for directionally

Published by Woodhead Publishing Limited, 2013



6.18 Aero-engine cooling effectiveness over heat load parameter.

solidified materials and later for single crystal alloys. Investment casting opened the opportunity of using multi-pass cooling systems. Initially, area enhancing features were used, and towards the end of the 1970s angled rib turbulators appeared in the open literature (Han, 1978) to improve the heat transfer in between the bulk cooling flow and the near wall flows. Angled rib turbulators introduce longitudinal vorticity into the cooling flow path, and thereby enhance the flow exchange.

Film cooling technology, introduced in the beginning of the 1980s, was cylindrical in shape first. With the F-class engines, fan shaped cooling hole technology through laser or EDM hole drilling was introduced. Due to unavoidable mismatch in pressure between the cooling and the hot gas flows, the large momentum of the films led to film lift off from the metal surface and loss of film cooling protection. Fan shaped cooling holes reduce the momentum and avoid film lift off, and thereby improve film cooling effectiveness.

Thermal barrier coatings, which had first been tested at NASA in 1978 (Miller, 1997) began to be commercially available for the heavy-duty gas turbine industry in the beginning of the 1990s.

Detailed data are difficult to obtain and difficult to generalise, since turbine design parameters, such as reaction vs impulse turbine scheme selection or materials used, may influence the specific requirements when the technology elements are needed. Estimates are given subsequently. Turbines with inlet temperatures of up to 850°C can remain uncooled. At around 875°C vane cooling and, above 900°C, first stage blade cooling is required. Temperature levels above 1100°C require first stage vanes to be cooled with showerhead film cooling and the second stage to be convectively cooled depending on the first stage

Published by Woodhead Publishing Limited, 2013

work extraction. The first F-class engine (GE 7FA turbine), which was shipped in 1988, was stated to be rated at 1250°C. Many cooling technology features introduced in the 1990s were first published with the NASA US E^3-aero-engine programme (Lakshminarayana, 1996).

Cooling technology is commonly classified using a set of parameters (Fig. 6.18), which are subsequently explained.

$$\Phi = \frac{(T_m - T_{\mathrm{HG}})}{(T_c - T_{\mathrm{HG}})} \quad \text{Cooling effectiveness}$$

Cooling effectiveness is defined as a normalised metal temperature. The metal temperature is normalised with the cooling air feed temperature and the driving hot gas temperature. At a value of one, the metal temperature is at the cooling air temperature, at a value of zero the metal temperature is at the hot gas temperature. The parameter defines the cooling requirements, that is, highly cooled versus weakly cooled.

$$\eta_c = \frac{(T_{c,\mathrm{out}} - T_{c,\mathrm{in}})}{(T_m - T_{c,\mathrm{in}})} \quad \text{Cooling efficiency}$$

The cooling efficiency refers to that of the internal heat exchanger. The average cooling air temperature at which the cooling fluid leaves the cooled part is normalised with the cooling air feed (cooling inlet temperature to the part) and the average metal temperature. At a value of one, the cooling air leaves the cooling system at the metal temperature, that is, maximum heat pick-up, maximum potential used. At a value of zero the cooling fluid leaves the cooling system at the cooling air inlet temperature, that is, no heat pick-up. It defines the cooling technology level achieved, that is, well cooled or badly cooled.

$$m^* = \frac{c_{p,c} \cdot m_c}{A_{\mathrm{HG}} \cdot \mathrm{HTC}_{\mathrm{HG}}} \quad \text{Heat load parameter (Mass flow function)}$$

The heat load parameter (sometimes called the mass flow function) sets the heat transported by cooling medium in relation to the heat input into blade.

$$\eta_{\mathrm{film}} = \frac{(T_{\mathrm{film}} - T_{\mathrm{HG}})}{(T_c - T_{\mathrm{HG}})} \quad \text{Film cooling effectiveness}$$

The film cooling effectiveness is defined as a normalised film temperature. The film temperature is normalised with the cooling air feed temperature and the driving hot gas temperature. At a value of one the film temperature is at the cooling air temperature, at a value of zero the film temperature is at the

Published by Woodhead Publishing Limited, 2013

hot gas temperature. The parameter defines the effectiveness of the cooling film, that is, non-mixed-out film vs mixed-out film. Above certain temperature levels, film cooling is required for reducing the hot gas temperature to the film temperature. Without film cooling the driving hot gas temperature is limited to what is achievable by convective cooling. With thermal barrier coatings the base metal interface temperature requirements remain similar, but the cooling mass flows can be reduced.

The four parameters mentioned above are interlinked. The cooling effectiveness is an engine-level constraint determined by the chosen cycle and part material. The higher the cooling effectiveness requirements are, the higher the cooling efficiency that can be achieved. A large driving temperature difference allows more heat to be taken out. At a certain limit, film cooling is required, since convective cooling is limited. Thinner walls significantly improve the convective cooling efficiency achievable.

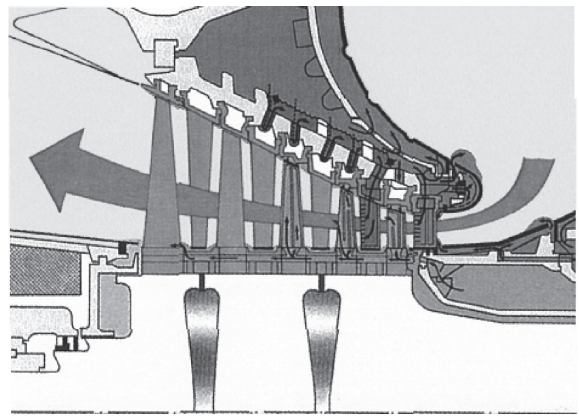
In practice for some designs a local cooling effectiveness to be achieved drives the total cooling flow amount, that is, the whole blade needs to be flowed to achieve the cooling requirements at a local geometry. On the other hand, bringing cooling fluid directly to such a location may result in no heat pick-up of the cooling fluid and consequently a low cooling efficiency. Using advanced cooling technology measures, this can be overcome, for example, near wall cooling, wall cooling, and transpiration cooling.

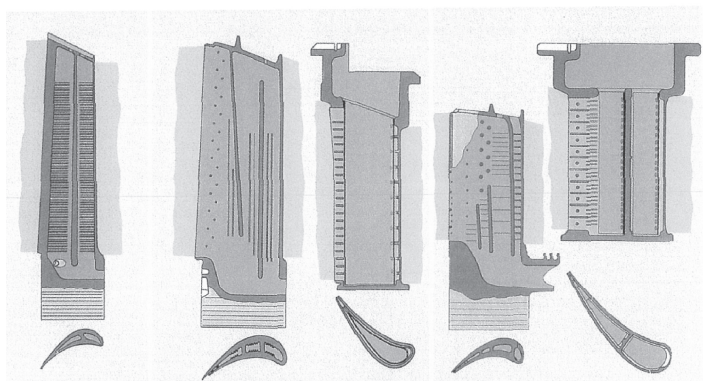
Figure 6.16 shows the evolution of blade cooling systems for aero-engines. Figure 6.18 shows a corresponding cooling effectiveness chart. Typical cooling schemes of a heavy-duty gas turbine from the beginning of the 1980s are shown in Fig. 6.19.

6.5 Durability and damage mechanisms

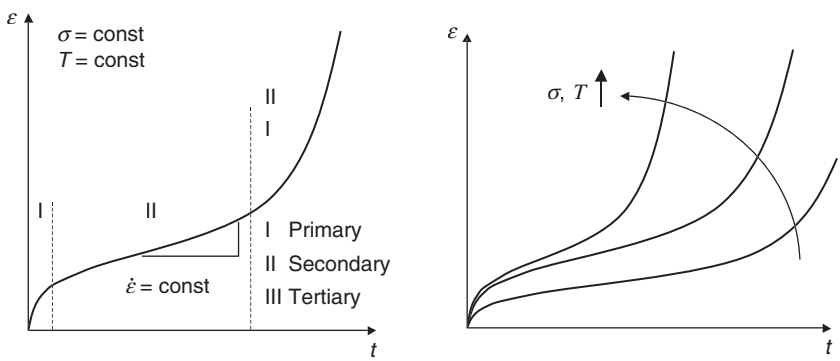
The main damage mechanisms for turbine blades and vanes are creep, high cycle and low cycle fatigue, as well as oxidation. Creep occurs when a component is exposed to high loads at high temperature for a long time, resulting in a time-dependent deformation (Webster and Ainsworth, 1994). Under the stresses prevalent in turbines, creep can be split into three phases: primary, secondary and tertiary creep (Dowling, 1999; Webster and Ainsworth, 1999). In the primary creep phase, the creep rate decreases in time. In the secondary phase, the strain rate is approximately constant and first voids start to form. In the tertiary strain phase, the strain rate increases progressively in time and creep cracks start to develop, eventually leading to rupture failure. Creep damage is accelerated with higher mechanical loads and with higher metal temperature (Fig. 6.20). For a safe design it is generally considered that creep should remain within the secondary phase throughout the lifetime of a blade. Creep can lead to failure before rupture is reached. Excessive creep deformation can, for example, lead to a clash

Published by Woodhead Publishing Limited, 2013





6.19 Beginning of 1980s Alstom GT13E: Typical five stage turbine layout out and corresponding cooling systems.



6.20 Creep strain relation.

with neighbouring parts, to the loss of shroud coupling or the failure of a sealing feature to perform its duty.

In fatigue, cracks can form under repeated application of a stress that is well below the tensile strength. High cycle fatigue is generally characterised by low strain within the elastic range, but with a high number of cycles. High cycle fatigue in turbines is typically caused by vibrations with vanes or blades either running in resonance to some outside excitation or by self-excited vibrations in the case of flutter. Low cycle fatigue, on the other hand occurs after relatively few cycles covering a high strain range leading to elastic–plastic material behaviour. In thermal fatigue, the stresses are generated by local temperature gradients, which vary between idle, part load, base load and engine off conditions. The strain range covered through a transient cycle may be larger than that between the two end states of the cycle, depending on the ratio of the time scale of the change to the characteristic thermal time scale of a part. For example, a rapid increase in hot gas temperature will initially lead to a high temperature gradient between the blade surface and the remainder of the wall and, therefore high thermal stresses. In time thermal conduction will even out the temperature gradient so that the thermal stresses in the end state may be lower than during the transient (Moustapha *et al.*, 2003).

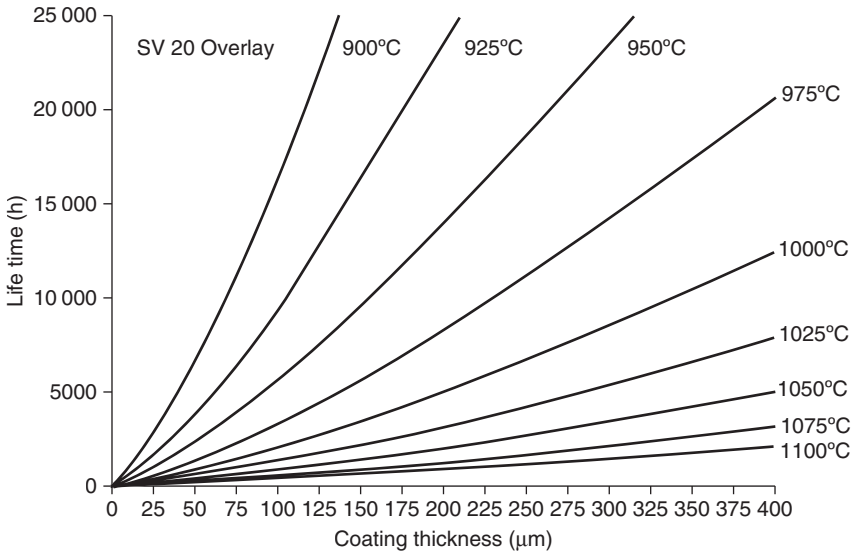
Oxidation occurs when metal is exposed to high temperatures and a reaction between the metal surface and the remaining oxygen in the hot gas path takes place. This reaction leads to a reduction of wall thickness. Coatings are usually applied to reduce oxidation. Even though these coatings have higher oxidation temperatures than the base metal, coating becomes depleted over time, at which point base metal oxidation will start (Fig. 6.21). Typical areas where oxidation is a major concern are the tips of unshrouded blades, where at best excessive amounts of cooling air may be required to sufficiently reduce the metal temperature. At worst, certain areas cannot be cooled sufficiently at all.

With the exception of high cycle fatigue, all these damage mechanisms are strongly dependent on the metal temperatures at the critical locations. Table 6.1 shows the sensitivities to metal temperature from Dailey (2000). The life of a blade is doubled or halved with a change of 15°C and 30°C, depending on the failure mechanism, highlighting the importance of accurate temperature predictions.

An understanding of the importance of stresses due to centrifugal loads can be obtained by looking at the parameter AN^2, which correlates to the hub stress of blades for a given taper ratio. In aircraft engine high-pressure turbines, AN^2 is typically in the range $5000 < AN^2 \leq 9000$ (Moustapha *et al.*, 2003) whereas in modern power gas turbines usually $2000 < AN^2 \leq 4500$. In last stage blades of power gas turbines, on the other hand, values of $AN^2 \approx 15\,000$ and higher are reached, whereas the typical range for aircraft engine low pressure turbines is

Table 6.1 Failure mechanism and sensitivity to metal temperature at critical locations

Mechanism	Metal temperature change to double/halve life
Creep	15°C
Corrosion (oxidation and sulphidation)	20°C
Low cycle fatigue	30°C
High cycle fatigue (vibration)	Not primarily temperature driven



6.21 Oxidation of overlay coating.

$11\,000 < AN^2 \leq 14\,000$. At the same time, the last stage turbine blades in power gas turbines are running at much higher temperature levels since the exhaust temperatures (Fig. 6.3) are 150–200°C higher than in aircraft engines.

As a consequence, the stresses in aircraft engine high-pressure turbine blades are typically about evenly split between centrifugal stresses and thermal stresses. In power gas turbines, on the other hand, thermal loads account for about 90% of the stresses in a first stage blade. Due to the lower centrifugal loads, blade creep is usually not an issue in such turbine blades and, due to the fixed rotation speed, high cycle fatigue can be avoided by tuning the blade eigenfrequencies to be out of resonance with known sources of excitation, although blades can briefly run through resonance at start-up and shut-down. Thus, the main concerns are oxidation and thermal fatigue.

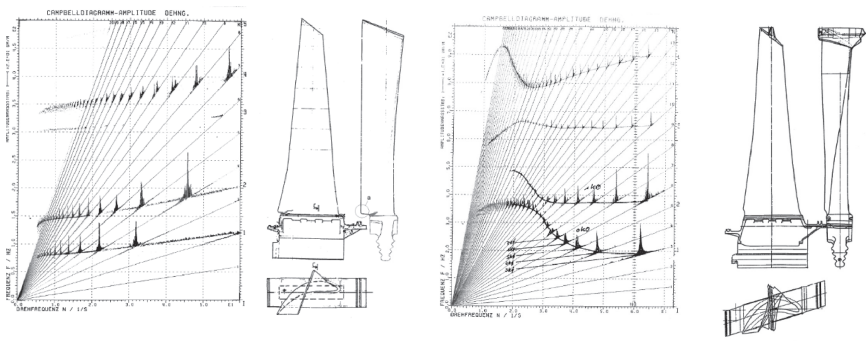
Published by Woodhead Publishing Limited, 2013

In the rear stages, on the other hand, creep becomes the relevant damage mechanism in turbine blades for power generation.

Power gas turbines differ from aircraft engines not only in the major damage mechanisms, but also in their lifetime requirements and operating concepts. In order to keep within emission regulations at part load (CO), combined-cycle part load efficiency at higher part load and in order to keep temperatures sufficiently high for the water steam cycle, power gas turbines operate with the turbine inlet temperature at or near the base load values throughout much of the operating range (Bauer and Rofka, 2002; Eppler *et al*., 2008). Thus, there is roughly an order of magnitude difference in terms of time spent at peak temperature between aircraft engines and power gas turbines (Bunker, 2004). With the increased flexibility required by the current market, gas turbines will run anywhere from daily start–stop cycles to long periods of continuous base load, where continuous operation for half to three-quarters of a year is not uncommon.

As noted above, high cycle fatigue due to resonance can usually be avoided by appropriate frequency tuning. However, with the high mass flow in modern power gas turbines, last stage blades become very long, with airfoil heights up to about 0.8 m. With increasing airfoil height, the eigenfrequency of the blade will drop. Once frequencies are below a certain threshold, self-excited aeroelastic vibrations may occur, leading to high cycle fatigue damage. Typically a blade design is deemed to be safe if the Strouhal number $Str = (fL)/U$ for the first bending mode is above $Str \approx 0.3$ to $Str \approx 0.35$, depending on the source. Higher values above $Str \approx 1$ are required for the first torsional mode. Since it is difficult to achieve sufficiently high frequencies to reach these Strouhal numbers, most engine manufacturers have chosen to use shroud coupling on their rear stages. Shroud coupling will increase the frequency and, with sufficient shroud stiffness, reduce the torsional component of the eigenmode. Siemens, as the only exception, at least for engines of the E- and F-class, have used hollow blades with a long axial chord, raising both the frequency due to stiffness at the inner diameter and increasing the Strouhal number with a higher tip chord. Typical Campbell diagrams for a free standing and a coupled blade are shown in Fig. 6.22. Here, blade vibrations were recorded via strain gauge measurements during start-up and over-speed in a spin pit test. In the free standing blade, there is a single eigenmode per family of modes for which the frequency increases with rotational speed due to centrifugal load stiffening. Thus the frequency recorded in this test is increasing with speed. For the coupled blade, each modal family has a different eigenmode and frequency for each possible nodal diameter or inter-blade phase angle. When running through a resonance, the nodal diameter number and the number of excitations per revolution coincide. Thus, the higher nodal diameters reach resonance early in the run-up. Since higher nodal

Published by Woodhead Publishing Limited, 2013



6.22 Typical Campbell diagram for uncoupled and coupled blades.

diameters have higher resonance frequencies, there is a general trend of lower eigenfrequencies with higher speed.

6.6 Typical parts and interfaces

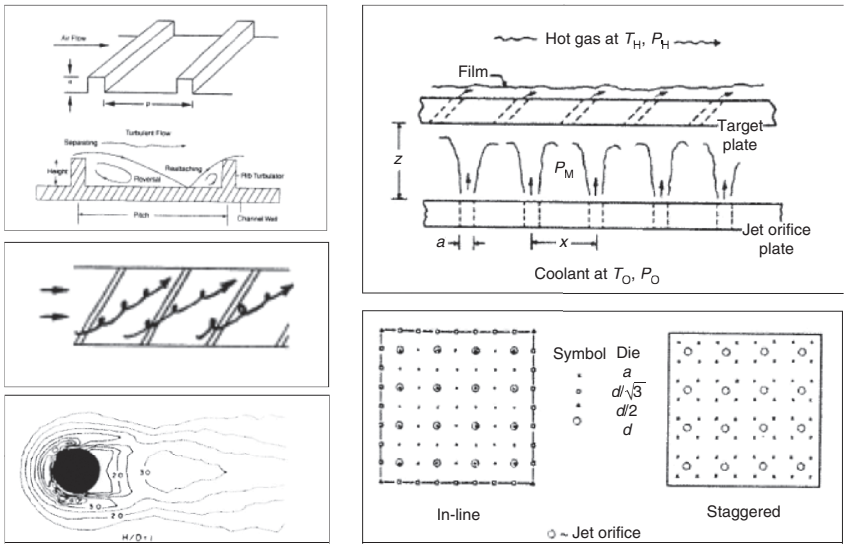
In the following section a brief summary is given on cooling features and turbine parts commonly used in today's modern gas turbine systems, and some key areas of concern. On each of the features, a large number of publications exist (Han *et al.*, 2000):

- The leading edge of an airfoil is of particular interest, since optimised aerodynamic design requires a small radius, which results in a high heat load in the leading edge laminar stagnation region due to its thin boundary layer. For many applications the leading edge is a critical area of concern, with showerhead film cooling applied on the front stages to reduce the heat load.
- Today's manufacturable wall thicknesses limit the range where pure convective cooling can be applied, and film cooling technology is a common feature to reduce the heat load. For film cooling a secondary cooling fluid is introduced into the main stream gas and kept attached to the exposed walls to protect the walls. Slot film cooling does not meet mechanical requirements, such that discrete hole film cooling is required. Many studies have been conducted to avoid the disturbance of the thin protecting film and achieve protection significantly downstream from the place of injection ($s/d > 50$). The intention is to have as little mixing as possible between the cooling and the mainstream flow. The injection locally disturbs the thermal boundary layer and therefore results in a heat transfer coefficient (HTC) enhancement, which has to be balanced with the temperature effect benefit of the film. Film cooling holes need to have a positive outflow, including margin (often called back flow margin – BFM),

under all operating and transient conditions (e.g. vane wake) and therefore impose constraints on the layout of a cooling system. An area of particular importance is the leading edge area where the film cooling holes cannot be angled into the flow direction of the mainstream gas (typical values 30°) and need to be pointed against the mainstream. Generally, the cooling system leading edge region is reliant on the film cooling hole internal convective cooling effect. This effect is of less benefit if the film effect is increased. The leading edge hole length can be increased to raise the convective effect by introducing an angle away from the GT machine axis, often called compound film cooling.

- For turbine internal convective cooling, the following methods are commonly used, or a combination thereof: multi-pass cooling, jet impingement cooling, rib-turbulated cooling and pin-fin turbulated cooling. Many more features have been examined as for example vortex generators, dimples and others. A summary can be found in Han *et al*. (2000).
- Multi-pass cooling is a method that was introduced when the manufacturing method of investment casting offered a technological benefit in terms of cooling efficiency increase compared to the formerly used forging method. Forging mostly resulted in single pass cooling channels, and connecting two with a connecting bend and turning the flow towards its original flow direction allowed the reuse of the cooling fluid and is well suited to form a geometry useable for a ceramic core. Still, the hole blade cross-section has to be flowed, putting constraints on the achievable internal Ma number at a given amount of cooling mass flow and therefore the achievable HTC. Increasing the number of multi-pass channels can increase the achievable HTC levels (Dailey, 2000) and thereby the cooling efficiency. Walls that are not connected to the hot gas side (often called webs) remain relatively cold. Increasing the number of passages results in increased channel aspect ratios and results in low bulk flow exchange with the hot near wall flow, and thus limits the achievable cooling efficiency.
- Jet impingement cooling (Fig. 6.23) with cast-in holes, or with holes formed by an insert, allows the hot near wall flow region to be cooled by an internal jet film (Goldstein, 2000). Thus, not the whole cross-section needs to be flowed, and the achievable internal HTC-levels/cooling efficiency tends to be higher. The use of inserts is limited for rotating parts. For static parts, inserts are commonly used but put a constraint on the allowable 3D aerodynamic external shape, since inserts need to able to fit in. Recent developments have therefore been undertaken to cast-in the jet impingement cooling holes not only into the split plane of the core (required to separate the core die tool after injection) but also in other areas. After the use of the cooling fluid for jet impingement cooling, the fluid is often reused as film cooling fluid subsequently.

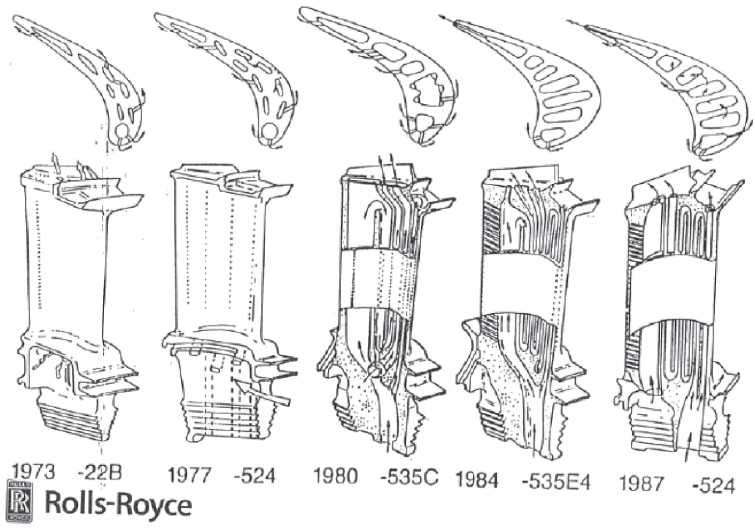
Published by Woodhead Publishing Limited, 2013



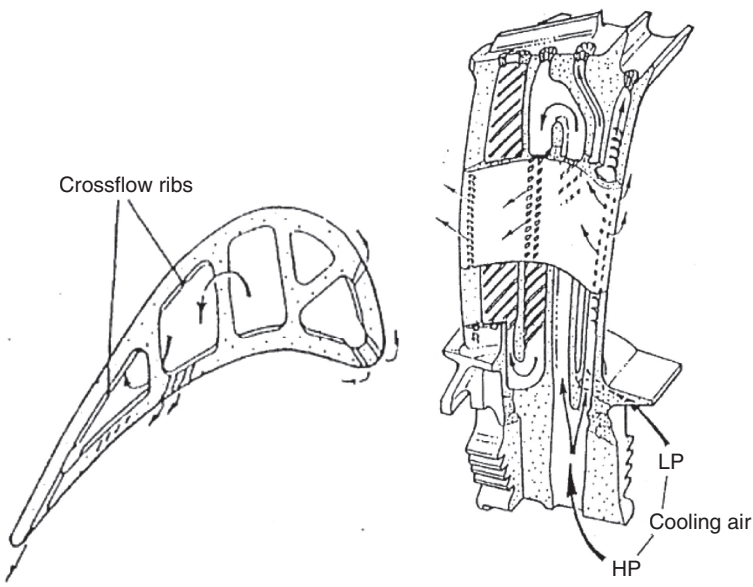
6.23 Internal cooling feature. Top left and middle left: rib-turbulated cooling, bottom left: pin-fin cooling. Right: jet impingement cooling.

- Rib-turbulated cooling (Fig. 6.23) was first used as roughness elements by placing them normal to the flow direction or as area enhancement ribs to increase the internal heat exchanger area onto the hot side walls (pressure or suction side). Angling the ribs towards the flow results in vortex pairs and enables a bulk flow heat exchange with the close wall region (Han *et al*., 1978). Today's angled rib turbulators are a common technology used in many turbine parts, mainly on rotating components but also on static parts.
- From the leading edge towards the trailing edge of an airfoil the thickness of the profile significantly reduces. For mechanical reasons it is often required to combine cooling features with geometrical features that are able to carry load. Pin-fin turbulated cooling is a method (Fig. 6.23) that offers heat transfer enhancement and can carry mechanical load. Half-pins can also be used to set the impingement to wall stand-off distance if jet impingement cooling is used, and therefore the feature is commonly applied in turbine cooling.

Typical cooling schemes for front stage parts can be seen in Figs 6.24–6.28 and Plate XII (see colour section between pages 346 and 347). Figures 6.25 and 6.26 show the front stage vane and blade of an aero-engine (Rolls-Royce Trent 800). In Plate XII and Fig. 6.27 a front stage vane and blade cooling system of a heavy-duty gas turbine and in Fig. 6.28 the cooling system of a front stage heat shield of an unshrouded blade are shown.

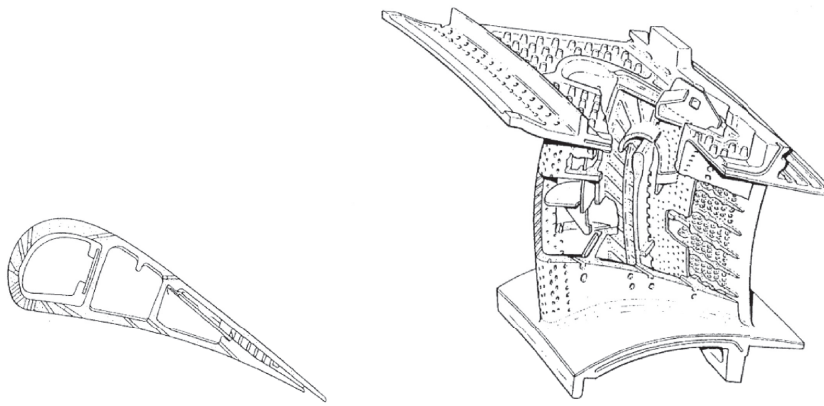


6.24 Aero-engine (Rolls-Royce) evolution of front stage rotating blade cooling schemes.

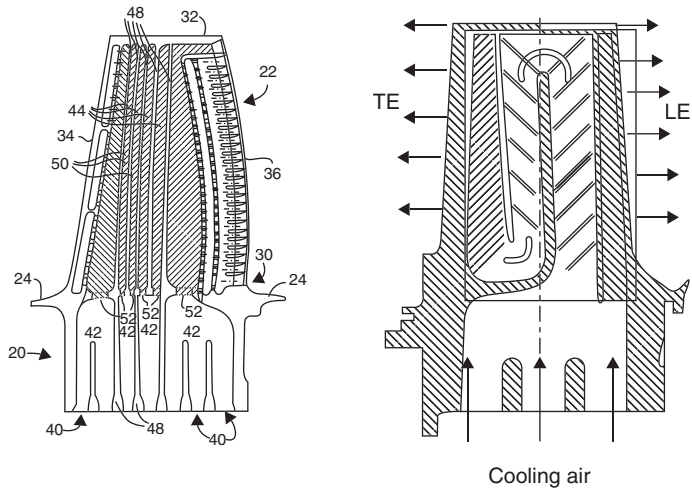


6.25 Aero-engine (Rolls-Royce) front stage rotating blade cooling scheme.

Published by Woodhead Publishing Limited, 2013



6.26 Aero-engine (Rolls-Royce) front stage vane cooling scheme.



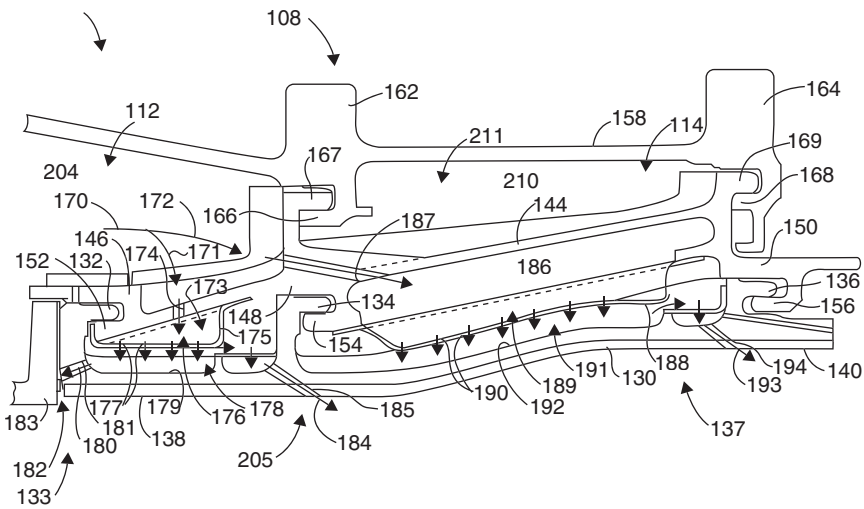
6.27 Left: Siemens first stage unshrouded blade, right: Alstom front stage blade.

Front stage vanes commonly use impingement cooling in combination with film cooling. Thermal barrier coating is sprayed to the external surface. At the leading edge shower head film cooling is used. The trailing edge is thin, and pin-fin turbulators are implemented. Some engines use vane twins to reduce costs. Not all surfaces may be available for thermal barrier coating (TBC) or film cooling hole drilling then.

Two principle configurations are shown for the front stage blade (Fig. 6.27):

1. A large multi-pass (1–3-3–1) type blade with split plane leading edge impingement and in some cases trailing edge impingement, which evolved

Published by Woodhead Publishing Limited, 2013



6.28 Right General Electric front stage heat shield (shroud) of an unshrouded blade.

from the US aero-engine technology. Such schemes are commonly used by General Electric (7FA) and Siemens (SGT5–4000, SGT6–5000).

2. A common multi-pass (1–3) type blade commonly used by Alstom (GT26), with advanced film cooling on the leading edge and the blade tip, which evolved from the European aero-engine technology (Rolls-Royce).

All front stage blades use film cooling with thermal barrier coating. Some blades are made out of single crystal, others use directionally solidified materials. Front stage heavy-duty gas turbine blades have no shrouds, due to the size and the loading of the blades. On multi-pass blades, core withdrawal of the ceramic core out of the core die tool imposes constraints on the cooling geometry feasible.

Modern blades often use tip squealer arrangements with TBC coating to reduce the heat load and overtip leakage (Bunker, 2004). Highly loaded tips may require cold cooling air supplied directly to the tip and tip flag features can be used.

A typical front stage heat shield can be seen in Fig. 6.28. The cooling technology used is very similar to the front stage vane. Film cooling is limited due to the disturbance of the passing blade. TBCs applied need to be rub resistant to allow aerodynamic clearance optimisation. In many cases high temperature abradable systems are used on the blade and heat shield to form a sealing system.

6.7 Future trends

Future trends in turbine component design can only be estimated. Some engine parameters can be envisioned as follows.

Gas turbine flexibility in operation is an important driver. Turbine extended operation is required. Examples are grid frequency stabilisation and fast start-up capability to balance alternative energy generation, for example, due to fluctuations in wind. Emission requirements for NO_x, CO, CO_2 capture achievability, for example, through flu gas recirculation, fuel flexibility for coal gasification or hydrogen fuels, require flexibility on the combustor interface in terms of temperature operation range and gas composition.

Performance improvements in terms of power output and combined-cycle efficiency will continue. The turbine hot gas temperature will increase beyond today's level, and improved cooling schemes to further reduce cooling air consumption in spite of the hot gas temperature increase will be required.

Published research, technologies used in aircraft engines, and patent applications may offer an insight into the next 20 year range. Often, relevant technology features are hidden and not published in patents if they are not directly accessible. From the many available examples, some advanced technology features have been taken and will be discussed below.

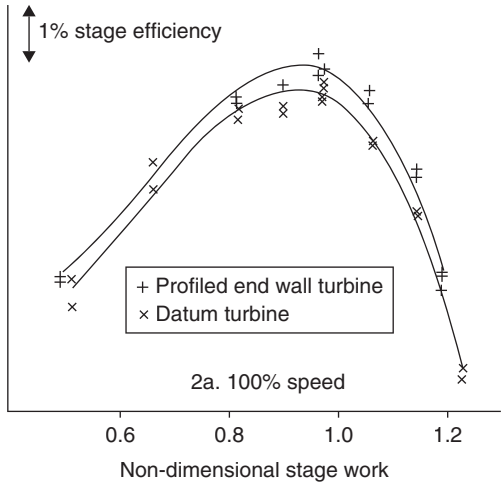
Examples of advanced technology features:

- Three-dimensional design features.
- Loaded endwall designs.
- Advanced convective cooling schemes for large components.
- Advances in tip clearance reduction.
- Advances in film cooling.
- Advances in material technology.
- Advances in coating technology.
- Advances in manufacturing technology.

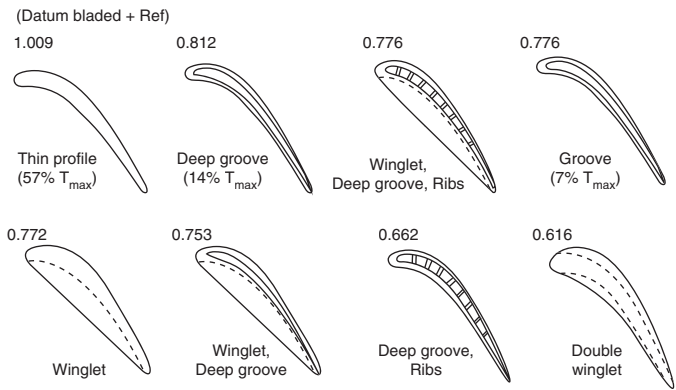
6.7.1 Aerodynamics

A large amount of research has been carried out in the field of non-axisymmetric endwall contouring (e.g. Rose, 1994; Rose *et al.*, 2001; Hartland and Smith, 2002; Paisner *et al.*, 2007). The first applications were aimed at reducing the transverse pressure amplitude at the trailing edge of a vane platform (Rose, 1994). Later it was recognised that there is a potential for reducing secondary flow losses by the application of non-axisymmetric endwall contouring. This feature has been applied in commercial civil aircraft engines (Rose *et al.*, 2001), but not to power generation gas turbines. One would expect that eventually contoured endwall technology will be transferred from aircraft engines to power generation turbines (Fig. 6.29).

Published by Woodhead Publishing Limited, 2013



6.29 Stage efficiency improvement due to profiled end walls (Rose *et al.*, 2001).



6.30 Different shapes of blade tip winglets.

The other main area of aerodynamic research that might in the future be applied to power gas turbines is the work on tip leakage reduction for unshrouded blades. Much of the work looks into the application of a so-called winglet or mini-shroud (Booth, 1981, 1985; Staubach *et al.*, 1996, Sjolander, 1997; Harvey and Ramsden, 2001; Harvey *et al.*, 2006). Such concepts have been applied in demonstrator engines and Harvey *et al.* (2006) report that the performance of their winglet design matched the one of a shrouded blade with two fins. This technology is still in the research stage even for aircraft engines (Fig. 6.30). Further discussion can be found in Denton and Xu (1999), Moustapha *et al.* (2003) and Harvey (2004).

Blade tip clearance control is to some extent in direct competition with advanced tip designs. In the first stages of power generation turbines, typical relative tip clearances were 3% and more of the blade height. However, several manufacturers have recently introduced clearance control measures by either controlling the radial position of the casing or by axial movement of the rotor relative to the stator (Fukuizumi *et al*., 2003). Other means of reducing the radial clearance is the application of an abradable coating to the stator heat shield (sometimes called shroud). If the steady state tip clearance can be reduced to sufficiently low levels, the application of a winglet may no longer be attractive.

6.7.2 Cooling and manufacturing

A significant turbine part improvement relies on the advancement in manufacturing technology. Today the manufacturing processes, mostly casting, limit possible advancements in cooling technology. Some insights on the pathways into the future can be drawn from the published patents and patent applications:

- More complex cores through:
  - Build cores out of several more detailed cores.
  - Dissolvable cores to manufacture the ceramic that are used in the casting process.
- Build parts with:
  - Joining at the cold less-loaded side removing the constraints for the hot fillets that join the airfoil and endwalls.
  - Shelves.
  - Hybrid parts with combinations of ceramic and standard super-alloy materials to have, for example, leading edge inserts.
- Rapid prototype manufacturing technology for part manufacture.
- Layered coatings which include transpiration cooling features.
- Minimisation of cooling features and reduction in wall thickness.
- TBC technology spraying to allow increased temperature deltas across the ceramic layer moving towards a pure ceramic part.

6.8 References

Anon, (2008), '32nd Power generation order survey', *Diesel & Gas Turbine Worldwide*, October, p. 32.

Aoki S, (2000), 'Trend and key technologies for gas turbine combined cycle power generation in a globally competitive market and environmental regulations', *Proceedings of the 2000 International Joint Power Generation Conference*, July 23–26, Miami Beach, Florida.

Bals H, (2002), 'Axialturbinen', in Lechner C and Seume J, eds, *Stationäre Gasturbinen*, Berlin, Springer, 357–382.

Bauer A and Rofka S, (2002), 'Stationäres betriebsverhalten', in Lechner C and Seume J, eds., *Stationäre Gasturbinen*, Berlin, Springer, 939–959.

Booth T C, (1981), 'Rotor-tip leakage part 1 – basic methodology', *ASME Turbo Expo 1981*, March 8–12, Houston, Texas, 81-GT-71.

Booth T C, (1985), 'Importance of tip clearance flows in turbine design', *VKI Lecture Series 1985–05: Tip Clearance Effects in Axial Turbomachines*, Von Karman Institute for Fluid Dynamics, Belgium.

Bunker R S, (2004), 'Blade tip heat transfer and cooling techniques', *VKI Lectures Series 2004–02: Turbine Blade Tip Design and Tip Clearance Treatment*, Von Karman Institute for Fluid Dynamics, Belgium.

Cohen H, Rogers G F C and Saravenemuttoo H I H, (1987), *Gas Turbine Theory*, 3rd edn, Harlow, Longman Scientific & Technical.

Dailey G, (2000), 'Design and calculation issues', *VKI Lectures Series 2000–03: Aerothermal Performance of Internal Cooling Systems in Turbomachines*, Von Karman Institute for Fluid Dynamics, Belgium.

Denton J and Xu L, (1999), 'The exploitation of three-dimensional flow in turbomachinery design', in Denton J, ed., *Developments in Turbomachinery Design*, Professional engineering Publishing Ltd, Suffolk.

Dowling N E, (1999), *Mechanical Behaviour of Materials*, Upper Saddle River, New Jersey, Prentice-Hall Inc.

Dyschlevskij V, (1965), in Abianz V K, ed., *Theory of Aviation Gas Turbines*, Chapter VI. Losses in Turbine Flow Path, Moscow, Mashinostroenie.

Eppler V, Lindvall K and Marx P, (2008), 'GT26 with sequential combustion – combining operational flexibility and clean, reliable power', *VDI Fachtagung Stationäre Gasturbinen*, 26 Nov, Leverkusen, Germany.

Fukuizumi Y, Masada J, Kallianpur V and Iwasaki Y, 'Application of "H gas turbine" design technology to increase thermal efficiency and output capability of the Mitsubishi M701G2gas turbine', ASME Turbo Expo 2003, June 16–19, Atlanta, Georgia, USA, GT2003-38956.

Gailloreto S, (2009), '33rd Power generation order survey', *Diesel & Gas Turbine Worldwide*, October, p. 32.

Goldstein R J, (1971), 'Film cooling', in Irvine, T F and Hartnett, J P, eds, *Advances in Heat Transfer*, Issue 7, Elsevier.

Gritsch M, Schulz A and Wittig S, (1997), 'Adiabatic wall effectiveness measurements of film cooling holes with expanded exits', *ASME Turbo Expo 1997*, June 2–5, Orlando Florida, USA, 97-GT-164.

Hartland J and Gregory-Smith D, (2002), 'A design method for the profiling of end walls in turbines', *ASME Turbo Expo 2002*, June 3–6, Amsterdam, The Netherlands, 2002-GT-30433.

Han J C, Glicksman L R and Rosenow W M, (1978), 'An investigation of heat transfer and friction for rib roughened surfaces', *Journal of Heat & Mass Transfer*, **21**, 1143–1156.

Han J-C, Dutta S and Ekkad S V, (2000), *Gas Turbine Heat Transfer and Cooling Technology*, London, Taylor & Francis.

Harvey N W and Ramsden K, (2001), 'A computational study of a novel turbine rotor partial shroud', *ASME J of Turbomachinery*, **123**, 534–543.

Published by Woodhead Publishing Limited, 2013

Harvey N W, (2004), 'Aerothermal implications of shroudless and shrouded blades', *VKI Lectures Series 2004–02: Turbine Blade Tip Design and Tip Clearance Treatment*, Von Karman Institute for Fluid Dynamics, Belgium.

Harvey N W, Newman D A, Haselbach F and Willer L, (2006), 'An investigation into a novel turbine rotor winglet. Part 1: Design and model rig test results', *ASME Turbo Expo 2006*, May 8–11, Barcelona, Spain, 2006-GT-90456.

Haselbach F, Schiffer H-P, Horsmann M and Dressen S, (2001), 'The application of ultra high lift blading in the BR715 LP turbine', *ASME Turbo Expo 2001*, June 4–7, New Orleans, Louisiana, 2001-GT-0436.

Haight B, (2010), '2010 Power generation order survey', *Diesel & Gas Turbine Worldwide*, May, p. 26.

Horlock J H, (1966), *Axial Flow Turbines*, London, Butterworths, 127.

Japikse D and Baines N C, (1997), *Introduction to Turbomachinery*, Oxford, Oxford University Press.

Krückels J, Arzel T, Kingston T R and Schnieder M, (2007), 'Turbine blade thermal design process enhancements for increased firing temperatures and reduced coolant flow', *ASME Turbo Expo 2007*, May 14–17, Montreal, Canada, 2007-GT-27457.

Lakshminarayana B, (1996), *Fluid Dynamics and Heat Transfer of Turbomachinery*, New York, John Wiley & Sons.

McNeely M, (2007), '31st Power generation order survey', *Diesel & Gas Turbine Worldwide*, October, p. 30.

Meyer A, (1939), 'The combustion gas turbine: Its history, development and prospects', *The Brown Boveri Review*, **26**(6), 127–140.

Michàlek J, Monaldi M and Arts T, (2010), 'Aerodynamic performance of a very high lift low pressure turbine airfoil (T106C) at low Reynolds and high Mach number with effect of free stream turbulence intensity', *ASME Turbo Expo 2010*, June 14–18, Glasgow, UK, 2010-GT-22884.

Miller R A, (1997), 'Thermal barrier coatings for aircraft engines: History and directions, *Journal of Thermal Spray Technology*, **6**(1), 36–42.

Moustapha S H, Okapuu U and Williamson R G, (1987), 'Influence of rotor blade aerodynamic loading on the performance of a highly loaded turbine stage', *Transactions ASME Journal of Turbomachinery*, **109**, 155–162.

Moustapha H, Zelesky M F, Baines N C and Japikse D, (2003), *Axial and Radial Turbines*, Concepts NREC, White River Junction.

Patel K V, (1980), 'Research on a high work axial gas generator turbine', *SAE 800618*.

Praisner T J, Allen-Bradley E, Grover E A, Knezevici D C and Sjolander S A, (2007), 'Application of non-axisymmetric endwall contouring to conventional and high-lift turbine airfoils', *ASME Turbo Expo 2007*, May 14–17, Montreal, Canada, 2007-GT-27579.

Rose M G, (1994), 'Non-axisymmetric endwall profiling in the HP NGV's of an axial flow gas turbine', *ASME Turbo Expo 1994*, June 13–16, The Hague, The Netherlands, 94-GT-249.

Rose M G, Harvey N W, Seaman P, Newman D A and McManus D, (2001), 'Improving the efficiency of the Trent 500 HP turbine using non-axisymmetric end-walls: Part II – experimental validation', *ASME Turbo Expo 2001*, June 4–7, New Orleans, Louisiana, 2001-GT-0505.

Published by Woodhead Publishing Limited, 2013

Seippel C, (1966), 'The evolution of compressor and turbine bladings in gas turbine design', *ASME Turbo Expo 1996*, March 13–17, Zürich, Switzerland, 66-GT-106.

Seippel C and Bereuter R, (1960), 'The theory of combined steam and gas turbine installations', *The Brown Boveri Review*, **47**, 783–799.

Sjolander S A, (1997), 'Overview of tip-clearance effects in axial turbines', *VKI Lecture Series 1997–01: Secondary and Tip Clearance Flows in Axial Turbines*, Von Karman Institute for Fluid Dynamics, Belgium.

Smith S F, (1963), 'A simple correlation of turbine efficiency', *Journal of the Royal Aeronautical Society*, **69**, 467–470.

Somerscales E F C and Hendrickson R L, (1984), '3500 kW gas turbine at the Schenectady plant of the General Electric Company', *ASME National Historic Landmark Dedication Brochure.* http://www.asme.org/about-asme/history/landmarks

Staubach J B, Sharma O P and Stetson G M, (1996), 'Reduction of tip clearance losses through 3-D airfoil designs', ASME Turbo Asia Conference: November 5–7, Jakarta, Indonesia, *Paper No. 96-TA-13.*

Sunden , B and Faghri, M, eds, (2001), *Heat Transfer in Gas Turbines*, Southhampton, WIT Press.

Van der Linden S, (1988), 'The World's First Industrial Gas Turbine Set at Neuchâtel (1939)', *ASME International Historic Landmark Commemorative Brochure.* http://www.asme.org/about-asme/history/landmarks

Webster G A and Ainsworth R A, (1994), *High Temperature Component Life Assessment*, London, Chapman & Hall.

Wilson D G and Korakianitis T, (1998), *The Design of High-efficiency Turbomachinery and Gas Turbines*, 2nd edn, Upper saddle River, New Jersey, USA, Prentice-Hall Inc.

Zweifel O, (1945), 'The axial spacing of turbomachine blading, especially with large angular deflection', *Brown Bovery Review*, **32**(12), 436–444.

Published by Woodhead Publishing Limited, 2013

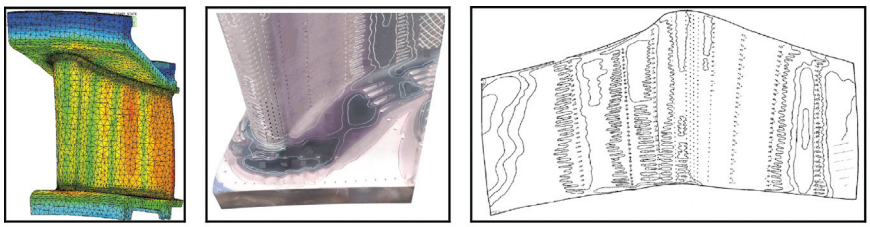


Plate XII (Chapter 6) GT26 LPT front stage vane.

© Woodhead Publishing Limited, 2013

7

Heat exchangers and heat recovery processes in gas turbine systems

B. SUNDÉN, Lund University, Sweden

DOI: 10.1533/9780857096067.2.224

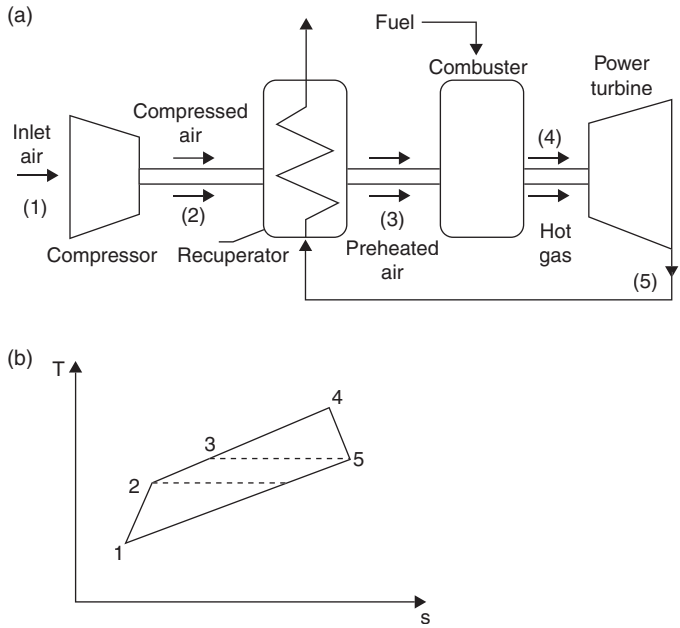
Abstract: This chapter presents an overview of heat exchangers and heat recovery processes in gas turbine systems. Various types of heat exchangers and their design are described. Some examples of commercially available compact heat exchangers are presented. Trends and future needs of research and development are brought up. High temperature heat exchanger materials are discussed. The applicability of modern computational and experimental tools is discussed.

Key words: recuperators, intercoolers, reheat, materials, thermal-hydraulic characteristics, applications.

7.1 Introduction

To improve the thermal efficiency and performance of modern gas turbine systems, many alternative methods exist. One methodology is to introduce a regenerator or a recuperator, i.e. a heat exchanger recovering heat from the hot exhaust gases from the turbine. If this heat is delivered to the compressed air before it enters the combustor, the cycle thermal efficiency will be increased without changing the net cycle work. At a given input, the net output will, of course, then increase. Other improvements may be achieved by introducing intercooling and reheating. Both of these methods increase the net cycle work. Reheating means that the expansion in the turbine is split up in several stages and, between each stage, the gas is heated. This increases the turbine work without changing the compressor work. Intercooling means that the air stream is cooled between two or more stages in the compressor. By intercooling, the compressor work decreases without changing the turbine work. However, it should be noted that intercooling and reheating, if used alone, may decrease the thermal efficiency in comparison with a basic cycle with the same compressor inlet temperature, turbine inlet temperature and overall pressure ratio. This can be found from theory of thermodynamics, see, e.g., Cengel and Boles (2006). Therefore, it is more appropriate to combine intercooling, reheating and regeneration/

© Woodhead Publishing Limited, 2013



7.1 Recuperated simple gas turbine cycle. (a) Components in the simple cycle, (b) temperature versus entropy chart illustrating the thermodynamic cycle.

recuperation in cycles, which can also be deduced from basic thermodynamics, see, e.g., Cengel and Boles (2006). Figure 7.1 presents a general sketch of the introduction of heat exchangers into a gas turbine cycle. Analysis shows that the recuperated cycle and the cycle with both intercooling and recuperation have much higher thermal efficiencies in the low pressure ratio regime than the simple gas turbine cycle, see Fig. 7.2. For the intercooling and regeneration/recuperation, heat exchangers are used. Thus compact, efficient and cheap heat exchangers are of interest. Reheating can be performed in different ways, and it is not necessary to use a heat exchanger if a second combustor is used.

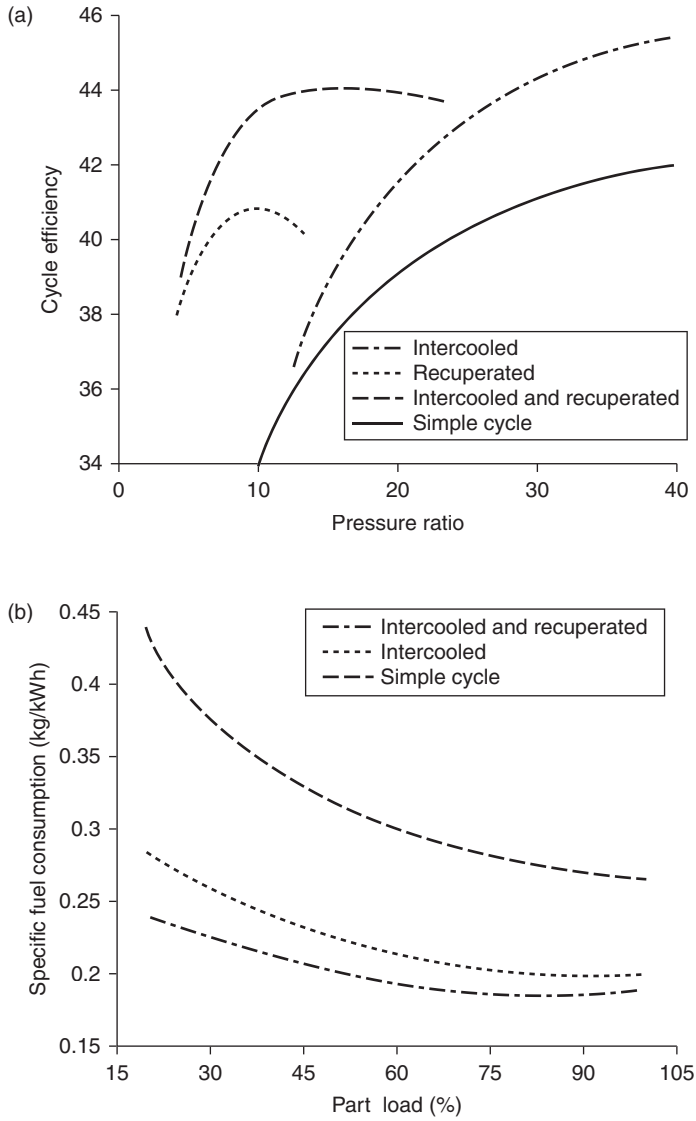
7.2 Heat exchange processes

In a gas turbine there are several processes where heat exchange is important. These are introduced here briefly.

7.2.1 Inlet cooling

Gas turbines ingest a constant volume of air at a given rotational speed, and the power output varies every day as the ambient temperature changes.

© Woodhead Publishing Limited, 2013



7.2 (a) Cycle efficiency versus cycle pressure ratio for various gas turbine cycles and (b) part load performance for various cycles.

Inlet cooling can provide significant power and thermal efficiency improvements. Cooler air is denser, which increases the mass flow rate through the turbine. Although the inlet cooling produces benefits down to very low temperatures, the condensation that occurs when air is cooled below the dew point presents a practical limit. Evaporative cooling and chiller coil systems

© Woodhead Publishing Limited, 2013

might be used for the cooling of the inlet air. Turbine inlet cooling provides a cost-effective, energy-efficient and environmentally beneficial means to enhance power generation capacity and efficiency.

7.2.2 Intercooling

Intercooling between compressor stages decreases the compressor work without changing the turbine work. Thus the network from the cycle is increased. In a two-spool compressor, the first stage compresses the air from ambient pressure to an intermediate pressure level. The air leaving the first compressor enters the intercooler, where heat is removed. Ideally no pressure drop occurs in the intercooler, and the temperature of the air as it leaves the intercooler is the same as the temperature at the inlet from the first compressor. In reality there is a pressure drop in the intercooler, and the air temperature after the intercooler is considerably above the inlet air temperature at the first compressor, because the intercooler is commonly an air-to-air heat exchanger and it is impossible to cool the air back to its inlet temperature. The second compressor completes the compression process to the desired final pressure.

7.2.3 Recuperators

A great increase in the thermal efficiency of the gas turbine cycle can be achieved by adding a heat exchanger, called a recuperator or regenerator, to transfer energy from the hot turbine exhaust gas to the air leaving the compressor. The specific application for the gas turbine will determine which type of heat exchangers should be employed. The gain in thermal efficiency must be weighed against the disadvantages of added cost, size, weight and increased service requirements.

7.2.4 Reheat

By adding a reheat process in the gas turbine expansion process, the turbine work can be increased without changing the compressor work. The hot gas expands from the maximum cycle pressure to an intermediate pressure level, and then it is reheated at constant pressure in, e.g., a second combustor (afterburner in a jet engine), to the maximum cycle temperature, and finally the gas expands in a second turbine stage to the minimum cycle pressure. A heat exchanger is not necessarily involved.

7.2.5 Heat recovery steam generator (HRSG)

In combined cycles, usually one or more gas turbines are releasing the exhaust gases into an HRSG. The exhaust gas is then used as the energy

© Woodhead Publishing Limited, 2013

source in the HRSG, whereby energy is transferred from the hot exhaust gas to the feed water of a boiler. Commonly shell-and-tube heat exchangers are used, where the hot gas flows on the shell side while the water flows on the tube side. The water at the exit of the HRSG is normally high pressure steam, which might be injected together with the fuel in the combustion chamber. Reduction in emissions and improvement of the thermal efficiency can be achieved.

7.2.6 Fuel preheating

If oil is used as the fuel in the gas turbine, it is commonly heated and then goes through vaporization and atomization. Steam can be used in the preheating of the fuel oil. This steam might be provided by a separate steam boiler, or by recovering heat from the exhaust gas. Thus heat exchangers can be useful (but costly) in such processes as well.

7.3 Heat transfer equipment

Heat exchangers are used in many commercial applications, and numerous types can be found from a large number of manufacturers. High temperature heat exchanger technology has become important for improving the performance of power generation, Sunden (2005, 2007) and Selimovic *et al*. (2005, 2008). Reviews have also shown that the use of gas turbines embodying internal heat recovery within the thermodynamic cycles is not widely applied. However, reducing the specific fuel consumption is necessary to meet environmental requirements, which are gradually being tightened. One such requirement is reduction in carbon-dioxide emissions, which can be attained by increasing the engine thermal efficiency. One way to do this is to increase the compressor and turbine efficiencies. This can be done by improving the heat exchange or cooling, but also to some extent by improvement of the aerodynamics. Despite decades of continuous research and development, there are numerous design and operating problems originating from a lack of understanding of basic flows and heat transfer phenomena such as flow distribution in manifolds, flow-induced vibration in two-phase flows, heat transfer enhancement, fouling, etc. In the following sections, mainly recuperators and intercoolers are discussed.

7.3.1 Recuperators

Introduction of a recuperator for recovering the heat energy of the exhaust gas by preheating the combustion air may increase the thermal efficiency of a small gas turbine considerably. Although, recuperators have been in

© Woodhead Publishing Limited, 2013

development for several years, the thermal design is still evolving, which is a complex and challenging task. There is a wide variety of efficient surface geometries that can be considered for compact high effectiveness counter-flow heat exchangers. The thermal analysis has to ensure that the design meets all performance requirements, and is structurally robust and yet compact and lightweight. A suite of analytical and experimental tools is often employed to achieve these desired objectives. Two key design parameters, which need to be identified in the preliminary phase, are (1) recuperator geometry and heat transfer surface selection, and (2) material. These topics are discussed next.

Design of recuperators

The first generation of recuperators was constructed based on boiler standards. With tube diameters of 25 mm, the recuperator proved to be bulky, large and heavy, with a low effectiveness. The surface compactness was less than 100 m^2/m^3 and the thermal density was less than 0.5 MW/m^3. The design trend today is to increase the compactness and/or improve the heat transfer coefficients in the ducts of the unit. By doing so, a low weight and small volume of the recuperator may be achieved. In this way, the material cost also is reduced. In a highly efficient and compact recuperator (thermal effectiveness $\varepsilon > 90\%$, area density >1600 m^2/m^3), the hydraulic diameter is about 1 mm and the metal wall thickness is less than 0.1 mm. These sizes indicate that efforts to find low cost manufacturing methods are needed, especially for non-straight ducts.

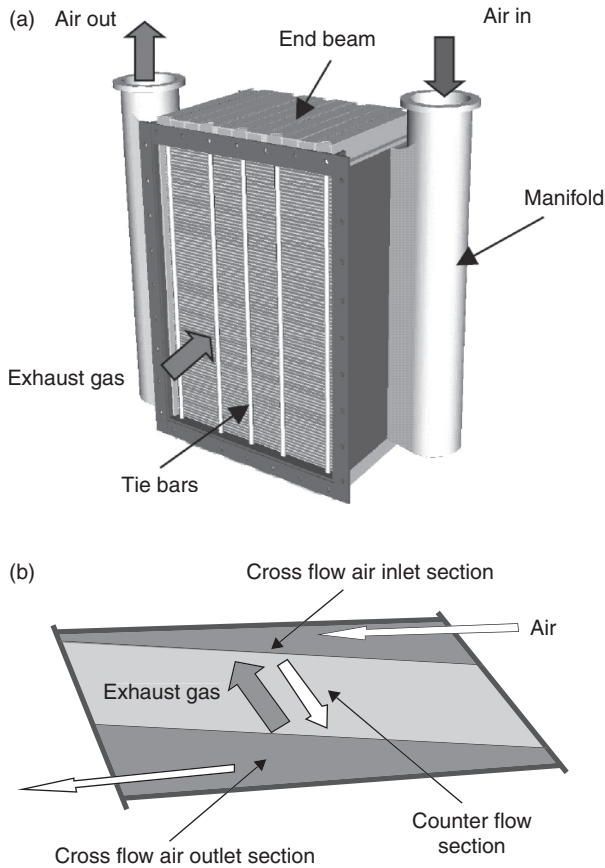
Plate-fin recuperator

This recuperator type was originally developed to meet weight and size requirements for various aircraft systems. The compactness and the high heat transfer coefficients result in a large decrease of the recuperator size as compared to a tubular design. Several types of fin configurations are available, e.g., in-line and offset strip fin, louvered fin, wavy fin, etc.

Primary surface geometries

A primary surface heat exchanger is one which does not involve any secondary surfaces, such as fins, ribs, dimples, etc. A primary surface recuperator (PSR) is a counter flow heat exchanger with a core manufactured from thin corrugated metallic foils. Examples have been described having an effectiveness in the range of 80–93%, and pressure drops of 3–5% on the hot gas side and about 1% on the air-side. A compactness or area density of more than 1600 m^2/m^3 has been reported. Examples of recuperators are shown in Figs 7.3 and 7.4, from Lagerstrom and Xie (2002) and Muley and Sunden (2003).

© Woodhead Publishing Limited, 2013



7.3 (a) Overall view of RSAB recuperator and (b) plate pattern of the RSAB recuperator (Lagerstrom and Xie, 2002).

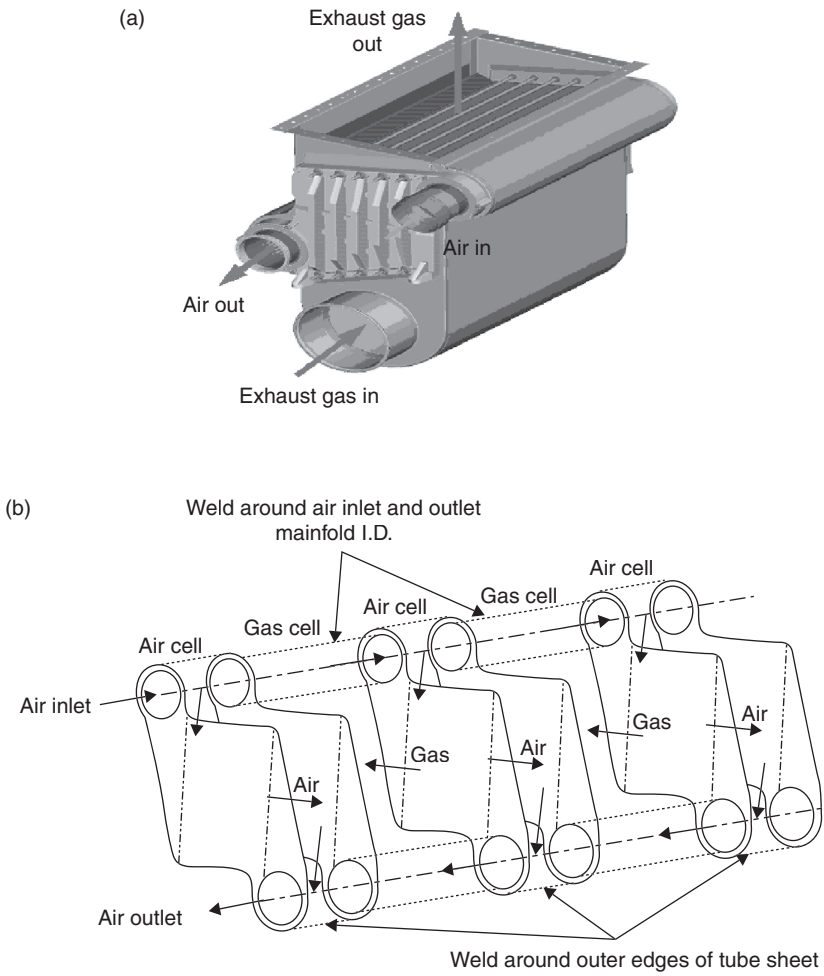
Tubular heat exchangers

The first generation of recuperators was often designed with tubular geometries, but the compactness and efficiency were low. To improve the compactness, small diameter tubes with some enhancement method are used. The heat transfer area can be increased by fins, surface roughness, etc., or by creating secondary flows promoting the heat transfer. This can be achieved by surface dimples, twisted tape inserts, or regular narrowing of the tubes. Shell-and-tube heat exchangers in ceramic materials have also been presented.

Plate type heat exchangers

This type of heat exchanger is simple and may be manufactured at a low cost, but utilization is constrained to low temperatures because polymeric

© Woodhead Publishing Limited, 2013



7.4 (a) Honeywell recuperator and (b) details of heat exchange process in Honeywell recuperator (Muley and Sunden, 2003).

materials are used as sealing elements. However, this problem might be resolved by welded or semi-welded plates, see Wang *et al*. (2007).

Recent investigations

A recent investigation of the performance of a recuperator for an aeroengine application was presented by Albanakis *et al*. (2009). The recuperator was of tubular type with elliptical tubes. A feature study of intercoolers and recuperators for jet engines was performed by Kroon (2002). Counterflow tubular heat exchangers were considered. It was found that opportunities

© Woodhead Publishing Limited, 2013

exist for improving the cycle, but it was also stated that the compactness and effectiveness of the heat exchangers were important issues. A performance study of the prime surface recuperator of a Turbec 100 microturbine was presented by Ferrari *et al*. (2009).

Materials issues

Most compact recuperators are manufactured from different metallic alloys, such as 300 series stainless steel and heat resistant Nickel-based alloys such as 625. For temperatures below 675°C, commonly stainless steels (300 series) have been used for metallic recuperators. However, at higher temperatures these materials are susceptible to creep deformation and oxidation, which may deteriorate the proper functioning of the recuperator, i.e., reduction of effectiveness, leakage and reduced life time. Most current compact recuperator design requires thin-section metallic alloys, which can offer good resistance to oxidation resistance in moist air. They should provide sufficient ductility at room temperature for various fabrication processes, such as stamping, roll forming, etc. Another desired property of these alloys is low thermal expansion. Maziasz and Swindeman (2002) identified two alloys, 120 and modified 803, which offer cost-effective improvements in creep strength and thermal expansion relative to type 347 stainless steel. Due to increased Cr and Ni content, alloy 803 provides good resistance to oxidation. With attempts to increase the overall efficiency, higher temperature levels are required and this calls for advanced metallic or ceramic recuperators.

Ceramic recuperators offer significant advantages, especially for portable systems, compared to metallic ones, namely:

- superior high temperature capability enabling system to operate at its maximum temperature level, minimizing fuel consumption;
- low cost, non-strategic construction materials; and
- significant potential for weight reduction.

Although research to evaluate various candidate materials has been going on, see, e.g., Maziasz and Swindeman (2002), Lara-Curzio *et al*. (2002) and Pint *et al*. (2002), substantial development work is required before high temperature metal alloys and ceramics can be used for recuperator fabrication on commercial scale. Recently Matthews *et al*. (2009) studied a stainless steel material with higher chromium and nickel contents than the frequently used stainless steel type. Improvement of the oxidation resistance was achieved. Pint *et al*. (2009) considered austenitic stainless steels with Al and Cr concentrations optimized to maintain better corrosion and creep behavior.

© Woodhead Publishing Limited, 2013

7.3.2 Rotary regenerators

Small stationary or automotive gas turbine engines are often designed with a recuperator in the form of a rotary regenerator. A ceramic core matrix is used. The exhaust gas heats up the matrix of the regenerator during a certain time period and then, over the next time period, the matrix gives up the heat to the air. Usually a high efficiency can be achieved, and a relatively compact unit may be built. However, this heat exchanger type has severe problems with leakage between the cold and hot stream sides in gas turbine applications. Leakage of about 15% of the compressor flow has been reported.

7.3.3 Recuperators versus regenerators

Whether a recuperator or a regenerator should be chosen with respect to the gas turbine engine performance depends on the engine cycle, space restrictions, power, etc. In the past recuperators suffered from fatigue problems due to thermal cycling and fouling on the hot gas side. However, a lot of efforts have been spent to make recuperators more resilient to thermal cycling. Fouling problems have also been reduced as low emission combustors have been developed. For rotary regenerators there is a limit on the disc diameter, and this means that regenerators are only practicable for low mass flow rates, say less than 2 kg/s, and power output less than 500 kW. Higher power output gas turbines then should use a recuperator. Commonly, recuperators require a higher volume than regenerators.

7.3.4 Intercoolers

The power for compression of the air in a gas turbine system can be reduced if the compression process is split up and a heat exchanger or intercooler is installed between the compressor stages. It can be shown theoretically that the power input to a two-stage compressor is minimized when equal pressure ratios are maintained across each stage. The introduction of only an intercooler in a gas turbine system may not increase the efficiency of the gas turbine significantly, but it may result in an increase of the specific power. At high pressure ratios, the introduction of an intercooler in a gas turbine cycle increases the efficiency, while in a cycle with both an intercooler and a recuperator the efficiency is increased even at low pressure ratios. Similarly, the introduction of recuperators, intercoolers and reheaters in combined gas and steam turbine cycles increases the overall thermal efficiency.

The current prognosis for most future systems is that intercoolers will play an essential role at least for a power up to 200 MW, see Saidi *et al.*

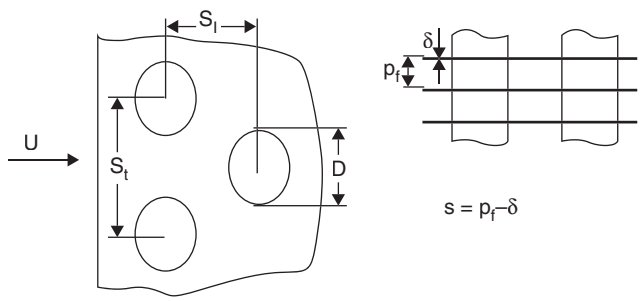
© Woodhead Publishing Limited, 2013

(2000, 2002). Often an intercooler is a gas-to-liquid conventional heat exchanger, with various types of extended surfaces on the air-side. In marine applications, a secondary cooling circuit including another heat exchanger is commonly employed. However, the current intercoolers are bulky and expensive. Thus, there is an industrial need to develop compact and efficient intercoolers. Because the thermal resistance on the air-side is dominating, the natural first step in the development process for compact units is to consider the thermal-hydraulic performance of various heat transfer surfaces on the air-side. Other types of intercooling include evaporative cooling, where a water mist is sprayed between the low pressure and high pressure stages. Another cooling type is isothermal cooling, where a refrigerant may be circulating through the stator vanes.

Types of intercoolers

At low pressure ratios, an air-water intercooler may be regarded as a conventional industrial heat exchanger. For single phase fluids with modest heat transfer coefficients, large surface areas are required. Tubular geometries are desirable to provide both a water-side cleaning capability (to remove fouling products), and the possibility for individual tube plugging in case of leakage. For each application detailed design investigations are necessary to establish optimum configurations such as helical bundle, straight tubes, U-tubes, etc., but in each case enhanced surface geometries will be necessary to optimize the heat transfer surface area. Candidate surface geometries include finned tubes, spiral geometries, various surface roughnesses, etc. Figure 7.5 shows a tube-fin configuration which might be suitable as an air–liquid intercooler. A major goal is to minimize the size of the intercooler and to make it compatible with the compact nature of the gas turbine prime-mover.

A practically employed intercooling system is the so-called WR-21 gas turbine for marine applications. This was presented some time ago by Crisalli



7.5 Possible tube-fin heat exchanger layout suitable for air–liquid intercooler (Saidi *et al.*, 2002). (a) view from above, (b) side view.

© Woodhead Publishing Limited, 2013

and Parker (1993). This system consists of an on-engine intercooler that uses a fresh-water-based coolant to cool the compressed air, and an off-engine intercooler to cool the primary coolant with sea water. The on-engine intercooler is a plate-fin heat exchanger with fins of rectangular offset strip type. The water enters and exits the intercooler through triangular sections that enable a counter flow arrangement in the major part of the heat exchanger. The off-engine intercooler is a plate heat exchanger.

Due to the influence of liquid particles on blade erosion of axial compressors, some efforts have been made to control condensation, see Kiang and Bowen (1995). The solution to this problem was to reduce the coolant flow rate to the seawater heat exchanger as temperatures close to the dew point were reached. The dew point is determined by measurement of humidity, pressure and temperature at the inlet of the engine.

Other intercooler designs have also been presented in the open literature and a number of patents exist. Not only should the intercooler be a compact heat exchanger with a high thermal efficiency, it also should be cheap and relatively simple to manufacture. More research is needed to achieve all these properties.

The above presentation shows that intercoolers often are gas-to-liquid heat exchangers with different type of extended surfaces on the air-side. By definition a compact heat exchanger is one which incorporates a heat transfer surface with an area density of above 700 m^2/m^3 on at least one of the fluid sides which usually is the gas side. The intercooler in the WR-21 marine gas turbine system satisfies this criterion. To increase the compactness of an intercooler it is necessary to consider closely the types of extended surfaces that have been used. Another objective might be to increase the volume goodness factor (heat transfer coefficient versus pumping power) of the intercooler, namely increase the heat transfer rate of an intercooler concept maintaining the lowest pumping power per unit heat transfer area. The dominant part of the thermal resistance for liquid-to-gas heat exchangers occurs on the gas- or air-side. Thus it is worthwhile to focus attention to different concepts of the air-side in the intercooler.

There are many types of extended surface concepts that can be used in intercoolers. For example, the extended surface type used in the WR-21 marine gas turbine is an offset strip fin geometry. Other types of extended surfaces, such as louvered fins and herringbone corrugated fins, are of interest. To recognize and implement the best possible concept for intercooler applications, it is necessary to study the thermal and the hydraulic behaviors, and to perform eventual modification or optimization of these. Tube-and-fin-heat exchangers with plain or wavy fins may present an opportunity for utilization as intercoolers. These heat exchangers are space-consuming compared to compact heat exchangers at the same nominal ratings, namely the same heat duty, but generally they are cheaper and introduce a lower

© Woodhead Publishing Limited, 2013

pressure drop penalty that might be an essential design factor. Thus, the decision to choose such a heat exchanger as an intercooler depends on the tradeoff analysis of cost, thermal demand and pressure drop limitations, as well as the allowable space and weight for the whole system.

Analysis of thermal-hydraulic characteristics

In general, it has now been recognized that to meet the requirements of a compact heat exchanger with a low weight, suitable for mass production and with acceptable pressure drop, PSRs with small hydraulic diameter and operating in counterflow arrangement should be attempted. There is a wide variety of efficient geometries that can be considered for compact high effectiveness counterflow heat exchangers. The investigation by Utriainen and Sunden (2002) revealed that cross-corrugated heat transfer surfaces, such as those in plate heat exchangers, were good candidates for achieving improved thermal efficiency and reducing the specific matrix volume. Also, patterns formed like cross wavy ducts were found promising. Surfaces of this type are shown in Fig. 7.6. Later studies have confirmed these conclusions.

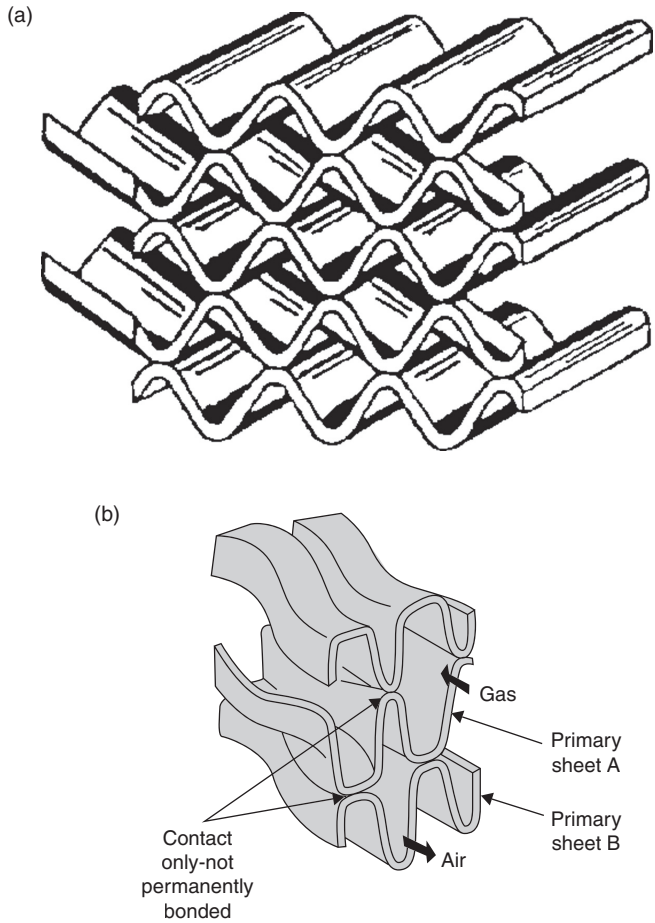
Fir the heat transfer surfaces to be analyzed, the convective heat transfer coefficients are needed. Generally, the hot and cold gases are flowing in ducts or channels of various design and with small hydraulic diameters. Thus, duct flow or internal flow is very important in the field of heat exchangers. These heat transfer coefficients are dependent on flow velocity, fluid properties, duct cross-sectional shape and size, and duct length. For some geometries such coefficients are available in the literature, e.g., Kakac *et al*. (1987), for single phase flow at laminar, turbulent or transitional conditions. However, in most recuperator applications for micro gas turbines, the Reynolds number is so low that laminar flow prevails. Usually non-dimensional formulations are presented. The general form is

$$\mathrm{Nu} = \frac{hD_h}{k} = f\left(\frac{\mathrm{Re}, \mathrm{Pr}, D_h}{L}\right) \qquad [7.1]$$

The functional relationship depends on the considered geometry. Sometimes the relationship is expressed in terms of the Colburn *j*-factor, instead of the Nusselt number, Nu.

In the development of compact recuperators (high ratio of heat transfer surface area to volume) the heat transfer coefficients play a significant role. The concept of enhanced heat transfer becomes very relevant for research and development of gas turbine heat exchangers. Several ideas for new primary surface heat exchangers have been presented over last few years, but also extended surface concepts, such as offset fins and pure straight ducts in

© Woodhead Publishing Limited, 2013



7.6 Primary surface cross wavy corrugated plates (Utriainen and Sunden, 2002). (a) Traditional cross wavy corrugated plates in plate heat exchangers, (b) new design of cross wavy heat exchanger core aimed for exhaust gas to air heat exchange.

ceramic material, have been considered. For those new surfaces correlations like Equation [7.1] are not available.

Because pressure drop in the recuperator presents a loss in gas turbine efficiency, it has to be considered accurately as well. In most cases the pressure drop is split into three parts, the inlet section (i.e., inlet manifold and distribution section) pressure drop, the pressure drop over the core heat transfer surface, and the outlet section (manifold) pressure drop. For the heat transfer core, commonly the Fanning friction factor is used to express the pressure drop. Similar to the heat transfer coefficients, correlations are available for some simple surfaces.

© Woodhead Publishing Limited, 2013

Numerical methods for heat transfer and fluid flow analysis

From the previous sections it has become evident that the heat transfer coefficient and friction factor are important parameters as recuperator surface concepts are designed and analyzed. For many years experimental methods were the only means to determine these properties. However, because the flow passages in recuperators may be very complex in geometry and of small dimension, detailed and accurate measurements of temperature and velocity fields become very difficult. The available experimental information thus concerns mainly overall pressure drop and heat transfer coefficients.

With the rapid development of methods for numerical solution of nonlinear partial differential equations and advanced computer power, predictions of temperature and flow fields and associated heat fluxes and mechanical stresses have been possible in many situations. However, turbulence modeling still presents a major problem, as accurate and reliable predictions of flow separation, reattachment or impinging and recirculating flow regions are required. Nevertheless, due to the small Reynolds numbers encountered in, e.g., recuperators, laminar flow prevails and the turbulence modeling is not such a critical issue. Instead, numerical grid generation for complex geometries and solutions not affected by the selected grid are major issues. Numerical computations may be useful to supplement experimental investigations by, e.g., providing details of local phenomena and fundamental mechanisms.

All the governing equations (mass conservation, momentum and energy) can be cast into a general differential equation as

$$\frac{\partial \rho \phi}{\partial t} + \frac{\partial}{\partial x_j} \rho \phi u_j = \frac{\partial}{\partial x_j} \left(\Gamma \frac{\partial \phi}{\partial x_j} \right) + S \qquad [7.2]$$

where ϕ is an arbitrary variable, S the source term, Γ the diffusivity, u_j the velocity vector and x_j the coordinate.

Commonly the so-called finite volume method, see Minkowycz *et al.* (2006), Ferziger and Peric (1996) and Versteeg and Malalasekera (2007), is used to discretize the equation in this method. The equations are integrated over control volumes formed around the nodes. Various schemes exist for handling convection–diffusion terms, pressure–velocity coupling, etc.

In heat transfer equipment like heat exchangers, both laminar and turbulent flows are of interest. While laminar convective flow and heat transfer can be simulated by Equation [7.2] (or transformed variants for arbitrary geometries), turbulent flow and heat transfer normally require modeling approaches in addition to Equation [7.2]. By turbulence modeling, the goal is to account for all of the relevant physics by using as simple a mathematical model as possible. The most common turbulence models for industrial applications

© Woodhead Publishing Limited, 2013

are classified as (a) zero-equation models, (b) one-equation models, (c) two-equation models, (d) Reynolds stress models, (e) algebraic stress models and (f) large eddy simulations (LES). A specific problem related to turbulence modeling is the treatment of wall effects. There are two standard procedures to account for wall effects in numerical calculations of turbulent flow and heat transfer. One is to employ low Reynolds number modeling procedures, and the other is to apply the wall function method. The wall functions approach includes empirical formulas and functions linking the dependent variables at the near-wall cells to the corresponding parameters on the wall. The functions are composed of laws of the wall for the mean velocity and temperature, and formulas for the near-wall turbulent quantities. The accuracy of the wall function approach is increasing with increasing Reynolds number. In general the wall function approach is efficient and requires less CPU time and memory but it becomes inaccurate at low Reynolds numbers. When low Reynolds number effects are important in the flow domain, the wall function approach ceases to be valid. So-called low Reynolds number versions of the turbulence models are introduced, and the molecular viscosity appears in the diffusion terms. In addition, damping functions are introduced. Also so-called two-layer models have been suggested where the transport equation for the turbulent kinetic energy is solved, while an algebraic equation is used for, e.g., the turbulent dissipation rate.

Nowadays, several commercial computer codes such as ANSYS-FLUENT, STAR-CD, ANSYS-CFX, etc. are available, and such codes are being more frequently applied in industry. The computational method is commonly referred to as computational fluid dynamics (CFD). Nevertheless, the need for research and development of numerical methods for heat transfer and fluid flow analysis remains. Narrow flow passages and complex geometries are examples of relevance for recuperators and other heat exchangers. CFD can be applied to heat exchangers in some different ways. In the first way the entire heat exchanger or the heat transferring surface is modeled. This can be done by using large scale or relatively coarse computational meshes, or by applying a local averaging or porous medium approach. For the latter case, volume porosities, surface permeabilities, as well as flow and thermal resistances, have to be introduced. The porous medium approach was first introduced by Patankar and Spalding (1974) for shell-and-tube heat exchangers, and has later been followed up by many others. Another way is to identify modules or group of modules that repeat themselves in a periodic or cyclic manner in the main flow direction. This will enable accurate calculations for the modules, but the entire heat exchanger, including manifolds and distribution areas, is not included. The idea of streamwise periodic flow and heat transfer was introduced by Patankar *et al*. (1977). Recent reviews of applications of CFD for heat exchanger design and analysis have been presented by Sunden (2007a, 2007b, 2010).

© Woodhead Publishing Limited, 2013

It should be noted that experimental methods also have been developed and improved significantly. So, for instance, laser Doppler velocimetry (LDV) and particle image velocimetry (PIV) techniques are useful for fluid flow analysis, and liquid crystal thermography (LCT) as well as infrared thermography (IR) may be employed for surface temperature measurement, thus being useful in determining heat transfer coefficients.

Heat exchanger sizing procedure

The overall heat exchanger design methodology would normally include thermal design, mechanical design and manufacturing consideration for the specific application. One of the key requirements in the design of a heat exchanger is to perform the heat transfer and pressure drop analyses. Several non-dimensional methods exist for thermal-hydraulic design, see Kays and London (1984), Shah and Sekulic (2003), Sunden (2007) and Wang *et al.* (2007). The two most commonly used are the ε-NTU and LMTD methods. In this section a PSR recuperator of the plate type is discussed using the ε-NTU method. The recuperator design task is a heat exchanger sizing problem, which is basically a determination of the recuperator plate size, the number of plate pairs to meet the specified heat transfer and pressure drop requirements. The iterative procedure essentially consists of the following steps:

- Select overall plate dimensions including length and width of the cross and counterflow sections and flow channel size.
- Calculate the fluid outlet temperatures for the specified or desired heat exchanger effectiveness.
- Obtain fluid the mean temperature on the hot and cold sides, and evaluate the fluid bulk mean thermophysical properties, e.g., μ, c_p, ρ, k, Pr.
- Calculate C_R and ε and determine the number of transfer units (NTU) of the heat exchanger.
- Determine the heat exchanger surface area using the fact that it is identical for the hot and cold sides, and the approximate relationship between the air- and gas-side heat transfer coefficients. Typically air-side heat transfer coefficients are 30–50% higher than those on the gas side, due to smaller hydraulic diameter. Calculate the number of plate pairs needed to meet this area requirement.
- Calculate mass flux, Re, f (friction factor) and j (Colburn factor) for the air and gas side flows.
- Calculate hot and cold side pressure drops in counterflow and cross-flow sections using the procedure outlined in, e.g., Kays and London (1984).
- Calculate total relative pressure drop $(\Delta p/p)_{\text{total}}$ and check whether it meets the specified requirement. If the $(\Delta p/p)_{\text{total}}$ is not within the requirements, then return to the beginning and modify the plate dimensions.

© Woodhead Publishing Limited, 2013

7.4 Applications

In this section, brief comments on applications of gas turbines in industries, such as microturbines and in aeroengines are presented.

7.4.1 Industrial gas turbines

Industrial gas turbines range in size from truck-mounted mobile plants to very big and complex systems. If waste heat from the gas turbine is recovered by an HRSG to power a conventional steam turbine in a combined cycle, the thermal efficiency might be up to 60%. Large scale single-cycle gas turbines may produce power in the order of 100–300 MW, and have a thermal efficiency in the range of 35–40%.

7.4.2 Microturbines

Microturbines are basically compact gas turbine generators. Microturbines were derived from turbocharger technologies in large trucks or the turbines in aircraft auxiliary power units. A microturbine usually consists of a single stage radial compressor, a single stage radial turbine, and a recuperator. The rotating speed is high. Some early product introductions featured unrecuperated designs (with lower efficiencies but also lower capital cost). In terms of produced power, they range from a few kilowatts to tens or hundreds of kilowatts. Typically, the microturbine efficiency ranges from 25% to 35%. Recently Ferrari *et al*. (2009) presented performance tests of a microturbine recuperator.

7.4.3 Aeroengines

Jet engines have in general a high technological level but there are demands on lower fuel consumption and reduced pollutant emissions. To achieve this alternate thermodynamic cycles recovering the thermal energy of the exhaust gas are considered. Heat exchanged jet engines are in the line of developments that may lead to improved performance and contribution to the overall optimization of jet engines. Thus, interests in intercooled and recuperated jet engines have come back. The presence of the heat exchangers may impose significant pressure losses to the exhaust gas side, and affect the operation of the jet engine and the potential benefit from the use of alternate thermodynamic cycles. In addition, the complexity with installation. and the heat exchanger weight and volume. are the main reasons why mainly theoretical investigations have been carried out so far. Because of the strictly limited space in the engine, the location of the intercooler and

© Woodhead Publishing Limited, 2013

recuperator can be very problematic. Recent studies have shown that the specific fuel consumption (SFC) – fuel consumption in relation to thrust – can ideally be reduced in the order of 25%, see Kroon (2002).

7.5 Future trends

The future trends in terms of heat exchanger development include improvement of the high temperature strength properties for both metal and ceramic materials, cheap manufacturing technique, increased compactness or thermal density of the heat exchangers by decreasing the hydraulic diameter and applying heat transfer enhancement techniques, and improvement of the reliability and cleanability.

There is renewed interest in using heat exchangers in aero-jet engines, but a lot of research and development work is still needed before this application becomes massive, see Kroon (2002) and McDonald and Rodgers (2009).

Some renewed interest has also been shown in externally fired gas turbines for combined heat and power generation, see Masgrau (2008). Most gas turbines are internal combustion engines, but it is possible to build an external combustion gas turbine, which in principle is a hot air engine, see Masgrau (2008). For fuels such as pulverized coal, municipal waste and biofuels, external combustion might be a good option. Using biofuels may significantly contribute to reduced CO_2 emissions. In such indirect systems, a heat exchanger is used and only clean air with no combustion products is traveling through the power turbine. Usually the thermal efficiency is lower than that for the direct types. However, the turbine blades are not exposed to corrosive substances or abrasive particles, and dirty fuel can be used. The performance of the heat exchanger might be a limiting factor. Some developments have been proposed to increase the thermal efficiency by adding extra heat from the combustion to the working fluid (air) prior to the turbine inlet. The concept is to integrate the combustor with a heat exchanger and make use of the high temperatures reached during combustion. Then more heat can be transferred to the air and thus the turbine inlet temperature is increased. Thermal radiation and convection are the modes for the heat transfer process. A key component then is a combined combustor–heat exchanger. Another improvement may be to introduce a radiant burner instead of a conventional one. The efficiency will probably be lower than for the direct cycle, but on the other hand the environmental problems are reduced significantly. Alternate fuels might also be needed and then effects of, e.g., syngas operation on the thermal characteristics will call for attention.

Open cell porous metal and graphite foams have received increased attention for application in compact heat exchangers, due to their increasing

© Woodhead Publishing Limited, 2013

availability and improved thermal performance. Novel foam materials offer a means to achieve goals of lightweight, high compactness and high performance heat exchange. Heat exchangers based on metal foam may find application in gas turbine processes, see Muley *et al*. (2009) and Dai *et al*. (2009).

7.6 Conclusion

Demanding requirements on reduced emissions and low fuel consumption are moving the development of gas turbines towards higher cycle efficiencies. To achieve this, heat exchangers are necessary, and probably a combination of several heat exchangers (recuperator, intercooler, precooler, reheater, etc.) is needed. Heat exchangers add investment and operating costs to the plant, and might also be bulky. To meet all the requirements, and to provide tools for design and optimization, calls for continued research and development.

7.7 Sources for further information and advice

In this section a list of books or chapters for heat exchanger description and design as well as for gas turbine fundamentals or applications are provided.

Bathie W W (1996), *Fundamentals of Gas Turbines*, 2nd ed., New York, J Wiley & Sons.

Saravanamuttoo H I H, Rogers G F C, Cohen H and Straznicky P V (2009), *Gas Turbine Theory*, 6th ed., New Jersey, Pearson Ltd, Prentice Hall.

Shah R K and Sekulic D P (2003), *Fundamentals of Heat Exchanger Design*, New Jersey, J Wiley & Sons, Inc.

Sunden B (2007), Heat transfer and heat exchangers, *Kirk-Othmer Encyclopedia in Chemical Technology*, New York, J Wiley & Sons. (on line publication).

Walsh P P and Fletcher P (2004), *Gas Turbine Performance*, 2nd ed., Boston, Blackwell Publishing.

Webb R L and Kim N H (2005), *Principles of Enhanced Heat Transfer*, 2nd ed., New York, Taylor & Francis.

7.8 Acknowledgement

Research projects related to this chapter have been financially supported by the Swedish Energy Agency, Swedish Scientific Council, Siemens Industrial Turbines, Volvo Aero Corporation.

7.9 References

Albanakis C, Missirilis D, Storm P, Yakinthos K and Goulas A (2009), 'Experimental investigation of the effect of heat transfer on pressure drop for a heat exchanger for aero engine applications', *ExHFT-7*, paper AT-5, 609–616.

Cengel Y A and Boles M A (2006), *Thermodynamics – An Engineering Approach*, 5th ed., New York, McGraw-Hill.

© Woodhead Publishing Limited, 2013

Crisalli A J and Parker M L (1993), 'Overview of the WR-21 intercooled recuperated gas turbine for a modern fleet', In Proceedings of ASME IGTI International Gas Turbine Conference, *ASME paper 93-GT-231*.

Dai Z, Nawaz K, Park Y, Chen Q and Jacobi A M (2009), 'A comparison of metal-foam heat exchangers to compact multi-louver designs for air-side heat transfer applications', *7th International Conference on Enhanced, Compact and Ultra Compact Heat Exchangers: Science, Engineering and Technology*, CHE2009–06, CD ROM Proceedings.

Ferrari M L, Pascenti M, Magistri L and Massardo AF (2009), 'Micro gas turbine recuperator: steady state and transient experimental investigation', In Proceedings of ASME IGTI International Gas Turbine Conference-TurboExpo2009, *GT2009–59172*.

Ferziger J H and Peric M, (1996) *Computational Methods for Fluid Dynamics*, Berlin, Springer-Verlag.

Kakac S, Shah R K and Aung W (Eds) (1987), *Handbook of Single-Phase Convection Heat Transfer*, New York, Wiley Interscience Publication.

Kays W M and London A L (1984), *Compact Heat Exchangers*, 3rd ed., New York, McGraw-Hill.

Kiang R L and Bowen T L (1995), 'Application of advanced heat exchanger technology in a 22 megaWatt naval propulsion gas turbine', *ASME/JSME Thermal Engineering Conference*, Vol. **4**, 347–357.

Kroon D (2002), 'Possibility of intercooled and recuperated jet engines', M. Sc. Thesis 02/5004, Department of Energy Sciences, Lund University.

Lagerstrom G. and Xie M (2002), 'High performance and cost effective recuperator for micro gas turbines', In Proceedings of ASME IGTI International Gas Turbine Conference, *ASME GT2002–30402*.

Lara-Curzio E, Maziasz P J and Pint B A (2002), 'Test facility for screening and evaluation candidate materials for advanced microturbine recuperators', In Proceedings of ASME IGTI International Gas Turbine Conference, *ASME GT2002–30581*.

Masgrau M (2008), 'Design of a combined combustor-heat exchanger for an externally fired gas turbine', M. Sc. Thesis 08/5143, Department of Energy Sciences, Lund University.

Matthews W J, More K L and Walker L R (2009), 'Comparison of three microturbine primary surface recuperator alloys', In Proceedings of ASME IGTI International Gas Turbine Conference-TurboExpo2009, *GT2009–59041*.

Maziasz P J and Swindeman R W (2002), 'Selecting and developing advanced alloys for creep resistance for microturbine recuperator applications', In Proceedings of ASME IGTI International Gas Turbine Conference, *ASME GT2002–30541*.

McDonald C F and Rodgers C (2009), Heat exchanged propulsion gas turbines: a candidate for future lower SFC and reduced emission military and civil aeroengines, In Proceedings of ASME IGTI International Gas Turbine Conference-TurboExpo2009, *GT2009–59156*.

Minkowycz W J, Sparrow E M and Murthy J Y (2006), *Handbook of Numerical Heat Transfer*, 2nd ed., New York, Wiley Interscience.

Muley A, Kiser C, Sunden B and Shah R K (2009), 'Foam heat exchangers: A technology management assessment', *7th International Conference on Enhanced, Compact and Ultra Compact Heat Exchangers: Science, Engineering and Technology*, CHE2009–07, CD ROM Proceedings.

© Woodhead Publishing Limited, 2013

Muley A and Sunden B (2003), Advances in recuperator technology for gas turbine systems, In Proceedings of ASME International Mechanical Engineering and Exposition Congress 2001, *IMECE2003–43294*.

Patankar S V, Liu C H and Sparrow E M (1977), 'Fully developed flow and heat transfer in ducts having streamwise-periodic variations of cross-sectional area', *ASME Journal of Heat Transfer*, Vol. **99**, 180–186.

Patankar S V and Spalding D B (1974), 'A calculation procedure for transient and steady state behavior of shell-and-tube heat exchangers', in *Heat Exchanger Design and Theory Source Book*, eds. N F Afgan and E U Schlunder, New York, McGraw-Hill.

Pint B A, Brady M P, Yamamoto Y, Santella M L, Howe J Y, Trejo R and Maziasz P J (2009), 'Development of alumina-forming austenitic alloys for advanced recuperators', In Proceedings of ASME IGTI International Gas Turbine Conference-TurboExpo2009, *GT2009–60197*.

Pint B A, More K L and Tortorelli P F (2002), 'The effect of water oxidation on performance of alloys used in recuperators', In Proceedings of ASME IGTI International Gas Turbine Conference, *ASME GT2002–30543*.

Proeschel R A (2002), 'Proe 90TM recuperator for microturbine applications', In Proceedings of ASME IGTI International Gas Turbine Conference, *ASME GT2002–30406*.

Saidi A, Eriksson D and Sunden B (2002), 'Analysis of some heat exchanger concepts for use as gas turbine intercoolers', *International Journal of Heat Exchangers*, Vol. **III**, no 2, 241–260.

Saidi A, Sunden B and Eriksson D (2000), 'Intercoolers in gas turbine systems and combi-processes for production of electricity', In Proceedings of ASME IGTI International Gas Turbine Conference, *GT2000–234*.

Selimovic F, Bruun T and Sunden B (2005), 'Computational analysis of gas flow and heat transport in monolithic structures for high temperature processes', In Proceedings of ASME Summer Heat Transfer Conference, *ASME HT2005–72183*.

Selimovic F and Sunden B (2008), 'Numerical simulation of fluid flow in a monolithic exchanger related to high temperature and high pressure operating conditions', in *Advanced Computational Methods and Experiments in Heat Transfer X*, eds. B Sunden and C Brebbia, 25–35, Southampton, WIT Press.

Sunden B (2005), 'High temperature heat exchangers', CHE2005–29, in *5th International Conference on Enhanced, Compact and Ultra-Compact Heat Exchangers: Science, Engineering and Technology*, eds. R K Shah, M. Ishizuka, T M Rudy and V V Wadekar, 226–238, CD-ROM Proceedings.

Sunden B (2007), 'High temperature heat exchangers', in *Advances in Compact Heat Exchangers*, eds. B Sunden and R K Shah, 38–58, Supplemental issue 1 of Int. J. Heat Exchangers, Philadelphia, R.T. Edwards, Inc.

Sunden B (2007a), 'Computational fluid dynamics in research and design of heat exchangers', *Heat Transfer Engineering*, Vol. **28**, no 11, 898–910.

Sunden B (2007b), 'Computational heat transfer in heat exchangers', *Heat Transfer Engineering*, Vol. **28**, no 11, 895–897.

Sunden B (2010), 'Simulation of compact heat exchanger performance', *International Journal of Numerical Methods for Heat & Fluid Flow*, Vol. **20**, no 5, 551–569.

Utriainen E and Sunden B (2002), 'Evaluation of cross corrugated and some other candidate heat transfer surfaces for microturbine recuperators', *ASME Journal of Engineering Gas Turbines and Power*, Vol. **124**, 550–560.

© Woodhead Publishing Limited, 2013

Versteeg H K and Malalasekera W M (2007), *An Introduction to Computational Fluid Dynamics-The Finite Volume Method*, 2nd ed., Boston, Pearson-Prentice Hall.

Wang L, Manglik R M and Sunden B (2007), *Plate Heat Exchangers: Design, Applications and Performance*, Southampton, WIT Press.

7.10 Appendix: nomenclature

List of abbreviations

c_p	Specific heat (J/kgK)
C_R	Ratio of heat capacity flow rates
D	Tube diameter (m)
D_h	Hydraulic diameter (m)
f	Fanning friction factor
h	Heat transfer coefficient (W/m^{2}K)
j	Colburn j-factor
k	Thermal conductivity (W/mK)
L	Characteristic length (m)
LMTD	Logarithmic mean temperature difference (K)
NTU	Number of transfer units
Nu	Nusselt number
p	Pressure (Pa)
p_f	Fin pitch (m)
Pr	Prandtl number
Re	Reynolds number
s	$p_{f\text{-}\delta}$, free air flow space (m) (Fig. 7.5)
S	Source term in Equation [7.2]
S_l	Longitudinal tube pitch (m)
S_t	Transverse tube pitch (m)
t	Time variable (s)
u_j	Velocity vector (m/s)
x_j	Cartesian coordinates (m)

Greek symbols

δ	Fin thickness (m)
Δp	Pressure drop (Pa)
ε	Heat exchanger thermal effectiveness (actual heat transfer rate divided by maximum heat transfer rate)
ϕ	Arbitrary variable
Γ	Diffusivity (m^2/s)
μ	Dynamic viscosity (kg/ms)
ρ	Density (kg/m^3)

© Woodhead Publishing Limited, 2013

8

Turbogenerators in gas turbine systems

B. GELLERT, Alstom Power Thermal Products, Switzerland

DOI: 10.1533/9780857096067.2.247

Abstract: The functioning of turbogenerators is explained as the final link between the turbine and the grid. Basic physical laws are given, and principles to calculate the performance and application of generators to gas turbines are derived. It is shown how generators developed with the progress of gas turbines. Modern designs are described and latest test results of generators are reported. Finally, an outlook is given about the future trends in technology and products. The chapter utilizes the author's in-house experience, and describes also achievements of other manufacturers.

Key words: turbogenerator, turbine generator, design concepts, generator history, development principles for gas turbine application, trends in technology and products.

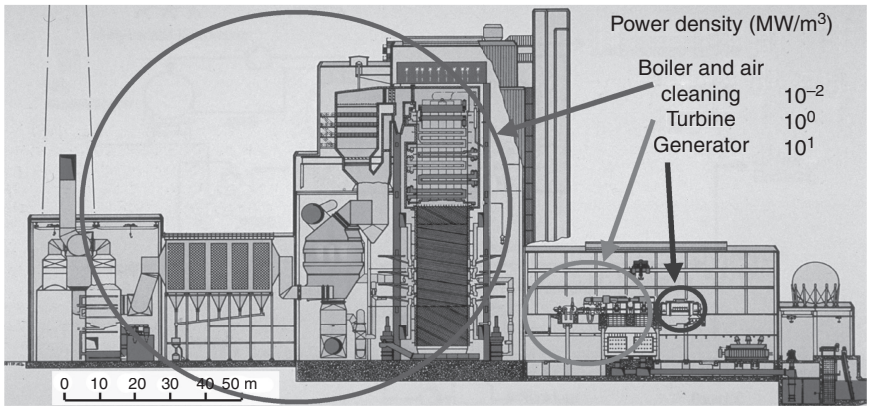
8.1 Introduction

In this chapter the basic integration of turbogenerators into gas turbine systems is shown. It is described how the reactive power is controlled. The power chart is introduced showing the interaction between the active and reactive power.

8.1.1 Rotating electrical machines

The main task of a rotating electrical machine is to convert mechanical energy into electrical energy, or electrical into mechanical. The first application is called generator operation, whereas the second is motor operation. In principle, every rotating electrical machine can be operated in both modes, even though it is designed and declared as a generator or a motor. The conversion of energy is based upon electromagnetic physical effects. They express themselves on the mechanical side as forces in magnetic fields, and on the electrical side as voltages induced by magnetic fields. The further transport of the energy is performed on the mechanical side via a torque, which is applied to a shaft. On the electrical side, a single-phase AC or multi-phase AC current system performs the required stationary energy transport. The three-phase AC system has established itself as the main system worldwide.

Published by Woodhead Publishing Limited, 2013



8.1 An example of a steam power plant indicating the size of the various components that are involved.

In conventional thermal power plants another step is added: the conversion of chemical energy by combustion into mechanical energy to drive either a steam or a gas turbine. High-speed generators for these power plants are called turbogenerators or turbine generators. Figure 8.1 shows an example of a steam power plant indicating the size of the various components that are involved

Chemical → mechanical → electrical energy
Boiler → turbine → generator

Due to the different sizes the components have to deal with very different physical and material effects, which are reflected in the different power densities involved:

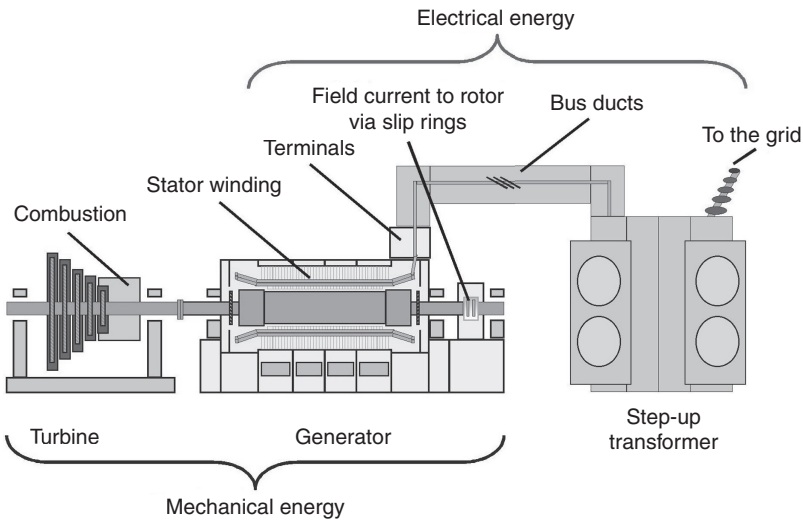
Boiler → turbine → generator
10^{-2} MW/m^3 → 10^{0} MW/m^3 → 10^{2} MW/m^3

The following deals with the final link of power generation to the grid: the generator, which is a small component in the plant, deals with the highest power densities, and is the one that realizes the only goal of a power plant: to generate electricity. The focus will be on a power range of some 50–500 MW, which is relevant for gas turbine applications.

8.1.2 Electricity generation

A generator is built up of a stationary part (the stator), a rotating part (the rotor), and the generator externals. The electrical energy is generated in the key component of the generator, the **stator winding** (armature winding), which connects to the generator **terminals** (bushings) (Fig. 8.2). The stator

Published by Woodhead Publishing Limited, 2013



8.2 The electrical energy is generated in the key component of the generator, the stator winding (armature winding), which connects to the generator terminals (bushings).

winding outputs a three-phase alternating current at the power frequency (50 or 60 Hz) and at a voltage of 10–27 kV, depending on power rating. **Bus ducts** connect the generator terminals to the step-up transformer, which adapts the generator voltage to the **grid voltage**.

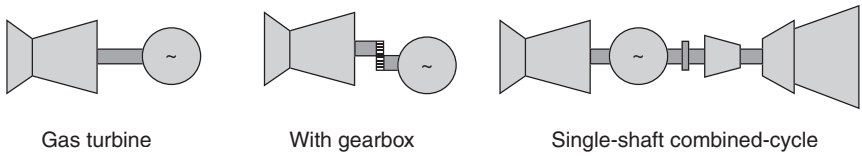
By the synchronous generator principle, the speed of the turbo set is given by the pole pair number. The speed for the full-speed generators used for GT application is 3000/3600 rpm (50 Hz/60 Hz), which corresponds to a one-pole pair.

For steam turbine and open-cycle gas turbine sets, the generator rotor is connected at the main drive end to the turbine. Smaller units may connect to turbine drives via a speed-reducing **gearbox**. Larger units connect directly to **gas turbines**. For **single-shaft combined-cycle** sets, the generator rotor is coupled at the main drive end to the gas turbine, and on its other drive end to the steam turbine (Fig. 8.3). The generator stator is, like the turbine frames, bolted to the foundation to sustain the reaction torque.

The rotor is designed for high-speed operation and has a rotor winding ('field winding'). The excitation current in the rotor winding is controlled by a stationary control unit, called the **Automatic Voltage Regulator (AVR)**.

The generator requires connection to a number of auxiliary systems, such as bearing-oil and jacking-oil supply, plant cooling water and, on larger units, to its hydrogen and stator winding cooling-water auxiliaries. For gas turbine starting, the generator may also operate as a drive motor, supplied from a static frequency converter (static starting device) connected to the generator terminals during gas turbine start-up.

Published by Woodhead Publishing Limited, 2013



8.3 For single-shaft combined-cycle sets the generator rotor is coupled at the main DE to the gas turbine, and on its other DE to the steam turbine.

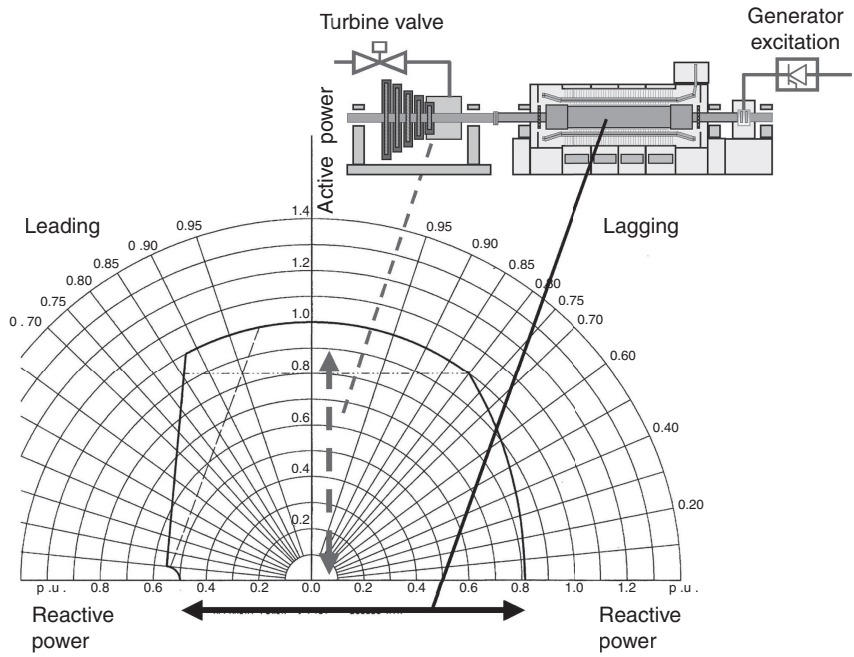
Principles of control – the power chart

The essential task of a power plant is to deliver power into the grid. Normally, several turbine units are acting on the grid. The unit operator ensures that the sum of the generated power is balanced against the sum of the consumed power. The grid parameters of concern are **voltage** and **frequency**.

The plant parameter to influence the frequency is the **active power** delivered into the grid. In the grids, which are usually large in size, the **turbine valve** is governed by continuously comparing the actual grid frequency with a reference value (50/60 Hz). If the demand for power in the grid increases, the speed of the turbines supplying the grid slows down, as power is then taken from the energy of the rotating masses. Since the synchronous generator locks the speed with the grid frequency, this frequency decreases. The response of the turbine governor is to open the steam or fuel valves to increase the power output from the turbines to maintain the grid frequency at the reference value.

The plant parameter to control the grid voltage is the **reactive power** delivered into the grid. The reactive power results from the current component, which is out of phase with the voltage. The **generator excitation** is responsible for the control of reactive power. Interaction between active and reactive power is shown in the power chart (Fig. 8.4). The excitation current can be controlled such that the grid current is in-phase with the voltage (so-called power factor pf = 1). Increasing the excitation current results in a phase shift of the grid current to the voltage (pf < 1, **overexcited** or **lagging** current mode). Decreasing the excitation current results in a reverse phase shift (pf < l, **underexcited** or **leading** current mode). Overexcited mode tends to increase the grid voltage, and underexcited tends to lower it. The stability of the turbo set on the grid is heavily influenced by the excitation; usually an overexcited mode makes the system more stable. This is the reason why, in the case of a disturbance on the grid, the generator excitation is driven to a ceiling value for a short duration. In the case of severe disturbances on the grid, the generator may fall out of step, that is, with a rotor speed running away from synchronous speed. In that case the generator is disconnected from the grid and resynchronized.

Published by Woodhead Publishing Limited, 2013



8.4 Interaction between active and reactive power is shown in the power chart.

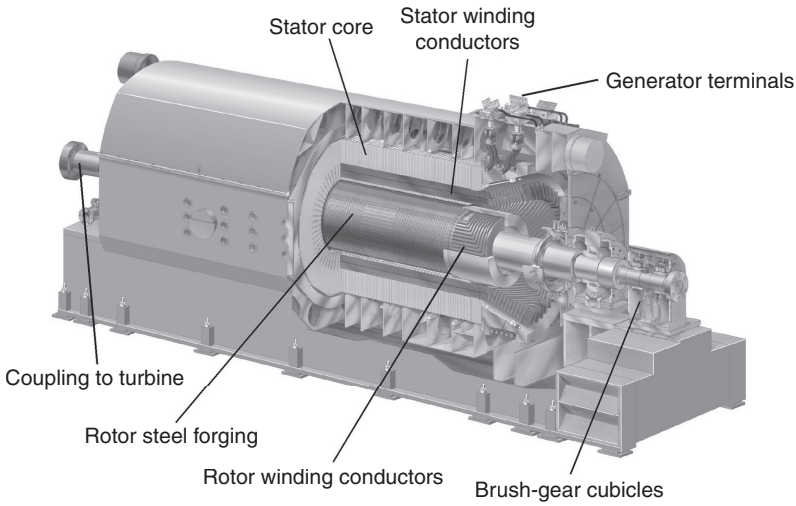
The control for generator excitation is performed by the **AVR**. It is a closed-loop regulator sensing the generator terminal voltage, comparing it with a set value and controlling the excitation current to counteract any deviation in voltage. An important additional component is the **Power System Stabilizer** (PSS), which dynamically modulates the excitation current to counteract low-frequency oscillations between the grid and the turbine generator.

Operation of a single generator supplying a local grid is called island-operating mode. In that mode the turbine valve governor acts directly for the constant speed of the turbo set, and thus for constant frequency. The AVR maintains the grid voltage.

8.2 Generator component design

The main components are shown in Fig. 8.5.

The **rotor** has a cylindrical central part with aligned shaft ends, commonly a single-forging design. The cylindrical central part of the rotor is furnished with slots, which carry the **rotor winding** (field winding); DC **rotor current** (excitation current) flows through these windings, provided by an excitation



8.5 The main generator components.

system. The rotor winding produces a **magnetic field,** which rotates with the speed of the rotor. The magnetic field lines bridge the air gap (up to 100 mm and more) between rotor surface and stator bore, and close in the stator core.

The **stator core** is a cylinder built up from a stacking of up to 250 000 insulated electrical steel sheets, which are clamped by bolts. Slots are formed in the inner surface to support the **stator winding** (armature winding). The outer cylindrical part of the core is called the yoke and carries the circumferential component of the magnetic fields.

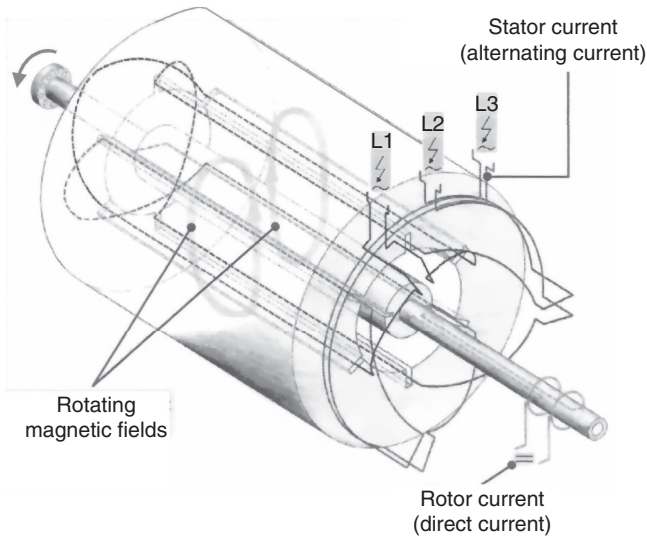
The **stator winding** is built up by series connection of the **conductor bars** in the stator slots. Matching the three-phase electrical system, the stator winding consists of three individual windings, one for each phase. It carries the main AC current in the generator and connects directly to the **generator terminals**. The terminals are connected by bus ducts to the step-up transformer, which matches the grid voltage.

Fans on both shaft ends serve for circulation of the gaseous coolant air (large units: hydrogen) through the generator parts to remove the dissipated heat.

In the **brush-gear cubicle,** arrays of carbon brushes contact the two slip rings on the rotor shaft end in order to supply the DC excitation current to the rotor winding.

Bearings are arranged on both shaft ends of the rotor, for air-cooled turbogenerators integrated in the frame independently (pedestal bearings) or integrated in the housing structure (end-shield bearings). Commonly a third bearing is arranged at the slip ring end.

Published by Woodhead Publishing Limited, 2013



8.6 The rotating magnetic field induces an alternating voltage in the stator winding.

For **air-cooled turbogenerators**, stator and rotor are supported on a common frame. The design allows transport with the rotor installed. The **rotating magnetic field** induces an alternating voltage in the stator winding (see Fig. 8.6). When the speed of the generator rotor is synchronized with the grid frequency, connection is made via the transformer to the grid. As the load on the generator increases and the **stator current** rises, the excitation current in the rotor winding must be adjusted by the AVR to maintain the voltage in the stator winding.

For static excitation the AVR controls a stationary thyristor-controlled rectifier, which feeds the excitation current via a brush-gear and slip rings (collectors) to the rotor winding. For brushless excitation (rotating excitation) the AVR controls the input of an exciter machine, which is mounted on the non-driven end of the main generator and in which a rotating diode wheel is integrated.

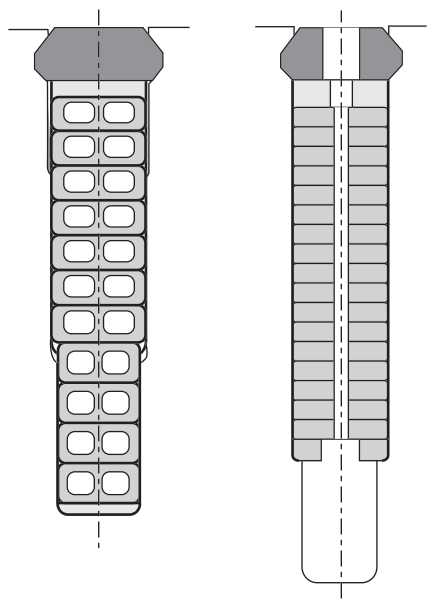
Because the windings are the most essential parts of a generator, an overview of their characteristic features will be given in more detail. The rotor winding consists of rectangular copper conductors, commonly silver-alloyed to retain mechanical strength at the elevated operational temperatures. Milled slots in the cylindrical part of the rotor carry stacked sets of these conductors; the slots are closed with metallic non-magnetic wedges to withstand the high centrifugal forces. The corresponding conductor ends are brazed together to achieve a series-connected concentric coil arrangement. Insulation strips are arranged full length between all conductors. The

Published by Woodhead Publishing Limited, 2013

conductors are stacked loose and pressed against the wedge by springs arranged in the bottom of the slot. Another possibility is to prepare compacted coil sides and mount them into the slots (so-called 'consolidated coils'). A slot wall insulation and a creepage block to the slot wedge enable insulation. The slot filling allows for thermal elongation against the slot wedge. The two end windings (winding heads) are embedded in retaining rings (end bells), which themselves are fixed to the rotor ends by shrink fits. Since they are subjected to highest mechanical stress, the retaining rings are made of specifically designed cold-worked austenitic steel. The electrical connection between the winding and the slip rings is provided by two semicircular conductors arranged back-to-back in a central bore of the shaft end, connected by radial bolts.

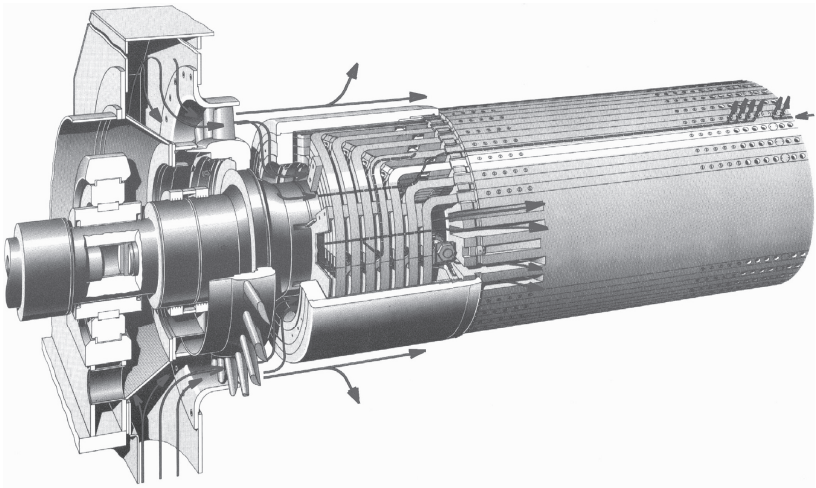
The rotor winding experiences current heat losses. In order to limit the temperature, axial cooling is provided (Fig. 8.7). The conductors are equipped with channels that carry the cooling gas (air) from the rotor ends to gas outlets in the rotor center, where the gas is discharged into the air gap (Fig. 8.8). To achieve more efficient cooling this may be done repeatedly over the rotor length, with the gas supplied by sub-slots. For radial cooling the gas is supplied from the sub-slot to the conductors through an array of aligned slits.

For the stator each slot contains two winding bars. The winding bars are bent at the end along a conical surface to be interconnected to windings and



8.7 The rotor winding experiences current heat losses. In order to limit the temperature, axial or radial cooling is provided.

Published by Woodhead Publishing Limited, 2013



8.8 The conductors are equipped with channels that carry the cooling gas (air) from the rotor ends to gas outlets in the rotor center, where the gas is discharged into the air gap.

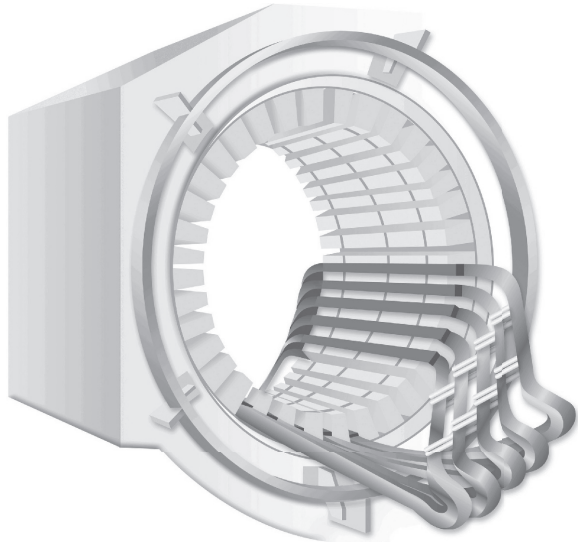
coils (Fig. 8.9). The unavoidable electromagnetic forces (EMFs), especially in short circuit, are counteracted by a wedging system in the slot and an end-winding support, which clamps the bars rigidly while allowing thermal expansion of the bars. Both need at least periodical inspection (preferentially with rotor *in-situ*), and designs that allow a fast retightening. Each phase may be built up of parallel and/or serially connected coils to provide the rated stator voltage at the generator terminals.

The stator bars are commonly designed as Roebel bars, built up of two parallel (or, for large units, four) stacks of insulated copper strands. The strands end in massive bar connections (lugs), or they are connected individually to the next bar (Fig. 8.10).

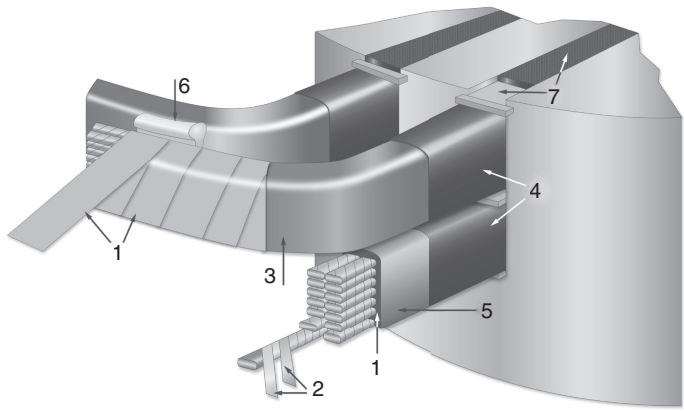
The main insulation of the stator winding bar usually consists of an application of mica tape (mica flakes on a glass/polyester carrier) being wound in multiple layers over the copper. Several recognized methods are in use to impregnate the wound tape with a synthetic resin (epoxy or polyester):

- Vacuum pressure impregnation (VPI). The bar with the wound tape is pressed in a form. Air is evaporated and resin is injected under pressure, the resin then being cured by a heating process. Later the bars are mounted individually into the stator slots.
- Global VPI. All bars are applied with wound tape and pressed in the stator slots, and the end winding is completed. In a giant vessel the complete stator core is then vacuum-treated and flooded with resin. The

Published by Woodhead Publishing Limited, 2013



8.9 For the stator each slot contains two winding bars. The winding bars are bent at the end along a conical surface to be interconnected to windings and coils.



8.10 The stator bars are commonly designed as Roebel bars, built up of two parallel (large units also 4) stacks of insulated copper strands. The strands end in massive bar connections (lugs) or they are connected individually to the next bar.

excess resin is pumped back, and the resin remaining in the stator is cured in a heating process.

- Resin Rich (RR) technology. The mica tape is delivered with the resin implemented in a dried condition and wound on the copper in the

described manner. The bars are shaped to their final dimension by hot form pressing or hydrostatic pressing. The resin is designed to become liquid again before the final curing takes place.

An anti-corona layer is applied to the surface of the main insulation to protect against electrical discharges. Special measures serve for a sustainable electrical coupling of this layer with the slot walls of the laminated core.

The stator winding bears current heat losses similar to the rotor. Contrary to the rotor winding, the stator winding (apart from some of the largest turbogenerators) is cooled indirectly, that is, the heat is removed through the main insulation.

The winding insulation is subjected to the laws of aging over time and temperature. It is established practice to define the temperature limits as thermal classes, as set in the standards. A rated operation in class 130 (130°C, formerly class B) is very common, while the main insulation system is qualified for class 155 (155°C, formerly class F). The difference gives a margin in lifetime, and may be used for overload operation (peaking reserve).

8.2.1 Important physical laws

To describe, calculate and design turbogenerators, the following basic physical laws are applied. The symbols in **boldface** denote vector quantities.

Maxwell's equations

For electrical machines that are in use for industrial application at 50 or 60 Hz, where the displacement current and further external fields can be neglected, Maxwell's equations reduce to

$$\text{rot}\,\boldsymbol{H} = \boldsymbol{J}\ \text{(Ampere's law)} \qquad [8.1]$$

$$\text{rot}\,\boldsymbol{E} = -\frac{\partial B}{\partial t}\ \left(\text{Faraday's law of induction}\right) \qquad [8.2]$$

$$\text{div}\,\boldsymbol{B} = 0\ \text{(Fundamental law of magnetostatics)} \qquad [8.3]$$

The relations that consider more specifically the material and complete the system of equations are:

$$\boldsymbol{B} = \mu\boldsymbol{H}\ \text{(Magnetic material with negligible hysteresis)} \qquad [8.4]$$

$$\boldsymbol{E} = \rho\boldsymbol{J}\ \text{(Basic Ohm's law)} \qquad [8.5]$$

Published by Woodhead Publishing Limited, 2013

Ampere's law

A coil with $\boldsymbol{N}$ windings that carries a current I is surrounded by a magnetic field $\boldsymbol{H}$ of closed loops

$$\oint_c \boldsymbol{H} \cdot \mathrm{d}\boldsymbol{s} = \int_A \boldsymbol{J} \cdot \mathrm{d}\boldsymbol{A} = \sum \boldsymbol{N} \times \boldsymbol{I} \qquad [8.6]$$

Lenz's rule of action and reaction

Lenz's law is an extension of the law of conservation of energy to the non-conservative forces in electromagnetic induction. It can be used to give the direction of the induced **electromotive force (EMF)** and current resulting from electromagnetic induction. Heinrich Lenz postulated:

> "An induced current is always in such a direction as to oppose the motion or change causing it."

The law provides a physical interpretation of the choice of sign in Faraday's law of induction, indicating that the induced EMF and the change in flux have opposite signs.

Biot–Savart's law

The Biot–Savart law is used to compute the magnetic field generated by a **steady** current, that is, a continual flow of charges, for example through a cylindrical conductor like a wire, which is constant in time and in which charge is neither building up nor depleting at any point. The equation is as follows:

$$B = \frac{\mu_0}{4\pi} \int \frac{I \cdot \mathrm{d}l \times r}{r^3}, \qquad [8.7]$$

where

I is the current,
$\mathrm{d}\boldsymbol{l}$ is a vector, whose magnitude is the length of the differential element of the wire, and whose direction is the direction of the current,
$\boldsymbol{B}$ is the net magnetic field,
μ_0 is the magnetic constant,
$\boldsymbol{r}$ is the displacement vector in the direction pointing from the wire element towards the point at which the field is being computed.

To apply the equation, you choose a point in space at which you want to compute the magnetic field. Holding that point fixed, you integrate over the path of the current(s) to find the total magnetic field at that point. The

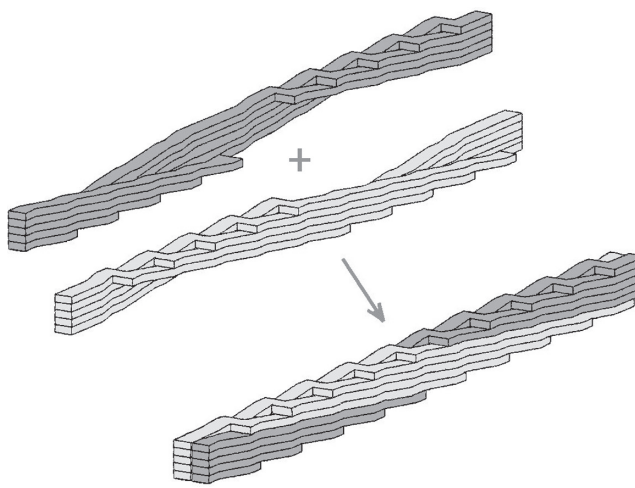
application of this law implicitly relies on the superposition principle for magnetic fields, that is, the fact that the magnetic field is a vector sum of the field created by each infinitesimal section of the wire individually. Therefore this is only applicable in materials with linear magnetic characteristics.

The Biot–Savart law is fundamental to magnetostatics, playing a similar role to Coulomb's law in electrostatics.

8.2.2 Turbogenerator calculations: some typical examples

The equations can be used to calculate the current distribution in all kinds of conductors. AC carrying stator bars are special types of conductors in generators. Whereas for a DC application a massive copper bar is most suitable, detailed calculations for AC currents result in current displacements. The key idea in generators is to use continuously twisted strands over their length in the active part of the machine. That couples each strand to the same transversal field along a slot. The strands may then be connected together at the ends of each winding half (conductor bar). The circulating currents are minimized, and a uniform distribution of the current in the conductor results. Only eddy currents due to the finite extension of the strand height (typically 1–2 mm) contribute to losses.

The most important invention to achieve an optimized design was by Ludwig Roebel in 1912. Figure 8.11 shows the design principle of a Roebel bar. Flat strands are located in a plane side-by-side and twisted along their



8.11 The design principle of a Roebel bar.

active length. Each strand completes a full 360° rotation at the same slope, so that all strands are led around each other once and uniformly.

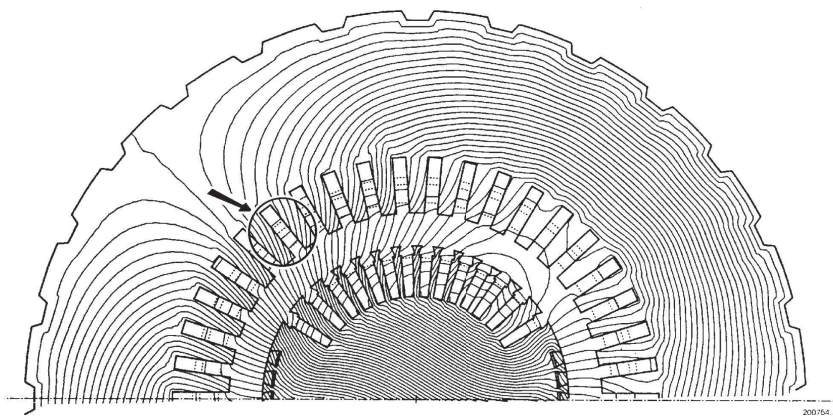
As an important typical example, in the following chapter eddy currents are calculated, which are one of the most important loss phenomena, impacting strongly on the efficiency of turbogenerators and requiring additional cooling.

Eddy-current losses are produced in electrically conducting material subjected to a varying magnetic field. The magnetic field may be externally generated, or may be produced in conductors carrying alternating currents. Eddy currents are present in all kinds of electrical machines. In synchronous machines, eddy currents are significant in stator winding copper, produced by the stator bar current, and in the stator core, produced by the rotating main field. The harmonics of the air-gap field to a certain extent produce eddy currents in the rotor surface. Since the beginning of electrical machine design eddy currents have been reduced, but have never been eliminated completely.

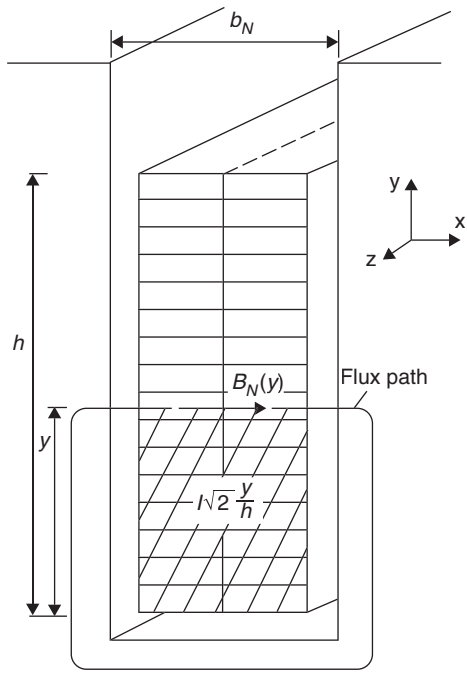
The eddy-current losses in the strands of stator bars in the slotted region are derived starting with the situation schematically shown in Fig. 8.12. A single bar of insulated twisted strands is assumed in a stator slot for the following calculation (Fig. 8.13). It carries an alternating current of rms value I in z direction.

The following considerations simplify the approach:

- Only the magnetic field produced by stator bar currents is considered. This simplifies the field calculation.



8.12 Magnetic field pattern in the active part of a two-pole turbogenerator under load. The arrow indicates the typical analysed stator slot.



8.13 A single bar of insulated twisted strands is assumed in a stator slot for the following calculation. It carries an alternating current of rms value *I* in z direction.

- The magnetic permeability of the stator core laminations is considered to be considerably larger than that of the slot itself. This results in a pure transversal field in the slot.
- The main current is evenly distributed over the conductor (postulating the result of the Roebel principle).

As a first step, we derive the magnetic field in the slot. Using the integral form of Ampere's law

$$\oint H \cdot \mathrm{d}\boldsymbol{s} = \int J \cdot \mathrm{d}A \qquad [8.8]$$

and taking the magnetic material equation, we can follow an assumed flux path which is linked to a portion of the effective value I of sinusoidal bar current (B shown as crest value)

$$\frac{1}{\mu_{\mathrm{Fe}}} B_{\mathrm{Fe}} \cdot l_{\mathrm{Fe}} + \frac{1}{\mu_0} B_N(y) \cdot b_N = I\sqrt{2}\frac{y}{h} \qquad [8.9]$$

Since core permeability μ_{Fe} is inherently considerably larger than the permeability of vacuum μ_0 in the slot, we can neglect the term of core magnetization, arriving at a transversal magnetic induction in the slot:

$$B_N(y) = \mu_0 I\sqrt{2}\,\frac{y}{h}\,\frac{1}{b_N} \qquad [8.10]$$

As a first result, the magnetic field increases linearly over the slot height.

The analysis of a single strand (Fig. 8.13) can be simplified by assuming a constant induction B_N over the height of the single strand, varying sinusoidally, as driven by the bar current.

Applying the integral form of Faraday's law

$$\frac{1}{\mathrm{d}A}\oint E\cdot \mathrm{d}s = \frac{\partial B}{\partial t} \qquad [8.11]$$

results in the electrical field $E_W(y)$ in the assumed conductive strip in the strand (Fig. 8.14) (observe changed $y = 0$ in center of the strand)

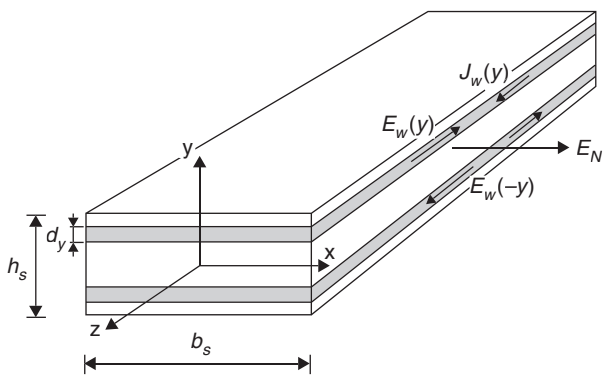
$$\frac{1}{y}E_w(y) = \frac{1}{\sqrt{2}}B_N\omega \qquad [8.12]$$

where $\omega = 2\pi f$ is the angular frequency of the bar current.

Applying Ohm's law leads to the specific eddy-current losses p_w in the conductive strip

$$p_w = \frac{1}{2}E_w(y)\cdot J_w(y) = \frac{1}{2}\frac{1}{\rho}E_w(y)^2 \qquad [8.13]$$

By substituting E_w, integrating over half the height h_s, doubling for symmetry over strand height and multiplying by the strand width b_s one obtains the eddy-current losses of one individual strand:

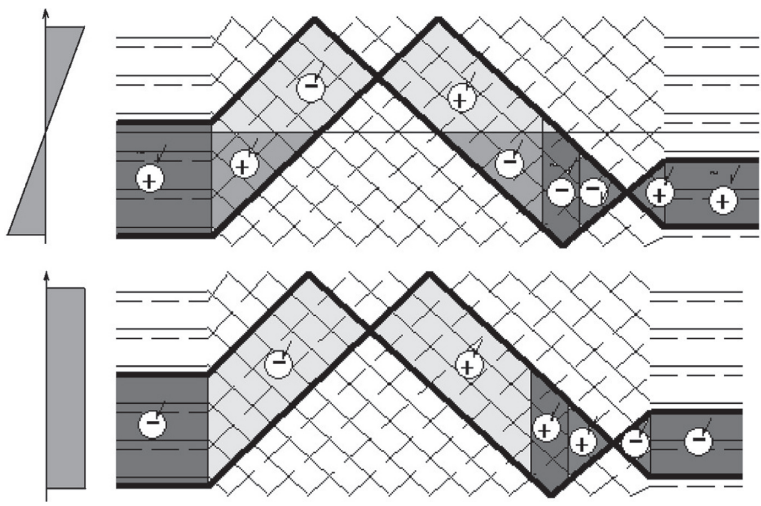


8.14 Simplified analysis of a single strand.

$$Pw = 2b_S \int_0^{hs/2} \frac{1}{\rho}\frac{1}{2} B_N{}^2 \omega^2 y^2 \mathrm{d}y = \frac{1}{\rho}\frac{1}{24} b_S h_S{}^3 B_N{}^2 \omega^2 \,[\mathrm{W/m}] \qquad [8.14]$$

The total eddy-current losses in a single slot result by applying the above formula for all strands using the corresponding magnetic induction B_N from Equation [8.10] and summing the individual eddy-current losses. Thus, for a fixed slot height, eddy-current losses grow with the square of strand height. The usual double-layer windings need corrections in losses for those slots in which the two bars carry phase-shifted currents. It is obvious that there is a limit to minimizing strand height, because increasing the amount of strand insulation decreases copper content, and thus increases ohmic losses.

The eddy currents in the slotted region of the stator core are a considerable contributor to current heating losses. The bars in the slot region are also subjected to losses produced by radial air-gap field penetrating into the slot. Another source of eddy-current losses in stator bars is the magnetic fields in the end regions – on the one hand producing eddy currents in the end regions, and on the other hand generating loop currents between strands inside a stator bar. One area of recent progress is the reduction of circulating currents in stator bars, which are not transposed in the end regions. A properly adjusted incomplete transposition (not 360°) in the slotted part of the stator establishes a compensation of the non-transposed end parts. Figure 8.15 shows the manner of minimizing the total flux (including the



8.15 The manner of minimizing the total flux (including the winding sense of each local loop) by cancelling-out of fluxes for both constant and ramping transversal magnetic field.

winding sense of each local loop) by cancelling-out fluxes for both constant and ramping transversal magnetic field.

In a similar way, losses in all metallic parts of the machine can be analyzed. For further study the reader is referred to specialist literature, for example, Haldemann (2004).

8.2.3 Characteristic parameters for turbogenerator operation

A rotor with p pairs of north and south poles generates a $2p$ pole magnetic field (Fig. 8.16), which interacts with the stator winding and – rotating at n revolutions per second – induces a voltage with frequency

$$f = p\, n \qquad [8.15]$$

On the other hand, the three-phase winding on the stator generates a magnetic field with frequency f, rotating also with n revolutions per second. The magnetic forces lock the fields, resulting in a synchronous rotation. That is why these machines are called synchronous. The number of revolutions n is therefore fixed to the frequency of the stator current. At constant grid frequency it is not influenced by the load. Only the rotor shifts or de-phases angularly across the air-gap field. The direction of the shift depends on the mode in which the machine is being operated. In generator mode driving torques accelerate, whereas in motor mode the rotor experiences braking forces. The production of torque in the synchronous machine results from the natural tendency of two magnetic fields to align. The magnetic field produced by the stator winding is denoted as Φs. The magnetic flux produced by the rotor winding is Φ_f. The resultant magnetic field is

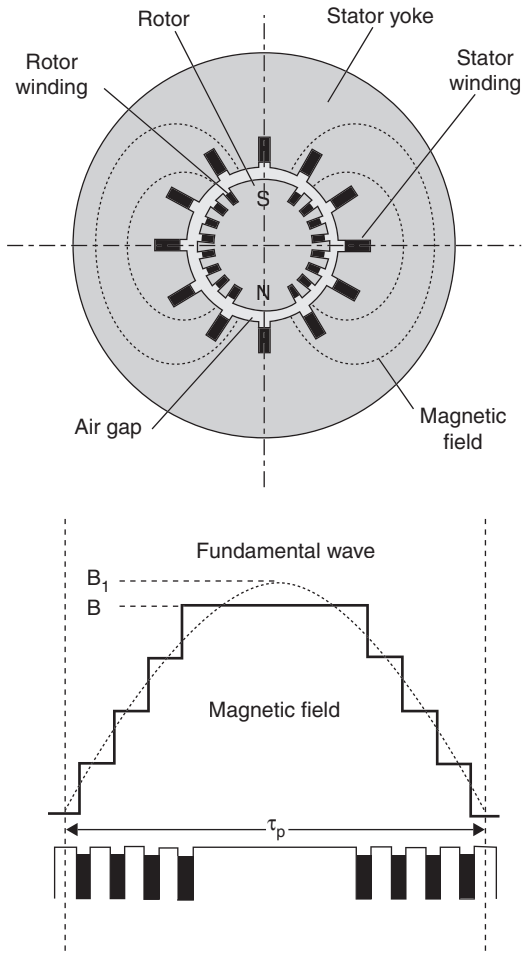
$$\Phi_r = \Phi_s + \Phi_f \qquad [8.16]$$

When the torque applied to the shaft equals zero, the magnetic fields of the rotor and the stator become perfectly aligned. When the torque is introduced to the shaft, either in a generating mode or in a motoring mode, a certain angular shift is produced between the stator and rotor fields.

If the machine at the grid is excited more than necessary to establish the magnetic field for a given active power (over-excitation), it delivers excess magnetization energy as inductive reactive power to the grid. Its effect is that of a capacitance. At under-excitation, however, it needs reactive power and has an effect similar to an inductance.

The corresponding phasor diagrams can depict these phenomena (Fig. 8.17). The plots below show the operating modes. The angle shown is the load angle δ. The phase angle φ_1 determines the power factor (pf) as

$$\text{pf} = \cos \varphi_1 \qquad [8.17]$$

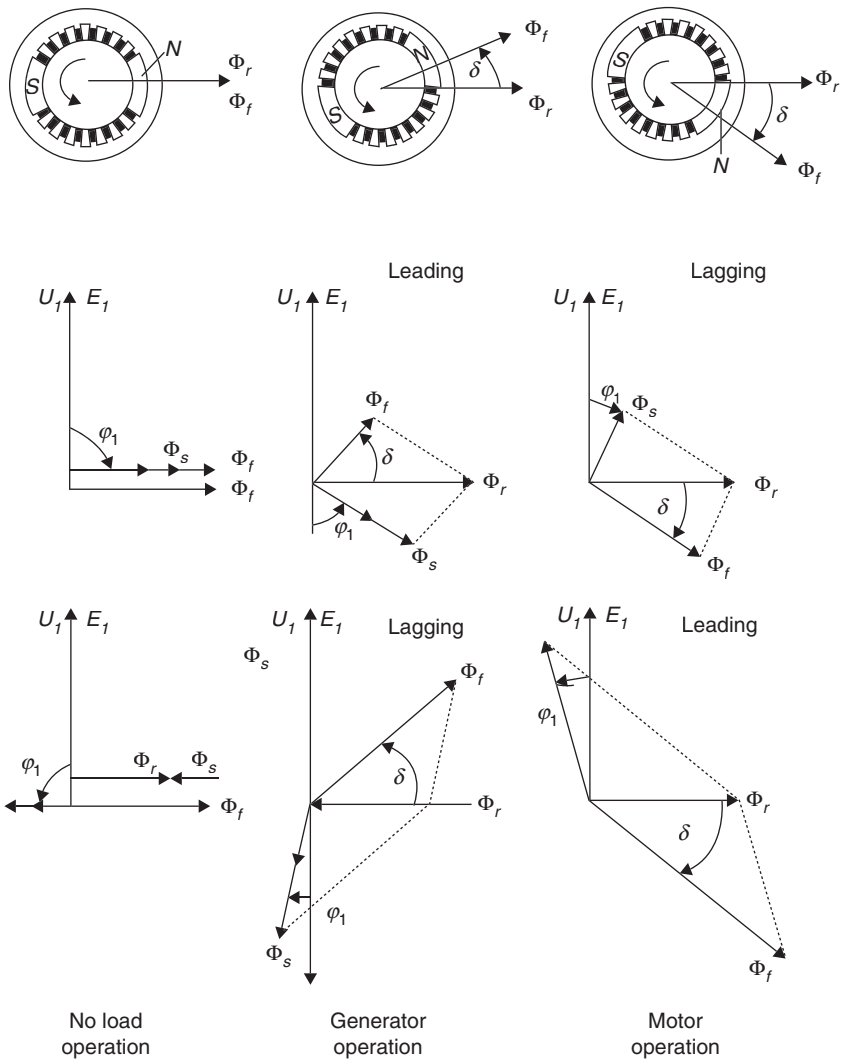


8.16 A rotor with *p* pairs of north and south poles generates a 2*p* pole magnetic field.

The load angle is the angle between the rotor flux Φ_f and the resultant flux Φ_r. It establishes the torque limits a machine can attain in a simple manner.

E_1 = excitation voltage
U_1 = terminal voltage

To describe and characterize rotating electrical machines and their operational behavior, it is customary to use internationally standardized reference quantities (see turbogenerator standards). This means that variable and characteristic quantities are referred to reference values in the same units, which are derived from the data obtained under rated operating



8.17 Phasor diagrams.

conditions (per unit (pu) quantities). By that, characteristic quantities result, mainly independent of generator size.

U_n	rated armature voltage, voltages are referred to U_n
I_n	rated armature current; currents are referred to I_n
$S_n = \sqrt{3}\ U_n\ I_n$	rated apparent power
$Z_n = U^2_n/S_n$	rated armature impedance; reference value for all resistances and reactances

When converting to per unit quantities, the numerical values of inductance and reactance become identical. It is common to refer to both as reactance.

Excitation current and excitation voltage are often referred to the following quantities:

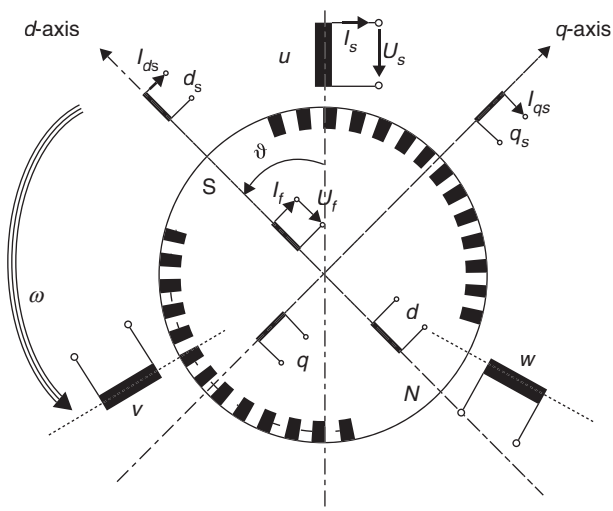
I_{f0} open-circuit excitation current for rated voltage on the air-gap line
U_{f0} open-circuit excitation voltage for rated voltage on the air-gap line

Because the design of a rotor is not fully rotationally symmetric, the behavior of the machine differs depending on the location of the stator field relative to the rotor. The characteristic *d*-/*q*-axis modeling is introduced to reduce the complexity of calculations (Fig. 8.18).

The direct-axis (*d*-axis) runs through the poles, whereas the quadrature-axis (*q*-axis) shifted by 90° crosses the rotor coils. That can transform the description of the three-phase system to just two equivalent currents I_{ds} and I_{qs}, the axis of which are the direct- and the quadrature-axis.

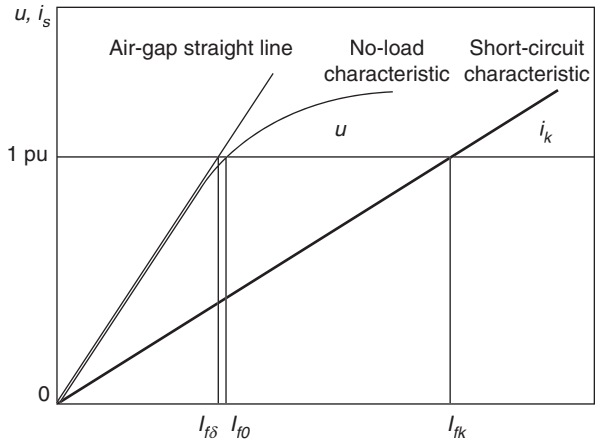
In no-load operation of a synchronous machine, only the field winding carries current and induces a three-phase voltage in the open windings of the stator. The relationship between the field current I_f and the stator voltage U is given by the no-load characteristic U (I_f) (see Fig. 8.19).

The curve increases with increasing excitation linearly and then evolves into a flat top part. The linear area is dominated by the air gap in the magnetic circuit, whereas the top part shows the influence of the magnetic saturation of the rotor and stator core. The tangent to the first part is called the



8.18 The characteristic *d*-/*q*-axis modeling is introduced to reduce the complexity of calculations.

Published by Woodhead Publishing Limited, 2013



8.19 The relationship between the field current *If* and the stator voltage *U* is given by the no-load characteristic *U* (*If*).

air-gap straight line and used as a reference for the modeling of the machine. Without saturation the rated voltage U_n would be reached at the field current $I_{f\delta}$ – when considering saturation at I_{f0}.

A no-load state is also an operation at the grid without excitation. With open field circuit ($I_f = 0$) the stator winding receives a three-phase current and creates a corresponding field to which the unexcited rotor reacts. In this case the stator current acts as the exciting medium and generates a pure magnetization current. The resulting machine reactance vs. the grid is the synchronous reactance x_d of the *d*-axis. Neglecting ohmic losses in the stator winding the stator current is then given by

$$i = \frac{-u}{x_d} \qquad [8.18]$$

The negative sign is due to the fact that energy is withdrawn:

$$i = \frac{I}{I_n} \qquad [8.19]$$

$$u = \frac{U}{U_n} \qquad [8.20]$$

In a three-phase sustained short circuit the machine is excited from the rotor and carries a short-circuit current in the stator. Field current I_f and short-circuit current I_k are linearly related to each other as shown in the

Published by Woodhead Publishing Limited, 2013

short-circuit characteristic of Fig. 8.19. For a rated current I_n the field current I_{fk} is required.

By that the synchronous reactance can be calculated from no-load and short-circuit tests, as shown in Fig. 8.19 as

$$x_d = \frac{I_{fk}}{I_{f\delta}} \qquad [8.21]$$

This is an unsaturated parameter, because under short-circuit conditions only the weak stator stray field exists. A saturated reactance is derived by replacing $I_{f\delta}$ with I_{f0}

$$x_{d\,\mathrm{sat}} = \frac{I_{fk}}{I_{f0}} \qquad [8.22]$$

The reciprocal of this reactance is called the short-circuit ratio (SCR) of the generator

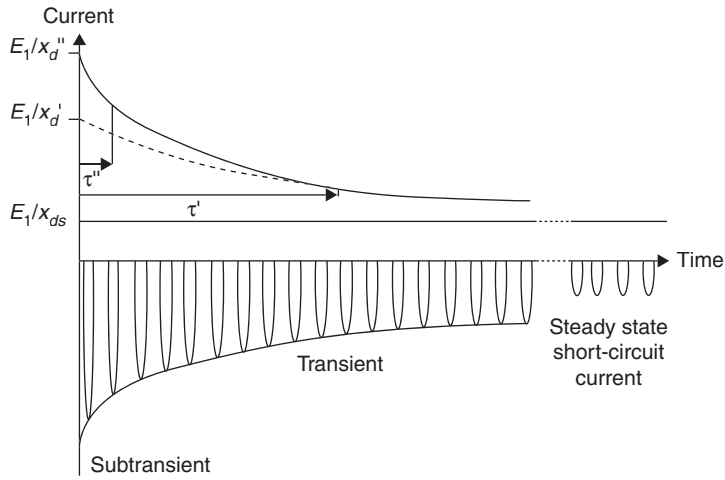
$$\mathrm{SCR} = \frac{1}{x_{d\mathrm{sat}}} = \frac{I_{f0}}{I_{fk}} = \frac{\text{no load excitation current for the rated stator voltage}}{\text{short circuit excitation current for the rated stator current}} \qquad [8.23]$$

Normally the value of the SCR is between 0.4 and 0.6. The SCR is of importance for the operation of a generator in the grid, in particular for underexcited operation. A high SCR contributes to grid stability, and becomes of more and more importance in today's grids. Machines with high utilization usually have low SCRs. Increasing the air gap (high I_{fo}) results in a higher SCR (limited by rotor winding losses).

In order to fully describe the performance of a rotating synchronous machine, further parameters are used, which can be measured from generator running tests (see Fig. 8.20 sudden short-circuit test). The main characteristics of a generator are described by the reactances as defined below (refer to standards in Chapter 4 and Table 4.1).

x_d': direct-axis transient reactance

x_d' is defined as the quotient of the initial value of a sudden change in that fundamental AC component of armature voltage that is produced by the total direct-axis armature flux, and the value of the simultaneous change in fundamental AC component of the direct-axis armature current, the machine running at rated speed and the high decrement components during the first cycles being excluded. In order to measure x_d' the method of the sudden three-phase short circuit is preferred. It permits saturated and



8.20 Sudden short-circuit test.

unsaturated values of x_d' to be determined. A more detailed description of the fundamentals can be found in Canay (1961).

The development of the short-circuit current is given by (symmetrical case, envelope only)

$$I(t) = \frac{E_1}{x_{ds}} + \left(\frac{E_1}{x_d'} - \frac{E_1}{x_{ds}}\right) \exp\left(-\frac{t}{\tau'}\right) + \left(\frac{E_1}{x_d''} - \frac{E_1}{x_d'}\right) \exp\left(-\frac{t}{\tau''}\right) \quad [8.24]$$

x_d'': direct-axis subtransient reactance

The direct-axis subtransient reactance x_d'' is the quotient of the initial value of a sudden change in that fundamental AC component of armature voltage which is produced by the total direct-axis armature flux, and the value of the simultaneous change in fundamental AC component of direct-axis armature current, the machine running at rated speed. For measurement of x_d'' again the method of the sudden three-phase short circuit is preferred, since it permits saturated and unsaturated values of x_d'' to be determined.

More sophisticated methods are used to determine the quadrature-axis reactances.

8.2.4 Fundamental rules for turbogenerator design

The main task of a designer is to design a turbogenerator for a given apparent power S and a given rotating speed

$$S = 3UI = \frac{P}{\text{pf}} \quad [8.25]$$

Where

U = phase voltage (rms)
I = armature current (rms)
P = active power
pf = power factor

Rated voltage at generator terminals is always defined as appearing between the phases and since commonly the windings of the three phases are connected in Y configuration the rated terminal voltage U_v is:

$$U_v = \sqrt{3}\,U$$

For a cylindrical rotor the fundamental component of the magnetic flux per pole is (see Fig. 8.16)

$$\Phi_1 = \frac{2}{\pi}\tau_p B_1 l_i = \frac{2}{\pi}\tau_p \frac{l_i}{\beta} B \qquad [8.26]$$

Where

τ_p = pole pitch = $d_i\,\pi/2p$
d_i = mean air-gap diameter
l_i = ideal air-gap length (slightly larger than core length)
$\beta = B/B_1$ = flux density ratio
B_1 = air-gap flux density of the fundamental wave
B = air-gap flux density at the pole center.

The flux depends on the air-gap flux density with the shown typical distribution in Fig. 8.16.

The rms value of phase voltage U that is induced in the armature (stator) winding by the fundamental wave of the flux is then given by

$$U = \pi\sqrt{2} f \Phi_1 W_s \xi_1 \qquad [8.27]$$

f = electrical frequency
w_s = number of turns in series in one phase of the armature winding
ξ_1 = winding factor for the fundamental of the air-gap flux.

The winding factor (<1.0) is the ratio of the induced voltage of the real distributed and skewed coil winding to an ideal full-span concentrated coil winding.

The no-load excitation current in the rotor winding can be determined using Ampere's law (Equation [8.8]) following the closed flux lines (see Fig. 8.16) and iterating for appropriate magnetic permeability of rotor and stator core. Equivalent magnetic networks were developed and adjusted according to measured no-load saturation curves from running tests, and are still providing satisfactory results today.

Published by Woodhead Publishing Limited, 2013

The excitation current for sustained short circuit can be analytically calculated by equalizing the magnetic flux of stator and rotor, taking into consideration stray flux loss in the stator winding. Here magnetic saturation can be neglected.

No-load and short-circuit excitation currents can be added in the generator phasor diagram to get excitation currents under load conditions, adjusted for saturation effects. Established graphical methods are described in the standards.

Today, the method of extrapolating measured no-load saturation curves is superseded by numerical two-dimensional (2D)-magnetic field calculations with precise results, even for load cases. A typical field plot is shown in Fig. 8.12 showing the distorted field pattern under load.

Apart from the magnetic flux density, the linear armature current density A is used to characterize the current loading. It is defined as the algebraic sum of all stator slot currents (rms) referred to the circumference of the stator bore.

$$A = \frac{N_{\text{slot}} I_{\text{slot}}}{\pi d_s b} \quad [\text{A/m}] \qquad [8.28]$$

The overall utilization coefficient c ('Esson coefficient' in kVAmin/m^3) is defined as the apparent power referred to 'rotor volume' and mechanical speed.

The apparent power is then given by

$$S = c\, d_r^2\, l\, n = \text{const}\, A B\, d_r^2\, l\, n \qquad [8.29]$$

Because $c \approx \text{const}\, A\, B$, the coefficient expresses the electromagnetic machine utilization, determined by the stator-current loading A (stressing the stator winding) and by the air-gap flux density B (reflecting the magnetic loading of the materials within the magnetic circuit). Corresponding design principles are described in Chapter 4 for the development of turbogenerators with a driving gas turbine.

Typical values of overall utilization and electromagnetic loading

The utilization coefficient c depends strongly on the machine design, unit rating, operating conditions and especially on the cooling design, therefore characterized here in brief.

Cooling is needed to keep temperatures in the standardized temperature classes (see Chapter 2). In principle, all generators could use air as a cooling medium, as grown historically and today possible for simple and reliable application up to high unit ratings (400 MVA) (Keller, 2008). Shaft-driven fans push the air through the generator, either in an open-ventilated (OV)

Published by Woodhead Publishing Limited, 2013

Table 8.1 Comparison of the cooling media air and hydrogen

	Air 1 bar abs.	Hydrogen 6 bar abs. 98% purity
Heat transfer	1 pu	6.5 pu
Heat flow	1 pu	6 pu
Air-gap friction loss	1 pu	0.5 pu

arrangement taking air from ambient, or in totally enclosed air–water cooling (TEWAC) using built-in air–water heat exchangers (coolers). Conduction losses of the rotor winding are commonly removed by air in direct contact with the copper, either axially through channels in the conductors or radially through aligned openings in the conductors.

The stator winding is cooled indirectly, that is, the copper losses are removed through the winding insulation. The air circulates through radial ducts in the stator core and thereby removes both losses of conductors and core. However, the larger is the rated power, the larger becomes the size, and thereby the costs, of the machine. Transport would not be possible without complex assembly on site. That is why other gaseous coolants were investigated. Hydrogen has established itself as an excellent solution for medium-size turbogenerators, especially for 60 Hz, because of low losses (down to 100 MVA) and for extending the limits of ratings (up to 700 MVA). Hydrogen is used with higher pressure of several bars, and is a very efficient extension of air, despite all the effort required for sealing, auxiliaries and safety precautions. Table 8.1 compares the values that contribute to cooling performance.

Largest units (600 MVA upwards) have direct cooling of the stator winding conductors, making use of embedded 'hollow conductors' in the stator bars, carrying hydrogen or by demineralized water.

The armature linear current density A, for generators with air cooling, is in the order of 80–130 $\times$ 10^3 A/m, depending on size, rotational and peripheral speed, mode of ventilation, temperature class, etc.

For large turbogenerators with hydrogen, current loadings are up to 200 $\times$ 10^3 A/m, and go up to 300 $\times$ 10^3 A/m when supplemented by water cooling in the stator winding. Consequently, the values of A depend strongly on the cooling system and the unit rating.

The air-gap flux density B usually lies in the range of 0.8–1.1 T. This requires careful dimensioning of the iron paths for the magnetic circuits, accurate calculation of the magnetic circuit in regard to the excitation demand, air-gap field and voltage waveform and use of appropriate magnetic materials: forged special-alloy steels having high permeability and strength for the rotors; cold-rolled low-loss electrical steel sheets for the stator core (2.7–3.5 W/kg at 50 Hz). Some manufacturers rely on grain-oriented electrical steel sheets, allowing higher flux density in the stator core yoke.

Published by Woodhead Publishing Limited, 2013

The overall utilization coefficient mainly depends on generator power range and cooling and is in the range of 10–15 kVAmin/m^3 for air-cooled generators, and up to 40 kVAmin/m^3 for the largest generators with hydrogen/water cooling.

Application: determination of main dimensions

For a given output and speed, the active (rotor) volume can be predetermined approximately by means of the basic design relation [8.29] and by using a suitable value for the utilization coefficient. For turbogenerators, the limiting feature is the centrifugal force, that is, peripheral speed $v_{R\max}$ at overspeed $n_{\max}$, which, as a first approach, determines the largest allowed rotor diameter $d_{\max} = v_{R\max}/\pi n_{\max}$. In the lower range of rotor diameters, the choice may be according to the manufacturer's offered generator series.

In large two-pole turbogenerators, the rotor diameter is limited by the mechanical strength of both the rotor-body forging steel and the end-bell alloy. Actually, the highest peripheral speeds possible at the active rotor surface are up to $v_{R\max} \approx$ 215–235 m/s at the over-speed of $n_{\max} = 1.2\ n$. Thus, rotor diameters reach a maximum of 1.25 m in the largest turbogenerators operating at 50 Hz (the limits for 60 Hz are lower). The active length is chosen to achieve the rated power. However, the length is restricted by shaft dynamics (critical speeds) and slenderness.

8.2.5 Efficiency

Apart from maximizing the apparent power within a given volume, another target is to design for highest efficiency. Efficiency for generators is defined as

$$\eta = \frac{\text{Delivered electrical power}}{\text{Consumed mechanical power at coupling}} = \frac{P_d}{P_c} \qquad [8.30]$$

The difference between P_c and P_d is the generator losses. In a real electrical machine, loss develops in all electrical circuits as:

- Current heat losses.
- Magnetization losses.
- Friction losses.

Current heat losses are usually sub-divided into:

- Stator winding losses.
- Excitation losses.
- Brush-gear transmission losses.

Published by Woodhead Publishing Limited, 2013

Stator winding losses are those ohmic losses that originate mainly in the windings of the stator.

$$P_{vw} = I^2 R \qquad [8.31]$$

Additional contributions arise from circulating currents and eddy currents.

Excitation losses mainly occur in the circuit of the field winding

$$P_{ve} = U_f I_f \qquad [8.32]$$

An additional contributor to excitation losses is the excitation unit (static exciter or rotating exciter machine), commonly considered based on an exciter efficiency of some 95%.

Brush-gear transmission losses are losses originating from the voltage drop from brushes to slip rings. The voltage drop U_b is not proportional to the current. For two brushes of natural graphite in series, a typical value of U_b = 4 to 5 V can be used. For the complete brush-gear the following estimate results

$$P_{vb} = U_b I_f \qquad [8.33]$$

Magnetization losses P_{vu} develop in the stator core. For a volume V_m with a constant loss density v_u of the magnetization losses

$$P_{vu} = v_u V_m \qquad [8.34]$$

The magnetization losses consist of hysteresis losses and eddy-current losses

$$P_{vu} = P_{vhyst} + P_{vwb} \qquad [8.35]$$

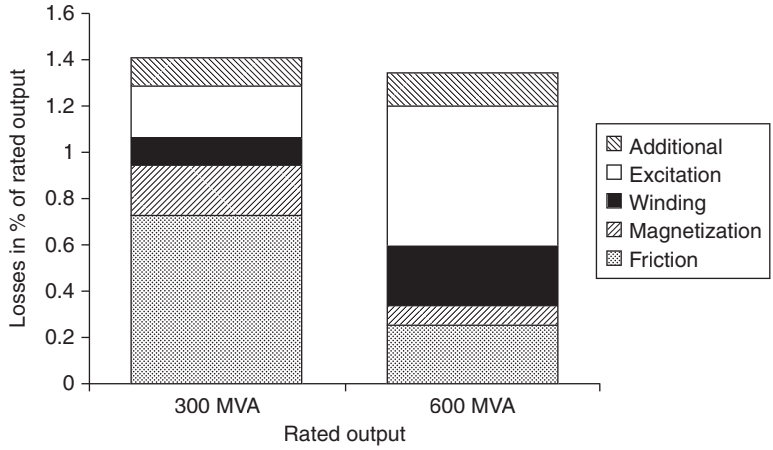
P_{vu} is approximately proportional to the square of the amplitude of the induction B that exists in the considered volume. Hysteresis losses vary linearly, and eddy-current losses vary quadratically with the frequency. Empirically derived correction factors apply for the consideration of the rotating magnetization.

Friction losses P_{vrb} appear as losses

- in bearings,
- in the brush-gear system,
- in the cooling gas.

The last contains not only the friction loss in the air gap, but also the losses due to ventilation, for example, by the fans which boost the flow-rate of cooling gas in the air gap, the rotor winding and the stator core.

Published by Woodhead Publishing Limited, 2013



8.21 The typical contributions of the various losses using air-cooling (300 MVA) and hydrogen cooling (600 MVA).

Finally, additional losses must be considered that are of parasitic mode and cannot be modeled easily. An example is eddy currents in parts of the generator components.

The total loss of a machine is therefore the sum of all losses. They can be divided into no-load losses P_{vn1} and load losses P_{vl} (load independent/load dependent losses):

$$P_v = P_{vn1} + P_{vl} \qquad [8.36]$$

No-load losses are magnetization losses, friction losses, and part of the excitation and additional losses. They occur already in no-load operation of the machine and are, to a great extent, independent of the load current.

Load losses are stator winding losses, the main part of the excitation losses as well as the main part of the additional losses. They increase mainly quadratically with the current.

The total efficiency of a machine is calculated as

$$\mu = \frac{P_d}{P_c} = \frac{P_d}{(P_d + P_v)} = \frac{(P_c - P_v)}{P_c} \qquad [8.37]$$

Typical efficiencies are in the range of 98.4–99.0%.

Figure 8.21 shows the typical contributions of the various losses.

8.3 The history of turbogenerator development

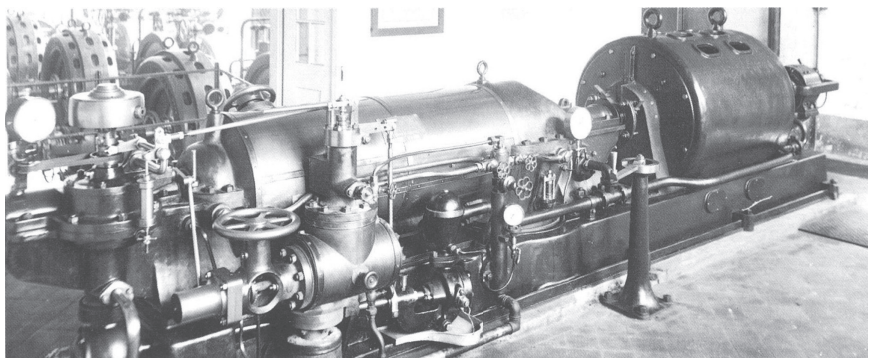
Knowing the working principles, basic design and main equations, it is of interest now to look into the history – how turbogenerators developed for

gas turbine applications. The author describes the principle evolution of the technology based on the particular example of the development in Europe by BBC/ABB/ALSTOM, with an additional chapter of pioneering work by other manufacturers.

8.3.1 Early turbogenerators developed for steam turbines

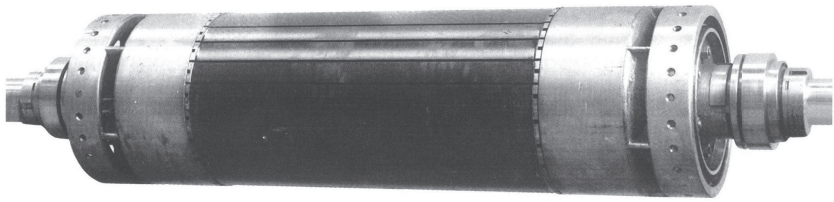
At the beginning of the twentieth century, steam turbines started to compete with steam engines. The speed was considerably higher and required new designs for a direct driven generator (Fig. 8.22). Rotors thus were getting smaller in diameter and longer in length. Triggered by the invention of the cylindrical rotor by Charles Brown in 1901, this became the acknowledged design for turbogenerators. In this design, the rotor body consists of a cylindrically shaped steel forging – remaining the preferred solution up to the present day (Fig. 8.23).

From the start, the highest achievable speed with synchronous machines was anticipated. The frequencies in the early years were different from later standards, according to individual local grid preferences, but were soon standardized to 50 Hz in Europe and 60 Hz in the USA, a prerequisite for the ensuing interconnection of grids. Voltages were up to 3 kV, and coil insulation was mainly by mica-paper slot channels, impregnated with shellac. Unit ratings developed to some few MW in the first ten years. Cooling in those times was by convection to ambient air. From the beginning, inside air flow was maintained to support cooling, provided by blowers integrated in the main shaft. The excitation current was produced by a dynamo exciter machine, located at the non-driven generator end, feeding the DC current via slip rings in the rotating field winding.

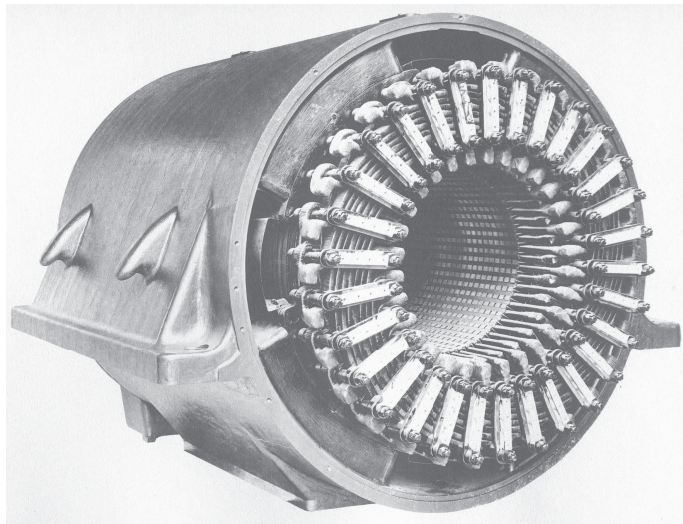


8.22 At the beginning of the twentieth-century steam turbines started to compete with steam engines. The speed was considerably higher and required new designs for a direct driven generator.

Published by Woodhead Publishing Limited, 2013



8.23 The rotor body consists of a cylindrically shaped steel forging – remaining the preferred solution up to today.

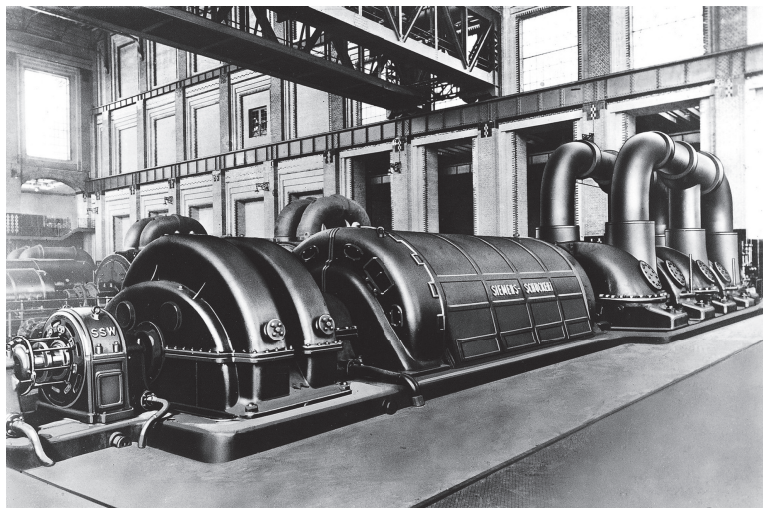


8.24 The design limitation was the stator winding, which was changed from coil to single bar design.

Steam turbine unit ratings were quite rapidly increasing and the generator evolved accordingly. The design limitation was the stator winding, which was changed from coil to single bar design (Fig. 8.24). The breakthrough came with the invention of Roebel in 1912, considerably lowering the additional losses, and thus paving the way for higher current loading (Roebel, 1912) (see also Section 1.3.2).

The 1920s were the high-point of air cooling, with quite sophisticated enclosed air circulation and brute-force support by external air blowers. A multi-chamber cooling, as used in modern air-cooled generators, was already applied. Remarkably, the cooling of rotor and stator winding was done indirectly, meaning that the copper losses had to be fully removed through the main insulation. Supported by progress in main insulation technology, the rated voltage went up to 16 kV.

Published by Woodhead Publishing Limited, 2013



8.25 At the beginning of the 1930s full-speed rating achieved 80 MVA.

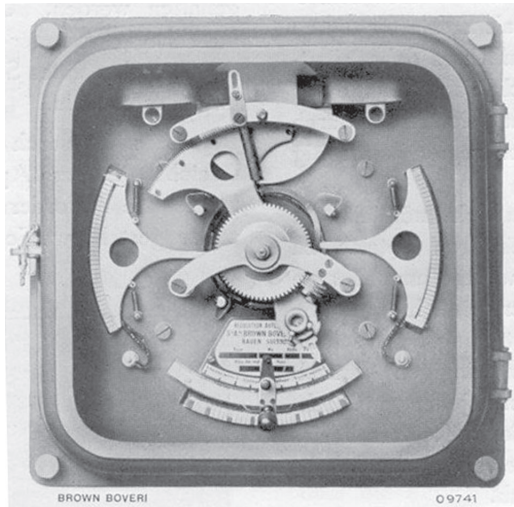
At the beginning of the 1930s, full-speed rating achieved 80 MVA (Fig. 8.25). To cope with forging supply limitations, rotors had to be designed as axially bolted multiple forgings, a technology kept until after World War II, and reintroduced in the nuclear power era. Through continuous joint development with the forge masters, rotor retaining ring material developed to forged non-magnetic steel, which was a prerequisite for an increase in rotor diameter. Excitation systems were still using DC exciter machines, but now supported with fast-acting mechanically-based rolling-sector regulators, used up to the 1960s (Fig. 8.26).

The race slowed down in the industrial crisis of the 1930s up until World War II. However, it is worth mentioning that at this time US manufacturers had started to introduce hydrogen cooling of turbogenerators, not yet using it for significant further increase beyond 100 MVA.

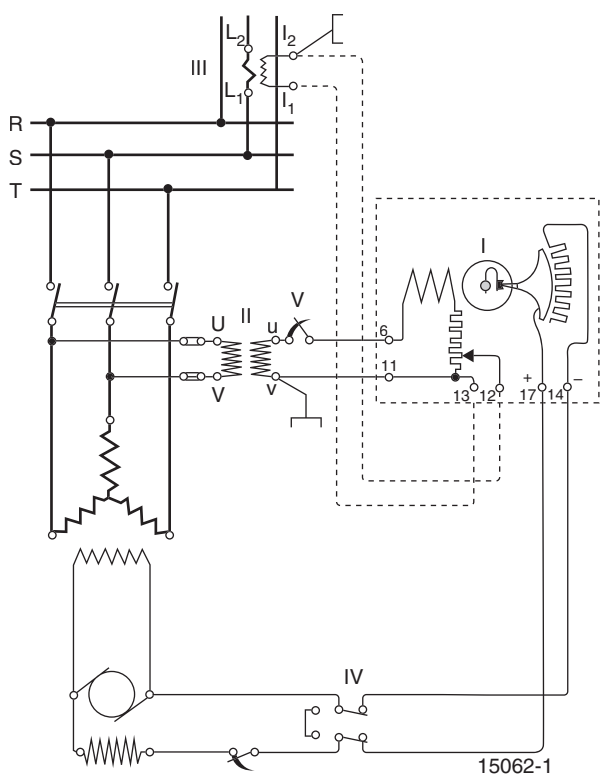
By 1950 European development was then catching up with US efforts to bring hydrogen-cooled generators to industrial standards. Supporting reasons for hydrogen were: the booming economy, requiring considerably higher unit ratings of steam turbines, later pushed by the nuclear power business, requiring steam turbine units from 300 up to 1000 MW. Although a gain of 0.5% in efficiency resulted (at that time: 98–98.5%), reduction of losses was of secondary priority compared to the intention to develop highest unit ratings. The first evolution of hydrogen-cooled generators was with indirectly cooled stator windings, using similar cooling principles as air-cooled generators. To enable further growth, directly cooled stator windings were introduced (Fig. 8.27).

Published by Woodhead Publishing Limited, 2013

(a)

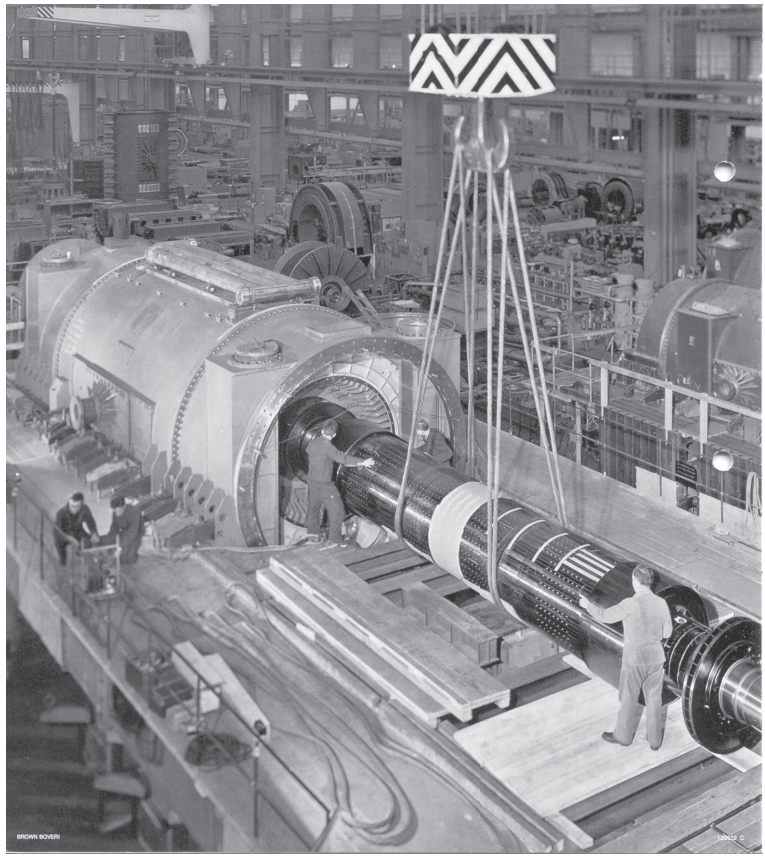


(b)



8.26 DC exciter machines, supported with fast-acting mechanically-based rolling-sector regulators, were used until the 1960s. (a) Photo of the mechanical arrangement, (b) electrical circuit of the device.

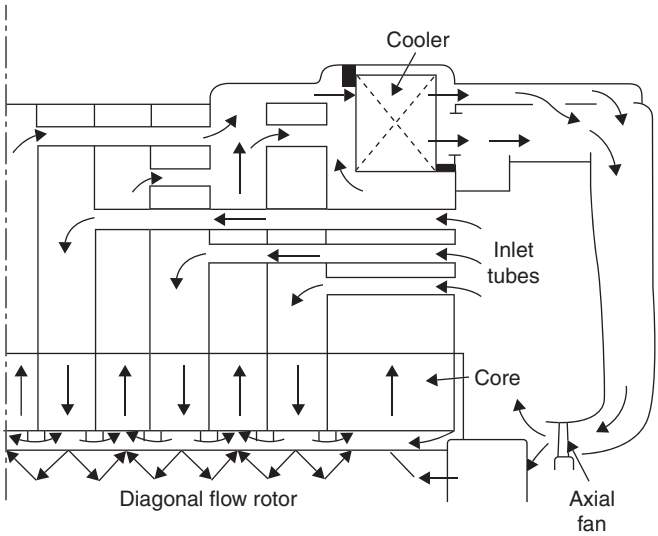
Published by Woodhead Publishing Limited, 2013



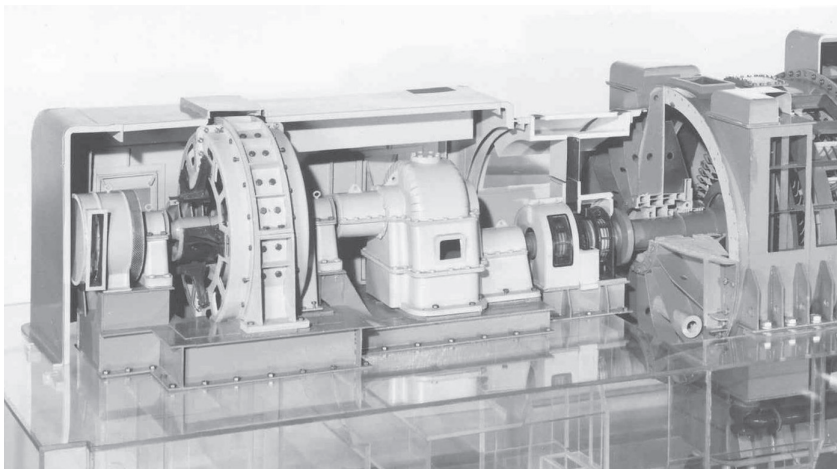
8.27 To enable further growth directly cooled stator windings were introduced.

Generator housings had to resist hydrogen overpressure of up to 6 bar, and were changing in design from cast steel to welded steel. Hydrogen-tight shaft seals had to be developed, as well as auxiliaries for hydrogen management. The water–air heat exchangers (coolers) were integrated into the housing. A new feature was the direct copper cooling of the field winding in the rotor, allowing higher current densities in the winding conductors. The US manufacturers developed sophisticated modular cooling systems (Fig. 8.28). A giant step was taken in insulation technology. Following worldwide research and development, around 1960 the manufacturers changed their insulation system to mica tape with synthetic resin impregnation, a technology for thermal qualification at 155°C (class F), and which has lasted to the present day, covered by trade names such as MICADUR, MICALASTIC, MICAPAL, etc. Rated voltages could be raised considerably and were extended to 27 kV.

Published by Woodhead Publishing Limited, 2013



8.28 The direct copper cooling of the field winding in the rotor, which allowed higher current densities in the winding conductors.



8.29 By the end of the 1960s, the DC excited machine was superseded by static excitation.

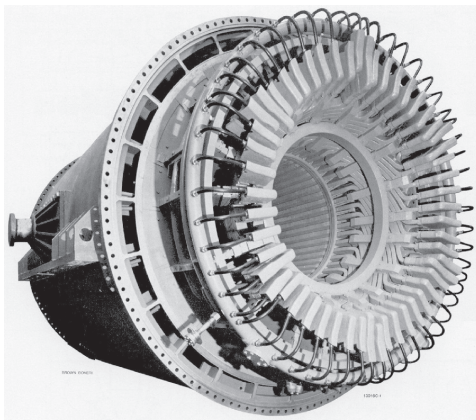
This insulation improvement was also an indispensable base for the later success of air-cooled generators. Similar developments took place for the rotor insulation.

By the end of the 1960s, when power semiconductors became mature, the DC excited machine (Fig. 8.29) was superseded by static excitation.

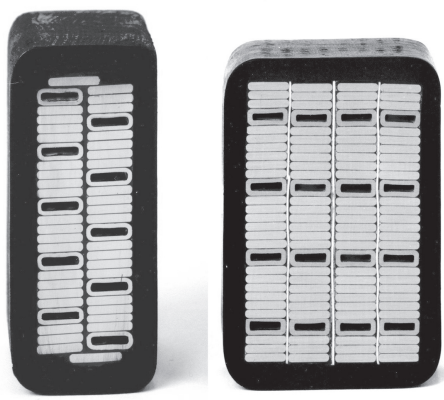
Published by Woodhead Publishing Limited, 2013

A parallel approach was that of rotating diode excitation. Both systems achieved worldwide acceptance, and have become the preferred standards today.

Hydrogen cooling with indirectly cooled stator winding arrived at unit ratings of 300 MVA. However, at that time it had not been exploited to its size limits, a task undertaken later to serve the single-shaft combined-cycle market. To overcome the limits for current densities in the mid-1960s, direct water cooling of the stator winding was introduced, first with hollow-copper conductors, embedded in the stator bar and carried by deionized water, later superseded by corrosion-resisting stainless steel tubes (Figs 8.30 and 8.31).



8.30 Direct water cooling of the stator winding, with hollow-copper conductors, embedded in the stator bar and flown by deionized water.

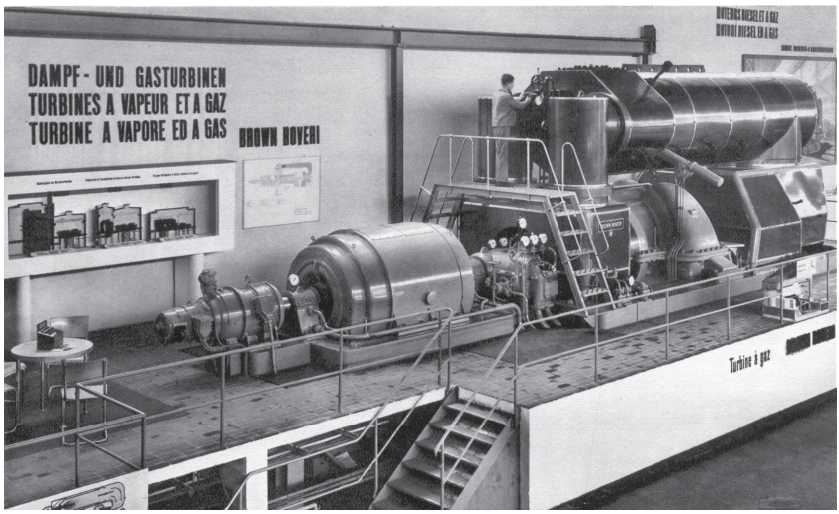


8.31 Direct water cooling of the stator winding through corrosion-resisting stainless steel tubes.

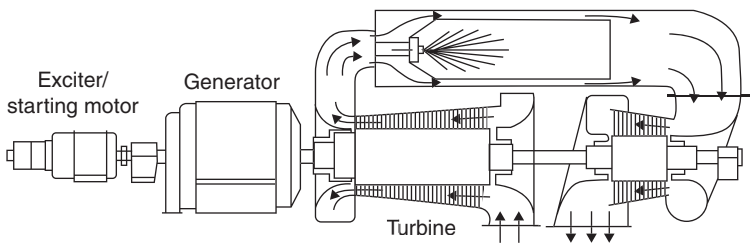
Published by Woodhead Publishing Limited, 2013

8.3.2 Turbogenerators developed for gas turbines

Air-cooled generators were the only choice to cover the needs of the emerging combustion gas turbine activity in 1939. At that time, BBC had developed a 4 MW prototype gas turbine for emergency power generation for the Neuchatel cavern power station (Figs 8.32 and 8.33). With 5 MVA the air-cooled generator was small in relation to the existing air-cooled generators. The generator was directly coupled to the turbine-compressor shaft, rotating at 3000 rpm. On the same shaft, behind the generator, were the DC exciter machine and the gas turbine starting motor. The unit served for pioneering operational experience, and remained operational until 2002.



8.32 Photograph of the 4 MW prototype gas turbine for emergency power generation for the Neuchatel cavern power station, developed by BBC.



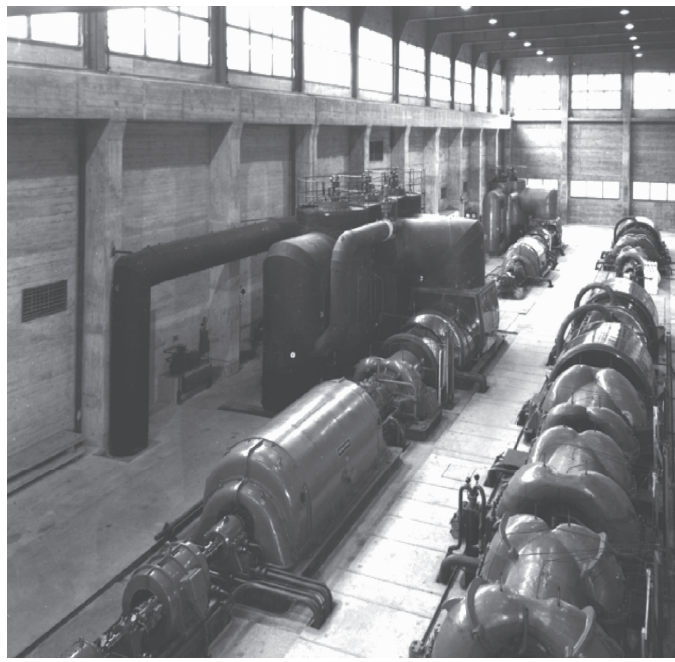
8.33 Schematic of the 4 MW prototype gas turbine for emergency power generation for the Neuchatel cavern power station, developed by BBC.

In the beginning gas turbines were offered up to 5 MW, and the industrial gas turbine business was growing, all equipped with air-cooled generators, partly also with gearboxes to adapt to synchronous speed (3000/3600 rpm).

In 1948/49 the first dual-shaft sequential-combustion gas turbine plant unit was installed in Döttingen/Beznau, Switzerland, with the intention of supporting hydro-pump storage in daily load leveling (Fig. 8.34). The two units produced 40 MW, the two air-cooled generators, one with a gear box 4700/3000 rpm designed for 13 MW–16 MVA and the other with direct drive at 3000 rpm for 27 MW–33 MVA, were of the classical design with the coolers arranged in the foundation. The unit is still operational as a reserve.

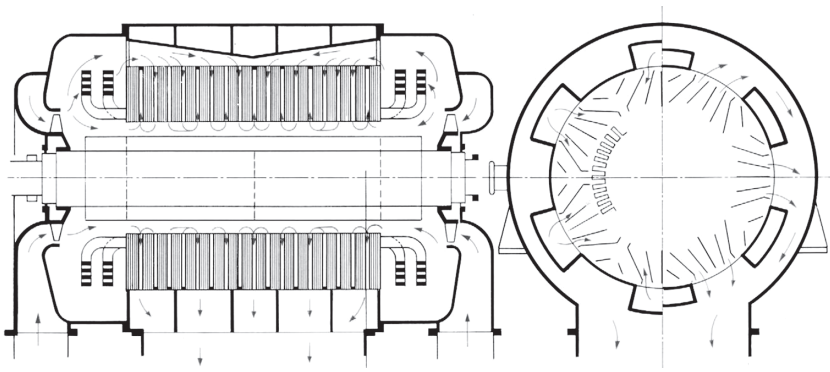
In 1963 BBC made an important step toward today's gas turbines with the introduction of the 15 MW GT11L, designed as a single-shaft package solution with overhead combustor, considerably simplifying the installation.

The gas turbines in the 1950s and 1960s were all equipped with technologies of established air-cooled generators. Stator bar insulation was of class 130 Mica foil type in the slot region, and rotor cooling was still indirect,



8.34 In 1948/49, the first dual-shaft sequential-combustion gas turbine plant unit was installed in Döttingen/Beznau, Switzerland, with the intention of supporting hydro-pump storage in daily load leveling.

Published by Woodhead Publishing Limited, 2013



8.35 Generators up to 60 MVA were designed with a sophisticated alternating stator core cooling.

at large ratings supported by slotted cooling channels in the rotor body. Generators up to 60 MVA were designed with a sophisticated alternating stator core cooling (Fig. 8.35). A version with integrated coolers and air distribution inside the housing was available. In 1969 this design was extended to the new gas turbine GT11.

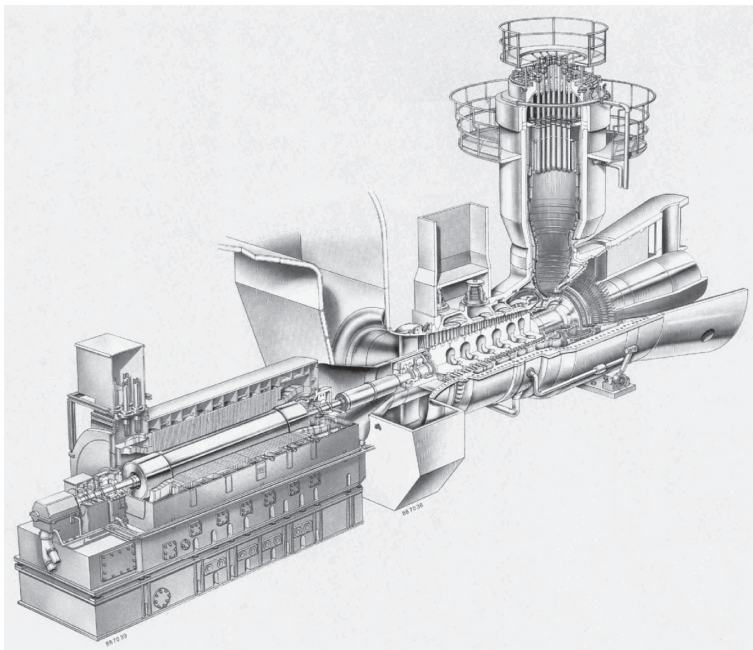
In 1969 BBC launched a new set of utility gas turbines, starting with the introduction of the GT11, rated 32 MW at 3600 rpm. The new design was a single-shaft frame with vertical combustor. In 1974 the GT9 (31 MW at 4482 rpm using a gearbox) and the GT13 (79 MW at 3000 rpm) were introduced, both now with combustor on top of the gas turbine. The ratings were now arriving at the limits of the existing air-cooled generator series. At the same time, the new plant layout required quite a high shaft line with alignment of turbine and generator on the normal foundation. This was the moment when BBC decided to introduce a new air-cooled series primarily designed for gas turbines (Fig. 8.36) with a special new type name WY. Early development was started in the Oerlikon facilities (the former Maschinenfabrik Oerlikon), and later the activities were continued in the Birr works. A first approach covered the range up to 130 MVA (Table 8.2).

The series was then expanding with the subsequent GT types. Thanks to a clever initial modular approach in design and cooling, it has been followed up to the present day, keeping the essential design principles. The growth in unit rating was realized by the increase in rotor size, as a rule first exploiting maximum length, and secondly by increase in diameter. The design always allowed a package solution, which enabled the complete generator to be delivered on site. In 1980 a first significant expansion was realized, preparing for the coming GT13E of 120 MW at 3000 rpm, although ahead of its time, introduced for a steam turbine application.

Published by Woodhead Publishing Limited, 2013

Table 8.2 A new air-cooled turbogenerator range, first time specially developed for gas turbines

Type	WY14	WY16	WY18	WY21
First unit operation	1974	1976	1978	1984
Max. rating 50/60 Hz	38/45	70/84	130/130	200/230
For gas turbine type	GT9	GT9	GT11, GT13	GT13E+

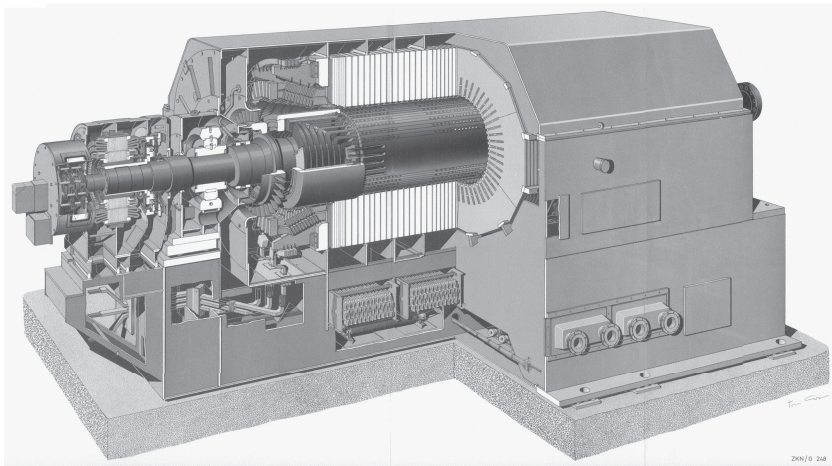


8.36 The BBC air-cooled series primarily designed for gas turbines.

Overall design

The overall design is characterized by a fully welded housing with a pre-manufactured 'built-in' stator. The new gas turbine arrangement standing on the foundation results in a high shaft line. The WY matches the corresponding requirements by transversal arrangement of the coolers in the bottom part of the housing to provide complete air circulation inside the generator, giving the generator its unique design (Fig. 8.37). The pedestal bearings for the generator rotor are arranged on housing extensions, which are an integral part of the housing. This gives the generator a sturdy appearance, and allows shipping as a package with the rotor inside.

Published by Woodhead Publishing Limited, 2013



8.37 The transversal arrangement of the coolers in the bottom of the housing provides complete air circulation inside the generator.

Static starting system

The preferred starting system was introduced by using the generator as a synchronous starting motor, fed by a static frequency converter (SFC). In the case of brushless excitation, auxiliary slip rings with a liftable brush-gear serve for excitation when the generator is fed by the SFC.

Transportation and installation

Transport of the complete generator is usually on flatbed car by road (Fig. 8.38) or by rail. Since the generator inherently is sealed against ambient, no additional measures need to be taken. Open air installations were common practice in Middle Eastern plants.

Combined-cycle arrangements

Although the technology was known long before, the 1973 energy crisis initiated the introduction of the combined-cycle plants. In the 1970s and 1980s this was done by adding separate steam turbine-generator units (steam tails), adding approximately a third of the gas turbine power, no problem for an air-cooled generator. The so-called KA plants were modularly extendable, for example four gas turbines serving one steam tail. In cases where the output exceeded air-cooling capability, hydrogen-cooled generators were chosen.

French designs

As a response to the growing gas turbine market in the 1980s, Alsthom in Belfort started the development of a low-cost air-cooled generator series

Published by Woodhead Publishing Limited, 2013



8.38 Complete generators are usually transported on flatbed cars by road or rail.

(TA types "turboalternateur"). The range was soon covering 25–100 MW. Alsthom was at that time serving the GE gas turbine program as a packager mainly for the 50 Hz market. The design was extended to 180 MW in the late 1990s, and remained there up to the merging with the ABB program in 1999 (Table 8.3). From that beginning the Belfort air-cooled series was shaped, to today's Alstom air-cooled generator program, up to 150 MW (Iseli, 2002).

The design is characterized by a modular package with a high degree of integration. The active part is built on a base frame. The frame is fully covered by an enclosure (Fig. 8.39), which serves for air circulation and noise attenuation, including the package integration options. It is suitable for outdoor installation. The compact overhung exciter is the standard solution (Fig. 8.40). Optionally, a gear box can be integrated. The package is shipped by flatbed trailer.

Swedish designs

ASEA had introduced an air-cooled generator series in early 1980 and brought this into the merger of BBC and ASEA to ABB (Fig. 8.41). The range covered 20–200 MVA. The welded rectangular-shaped housing and end-shield. There were an impressive number of variants available. Around 80 units were manufactured in the 1990s, some up to 200 MVA. For gas turbines there was a close collaboration with ABB Stal. The series was discontinued in early 2000.

Published by Woodhead Publishing Limited, 2013

Table 8.3 Development steps of the small air-cooled range

Type (Speed-MW)	TA30–40	TA30–131	TA30–150	TA30–180
Main development steps 50 Hz				
First unit operation	1975	1992	1997	1999
For gas turbine type	LM6000	MS9001	M701D V94–2A	Steam
Main development steps 60 Hz				
Type (Speed-MW)	TA36–22	TA36–40	TA36–82(90)	
First unit operation	1980	1980	2000	
For gas turbine type	MS5	MS6B LM5000 LM6000	MS6001FA	



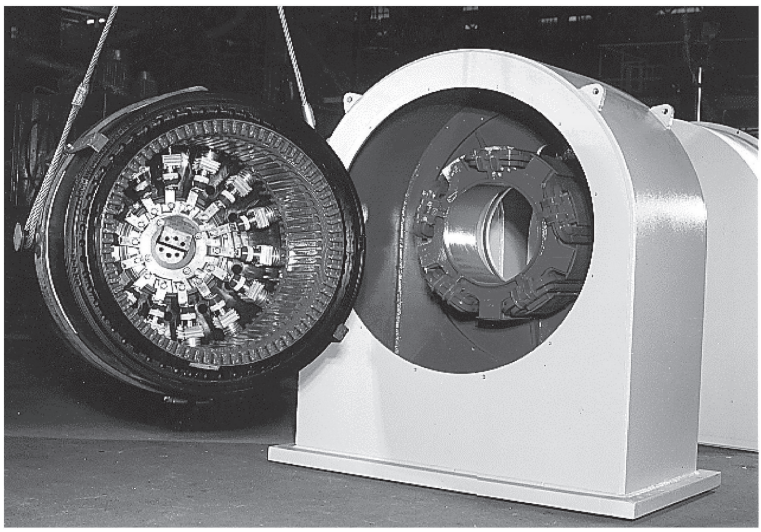
8.39 The active part of the Alstom air-cooled generator is built on a base frame, which is fully covered by an enclosure.

8.3.3 Further international developments

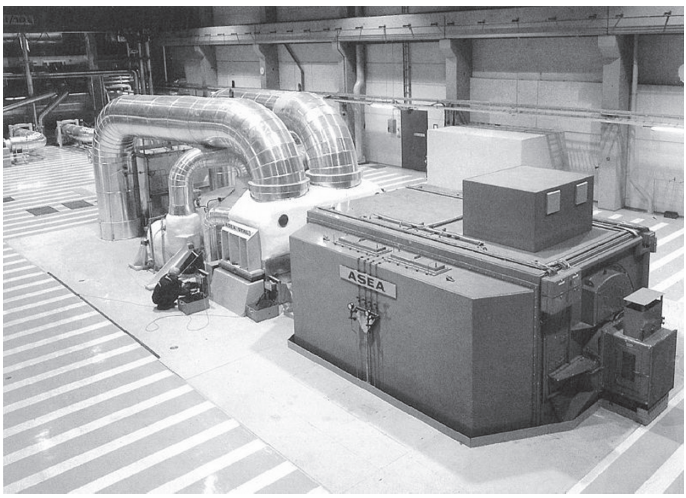
Design solutions of other manufacturers will be briefly described with examples to show independently developed unique designs, to complete the historical overview.

The US package approach for generators to gas turbines is demonstrated by two solutions of General Electric. Based on the 60 Hz market and the inherently lower efficiency, GE was limiting air-cooled developments to

Published by Woodhead Publishing Limited, 2013



8.40 The compact overhung exciter in an Alstom air-cooled generator.

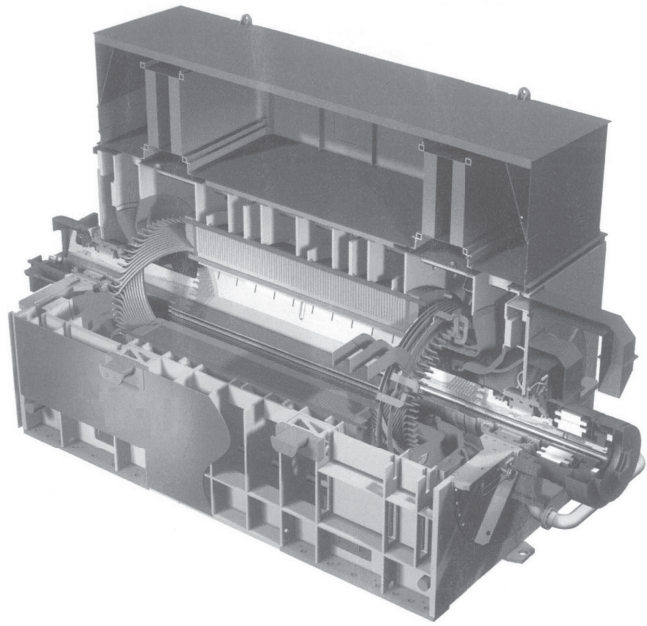


8.41 The ABB air-cooled generator.

some 200 MVA and has developed hydrogen-cooled generator solutions for applications in the range up to 500 MVA.

The air-cooled 9A4 generator (Fig. 8.42) represents a robust and modular package solution, developed for the gas turbine model 9E. It has found widespread use for the 60 Hz as well as the 50 Hz market in the range of 140–200 MVA. The characteristic robust rectangular-shaped structured

Published by Woodhead Publishing Limited, 2013

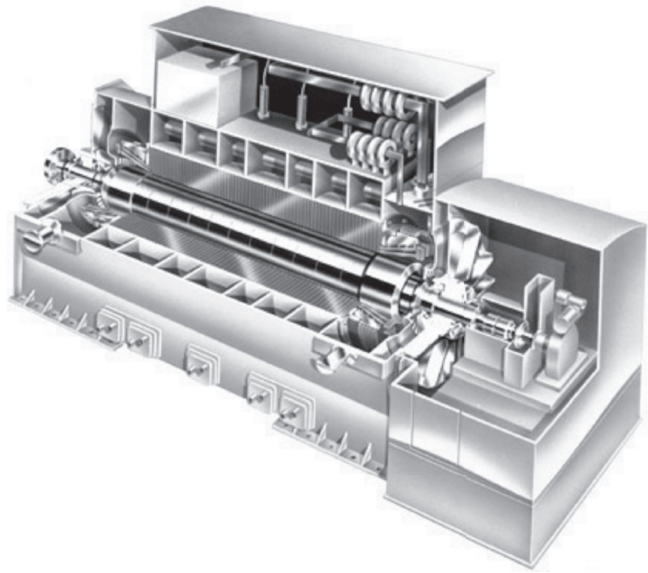


8.42 The air-cooled 9A4 generator, developed by General Electric (*Source*: GE).

housing with end-shield bearings for the rotor has a resemblance to large motor designs. This allows easy handling during transportation and weather-proof outdoor installation on site. The default rotating exciter is flanged to the end-shield. Cooling is possible in TEWAC and OV in a couple of developed variants. The type has been subcontracted for further development to match other OEM turbines. Similar designs from other manufacturers corroborate the advantages.

GE's hydrogen-cooled 7FH2 generator demonstrates a package solution with a very high integration of auxiliaries. The application is for the model 7F gas turbines in the range 190–270 MVA, and was extended to 50 Hz applications. The rated hydrogen pressure is adapted over a range to the generator rating, while the basic dimensions are kept fixed. The design is characterized by a closed frame with end-shield bearing and hydrogen–water coolers arranged in the bottom part (Fig. 8.43). An integrated collector compartment contains the brush-gear, hydrogen auxiliaries and turning gear. The generator is transported with built-in rotor and, if transportation allows, with attached collector compartment. This makes the generator a simple handling package (Fig. 8.44). The use of grain-oriented electrical steel in the stator core reduces the core diameter and, despite a heavier housing, makes the weight comparable with air-cooled units.

Published by Woodhead Publishing Limited, 2013

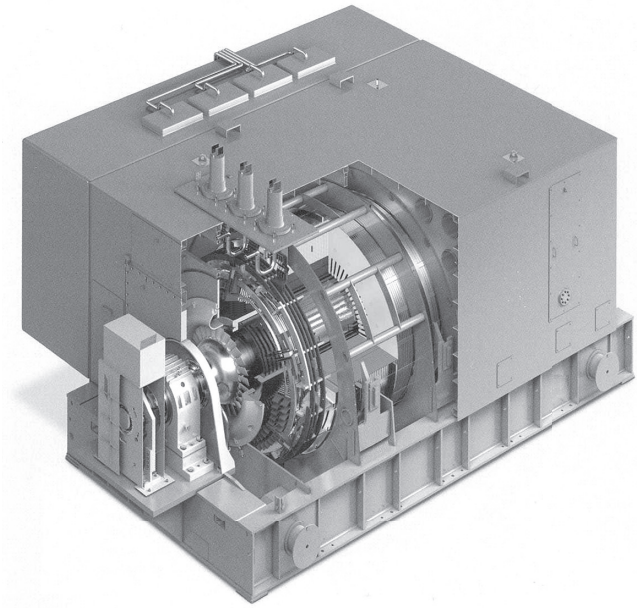


8.43 The closed frame design of General Electric's 7FH2 generator, with end-shield bearing and hydrogen–water coolers arranged at the bottom (*Source*: GE).



8.44 The 7FH2 generator is transported with a built-in rotor and, if the method of transport allows, with the collector compartment attached (*Source*: GE).

Published by Woodhead Publishing Limited, 2013



8.45 In the German Siemens type SGen-100A-2P (TLRI), the stator is suspended on a frame base, as well as the pedestal bearings of the rotor (*Source*: Siemens).

The German approach for air-cooled turbogenerators is the Siemens type SGen-100A-2P (TLRI). The wide range from industrial application to power generation application is between 25 and 250 MVA, 50 and 60 Hz. The stator is suspended on a base frame, as well as the pedestal bearings of the rotor (Fig. 8.45). The housing serves for protection, noise attenuation, and cooling air circulation. For gas turbine application, the coolers are flanged to the side wall in the vertical position. This allows the arrangement of the generator terminals on top. Steam turbine versions do exist with coolers either on top or in a foundation recess. Excitation is brushless as the default solution. As the standard solution for that range of power, the complete stator is pre-manufactured using the Global VPI system. The design shows similarities to the French design. Many similar design versions are used over the world.

8.4 Design concepts of turbogenerators for modern gas turbines

New generator types for gas turbine applications are commonly introduced together with the new turbine of the same manufacturer. Meanwhile, as

Published by Woodhead Publishing Limited, 2013

generators for GT applications have become a commodity, the generator types and series can be combined with gas turbines from other manufacturers. The preferences are commonly set out in the customer's plant specifications. Generator manufacturers are thus driven to make their products attractive for the whole market. The following gives a rough overview of the scope.

Basic generator features are speed/frequency, cooling system and excitation. The generator speed is determined by the number of magnetic poles (a basic generator design feature) and the grid frequency of 50 or 60 Hz. Two-pole generators run at 3000/3600 rpm and are the general choice for gas turbines and steam turbines in the power range 40 to > 400 MW (Baumgartner, 2001).

Hydrogen cooling is applied above 200–300 MW. Besides the physical limits of air cooling the generator, efficiency plays an important role. Hydrogen combines high cooling capacity with low gas friction loss. The frequency of 60 Hz favors hydrogen cooling because of the inherent higher friction and ventilation losses of air. On larger generators (above 400–500 MW), for example, for steam tails of combined-cycle plants, hydrogen-cooled generators are equipped with water-cooled stator windings.

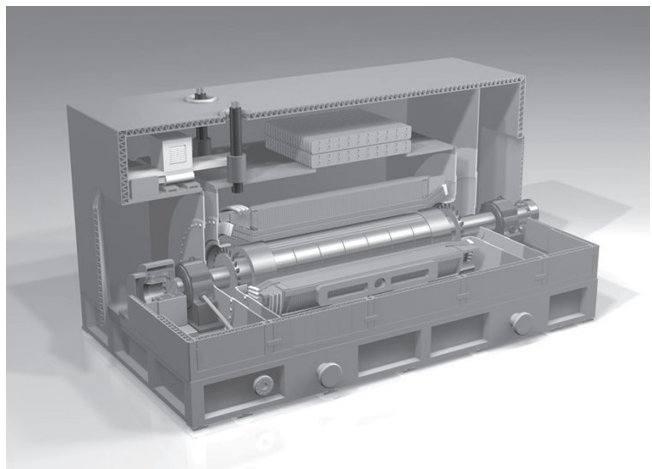
Depending on design constraints and grid requirements, generators are equipped either with static excitation or rotating (brushless) excitation. Design rules vary between manufacturers, and both systems can be found at all ratings. Static excitation results in faster response (grid stability) while rotating excitation has minimum maintenance requirements.

8.4.1 Turbogenerator layout

In this chapter we distinguish between small and large air-cooled, hydrogen-cooled and hydrogen/water-cooled generator types as used today. Advances in the latest history are described in more detail elsewhere (Joho, 2002).

Small air-cooled units (Fig. 8.46) have a rectangular base frame on which generator stator, pedestal bearings, and exciter stator are mounted. The base frame transfers all mechanical forces from bearings and stators to the foundation. The base frame supports a box-shaped cover (acoustic enclosure), which serves for internal air flow, noise protection and, when requested, weather protection. The top of the enclosure is prepared for both open ventilation (air filters) and totally enclosed air-circuit with air–water heat exchangers (TEWAC). All essential components are inside the enclosure. This applies for the bearings, the exciter, wiring, and piping. Further components may be integrated inside the enclosure, including a gearbox to the turbine, and medium voltage equipment such as voltage and current transformers, neutral point circuitry, and overvoltage protection. The only external component is the generator excitation control module (AVR). These generators are widely used on various OEM industrial steam turbine plants as well.

Published by Woodhead Publishing Limited, 2013



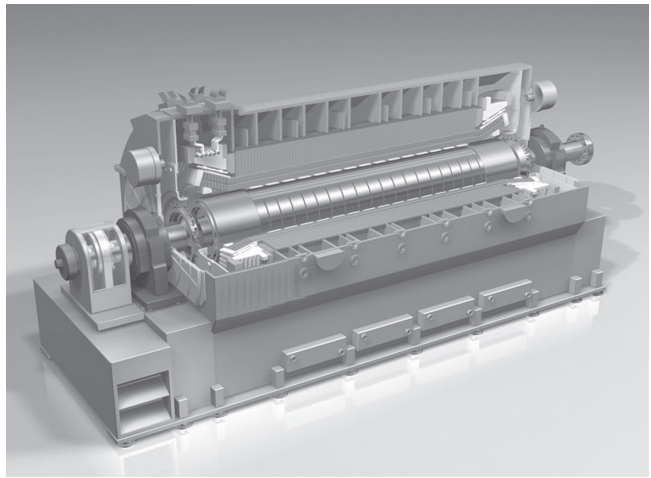
8.46 Small air-cooled units.

Large air-cooled units (Fig. 8.47) consist of a two-part housing: housing frame and housing cover. The housing frame carries the heat exchangers, the inner stator and, on integral housing extensions, the bearing pedestals and the brush-gear or rotating exciter. To keep the railway profile, the housing cover and bushings are installed on site. The normal cooling is TEWAC, with the heat exchangers located at the bottom of the housing frame. An additional outer enclosure can be provided for noise protection. The main interfaces to the plant surroundings are the stator winding terminals mounted on top of the housing, the individual bearing-oil supplies, and the excitation current leads of the brush-gear (see Fig. 8.5). The external components are the AVR and the static excitation cubicles, where applicable. Current and potential transformers are also mounted outside the generator.

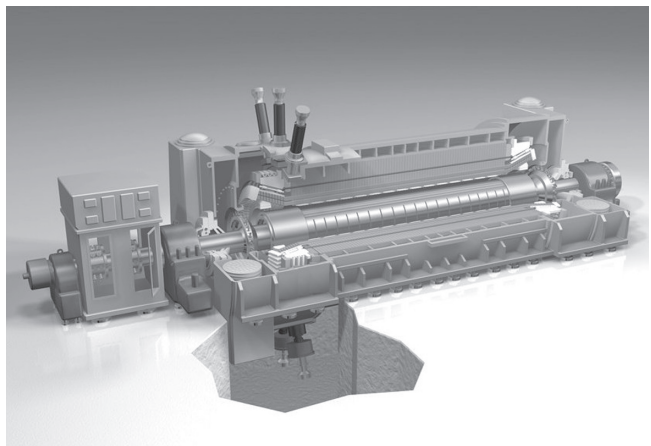
Hydrogen and hydrogen/water-cooled turbogenerators (except four-pole) are all equipped with bearing pedestals supported on the foundation. Transport is by components, the main components being the stator central housing and rotor.

Hydrogen-cooled units (Fig. 8.48) consist of a central housing part, two end covers (which support the gas/water heat exchangers) and pedestal bearings. Since the housing contains the hydrogen, it is of heavy design and contributes significantly to the overall weight of the generator. The openings for the shaft in the end covers are fitted with hydrogen-tight oil seals located inboard of the generator bearings. The generator is designed for table mounting and needs a recess in the foundations to clear its lower half. Flanges on each side of the central housing transmit the static and dynamic forces to the table.

Published by Woodhead Publishing Limited, 2013



8.47 Large air-cooled units.

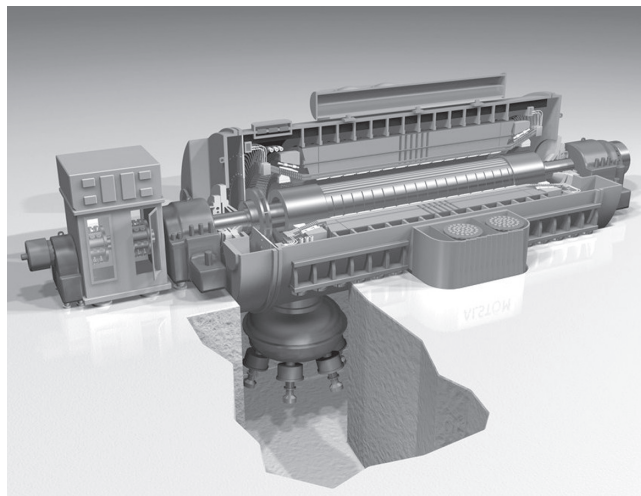


8.48 Hydrogen-cooled units.

Three generator terminals are mounted three on top, and three below, allowing flexibility for the bus-duct arrangement. A brush-gear cubicle is arranged separately on the foundation, which connects to an external static excitation unit.

Hydrogen-cooled generators require an additional **auxiliary unit** to control the air and the CO_2 used for purging. Furthermore, an external source of hydrogen is needed, usually a battery of bottled gas in a safe area. A second auxiliary unit is fitted to circulate seal oil and control pressure differentials in the shaft seals. This unit continuously degasses the oil recirculating from the shaft-seals.

Published by Woodhead Publishing Limited, 2013



8.49 Hydrogen/water-cooled units.

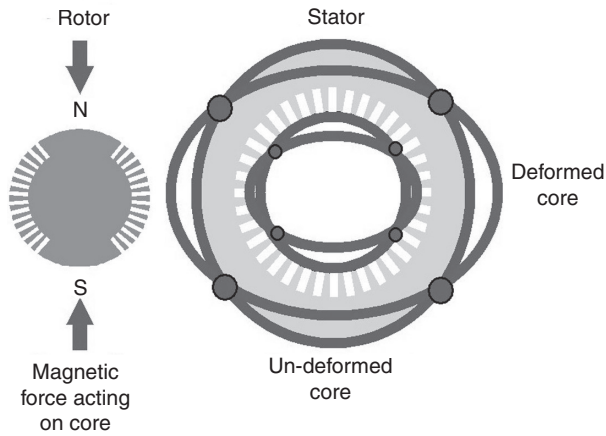
Hydrogen/water-cooled units (Fig. 8.49) differ from hydrogen-cooled designs by having central housing extensions for the heat exchangers. In addition, a **deionized-water** auxiliary is needed for the supply of cooling water to the stator winding and bushings. The generator terminals are arranged in a bottom housing extension.

8.4.2 Component design

Stator

The inner stator consists of a cylindrical magnetic core with the stator winding embedded in the slots in the inner surface of the core (Figs 8.9 and 8.10). The **stator core** consists of stacked silicon–steel laminations. The laminations are typically 0.5 mm thick and chosen to balance magnetic properties, core loss and mechanical properties. The laminations are overlapped, like bricks in a wall, and clamped in the axial direction by key bars at the core back and, in some designs, by tie bolts through the core. This forms a rigid cylindrical structure to resist the rotating **2f-Ovalization** forces (Fig. 8.50) produced by the magnetic fields in the air gap. The stator core connects to the bedplate or housing via a spring support system to attenuate vibrations transmitted to the foundation. Press-plates are fitted at the ends of the core to transmit axial pressure from the key bars and tie bolts, and to protect the end laminations from axial magnetic fields that induce eddy currents in the core ends. There are various designs of the press-plate and core end screen including steel plates with a copper screen, aluminum plates or conical rings of bonded lamination material.

Published by Woodhead Publishing Limited, 2013



8.50 The stacked silicon–steel laminations in the stator core form a rigid cylindrical structure able to resist the 2f-ovalization forces produced by magnetic fields in the air gap.

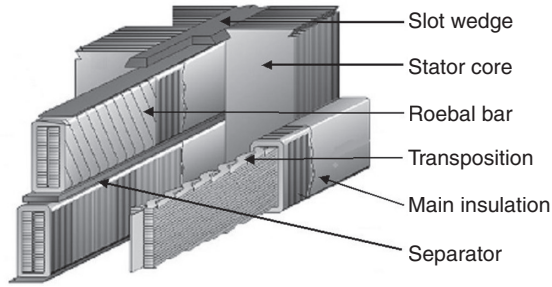
The **stator winding system** (Fig. 8.51) consists of a two-layer arrangement of Roebel bars (Chapter 2) located in the slots. The bars are series-connected upper bar to lower bar, to form coils. For two-pole windings, connection is made between nearly opposite slots. Thus, the array of all connections forms a cone-shaped end winding. The line and neutral ends of the three phases of the stator winding are connected to the generator terminals by the phase ring connections. Usually, rated generator voltage is defined phase-to-phase and, depending on size, is in the range of 10–27 kV. Terminal currents are in the range of 2–30 kA.

To support the bars against magnetic forces, the slot is closed by fibreglass wedges. The tightness of these wedges is maintained either by fibre-reinforced ripple springs between top bar and wedge, or by a double-tapered wedge, which inherently acts as a spring.

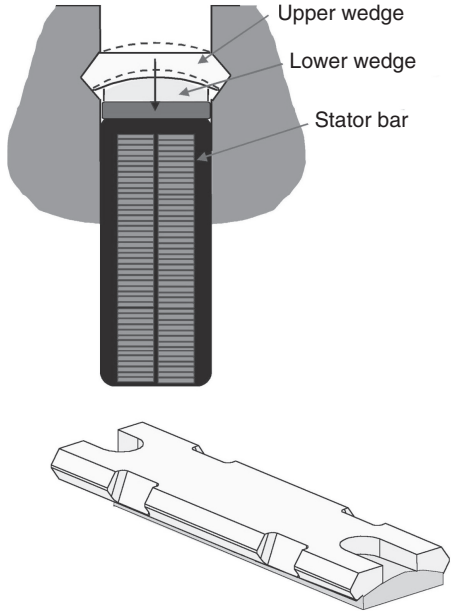
The stator concave/convex wedging system (Fig. 8.52) provides a sustained pressure on the stator bars and can compensate for the initial settling and thermal expansion of the bars during operation. This wedging system has demonstrated excellent performance and its testing can be performed with a robot, without rotor removal. The wedging system can be simply retightened by adjusting the position of the lower wedge, avoiding in many cases a re-wedging.

Like the other sections of the bar, the **stator end winding** (Fig. 8.53) is subject to double-frequency magnetic forces. To keep the vibrations within acceptable levels, and to prevent deformation under short-circuit conditions, the bars are fixed to an end-winding support structure. For **indirect-cooled windings** the support must allow enough space for coolant flow around the

Published by Woodhead Publishing Limited, 2013



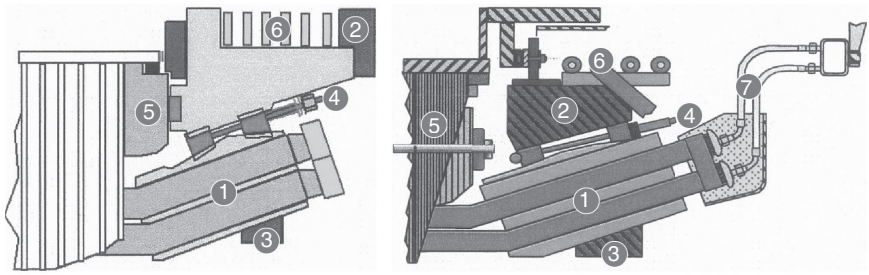
8.51 The stator winding system.



8.52 The stator concave/convex wedging system.

bars. In general, this is done by taping the bars in the cone to triangular brackets, which are in turn suspended by a system of concentric rings. A well-designed support structure allows for axial expansion of the bars whilst keeping the end winding stiff in the radial and tangential directions. In larger air-cooled machines and hydrogen-cooled machines, the cone inner surface is additionally supported by an inner ring. For larger generators with **water-cooled (direct-cooled)** windings, the bracket support structure may be replaced by a massive cone-shaped fibreglass ring. Usually, the phase ring connections are also supported by the end-winding support.

Published by Woodhead Publishing Limited, 2013



8.53 The stator end winding for an air-cooled (left) and a hydrogen-cooled generator (right). (1) Stator bars, (2) outer support ring, (3) inner support ring, (4) retightening, (5) press-plate, (6) phase ring connectors, (7) water-cooling circuit.

The stator winding insulation materials are specified to allow conductor temperatures up to at least 155°C, according to class 155 (former class F) of the electric machine standards. According to long standing practice, rated thermal utilization is well below 130°C, according to class 130 (former class B).

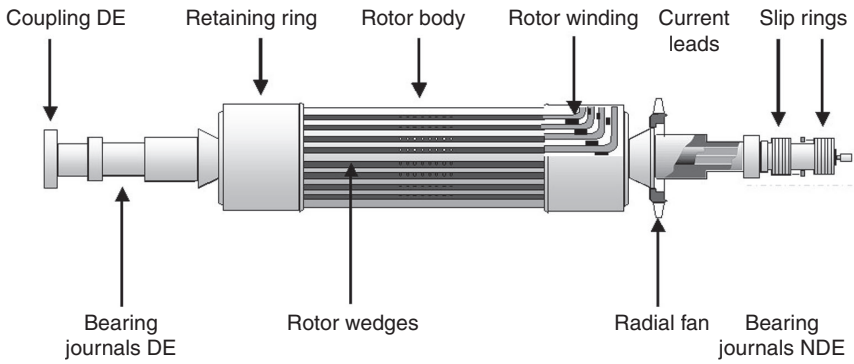
Rotor

The main components of the rotor of a turbogenerator are: a cylindrical-shaped steel forging (rotor body), the rotor winding contained in slots in the rotor body, the retaining rings (end bells) to support the winding heads, and one or two fans for coolant drive (Fig. 8.54).

The **rotor body** consists of a steel forging with shaft extensions on both ends. The driven end (DE) is fitted with a coupling to the turbine; the non-driven end (NDE) carries the slip rings or the rotating exciter. On two-pole units, the center part of the rotor is divided circumferentially into two-pole zones with winding zones in between. The winding zones are provided with axial slots which contain the rotor winding. The pole zones usually have transversal slots (inertia slits) to equalize the stiffness in bending on the pole and quadrature-axis. On four-pole rotors the circumference is divided into four-pole zones with winding sections between.

The **rotor winding** consists of a stack of copper conductors (temperature resistant silver-alloyed copper) in each slot. The slot ends are connected together in series across the pole faces to form the rotor coils and winding. The conductors are insulated from the rotor body by the slot wall insulation, and the stacked conductors are separated by layers of an interturn insulation. The excitation current is supplied via copper semicircular conductors in the center of the shaft at NDE. Connection to the winding is made via radial studs through the shaft with flexible connectors to the ends of the winding. Depending on unit size, the rated field current is in the range of 1000–6000 A, and the rated field voltage is in the range of 200–750 V.

Published by Woodhead Publishing Limited, 2013



8.54 The main components of the rotor from a turbogenerator.

The slots are closed by metallic wedges, usually of non-magnetic steel or a high-strength copper-nickel alloy or aluminum. The latter two normally consist of single-piece wedges running the full length of the rotor. The rotor is fitted with a damper winding to limit rotor heating under system fault conditions and to dampen rotor angle oscillations. This can be achieved by single conductors located beneath the slot wedges closed by a circumferential copper coronet at the slot ends, or formed by connecting full-length slot wedges to a copper coronet or to the retaining ring at the slot ends.

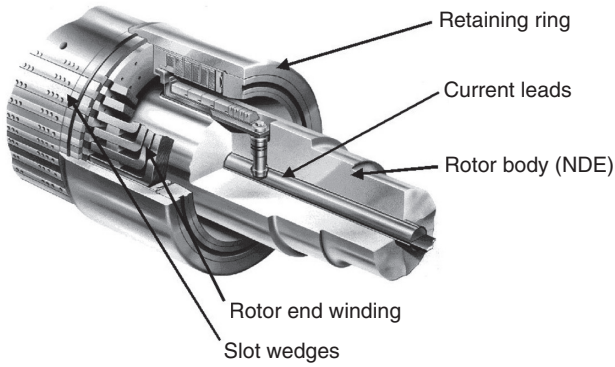
The winding conductors are usually provided with ducts or openings for cooling gas flow. Depending on design the slots are equipped with sub-slots between the copper and slot bottom to feed cooling gas into the conductors. The cooling gas escapes through an array of openings in the wedges. Additional baffling is provided in the rotor end windings to direct gas into the conductors.

The rotor end windings (Fig. 8.55) are enclosed by a retaining ring, which is held in place by a shrink fit onto the rotor body. The retaining ring serves to hold the winding heads against the centrifugal forces. It is made of non-magnetic, cold-worked, austenitic steel (18Mn-18Cr). Older units may be operating with ring material that is susceptible to stress corrosion cracking and need special supervision.

Usually the rotor is equipped with a fan on one or both shaft ends to circulate the air or hydrogen cooling gas within the generator. Normally this is an axial fan. However, larger units may be equipped with radial fans or multi-stage axial blowers.

The modern rotor insulation materials are specified to allow conductor temperatures up to at least 155°C, according to class 155 (class F) of the electric machine standards. According to long standing practice, the rated operating temperatures are much lower, corresponding to Class 130 (class B).

Published by Woodhead Publishing Limited, 2013



8.55 The rotor end windings for small generators.

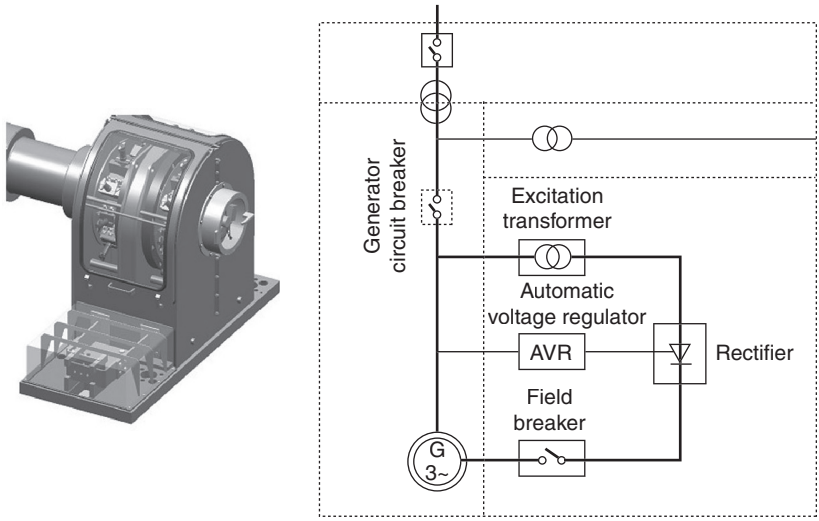
Exciter

Two excitation systems, static excitation (see Fig. 8.56) and rotating excitation (see Fig. 8.57), have grown in parallel. Their use depends on generator type and, for some generator types, on customer preference. Both system are discussed in futher detail below.

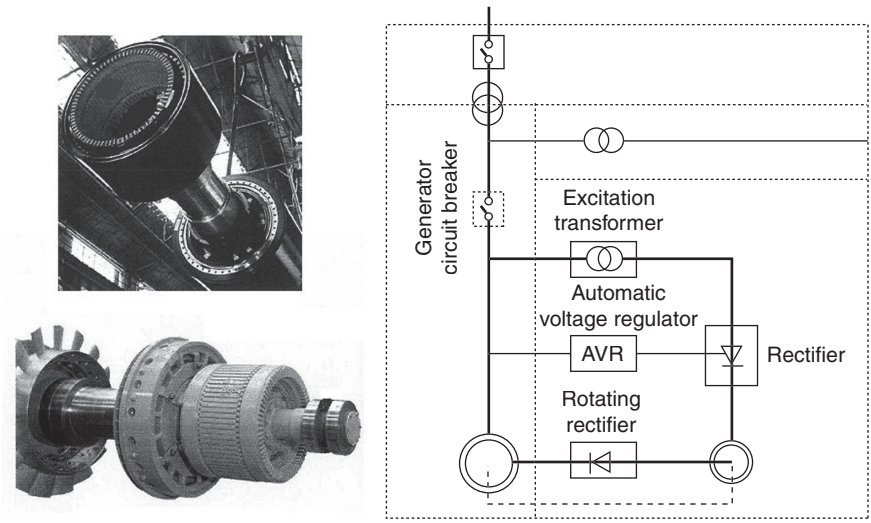
Static excitation

In general, the power for the generator excitation is tapped from the generator bus ducts and fed to an excitation transformer. The excitation transformer steps down the voltage to the level required by the AVR to maintain rated generator field voltage and specified voltage margin (ceiling factor). The output of the excitation transformer is connected to a thyristor-controlled rectifier which is located in the excitation cubicle. The DC output is fed by cables or bus bars to the generator **brush-gear**. In the brush-gear, an array of brushes contact two slip-rings located on a rotor shaft extension which carry the excitation current to the rotor winding. The slip-rings are normally of steel, but some older units may use bronze. The brushes are of natural graphite and are mounted in brush holders, which allow an exchange of worn brushes in operation. The normal lifetime of brushes is one year, but this may be considerably lower with non-optimal air conditions (humidity, salt, chemical pollution). Usually, a small fan provides air flow in the brush-gear. Large units have air-conditioned brush-gear with closed air circulation and built-in air–water heat exchangers. Depending on shaft dynamics a third bearing is needed behind the slip rings. The AVR that controls the rectifier is normally integrated in the rectifier cubicle. In operation the static excitation is characterized by its fast response under system fault conditions, but is also susceptible to low voltage at the generator terminals in system fault conditions.

Published by Woodhead Publishing Limited, 2013



8.56 Static excitation.



8.57 Rotating excitation.

Rotating excitation

The excitation power is produced by a rotating exciter machine, which is driven from the generator shaft end. The rotating winding of the exciter feeds into a rectifier equipped with silicon diodes. The rotating rectifier supplies the rotor winding of the generator. There are two basic designs of

rotating exciters: the conventional exciter, where a three-phase winding supplies a rectifier bridge with fused parallel diodes in the branches, and an overhung-bell exciter, where a multi-phase winding supplies a multi-phase bridge of individual diodes. The latter is generally without fuses, and is characterized by its short axial extension, which eliminates the need for a third bearing. In a conventional exciter the stator surrounds the exciter rotor, and in the overhung-bell design the stator is arranged inside the exciter rotor. The AVR supplies the field current to the exciter stator. Since the excitation power is generated mainly by the exciter, running as a small generator, the required control power from the AVR is quite low and can be provided by a small thyristor-controlled rectifier. Rotating exciters do not require maintenance during operation.

8.4.3 Cooling gas circuits

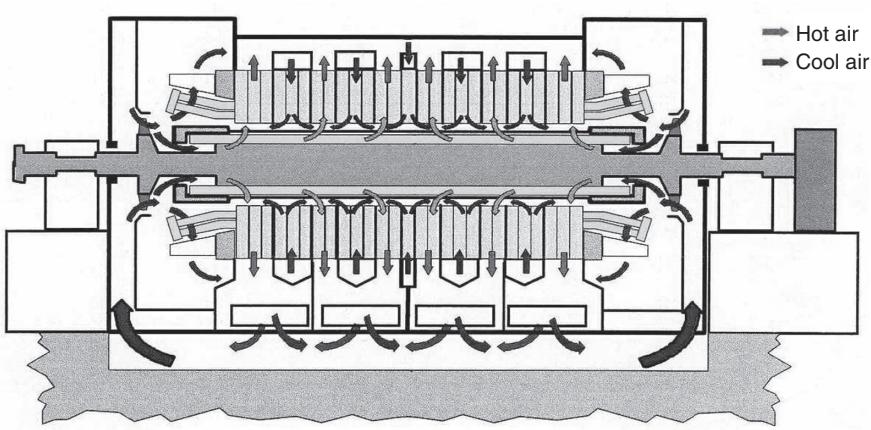
The cooling gas serves to remove the losses produced in the stator and rotor, and to maintain the conductor iron temperatures at acceptable levels.

In **small air-cooled generators**, the air is driven by axial fans located at the rotor shaft ends. The air flows through the rotor conductors (direct cooling) and radially out through the slot wedges into the air gap, where it mixes with cold air coming from the open ends of the air gap. This air mix enters the stator core through a multitude of radial cooling ducts. By means of this system, the air cools the stator core and thus removes the losses from stator core and winding. Losses from the stator winding conductors are all removed through the main insulation (indirect cooling). The hot air escapes through the core back. On open air ventilated units, ambient air is drawn into the fans through filters, and the hot air from the core back is exhausted through silencers. On closed air flow machines (TEWAC), the hot air from the core back is passed through air/water heat exchangers and the cooled air returns to the fan inlets.

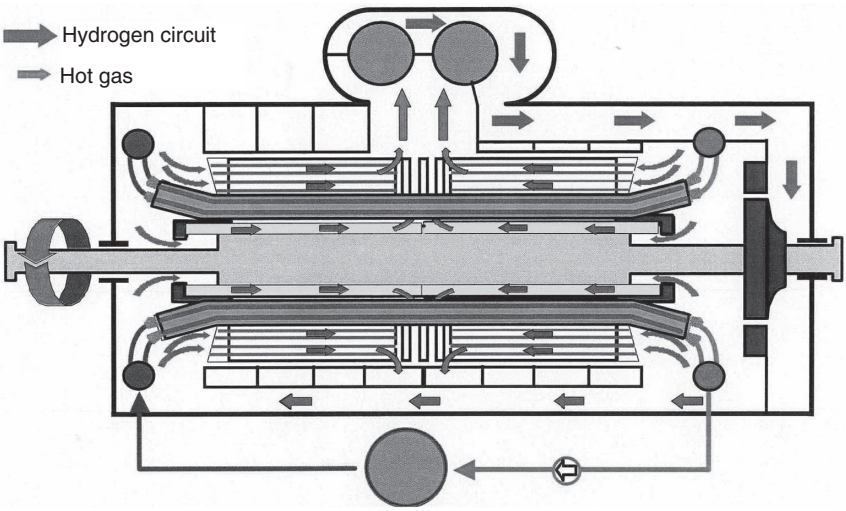
In **large air-cooled generators** the stator core is equipped with a series of cold and warm air chambers (Fig. 8.58). Fresh air is supplied into the air gap by centripetal flow in the cold air chambers. The warm air chambers expel the heated air at the core back, where it is fed by a series of ducts to the air–water heat exchangers. The system results in uniform stator winding temperatures and reduces the total air flow, thus increasing efficiency.

Hydrogen-cooled **generators** are similar in cooling to the largest air-cooled generators. The hydrogen is subject to a static overpressure in the range 4–6 bar, and thus combines highly efficient cooling with low windage loss.

Published by Woodhead Publishing Limited, 2013



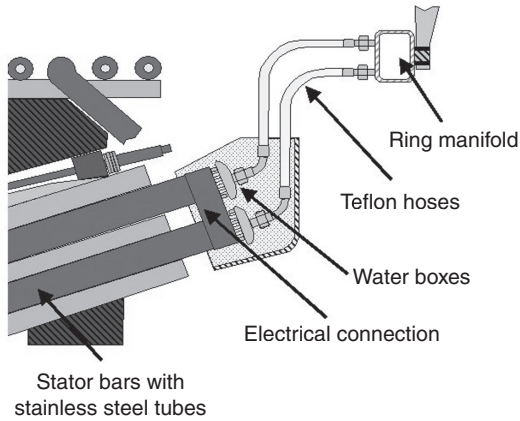
8.58 Cooling principle in large air-cooled generators where the stator core is equipped with a series of cold and warm air chambers.



8.59 Hydrogen/water-cooled turbogenerators have independent direct water cooling of the stator winding.

Hydrogen/water-cooled turbogenerators (Fig. 8.59) have independent direct water cooling of the stator winding. The ventilation of the rotor is similar to indirect-cooled machines. However, the ventilation of the stator core can vary. Some designs use radial cooling ducts, similar to indirect-cooled machines, while others employ axial cooling channels in the stator core, formed by special punching of the laminations.

Published by Woodhead Publishing Limited, 2013



8.60 Large generators are equipped with water-cooled stator bars.

8.4.4 Water-cooled stator bars

Large generators are equipped with **water-cooled stator bars** (Fig. 8.60). Water cooling allows an increase in electric loading far beyond the values of indirect cooling. To achieve this water-flow, rectangular tubes of the same width as the strands are dispersed into the Roebel bar stacks. Most designs of generators use copper tubes. This requires rigid control of the cooling-water quality to avoid oxidation of the copper leading to blockage of the cooling tubes. In modern generators the tubes are made of stainless steel, which avoids the risk of copper corrosion. The ends of the stator bar connect to water boxes. On bars with conventional copper tubes, the strands and tubes of the stator bar are brazed together to form a combined electrical connection and the water box. This brazed connection is a weak point of design on many generators, since microscopic failures in the brazed joint can allow water to leak into the stator winding insulation. This problem is avoided on modern units by making the electrical connection of the copper strands between copper plates and the hydraulic connection of the stainless steel tubes in a separate, welded water box.

The water passes through all bars in parallel. This is achieved by a ring manifold at one end of the generator supplying water via electrically insulating Teflon hoses to each bar. The water is collected on the other end in a similar manner. Usually, sensors are fitted to measure the water outlet temperatures to help detect corrosion or blockage of the cooling tubes.

A separate auxiliary unit serves for circulation and cooling of the water, and for maintaining the water quality. Regeneration of the water is normally done in a ion-exchanger. The water quality is permanently monitored by sensing the electrical conductivity. The water pressure is kept below

Published by Woodhead Publishing Limited, 2013

hydrogen pressure, so that in case of leaks water does not break into the machine.

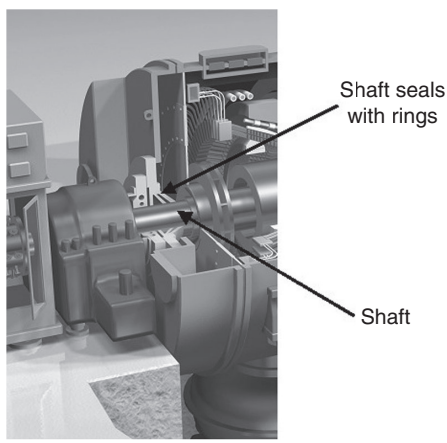
8.4.5 Hydrogen management and seal oil system

Hydrogen-cooled generators need rigid hydrogen management to maintain operational performance and safety. This is achieved by design of the generator itself, and by auxiliary equipment connected to the generator.

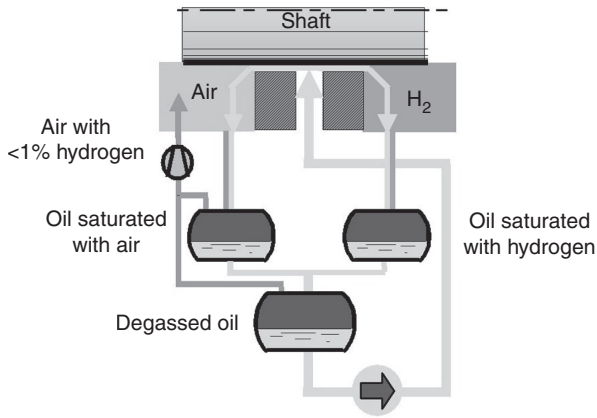
The generator housing is pressure tested and equipped with **shaft seals** (Fig. 8.61). A shaft seal consists of two rings that are assembled from segments. The rings are floating, and close around the shaft with a small clearance. The seal oil enters the gap between the rings and fills the clearance between ring and shaft. Since the oil pressure is kept slightly above hydrogen pressure, the seal oil flows through the clearance in the hydrogen-side ring and prevents hydrogen from escaping. The same, with more pressure drop and thus more flow, applies to the air-side ring. An array of baffling rings collects the oil flow.

This single-circuit seal is very common (Fig. 8.62). To combine the highest pressure with the lowest hydrogen leakage rate, more complex twin-circuit or triple-circuit seals are available.

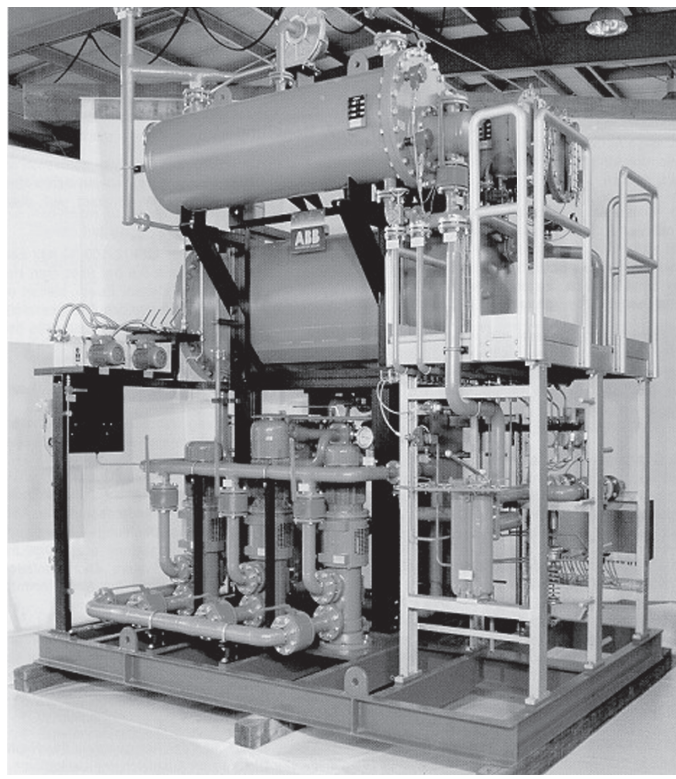
The drain oil flow from the seals passes to the **seal oil auxiliary** package unit (Fig. 8.63), which essentially is comprised of a pump and degassing tanks. The degassed seal oil (vacuum oil) is pumped back into the shaft seal. Since the reliable option of the seal oil system is a vital safety issue, its components are arranged with various levels of redundancy. The seal oil unit operates as long as hydrogen is in the generator, and it also operates when



8.61 The generator housing is pressure tested and equipped with shaft seals.

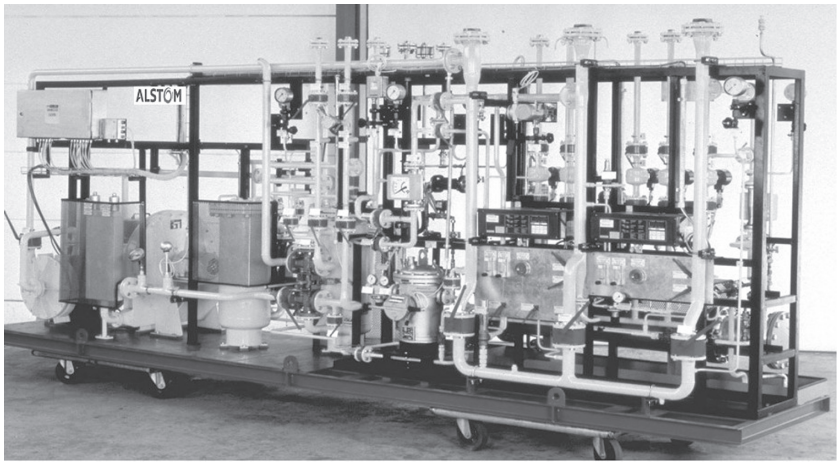


8.62 A common type of single-circuit seal.



8.63 The drain oil flow from the seals passes to the seal oil auxiliary unit, which is comprised of a pump and degassing tanks.

Published by Woodhead Publishing Limited, 2013



8.64 A gas unit is connected to the generator, for maintaining the hydrogen supply and hydrogen evacuation.

the generator is at a standstill. The seal oil unit is usually a few meters below generator level, and the drain seal oil returns in slightly inclined ducting to prevent production of foam.

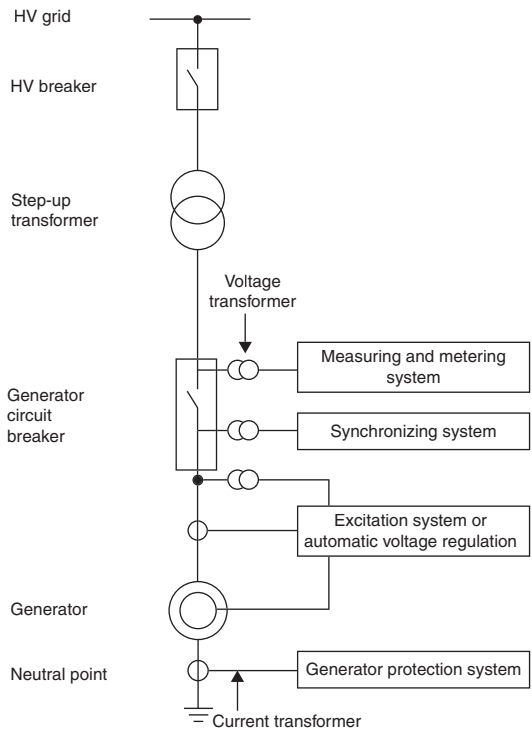
A **gas unit** is connected to the generator (Fig. 8.64). The gas unit serves for safe filling with hydrogen, for maintaining hydrogen supply, and for evacuation of the hydrogen. The gas unit is connected to a hydrogen supply, commonly consisting of a battery of gas bottles in a free area, and a purging medium supply, commonly an array of CO_2 bottles. Hydrogen filling of the generator is preceded by a purging of air by CO_2 and a following drive out of CO_2 by hydrogen. Evacuation of hydrogen is done in the reverse fashion. This avoids any explosive mixture of gases. Hydrogen pressure, purity and consumption (leakage) are continuously monitored when the generator is operational. An alternative for CO_2 purging is to use nitrogen or argon instead (European patent No. 923803, allocation year 1996).

8.4.6 Automatic voltage regulator and electrical generator protection

The **electrical output** of the generator is continuously monitored by current and voltage (potential) transformers connected to the generator terminals. The measured current and voltage signals are used for control and protection purposes (Fig. 8.65). Small generators have this equipment integrated within the casing, while larger units have the equipment outside the generator.

Some of the current and voltage transformers are used to determine the **generator active power** output. This value is passed to the turbine control

Published by Woodhead Publishing Limited, 2013



8.65 The electrical output of the generator is continuously monitored by current and voltage potential transformers connected to the generator terminals, for control and protection purposes.

and compared with a set-point value. The difference signal is used to control the turbine valves and hence output power.

The measured voltages are also passed to the AVR. Usually, the signal is compared with a set-point value for the voltage and deviations act on the generator excitation equipment (constant voltage regime). Other practices are to compensate further with an additional current signal to determine the **actual reactive power** and to work on constant reactive power delivery. The AVR control part is often integrated in the static excitation cubicle where it acts on the gates of a silicon-controlled rectifier (six-pulse thyristor bridge) to control the DC current supplied to the generator rotor winding. For rotating excitation the AVR acts on a small silicon-controlled rectifier, which supplies the DC current to the exciter field winding, which in turn controls the generator rotor current.

Modern AVRs are prepared to be equipped with an optional **power system stabilizer (PSS)**. The PSS senses low-frequency oscillations in the electric power and counteracts by modulating the gating of the thyristor bridge.

Some current transformers are used for protection purposes. Currents are compared at each end of the winding (differential protection), between phases (phase imbalance) and summed over phases (earth leakage current). These signals can indicate different types of electrical faults in the stator winding.

8.5 Turbogenerator development for gas turbines

How is the best fitting generator specified to a given gas turbine? In very simple terms the power delivered from the turbine reduces to

$$P = M\,\omega = \text{torque} \times \text{angular frequency} \qquad [8.38]$$

This is the mechanical power driving the generator at the coupling. The mechanical energy is converted into electrical energy, resulting in a power delivered to the grid of

$$P = U\ I\sqrt{3}\ \cos\varphi \qquad [8.39]$$

According to Equation [8.29] this is equivalent to

$$P = \text{const}\ A\ B\ d^2\ l\ \omega \cos\varphi = f\,(d^2\ l) \qquad [8.40]$$

which relates the torque of the turbine to the important design parameters of the generator

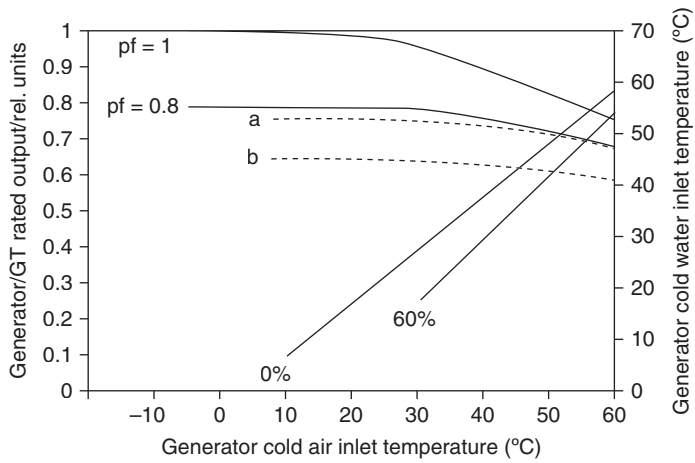
$$M = \text{const}\ A\ B\ d^2\ l \cos\varphi \qquad [8.41]$$

This represents the utilized effective electrical reactive torque of the generator. As shown above, the generated electrical power is a function of the volume and the cooling:

$$P = f\,(d^2\ l\ A) = f\,(\text{volume, cooling}) \qquad [8.42]$$

A larger power requires a larger volume. Because the size of a generator determines its costs and possibility of transport, alternative cooling technologies are applied utilizing the better heat capacity of hydrogen gas compared to air as a cooling medium. With further increasing output even generators pressurized to several bar need to find ways to overcome the size limitation. For that purpose, additional water cooling of the stator bars is introduced. As a consequence, air-cooled generators are used for all lower rating GTs, hydrogen-cooled generators for medium and large-size gas turbines, and hydrogen/water-cooled generators are delivered for very large GTs.

Published by Woodhead Publishing Limited, 2013



8.66 A typical example of a capability chart.

How can the generator be engineered in such a way that the electrical power is best fitted to a given turbine output? In the plant, the generator and the turbine operate at specific local boundary conditions. Apart from the altitude above sea level, the cold air inlet temperature impacts strongly on the performance of the coupled turbine-generator system. A typical example of a capability chart is shown in Fig. 8.66.

The local ambient air temperature that determines the gas turbine performance has to be related to the turbogenerator cold-water inlet temperature of the coolers and the corresponding cold gas inlet temperature. The generator has to be able to deliver the corresponding power output, which means that the characteristic curve of the generator for a certain power factor pf in Fig. 8.66 has to be above all turbine values. Depending on the minimum local temperatures, different percentages of glycol are usually used in the coolant water. In that way, the operating regimes of a generator can be optimized.

Development has to consider all trends of power augmentation or other retrofit possibilities of the future as indicated by two turbine performance curves a and b. Further main targets are given by costs and size requirements. Apart from that, various other aspects have also to be considered. Typical considerations cover, among others, the following items:

- Plant types and operation conditions:
  - single-shaft or multi-shaft combined-cycle train arrangement
  - power-augmentation performance
  - outdoor or semi-indoor generator enclosure
  - base-load and peaking operation capability (load profiles)
  - ambient temperature operating ranges
  - environmental operating conditions, for example, seismic zones.

- Cooling water specification/requirements:
  - air-cooled cooling water
  - direct cooling (river/sea water)
  - cooling tower.
- Transportation requirements.
- Generator noise emissions (sound pressure level/power in dBA).
- Generator component lifetime and RAM (Reliability, Availability, Maintainability).
  - number of guaranteed start/stop cycles, cold starts of the GT
  - RAM and lifetime guarantees.
- Maintenance types and inspection intervals.
- Start-up of GT requirements.
  - During start-up, the synchronous generator operates as a synchronous motor, the generator circuit breaker is open and the starting disconnect switch is closed, and start-up power is taken from the HV grid via the start-up transformer. The input voltage is first rectified and then transformed into a three-phase voltage with variable frequency. The starting excitation system supplies DC current to the field windings of the generator rotor, producing the magnetic fields, which enables the generator to run as motor. At about 50% of rated speed the turbine contributes to the starting torque.
- Grid code compliance:
  - Over-speed and negative sequence current operation.
  - Frequency response.
  - Voltage–frequency operation ranges.
  - Island mode operation, load rejection, black start and restoration, etc.

8.5.1 Turbogenerator standards

As in all technical businesses, the world of generators is governed by international standards. The standards guarantee a clear and sustainable platform for specifications. They describe a minimum of performance – customer and manufacturer may agree on more stringent or additional specifications. The two worldwide institutions dominating the field are the International Electrotechnical Commission (IEC) and the Institution of Electrical and Electronics Engineers (IEEE). The table shows in summary the most important standards and does not claim full coverage. The basic standards are listed in topic "Design, markings, performance" (Table 8.4). Parts of these basic standards add to many of the other topics (not all shown). The list does not cover basic material specifications and

Published by Woodhead Publishing Limited, 2013

Table 8.4 Overview about standards

Topic	IEC (more likely in 50 Hz countries)	IEEE (more likely in 60 Hz countries)
Design, markings, performance	60034–1 Rotating el. machines 60034–3 Turbogenerators 60034–5 IP codes (encapsulation) 60034–6 IC codes (cooling) 60034–7 IM codes (mountings) 60034–8 Generator terminals	C50.13 Cylindrical rotor synchronous generators
Excitation systems	60034–16 Definitions, Models, Dynamic performance	421 Definitions, Dynamic performance, High pot tests, Excitation systems specifications
Testing	60034–2 Efficiency and losses 60034–29 Temperature rise by testing	115 Test procedures
Electrical modeling, parameters	60034–4 Defining electrical parameters, testing	1110 Modeling practices
Protection		37.102 Generator protection 37.101 Neutral grounding
Insulation systems	60034–18 Testing, many parts! 60034–27 PD measurements 62114 Thermal classification	434 Functional evaluation 1043 Voltage endurance testing 1310 Thermal cycle testing 43 Insulation resistance testing
Operation, maintenance	60034–23 Refurbishing	67 Guide for operation + maintenance 62.2 Diagnostic field testing

evaluations. For details the reader is referred to the official websites of the standards organizations.

8.5.2 Development methods and validation

To fulfill increased performance criteria from up-rated gas turbines, generator development activities make use of technological progress in all fields of science and technology. Based on the refinement of calculation tools and simulation possibilities, OEMs can nowadays use most complex tools such as three-dimensional (3-D) design, FE calculation in various dimensions connected to huge models, fast solvers for differential equations, computational fluid dynamics (CFD) simulation of flows, etc. Cooling circuits are

determined in detail by numerical flow calculation systems supported by CFD tools. Inserting the calculated values of cooling air distribution permits determination of the expected temperature. However, results are only as good as the model parameters. In the case of a stator cooling system with several cooling chambers and outlet zones for the rotor cooling air, and with Mach numbers (critical velocity ratios) up to 0.7, the air gap is a section of the cooling circuit that is difficult to model. Fundamental innovations have been developed over time and introduced into the development to reduce windage loss and to improve precalculation of coolant distribution, and also with respect to cooling of the generator active parts. A refined segmentation allows the generation of a quite homogeneous axial temperature distribution in the indirectly cooled stator winding, leading to an equalized thermal utilization of the insulation. The latter aspect is a basic condition to reach today 400 MVA by air cooling. The losses of the entire system are removed by typically four or six water/air coolers (TEWAC).

The reverse cooling concept has the fans arranged upstream of the coolers. This eliminates a 10 K-preheating of the cold air by the fans. As for the standard design, there are two symmetric, closed-loop cooling circuits, each responsible for one half of the machine.

The more experienced an OEM supplier is, the more input he can use to adapt boundary conditions to real operational conditions. Experience feedback from the fleet of installed generators is used in cooperation with customers. Major OEMs continuously develop large in-house computer programs utilizing most modern IT and numerical progress. For those effects that are still not predictable, usually laboratory tests are performed. Examples are, for example, lifetime tests or new material evaluations.

Finally, the running test is conducted as a type test that proves the correctness and reliability of the design.

Below are data taken from the latest running tests of a large air-cooled and a hydrogen-cooled generator.

The air-cooled generator for an up-rated GT achieves the following machine data:

Rated output	S_N	400 MVA
Frequency	f	50 Hz
Rated power factor	pf	0.8
Rated voltage	U_N	21 kV
Rated current	I_N	10.997 kA

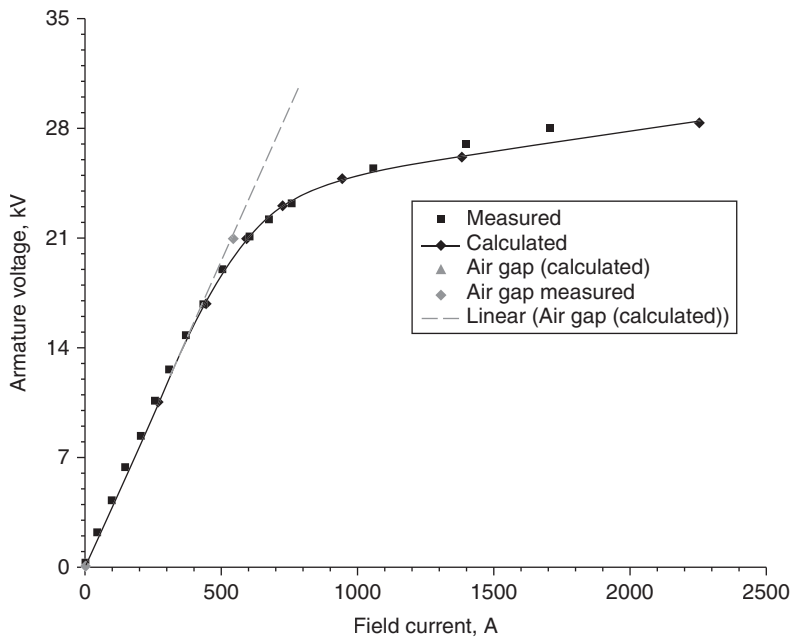
The test resulted in the values given in Table 8.5.

Also shown is the measured armature voltage as a function of the field current (Fig. 8.67).

Published by Woodhead Publishing Limited, 2013

Table 8.5 Running test results of a 400 MVA air-cooled generator for gas turbine application

Parameter	Measured	Calculated	Difference (%)
If_0	610A	591A	3.3
SCR	0.533	0.516	3.3
xd	2132	2134	−0.0094
xd′	0.230	0.218	5.5
xd″	0.18	0.166	8.43
Total losses	3961 kW	3987 kW	−0.65



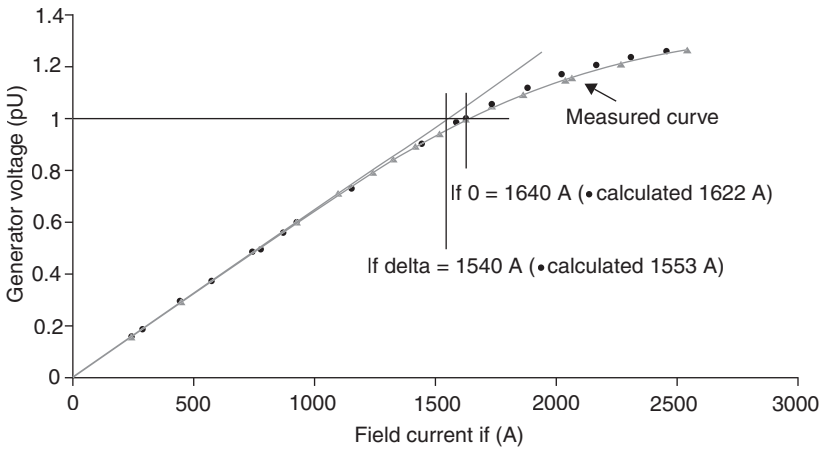
8.67 The measured armature voltage as a function of the field current.

For single-shaft combined-cycle operation, a hydrogen-cooled generator uprate was developed with the performance data:

Rated output	S_N	530 MVA
Frequency	f	50 Hz
Rated power factor	pf	0.8
Rated voltage	U_N	21 kV
Rated current	I_N	14 571 kA

Table 8.6 Running test results of a 530 MVA indirect hydrogen-cooled generator for gas turbine application

Parameter	Measured	Calculated	Difference (%)
If_0	1640A	1622A	1.1
SCR	0.509	0.507	0.3
xd	2.094	2.065	1.4
xd′	0.360	0.350	2.9
xd″	0.305	0.270	13
Total losses	4732 kW	4830 kW	–2.0



8.68 The measured generator voltage as a function of the field current.

The test resulted in the parameters shown in Table 8.6.

It is obvious to note that all the measurements match very well with predicted values and are conservative within the predicted values (Fig. 8.68).

8.6 Recent developments

Over the recent years, air-cooling and hydrogen-cooling technology have become available in the 500 MVA range. Depending on the specific application and considering the site conditions the one or the other technology may be of more advantage. For single-shaft combined-cycle applications the hydrogen-cooled generator has proved to be the preferred solution, while the air-cooled generator has advantages for a single gas turbine.

Published by Woodhead Publishing Limited, 2013

Table 8.7 Steps in the development of large air-cooled turbogenerators

Range MVA	Introduction year	Application
Up to 250	1984	Medium-size gas turbine, large-size 60 Hz gas turbine
Up to 300	1995	Large-size 50 Hz gas turbine, large-size single-shaft 60 Hz CC
Up to 400	1998	Combined-cycle steam turbine 50 Hz

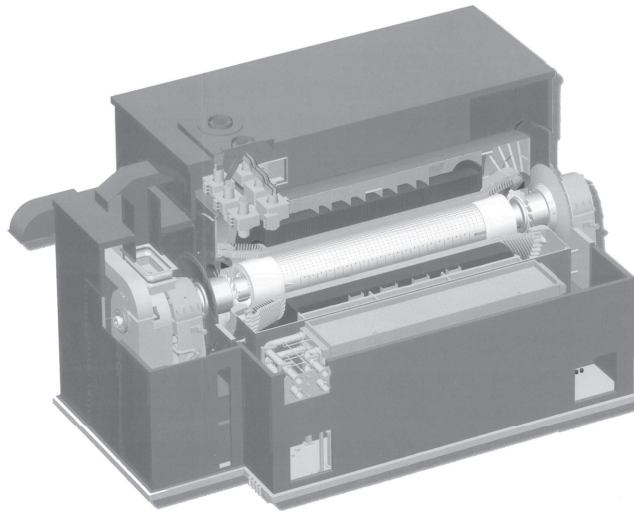
8.6.1 Achieving higher ratings with air-cooled turbo generators

The increase in unit ratings has clearly been driven by the evolution of gas turbines and combined-cycle units. Table 8.7 shows the achievements concerning increased unit ratings over time.

To understand the trends, the basic Equation [8.29] can be used. Concerning the magnetic induction, there has been no visible progress related to a significant improvement of magnetic material properties. Any attempt to increase the magnetic induction would drive the rotor and stator core into magnetic saturation, resulting in an excessive increase of excitation losses. On the other hand, the physical dimensions permit a limited increase in output. For example, if the active length and the rotor diameter were to be enlarged by 10%, that is, length-to-diameter ratio is maintained, then according to Equation [8.29] an approximate 33% increase of output would be possible, all other quantities remaining unchanged. Based on an output of, for example, 225 MVA (Stephan, 1995), an output of 300 MVA would thus be possible. However, there are limitations in size: rotor slenderness due to critical speeds, and core diameter due to housing size limitations due to transport restrictions. An approach to overcoming this limitation is a design with an inner stator frame as the transported unit and an outer housing for air circulation and enclosure, added on site (Fig. 8.69). The stator frame ends at the core outer diameter, however, it still contains the rotor, and the resulting package is smaller than for conventional solutions (www.siemens.com/energy, 2008).

By linearly increasing all dimensions, the slot volume also increases, permitting the accommodation of more copper. However, limits are imposed on a corresponding increase of linear current density, by the temperature rise. Increasing the dimensions, based on today's maximum rating machines, results in more magnetic flux and thus higher rated voltage, and consequently in thicker stator winding insulation that adversely affects the indirect cooling in the stator. The windage loss, which is a significant part of the total loss, increases with the rotor diameter to the power of four. Therefore, additional measures have to be taken to improve the cooling system in order to achieve the highest possible utilization. An approach to the largest

Published by Woodhead Publishing Limited, 2013



8.69 A design with an inner stator frame as one transport unit and an outer housing for air circulation (*Source*: Siemens).

air-cooled technology is the reverse cooling concept (Joho, 2000), in which the sequence of flow of cooler to fan is reversed. By this means the inevitable preheating of the cooling air when passing the shaft fan is neutralized in the following cooler. This measure is combined with a refinement in the modular multi-chamber stator cooling, and a multi-path axial cooling in the rotor winding, using sub-slots.

Air cooling has an overall customer benefit, when compared with hydrogen cooling, which is quantified for the 250 MW range in Table 8.8. Even when including an efficiency penalty of 0.1% (50 Hz) to 0.35% (60 Hz) with a rating of 1000 USD/kW (0.25–0.9 Mio USD) there remains a clear overall cost benefit for air-cooled technology (Joho, 2000).

In Europe the handling of hydrogen as the cooling medium is more and more subject to new safety regulations. This will incur extra costs for protective measures and the requirement for specially trained staff, which will further add to the advantages of air cooling.

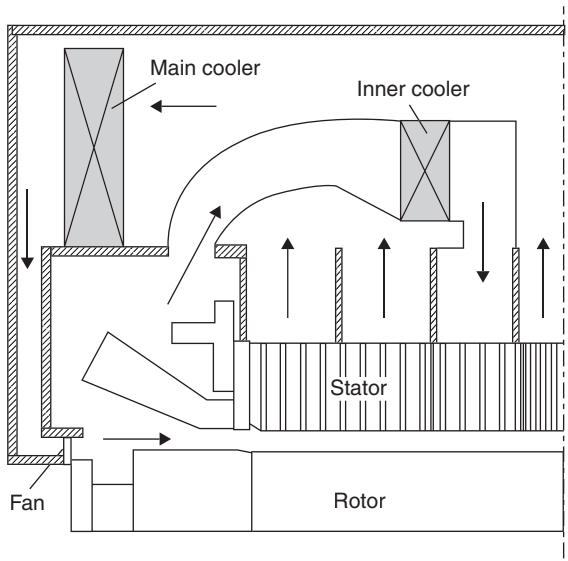
The situation is less favorable for 60 Hz applications in view of the larger difference in efficiency (Gellert, 1999). A considerable amount of losses are accountable to the shaft fans pressing air through the generator active part. A new approach (Hattori, 2006) introduces intercoolers in the cooling path (Fig. 8.70). By that concept, for the same cooling capacity the fan driving power for air circulation can be significantly lowered. Efficiencies in the same range as for hydrogen-cooled generators can be achieved.

Thanks to its simplicity and the general use of a closed air cooling (TEWAC), the air-cooled generator fleet shows excellent RAM values (EPRI Project RP-3577–02), as shown in Fig. 8.71 (Azad, 1999).

Published by Woodhead Publishing Limited, 2013

Table 8.8 Cost savings of an air-cooled generator in comparison with hydrogen-cooled generator

First costs	Running costs
No auxiliary units and less piping	No H_2/CO_2 bottles and supply system
Less space and simpler foundation	Less spares and less complex spares
Less interfaces to other systems	Less maintenance and supervision
Simpler layout, lower engineering	Better availability → better earnings
Quicker and simpler erection/ commissioning	Safer and simpler operation
⇓	⇓
Cost benefit ≈1 Mio US$ per unit	Cost benefit ≈ 0.5–2.5 Mio US$ per unit

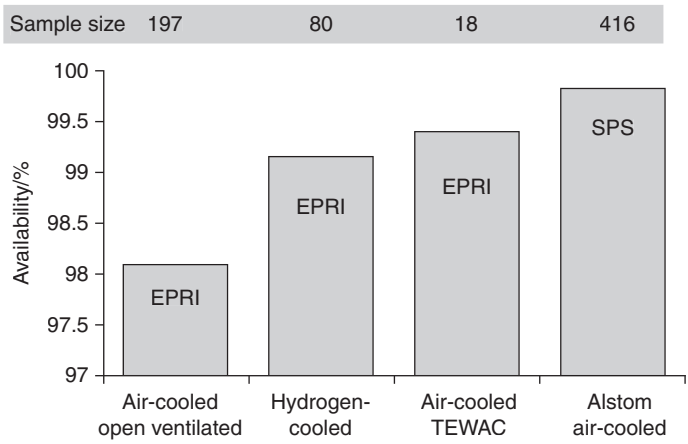


8.70 A new cooling approach that uses intercoolers to achieve the same cooling capacity for lower fan driving power (*Source*: Hitachi).

Due to all these commercial advantages and technology potentials, air-cooled generators will continue to supersede hydrogen-cooled generators for GT applications (Joho, 2001).

8.6.2 Achieving higher ratings with gas-cooled turbogenerators

Apart from optimization of cooling principles, an increase in linear current density can also be attained by improving the heat flow in the insulation of the indirectly cooled stator winding. That is because the better the contact



8.71 Thanks to its simplicity and the general use of a closed air cooling (TEWAC) the air-cooled generator fleet shows excellent RAM values.

between the conductor bundle and the slot walls is, the higher may be the conductor losses for the same permissible temperature rise, and hence the higher the linear current density. In hydrogen-cooled generators, with intrinsically excellent coolant, the stator bar insulation is the main thermal barrier. For gas-cooled generators improvements of thermal properties of insulation have been investigated in recent years. An effective means is the reduction of insulation thickness. The field strength at the edges of the bar insulation, which is the decisive factor for insulation thickness, is reduced, for example, by increasing the copper edge radius (Bock, 2002). Other means are new insulation systems that can hold higher electrical field strengths and thus allow lower insulation thickness or have better specific thermal conductivity by fillers thermally bridging the resin content. A preferred filler is boron nitride, which may be added as microscopic powder to the impregnation resin. A doubling in thermal conductivity is achieved. Such insulation systems have been developed and applied already, with the assistance of mica-tape suppliers (Kitajima, 2004).

8.7 Future trends

Since its introduction at the end of the 1950s, the synthetic resin mica-tape insulation is the established technology for stator winding insulations. Over the past years a worldwide re-evaluation has begun. On the far horizon, polymer insulations might replace the mica tape (Bock, 2002). However, when benchmarking with mica-tape insulation, the required tight quality control in manufacturing and the lower fault tolerance for inner electrical

discharges become obstacles. Therefore it seems that steps in today's proven insulation technology will be realized earlier. Such novelties close to introduction are:

- Improved further modified tapes with even higher thermal conductivity using fillers (see 6.2), and higher mica content, for example, by denser mica carriers. Such technologies are in the trial phase.
- Improving the insulation system to a higher thermal class (class 180). This technology is in the final verification stage (Bock, 2002).

As specified by standards, insulation verification tests are commonly based on stringent comparative tests of specific characteristics. Any modified insulation system, at the specified higher utilization, must be at least as good in all other characteristics as the established technology. These other characteristics are: sensitivity to manufacturing variances, production throughput time, environmental compliance, and supplier availability for the components.

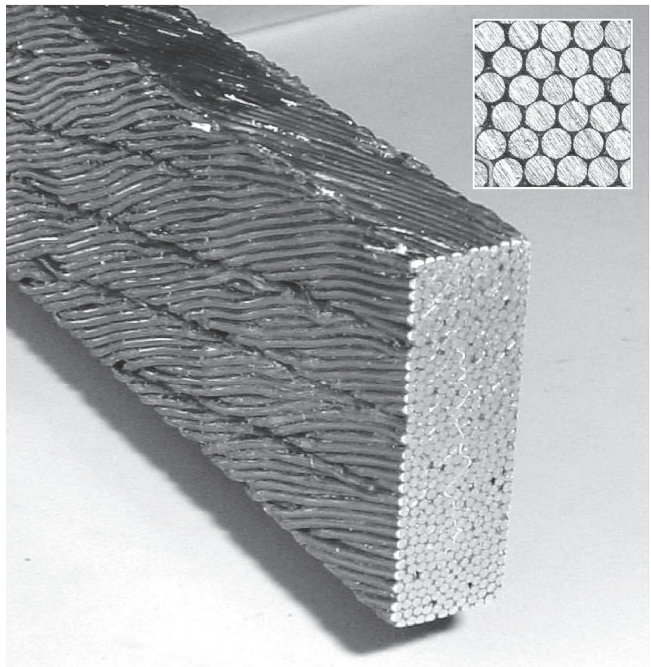
All these improvements for the stator winding insulation look likely to shift the design limitation into the rotor. Fortunately, the rotor material technology brings along all prerequisites to be upgraded into class 180 technologies. In the case of class 180, allowing class 155 operation, and probably in a later stage peaking in class 180, it is of utmost importance that both stator and rotor winding designs can accommodate their elongation due to thermal expansion.

With generally rising fuel costs, an upcoming driver of development is foreseen in all further efficiency improvements. Insulation technology improvements contribute to higher generator efficiencies. Another trend is the reduction of additional losses by refinement in stator windings (Haldemann, 2004). This will be done by optimized strand transposition schemes in stator bars, and may lead to novel stator bar designs, and refinement of conductor strands into Litz wires (Fig. 8.72).

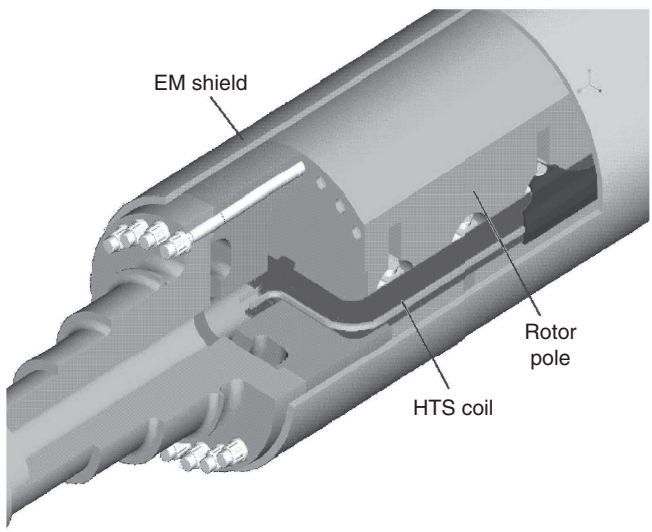
Another approach to a reduction of losses with high impact will be the introduction of superconducting rotor coils. The topic has arisen again with the announcement of high-temperature superconductors of the second generation by several suppliers, maybe even allowing liquid nitrogen cooling. Thanks to the eliminated rotor coil losses, the overall efficiency would increase by approximately 0.3–0.5%. Another benefit would be the higher SCR and thus enhanced stability on the grid. The challenge lies in the fixing and cooling of the rotor winding, and the supply and transfer of the coolant in the rotor (Fig. 8.73) (Fogarty, 2004; Joho, 2005; Frauenhofer, 2008).

Generally speaking, the air-cooled generator, after a stormy expansion phase up to 500 MVA, is approaching its limits in physical size, and is currently moving into a phase of consolidation. This consolidation includes the implementation of the aforementioned technology upgrading packages of novel insulation and lower loss designs. It remains up to the

Published by Woodhead Publishing Limited, 2013



8.72 Refining stator windings to reduce fuel costs could be achieved by optimizing strand transposition schemes in stator bars, and may lead to novel stator bar designs, and refinement of conductor strands into Litz wires.



8.73 Rotor coils incorporating high-temperature superconductors could be used to reduce rotor coil losses (Fogarty, 2004).

market to assess the more and more reduced difference in the efficiency between air- and hydrogen-cooled generators, considering the simplicity of air-cooled technology and the emerging stringent regulations with hydrogen.

Finally, system aspects become of more and more importance. The generator is the link between the utility grid and the turbine. Stability issues are addressed by grid codes. In view of renewable power generation, the traditional large units take over an important role in maintaining operational stability of the grid. Instead of over-dimensioning the generator to get the required SCR, leading to high initial and operational cost, there is still potential for new ideas, for example, involving the excitation system (Rouco, 2010). Efficiency and operational optimization with regard to the generator and all other plant components in the distant future might lead to solutions where plant components are specially developed for best overall performance. This could include further parameters for generators, such as coolant pressure, speed deviation, direct grid voltage connection or power stabilizers. Resulting operational benefits would be a fast load response, grid stability, customized power quality in a smart grid and an optimized overall power plant efficiency.

8.8 Acknowledgement

I would like to thank R. Joho for his outstanding help and expertise supporting this contribution, in particular referring to the history of generators.

8.9 Standard literature

Bozzuto, C. *Clean Combustion Technologies* 5th edn, ALSTOM Windsor, Transcontinental Printing (1996).

Klempner, G. and Kerzenbaum, I. *Handbook of large Turbo-generator operation and Maintenance*, 2nd edn, IEEE press, Wiley & Sons Inc, New York, (2008).

Müller, G. *Elektrische Maschinen – Grundlagen, Aufbau und Wirkungsweise*, VDE-Verlag GmbH Berlin (1985).

Müller, G. *Elektrische Maschinen – Betriebsverhalten rotierender elektrischer Maschinen*, VEB Verlag Technik Berlin (1989).

Neidhöfer G. in *Handbuchreihe Energie* (edited by Thomas Bohn) *Elektrische Energietechnik*, Verlag TüV Rheinland (1987).

Say, M. G. *Alternating Current Machines*, 5th edn, Longman Scientific & Technical (1983).

VDI/VDE Richtlinien Control of Synchronous machines, VDI/VDE 3680, October (2002) ICS 29.160.01.

Wiedemann/Kellenberger, *Konstruktion elektrischer Maschinen*, Springer-Verlag, Berlin/Heidelberg/NY (1967).

8.10 References

Azad, T., Stephan, C.-E. and Gellert, B. *New test results and operation experiences of the largest air-cooled turbogenerator technology with multi-million dollar benefits*, PowerGen Europe, Frankfurt, Germany, June (1999).

Bock, A., Joho, R., Baumann, T. and Stephan, C.-E. *Trends in insulation systems for generator HV-windings*, CIGRE session, (2002), paper 11–102.

Canay, M. Archiv für Elektrotechnik **46**. *Band*, 2. Heft, (1961), p. 83–102.

EPRI Project RP-3577–02 Large Air-cooled Generators driven by Combustion Turbines – Generic Issues', December 1996 (ORAP Data) data for all manufacturers and years 1971–1993.

Fogarty, J. M. *Development of a 100 MVA High Temperature Superconducting Generator*, IEEE PES General Meeting 2004, Denver and DOE Peer Review, Washington DC, July 27–28, (2004).

Frauenhofer, J., Grundmann, J., Klaus, G. and Nick, W. Basic Concepts, Status, Opportunities, and Challenges of Electrical Machines utilizing High-Temperature Superconducting Windings, EUCAS (2007), *Journal of Physics*, conference series vol. **97** - 012189, (2008), p 1–10.

Gellert, B., Stephan, C.-E. and Baer J. Der weltgrösste luftgekühlte Turbogenerator, *Technica*, **1**, (1999), p. 16–21.

Haldemann, J. Transposition in stator bars of large turbogenerators, *IEEE transactions* September (2004), vol. **19**, no. 3, pp. 553–560.

Hattori, K., Okabe, H., Ide, K., Kobashi, K. and Watanabe, T. Performance evaluation and measurement of the 250-MVA class air-cooled turbo generator. CIGRE session (2004), paper A1–107.

Iseli, M., Mayor, K., Sabater, Y., Verrier, M. and Zimmerli, B. *Air-cooled turbogenerator series for a changing market*, CIGRE 11–207 session, (2002).

Joho, R. *Air-cooled turbogenerators superseding hydrogen-cooling domain*, Proceedings of the IEMDC, MIT Cambridge, (2001).

Joho, R. Advances in synchronous machines: a turbogenerator view, *IEEE Power engineering Review* July (2002), vol. **22**, no. 7. pp. 7–10

Joho, R. *Highlights of a Superconducting Generator Study*, CIGRE SC A1 Colloquium 2005, Lausanne.

Joho, R. Baumgartner, J. *Breaking the 400MW barrier with air-cooled turbogenerators*, Power Gen International, Orlando, Florida, November (2000).

Joho, R. Baumgartner, J. *The advantage of large air-cooled turbogenerators in thermal power plants*, Proceedings of the IEEC, Bilbao, (2001).

Keller, S., Mayor, K. and Iseli, M. *Reliability and availability of modern air-cooled turbogenerators under stringent middle east ambient conditions*, PowerGen Middle East, February (2008), Manama Bahrain.

Kitajima, T., Ito, H., Nagano, S. and Kazao, Y. The world's largest capacity turbine generator with indirect hydrogen cooling. CIGRE session (2004), paper A1–106.

Roebel, L. Roebel bar, Vorrichtung zur Verbesserung des Wirkungsgrades und zur Erhöhung der Leistung elektrischer Großmaschinen, German Patent D.R.P. Nr. 277012, March 19, (1912).

Rouco, L., Ginet, C., Chan, K., Mayor, K., Malcher, O., Diez-Maroto, L. and Cherkaoui, R. *Improvement of the voltage ride through capability of synchronous generators by excitation control*. CIGRE session (2010), paper A1–106.

Stephan, C.-E. and Iseli, M. A new air-cooled turbogenerator with highest unit rating, *Power Gen Europe* 27, September (1995).

www.siemens.com/energy: Siemens Air-Cooled Generators, (2008).

9

Materials and coatings developments for gas turbine systems and components

M. KONTER and H-P. BOSSMANN,
Alstom (Schweiz) AG, Switzerland

DOI: 10.1533/9780857096067.2.327

Abstract: The efficiency increase of advanced gas turbines (GTs) is often accompanied with increased thermal, mechanical and environmental loading of turbine, combustor and rotor materials. The development of alloys suitable for such applications has been described with regard to metallurgical rationales and manufacturing processes. Combustor and turbine hot parts materials are developed to manage thermo-mechanical loading. To control thermal and environmental loading, thermal barrier coating and oxidation/corrosion resistant coating have been used. The lifetime prediction based on laboratory tests has been validated by engine experience evaluation of coated parts. Failure mechanisms as well as optimised manufacturing have been discussed in detail to indicate future needs.

Key words: Ni-base alloy, rotor steel, protective coating, thermal barrier coating, ceramic, manufacturing process, failure mechanism, lifetime prediction, engine experience.

9.1 Introduction

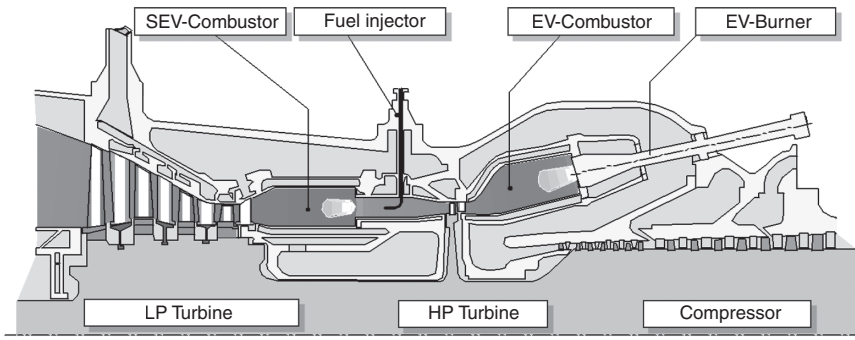
The efficiency of single cycles and combined cycles has improved during the last decades. Increased material temperatures, realised by less cooling and higher firing, and increased hot gas temperature were the major drivers, and will be for the next generation of gas turbines (GTs).

Especially parts of the hot gas path from turbine and combustor, but also the rotor, are affected by increased hot gas temperature. These parts are the focus for development for new materials and coatings with higher strength and higher temperature capability.

9.2 Turbine parts

Turbine parts, especially first stage blades, are exposed to high thermal and mechanical loading during operation, and to high thermo-mechanical loading

Published by Woodhead Publishing Limited, 2013



9.1 Hot gas path of Alstom's GT24/GT26.

during start-up and shut-down of the GT. High heat transfer at thin-walled blades results in high base material (BM) temperature. In the case of thermal barrier coating (TBC) spallation, the metallic bond coat (BC) has to protect the thin-walled blade against environmental attack at elevated temperature.

9.2.1 Turbine loading

The hot gas leaving the combustion chamber, with an average temperature called turbine inlet temperature (TIT) of about 1200–1400°C and a maximum pressure of more than 30 bars, is guided by vanes and driving blades (Fig. 9.1). These parts are internally cooled with compressed air at 350–550°C. The vanes and blades have to withstand 25 000–80 000 h service 'multiple loadings':

- mechanical load at high temperatures, including vibrations due to the expanding combustion gas and, for blades additionally, the centrifugal force of about 10 000 g,
- metal temperature of 700–900°C, and temperature gradients of the materials due to locally different heat transfer of combustion gas and cooling air of the complex shaped parts,
- temperature transients due to start/stop cycles, and
- environmental loading due to the hot combustion gas.

If these loadings are too high, the parts will fail, due to typical high-temperature failure mechanisms such as creep, fatigue, oxidation and corrosion.

9.2.2 Alloys for turbine blading

Ni-base superalloys

Alloys that are designed to survive at the above-mentioned conditions are called 'superalloys'. Most 'superalloys' are Ni-based alloys, hardened with intermetallic γ' phase on a basis of Ni_3Al (40–70 vol-%), and carbides and

borides along grain boundaries. Superalloys typically contain ten or more alloying elements, grouped according to their function into three categories:

1. Solid solution elements (Co, Cr, W, Mo, Re) are elements predominantly present in the austenitic γ matrix. W, Mo, Re are effective solid solution strengtheners due to their large atomic diameter; the main role of Cr is to provide corrosion and oxidation resistance through the formation of dense oxide scale; Co, being a minor matrix strengthener, stabilise γ' phase and increases γ' solvus temperature. These elements also replace Ni atoms in γ' phase lattice with a similar strengthening effect.
2. Gamma prime formers (Al, Ti, Ta, Nb, Hf) form an intermetallic γ' phase, replacing Al and, due to larger atomic diameter, strengthening this phase.
3. Grain boundary strengtheners (C, B, and Zr, Hf, Ti, Ta, Nb) form stable carbides and borides along grain boundaries.

This system has been successfully deployed in GTs during the last 50 years, due to the unique properties of the γ' phase. While most materials lose strength with increase of temperature above 600°C, the strength of γ' phase increases in temperature range from 600°C to about 800°C. Above this temperature range, the strength lightly decreases, but up to solutioning temperature, it remains higher than that of the matrix. The γ' phase has a crystallographic lattice, coherent with that of the matrix. Typical compositions of Ni-base superalloys for industrial GTs are presented in Table 9.1.

Consideration of the physical metallurgy of superalloy deformation at different temperatures illustrates the concept of the superalloy alloying approach:

- At temperatures below ~700°C, the predominant deformation mechanism is the cutting of the γ' phase by dislocations. The strength and volume fraction of γ' and the lattice mismatch between γ' and γ determine the alloy's deformation resistance.
- At temperatures above 700–750°C, the γ' phase becomes stronger than the matrix, while diffusion becomes much easier with increasing temperature. Diffusion-controlled climbing over γ' particles becomes a predominant mechanism of dislocation movement. Thus, solid solution strengthening plays the main role at these temperatures, along with the very high volume of γ' phase (>60%), resulting in a high density of dislocations in matrix channels between cuboidal γ' particles.
- The homological temperature $T_h = 0.8\ T_{\text{melting}}$ is that temperature of the material at which the grain boundary becomes weaker than the grain. Above this temperature, the predominant deformation mechanism is grain boundary sliding. Fine precipitates of carbo-borides along grain boundaries are strong barriers for this type of deformation. The ultimate solution for strength at this temperature is avoidance of grain

Table 9.1 Chemical composition of IGT superalloys

Type	Ni	Cr	Co	Mo	W	Re	Al	Ta	Nb	Ti	C	B
		Solid solution strengthening					γ' forming				Grain boundaries strengthening	
IN 738 LC	BAL	16	8.3	1.75	2.6	0	3.4	1.75	0.9	3.4	0.1	0.001
GTD 111	BAL	14	9.5	1.5	3.8	0	3	2.8	0	4.9	0.1	0.01
IN 792	BAL	12.7	9	2	3.9	0	3.2	3.9	0	4.2	0.2	0.02
IN 939	BAL					0						
GTD 222	BAL	22.5	19	2.3	2	0	0.8	0	0	1.2	0.08	0.1
FSX 414	10	28	BAL	0	7	0	0	0	0	0	0.25	0.01
MarM 247LC	BAL	8.5		0.5	9.5	0	5.5	3.2	Hf 1.3	1	0.15	0.015
CM 247 LC	BAL	8		0.5	9.5	0	5.5	3.2	Hf 1.4	1	0.07	0.01
Rene N4	BAL	9	8	2	6	0	3.7	4	0.5	4.2		
Rene N5	BAL	7	8	2	5	3	6.2	7	0	0		
CMSX 4	BAL	6.5	9	0.6	6	3	5.6	6.5	0	1		
MK 4	BAL	6.5	9	0.6	6	3	5.6	6.5	0	1		
PWA 1483	BAL	12.8	9	1.9	3.8	0	3.6	4	0	4		
MD 2	BAL	8	5	2	8	0	5	6	0	1.5		
CMSX-8	BAL	5.4	10	0.6	8	1.5	5.7	8	Hf 0.3	0.7		

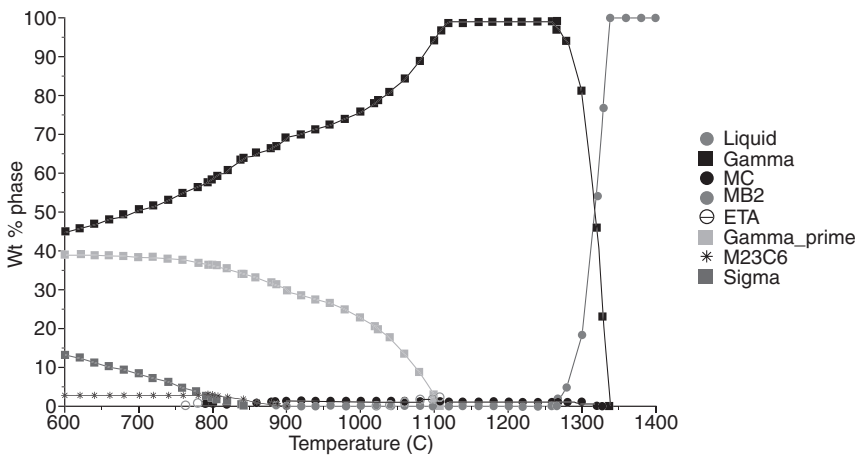
Published by Woodhead Publishing Limited, 2013

boundaries along the direction of main stress, or avoidance of boundaries at all. Directionally solidified and single crystal materials, following this route, will be discussed later.

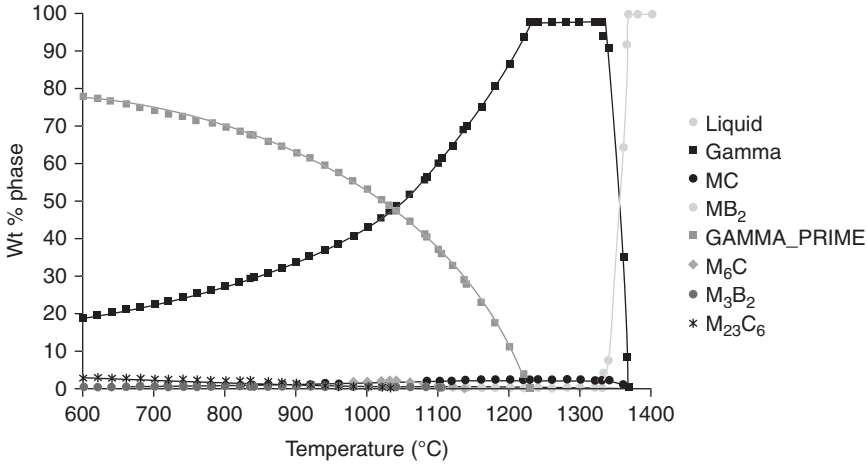
Phase stability is a significant limitation in design of saturated multi-alloyed systems. A number of undesirable phases can precipitate in over-alloyed Ni-base superalloys:

- Plate-like topologically closed packed (TCP) phases are considered as brittle; TCP phases on the basis of $(Cr,Mo)_x(Ni, Co)_y$ include more dangerous Cr-rich σ phase and rather more ductile Mo-rich μ phase.
- Hf, Zr rich eutectic on γ' base, prone to incipient melting during heat treatment.
- M_6C carbides, typically $(Ni,Co)_{3-2}(W, Mo)_{3-4}C$, which do not contribute to grain boundary strengthening, but consume valuable W and Mo.
- Weak α-Cr, Laves phases, etc.

Phase calculation methods help to avoid phase instability. PHACOMP methods are based on electron-hole calculations, with Nv numbers assigned for each element. PHACOMP is especially useful in superalloy metallurgy, when a quick decision on alloying of the batch is needed. In alloy design in recent decades, PHACOMP has been replaced by thermodynamically-based modelling of phase diagrams (e.g. ThermoCalc, JMatPro). Two examples (Figs 9.2 and 9.3) illustrate the JMatPro modelled phase structure of high Cr alloy IN939 and low Cr alloy MarM247LC. In the first case, one can see a pronounced presence of σ phase at temperatures below 800°C. In practice using PHACOMP, industrial IN939 melts are σ-free, or contain only traces of this phase. In the second



9.2 Phase structure vs. temperature for alloy IN939.



9.3 Phase structure vs. temperature for alloy MarM247LC.

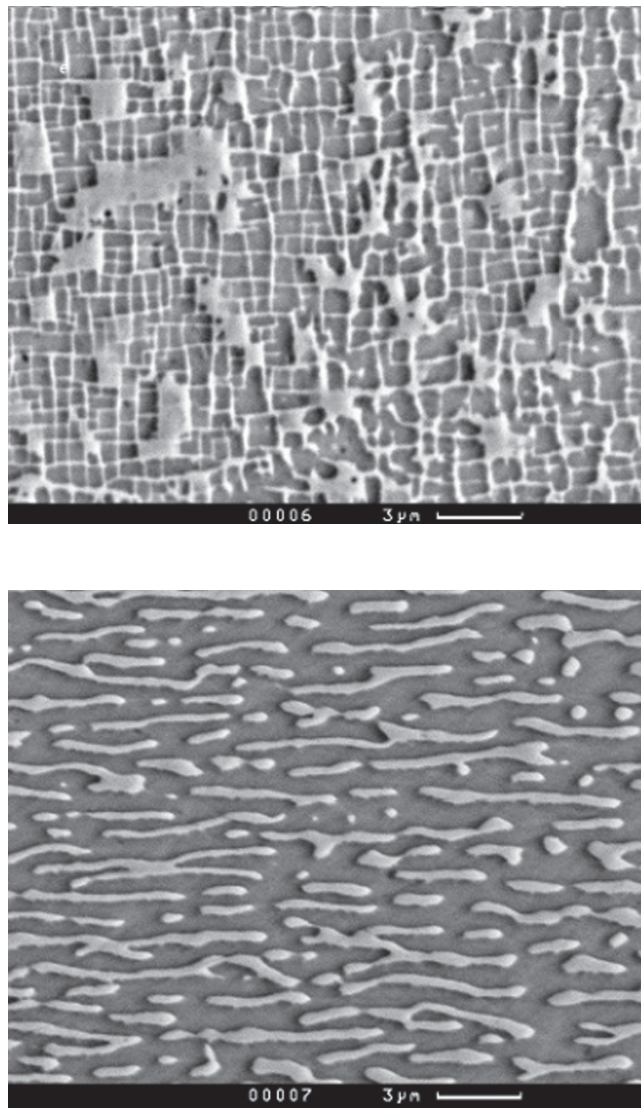
example, MarM247, being strongly alloyed with W and Mo (see Table 9.1), forms M_6C carbides, which at higher temperature transform to MC carbides and MB_2 borides. Current examples (Figs 9.2 and 9.3) demonstrate also the limitations of equilibrium phase modelling, as real structures are in non-equilibrium. For example, very high volumes of γ' at lower temperature are never reached, phase balance occurs in reality only at temperatures above 800°C.

Stability of alloy structure does not only include phase stability, but also stability of the cuboidal morphology of the γ' phase. Alloys with a very high fraction of γ' phase (usually >60 vol-%) tend to degrade, forming elongated, so-called 'rafted', structures perpendicular to stress axes and even to a reverse structure of γ in γ' matrix. A rafted structure is characterised by lower creep properties, and the inverse structure is prone to cracking (Fig 9.4).

Another aspect of alloy service properties is resistance to oxidation and corrosion. This resistance is determined by the ability of the alloy to form a dense, stable oxide layer at the beginning of the exposure, which then protects metal from further oxidation/corrosion. Alloys with insufficient environmental resistance form porous Ni oxides. Cr_2O_3 formers are corrosion resistant, and Al_2O_3 formers have good resistance to oxidation. Besides Cr and Al, other alloying elements also influence the type of TGO. One attempt to visualise the effect of main elements on corrosion and oxidation properties is a ternary diagram utilising Ni-, Cr-, and Al-equivalents (Fig. 9.5).[1]

The right corner of the diagram represents pure Ni+Co system, with increase in Cr-equivalent and Al-equivalent content along the horizontal and diagonal axes respectively. This picture illustrates very well the point that it is essential to have Cr content above 10 at-% to get a good Al_2O_3 former.

Minor elements, especially those segregating to the surface, significantly affect adhesion and stability of the oxide scale and the oxidation/corrosion

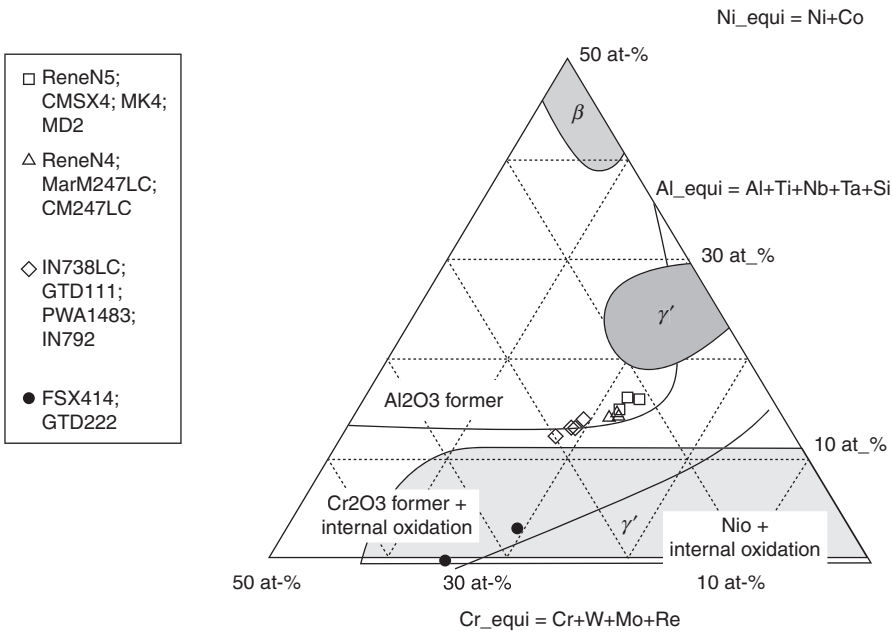


9.4 Cubical (a) and rafted (b) morphology of γ′ phase in highly alloyed superalloy. (a) Initial condition (fully heat treated), (b) continuous γ′ after creep at 950°C.

behaviour. While Hf and rare earth elements are believed to be beneficial, S and P are extremely detrimental.[2] Tight metallurgical control over these elements allows significantly increasing the environmental resistance of superalloys.

Until now, all the characteristics and approaches discussed were valid for both aircraft and power generation applications. In the past, material

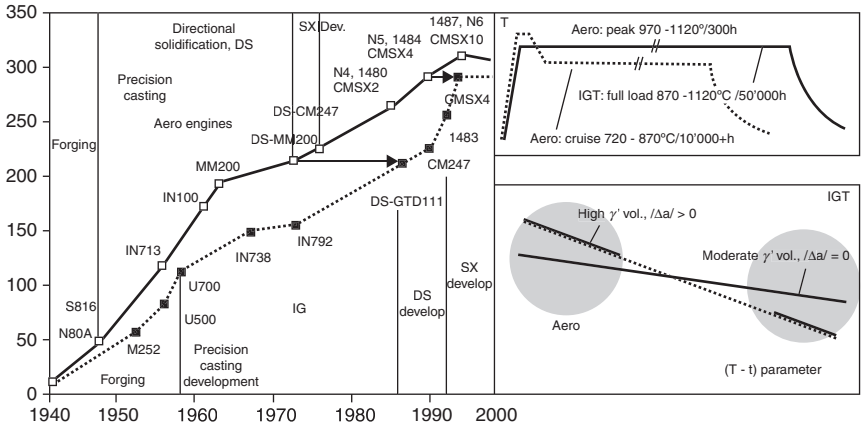
Published by Woodhead Publishing Limited, 2013



9.5 Oxide formation ternary diagram using Ni-, Cr- and Al-equivalents.

technology for power generation GTs has followed the aircraft technology with a delay of about two decades.[3] From the late 1990s, increasing competition in the power equipment sector has reduced this technological gap to less than 10 years (Fig. 9.6). Aero alloys MarM247LC, CM247LC, CMSX4 and their derivatives have found wide utilisation in industrial GTs.

However, there is a significant difference between aero and industrial GT operation conditions, illustrated at Fig. 9.6. Maximum temperature and load at peak in aero engines is much higher than temperatures and load in IGT. However, the main time aero engine operates in cruise mode at temperatures significantly lower than those of the base load of IGT. Thus, aero alloy needs rather high resistance to creep and thermal fatigue at very high temperature, but for a relatively short time, as well as high oxidation resistance. An ideal alloy for IGT needs, in a turn, long-term resistance to creep and fatigue at 'moderate' temperatures, long-term stability of the properties – and therefore structure – and a combination of oxidation and corrosion resistance. Here we come to the main ideological difference between ideal aero- and IGT superalloys. In order to achieve the best resistance to dislocation movement (both sliding/cutting and climbing) an aero alloy needs a certain mismatch between lattice parameters of γ and γ' phases. In



9.6 Progress in aero- and IGT blade material, specific IGT service conditions, and trends in IGT vs. aero alloy development.

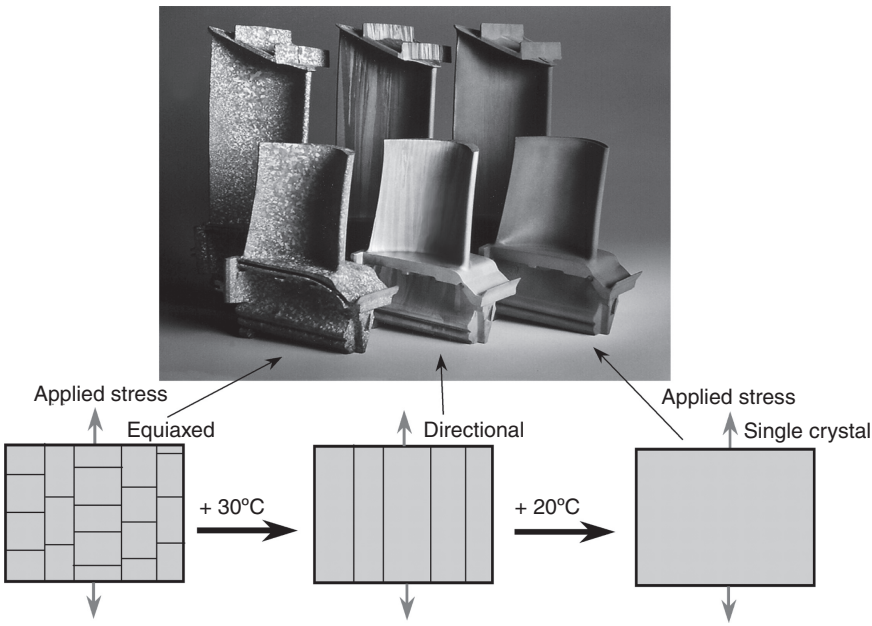
contrast, at long-term high temperature exposure under stress, mismatch between γ and γ' lattice parameters results in an accumulation of dislocation on the interface and finally loss of coherency, with coagulation of γ' particles in lower alloyed alloys and rafting on higher alloyed alloys. Therefore, an 'ideal' IGT alloy should have a lattice mismatch close to zero, resulting in a stable γ' morphology over operation time.

Directionally solidified and single crystal technology

In modern IGTs the TIT exceeds 1300°C, efficiency requirements limit the amount of compressor air available for cooling, and the life target for highly loaded front stage components is 25 000–50 000 h at metal temperatures above 900°C. To satisfy these requirements, modern IGTs employ advanced cooling schemes, thermal barrier ceramic coatings, and use directionally solidified and single crystal blades and vanes.

Directionally solidified and single crystal structures are illustrated in Fig. 9.7. The directionally solidified part is grown along the vertical axe so that single grains extend from the bottom to the top of the part. Consequently, a part has no grain boundaries in the direction normal to the main stresses (for example, from the axial load).

For the single crystal component, the entire part is one single grain, and grain boundaries are fully abandoned. An additional increase in temperature capability comes mostly from better thermo-mechanical fatigue (low elastic modulus of the crystal with <001> orientation) and load from the thermal gradient in the transverse direction. One additional factor, very significant for thin wall parts, is the avoidance of catastrophic grain bound-



9.7 IGT Blades with conventional, DS, and single crystal grain structure (in grain boundaries etched condition).

ary failure in one-grain cross-sections due to grain boundary sliding at high temperature.

Single crystal (SX) components for industrial GTs are significantly larger and heavier compared to the aircraft parts. This certainly reflects in manufacturing yield and in component costs. Does the industry really need them? The very high costs of IGT SX components gives particular significance to this question. Each new turbine design needs a benchmark of SX against conventional and directionally solidified (DS) parts. Despite the high costs of SX technology, most IGT producers are using SX components in the front stages.

One important advantage of SX over conventional material is its stability against the so-called 'thin wall' factor. At a wall thickness below 1 mm, conventionally cast material shows catastrophic reduction in high temperature creep life, due to through-going grain boundaries and grain boundary sliding. In large IGT components, the wall thickness are often above 1.5 mm and the maximum metal temperature is below the limit of grain boundary sliding.

The driving force to use SX technology in IGT is the excellent resistance of its properly oriented single crystals to thermo-mechanical fatigue (TMF). In the <001> direction, its E is one-half of those for conventionally cast

materials, which reduces thermally induced stress and extends TMF life significantly. The main advantage of SX over DS parts is an absence of grain boundaries in the platform areas, and better control over orientation. Since most IGT blades and vanes are life-limited by TMF rather than creep, in many cases SX technology is the only way to achieve life target.

Single crystal IGT blading is made of cast Ni-based superalloys, often Re-containing. Re is not only a very effective solid solution and γ/γ' interface strengthener, but also extends the stability of the precipitation hardening γ' phase towards higher temperatures. CMSX4,[4] MK-4[5] and Rene N5[6] are examples of such high strength- and high oxidation-resistant aircraft type alloys used in power generation turbines. IGT SX materials of another class are derivatives from traditional power generation alloys, such as IN792SX, PWA 1483, GTD 111 and CMSX11.[7] These Re-free so-called 'first generation' single crystal superalloys have lower temperature capability, but are significantly less expensive and demonstrate good phase stability during operation, and balance between oxidation and corrosion resistance.

The modern trend in IGT alloy development reflects the specific power generation requirements: IGT components operate at base load temperature much longer than do those in aircraft engines, although the peak temperature is lower (Fig. 9.6). Consequently, the stability of the alloy structure and properties in long-term, high temperature operation gains in importance compared to ultimately high strength at very high temperature, which was a dominant optimisation parameter in aerospace alloy design.

Application of SX parts must be supported by specific manufacturing, reconditioning and repair technologies, and by consideration of IGT-specific material requirements.

Single crystal alloys

Further life extension of IGT blading material beyond the level achieved today will require alloys with very high levels of γ and γ' solid solution strengthening, but probably a lower precipitate volume fraction and a more stable γ–γ' structure (low lattice mismatch).

Compared to the 'ideal' approach to IGT alloy design mentioned above, the 'real' approach is governed by a compromise between contradictory requirements.

On the one hand, a low γ/γ' lattice mismatch in alloys, highly alloyed with solid solution strengtheners and having high γ lattice parameter, can be achieved only by the replacement of Al atoms in γ' phase with atoms of Ti and Ta. The γ/γ' lattice mismatch causes an additional strengthening. However, the lattice mismatch, as well as very high γ' volume fraction, promotes the formation of a rafted structure,[8] especially detrimental when γ' becomes a continuous phase or inverted matrix. Though the detrimental

Published by Woodhead Publishing Limited, 2013

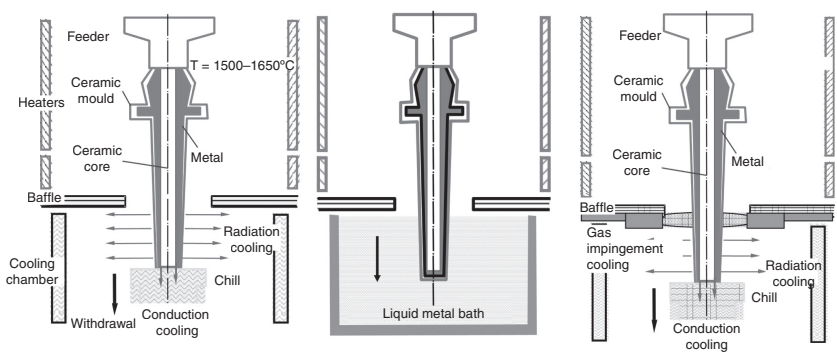
effect of rafting and γ/γ' inversion on creep properties is being disputed (several publications show no reduction in creep properties due to these types of degradation), ductility and TMF life deteriorate.

On the other hand, cooled high temperature IGT components cast in alloys with relatively high Ti and low Al content, such as IN-792 derivatives, suffer from internal oxidation and nitridation if not internally coated. Overall, oxidation resistance of IGT alloys plays a very important role and being promoted by clean processing, desulphurisation and addition of rare earth elements.[9]

Next generation IGT blade alloys will most probably combine the high oxidation and fatigue resistance of aircraft materials with significantly increased structural degradation resistance. Alloys with higher resistance to rafting and γ/γ' inversion, namely those with moderate γ' volume fraction and low lattice mismatch, fit the IGT requirements better. Their temperature capability, oxidation and creep resistance have to be further improved compared to commercial alloys of the 'corrosion resistant' class, such as CMSX11 and IN792SX. High potential for land-based GTs has also developed alloys lately with nominal Re content at 1.5 wt.%, compromising somewhat lower high temperature strength compared to 3%Re alloys in favour of better long-term phase- and morphology stability and lower costs, such as Rene N515 and CMSX-8.[10]

Single crystal/directional solidification casting process

Large IGT single crystal components give rise to high manufacturing costs when using traditional SX casting technology. Figure 9.8a illustrates the current Bridgman process. The mould with molten metal moves gradually from the heating chamber to the cooling chamber, separated by a baffle.



9.8 Bridgman (left), LMC (middle) and gas cooling (right) casting processes.

Heat is removed by radiation in vacuum from the mould towards the water-cooled chamber walls. Good isolation between the cooling and the heating zones provided by the baffle results in a vertical temperature gradient. This gradient provides the directional solidification of the component. When the temperature gradient in the primary growth direction (vertical) is sufficiently high, a microstructure with no grain defect is formed. This is usually the case when relatively small aircraft components are cast. For massive IGT parts, the heat radiation in vacuum is at the limit of its heat extraction capability, and therefore also at the lower limit of the required temperature gradient. When the temperature gradient is insufficiently low, the solidification rate will be either too high or too low. Both could result in various casting defects, such as freckles, columnar grains and porosity.

Several measures are being currently implemented to increase the SX yield of large components. Computer simulation of the solidification process is used by both vendors, to optimise the casting process parameters, and turbine producers, as a part of design for manufacturing. Latest versions of computer codes allow the prediction of casting stresses and formation of low angle grain boundaries.

More advanced is development of single crystal casting techniques with a high cooling rate, such as the liquid metal cooling (LMC), Fig. 9.8b,[11] and the gas cooling casting (GCC) process, Fig. 9.8c.[12] In the LMC process, the mould is immersed in a bath with liquid tin or aluminium. The advantage of this process, besides the higher temperature gradient, is that in the bath elements of the mould see no heat input from the adjoining parts. Therefore, the mould size (number of blades per mould) is only limited by the mould strength and size of the equipment. Limitations of the process are the effectiveness and stability of the aluminium bath in Al process, and shell cracking (tin poisoning of superalloy) in the tin process. In the GCC process gas impingement cooling is provided below the baffle, in addition to the 'standard' cooling by radiation. One significant advantage over the Bridgman and LMC processes is that the inert gas penetrates the mould, and fills in the mould pores and the vacuum gap formed between metal and mould due to contraction during the solidification. This significantly increases the heat transfer coefficient of the system. The process is at least as effective as LMC, easy to control, but the cluster size is limited, similarly to the conventional process, by heat input from adjoining mould elements.

Another way to increase the casting yield is the alloy design for castability. The density balance, between the liquid metal in the mushy zone and the bulk liquid metal above the liquidus line, significantly reduces metal convection during solidification. This prevents formation of freckles and increases tolerance to the inclination of solidification front with respect to formation of secondary grains. Balance of elements such as Hf and C controls the metal–mould reaction (wrinkles, surface scale, etc.) and reduces freckling.[13]

Published by Woodhead Publishing Limited, 2013

Addition of grain boundary active elements increases tolerance to the low angle grain boundaries misfit from 5–6° to 9–12° and above.

Reconditioning of single crystals

The service life of conventionally cast blades and vanes should be extended by rejuvenation heat treatment after the first 20 000–30 000 h of operation. During this treatment of ex-service parts, the coarsened γ' is fully or partially dissolved and newly precipitated in a fine form. Sometimes this step is combined with a hot isostatic pressure treatment (HIP) to close voids and micro-cracks accumulated during the service. Single crystal components, which locally accumulate more than 1–2% strain, are sensitive to recrystallisation after solutioning of γ' phase, which leads to loss of properties. For the same reason, it is impossible to HIP the SX parts.

The difficulty in finding a heat treatment that does not result in recrystallisation but transforms degraded γ' phase of ex-service parts back to cubical morphology was described earlier. Fortunately, the rafted morphology of γ' phase is thermodynamically unstable in isothermal unloaded condition. In addition, experimental investigations on ex-service blades have shown that a combination of stress relief steps and an isothermal heat treatment below γ' solvus temperature restores the cubical morphology, though coarser than in the initial condition. Coarse cubic γ' structures possess creep and fatigue properties significantly higher than those of the inverse γ' matrix, but still lower than that of fine γ' structure of virgin material before operation in a GT. The virgin SX material properties, therefore, can be only partially restored by a rejuvenation treatment. However, even the partial rejuvenation component gives an additional life of more than 50% compared to that of the initial component.

Single crystal brazing for manufacturing and repair

Problems with casting of large internally cooled SX components keep interest in alternative manufacturing technologies. One example is the concept of the so-called 'constructed blade', where parts of the blade are cast separately and then joined together. Already in the 1970s, there were trials on diffusion welding of two SX blade halves with open cooling configuration. Drawbacks of this technology were the absence of adequate non-destructive testing (NDT) techniques and the very high geometric precision requirements for joining the parts. Today, advanced NDT methods and the application of transient liquid phase (TLP) brazing allows to production of at least prototypes of very heavy blades with complex cooling geometry. TLP brazing, giving more flexibility to joining process, usually results in equiaxed or eutectic cellular structures. However, only an SX structure of the braze zone, epitaxial to the BM can provide 'as-cast' life of a component. Even

Published by Woodhead Publishing Limited, 2013

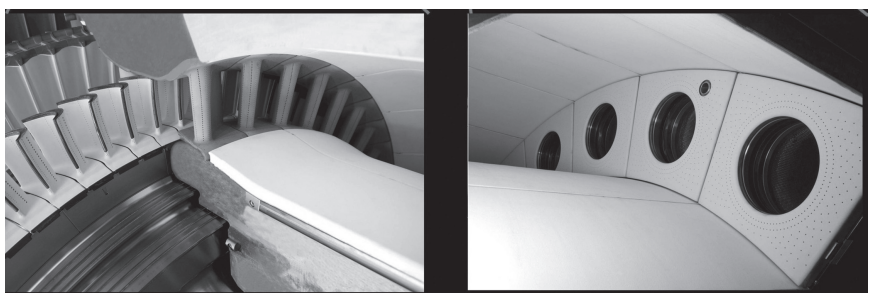
higher demand for epitaxial SX brazing comes from repair needs. Epitaxial closure of cracks in base metal and rebuild of the blade tip area can extend service life of SX components by 80% (in combination with rejuvenation heat treatment and recoating).

The principles of directional solidification known from casting have helped to develop the epitaxial SX brazing process. Using the constitutional undercooling equations[14], the temperature gradient and velocity of the solidification front can be described in terms of the concentration gradient and the diffusivity of the alloying elements. Diffusion modelling enables definition of a composition of the braze alloy that at the chosen temperature produces an epitaxial single crystal joint for commercial SX superalloys (Plate XIII, see colour plate section between pages 346 and 347). The next important step, after solidification, is the homogenisation heat treatment, which binds melting point depressants into stable, widely spread precipitates with fine morphology. Wrongly precipitated boron- and silicon-rich phases, for example with plate-like morphology, embrittle the material. In contrast, fine nano-sized particles reduce neither the ductility nor the strength of the base alloy.

9.3 Combustor parts

9.3.1 Combustor loading

Combustor parts for industrial GTs, such as burner or liner, are large, thick-wall elements, which are casted or welded Ni- or Co-base alloys (Fig. 9.9). The walls of these parts are on one side in direct contact with combustion gas, and subjected to firing temperatures of 1400–1700°C.[15] On the other side, the walls are cooled by compressed air to limit the materials' temperature to an acceptable level of about 900°C for mechanical and environmental loading requirements.



9.9 Coated parts in HGP: Combustion chamber with liner segments and burner and turbine with coated vanes and blades.

Table 9.2 Typical BMs for combustor parts

Type	Fe	Ni	Cr	Co	Mo	W	Ta	Nb	Ti	Al	C	B
Hastelloy X	19	BAL	22	1.5	9	0.7	0	0	0	0	0.07	0.005
IN617	3 max	BAL	22	12.5	9	0	0	0	0	1.2	0.1	0.005
1N738LC	0	BAL	16	8.3	1.75	2.6	1.75	0.9	3.4	3.4	0.1	0.001
AISI 309	BAL	13	23	0	0	0	0	0	0	0	0.1	0
Nimonic 263	0.4	BAL	20	20	6	0	0	0	2.1	0.4	0.06	0
HS-188	1.5	22	22	BAL	0	14	0	0	0	0	0.05	0.01

9.3.2 Combustor materials

Typically, combustor BMs are lower alloyed as compared to materials used for blades and vanes in the turbine. They vary from solution-strengthened alloys with excellent weldability and manufacturability, such as Hastelloy X or even 23–13 austenitic steel, through Co and Ni alloys with a small volume of precipitation hardening phases, to relatively high strength superalloys such as IN738LC (Table 9.2). Cycling in high velocity and high temperature combustion gas leads to a significant degradation of the material and loss of wall thickness (0.14 mm for 1000 h at 980°C).[16,17] This might affect the mechanical integrity of the parts. Impurities, coming with the fuel, the intake air or the water injected into the compressor or combustor, will accelerate the material degradation and loss due to hot corrosion under deposits. Appropriate metallic coatings are about 10–30 times more resistant and will protect the coated BM from oxidation and corrosion.

Mechanical integrity is also a matter of thermal and thermo-mechanical loading. Large thick-walled parts will see an inhomogeneous temperature distribution, resulting from locally different heat fluxes. Thermal gradients will lead to thermal stresses during steady state operation, and even more during transient operation, namely start-up and shut-down. Increasing surface temperature, and higher heat flux through thick walls, results in cracking of parts. A TBC is used to reduce heat flux as well as the temperature of the metal wall. Consequently, the transient and gradient stresses are also reduced.

9.4 Coatings for hot gas path parts

Enabling reliable operation despite of multiple loadings, most parts of the hot gas path (Fig. 9.9) have been coated to separate the functionalities, primarily with respect to mechanical integrity, environmental protection and temperature capability of the materials. The BM has to take the mechanical and thermo-mechanical loads, while a metallic MCrAlY coating has to protect the parts against oxidation or corrosion and the TBC that has to reduce

the metal temperature of the cooled parts. In the latter case, the metallic coating has additionally to act as BC for good adherence of the TBC.

9.4.1 Coated parts

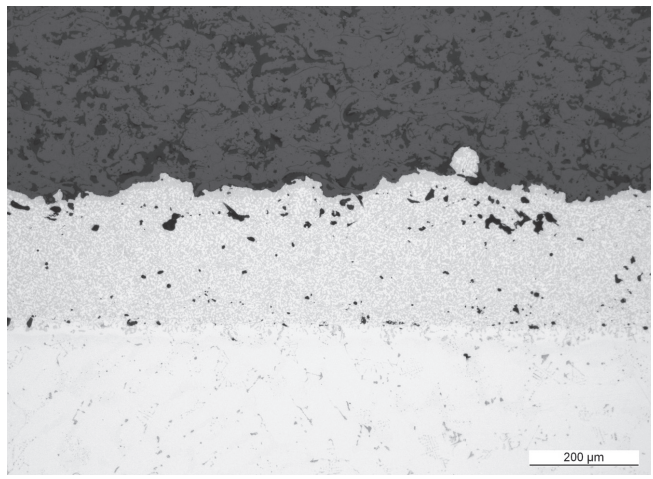
Typically for industrial GTs, the first stages of the turbine blading are made out of Ni-base superalloys, cast as a single crystal, directionally solidified or polycrystalline microstructure. On top of this BM, a layer of MCrAlY is applied by VPS or LPPS as a protective coating. In many cases, this MCrAlY layer also acts as BC and a second layer of 7YSZ TBC is applied by APS (Fig. 9.10a). The standard system for aero turbines, a smooth PtAl-BC applied by PVD combined with a thin 7YSZ TBC applied by EB-PVD, is more seldom used for IGTs, due to thickness limitations and cost.

Combustor parts, such as liner, burner or transition pieces, are predominantly thermally less mechanically loaded. They are made of solid solution strengthening Ni-base alloys or precipitation strengthened alloys. In principle, the coatings applied on combustor and turbine parts do have comparable functions. Due to the size of the parts, they may differ with respect to coating process, thickness and post processing. Typically, combustor parts of IGTs are coated by APS for the BC as well as for the TBC (Fig. 9.10b). The materials MCrAlY for BC and 7YSZ for TBC are the same or similar to that of the turbine parts. The thermal performance and lifetime of the BC/TBC systems strongly depends – beside loading and design of the part – on the materials and the manufacturing process. Failure of the coated system can be seen as delamination or spallation of more or less large TBC areas.

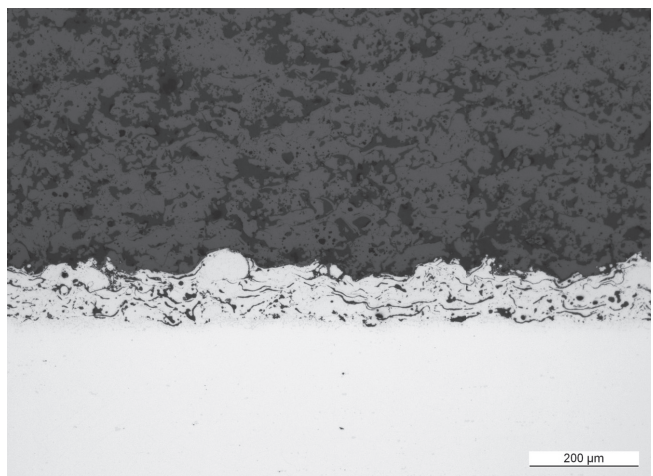
9.4.2 MCrAlY as protective coating

The performance of the BM as well as the MCrAlY coating is dependent on the loading and the composition. For material temperatures from about 700°C to 900°C, failure by hot corrosion could occur in a sulphur containing environment; at higher temperatures, oxidation will occur. As a rough guideline, good corrosion life can be achieved with a composition having a high Cr-equivalent (= sum of Cr, W, Mo, Re/at-%/), good oxidation life requires a composition with a high Al-equivalent (= sum of Al, Ti, Nb, Ta, Si/at-%/). However, both must be balanced with the Ni-equivalent (= sum of Ni, Co/at-%/), to establish appropriate physical properties and good mechanical behaviour. The comparison of the ternary equivalent compositions of coatings developed by various companies and typical blading materials demonstrate clearly their different roles (Fig. 9.11): in general, Al-equivalent and/or Cr-equivalent are significantly higher in the coating than in the BM, reflecting their intended application against oxidation or corrosion.

Published by Woodhead Publishing Limited, 2013



(a)



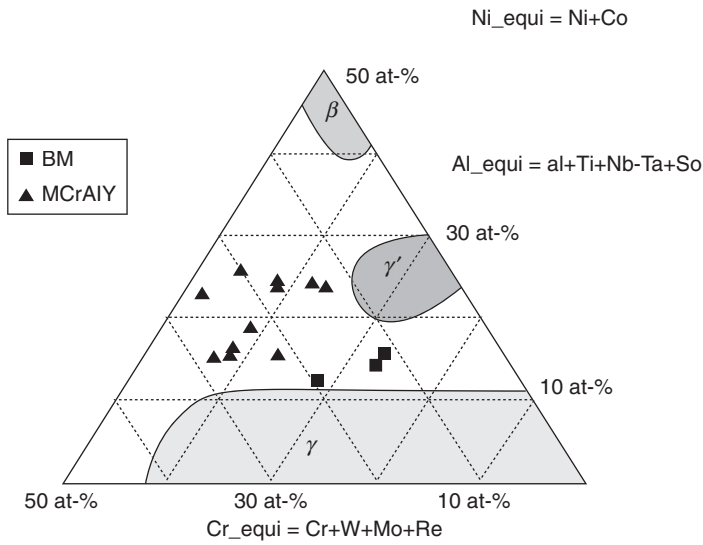
(b)

9.10 (a) BM/LPPS BC/APS TBC and (b) BM/APS BC and APS TBC.

Other elements are less than 2 at-%.

The MCrAlY coatings show different oxidation and corrosion behaviour as compared to the BMs typically used for turbine blading:

- At high temperatures above 1000°C, BMs often reveal accelerated oxidation due to increased TGO spallation, internal oxidation (formation of Al_2O_3) and nitridation (formation of TiN and AlN) especially during superimposed thermo-cyclic loading.[18] Optimised MCrAlY with high Al- and Cr-activity instead do not show any or only irrelevant internal



9.11 Ternary equivalent composition of blading BM and coating developed by various GT companies.

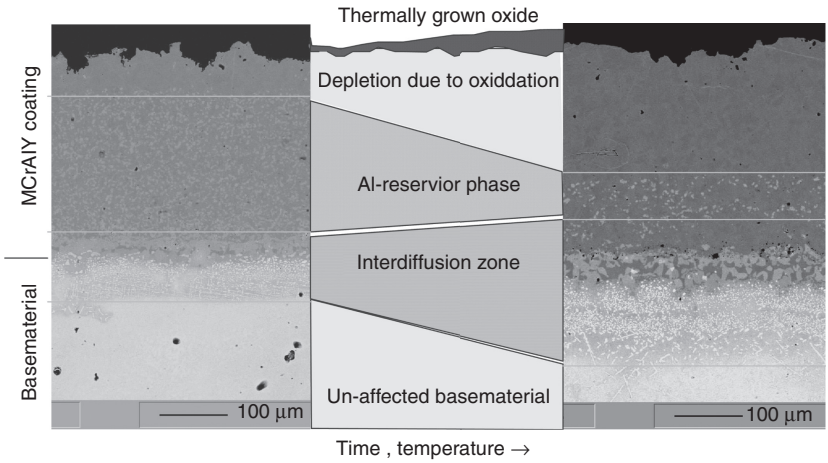
oxidation or nitridation at temperatures up to 1050–1100°C. In addition, TGO growth or spallation of such coatings is reduced.

- Sulphur-induced hot corrosion is often a problem for high strength superalloys, due to their low Cr-activity. In laboratory tests CMSX4 or CM247LC showed already after 500 h corrosion depths of 200 μm for Type II (700°C) or more than 1000 μm for Type I (850°C), while the MCrAlY coated BM revealed for both corrosion types only some negligible attack of about 20 μm.[19]

Coating consumption

Hot corrosion and oxidation life of MCrAlY have been prolonged by increasing the level of sacrificial elements Cr and/or Al, and by addition of other elements to reduce growth rate and spallation of the TGO. Detailed studies have shown that even minor changes of some elements (i.e. sulphur)[20] could have a significant influence on oxidation or corrosion resistance. Oxidation and hot corrosion mechanisms have been well described by thermodynamic models, but their growth rates are very difficult to predict, due to the effect of minor elements in complex alloys.

At the interface of MCrAlY to BM an interdiffusion takes place at high temperature, where elements from the coating diffuse into the BM and vice versa. Depending on the activity and mobility of these elements, new



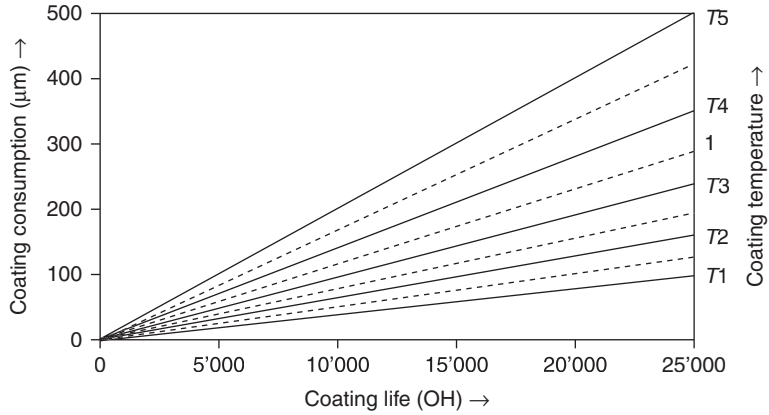
9.12 Consumption of coating due to oxidation and interdiffusion In the coating the dark dots in grey matrix represent Al-rich beta phase (about 17–20 wt-% Al) in γ-matrix (about 2.5–6 wt-% Al).

phases can be formed or existing phases can coarsen. Thermodynamic and kinetic models can describe the interdiffusion zone with the phases formed and the depth profile to evaluate the chemical compatibility of BM and coating.

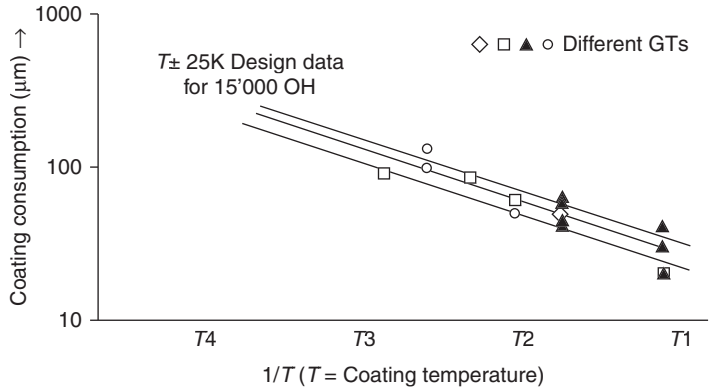
At temperatures above 900°C, the oxidation of the coating will predominantly form a TGO, predominantly out of alumina, and an aluminium-depleted layer at the outer surface; both are growing with time and temperature (Fig. 9.12). In the interdiffusion zone, Al-rich and Cr-rich phases will be formed, often increasing the local hardness in this zone.

The consumption of the coating due to oxidation can be seen by the depletion zones, or be the remaining layer, which contains Al-reservoir phases like γ'-Ni_3Al and/or β-NiAl. The long-term behaviour follows a nearly linear time dependence and exponential temperature dependence, where an approximately 30K higher temperature leads to twice the consumption in the temperature range of interest (Fig. 9.13).

Test and validation of coated parts is a key discipline for reliable design and operation of the turbine. For example, coated blades running for 15 000 h in four different GTs have been investigated.[21] The coating consumption has been plotted against the temperature of the BM close to interdiffusion zone by evaluating the coarsening of the γ' phase of the BM (Fig. 9.14). The centreline represents the oxidation data generated in the lab furnace at various temperatures; the outer lines represent the oxidation data for 25K higher or lower temperature to consider the accuracy of γ'-evaluation. The good correlation from laboratory and engine data reveals that



9.13 Consumption of the coating due to oxidation in lab furnace.

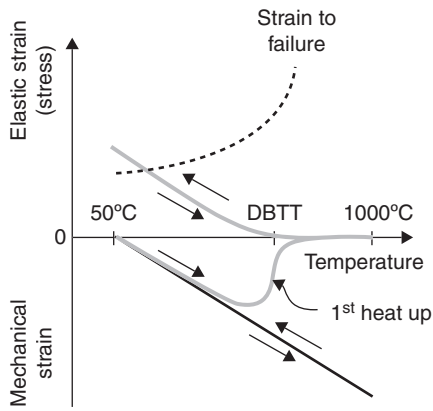


9.14 Validation of coating consumption based on assessment of blades of four different GTs operating for 15 000 h.

for these blades, oxidation was not affected by other consumption-relevant parameters, such as corrosion and thermo-mechanical loading.

Thermo-mechanical behaviour

Besides the above-described environmental loading of hot combustion gas, the thermo-mechanical loading due to the start/stop cycles of the GT is important for the performance of the BM and the coating. Thermal stresses or strains induced by temperature gradients across the wall thickness, plus part-specific mechanical stresses or strains, result in deformation of the coating. This can be simulated by TMF tests, which reproduce the temperature and strain as in-phase or out-of-phase cycles to represent different locations of a component (Fig. 9.15). The coating is repeatedly cycled from



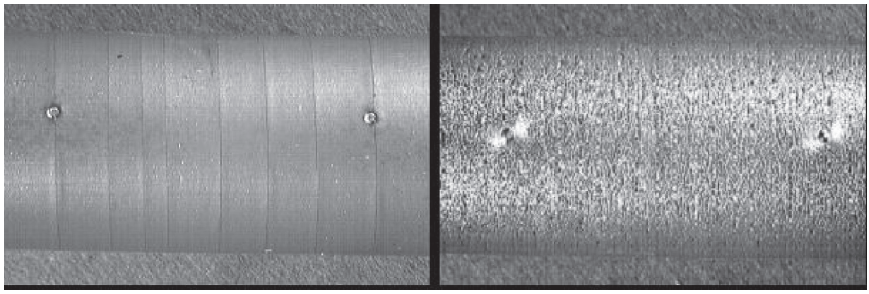
9.15 Thermo-mechanical loading of coated turbine blade.

T_{min} to T_{max} passing the DBTT. This is of particular relevance to the coated parts or specimens, since the coatings investigated show brittle deformation behaviour below DBTT and super-plasticity above DBTT. Different Young's moduli and thermal expansions of the coating and the BM result in additional stresses. Isothermal low or high fatigue tests cannot reproduce such loading and damage mechanisms.

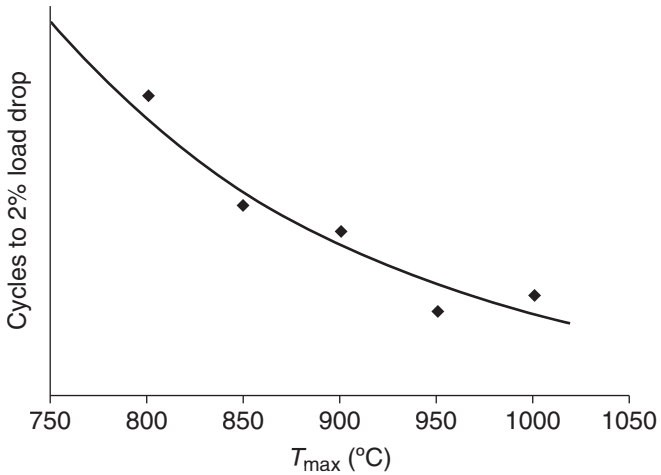
The complex failure mode can lead to quite different behaviour even for coatings belonging to the same composition class. While one coating showed fast propagating, brittle cracking in the early test phase, the other showed multiple crack initiation and a high density of slowly propagating cracks (Fig. 9.16). The material behaviour around DBTT can explain completely neither this different crack initiation or propagation nor the influence of the upper dwell temperature T_{max}, which is generally far above DBTT: increasing T_{max} from 800°C to 1000°C, the cycles to 2% load drop reduce clearly by a factor of 3 (Fig. 9.17). Additionally, the appearance of the coating surface changes from a smooth surface with fine near surface cracks to a rumpled surface with cracks crossing the coating thickness (Fig. 9.18). In the lower range of T_{max} a single crack is propagating into BM during the final stage of the TMF testing.

Future coatings for superalloys

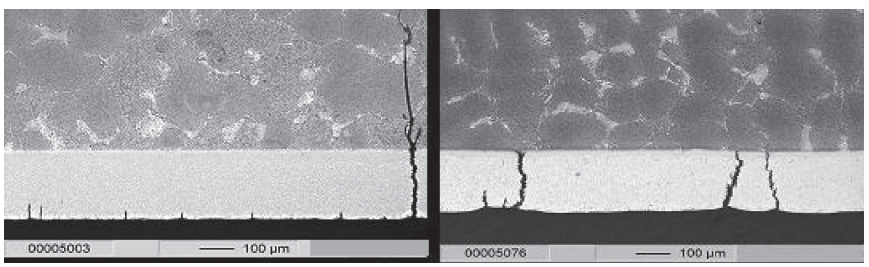
Future GTs with increased efficiency will be designed for higher thermal loading of coated blades. To evaluate a coated system, not only the maximum temperature but also the wide temperature range has to be considered for the relevant failure mechanisms. To shorten development times for advanced coating systems a composition- and phase-based lifing model has been generated based on detailed oxidation and TMF testing of many



9.16 TMF test samples with T_{max} = 800°C (T_{min} = 50°C, 0.6% strain; out-of-phase, 5 min hot dwell time). Left: NiCoCrAlY-Coating after 600 cycles, right: NiCrAl-Coating after 2000 cycles.



9.17 TMF of 200 μm thick MCrAlY coating (T_{min} = 50°C, 0.6% strain; out-of-phase, 5 min hot dwell time).

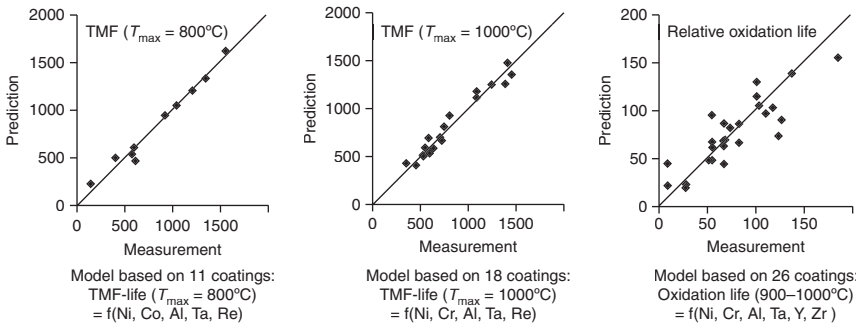


9.18 Cross section through TMF test samples with same MCrAlY coating (T_{min} = 50°C, 0.6% strain; out-of-phase, 5 min hot dwell time). Left: T_{max} = 800°C, right: T_{max} = 1000°C.

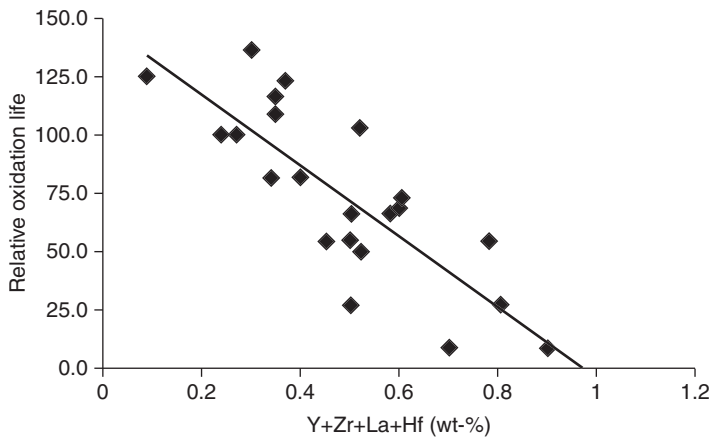
different coatings. The model is based on linear regression of the concentration of all elements and their interaction (Fig. 9.19).

For β phase containing NiCoCrAlY coatings, a high amount of β phase or Al-equivalent improves oxidation life and TMF at $T_{max} = 1000°C$. High amounts of Ni-equivalents are detrimental for oxidation but beneficial for TMF at $T_{max} = 800°C$. A high amount of γ phase is beneficial for TMF at $T_{max} = 800°C$ but not favourable for TMF at $T_{max} = 1000°C$.

The effect of reactive elements is important for the metal/oxide interface to reduce void formation, to act as a mechanical key and to tie up sulphur before segregation at the metal surfaces and weakening the TGO adherence. Large concentrations of the most reactive elements result in phases that can harm the mechanical properties.[22] In addition, a high concentration of reactive elements is harmful for oxidation resistance or life (Fig. 9.20).



9.19 Comparison of experimental results with prediction.



9.20 Effect of reactive elements in oxidation of beta phase containing NiCoCrAlY coatings.

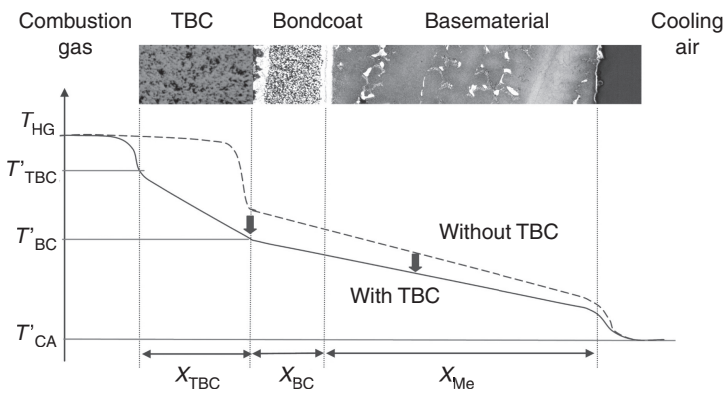
Advanced testing, modelling and validation tools will be required to develop an improved coating for next generation of GTs. The complex loading of turbine parts with respect to oxidation, corrosion and TMF requires an optimised coating with a balanced composition. Part-specific loads may require tailor-made coatings with increased capability in one or the other direction.

9.4.3 Thermal Barrier Coating (TBC) coated substrate

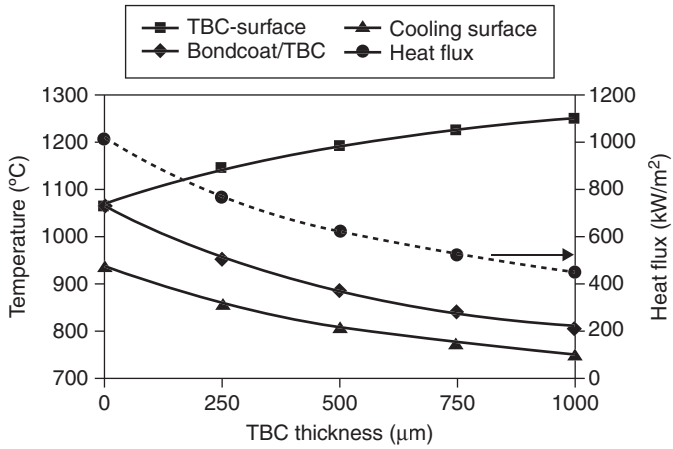
Reduction of the service temperature of a cooled wall can be achieved by reducing the heat conductivity or by increasing the thickness of the TBC (Fig. 9.21). The heat conductivity of porous 7YSZ TBC applied by APS is about $k_{TBC} \approx 1.0$ W/(m·K)[23] (average between 900°C and 1100°C), while that of CMSX4 and MCrAlY is about $k_{Me} \approx 22$–28 W/(m·K) (between 700°C and 1000°C). The one-dimensional heat flux can be described by the following equation (neglecting the interlayer surface resistance)

$$\dot{q} = \frac{1}{\left(1/\mathrm{HTC}_{HG}\right) + \left(X_{TBC}/k_{TBC}\right) + \left(X_{BC}/k_{BC}\right) + \left(X_{Me}/k_{Me}\right) + \left(1/\mathrm{HTC}_{CA}\right)} \times \left(T_{HG} - T_{CA}\right) \quad [9.1]$$

where $\dot{q}$ = heat flux, HTC = heat transfer coefficient of hot gas (HG) or cooling air (CA), X = thickness and k = heat conductivity of TBC, BC or metallic substrate (Me). Often the BC will be integrated to the Me term. The HTC_{HG} has to include convective and radiative heat transfer. The latter is complex to determine, due to the thickness-dependent semi-transparency



9.21 Temperature profile through the wall of cooled GT part (schematic).



9.22 The effect of TBC on material temperature and heat flux (basis for calculation: metal wall thickness 3 mm; hot gas temperature 1400°C, cooling air temperature 600°C; k_{Me} = 24 W/(m·K), k_{TBC} = 1 W/(m·K), $HTC_{HG} = HTC_{CA}$ = 3000 W/(m²·K)).

of 7YSZ for wavelengths less than about 5 μm.[24] For materials purposes, the equation (see Fig. 9.21) can be simplified to

$$\dot{q} = \frac{1}{\left(X_{TBC}/k_{TBC}\right)+\left(X_{Me}/k_{Me}\right)} \times \left(T''_{TBC} - T'_{Me}\right) \qquad [9.2]$$

or, considering only the TBC

$$\dot{q} = \frac{1}{\left(X_{TBC}/k_{TBC}\right)} \times \left(T''_{TBC} - T''_{BC}\right) \qquad [9.3]$$

For 500 μm thick TBC, the heat flux or the amount of required cooling air will be reduced by 40%. Additionally the SX mean temperature will be 130 K and the SX surface temperatures 180 K lower than the uncoated CMSX4 (Fig. 9.22). The temperature gradient of TBC coated SX will be high within TBC (620 K/mm) but low within the metal (25 K/mm) which is much lower than that of uncoated CMSX4 (42 K/mm). Using the example above, the thickness to conductivity ratio for TBC is about four times higher than that of the CMSX4 substrate, which shows that the overall heat flux is determined predominantly by the TBC conductivity and thickness.

The calculation of the local stress/strain of TBC coated parts is very complex when operational conditions with mechanical constrains, gradients, transients and, finally, degradation of material properties have to be considered. Nevertheless, trends can be modelled for simplified boundary

conditions (in-plane stress for a thin ceramic coating at a planar interface Equations [9.4] + [9.5]).

$$\Delta\varepsilon(T) = \Delta\mathrm{CTE}(T) \times \Delta T \quad [9.4]$$

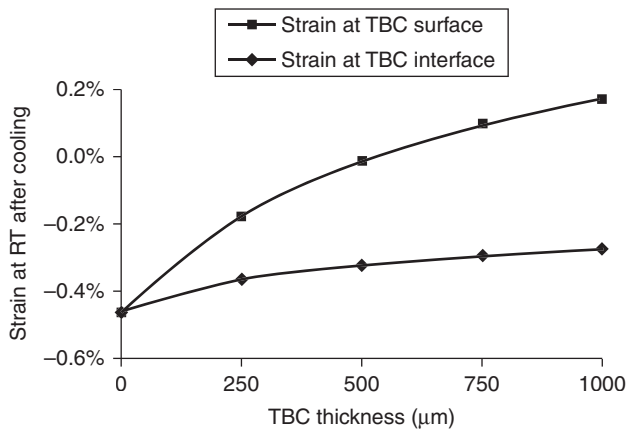
$$\sigma(T,t) = \frac{\Delta\varepsilon(T)}{1-\nu} \times E(T,t) \quad [9.5]$$

where $\Delta\varepsilon(T)$ = temperature dependent mismatch strain, ΔCTE = difference between the coefficients of thermal expansion of TBC and BM, $\Delta T = T - 25°C$ with T = hot dwell temperature before cooling to room temperature, $\nu = 0.30$ Poisson's ratio, $E(T,t)$ = stiffness depending on sintering temperature and time, and $\sigma(T,t)$ = residual stress.[25–27]

The effect of the mismatch of thermal expansion can be easily estimated with the assumption that at high temperature the substrate/BC/TBC has relaxed all stresses and no constraints will affect the thermal expansion of the BM. Cooling from the operation temperature (as given in Fig. 9.22) to room temperature will lead to compressive strains at the TBC interface. For thicker TBCs, the outer surface will be under tensile strain after cooling (Fig. 9.23).

The residual stress/strain is direct proportional to the stiffness of the TBC, depending on porosity and micro-/macro-cracks. With time and temperature, progressing sintering will increase the stiffness (i.e. apparent elastic modulus) and the stress level.

Several experimental and theoretical approaches were made to reduce the mismatch stress. The roughness of the BC was optimised to generate



9.23 Thermal strain of relaxed BM/BC/TBC at operation temperature as given in Fig. 9.23 before cooling to room temperature.

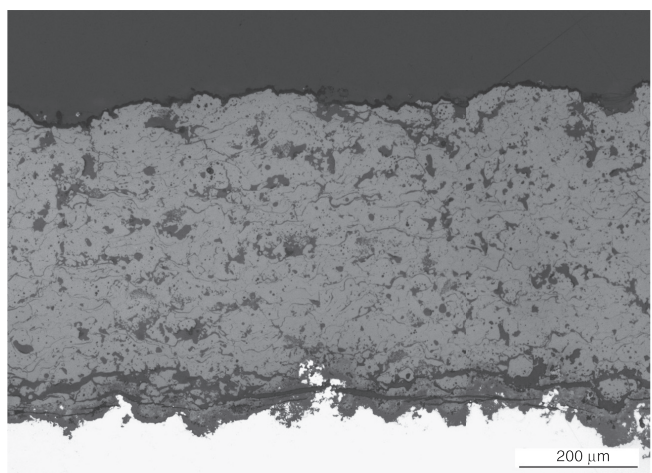
alternating tensile and compressive stresses at the BC/TBC interface to reduce crack propagation.[28] TBC was optimised for low stiffness either by high porosity or by sinter-inhibitors. In addition, dense vertically cracked microstructures have been developed to increase the strain tolerance of TBC coated systems.[29]

Role and limitation of the Bondcoat (BC)

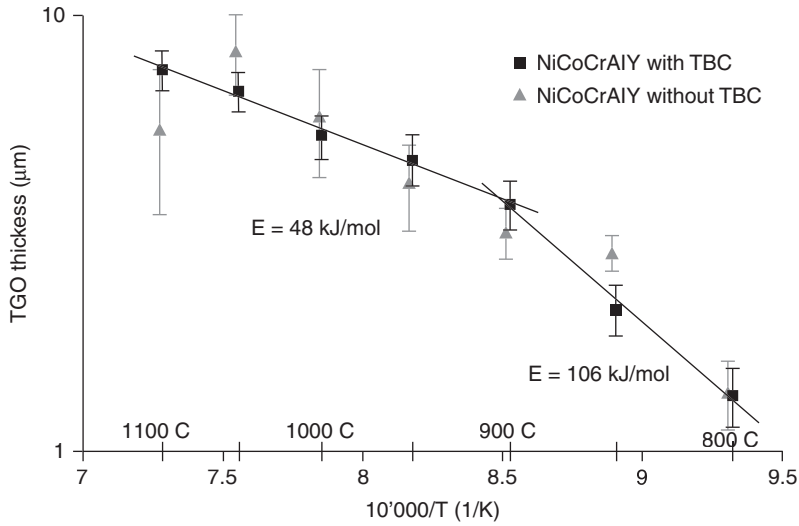
The BC is an important part for the oxidation life and the temperature capability of the BC/TBC system. An oxide scale or a corrosion product of the BC will be formed at the interface with the TBC (Fig. 9.24). This will result in a compressive oxidation growth stress with subsequent TGO or TBC spallation. The TBC is not preventing the oxidation or corrosion of the BC, but it will happen at a lower temperature and, typically, at a lower rate. At high temperature, the BC will form a TGO at this rough interface independently of the TBC. Even the thickness of the TGO is same for MCrAlY-BC, with or without 7YSZ-TBC (Fig. 9.25).

Typically for large combustor parts, BC and TBC are open porous layers when applied by APS without any specific post-heat treatment. In this case, both coatings will not prevent the oxidation or corrosion of the BC and the BM, but it will happen at a lower temperature and at a lower rate compared to uncoated BM. The BC is an important part for the oxidation life and the temperature capability of the BC/TBC system.

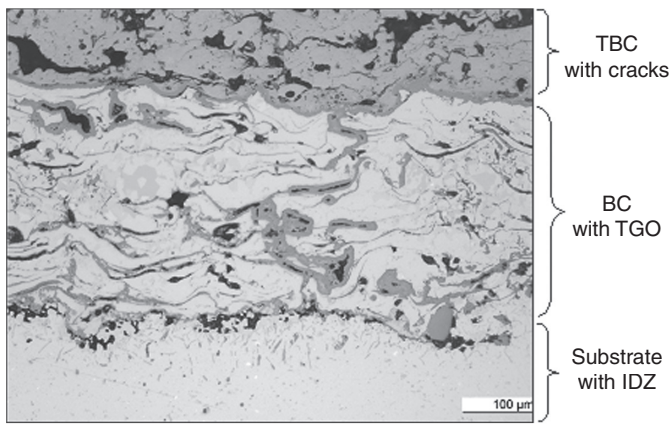
An oxide or a corrosion product of the BC will be formed at the interface with the TBC but also within the porous BC and at the BC/BM interface (Fig. 9.26). This results in a compressive stress within the whole BC and at



9.24 Cross section of coating system (BC/TGO/TBC) after operation.



9.25 TGO thickness on rough MCrAlY coating with or with TBC after 1000 h oxidation under isothermal conditions.



9.26 Cross section of coating system after operation.

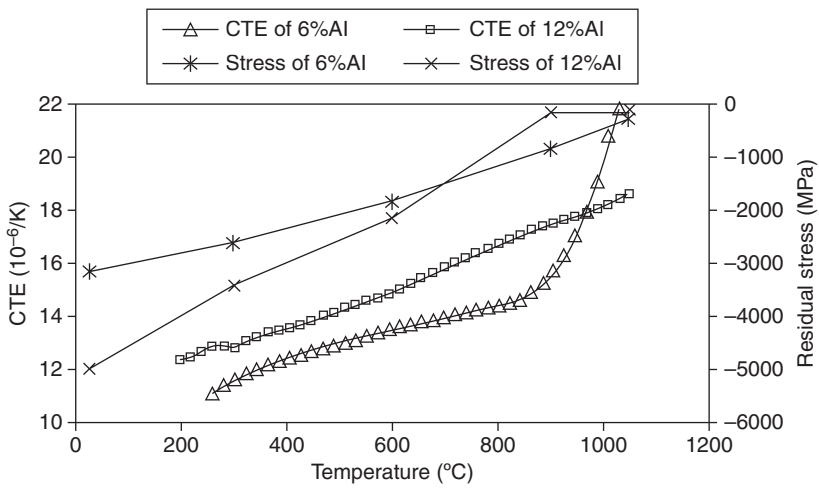
the two interfaces. As long as the metallic BC is not severely oxidised, these oxide growth induced stresses will relax to a great extent during operation at high temperature. Depending on the porosity level and microstructure, the APS sprayed BC could oxidise, due to the enlarged open surface, around ten times faster than the same BC composition coated by LPPS. A general coating consumption curve, similar to Fig. 9.12, cannot be given since the relevant microstructure description (i.e. effective open surface and thickness of the BC, etc.) is included.

Published by Woodhead Publishing Limited, 2013

Similar to the protective coatings, most BC are MCrAlY type coatings, where M = Ni and/or Co. Further elements, such as Si, Ta, Zr, B, Re, etc., were added to improve the adhesion and growth rate of the oxide scale.[30,31] Typically, these MCrAlY coatings contain high amounts of Al (typically 8–12%) to form an alumina TGO at the interface with the TBC. Especially α-alumina is preferred, due to its low oxidation growth rate and a slow growing oxide scale. Nevertheless, all kinds of TGO will spall sooner or later, depending on many parameters affecting oxide scale adherence.

The Pilling–Bedworth ratio (PBR) is the relative volume increase due to oxidation, which leads to strains or stresses of the oxide layer on top of the metal surface. The PBR of Al_2O_3 (PBR = 1.28) is much lower than that of NiO (1.65), CoO (1.86) and Cr_2O_3 (2.05). In all these cases where PBR > 1, oxidation leads to compressive growth stress in the TGO despite relaxation at high temperature. This can result in the spallation of parts of the TGO during oxidation at high temperature.

For two different MCrAlY coatings with 6 wt-% Al or 12 wt-% Al, oxidised for 100 h at 1050°C, a compressive residual stress of the α-alumina TGO of about 200 MPa was measured with *in situ* X-ray diffraction at 1050°C (Fig. 9.27). When cooling down these samples, additional compressive stresses have been generated due to the different CTEs of the TGO and the coated substrates. In agreement with experimental findings, the TGO will spall off preferentially during the cooling phase of thermal cycling. For a cooling rate of 10 K/s, the absolute stress value at room temperature increased to 3000 MPa for 6 wt-% Al or 5000 MPa for 12 wt-% Al respectively. The MCrAlY with lower CTE over most of the temperature range



9.27 Temperature dependence of Residual stress of the TGO and Thermal expansion of MCrAlY with 6% Al or 12% Al, respectively.

showed clearly a lower residual stress level. The different DBTT of both coatings (450°C or 600°C, respectively) does not really affect the stress formation during cooling.[32]

IGTs mostly use BC with a surface roughness of typically Ra = 7–15 μm for mechanical interlocking with an open porous micro-cracked TBC. This roughness can be achieved by adjusting different coating process parameters or BC material compared to the above-described protective MCrAlY coating.

The positive effect of high roughness on TBC adhesion results in a negative one for the oxidation behaviour of the BC. The increased effective surface area will increase the coating consumption and, more importantly, it will increase the overall TGO volume compared to less rough BC surfaces. In addition, the morphology of the roughness profile with smooth or sharp edged structures has a significant influence on TGO adhesion, which is directly linked to TBC spallation.

For more than 20 years, the role of roughness and TGO thickness has been a topic of many theoretical and experimental studies:

- With piezo-spectroscopy, the compressive in-plane stress of about 2–4 GPa for short-term oxidation has been determined with high spatial resolution and BC oxidation and depletion models to predict TGO growth and spallation.[33]
- Experimental studies were performed for various BC compositions to measure the TGO growth rate and phase composition by *in situ* XRD, the critical thickness for TGO and/or TBC spallation for various BC roughness profiles.[32]
- FEM calculations for stress analysis and crack growth along BC/TGO interface considering local relaxation in BC/TGO/TBC were used to predict crack growth.[34]
- Thermal stresses and oxidation-induced stresses have been calculated for thermal cycling loading. Creep effects and the growth of the TGO for simplified roughness profiles of the interface between the bondcoat and the TBC have been simulated. The time-dependent stress distribution in such a model qualitatively explains the influence of BC oxidation and BC roughness on the lifetime of TBC systems.[35]
- Failure by shift of the tensile zone during burner rig thermal cycling was used to explain TBC spallation. Early in life, creep was identified as the prime driver for delamination cracking at the BC peak region. Later, oxidation of the BC will dominate the stress generation, increasing delamination stresses over BC valleys. These results indicate that oxidation is the driver for the continued cracking necessary to cause ceramic layer spallation.[36]

Published by Woodhead Publishing Limited, 2013

- Failure by ratcheting, as of thermal cyclic straining of the BC, leads to crack initiation by fatigue. In this case the number of thermal cycles was seen as the prime driver for TBC spallation.[37]

All these investigations contribute to explain, and to predict, TBC spallation under narrow boundary conditions. A description of performance or dominant failure mechanisms has to consider the loading conditions of oil or gas fired GTs, i.e. oxidation time and temperature, the composition of the combustion gas, the cycling type and frequency or the mechanical and thermal strain. A general temperature capability for a BC, defined as the maximum temperature for the required operational time, cannot be given without defining thermal, mechanical and cyclic loading.

Role and limitation of the TBC

Almost all IGTs are using 7YSZ as TBC material, as it was identified as being the most suitable for cyclic loading. It consists of a metastable t' phase, which can transform with time and temperature to stable tetragonal and cubic phases (thermally induces transformation).[38] In air or clean combustion gas, long-term operation up to about 1200°C seems to be possible, especially when other TBC parameters such as porosity and stiffness are manufactured in the right range. However, in dirtier environments, impurities from fuel, water or intake air form deposits on the TBC surface. At temperatures above 1100°C, the TBC material (7YSZ) can react with these deposits, and impurities such as Ca or Mg can act as unwanted stabiliser forming more cubic phases (environmental induced transformation).[39] For TBC surface temperatures above 1200°C a liquid deposit could infiltrate the porous TBC structure, known as the CMAS effect. In both cases, the stresses during thermal cycling will increase and the strain-to-failure will be reduced.

Sintering of TBC is often described as a root cause for TBC spallation. In general, sintering increases with time and temperature, and leads to densification. The onset sintering temperature for APS coated 7YSZ TBC is between 1000°C and1100°C. Even short-term heat treatment affects healing of micro-cracks and increases stiffness of the ceramic. The sintering of detached TBC (unconstrained free standing bodies) is higher than for a TBC attached to a BC and substrate, which is under tensile stress at high temperature.[40] The sintering of TBC on top of BC/BM occurs at lower sintering temperature, primarily by micro-crack closure and macro-crack opening. At higher sintering temperature the mean pore size and density will change additionally. The overall TBC porosity is nearly unchanged for IGTs with current boundary conditions.

The TBCs applied on combustor parts are very similar to that on turbine part. Due to the generally lower heat transfer on combustor parts, the

Published by Woodhead Publishing Limited, 2013

applied TBC will be much thicker, but the resulting material temperature and mismatch strains are also comparable for both coated systems.

TBC material and microstructure

During the last decades, many oxide ceramics for TBC applications have been investigated concerning thermal expansion, thermal conductivity, thermal shock resistance, thermal stability, sintering, corrosion, manufacturability, etc.[41] Except for a few applications, 7YSZ has remained the material of choice for combustor parts as well as for turbines of industrial GTs.

For current IGT loading, it beneficially combines high thermal expansion, high fracture toughness and moderate intrinsic thermal conductivity. On the other hand, its phase stability, corrosion and sintering behaviour is not appropriate for future efficiency requirements with increased firing and surface temperatures. New compositions with different crystal structures such as Perovskites (i.e. $(Gd,La)AlO_3$), Pyrochlores (i.e. $La_2Zr_2O_7$), Spinels (i.e. $MgO\text{-}Al_2O_3$), or zirconia with all kinds of stabilisers[42] are being tested worldwide within various public funded programmes as single layer, multilayer or graded TBC.[29,43–45] Many invention disclosures reveal activities of companies and research institutes and demonstrate the TBC improvement requirements for future GTs.

Beside the intrinsic material properties, the TBC behaviour strongly depends on the manufactured microstructure with porosity, micro-/macrocracks, grain size and their orientation or special distribution. A wide range of microstructures are realised due to thermal spraying processes, which is the typical application method for IGTs. The use of different powders and powder size distribution (i.e. agglomerated and sintered, 'HOSP' hollow spherical powder, fused and crushed powder, or suspension with nano-sized powder), applied by different methods and parameters, will make a large contribution. Special TBCs with some special microstructural features have been developed (i.e. 'DVC' dense vertically cracked, 'SPS' solution plasma spayed TBC, 'LPPS-TF' low pressure plasma spray thin film, etc.) to improve TBC life or temperature capability.[29]

Lifetime prediction

Many different laboratory tests have been used to predict the behaviour of TBC coated turbine parts with their inherent thermal, mechanical and environmental loadings during long-term operation. None of these tests can reproduce the complex loading scheme of a turbine blade, but they can evaluate specific boundary conditions for failure, i.e. TBC spallation caused by BC oxidation, TBC sintering, material related stresses or strains, thickness and temperature gradients or transients, etc.

Published by Woodhead Publishing Limited, 2013

Most tests for BM/BC/TBC coated systems use cooled samples in a BRT (burner rig test) or uncooled samples in an FCT (furnace cycling test).

In a BRT the heat transfer often varies so severely during heat-up and cooling that, in most cases, a long-term stable temperature gradient over the whole sample cannot be achieved. Thermo-cycling is reduced to transient loading without taking the high temperature degradation and relaxation mechanisms sufficiently into account. For economic reasons, a BRT is done typically on small sample series, which makes a statistical evaluation difficult.

The FCT considers long-term exposure at high temperature with moderate transients during cooling. The large number of samples allows a statistical evaluation, required to separate the various contributions from the coating quality (i.e. TBC porosity, BC roughness and thickness, coating process parameter), BM, thickness and curvature of complex shaped parts.

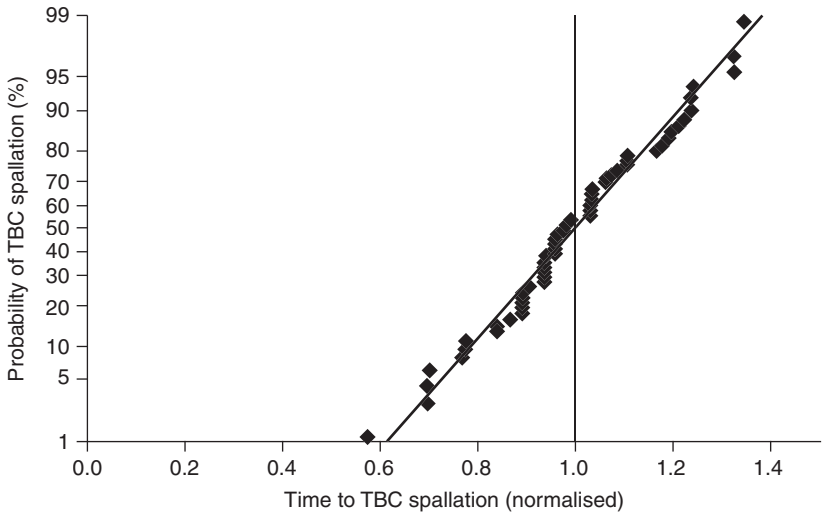
In a BRT with cooled samples but, more importantly, in an FCT with uncooled samples, the temperature has to be adjusted to reflect the typical thermal conditions during service. In TOPPCOAT[29] an average reduction of 250K/mm TBC has been assumed. For benchmarking of different systems, samples with 100 μm thin TBC have been thermo-cycled between 1100°C and RT and compared with 500 μm thick TBC thermo-cycled between 1000°C and RT.[46]

For lifetime prediction, the FCT has been applied over a wide temperature range. Typically, TBC coated buttons or rods, or specimens cut from real turbine blades, have been thermo-cycled until a certain fraction of TBC has been spalled off. This thermo-cyclic life can be described statistically by a Weibull distribution or (in the case of a high shape factor) by a normal distribution (Fig. 9.28) with a minimum lifetime (i.e. probability of TBC spallation less than 1%). On the other hand, the top 10% of this distribution reveals room for improvement to double thermo-cyclic life for the given BC/TBC system (Fig. 9.29).

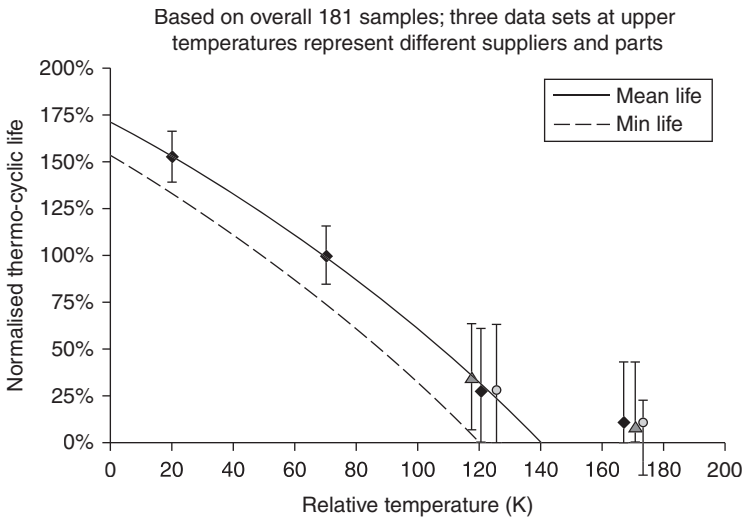
For the typical temperature range of BC, the thermo-cyclic life will be reduced with increasing temperature (about 10–15% relative reduction of life for 10K increase of BC temperature). Additionally, a temperature limit can be seen for mean or minimum life using statistical scattering. To improve the reliability, the maximum BC temperature has to be reduced by 20K for 1σ (84% probability of TBC survival), 40K for 2σ (97.7% probability) or 60K for 3σ (99.86% probability).

Often the TGO thickness before spallation has been considered as a prime parameter for lifetime prediction. The analysis of scatter and the temperature dependence could not confirm this correlation for a broader set of TBC coated samples with the same BC. The TGO thickness correlates well with the BC depletion, both following the parabolic time dependence of Fick's law. After 10 000 h, the oxidation results in a depletion zone of 120 μm and

Published by Woodhead Publishing Limited, 2013

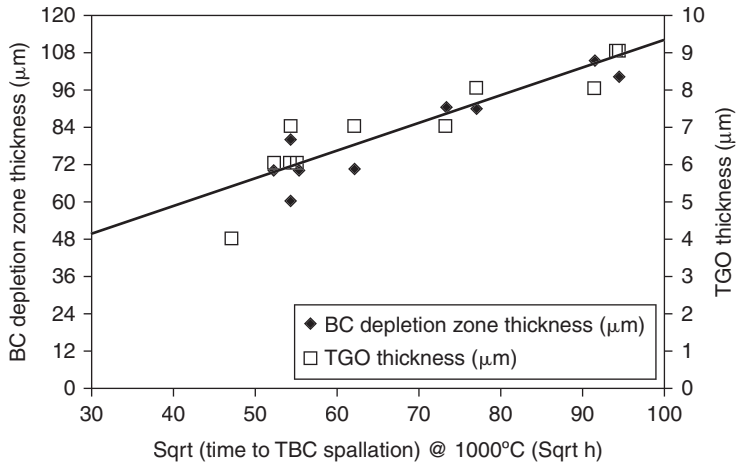


9.28 FCT results for samples machined from 'engine ready' turbine blades.



9.29 Temperature dependence of FCT results for samples, machined from 'engine ready' turbine blades.

a TGO of 10 μm. Some samples exhibit spallation already after 3000 h with 6 μm TGO thickness, while others last 9000 h with 9 μm TGO thickness. root cause analysis of spallation has revealed different mechanisms changing with TBC porosity and thickness. For the typical temperature range of



9.30 TGO and BC depletion zone thickness of spalled TBC samples on same BC.[17]

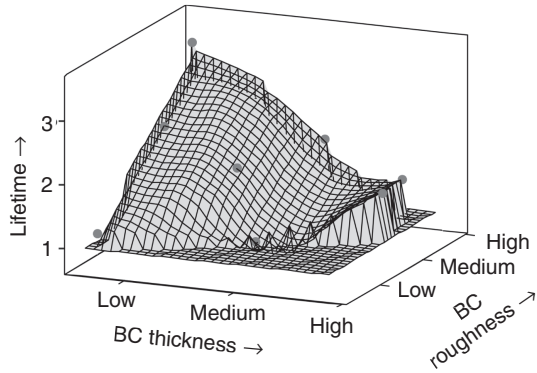
BC used in industrial GT, the TBC quality parameters appear to be more sensitive for TBC spallation than those of the BC. Exceeding a critical BC temperature the TBC spalled off very early without a suitable correlation with the known TBC quality parameter (Fig 9.30).

Optimised BC/TBC system for blading

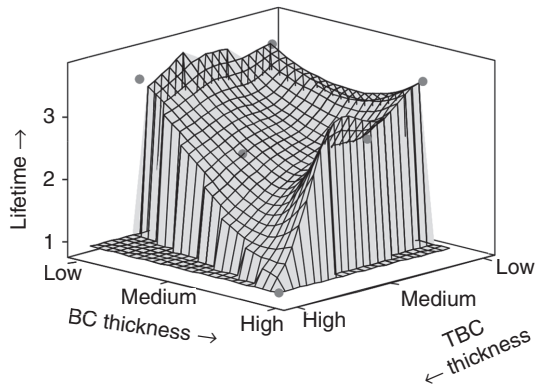
The main task of a BC/TBC system on a turbine part is to enable its efficient operation in hot combustion gas without excessive cooling. Reduced cooling will result in a reduced heat flux through the TBC coated wall and an increased temperature of BC and BM (see Equation [9.1]). A shorter life of the coated part due to LCF, TMF or creep of the BM and/or TBC spallation can be expected. To mitigate these effects, the TBC thickness could be increased and/or the conductivity reduced.

A DoE study revealed the importance of various BC and TBC parameters. Initiation and propagation of TBC spallation of coated blade have been investigated by a long-term FCT to evaluate their life span.[47] The study demonstrated that for an established BC/TBC system and manufacturing process, no individual parameter but an interaction of various BC and TBC parameters is most critical for failure. Consequently, the optimisation of this parameter set offers potential for significant life extension.

The influence of BC thickness or BC roughness on the TBC lifetime can be seen in (Fig. 9.31): For high BC thickness, the variation of BC roughness over a wide range does not interfere and vice versa. On the other hand, for low BC thickness, the variation of BC roughness is very important and the lifetime increased three-fold, doubling the roughness.



9.31 The influence of BC thickness and BC roughness on TBC lifetime.

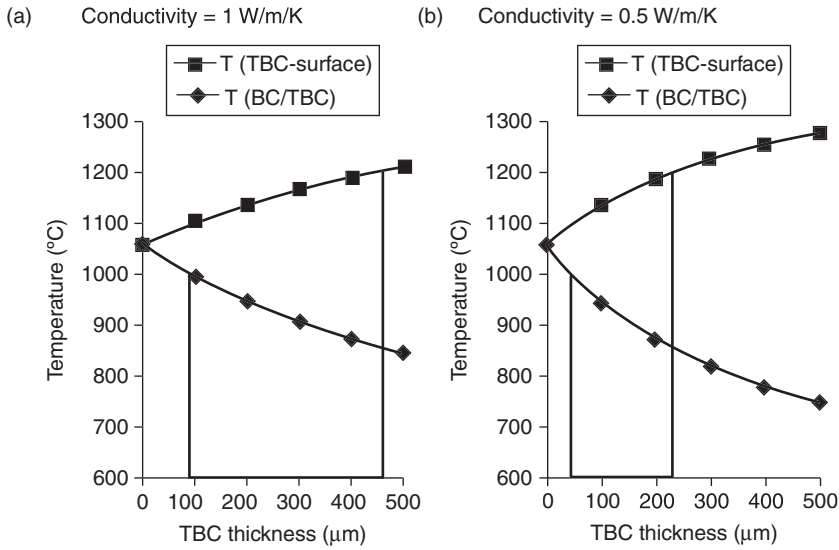


9.32 The influence of BC thickness and TBC thickness on TBC lifetime.

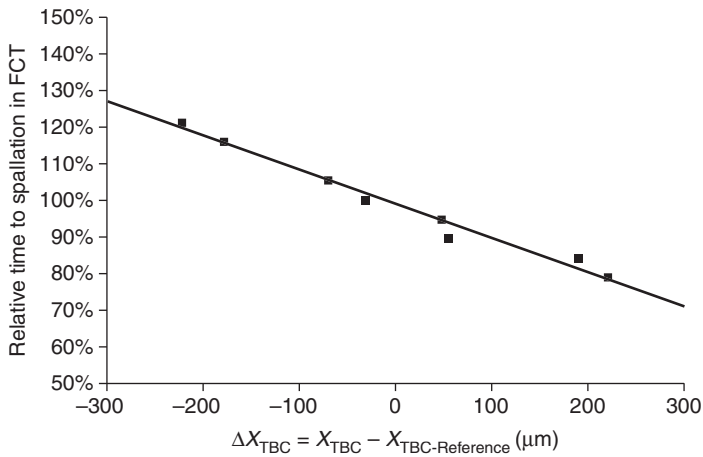
A second example demonstrates the risk of early TBC spallation when a couple of coating parameters is not optimised (Fig. 9.32): For a low BC thickness, the variation of TBC thickness over a wide range does not interfere, and vice versa. Only by increasing BC and TBC thickness, the time to TBC spallation dropped dramatically. Further parameters, such as porosity, conductivity and stiffness of the TBC, exhibit similar cross dependencies.[47]

For the given BC/TBC system of a blade, the highest lifetime can be achieved with thin and rough BC, coated with porous, thick TBC.

Beside the BC and TBC qualities, their temperature capabilities have to be considered. Using typical turbine numbers as given in Fig. 9.22, and assuming a maximum temperature for the BC of 1000°C and 1200°C for the TBC for long-term operation in turbines, the TBC thickness must be in the range between 100 and 450 μm for a standard TBC with a conductivity of 1 W/(m·K) (Fig. 9.33). In the case of TBC with half the conductivity, it must be much



9.33 TBC thickness range depending on BC and TBC temperature capability for standard TBC (a) and low conductivity TBC (b).



9.34 Influence of TBC thickness on time to TBC spallation for a given BC temperature.

thinner and tolerates less thickness variation. Within those limits, high TBC thickness results in low BC temperature, which is assumed to be favourable for the time to TBC spallation. On the other hand increasing the TBC thickness will reduce the TBC life considering the same BC temperature (Fig. 9.34).

Published by Woodhead Publishing Limited, 2013

To cash in the benefit of TBC coated blades for longer life and/or less cooling requirements, the BC/TBC system must be well balanced concerning the pros and cons of TBC thickness as well as those of TBC conductivity.

The effect of TBC coated substrate

The heat transfer on combustor parts is generally lower than on turbine parts, such that the BC/TBC system has to be adapted to the thermal boundary conditions of combustor parts. The reduction of the temperature for a cooled wall can be achieved by adjusting the heat conductivity or the thickness of the TBC. The heat conductivity of porous 7YSZ TBC applied by APS is about $k_{TBC} \approx 1.0$ W/(m·K)[48] (average between 900°C and 1100°C), while that of Hast X between 700°C and 900°C is $k_{Hast\ X} \approx 23–27$ W/(m·K).[49] The heat flux and the temperatures have been calculated according Equation [9.1] using HTC = 1500 W/(m²·K), $T_{hg} = 1450$°C, $T_{ca} = 500$°C.

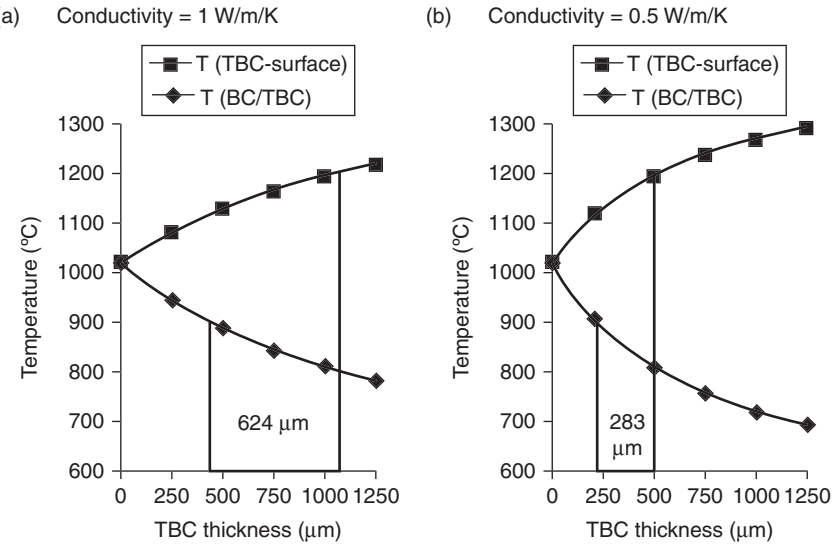
For 1 mm thick TBC, the heat flux or the required amount of cooling air will be reduced by 40%. This leads to a Hast *X* temperature reduction of 170 K compared to uncoated Hast *X*. The temperature gradient will be high in the TBC (385 K/mm) and low in the metal (16 K/mm), which is lower than for uncoated Hast *X* (27 K/mm). Using the example above, the thickness to conductivity ratio for TBC is about seven times higher than that of the Hast *X* substrate, and the overall heat flux is determined predominantly by the conductivity and thickness of the TBC.

Similar to the limitations of the BC/TBC for turbine parts, the TBC thickness must be adjusted to the temperature capability of the BC of large combustor parts. This BC is typically applied by APS and is less oxidation resistant due to some open porosity. A maximum temperature of 900°C for the BC and 1200°C for the TBC for long-term operation is assumed for the calculation of BC and TBC thickness (Fig. 9.35). The lower heat transfer allows a wide scatter for TBC thickness for a given conductivity, but only a small manufacturing range in case of conductivity variation.

9.4.4 Engine experience

TBC coated combustor parts are designed for long-term operation without replacement. Ex-service parts have been investigated to identify the degradation or failure modes for remnant life assessment and to develop and validate lifetime prediction models. Investigation methods, especially for ex-service parts, have been developed to determine the average TBC surface temperature during operation, the stiffness over the TBC and the strain-to-failure of the aged and degraded BC/TBC system:

- Temperature has been determined by XRD. Rietfeld refinement was used to quantify the four phases resulting from phase transformation of



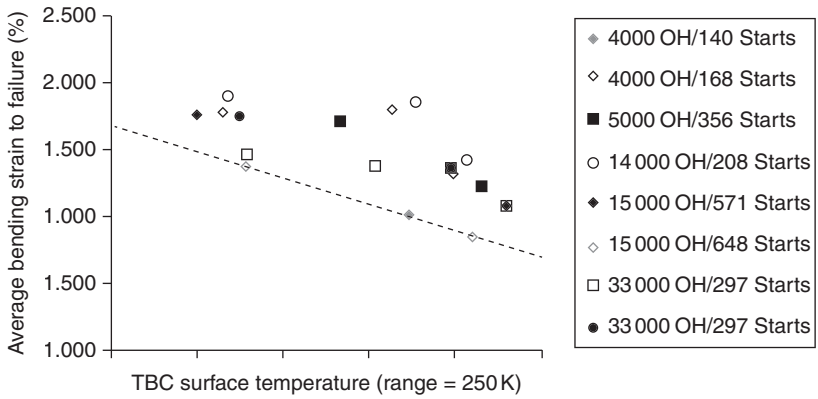
9.35 TBC thickness range depending on BC and TBC temperature capability for standard TBC (a) and low conductivity TBC (b).

the metastable 7YSZ.[50] This method has been developed for an accuracy of about ±25 K.

- The stiffness of the TBC has been measured with Knoop hardness indentation, considering the different elastic–plastic deformation of the short and long axis of the imprint.[51] Loads of 10 N have been applied to generate imprints of typically 200 µm, covering a part of the splat-like TBC microstructure. Values are in good agreement with other methods.[29,52]
- Strain-to-failure has been evaluated by four-point bending equipped with acoustic emission to detect the critical strain of start of TBC delamination, macro-cracking or spallation. To simulate the loading during cooling the TBC was tested under compressive loading (Fig. 9.36).

The average TBC surface temperature during operation was determined by measuring the thermal and environmental phase transformation of 7YSZ. Samples for four-point bending have been taken from different temperature zones of the combustor liners of GTs with different histories. The BC/TBC interface strain, which led to TBC spallation at room temperature, decreases by 10% (relative) with 50 K increased surface temperature. This behaviour is more or less independent of the operational periods and cycles of the considered GTs. In this case, none of the liners has shown life limitation due to oxidation. The dominant temperature dependence of strain-to-spallation indicates degradation of the TBC (Fig. 9.36).

Published by Woodhead Publishing Limited, 2013



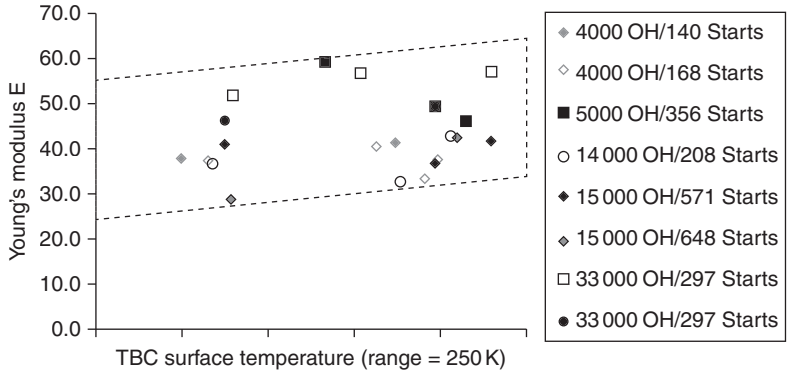
9.36 Strain-to-failure of 4-point-bend samples, taken from ex-service combustor liner of various GTs with different operation schemes (operation hours [OH]/cycles [Starts]).

The stiffness of the TBC surface indicates a slight increase with temperature and operation time. This is superimposed by thermo-cycling (starts), which promotes micro-/macro-cracks and reduces the stiffness of the TBC (Fig. 9.37).

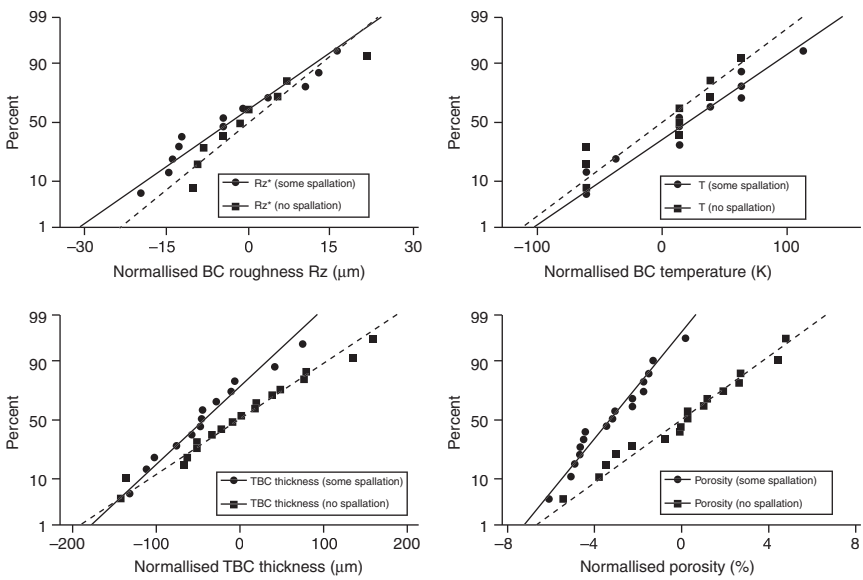
The thermo-mechanical loading of turbine blades and vanes spreads over a wide range of temperatures, strains, stresses and shape with convex and concave radii. Based on the various loading schemes different failure mechanisms and lifetimes can be expected. To identify the most important coating quality parameters, a statistical evaluation has been used:

- Effect of coating quality parameters for same loading (Fig. 9.38):
  Blades with some TBC spallation have been compared with those without TBC spallation, originating from the same turbine and operation conditions. For this set of blades the TBC porosity distribution demonstrates a lower porosity (in average about 3%) for the parts with some spallation than without spallation. The other assessed parameters are quite similar for both groups.
- Effect of coating quality parameter for different loading (Fig. 9.39):
  Blades of two different stages of the same turbine, but with the same coating system, have been compared. The HPB revealed no spallation, and the LPB some spallation. TBC porosity and BC roughness were quite comparable for both systems. The main difference was found for BC and TBC thickness, which in average were about 40% thicker for parts showing some TBC spallation,

For industrial GTs operating in a 'dirty environment', a BC/TBC failure mechanism based on fuel or air borne impurities has been seen. The TBC

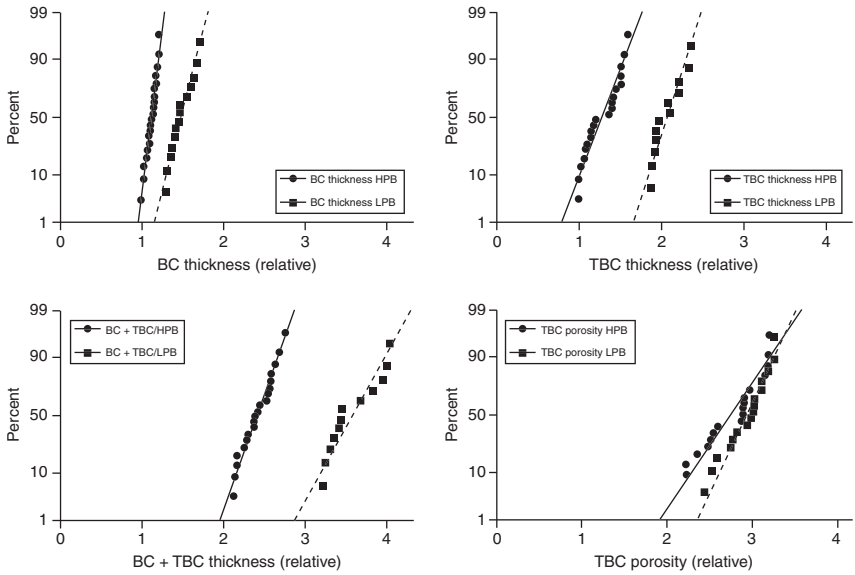


9.37 Stiffness (measured by knoop hardness) and temperature at TBC surface of ex-service combustor liners of various GTs with different operation schemes (operation hours [OH]/cycles [Starts]).

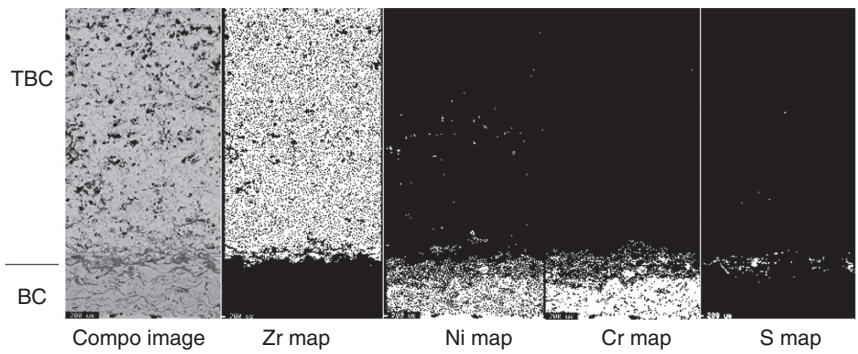


9.38 Comparison of coating parameters of parts with spallation (□) and without spallation (○) from same turbine stage.

material 7YSZ can be destabilised by combustions products, formed due to the injection of dirty fuel or water or the ingestion of fine dust and salts, even through the filter systems of the air intake. High concentration of Na, K and S in the fuel or water will form alkali sulphates in the combustion gas,



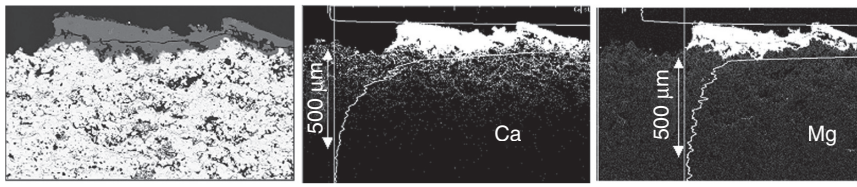
9.39 Comparison of coating parameters of parts with spallation (□) and without spallation (○) from different turbine stages.



9.40 Hot corrosion attack of BC/TBC.

migrating through the open porous TBC to condense as a solid deposit at the BC/TBC interface up to about 900°C. The MCrAlY will be attacked by the sulphur-induced hot corrosion, forming voluminous corrosion products at the interface (Fig. 9.40).

At high temperature, molten deposits of calcium-magnesium-alumina-silicate (CMAS) deposits can be formed, which interact with the 7YSZ by either infiltration or accelerated phase transformation.



9.41 CMAS deposit on TBC, infiltration and reaction at top TBC part Semi-quantitative concentration profiles of Ca and Mg.

The infiltration, filling pores and micro-cracks with molten CMAS, leads to an increased stiffness due to the densification of the TBC and finally results in an increased compressive stress in the TBC at room temperature.[53]

The transformation of the metastable t' phase to tetragonal and cubic phases is accelerated because in additional to the thermal induced transformation (described above), an environmentally induced transformation is taking place.[54] The example of Fig. 9.41 shows that nearly no infiltration of the TBC has occurred. The temperature of the TBC has been lower than the melting point of CMAS (1200–1230°C). Nevertheless, CMAS lead to a corrosive reaction with the TBC for the outermost 500 µm. This outer part of the TBC consists predominantly of cubic phase due to the reaction with Ca and Mg, while the inner part remains nearly completely composed of metastable t' phase.

All three effects, hot corrosion, infiltration and phase transformation, do change the cyclic behaviour of the TBC, which finally leads to spallation.

9.5 Ceramics for hot gas path parts

Ceramics for GT components have been under development for half a century, with intensifying research activities during last two decades. The motivation for the introduction of ceramics is based on their high temperature capability, low thermal conductivity, and low density. For such application, monolithic parts of non-oxidic ceramics (i.e. silicon carbide or nitride) or oxidic ceramics (i.e. alumina, zirconia or mullite) have been investigated. Despite generous public funding in the USA, Japan and Europe, the commercial break-through is limited to a few users, suppliers and applications, which can be explained by the boundary conditions of product development.

The interesting GT products and materials to be substituted by ceramics were continuously optimised concerning design, materials, manufacturing and cooling technologies to enable higher temperature capability and product reliability. The hurdle to introducing ceramic parts is steadily increasing because of the continuous improvements made with the current products, i.e. efficiently cooled TBC coated parts for high temperature.

Published by Woodhead Publishing Limited, 2013

On the other hand, the GT environment with increasing firing temperature, high humidity of the combustion gas, and high thermo-mechanical gradients and transients has revealed limitations of several ceramic materials that already have been successfully used for other high temperature applications, such as the protection of rockets or cement calcination devices. The effect of humidity at high temperature and pressure was initially underestimated. Especially the silicon containing ceramic materials require oxidation protection.[55]

Manufacturing processes and proof test methods have been developed to reduce the effect of surface and volume flaws for newly designed monolithic ceramic vanes.[56] To improve the reliability, especially for larger ceramic parts, CMC has been used either as whole part or as hybrid part where a CMC support structure is combined with monolithic ceramic layer for protection or economic reasons. The gain of higher fracture toughness compared to fully monolithic ceramic parts must be balanced with lower high temperature strength and significantly higher costs. Long-term field tests have been performed for stationary GTs to demonstrate the feasibility of CMC components with enhanced life for large combustor parts.[57]

However, the various ceramic materials and manufacturing processes reveal inherent strength and weaknesses, which have to be balanced for reliable and competitive products:

Monolithic ceramic parts need further improvements on:

- fracture resistance (i.e. by increased material toughness, strain tolerant design, stable manufacturing processes),
- long-term oxidation/corrosion resistance in combustion gas environment (i.e. by chemical stability of the ceramic material or protective coatings), and
- cost reduction for material and manufacturing (i.e. low-cost powders/precursors, near-net-shape manufacturing for low final machining, reliable non-destructive quality or proof test).

For CMC and hybrid parts, the fracture resistance has been improved, but further improvements are necessary for:

- high temperature behaviour (>1200°C) of strength, thermal stability and oxidation/corrosion,
- understanding of constitutive behaviour and failure mechanisms, requiring different solutions for short or continuous fibres (i.e. interaction with matrix, oxidation/corrosion and protection by coatings),
- cost reduction for materials (especially for continuous fibres) and manufacturing, each with similar approaches as described for monolithic ceramics.[58,59]

Published by Woodhead Publishing Limited, 2013

The selection of material for fibres, matrix or coating suitable for combustion gas environment at temperatures in the range of 1200–1500°C appears very challenging. Additives used for improved manufacturing (i.e. boron, carbon, alumina in SiC or refractory oxides in Si_3N_4) dominate the oxidation and corrosion behaviour, resulting in high rate of external and internal degradation.[60]

Finally, the assembly or joining within a metallic combustor or turbine part has to be solved. Mechanical clamping can be used only for moderate temperatures and restricts the temperature capability of most ceramics. Joining of metal to ceramic also reveals deficits on high temperature stability in combustion gas environments.[61,62]

For reliable use of ceramics under all loading conditions, new design rules, data and procedures must be developed, generated and validated. Although ceramics have been successfully used in several areas and products, they still require development for use in advanced GT applications.[63]

9.6 Rotor parts

IGT rotors are constructed from forged discs, which are either joint mechanically (bolted) utilising hollow shafts, and centre shaft (rod), or are welded together. Independently of the design approach, turbine disks are typically the most critical components of the rotor, due to a combination of elevated temperature exposure with high circumferential load from the blades. In order to limit the metal temperature, the rotor design widely uses air-cooling through the bored channels.

Compared to aircraft engines, the discs are of large size, and thus manufacturability and detectability of defects become major material selection criteria.

Manufacturing of IGT rotor disks is considered as a high technology of the steel industry, due to the very tight requirements with respect to alloy impurities and homogeneity of the structure of large forgings. Rotor alloys are produced using vacuum arc remelting (VAR), electro-slag remelting (ESR), or vacuum degasation processes. Subsequently, the disks are forged in an open-die or closed-die process, and heat-treated to provide the final structure and properties. After a first machining and welding (in the case of welded rotor design), a final rotor machining is required.

The quality inspection consists of:

- NDT of each forging using ultrasonic and magnetic particles techniques,
- tensile, impact, fatigue and rupture tests of material from disc forging,
- spin test of discs and spin test of assembled rotor,
- NDT of rotor before and after spin test.

Published by Woodhead Publishing Limited, 2013

Table 9.3 Chemical composition of rotor materials, wt%

Type	Fe	Ni	Cr	Mo	W	Nb	Ti	Al	C	N
St 572S	94.4	3	1.8	0.6	0	0	0	0	0.25	0
Cr-Mo-V	96.7	0.5	1	1.25	0	V0.25	0	0	0.3	0
St1OTS	87.5	0.5	10	1	1	V 0.22	0	0	0.12	0.05
St13TNiEL	84.5	2.4	11.5	1.6	0	V0.25	0	0	0.12	0.05
M152	83.7	2.5	12	17	0	V0.3	0	0	0.12	0
IN 706	36	42	16	0	0	3	1.8	0.5	0.06	0
IN 718	20	52	19	3	0	4.2	1	0.4	0.08	0

9.6.1 Rotor steels

Rotors of older turbines as well as compressor side disks and other low temperature components (rods, front and rear hollow shafts, spacers) in advanced turbines are made of low-alloy martensitic, carbide-strengthened Cr-Mo-V or Ni-Cr-Mo-V steels. Typical grades are 26NiCrMoV115 (St572S) used in Siemens and Alstom turbines, and Cr-Mo-V steel used by GE (Table 9.3).

Low-alloy rotor steels are quenched and tempered, which provides a combination of good toughness, especially important in bore area, with sufficient creep and fatigue properties at operation temperatures. These steels have also been proved to be stable against embrittlement at elevated temperatures after hundreds of thousands of hours of service.

Parts that operate at higher temperatures, such as high-pressure compressor disks (with compressor air discharge temperature 400–600°C), turbine disks and drums in advanced turbines, require more temperature-resistant materials. Over past decades, there has been a significant international effort in the development of high temperature 10–12% Cr rotor ferritic steels (driven by steam turbine developments) within European COST, US EPRI and Japanese EPDC programs. The conflicting requirements, such as high strength, high toughness, creep resistance at temperatures up to 600°C, and long-term stability of the microstructure and properties have made the optimisation of steel chemistry and processing quite complex. This class of steels is also alloyed with Mo and V, which form fine M_2C carbides and slow down the formation of coarse $M_{23}C_6$ carbide structure and improve tempering resistance, but promote the formation of delta ferrite, reducing its strength. Ni suppresses delta ferrite but reduces the tempering resistance.

For IGT rotors, the two most widely used commercial steels of this type are St10TS (or similar X12CrMoWVNbN1011), M152 and St13TNiEL (Table 9.3). Both steels are austenitised at 1060–1070°C. Compared to St13TNiEL, the steel St10TS has a higher tempering temperature (690°C compared to 640°C), and at 550°C, a higher strength and creep resistance.

Published by Woodhead Publishing Limited, 2013

On the other hand, St13TNiEL has higher properties up to 500°C, higher fracture toughness and lower fracture appearance transition temperature (FATT).

10–12% Cr steel disks are used in both bolted rotors (Siemens and Mitsubishi designs) and in welded ones (Alstom design). Welded ferritic rotors have proved to be extremely robust, with failure-free life beyond 150 000 h.

9.6.2 Ni-base alloys

Nickel-based, precipitation-hardened superalloys are widely used for aircraft rotors. The most typical example is IN718 (Table 9.3), which has also been used for decades for rotor wheels in small air-derivative IGT turbines. This alloy has an Ni-based austenitic matrix with Cr, Mo atoms acting as solid solution strengtheners, and precipitates of disc-shaped $Ni_3(Nb,Ti)$ γ'' phase as well as small amounts of Ni_3Al–based γ' phase coherent with the matrix. Nb, Ti and Cr also form MC and $M_{23}C_6$ carbides, which strengthen the grain boundaries. The precipitates provide effective long-term stable hardening of the alloy at temperatures up to 650°C. Above this temperature, thermodynamically unstable γ'' transforms into the stable but needle-like, brittle δ phase.

In the past, there have been some hurdles for the introduction of superalloys for the production of large IGT parts, namely the segregation tendency and metastable phase structure, which was very difficult to control in large IN 718 forgings and leading to problems in hot workability and machinability.

The alloy IN706 (Table 9.3) was developed to resolve the main problems: without Mo and only reduced Cr content, the matrix of IN706 is less saturated with solid solution elements, a part of Nb is replaced by Ti, the carbon content is reduced, and, finally, increased Fe content reduces raw material costs. This allowed GE to introduce IN706 as the main material for turbine disks in F–class engines.

The high temperature properties of IN706, although lower than those of IN718, are clearly superior to the mechanical properties of rotor steels. The positive effect, however, is at least partially consumed by the higher stresses in Ni-base parts, due to less beneficial physical properties (E-modulus, thermal expansion). Additionally, rotor Ni-base alloys need a very tight metallurgical control, as at temperatures above 550–600°C they can be sensitive to stress assisted grain boundary oxidation (SABGO) problems. Thus, application of Ni-base rotor alloys in large IGT engines remains a subject of design philosophy, with no common position in the industry.

Published by Woodhead Publishing Limited, 2013

9.7 References

1. Barrett, C. A. and Lowell, C. E. (1977), Resistance of Ni-Cr-Al alloys to cyclic oxidation at 1100 and 1200°C. *Oxidation of Metals,* **11**(4), pp. 199–223.
2. Smialek, J. L. (1998), Toward optimum scale and TBC adhesion on single crystal superalloys. *High temperature materials chemistry*, 3–8 May, San Diego, CA, United States. Herausgegeben von Glenn Research Center. #2808.
3. Schlachter, W. and Gessinger, G.H. (1990), *High temperature materials for power engineering*, Ed. Bachelet, E., *et al*., Kluwer, Liege, pp. 1–22.
4. Harris, K. and Erickson, G. (1987), Patent US4643782 (A) Single crystal alloy technology. 1987–02–17.
5. Konter, M., Newnham, M. and Tönnes, C. (1990), Patent EP0914484 (A1) Nickel base superalloy. 1999–05–12.
6. Reed, R. G. (2006), *The Superalloys, Fundamentals and Applications*. Cambridge University Press, p. 22.
7. Erickson, G. L. (1996), Superalloys, Ed. Kissinger, R. D. *et al*., *8th International Symposium on Superalloys 1996*, Champion, Pennsylvania, 1996, TMS.
8. Fährmann, M., Fährmann, E., Paris, O., Fratzl, P. and Pollock T. M. (1996), Superalloys, Ed. Kissinger, R. D. *et al*., *8th International Symposium on Superalloys 1996*, Champion, Pennsylvania, 1996, TMS.
9. Ford, D. A. and Arthey R.P. (1998), *Materials for Advanced Power Engineering*, Ed. Lecomte-Beckers *et al*., FZ Jülich Publ., Liege, p. 679.
10. Wahl, J. B. and Harris, K. (2012), New single crystal superalloys, CMSX-7 and CMSX-8. Pre-print of article submitted to Superalloys 2012, *12th International Symposium on Superalloys*, Champion, Pennsylvania.
11. Hugo, F., Mayer, H. and Singer, R. F. (1994), Directional and single crystal solidification using liquid metal cooling, *Investment Casting Institute 42nd Annual Meeting 1994*, Atlanta, Georgia, USA, 25–28 September 1994, Investment Casting Institute.
12. Konter, M., Kats, E. and Hofmann, N. (2000), A novel casting process for single crystal gas turbine components, Superalloys 2000, *9th International Symposium on Superalloys 2000*, Champion, Pennsylvania, 17–21 September 2000, TMS.
13. Konter, M., Guido, M., Roesler, J. and Baumann, R. (1994), Castability of directionally solidified ni-base superalloys. In: *Materials Research for Engineering Systems*, Ed. Ilschner, B., *et al*., TechnischeRundschau, Hallwag AG, Bern.
14. Flemings, M. C. (1974), *Solidification Processing*. McGraw-Hill College Pbl., pp. 47–49.
15. Tukagoshi *et al*. (2005), Latest technology for large-capacity gas turbine, Mitsubishi Heavy Industries, Ltd., *Technical Review* Vol. 42 No. 3 (October 2005).
16. Haynes International, Inc. (Hg.) (1992), Oxidation resistance of HAYNES high-temperature alloys. Haynes International – Technical Information. Kokomo, Indiana.
17. Srivastava, S. K., Newburn, M. J., Cotner, J. P. and Richeson, M. A. (2007), Long-term oxidation behavior of selected high temperature alloys. GT2007–28269. *American Society of Mechanical Engineers (ASME) (Hg.): ASME Turbo Expo 2007: Power for Land, Sea and Air. Proceedings of the GT2007,* 14–17 May 2007, Montreal, Canada.

Published by Woodhead Publishing Limited, 2013

18. Chang, S. Y., Krupp, U. and Christ, H.–J. (1999), The influence of thermal cycling on internal oxidation and nitridation of nickel-base alloys. In Michael Schütze, W. J. Quadakkers (Eds.): *Cyclic Oxidation of High Temperature Materials. Mechanisms, Testing Methods, Characterisation and Life Time Estimation; Proceedings of an EFC Workshop,* Frankfurt/Main, London: Published for the European Federation of Corrosion by IOM Communications, pp. 63–81.
19. Bordenet, B. and Bossmann, H. P. (2004), Development of a new test method of high temperature corrosion in gas turbines based on thermodynamic modelling. In Pierre Steinmetz, Ian G. Wright (Eds.): *High Temperature Corrosion and Protection of Materials. 6. Proceedings of the 6th International Symposium on High Temperature Corrosion and Protection of Materials*, Les Embiez, France, 16–21 May 2004. Uetikon-Zürich: Trans Tech Publ. (Materials science forum, 461/464).
20. Smialek, J. L. (1998), *Toward Optimum Scale and TBC Adhesion on Single Crystal Superalloys. High Temperature Materials Chemistry*, 3–8 May 1998, San Diego, CA, United States. Herausgegebenvon Glenn Research Center.
21. Bossmann, H. P., Witz, G. and Baumann, R. (2011), Development of reliable thermal barrier coatings for high-loaded turbine and combustor parts. In VGB Power Tech e.V. (Ed.): *Gas Turbines and Operation of Gas Turbines 2011*. VGB Fachtagung am 11./12. Mai 2011 in Offenbach/Main.
22. Birks, N., Meier, G. H. and Pettit, F. S. (1994), Forming continuous alumina scales to protect superalloys. *Journal of Metals* (JOM), **12**, 43–46.
23. Brito, M. E. (Hg.) (2005), Developments in advanced ceramics and composites. A collection of papers presented at the *29th International Conference on Advanced Ceramics and Composites*, 23–28 January 2005, Cocoa Beach, Florida. Westerville, Ohio: American Ceramic Soc. (Ceramic engineering and science proceedings, 26,8).
24. Eldridge, J. I., Spucklearn, C. M., Street, K. W. and Markham, J. R. (2002), Infrared radiative properties of yttria-stabilizezd zirconia thermal barrier coatings. *26th Annual Conference on Advanced Ceramics and Composites,* 13–18 January 2002, Cocoa Beach, FL, United States. Edited by NASA Glenn Research Center.
25. TBC Interagency Coordination Committee (1997), TBC Workshop 1997. Various Reports. TBC Interagency Coordination Committee. Cincinnati.
26. Chang, G. C., Phucharoen, W. and Miller, R. A. (1985), *Thermal expansion mismatch and oxidation in thermal barrier coatings*. In Its Turbine Engine Hot Section Technology, 1985, 405–425 (See N88–11140 02–39). Herausgegeben von Glenn Research Center.
27. Chang, G. C., Phucharoen, W. and Miller, R. A. (1987), *Thermal expansion mismatch and plasticity in thermal barrier coating*. In Its Turbine Engine Hot Section Technology, 1987, 357–368 (See N89–17298 09–39). Herausgegeben von Glenn Research Center.
28. Brindley, W. J. and Miller, R. A. (1990): Thermal barrier coating life and isothermal oxidation of low-pressure plasma-sprayed bond coat alloys. *Surface and Coatings Technology,* **H. 43/44**, S. 446–457.
29. TOPPCOAT, Final report, Project no. AST4-CT-2005–516 149; Project co-funded by the European Commission within the Sixth Framework Programme (2002–2006).
30. Vosberg, V. R., Clemens, D., Berger, M., Quadakkers, W. J., Fischer, W. and Nickel, H. (24–27 June 1996), Stresses in alumina scales on high temperature

alloys measured by X-ray and optical methods. 9. Arbeitstagung Angewandte Oberflächenanalytik. ForschungszentrumJülich GmbH (KFA).
31. Huntz, A. M., Zhao, J. G., Boumaza, A. and Moulin, G. (1988), Parameters affecting oxide adherence in nickel based alloys and techniques allowing estimation of adherence. *Materials Science and Technology,* **H. 4**, S. 470–478.
32. Alstom propriety investigation and data.
33. Lipkin, D. M. and Clarke, D. R. (1996), Measurement of the stress in oxide scales formed by oxidation of alumina-forming alloys. *Oxidation of Metals,* **H. 45**(3/4), S. 267–281.
34. Beck, T., Trunova, O., Herzog, R. and Singheiser, L. (November 2009): Damage evolution and lifetime prediction of APS TBCs under isothermal and thermocyclic loadings. 11. *Jülicher Werkstoff Symposium – Processes and materials for tomorrow's thermal barrier coatings*. Veranstaltungvom November 2009. Jülich.
35. Kerkhoff, G., Vassen, R. and Stöver, D. (1999), Numerically calculated oxidation induced stresses in thermal barrier coatings on cylindrical substrates. In: Schütze, Michael; Quadakkers, W. J. (Hg.): *Cyclic Oxidation of High Temperature Materials. Mechanisms, Testing Methods, Characterisation and Life Time Estimation; Proceedings of an EFC Workshop,* Frankfurt/Main. London: Published for the European Federation of Corrosion by IOM Communications, S. 373–382.
36. Freborg, A. M., Ferguson, B. L., Petrus, G. J. and Brindley, W. J. (1998), *Residual stresses modeled in thermal barrier coatings*. Herausgegebenvon Glenn Research Center.
37. Evans, A. G., He, M. Y. and Hutchinson, J. W. (1997), Effect of interface undulations on the thermal fatigue of thin films and scales on metal substrates. *ActaMaterialia*, **H. 45**(9), S. 3543–3554.
38. Witz, G., Shklover, V., Steurer, W., Bachegowda, S. and Bossmann, H-P. (2007), Monitoring the phase evolution of yttria stabilized zirconia in thermal barrier coatings using the rietveld method. *Proceedings of the 31st International Conference on Advanced Ceramics and Composites*, S. 41–51.
39. Witz, G., Steurer, W., Shklover, V., Bossmann, H-P. and Bachegowda, S. (2009), High-temperature interaction of yttria stabilized zirconia coatings with 2 CaO–MgO–Al_2O_3–SiO_2 (CMAS) deposits. *Surface & Coatings Technology*.
40. Thompson, J. A. and Clyne, T. W. (2001), The effect of heat treatment on the stiffness of zirconia top coats in plasma-sprayed TBCs. *Acta Materialia*, **H. 49**, S. 1565–1575.
41. Cao, X. Q., Vassen, R. and Stoever, D. (2004), Ceramic materials for thermal barrier coatings, *Journal of the European Ceramic Society*, **24,** 1–10.
42. Zhu, D. and Miller, R. A. (2004), Development of advanced low conductivity thermal barrier coatings. *International Journal of Applied Ceramic Technology* **1**(4), 86–94.
43. TBC Plus – Final Technical Report: New increased temperature capability thermal barrier coatings. Contract N°: G4RD-CT-2001–00504 – PROJECT N°: GRD1–2000–26800. Project funded by the European Community under the 'Competitive and Sustainable Growth' Program (1998–2002).
44. US Department of Energy National Energy Technology Laboratory Morgantown, WV 26507–0880. DOE Contract Nos. DE-AC21–93MC30247 – DE-FC21–95MC32267.: Advanced Turbine Systems Program.

Published by Woodhead Publishing Limited, 2013

45. Activities shown on 1st German-Japanese TBC Workshop, Darmstadt 2006, M. Okazaki: Recent Activities for Superalloys and Coatings in The Society of Materials Science, Japan (JSMS) 2nd German-Japanese TBC Workshop, Kyoto 2009, M. Okazaki: Current activities to evaluate mechanical properties of TBC in The Society of Materials Science, Japan (JSMS) and Japan Society of Mechanical Engineers (JSME).
46. Bossmann, H. P., Witz, G. and Baumann, R. (2011), Entwicklung zuverlässiger Wärmedämmschichten für hochbeanspruchte Turbinen- und Brennkammerbauteile. TGT11-V02. In VGB PowerTech e.V. (Ed.): *Gasturbinen und Gasturbinenbetrieb 2011*. Gas Turbines and Operation of Gas Turbines 2011. VGB Fachtagung am 11./12. Mai 2011 in Offenbach/Main.
47. Bossmann, H-P., Bachegowda, S. and Schnell, A. (2008): Manufacturing optimization for bondcoat/thermal barrier coating systems. GT2008–51366. *Proceedings of ASME Turbo Expo 2008: Power for Land, Sea and Air,* 9–13 June 2008, Berlin, Germany.
48. Brito, M. E. (Hg.) (2005), Developments in advanced ceramics and composites. A collection of papers presented at the *29th International Conference on Advanced Ceramics and Composites,* 23–28 January 2005, Cocoa Beach, Florida. Westerville, Ohio: American Ceramic Society. (*Ceramic Engineering and Science Proceedings*, 26, 8).
49. Haynes International, Inc. (Hg.) (1997), HASTELLOY® X ALLOY. A nickel-base alloy with an exceptional combination of oxidation resistance, fabricability and high temperature. Product Flyer/Techn. Documentation H-3009A from Haynes.
50. Witz, G., Shklover, V., Steurer, W., Bossmann, H-P. and Bachegowda, S. (2007), Phase evolution in yttria-stabilized zirconia thermal barrier coatings studied by rietveld refinement of X-ray powder diffraction patterns. *Journal of the American Ceramic Society,* **90**(9), 2935–2940.
51. Eldridge, J. I., Zhu, D. and Miller, R. A. (2001), Mesoscopic nonlinear elastic modulus of thermal barrier coatings determined by cylindrical punch indentation. *Journal of the American Ceramic Society,* **84**(11), 2737–2739.
52. Heckmann, S., Herzog, R., Steinbrech, R., Schubert, F. and Singheiser, L. (2002), *Visco-plastic properties of separated thermal barrier coatings under compression loading*. *Proceedings of the 7th Liege Conference 2002*, Forschungszentrum Jülich GmbH - Institute for Materials and Processes in Energy Systems. Liege, Belgium.
53. Borom, M. P., Johnson, C. A. and Peluso, L. A. (1996): Role of environmental deposits in spallation of thermal barrier coatings on aeroengine and land-based gas turbine hardware. *Presented at the International Gas Turbine and Aeroengine Congress & Exhibition,* Binningham, UK, 10–13 June 1996. Herausgegeben von The American Society of Mechanical Engineers (ASME).
54. Witz, G., Steurer, W., Shklover, V., Bossmann, H-P. and Bachegowda, S. (2009), High temperature interaction of yttria stabilized zirconia coatings with 2 CaO–MgO–Al_2O_3–SiO_2 (CMAS) deposits. *Surface & Coatings Technology*. DOI: 10.1016/j.surfcoat.2009.07.034.
55. van Roode, M. (2007), Applications of ceramics for gas turbine engines. *Global roadmap for ceramic and glass technology 1st International Congress on Ceramics (ICC)*, Toronto, Canada, 25–29 June 2006. 1 volume. Eds.: S. Freiman

and R. Cook. Hoboken, NJ, Wiley (*Global Roadmap for Ceramic and Glass Technology*, 1).
56. Easley, M. L. and Smyth, J. R. (1996), Ceramic gas turbine technology development. *Presented at the International Gas Turbine and Aeroengine Congress and Exposition*. Edited by The American Society of Mechanical Engineers. Birmingham, UK (96-GT-367).
57. van Roode, M. (15 November 2005), Results of hybrid oxide CMC combustor liner testing. *Environmental Barrier Coatings Workshop*. Nashville, TN, 15 November 2005.
58. United States Advanced Ceramic Association and U.S. Department of Energy (2000), Advanced Ceramics Technology Roadmap. Charting Our Course. Priority Research, Development and Demonstration Needs to Advance Monolithic Ceramic, Ceramic Matrix Composites, and Ceramic Coating Systems.
59. Krenkel, W. (2008), *Ceramic Matrix Composites. Fiber Reinforced Ceramics and Their Applications*. Weinheim, Wiley-VCH.
60. Jacobson, N. S., Fox, D. S., Smialek, J. L., Opila, E. J., Tortorelli, P. F. and More, K. L., Nickel, K., Hirata, T., Yoshhida, M. and Yuri, I. (2000), *Corrosion Issues for Ceramics in Gas Turbines*. Edited by Glenn Research Center. Available online at http://ntrs.nasa.gov
61. Lewinsohn, C. A. (Ed.) (2003), Advances in joining of ceramics. *Proceedings of the Joining of Ceramics Symposium held at the 104th annual meeting of the American Ceramic Society*, 28 April–1 May 2002, St. Louis, Missouri. American Ceramic Society; Joining of Ceramics Symposium. Westerville, Ohio American Ceramic Society (Ceramic transactions, 138).
62. Mei, J. and Xiao, P. (1999), Joining metals to zirconia for high temperature applications. *Scripta Materialia* **40**(5), 587–594.
63. van Roode, M. (2008), Ceramic gas turbine development – need for a 10-year plan. GT2008–51378. In The American Society of Mechanical Engineers (Ed.): *Proceedings of the ASME Turbo Expo 2008. Power for Land, Sea & Air* 9–13 June 2008, Berlin, Germany.

9.8 Appendix: nomenclature

7YSZ	7wt-% yttria stabilised zirconia
at-%, vol-%, wt-%	atomic-%, volume-%, weight-%
APS	Air plasma spraying
BC	Bond coat
BM	Base material
BRT	Burner rig test
CC	Conventionally cast
CMAS	Calcia-magnesia-alumina-silica (compound)
CTE	Coefficient of thermal expansion
CVD	Chemical vapour deposition
DBTT	Ductile–brittle transition temperature
DoE	Design of Experiment
DS	Directionally solidified

E	Young's modulus or stiffness
ε	Strain
EB-PVD	Electron beam physical vapour deposition
FCT	Furnace cycling test
g	Gravitational acceleration
γ, γ', γ'', α, β, δ, μ	Various phases in BM or coating
GCC	Gas cooling casting
GT	Gas turbine
HIP	Hot isostatic pressure
HTC	Heat transfer coefficient
IGT	Industrial GT
LMC	Liquid metal cooling
MCrAlY	Coating composition with M (= Ni and/or Co), Cr, Al, Y plus other minor elements
ν	Poisson ration
NDT	Non-destructive testing
RT	Room temperature
σ	Stress
SX	Single crystal
TBC	Thermal barrier coating
TGO	Thermally grown oxide
TLP	Transient liquid phase
TMF	Thermo-mechanical fatigue
T_{min}, T_{max}	minimum and maximum temperature of the TMF cycles

Published by Woodhead Publishing Limited, 2013

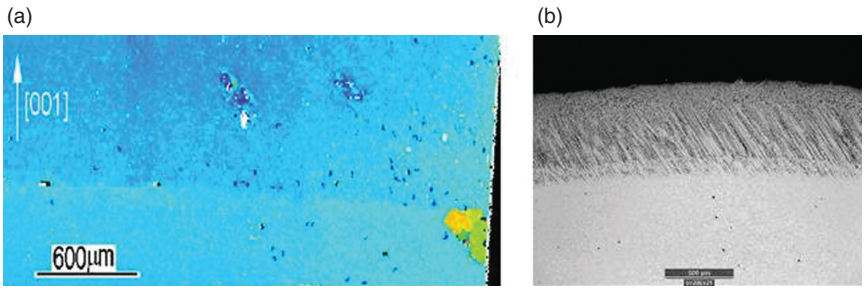


Plate XIII (Chapter 9) (a) Kikuchi crystal orientation map of SX brazed joint; (b) laser cladded SX coating.

© Woodhead Publishing Limited, 2013

10

Gas turbine operation and combustion performance issues

B. PRADE, Siemens AG Energy, Germany

DOI: 10.1533/9780857096067.3.383

Abstract: This chapter examines operational issues in gas turbine systems, which are caused by, or have an impact on, the performance of the combustion system. Based on a typical gas turbine operation schedule, and with a focus on natural gas based fuels, the chapter assesses the impact of various thermodynamic boundary conditions on the physics of the combustion processes. The chapter begins by summarising the fundamental requirements of a gas turbine combustion system, followed by more detailed discussions on flame stabilisation mechanisms, and the impact of operational conditions of a gas turbine on exhaust gas emissions (especially NO_x and CO). The concluding sections review the fundamentals of thermo-acoustics and consider potential future technologies, such as exhaust gas recirculation (EGR), which will have impact on gas turbine combustion.

Key words: flame stabilisation, auto ignition, flash back, gas turbine exhaust emission, combustion dynamics, pressure fluctuation, exhaust gas recirculation.

10.1 Introduction

In simplified terms, gas turbines for power generation may be split into two categories. Engines with a power output of from 20 to 40 MW are often based on aero engine designs. The compressor and turbine are not arranged on a single shaft, but are run at different speeds. Both fuel flow and speed can be used to control the gas turbine operational conditions or air mass flow. Larger engines (>60 MW) predominantly use a single-rotor design, with the compressor and turbine on one shaft running at the same speed. Variable inlet guide vanes have become the standard device used in compressors to control engine operation by modulating the mass air flow. This chapter focuses on this second type of engine, to highlight the relationship between operational performance and combustion. The performance of the combustion system can be linked to the compressor exit pressure and related temperature, as well as to the air and fuel mass flow entering the

© Woodhead Publishing Limited, 2013

combustion system. In this respect, the combustion system of a multi-shaft gas turbine is not fundamentally different.

A set of thermodynamic parameters, given by the operational status of the engine, along with some additional requirements, are the controlling boundaries for combustion systems in gas turbines. These can be summarised as follows:

1. Fuel conversion to heat at a high efficiency, characterised by the complete burnout of the fuel over a wide load range with minimal heat loss and an acceptable pressure drop. Complete burnout is commonly characterised by emissions of carbon monoxide (CO) and/or unburned hydrocarbons (UHCs).
2. Low emissions of NO_x, supporting the option to minimise power plant capital and operational cost by avoiding/reducing the need for post combustion emission reduction (SCR).
3. Flexibility and robustness regarding stable operation in the complete operation range. This is related to such phenomena as flash back, flame blow off, and acoustical vibrations excited by the combustion system (also known as combustion dynamics, screech, humming, etc.).
4. Flexibility regarding stable operation considering fuel variations.
5. Low life-cycle cost, represented by first-time cost and low operational costs (fuel), inspection, repair and exchange.

In the late 1980s gas turbine design technology reached a level at which turbine inlet and outlet temperatures were sufficient for it to make commercial sense to integrate the turbine into a power plant with an exhaust heat recovery steam generator (HRSG) system and a steam turbine. As a result, gas turbine combustion technology experienced a major revolution. Driven by the needs of a combined cycle power plant (CCPP), gas turbine compressors were equipped with variable inlet guide vanes (IGV), which modulated the mass air flow, in order to keep the gas turbine exit or HRSG inlet temperature at a high level (up to 600°C) over a wide load range. This considerably increased the load range at which stable lean premixed combustion with complete burnout is possible, which was of considerable benefit to gas turbine combustion because changes in the average mixture fraction of fuel to air become small in this load range.

The ratio of fuel to air is commonly characterised using the so-called equivalence ratio EQR (φ), which is the ratio of fuel to air normalised by the ratio of fuel to air needed for complete stoichiometric combustion.

$$\text{EQR} = \frac{\text{fuel-to-air ratio}}{\text{fuel-to-air ratio at stoichiometric condition}} \qquad [10.1]$$

An EQR of 0 represents pure air, values below one characterise conditions with excess air and values of greater than one represent conditions under

© Woodhead Publishing Limited, 2013

which complete combustion is not possible due to the lack of oxygen. Pure fuel has an EQR equal to infinity. The reciprocal of EQR, which is called the air excess ratio (λ), is often used in combustion systems as well.

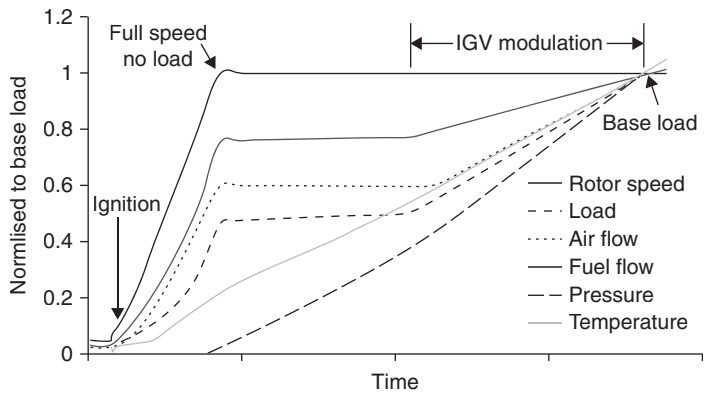
The temperature capability of turbine materials and the need for the minimisation of turbine cooling air to maximise efficiency provides an additional benefit for combustion systems, since these conditions allow current modern gas turbines to operate at a comparatively low equivalence ratio, leaving a high excess of air available for combustion. Typical equivalence ratios in the combustion system of a gas turbine operating at base load are in the range of about 0.45–0.6. This is significantly lower than for other combustion systems, such as directly fired boilers, and favours the concept of lean premixed combustion, which is the state of the art in stationary gas turbines today.

The wide range of operational conditions (shown in Fig. 10.1) makes gas turbine combustors different to many other combustion systems. A translation of Fig. 10.1 into parameters, which more clearly highlight the operational challenges of such a system, is given in Fig. 10.2.

Taken together, Figs 10.1 and 10.2 highlight how significantly combustion performance parameters are changing over the complete operational range. The combustor inlet temperature and pressure and the fuel-to-air ratio, characterised by the equivalence ratio and the velocity of the fuel air mixture in the burner passages, are of fundamental importance for the design and performance of a combustor.

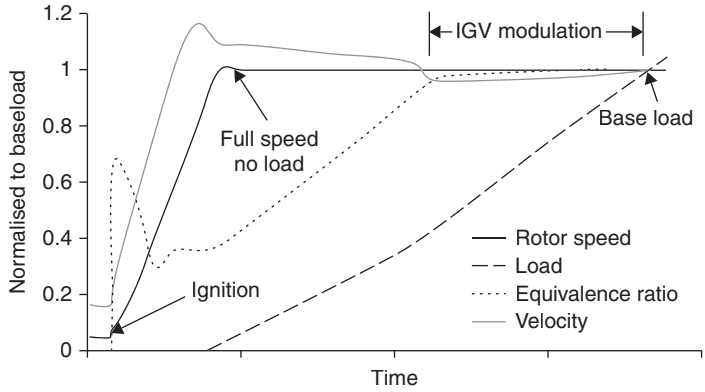
The example of Figs 10.1 and 10.2 shows that the:

- Combustor inlet pressure ranges from an ambient pressure to approximately 20 bar. This value can be higher with special gas turbines, especially in the case of aero derivates when the level can even be twice as high.



10.1 The wide range of operational conditions required for a gas turbine combustor.

© Woodhead Publishing Limited, 2013



10.2 Parameters that highlight the operational challenges of gas turbine combustion systems.

- Combustor inlet temperature accordingly spans from an ambient temperature at ignition to approximately 450°C at base load.
- Flow velocity at the burner inlet varies significantly, with approximately only 15% at ignition compared to the base load. The largest velocity, however, is seen slightly below 'full speed no load' (FSNL), which is unfavourably coincident with the next point.
- Very low equivalence ratio. The range of the equivalence ratio varies but can be as low as 30% of the base load equivalence ratio. In the given example, this means an absolute number of only 0.15.

The combination of these parameter variations means that highly flexible systems are now necessary to address the related issues which can occur in this wide range. These include:

- flame blow off of single burners, leading to increased emissions of CO or hydrocarbons and a non-uniform temperature distribution at the turbine inlet, or even,
- a flame out of all burners followed by an immediate engine trip,
- flash back possibly associated with severe damage of burner/combustor parts,
- high emissions of CO or NO_x caused by a too low or too high a flame temperature,
- combustion dynamics at very lean conditions (so-called 'cold' tones) or at high load ('hot' tones). Such acoustic pressure vibrations can cause severe combustor damage.

The following sections examine flame stabilisation mechanisms, emissions variations and combustion dynamics in gas turbine systems.

© Woodhead Publishing Limited, 2013

10.2 Flame stabilisation mechanisms

Flames stabilise in one of two ways (i) by propagation of a reaction front equivalent to the local flow direction, which is supported by the diffusive or convective transport of heat and/or reactive molecules (radicals), or (ii) by self-ignition (auto ignition), which occurs when the temperature is sufficiently high for the reaction chain branching to outweigh the chain termination. The level of temperature necessary for self-ignition is called 'auto ignition temperature' and largely depends on fuel composition and pressure and, to a certain extent, also on the fuel-to-air ratio. In most gas turbine combustors the temperature level is not sufficiently high to permanently support auto ignition flame stabilisation. The main focus of the following section will, therefore, be on flame stabilisation by flame propagation.

10.2.1 Flame stabilisation by flame propagation

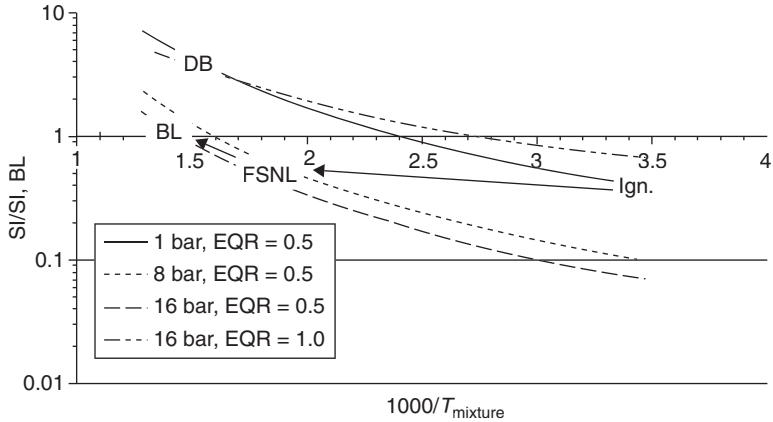
This mechanism can be simply described as a reaction front propagating in the opposed direction into the fresh unburnt fuel/air mixture coming from the burner. The relevant flame propagation velocity is often called flame speed (S) (Beér and Chigier, 1972). At laminar flow conditions the laminar flame speed is basically defined by the fuel, the fuel/air ratio and the thermodynamic conditions in the burner (Williams, 1985).

$$S_l = \text{function (fuel composition, mixture temperature and pressure, EQR)} \quad [10.2]$$

Figure 10.3 illustrates some characteristic engine operation points in the laminar flame speed vs compressor discharge temperature graph. The laminar flame speed is normalised by the flame speed at base load, assuming a constant stoichiometry at an equivalence ratio of about 0.5, which is a typical value for F-class base load conditions. The general trend of laminar flame speed for natural gas is a strong increase with the increasing mixture (equivalent to compressor discharge) temperature and, during lean conditions, an increase with increasing EQR and a moderate decrease with increasing pressure.

Figure 10.3 shows that – assuming that EQR can be maintained at a burner throughout the operation range – the flame speed would vary by approximately 250% between the base load and ignition. The figure includes a curve for a stoichiometric mixture at base load conditions, which can be interpreted as a diffusion-based combustion system (state of the art prior to the introduction of lean premixed technology). It very clearly shows that the implementation of the premix technology meant dealing with a significant reduction of flame speed compared to the diffusion flame. Such a flame

© Woodhead Publishing Limited, 2013



10.3 Characteristic engine operation points ignition, FSNL and base load in the laminar flame speed vs compressor discharge temperature graph.

stabilises at the point where the flame speed has the highest value, which is typically close to the stoichiometric mixture.

The effective flame speed, which is relevant to design gas turbine combustors, fortunately is not the laminar but the turbulent flame speed S_t. Flow velocity and pressure in gas turbine combustors are normally high, and therefore the Reynolds number of a flow into a gas turbine burner is large enough to ensure that the flow is fully turbulent. The level and structure of the turbulence of the flow has a large impact on the effective flame speed, and is, therefore, very relevant for the design of burners. Correlations for calculating the turbulent flame speed (Zimont *et al*., 1998; Peters, 1999, 2000; Chomiak and Lapatnikov, 2005; Siewert, 2006) are a hot topic for several reasons. In the recent past the use of fuels, which are different from normal natural gas, has become increasingly popular and this trend will continue in the future. Fuels containing hydrogen in particular have significantly increased flame speeds. Additionally, the turbulent flame speed has become an important input for computational fluid dynamic (CFD) design as an alternative method to describe the reaction progress (i.e. fuel consumption).

$$S_t = \text{function}\ (S_l, \text{turbulence characteristics, fuel, etc.}) \qquad [10.3]$$

As a rule, it can be estimated that, for aliphatic hydrocarbon-based fuels, the effective turbulent flame speed can increase from the laminar flame speed by more than one order of magnitude, which still leaves a significant gap (up to another order of magnitude) to the net flow velocity at the burner exit. In typical gas turbine combustor conditions the average flow velocity

© Woodhead Publishing Limited, 2013

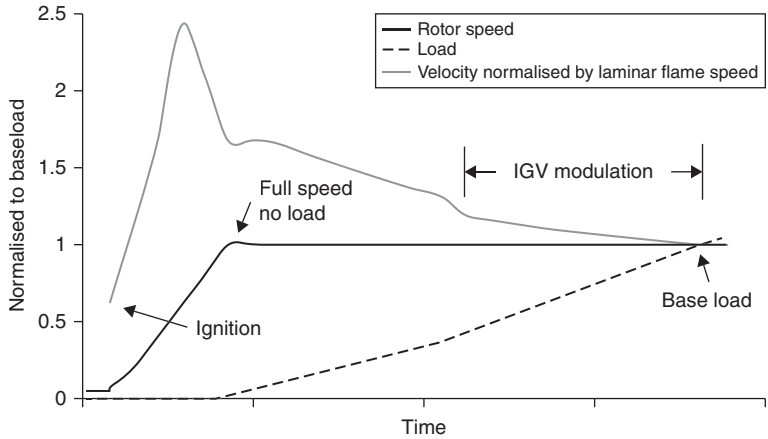
at the burner exit is in the order of approximately 100 m/s, which is more than one order of magnitude larger than the maximum turbulent flame speed. Therefore, burners have to be designed to provide regions in the flow field, where favourable conditions do locally exist, where a flame front can stabilise.

Two fundamental operational combustion issues, flash back and blow off, are directly linked to this mechanism and are caused by the following conditions:

- The flame speed is lower than the lowest flow velocity:
  This leads to a critical condition regarding flame blow off. Blow off of single burners may be accepted in a gas turbine during some transient conditions, but it must be avoided in steady state operation at higher loads. Procedure must, therefore, be in place to quickly reignite a burner in the event of a blow off occurring. This can be achieved via different means, such as cross-ignition by a neighbouring burner in a multi-burner combustor, cross-ignition tubing between can-annular combustors or even by using an ignitor. A permanent blow off at steady state is usually unacceptable because of the high life-cycle consumption (due to large temperature gradients) especially of vanes and blades. Engine operation will be terminated by a trip (immediate) or a fired shut down in such a situation.

  Combustor health regarding flame blow off can become a severe safety issue because the fuel of single burners may be being carried over into the HRSG or exhaust section, where critical conditions up to deflagration can occur. Thus 'flame on'-monitoring has become mandatory following national standardisation institutions such as TUEV and ASME. The national requirements and solutions may vary by country, but optical systems, possibly supported by turbine exit temperature monitoring and control software solutions, are often used for flame monitoring and this monitoring is usually required to be failsafe.
- The flame speed is higher than the burner exit velocity:
  This situation means that the reaction front can propagate into the burner passage, which significantly increases the potential for damage of the burner and subsequently even turbine components. Monitoring of the 'flash-back health' of a burner can be performed to protect engine hardware. This can be undertaken using standard instrumentation (thermocouples), but special instrumentation is often implemented for validation purposes during the first application designs or where there are special operational conditions such as off-design fuels. As flash-back damage does not usually impact on safety, there are no mandatory regulations covering flash-back monitoring and it can often be avoided by optimising the aerodynamic design of the burner.

© Woodhead Publishing Limited, 2013



10.4 The challenges involved in stabilising a flame at the burner during gas turbine operation.

- The flame speed is equal to the fresh mixture approach velocity: This condition is required locally for obtaining a steady and stable flame front. Due to the unsteady nature of turbulent flows this is usually achieved only on a time average ('dynamic equilibrium').

Figure 10.4 illustrates the challenge involved in stabilising a flame at the burner during gas turbine operation. A parameter – relative bulk velocity – which can help to characterise the flame stabilisation condition is given by the ratio of the bulk flow velocity divided by the flame speed of the mixture. Both bulk flow velocity and flame speed are normalised by the respective conditions at base load.

Bearing in mind that the chart shows a very simplified version of the process, it does highlight several relevant operational challenges:

- During operation in the 'normal' load range (25–100% load) the burner has to provide proper flame stabilisation over a range of up to 50% higher velocity ratio compared to base load.
- Thus the highest risk stage for a flame to move into the burner (flash back) is during the high load range close to base load. Compressor discharge pressure and flame temperature are at their highest levels during this stage, so the risk of severe damage to the burner is also highest at this stage.
- The chart also shows that, at or shortly after ignition, the relative bulk velocity at the burner exit is significantly lower than at base load. This is primarily because of the low volumetric flow during acceleration at the comparatively low compressor discharge temperature, in conjunction with the compressor bleed systems normally being active during

© Woodhead Publishing Limited, 2013

this operation mode. The thermodynamic conditions (low temperature and pressure) of the gas turbine in this range, however, help the burner to better withstand and possibly even survive a flash-back event.

- With increasing rotor speed the relative bulk flow velocity increases strongly, up to approximately 250% higher than the base load conditions. This helps to prevent flash back or even pushes a flame out of the burner, if it has been in a flash-back condition at ignition. The burner must still stabilise the flame at these conditions to avoid a blow off, however. The most critical condition regarding such problems in most large industrial gas turbines occurs just below full speed no load (FSNL), which means during the so-called run-up time.

Furthermore, the aforementioned operational challenges assume that the gas turbine burner is exposed to a constant equivalence ratio at different operational conditions. If this cannot be assured, then the challenge to stabilise a flame properly over the whole operation range becomes even greater.

Several methods to support flame stability against blow off can be applied to the process. These can basically be split into the main categories of aerodynamic design features and staging options of fuel and air. Staging includes a variety of different methods for improving combustion stability, which, in turn, is closely related to the emissions of CO and UHC.

Staging of air seems to be an obvious method of controlling the equivalence ratio in a gas turbine combustor. To produce a significant effect, however, large modulation valves for air bypass or blow off are required. Design requirements on such valves have become more stringent for F-class and higher performance class engines. In these engine classes there can be little tolerance for uncontrolled leakage due to the effect on emissions. With recent increases in the firing and compressor discharge temperatures the conditions for flame stabilisation have slightly improved, and, as a result, most modern gas turbine OEMs have moved away from variable combustor air bypass in large F-, G- and H-class gas turbines.

Staging of fuel, on the other hand, offers several different options:

- Splitting the fuel, and possibly also the air passage of a burner into separate systems allows fuel to be added to the burner via independently controllable manifolds (galleries). This allows for the creation of areas of different stoichiometry and/or mixing quality in the combustor, or, in other words, a zone with increased reactivity. This is called piloting and can ultimately even result in the production of a small separate (possibly even a diffusion type) pilot flame.
- Splitting of the fuel into separate manifolds which are connected to groups of burners even allows for the possibility of completely closing the

© Woodhead Publishing Limited, 2013

fuel supply of a specific burner group and helping to keep the preferred equivalence ratio range almost constant over the load range for the rest of the burners. This, however, requires consideration regarding reignition and the interaction with neighbouring burners. This fuel staging concept is completed in a parallel flow arrangement, but it is also possible for it to be used in a sequential arrangement, as implemented in ALSTOM's reheat systems (GT24 and GT26), in which a considerable amount of the fuel is injected into the hot flow of vitiated air/exhaust gas (>1200K) coming from an upstream burner or combustor. The high temperature in this hot flow causes the reactivity of the fuel to increase drastically (Fig. 10.3), which is sufficient to sustain a stable flame with appropriate aerodynamic design features. This mechanism can be exploited as soon as the primary combustor stage exit temperature (equivalent with the gas turbine load) is sufficiently high.

Aerodynamic design features are, nevertheless, the most important methods of supporting flame stability against blow off. Creating zones with low local flow velocity in the combustor close to the burner exit is the most common design feature. More specifically, this can be achieved by sudden area expansions (dump combustor) and/or blockage (bluff) bodies, both resulting in flow separation in the wake of the blockage or dump. The application of swirl generators to burners, however, has become state of the art in industrial combustion systems. An advantage of swirl generation (an additional tangential component of the flow vector) is that the reverse flow feature can be induced by aerodynamic forces without the need for exposing a blockage to the reacting mixture associated with the risk of producing an attached flame and, consequently, the overheating of this element. Aerodynamics and flame characteristics of such systems are widely described in literature (Beér and Chigier, 1972; Leuckel, 1968; Gupta *et al* ., 1984). Very briefly summarised, it is necessary to provide a minimum amount of tangential momentum relative to the axial momentum of the flow for achieving a stable reverse flow pattern (vortex break down), a so-called internal recirculation zone. The swirl number S, which is the ratio of tangential/axial momentum of the flow, is commonly used to evaluate the strength of the swirl. This parameter is made non-dimensional by the burner exit diameter D. In gas turbine burners with a very high Reynolds number, this parameter is independent of mass flow and can be expressed sufficiently accurately by geometry dimensions. In literature a level for S of approximately 0.6 can be found as a critical swirl number, above which a swirl generator would provide a stable internal recirculation zone. This characterises the bi-stable nature of swirling flows. The value of 0.6 should be considered as a guideline only. Considerable impact on the formation of a stable vortex breakdown can be achieved by a combination of swirling flow and diffuser or dump geometries.

© Woodhead Publishing Limited, 2013

$$\text{Swirl number, } S = \frac{\text{tangential momentum of flow}}{\text{burner diameter} \times \text{axial momentum of flow}} \quad [10.4]$$

As previously mentioned, one of the design tasks for gas turbine burners is the avoidance of flash back and the, often almost immediate, damage that can result from it. Fundamentally flash back is related to the very similar physical/chemical mechanism of flame stabilisation/blow off. In the current state of the art, lean premix burner precautions have to be taken to avoid flame propagation in the premixing passage, since most passages do not have cooled walls. Cooling of the walls would deteriorate the fuel/air mixing quality and thus increase NO_x emissions. Here the flame speed is a very important parameter, and it is also relevant for all the different mechanisms for flash back:

- Flame propagation against the main flow in the core of the flow:
  This mechanism for flash back is normally the easiest task for the designer to handle, as typically the average flow velocity in the burner itself is large enough to prevent a flame from propagating against the flow. Nevertheless this becomes more relevant with increasing thermodynamic operating conditions (pressure and temperature), and especially for fuels containing high amounts of hydrogen (H_2) with a largely increased flame speed. It is important to note that the flow path needs to be designed in such a way that even if, during unplanned design conditions, a flame moves into the passage it can swiftly be pushed out again.
- Flame propagation at the walls of the premixing passage (in boundary layers or in flow separation zones):
  Critical boundary layers in gas turbine burners can usually be avoided with reasonable effort, especially at the outer wall in a channel with a swirling flow, by designing ducts which have a slightly accelerated flow. On the other hand flow separation (even unsteady) at an inner wall of a swirl burner passage may occur because of the bi-stable nature of swirling flows. The swirl component – needed to increase blow off stability of the burner – is a main contributor for enhanced flash-back risk in the premixing section. Radial profiling of the tangential velocity component and the fuel concentration can be applied to reduce or possibly eliminate this risk.

10.2.2 Self- or auto ignition

Another important mechanism, which contributes to the risk of burner overheating and potential damage, is the effect of self- or auto ignition. Auto ignition, in comparison to flame speed, is a purely chemical kinetic characteristic

© Woodhead Publishing Limited, 2013

of the fuel/oxidiser mixture and is therefore defined by the thermodynamic status (pressure, temperature, molecular composition). Auto ignition can occur, when the number of chain branching reactions (producing additional radicals) becomes larger than the number of chain terminating reactions (consuming radicals). If auto ignition occurs, it can basically be understood as a continuous ignition source and thus needs to be very well controlled in order to avoid unwanted reactions in the premix passage.

Two parameters are often used to characterise the relevance of auto ignition: (i) the auto ignition temperature (AIT), which is defined as the temperature, at which a mixture ignites without the aid of additional energy from external sources such as an electric spark or convection; (ii) the ignition delay time of an initially given mixture temperature, which is defined as the time after which the temperature begins to increase rapidly and reaches a certain level (most commonly 90% of the adiabatic flame temperature). Besides, taking experimental data, which is often not readily available, both parameters can be easily calculated using commercial or open source codes for chemical kinetics calculations for all kind of variable conditions. Detailed reaction mechanisms are available in the literature, which can be adapted and validated to special thermodynamic conditions and fuel compositions. All data presented in this chapter are based on a mechanism (Bikas, 2001) and therefore the impact of some relevant higher hydrocarbons (up to 7 C-atoms) on auto ignition delay time or AIT can be assessed.

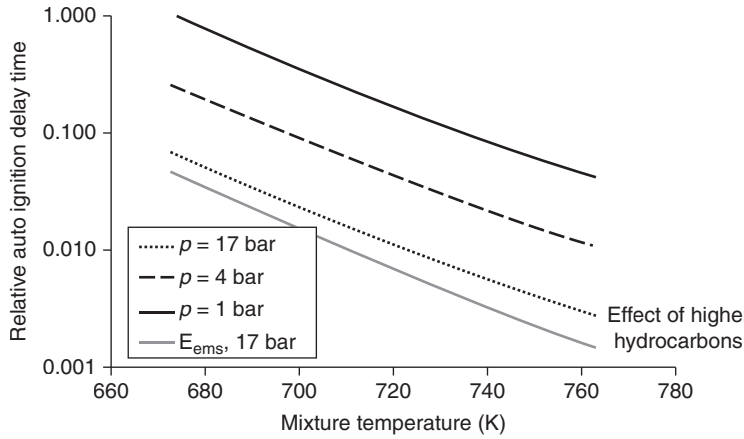
The main factors in gas turbine combustors, which dominate the problem of auto ignition, are combustor inlet temperature and pressure, fuel composition and equivalence ratio.

10.2.3 Combustor inlet temperature

As with the flame speed, the most important factor in controlling combustor inlet temperature is the temperature of the fuel/air or oxidiser mixture. Again, an approximately exponential increase of reactivity in the temperature is the reason for the strong decrease in the auto ignition delay time following the increased mixture temperature. Figure 10.5 shows this dominant trend, which is of essential importance for combustor design. As a rule, it can be estimated for natural gas that the auto ignition delay time drops by one order of magnitude if the mixture temperature increases by 70–80 K. In practice this means that:

- For a premixer of a gas turbine burner, which is operating at compressor exit conditions of approximately 20 bar and 450°C, the auto ignition time for pure methane is in the range of hundreds of seconds. This means auto ignition is not then a concern, because typically the residence time

© Woodhead Publishing Limited, 2013



10.5 Auto ignition delay time decreases substantially with increasing mixture temperature.

in the mixing passage is in the range of a millisecond (ms) only. Recall that the typical flow velocity is approximately 100 m/s and the typical dimension of a length of a premixer is probably less than 0.2 m, resulting in about 2 ms.

- When injecting fuel in hot exhaust gas (as for GT26/GT24), where the temperature is in the order of approximately 1000°C, the calculated autoignition delay time drops down to a level of one ms or less.

10.2.4 Combustor pressure

Compared to the laminar flame speed the impact of pressure on auto ignition is of higher relevance. The AIT and auto ignition delay time of a mixture significantly decreases with the increasing pressure. With good approximation the auto ignition delay time is proportional to the inverse of the pressure. The examples given in Fig. 10.5 show the drop in auto ignition delay time to almost 25%, if the pressure increases by a factor of 4.

10.2.5 Fuel composition

The fuel composition of natural gases is of higher relevance for auto ignition than for flame speed, which is essentially important for cases in which natural gas carries small amounts of higher hydrocarbons (C_nH_m, paraffin). Higher hydrocarbons are characterised as having several simple C–C (carbon–carbon) bonds. With an increasing number of such bonds it becomes easier to split such a molecule in parts, which is equivalent to a decrease in the AIT. This trend is well documented in literature (Zabetakis, 1965).

© Woodhead Publishing Limited, 2013

At atmospheric pressure the AIT for CH_4 is in the range of 550–600°C. The AIT for hydrocarbons with more than 4–5 carbon atoms falls below 300°C, which is below the compressor discharge temperature in modern gas turbines over a wide load range. In spite of normally low levels of C_nH_m, the auto ignition time of natural gas can be significantly shorter than for methane. This is shown in Fig. 10.5, where the auto ignition time of pure CH_4 is compared to a typical natural gas from the Netherlands (Eems). The Eems gas in this calculation was taken to have about 6%-Vol. ethane, 1%-Vol. propane and 0.5%-Vol. butane. There is a considerable drop of approximately one-third in the auto ignition delay time compared to methane (CH_4). This effect becomes especially relevant for gas turbine combustors, which are running at a high combustor inlet temperature (e.g. as the second combustor of GT24/26) as then the auto ignition delay time is in the order of the flow residence time. It would also require attention when using standard F-class gas turbine combustors, if they are intended to be operated on fuel oil in a quasi-premixed configuration – so-called partially premixed or lean prevaporised premixed (LPP) mode. Fuel oil can be approximately modelled as a hydrocarbon with a chain length of 10–12 carbon atoms, leading to an AIT in the range of approximately about 200°C. Such operation offers a large potential for reduced NO_x emission for oil compared to diffusion combustion. The auto ignition delay time of a fuel oil/air mixture is only in the range of 0.1–1% of that of natural gas. As a consequence, flow separation in the mixing passage has to be absolutely avoided in cases of fuel oil based operations.

10.2.6 Fuel/air stoichiometry

The equivalence ratio of the fuel/air mixture also changes the auto ignition characteristics. For state-of-the-art premixing technology, however, the mixing intensity is so high that good premixing occurs within a short length of time. Nevertheless, the auto ignition delay time clearly reduces with fuel rich mixtures. Again, this can be considered of higher relevance in systems in which fuel is injected into a very hot environment, as in the secondary combustor of a reheat system. If the time scale of the chemical reaction becomes shorter than the time scale of mixing, the local mixture fraction can become a design parameter of high relevance for safe and stable operational characteristics.

10.3 Emissions variations

Most of the technology development efforts taken regarding gas turbine combustion since the 1980s have been driven by the need to reduce power plant emissions. The essential products of hydrocarbon combustion are CO_2

© Woodhead Publishing Limited, 2013

(carbon dioxide) from the fuel's carbon content, H_2O (water vapour) from the fuel's hydrogen content, air humidity and in 'conventional' diffusion flame-based combustion systems from steam or water, which is injected for NO_x emission control, N_2 mostly from air with a minor contribution from the fuel as well, O_2 (oxygen) from the air, which is available in gas turbine combustion systems in excess. In addition to these end products there are by-products generated, which are mostly considered to be pollutants:

- CO (carbon monoxide) created from incomplete combustion; CO will be discussed in detail in this chapter.
- C_nH_m/UHC (unburned hydrocarbons), such as CO, related to incomplete combustion.
- Smoke, mostly made up of particle (soot) emissions. This is especially relevant to fuel oil combustion.
- NO_x as the sum of NO (nitrogen oxide) and NO_2 (nitrogen dioxide). NO_x will be discussed in detail in this chapter.
- SO_x as the sum of SO_2 (sulphur dioxide) and SO_3 (sulphur trioxide). SO_x emission is directly caused by the sulphur content in the fuel.

A key component in this cossntext is the emission of NO_x gases, which have to be considered as strong greenhouse gases. CO and UHC are normally closely related to one another as they both represent incomplete burn out and are especially relevant at low part load. The SO_x emission level of a gas turbine is normally caused by the fuel quality. In gas turbine conditions, each sulphur atom will essentially be oxidised to SO_x, almost independently from its original molecular form. Elevated levels of sulphur have to be considered carefully, because of the known related issues of corrosion of components in the hot gas path.

These combustion by-products are regulated or limited by local rules in most countries. CO_2 is not yet commonly considered as a regulated emission component, but this is a topic which may become relevant soon in light of recent climate change discussions. Similarly to SO_x, the level of CO_2 emissions is mainly dependent on fuel composition and additionally on cycle efficiency. NO_x and CO emissions are the main topics discussed in the following sections.

10.3.1 Nitrogen oxides

NO_x is considered to be among the most important greenhouse gases. NO_x includes the nitrogen oxide molecules of NO and NO_2. Worldwide emission regulations of NO_x are in the range of 2 to <100 ppmV depending on local regulations. NO, which usually accounts for the larger portion in combustion exhaust gases, is oxidised to NO_2 in atmospheric conditions. If NO_x is

© Woodhead Publishing Limited, 2013

regulated on a mass base (as mg/m³), NO_x is normally calculated as NO_2. NO_2 itself only accounts for a small portion of the exhaust of a gas turbine, especially at high loads. It can, however, be of separate importance for regulations because, depending on concentration and stack size, it can cause a visible plume at the power plant stack.

The formation mechanisms of nitrogen oxides have already been studied for a long time and fundamental work on this topic has been done by Zeldovich (1964), but further detailing of the research is still going on, because of the still strongly demanding legal requirements, and also the attempts of gas turbine manufacturers to increase the thermodynamic cycle efficiency. Thermodynamic parameters, which are relevant for the increase of plant efficiency, are unfortunately also strongly chemically linked to NO_x emissions and thus research into low NO_x emission combustion is still a major topic.

The most important pathways, which are relevant for NO_x formation in gas turbine combustors, are:

- thermal NO formation, also called Zeldovich mechanism,
- N_2O,
- prompt NO formation,
- fuel bound nitrogen (FBN) formation.

Only little relevance is given to the FBN pathway (Fenimore, 1971) for typical gas turbine fuels, especially for natural gas. Nitrogen, which is chemically bound to other atoms in one molecule, normally only occurs to a very small extent in oil or in gasification-based synthetic fuels (ammonia/NH_3), but not in natural gases. FBN-based NO_x formation will not, therefore, be discussed in detail in this chapter. To provide a brief overview, however, ammonia, or other molecules with simple chemical nitrogen–hydrogen bonds, can react quickly to NHi radicals or with CH radicals to HCN as an intermediate product, which almost completely transforms into NO_x in regions where O_2 is available. The excessive availability of O_2 is largely the fundamental basis of lean premixed combustion systems, so the minimisation of NO_x emissions from FBN fuels requires a different technology. The staging of air (rich–lean) or air and fuel has become a popular design solution in boilers to handle fuels carrying larger amounts of FBN.

The promptNO_x mechanism is chemically similar to the FBN mechanism. The main difference is the chain initiation step. Again, the CH radical plays an important role by cracking the strong triple bond N_2 molecule and forming HCN. The prompt NO_x mechanism takes place in the front of the flame where relatively high CH concentrations can be found. The following reaction steps to NO are almost identical to the Fenimore mechanism for FBN.

© Woodhead Publishing Limited, 2013

The contribution of the prompt NO_x mechanism to the overall NO_x emissions is <2 ppmV and can hardly be reduced in gas turbine combustors.

The N_2O pathway is becoming more important in gas turbine combustors of the current technology level, because the initiating reactions of this pathway are so-called three-body reactions, which means that a collision of three molecules (O, N_2 and M – 'M' can be any molecule) is needed to initiate it (see Equation [10.5]).

$$O + N_2 + M <-> N_2O + M \quad [10.5]$$

The probability for such three-body reactions to occur increases with the pressure. Increasing pressure is also one of the two most important thermodynamic boundaries for increasing the gas turbine cycle efficiency.

N_2O can transform into NO in subsequent reactions with O or H. In current gas turbine combustors, thermal NO formation appears to be the dominant mechanism used. The high stability of the molecule means that a great deal of energy is needed to break it into radicals, which then can react to NO_x. Reactions [10.6]–[10.8] show the three fundamental reactions of the thermal NO_x formation.

$$O + N_2 <-> NO + N \quad [10.6]$$

$$N + O_2 <-> NO + O \quad [10.7]$$

$$N + OH <-> NO + H \quad [10.8]$$

The first two of these equations are the fundamentally defined reactions, and are generally known as the Zeldovich mechanism. Reaction [10.6] starts the reaction chain by producing NO and a nitrogen radical (N), which itself then forms another NO molecule leaving an oxygen radical (O) to close the loop. Reaction [10.7] was added in the late 1980s/early 1990s, after the importance of the hydroxyl radical (OH) in many high temperature reactions was considered, and this relevance was confirmed for the thermal NO_x formation.

The reaction shown by Reaction [10.5] in particular only occurs at very high temperatures because of its rather high activation energy. Thermal NO_x formation in gas turbines can be assumed to be the dominating NO_x contributor, if the average temperature in the combustor exceeds approximately 1300–1400°C. As this range of temperatures is found in the complete combustion system volume downstream of the flame front, the NO_x contribution created by this mechanism is sometimes called post-flameNO_x . A closer study of Reaction [10.6] highlights the relevance of gas turbine operational parameters on the thermal NO_x formation. Assuming that the NO_x concentration in the combustor is low compared to the equilibrium concentration, and thus backwards reactions from NO to N_2 can be neglected, the reaction

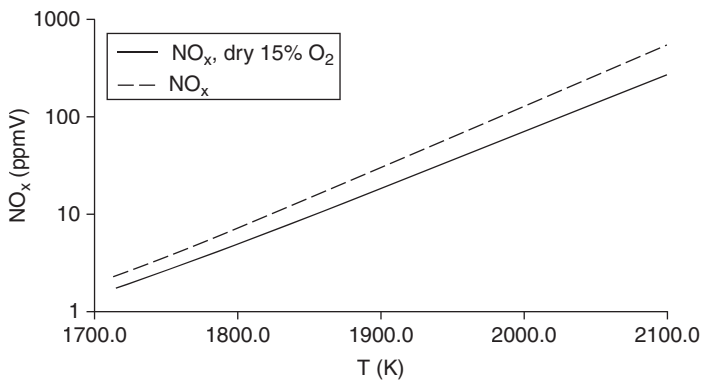
© Woodhead Publishing Limited, 2013

rate for the starting reaction [10.6] can be written as a first order law for the reaction, with an exponential Arrhenius temperature term.

$$\frac{\mathrm{d}[\mathrm{NO}]}{\mathrm{d}t}(\mathrm{mol/m^3/s}) \propto [\mathrm{O}](\mathrm{mol/m^3}) * [\mathrm{N_2}](\mathrm{mol/m^3}) * \exp\left(\frac{-E_A}{R * T}\right) \quad [10.9]$$

For this reaction the activation temperature, which is equivalent to the activation energy divided by the universal gas constant, is at the very high 38 000 K. Thus, from Equation [10.9] it can be concluded that the NO_x formation is mainly determined by a strong exponential dependence on temperature. Beside this, a linear correlation with residence time is shown. The impact of residence time on total NO_x emission is, therefore, of lower relevance compared to an increase in the turbine inlet temperature, which is required to achieve increasing cycle efficiency. Additionally, this equation indicates a pressure impact on the NO_x emissions. For the total thermal NO_x formation, however, a number of different reactions have to be taken into consideration, which finally weakens the overall pressure impact. Values for the pressure exponent of the NO_x formation, experimentally validated, mostly lie between 0.2 and 0.5.

In the literature, several sources can be found, suggesting an overall thermal NO_x formation rate. These correlations are fitted to certain special conditions and may completely fail, if they were applied to alternative conditions from the validated range of boundary conditions. For example, Fig. 10.6 shows the NO_x emission, calculated for a perfect mixture of CH_4 and air at an initial temperature of 700 K at 20 bar reacting for 20 ms. The detailed reaction mechanism [GRI3] was used for the chemical kinetics simulation. NO_x emissions of gas turbines in



10.6 NO_x emission, calculated for a perfect mixture of CH_4 and air at an initial temperature of 700 K at 20 bar reacting for 20 ms.

© Woodhead Publishing Limited, 2013

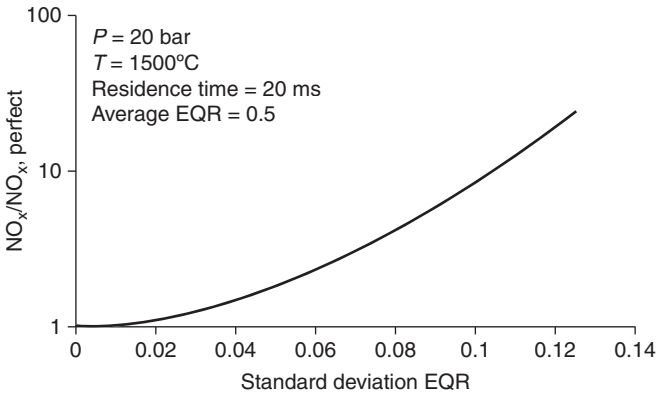
most countries are presented as dry emissions normalised to an oxygen level of 15%. The relevant curve is included in this chart. The reaction mechanism includes NO_x forming reactions, which are not part of the thermal mechanism, but, for the used fuel and the temperature range above 1500–1600°C, it can be assumed with acceptable accuracy that the thermal NO_x formation is dominant. As a simple rule of thumb, the NO_x emissions double if the flame temperature increases by 50–55 K. Changes to the thermodynamic cycle conditions, or to the design of the cooling system of combustor and turbine, both lead to changes in the combustion temperature. This allows for a rough estimate of the impact of the changes on NO_x emissions and easily explains the relevance of cooling air savings, not only for cycle efficiency but also for NO_x emissions. Knowing that only one percentage point of cooling air is worth a change in combustion temperature of roughly 12 K, it is equivalent to an increase or decrease of NO_x emissions of almost 20%!

The strong dependence of thermal NO_x formation on temperature also highlights the importance of using a high quality fuel–air mixture (Biagioli and Güthe, 2007). Localised areas with high equivalence ratios, and thus high local temperatures, are especially significant in contributing to overall NO_x emissions. The design for highest homogeneity is, therefore, one of the most important tasks in a premixed combustion system. Figure 10.7 shows a simulation of the impact of an inhomogeneous mixture compared to a perfect mixture of fuel and air on NO_x emission.

The simulation, based on the GRI3 reaction mechanism, calculates the NO_x emissions of a methane/air mixture for Gaussian distributions of the equivalence ratio with changing standard deviation, which is equivalent to the width of the distribution. At an average equivalence ratio of 0.5, an average temperature of 1500°C at 20 bar and a residence time of 20 ms for example, a standard deviation of 0.1% or 20% leads to an increase in NO_x emissions relative to the perfect mixture by a factor of almost 10!

Real gas turbine combustors can only achieve a technical mixture quality. Technical mixture quality can be in the range of approximately 5–15% standard deviation. Figure 10.7 shows why industries are putting so much effort into improving the homogeneity of the fuel air mixture. The effects, which have to be taken into consideration, are large scale variations in the burner and variation of the burner air or fuel flow. The fuel–air distribution within one burner cannot be made perfectly equal over the complete burner exit cross-section. A simple reason for this is the limited space available for mixing devices and the increasing complexity and thus cost of the burner design. Imperfect flow conditions and manufacturing tolerances (especially considering the small dimensions of fuel injection devices) significantly contribute to the lowest achievable fuel/air mixture homogeneity. A more complex reason for not attempting to achieve a perfect air mixture is that

© Woodhead Publishing Limited, 2013



10.7 A simulation of the impact of an inhomogeneous mixture compared to a perfect mixture of fuel and air on NO_x emission.

the pattern of the fuel/air mixture is a sensitive parameter driving thermo-acoustic oscillations; thermo-acoustic oscillations will be discussed later in this chapter. This, however, means that there is a trade-off between achievable NO_x emissions and combustion dynamics.

Most technical injectors for natural gas in premix burners are currently based on the jet in cross-flow injection with a fixed geometry. The mixing quality of such systems can be related to the jet penetration depth of the fuel jet into the cross-flowing air flow at a certain distance from the injection spot. An acceptable trend correlation to assess the impact of the operation condition on the mixing quality can be completed via the penetration depth (Callaghan and Rugheri, 1948):

$$x/d \sim \sqrt{\frac{\rho_{FG} * c_{FG}^2}{\rho_{Air} * c_{Air}^2}} \qquad [10.9]$$

where x is the jet penetration depth normalised by the nozzle diameter d. The driving parameter is the ratio of the momentum fluxes of fuel (index FG) to air. Since geometry in technical systems is not variable with power output, this ultimately means that the jet penetration depth, and thus the mixing quality, are linked to the operational conditions.

With some approximation Equation [10.9] can therefore be written as follows:

$$x/d \sim \mathrm{EQR} \qquad [10.10]$$

Comparing this equation to Fig. 10.2 shows that the jet penetration or, equivalent to this, the mixing quality can be maintained with a relatively small variation over the IGV control operation range.

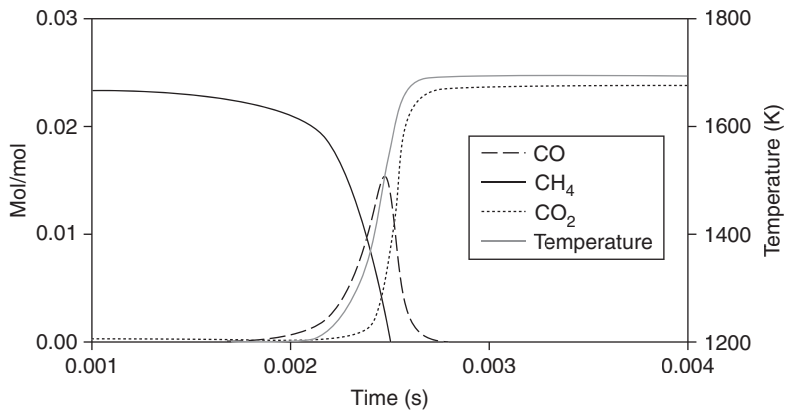
© Woodhead Publishing Limited, 2013

A change in the combustor or flame temperature runs parallel to this, which in this range is almost equally driven by the increase of both compressor discharge temperature, with increasing mass flow and pressure, and by the change in the equivalence ratio. A combustor temperature increase in current F-class gas turbines from the beginning of the IGV modulation (40–50% of relative load) to the base load and full mass flow is in the range of roughly only 100 K, still typically results in a strong change in NO_x emissions (Fig. 10.6). A further decrease in the load during closed IGV, as shown in Fig. 10.2, results in a significant change in the EQR and thus also in both the flame temperature and the mixing quality. Pilot fuel is also often injected in a less well-mixed condition in order to enhance flame stabilisation in very lean conditions. The combination of increasing the pilot fuel flow and a poor fuel/air mixing quality in the very low part load range can compensate for the decrease of combustor temperature regarding the overall resulting NO_x emission, i.e. NO_x emissions may still increase even during low load conditions.

10.3.2 Carbon monoxide (CO)

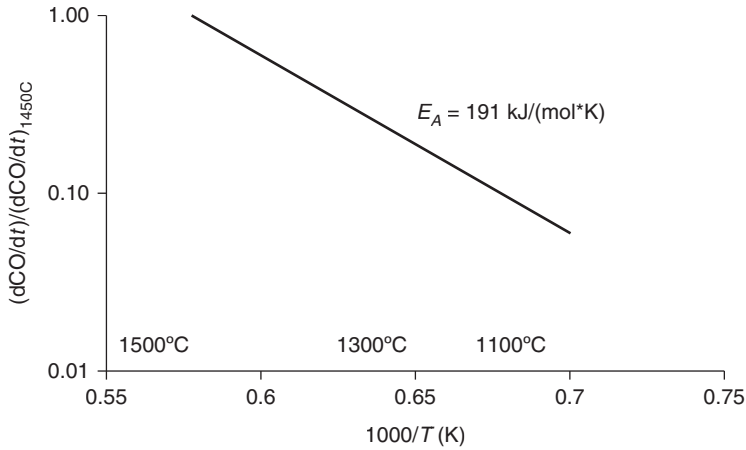
Carbon monoxide is an intermediate species of hydrocarbon oxidation reactions. Figure 10.8 shows the progress of temperature with CH_4 as educt, CO as an intermediate species, and CO_2 as a product of the CH_4/air mixture reaction.

Approaching the flame front, the oxidation of CH_4 correlates with an initial increase in CO. CO_2 production follows slightly later. The maximum intermediate CO level, typically reached, is in the range of 1–2%-Vol. Close



10.8 The progress of temperature, CH_4 as educt, CO as intermediate species and CO_2 as a product of the CH_4/air mixture reaction.

© Woodhead Publishing Limited, 2013



10.9 An averaged energy of activation for the CO oxidation can be estimated with approximately 191 kJ/(mol*K).

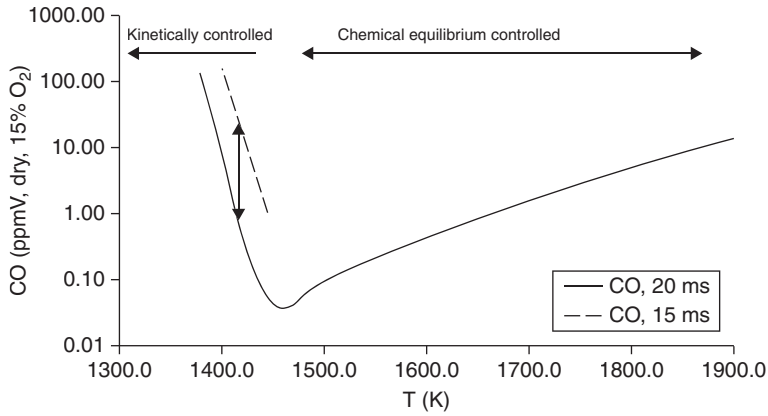
to the point where the maximum CO emission is reached, CH_4 is already completely oxidised, but the temperature is still significantly below the adiabatic flame temperature, because the concentration of CO is still high and the volumetric heating value of CO is approximately one-third of the heating value of CH_4. At temperature levels above 1400°C the overall time, in which CO is formed and oxidised, is in the range of less than one millisecond. The oxidation of CO itself, however, is a strongly temperature dependent set of reactions. An averaged energy of activation for CO oxidation can be estimated at approximately 191 kJ/(mol*K) as shown in Fig. 10.9.

The reaction rate at a temperature of 1100°C, which is still a temperature occurring in the load range of a gas turbine, is considerably reduced down to only one-tenth of the level at 1450°C. This is equivalent to the time needed for a complete CO oxidation of approximately 10 ms and it rapidly increases with the further decreasing flame temperature.

Current F-class gas turbine combustors are dimensioned such that the typical range of total residence time is between 10 and 30 ms. This includes the space (or as a consequence the time), which is needed to complete the mixing of fuel and air, mixing and preheating with circulating hot gases and radical formation for reaction initiation (ignition delay).

Figure 10.10 shows the CO emission of a perfectly premixed flame, calculated with the GRI3 reaction mechanism for a combustor residence time of 20 ms. The increasing CO emissions which reach above approximately 1450 K are caused by the fast CO_2 <–> CO reactions and thus reach the chemical equilibrium of CO and CO_2. This part of the curve, however, is not of particular relevance for gas turbine plants because, even in cases

© Woodhead Publishing Limited, 2013



10.10 The CO emission of a perfectly premixed flame, calculated with the GRI3 reaction mechanism for a combustor residence time of 20 ms.

with an extremely high combustor exit temperature (>1850 K) the reaction rates in both directions are so high that reduced equilibrium CO values are achievable even in the downstream turbine section where the temperature decreases due to expansion and cooling air injection. The left section of the curve, however, is of high relevance for gas turbine combustors in which CO strongly increases with decreasing temperatures below about 1450 K. For these temperature conditions, the CO oxidation is kinetically limited and thus chemical equilibrium cannot be reached because of the limited residence time in the combustor.

The impact of residence time on CO formation in this temperature range is much stronger than for the NO_x formation at high temperatures (see Equation [10.9]), because the CO oxidation rate depends on the actual CO molar fraction itself.

$$\frac{\mathrm{d[CO]}}{\mathrm{d}t}(\mathrm{mol/m^3/s}) \propto [\mathrm{CO}](\mathrm{mol/m^3})^{*} \exp\left(\frac{-E_A}{R^{*}T}\right) \qquad [10.11]$$

Thus total CO emission roughly exponentially depends on both temperature and residence time.

Figure 10.10 shows the impact of the residence time of the combustor for a perfect mixture. The decrease in residence time from 20 to 15 ms leads to an increase of CO emissions to a factor of almost 20!

It is important to note that in the lower load range of the gas turbine operation the emission of unburned hydrocarbons can occur too. The level of these emissions is usually clearly lower than that of the CO emission, but is strictly limited by legal regulations as well. In practice the shown curves for CO emissions at low temperature (turndown) cannot be reached, because,

© Woodhead Publishing Limited, 2013

as with the NO_x formation, no perfect fuel–air mixture can be achieved. In particular, fuel lean or colder streaks in the combustor do require a significantly larger residence time for complete oxidation.

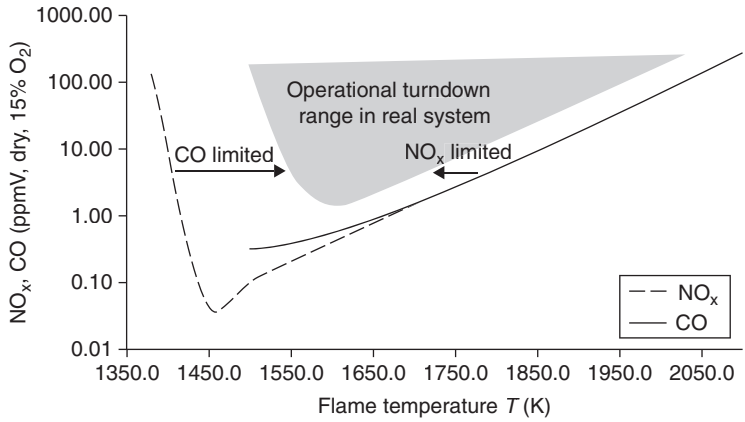
For example, metallic F-class combustors, in spite of the use of thermal barrier coatings, require wall cooling. The wall temperature is, therefore, normally significantly lower than the flame temperature. In addition, leakage or cooling of open cooled combustors further reduces temperature locally and therefore the CO burn out reaction rate. In practical combustors, therefore, a turndown temperature of even 1600 K for a CO emission target of 10 ppmV is not achievable without significant alterations to the standard combustor design. This is equivalent to a relative gas turbine load of about 40–50%. The minimum load range, where CO and NO_x emissions can both be kept low, often is called 'critical turn down ratio'.

Modern gas turbines can offer design features, which are not part of the combustion system but still support low CO turn down through the use of air management, as can the use of IGVs, which reduce the total air flow provided by the compressor. Bypass systems are also used to further reduce the burner air by dumping the bypassed air into the combustor far enough downstream so that CO burnout in the hot flame zone can be completed. More engine/plant integration options exist, such as air preheat and gas turbine air bleed systems, in which compressed air bypasses the combustor or even the complete turbine at the cost of a significant loss of efficiency. Staging options on the fuel side, however, often are easier to implement and do not affect efficiency with the use of separate pilot flames or piloting parts of the flame by direct injecting fuel are commonly used approaches. These piloted flames are operated at higher temperatures to stabilise combustion at low part load. Shut-off of complete stages and even burners can also be found in the different gas turbine frames. Such fuel staging options may, however, come at the cost of increased NO_x emissions due to locally increased temperature.

10.3.3 Low NO_x and CO emission (turndown) operation range

The operation range, which is given by a low concentration of the two components CO and NO_x in the exhaust of a combustion system of fixed dimension, is generally characterised by the flame temperature range, which, in turn, is given by the thermodynamic conditions of the gas turbine. The curves for NO_x and CO particularly can be shifted by optimisation of the fuel air mixing in the premix burner passages, combustor cooling design and combustor size. The fundamental limitation for lean premixed combustion systems regarding the temperature range, where emissions of lower CO and

© Woodhead Publishing Limited, 2013



10.11 The fundamental limitation for lean premixed combustion systems regarding the temperature range, where emissions of lower CO and NO_x can be met, is indicated by the arrows and the marked area.

NO_x can be met, is indicated in Fig. 10.11 by the arrows and the marked area. This area corresponds to an operation range with a flame temperature of approximately 200 K variation, within which such low emission values can be maintained.

The thermo-acoustic stability of a combustion system is another important aspect of gas turbine combustion systems, which has a significant impact on emissions. Driven by thermo-acoustical boundaries, combustion systems often have to be operated at fuel/air equivalence ratio adjustments, which are outside the optimal range for the lowest emissions in order to keep the acoustic pressure fluctuations at a low and acceptable level.

The topic of thermo-acoustic fluctuations is discussed in greater detail in the following sections.

10.4 Combustion dynamics

Acoustic pressure fluctuations are known to occur in technical combustion systems for a long time. This phenomenon – also called combustion dynamics or pulsations – is not limited to gas turbine combustors; it can also become an operation limiting issue in boiler systems, because of the very large surfaces exposed to the pressure fluctuations, or even in house firing applications because of noise emission.

Though only a small fraction (approximately 10^{-5}) of the total heat release in a combustor is normally transferred into acoustic energy, the equivalent pressure fluctuations can nevertheless become significant. The pronounced peaks – occurring at the natural frequencies (eigenmodes) of

© Woodhead Publishing Limited, 2013

the combustion system – are typical for thermo-acoustic oscillations. The eigenmodes of a combustion system are mainly defined by geometry and the spatial distribution of the Mach-number (temperature) therein. The acoustic pressure fluctuations in gas turbine combustors particularly can reach very high levels because of the relatively high volumetric heat release density and the high static pressure level. Such pressure fluctuations can have severe negative consequences on the operation of a gas turbine.

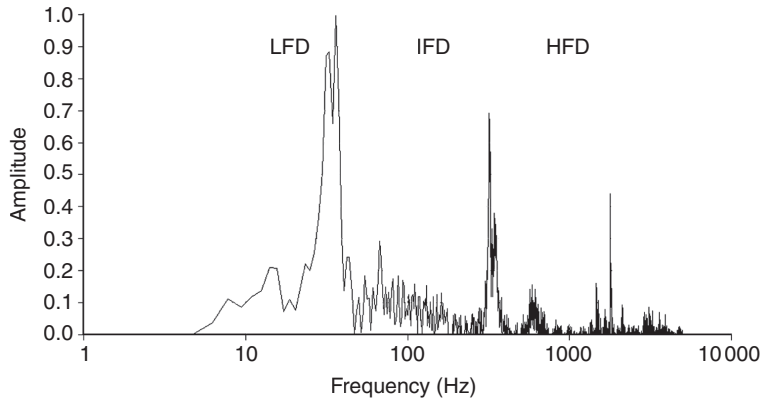
The change from a quasi-stationary to an unsteady volumetric flow of air due to the fluctuating pressure has a significant impact on the combustion system performance. As a result temporal fluctuations of the equivalence ratio occur, because the fuel injection systems are very often designed for a higher pressure drop than the air side pressure drop of the burner. Analogous to the spatial lack of mixing of the fuel/air mixture, this will lead to an increase in NO_x emissions.

The mechanical vibrations of parts, which can be induced by the acoustic pressure fluctuations, however, often have a more severe impact than the increase of emissions in the exhaust gas, because parts can reach their mechanical life limit and accordingly fail due to high cycle fatigue (HCF) in a very short time. To protect engine component parts in advanced gas turbines it is common practice to monitor the level of combustion dynamics by the direct detection of part accelerations. Several alternative indirect protection methods can also be found. The measurement of the pressure amplitude or amplitude of heat release fluctuation (for example by OH radiation) is often used. These methods can be implemented for lower cost and higher reliability, but they require the formulation of rules to translate the resulting signal into mechanical vibrations. The measurement of the dynamic pressure or better still, the dynamics of the heat release, in comparison to the measurement of the acceleration of parts, especially, is more often used in research and development, because these signals represent a direct link to the driving mechanism, which is the combustion dynamics. In order to avoid resonance effects it is important to measure the spectral distribution of the amplitudes of the combustion pulsation. Thus the monitoring systems for combustion dynamics mostly evaluate the complete spectral information of the signal. This chapter will not discuss the methods of using signal and spectrum processing; however, since the information, which is taken from the spectral data, is of high importance, it needs to be mentioned that a large variety of definitions and units can be used to characterise the level of amplitude.

Figure 10.12 shows an example of a typical pressure fluctuation signal in a gas turbine combustion system.

The spectral signal information, which is shown in Fig. 10.12, is obtained from a single burner test rig running at full pressure – very close to the lean blow off limit of the burner. Three peaks of the dynamic pressure signal

© Woodhead Publishing Limited, 2013



10.12 An example of a typical pressure fluctuation signal in a gas turbine combustion system.

clearly dominate the appearance of the spectrum. The segmentation of the spectrum into the three parts low frequency dynamics (LFD), intermediate frequency dynamics (IFD) and high frequency dynamics (HFD), which is shown in the figure, is arbitrary. Nevertheless, such segmentation is often used and even needed to set up specific operation/control algorithms.

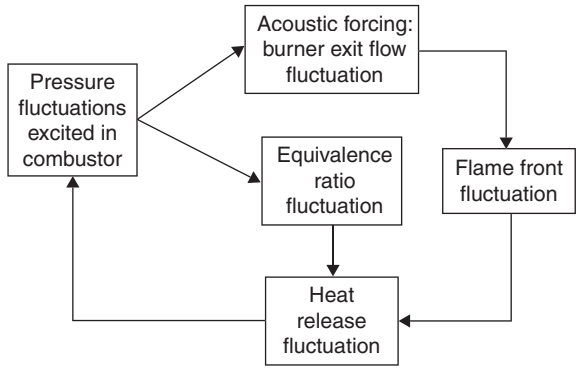
Background for this segmentation is based on the following:

- LFD are frequently referred to as 'breathing', 'bulk' or 'Helmholtz' modes. They are not characterised by the classical feedback loop between flame and combustor acoustical boundaries.
- IFD occurs at frequencies between 50 and 1000 Hz. Generally, the first natural eigenmode in a large gas turbine combustor is from 50 to 300 Hz, depending on the geometry and flame temperature. The next following low-order natural eigenmodes can be distinguished from neighbouring modes with acceptable accuracy.
- HFD in the range above 1000 Hz typically are higher order three-dimensional acoustic modes. Often it is not possible to distinguish exactly between neighbouring modes because of the small differences in frequency.

Combustion dynamics is a complex phenomenon arising from the interaction of the flame and the acoustical/geometrical boundaries, which can occur in all kind of combustion systems.

A sketch of the feedback loop for thermo-acoustical pressure fluctuations in a combustor is given in Fig. 10.13. A fluctuation of the combustor pressure (p_{com}) results in a fluctuation of the mass flow at the exit of the burner (m_{bu}) and, in technical not perfectly premixed systems, possibly in

© Woodhead Publishing Limited, 2013



10.13 The feedback loop for thermo-acoustical pressure fluctuations in a combustor.

equivalence ratio fluctuations as well. The mass flow fluctuation term is often called acoustic forcing. This term leads to fluctuations of the flame front location and thus the heat release. Equivalence ratio fluctuations also result in heat release fluctuations. For well premixed burner systems, however, this term is sometimes considered of less relevance than acoustic forcing. The heat release fluctuation itself again causes combustor pressure fluctuations, which closes the feedback loop. Modelling of such a system is unfortunately complex, because several boundary conditions need to be considered. Wall damping is of high relevance, because of the potential capability to dissipate acoustic energy, but also because of the ability of the flame to react on flow fluctuation and to respond with heat release variation (flame response function) and subsequently with pressure fluctuations, is very often not known well; both, however, are essential inputs for the thermo-acoustic modelling of the combustor.

The acoustic model needs to include the properties of acoustic resistance (or impedance) of the components of the combustion system (burner air passage, fuel injectors), compressor exit and turbine inlet. These together define the boundaries for the acoustic wave propagation and thus the eigenmodes of the combustion system, which are needed to perform the analysis of the thermo-acoustic stability of the combustion system. In most technical designs an exact description of the characteristics of components is not possible and instead strongly simplified models are sometimes used instead. The following methods, which are used to assess thermo-acoustical features, will not be described in full detail, but are mentioned briefly. More detailed information can be found in Van Kampen (2006), Krebs *et al*. (2002), Prade *et al*. (2002) and Sattelmeyer (2000):

© Woodhead Publishing Limited, 2013

- Low dimensional order stability analysis:
  A network of elements is created and analysed analogous to control system identification. The single elements are characterised by a transfer matrix, often based on correlations, which couples the output with the input of a single element regarding amplitude and phase in the frequency domain. This method can only provide qualitative trends due to the strong simplifications; however, because of the simplicity, it is a fast approach compared to other methods.
- Three-dimensional (3D) stability analysis:
  Finite Element Analysis (FEA) is used to solve the equations for the acoustic wave propagation in the combustor volume. An acoustical source needs to be coupled to this analysis; the acoustical source in turn is generally modelled using the distribution of heat release, which for example can be obtained from CFD. This method is expensive in terms of calculation and processing time and yet cannot be considered as state of the art. No integrated commercial software package for this process is available.
- 3D unsteady CFD:
  Unsteady CFD methods have become more popular in recent years because of the considerable progress in computational resources, and further progress is to be expected. Large eddy simulation (LES) has already proven that it has the potential to predict combustion dynamics related to self-excitation. The method basically evaluates the flame response function and requires a stability analysis to be performed as a post processing step. Currently LES is still expensive, due to the computational effort involved, and is thus not yet cost effective for evaluating small design changes with respect to their impact on combustion dynamics.
- Time lag modelling:
  The time lag modelling approach is based on the Rayleigh criterion (see below). In order to evaluate design changes a simplified flame response function or time lag function is generated, generally via CFD methods. This method can be used to assess the status of the Rayleigh integral, if the acoustic eigenmodes of a system are known. This method has been successfully applied in the past and is described in more detail in the following sections.

The first attempts to explain the phenomena of thermo-acoustics were made by Rayleigh (1878); based on his observations (Putnam, 1953, 1971) formulated the so-called Rayleigh integral, which is a necessary, but not sufficient, criterion for self-induced combustion oscillations. According to this criterion, the combustion system can run into unwanted and often unstable

© Woodhead Publishing Limited, 2013

self-excited pressure fluctuations if only the integral parts of the product of pressure and heat release fluctuations over a full period T are positive.

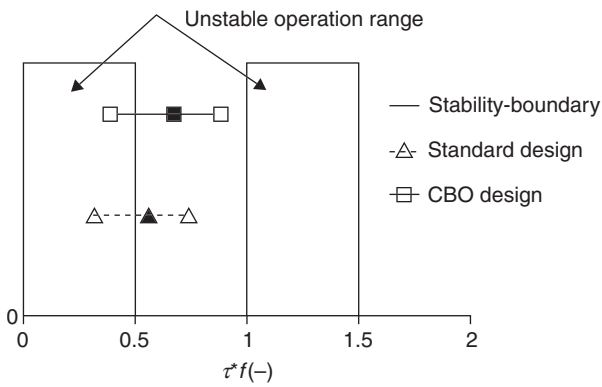
$$\int_0^T q'(t) * p'(t) * \mathrm{d}t > 0 \qquad [10.12]$$

In technical systems, the value of this integral has to be integrated over the combustor volume to evaluate its cumulative effect as q and p are functions of both space and time.

$$\int_V \int_0^T q'(t,\vec{x}) * p'(t,\vec{x}) * \mathrm{d}t * \mathrm{d}V > 0 \qquad [10.13]$$

For heat release (q') and pressure (p') oscillations of single frequencies this criterion is fulfilled for phase shifts smaller than 90°, i.e. smaller than one-quarter of the acoustic period T. The phase shift can be interpreted as a time delay (or time lag) between the pressure fluctuation and the heat release fluctuation (Blackshear, 1952; Crocco and Cheng, 1956; Putnam, 1971). In technical combustion systems with good premixing capability it is often assumed that acoustic forcing (Fig. 10.13) is the dominant mechanism, thus the Rayleigh criterion can be reformulated using the so-called burner time lag τ and the combustor frequency f (Equation [10.14]). The combustion system can become unstable, if pressure and heat release fluctuations are sufficiently in phase and if the following criterion is met (n being the n-th eigenmode of the system):

$$n < \tau * f < n + 0.5 \quad \text{with} \quad n = 0, 1, 2, \ldots \qquad [10.14]$$



10.14 The change in time lag resulting from the burner design with CBO.

© Woodhead Publishing Limited, 2013

This criterion can be used to investigate if design changes move the product τ^*f away from an unstable situation in the stability chart. In technical combustion systems it is obvious that the time lag for fluid elements from the point of injection to the flame front is a distribution and not a single value. Sattelmeyer (2000) and Krebs *et al*. (2002) discuss the procedure of determining the time lag distribution in more detail.

An example of a technical design change, which was successfully implemented in several large Siemens gas turbine combustion systems (Prade *et al*., 2002), is the addition of a cylindrical burner extension to the burner (called CBO design), which resulted in a significant change in the flame shape and thus of the time lag distribution (Plate XIV, see colour section between pages 346 and 347). The flame shape in Plate XIV is characterised by the strong temperature gradient from blue to red.

Plate XIV shows that the burner design with CBO changes the flame shape significantly. The flow field appears slim and consequently more fluid elements cross the flame front at a longer time lag. The corresponding change in the time lag stability chart is shown in Fig. 10.14. For two burner designs, without CBO and with CBO, three cuts (20%, 50% and 80%) of the τ^*f distribution are shown relative to the stability limit, highlighting that the CBO design variant has moved the time lag distribution out of the unstable boxes. This result has been confirmed by experimental proof in engines in which the CBO system could run with significantly lower combustion dynamics.

There is still no completely accurate method existing, which can predict combustion dynamics. The experimental validation of design changes in regard to the thermo-acoustical performance is, therefore, still necessary. It is important to note that the testing of combustion systems with respect to combustion dynamics requires significant effort to generate data, which can later be transferred to the engine geometry with acceptable significance. Large engine combustors normally have to be tested in a single burner arrangement, which results in obvious differences regarding acoustical and geometrical boundary conditions (annular in engine–segment in rig, single can in rig–can-to-can interaction in engine). Care therefore has to be taken when translating the rig tested combustion dynamics performance to the respective engine performance.

Other successful examples to counteract combustion dynamics can be found in industrial gas turbines, but will not be discussed in detail here. A short listing of examples is:

- Increase of damping or dissipation of acoustical energy:
  Resonators, such as Helmholtz resonators or quarter wave tubes, are used in several gas turbine frames. Resonators are passive elements and can be easily adapted to the target frequency range and have a good predictability. It is important to consider the mode shape of the combustor, because it is essential for the efficient functioning of a resonator that it is

© Woodhead Publishing Limited, 2013

located in a pressure anti-node. It is still not possible to accurately predict the amount of damping that is needed for safe operation. It is therefore still necessary to optimise the number and location of resonators in a new combustion system. Resonators are very effective for damping pressure fluctuations, but normally only work within a very narrow frequency range. The application of resonators is especially beneficial in the high frequency range, because the size of a resonator is inversely proportional to the frequency it is designed for. The use of a multitude of such resonators allows the widening of the system damping capability with regard to frequency, if the single resonators are designed for slightly different frequencies.

- Air/fuel profile variation:
  Similarly to the time lag modification approach described previously (CBO), the profile of the fuel/air mixture has a large impact on the shape of the flame. Thus the fuel/air mixing profile impacts on the time lag distribution as well. Both methods have been applied in industry, distributed air as well as fuel injection, to fit the flame response of the combustion system to its acoustic eigenmodes.

Unlike the aforementioned mentioned passive (fixed geometry and settings) measures is the category of active measures, which change operational settings of fuel or air supply using standard or additional equipment. Such active measures have also proven to be effective in large scale technical applications for helping with combustion dynamics. There are two fundamentally different categories, which are the open loop and the closed loop approach:

- A gas turbine combustion system normally has more than one fuel stage in order to mix the fuel with the combustion air. Single stages can be designed in such a way that changing the fuel split between the stages results in different fuel/air mixing profiles or even a different flow field. The flame shape, and thus the heat release and time lag distribution, can therefore be impacted by controlling the fuel valves. This is especially effective and flexible if it is arranged in a closed loop control system. Often, however, even an open loop integration of preset and fixed settings for different load ranges into the control system is sufficient to significantly reduce combustion dynamics.
- It has also been demonstrated on large scale that active instability control is an option for the reduction of gas turbine combustion dynamics (Seume *et al*., 1997). This technology applies the theoretically obvious, but practically more difficult to achieve, method of compensating for pressure fluctuations by modulating flows with the same frequency, but shifted by 180° in phase ('anti-sound'), so that the resulting amplitude is

© Woodhead Publishing Limited, 2013

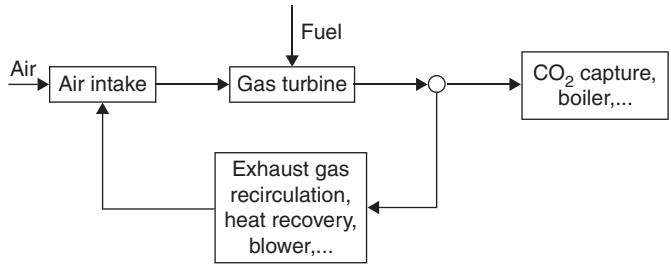
reduced. In large gas turbines such systems, besides the sensor and signal processing technology, especially require actuators, which are able to provide both actuation frequency and energy. Such equipment for large gas turbines is thus expensive and may not be considered as a standard equipment option. It is, however, efficient in 'buying time' for problem resolution.

10.5 Future trends

The combustion technology of turbines in the future will be strongly impacted by market requirements. There are a large variety of long-term forecasts available, which speculate on the potential future trends in the energy market. Long-term forecasting has proven very uncertain in the past, however, and it has become more common to discuss potential future scenarios including EER (2006, 2009), BP (2009) and Enerdata (2008). The most important scenario factors, which will impact on future gas turbine and thus combustion technology, therefore are:

- Natural gas price/availability:
  The price of fuel is the primary driving factor for the value of efficiency in power plants. All current studies forecast increasing fuel prices in the long-term perspective. Gas turbine efficiency will therefore become even more important than it is currently. For thermodynamic reasons this will result in gas turbines operating at higher pressure ratio and at a higher turbine inlet temperature. It will, therefore, become even more challenging to achieve low NO_x emissions, and the resulting technological developments will be a cornerstone of future research efforts. The topic of thermo-acoustic oscillations will be impacted by this trend as well because of the increasing heat release density in such future combustion systems.
- CO_2 emission reduction cost:
  The cost models for the CO_2 emissions of power plants are currently an undecided factor worldwide. All forecasting agencies have, therefore, evaluated scenarios considering different CO_2 cost levels. Since combustion in most gas turbine power plants is, and will continue to be, based on natural gas, the specific CO_2 emissions relative to power output are already small. Nevertheless, depending on the cost of CO_2 it will become attractive for gas turbine power plants to further reduce CO_2 emissions. The consequences for gas turbine combustion are twofold. As with the impact of increasing fuel prices, this will lead to attempts to increase efficiency, but an alternative option is to separate CO_2 from the exhaust. Due to the relatively low CO_2 content in the exhaust of a gas turbine the respective sequestration processes are less efficient when compared

© Woodhead Publishing Limited, 2013



10.15 A simplified sketch of an EGR cycle.

to boilers for example. Studies of variations in the normal thermodynamic gas turbine cycle have been performed and are still on-going in both academia and industry. Currently a cycle variation based on EGR (see Fig. 10.15) is being evaluated in more detail. The implementation of such cycles would have a huge impact on the required combustion technology.

- Due to the large reserves of coal worldwide, clean coal combustion will be a topic of the future as well. The so-called integrated coal gasification cycle (IGCC) process can be considered to be proven technology. Several large scale power plants, which have already been in service for some years, are the basis for improvement of the total plant efficiency and the much needed plant reliability. The IGCC process includes gasification equipment, which converts coal, pet coke or other lower quality fuels into synthetic fuel (syngas), which essentially consists of H_2 and CO. This fuel can either be burnt directly or, in the event of the CO_2 costs becoming high, converted into a high H_2 fuel with only small amounts of CO (and therefore CO_2 in the exhaust) remaining. Power plants, which can operate on such hydrogen rich fuel mixtures, are not common, but are already the subject of development for demonstration projects. Chapter Xon fuel flexibility in this book will discuss the impact of these fuels on combustion in detail.
- Market penetration by regenerative energy:
  All forecast agencies predict an increasing share of regenerative energy in the future, particularly in wind and solar energy. Both, however, come with a need for fast starting balancing (reserve) power plants. Most likely this will be an important reason for the on-going success of gas turbines in the power market for the foreseeable future. A faster start capability has some severe implications on gas turbine design, but with only a little impact on the combustion system. There are even scenarios based on a very high market penetration with regenerative energy, which result in the requirement for energy storage systems. Several options for storage systems – such as compressed air (CAES), pumped hydro or Li-Ion

© Woodhead Publishing Limited, 2013

battery – are currently being evaluated. Another more unusual scenario is based on water electrolysis producing H_2 and consequently storing this in large caverns. This fuel would most likely be burnt in gas turbines again. The combustion technology required for this fuel may be similar to what is needed for the gas composition from an IGCC process with carbon capture. On the other hand H_2-fuel, which is based on electrolysis, will be extremely clean and more cycle options will be possible and will have to be evaluated. As an alternative, this H_2 also could be fed into the existing natural gas pipeline infrastructure up to a certain volumetric content. Even further processing of H_2 into CH_4 is under consideration; both as possibly a simpler way to store huge amounts of power compared to direct storage of electricity.

In the following sections, examples of technology concepts to produce higher combustor temperatures and pressure will be briefly discussed, and the concept of EGR will be summarised.

10.5.1 Efficiency increase

As previously discussed, the future increase of gas turbine cycle efficiency will go along with an increase in pressure ratio and turbine inlet temperature. Improvements in the technology of materials, coatings and seals, which are resulting in a relative reduction of cooling and leakage air in the turbine, will most probably not be sufficient to prevent a future increase in the combustor exit temperature. This will not only impact on NO_x emission formation (see Section 10.3), but also on the development of resulting technologies, such as mixing improvement, peak temperature reduction and residence time optimisation.

10.5.2 Catalytic combustion

Combustion concepts like catalytic combustion may become attractive again, if the identified main hurdles like robustness regarding overheating, fast catalyst ageing and high cost could be overcome in the future. Different catalytic combustion concepts have already been successfully applied, either in low temperature class gas turbines or full scale combustion test rigs and have demonstrated some NO_x emission reduction potential. Based on the temperature limitations of the currently used materials in the catalytic reactor it is, on the other hand, clear that catalytic combustion systems in high efficiency and thus high temperature combustion systems could only be successful in the future, if these temperature limits could be increased significantly in order to increase the share of the fuel conversion in the catalytic

© Woodhead Publishing Limited, 2013

sector and, consequently, to reduce the size of the burn out section and thus the thermal NO_x formation downstream of the catalytic reactor. This, however, may be in competition with the increasing relevance of fuel flexibility. The quality of liquid fuels, which are often backup fuels or syngas from gasification plants, may not be sufficient for use in catalytic combustors without additional sophisticated fuel treatment.

In addition to this, it is expected that the challenges related to combustion dynamics will also increase with the increasing pressure ratio and flame temperature. Based on the equations for energy conservation (Poinsot and Veynante, 2001) it may be expected that the acoustic energy in the system, which is equivalent to pressure fluctuations, will increase with the source term for energy fluctuation $\tilde{p}\,\tilde{\omega}$, with $\tilde{p}$ the pressure fluctuation and $\tilde{\omega}$ the heat release fluctuation. Both may be assumed to increase in future engines at an increasing pressure ratio and flame temperature. The development of systems with higher acoustical damping, but without excessive usage of cooling air for the damping elements will, therefore, be a critical task in the design process of future combustion systems. Hand in hand with this the mechanical design regarding fluid–structure interaction and the implementation of predictive thermo-acoustical stability analysis of a combustion system will need to be advanced. These topics, especially would benefit significantly from the enhanced availability of computational resources.

So-called mild combustion systems are based on the idea of stretching out the reaction or heat release zone on the basis that these flames will be more insensitive regarding combustion dynamics. These concepts are finally based on lifted flames in different geometrical arrangements, but the fuel–air jet always contains relatively large amounts of exhaust gas before the flame front is reached and therefore the effect of imperfectly mixed fuel air pockets on emissions can be reduced. The main incentives for looking into these concepts, however, are combustion dynamics while the reduction of NO_x emissions in gas turbine combustors with the aforementioned concepts is expected to be mainly a secondary effect. The transfer of such concepts from boilers and furnaces (Wünning and Wünning, 1997), which are mostly based on non-premixed burners, into gas turbine combustors is an on-going research topic and has not yet been implemented into large gas turbine combustors (Rao *et al.*, 2008).

CO_2 capture from gas turbines running on natural gas – EGR

The introduction of CO_2 emission reduction from the exhaust of a gas turbine via carbon capture will involve significant changes in the design of the core and particularly of the combustion system. This section will discuss the natural gas fired gas turbine cycle with EGR. This concept has been under evaluation for some years, with a focus on thermodynamical cycle studies and the resulting impact on combustion systems (ElKady *et al.*, 2008; Guethe *et al.*, 2009). Pre-combustion capture cycles, which are based

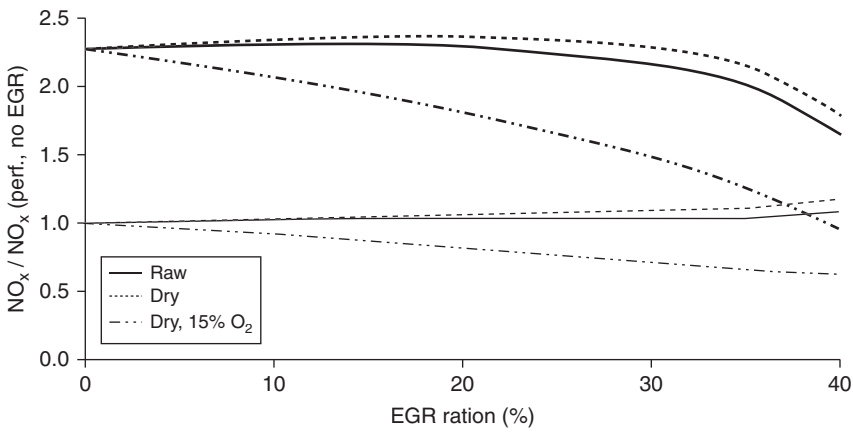
© Woodhead Publishing Limited, 2013

on hydrogen rich fuels – similar to fuel from IGCC cycles with carbon capture – are not covered in this chapter.

Figure 10.15 shows a simplified sketch of an EGR cycle. The fundamental idea of the EGR cycle is to increase the CO_2 content in the gas turbine exhaust to a level, at which CO_2 washing/capture technologies become more efficient. It is expected that the capital cost of the total plant can be significantly reduced, in case CO_2 capture is needed for natural gas fired gas turbines. Current studies have not yet been able to produce a very clear picture regarding the rate of EGR, but it is likely that flow rates in the order of one-third of the total exhaust flow will have to be circulated in such cycles. This approximately results in oxygen content in the combustor exit of only 3–4% compared to approximately 10% in a normal gas turbine cycle. Because the oxygen content in the vitiated air, which is supplied by the compressor, is significantly reduced, it will cause considerable design changes to the combustor and especially to the burner.

The regulation of emissions from gas turbine power plants is often defined on a parts per million by volume basis; in many countries the emissions of gas turbines are normalised to an oxygen content of 15%-Vol in the dry exhaust gas. In the case of EGR, however, it is likely that emissions legislation will finally change to be based on mass basis finally, possibly tons per Gigajoule or tons per year, in order to eliminate the effect of the oxygen dilution due to the circulating exhaust.

Figure 10.16 shows NO_x emissions calculated from a kinetic model of a combustor, which is exposed to a premixed fuel/oxidiser mixture at a variable EGR rate. The calculations are all made for a constant combustor exit temperature of 1700°C using the GRI3 mechanism. Two fuel/air mixing



10.16 NO_x emissions calculated from a kinetical model of a combustor, which is exposed to a premixed fuel/oxidiser mixture at a variable EGR rate.

© Woodhead Publishing Limited, 2013

quality scenarios are compared in Fig. 10.16, one scenario assuming a perfect fuel oxidiser mixture quality (thin lines starting at relative NO_x of 1 at EGR = 0) and the other scenario assuming a real quality mixture (bold lines starting at relative NO_x of 2.3 at EGR = 0). The figure shows that in the perfect mixture case there is no NO_x emission benefit to be expected in the exhaust. The values corrected to 15% oxygen suggest a reduction of NO_x emission content; however, this is mainly due to the significant dilution with increasing EGR rate. On the other hand for the real fuel/oxidiser mixture scenario there is a positive NO_x emission effect visible at high EGR rates, when compared to the perfect mixture. This is mainly due to the decrease of the adiabatic flame temperature in the fuel rich and thus hot pockets of the flame. This fits accurately with the real-life test results, which have been made in the past with EGR systems in boilers or automotive engines, and is also equivalent to the peak temperature reduction by dilution (steam or water injection) in diffusion flames.

It has also been highlighted by Guethe *et al*. (2009) that in an EGR environment, especially at high recirculation rates, CO burnout can become a major technical hurdle. This is not only because of the increased carbon content in the combustor, but it is also related to the lack of mixing in real burners. Compared to normal lean premixed gas turbine cycles, it is much more likely that fuel rich parts of the flame may even be exposed to regions with an oxygen deficit.

It is additionally essential to note that the reactivity of the EGR fuel/oxidiser mixture is largely reduced compared to mixtures with regular air. The reduction of reactivity is in the range of one order of magnitude. Thus aero design adaptations to the burner will be required as well as fuel/oxidiser staging modifications in order to maintain stable operation with a sufficient blow off margin all over the load cycle.

10.6 References

Biagioli F and Güthe F, (2007), Effect of pressure and fuel-air unmixedness on NO_x emissions from industrial gas turbine burners, *Combustion and Flame*, **151**, pp. 274–288.

Beér J and Chigier N, (1972), *Combustion Aerodynamics*, Malabar, Robert E. Krieger Publishing Company.

Bikas G, (2001), *Kinetic* Mechanism *for Hydrocarbon Ignition*, Rheinisch-Westfälische Technische Hochschule Aachen, Fakultät für Maschinenwesen.

Blackshear P, (1952), *Driving Standing Waves by Heat Addition*, 4th International Symposium on Combustion, Cambridge, Massachusetts.

BP, 2009, *Statistical Review of World Energy* June (2009), www.bp.com/statisticalreview

Callaghan EE and Rugheri RS, (1948), *Investigation on the penetration of an air jet, directed perpendicular to an air stream*, NACA Technical Note 1615.

© Woodhead Publishing Limited, 2013

Chomiak J and Lapatnikov A, (2005), Molecular transport effects on turbulent flame propagation and structure, *Progress in Energy and Combustion Science,* **31**, pp. 1–73.

Crocco L and Cheng S, (1956), *Theory of Combustion Instability in Liquid Propellant Rocket Motors*, Butterworths.

EER, (2006), *Lessons to be Learned from the Renewable Generation Strategies of Europe's Utilities*, Orlando, Power Gen International.

EER, (2009), *Global Carbon Sequestration Markets and Strategies, 2009–2030*, Cambridge, Emerging Energy Research.

ElKady A, Evulet A, Brand A, Ursin T and Lynghjem A, (2008), *Exhaust Gas Recirculation in DLN F-Cass Gas Turbines for Post-Combustion CO_2 Capture*, Proceedings of ASME Turbo Expo 2008, GT2008–51152, Berlin.

Enerdata, (2008), *The world energy demand in 2007*, www.enerdata.fr

Fenimore C, (1971), Formation of nitric oxide in premixed hydrocarbon flames, *Proceedings of the Combustion Institute* **13**, pp. 373–380.

Frenklach M, Bowman T, Smith G and Gardiner G, GRI3.0, http://www.me.berkeley.edu/grI_mech/

Guethe F, de la Cruz García M and Burdet A, (2009), *Flue Gas Recirculation in Gas Turbine: investigation of Combustion Reactivity and NO_x Emission*, Proceedings of ASME Turbo Expo 2009, GT2009–59221, Orlando.

Gupta A, Lilley D and Syred N, (1984), *Swirl Flows*, England, Abacus Press.

Krebs W, Flohr P, Prade B and Hoffmann S, (2002), Thermoacoustic stability chart for high intense gas turbine combustion systems, *Combustion, Science and Technology*, **174**, pp. 99–128.

Leuckel W, (1968), *Swirl intensities, swirl types and energy losses of different swirl generating devices*, Ijmuiden, Doc. No. GO2/a/16, IFRF.

Peters N, (2000), *Turbulent Combustion*, Cambridge University Press.

Peters N, (1999), The turbulent burning velocity for small scale and large scale turbulence, *Journal Fluid Mechanics*, **384**, pp. 107–132.

Poinsot T and Veynante D, (2001), *Theoretical and Numerical Combustion*, RT Edwards, ISBN: 1–930217–05–6

Prade P, Gruschka U, Hermsmeyer H, Hoffmann S, Krebs W and Schmitz U, (2002), V64.3A Gas turbine natural gas burner development, ASME Paper GT-2002–30106.

Putnam A, (1971), *Combustion Driven Oscillations in Industry*, American Elsevier Publishers, New York.

Putnam A and Dennis W, (1952), *Organ Pipe Oscillations in a Flame-filled Tube*, 4th International Symposium on Combustion, Cambridge, Massachusetts, pp. 566.

Rao G, Levy Y and Gutmark E, (2008), *Chemical Kinetic Analysis of a Flameless Gas Turbine Combustor*, Berlin, Proceedings of ASME Turbo Expo 2008, GT2008–50619.

Rayleigh, JWS, (1878), the explanation of certain acoustical phenomena, *Nature*, **XVIII**, pp. 319–321.

Sattelmayer T, (2000), *Influence of the combustor aerodynamics on combustion instabilities from equivalence ratio fluctuations*, ASME Paper 2000-GT- 0082.

Seume JR, Vortmeyer N, Krause W, Hermann J, Hantschk C-C, Zangl P, Gleis S, Vortmeyer D and Orthmann A, (1997), Application of Active Combustion Instability Control to a Heavy Duty Gas Turbine, ASME Paper 97-AA-119.

© Woodhead Publishing Limited, 2013

Siewert P, (2006), *Flame front characteristics of turbulent lean premixed methane/air flames at high pressure*, PhD thesis ETH Zurich.

Smith GP, Golden DM, Frenklach M, Moriarty NW, Eiteneer B, Goldenberg M, Bowman CT, Hanson RK, Song S, Gardiner Jr WC, Lissianski VV and Zhiwei Q, http://www.me.berkeley.edu/gri_mech/

Van Kampen J, (2006), *Acoustic Pressure* Oscillations Induced *by* Confined Turbulent Premixed Natural Gas Flames, Febodruck PV, Netherland, ISBN 90–365–2277–3

Williams F, (1985), *Combustion Theory*, 2nd Edition, Princeton University.

Wünning JA and Wünning JG, (1997), Flameless oxidation to reduce thermal NO-formation, *Progress in Energy and Combustion Science*, **23**, pp. 81–94.

Zabetakis MG, (1965), Flammability characteristics of combustible gases and vapors, Bulletin 627, Bureau of Mines.

Zeldovich Y, (1946), USSR, The oxidation of nitrogen in combustion and explosion, *Acta Phisicochim*, **21**, pp. 577–628.

Zimont V, Polifke W, Bettelini M and Weisenstein W, (1998), An efficient computational model for premixed turbulent combustion at high Reynold numbers based on turbulent flame speed closure, *Transactions of the ASME*, **120**, pp. 526–532.

© Woodhead Publishing Limited, 2013

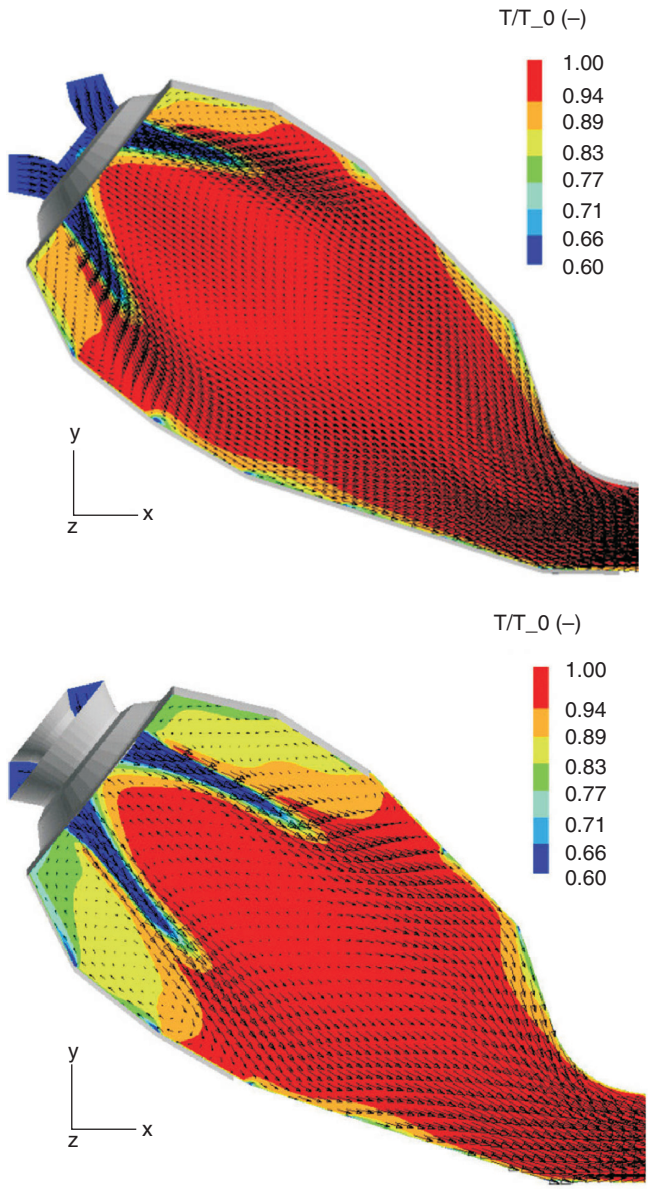


Plate XIV (Chapter 10) Flame shape, characterized by a strong temperature gradient from dark to white. The burner design with CBO changes the flame shape significantly; the flow field appears slim and consequently more fluid elements cross the flame front at a larger time lag.

© Woodhead Publishing Limited, 2013

11

Gas turbine performance modelling, analysis and optimisation

A. M. Y. RAZAK, Gas Path Analysis Ltd, UK

DOI: 10.1533/9780857096067.3.423

Abstract: This chapter discusses the performance of both industrial and aero gas turbines. This includes both steady-state and transient performance of gas turbines. Methods to determine steady-state and transient performance are discussed in detail, including the prediction of thermodynamic properties of air and products of combustion. Various engine configurations, including complex cycle, which employ reheat (afterburning), intercooling and regeneration are included. Methods for controlling dry low emission combustion are also discussed.

Key words: design and off-design-point performance, industrial and aero gas turbine, steady-state and transient performance, adaptive model-based control, future trends, geared turbo-fan.

11.1 Introduction

Although other aspects of gas turbine engineering are of paramount importance, as they are largely responsible for the excellent reliability and performance of gas turbines, it is performance that users purchase as the end product. This is because performance directly impacts on the profitability of industries that employ them. Poor performance results in increased life cycle costs – primarily due to higher fuel/energy costs – and potentially reduced production.

In this chapter, we will discuss the predictions of various gas turbine cycles, both at design-point and off-design operation including transient performance. However, we will start the discussion by first considering the thermodynamics of air and the products of combustion, as they are extensively used in the prediction of the performance of gas turbines, which will require a brief discussion of the laws of thermodynamics. We will then consider the thermodynamics of various gas turbine components, such as compressors, combustors and turbines.

We will then be in a position to discuss the design-point performance of various gas turbine cycles. This will vary from simple cycle engines to complex cycles, which employ regeneration, intercooling and reheat cycles. Also,

© Woodhead Publishing Limited, 2013

we will include the design-point performance of aero gas turbine cycles such as turbo-fans, turbo-jets and turbo-shaft engines, which are currently employed in industry.

These cycles have different engine configurations, namely the number of shafts, and we will discuss the rationale for such arrangements. This will require an introduction to engine component characteristics for compressors, combustors and turbines, as they have a profound impact on the off-design prediction and behaviour of gas turbines.

The above discussion will enable us to consider methods for predicting the off-design performance of the various gas turbine cycles, including the different mechanical arrangements used. We will also introduce numerical methods required for the prediction of off-design performance of gas turbines.

The above discussion of gas turbine performance is concerned with the steady-state performance prediction of gas turbines. However, gas turbines have to operate satisfactorily during transients such as start-up, shutdown and change in load/power demand. Also, changes in ambient conditions influence transient operation. Therefore, methods to predict the transient performance of gas turbines are also included.

Although much of the above discussion is associated with the prediction of gas turbine performance, both at steady and transient conditions, we will discuss the behaviour of these gas turbine cycles with change in load and ambient conditions. Also the means to augment power will be included here.

As gas turbines operate over wide range of ambient conditions they invariably impact the performance of the engine. We will consider means to optimise the gas turbine performance by introducing variable geometry to different components, namely the compressors and turbines. This will be influenced by the number of shafts employed in the construction of the gas turbine. Modern gas turbines employ combustion systems to reduce harmful or toxic emissions such as NO_x, CO and UHCs, known as DLE combustors. The method employed to control such combustion systems also impact on the performance of the gas turbines. The means to optimise the performance of gas turbines employing such combustion systems will also be included. Gas turbines drive various loads, such as electric generators, compressors and pumps. Therefore, in optimising the performance it is essential to consider not only the gas turbine but the whole process. We will introduce model-based control to optimise the process.

Future trends in gas turbine performance technologies and the factors driving such technologies will be discussed.

11.2 Design-point modelling of gas turbine cycles

Gas turbines are heat engines and the laws of thermodynamics govern their performance. The first and second laws of thermodynamics are the laws we

© Woodhead Publishing Limited, 2013

apply in describing their performance. In this section we will briefly review these laws and discuss the design-point performance of gas turbines. The reference to pressures and temperatures in this chapter refer to total or stagnation pressures and temperatures, rather than to static values. This is because the total energy (enthalpy) in continuous flow systems refers to stagnation values for pressures and temperatures, as they include the dynamic pressures and temperatures of a flow gas.

11.2.1 First law of thermodynamics

The first law of thermodynamics is based on the law of conservation of energy, which states that energy cannot be created or destroyed, but can be transferred from one form to another. As gas turbines are heat engines, converting heat into work, the first law requires that we cannot produce more work than the heat supplied. This restriction implies that the thermal efficiency of a heat engine, which is defined as the ratio of the work done to the heat supplied, cannot be greater than 100%.

11.2.2 Second law of thermodynamics

There are many definitions of the second law of thermodynamics. From a heat engine perspective, the most useful definition is that the thermal efficiency of a heat engine must be less than 100%. We may define a heat engine as a device operating in a cycle, producing work from a heat source and rejecting heat to a heat sink. As a thermodynamic system, a heat engine operates in a cycle, the initial and final states being identical. Therefore, if we supply a quantity of heat (Q_1) to produce work (W) and reject heat to a heat sink or surroundings (Q_2), then the second law of thermodynamics requires that the heat rejected (Q_2) cannot be zero. Thus the thermal efficiency (η_{th}) may be defined as:

$$\eta_{th} = \frac{W}{Q_1} \qquad [11.1]$$

Since the net heat supplied is $Q_1 - Q_2$, the first law of thermodynamics requires the work done (W) must equal the net heat supplied. Therefore the thermal efficiency can be defined as:

$$\eta_{th} = 1 - \frac{Q_2}{Q_1} \qquad [11.2]$$

The French physicist Nicolas Léonard Sadi Carnot in 1824 showed that the maximum thermal efficiency of a heat engine occurs when all the heat

© Woodhead Publishing Limited, 2013

supplied (Q_1) is at a constant temperature (T_1) and when all the heat rejected (Q_2) is also at a constant temperature (T_2). The maximum thermal efficiency is then determined by:

$$\eta_{max} = 1 - \frac{T_2}{T_1} \quad [11.3]$$

This is another definition of the second law of thermodynamics.

Entropy

The availability and accessibility of energy is important in producing work from a heat engine, such as a gas turbine cycle. The more accessible the energy is, the lower is its entropy. Consequently, the less available the energy, the higher is its entropy. Entropy is a thermodynamic property, given the symbol S, and the change in entropy during a thermodynamic process is defined as:

$$\Delta S = \int \frac{dQ}{T} \quad [11.4]$$

What prevents the heat engine from achieving 100% thermal efficiency is this increase in entropy or degradation of energy, thus preventing the heat rejected to the heat sink (Q_2) reducing to zero. Therefore, some heat must always be rejected from a heat engine (i.e., Q_2 cannot be zero). Further details on the laws of thermodynamics are given by Rogers and Mayhew (1992) and Eastop and McConkey (1993).

11.3 Steady flow energy equation

Gas turbine cycles are continues flow processes and differs from other internal combustion (piston) engines, which are intermittent flow processes. Therefore the governing thermodynamic equation for modelling of such continues flow processes that satisfy the first of thermodynamics is the steady flow energy equation or SFEE.

$$Q - W = \Delta H \quad [11.5]$$

where Q represents the heat input into a steady flow thermodynamic system, W represents the work done by the thermodynamic system and ΔH represents the change in the energy of the gas in the system. ΔH has capacity to hold heat (specific heat) and is referred to as the change in the stagnation or total enthalpy in the thermodynamic system.

© Woodhead Publishing Limited, 2013

11.4 The ideal simple gas turbine cycle

Most gas turbines use the simple or open gas turbine cycle. It consists of the following thermodynamic processes:

1. Compression.
2. Combustion.
3. Expansion.
4. Heat rejection.

The compression is carried out using axial and centrifugal compressors, while the expansion is usually carried out using axial turbines but some small gas turbines use radial turbines. The combustion process is normally achieved by burning hydrocarbon fuels in a combustion chamber, and various stages or zones are required to achieve satisfactory combustion. At least two stages are required, corresponding to the primary zone, where the fuel is burnt and heat is released, and a dilution zone, where the temperature of the products of combustion is reduced to meet the required operating temperature of the turbine. The compressor and the turbine are mechanically linked by a shaft, as shown in Fig. 11.1, and are a schematic representation of a single-shaft gas turbine. Referring to Fig. 11.1, the thermodynamic processes involved in an ideal gas turbine cycle, which is known as the Joules cycle or Brayton cycle, are:

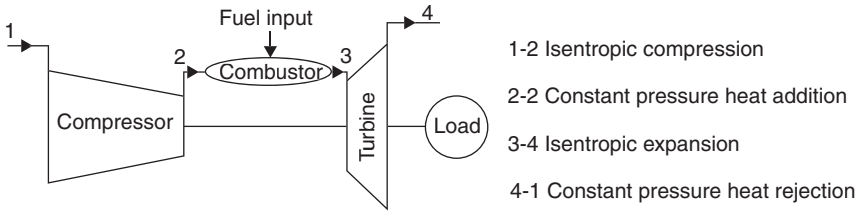
1. Isentropic compression.
2. Constant pressure heat addition.
3. Isentropic expansion.
4. Constant pressure heat rejection.

The thermodynamic cycle can be represented on a pressure–volume (PV) diagram, as shown in Fig. 11.2. However it is more useful to represent the cycle on a temperature–entropy (TS) diagram, as shown in Fig. 11.3. As stated in Section 11.2.2, the thermal efficiency of a thermodynamic cycle is given by the ratio of the net work done and the heat supplied, and for an ideal simple gas turbine cycle the ideal thermal efficiency can be described by Equation [11.6].

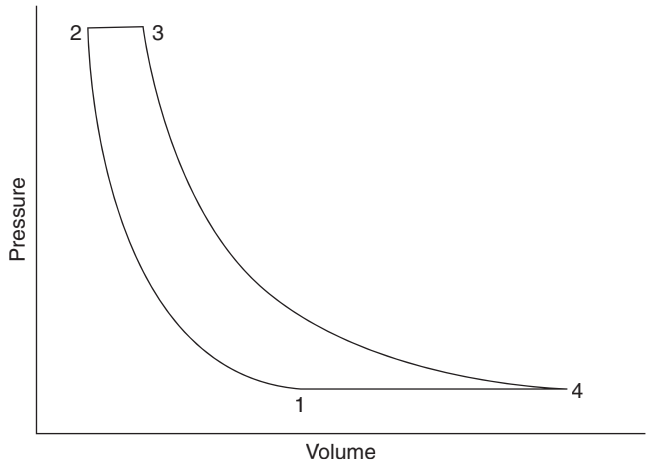
$$\eta_{\text{th}} = 1 - \frac{1}{\text{Pr}^{(\gamma-1)/\gamma}} \qquad [11.6]$$

where η_{th} is the thermal efficiency, Pr is the compressor pressure ratio, γ is the isentropic index, and is defined as the ratio of specific heats (cp/cv), where cp is the specific heat of the gas at constant pressure and cv is the specific heat at constant volume.

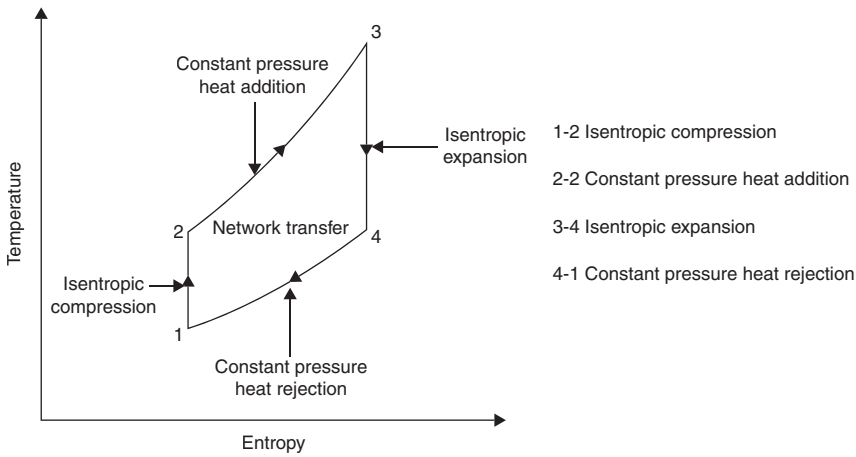
© Woodhead Publishing Limited, 2013



11.1 A schematic representation of a simple cycle gas turbine.



11.2 PV diagram of a simple gas turbine cycle.



11.3 Representation of a gas turbine cycle on a temperature–entropy diagram.

© Woodhead Publishing Limited, 2013

From Equation [11.6] the thermal efficiency depends on the pressure ratio and the isentropic index of the gas, and increases with pressure ratio and the isentropic index. However, thermal efficiency cannot increase indefinitely with pressure ratio, as this would violate the second law of thermodynamics, which states that the thermal efficiency of any heat engine cannot exceed the Carnot cycle efficiency. Therefore, there is an upper limit for the compressor pressure ratio, and it is dependent on the maximum-to-minimum cycle temperature ratio (T_3/T_1). It can be shown that the compressor temperature ratio (T_2/T_1) can be given by:

$$\frac{T_2}{T_1} = \mathrm{Pr}^{\frac{\gamma-1}{\gamma}} \qquad [11.7]$$

Therefore, Equation [11.6] can also be represented in terms of the compressor temperature ratio as:

$$\eta_{\mathrm{th}} = 1 - \frac{T_1}{T_2} \qquad [11.8]$$

For a given maximum-to-minimum temperature ratio (T_3/T_1) the maximum pressure ratio ($\mathrm{Pr}_{\mathrm{max}}$) is:

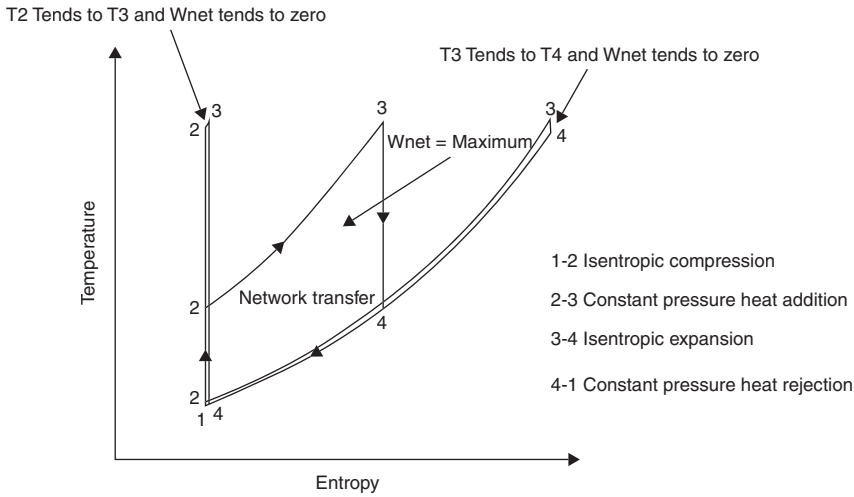
$$\mathrm{Pr}_{\mathrm{max}} = \frac{T_3}{T_1}^{\frac{\gamma}{\gamma-1}} \qquad [11.9]$$

Therefore, the corresponding thermal efficiency when operating at the maximum or limiting compressor pressure ratio will be equal to the Carnot efficiency. In this limiting case, all the heat is supplied at the maximum cycle temperature and all the heat is rejected at the minimum cycle temperature. This is the Carnot cycle requirement to achieve the Carnot cycle thermal efficiency, and the ideal simple gas turbine cycle cannot exceed the Carnot cycle efficiency, as required by the second law of thermodynamics. Figure 11.4 shows the gas turbine cycle for this limiting case on the temperature–entropy diagram.

Another performance parameter associated with the performance of an ideal simple cycle gas turbine is the specific work, and is defined as the net work done by the cycle per unit mass flow rate of gas through the cycle, which is usually air. The specific work is therefore equal to the turbine work produced less the compressor work absorbed and is given by:

$$W_{\mathrm{net}} = cp\left(T_3 - T_4\right) - cp\left(T_2 - T_1\right) \qquad [11.10]$$

© Woodhead Publishing Limited, 2013



11.4 Effect of pressure ratio on the temperature–entropy diagram for an ideal gas turbine cycle when T_3 is constant.

Equation [11.10] can also be represented in terms of pressure ratio and maximum-to-minimum cycle temperature ratio as:

$$W_{\text{net}} = cpT_1\left(\frac{\text{Pr}^{\frac{\gamma-1}{\gamma}}-1}{\text{Pr}^{\frac{\gamma-1}{\gamma}}}\right)\left(\frac{T_3}{T_1}-\text{Pr}^{\frac{\gamma-1}{\gamma}}\right) \qquad [11.11]$$

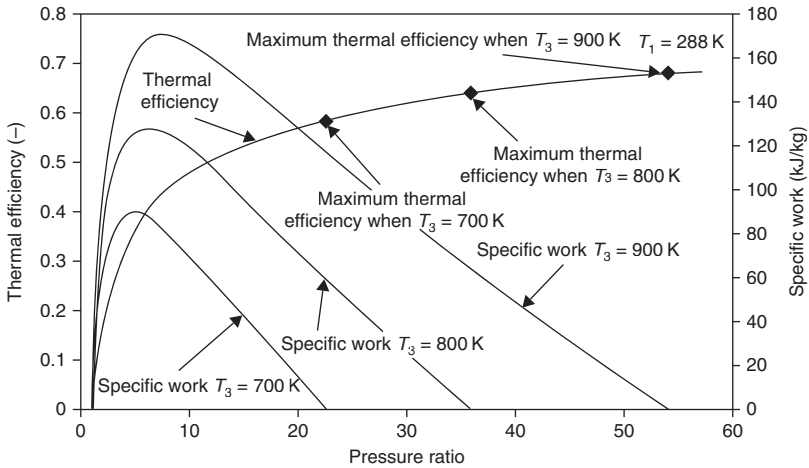
From Equation [11.11] it can be seen that the specific work tends to zero when the compressor pressure ratio (Pr) tends to unity and when Pr tends to (T_3/T_1). It is also evident from Equation [11.6] when Pr tends to unity the thermal efficiency tends to zero, and when Pr tends to T_3/T_1 the thermal efficiency tends to the Carnot efficiency. Thus, the maximum specific work lies between these two limit values of Pr. By differentiation of Equation [11.11] with respect to Pr it can be shown that the maximum specific work occurs when the compressor pressure ratio (Pr_{opt}) is equal to:

$$C_{\text{opt}} = \sqrt{\frac{T_3}{T_1}} \qquad [11.12]$$

where $C_{\text{opt}} = \text{Pr}^{\frac{\gamma-1}{\gamma}}$.

The temperature-entropy diagram for the maximum specific work case is also shown in Fig. 11.4.

© Woodhead Publishing Limited, 2013



11.5 Variation of thermal efficiency and specific work with compressor pressure ratio.

The variation of thermal efficiency and specific work of an ideal simple cycle with pressure ratio, for a series of maximum (T_3) and a given minimum temperature (T_1), is shown in Fig. 11.5.

11.5 Reversibility and efficiency

The discussion above has considered the ideal or reversible thermodynamic processes for the compression, expansion, heat addition and heat rejection present in a gas turbine (Joule) cycle. However, such reversible processes do not exist in a practice. In this section, we consider the prediction of the design-point performance of practical gas turbine cycles (i.e., when the thermodynamic processes are irreversible).

11.5.1 Compressor and turbine irreversibility and efficiency

Irreversibilities in thermodynamic processes reduce the accessibility of energy, or the energy is degraded during the thermodynamic process. Therefore, for an adiabatic compression process, additional energy has to be supplied to achieve the required pressure ratio. Similarly, during an adiabatic expansion process the degradation of energy results in the ideal work done by the expander (turbine) to be always greater than the actual work done. The presence of irreversibilities during adiabatic compression and expansion processes increases the entropy associated with these processes and gives rise to the concept of efficiency.

© Woodhead Publishing Limited, 2013

Isentropic efficiency

The isentropic efficiency of a compression process is defined as the ratio of the ideal work done to the actual work done. Therefore, the isentropic efficiency (η_c) is given by:

$$\eta_c = \frac{cp\left(T_2' - T_1\right)}{cp\left(T_2 - T_1\right)} \qquad [11.13]$$

where T_2' is the ideal compressor exit temperature. T_1 is the compressor inlet temperature and *cp* is the specific heat at constant pressure – we shall assume a constant specific heat, and the effect of the variation of specific heats will be discussed later in the chapter. Equation [11.13] can be represented in terms of the compressor pressure ratio as:

$$\eta_c = \frac{T_1(c-1)}{T_2 - T_1} \qquad [11.14]$$

where $C_{\text{opt}} = \text{Pr}^{\frac{\gamma-1}{\gamma}}$ and Prc is the compressor pressure ratio.

Therefore the compressor exit temperature can be determined by:

$$T_2 = T_1 + \frac{T_1}{\eta_c}(c-1) \qquad [11.15]$$

Similarly, for an expansion process the isentropic efficiency (η_t) is given by:

$$\eta_t = \frac{cp(T_3 - T_4)}{cp(T_3 - T_4')} \qquad [11.16]$$

where T_4' is the ideal expander/turbine exit temperature, T_3 is the expander/turbine inlet temperature and *cp* is the specific heat at constant pressure – again we shall assume a constant specific heat and the effect of the variation of specific heats will be discussed later.

In a manner similar to the compressor isentropic analysis above, it can be shown that the expander/turbine exit temperature is given by:

$$T_4 = T_3 - T_3\eta_t\left(1 - \frac{1}{c}\right) \qquad [11.17]$$

where $c = \text{Prt}^{\frac{\gamma-1}{\gamma}}$ and Prt is the expander/turbine pressure ratio.

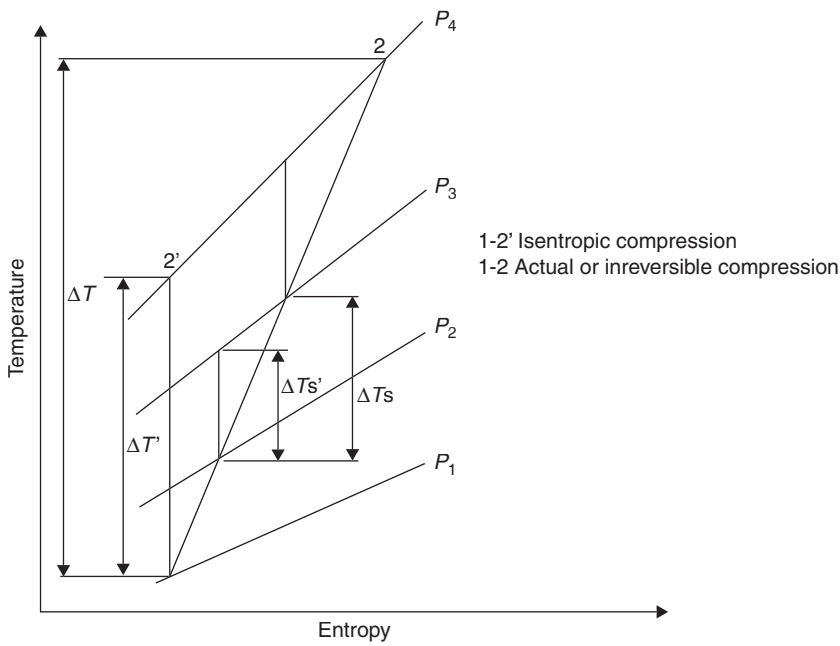
© Woodhead Publishing Limited, 2013

Polytropic efficiency

The isentropic analysis discussed above only considers the start and end states of a compression or expansion process. However, unlike temperatures, pressures, enthalpy and entropy, work and heat transfer are not thermodynamic properties and the amounts of work and heat transfer are dependent on the thermodynamic path. To determine the work transfer during a polytropic process, the compression or expansion process is assumed to occur in small steps (infinitesimally small steps), as illustrated in Fig. 11.6. The work transfer for a polytropic process is now the sum of all the work transfers of the individual steps or stages. To determine the work for each infinitesimally small step, we treat each step/stage using the isentropic analysis discussed above (i.e. the polytropic efficiency (η_p) is equal to the stage isentropic efficiency). Therefore for a compression process:

$$\eta_p = \frac{\mathrm{d}T'}{\mathrm{d}T} \qquad [11.18]$$

where $\mathrm{d}T'$ is the ideal temperature rise, $\mathrm{d}T$ is the actual temperature rise for each step.



11.6 Polytropic process of a multi-stage compressor.

© Woodhead Publishing Limited, 2013

For an isentropic process in differential form:

$$\frac{\mathrm{d}T'}{T} = \frac{\gamma - 1}{\gamma} \times \frac{\mathrm{d}P}{P} \qquad [11.19]$$

Substituting Equations [11.19] into [11.18] we get:

$$\eta_p \frac{\mathrm{d}T}{T} = \frac{\gamma - 1}{\gamma} \times \frac{\mathrm{d}P}{P} \qquad [11.20]$$

Integration Equation [11.20] the polytropic efficiency (η_p) can be expressed as:

$$\frac{T_2}{T_1} = \left(\frac{P_2}{P_1}\right)^{\frac{\gamma-1}{\gamma\eta_p}} \qquad [11.21]$$

where T_1 and T_2 are the compressor inlet and actual exit temperatures respectively, and P_1 and P_2 are the compressor inlet and exit pressures.

A similar analysis can be carried out for an expansion process and it can be shown that the polytropic efficiency (η_p) for an expansion process is given by:

$$\frac{T_4}{T_3} = \left(\frac{P_4}{P_3}\right)^{\frac{(\gamma-1)\eta_p}{\gamma}} \qquad [11.22]$$

where T_3 and T_4 are the expander/turbine inlet and actual exit temperatures, and P_3 and P_4 are the expander/turbine inlet and exit pressures.

For a polytropic compression process the actual specific work done (W) is:

$$W = cp\left(T_2 - T_1\right) = cpT_1\left(\left(\mathrm{Prc}\right)^{\frac{\gamma-1}{\gamma\eta_p}} - 1\right) \qquad [11.23]$$

For the same actual specific work (W) the corresponding isentropic analysis yields:

$$W = cp\left(T_2 - T_1\right) = cp\frac{T_1}{\eta_c}\left(\left(\mathrm{Prc}\right)^{\frac{\gamma-1}{\gamma}} - 1\right) \qquad [11.24]$$

Therefore, we can relate the compressor isentropic efficiency to the polytropic efficiency by equating Equations [11.23] and [11.24]:

© Woodhead Publishing Limited, 2013

$$\eta_c = \frac{(\mathrm{Prc})^{\frac{\gamma-1}{\gamma}} - 1}{(\mathrm{Prc})^{\frac{\gamma-1}{\gamma\eta_p}} - 1} \quad [11.25]$$

Therefore, for a given polytropic efficiency (η_p) and for the case $\eta_p < 1$ and $\mathrm{Prc} > 1$, the isentropic efficiency (η_c) decreases as the pressure ratio increases. The reason for the decrease in the isentropic efficiency with pressure ratio is due to the increase in stage inlet temperature, due to irreversibilities, as we move along the compression process. This increase in inlet temperature increases the work required to achieve the required stage pressure ratio.

A similar analysis can be carried out for expanders/turbines where it can be shown that the isentropic efficiency (η_t) is related to the polytropic efficiency by the equation:

$$\eta_t = \frac{1 - (1/\mathrm{Prt})^{\frac{(\gamma-1)\eta_p}{\gamma}}}{1 - (1/\mathrm{Prt})^{\frac{\gamma-1}{\gamma}}} \quad [11.26]$$

where η_t and Prt are the expander/turbine isentropic efficiency and pressure ratio respectively. Examining Equation [11.26], and for $\eta_p < 1$ and $\mathrm{Prt} > 1$ and a given polytropic efficiency (η_p), the isentropic efficiency of an expander/turbine increases with pressure ratio. This is the opposite effect to that observed for compressors and for expanders/turbines. During expansion the increase in temperature to the downstream stage, due to irreversibilities, for a given stage pressure ratio, the work done by the downstream stages increases as we process along the expansion process.

When the pressure ratio is unity Equations [11.25] and [11.26] are indeterminate. However, applying L'Hôpital's rule to Equations [11.25] and [11.26] it can be shown that for these limiting pressure ratio cases the compressor and turbine isentropic efficiency equals the polytropic efficiency. The impact of pressure ratio on isentropic efficiency for a given polytropic efficiency are graphically illustrated in Fig. 11.7.

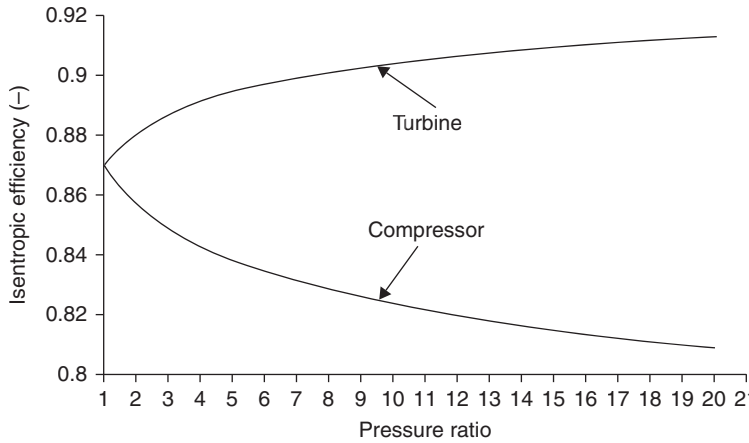
It is worth pointing out that for an adiabatic process the polytropic efficiency is related to the change in entropy by the following simple relationships.

For compressors:

$$\Delta s = R\left(\frac{1}{\eta_p} - 1\right)\ln \mathrm{Prc} \quad [11.27a]$$

where R is the gas constant, η_p is the polytropic efficiency and Prc is the compressor pressure ratio.

© Woodhead Publishing Limited, 2013



11.7 Variation of isentropic efficiency with pressure ration for a polytropic efficiency of 0.87.

From Equations [11.27a] and [11.27b] the change in entropy for an adiabatic process always increases when the polytropic efficiency is less than unity. When the polytropic efficiency is unity then the entropy change is zero, as the thermodynamic process is now reversible and adiabatic (isentropic).

For expanders/turbines:

$$\Delta s = R\left(1 - \eta_p\right)\ln \mathrm{Prt} \qquad [11.27b]$$

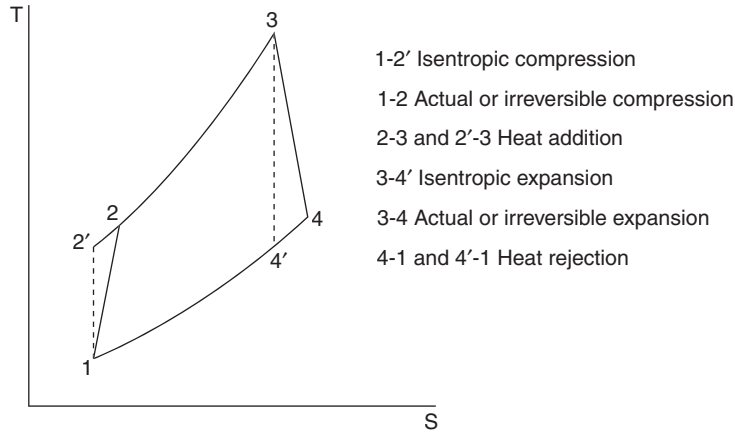
where Prt is the expander/turbine pressure ratio.

Again, when an adiabatic process is irreversible the entropy increases and the entropy change of a reversible process is zero.

11.5.2 The effect of irreversibilities during compression and expansion on thermal efficiency

The presence of irreversibilities has an adverse effect on thermal efficiency. We can now analyse the impact of irreversibilities during the compression and expansion processes on simple cycle gas turbine thermal efficiency. We shall assume the heat addition and rejection are still ideal processes and the effect of irreversibilities on heat addition and rejection will be considered later in the chapter. The temperature–entropy diagram when irreversibilities are present in the compression and expansion processes, are as shown in Fig. 11.8.

© Woodhead Publishing Limited, 2013



11.8 Gas turbine cycle on a temperature–entropy diagram when irreversibilities are present.

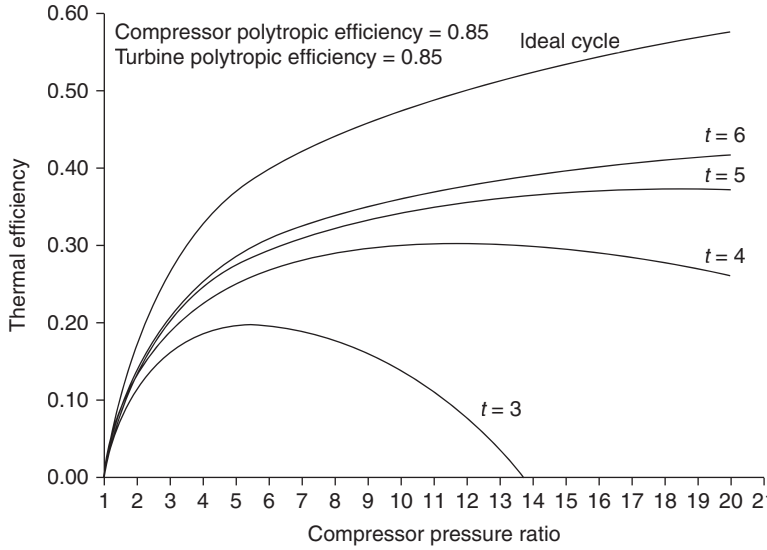
Using isentropic efficiencies it can be shown for an irreversible compression and expansion process the thermal efficiency (η_{th}) of a simple cycle gas turbine is given by:

$$\eta_{th} = \left(1 - \frac{1}{c}\right)\left(\frac{t\eta_t - (c/\eta_c)}{t - 1 - ((c-1)/\eta_c)}\right) \qquad [11.28]$$

where t is the maximum-to-minimum temperature ratio (T_3/T_1), η_c and η_t are the isentropic efficiencies of the compression and expansion processes, respectively, c is the pressure ratio function $\mathrm{Pr}(\gamma-1/\gamma)$ and γ is the isentropic index (cp/cv). It should be noted that the compressor pressure and the expansion ratios are in this case equal to Pr. This is because we have assumed ideal heat addition and rejection processes, and therefore the heat addition and rejection occurs at constant pressure.

From Equation [11.28] we observe that the thermal efficiency of a simple cycle gas turbine when irreversibilities are present is equal to the ideal thermal efficiency $(1-(1/c))$ multiplied by a function of t, η_c, η_t and c. Examining Equation [11.28] the thermal efficiency is more sensitive to the turbine isentropic efficiency than the compressor isentropic efficiency. Referring to Fig. 11.8, the inefficiency in the compression process results in a reduction in net (cycle) specific work and heat addition. However, when inefficiencies are present in the expansion process, there is only a reduction in net specific work and no change in the head addition. Thus, the sensitivity of the simple cycle thermal efficiency is greater to expansion inefficiencies. The impact of irreversibilities on thermal efficiency is illustrated in Fig. 11.9,

© Woodhead Publishing Limited, 2013



11.9 Variation of thermal efficiency with pressure ratio of a simple cycle gas turbine when irreversibilities are present in the compression and expansion processes.

which shows the thermal efficiency of a simple cycle gas turbine with pressure ratio when inefficiencies exist during compression and expansion processes. The thermal efficiency curve for the ideal simple cycle is also shown for comparison.

Differentiating Equation [11.28] with respect to t we get:

$$\frac{\mathrm{d}\eta_{\mathrm{th}}}{\mathrm{d}t} = \left(1 - \frac{1}{c}\right) \frac{\left((c + \eta_t) - \eta_t(\eta_c + c)\right)}{\eta_c \left(t - 1 - \left((c-1)/\eta_c\right)\right)^2} \qquad [11.29]$$

For $\eta_t < 1$ and $\eta_c < 1$ and Pr > 1 we can state that:

$$c > c\eta_t \qquad [11.30]$$

Also

$$\eta_t > \eta_t \eta_c \qquad [11.31]$$

Adding the Inequalities [11.30] and [11.31] and manipulating we get:

$$(c + \eta_t) - \eta_t(\eta_c + c) > 0 \qquad [11.32]$$

Inequality [11.32] is the numerator of Equation [11.29]. Therefore, from Equation [11.29] the thermal efficiency of the simple cycle gas turbine

© Woodhead Publishing Limited, 2013

increases with the maximum-to-minimum cycle temperature ratio (t). This differs from the ideal cycle, where the thermal efficiency is independent of (t), which can also be inferred from Equation [11.32] for the reversible compression and expansion cases (i.e. when $\eta_c = \eta_t = 1$), when Equation [11.32] is zero.

A similar analysis can be carried out using polytropic efficiencies and it can be shown that the thermal efficiency when irreversibilities are present is given by:

$$\eta_{\text{th}} = 1 - \frac{1}{c_t}\frac{(t - c_t)}{(t - c_c)} \qquad [11.33]$$

where t is the maximum-to-minimum temperature ratio (T_3/T_1), $c_t = \text{Pr}^{(\gamma-1)\eta p_t/\gamma}$ and $c_c = \text{Pr}^{(\gamma-1)/\gamma\eta p_c}$, Pr is the compressor and expander/turbine pressure ratio, and ηp_t and ηp_c are the compressor and turbine polytropic efficiencies respectively.

Differentiating Equation [11.33] with respect to (t) we get:

$$\frac{\text{d}\eta_{\text{th}}}{\text{d}t} = \frac{c_c - c_t}{c_t(t - c_c)^2} \qquad [11.34]$$

From Equation [11.34] it can be shown that $c_c - c_t > 0$ when irreversibilities are present, and therefore for all values of t the thermal efficiency η_{th} increases with t.

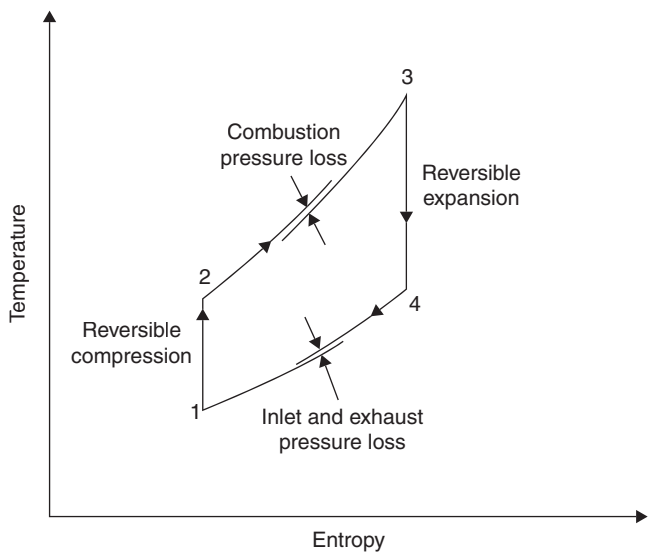
The change in thermal efficiency with pressure ratio for various values of maximum-to-minimum temperature ratio (t) is shown in Fig. 11.9. Although there is a marked increase in maximum thermal efficiency with (t) this increase in thermal efficiency diminishes as t increases and this is due to the presence of the temperature ratio term (t) in the denominator in Equations [11.29] and [11.34]. This implies that as (t) increases the rate of change in thermal efficiency decreases, as observed in Fig. 11.9. Furthermore, we observe that for a given value of (t), the thermal efficiency initially increases before decreasing with the increase in pressure ratio. The initial increase in thermal efficiency is due to the initial increase in pressure ratio, as the thermal efficiency increases with pressure ratio. However, at high pressure ratios the thermal efficiency decreases and this is due to the compression and expansion processes approaching each other, when the effects irreversibilities are profound, and this reduces the thermal efficiency. For a given turbine inlet temperature, we can imagine an extreme case when the expander/turbine inlet temperature is equal to the compressor exit temperature (i.e. when the combustor temperature rise will be zero) and the work done by the cycle to be negative – as the turbine work is less than the compressor work. Therefore at some lower pressure ratio the turbine work can equal the

© Woodhead Publishing Limited, 2013

compressor work, and at this condition the thermal efficiency will be zero. At pressure ratios below this (critical) value, the thermal efficiency will be positive. Therefore, for a given maximum-to-minimum cycle temperature ratio (t), there is a pressure ratio when the thermal efficiency is a maximum and this optimum pressure ratio increases with (t), as seen in Fig. 11.9.

11.5.3 The effect of pressure losses during heat addition and heat rejection on thermal efficiency

In the above discussion we have assumed that heat addition and rejection occurs at constant pressure. In practice, these thermodynamic processes are also irreversible and experience pressure losses. Furthermore, irreversibilities during the heat addition process result in inefficiencies, thus increasing heat input above the ideal value. It can be shown using a similar analysis to the above that when irreversibilities are only present during in the heat addition and rejection process the simple cycle thermal efficiency is dependent on the maximum-to-minimum cycle temperature ratio (t). When irreversibilities exist in the heat addition and rejection processes only the temperature–entropy diagram is shown in Fig. 11.10. We can express the thermal efficiency when irreversibilities exist during heat addition and heat rejection as $\eta_{\text{th}} = 1 - \frac{1}{c_t}\frac{(t-c_t)}{(t-c_c)}$. Referring to Fig. 11.10 $c_t = \left(P_3/P_4\right)^{(\gamma-1)/\gamma}$ and $c_c = \left(P_2/P_1\right)^{(\gamma-1)/\gamma}$. Since $\left(P_2/P_1\right) > \left(P_3/P_4\right)$ then $c_c > c_t$. The η_{th} increases as t



11.10 The temperature–entropy diagram for a practical simple cycle gas turbine.

© Woodhead Publishing Limited, 2013

increases, and thus the thermal efficiency of a simple cycle increases with t when the heat addition and reject process are irreversible.

11.6 Thermophysical properties of air and products of combustion

The above discussion has considered the working fluid/gas to act as an ideal gas, where the specific heat and isentropic index were constant. In a practical open cycle gas turbine this is not the case, and these values are strictly dependent on temperature and pressure because air, which is the usual working medium of such engines, is a real gas.

In the analysis of gas turbine performance using real gases the evaluation of various thermodynamic properties are required. Two such properties are enthalpy and entropy. It can be shown for a real gas the enthalpy change during a thermodynamic process is given by:

$$\Delta h = \int cp\,\mathrm{d}T - \int \frac{RT^2}{P}\left(\frac{\partial Z}{\partial T}\right)_P \mathrm{d}P \qquad [11.35]$$

Similarly, the change in entropy for a thermodynamic process is given by:

$$\Delta s = \int \frac{cp}{T}\,\mathrm{d}T - \int \frac{ZR}{P}\,\mathrm{d}P - \int \frac{RT^2}{P}\left(\frac{\partial Z}{\partial T}\right)_P \mathrm{d}P \qquad [11.36]$$

where h is the specific enthalpy, s is specific entropy, cp is the specific heat at constant pressure, R is the gas constant, P is pressure and Z is the compressibility factor.

The term $\left(RT^2/P\right)\left(\partial Z/\partial T\right)_P \mathrm{d}P$ is known as the residual properties or terms and their evaluation requires the employment of an equation of state. The most widely used equations of state are the Peng Robinson and Benedict Web Ruben equations. However, at normal operating pressures (about 1–60 bar) and temperatures (220–1800 K) that occur in gas turbines, the residual term for air and products of combustion is to a good approximation zero. It should be noted that, as the pressure decreases and temperature increases, the gases tends to be more like a perfect gas. Further details regarding equations of state and their evaluation are given in Assael *et al*. (1996).

Therefore, Equations [11.35] and [11.36] reduce to:

$$\Delta h = \int cp\,\mathrm{d}T \qquad [11.37]$$

and

$$\Delta s = \int \frac{cp}{T}\,\mathrm{d}T - \int \frac{R}{P}\,\mathrm{d}P \qquad [11.38]$$

© Woodhead Publishing Limited, 2013

Table 11.1 The coefficient for calculation the specific heat of air and products of combustion

Coefficients→	*a*	*b*	*c*	Molecular weight
O_2	936	13.1	–523	31.999
N_2	1020	13.4	–179	28.013
H_2O	1695	57.1	0.0	18.030
CO_2	1005	20.0	–1959	44.010
Ar	521	0.0	0.0	39.948

The specific of constant pressure (cp) can be defined as a function of temperature only (perfect gas). Various sources are available for such a function and include Rogers and Mayhew (2007) and Walsh and Fletcher (2004), but we quote the function given by Harman (1981):

$$cp = a + b\frac{T}{100} + c\left(\frac{T}{100}\right)^{-2} \qquad [11.39]$$

where the *cp* is the specific heat constant pressure (kJ/kg), *T* is temperature (K) and *a*, *b* and *c* are constants as defined in Table 11.1.

Substituting Equation [11.39] into Equations [11.37] and [11.38] and integrating, we get:

For enthalpy

$$h = a(T - T_0) + \frac{b}{200}(T - T_0)^2 - c \times 200^{-2}(T - T_0)^{-1} \qquad [11.40]$$

For entropy

$$s = a\ln\frac{T}{T_0} + \frac{b}{100}(T - T_0) - c \times 200^{-2}(T - T_0)^{-2} - R\ln\frac{P}{P_0} \qquad [11.41]$$

where *h* is the change in specific enthalpy (kJ/kg), *s* is the specific entropy (kJ/kgK) and T_0 and P_0 are the reference temperature and pressure respectively when the enthalpy and entropy are assumed to be zero (it should be noted that the second law of thermodynamics do not permit the evaluation of the absolute enthalpy and entropy). It is usually assumed that the entropy and enthalpy are equal to zero when $P_0 = 1.013$ bar and $T_0 = 273$ K (0°C).

Air is a mixture of gases whose gravimetric or mass fractions of various components for dry air are given in Table 11.2. However, air also contains water vapour, which has to be included as its influence is quite noticeable at high ambient temperatures (above 28°C). Also, the combustion process adds

© Woodhead Publishing Limited, 2013

Table 11.2 The composition of dry air on a gravimetric basis

Component	Gravimetric or mass fraction
N_2	0.7553
O_2	0.2314
Ar	0.0128
CO_2	0.0005

water vapour, and the amount is dependent on the fuel used (e.g. kerosene, diesel or natural gas). To determine the amount of water vapour present in air, we need to know the ambient pressure, temperature and humidity. With respect to humidity, it is usual to quote it as relative humidity, which is the mass of water required to saturate the air. Another definition of humidity is the specific or absolute humidity, which is the mass of water vapour present in a unit mass of dry air, and it is the specific humidity that influences gas turbine performance.

Given the ambient pressure, temperature and relative humidity (ϕ), the specific humidity can be determined, thus determining the mass fraction of water vapour in moist air as follows:

$$\phi = \frac{p}{p_s} \times 100 \qquad [11.42]$$

where p and p_s are the water vapour pressure and saturated vapour pressures, respectively, and normally quoted in mbar.

The saturated vapour pressure (p_s) can be determined by:

$$p_s = 6.112 \times e^{\frac{17.67T}{T+243.5}} \qquad [11.43]$$

where T is the ambient temperature in Celsius.

The specific humidity (ω), which relates water vapour in the air as a mass fraction, is given by:

$$\omega = \frac{\text{mass}_w}{\text{mass}_a} \qquad [11.44]$$

We can relate the specific humidity to water vapour pressure and ambient pressure using Dalton's law of partial pressures as:

$$\omega = 6.112 \frac{p}{P - p} \qquad [11.45]$$

© Woodhead Publishing Limited, 2013

where P is the ambient pressure in mbar.

Thus, we can determine the mass fraction of water in dry air, which can be added to the mass fraction of the various gas component of dry air and normalised to determine the mass fraction of moist air.

The procedure to determine the enthalpy and entropy of moist air is to determine the enthalpy of each component (CO_2, O_2, N_2, Ar and H_2O) using the corresponding component constant defined in Table 11.1. The gas constant R for each gas component can be determined by $R = R_0/\text{MW}$, where R_0 is the universal gas constant and MW is the molecular weight (Mole Wt) of each gas component, which is required to determine the entropy of each gas component. Thus the enthalpy (h_a) of air is determined by using the mixing rule $h_a = \sum_{i=1}^{n} m_i h_i$, where m_i and h_i are the mass fraction of each gas component in air and h_i is their corresponding enthalpy, n is the number of gas components – usually four. Similarly, the entropy of air can be determined as: $s_a = \sum_{1}^{n} m_i s_i$.

11.7 Thermodynamic modelling of gas turbine components applicable for practical gas turbine cycles

Using the analysis discussed in Section 11.6, the actual thermodynamic performance of various gas turbine components, such as compressors, combustors, turbines, heat exchangers and coolers, can be determined. Combining the performance of such individual components will determine the design point performance of the actual gas turbine cycle. Before doing so we shall discuss the detailed modelling of each of the engine component.

11.7.1 Compressor

Applying the steady-state energy equation for an adiabatic process, the specific work (wc) for compression is given by:

$$wc = h_2 - h_1 \qquad [11.46]$$

where h_2 and h_1 are the compressor inlet and exit specific stagnation enthalpies, respectively.

Given the compressor inlet pressure, temperature, humidity, exit pressure and the isentropic efficiency (η_c), the process of determining the specific work and compressor exit temperature is implicit or iterative, as follows:

© Woodhead Publishing Limited, 2013

1. Calculate the enthalpy and entropy at the compressor inlet (h_1 and s_1 respectively).
2. Estimate or guess the isentropic compressor exit temperature (T_2').
3. Calculate the compressor isentropic exit enthalpy and entropy (h_2' and s_2' respectively).
4. Check if s_1 from step (1) equals s_2' from step (3) and, if they are unequal, return to step (2) and estimate a new value for T_2' until they are equal.
5. Calculate the compressor exit enthalpy $h_2 = h_1 + (1/\eta_c)(h_2' - h_1)$ (it should be noted that the compressor isentropic efficiency is $\eta_c = ((h_2' - h_2)/(h_2 - h_1))$.
6. Estimate the compressor exit temperature (T_2).
7. As the compressor exit pressure is given, using the estimated compressor exit temperature T_2 calculate the compressor exit enthalpy.
8. If the compressor exit enthalpy calculated in step (7) does not equal to the enthalpy calculated in step (5) return to step (6) and estimate a different compressor exit temperature until the enthalpies calculated in steps (7) and (5) are equal.

In determining the compressor specific work and exit temperature the above employed the compressor isentropic efficiency. A similar process exits when the compressor polytropic efficiency is polytropic is specified, as given by Palmer.

For a polytropic process we define the isentropic pressure ratio (π) as the pressure ratio for isentropic compression (or expansion) from the standard temperature and pressure (T_0 = 273 K, P_0 = 1.013 bar) to a given temperature. Using this definition of isentropic pressure ratio for a polytropic process, the procedure to determine the compressor exit temperature and specific work is as follows:

1. Determine π_1 at the compressor inlet using the compressor inlet temperature T_1.
2. Determine π_2 at the compressor exit using the identity $\pi_2 = \pi_1 \times (P_2/P_1)^{\eta_p}$ where η_p is the compressor polytropic efficiency.
3. Using π_2 we can now determine the compressor exit temperature T_2 using the definition of isentropic pressure ratio (π) for a polytropic process. This will require an iterative process, where the compressor exit temperature (T_2) is estimated and the entropy at compressor exit is determined using the compressor pressure ratio of $\pi_2 \times 1.013$. The compressor exit temperature is adjusted until the entropy at standard pressure and temperature (1.013 bar and 273 K, respectively) matches the entropy at the compressor exit.
4. Knowing the compressor exit temperature the enthalpy at the exit of the compressor can be determined and thus the specific work is calculated

© Woodhead Publishing Limited, 2013

as $h_2 - h_1$, where h_1 is the compressor inlet enthalpy at the specified inlet pressure and temperature.

11.7.2 Combustor

The power output of the gas turbine is determined by the heat input, which is achieved by burning fuel in a combustion chamber or combustor. The fuel type may be liquid, such as kerosene or diesel, or natural gas, which is a mixture of hydrocarbons. Natural gas can also contain significant amounts of non-combustible components, such as CO_2 and N_2. The combustion process is usually achieved in stages, and much detail about gas turbine combustion can be found in Lefebvre (1998).

From a performance point of view we are interested primarily in the overall combustion temperature rise and fuel input (heat input). Tables and correlations have been developed to determine these parameters but they are limited mainly to liquid fuels, such as kerosene, which is widely used in aircraft gas turbines. However, many industrial gas turbines operate with natural gas and their fuel composition can vary significantly. Although correlations developed for liquid fuels can be adapted for natural gas, the steady-state energy equation can be employed to determine the performance parameters associated with the gas turbine combustor.

Since there is no work done by a combustor, the heat input $q = h_3 - h_2$, where h_2 and h_3 are the stagnation specific enthalpies at the inlet and exit of the combustor respectively. Given a combustor inlet and exit temperature, this equation can be represented in terms of the lower heating value of the fuel, fuel–air ratio and enthalpies for air and products of combustion, as follows:

$$f \times Q_{\text{net}} = (1+f)\left(h_3 - h_{3\,\text{at}\,298}\right) + \left(h_{2\,\text{at}\,298} - h_2\right) + f\left(h_f - h_{f\,\text{at}\,298}\right) \qquad [11.47]$$

where f is the fuel–air ratio, Q_{net} is the lower heating value of the fuel, h_2 is the enthalpy of air at the combustor inlet pressure and temperature, $h_{2\,\text{at}\,298}$ is the enthalpy for air at 298 K (25°C), h_3 is the enthalpy of products of combustion at the combustion exit, $h_{3\,\text{at}\,298}$ is the enthalpy of products of combustion at 298 K, h_f is the enthalpy of the fuel at the fuel temperature and pressure, $h_{f\,\text{at}\,298}$ is the fuel enthalpy at 298 K. Since the heat of combustion of fuels is referred to a temperature of 298 K (25°C) the enthalpy change of air, the products of combustion and fuel is determined over the respective temperature ranges stating at 298 K. It should also be noted that Q_{net} is usually quoted as a negative number at 25°C (e.g. for kerosene $Q_{\text{net}} = -43\,100$ kJ/kg at 25°C).

To determine the enthalpy at the combustor inlet requires the composition of the combustion air, which will normally correspond to moist air, as

© Woodhead Publishing Limited, 2013

discussed in Section 11.6. The gas composition at the exit of the combustor will be different, due to the combustion of hydrocarbon fuels, and they have to be determined. The fuel composition should also be known, which can be expressed as C_xH_y, where x and y are the numbers of atoms of carbon and hydrogen, respectively, in one molecule (mole) of fuel, and x/y is known as the carbon–hydrogen ratio. The combustor exit temperatures seldom exceed 1800 K, to limit emissions of pollutants such as NO_x, CO and UHCs. Thus, combustion in gas turbines occurs in excess air, which will result in O_2 being present in the products of combustion. The combustion of hydrocarbon fuels in excess air can be expressed as:

$$C_xH_y + m\left(O_2 + \frac{a2}{a1}N_2 + \frac{a3}{a1}H_2O + \frac{a4}{a1}CO_2\,\frac{a5}{a1}Ar\right) = n1CO_2 + n2H_2O + n3O_2 + n4N_2 + n5Ar \quad [11.48]$$

where m is the number of moles of excess air, $a1$ is the number of moles of O_2, $a2$ is the number moles of N_2, $a3$ is the moles number of H_2O, 4 is the moles of CO_2, Ar is the number of moles of Argon. $n1$, $n2$, $n3$, $n4$ and $n5$ are the number of moles of CO_2, H_2O, O_2, N_2 and Ar in the products of combustion respectively. For dry air the mole fractions for O_2, N_1, CO_2 and Ar are 0.2095, 0.7809, 0.0003 and 0.0093, respectively. The humidity of the air is required to determine the mole fraction of water vapour (H_2O), which can be determined using the procedure, discussed Section 11.6. It should be noted that the mole fraction is equal to mass faction divided by the mole weight of the gas component.

Equating coefficients, from Equation [11.48] we get:

$$n1 = x + m\frac{a4}{a1} \quad [11.49]$$

$$n2 = \frac{y + m(a3/a1)}{2} \quad [11.50]$$

$$n3 = \frac{m\left(2 + (a3/a1) + (2a4/a1)\right) - 2n1 - n2}{2} \quad [11.51]$$

$$n4 = \frac{ma2}{a1} \quad [11.52]$$

$$n5 = \frac{ma5}{a1} \quad [11.53]$$

© Woodhead Publishing Limited, 2013

The moles for excess air (m) can be determined from the fuel–air ratio (f) and defined as:

$$f = \frac{12.01x + 1.008y}{m\left(31.99 + 28.013\left(a2/a1\right) + 18.015\left(a3/a1\right) + 44.01\left(a4/a1\right) + 39.948\left(a5/a1\right)\right)} \quad [11.54]$$

where 31.99, 28.013, 44.01, 18.015, 39.948 are the molecular weights of O_2, N_2, H_2O, CO_2, Ar, respectively in Equation [11.54].

The products of combustion can be determined iteratively using Equations [11.48] to [11.54], as follows:

1. Assume the gas composition at the exit of combustion is the same as the inlet of the combustor (usually air).
2. Calculate fuel–air ratio f using Equation [11.47].
3. Using the fuel–air ratio (f) in step (2) calculate the moles of excess air using Equation [11.54].
4. Calculate the products of combustion using Equations [11.48]–[11.53].
5. Using the products of combustion from step (4) repeat from step from (2) until the current fuel–air ratio matches the previous value.

The values of x and y are readily available for hydrocarbons, such as kerosene, which is widely used and can be represented as $C_{12}H_{24}$. Similarly, methane can be represented as CH_4. Although natural gas contains a substantial amount of methane, significant amounts of other hydrocarbon components (such as ethane propane, etc.) exist in natural gas, including small amounts of hydrogen sulphide (H_2S). Furthermore, there may also be significant amounts of inert or non-combustible gases in natural gas such as CO_2 and N_2. When performing combustion calculations using natural gas as fuel, we have to account for these components present in the fuel gas. However, such mixtures of hydrocarbons can be reduced to the form of C_xH_y, provided the gas composition is known. As an example, we shall consider a fuel gas made up gas components, as defined as defined in Table 11.3, where various

Table 11.3 A fuel gas composition mode up of hydrocarbons and inert components as mole fractions

Component	Molecular or mole fraction
CH_4	0.7
C_2H_6	0.15
C_3H_8	0.05
CO_2	0.03
N_2	0.02

© Woodhead Publishing Limited, 2013

components are defined as mole fractions. The 'x' value can be determined by the summation series $x = \Sigma_{i=1}^{n} \mathrm{mf}_i x_i$ where mf_i and x_i are the mole fraction and the number of carbon atoms in each hydrocarbon component present in the fuel gas respectively, and n is the number of hydrocarbon components. Similarly, $y = \Sigma_{i=1}^{n} \mathrm{mf}_i y_i$ where y_i is the number of hydrogen atoms in each hydrocarbon component. Using the gas composition defined in Table 11.3, the first term in Equation [11.48] becomes:

$$C_xH_y = C_{1.15}H_{4.1} + 0.03\ CO_2 + 0.02\ N_2$$

When equating coefficients, as discussed above in Equations [11.49]–[11.53], the quantities of CO_2 and N_2 present in the fuel gas should also be taken into account.

The lower heating value (Q_{net}) in Equation [11.47] can be also determined for natural gas using the Q_{net} value for each gas component, which is also known as the heat of combustion of each component in fuel gas, as:

$$Q_{\mathrm{net}} = \frac{\sum_1^n Q_{\mathrm{net}_i} \mathrm{mf}_i}{\mathrm{MW}} \qquad [11.55]$$

where Q_{net_i} is the lower heating value or heat of combustion of combustible components on a molar basis and mf_i is the mole fraction. MW is the molecular weight of the fuel gas. It should be noted that the Q_{net_i} for non-combustibles such as CO_2 and N_2 are zero, but they should be included when calculating the molecular weight of the fuel. n is the number of component is natural gas.

The heats of combustion of many hydrocarbons are readily available. They can also be calculated using the heats of formation of the combustible component. We will illustrate this for hydrogen sulphide, which may be present in small quantities in fuel gas, as follows:

$$2H_2S + 3O_2 \rightarrow 2H_2O + 2SO_2 \qquad [11.56]$$

The heat of formation of H_2S = –20.63 kJ/kmol.
The heat of formation H_2O = –241.83 kJ/kmol.
The heat of formation of SO_2 = –279 kJ/kmol.

Substituting the heats of formation of each component into Equation [11.56] the heat of combustion of H_2S (Q_{net_i}) is:

$$Q_{\mathrm{net}_i} = \frac{2 \times -241.83 + 2 \times -297 + 20.63}{2} = -518.19\ \mathrm{kJ/kmol}$$

© Woodhead Publishing Limited, 2013

Since the mole weight of H_2S is 34.08 the lower heating value of H_2S (on a gravimetric basis) is –518.19/34.08 = –15.21 kJ/kg.

Sandler (1997) gives further details on enthalpies of formation and heats of combustion of many compounds.

Gas turbines also employ reheaters and after-burners, which are positioned between the turbine components of the engine, or upstream of the propelling nozzle in the case of aircraft propulsion. The method described above for modelling the combustion performance is also applicable to reheaters and after-burners. However, the gas composition at the inlet to the reheater or after-burner is not air but products of combustion, as determined above, and should be used rather than air at the inlet to the reheater/after-burner.

In the above analysis, in determining the fuel–air ratio we have assumed that the products of combustion are CO_2 and H_2O; however, this would only be the case if the combustion efficiency were 100%. The presence of pollutants, such NO_x, CO and UHC, among the products of combustion implies that combustion is not 100%. But the combustion efficiency of gas turbines is very high, typically above 99%, particularly for modern gas turbines.

The combustion efficiency is defined as the ratio of the actual fuel–air ratio (fa) to the ideal of theoretical fuel–air ratio (f), as determined above, for the same combustion temperature rise. Therefore the combustion efficiency (η_b) is given by:

$$\eta_b = \frac{f \text{ for a required } \Delta T}{fa \text{ for the same } \Delta T} \qquad [11.57]$$

Therefore the actual fuel–air ratio is:

$$fa = \frac{f}{\eta_b} \qquad [11.58]$$

Using the actual fuel–air ratio, the actual products of combustion can be determined using Equations [11.48] to [11.54]. We can also include the pollutants in determining the products of combustion. They can be taken into account by the use of parametric models where combustion parameters such as pressures, temperature and fuel–air ratios are used to predict these pollutants. Hung (1974) and Lefebvre (1998) describe such parametric models, and they can be employed to determine the mole fractions of pollutants present in the products of combustion. However, the inclusion of these pollutants in the combustion analysis will not improve the accuracy of the calculations significantly.

The combustion process introduces pressure losses due to the turbulence and flame stabilisation devices. This pressure loss is called the cold loss, and is proportional to the combustor inlet dynamic pressure ($1/2\rho u^2$). The heat

© Woodhead Publishing Limited, 2013

addition process reduces the gas density, thus increasing the gas velocity, which also contributes to the combustion pressure loss known as Rayleigh flow, and is known as the hot or fundamental pressure loss. Combining the two sources of combustion pressure loss we can define the total combustion pressure loss as:

$$\frac{\Delta P}{P_1} = \text{PLF}\left(\frac{W\sqrt{RT_1}}{P_1}\right)^2 \qquad [11.59]$$

where

ΔP is the combustor stagnation pressure drop,
W is the combustion air flow rate,
P_1 is the combustor inlet pressure,
T_1 is the combustor inlet temperature,
T_2 is the combustor exit temperature,
PLF is the combustor pressure loss factor,
R is the gas constant of air,

The combustion pressure loss factor is defined as:

$$\text{PLF} = K_1 + K_2\frac{T_2}{T_1} \qquad [11.60]$$

K_1 and K_2 are constant and determined experimentally for a given combustion chamber.

Combustor pressure loss is about 3% and about 6% for industrial and aero gas turbines respectively. For aero gas turbine applications, engine size and weight considerations result in smaller combustion volume. This requires a higher combustion pressure loss to achieve a suitable combustion stability loop. Lefebvre (1998) give more details on gas turbine combustion.

11.7.3 Turbines

As with a compression process, expansion process in a turbine can also be assumed to be adiabatic. From the steady flow energy equation the heat transfer is zero. Therefore the specific work (wt) is given by:

$$wt = h_3 - h_4 \qquad [11.61]$$

where h_3 and h_4 is the inlet and exit stagnation specific enthalpies, respectively.

Given a turbine inlet pressure, temperature, gas composition, exit pressure and the isentropic efficiency (η_t), the process of determining the specific

© Woodhead Publishing Limited, 2013

work and turbine exit temperatures is implicit or iterative, and is similar to that discussed for a compressor in Section 11.7.1. For completeness the process is as follows:

1. Calculate the enthalpy and entropy at the turbine inlet (h_3 and s_3 respectively).
2. Estimate or guess the isentropic turbine exit temperature (T_4').
3. Calculate the turbine isentropic exit enthalpy and entropy (h_4' and s_4' respectively).
4. Check if s_3 from step (1) equals s_4' from step (3) and, if they are unequal, return to step (2) and estimate a new value for T_4' until they are equal.
5. Calculate the compressor exit enthalpy $h_4 = h_3 + \eta_t(h_3 - h_4')$ (it should be noted that the turbine isentropic efficiency is $\eta_t = (h_3 - h_4)/(h_3 - h_4')$.
6. Estimate the turbine exit temperature (T_4).
7. As the turbine exit pressure is given, using the estimated turbine exit temperature T_4 to calculate the compressor exit enthalpy.
8. If the turbine exit enthalpy calculated in step (7) is not equal to the enthalpy calculated in step (5), return to step (6) and estimate a different turbine exit temperature until the enthalpies calculated in steps (7) and (5) are equal.

In determining the turbine specific work and exit temperature for a polytropic process the method is similar to that discussed for a compressor and described by Palmer. Again, for completeness, we will describe the process to determine the turbine exit temperature and specific work due to polytropic expansion, as follows:

1. Given the turbine inlet temperature determine π_3 at the compressor inlet using the compressor inlet temperature T_3.
2. Determine the isentropic pressure ratio π_4 at the turbine exit using the identity $\pi_4 = \pi_3 \times (p_4/p_3)^{\eta_p}$, where η_p is the turbine polytropic efficiency and P_4 is the turbine exit pressure, and where π_3 is the isentropic pressure ratio based on the inlet conditions of the turbine, as defined in Section 11.7.1 for a polytropic compression process.
3. Using π_4 we can now determine the turbine exit temperature T_4 using the definition of isentropic pressure ratio (π) for a polytropic process.
4. Knowing the turbine exit temperature, the enthalpy at the exit of the turbine can be determined, and thus the specific work ($h_3 - h_4$).

Turbine entry temperature and stator outlet temperature

The gas temperatures at entry to the turbine in advanced gas turbines are very high and turbine blade materials suffer from a phenomenon called

© Woodhead Publishing Limited, 2013

creep where stressing and un-stressing of the turbine blade material (within the elastic limit) leaves a permanent deformation called creep, which can lead to blade rupture. The higher the temperature and stress in the turbine blade material, the higher is the creep, and turbines operating at such high temperatures require cooling, normally using air, which is usually bled from the compressors and fed into the various components of the turbine. These components consist of the nozzle guide vane, rotor and turbine disk. Cooling air that is directed to the nozzle guide vanes invariably mixes with the combustion gases leaving the nozzle guide vane (after carrying out the cooling function). This results in the rotor inlet temperature decreasing. Therefore, the turbine rotor inlet temperature is an important temperature (also referred to as the stator outlet temperature) because the work of extraction from the gas stream occurs in the rotor of the turbine and the enthalpy at inlet to the turbine, as discussed in Section 11.7.3, should use the stator output temperature when determining the turbine work output when turbine cooling is employed. This achieved by carrying out an enthalpy balance between the cooling air and the gases entering the turbine. We can assume that the work and heat transfer are zero during the mixing, and the rotor inlet enthalpy can be determined by $h_m = (m_g h_g + m_c h_c)/(m_g + m_c)$, where h_m is the enthalpy of the gas after mixing of the combustion gases and cooling air and entering the turbine rotor, h_g is the enthalpy of the combustion gases at entry to the turbine, m_g gas mass flow rate at entry to the turbine, h_c is cooling air enthalpy and m_c is the cooling air mass flow rate. Knowing the stator output enthalpy, the stator outlet temperature (t_m) can be implicitly determined, as the enthalpy is a function of temperature (for a perfect gas). It should be noted that the gas composition at the inlet to the rotor will be different from that at the inlet to the turbine (i.e., at the inlet to the nozzle guide vane) because of the dilution of the products of combustion by the cooling air. As we know the cooling air composition and that of the products of combustion, together with the cooling air flow and gas flow, the gas composition at inlet to the rotor can be readily determined. Also, the combustion air will be reduced by the cooling air flow, as it will bypass the combustor and has to be allowed for when performing the combustion calculations.

Various methods of turbine cooling have been developed and successfully applied. These methods vary in complexity from the older methods such as convective cooling where the cooling air is introduced into the various turbine components and largely removed from the main gas path after carrying out the turbine cooling function. Film cooling, on the other hand, allows the cooling air to enter the gas path and to form a film around the turbine blades, thus further protecting the turbine blades from the high gas temperatures entering the turbine component. The type of cooling technology also affects the performance of the turbine component, with film cooling

© Woodhead Publishing Limited, 2013

having the worst effect on turbine efficiency but requiring less cooling air, and the effect of the lower cooling air requirements prevails, giving the best thermal efficiency. More recently, steam and mist cooling methods have also been developed, where these methods of cooling are external to the gas turbine and have found application in combined cycle plants. Apart from turbine cooling, compressor bleed air is also used for sealing the combustion gases from entry turbine disk cavities and other cooler engine components. Sealing air can be modelled by allowing air extraction at the exit from the appropriate compressor section (e.g. compressor discharge) and the sealing air is ignored or removed from the components downstream (e.g. combustor) as it is largely lost from the gas path flows (similar to modelling convective cooling).

A factor affecting cooling air requirements is the cooling air temperature. Modern large industrial gas turbines have implemented external cooling systems to reduce the cooling air, as the cooling air temperature has a significant effect on the amount of cooling air required (i.e. lower the cooling air temperature smaller is the amount of cooling required). The cooling medium to reduce the cooling air temperature can be the fuel, particularly for natural gas fired gas turbines, as the resultant increase in fuel temperature increases the thermal efficiency of the gas turbine. Such cooling air systems can be considered for other gas turbine applications (e.g., aircraft applications); however, the increase in engine weight due to the heat exchanges and pressure losses of the cooling air has to be carefully evaluated against the performance improvements. Since the fuel for air aircraft propulsion is kerosene, the fuel temperature should be low enough to prevent thermal cracking of the fuel.

For aircraft applications, the amount of cooling air during cruise can be reduced as the engine thrust is lower and therefore the turbine entry temperatures are also lower compared to takeoff and climb. This will improve the cruise fuel efficiency of the engine. In fact, it was considered for the Olympus turbo-jet powering Concorde, where the subsonic thrust was low enough so that the turbine cooling air could be shut off, thus improving the subsonic fuel efficiency. However, the risks involved were considered to be too great. Nevertheless, such changes to the cooling air requirements with different flight regimes will be considered, particularly when the pressures to improve cruise fuel consumption increase.

Intakes and exhaust systems

Intake systems

Practical gas turbines are normally open cycle systems, where air is continually drawn in before undergoing different thermodynamic processes, such as

© Woodhead Publishing Limited, 2013

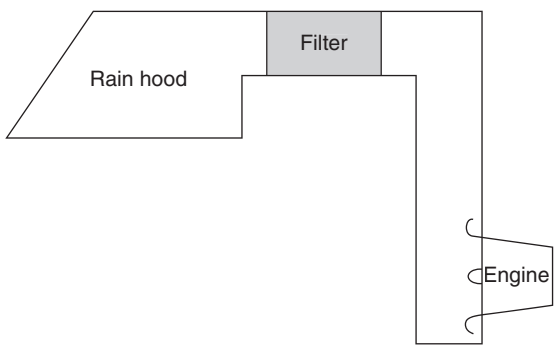
compression, combustion and expansion. For industrial and land-based gas turbines, the inlet system usually incorporates a filter, which removes dirt and dust from the air. This is necessary to prevent fouling of the compressor thus reducing engine performance. Such filtration systems incur pressure losses that also adversely affect engine performance. However, the loss in engine performance due to compressor fouling is much greater, as much as 5% loss in power output. Such pressure losses are kept to a minimum, and a typical inlet pressure loss is about 100 mm of water gauge, where the power loss is about 1.5%. Since the Mach numbers are very low in such inlet systems the non-dimensional pressure loss in air intake/inlet systems is proportional to the dynamic pressure and can be represented as:

$$\frac{\Delta P}{P_1} = k\left(\frac{W\sqrt{RT_1}}{P_1}\right)^2 \qquad [11.62]$$

where ΔP is the stagnation pressure drop across the inlet, W is the air flow rate, P_1 is the inlet pressure, T_1 is the inlet temperature, k is the pressure loss coefficient of the inlet system and R is the gas constant of air.

A schematic representation of an inlet system for industrial gas turbines is shown in Fig. 11.11.

Gas turbines are also widely used in aircraft propulsion, and inlet systems for aero engines are quite different from their land-based counterparts. This is because the inlet Mach numbers for aero engines are much higher, varying from about 0.85 for subsonic flight to about 3.0 for supersonic flight. Since flight Mach numbers are much higher than those required at the compressor inlet, the aircraft inlet systems have to diffuse the intake air such that the Mach number at the compressor inlet is no higher than about 0.4. Given an altitude (i.e. ambient pressure and temperature), flight speed and intake



11.11 Schematic representation of a typical industrial gas turbine inlet system.

© Woodhead Publishing Limited, 2013

isentropic efficiency, the stagnation enthalpy at compressor inlet can be determined from Equation [11.63]. Since the stagnation enthalpy and temperature at the compressor inlet is the same as the stagnation temperature at entry to the intake (i.e., no work or heat transfer occurs in the intake – the thermodynamic process is assumed to be adiabatic) the actual stagnation pressure at the compressor inlet can be determined as follows:

The isentropic stagnation enthalpy (h_1) at compressor inlet is:

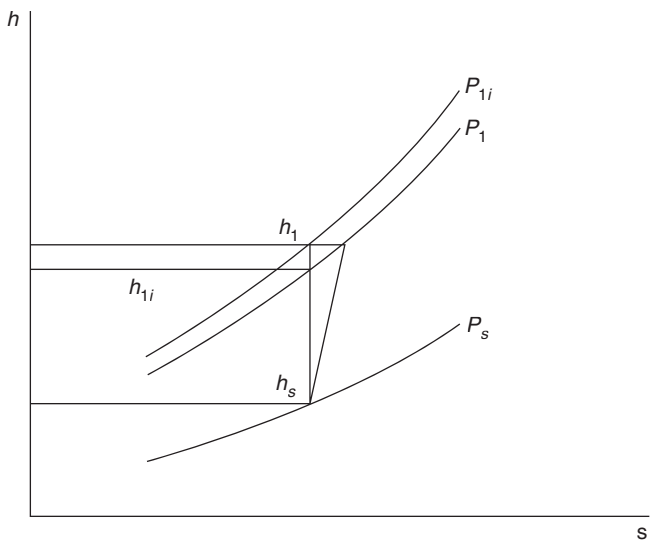
$$h_1 = hs_1 + \frac{1}{2}u^2 \qquad [11.63]$$

where hs_1 and u are the ambient or static enthalpy and flight speed respectively.

Referring to Fig. 11.12, which describes the enthalpy–entropy diagram, for a subsonic inlet:

1. As the enthalpy is only a function temperature (assuming air acts as a perfect gas) determine the stagnation temperature at the inlet to the compressor using the value for enthalpy determined by Equation [11.63]. Determine the isentropic enthalpy (h_1') using Equation [11.64]:

$$\eta_i = \frac{h_1' - hs_1}{h_1 - hs_1} \qquad [11.64]$$



11.12 Enthalpy–entropy diagram of a subsonic intake system.

© Woodhead Publishing Limited, 2013

where h_1 is the actual stagnation enthalpy at the compressor inlet and the isentropic efficiency (η_i) of the intake.

2. Estimate the stagnation pressure (P_1) at the compressor inlet, and thus the stagnation-to-static pressure ratio (P_1/Ps_1), where Ps_1 is the static or ambient pressure at entry to the inlet.
3. Determine the isentropic enthalpy (h'_1) at the compressor inlet using the procedure described in Section 11.7.1.
4. If the value for h'_1 determined in step (3) does not match the enthalpy determined from Section 11.7.1, then return to step (2) and repeat with a revised value for P_1 until the enthalpies match, which will then correspond to the actual stagnation pressure at compressor inlet.

For supersonic intakes the implied assumption we have made for subsonic intakes, where the inlet isentropic efficiency is independent of the flight speed or Mach number, is invalid. This is because of the stagnation pressure loss that occurs across a shock wave in such intakes, is dependent on the flight Mach number. The calculation of the stagnation pressure loss across shock waves is dependent on the intake system, and much of it is classified, but Seddon and Goldsmith (1985) give some information on supersonic take systems. However, the US Department of Defence quotes the following correlation to estimate the stagnation pressure loss in a supersonic inlet system.

$$\mathrm{Pr}_{\mathrm{shock}} = 1 - 0.075(M-1)^{1.35} \qquad [11.65]$$

where $\mathrm{Pr}_{\mathrm{shock}}$ is the stagnation pressure ratio across the shock wave, which is $<= 1$, and M is the flight Mach number. The Mach number range for which Equation [11.65] is valid is between 1 and 5 (i.e. $1 < M < 5$).

The stagnation pressure at the compressor inlet can be determined by multiplying the pressure ratio across the shock wave by the isentropic pressure ratio, as determined for a subsonic intake described above. Since a supersonic intake is considered to be an adiabatic process and without work transfer, the stagnation temperature at the compressor inlet is the same as the inlet stagnation temperature, and determined as that for a subsonic intake.

Exhaust systems

Exhaust systems in industrial and land-based gas turbines are responsible for removal of the products of combustion into the atmosphere. They are duct work positioned downstream of the turbine and introduce a pressure drop requiring the turbine exit pressure to be slightly greater than the atmospheric pressure. The pressure drop can be modelled using Equation [11.62],

© Woodhead Publishing Limited, 2013



11.13 Schematic representation of convergent and convergent–divergent propelling nozzles.

where the loss coefficient corresponds to the exhaust system. Typical pressure loss in the exhaust systems of industrial and land-based gas turbines is about 50 mm of water gauge, and reduces the power output of the engine by about 0.5%.

In aero gas turbines, such as turbo-jets and turbo-fans, the performance of exhaust systems is of paramount importance, as they are primarily responsible for generating the gross thrust of the engine. The exhaust systems are nozzles (or propelling nozzles), either of the convergent type, which are common on aero engines powering subsonic aircraft, or convergent–divergent nozzle type, as found on engines on supersonic aircraft. Additionally, such convergent–divergent nozzles are normally of fully variable area nozzle, and they can also change in configuration from being convergent, during subsonic flight, to convergent–divergent nozzle during supersonic flight. Schematic representations of convergent and convergent–divergent nozzles are shown in Fig. 11.13.

The steady flow energy equation can be applied to determine the thrust developed by such propelling nozzles. Since the process is adiabatic, and there is no work done by the nozzle, the steady flow energy equation relative to the aircraft is:

$$h_2 = hs_2 + \frac{1}{2}u_2^2 \qquad [11.66]$$

where h_2 is the stagnation enthalpy at the exit to the nozzle, hs_2 is the static enthalpy at the exit of the nozzle and u_2 is the exit velocity at the exit of the nozzle.

Assuming the nozzle is fully expanded (i.e. the exit pressure is equal to the ambient pressure irrespective of the nozzle inlet pressure), the isentropic efficiency of the nozzle (η_n) can be defined as:

$$\eta_n = \frac{h_1 - hs_2}{h_1 - hs_2'} \qquad [11.67]$$

where h_1 is the stagnation enthalpy at the inlet to the nozzle, hs_2 is the actual static enthalpy at the exit of the nozzle and hs_2' is the isentropic enthalpy at the exit of the nozzle.

© Woodhead Publishing Limited, 2013

Given the nozzle isentropic efficiency, inlet stagnation enthalpy, nozzle inlet pressure and temperature and exit pressure, the actual static enthalpy can be determined from Equation [11.67], as follows.

The isentropic analysis described in Section 11.7.1 enables the evaluation of the isentropic nozzle exit static enthalpy. Knowing the nozzle inlet stagnation enthalpy, the velocity of the gases at exit of the nozzle can be determined from Equation [11.66].

The momentum thrust (T_m) from the nozzle is now determined by:

$$T_m = m \times u_2 \qquad [11.68]$$

where exhaust m is the mass flow rate.

The assumption that the nozzle is fully expanded may be invalid in a practical nozzle, particularly for a convergent nozzle. This is because the flow can be choked at the exit or throat of a convergent nozzle (i.e. the velocity at the exit of a convergent nozzle is sonic). The static pressure at the exit of the nozzle under choked conditions will be above the ambient pressure to which the nozzle is exhausting. There is now an 'uncontrolled' or further expansion to the ambient pressure just downstream of the exit of the nozzle, and this uncontrolled expansion provides an additional thrust, known as the pressure thrust. The pressure thrust can be defined as $A_2(p_2 - p_a)$, where A_2 is the nozzle exit or throat area, and p_2 and p_a are the nozzle exit static pressure and ambient pressure, respectively. Thus, the gross thrust (T_g) generated by the convergent nozzle is:

$$T_g = ma + (p_2 - p_a)A_2 \qquad [11.69]$$

where a is the velocity of sound at the exit or throat of the convergent nozzle.

The velocity of sound is defined as $a = \sqrt{\gamma_c R_g T_c}$, where γ_c is the isentropic index at the exit of the nozzle, R_g is the gas constant and T_c is the static temperature at the exit of the nozzle (and is also known as the critical temperature). For adiabatic flow (either reversible or irreversible), the stagnation-to-static temperature ratio at the exit of the nozzle is given by:

$$\frac{T_1}{Ts_2} = \frac{T_2}{Ts_2} = 1 + \frac{\gamma - 1}{2} M^2 \qquad [11.70]$$

where M is the Mach number.

Since the Mach number of a choked nozzle at the exit is unity, the stagnation-to-static temperature as defined by Equation [11.70] becomes:

$$\frac{T_2}{Ts_2} = \frac{\gamma + 1}{2} \qquad [11.71]$$

© Woodhead Publishing Limited, 2013

For a given inlet nozzle stagnation inlet temperature (T_2), the static temperature (Ts_2) at the exit of the nozzle can be determined by Equation [11.71]. Since the enthalpy for a perfect gas is only a function of temperature, the static enthalpy at the exit of the nozzle can be determined by Equation [11.71]. The isentropic enthalpy at the exit of the nozzle can now be determined using Equation [11.67], which relates the actual and isentropic enthalpy drops to the nozzle isentropic efficiency. The isentropic pressure ratio, which is also the critical isentropic pressure ratio since the nozzle at exit is choked, is determined implicitly or iteratively. The process involves estimating the nozzle exit pressure (p_2) and using the isentropic analysis described above (Section 11.7.3) to determine the isentropic enthalpy at the nozzle exit. This is compared with the isentropic enthalpy, as determined from Equation [11.67], and repeated by altering the nozzle exit pressure until they match.

The nozzle exit area (A_2) can now be determined from the continuity equation $\left(A_2 = mR_gT_2/p_2a\right)$.

Thus, given a nozzle inlet pressure, temperature, flow and ambient pressure, the gross thrust can now be calculated using Equation [11.39].

An alternative method for determining the nozzle exit velocity, the gross momentum thrust and the pressure thrust is to employ the nozzle velocity coefficient (*cv*) and discharge coefficient (*cd*). The velocity coefficient (*cv*) is defined as the ratio of the actual velocity to the ideal velocity at the exit of the nozzle. Similarly, the discharge coefficient (*cd*) is defined as the ratio of the actual area, which accounts for the displacement thickness of the boundary layer, to the geometric area at the exit of the nozzle. The isentropic nozzle exit velocity can be determined from the methods discussed above, and for a choked nozzle it can be determined by $a = \sqrt{\gamma_c R_g T_c}$. Given a velocity coefficient for the nozzle, the actual nozzle exit velocity can be readily determined. The nozzle velocity coefficient is dependent on the nozzle area contraction and nozzle pressure ratio. However, their value is usually very high, and typically has values of around 0.99.

Similarly, the actual nozzle exit area can be determined from the nozzle discharge coefficient, and its value is also dependent on the nozzle area contraction and pressure ratio. Typical values for discharge coefficients are about 0.98. For choked nozzles, the nozzle exit static pressure is determined assuming the expansion is isentropic and the methods described above for nozzle performance calculations may be adjusted accordingly. Both methods (i.e., isentropic analysis and the approach using velocity and discharge coefficient) are applicable in determining aero engine performance; however, it is easier to measure velocity and discharge coefficients in a test rig, and manufacturers of aero engines often use the coefficient method rather than isentropic analysis for evaluating nozzle performance. It should be noted that, for an un-choked nozzle, the nozzle isentropic efficiency equals the square of the velocity coefficient.

© Woodhead Publishing Limited, 2013

Although convergent nozzles are primarily used in aero engines powering subsonic aircrafts, for supersonic aircraft, particularly aircraft operating at sustained supersonic cruise, such as Concorde, convergent–divergent nozzles give a significant gain in performance. The procedure to determine the gross thrust of convergent–divergent nozzles is similar to that discussed for fully expanded nozzles above. The nozzle (overall) pressure ratio will be greater than the critical pressure ratio, and the gas velocity at the exit of the nozzle will be greater than the speed of sound. However, if the nozzles are under-expanded (i.e., the nozzle exit pressure is greater than the ambient pressure to which nozzle is exhausting too) the nozzle exit area has be calculated and checked against the actual nozzle area. The (overall) nozzle pressure ratio is adjusted iteratively, until calculated and actual exit nozzle areas match. Such nozzles normally incorporate variable geometry to prevent the nozzle from over expanding. Should a convergent–divergent nozzle become over-expanded, shock losses will occur in the divergent part of the nozzle and adversely affect the nozzle efficiency.

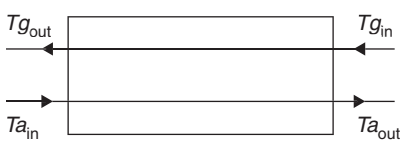
11.7.4 Heat exchangers and coolers

Means to improve the thermal efficiency of the simple cycle gas turbines can involve the incorporation of devices such as heat exchangers to reduce the net heat input. This is achieved by transferring some of the exhaust heat to the combustion air just downstream of the compressor. Similarly, the specific work, and thus the power output, of the simple cycle gas turbine can be increased by intercooling the compression process. Again, heat exchangers are employed to cool the compressor discharge air prior to compression by the high pressure compressor stages. The performance of such intercooled-regenerative cycles will be discussed in the next section.

A schematic representation of a heat exchanger is shown in Fig. 11.14. The parameter used to represent the performance of a heat exchanger is the effectiveness (ε) or thermal ratio, which is defined as:

$$\varepsilon = \frac{Ta_{\text{out}} - Ta_{\text{in}}}{Tg_{\text{in}} - Ta_{\text{in}}} \qquad [11.72]$$

Referring to Fig. 11.14:



11.14 Schematic representation of a heat exchanger.

© Woodhead Publishing Limited, 2013

Ta_{out} is the air temperature at the exit from the heat exchanger (and will become the combustor inlet temperature) (K or Celsius), Ta_{in} is the heat exchanger inlet temperature (which is normally the compressor discharge temperature) (K or Celsius) and Tg_{in} is the heat exchanger gas inlet temperature (which is also the turbine exit temperature) (K or Celsius).

To determine the gas temperature (Tg_{out}) at the exit of the heat exchanger, we need to determine the enthalpy of the gas (hg_{out}) at the exit from the heat exchanger. This is achieved by performing an enthalpy balance between the heat transfer of the cold and hot side of the heat exchanger as:

$$hg_{out} = hg_{in} - \frac{ma}{mg}\left(hc_{out} - hc_{in}\right) \qquad [11.73]$$

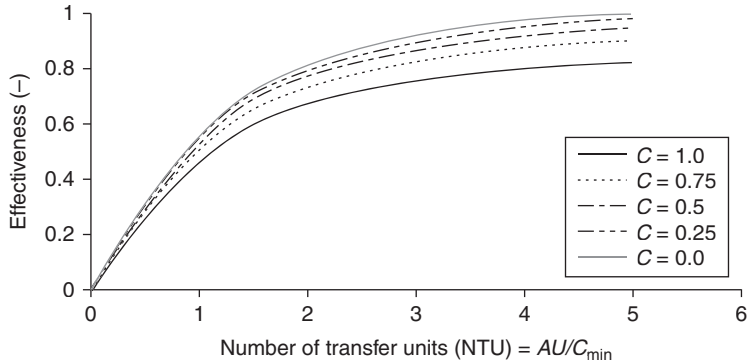
where hg_{in} is the enthalpy of the gas at the inlet to the hot side of the heat exchanger, hc_{out} is the enthalpy of the air at the exit of the cold side of the heat exchanger, hc_{in} is the enthalpy of the air at the inlet to the cold side of the heat exchanger, *ma* is the air flow rate at the inlet of the cold side of the heat exchanger and *mg* is the gas flow rate at the inlet to the hot side of the heat exchanger.

Since the enthalpy of air or gas is a function of temperature, as defined in Section 11.6, the temperature of the gas at the exit from the heat exchanger can be determined implicitly.

Furthermore, the thermal capacity ratio *C*, which is defined as $macp_{am}/mgcp_{gm}$, must be less than unity to satisfy the second law thermodynamics, where cp_{am} and cp_{gm} are the mean specific heats at constant pressure of the cold and hot sides of the heat exchanger respectively. It must be noted that the thermal ratio (*C*) is assumed to be less than unity, as thermal capacity of the cold flow is normally less than the thermal capacity of the hot or exhaust flow in a gas turbine.

The evaluation of heat exchanger effectiveness depends on the type of heat exchanger. The types of heat exchangers that have been employed by gas turbines are counter- and cross-flow recuperators, where the heat exchange takes place through a separating (conducting) wall. With regenerators, the hot exhaust gases heat a matrix, after which the cold air is passed through the matrix to absorb the heat given up by the hot gases. Thus, with regenerators the matrix requires a large thermal capacity, whereas with recuperators the separating wall requires a small thermal capacity and high thermal conductivity. The effectiveness of the heat exchanger may be determined from its performance curves, which depend on the type of heat exchanger, as discussed above. The performance curves for a heat exchanger are shown in Fig. 11.15, where the effectiveness of the heat exchanger is plotted against the number of transfer units (NTU), for a series of thermal capacity ratios (*C*) of the cold and hot fluids. NTU is defined as:

© Woodhead Publishing Limited, 2013



11.15 Performance curve of a typical counter flow heat exchanger.

$$\text{NTU} = \frac{UA}{C_{\min}} \qquad [11.74]$$

where U is the overall heat transfer coefficient (kW/m^{2}K), A is the heat transfer area of the heat exchanger (m^2) and $C_{\min}$ is the smallest thermal capacity of the two fluids (kW/K).

The calculation of the overall heat transfer coefficient is given in detail in Kays and London (1964) and in Simonson (1975). It should be noted that the effectiveness of the heat exchanger depends on C – the ratio of the thermal capacities of the air and combustion gases. In gas turbines the exhaust flow normally has a higher thermal capacity, due to the higher temperatures, and different gas composition, due to combustion. Typically, the values of thermal capacity ratio, C, for gas turbines are in the range of 0.97–1.0, and this restricts the effectiveness of the heat exchanger to about 0.9.

11.8 Determining component performance using specific heats

Much of the discussion above employs enthalpy and entropy for determining the performance of various components employed by gas turbines. Although this approach is considered as the rigorous method of calculation, the use of mean values of specific heats and isentropic index between the inlet and exit of the thermodynamic process also yields accurate results. The error is quite small (less than 1% for overall pressure ratios less than about 10) when compared with the enthalpy/entropy method. The reason for this is that air products of combustion behave as a perfect gas (i.e. the compressibility factor Z is close to unity). However, using the mean specific heat

© Woodhead Publishing Limited, 2013

method, the calculations are very much simplified, and discussed by Walsh and Fletcher (2004) and Razak (2007).

The method starts by assuming the specific heat at constant pressure (*cp*) at the exit of the process is the same as the inlet. The exit temperature is calculated and the exit *cp* is now evaluated. The average *cp* is now used to determine the revised exit temperature of the process, and repeated until the difference between the current and the previous exit temperatures is small ($<10^{-6}$). For compressors, the exit temperature is calculated using Equation [11.15], where the average isentropic index (γ) is defined as $\gamma = cp/cp - R$ and *cp* is determined from Equation [11.39]. The specific compression work (w_c) is given by $w_c = cp(T_2 - T_1)$. A similar analysis is applicable for turbines and combustors, and the average *cp* is evaluated using the gas composition resulting from the products of combustion.

11.9 Design-point performance modelling, analysis and performance optimisation of practical (shaft power) gas turbines

We have discussed ideal simple cycle gas turbine performance and considered the effects of irreversibilities on the performance of a simple cycle performance. We have also discussed the calculation of the thermodynamic performance of the various components that can be present in a gas turbine. Using the above analysis the design-point performance of various practical gas turbine cycles can be done as follows.

11.9.1 Simple cycle

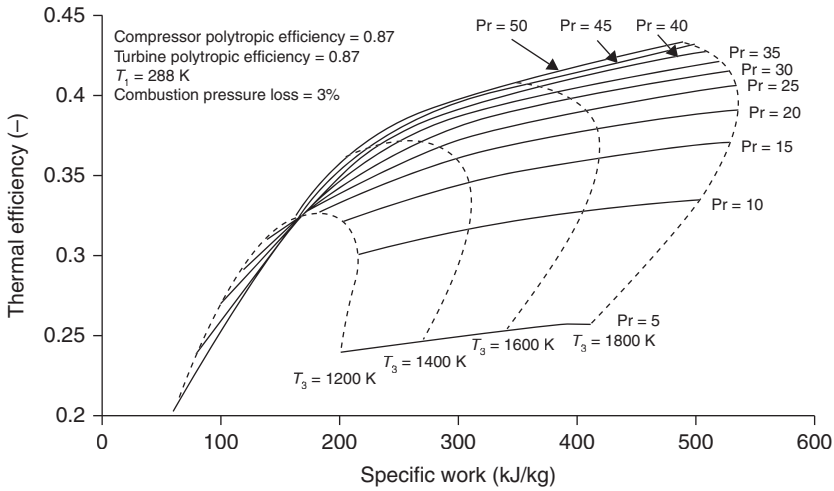
In carrying out the design-point performance of a simple cycle gas turbine, the compressor pressure ratio, turbine entry temperature or maximum cycle temperature, compressor and turbine isentropic or polytropic efficiency, and combustor pressure loss must be specific. Referring to Fig. 11.1, which shows a schematic representation of a simple cycle gas turbine with the salient points, the thermal efficiency can defined as the ratio of the net specific work to the thermal or heat input as:

$$\eta_{\text{th}} = \frac{(h_3 - h_4) - (h_2 - h_1)}{f \times Q_{net}} \qquad [11.75]$$

where $f \times Q_{net} = h_3 - h_2$.

The analysis can be carried out for various cycle pressure ratios, maximum cycle temperatures and component efficiencies including the effects of pressure losses in the heat addition and exhaust processes. Such analysis

© Woodhead Publishing Limited, 2013



11.16 Performance of a practical simple gas turbine cycle as a carpet plot for a series of maximum cycle temperatures and pressure ratios.

can be summarised using a carpet plot, as shown in Fig. 11.16. We observe that for a given maximum cycle (T_3) the increase in pressure ratio initially increases both the thermal efficiency and specific work. However, at high pressure ratios the specific work decreases while the thermal efficiency continues to increase (for maximum cycle temperature greater than or equal to 1800 K). For a required power output of the gas turbine, the decrease in specific work mean an increase in size and weight of the engine at these high pressure ratios. For industrial and land-based gas turbines size and weight is generally of little importance, and the optimisation process endeavours to employ the optimum compressor pressure ratios to achieve the highest thermal efficiency. At a low maximum cycle temperature (e.g. about 1200 K) the effect of irreversibilities become dominant at high pressure ratios, and at such high pressure ratios the thermal efficiency and specific work decreases with increase in pressure, as can be seen in Fig. 11.16.

Modern gas turbines that operate using a simple cycle can achieve pressure ratios of the order of about 40:1 and maximum cycle temperatures about 1800 K. At such design conditions, the thermal efficiency of such gas turbines can exceed 42%, which make them a formidable competitor compared with other types of power plants. Although the compressor ratio of modern gas turbines can be increased further, thus increasing the simple cycle thermal efficiency further, the maximum cycle temperature is unlikely to increase beyond 1800 K for industrial and land-based gas turbines. This is because, as the maximum cycle temperature exceeds 1800 K, the emissions of pollutants, particularly NO_x, increases appreciably and therefore

© Woodhead Publishing Limited, 2013

emissions of such pollutants are likely to impose the maximum limit of maximum cycle temperature. It should be noted that the rate of increase in thermal efficiency decreases as the maximum cycle temperature is increased and this can be readily deduced from Fig. 11.9. High maximum cycle temperatures will also increase the cooling air requirements, which can reduce the turbine efficiency, and therefore may impose a lower maximum cycle temperature for a simple cycle gas turbine, particularly when the costs of better turbine materials are also taken into account. However, complex cycles, which incorporate regeneration, discussed in Section 11.9.2, may justify higher maximum cycle temperature as the rate of increase in thermal efficiency with maximum cycle temperature is greater with such complex cycles.

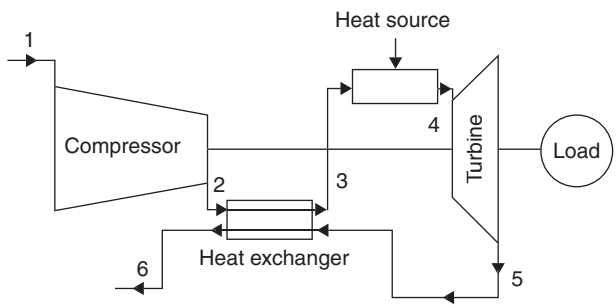
11.9.2 Regenerative cycle

The principle of a regenerative cycle is to recover some of the exhaust heat and transfer it to the combustion air. This can only be achieved if the turbine exhaust temperature is greater than the compressor exit temperature, and therefore implies that the optimum cycle pressure ratios are lower than those of the optimised simple cycle gas turbines, as discussed in Section 11.4. A schematic representation of the regenerative gas turbine cycle is shown in Fig. 11.17. Referring to Fig. 11.17 and specifying the heat exchanger effectiveness in addition to the design-point parameters for a simple cycle gas turbine, the thermal efficiency of a regenerative cycle is given by:

$$\eta_{\text{th}} = \frac{(h_4 - h_5) - (h_2 - h_1)}{f \times Q_{\text{net}}} \qquad [11.76]$$

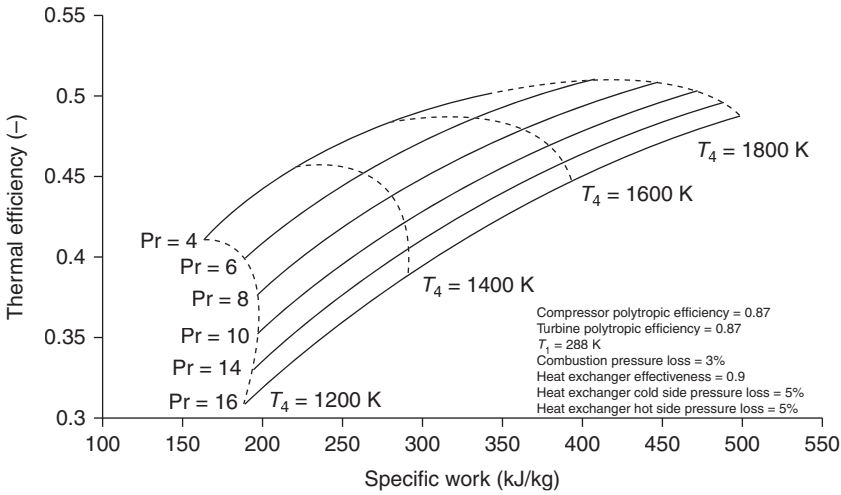
where $f \times Q_{\text{net}} = h_4 - h_3$.

Performing the analysis for various cycle pressure ratios and maximum cycle temperatures the data can be represented as shown in Fig. 11.18. As



11.17 Schematic representation of a regenerative gas turbine cycle.

© Woodhead Publishing Limited, 2013



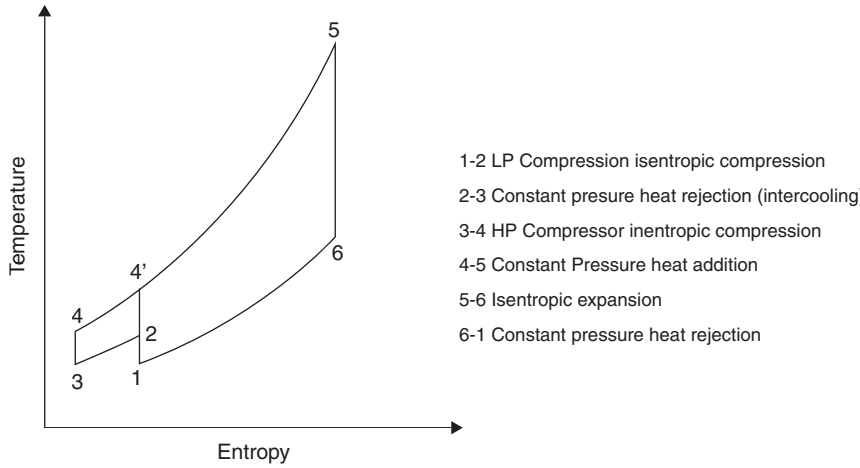
11.18 Performance as a carpet plot for a regenerative gas turbine cycle.

stated above, the optimum pressure ratio where the maximum thermal efficiency occurs is much lower than that for a simple cycle gas turbine. This also results in a significant decrease in the specific work due to the low pressure ratios, but thermal efficiencies of about 50% are possible with the regenerative gas turbine cycle, which compares with about 42% maximum thermal efficiency for a simple cycle. Another feature of a regenerative cycle is that the increased pressure loss in the heat exchangers reduces the specific work, but it also increases the exhaust temperature. Thus, the heat available for recovery by the heat exchangers increases, and this makes the regenerative cycle thermal efficiency less sensitive to such pressure losses compared with a simple cycle gas turbine.

11.9.3 Intercooled cycle

The addition of intercoolers in gas turbine cycles reduces the compression work, and this is achieved by dividing the compression processes into two or more stages, and the exit air/gas from each stage is cooled by the intercooler/heat exchanger to the minimum cycle temperature. This increases the specific work output of the gas turbine. There can also be an increase in thermal efficiency of a practical cycle; however, there is always a decrease in the thermal efficiency of the ideal (reversible) intercooled gas turbine cycle compared with the simple cycle. This is because we are in effect adding a lower efficiency simple cycle (the simple cycle 2–3-4–4′) to the compression process of a simple cycle gas turbine, as shown in Fig. 11.19.

© Woodhead Publishing Limited, 2013



11.19 Temperature–entropy diagram of an ideal, intercooled gas turbine.

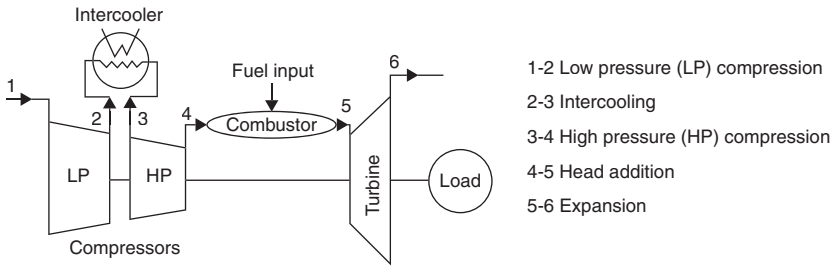
This also makes the ideal intercooled cycle thermal efficiency increase with the maximum cycle temperature, which differs from the ideal simple cycle whose thermal efficiency is independent of the maximum cycle temperature, as discussed in Section 11.4. A schematic representation of an intercooled gas turbine cycle is shown in Fig. 11.20. In practice, it is unusual to have more than one stage of intercooling. The split in pressure ratio between the low pressure (LP) and HP compressor, which has to be specified, influences the compression work and the minimum compression work occurs when the LP and HP pressure ratios are equal, provided the efficiency of the LP and HP compressors is also equal. This corresponds to the case when the specific work of the intercooled cycle is a maximum. If the LP and HP compressor efficiencies are unequal, then the pressure ratio of the higher efficiency stage has to increase to achieve minimum compressor work requirement.

However, when such intercooled compressors are considered in a practical (irreversible) gas turbine cycle, the optimum pressure ratio may not be equal even if the efficiencies of the LP and HP compressors are equal. This will depend of whether we optimise on maximum thermal efficiency or specific work. Referring to Fig. 11.20 the thermal efficiency of an intercooled gas turbine cycle can be given by:

$$\eta_{th} = \frac{(h_5 - h_6) - \big((h_2 - h_1) + (h_4 - h_3)\big)}{f \times Q_{\text{net}}} \qquad [11.77]$$

where $f \times Q_{\text{net}} = h_5 - h_4$.

© Woodhead Publishing Limited, 2013



11.20 Schematic representation of an intercooled gas turbine.

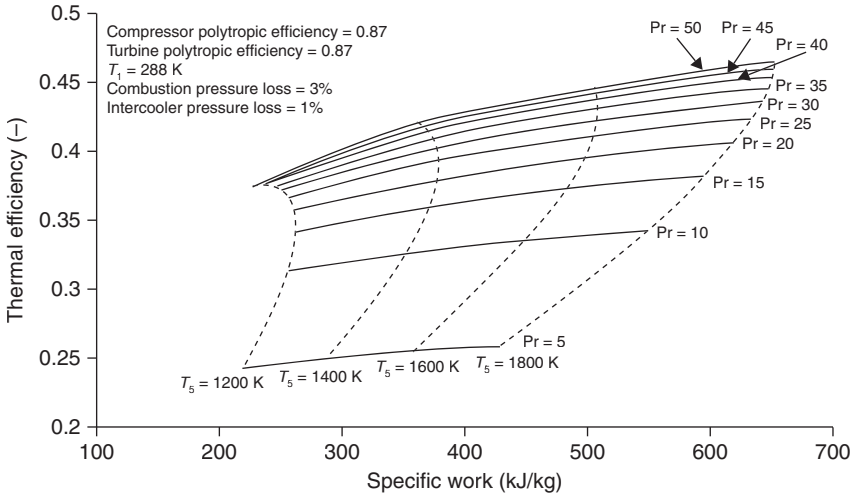
Again, the analysis can be carried out for a series of overall pressure ratios and maximum cycle temperatures while optimising the LP and HP pressure ratio split for maximum thermal efficiency or maximum specific work. When optimising for maximum thermal efficiency, the LP compressor pressure ratio contributes less to the overall pressure ratio and its contribution decreases as the maximum cycle temperature increases. This is because the effects of irreversibilities on performance decrease as the maximum cycle or firing temperature increases. Thus, the intercooled cycle tends towards the simple cycle when the thermal efficiency is at maximum, which requires the HP compressor ratio to increase relative to the LP compressor ratio. The optimised thermal efficiency varying with specific work for an intercooled cycle for a series of overall pressure ratios and maximum cycle temperatures is shown in Fig. 11.21. It can be seen that thermal efficiency of about 45% can be achieved, and this is higher than for a practical simple cycle gas turbine, where the maximum cycle efficiency is about 40%. Some interesting information on the application of such cycles by one major manufacturer is given in Diesel and Gas Turbine Worldwide, January–February (2004).

Optimising the intercooled compressor pressure ratio for maximum specific work results in the pressure ratios being equal, as we have assumed the efficiency of the LP and HP compressors is equal. Figure 11.22 shows the variation of thermal efficiency with specific work, when optimised for specific work. The thermal efficiency, although respectable, is somewhat lower compared when optimised for maximum thermal efficiency.

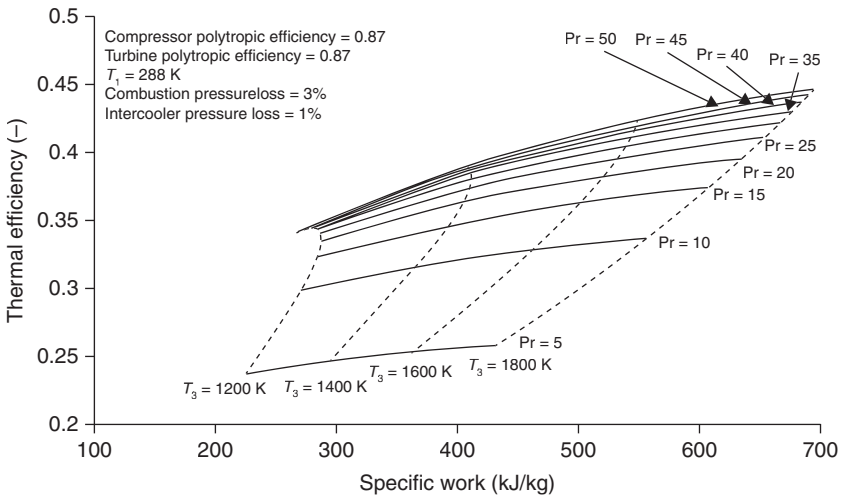
11.9.4 Reheat cycle

The specific work of a simple cycle gas turbine can also be augmented by applying reheat to the turbines. The expansion process in the turbine can be divided into two or more stages where the gases at the exit from each stage are normally increased to the maximum cycle temperature before further expansion

© Woodhead Publishing Limited, 2013



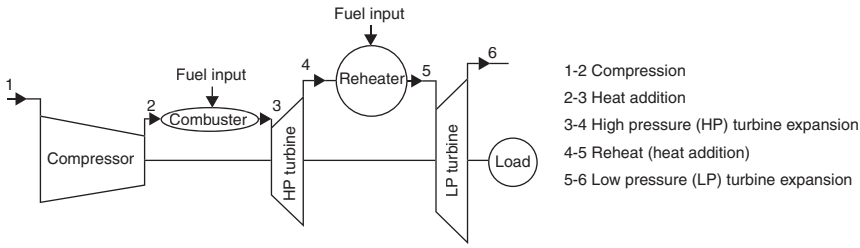
11.21 Variation of thermal efficiency with specific work for a practical intercooled gas turbine when optimised for maximum thermal efficiency.



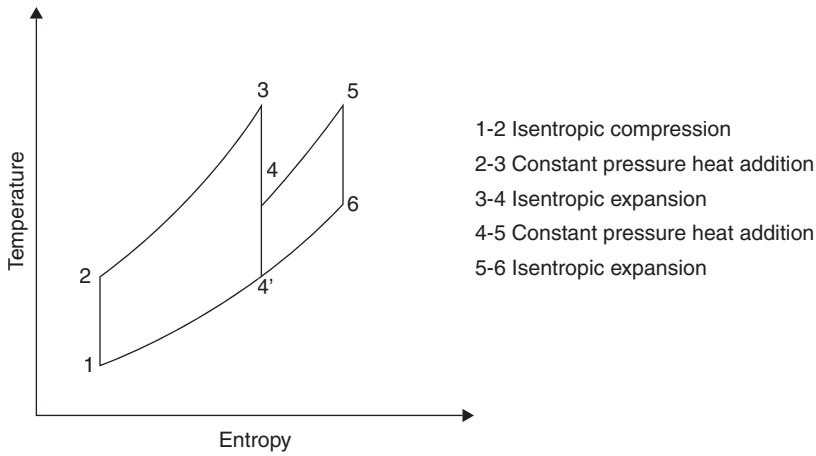
11.22 Variation of thermal efficiency with specific work for a practical intercooled gas turbine, when LP compressor pressure ration is optimised for maximum specific work.

in the subsequent turbine stage (Fig. 11.23). As we found with intercooling, the thermal efficiency of a practical reheat gas turbine cycle can also be increased with reheat. However, ideal (reversible) reheat cycle always results in a lower thermal efficiency compared with the simple cycle gas turbine. This is again

© Woodhead Publishing Limited, 2013



11.23 Temperature–entropy diagram for an ideal, reheat gas turbine cycle.



11.24 Schematic representation of a reheat gas turbine.

due to the fact that reheat effectively adds a lower efficiency simple cycle (4'4–4-5–6), as shown in Fig. 11.24. Its contribution to the increased work output, for a given cycle pressure ratio, is greater than the corresponding intercooled cycle, as shown in Fig. 11.19. Thus the ideal thermal efficiency of the ideal reheat cycle is less than the corresponding intercooled cycle. It can also be shown that the maximum turbine work occurs when the split in the HP and LP turbine pressure ratios are equal provided that the efficiency of each stage is equal. As we found with intercooling, if the efficiencies of the HP and LP turbine efficiencies are different, then the optimum turbine stage pressure would be biased to the higher efficiency turbine stage. Referring to Fig. 11.23 the thermal efficiency of a reheat cycle can be given by:

$$\eta_{\text{th}} = \frac{\left((h_3 - h_4) + (h_5 - h_6)\right) - (h_2 - h_1)}{f \times Q_{\text{net}}} \qquad [11.78]$$

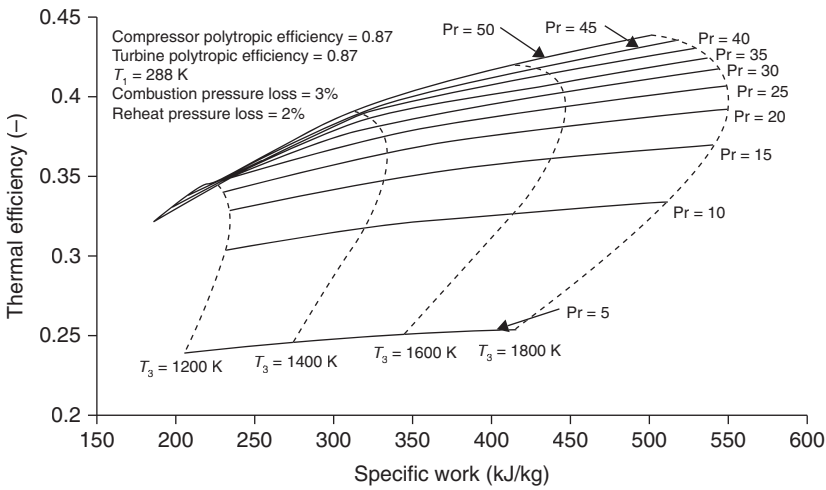
where $f \times Q_{\text{net}} = h_3 - h_2$.

© Woodhead Publishing Limited, 2013

The presentation of the variation of the thermal efficiency with specific work for a series of cycle pressure ratios and maximum cycle temperatures is shown in Fig. 11.25, which correspond to the case when the split in the HP and LP turbine pressure ratios is optimised for maximum thermal efficiency. The optimisation of the HP and LP turbine pressure ratios for this case results in the HP turbine being smaller and decreasing as the maximum cycle temperature increases. The maximum thermal efficiency is about 43%, somewhat less than the case with compressor intercooling. Optimising the HP and LP turbine pressure ratio split for maximum specific work is shown in Fig. 11.26. The specific work is considerably greater for this case, but the thermal efficiency is significantly lower compared with the corresponding case when the HP and LP turbine pressure ratios are optimised for maximum thermal efficiency.

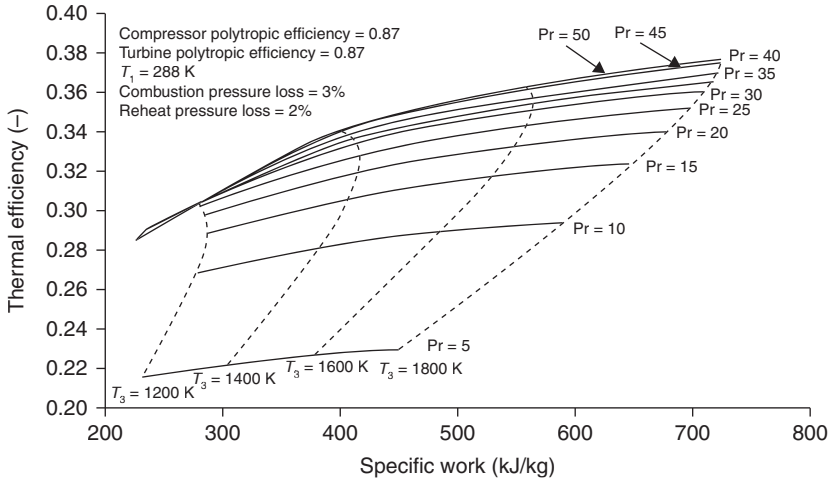
11.9.5 Intercooled, reheat and regenerative cycle

The intercooled and reheat cycles can each include regeneration to recover some of the exhaust heat to improve the thermal efficiency of these respective cycles, and indeed there will be significant increase in the thermal efficiency of these cycles. The optimisation of the pressure ratio split for the compressors and turbines in this case would be approximately equal, and will correspond to the maximum specific work case. However, it is the inclusion of regeneration into a combined intercooled-reheat cycle that gives the largest improvement in thermal efficiency, and a schematic representation of such a cycle is shown in Fig. 11.27.

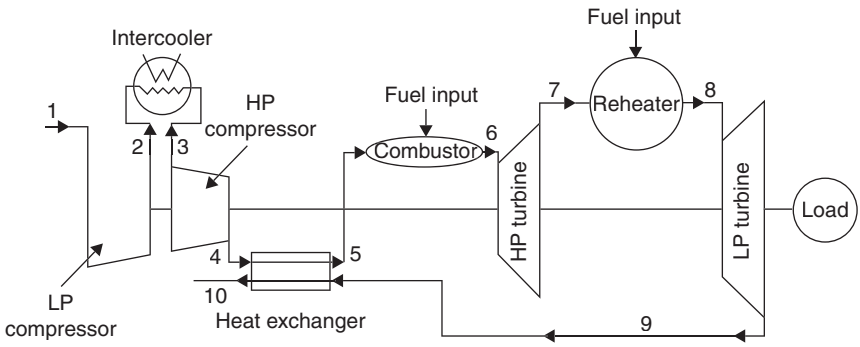


11.25 Variation of thermal efficiency with specific work when optimised for maximum thermal efficiency.

© Woodhead Publishing Limited, 2013



11.26 Variation of thermal efficiency with specific work when optimised for maximum specific work.



1-2 Isentropic LP compression

2-3 Intercooling

3-4 Isentropic HP compression

4-5 Constant pressure heat addition via heat exchanger

5-6 Constant pressure heat addition via external heat source

6-7 Isentropic HP turbine expansion

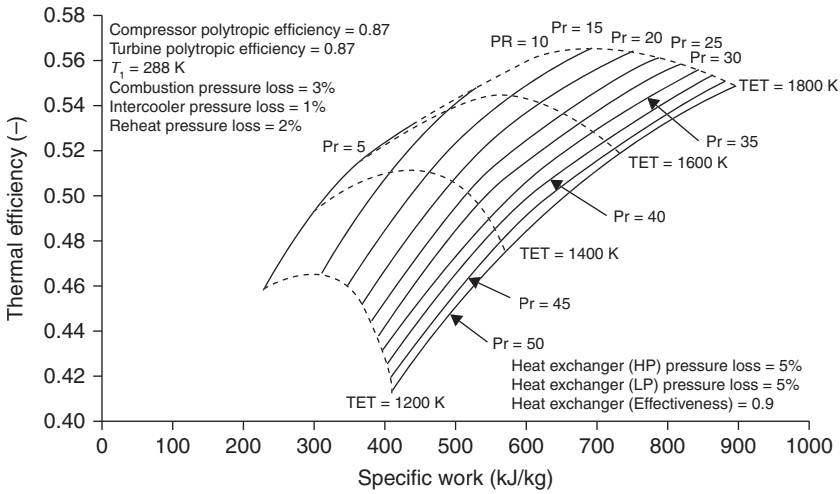
7-8 Reheat (heat addition–external heat source)

8-9 Isentropic LP turbine expansion

9-10 Constant pressure heat transfer for heating process 4–5

11.27 Schematic representation of an intercooled, reheat and regenerative cycle.

© Woodhead Publishing Limited, 2013



11.28 Variation of thermal efficiency with specific work for practical intercooled, reheat and regenerative cycle.

Referring to Fig. 11.27 the thermal efficiency of the intercooled/reheat/regenerative cycle can be given by:

$$\eta_{\text{th}} = \frac{\left((h_6 - h_7) + (h_8 - h_9)\right) - \left((h_2 - h_1) + (h_4 - h_3)\right)}{f \times Q_{\text{net}}} \qquad [11.79]$$

where $f \times Q_{\text{net}} = h_6 - h_5$.

The variation of thermal efficiency with specific work for a series of overall pressure ratios and maximum cycle temperature is shown in Fig. 11.28. Such complex cycles are capable of achieving thermal efficiencies as high as 57%. This corresponds nearly to the thermal efficiencies achieved by combined cycle power plants. Increasing the number of intercooled and reheat stages, the thermal efficiency can exceed 60% and the cycle approaches the Ericsson cycle. The Ericsson cycle is of special importance in thermodynamics, because it is ideally capable of achieving the Carnot cycle thermal efficiency. In the Ericsson cycle, the compression and expansion processes are isothermal.

11.10 Design-point performance modelling of aero gas turbines, analysis and optimisation

With the exception of light aircraft gas turbines are widely used in the aircraft propulsion, and it was this industry that first employed gas turbines on a large scale. In this section we will discuss the design-point performance of various gas turbines cycles used in aircraft propulsion.

© Woodhead Publishing Limited, 2013

Before we do so we will define some efficiency terms, as they are somewhat different from shaft power cycles. Aircraft engines, whether turbo-jets, turbo-fans or turbo-props (also known as propeller turbines), produce thrust to propel the aircraft and the work done is the thrust power (TP), which is defined as the thrust multiplied by the aircraft speed or flight speed. Thus the thermal efficiency or overall efficiency (η_o), as it is known in aircraft propulsion, is defined as:

$$\eta_o = \frac{\text{TP}}{Q_{\text{in}}} = \frac{FC_a}{Q_{\text{in}}} \qquad [11.80]$$

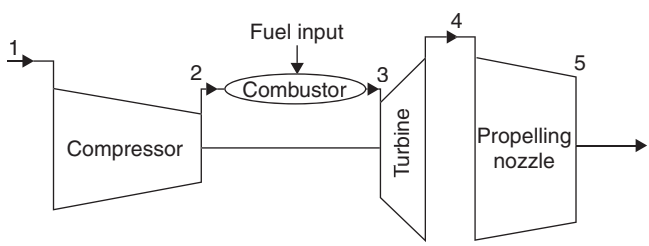
where Q_{in} is the thermal or heat input and is equal to the fuel flow × lower heating value of the fuel. F is the trust and the C_a is the aircraft or flight speed.

11.10.1 Turbo-jet engine

A schematic representation of a turbo-jet is shown in Fig. 11.29 and consists of the following components:

1. Intake.
2. Compressor.
3. Combustor.
4. Turbine.
5. Propelling nozzle.

Given a flight Mach number and intake efficiency, the stagnation pressures and temperatures at the inlet to the compressor can be determined using the analysis described in the section Intakes and exhaust systems. The turbine in a turbo-jet provides just enough power to drive the compressor, and the energy left in the gases downstream of the turbine is used by the propelling nozzle to increase the gas velocity and generate thrust. The compressor, combustor and turbine are collectively known as the gas generator. Referring to Fig. 11.29, and carrying out an energy balance between the



11.29 Schematic representation of a turbo-jet.

© Woodhead Publishing Limited, 2013

compressor and turbine, the enthalpy at the exit of the turbine (h_4) can be determined as $((h_2 - h_1) - h_3)$. Given either the isentropic efficiency or polytropic efficiency, the isentropic enthalpy at the exit of the turbine can be determined. Carrying out an isentropic analysis between the turbine inlet and exit, the turbine pressure ratio is determined, and hence the turbine exit pressure. This is achieved by using a scheme similar to that described in Section 11.7.3. An additional iterative loop is required in determining the turbine pressure ratio. This involves estimating or guessing the turbine pressure ratio and performing the isentropic analysis described in Section 11.7.3. This will generate the actual enthalpy, and is compared with the enthalpy determined by the energy balance $((h_2 - h_1) - h_3)$. If they do not match, we alter the estimate of the turbine ratio and repeat until there is a match.

The thermodynamic analysis carried out for the gas generator turbine will yield the turbine exit pressure and temperature, and using the analysis discussed in Section 11.7.3 for nozzles, the gross thrust can be calculated. A turbo-jet can be considered in its entirety as a propulsive duct and the thrust F can be defined as:

$$F = C_j m_j + A_e(p_e - p_a) - C_a m_a \qquad [11.81]$$

where C_j and C_a are the jet velocity and aircraft velocity relative to the engine respectively, m_j is the mass flow rate of the exhaust or propelling nozzle exit flow rate, m_a is the airflow rate at inlet to the engine, p_e and p_a are the static pressure at the exit of the nozzle and ambient pressure, respectively, and A_e is the nozzle exit area (assuming a choked convergent propelling nozzle).

If we assume a fully expanded nozzle, then the pressure thrust term $A_e(p_e - p_a)$ will be zero and, also assuming that the airflow rate at inlet to the engine is equal to the exit of the nozzle (i.e. $m_a = m_j = m$) Equation [11.81], will reduce to:

$$F = m(C_j - C_a) \qquad [11.82]$$

Therefore, for a turbo-jet the overall efficiency can be defined as:

$$\eta_o = \frac{mC_a(C_j - C_a)}{Q_{\text{in}}} \qquad [11.83]$$

From Equation [11.83] it is evident that the overall efficiency will be zero when aircraft velocity (C_a) is zero, and increases with C_a until the aircraft velocity equals the jet velocity (C_j), at which condition the overall efficiency will again be zero, as the thrust will be zero.

© Woodhead Publishing Limited, 2013

We can also define an efficiency which indicates how efficiently the kinetic energy changes are taking place across the turbo-jet, as:

$$\eta_e = \frac{m(C_j^2 - C_a^2)/2}{Q_{\text{in}}} \quad [11.84]$$

where η_e is known as the kinetic energy conversion efficiency, or energy conversion efficiency.

It can be seen from Equation [11.84] that η_e is a maximum when $C_a = 0$ and zero when $C_j = C_a$. We can also define an efficiency which relates how efficiently propulsion takes place, called the propulsive or Froude efficiency (η_{pr}). It is defined as the ratio TP to the TP plus the unused kinetic energy, as:

$$\eta_{\text{pr}} = \frac{mC_a(C_j - C_a)}{mC_a(C_j - C_a) + (C_j - C_a)^2/2} \quad [11.85]$$

which can be shown to be:

$$\eta_{\text{pr}} = \frac{2C_a}{C_a + C_j} \quad [11.86]$$

The propulsive efficiency is zero when $C_a = 0$, and unity or 100% when $C_j = C_a$. From the above analysis it should be evident that the overall efficiency is equal to the energy conversion efficiency multiplied by the propulsive efficiency, as:

$$\eta_o = \eta_e \eta_{\text{pr}} \quad [11.87]$$

From Equations [11.83] and [11.84] the overall efficiency and the energy conversion efficiency are zero when the aircraft velocity (C_a) is equal to the jet velocity (C_j), and from Equation [11.86] the propulsive efficiency is 1 or 100% at this flight condition. Thus, the optimisation process would result in determining the flight velocity such that the overall efficiency is a maximum. For aircraft that are powered by turbo-jet engines, the optimum flight velocity is usually very high, typically Mach 2 or 3.

We have stated above that when the flight velocity is zero the overall efficiency is zero. This makes comparing the performance of turbo-jets at sea level static (SLS) difficult and has given rise to the concept of specific fuel consumption or *sfc*, which is defined as the ratio of the fuel flow to thrust. Thus, the *sfc* is defined as:

$$sfc = \frac{mf}{m(c_j - c_a)} \quad [11.88]$$

© Woodhead Publishing Limited, 2013

Equation [11.88] is effectively the ratio of fuel–air ratio ($f = mf/m$) to specific thrust ($c_j - c_a$) and be defined as:

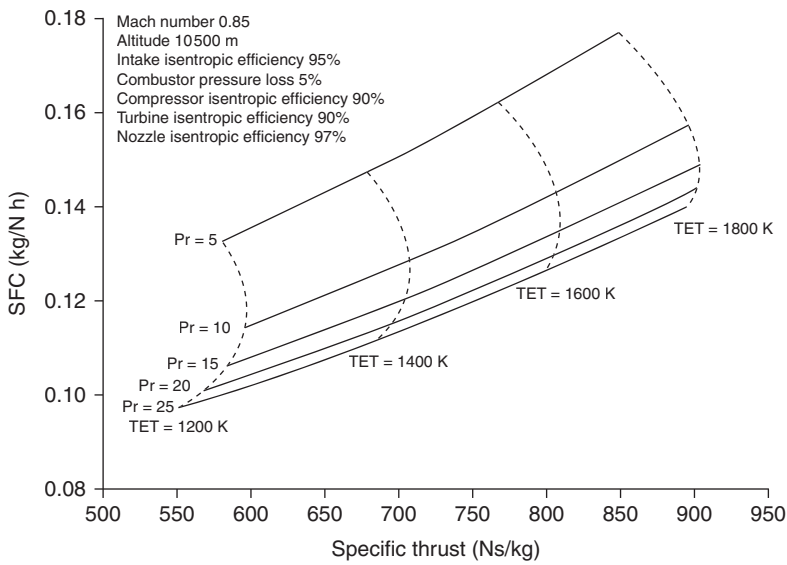
$$sfc = \frac{f}{Fs} \qquad [11.89]$$

Equation [11.88] can also be defined in terms of flight velocity and overall efficiency as:

$$sfc = \frac{c_a}{\eta_o} \times Q_{\text{net}} \qquad [11.90]$$

where Q_{net} is the lower heating value of the fuel.

The above analysis can be carried out for a turbo-jet engine for a series of compressor–pressure ratios and maximum cycle temperatures (also known as the turbine entry temperature (TET)), as shown in Fig. 11.30. We observe that the increase in pressure ratio results in a decrease in *sfc*. The specific thrust initially increases with pressure ratio before decreasing, and this occurs for a similar explanation given for the case of the turbo-shaft gas turbine above. However, the increase in TET for a given pressure ratio results in an increase in *sfc*, which differs from turbo-shaft cycle where there is an improvement in thermal efficiency, but results in a significant increase in



11.30 Variation of SFC with specific thrust of a turbo-jet for a series of TETs.

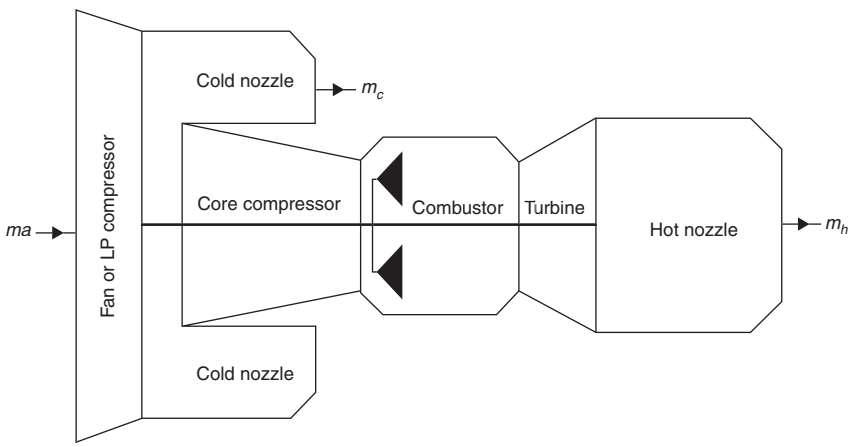
© Woodhead Publishing Limited, 2013

specific thrust. This is because there is an increase in jet velocity with TET, which decreases the propulsive efficiency and is responsible for the increase *sfc*. The increase in specific thrust results in a decrease in engine weight, which is paramount in aircraft propulsion, and for this reason every endeavour is made to increase the TET of turbine jets.

11.10.2 Turbo-fan

Turbo-jets were first employed in subsonic transport but it was soon realised that the low propulsive efficiency of turbo-jets gave rise to high fuel consumption (i.e. flight speed is not optimised). Means to improve the propulsive efficiency of turbo-jets, and thus fuel consumption, gave rise to the concept of turbo-fan or bypass turbo-jets. Here the compressor is divided into two parts, and the air leaving the first (stage) compressor is split, whereby one portion bypasses the (core) compressor and is exhausted via a separate or cold nozzle. The core flow is further compressed in the second stage of the compressor and enters the combustor, where fuel is burnt, and drives the turbine, which produces power to drive the compressors. The energy in the gases leaving the turbine is exhausted through the core or hot nozzle, as shown schematically in Fig. 11.31. Since only part of the airflow enters the core of the engine the turbine specific work has to increase to provide the compression work of the bypass air and this reduces the jet velocity of the hot nozzle. As the velocity at exit of the cold nozzle is small, there is increased propulsive efficiency, which now improves the fuel consumption.

The modelling of the design performance of a turbo-fan is similar to that of a turbo-jet, but the designer has two further parameters available. These



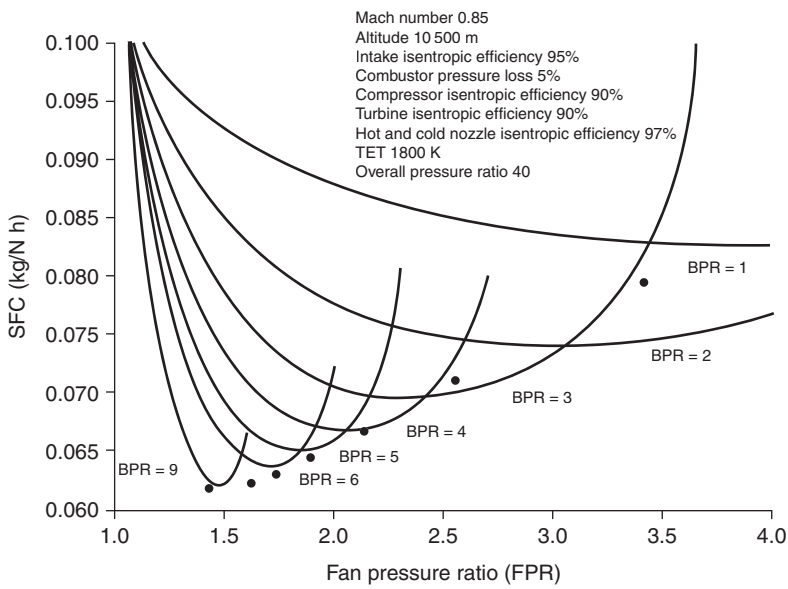
11.31 Schematic representation of a turbo-fan.

© Woodhead Publishing Limited, 2013

correspond to the fan or LP compressor pressure ratio or fan pressure ratios (FPR) and the bypass ratio (BPR), which is defined as the ratio of the cold flow (m_c) to the core or hot flow (m_h). Referring to Fig. 11.31 the BPR is given by:

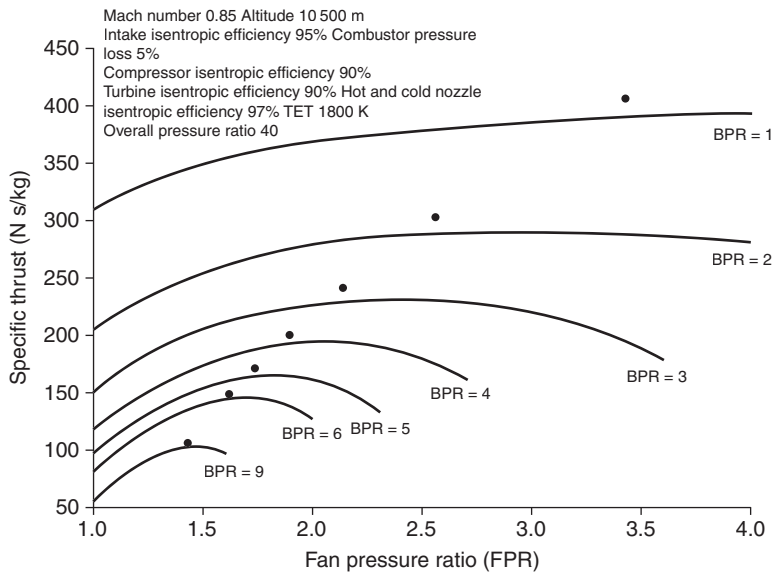
$$\text{BPR} = \frac{m_c}{m_h} \qquad [11.91]$$

The design-point performance analysis can be carried out for a given overall compressor pressure ratio, TET, component efficiencies for a series of bypass ratios, and fan pressure ratios, as shown in Figs 11.32 and 11.33, which show the variation of *sfc* and specific thrust with FPR for a series of BPRs. Increasing the FPR initially results in a decrease in *sfc* followed by an increase, and this is due to the initial improvement in propulsive efficiency at low FPRs, as shown in Fig. 11.32. However, at higher FPRs there is an increase in *sfc*, and this is due to the decrease in propulsive efficiency at these higher FPRs. A similar trend in specific trust is also observed, as shown in Fig. 11.33 and the FPR when the *sfc* is a minimum also corresponds to the FPR when the specific thrust is a maximum. For a given BPR the fuel input is fixed, therefore the minimum *sfc* and maximum specific thrust correspond to the same FPR. Other features shown in Figs 11.32 and 11.33



11.32 Variation of SFC with fan pressure ratio for an unmixed and mixed turbo-fan for a series of BPRs.

© Woodhead Publishing Limited, 2013



11.33 Variation of specific thrust with fan pressure ratio for an unmixed and mixed turbo-fan for a series of BPRs.

illustrate that the optimum FPR decreases with increase in BPR. The effect of overall pressure ratio and TET also influences the optimum FPR. It can be shown that increasing overall pressure reduces the optimum FPR when the *sfc* is a minimum and the specific thrust is a maximum, while increasing the TET results in the optimum FPR to increase. For an ideal turbo-fan cycle (i.e. reversible compression and expansion in the compressors, turbines and nozzles (assuming fully expanded nozzles) and assuming the gas is ideal) the maximum propulsive efficiency occurs when the jet velocities of the cold and hot nozzles are equal. However, in a practical cycle when such ideal conditions are absent, the maximum propulsive efficiency occurs when the hot nozzle exit jet velocity is somewhat higher than the cold nozzle exit jet velocity. It can be seen from Figs 11.32 and 11.33 that the increase in the BPR results in a significant decrease in specific thrust and *sfc*. Although the decrease in specific thrust results in the increase in engine weight, the decrease in *sfc* decreases the fuel consumption, and thus fuel weight, for a given flight. This is particularly important for long-haul flights where it is the weight of the engines and fuel that is important. This has resulted in engines designed to operate with BPRs high as 9 to be developed. These advanced engines also have overall pressure pressures of the order of 40:1 and TET of the order of 1800 K at takeoff conditions.

The turbo-fan cycle discussed above corresponds to unmixed jets (i.e. the cold and hot flows have their own or separate exhaust nozzles). It is possible

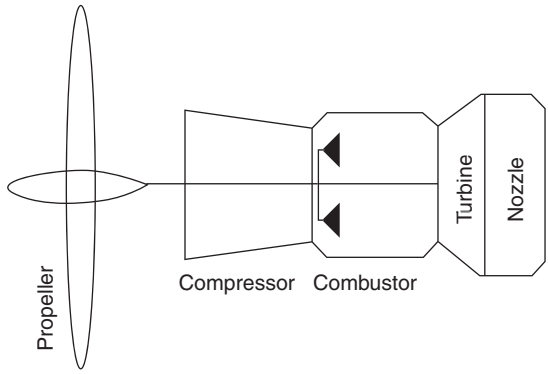
© Woodhead Publishing Limited, 2013

to mix the two flows and exhaust the gases through a single nozzle, and such a turbo-fan engine is normally referred to a mixed turbo-fan engine. Mixing effectively increases the cold jet velocity while decreasing the hot jet velocity, resulting in a lower optimum FPR. In a practical cycle, the lower FPR results in smaller losses due to irreversibilities in the compression and expansion processes of the fan and cold nozzle, and this gives a small but significant improvement in both *sfc* and specific thrust. However, for a given set of design parameters, the performance of an ideal mixed turbo-fan cycle (optimum *sfc* and specific thrust) is identical to an unmixed turbo-fan cycle. The main difference is that the ideal mixed turbo-fan cycle requires a smaller FPR, and this result in a simpler and lighter fan. Figures 11.32 and 11.33 illustrate these features of mixed and unmixed jets, where the mixed performance is shown as circles in these figures. It can be seen that the optimum FPR is less for the mixed turbo-fan cycle, and the difference decreases with pressure ratio. Also, the improvement in performance with the mixed turbo-fan cycle decreases as the BPR increases. The mixing of the cold and hot flows introduces pressure losses, and at high BPRs any benefit in performance due to mixing can easily be lost and the mixing losses for high BPR engines must be tightly controlled. Saravanamutoo *et al*. (2001) and Frost (1966) gives details on the pressure loss calculation due to mixing. Today's high pass engines rarely use mixed configuration, and high bypass turbo-fan engines primarily use the unmixed configuration. In the performance analysis of mixed turbo-fan cycles the gas composition at the entry to the final nozzle will not correspond to the products of combustion and the actual gas composition is now a mixture of air and products of combustion, which can be determined for a given BPR. Low bypass engines, of the order of 0.5–1, are used by high speed military aircraft where a small amount of time is spent at supersonic speeds. The low BPR helps keep the engine's frontal areas low, which is important in minimising the drag at supersonic speed but helps improve the *sfc* at subsonic speed where a substantial amount of the flight occurs with these aircraft. However, aircraft that operate at sustained supersonic speed, such as Concorde, a turbo-jet is probably the best option, because at such high airspeeds the propulsive efficiency of turbo-jets is high.

11.10.3 Turbo-props or propeller turbine engines

Before concluding this section on aircraft gas turbines, we should mention the turbo-prop engine, which is shown schematically in Fig. 11.34. Here the engine produces shaft power, which is used to drive a propeller to generate thrust. The design-point performance analysis is very similar to that discussed above for shaft power cycle. However, turbo-props produce a small but significant amount of jet thrust, and the amount of jet thrust

© Woodhead Publishing Limited, 2013



11.34 Schematic representation of a turbo-propeller engine or turbo-prop.

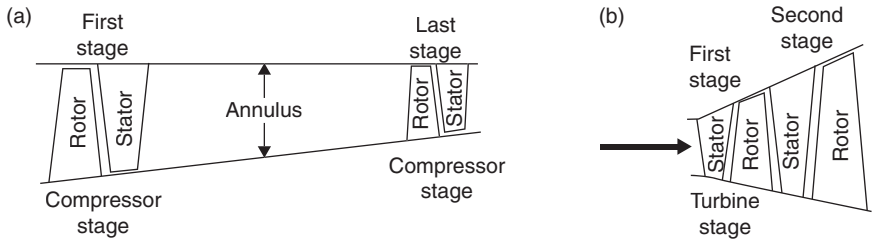
is determined by the pressure ratio split between the turbine section and the nozzle. Increasing the jet thrust results in a lighter turbine but would increase the *sfc*. Such optimisation depends on the range of aircraft that employ such engines, with short-haul aircraft biased towards higher jet thrust. Turbo-props are employed to power low speed aircraft, where their propulsive efficiency is superior to turbo-fans or turbo-jets. A gearbox is also used to reduce the gas turbine shaft speed suitable for the propeller.

11.11 Component characteristics

We have discussed the various thermodynamic processes present in a gas turbine, whose performance calculations are carried out using the steady flow energy equation but without any reference to the machines (hardware) required to perform these processes. Gas turbines almost exclusively employ dynamic compressors and expanders, and they correspond to axial and radial compressors and expanders. Examples of axial compressors and expanders are shown in Fig. 11.35. The design of these components is a specialist activity, and is outside the scope of this chapter. Details on the design of such turbomachinery may be found in Saravanamutoo *et al*. (2001), Cumpsty (1989), McKenzie (1997) and Horlock (1958).

The performance of these components can be represented in terms of pressures, temperatures, mass flow, efficiency and speed. However, proper presentation of these parameters for all operating conditions is impractical and dimensional analysis is employed to generate non-dimensional terms, which allow concise representation of the performance of such components. The non-dimensional terms of importance are non-dimensional flow $\left(W_1\sqrt{R_1T_1}/\gamma_1\right)\Big/A_1P_1$, pressure ratio, P_2/P_1, efficiency (usually isentropic efficiency) and non-dimensional speed $N_1D_1\Big/\sqrt{\gamma_1R_1T_1}$. The

© Woodhead Publishing Limited, 2013

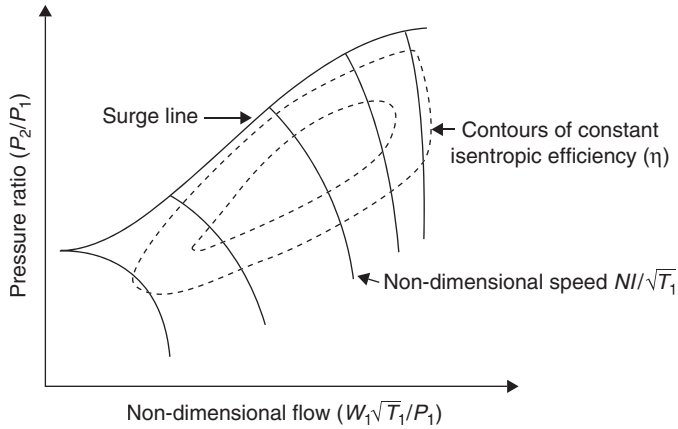


11.35 An axial compressor showing the first and last stages (a) and showing an axial turbine comprising two stages (b).

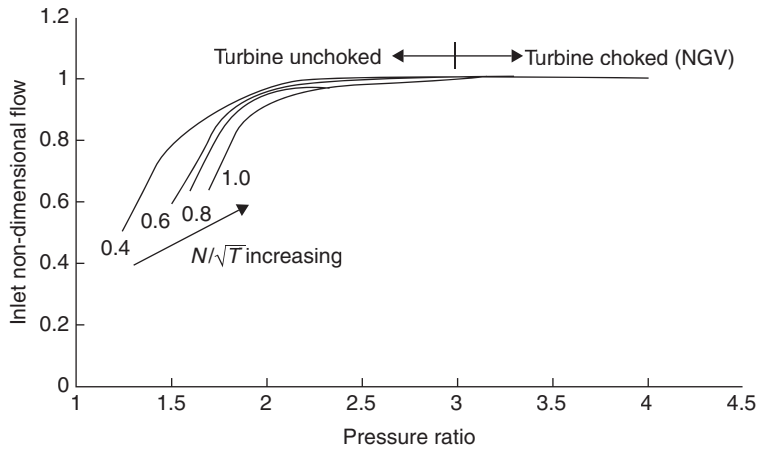
suffixes 1 and 2 refer to the inlet and exit of the compressor and turbine. The temperature ratio, which is also of importance, can now be determined using the pressure ratio and efficiency. It can readily be deduced that non-dimensional flows and speeds are Mach numbers at the inlet to these components.

Compressor and turbine characteristics are shown in Figs 11.36, 11.37 and 11.38, including some typical features of these characteristics and usually found in axial compressors and turbines, which are widely used in gas turbine applications. For compressors we observe that the flow becomes quite steep and even vertical at high speed operation. As we increase the compressor speed from design the front stages of the compressor chokes and this is primarily responsible for the speed line describing the variation of flow with pressure ratio becoming steep. The choking of the front stages also causes the rear stages to operate near stall, which can lead to compressor surge, a violent aerodynamic vibration, and is associated with rear stages stalling at high speed compressor operation. Low compressor speed operation results in lower pressures at the rear stages of the compressor increasing the velocity in these stages, resulting choked operation of the rear stages. This will cause the front stages of the compressor to operate nearer to stall, and compressor surge at low speed operation is associated with stalling of the front stages of an axial compressor. The effect of such choking and stalling is most profound with compressors designed to operate at high pressure ratios, typically above 8:1, when the area ratio of the front to the rear of the compressor increases, and therefore the severity of stage matching problems is greater. Various means are used to overcome surge, and they vary from using variable stators and inlet guide vanes to unload the front stages during low speed operation, and imposing speed limits to prevent compressor surge at high speed operation. Other methods include dividing the compressor into parts, each driven by its own turbine, to prevent such extreme conditions occurring in the compressor when operating at off-design conditions. At low operating speeds blow-off values are also used at some intermediate stage/point between the inlet and the exit of the

© Woodhead Publishing Limited, 2013



11.36 Typical compressor characteristic.

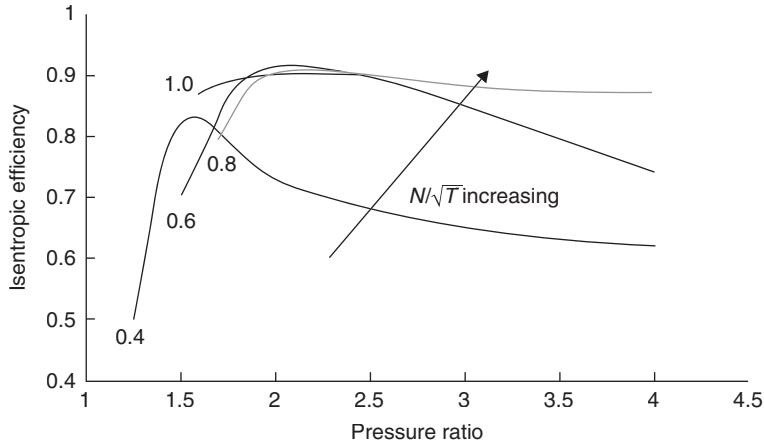


11.37 Typical flow turbine characteristic when NGVs are choked.

compressor to alleviate the choking effects of the rear stages of the compressor. Further details on such off-design operation of compressors can be found in Saravanamutto *et al.* (2001), Walsh and Fletcher (2004), Cumpsty (1989) and McKenzie (1997).

With turbines, the non-dimensional flow initially increases with pressure ratio, after which it remains constant. The pressure ratio at which the flow becomes constant is referred to as the choking of the turbine, and is dependent on the non-dimensional speed of the turbine. The higher the non-dimensional speed of the turbine, the higher is the pressure ratio when the turbine chokes. However, if choking occurs in the rotors of the turbine then

© Woodhead Publishing Limited, 2013



11.38 Typical turbine efficiency characteristic.

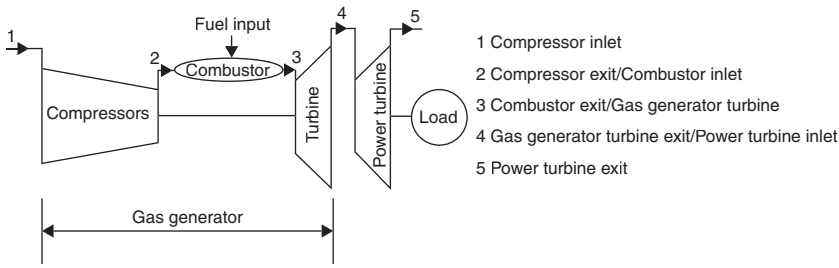
there is some variation of non-dimensional flow with speed but this is usually small. Unlike compressors, turbines do not suffer from surge problems, and this is due to the favourable pressure gradient present in turbines (i.e., the pressure decreases along the turbine).

11.12 Engine configurations

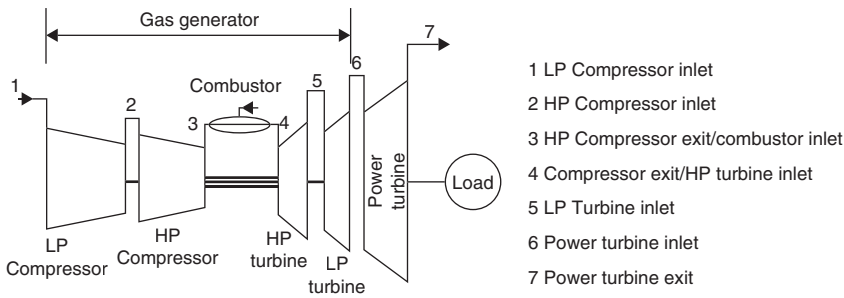
The schematic representation of a gas turbine, as shown in Fig. 11.1 was used in describing the design-point performance analysis, discussed above, and is indeed the configuration of a single-shaft gas turbine. Part of the power generated by the turbine section drives the compressor and the remaining power, typically about 50%, drives the load, which in the case of electrical power generation is a generator. The single-shaft configuration is most suitable for applications where the generator and thus the gas turbine speed is fixed, as we find in base-load power generation. Such a gas turbine configuration has the advantage of preventing over-speed conditions should the loss of electrical load occur. This is due to the large inertia of the rotor which acts as an effective brake.

The expansion process in the turbine can be split into two parts. where the HP or gas generator turbine drives the compressor, while the second stage, which is often referred to as the free power turbine, drives the load. A schematic representation of a two-shaft gas turbine operating with a free power turbine is shown in Fig. 11.39. Its application is most suitable when the speed of the load is changing with power demand, such as gas compression (also known as mechanical drives) or marine applications where the power turbine drives a fixed pitch propeller. The compressor and HP turbine (i.e. the

© Woodhead Publishing Limited, 2013



11.39 Schematic representation of a two-shaft gas turbine operating with a free power turbine.



11.40 Schematic representation of a three-shaft free turbine gas turbine.

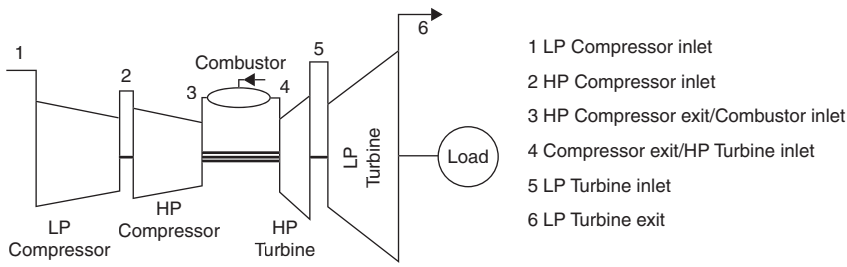
gas generator) produces high pressure high temperature gases, and this is utilised by the power turbine to develop the power output of the engine. Although we have stated that two-shaft gas turbines operating with a power turbine are most suitable for mechanical drives, they are also used in industrial power generation particularly if the power required is unavailable in a single-shaft configuration.

The gas generator shown in Fig. 11.39 can be divided into two parts, where the HP turbine drives the HP compressor, and the LP turbine drives the LP compressor, as shown in Fig. 11.40, and is referred to as a three-shaft gas turbine operating with a free power turbine. Again, such configurations are quite suitable for mechanical drive application. The advantage of splitting the compressor into two parts is that the effects of choking and stalling, which increase the potential of compressor surge, can be eased at low speed operation, particularly for gas turbines designed to operate at high compressor pressure ratios. At low speed operation, the HP compressor can operate at a higher speed, thus allowing more flow through the HP compressor, and thus alleviating the choking effects of the HP stage which would occur if the compressor were a single integral compressor. It should

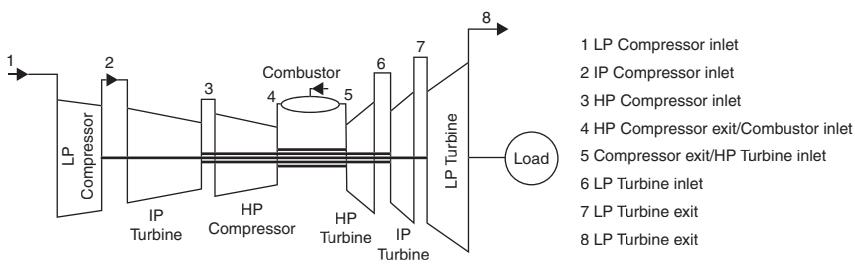
© Woodhead Publishing Limited, 2013

not be thought that such engine configurations find exclusive application for gas turbines designed to operate at high pressure ratios. High pressure ratio designs using a single compressor have been successfully designed, but they use many stages of variable stator vanes to unload the LP stages. However, there is a limit to the pressure ratio generated by such compressor using currently technology and the maximum pressure ratio achievable using a single spool is about 20:1 (Cumpsty, 1989), although recent engines have single spool compressors designed to operate at pressure ratios as high as 24:1.

Variations of the three-shaft gas turbines operating with a power turbine have been developed for industrial gas turbines, and they are referred to as the two-shaft and three-shaft gas turbines. These configurations do not have power turbines, and the LP compressor and the LP turbine are mechanically linked, which also drives the load. Schematic representation of the two and three-shaft gas turbine configurations are shown in Figs 11.41 and 11.42, respectively. These configurations are primarily developed for power generation where the LP compressor, turbine and load act as a brake in case the electrical load is shed. However, the multi-spooling of the LP and HP compressor enables very high design pressure ratios to be achieved, thus enhancing the engine performance. Complex cycles employing intercooling, regeneration and reheat are rare but a few manufacturers have developed industrial gas turbines using intercooling and reheat.



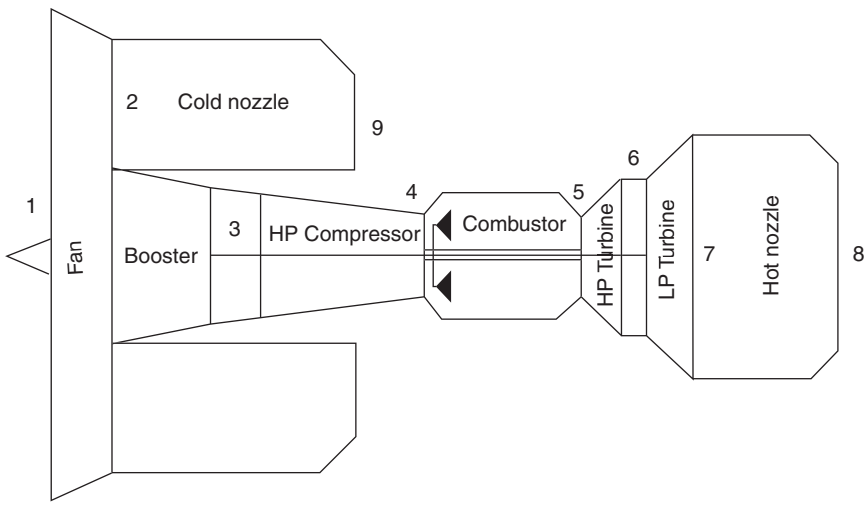
11.41 Schematic representation of a two-shaft gas turbine.



11.42 Schematic representation of a three-shaft gas turbine.

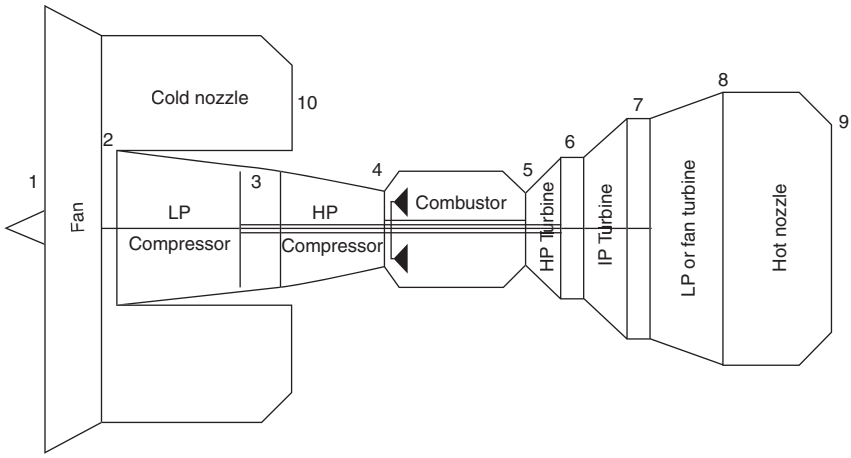
© Woodhead Publishing Limited, 2013

Turbo-jets can be regarded as similar to a two-shaft gas turbine operating with a free power turbine where the power turbine is replaced with a propelling nozzle. The gas generator, which consists of the compressor and turbine, can be divided into two parts in a manner similar to a three-shaft gas turbine operating with a free power turbine. Again, the power turbine is replaced with a propelling nozzle. Although a single spool turbo-jet could be considered as a satisfactory configuration for high speed flight (Mach numbers 3+), multi-spooling is essential for bypass engines, particularly for high to very high bypass engines, to prevent compressor instabilities such as stall and surge due to the high pressure ratios often employed by these engines. High pass ratio turbo-fan engines find application where the flight Mach number is about 0.85. Common configurations for high BPR engines are shown in Figs 11.43 and 11.44. The so-called booster compressor in the twin spool configuration shown in Fig. 11.43 contributes little to the overall pressure ratio, as the rotational speed of the boost compressor is constrained by the fan-tip speed to maintain a suitable fan-tip Mach number. The triple spool configuration shown in Fig. 11.44 is a better option, as both the IP and HP compressor can contribute usefully to the overall compressor pressure ratio. For moderate or low BPRs a twin speed arrangement, as shown in Fig. 11.45, is suitable, although triple spool arrangements have also been developed for low BPR engines. As stated above, low BPR engines are primarily used in fighter aircraft to improve subsonic fuel consumption. Turbo-props may use a single or split shaft configuration, as shown in Figs 11.34 and 11.46, and they find application where the flight Mach number is

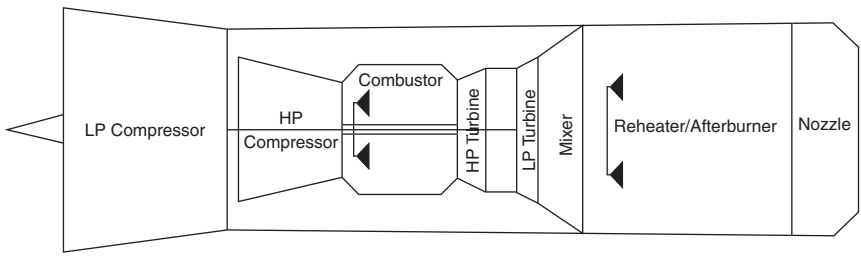


11.43 Schematic representation of a twin spool high bypass turbo-fan engine.

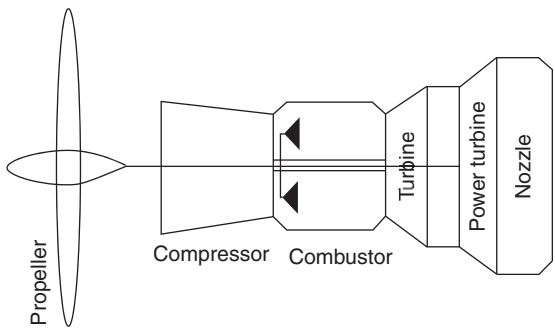
© Woodhead Publishing Limited, 2013



11.44 Schematic representation of a triple spool high bypass turbo-fan engine.



11.45 Schematic representation of a twin spool low bypass mixed turbo-fan engine.



11.46 Schematic representation of a two-shaft turbo-prop operating with a free power turbine.

© Woodhead Publishing Limited, 2013

low (typically about 0.4), as at these flight conditions the propulsive efficiency of turbo-props is much better than turbo-fans or turbo-jets. Note the presence of the propelling nozzle, as these engines produce a small amount of jet thrust although a substantial amount of the thrust is generated by the propeller.

11.13 Off-design performance prediction

The above discusses the design-point performance calculation of various gas turbine cycles, and engines designed on these principles would normally achieve their design-point performance. Information from design-point calculations, such as air mass flow rate, which is obtained from the power required and the specific work, cycle pressure ratios, and maximum cycle temperature are employed in the design of the turbo machinery and combustion system. However, gas turbines have to operate for prolonged periods at off-design conditions and the performance of gas turbines at off-design conditions is also of paramount importance. Off-design operation results from a change in load and ambient conditions. In this section, we will discuss methods of predicting the off-design performance of single-shaft, two-shaft gas turbine operating with a free power turbine and a high bypass turbo-fan engine. The methods for predicting the off-design performance of other engine configurations may be found in Walsh and Fletcher (2004) and Razak (2007).

To predict the off-design performance of gas turbines we require the component characteristics and these are usually generated during the design of the turbomachinery. The process of predicting the off-design performance employs the methods for calculating the thermodynamic performance of engine components, as discussed above, but on this occasion we need to satisfy the flow, work or power and speed compatibility of the various engine components.

Referring to Fig. 11.1, which is a schematic representation of an industrial single-shaft gas turbine, the prediction of the off-design performance is described as follows. The required power output, gas turbine speed (N_1), ambient pressure (P_a), ambient temperature (T_a) and humidity are specified.

Step 1.0 Inlet

Step 1.1 Estimate the inlet airflow W_1 and calculate the compressor inlet pressure P_1 using Equation [11.62]. The compressor inlet temperature T_1 will be equal to the ambient temperature T_a as the inlet is assumed to be an adiabatic duct.

Step 2.0 Compressor

Step 2.1 Estimate the compressor pressure ratio P_2/P_1 and combustion exit temperature (T_3).

© Woodhead Publishing Limited, 2013

Step 2.1 Calculate the compressor inlet non-dimensional flow $\left(W_1\sqrt{R_1T_1/\gamma_1}\right)\Big/P_1$.

Step 2.2 Using the compressor non-dimensional flow and pressure ratio P_2/P_1 determine the compressor non-dimensional speed $N_1\Big/\sqrt{\gamma_1R_1T_1}$ and compressor isentropic efficiency $\eta 12$ by interpolation using the compressor characteristic (Fig. 11.36).

Step 2.3 Calculate the compressor exit mass flow pressure, temperature and speed using the following

$$W_2 = W_1 - W_c$$

where W_c is the cooling air bleed

$$P_2 = P_1 \times \frac{P_2}{P_1}$$

Calculate T_2 using the procedure described in Section 11.7.1.

$$N_1 = \sqrt{\gamma_1 \times R_1 \times T_1}\sqrt{\frac{N_1}{\gamma_1R_1T_1}}$$

Step 2.4 Calculate the compressor power absorbed using:

$$cpow = W_1 \times (h_2 - h_1)$$

where h_1 and h_2 are the enthalpy at inlet and exit of the compressors.

Step 3.0 Combustor

Step 3.1 Using the estimated combustor exit temperature T_3 calculate the fuel flow (*mf)* using the process described in Section 15.8.2.

Step 3.2 Calculate the combustor exit pressure ($P3$), as described in Section 11.7.2.

Step 3.3 Calculate the exit mass flow:

$$W_3 = W_2 + mf$$

Step 4.0 Turbine

Step 4.1 Calculate the turbine inlet non-dimensional flow and non-dimensional speed $\left(W_3\sqrt{R_3T_3r/\gamma_3}\right)\Big/P_3$ and $N_3\Big/\sqrt{\gamma_3R_3T_3r}$ respectively, where T_3r is the turbine stator outlet temperature and determined as discussed in Section TET and stator outlet temperature.

Step 4.2 Estimate or guess the turbine pressure ratio P_3/P_4 and the calculated non-dimensional speed $N_3\Big/\sqrt{\gamma_3R_3T_3r}$ in step 4.1, determine the turbine inlet non-dimensional flow $\left(\left(W_3\sqrt{R_3T_3r/\gamma_3}\right)\Big/P_3\right)$ isentropic

© Woodhead Publishing Limited, 2013

efficiency $\eta 34$ by interpolation using the turbine characteristic (Figs 11.37 and 11.38). Also, we can calculate the turbine exit pressure:

$$P_4 = \frac{P_4}{P_3} \times P_3$$

Step 4.3 Calculate the turbine exit temperature and power output procedure described in Section 11.7.3.

Step 5.0 Check1

Given the calculated exit temperature and pressure from the turbine we can determine the exit non-dimensional flow $\left(W_4\sqrt{R_4T_4 / \gamma_4}\right)\Big/P_4$, and determine the pressure loss in the exhaust stack. Check that the exit pressure equals the ambient pressure. If they do not match then return to step 4.2 and estimate the turbine pressure ratio and repeat from step 4.2 until the exhaust stack pressure matches the ambient pressure.

Step 6.0 Check 2

Step 6.1 Compare the calculated turbine inlet non-dimensional flows $\left(W_3\sqrt{R_3T_3r / \gamma_3}\right)\Big/P_3$ in step 4.1 and the turbine inlet non-dimensional flow determined from the turbine characteristic, in step 4.2. If they do not agree return to step 3.0 and estimate a different T_3 and repeat to step 5.1 until the two values for turbine inlet non-dimensional flows agree.

Step 7.0 Check 3

Step 7.1 Calculate the net turbine power output (*pnet*) using $pn_{et} = tp_{ow} - cp_{ow}$

Step 7.2 Compare the calculated turbine power output with the required power output from the gas turbine. If they do not agree return to step 2.0 and estimate a different compressor pressure ratio (P_2/P_1) and repeat to 7.2 until the powers agree.

Step 8.0 Check 4

Step 8.1 Compare the compressor speed (N_1) calculated in step 2.0 with the speed required by the load. If they do not agree, estimate a different compressor inlet mass flow (W_1) and return to step 2.0 and repeat to step 8.1 until the speeds agree.

The above describes the off-design performance of a single-shaft gas turbine, using a series of guesses or estimates such as compressor, pressure ratio and temperatures. The validity of these estimates were checked against turbine flow, speed and power compatibility and the estimates are adjusted until the flow, speed and power compatibility are achieved. We can indeed extend such schemes of guesses in checking other engine configurations and

© Woodhead Publishing Limited, 2013

thereby determine the off-design performance of such engine configurations. However, in practice we can use matrix manipulation where Newton's method of approximation or Newton Raphsons is applied to determine the off-design performance of gas turbines. Methods employed by computer programs often use such matrix manipulations, using the estimates and checks described above to solve a set of non-linear equations. In matrix notation the solution of a set of equations is given by:

$$\mathbf{J} \cdot \delta\mathbf{x} = -\mathbf{F} \qquad [11.92]$$

where **J** is a matrix which represents the rates of change of the variables used in the calculation of the checks above, such as non-dimensional flows and power balance with respect to the estimated variables such as compressor pressure ratio and TET, as discussed above describing the step-by-step approach in predicting the off-design performance of a single-shaft gas turbine. $\delta\mathbf{x}$ is a column matrix or a vector containing step changes in the estimated values used to calculate the rates of change in the matrix **J**. **F** is a vector containing the function values (check values described earlier) and will represent the errors since we are solving these equations for the case $\mathbf{F} = \mathbf{0}$. Solving Equation [11.92] will determine the vector $\delta\mathbf{x}$. Thus a new set of values of **x** can be determined via $\mathbf{xnew} = \mathbf{xold} + \delta\mathbf{x}$. These values are now used in Equation [11.92] and the process repeated until $\mathbf{F} = \mathbf{0}$ or the value of **F** is within an acceptable error tolerance, usually within 10^{-6}. Vetting and Flannery (1992) and Gerald and Wheatly (1997) give further details.

For a single-shaft gas turbine the solution is started by providing Equation [11.92] with a set of initial estimates, which are:

1. Compressor inlet flow, W_1.
2. Compressor pressure ratio, P_2/P_1.
3. Combustor exit temperature, T_3.
4. Turbine pressure ratio, P_3/P_4.

Using these estimates, every engine parameter can be calculated (pressure, temperatures, speeds, flows and powers for each engine component). While the calculated powers, flows and speeds may not necessarily satisfy the flow, power and speed compatibility, these errors or differences can be used to determine the check vector *F* employed by Equation [11.92]. This is achieved by considering:

1. Turbine flow compatibility $\left(W_3\sqrt{R_3T_{3r}/\gamma}\right)\Big/P_3$.
2. Power compatibility (i.e. difference between gas turbine calculated power and required power).
3. Pressure difference between the exhaust stack exit pressure and ambient pressure.

© Woodhead Publishing Limited, 2013

4. Speed compatibility (i.e., difference between gas turbine speed and the speed required by the load).

It is important that the number of estimates is at least equal to the number of checks. For the single-shaft gas turbine, four estimates and checks have been described. A required fuel flow or compressor pressure ratio can be specified instead of a required power output in which case the power output will be calculated. The solution will result in the evaluation of all relevant thermodynamic parameters (e.g., pressures, temperature and flows).

For a two-shaft gas turbine operating with a free power turbine, as shown in Fig. 11.39 the vector data is as follows.

The estimated vectors are:

1. Compressor inlet flow, W_1.
2. Compressor pressure ratio, P_2/P_1.
3. Combustor exit temperature, T_3.
4. Gas generator pressure ratio, P_3/P_4.
5. Power turbine pressure ratio, P_4/P_5.

And the check vectors are:

1. Gas generator flow compatibility $\left(W_3\sqrt{R_3T_{3r}/\gamma}\right)\Big/P_3$.
2. Power balance between the compressor and gas generator turbine $W_1 \times (h_2 - h_1)$ and $W_3 \times (h_{3r} - h_4)$, respectively, where h_{3r} is the stagnation enthalpy at the turbine stator outlet.
3. Power turbine flow compatibility $\left(W_4\sqrt{T_4/\gamma_4}\right)\Big/P_4$.
4. The difference between the power output from the power turbine and the required power output.
5. Pressure difference between the exhaust stack exit pressure and ambient pressure.

There are five estimates and checks for a two-shaft gas turbine operating with a power turbine. Fuel flow, gas generator speed, compressor non-dimensional speed or compressor pressure ratio can be specified as a check vector instead of the required power output.

Similar schemes for initial estimate vectors and check vectors can be developed for other engine configurations and have been discussed by Razak (2007). We shall develop these vectors for a triple spool turbine fan, as shown in Fig. 11.44, as follows:

The initial estimates are:

1. Fan inlet flow, $W_{1.}$
2. Fan pressure ratio, $P_2/P_{1.}$

© Woodhead Publishing Limited, 2013

3. Bypass ratio, BPR.
4. IP compressor pressure ratio, P_3/P_2.
5. HP compressor pressure ratio, P_4/P_3.
6. Combustor exit temperature, T_5.
7. HP turbine pressure ratio, P_5/P_6.
8. IP turbine pressure ratio, P_6/P_7.
9. LP turbine pressure ratio (P_7/P_8).

The check vectors are:

1. HP turbine flow compatibility $\left(W_5\sqrt{R_5T_5/\gamma_5}\right)\Big/P_5$.
2. Power balance between the HP compressor and HP turbine $W_3 \times (h_4 - h_3)$ and $W_5 \times (h_5 - h_6)$, respectively.
3. IP turbine flow compatibility $\left(W_6\sqrt{R_6T_6/\gamma_6}\right)\Big/P_6$.
4. Power balance between the IP compressor and IP turbine $W_2 \times (h_3 - h_2)$ and $W_6 \times (h_6 - h_7)$, respectively.
5. LP turbine flow compatibility $\left(W_7\sqrt{R_7T_7/\gamma_7}\right)\Big/P_7$.
6. Power balance between the fan and LP turbine $W_1 \times (h_2 - h_1)$ and $W_7 \times (h_7 - h_8)$, respectively.
7. Hot nozzle flow compatibility $\left(W_8\sqrt{R_8T_8/\gamma_8}\right)\Big/P_8$.
8. Cold nozzle flow compatibility $\left(W_9\sqrt{R_9T_9/\gamma_9}\right)\Big/P_9$.
9. Difference in the net trust from the engine and the required thrust.

There are nine estimates and checks for a triple spool unmixed turbo-fan engine, as discussed earlier. Instead of specifying the net thrust required in item (9) for the check vector a required fuel flow or fan speed or IP spool speed or HP spool speed can be specified. The speeds can be either mechanical or non-dimensional speeds. Also fan, IP or HP compressor pressure ratios can be specified as the ninth check vector discussed above. It should be noted that the TETs (T_5, T_6 and T_7) should be the stator outlet temperatures if cooled, and can be determined using the procedure discussed in the section TET and stator outlet temperature. Also the enthalpy at which work is extracted from these turbines should be determined at the stator out let temperatures.

11.14 Transient performance modelling

Much of the discussion above has considered gas turbines operating at steady-state conditions. In this section, we will discuss the modelling of the transient performance of gas turbines. Although our discussion will be restricted to a single-shaft gas turbine, the methods described in this section can be adapted and applied to any gas turbine configuration (both industrial and aero engines).

© Woodhead Publishing Limited, 2013

The gas turbine is divided into elements, such as compressor, combustors, turbines and interconnecting ducts or transition ducts that connect these various components so that the air and gases can flow from one component to another. A schematic representation of such an elemental representation of a single-shaft gas turbine is shown in Fig. 11.48. When considering the simulation of the transient performance of the gas turbine we need to consider the dynamic form the continuity, momentum and energy equations. Referring to a generalised element, as shown in Fig. 11.47, which can be a compressor or turbine element, assuming the Mach numbers at the inlet and the exit of the element are less than 0.3, the dynamic form of the continuity equation can be described as:

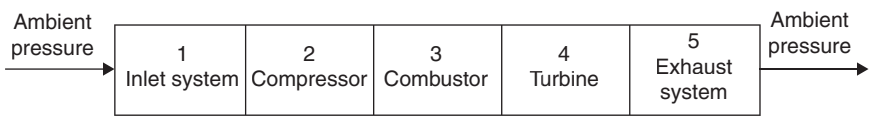
$$\frac{\mathrm{d}P_2}{\mathrm{d}t} = \frac{RT_2}{V}\left(W_1 - W_2 \pm W_3\right) \qquad [11.93]$$

where P_1 and P_2 is the element inlet and exit stagnation pressure respectively. R is the gas constant, W_1, W_2 and W_3 is the inlet and exit element flow rates respect, and V is the element volume.

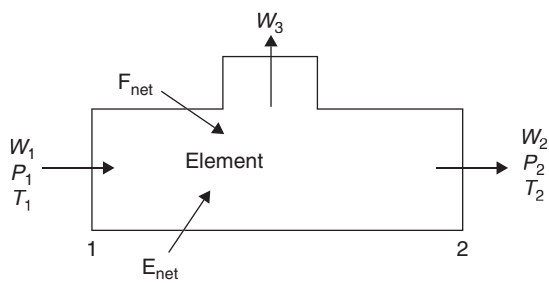
The dynamic form of the momentum equation can be stated as:

$$\frac{\mathrm{d}W_1}{\mathrm{d}t} = \frac{A_m}{\Delta x}\left(P_1 - P_2 + F_{\mathrm{net}}\right) \qquad [11.94]$$

where A_m is the area mean flow area and F_{net} is the instantaneous net external forces acting on the element. For the compressor or turbine, F_{net} corresponds to the pressure rise or pressure drop across the compressor or turbine



11.47 Diving flow or blow-off element.



11.48 Elemental representation of a single-shaft gas turbine.

© Woodhead Publishing Limited, 2013

and is determined from the steady-state characteristic of the compressor and turbine. Often stage characteristics are employed in determining F_{net}.

The dynamics of the energy equation can be described as:

$$\frac{dU}{dt} = W_1 h_1 - W_2 h_2 + E_{net} \quad [11.95]$$

where U is the internal energy within the element and E_{net} is the instantaneous net heat entering the element; for compressors and turbines E_{net} is zero as the process is assumed to be adiabatic but for combustors E_{net} corresponds to the instantaneous heat input ($mf \times$ LHV). h_1 and h_2 are the specific enthalpy at inlet and exit of the element respectively.

By solving differential Equation [11.95] the internal energy at the present time can be determined. The specific internal energy (U) can be defined as $U = \int cv\,dT$, where cv is the specific heat at constant volume, and for a perfect gas cv can be considered to be a function of temperature, thus the temperature at exit of the element can be determined implicitly.

The equations described above to simulate the transient performance of gas turbines assume a lumped distribution of the calculated parameters, where they are assumed to remain constant across the element and are based on the work of Elder and Cobert (1975). They report that the simulated results for the lumped and linearly distributed models were in good agreement, but that the linear model required a significant increase in computational effort (some 2.3 times more computing time). Thus, lumped models are often employed in the prediction of the transient performance of gas turbines. However, the assumption in the lumped parameter model imposes frequency limitations, because second- or higher-order equations are being solved. Such systems of equations employed in predicting transient performance gas turbines and gas compression systems are capable of simulating longitudinal waves. For air, the element length, Δx, in Equation [11.94] should be less than about 34 m ($\Delta x << 34$ m), as determined by Corbett and Elder (1975). This is usually the case with gas turbine components.

It should be noted that these models are capable of simulating compressor surge cycles. Elder and Macdougal (1983) developed a frequency parameter model to account for surge and pre-surge oscillations during the transient response of the compressor element. They related a frequency parameter to the phase change across the compressor element in terms of an expected error when comparing the lumped parameter model with the true solutions. Using an expected frequency of interest, fx, and Mach number, Mx, of 0.3 or less, a suitable element length for the compressor could be determined using: $2\pi\, fx\Delta x < a(1 - Mx)$ where a is the velocity of sound.

Although the above analysis improves the simulation, the elements do not communicate in a realistic manner if the adjacent element volumes are

© Woodhead Publishing Limited, 2013

significantly different. In order for elements to interact in a realistic manner, a criterion of approximately equal volumes is used, in conjunction with the frequency parameter model. Other researchers in the field of transient analysis of gas turbines include Greitzer (1978) and Fawke and Saravamuttoo (1971). Although Greitzer (1978) used a similar approach to that described by Elder and Colbert (1975) and discussed above, Fawke and Saravamuttoo (1971) restricted their models to continuity-only. Surge simulations are unavailable using the continuity-only model.

11.14.1 Boundary conditions

Solving Equations [11.93]–[11.95] determines the element inlet mass flow rate, discharge or exit pressure and exit temperature for each element during transients. Therefore, we need to specify the pressure and temperature at inlet to the first, and the mass flow rate at exit from the last element. In industrial gas turbines, the inlet pressure at the entry to the system, which is usually the inlet system, is the ambient pressure and therefore can be used as the inlet boundary condition. This is shown in Fig. 11.47. The inlet temperature at the entry to the system would also correspond to the ambient temperature. For aero gas turbines, the inlet pressure and temperature will also correspond to the ambient pressure and temperature, which is upstream of the inlet system.

The last element of an industrial gas turbine would normally be the exhaust system as shown in Fig. 11.47. This element incurs a small pressure loss, typically of the order of about 100 mm water gauge, and could be used to determine the flow at the exit from the last dynamic element, which is the turbine as shown in Fig. 11.47. Since the pressure and temperature at the exit from the turbine element (which is the inlet to the exhaust system) are known, calculation of the mass flow rate at the exit from the turbine element is possible using the equation describing the pressure loss in the exhaust system. The pressure loss equation for the exhaust system is similar to Equation [11.62] in Section 11.7.3, but the temperature rise is zero. Since the pressure at the exit of the exhaust system is the ambient pressure, the pressure loss in the exhaust system is readily known. From Equation [11.59], the mass flow rate can be calculated. For aero gas turbines the propelling nozzle(s) can be used to determine the exit mass flow of the last dynamic element, as discussed in Section 11.7.3.

Again restricting our discussion to single-shaft gas turbines, the compressor–turbine and the driven load may vary in speed during transients. This will depend on the power absorbed by the compressor and load, and the power developed by the turbine. Also, the gas turbine configuration and control system performance will influence the changes in speed of these components. The power absorbed by the compressor and the power developed by the turbine are readily calculated as discussed above. For a given

© Woodhead Publishing Limited, 2013

compressor and turbine speed, the torque at the compressor and turbine are readily calculated using the relationship:

$$\text{Power} = \text{Torque} \times \text{Angular velocity}$$

Therefore, at any instance the torque at the compressor and turbine can be calculated. Furthermore, for a given power output and load speed the torque at the load is also known. For a single-shaft gas turbine rotor, as shown in Fig. 11.1, the net torque, T_{net}, is given by $T_{net} = T_{Turb} - (T_{comp} + T_{load})$, where T_{Turb}, T_{comp} and T_{load} are the torque at the turbine, compressor and load, respectively.

Applying Newton's second law of motion:

$$\alpha = \frac{\mathrm{d}\varpi}{\mathrm{d}t} = \frac{T_{net}}{I} \qquad [11.96]$$

where α and I are the angular acceleration or deceleration of the rotor system and polar moment of inertia of the rotor, respectively.

Given an initial angular velocity, the current angular velocity can be calculated from the angular acceleration calculated from Equation [11.96]. The analysis can be extended to other engine configurations discussed in Section 11.12.

Equations [11.93]–[11.96] are referred to as first-order ordinary differential equations. These are non-linear differential equations and therefore no analytical solutions exist. In these situations the only means of finding a solution is numerically. Many such methods have been developed, from simple Euler to more advanced methods such as Rung–Kutta–Felberg and Gears method. Press *et al*. (1992) and in Gerald and Wheatly (1997) discuss the application such methods in detail.

11.15 Off-design performance behaviour of gas turbine cycles

In Section 11.13, we described the procedure for prediction of the off-design performance of gas turbines. Although the process is rather tedious and computer programs are often employed in determining the off-design performance, making certain assumptions the off-design behaviour of gas turbine can be more easily understood. We will restrict our discussion to the single- and two-shaft gas turbine in this section and the concepts can be extended to cover other engine configurations.

Neglecting the gas property terms and referring to Fig. 11.1 the flow compatibility equation for a single-shaft gas turbine between the compressor and turbine can be written as:

© Woodhead Publishing Limited, 2013

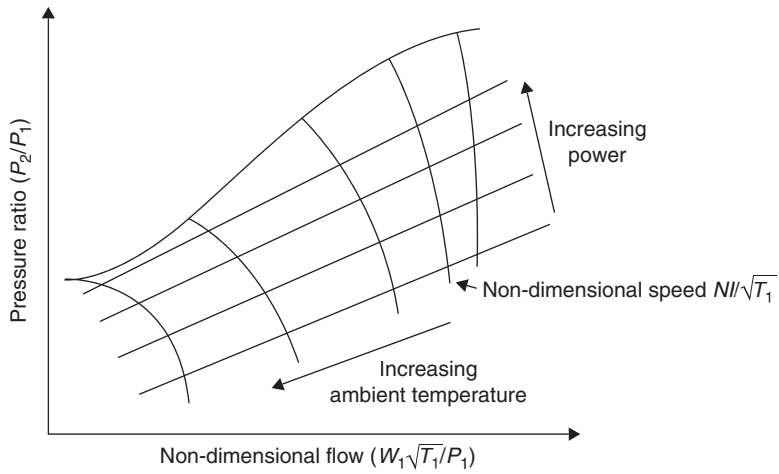
$$\frac{W_3\sqrt{T_3}}{P_3} = \frac{W_1\sqrt{T_1}}{P_1} \times \frac{P_1}{P_2} \times \frac{P_2}{P_3} \times \sqrt{\frac{T_3}{T_1} \times \frac{W_3}{W_1}} \qquad [11.97]$$

Assuming the turbine is choked, which is normally the case at high operating powers, the turbine non-dimensional flow will remain approximately constant with turbine pressure ratio. Thus the term $\left(W_3\sqrt{T_3}\right)\Big/P_3$ is a constant. If we also assume that the compressor speed line is near choke conditions, especially at high operating speeds, the variation of the compressor inlet non-dimensional flow $\left(W_1\sqrt{T_1}\right)\Big/P_1$ with pressure ratio for a given compressor non-dimensional speed will be small. Furthermore, if the combustion pressure loss and bleeds are assumed constant, then P_2/P_3 and W_3/W_1 will also be constant. Hence, an increase in compressor pressure ratio must be accompanied by an increase in T_3/T_1 to satisfy the flow compatibility in Equation [11.97].

For a given compressor non-dimensional speed the compressor temperature ratio (T_2/T_1) is approximately constant with varying compressor pressure ratio, as discussed by Saravanamutoo *et al.* (2001), and this is due to the change in compressor efficiency as the compressor operates at off-design conditions, particularly as the compressor pressure ratio decreases. Thus the compressor specific work is approximately constant. As the compressor pressure ratio increases the turbine pressure ratio and the TET (T_3) increases. Thus the gas turbine, the power output, and the thermal efficiency also increase. The analysis can be carried out for different compressor non-dimensional speeds. For a constant speed engine, as we would find in power generation, the higher the ambient temperature (T_1) the compressor non-dimensional speed and inlet non-dimensional flow decreases, as shown in Fig. 11.49. Carrying out a similar analysis, it can be shown that the pressure ratio and TET decrease as the ambient temperature increases, which results in a decrease in engine performance. A series of constant power running lines can be produced on the compressor characteristic, as illustrated in Fig. 11.49.

It should be evident from the above analysis that the increase in ambient temperature will have a detrimental effect on engine performance, where the maximum power available and thermal efficiency decrease. Other environmental effects that affect engine performance are ambient pressure and humidity. For a given ambient temperature and gas turbine speed, the compressor non-dimensional speed and flow will be constant. This results in the specific work and thermal efficiency also being constant. However, as the ambient pressure decreases the compressor inlet flow decreases (i.e. $\left(W_1\sqrt{T_1}\right)\Big/P_1$ is constant but, as the ambient pressure decreases, P_1 decreases the compressor inlet flow W_1 also decreases). Thus the power output decrease is approximately proportional to the decrease in ambient pressure. An increase in humidity increases the amount of water vapour in the air

© Woodhead Publishing Limited, 2013



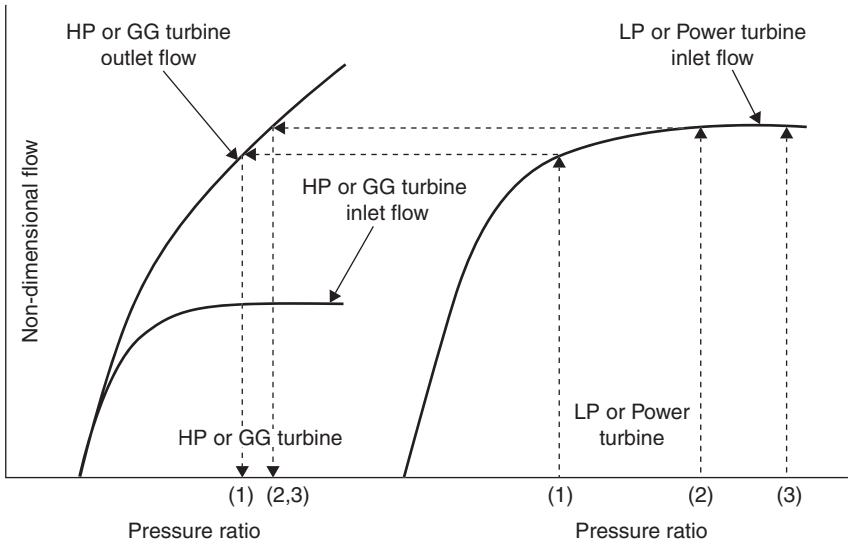
11.49 Series of running lines due to power and ambient temperatures for a single-shaft gas turbine.

and thus the gas constant of air. Allowing for gas property terms in the non-dimensional speed $N_1/\sqrt{\gamma_1 R_1 T_1}$, the increase in humidity increases the gas constant R_1 (assuming a constant mechanical speed (N_1) as we would find in power generation). Although there is also a decrease in the isentropic index (γ_1) the increase in gas constant is greater and the compressor non-dimensional speed decreases with increased humidity. A decrease in compressor non-dimensional speed, as seen from above decreases the power output and thermal efficiency of the gas turbine. The effects of humidity on gas turbine performance are more noticeable at high ambient temperatures as air can hold more water vapour at high ambient temperatures.

To understand the off-design behaviour of a two-shaft gas turbine operating with a free power turbine we need to consider the matching of turbines operating in series. Referring to Fig. 11.39, which shows a schematic representation of a two-shaft gas turbine operating with a free power turbine, the matching of the gas generator (GG) or HP turbine, and the power or LP turbine characteristics are shown in Fig. 11.50. It can be seen that when the power turbine is choked, the GG turbine pressure is fixed and determined by the swallowing capacity of the power turbine. Since GG turbine efficiency does not change a great deal, particularly at high turbine non-dimensional speed, which will correspond to high power operation, the turbine temperature ratio (T_3/T_4) will also be essentially fixed and therefore $\Delta T_{34}/T_3$ will also be constant. The power balance between the compressor and the GG turbine can be written as:

$$\frac{\Delta T_{21}}{T_1} = \frac{\Delta T_{34}}{T_3} \times \frac{T_3}{T_1} \times \frac{cp_g}{cp_a} \times \frac{W_3}{W_1} \qquad [11.98]$$

© Woodhead Publishing Limited, 2013

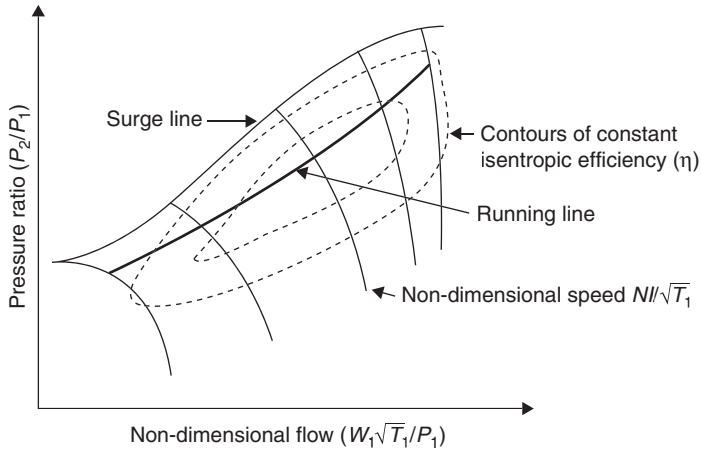


11.50 Characteristics of turbines operating in series.

Since for a choked power turbine the GG temperature ratio $\Delta T_{34}/T_3$ will be constant and for a given compressor non-dimensional speed $\Delta T_{21}/T_1$ is also constant, as discussed when considering the single-shaft gas turbine, assuming the specific ratio cp_g/cp_a and the ratio of the GG turbine inlet flow to compressor inlet flow ratio (W_3/W_1) is also constant, then for a given compressor non-dimensional speed the maximum-to-minimum cycle temperature (T_3/T_1) will also be constant. Referring to the flow compatibility equation between the compressor and GG turbine, as defined in Equation [11.97], the compressor pressure ratio will be fixed. The above analysis for a two-shaft gas turbine can be carried out at different compressor non-dimensional speeds, and this will determine a unique compressor pressure ratio for each compressor non-dimensional speed. Connecting these pressure ratios on the compressor characteristic will generate the unique running line on the compressor characteristic, as shown in Fig. 11.51. This differs from a single-shaft gas turbine where there is no unique running line and the running line is dependent on the power output. (It should be noted that the unique running line only occurs if we assume that the gas property terms are fixed. When changes in gas property terms are considered the running line will vary with operating conditions; however, this is usually small.)

For a given maximum cycle temperature (T_3), an increase in ambient temperature (T_1) would result in a decrease in T_3/T_1 and compressor pressure ratio, that is, the operating point will move down the running line on the compressor characteristic (Fig. 11.51). Thus the thermal efficiency and power output decreases. As discussed for a single-shaft gas turbine, high

© Woodhead Publishing Limited, 2013



11.51 Running line on the compressor characteristic for a two-shaft gas turbine.

ambient temperatures also affect the performance of two-shaft gas turbines adversely. The ambient pressure also affects the performance of a two-shaft gas turbine operating with a free power turbine and a decrease in ambient pressure decreases the power output but has little effect on the thermal efficiency of the engine. The impact of humidity on the performance of a two-shaft engine is different from that of a single-shaft engine. Since the GG speed is not fixed, an increase in humidity will result in an increase in the GG speed while maintaining the temperature ratio T_3/T_1. This results in an increase in power output, but would decrease the thermal efficiency of a two-shaft gas turbine operating with a free power turbine.

A similar analysis can be carried out for out for other engine configurations, including aero engine. Saravanamuttoo *et al*. (2001), Walsh and Fletcher (2004) and Razak (2007) gives further details on such complex engine configurations. Razak (2007) also include gas turbine simulators, which are effectively virtual engines and can be used to understand the off-design behaviour of single- and two-shaft gas turbines. It also covers the simulation of performance deterioration, emissions, turbine creep life usage and engine control systems.

11.16 Adaptive model-based control

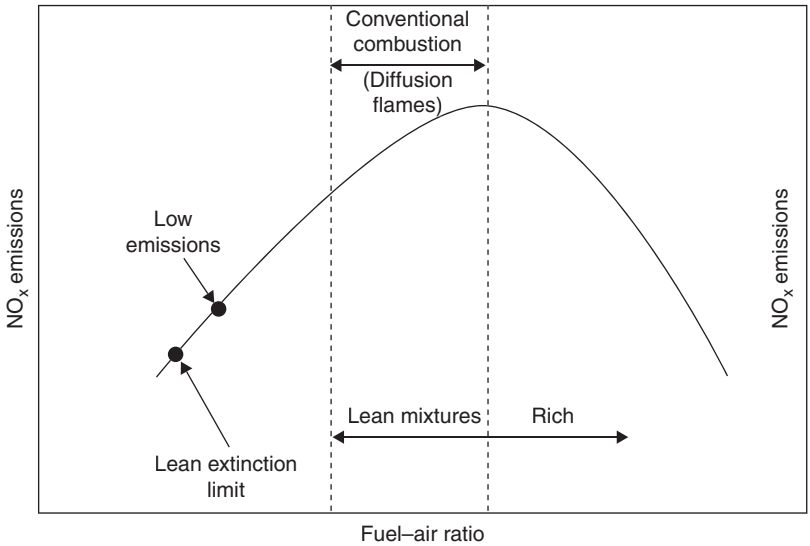
In Section 11.14, we discussed the transient performance modelling of gas turbines, which occur when operating conditions change. It is the responsibility of a control system is to ensure that the change in operating conditions occurs safely. Engines have various limiting operating values, such as exhaust gas temperature, which prevent the overheating of the turbine, and

© Woodhead Publishing Limited, 2013

operating speed limits are not exceeded so that the stresses in rotating members are within design limits, while the required power demand from the gas turbine is achieved provided that any component operating limits such TET is not exceeded. Other important operating conditions, which the control system should prevent, includes compressor surge. Although the details of the performance and behaviour of controls system are outside the scope of this chapter, engine control systems normally employ **P**roportional, **I**ntegral and **D**erivative (PID) controllers. There may be more than one PID controller required to ensure satisfactory control of a gas turbine. However, all controllers require a set point, which can be the required power demand from the gas turbine or limit values at certain salient points in the gas turbine cycle. Set points can be viewed as the required or desired steady-state value at salient points in the engine. There can be many such set points, and low or high signal selection is used to select the required set point. For example, if the maximum exhaust temperature will be exceeded, thereby overheating the turbine blades, low signal selection would ensure that the maximum exhaust gas temperature will be selected as the set point. During normal engine operation low signal selection will select the power demanded from the gas turbine as the set point. Thus we see that set points for control systems are determined from the design of the gas turbine. Razak (2007) gives further details on the control system in general, which are also applicable to gas turbines.

Set points for control systems can also be derived from engine models, since set points are the desired steady-state values during operation and model derived set points are usually determined from steady-state models rather than transient models. However, other types of models can also be employed, including data driven models or neural networks. In this section we will employ a steady-state performance model of the gas turbine for DLE combustion control. We shall consider a two-shaft industrial gas turbine operating with a free power turbine. The principle of a DLE combustion system is to maintain the fuel–air ratio near the weak extinction limit over the significant part of the power range of the gas turbine. At such low fuel–air ratios, emissions of oxides of nitrogen (NO_x), carbon monoxide (CO) and un-burnt hydrocarbons (UHC) are very low (typically about 15 ppmv or less), as illustrated in Fig. 11.52. A change in operating conditions, such as a reduction in power output, will result in a decrease in the fuel–air ratio, and this could lead to a flame-out of the engine if the ratio decreases below the weak extinction limit. We have also discussed that turbine operating in series will maintain the GG turbine pressure ratio at off-design conditions during choked power turbine operation, as illustrated in Fig. 11.50. The fixed GG turbine pressure ratio also maintains approximately constant GG turbine efficiency. If we maintain the exhaust gas turbine temperature at part loads, the constant GG turbine pressure ratio efficiency will result in a

© Woodhead Publishing Limited, 2013

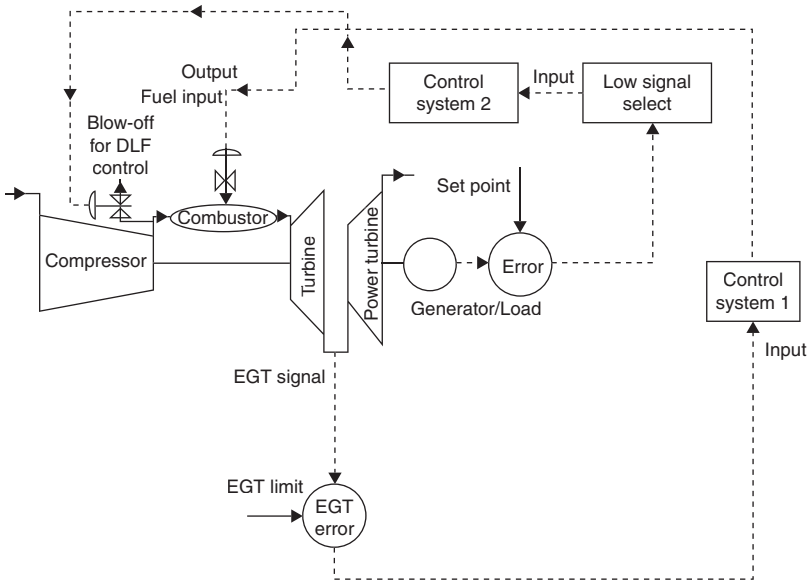


11.52 Running line on the compressor characteristic for a two-shaft gas turbine.

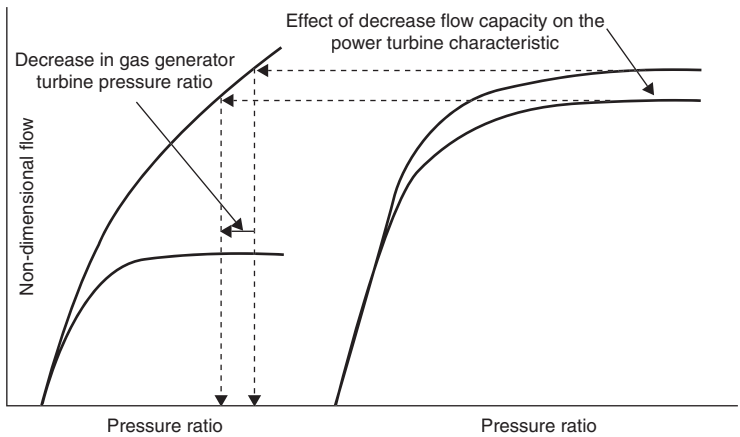
constant TET and thus a constant combustion temperature. This means that the fuel–air ratio is also constant, thus maintaining low emissions. However, we need to blow-off air at the combustion inlet at part load or off-design operating conditions, as illustrated in Fig. 11.53, which also shows an engine control system strategy including DLE combustion control. In effect, we are varying the load by increasing or decreasing the amount of blow-off.

Clearly, the use of blow-off for engine control is inefficient and manufacturers of such control systems set the design-point fuel–air ratio to be slightly higher and reduce engine load by reducing the EGT and when the EGT decreases below a certain value (set point) the blow-off valve is modulated to maintain the EGT at the set point. Thus, for much of the useful operating range of the engine (approximately 80–100% power range) there is no performance penalty using a DLE control system as described above. A better strategy would be to employ a variable geometry power turbine, and the power turbine capacity is decreased by closing the variable area nozzle guide vanes; such a control strategy will eliminate the use of blow-off. However, the closure of the power turbine nozzle guide vanes (NGV) results in the rematching of the turbines, as illustrated in Fig. 11.54 due to closure of the power turbine NGV, and this will decrease GG turbine pressure ratio and thus TET for a given exhaust gas temperature. The decrease in TET will decrease the fuel–air ratio and increase the risk of flame-out due to the fuel–air ratio exceeding the weak extinction limit. A steady-state performance model of the engine can be employed to prevent this. However,

© Woodhead Publishing Limited, 2013



11.53 The control strategy for DLE combustion using a single-combustion stage requiring the use of blow-off.



11.54 Effect of decreasing the power turbine area on the GG pressure ratio.

for a specified power required from the gas turbine, we solve the necessary flow and work compatibility equations as follows.

The estimated vectors are:

1. Compressor inlet flow, W_1.
2. Compressor pressure ratio, P_2/P_1.

© Woodhead Publishing Limited, 2013

3. Combustor exit temperature, T_3 (i.e., TET).
4. GG pressure ratio, P_3/P_4.
5. Power turbine pressure ratio, P_5/P_6.

And the check vectors are:

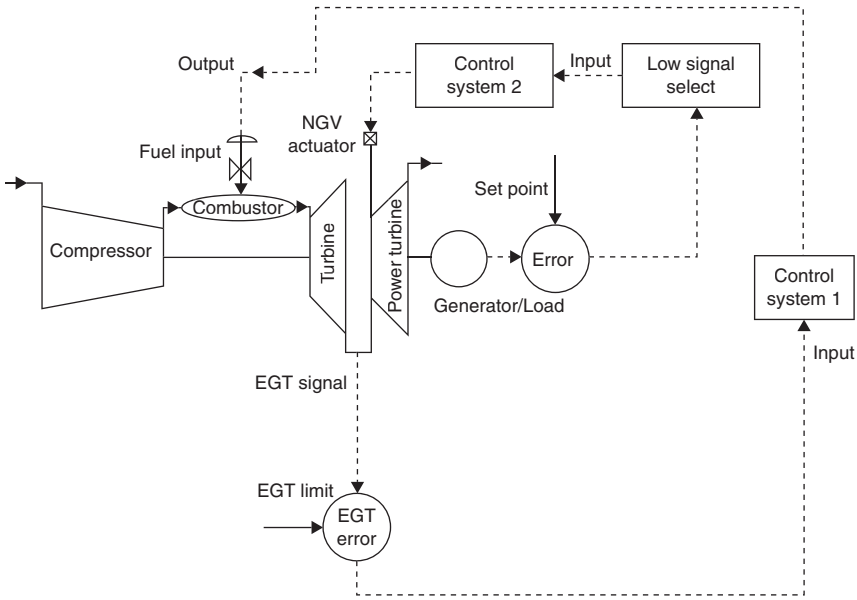
1. GG flow compatibility $\left(W_3\sqrt{R_3T_{3r}/\gamma}\right)\Big/P_3$.
2. Power balance between the compressor and GG turbine $W_1 \times (h_2 - h_1)$ and $W_3 \times (h_{3r} - h_4)$, respectively.
3. Difference between the calculated TET and that required for minimum emissions (usually this would correspond to the design-point value of the TET).
4. The difference between the power output from the power turbine and the required power output.
5. Pressure difference between the exhaust stack exit pressure and ambient pressure.

In the above scheme, solving the equations for the power turbine flow compatibility is not required, and the model will determine the power turbine flow capacity and the EGT, which will become the set point of the DLE combustion system. A schematic representation of a two-shaft gas turbine operating with a free power turbine using such a control scheme is shown in Fig. 11.55. Razak (2007) gives further details of such a control scheme, which has the potential to achieve all the requirements of variable geometry combustion systems. Such a method of adaptive model-based control for gas turbine emissions control can be extended to other engine configurations, including aero gas turbines. With respect to aero gas turbines, the variable geometry could be applied to the propelling nozzle rather than to the turbine sections.

Adaptive control can also be applied to compressor variable stators (VSV), to improve thermal efficiency at part load operation due to better compressor efficiency when operating under these conditions. However, VSVs are primarily provided to prevent compressor surge. Although such variable stators can be adjusted where suitable set points can be determined from a steady-state model in a manner similar to that for DLE control, as described above, it is unlikely such VSV adjustments during off-design operation will give a worthwhile gain in thermal efficiency. It should be noted that such VSV control will significantly increase the complexity of the VSV control system.

As an alternative to VSVs to optimise engine performance during part load operation, statorless turbines can also be used in off-design conditions. Unlike conventional turbines, where the turbine flow capacity is largely

© Woodhead Publishing Limited, 2013



11.55 The control strategy for DLE combustion using a single-combustion stage without the use of blow-off.

constant with turbine non-dimensional speed, particularly during choked operation, with statorless turbines there is an increase in turbine flow capacity with increase in turbine non-dimensional speed. The closure of VSVs will increase the GG speed and, for a given TET (T_3), will also increase the statorless turbine non-dimensional speed. The resultant increase in non-dimensional capacity of the statorless turbine will, for a given TET, decrease the compressor pressure ratio. Although such a scheme can be used for DLE control, rather than a variable geometry power turbine, as discussed above, the lower compressor pressure ratio will result in a lower thermal efficiency when compared with the variable geometry power turbine method. However, the higher operating temperatures of power turbines make variable geometry power turbines less reliable than VSVs. A similar control strategy is proposed by Lei and Grönstedt (2009), where statorless turbines are used to improve the sfc of high BPR turbo-fan engines during cruise. Here the HP compressor VSVs are opened to decrease the HP spool speed, which results in an increase in overall pressure ratio due to the decrease in HP turbine capacity, and they claim about 0.5% reduction in sfc. A similar concept may be considered for afterburning turbo-fans/turbo-jets, where the VSV is controlled so that no variable area nozzle is required (i.e. assuming a twin spool GG the LP compressor VSVs are opened during afterburning).

© Woodhead Publishing Limited, 2013

11.17 Future trends

Ever since the advent of the gas turbines, the performance has been steadily increasing over the years making it a formidable competitor as a source of mechanical power both for industrial and aircraft propulsion. As seen from the discussion above, simple cycle gas turbines are capable of achieving thermal efficiencies in excess of 40%, while complex cycles incorporating intercooling, reheat and regeneration can achieve thermal efficiencies of nearly 60%.

Gas turbines are therefore well placed to help combat global warming, which is thought to be due to the emissions of man-made carbon dioxide (CO_2) into the atmosphere. Nuclear power has been developed and applied successfully in power generation; however, the costs of building, operating and disposing of nuclear waste is quite high, making such power generation system less competitive. However, such power plants are zero or near zero CO_2 emitters. The higher the efficiency of such nuclear power plants, the lower the costs and less nuclear waste. If high temperature reactors can be developed, then high efficiency gas turbines can be employed rather than the traditional steam plant to generate power. The gas turbine would be used in conjunction with a steam turbine as a combined cycle power plant, and the efficiencies of such nuclear power plant could exceed 55% resulting in significant reduction in costs and nuclear waste. Alternatively, complex cycles employing intercooling, reheat and regeneration can be considered for nuclear power generation.

Air can be heated to very high temperatures, 1800 K or higher, using solar power. This is achieved by employing parabolic reflectors or mirrors. At such high temperatures, gas turbines are very efficient and have been considered as part of a power generation system. They can be part of a combined cycle plant where the performance is increased further. This will result in lower capital cost. Additionally, thermal storage could also be incorporated, so that power generation could continue overnight. Maximum cycle temperatures up to about 1800 K using air as a working fluid could be considered. However, at higher temperatures, thermal NO_x emissions would be excessive and closed cycle gas turbines might be considered, wherein the working fluid could be helium, which would be free of such emissions. Thus, even higher performance is now possible to help in reducing the capital cost of such power plants. For large power plants complex cycles or combined cycle system arrangements could be considered.

Gas turbines have been largely restricted to operating with clean fuels, where the amount of corrosive and erosive content of the fuel is negligible. Although gas turbine power systems have been developed to burn lower quality fuels, such as coal where the coal is converted to hydrogen

© Woodhead Publishing Limited, 2013

and carbon monoxide (integrate gas gasification combined cycle or IGCC), which is burnt in gas turbines, such a system is rather expensive. A direct coal-fired gas turbine cycle can be developed by the use of novel cycles in conjunction with special materials, such as ceramics, to minimise or eliminate turbine corrosion and erosion problems. Such a cycle would result in reduced capital costs. The high level of CO_2 emissions would have to be tackled using techniques such as carbon capture and storage (CCS). Such gas turbine cycles can also be considered to burn other low quality fuels, such as residual fuel oil (which is widely used in marine propulsion). When combined with a bottoming cycle, such as a steam turbine, the thermal efficiency of such power plants could be of the order of 55%, thus resulting in significant reduction in CO_2 emissions but also significantly reducing operating costs.

Steam turbines have been almost exclusively used as part of bottoming cycles. Intercooled gas turbine cycles can also be considered as a bottoming cycle, and would result in much a lower capital and operating cost of power plant. Such gas turbine power plants have been proposed, and are referred to as air bottoming cycle or ABC, as described by Bolland and Førde (1996).

Hydrogen as a fuel for gas turbines has also been actively proposed, and is feasible. Since hydrogen is an element, it can be used directly for cooling the combustor and turbines. Of course, engines powered by hydrogen will be zero emitters of CO_2; however, the production of hydrogen would require the electrolysis of water, which would require nuclear power generation to ensure that CO_2 emissions remain zero. Chiesa and Lozza (2005) give details of a study evaluating the practicalities of using hydrogen as a fuel for gas turbines.

Due to the lack of abundant hydrogen, fuel cells employ hydrocarbon fuels, typically natural gas, to produce hydrogen using the water gas reaction in a reformer. The carbon monoxide (CO) produced in the process would be wasted, thus reducing the efficiency of the fuel cells. Gas turbines can be employed to burn the CO to generate power to augment the performance of the fuel cells. Such systems claim to achieve overall thermal efficiencies of the order of 70%. As fuel cell/gas turbine combinations are capable of achieving very high thermal efficiency, they will no doubt be considered as a serious competitor for power generation, particularly for distributed power generation. Samuelsen (2004) gives further details on such combined fuel cell/gas turbine cycles.

Gas turbines are chosen exclusively for aircraft propulsion. Indeed, the performance of such engines has increased considerably since they were first used to power such early operational jet aircraft as the Messerschmitt (Me) 262, powered by the Junkers Jumo 004, and the Gloster Meteor, powered by the Whittle 2/700, which were turbo-jets. Today virtually all

© Woodhead Publishing Limited, 2013

large subsonic transport aircraft employ turbo-fan engines because of their superior fuel efficiency and power-to-weight ratio. The future of aircraft propulsion will require a step improvement in fuel efficiency. Unlike today's aircraft engines, which are all based on the simple gas turbine cycle, engines incorporating regenerators and intercoolers to achieve significant improvements in fuel efficiency must appear in the future. The additional weight of regenerators and intercoolers are a major drawback with such complex cycles. More recently, propellers incorporating sweep back have been developed, which can maintain their propulsive efficiency at higher flight Mach numbers. Such turbo-propeller turbines, also known as the prop-fan engines, have been developed and demonstrated. They show that a 20% reduction in fuel consumption is possible. A variant of the prop-fan engine is the unducted fan engine, which employs two counter rotating propellers, thus eliminating the need for the heavy gear box that would be required by a prop-fan engine. Such engines, employing a complex cycle to further improve their performance, may be considered, particularly if the reduction in fuel consumption can justify the increased weight of the engine because of the presence of regenerators and intercoolers (Boggia and Rüd, 2004).

In the intermediate term a geared turbo-fan engine is actively being considered. As the BPR increases, the sfc decreases, although at a decreasing rate. However, with improved core performance, such very high BPR engines of the order of 12 or higher can be justified. At such high BPRs the LP turbine speed, which drives the fan, decreases as the fan-tip speed is often limiting and therefore the LP turbine require many stages, adding weight to the engine. If a light-weight gearbox could be developed, then the LP turbine speed would increase, reducing the number of LP turbine stages and hence the weight of the LP turbine. If the reduction in LP turbine weight were greater than the weight of the gearbox system, then the fuel burn would decrease. This is the justification for the geared turbo-fan engine. The concept of a geared turbo-fan is not new and such engines have been developed for business jets where the power requirements of the fan are considerably smaller when compared with civil turbo-fan engines and as a result the gearbox weight is not that great.

11.18 References

Assael M.J., Martin Trusler J.P. and Tsolakis T.F. (1996). *Thermophysical Properties of Fluids*, Imperial College Press.

Boggia S. and Rüd K. (2004). *Intercooled recuperated aero engine*, Advanced Project Design, MTU Aero Engines, München, Germany.

Bolland O. and Førde M. (April 1996). Air bottoming cycle: Use of gas turbine waste heat for power generation, *J. Eng. Gas Turbines Power,* **118**(2), 359.

© Woodhead Publishing Limited, 2013

Chiesa P. and Lozza G. (2005). Using hydrogen as gas turbine fuel, *J. Eng. Gas Turbines Power,* January.

Corbett A.G. and Elder R.L. (1975). Stability of an axial compressor with steady inlet conditions, *J. Mech. Eng. Sci.*, **16**(6).

Cumpsty N.A. (1989). *Compressor Aerodynamics*, Longmans.

Eastop T.D. and McConkey A. (1993). *Applied Thermodynamics for Engineers and Technologist*, 5th edn, Longmans.

Elder R.L. and Macdougal I. (1983). *Simulation of Centrifugal Compressor Transient Performance for Process Plant Application*, ASME Paper.

Fawke A.J. and Saravamuttoo H.I.H. (1971). *Digital computer methods for prediction of gas turbine dynamic response*, *Transactions of the Society of Automotive Engineers*.

Frost T.H. (1966). Practical bypass mixing systems for fan jet aero engines, *Aeronautical* Quarterly.

GE's LMS100, a game changer, Diesel & Gas Turbine Worldwide, January–February 2004.

Gerald C.F. and Wheatly P.O. (1997). *Applied Numerical Analysis*, 6th edn. Addison-Wesley.

Greitzer E.M. (1978). Surge and rotating stall in axial compressors Part II – Experimental results and comparison with theory, *J. Eng. for Power*, April.

Harman R.T.C. (1981). *Gas Turbine Engineering*, Macmillan Press.

Horlock A.J. (1958). *Axial Compressors*, Butterworth.

Hung W.S.Y. (1974). *Accurate Method of Predicting the effect of Humidity or Injected Water on NO_x Emissions from Industrial Gas Turbines*, ASME Paper 74-WA/GT-6.

Kays W.M. and London A.L. (1964). *Compact Heat Exchangers*, MacGraw-Hill.

Lefebvra A.H. (1998). *Gas Turbine Combustion*, Taylor and Francis.

Lei X. and Grönstedt T. (2009). *A Contra-Rotating Variable Cycle Turbofan Engine*, ISABE-2009–1161.

McKenzie A.B. (1997). *Axial Flow Fans and Compressor*, Ashgate.

Palmer J.R. *Thermodynamic Functions for Air and for Combustion Products of Standard Kerosine*, Cranfield University, Bedford, UK.

Press, W.H., Teukolsky S.A., Vetting W.T. and Flannery B.P. (1992). *Numerical Recipes in Fortran 77*, 2nd edn, The Art of Scientific Computing, W.H. Press, Cambridge University Press.

Razak A.M.Y. (2007). *Industrial Gas Turbines, Performance and Operability*, Woodhead Publishing.

Reflexions sur la puissance motrice du feu sur les machines propres a developper cette puissance. Par S. Carnot, Ancien Eleve De L'ecole Polytechnique. A Paris, Chez Bachelier, Libraire. Quai Des Augustins, N0. 55. 1824.

Rogers G.F.C. and Mayhew Y.R. (1992). *Engineering Thermodynamics, Work and Heat Transfer*, 4th edn. Longmans.

Rogers G.F.C. and Mayhew Y.R. (2007). *Thermodynamic and Transport Properties of Fluids*, Blackwell.

Samuelsen S. (2004). *Fuel Cell/Gas Turbine Hybrid System*, National Fuel Cell Research Centre, University of California, Irvine, CA 926997–3550. ASME International Gas Turbine Institute.

Sandler S.I. (1997). *Chemical and Engineering Thermodynamics*, John Wiley.

© Woodhead Publishing Limited, 2013

Saravanamuttoo H.I.H., Rogers C.F.G. and Cohen H. (2001). *Gas Turbine Theory*, 5th edn, Longmans.
Seddon J. and Goldsmith E.L. (1985). *Intake Aerodynamics*, AIAA Education Series.
Simonson J.R. (1975). *Engineering Heat Transfer*, Macmillan Press.
Smith J.M., Van Ness H.C. and Abbot M.M. (1996). *Introduction to Chemical Engineering Thermodynamics*, 5th edn, McGraw-Hill.
Walsh P.P. and Fletcher P. (2004). *Gas Turbine Performance*, Blackwell Publishing.

© Woodhead Publishing Limited, 2013

12

Advanced gas turbine asset and performance management

T. ÁLVAREZ TEJEDOR, Endesa Generación, Spain and
R. SINGH and P. PILIDIS, Cranfield University, UK

DOI: 10.1533/9780857096067.3.515

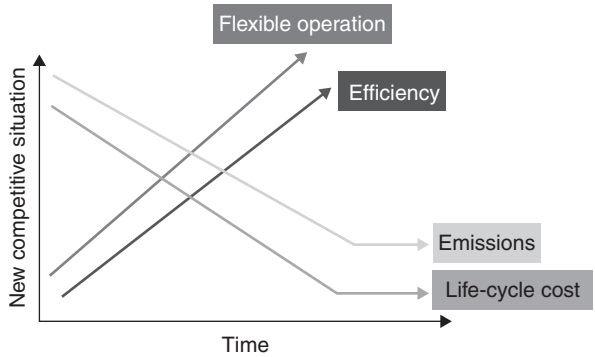
Abstract: A gas turbine degrades with use. The causes of degradation can often be related to the operating environment of the machine. Its consequent performance and other symptoms and changes are outlined in this chapter. Instrumentation in the engine can give, through a suitable analysis, useful clues that can benefit rectification of the causes of degradation. The interpretation of the information can be done effectively through specialist centres that can, remotely, receive information from different plants distributed widely geographically. They can handle disparate types of data coming through a range of streams. These features place complex requirements on information processing, analysis, staff preparation and management practice. This gives rise to the seven levels of gas path management: sensor, control and supervision, condition monitoring, performance and health assessment, prognostics, decision support and, finally, asset management.

Key words: gas turbine degradation, deterioration, data fusion, gas path analysis and management, remote monitoring centres, diagnostics, prognostics.

12.1 Introduction

The past thirty years have seen significant changes in conventional power plant requirements. Capacity and high efficiency used to be the key preoccupations of the conventional power sources. In the last ten years, the key focus has been the switch from base load to intermediate load operation, forced by the deregulation of electricity markets and an increasing, preferential share of renewable sources. This created the need for fast load ramps, minimum load, and decrease in start-up times.[45] Conventional power plants are, increasingly, required to take on ancillary services such as provision of control reserves and frequency support, as well as tertiary control reserves and load-follow operation in order to stabilize power grid dynamics and hence ensure secure and economic electricity supply. New gas turbine developments will be focused on (Fig. 12.1):

© Woodhead Publishing Limited, 2013



12.1 New competitive arena for power generation.

- Flexible operation (cyclic duty, auxiliary services, load-following).
- Competitive economics (i.e., higher efficiency and better life-cycle cost).
- Reliable operation in cyclic duty (repeated gas turbine startups and shutdowns).
- Increased dependability (see p. 561) (Reliability, Availability and Maintainability (RAM-D)).
- Compliance with emissions regulations while achieving high thermal efficiencies (turndown capability increase and part-load efficiency).
- Reliable fuel-switching capability and fuel flexibility.
- Becoming a low-carbon technology (CCS, hybrid CCPPs).

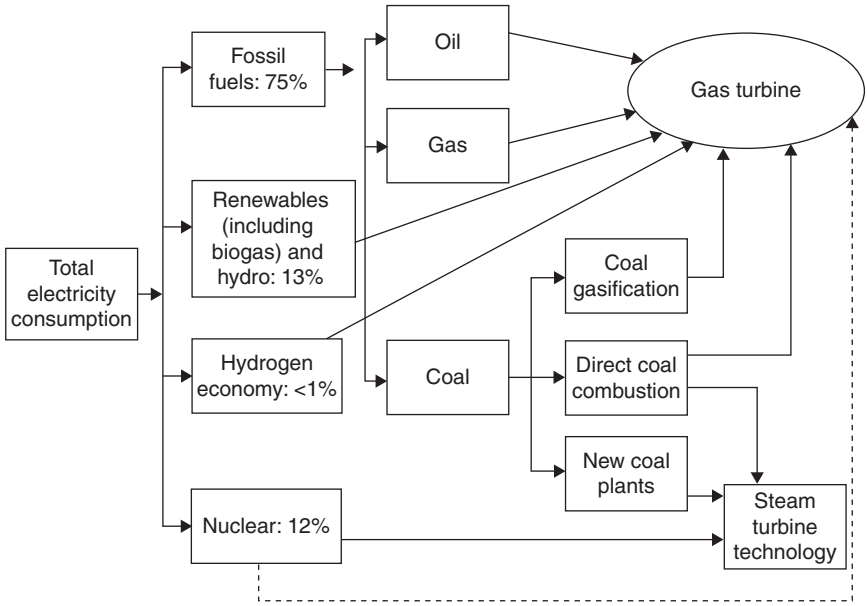
Additionally, newly-found vast gas supplies will push the transformation of the energy system. Substitution of coal (and oil) with gas in the short to medium term could help to reduce emissions with existing technologies until at least 2030 or 2035 (Fig. 12.2). On the other hand, renewable energy sources (RES) cannot grow without conventional energies supporting them (auxiliary services are required).

However, operational costs in the future may be higher than for carbon-free options, and gas-fired power stations will run for fewer hours. Shale gas and other unconventional gas sources will become very important new sources of supply in or around Europe to reduce operating costs.

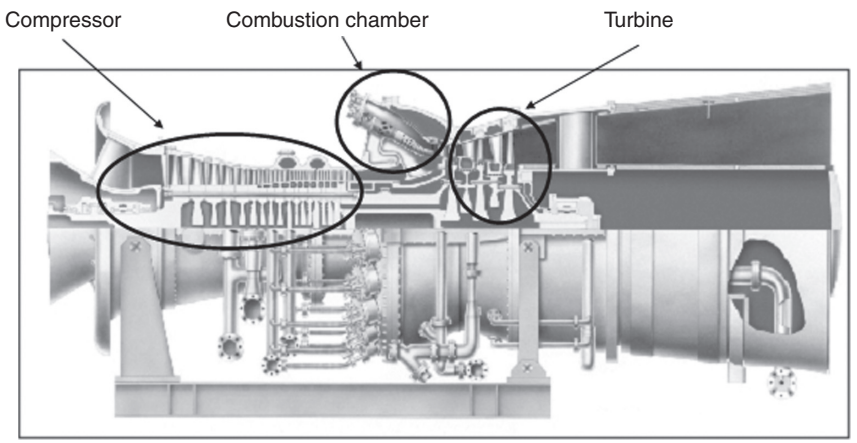
Higher operational flexibility will require new developments in reducing wear and tear of components, as well as to extend equipment lifespan, durability and maintenance interval. An essential prerequisite to ensure success in this new competitive arena is advanced technology for enhanced gas turbine asset and performance management.

The hot gas path of a gas turbine is the core of the engine, which includes the combustion chamber, the transition pieces and the turbine section (Fig. 12.3). A key technology driver for the gas turbine is the pursuit of

© Woodhead Publishing Limited, 2013



12.2 Gas turbine role in projected power generation (projected power generation in 2030 by fuel type – International Energy Agency 2004).



12.3 Gas turbine hot gas path section (courtesy of GE).

high turbine entry temperature for thermal efficiency and specific power. It brings with it cost, life and nitrogen oxide emissions challenges. To increase the durability of the blades and vanes in these extreme conditions in the turbine section, special metal superalloys and coatings have been developed.

© Woodhead Publishing Limited, 2013

Thus the goal of achieving 60% efficiency while staying below 10 ppm of NO_x emissions is constrained by the thermal, emission reduction and material limits of the turbine system. Several critical innovations are:

- Closed-loop steam cooling.
- Single crystal superalloys.
- Thermal barrier coating.
- Low NO_x combustors.

Gas turbine LCC is strongly affected by the hot gas path cost and maintenance. This gives rise to maintenance practices and inspection techniques to improve gas turbine dependability (see p. 561), that is, reliability, availability, maintainability and durability (RAM-D) ratios.

In a deregulated and more competitive market, power producers are continually seeking competitive edge. How can they improve their decision-making processes? How can they be more efficient and cost effective? How can they limit damage and improve availability? How can they reduce maintenance costs and extend service life? How can they know fixed asset remaining value along power plant life? A key to this is gas turbine asset and performance management.[1]

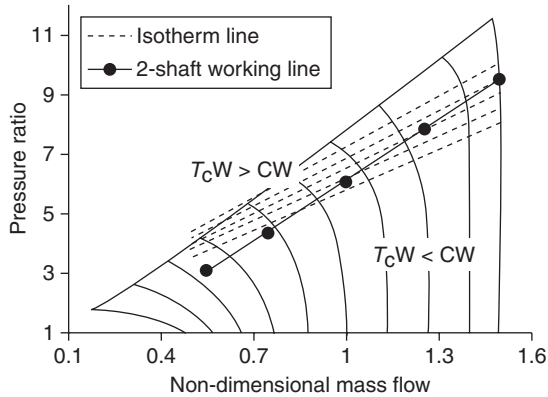
From the condition monitoring, instrumentation and control standpoint many contributions can be made to enhance hot gas path management. The final goal is to manage the hot gas path section by knowing its condition and its performance; the former is condition based maintenance (CBM) and the latter is performance monitoring (see p. 561).

To optimize gas turbine life-cycle (see p. 561), cost special attention must be given to the hot gas path components. Typically around 65% of the total maintenance cost corresponds to the scheduled maintenance parts and materials. This leads to establishing a mechanism for risk mitigation for, for example, long-term service agreements (LTSA), business interruption insurance, extended guarantees, and part costs guarantees.

12.2 Gas turbine degradation

The operating line (or steady state line, or running line) shows the sets of circumstances where the engine will operate in a steady manner.[2] Figure 12.4 shows the operating line of a two-shaft engine. In this machine the first turbine (or compressor turbine – T_c) delivers the power needed by the compressor (plus, often, some auxiliaries), and the second delivers the power for the load. In this case the pressure ratio of the first turbine is much lower than that of the compressor. The remaining pressure drop takes place mainly in the power turbine that delivers the output power. In this case, a specific point on the operating line is obtained by feeding the appropriate

© Woodhead Publishing Limited, 2013



12.4 Two-shaft engine operating line.[2] (CW: compressor work, TcW: compressor turbine work).

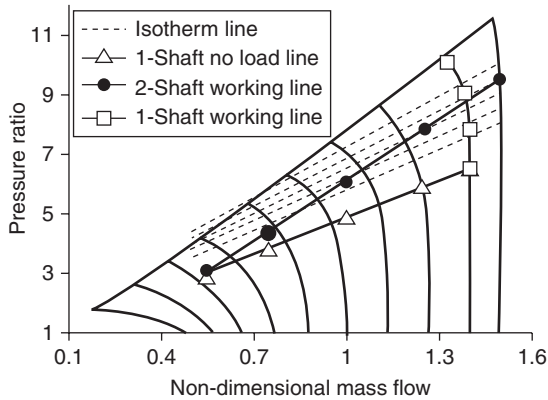
amount of fuel to the engine. The dotted lines on the chart correspond to turbine inlet temperature non-dimensional (T_4/T_2) isotherms. Higher values of turbine inlet temperature correspond to the higher isotherms.

Operating points above the operating line correspond to transient situations where the power delivered by the compressor turbine is larger than that of the compressor. Similarly, operating points below the operating line correspond to transient situations where the power delivered by the compressor turbine is less than that of the compressor.

Figure 12.5 shows an operating line of a single-shaft engine. In this machine there is only one turbine that delivers the power needed by the compressor and the power for the load. In this case, the pressure ratio of the turbineis very similar to that of the compressor. The difference is due to losses in other components. In this case the 'no load line' is where the compressor and turbine powers are equal, leaving no net power output. In theory, a single-shaft engine can operate on any point above the 'no load line'. If the excess turbine power is absorbed by the driven equipment, then the machine is in equilibrium. Many of these machines are used for constant frequency electricity generation. In this case the generator is coupled directly, or by means of a gearbox, to the generator and both need to rotate at a constant rotational speed. The operating line then follows a constant non-dimensional speed line if ambient temperature does not change. If ambient temperature rises, the machine operates along a lower non-dimensional speed line and vice-versa.

Degradation, for the purposes of this section, is the gradual deterioration of engine performance arising from normal wear and tear. This degradation in whole engine performance arises from the gradual loss of capability of the components. Many factors contribute to this – fouling, erosion, seal tip gap enlargement, hot section deformation, and others. The outcome is a

© Woodhead Publishing Limited, 2013



12.5 Single-shaft engine operating line.[2]

change in component flow capacities and efficiencies. Surge pressure ratio reduction occurs in the compressors.

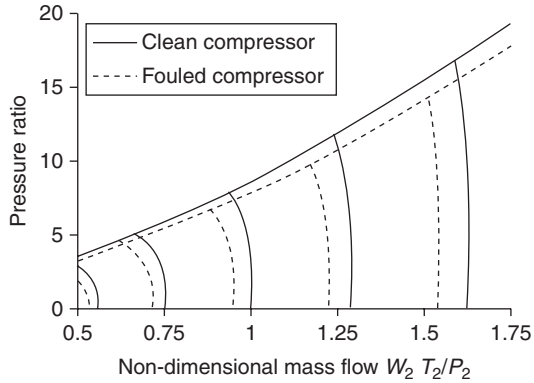
Figure 12.6 shows the effect of degradation on the compressor map. At a rotational speed the compressor will deliver a lower mass flow. The losses also lower the position of the surge line. The efficiencies (not shown) also fall and, for a given pressure ratio, the compressor requires more power per unit of flow. The turbine also degrades with time. The efficiency will fall. Non-dimensional mass flow, however, may rise or fall, depending on the nature of the degradation.

Figure 12.7 shows the effect of compressor degradation on the single-shaft engine operating line. The result of capacity reduction is a movement of the non-dimensional speed lines to the left of the map, delivering less air. Normally the engine would incorporate control laws to prevent operation beyond a maximum hot section firing temperature, on the grounds of material considerations. Therefore, the degraded operation point on the map has now moved on the same isotherm to the intersection with the new position of the compressor non-dimensional speed line corresponding to the rotational speed required by the generator. The engine is therefore operating with a lower pressure ratio, lower mass flow and the same turbine inlet temperature. The result of these degradations is, therefore, a reduction of power output and thermal efficiency.

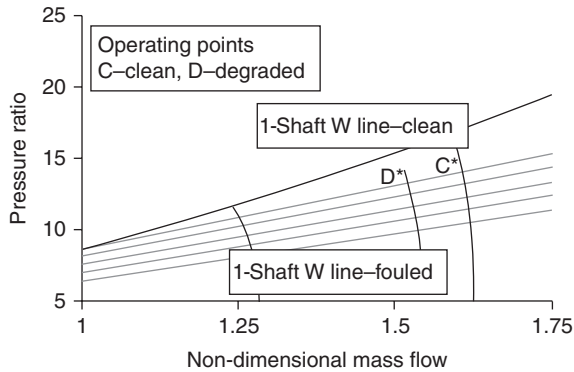
Figures 12.8 and 12.9 show degradation effects on the efficiency of a one-shaft engine. This picture shows hypothetical situations of single- and multi-component faults on a hypothetical single-shaft gas turbine in the 160 MW class.[3] These estimates were carried out with Cranfield's gas turbine performance code, TURBOMATCH.[4]

Figure 12.10 shows the effect of degradation on a two-shaft engine operating line. In this case the situation is somewhat different. Compressor

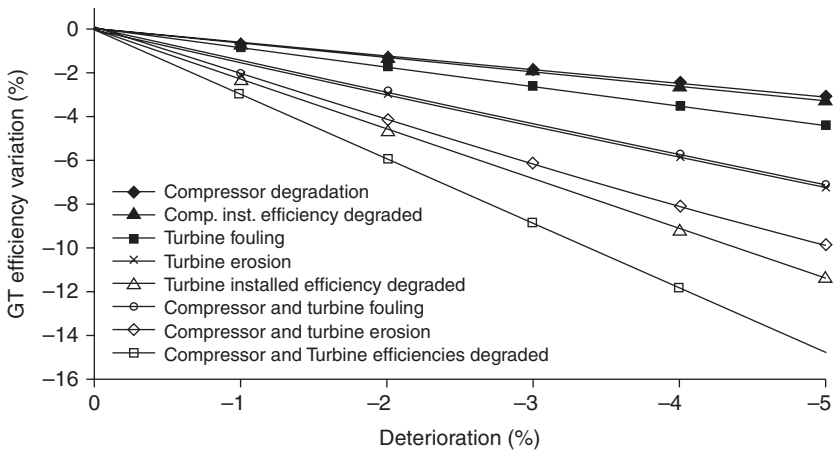
© Woodhead Publishing Limited, 2013



12.6 Effect of compressor degradation on map.

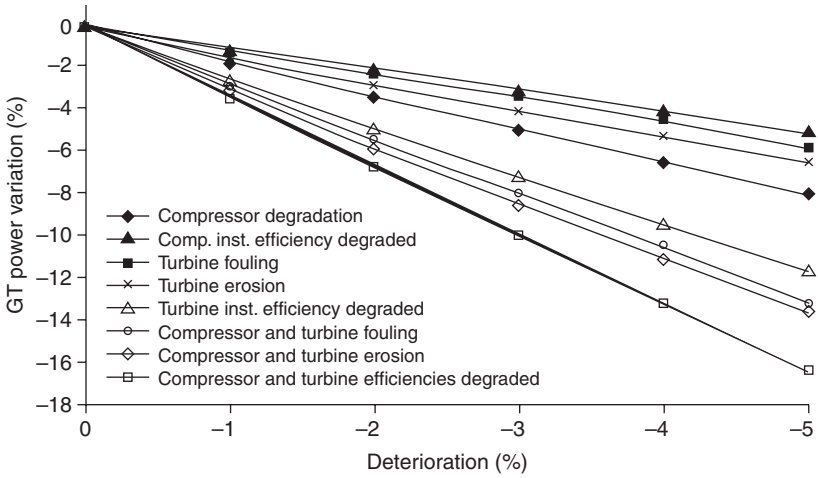


12.7 Effect of compressor degradation on a single-shaft engine operating line.

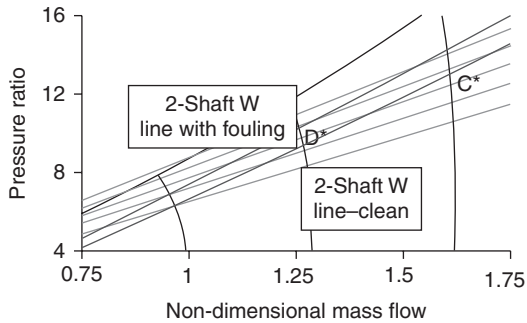


12.8 Effect of degradation on a single-shaft engine.[3]

© Woodhead Publishing Limited, 2013



12.9 Effect of degradation on a single-shaft engine.[3]



12.10 Effect of degradation on a two-shaft engine operating line.

efficiency degradations will move the operating line upwards, to regions of the map where the compressor turbine produces the increased power absorbed by the compressor operating less efficiently. The increased firing temperatures needed for this explain the higher pressure ratios needed from the compressor (despite its degradation) to enable the gas to flow through the restriction imposed by the turbine nozzle guide vanes. The degradations on the compressor will lower the position of the surge line on the map. Figure 12.10 does not show this movement of the surge line. This image shows the displacement of an operating point for the case where the reduction in surge margin is not unduly large.

As in the previous case there is a reduction in power and efficiency. However, given that the two shafts of the engine are not connected, in some circumstances the gas generator shaft may experience an increase in

© Woodhead Publishing Limited, 2013

rotational speed to compensate partly for the effect of capacity reduction. These effects are due to the relationships in the components, and the understanding of these phenomena gives rise to performance health monitoring techniques.[5–9]

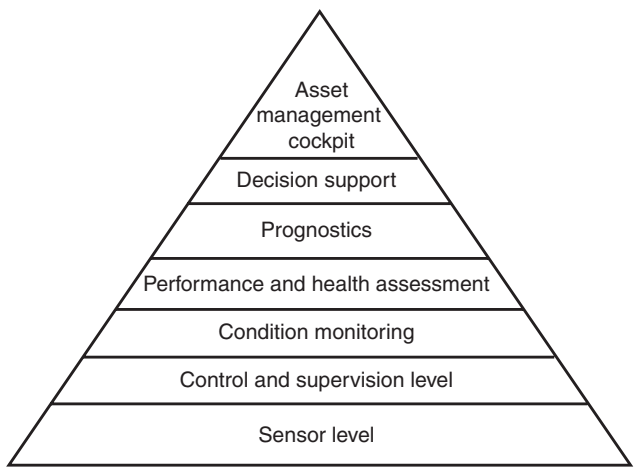
12.3 Hot gas path management

The hot gas path section can be managed by techniques such as CBM and performance monitoring. To get an in-depth knowledge of a hot gas path component condition, it is useful to combine on-line and off-line techniques. Jointly they will indicate the condition of the main components of the hot gas path section. For clarity, the process can be split into seven different levels (Fig. 12.11).

12.3.1 Level 1: sensor level

Gas turbine units are, usually, equipped with a relatively sparse instrumentation suite, to assure safe operation and to monitor performance and emission requirements. A question that should be asked is whether these sensors give information to enable us to:

- Optimize performance.
- Define risk of extending operating periods.
- Monitor component degradation.
- Provide early warning of faults in the system.
- Assess hot section environment and failure mechanisms.



12.11 Power generation asset and performance management.[10]

© Woodhead Publishing Limited, 2013

The range of possibilities can be divided into three broad categories: those based on permanently installed (on-line sensors), those based on temporarily installed sensors that are used to make specific measurements when desired (on-line measurement for condition assessment), and those based on off-line techniques aimed at off-line diagnostics (inspections).

Along with the ability to assess and monitor the actual performance of a gas turbine comes the need to detect and diagnose fault conditions when they occur. This need is addressed by the development of new special diagnostic instruments for one of the most highly stressed regions of a gas turbine: the hot section. Advanced gas turbine and diagnostic performance also relies on diagnostic instrumentation[11]:

On-line sensor:

- High intensity acoustic, turbulence, and pulsation measurements (high sensitivity pressure dynamic sensor).
- Flame temperature sensors (semiconductor photodiode).
- Fuel LHV measurement (low-heating-value sensor).
- Turbine blade surface temperature – optical pyrometers.
- Turbine blade vibration – optical probes.
- Turbine blade tip deflection – capacitance tip clearance probe.
- GT exhaust debris monitoring.
- Visual display of the inside of the combustion chamber and the combustion flame during operation (combustor viewing probe).
- Turbine circumferential temperature distribution (optical fibre thermometers, high-temperature RTD (Resistance Temperature Detector)).
- Compressor dynamic pressure.
- Compressor acoustic emissions.

Off-line sensor:

- Coating life degradation sensor (odometer, infrared sensor, eddy-current sensor).
- Superficial crack detection and sizing (visual and eddy-current inspection).
- Crack detection (ultrasonic sensor, thermosonic sensor, phase array and advanced ET (Eddy Current Testing) and UT (Ultrasonic Testing) technology).
- Coating delamination and wall thinning (thermography, X-ray tomography).
- Tip caps inspection (automatic submerged ultrasonic inspection).
- Blade dovetail (flexible eddy-current array probe).
- Rotor bore hole inspection (automated portable rotary gun).
- Material property degradation at critical locations (SMT – small punch test).

© Woodhead Publishing Limited, 2013

12.3.2 Level 2: control and supervision level

The output from the instrumentation is acquired and used locally as input to the unit's control station. The control station consists of a PC equipped with original equipment manufacturer (OEM) software that provides the operator with a series of Windows, UNIX, etc. based displays which present the measured and calculated data, alarm status, etc.

There are different factors that influence equipment life and they are responsible for the component degradation mechanisms. Each of these factors has an effect on gas turbine maintenance intervals and component parts' lives, and will vary depending on each unit's operation.

Each OEM has developed its own conventions such as 'factored hours' or 'equivalent operating hours' (EOH) to define maintenance intervals. It is not readily apparent from the OEM formulations which specific component location, for example, first row blade tip, leading edge, trailing edge, platform, etc. is indeed the weak link driving the maintenance action. This underlying uncertainty can result in higher repair fallout rates or possible lost production time. In other cases, the maintenance interval may be too conservative, leading to premature parts retirement. This approach could be improved with a more machine-specific condition based approach to determining the timing of maintenance. This approach relies on recording operational data and component condition.

Control systems play a critical role in the intermediate step of data collection, conditioning and analysis within the automated CBM infrastructure. Advanced process control systems include analysis algorithms that enable them to diagnose and report malfunctions to the CBM system, which ultimately supports system-wide asset management.

Data manipulation technology is critical for CBM success:

- Information technologies for data manipulation:
  - On-line data acquisition. The data acquisition module represents the module that provides system access to digitized sensor or transducer data. It may represent a specialized data acquisition module that has analogue feeds from sensors, or it may collect and consolidate sensor signals from a data bus.
  - Data processing and validation:
    - Signal processing approach.
      - Signal correlation.
      - High pass filtering.
      - Correlation matrix and response statistic.
    - Physics-based approaches:
      - Correlation matrix and response statistic.
      - Statistical neural network.
      - Fuzzy logic rule based.

© Woodhead Publishing Limited, 2013

  - Data fusion – which is a formal framework used to express the convergence data from different sources in which is expressed the means and tools for the merging of data that has originated from different sources.
  - Data mining tools – which provide new insights into wear and failure mechanisms in engine components:
    - Neural nets.
    - Statistical analysis.
    - Generic algorithms.
- Advanced control algorithms.
  - Predictive control algorithms for combustion instability.
  - Adaptive controller.
  - Closed-loop steam cooling control.
  - Active control technologies for enhanced performance and reliability and reduced emission.
  - Fault tolerant engine control (smart sensor and actuators).
  - Closed-loop optimization.

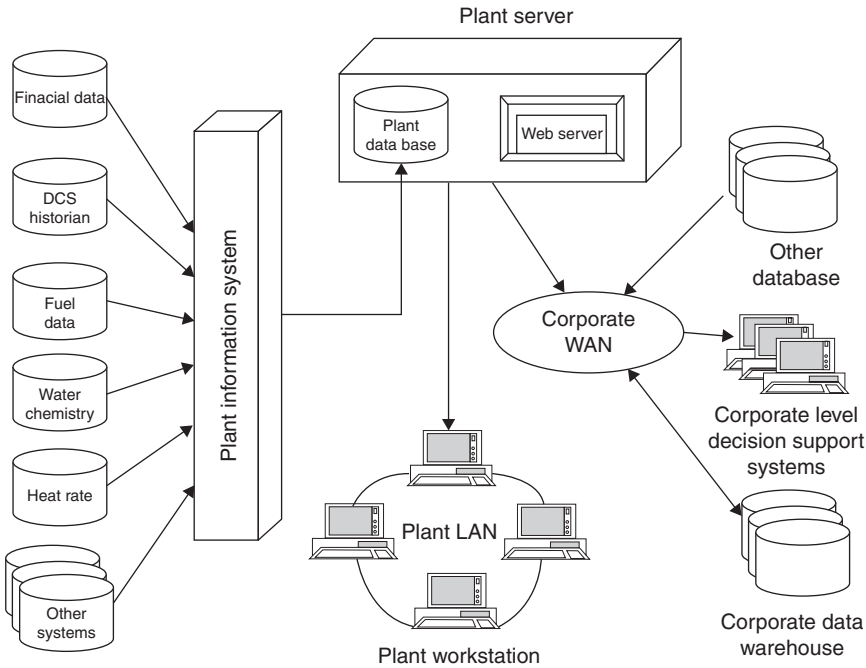
The idea is to produce useful information from these sources and make it available to operational, engineering, and management personnel in their day-to-day work. Data fusion provides one consistent source for validated data for reports, planning, analysis, monitoring and diagnostics. According to the system architecture shown in Fig. 12.12, key data are read from various source systems by the plant information system (which can then perform a number of operations on these data) and are loaded into the plant data base at each plant.

By means of the plant information systems, data are routed through the system, where processing tools can transform them into useful information. Interactive displays make that information available wherever it is needed. The process information can be stored in a nearly limitless amount of data. With the plant information system, personnel throughout the enterprise gain unprecedented access to real-time information, helping them to make better business decisions. The plant information system is an information management infrastructure that turns operational data into a powerful corporate asset, acquiring data from the power plant or process, usually from automated control systems or other sources.[13]

This data fusion platform must be open and flexible, to allow the multilevel and multifaceted process dealing with the automatic detection, association, correlation, estimation, and combination of data and information from single and multiple sources. The resulting information is more useful to the user when fusion is performed than simply delivering the raw data.[14]

Data fusion users at the plant connect to the plant database using data fusion client applications running on a digital operating system via the plant

© Woodhead Publishing Limited, 2013



12.12 Data fusion architecture.[12]

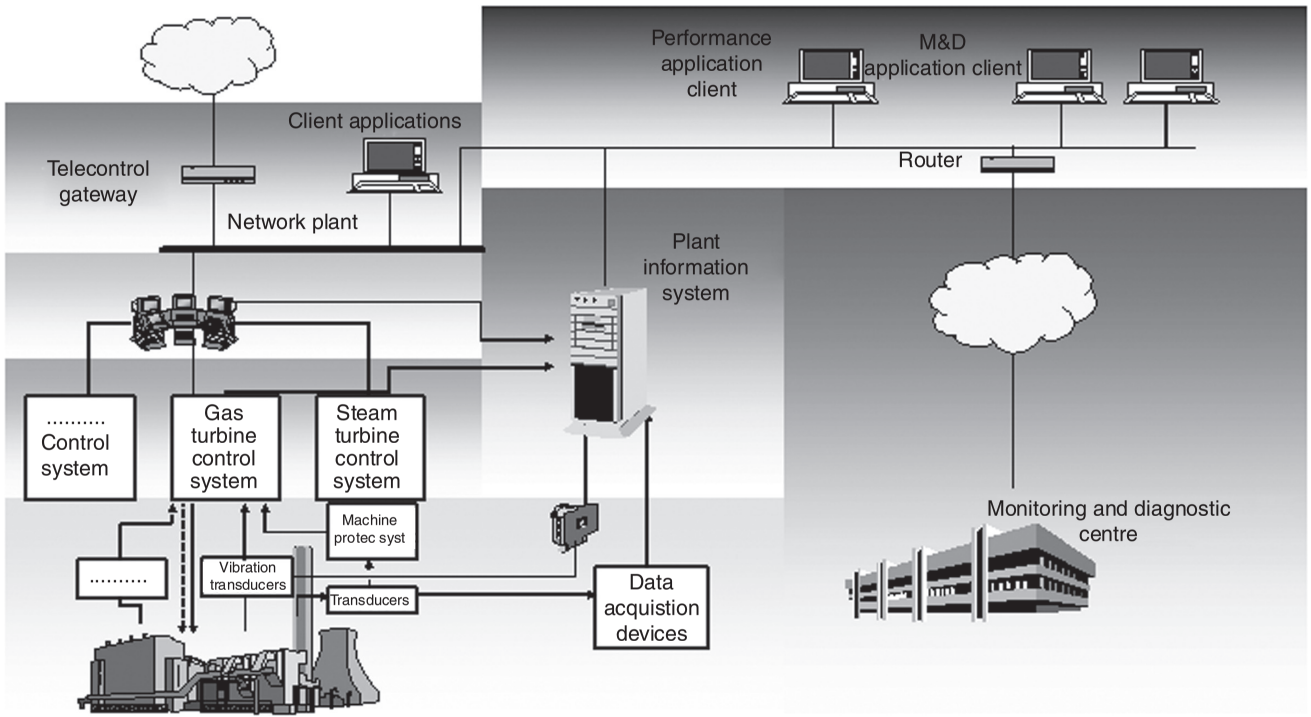
local area network (LAN) for data analysis and reporting. Users at other locations can also access the plant databases at the various plants via the corporate wide area network (WAN). A sub-set of the data at each plant is periodically loaded into the corporate data fusion data warehouse by the corporate information system. This corporate information system also rolls up plant data into the monthly and year-to-date values most often used for corporate-level reports.

A data fusion system could be developed as a client-server application with interconnections through the WAN (Fig. 12.13). It has the capability to have several hundred users at power plants and at the corporate office. A possibility is to have a web-based version (web data fusion system) which can be run over the intranet and provide integration with plant data historians. The web data fusion system is based on a complete system of interfaces, web services and client tools used to create a real-time user interface on the web.

12.3.3 Level 3: condition monitoring

Condition monitoring can be described as 'assessing the current state and estimating the future state of a system by means of measurements and

© Woodhead Publishing Limited, 2013



12.13 Data fusion system with interconnections via WAN.[15]

© Woodhead Publishing Limited, 2013

calculations'. The results of condition monitoring can be used to take corrective actions, to plan the availability and maintenance, and to optimize the plant's performance.[16] The main reasons to apply condition monitoring are:

- Prevention of damage.
- Increasing availability.
- Increasing reliability.
- Increasing time between outages (TBO).
- Changing from periodic maintenance to condition dependent maintenance.
- Fuel savings, by optimizing the process continuously.
- Reduction of production loss.
- Better operator process knowledge through more information and insight.

The condition monitoring level uses data from the data fusion platform and compares these data with expected values or operational limits and generates alerts based on these limits. Then, the primary function of the condition monitor is to compare features against expected values or operational limits and output enumerated condition indicators (e.g. level low, level normal, level high, etc.). The condition monitor may also generate alerts based on defined operational limits and when appropriate data are available the condition monitor may generate assessments of operational context (current operational state or operational environment).[17,18]

- Component life monitoring: through direct or indirect monitoring of component properties:
  - On-line monitoring of component life would allow some assessment of when the next shutdown might occur.
  - On-line indication of component degradation could alert operators to failures that could propagate through the unit. For example, on-line monitoring of the combustor status or blade coating integrity.
  - Off-line non-destructive evaluation (NDE) of component life would help to determine if component replacements are needed before the next scheduled shutdown.
    - Eddy-current metallic coating life (Al depletion vs conductivity).
    - TBC integrity (NDE methods).
    - Component physical condition referenced to baseline.
    - Component cyclic fatigue status.
    - Component coating wear and integrity status.
  - On-line risk assessment of extending the outage schedule would also be useful to determine whether it is possible to operate for extended periods.
  - On-line monitoring of exhaust gases for metal particles.

© Woodhead Publishing Limited, 2013

12.3.4 Level 4: performance and health assessment

This module includes the component/system's current health grade and diagnosed faults and failures with associated probabilities. A calculation of the current risk priority number (RPN) may also be performed. The output from this level includes:

- Estimates of current health grade.
- Diagnoses of faults and failures.
- Recommendations.
- Evidence and explanation.

The performance and health assessment level receives data from condition monitoring and prescribes if the performance and health in the monitoring component, sub-system or system are degraded in terms of their thermodynamic and mechanical condition.

If the health and performance are degraded, this level may generate a diagnostic record that proposes one or more possible fault conditions with an associated confidence. This level should take into account trends in the health history, operational status and loading, and the maintenance history. There is a variety of techniques for doing this. Some are described in References 9 and 19.

Different diagnostic modules are required to evaluate the health and performance of the monitored systems:

- Gas turbine performance degradation:
  - Determination of the degradation in the efficiency and power output.
- Combustion process diagnostic module:
  - Automated assessment of EGT spread, fuel flow manifold and supply pressure, vibration/dynamic pressure, emission data.
- Hot gas path analysis:
  - Determination of the gas path condition based on thermodynamic relationships which exist between the engine components and various gas path performance parameters.
- Hot section damage assessment:
  - Automated trending and fault pattern classification and fusion.
- Aero-thermal performance based module.

The final result would be the assessment of the condition of the hot gas path section automatically, reducing human inspection tasks and unnecessary maintenance that occurs in a traditional periodic maintenance scheme, and optimizing gas turbine performance (power output, emissions and efficiency). System assessment also would provide valuable real-time decision-support data for operational planning.

© Woodhead Publishing Limited, 2013

12.3.5 Level 5: prognostics

The primary function of the prognostics level is to project the current health and performance state of equipment into the future, taking into account estimates of future usage profiles. The prognostics level may report health and performance status at a future time, or may estimate the remaining useful life of an asset given its projected usage profile. Assessments of future health or remaining useful life may also have an associated diagnosis of the projected fault condition.

Assessments of future health or remaining life may also have an associated prognosis of the projected fault condition. A calculation of the future RPN may also be performed. This module includes the component/system's future health grade and future failure events with associated likelihood probability. The output from this level includes:

- Estimates of future health grade.
- Predictions of faults and failures.
- Estimates of remaining life.
- Recommendations.

So prognostics allow us to predict the onset of hot gas path component failure to match its used, or to enhance maintenance support. Prognostic capabilities expand support options and allow for cost-effective planning and management. Component remaining-life-assessment and plant modelling are required for prognostic purposes:

- Life consumption tracking module of hot gas path components:
  - Assessment model for coating degradation.
  - Assessment model for creep fatigue damage.
  - Assessment model for thermo-mechanical fatigue.
- Hot gas path components lifing prognostics.
- 'What if' analysis for performance and health of hot gas path components.

12.3.6 Level 6: decision support

The primary function of the decision-support module is to provide recommended actions and alternatives and the implications of each recommended action. Recommendations may include maintenance action schedules, modifying the operational configuration of equipment in order to accomplish mission objectives, or modifying mission profiles to allow mission completion.

Maintenance advice from this module should detail future maintenance work required, which may include the verification of monitoring data or the performance of additional monitoring. The structure of this advice should

© Woodhead Publishing Limited, 2013

be put into a 'work request' format for external maintenance work management systems. Based on this request, maintenance work management systems can schedule work in advance and locate spare parts and tools required for these jobs.

Operational advice from this module might be immediate in nature, such as the current notification of operators of alerts and resulting action steps. Other production-related advice might be more strategic, such as sending a notice to a production planning system about the high risk of failure on a production line, due to a soon-to-fail critical piece of equipment.[20] The output from this level includes:

- Operational and maintenance (O&M) advice.
- Capability forecast assessments.
- Recommendations.
- Evidence and explanation.

The decision-support module needs to take into account operational history (including usage and maintenance), current and future mission profiles, high-level unit objectives, and resource constraints. This module relies on IT systems and techniques (data fusion) for data converging and managing from different sources:

- Computer-based gas turbine condition and health monitoring predictive systems might offer the potential for giving decision support for the following:
  - Reduced nuisance shutdowns and unplanned outages.
  - Optimum engine operation.
  - Continuous real-time maintenance scheduling.
  - Extended time between overhauls based upon determination of remaining component life.
  - Protection against catastrophic failure via real-time fault assessment.
  - Estimating O&M cost based on condition monitoring.
- Automated logistics allows advanced scheduling and coordination of maintenance actions. Advanced triggering of logistics support events improves system availability and resources utilization.

12.3.7 Level 7: asset management cockpit

The primary function of asset management cockpit is the presentation of critical plant asset management information aimed at providing a groupware environment that helps managers, engineers, operators and maintenance staff to understand each other's plant issues.

© Woodhead Publishing Limited, 2013

The aim is to create an environment that encourages more efficient plant management and boosts team performance and collaboration between operations, maintenance and plant managers, via a reliable decision-making process.

This level is also the human/machine interface, and it can communicate with all others levels with multiple layers of access depending on the information needs of the user.

Typically high-level status (health assessments, prognostic assessments, or decision-support recommendations) and alerts would be displayed at this level, with the ability to drill down when anomalies are reported.

A friendly, human interface helps supply actionable information to the operator and maintenance staff:

- Actionable information for effective decision making by the users.
- Actionable information in the form of 'what happened', 'where', 'when', 'how bad is it' and 'what should be done about it'.

12.4 Centre for remote monitoring and diagnostics (CMD)

To gain competitive edge, power producers are rethinking how they manage their plant assets and what decision-making processes are needed to operate their plants more efficiently and cost-effectively.

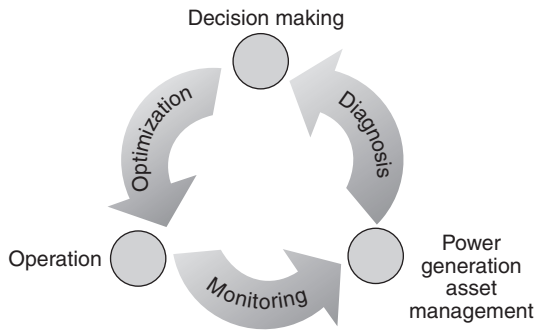
They look to minimize the risk of asset damage, and to improve availability and reliability (while reducing maintenance costs and extending service life), and to assessment of the remaining value of fixed assets.

In most cases, operation is almost exclusively focused on the process (in order to maximize performance), maintenance is focused on the maintenance tasks (to improve asset maintainability), while plant management is focused on producing electricity in a cost-effective manner.

The following questions then arise. Are operations and maintenance working in the same direction? Do they require the same information? Do they have the required information at the right time in order to make the best decisions? Are we managing our plant assets proactively, rather than reactively?

As shown in Fig. 12.14, a new approach is possible by integrating the critical requirement of power generation plant management: to integrate operations and asset management with a reliable decision-making process (methodology). This can be accomplished through the use of plant information systems and asset condition management systems capable of providing the exact information required by the right people and at the right time (Actionable Information ®[21]).

© Woodhead Publishing Limited, 2013



12.14 Integration process for the key factor of the power generation management.[21]

Continuous on-line condition monitoring systems, that collect, measure, and display key process and asset condition variables in real time, are used to link operations with asset management, resulting in combined cycle power plants (CCPP) networked worldwide by means of the CMD.

The purpose of the CMD is to provide real-time service to all power plants, analysing operation and maintenance data, and proposing recommendations aimed at improving the availability, reliability, maintainability and efficiency of the plants.

Through the monitoring and diagnosis system, based on automatic systems and modern information transmission techniques, the state of the plants can be continuously supervised, thus allowing the operation of the plant to be constantly monitored. The remote monitoring and diagnostic (RM&D) system collects and transmits machine operating data to a central facility staffed by experts in machine analysis, diagnostics, and maintenance planning, and backed up by specialized software for the analysis, extrapolation and interpretation of data.[22] Through this RM&D system, based on computerized systems and modern information transmission techniques, operational conditions can be kept under constant control. Maintenance is no longer carried out in a reactive way; with RM&D systems it is possible to plan maintenance and intervene proactively, before the deterioration of a component can induce damage in the plant, with production, and consequently financial, loss.[23]

To this end, a communications network is set up between plant staff (plant management, operators, maintenance personnel) and the CMD (diagnostic engineers, M&D experts), to enable on-line technical assistance and support in the operation and maintenance of CCPP. With all the above based on more reliable and precise information on plant equipment condition and whole-plant thermodynamic performance, we are able to maximize the efficiency, reliability and availability of the plant, and in this way, to lengthen the intervals between planned plant maintenance shutdown. [24,25]

© Woodhead Publishing Limited, 2013

Diagnostic specialists would be able to connect to the plant directly on-line, in order to examine operations and activities, to investigate the nature of a problem, or to provide on-line advice. From this centre, it is possible to detect promptly early deviations from regular operations concerning the thermodynamic and mechanical condition of the plant and its parts. This will lead to a reduction in the degradations in output, and a reduced risk of catastrophic equipment.

Diagnostic experts collect operational data from the facilities on a real-time basis, and subsequently analyse them in great detail. By means of tools based on knowledge and operational experience, they can offer operational recommendations to optimize the operation of the power plants.

The CMD is created as a supplement to the operational processes carried out by the plants, and it will enable the operational personnel and plant managers to gather operational information, which will help them when operating their plants and making decisions.

The immediate benefits for the facilities are basically the following:

- Extension of the intervals between regular maintenance shutdowns.
- Reduction in the length of the scheduled outages.
- Optimization of the plant operation.
- Prediction of life cycles.
- Reduction in non-programmed unavailabilities.
- Maximization of income and reduction in maintenance costs.

This system, through considered action, could lead to an increase in the efficiency, availability and extension of the life cycle of the plant. The main functions of the CMD are:

- Diagnosis of the key parameters – thermodynamic and mechanical monitoring.
- Detection of malfunctions before they lead to trips and serious faults in the plant.
- Archive and retrieval of M&D and O&M data.
- O&M monitoring and reliability tracking of the plant.
- Generation of reports on performance and incidents.
- Carrying out O&M recommendations.

12.4.1 Design process of the CMD

The performance of a gas turbine, its components and systems, includes reliability, availability and maintainability, intrinsic characteristics fundamental in defining the requirements of the gas turbine for its intended service, in other words, dependability of gas turbines. This has a large impact on

© Woodhead Publishing Limited, 2013

operating costs (O&M), keeping the gas turbine in operation, and acceptable costs throughout the life cycle of the gas turbine.

Reliability analysis takes place mainly during the concept and defining phases, the design and development phases, as well as in the maintenance phases, in order to determine and evaluate the dependability values of a system or installation. To this aim, the most used methods of analysis can be summarized as follows:

- Failure modes and effects analysis (FMEA).
- Failure modes, effects and criticality analysis (FMECA).
- Fault tree analysis (FTA).

There are also event tree analysis (ETA); reliability block diagram analysis (RBD); Markov analysis (MA); Petri net analysis; hazard and operability studies (HAZOP); reliability forecasting through the part count (PC); analysis of human reliability (HRA); analysis of force – resistance; truth table (structure function analysis); Boolean methods; and, statistical tests and estimation methods for reliability growth.

Only the first three methods will be briefly discussed. Further details on the others can be found in the bibliography.[26] Note that the aforementioned methods for reliability analysis are treated in the technical standards edited by the International Electrotechnical Commission (IEC) and in particular by the Technical Committee IEC TC 56 *Dependability*.

In general, there are two types of analysis: inductive (bottom-up analysis, such as FMEA and FMECA) and deductive (top-down analysis, such as FTA).

Inductive methods start at the lowest level, for example the failure of a single component (mechanical, electrical, etc.) that has an effect on the whole system. In such a case, a detailed knowledge of the system and its structure is required, in order to study the fault conditions and failure propagation, for example.

Deductive methods, instead, start from the final effect; for example, studying the causes of a particular and well-defined failure. The analysis is implemented starting at a system level and little by little progresses towards the lower levels (e.g., to the analysis of a single mechanical, electronic, etc. component).

FMECA is a process for identifying potential failure modes and classifying them according to both the severity of their effects on the system and the probability of their occurrence. FMECAs are often two-part processes wherein failure modes and their effects (FMEAs) are identified first, and both the severity and the probability of occurrence for the failure mode (criticality analysis (CA)) are defined in the second step of the process.

FMEA is a systematic procedure able to analyse a system with the aim of identifying potential failure modes, their cause and effect on performance

© Woodhead Publishing Limited, 2013

and, when applicable, their effect on the safety of the personnel, and on the environment, as well as on the system.[27–29]

An analysis of criticality is usually the objective of an in-depth FMECA analysis rather than a FMEA. Criticality is a way to quantify the attention that should be given to a determined failure, event or non-conformity, and depends both on the probability of its occurrence and the gravity of the consequences it may have. The attention to be dedicated to an event depends first of all on the effect it may have on the safety of personnel, on the damage it can cause in terms of subsequent losses, and its effect on the availability of service. Criticality is defined by means of a scale of values that permits evaluating the seriousness of consequences in function of the criteria taken into consideration.

A quantitative evaluation of criticality is possible when data relative to failure mode rates of systems or components to be analysed are available. Otherwise, a qualitative evaluation is applied.

The objective is to identify the items where modification to the design or the operating, inspection, or maintenance strategies may be required to reduce the severity of the effect of specific failure modes.

The FMECA process is typically undertaken in the following steps[26]:

- Define the system to be analysed and its required reliability performance.
- Construct a model or RBD of the system being analysed.
- Identify failure modes for all major sub-systems.
- Attempt to define primary and secondary effects of the failure mode.
- Classify the severity of the malfunction in terms of mission parameters.
- Based on systems knowledge, including fault detection systems and probabilities of detection for all detection systems and techniques, identify the probability of occurrence for the fault.
- Rank failure modes in terms of severity and criticality.
- Review the worksheets to identify the reliability-critical components and make recommendations for design improvements, inspection or maintenance strategies (monitoring).

The FMECA was applied in Table 12.1 for a gas turbine. Employing these techniques, a preliminary FMEA was obtained, which listed possible failure modes and their expected effect on sub-system and system availabilities, as well as an estimation of failure mode severity (RPN1 – Risk Priority Number), failure rate, detectability, and active repair time for the different components in the system (RPN2 to reflect the importance of the repair process to system availability).

This exercise also demonstrates its value for repairable systems, where it can supplement the information obtained from field data analysis both in identifying the critical failure modes (i.e., those failure modes which affect

© Woodhead Publishing Limited, 2013

Table 12.1 Gas turbine system FMECA[30]

Unit	Sub-unit	Failure mode	Local failure effect	System failure effect
Gas turbine/ generator	Air inlet	Filter fouling	Reduce output/ efficiency	Degraded output
		Filter blockage	Filter implosion	Potential catastrophic failure
	Compressor/ turbine	Overspeed	Major damage to rotor and casing	Potential catastrophic failure
		Rotor out of balance	High vibration and trip	Forced outage
		Rotor bend distortion	High vibration and trip	Forced outage
		High temperature	Distortion/material damage and HT trip	Forced outage
		High vibration	High vibration tip	Forced outage
		Tip rub	Reduced power output	Degraded output
		Blade failure or inlet guide vane failure	Damage to other blades and high vibration trip	Forced outage
		Thrust bearing failure	Major damage to rotor and stator	Forced outage
		Radial bearing failure	Major damage to rotor and stator	Forced outage
		Foreign object damage	Possible blade/ combustion chamber damage	Forced outage
	Bleed air system	Blockage of external cooler	Over-heating to blade or vane failure	Forced outage
		Valve stuck shut	Start system inhibited	Failure to start
		Valve stuck open	Turbine over temperature, gas generator overspeed	Forced outage
	Combustion chamber	Explosion in combustion chamber	Possible fire, distortion of hot gas path and debris in turbine	Forced outage
		Failure of refractory lining	Debris in turbine with consequential blade damage	Forced outage

© Woodhead Publishing Limited, 2013

Comment	Severity range (1–10)	Failure rate range (1–4)	Detectability (1–10)	Active repair time (h)	RPN1	RPN2	RPN1 rank	RPN2 rank
External atmospheric effect	3	3	8	8	27	216		
Ditto	3	3	8	6	27	162		
Sudden load change	10	1	10	1000	10	10000		2
Fouling/ degradation	4	1	7	200	16	3200		
Component degradation	6	2	4	200	84	16800	5	1
Sudden load change	3	3	9	8	18	144		
Fouling/ alignment change	3	3	9	8	18	144		
Component degradation	3	1	5	100	18	1800		
Component degradation	7	2	9	100	28	2800		
Component degradation	8	2	10	72	16	1152		
Ditto	3	3	9	8	18	144		
External event	4	1	3	100	32	3200		
Hostile local environment	4	3	5	24	72	1728		
No effect	5	2	5	8	60	480		
Corrosion/ oxidation	3	2	4	8	42	336		
Change in op. conditions	6	2	9	100	24	2400		
Component degradation	6	3	7	30	72	2160		

(*Continued*)

© Woodhead Publishing Limited, 2013

Table 12.1 Continued

Unit	Sub-unit	Failure mode	Local failure effect	System failure effect
	Burners	Combustion instability (pre-mix)	Pressure pulse humming and possible fatigue damage to turbine	Forced outage
		Flame out	Engine rundown and stop	Forced outage
		High temperature	Possible blade damage and HT trip	Forced outage
	Fuel system	Sensor/actuator failure leading to mis-scheduling of fuel flow	High flow – turbine overtemperature, gas generator overspeed, shaft overtorque	Forced outage
	Fuel pipework	Fuel leak	Low flow – failure to achieve power setting.	Degraded output
			Possible explosion or fire	Forced outage
	Inlet guide vane system	Sensor/actuator problems	Vanes malscheduling open – possible surge and compressor damage	Forced outage
			Vanes malscheduling closed – possible gas generator overspeed and turbine overtemperature	Forced outage
	Casing	Air leak	Reduced output/ efficiency	Degraded output
		Seal failure	Leakage of hot gases to atmosphere with possible fire	Forced outage
		Valve/pipework failure	Ditto	Forced outage
		Exhaust flexible joint failure	Ditto	Forced outage

© Woodhead Publishing Limited, 2013

Comment	Severity range (1–10)	Failure rate range (1–4)	Detectability (1–10)	Active repair time (h)	RPN1	RPN2	RPN1 rank	RPN2 rank
Change in op. conditions	4	3	8	10	36	380		
Change in op. conditions	4	3	9	8	24	192		
Ditto	3	4	9	8	24	192		
Component malfunction	3	3	4	8	63	504		
Ditto	3	3	4	8	63	504		
Component degradation	5	3	7	8	60	480		
Component malfunction	3	4	5	8	72	576		
Ditto	8	4	5	24	192	4608	1	4
Component degradation	4	3	5	48	72	3456		5
Ditto	5	2	8	8	30	240		
Component degradation	5	2	8	8	30	240		
Ditto	2	1	6	5	10	50		

(*Continued*)

© Woodhead Publishing Limited, 2013

Table 12.1 Continued

Unit	Sub-unit	Failure mode	Local failure effect	System failure effect
Power turbine	Rotating assembly	Blade failure	Damage to other blades	Forced outage
		Rotor bend	Vibration and major damage to rotating assembly and stator	Forced outage
		Tip rub	Reduced power/ vibration	Degraded output
		Thrust bearing collapse	Major damage to rotor and stator	Forced outage
		Radial bearing failure	High vibration and trip	Forced outage
Control and monitoring	Sensors	Spurious instrument fault	Spurious shutdown	Spurious trip Component degradation
		Instrument fault	Fail to detect off spec. condition	Potential catastrophic failure
	Control unit	Control hardware fault	Possible overspeed or reduced output	Forced outage/ degraded output
		Control software fault	Ditto	Forced outage/ degraded output
Lubrication system	Oil supply	Loss of supply or contamination	Bearing damage and vibration	Forced outage
		Fail to scavenge	Bearing chamber flooding. Rubs and damage due to out of balance forces. Internal oil fire and disc burst if leakage occurs into turbine	Forced outage

the operational reliability of the equipment), the failure mechanisms which are likely to cause component degradation, and the high-impact, low-probability events which can result in very long outage times. It is important to include and quantify the impact of the repair process on the operational reliability of the equipment, in addition to the identification and quantification of failures modes which can be hazardous to both personnel and plant.

An FMECA provides a complementary analysis of the failure characteristics of complex rotating machinery systems such as gas turbines, particularly

© Woodhead Publishing Limited, 2013

Comment	Severity range (1–10)	Failure rate range (1–4)	Detectability (1–10)	Active repair time (h)	RPN1	RPN2	RPN1 rank	RPN2 rank
Component degradation	8	2	9	100	32	3200		
Ditto	8	2	8	100	48	4800		3
Ditto	3	1	5	100	18	1800		
Ditto	8	2	10	82	16	1152		
Ditto	3	3	9	8	18	144		
Component degradation	3	4	5	2	72	144		
Ditto	3	4	3	6	96	576	2	
Ditto	3	1	7	5	12	60		
Ditto	4	2	6	5	40	200		
External malfunction	5	3	5	4	90	360	3	
Component degradation	4	3	4	8	84	672	4	

for identifying the failure mechanism likely to be associated with the critical sub-units and the infrequent high-impact, low-probability events which can result in very long outage times.

An analysis of failure mechanisms, actual failures, and their effects on operation shows up which mechanisms and factors in the past have led to significant failures or outages. The FMECA is a widespread aid for choosing the optimal mechanisms to monitor.

If a power plant has the instrumentation to know the state of the main parameters and the condition of main equipment process supervision can

© Woodhead Publishing Limited, 2013

be implemented. This will enable failure mode analysis of the principal elements and components based on FMECA techniques. There are many mechanisms of a component that are at risk of age-failure. A prudent choice of a small number of mechanisms to monitor, diagnose or inspect has to be made. Application of such intelligence and methods by users will enhance the pool of knowledge and experience in the power sector.

An FMECA is based on historical data, mostly handled statistically. It is based on the experience with a population of more or less identical components. In an FMECA, the main component is split up into sub-components. Of all sub-components, several statistical aspects of failures are determined. Based on the results of the FMECA, dominant failures and failure mechanisms are assigned. Coping with the dominant mechanisms is most efficient. The choice for techniques for monitoring, diagnosis and inspection should be well-grounded. A well-founded choice can be made, keeping the following aspects in mind:

- determination of dominant failure and ageing mechanisms;
- parameters to monitor for failure (ageing mechanisms are often perceptible);
- choice of technique for monitoring, diagnosis and inspection.

When a choice is made as to what factors to monitor, diagnose or inspect, the next step is to choose parameters to monitor. This choice can benefit from manufacturer recommendations. The manufacturer is familiar with the behaviour of the component in question, and therefore can pinpoint the most important parameters to monitor. This underlines the necessity for collaboration with the OEM. The choice for monitoring parameters has to be made based on various criteria:

- a clear relation between monitored parameter and failure or ageing mechanism is required;
- the monitoring technique should not interfere with operation;
- the technique to be used should be proven and reliable;
- lifetime expectancy should be as long as that of the equipment to be monitored;
- monitoring equipment failure should not endanger the power plant;
- compromises that are acceptable during implementation.

The following requirements are defined for the RM&D system that is made up of the monitoring and diagnostic system on site, the telecommunications system, and the monitoring and diagnostic centre. The monitoring and diagnostic system must comply with several requirements; for such a system to be effective it should be:

© Woodhead Publishing Limited, 2013

- automated and integrated,
- able to perform all actions, from data collection to diagnostic decisions derivation,
- robust, that is, not overly susceptible to noise or faulty input information,
- with wide coverage of detectable faults,
- able to allow for additions of new faults not included in the initial repertoire,
- have prognostic capabilities for maintenance and repair actions,
- able to assist with availability of long lead-time spares and reduce outages,
- able to derive information with high confidence,
- able to derive one conclusion by different methods,
- modular and flexible with open architecture to be adapted to operator needs,
- very user friendly, so that it can be used by non-specialized personnel.

In order to realize a monitoring system which possesses these features, the procedures to be implemented are as follows:

1. Measurement data acquisition.
2. Data evaluation to discard unreliable readings and detect sensor faults.
3. Data processing using appropriate techniques to derive diagnostic information.
4. Diagnostic inference to decide nature, location and severity of malfunctions.
5. Efficient management of long-term historical monitoring, data records.

The mission is to develop an analytical procedure to identify the degradation and malfunctions in the performance of power plants by means of symptoms and indicators of initial stage problems. Providing solutions and operational recommendations in time may allow improvements of the power plant performance. To accomplish this, a RM&D system can be implemented. The concept of an RM&D system implies access to, and collection of, O&M data of the power plant, its transmission to the RM&D centre, analysis and diagnosis by means of a combination of automatic analysis and the M&D specialists, editing of condition and performance reports, and provision of O&M recommendations.

Analysis of data and diagnosis inference in plant

By means of the use of appropriate techniques we can extract diagnostic information and know what is the nature, the location and the root cause of the present malfunction. The analytical system measures and analyses

© Woodhead Publishing Limited, 2013

a great quantity of data, it detects anomalies or anomalous states of the equipment by comparing conditions with the data base (baseline), diagnosis rules included in the base of knowledge of the system, and design specifications, and it communicates the information to the CMD. There are two levels of malfunction detection:

- The detection of malfunction at an initial stage by means of an immediate flagging system which is carried out by the plant information system.
- The detection of malfunction over a longer timescale is carried out by M&D experts in the RM&D centre.

The analysis module is made up of the following main sections:

1. Thermodynamic condition analysis.
2. Mechanical/rotordynamic condition analysis.
3. Fluid condition analysis.
4. Electrical equipment condition analysis.
5. Mechanical integrity and remaining-life assessment.
6. Dependability analysis.

Telecommunications system

This function of the system guarantees safe and reliable data communication between the power plant and the CMD. The communication can be:

- A warning from plant itself when the malfunction is automatically detected.
- In a continuous mode, 'in real time'.
- Periodic transmission of information at the selected frequency rate.

Monitoring and diagnostic centre

The CMD is a technology centre which will act as a core of technological competencies, that is, where the company knowledge, skill and facilities are concentrated to optimize power plant operation and maintenance (Fig. 12.14). With all the aforementioned, a communications network is set up between plant staff (plant manager, operators, maintenance personnel, etc.) and RM&D centre (diagnostic engineers, M&D experts, etc.) which will enable on-line technical assistance and support in the operation and maintenance of power plant. Therefore, the monitoring and diagnostics system has four levels:

1. Field level, classified in two groups based on instruments and monitoring device:

© Woodhead Publishing Limited, 2013

- *Standard instrumentation*: The selected variables are monitored by means of conventional field instrumentation and the data acquisition device is the one of the distributed control system (DCS).
- *Special diagnostic instrumentation*: The selected variables are monitored by means of special instrumentation and the data are directly acquired by means of the Data Acquisition System (DAS).

2. Acquisition level, with the devices that log data temporarily and transmit it to the main DAS, which can interact simultaneously with other devices (control system units, DCS, data loggers, etc.) in acquiring field data.
3. Monitoring level, for access, logging and treatment of the system information.
4. Diagnostic level, which provides the data analysis and deviations by means of trends, correlation with the process data and comparison with the base line for the identification of the potential equipment irregularities and analysis of the plant performance.

Finally, the choice of data platform and human interface software has to consider the following requirements:

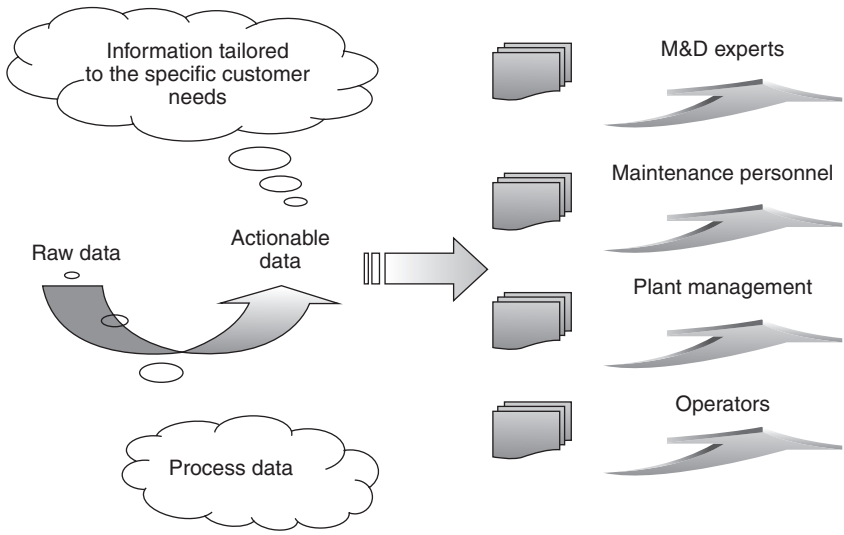
- The system should be user friendly.
- The information produced by the system should be easily transferable to widely used commercial packages.

12.4.2 CMD of combined cycle power plants

Integrating asset management and plant operation must be done in a way to secure safety. If carefully thought out it will also lead to reliability, availability, performance and manning improvements. To integrate effectively with asset management, the power plant operation needs to be monitored by a continuous on-line system to collect, measure and display the process variables.[1] Process data are gathered and displayed. Then they will be used to inform the decision-making process by means of diagnostic tools. The specialist for each main area of fundamental-cause evaluation and corrective action will apply custom rules for specific machinery and plant characteristics, as shown in Fig. 12.15. In this way, the information can be customized for the specific needs of each user and allow a better connection.

Factors, such as, Efficiency and Reliability, Availability and Maintainability (RAM) appear as key issues to be tracked. The way to confront these factors with guarantees for success, and as a differentiating and competitive element, is by means of a combination of information technologies, methods of both field data analysis and assessment, and knowledge management technology (advanced diagnostic tools, how to get knowledge from data, how to transform raw data into actionable data).

© Woodhead Publishing Limited, 2013



12.15 Actionable information.[15]

Therefore, the mission is to develop an analytical procedure which will allow us to identify the degradation and malfunctions in the performance of CCPP by means of symptoms and indicators of initial stage problems and, by providing solutions and O&M recommendations in time, allow the optimization of the CCPP performance. This mission is implemented through the concept of RM&D, which implies:

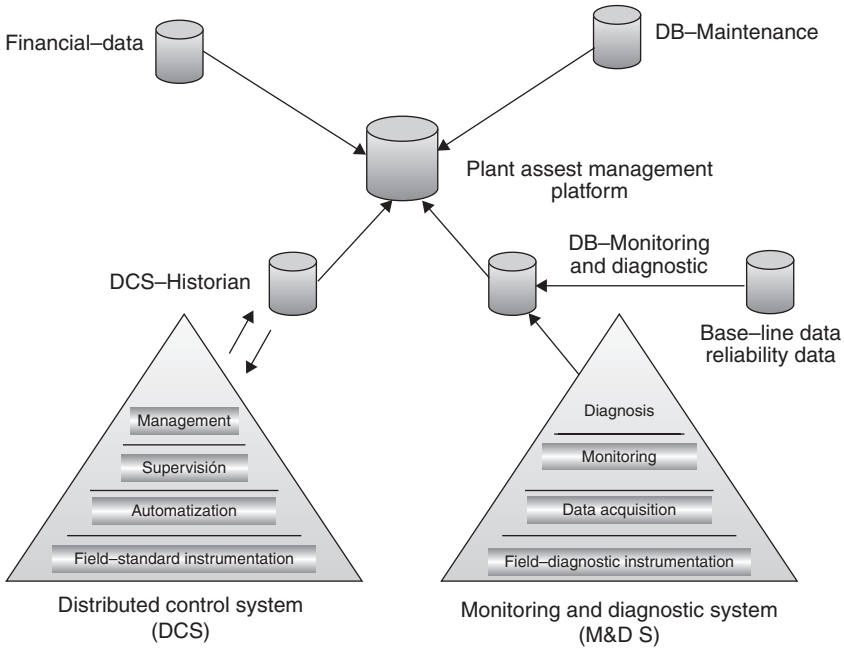
- access to and collection of operation and maintenance data of the CCPP,
- its transmission to the CMD,
- diagnosis by a combination of automatic analysis and M&D specialists,
- editing of condition and performance reports,
- provision of O&M recommendations.

The implementation of the monitoring and diagnostic system requires the following elements:

- Diagnostic instrumentation (special + standard).
- Plant information system (Fig. 12.16).
- Telecommunication system.
- RM&D centre (CMD).

Figure 12.17 shows a functional diagram of the RM&D system made up by on-line DAS. This is the link between the monitoring system and the plant, providing the necessary diagnostic data. Once the data are collected,

© Woodhead Publishing Limited, 2013



12.16 Power plant monitoring and diagnosis vs control system.[15]

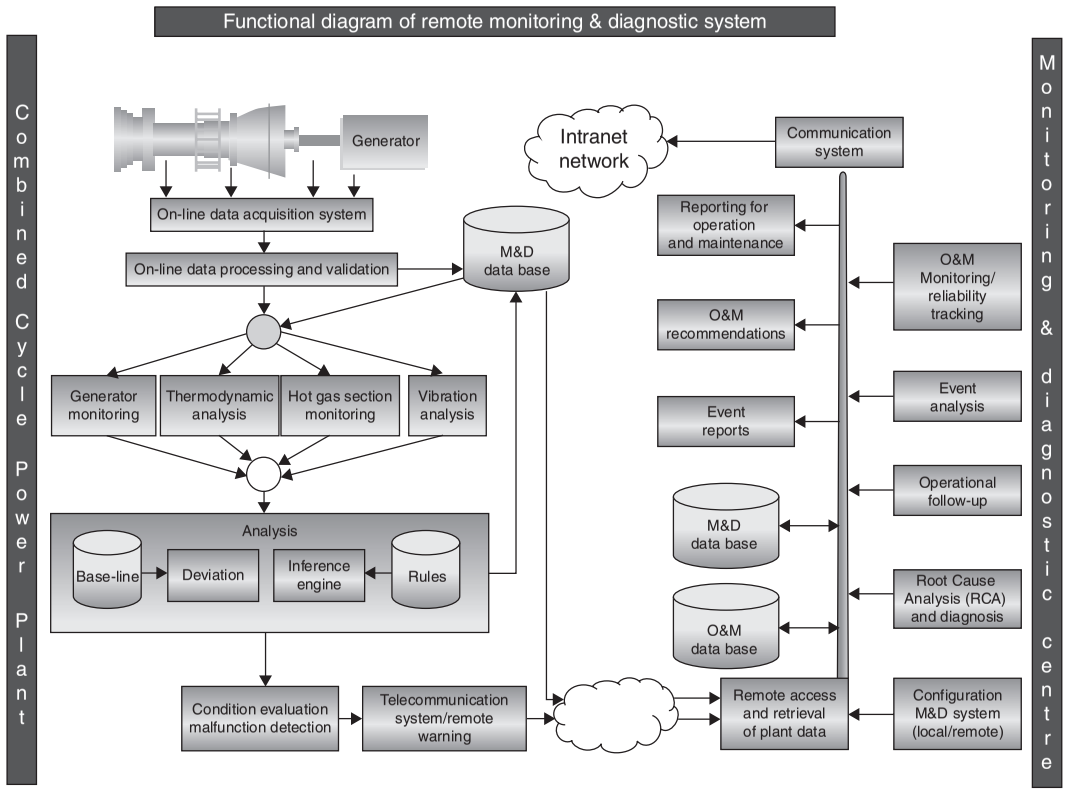
they are validated on-line and can be calculated as a mathematical function of the recorded data. The next step is the data analysis and diagnostic inference, carried out in two levels of malfunction detection by means of an immediate flagging system, which is carried out by the plant information system and, over a longer timescale, by M&D experts, and the analysis module, which is the most important element and which focuses on determining the mechanic/rotordynamic condition, thermodynamic and functional condition, RAM-on-line tracking, electrical generator and balance of plant (BOP) equipment monitoring.

To improve cost of operation, efficiency and availability, the traditional I&C must be reinforced by incorporation of systems for analysis and diagnosis of power plant performance and condition. These detect incipient deviations of both performance and condition from normal operations, at an early stage, avoiding or reducing performance losses and more serious equipment damage.

Analysis and diagnosis of components is also a central requirement for CBM, where the current condition of a component must be precisely known so that maintenance time and scope can be accurately determined.[31] Over the long term, this maintenance strategy results in longer intervals between service operations and shorter service duration.

© Woodhead Publishing Limited, 2013

© Woodhead Publishing Limited, 2013



12.17 Functional diagram of RM&D.[15] (M&D: Monitoring and Diagnosis, O&M: Operation and Maintenance).

Data fusion for combined cycle power plant (CCPP)

The data fusion is a tool that electricity utilities can use to analyse the performance of their plants, providing universal access to a multiplicity of information both at the plants and at the corporate level. The types of information include:

- At power plants:
  - Current and historical plant operating data and statistics.
  - Performance indices.
  - Trend and control charts.
  - Performance analysis and reports.
  - Financial analysis and reports.
  - Fuel usage and analysis, etc.
- At the corporate level:
  - System-wide operating performance and statistics.
  - Financial performance and statistics.
  - Information for process improvement and business planning, etc.

Data fusion provides the following benefits:

- Easy, centralized access to data from multiple sources for decision making.
- Regular and ad hoc reports for data analysis.
- Improved operating efficiency, by access to control and performance indicators.
- Lower labour costs for budgeting, scheduling, and reporting.

The potential data sources of interest in a typical power plants layout are shown in Table 12.2. It is easy to add standardized reports to a data fusion system since it has been designed with the functionality to efficiently retrieve, format, and report data, and it also contains a large library of utility specific equations which can be used to report calculated data. Calculations can also be done when data are first acquired and/or processed, with the calculated results stored for fast retrieval and reporting. A large number of standard reports have been developed that are discussed below:[32]

- Plant reports.
- Heat-rate reports.
- Water chemistry reports.
- Operating statistics performance reports.
- Operational plant report – summarizing key operational data including hydrogen usage, condenser air in leakage, hot well dissolved oxygen, start-up and shutdown data, etc.
- Plant maintain report – showing extensive data about work orders.

© Woodhead Publishing Limited, 2013

Table 12.2 Data sources for data fusion[12]

Operations	Documents
– Operating values – Maintenance equip. variable – Operator logs – Control chart	– Procedure – Drawings – Any data type
Maintenance – Repair description – Labour hours and cost – Parts cost – Maintenance procedures – Maintenance cost – Drawings	Vibration – Frequency aspect – Cascade plots – Orbit plot – Overall vibration
Performance test data	Heat rate Heat rate Control losses Performance On-line measurements
DCS or process computer	Procedure
Financial – Budget – Hour – Rates costs	Reliability – Available hours – Forced outage – Service hours
Boiler – Tuber records – Boiler Graphics – Tube conditions – Failure mechanism – Remaining life	Turbines – Outage inspection – Damage reports – Repair made – Design change
Water chemistry – Conductivity – pH – Silica – Procedure – Hydrazine – Sodium	Laboratory – Oil analysis – Particle count – Metals – Viscosity

- Vibration report.
- Control charts – allowing users to select and format charts as needed.
- Structure tree module – for root cause analysis.
- Ad hoc queries.
- Formatted ad hoc reports for groups of parameters for a unit or a group of units, with selected time period of interest.

Corporate reports present information for a plant or a group of plants. Corporate reports generally present monthly data and year-to-date data. The corporate report format is basically the same as that for plant reports:

© Woodhead Publishing Limited, 2013

- The system heat-rate deviation analysis report shows heat rate (Btu) and cost deviations for critical operating parameters such as throttle temperature and pressure, station service, exit gas temperature, etc.
- The system operating statistics report shows a system-wide overview of performance-related items such as generation, heat rate, boiler efficiency, station service, etc.
- The water chemistry percentage capable report shows an index of the percentage of defined water chemistry processes that are capable of being controlled.
- The fuels accounting summary presents generation and heat-rate data along with gas or distillate fuel for individual units and summarizes these data for all plants in the system.
- The system monthly target deviation performance report shows the deviation from defined targets for heat-rate related parameters.
- The efficient production index (EPI) report shows a calculated performance index for seven heat-rate indicators, showing whether or not these parameters meet specifications. The EPI represents the percentage of defects, with a lower EPI being better.

Typical data fusion users, the ways in which they use the system, and the benefits they derive are listed below:

- *Plant operators*: Hourly and shift reports and performance indicators. Control charts for critical operational parameters.
- *Plant engineers*: Daily, shift, and weekly data summaries; daily, shift, weekly and monthly performance indicators; customized ad hoc reports and data queries.
- *Plant managers*: plant-wide summaries.
- *Corporate specialists*: troubleshooting, data mining, performance monitoring.
- *Corporate managers*: plant and system performance/cost overview and comparison.

Condition monitoring and diagnostic system

The effectiveness of a power plant's production asset management is crucial in determining how profitable the plant can be in the increasingly competitive electricity industry. This therefore places special technical demands on the condition monitoring systems that are used in the operation and maintenance of such assets.

Thermodynamic condition analysis

Performance monitoring is a technique which uses measured and calculated thermodynamic properties to assess the condition of a machine or system.[33]

© Woodhead Publishing Limited, 2013

The rationale for performance monitoring systems as a part of preventive/predictive maintenance programmes is economic impact on the turnover of the power plant. The appendix 'An overview to the Monitoring & Diagnostic Techniques for Combined Cycles Power Plants' presents the basic principles of gas turbine thermodynamics, latest advances in gas turbine technology, performance test procedures, advanced performance monitoring, and several specific malfunction symptoms, such as rotating stall and surge for the compressor, are addressed.

Mechanic and rotor dynamic condition analysis

This item outlines rotating machinery malfunction diagnostics using vibration data in correlation with operational process data.[34] The advantages of vibration monitoring systems as a part of preventive/predictive maintenance programmes are:

- Reduced production losses.
- Enhanced efficiency, reliability, availability and longevity of machinery.
- Reduced maintenance costs (labour, spares inventory and, maybe, fuel).
- Improved work-load planning.
- Enhanced safety and environmental programmes.

The basic principles creating the foundation for machine malfunction diagnosis methodology applicable for both periodic and continuous monitoring are[35]:

- Know the mechanical, fluidic, thermal, and electric machine characteristics.
- Know the likely machine malfunction mechanisms and their symptoms.
- Monitor the key parameters that will indicate a change in machine condition.
- Reduce diagnostic data to interpretable formats.
- Compare with analytical predictions.
- Understand history and events that may have changed machine condition.
- Present data on the machine condition in as solid an engineering form as possible.
- Take prompt action based on machine diagnosis.

After presenting basic principles of machinery diagnostics the appendix 'An overview to the Monitoring & Diagnostic Techniques for Combined Cycles Power Plants', will deal with several specific symptoms of malfunction, supported by simple mathematical models. These malfunctions include imbalance, excessive radial preload, rotor-to-stator rubbing, fluid-induced

© Woodhead Publishing Limited, 2013

vibrations, loose stationary and rotating parts, coupled torsional/lateral vibrational excitation, and rotor cracking.

Fluid condition analysis

Analysing the fluids passing through equipment is essential in order to have a full picture of the condition of a power plant. In fact, we can consider a CCPP as a 'black box', in which some fluids act as inputs into the system and, after having carried out their mission, they leave it incorporating information about the condition and the performance of the system.

In order to guarantee the performance of the system it is essential to guarantee the condition of the intake fluid accords with the manufacturer specifications; similarly, the condition of fluids leaving the system allow analysis of the condition of the system. The main fluids to be considered are:

- Water/steam.
- Oil lubricant.
- Combustion air.
- Fuel gas.
- Exhaust gas.

Electrical equipment condition analysis

A modern power plant is a complex combination of mechanical and electrical equipment. In this item the focus will be on monitoring and diagnosis of electrical equipment. Generally speaking, modern electrical equipment is very reliable, demanding little maintenance at long intervals. Proper monitoring or diagnosis can aid in improving the overall reliability and availability of the electrical system, by:

- early detection of incipient faults, thereby reducing downtime,
- effective maintenance,
- reduced downtime for scheduled maintenance (because weak spots are known).

The main electrical equipment to be monitored are converters, transformers, generators, motors and drives, converts and switchgear.

Mechanical integrity and remaining-life assessment

Beyond the EOH or factored hour/start criteria, which assume a very generic approach in the repair/replacement HGP components, the alternative would be to have component-specific lifetime monitoring supplemented with some specific monitoring techniques to deal with the increased risk.

© Woodhead Publishing Limited, 2013

Components which operate at low temperatures below the creep regime are generally designed on the basis of yield strength, tensile strength, and fatigue strength, by applying suitable safety factors to these values. Because deformation and fracture are not time-dependent under these circumstances, there is no specific value of 'design life' associated with them.

In the case of high-temperature components operating in the creep regime, both deformation and fracture are time-dependent. They are therefore designed with respect to a target life usually based on a specified amount of allowable strain or rupture in 100 000 h.

Many metallurgical and operational factors can extend the actual component life beyond the design life. These include: use of minimum properties in design, safety factors in design, conservative operation of units, inaccuracies in data extrapolation, and overestimation of oxidation effects.

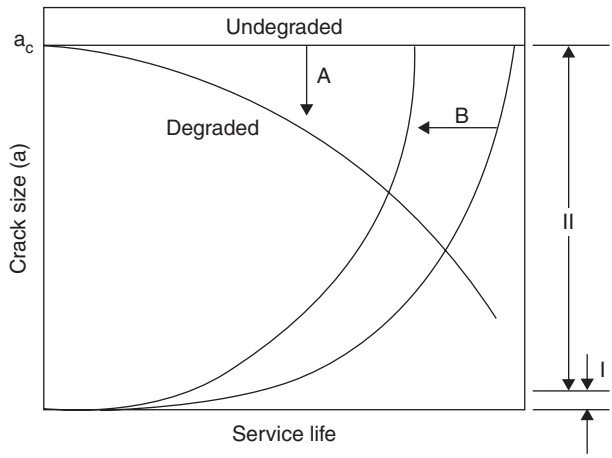
Alternatively, if these factors are adverse, actual life can be reduced; for instance, unanticipated stresses (e.g., residual, systems stresses), operation outside design limits (e.g., excessive temperatures, load cycling of baseload units), operational and environmental effects, degradation of material properties in service (e.g., temper embrittlement and softening).

Failure of a component can be defined as the inability to perform its intended function reliably, economically, and safely. Component retirement decisions can be based not just on economic justification. A logically and technically based decision may, for instance, involve a sequence of steps, such as remaining-life calculations based on operating history, inspections, material testing, assessment of remaining life, and final disposition of the component in terms of continued service, repair, or replacement.

The general approach of a remaining-life-assessment procedure for a commonly encountered failure scenario is illustrated in Fig. 12.18. Region I corresponds to incipient, microscopic damage events leading up to the initiation of a macroscopic crack. These events include dislocation rearrangements, coarsening of precipitate phases, and formation of creep cavities and microcracks. NDE techniques that are potentially capable of detecting these events include electron microscopy, replication metallography, X-ray diffraction, electrical resistivity measurements, positron annihilation measurements, ultrasonic velocity measurements and hardness measurements. Region II corresponds to propagation of the above-mentioned macrocrack. Conventional NDE techniques such as magnetic-particle inspection, dye-penetrant inspection, ultrasonic examination, X-ray radiography, and eddy-current testing apply to crack detection and sizing in Region II. In Region II, the crack grows until it reaches a critical size, defined as a_c, at which point rapid fracturing occurs.[36]

Techniques that use crack initiation as a failure criterion include calculations based on history, extrapolations of failure statistics, strain measurements, accelerated mechanical testing, microstructural evaluations, oxide scale growth, hardness measurements and advanced NDE techniques.

© Woodhead Publishing Limited, 2013



A – embrittlement phenomena, B – unanticipated factors (excess cycling, temperature excursions, corrosion, metallurgical degradation, improper material, excesive stresses).

12.18 Illustration of a remaining-life-assessment procedure for a common failure scenario involving crack in initiation and propagation.[36]

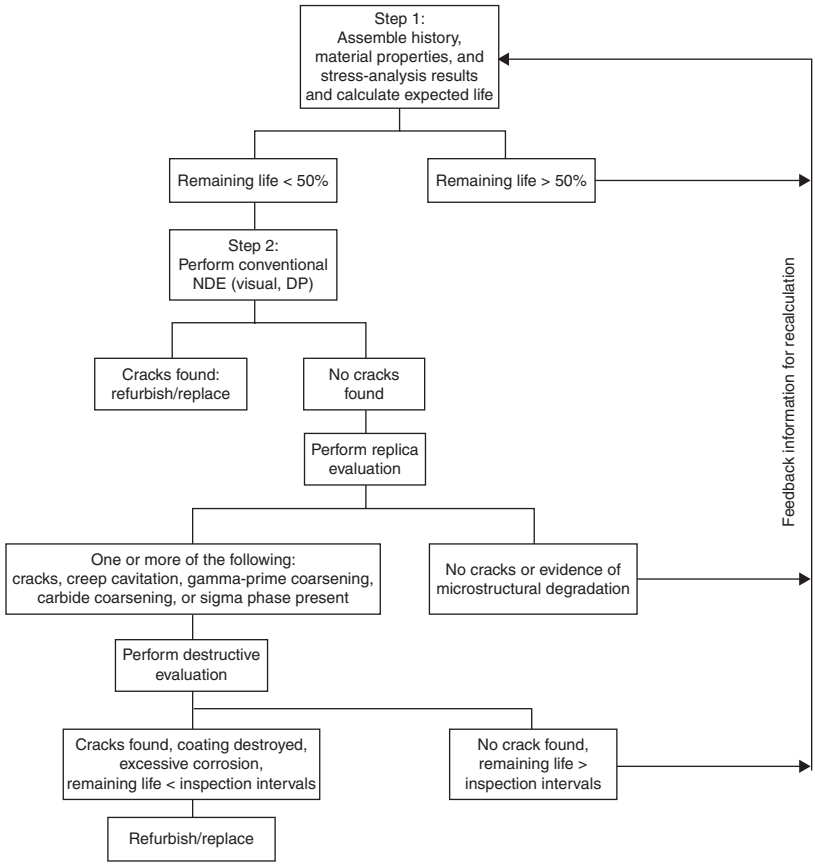
For crack-growth-based analysis, the NDE information, results from stress analysis, and crack-growth data are integrated and evaluated with reference to a failure criterion.

Typical examples are creep and fatigue monitoring for the heat recovery steam generator, the steam turbine and gas turbine major components.

The integrated methodology for life assessment of blades includes a three-step process involving calculations followed by NDEs, and culminating in destructive evaluations. A logic diagram showing the various steps and the decision points is shown in Fig. 12.19.

The calculation procedures should be utilized to set up an inspection schedule, and should not be used as a basis for repair/replacement decisions. There are various sources of uncertainties which should be taken into account. NDE evaluations begin with the conventional NDE techniques to detect cracks. If cracks are found, immediate repair/replacement is necessary. If cracks are not detected, replication should be carried out at several locations and on different blades. The purpose of the NDE is primarily to identify the need, and the critical locations and blades, for further destructive evaluations. If a comparison of the microstructures at the hot and cold locations shows no evidence of creep cavitation or microstructural changes, further destructive evaluations may not be necessary. If, on the other hand, evidence of such damage is found, sacrificial blades should be removed and subjected to the various destructive evaluations.

© Woodhead Publishing Limited, 2013



12.19 Logic diagram for blade disposition.[36]

RAM metrics

While low heat rates, lowest emissions and minimized first costs are prerequisites for participating in the competitive power generation market, the reliability, availability, maintainability, durability (RAM-D) and performance of modern gas turbine equipment are the key issues for the long-term, economically optimized operation of a CCPP.[37] RAM-D is a key element in efficient and cost-effective power generation and the benefits expected from the implementation of a monitoring and diagnostic system have to be measured in terms of RAM-D metrics, including such valuable measures as:

- plant availability and reliability factors.
- service factor and starting reliability.
- equipment outage factors down to the component level.

© Woodhead Publishing Limited, 2013

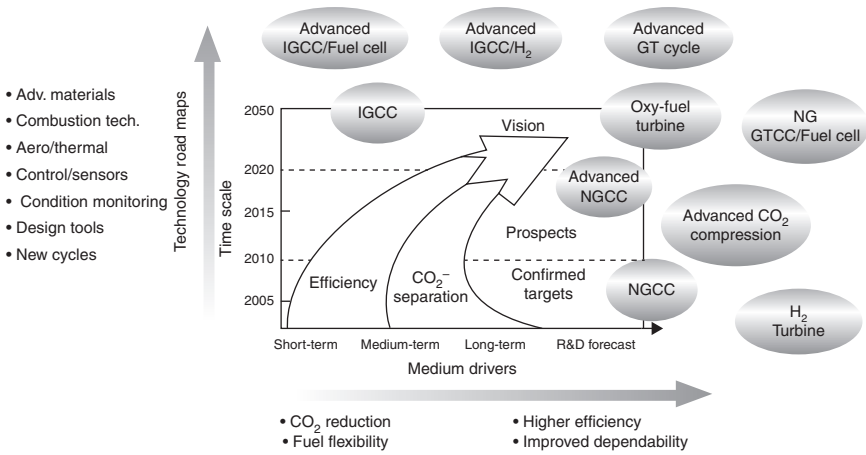
- failure rates and times to repair.
- symptoms, corrective actions, and root cause of failures.

RAM-D metrics allow each plant to establish rigorous, achievable goals for 'best in class' performance (benchmarking analysis).[38] The market place has become extremely competitive, and intensely focused on profitability and return on investment opportunity. The focus on profitability is keenly orientated on both the control and minimization of operating expenses, as well as maximizing top-line growth. For power plants, this equates to operating at times of high return (when the selling price of electricity is high), and minimizing the effect of both scheduled and unscheduled maintenance. This means that each operating plant must be concerned with effective risk and asset management. RAM-D is the 'key controlling variable' in the tenuous balance between risk and reward.

12.5 E-maintenance and future trends

Figure 12.20 shows the future of advanced thermal power plants where highly complex designs are needed to address environmental issues and where gas turbine technology will play a key role as the core technology for many different plant configurations. Gas turbine asset and performance management appear as a pathway to competitive skills for the new power generation arena, aimed at optimizing life-cycle cost by improving both gas turbine dependability and performance.[39]

Advanced maintenance has a critical role to play in improving the competitiveness of gas turbine technology. Technology will not be effective without excellent management. The reliability, maintainability and availability



12.20 Pathways to achieve advanced thermal power plants.[1]

© Woodhead Publishing Limited, 2013

of engines and equipment are crucial factors for competitiveness, particularly in applications where safety and availability are important.

This chapter has reviewed gas turbine performance monitoring and CBM strategy to optimize O&M management. CBM has been defined in detail and has been shown to be an advanced strategy, aimed especially at high criticality problems that are not adequately treated by traditional strategies of run-to-failure and time-based preventive maintenance.

The optimal solution is to know continuously the condition of the asset and its components and to take repair and service actions only when they are really needed. This is, of course, a big challenge. However, current technological developments offer new and advanced techniques and methods to support this approach. Currently, there is an improved understanding of the physical, mechanical and electrical phenomena initiating and triggering disturbances and failures. There is the potential to develop advanced sensors for monitoring the behaviour of a component or system. There are high capacity and advanced methods for condition data collection and processing, data validation and fusion, signal analysis, data mining and decision making. There are also methods for computer-based diagnostics and prognostics of asset conditions.

New wireless techniques and the internet offer the possibility of using mobile hand-held computers (personal digital assistants (PDA)) to have access, globally and on-line, to large bodies of information. This opens a new possibility in asset maintenance: *e-maintenance*. It has been defined as 'the network that integrates and synchronizes the various maintenance and reliability applications to gather and deliver asset information *where it is needed*'.[40] E-maintenance is a synthesis of two large trends in our society: on the one hand, the growing importance of maintenance as a key technology to keep machines running properly, efficiently and safely and, on the other hand, the very rapid development of information and communication technology. This has opened the way to completely new concepts and solutions. They benefit from more specialized equipment for performance and health information, more effective diagnostic/prognostic tools, plus user interfaces to ensure good reliability and availability of assets remotely and worldwide.

New maintenance philosophies and strategies available for e-maintenance are remote maintenance operations and decision making. By leveraging information, through wireless (e.g., Bluetooth) and Internet technologies, users may log in from anywhere and with any kinds of device. An e-maintenance platform may introduce unprecedented levels of efficiency into the entire company, by producing an integration of business and maintenance processes through proactive on-line maintenance, real-time remote monitoring of equipment status and CBM.[41,42] Applications in this area include equipment failure prognosis based on current condition and projected usage, or remaining life prediction of machinery components.

© Woodhead Publishing Limited, 2013

Prognostic and health management systems can offer a great opportunity in terms of reducing the overall LCCs of operating systems.[43]

12.6 Key definitions

Condition based maintenance

'The preventive maintenance initiated as a result of knowledge of the condition of an item from routine or continuous monitoring'. More informally, components are periodically inspected by manual or automatic systems in order that their condition may be assessed and their degradation rates identified. A decision is then taken regarding replacement, based upon an analysis of the monitored data.[44]

Performance monitoring

Performance monitoring is a technology which uses measured and calculated thermodynamic properties to assess the condition of a machine or system. The purpose of performance monitoring systems as a part of preventive/predictive maintenance programmes is to do with economic impacts on the turnover of the power plant.

Life-cycle cost

LCC is the total cost of ownership to the customer of acquisition, operation and maintenance and disposal of a product over the whole life cycle.

Dependability

Dependability is a collective term used only for non-quantitative descriptions of the following:

- Reliability (R): How often does it fail?. This can be expressed in terms of time as 'Mean Time Between Failure' (MTBF).
- Availability (A): Can it be used when you want it?. This is a measure of the ability to satisfy demand.
- Maintainability (M): How easy is it to fix?. This is expresses in terms of time as 'Mean Time To Repair' (MTTR).
- Durability (D): It is defined as the ability to continue to meet the performance goals after a specified extended period of time. It can be expressed in terms of time as 'Mean Time Between Overhaul' (MTBO).

12.7 Acknowledgement

The authors thank Mr P. Giannakakis for his help with this chapter.

© Woodhead Publishing Limited, 2013

12.8 Sources of further information and advice

Alvarez Tejedo, T. (2002) (Octubre 2007). *Tecnología y sistemas avanzados de mantenimiento en turbinas de gas.* Revista Mantenimiento (AEM-Asociación Española de Mantenimiento) Vol 208 pagina 16–28.

British Standard Glossary of Maintenance Management Terms in Terotechnology, British Standards Institution (1984).

Davies, A. (1990) *Management Guide to Condition Monitoring in Manufacture*, IProdE, London.

Harker, R. (2000). Understanding Machinery Management – Using Machine Condition and Process Information for Maximun Benefit. *Bently Nevada Orbit Magazine*, Third Quarter 2000.

Hastings, M. and Laagland, G.H.M. (1999). *Integrated monitoring strategy in the Oil & Gas Industry*; Presented at CCBT Conference, 17 March 1999, London.

Hodges, W. (1991) 'Terotechnology'. *Maintenance*, **6** (4), 22–25.

Laws, C.W. and Bosmans, R. (1998) *Machinery Condition Management for Power Plants – Integrated Systems Deliver Operational and Maintenance Benefits with Early Return on Investment*, Proceedings of Power-Gen Asia 1998, New Delhi, India, September 1998.

Lie, C.H., Hwang, C.L. and Tillman, F.A. (1977) 'Availability of maintained systems: a state of the art survey'. *AIIE Transactions*, **9** (3), 247–259.

Mountford, R. and Lee, Y. (1999) *Machinery Management – Review of Advances in Diagnostic Methodologies*, Proceedings of Power-Gen Asia 1999, Singapore, September 1999.

Nakajima, S. (1984) *Introduction to Total Productive Maintenance*, Productivity Press Inc., Cambridge, MA.

Thomson, A., and Kannan, V. (1996). *Getting Results from Your Machinery Management System,* Proceedings of the Twelfth Turbomachinery Maintenance Congress, Bangkok, Thailand, October 1996.

Wilmer, B. (1992) *Total Productive Maintenance (TPM)* at Nissan Motor Manufacturing (UK) Ltd.

12.9 References

1. Alvarez Tejedor, T. (June 2007) Towards the Future of Gas Turbine Asset and Performance Management. *Touch Briefings Magazine: Power Industry International* 2007.
2. Pilidis, P. and Palmer, J. (2008) 'Gas Turbine Theory and Performance', Thermal Power MSc Lecture Notes, Cranfield University, 2008.
3. Zwebek, A. and Pilidis, P. (2003) Degradation effects on CCGT plant performance: Part I: Gas turbine cycle component degradation effects. *ASME Journal of Engineering for Gas Turbines + Power*, **125**, 651–657.
4. Cranfield University (October 1999). *The Turbomatch Scheme*, User manual.
5. Zedda, M. and Singh, R. (2002) Gas turbine engine and sensor fault diagnosis using optimization techniques. *AIAA Journal of Propulsion and Power*, (5), 1019–1025.
6. Ogaji, S.O.T. and Singh, R. (2002) Neural network technique for gas turbine fault diagnosis. *International Journal of Engineering Intelligent Systems*, **10**(4), 209–214.

© Woodhead Publishing Limited, 2013

7. Marinai, L., Singh, R., Curnock, B. and Probert, D. (2003) *Fuzzy-Logic-Based Diagnostic Process for Turbofan Engines*. ISABE, International Symposium on Air Breathing Engines, Cleveland USA, 31 Aug. –5 Sept. 2003.
8. Ogaji, S.O.T. and Singh, R. (2003) Gas path fault diagnoses framework for a 3-shaft gas turbine. *Proceedings of the Institution of Mechanical Engineers: Journal of Power and Energy*, **217** (A3), 149–157.
9. Ogaji, S.O.T., Sampath, S., Singh, R. and Probert, S.D. (2002) Parameter selection for diagnosing gas-turbine performance deterioration. *Journal of Applied Energy*, Vol. **73**, no. 1, pp. 25–46.
10. Alvarez, T. (2006) *Gas Turbine User Needs assessment for improving Hot Gas Path Management*. The Future of Gas Turbine Technology, 3rd International Conference. 11–12 October 2006, Brussels, Belgium.
11. Battelle Columbus Division. (1989) *Gas Turbine Characterization and Diagnostic Instrument Evaluation*, EPRI July 1989.
12. Humphris, D.A., Petek, J., Russell-Jayne, B.R. and Gaither, T.P. (2002) *DataFuser – A Power Tool to Merge Utility Information*, VGB PowerTech 12/2002.
13. Bascur, O.A. and Kennedy, J.P.*"Real Time Information Management Infrastructure – Assets Optimization*. http://www.osisoft.com/resources/articles/Articles.aspx
14. Harker, R. (2000) *Process Data Correlation – The Secret Weapon for More Effective Machinery Management*. Bently Nevada Orbit Magazine, Third Quarter.
15. Alvarez Tejedor, T. and Mendivil, P. (June 2002) *IBERDROLA Centre for Monitoring, Diagnostic and Simulation of Combined Cycle Power Plants*. POWERGEN.
16. Laagland, G.H.M. and Peek, R.F. (1997) *Condition Monitoring – Different Approaches*, Paper presented at Power Plant Operations Maintenance, 16 May 1997, Amsterdam.
17. Roger, G., Harker, Steven and Sabin, *J. Machinery Management: The New Paradigm*. Paper No. GT2002-30431, pp. 1015–1024.
18. De Ruijter, J.A.F., Schaaafsma, C.T., Laagland, G.H.M. and Donauer, P. (1995) *Condition Monitoring of Thermal Power Plants*. Paper for PowerGen Europe 1995, Amsterdam.
19. Sampath, S. and Singh, R. (2006) 'An integrated fault diagnostics model using genetic algorithm and neural networks', *ASME Journal of Engineering for Gas Turbines and Power*, **128** (1), January 2006.
20. ISO/DIS 13374–2. Date: 2005–05–20. *Condition Monitoring and Diagnostics of Machines – Data Processing, Communication and Presentation – Part 2: Data-processing.*
21. Mendivil, P., Alvarez, T., Sandrea, R. and García, J.I. (2003) *IBERDROLA´s Center for Monitoring, Diagnostic and Simulation (CMDS) of Combined-Cycle Power Plants. An Asset Management Vision Becomes a Reality*. ORBIT Magazine, Bently Nevada. First Quater 2003.
22. Sandtorv, H. (1991) 'RCM-closing the loop between design, reliability and operational reliability', *Maintenance*, **6** (1), 13–21.
23. Calabro, S.R. (1962) *Reliability Principles and Practices*, McGraw-Hill, New York.
24. Kurnar, U. and Granholrn, S. (1990) 'Reliability centred maintenance – a tool for higher profitability', *Maintenance*, **5** (3), 23–26.

© Woodhead Publishing Limited, 2013

25. Moss, M.A. (1985) *Designing for Minimal Maintenance Expense*, Marcel Dekker Inc., New York.
26. Lazzaroni, M., Cristaldi, L., Peretto, L., Rinaldi, P. and Catelani, M. (2011) *Reliability Engineering*. Springer.
27. IEC 60812:2006 – *Analysis techniques for system reliability – Procedure for Failure mode and effects analysis (FMEA).*
28. IEC 60300–3-1:2003–01 – *Dependability management. Part 3–1: Application guide – Analysis techniques for dependability – Guide on methodology.*
29. ISO TC 108/SC 5. Date 2002–05–16. *Condition monitoring and diagnostics of machines — General guidelines.*
30. Andrews, J.D. and Moss, T.R. (2002) *Reliability and Risk Assessment*. Professional Engineering Publishing Limited London and Bury St Edmunds, UK. IMechE.
31. Williams, J.H., Davies, A. and Drake, A.R. (1994) *Condition-based Maintenance and Machine Diagnostics*, Chapman & Hall.
32. Carvalho, H.S., Heinzelman, W.B., Murphy, A.L. and Coelho, C.J.N. (2003) *A General Data Fusion Architecture*.
33. Tsalavoutas, A., Mathioudakis, K., Aretakis, N. and Stamatis, A. (2002) *Combining advanced data analysis methods for the constitution of an integrated gas turbine condition monitoring and diagnostic systems*. ASME TURBOEXPO 2000. 8–11 May 2000, Munich Germany.
34. Bently, D.E. (2003) *Fundaments of Rotating Machinery Diagnostics*, Bently Pressurized Bearing Press.
35. Lebold, M., Reichard, K., Hejda, P., Bezdicek, J. and Thurston, M. (2002) *A framework for next generation machinery monitoring and diagnostics*. April, pp. 115–126.
36. Viswanathan, R. (1993) *Damage Mechanisms and Life Assessment of High-Temperature Components*. ASM INTERNATIONAL Metal Park, Ohio 44073.
37. Boyce, M.P. (January 2001) *Handbook for Cogeneration and Combined Cycle Power Plants*. American Society Mechanical Engineers.
38. Madej, J., Longtin, K.A. and Smith, D.P. (1996) *Monitoring and Diagnostics Service Delivery System*. GE Power Generation.
39. Alvarez, T. (2007) Advanced gas turbine asset and performance management. *Revista: Orbit*, **27**(2), 51–61.
40. Baldwin, R.C. (2001) 'Enabling an E-Maintenance Infrastructure'. *Maintenance Technology*, 12, Available: http://www.mt-online.com/articles/1201_mimosa.cfm
41. Homberg, K., Adgar, A., Arnaiz, A., Jantunen, E., Mascolo, J. and Mekid, S. (2010) *E-Maintenance*. Springer-Verlag London Limited.
42. Crespo-Marquez, A. and Iung, B. (2008) A review of e-maintenance capabilities and challenges. *Journal on Systemics, Cybernetics and Informatics* **6** (1), 62–66.
43. Kacprzynski, G.J. (2000) *Health Management Strategies for 21st Century Condition Based Maintenance Systems*. International COMADEM Congress, Houston, TX, December 2000.
44. Seddon, G.N.D. (1984) Computer applications for condition based maintenance – data col1ection, trend monitoring, future prediction and system integration. *Maintenance Management International*, **4** (4), 229–236.
45. Alvarez Tejedor, T. (2012) *Situation of CC electric power generation in Europe*. Technical presentation at EPRI Program 79 – Combined Cycle Turbomachinery. 2012 Generation Sector Program Advisory Meetings (Nashville, US).

© Woodhead Publishing Limited, 2013

13

Maintenance and repair of gas turbine components

T. ÁLVAREZ TEJEDOR, Endesa Generación, Spain and
R. SINGH and P. PILIDIS, Cranfield University, UK

DOI: 10.1533/9780857096067.3.565

Abstract: Material selection is a key factor in gas turbine performance and lifecycle cost because it has a central influence in the maintenance of the gas turbine.[1] Further, the operation of a gas turbine does result in gas path degradation[2] that impacts lifecycle costs and eventually design, manufacture, material choice and maintenance.[3] A component repair programme that minimizes maintenance costs and maximizes equipment availability can be instituted to meet or improve lifecycle cost. This chapter presents the key factors influencing the need for maintenance and the choices available.

Key words: hot gas path, superalloy, non-destructive evaluation, metallurgical evaluation, remaining life evaluation, repair, welding, brazing, coating, heat treatment, compressor cleaning, compressor washing.

13.1 Introduction

The 'hot gas path' of a gas turbine is the core of the engine, and includes the combustion chamber, the transition pieces and the turbine section. The main hot gas path technology drivers are:

- gas turbine performance: highly dependent on a turbine inlet temperature that is beneficial to thermal efficiency and specific power, with the challenge of low nitrogen oxide (NO_x) emissions;
- gas turbine lifecycle cost: strongly affected by hot gas path first cost and maintenance.

A materials selection programme will define the corresponding maintenance programme for the gas turbine lifecycle. This gives rise to maintenance practices and inspection techniques that influence gas turbine dependability, i.e. its RAM–D. Key properties are long-term creep at the expected operating temperatures, tensile rupture, low- and high-cycle

© Woodhead Publishing Limited, 2013

fatigue, thermal-mechanical fatigue (TMF), toughness, and corrosion/oxidation resistance. Gas turbine duty will impact on the predominant failure mechanism. Symptoms include cracking due to thermal and low-cycle fatigue, thermal barrier coating (TBC) spallation, oxidation, corrosion, erosion, and foreign object damage.

Major gas turbine components have limited lives in comparison to the unit's useful life. The life of a component consists of a number of intervals limited, directly or indirectly, in terms of hours or cycles between prescribed overhauls of the whole equipment. Within each set of these overhauls, the repaired component needs to have acceptable integrity to meet the performance goals. A component repair programme that minimizes maintenance costs and maximizes equipment availability can be instituted within the installed base to meet or improve lifecycle cost.

13.2 Maintenance factors

There are different factors that influence life and are responsible for degradation of component mechanisms. These factors must be understood and accounted for in the owner's maintenance plans (Table 13.1).

These factors influence gas turbine maintenance intervals and component parts' lives, and vary with operation. Some failure modes are outlined in Table 13.2.

TMF is the predominant life-limiting factor for peaking machines, while creep, oxidation and corrosion are the dominant limiters for continuous-duty machines. The scope of typical maintenance inspections (combustion, hot gas path and major) are defined by the different original equipment manufacturers (OEM) in order to optimize cost and maximize availability of the unit.

Estimated repair and replacement cycles are provided by OEMs for some major components.

Table 13.1 Life-limiting factors for HGP components

Life-limiting factors
- Fuel - Firing temperatures - Steam/water injection - Continuous duty (centrifugal loads, temperature load, corrosive and oxidation environment, erosion, etc.) - Cyclic duty (thermal stress, etc.) - Peaking duty /TMF, etc.) - Random events (FOD, cooling air hole plugging, malfunction/operation, off-frequency operation, etc.)

© Woodhead Publishing Limited, 2013

Table 13.2 Typical failure modes for HGP components

Failure modes	
Continuous duty	Cyclic/peaking duty
- Rupture	- TMF
- Creep deflection	- High-cycle fatigue
- High-cycle fatigue	- Rubs/wear
- Oxidation	
- Erosion	
- Corrosion	
- Rubs/wear	

OEMs have developed their own conventions such as 'factored hours' or 'equivalent operating hours' (EOH) to define maintenance intervals. It is not readily apparent from the OEM formulations which specific component location, e.g. first row blade tip, leading edge, or trailing edge platform is actually the weak link driving the maintenance action. This underlying uncertainty can result in high repair fallout rates or possible lost production time. Much more often, the maintenance interval may be too conservative, leading to premature parts retirement.

One approach provides an hours-based and starts-based maintenance interval for inspection and replacement of the hot section parts. As discussed, typically starts may be related to the accumulated damage caused from TMF cycles, and hours may be related to coating degradation and/or creep damage accumulated over time. This approach assumes that there is no interaction between the starts-based and hours-based intervals. The maintenance action should be carried out if either interval is exceeded.

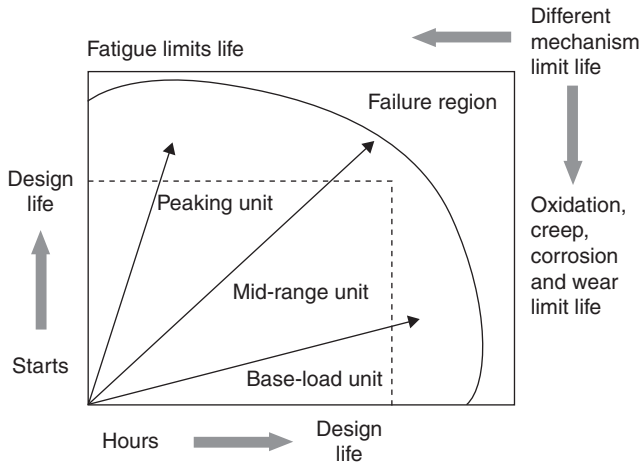
The term 'factored starts' means that actual starts are referenced to a baseline start, referred to as a normal base-load start. To account for damage accumulated for different types of starts or trips, factors are applied to the normal base-load start–stop cycle, reflecting GE's criteria of their relative severity (Fig. 13.1). For instance, hot gas path inspection based on factored starts is determined by GE as follows:

$$\text{Maintenance interval (starts)} = \frac{S}{\text{Maintenance factor}} \qquad [13.1]$$

where,

$$\text{Maintenance factor} = \frac{\text{Factored starts}}{\text{Maintenance factor}} \qquad [13.2]$$

© Woodhead Publishing Limited, 2013



13.1 Maintenance Interval for hot gas path inspection.[4]

and *S* stands for maximum starts-based maintenance interval.

Similarly, the term 'factored hours' means actual operating hours are referenced to a baseline of base-load operation with natural gas and no water or steam injection. For instance, hot gas path inspection based on factored hours is determined by GE as follows:

$$\text{Maintenance interval (hours)} = \frac{24\,000}{\text{Maintenance factor}} \qquad [13.3]$$

where,

$$\text{Maintenance factor} = \frac{\text{Factored hours}}{\text{Maintenance factor}} \qquad [13.4]$$

The assumption that there is no interaction between starts (fatigue) and operating hours (creep) is not supported by other OEMs. There is a large body of evidence that shows creep-induced damage will reduce the fatigue life of a metal, and that fatigue-induced damage will reduce the metal's creep life.

TMF life prediction models take into account the interaction between fatigue and creep at varying temperatures. The models used include damage-based criteria, stress-based criteria, strain-based criteria and energy-based criteria. The linear damage summation (DS) model (also called the linear life fraction, or linear cumulative damage) is the simplest expression for creep-fatigue-life prediction:

$$D_{\text{fatigue}} + D_{\text{creep}} = D_{\text{total}} \qquad [13.5]$$

© Woodhead Publishing Limited, 2013

D_{total} is the total damage, and $D_{fatigue}$ and D_{creep} are the fatigue damage and creep damage respectively. This approach combines the DSs of the time fraction rule or Robinson Rule (1952) for creep and of Miner for fatigue (1945) as follows:

$$\sum \frac{N}{N_f} + \sum \frac{t}{t_r} = D \qquad [13.6]$$

N/N_f is the cyclic portion of the life fraction, in which N is the number of cycles at a given strain range, and N_f is the pure fatigue life at that strain range.

t/t_r is the time-dependent creep-life fraction, where t is the time at a given stress and t_r is the time to rupture at that stress.

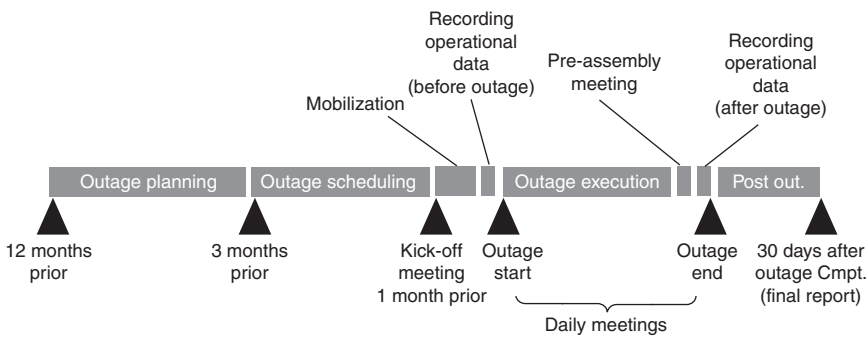
D is the cumulative damage index, when $D = 1$ represents failure.

13.3 Outage cycle

The effective planning and management of maintenance is considered as an increasingly critical business process. The operational and maintenance cost is about 17%, while the initial cost is about 8% of the total lifecycle cost of a gas turbine plant. So much effort has recently gone into technologies such as on-line monitoring and condition-based maintenance.

Plant outages are shut-downs in which maintenance activities are carried out between disconnection and connection of the unit to the electrical grid. A plant outage is normally considered a cyclical process with four phases, initiation, preparation, execution and termination, each with its own specific set of critical issues and activities. It is rightly referred to as a cycle, because the initiation phase of the next outage should follow on from the termination phase of the previous one.

Plant outages require many formal meetings, because a group of people need to transmit, check, challenge and validate information. Figure 13.2



13.2 Outage process.

© Woodhead Publishing Limited, 2013

shows a regular set of meetings after and before the outage to properly develop the so-called 'outage cycle'.

Initiation and preparation are important phases in the optimization of the outage duration, which should ensure safe, timely and successful execution of all activities in the outage. The post-outage review will provide important feedback for the optimization of the next outage planning, preparation and execution.

13.3.1 Outage planning and initiation

In this phase it is necessary to define in detail the strategic issues to be addressed and the activities required to move the process to the point where it can actually be planned and prepared. This phase is characterized by defining objectives, by setting policy, safety and technical requirements, and by appointing the necessary personnel to set up the preparation team and gather basic data.

A detailed outage execution plan should be prepared, including all necessary work files and support needed. This process begins by holding a meeting twelve months ahead of the outage (outage planning meeting). A timeframe is defined for the outage, preliminary work-scope, list of punch items to implement, order and delivery schedule for parts/repairs and services, major logistics needs, and outage responsibilities.

Safety targets on an outage must be uncompromising zero accidents, incidents, fires, etc. Working practices must be equally uncompromising in terms of safety.

13.3.2 Outage scheduling and preparation

Organizational structures need to understand the sequence of events that take place between shutting the plant down and starting it up again, and ensuring that the plans and schedules match the actual sequence.

A second meeting is usually held three to six months ahead of the outage. The main purpose is to schedule the outage, to review outage scope document with roles, responsibilities and technical advancement plan, to define the quality scorecard, to update parts inventory/orders and delivery schedules, to define outage staffing charts with key personnel identified and total manpower expected, to review lessons learned from previous and best practices outages, to determine required lockout/tagout (LOTO) needs and integrate them into the outage schedule, and to review the outage checklist and minutes from previous meetings.

In the detailed planning and preparation, the following items should be considered: (1) pre-outage milestones, including planning, materials, schedule development, external services contracts, etc.; (2) outage duration for

© Woodhead Publishing Limited, 2013

all main phases, shut-down, execution of work, and start-up; (3) final scope of work/activities; (4) outage schedule; and (5) work packages, including work orders and permits, instructions and procedures, materials, spare parts, consumables, human and material resources, special tools, post maintenance testing, and start-up programmes.

13.3.3 Kick-off meeting

One month prior to the outage execution, the kick-off meeting takes place wherein a review of all documents presented in the previous meetings are required, as well as to review the file of LOTO request forms and part receipt inspections, to review operational data, to finalize the outage quality scorecard, to finalize the outage checklist and quality control forms, to review lessons learned and best practices, and to document meeting minutes.

13.3.4 Recording operational and maintenance data

Before starting the outage, a recording of the operational data provides a reference point for comparison before and after the outage (Table 13.3). The purpose of this meeting is data collection and evaluation on the current gas turbine operating conditions.

Operating data allow an evaluation of the equipment performance and maintenance requirements. Typical data include load, exhaust temperature, vibration, fuel flow and pressure, exhaust temperature control and variation, and start-up time.

As well there is a review of such operational indicators as reliability, availability, maintainability, durability and safety (RAMD-S).

13.3.5 Outage execution

To assure that the 'outage cycle' is within a safe, timely and successful execution it is necessary to set up a quality assurance programme (QAP) aimed at:

- Monitoring the process of the outage cycle.
- Establishing quality indicators (scorecard).
- Ensuring the inspection plan is known by all parties involved.
- Identifying early quality deviations of the maintenance plan.
- Implementing best practices and lessons learned.
- Gathering information for future improvements.

The outage starts by setting formal daily meetings to keep the staff informed of the status of the outage planning. The purposes of these meetings include

© Woodhead Publishing Limited, 2013

Table 13.3 Operational and maintenance data

Operational data
• Vibration analysis (steady state, start-up and shut-down, transient state, etc.).
• Performance assessment (heat rate, auxiliary consumption, trends of operational parameters during start-up and steady state condition, etc.).
• Fluid condition (lube oil, fuel analysis, air filtering system condition, etc.).
• Hot gas path analysis.
• Start-up and cost down trends.
• Dependability evaluation metrics (MTTR, MTBF, etc.).
• Maintenance factor evaluation metrics (fired hours, fired starts, etc.).
• Main events from last outage (trip evaluation, etc.).
• Outage report from the previous inspection.
• Etc.

daily monitoring and jointly checking the quality control programme, as well as determining any deviation from the initial schedule and performing the corrective actions needed, and reporting any event and safety incidents. These meetings must be attended by the plant management and key personnel.

Before the reassembly of the unit, a pre-assembly meeting is required, to perform a visual inspection of the gas turbine and its auxiliary equipment, in addition to the verification of clearances, alignment, balancing, etc.

The next step is the commissioning of gas turbine after the outage by a set of control checking and tests conducted for setting the turbine control system and data collection to assess the condition of the gas turbine after the outage.

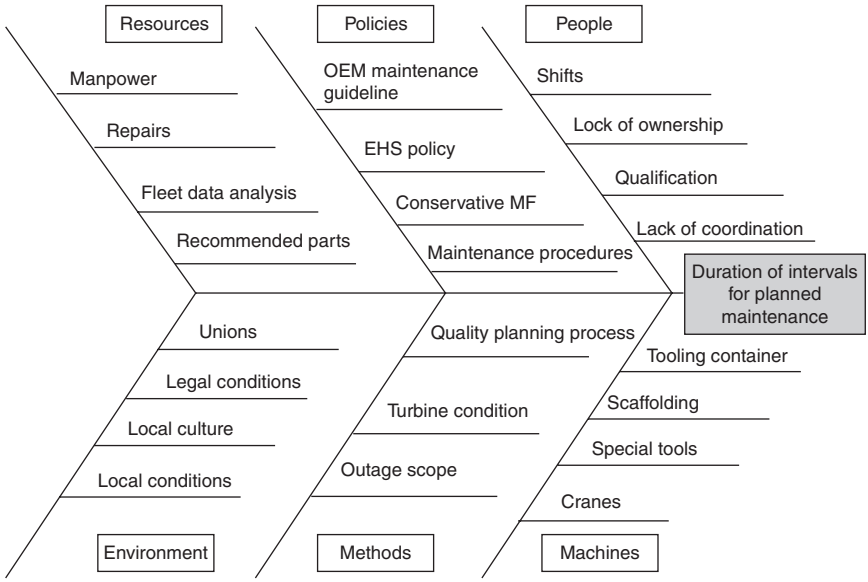
13.3.6 Post-outage review

After the conclusion of the outage, a review of all activities performed is essential to assess the work done and provide feedback to further optimize the next outages by:

- Recognizing key indicators of a successful outage.
- Gaining collective understanding of the outage plan quality programme.
- Gathering information to improve future performance.
- Focusing on key inputs to outage plan quality programme.
- Updating lessons learned and best practices.

Quality metrics is a ‘must’ in the post-outage review. It implies a revision of the scorecard set aimed at evaluating the outage duration/start, performance, safety, scope, QA/QC, etc. The post-outage review should consider the items mentioned in Table 13.4.

© Woodhead Publishing Limited, 2013



13.3 Fishbone analysis.

It is necessary to produce the outage report in one month, to provide timely feedback for the next outage. Another good practice is to arrange a meeting with the main players to discuss experiences and improvements. This post-outage assessment provides the basis for planning the next outage and optimizing the outage cycle.

On the other hand, analytical tools such as Fishbone Diagram (Fig. 13.3), Pareto Chart, process analysis, graphical analysis (Plots), hypothesis testing and regression analysis will help to visualize gaps for improvements.

13.4 Advanced component repair technology

Gas turbine components have a limited life under the OEM operating guidelines. During the maintenance cycle, owners and operators decide to use the component 'as is', repair the component, or replace the component. The damage has to be evaluated and the scope of repair has to be defined. The repair process is described below.

Advanced repair technology may include upgrades that will bring the part or component beyond its original capability. Financial benefits will follow when repair costs range from 10% to 30 % of the price of new components. This gives rise to a vigorous and aggressive aftermarket.

Gas turbine components are repaired by many processes that restore the metallurgical and dimensional properties of the component. The repair cycle

© Woodhead Publishing Limited, 2013

Table 13.4 Outage quality scorecard

Discussion points	Task	Definition	Plan	Metric		Comments
				On time (Y/N)	Quality (Y/N)	
Meetings	Outage kick-off meeting	Open issues Status Updates Schedule Goals	Date/time			
	Pre-outage safety meeting	Open issues Status Updates Schedule Goals	Date/time			
	Outage meetings	Open issues Status Updates Schedule Goals	Date/time			
	Pre-fire meeting	Open issues Status Updates Schedule Goals	Date/time			
	Post-outage meeting	Open issues Status Updates Schedule Goals	Date/time			
				On time (Y/N)		

© Woodhead Publishing Limited, 2013

Outage duration	Outage start agreement:	Conditions for outage start: LOTO completed	TBD		
	Outage end agreement:	Conditions for outage end: 72 h after unit released for LOTO clearance	TBD		
	Outage duration agreement	Time (hours/days)	TBD		
				Increased Work-Scope (Y/N)	
Scope	Variance to planned scope	Increased work items that should have been previously identified	Item tracking		
	Variance to extra work	Extra work added to original outage scope that was not previously identified	Track for lessons learned		
	Emergent work	Unplanned work found during outage with no prior lessons learned	Track for lessons learned		
				On-site and operational (Y/N)	
Outage schedule	Mobilization	Tooling	Date/time		
		Scaffolding Trailers Lighting Toilets			
				Arrived when required (Y/N)	Adequate heads (Y/N)
	Labour	Lead TA(s) Mechanical TA(s) Electrical TA(s) Craft labour	Date/time		
				On time (Y/N)	
	Disassembly	Disassembly milestone (casing removals, TP removal, etc.)	Date/time		

(*Continued*)

© Woodhead Publishing Limited, 2013

Table 13.4 Continued

Discussion points	Task	Definition	Plan	Metric		Comments
				On time (Y/N)	Quality (Y/N)	
	Reassembly	Reassembly milestone (mechanical completion, LOTO removed, etc.)	Date/time			
	Start-up	Unit fire	Date/time			
	Tuning	Post-outage unit re-tune	Date/time			
				Removed (Y/N)		
	De-mobilization	Tooling Scaffolding Trailers Lighting Toilets	Date/time			
				Satisfactory (Y/N)		
	General housekeeping	Pre-outage During outage Post-outage	Site condition			
				Event occurred (Y/N)		
Restart	Failure to start/ fire	Unscheduled failure to start/fire following outage completion	Non-occurrence			
	Trips	Any unit trips during restart (as measured by turbine controller logic)	Non-occurrence			
				Lower post-outage values (Y/N)		

© Woodhead Publishing Limited, 2013

Performance	Heat rate	Heat rate measurement (either per contract requirements or local measurements)	Value	
	Output	Output measurement (per contract requirements or local measurement)	Value	
				Increased post-outage emissions (Y/N)
	Emissions	Emission measurement (per contract requirements or local measurements (turbine or stack?)	CO, O_2, NO_x	
				Event occurred (Y/N)
Safety	Any recordable incidents	Recordable injury, lost time accident, permit violation, hazardous material spill, etc.	Non-occurrence	
	Near misses	Events which, if actually happened, could have resulted in EHS incident	Non-occurrence	
				Satisfied? (Y/N)
QA/QC	Were you satisfied with the QA/QC process that occurred during the outage	Indication of all equipment/material checks done	Item tracking	

(*Continued*)

© Woodhead Publishing Limited, 2013

Table 13.4 Continued

Discussion points	Task	Definition	Plan	Metric		Comments
				On time (Y/N)	Quality (Y/N)	
Final report out				On time (Y/N)	Quality (Y/N)	
	Closure report	Report complete and issued	Date/time			
				On time (Y/N)	Quality (Y/N)	
	Final report out meeting (30 days after outage completion)	Open issues Status Updates Schedule Goals	Date/time			
	Post-outage performance			Lower post-outage values (Y/N)		
	Heat rate	Heat rate measurement (either per contract requirements or local measurements)	Value			
	Output	Output measurement (per contract requirements or local measurement)	Value			
				Increased post-outage emissions (Y/N)		
	Emissions	Emission measurement (per contract requirements or local measurements (turbine or stack?)	CO, O_2, NO_x			
	Post-outage unit information			Event occurred (Y/N)		
	Rework	Any non-scheduled/planned post-outage rework	Non-occurrence			
	Trips	Any unit trips after restart (as measured by turbine controller logic)	Non-occurrence			

© Woodhead Publishing Limited, 2013

is part of a more complicated process, during which components receive a variety of actions in order to prepare them for the actual repair. The typical repair cycle of a gas turbine component is displayed in Fig. 13.4.

13.4.1 On-site assessment and inspection

Refurbishment of components begins with inspection and condition assessment at the plant before disassembly. The information compiled is helpful in selecting the repair and coating vendor, and developing the repair and bidding specifications.

Checking dimensions and damage mapping

On every removal of the turbine casing, the internal clearances should be verified. This will be compared to the unit's original clearance data so that a determination for corrective action, if any, can be made. The clearances should be taken and recorded on inspection forms (axial rotor clearances, axial seal clearances, rotor set dim, radial seal clearances, bucket tip clearance, shroud-to-bucket clearances, diaphragm radial seal clearances, etc.).

Hot section components are subject to deformations that change as-built clearances. This is especially true for unsupported components that are exposed to high temperatures and stresses, such as shrouded blades (buckets) and second-stage vane segments (also known as nozzles).

Nozzles are inspected for foreign object damage, erosion, corrosion, and cracks. Nozzles experience severe thermal gradients during starting, as well as high temperatures during loading operation. Such conditions frequently cause nozzle cracking and, in fact, cracking is expected.

Buckets or blades are inspected for cracks, dents, missing metal, wear, and corrosion. Each time the upper-half shell is removed, the turbine buckets should be carefully examined. Such examination can reduce the risk of major damage from the failure of a previously damaged bucket. At the same time, judgement is necessary to avoid replacement of adequate buckets.

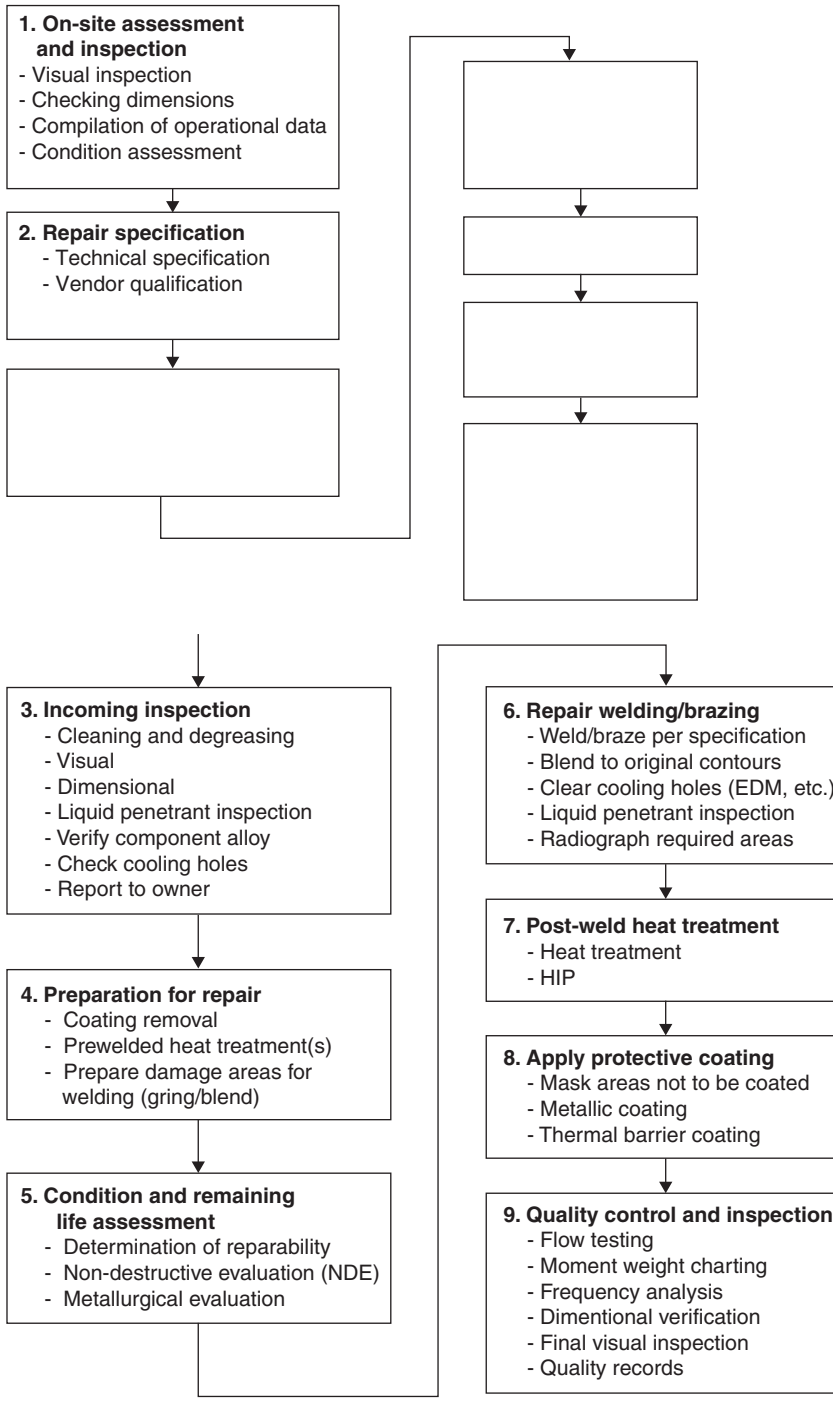
The results of inspections should be documented, along with the relative information on unit operation and fuels.

The information compiled also is valuable in the verification of dimensions taken during the repair vendor's incoming inspection, as well as damage evaluation, and mapping is important to define and validate the required repair process.

Condition-based maintenance (CBM)

Advanced repair and rejuvenation are processes undertaken to extend the useful life of a component. Repairs can be thought of as 'external' processes

© Woodhead Publishing Limited, 2013



13.4 Repair process (part 1, top). Repair process (part 2, bottom).

© Woodhead Publishing Limited, 2013

that return the component to its original size and shape, or replace the protective coating. Rejuvenation can be defined as the regeneration of a microstructure leading to the restoration of mechanical properties equivalent to those of the original component prior to initial service. These reconditioning technologies, together with the condition assessment and life assessment of components, will give way to a new vision of gas turbine asset and performance management.

On-line condition monitoring allows the continuous or periodic measurement and interpretation of operational data to indicate the condition of a component to determine the need for maintenance. Off-line inspection techniques allow (i.e. advanced non-destructive evaluation methods) non-destructive degradation assessment of hot gas path component coatings and base materials. This information constitutes the starting point for developing and tuning methods for predicting the life of critical high-temperature components of gas turbine.

This is the basis of CBM, which is defined as preventive maintenance which should be initiated as a result of knowledge of the condition on an item from routine and continuous monitoring. CBM based upon non-destructive flaw evaluation and fracture mechanics arises as a way of promoting lifetime extension and maintenance cost reduction.

13.4.2 Repair specification and vendor qualification

The assessment and selection of potential vendors to refurbish parts should take into account the customized scorecard with the specific requirements of the end users. At least, it should cover the evaluation of experience and reputation, the quality plan, in-house and subcontractor technical capabilities, and management systems. The next step is to define the repair specification, which has to cover the minimum requirements for the weld and heat treatment of turbine buckets, nozzles and combustion hardware, conditioning of contact surfaces to minimize wear, and the application of thermal barrier and metallic coating.

The flowchart (Fig. 13.4) lists some items to be included. Information compiled during visual inspection and checking of clearances is key to preparing the specification. To ensure quality work, it is important to divide the repair process and the specification into logical stages. Visits for verification should take place at different times along repair cycle[5]:

- Incoming inspection is the best time to verify the severity of the damage, agree the repair work-scope and cost, or make a decision to replace badly worm parts rather than repair them.
- Intermediate inspections along the repair cycle are also essential to assure the final result. The repair facility has to report its findings and

© Woodhead Publishing Limited, 2013

recommendations after each stage and not proceed with the work before the operator and/or its representative approves. The four main stages are:
  – Receive and conduct the initial inspection.
  – Disassemble components, clean/strip, heat treat, and inspect.
  – Repair, heat treat, and inspect.
  – Coat, reassemble, and make a final inspection.
- Final Inspections should take place after all repairs are complete, but before the parts are covered with protective oils or put in boxes.

13.4.3 Incoming inspection

The goal of the incoming inspections is to decide disposition for the repair/Scrap/Replace sub-parts/Heat Treat and Hot Isostatic Pressing (HIP):

- Visual – record results on damage forms.
- Dimensional – record results on dim forms.
- Cut samples (nozzle and buckets) and perform metallography analysis.
- Grit blast/clean parts.
- Incoming LPT or Fluor penetrant inspection (FPI) adds results to damage forms.

Dimensional integrity of all components should be checked as part of the detailed incoming inspection when the unit arrives at the repair shop. Typical dimensions to be checked are cooling-hole passages, cavity and wall thicknesses, distortion, downstream deflection, critical throats and pitches, and machining assembly tolerances. These dimensions should be compared to the 'as-new condition', the measured differences and deviations recorded, and the measurements evaluated with respect to allowable tolerances. As with internal damage, major loss of dimensional integrity may lead to a component becoming physically or economically unrepairable. On the other hand, it is important for operators to assess and evaluate the extent or level of damage to their components.

Cleaning and degreasing

Cleaning is required to allow proper inspection and repair process application. It is required prior to penetrant inspections to remove corrosion/erosion damage, heat treatments and welding or brazing process, to improve surface finish and remove excess weld and brace material.

Important factors in selecting a cleaning method for the repair process are the contaminant to be removed, the degree of cleanliness required, the substrate material to be cleaned, the purpose of the cleaning, environmental and safety factors, the size and geometry of the part, and production

© Woodhead Publishing Limited, 2013

and cost requirements. Chemical and/or mechanical processes are used to accomplish this cleaning. As part of the cleaning process, degreasing is required, and it is normally accomplished with solvents, or vapour, which uses less solvent and is most widely used.

Chemical cleaning processes

The most common processes used are[6]:

- Alkaline cleaning.
- Emulsion cleaning.
- Solvent cleaning.
- Acid cleaning.
- Ultrasonic cleaning.

Alkaline cleaning

An alkali can remove oils, grease, wax, and various types of particles (metal chips, silica, and light scale) from a metallic surface. It is a widely used industrial cleaning method. Alkaline solutions include sodium and potassium hydroxide (NaOH, KOH), sodium carbonate (Na_2CO_3) and borax ($Na_2B_4O_7$). The most common cleaning methods used are immersion or spraying, usually at temperatures of 50–95°C (120–200°F), followed by water rinsing to remove residue.

Acid cleaning

Acid, in the form of acid solutions combined with water-miscible solvents, and wetting and emulsifying agents, removes oils and light oxides from metal surfaces. Common application techniques are soaking, spraying, and manual brushing or wiping carried out at ambient or elevated temperatures. Cleaning acids include hydrochloric (HCl), nitric (HNO_3), phosphoric (H_3PO_4), and sulphuric (H_2SO_4).

Mechanical cleaning and surface preparation

This process consists in the physical removal of soils, scales, or films from the work surface by means of abrasives or similar mechanical action (fibre brushing). It often serves other functions, such as improving surface finish, and surface hardening. There are different types of mechanical surface cleaning techniques, the most common in use being:

- Abrasive blast cleaning.
- Manual grinding.
- Shot peening.

© Woodhead Publishing Limited, 2013

Abrasive blast cleaning

A surface is bombarded with abrasive particles propelled at high velocity by air, water, or centrifugal force. The effects of blasting are influenced by the type, hardness, particle size, velocity, and angle of impact of the abrasive. Blasting is a rapid method of removing rust and mill scale. The most well-known method is sand blasting, which uses sand grits as the blasting media. Other blasting media include hard abrasives such as aluminium oxide (Al_2O_3) and soft media such as nylon beads. The selection of the type and size of the blast cleaning material will depend on the size and shape of the parts to be cleaned, the finish desired, and the treatment or operation that may follow blast cleaning.

Shot peening

A high-velocity stream of small cast-steel pellets (called shot) is directed at a metallic surface to cold work and to induce compressive stresses into surface layers. Used primarily to improve the fatigue strength of metal parts. The purpose is therefore different from blast finishing, although surface cleaning is accomplished as a by-product of the operation.

Specialized cleaning processes

Several processes are used for the more aggressive cleaning required to remove oxides from surfaces:

- Salt bath cleaning.
- Heat treating in hydrogen or vacuum.
- Thermo-chemical processes.

These processes are specialized and are generally used prior to brazing.

13.4.4 Preparation for repair: coating removal

Most of the coating is generally removed by chemical stripping. Then the external surface can be inspected by heat tinting or macro-etching, so that any remaining coating and oxidation/corrosion products can be identified and eliminated by blending. It is important to specify tight control on stripping/cleaning processes to avoid unnecessary thinning of the component. Preparation of components should include standard pre-weld solution for nickel precipitation and cobalt-based superalloys. Occasionally, metallurgical evaluation also suggests the need for specialized heat treatment.

Both topcoat and bondcoat have to be properly removed. Remnants of old coating with oxides, corrosion products, porosity, and active element depleted zone do not allow good adhesion between the new coating and the substrate.[7]

© Woodhead Publishing Limited, 2013

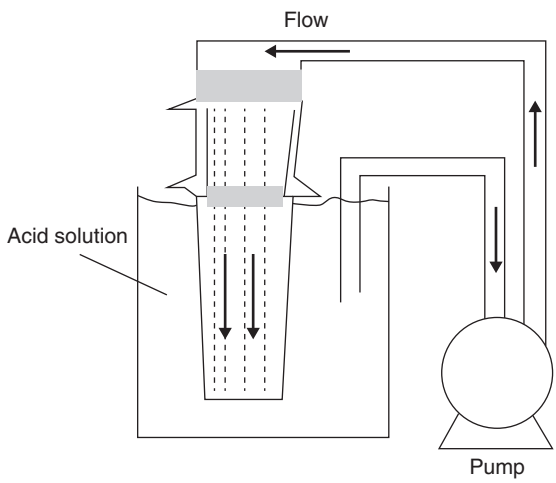
Removal of ceramic coatings

A number of processes have been evaluated for removal of ceramic coatings based on yttria stabilized zirconia (YSZ) composition. The ceramic layer of TBCs is removed by abrasive blasting and mechanical grinding is typically used to remove coatings in isolated areas not stripped in the chemical cycle. A high-pressure water jet without abrasive grits has also been successfully used to remove the ceramic coating of TBCs.[8,10]

Removal of metallic coatings

The problem of stripping MCrAlY coatings is that there are many different types in use. The standard procedure to remove MCrAlY coatings is removing the remaining aluminium-rich phase by etching and subsequent removal of the remaining coating skeleton by grinding. The complex shape of gas turbine blades and vanes means that a surprisingly large portion of the stripping process is just hand labour. Stripping internal cooling passage coatings (diffusion aluminides are used) on rotating blades has been a continuing challenge to the repair industry for many years. No stripping is required, but the surfaces must be clean.

A modern chemical stripping process (Fig. 13.5) must be able to flow the hot solution in a controlled manner through the internal cooling passages, in order to remove any internal coatings while simultaneously stripping the thicker external coatings. Special care must be taken to prevent chemical attack (IGA) on the critical blade root surfaces and inside internal cavities.



13.5 Schematic of stripping process.[9]

© Woodhead Publishing Limited, 2013

Verification of coating removal

There are two common ways to check for coating removal:

1. Abrasive blast clean and re-immersion in fresh acid (acid etch). Areas with residual coating turn black.
2. Heat tinting – parts are heated to 450–650°C in an air furnace. Colour differences occur between stripped areas and areas with residual coating.

For TBC-coated components, complete ceramic coating removal is generally ascertained by visual inspection. Once the old coating is removed, and the component is cleaned and conditioned properly, a new coating can be deposited.

13.4.5 Condition and remaining life assessment

Reconditioning scope is defined by operation (component loads and stresses, operating condition and history), design features (upgrade and improvement feasibility), base material and coating condition, component geometry (dimensional check, assembly check), repair allowances (repair limits), reconditioning experience and statistical data, capability of repair processes and economic aspects (reconditioning cost vs new part cost for the part remaining life).

To perform the condition evaluation to determine reparability and subsequently the lifetime assessment, a combination of non-destructive evaluation (NDE) and material evaluations is needed (see section metallurgical evaluation). Generally the lifetime assessment is divided into two broader categories based on the components and their service conditions.

1. Condition assessment.
2. Remaining lifetime assessment.

Condition assessment may be sufficient for components that operate at lower temperatures, or smaller components that are more readily replaceable (wear items). Other components may require a remaining lifetime estimate. This is estimated by a combination of NDE testing, materials inspection, and engineering analyses (computational methods) in conjunction with operational data. The continuous improvement of inspection techniques has moved the repair limits without jeopardizing integrity. Advanced repair procedures require multiple inspections during the repair cycle, as well as after completion of the repair, to assure a high quality standard.

Inspection and evaluation include the assessment of mechanical damage, surface degradation, microstructural deterioration, and creep damage. Mechanical damage is generally detected by non-destructive testing

© Woodhead Publishing Limited, 2013

techniques, while the rest of the damage is best detected by destructive examination. As a general guideline provided by ASM, the process is made up of the following different steps[11]:

1. Establish evaluation intervals based on the design life and service history of the blade.
2. Conduct NDE continuously monitoring turbine operation, and a rigorous inspection programme to periodically check for cracks by NDE and microstructural damage by microscopic examination of the surface material. Various NDE methods for inspection are discussed in the next sections.
3. Conduct destructive evaluation. Many life-limiting characteristics cannot be assessed just by NDE.

There are various methods available to determine blade life under a specified failure mode, that is, creep, high-cycle fatigue, low-cycle fatigue, TMF, and so on. Some of the techniques widely used are[11]:

- Qualification testing using the same tests used to qualify lots of new material. A pass/fail indication of serviceability is provided rather than a remaining life estimate. The same parameters used to qualify new material should be used. Blades that are returned to service should be re-examined at a determined percentage of the design life of the blade.
- Life fraction rule: remaining life is determined by comparing stress-rupture properties of new material with those obtained after service exposure. A conservative estimate of service stress and higher-than-service temperature should be used.
- Parameter-based approaches: these methods are based on a creep-property database developed by testing several specimens to obtain data from both long- and short-term tests. Two such methods that are widely used are the Larson-Miller parameter (Fig. 13.6) and the Monkmon-Grant parameter.

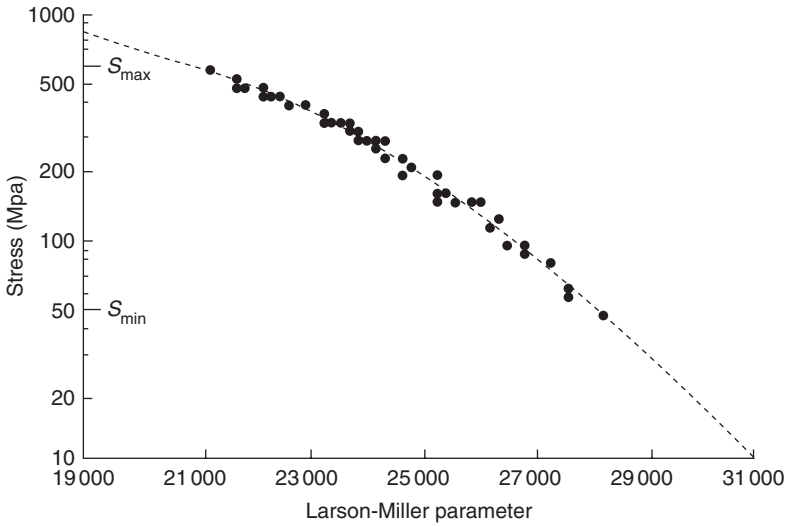
When trying to predict remaining life, the test should be carried out at conditions close to service conditions.

Determination of reparability

Basically, there are three types of damage to gas turbine rotating and stationary components[12]:

1. External physical damage.
2. Internal base material microstructural damage.
3. Loss of dimensional integrity.

© Woodhead Publishing Limited, 2013



13.6 Long-term creep prediction using the Larson-Miller time-temperature parameter for IN 738 alloy.[11]

External damage includes cracks (most often caused by low-cycle fatigue), surface oxidation/corrosion, foreign object damage (FOD), gas path erosion and fretting. This type of damage can generally be detected by good visual and liquid penetrant inspection. Repairs usually consist of grinding out defects, welding, blending and occasionally brazing. Coating loss can also be detected by good visual inspection and by heat tinting.

Internal microstructural damage consists of carbide precipitation along grain boundaries, changes in gamma prime, grain size and structure for nickel-based alloys, subsurface depletion, internal cooling-hole corrosion and others. Normally, the best means to detect this type of damage is to destructively remove pieces or section parts. After proper preparation, a superalloy experienced metallurgist should view samples microstructurally on optical and electron imaging microscopes at magnifications of 100× to 5000×. This type of damage or deterioration can be corrected with rejuvenating heat treatments. In many cases the component will require a physical repair for the external damage and an internal repair/rejuvenation for the microstructural damage. With newer units operating at much higher firing temperatures, and utilizing coatings more often, metallurgical evaluation has become a necessity, especially on turbine rotating blades/buckets.

Damage severity is usually divided into the following three categories[12]:

1. Minor: small cracks and FOD covering less than 10% of the part, usually repairable without heat treatments, recoating or much dimensional restoration.

© Woodhead Publishing Limited, 2013

2. Medium: large cracks 1/2 to l-inch long, corrosion and FOD covering up to 30% of the part, requiring weld repairs, reheat treatment, dimensional restoration and recoating. Seals and other consumable component pieces may also need replacement.
3. Major: heavy or extensive cracking, FOD, surface attack and wall thickness loss over more than 30% of the part. Normal weld repairs will not effectively repair the part. New exit/entry pieces, couponing, wall thickness build-up by superalloy overlaying and other special repair techniques will be required.

If component damage falls into the major category, consideration should be given to replacing the part with a new or a used/refurbished component.

Operating conditions

Start-up and shut-down cause substantial degradation and often damage, despite the use of superalloys and dedicated high-temperature coatings. This damage is often caused by a combination of factors that, by themselves, would not necessarily cause a problem.

The high-temperature strength of superalloys is based on a stable face-centred cubic (fcc) matrix combined with either precipitation strengthening (age-hardenable) and/or solid-solution hardening. In age-hardenable nickel-based alloys, the γ' intermetallic (Ni_3, Al,Ti) is generally present for strengthening, while the non-hardenable nickel-, cobalt-, and iron-based alloys rely on solid-solution strengthening of the fcc (γ) matrix. Cobalt-based superalloys may develop some precipitation strengthening from carbides (Cr_7C_3, $M_{23}C_6$), but no intermetallic phase strengthening equal to γ' strengthening in nickel-base alloys has been discovered in cobalt-based superalloys.[13]

The environment of a gas turbine blade contains oxygen and other elements, such as sulphur, that react readily with metals at operating temperatures. Hot corrosion is a severely accelerated form of environmental attack, which occurs by a combination of oxidation and sulphidation in contaminated operating environments. The most common contaminants, which lead to hot corrosion, are sodium and sulphur. However, other metallic impurities, such as potassium, vanadium, lead, and molybdenum, can lead to accelerated attack. Two distinct hot corrosion mechanisms have been recognized: Type 1 hot corrosion occurs between 800°C and 925°C (1470°F and 1700°F), while Type 2 hot corrosion occurs between 600°C and 750°C (1110°F and 1380°F). In both cases, the protective oxide layer is melted by a fluxing reaction, allowing greatly accelerated oxidation and sulphidation to occur.

Two generic coating types are used for blade protection: diffusion coatings and overlay coatings. Both result in a surface layer enriched in

© Woodhead Publishing Limited, 2013

oxide-forming elements to promote formation of a protective oxide layer. However, the protective coatings themselves are subject to degradation under engine operating conditions and thus have limited lives.

Degradation during operation

Material degradation is characterized by microstructural ageing and subsequent loss of creep strength. Material degradation occurs in turbine hot section components that run for long periods of time at high temperature and stress conditions.

Service damage is the time-dependent effect of 'ageing' and 'creep'. Ageing is metallurgical degradation resulting from increased diffusion of alloying elements at high service temperatures. Ageing in nickel-based superalloys is typified by coarsening of the strengthening gamma prime (γ') precipitates (with high operating temperatures stimulating the motion and diffusion of atoms within the alloy, diffusion results in precipitate coarsening, coalescing and rafting), carbide degeneration (during service at elevated temperature, MC carbides dissolve into the matrix and convert into $M_{23}C_6$ carbides enveloped in γ'), grain-boundary coarsening and the formation of undesirable topologically close packed (TCP) phases (several low ductility intermetallic phases having similar crystallographic structures).[14] While ageing is largely a temperature-related phenomenon, creep is a response to the loads acting on the parts, and is typified by slow diffusion-driven strains.

Since the root of a turbine blade is located farthest from the hot gas path, ageing should be slowest in this section and hence a section of the root can be examined and deemed to be representative of the pristine/as-manufactured microstructure. Aged microstructures can generally be identified by larger rounder primary γ' and limited, or no, secondary particles.

The rejuvenation process involves taking the alloy up to a temperature where both primary and secondary γ' dissolve into the austenite matrix and subsequent ageing at lower temperatures to re-precipitate the γ' into the desired morphology as explained in section heat treating and HIPping. Effective rejuvenation heat treatments must also employ cooling rates that create an optimal grain-boundary morphology for creep properties. Similar results have been achieved for a wide variety of other superalloys (Table 13.5). Rejuvenation heat treatments have been successfully used to restore the aged γ' microstructures of the alloys and have allowed components that would otherwise have been retired, to be returned to service.

The principal degradation mechanisms for coatings are the same environmental mechanisms that affect uncoated superalloys. Hot corrosion and oxidation attack occur on coated components and with the same general

© Woodhead Publishing Limited, 2013

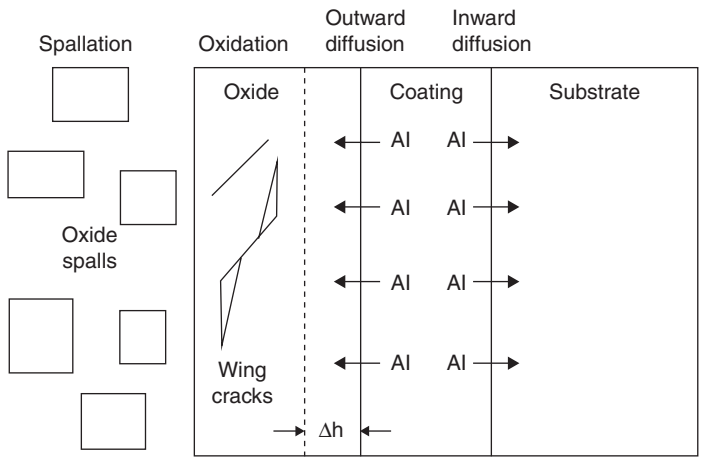
Table 13.5 Superalloy rejuvenation[14]

Alloy	Component
310 SS	RT45 2nd stg NGV, compressor airfoils
A286	Turbo-expander blades
C1023	Avon Vanes
FSX 414	CAES stage 4 vane, GE Industrial Stage 1 Vanes
GTD 111/GTD 111DS	GE Industrial Frame Stage 1 Blades, NP PGT HP blades
GTD 222	GE Industrial Frame Stage 2 Vanes
Hastelloy X	Combustion hardware
IN617	Combustion hardware
IN700	DR DJ290R, Siemens W501AA, W101, W191
IN738	Alstom 11N2, ELM116, GE Industrial Frame Blades GE LM1600, NP PGT LPT blades, RR Avon, RR Olympus HPT, Ruston Tornado CT2, Siemens EM610, Siemens V84.2, Siemens V94.2, Siemens W251, Siemens W501-D5A, Siemens W501F, TB5000 CT2, TB5400 CT2,
IN792	RR Avon, RR RB211
IN939	DR DJ270G, Ruston Tornado CT1, Siemens V84.2, DC990, Siemens V series vanes
Mar M002	RR RB211, RR Spey HP2
Mar M247	W501F, Allison 501K, Solar
N 155	BB
Nimonic 105	RR Avon, RR Spey
Nimonic 115	RR Avon
Nimonic 263	Combustion hardware
Nimonic 80a	Alstom EAS-1 PT, AEI AP1 PT, RR Spey LP2
Rene 80	Siemens V84.3A1, GE LM1600, GE LM2500
Udimet 500/Udimet 500 forged	GE Industrial Frame Stage 3 Blades, RT45 stg 2, NP PGT10, NP PGT16 LPT blades
Udimet 520	MHI 701D, Siemens W501-D5A, W101, W191
X45	Turbine Vanes
X-750	W101, W191, and legacy Westinghouse engines
Other Alloys	416 SS, C242 (Nimocast 242), C6Y Alloy, M252, Nimonic 108, Nimonic 90, Rene 77, S590

features as on uncoated blades. Although the resistance of coatings to attack is higher than for uncoated superalloys, coatings are often employed under very severe conditions of temperature or contamination. The coatings, therefore, have a limited life, after which the base metal is exposed, and accelerated attack can occur.

Gas turbine blades are generally coated with overlay (MCrAlY) or diffusion coatings (plain aluminide or platinum aluminide) to improve the oxidation and hot corrosion resistance. The effectiveness of the coating deteriorates with time after exposure to high temperature and repeated heat-up during start of the engine and cool-down during the engine shut-down cycle. The active element that provides the protection on the outer surface of the

© Woodhead Publishing Limited, 2013



13.7 Schematic of the degradation mechanisms.[11]

coating is aluminium, which forms a protective aluminium oxide, that is, alumina layer. When the aluminium is depleted during service exposure, the coating loses its ability to protect the substrate, because it loses its ability to form and maintain a continuous alumina layer. This leads to breaching of the coating by the environment. The loss of aluminium occurs by three mechanisms: oxidation, oxide fracture and spallation, and inward diffusion. A schematic diagram of these mechanisms is shown in Fig. 13.7.

Non-destructive evaluation (NDE)

Non-destructive testing (NDT) and NDE involve the use of non-invasive measurement techniques to gain information about defects and various properties of materials, components and structures, information that is needed to determine their ability to perform their intended function and to prevent failure.[11]

Many measurement techniques are employed in NDE. Those most widely used are visual, liquid penetrant, magnetic particle, eddy current, ultrasonic and radiographic testing. Table 13.6 shows that FPI is the most user-friendly and cheapest method to detect surface cracks.

Visual Inspection

Visual Inspection is an NDT technique that provides a means of detecting and examining a variety of surface flaws, such as corrosion, contamination, surface finish, and surface discontinuities. It is widely used for detecting and examining surface cracks, which are particularly important because of their relationship to structural failure mechanisms.[16]

© Woodhead Publishing Limited, 2013

Table 13.6 NDE methods[15]

	X-ray	Ultrasonic	Eddy current	FPI	MPI
Material	All	Many	Many	All	Ferromagnetic surface
Material flaw	Internal and surface	Internal and surface	Internal and surface	Surface cracks	Surface cracks
Flaw size	1% mat. thickness	Very small	Very small	Small	Very small
Test-piece shape	Arbitrary	Not to irregular	Not to irregular	Arbitrary	Arbitrary
Exp. Level req.	High	High	High	Limited	Limited
Costs	High	High	High	Low	Medium
Documentation	Direct	Indirect	Indirect	Direct	Direct

Liquid penetrant inspection

Liquid penetrant inspection is a non-destructive method of revealing discontinuities that are open to the surfaces of solid and essentially non-porous materials. Indications of a wide spectrum of flaw sizes can be found regardless of the configuration of the workpiece, and regardless of flaw orientations. Liquid penetrants seep into various types of minute surface openings by capillary action. Because of this, the process is well suited to the detection of all types of surface cracks, laps, porosity, shrinkage areas, laminations and similar discontinuities. It is extensively used for the inspection of wrought and cast products (Fig. 13.8).

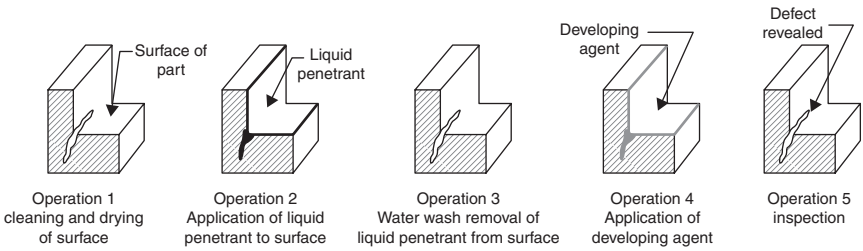
FPI is typically used only for rotating blades. Larger parts, vanes and combustion parts are typically inspected by LPT. The main limitation of liquid and fluorescent penetrant inspections is that they can only detect defects that break the surface and have some volume to hold the penetrant. They cannot detect cracks that are filled with oxides, or internal weld cracks, and sensitivity varies with the type of defect and surface condition.

Eddy current inspection

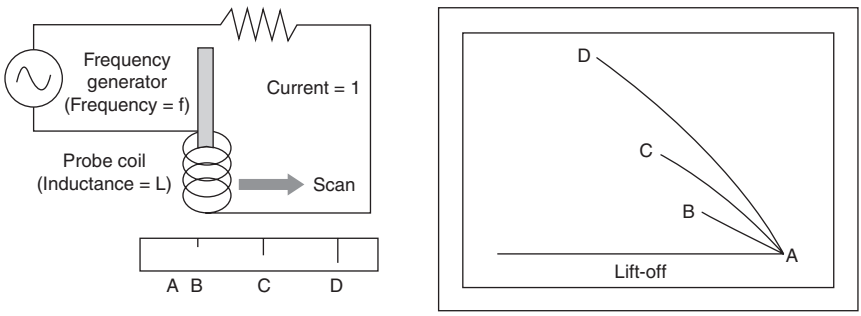
Eddy current inspection is based on the principles of electromagnetic induction and is used to identify or differentiate among a wide variety of physical, structural, and metallurgical conditions in electrically conductive ferromagnetic and non-ferromagnetic metals and metal parts.

The eddy current technique can detect cracks below the surface. When an alternating current is directed through a coil a magnetic field is generated. When the coil is positioned above a test-piece this magnetic field generates a current in this test-piece (see Fig. 13.9).

© Woodhead Publishing Limited, 2013



13.8 Visual inspection.[16]



13.9 Eddy current inspection.[15]

The main applications of eddy current inspections are:

- Crack detection.
- Coating thickness measurements and differences.
- Wall thickness measurements (thin materials).
- Material condition (hardened, heat treated).

and limitations:

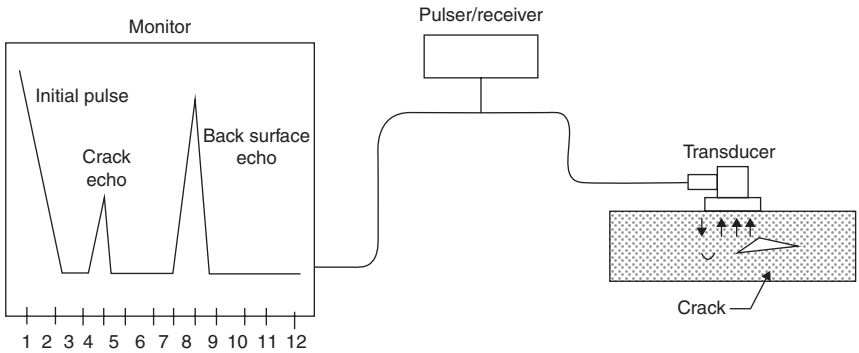
- Limited depth of penetration.
- Interpretation of results.
- Expensive inspection method.

Ultrasonic inspection

Ultrasonic inspection is a non-destructive method in which beams of high-frequency sound waves are introduced into materials for the detection of surface and subsurface flaws in the material.

Cracks, laminations, shrinkage cavities, bursts, flakes, pores, disbonds, and other discontinuities that produce reflective interfaces can be easily detected.

© Woodhead Publishing Limited, 2013



13.10 Ultrasonic inspection.[17]

Inclusions and other inhomogeneities can also be detected by causing partial reflection or scattering of the ultrasonic waves or by producing some other detectable effect on the ultrasonic waves.[16] Most ultrasonic inspection is done at frequencies between 0.1 and 25 MHz. Figure 13.10 shows the principle of ultrasonic inspection.

The main applications of ultrasonic inspection are[15]:

- Wall thickness measurement.
- Detection of flaw, cracks, inclusions, porosity.
- Delaminations of different materials.

and limitations:

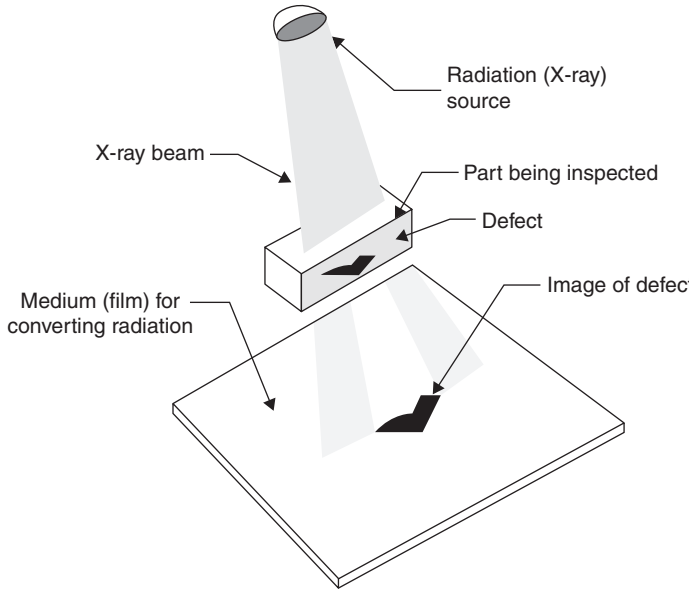
- Size of cavity.
- Orientation of cavity (cracks).
- Sound reflections from grain boundaries.
- Skill and training – more than some methods.
- Rough surfaces, small or thin parts and non-homogeneous materials difficult to inspect.

Radiographic inspection

Three basic elements of radiography include a radiation source, the test-piece or object being evaluated, and a sensing material. These are shown schematically in Fig. 13.11.

In general, radiography can detect only those features that have an appreciable thickness in a direction parallel to the radiation beam. In general, features that exhibit a 1% or more difference in absorption compared to the surrounding material can be detected. Radiographic inspection can be used

© Woodhead Publishing Limited, 2013



13.11 Radiographic inspection.[16]

for a number of different purposes in the gas turbine repair process, such as checking internal crack formation, cooling-hole clearance or connections, etc. In comparison to other generally used non-destructive methods, radiography has three main advantages[16]:

1. The ability to detect internal flaws.
2. The ability to detect significant variations in composition.
3. Permanent recording of raw inspection data.

The most common applications in the gas turbine repair process are to check on internal crack formation and on cooling-hole clearance or connections. The main limitations are:

- Penetration depth (power of X-ray).
- Resolution of image (cracks).
- Orientation of defects.

Thermography inspection

Active thermography as an inspection method comprises all techniques which heat a part specifically to induce a heat flow in the component to be tested. This heat flow also affects the surface temperature, which can be measured in non-contacting way by looking at the emitted thermal radiation with an infrared camera sensitive to this radiation.

© Woodhead Publishing Limited, 2013

The main applications of thermography inspection are inspection for delaminated coating, surface and subsurface defects, blocked cooling holes and thin wall thickness.

And the main advantages are:

- The non-contacting detection simplifies automating the measurement procedure.
- The imaging detection with the infrared camera provides not only the measurement at a single spot but a complete thickness map.
- The heat flow initiated by uniformly heating an area of the surface always traverses the material perpendicular to the surface. So the measurement can be done even if the surface is tilted with respect to the sensor. Thermography is therefore particularly useful for curved surfaces, such as the airfoil of a blade.

and its limitations are:

- Technology not yet well established for all applications.
- Interpretation depends on experience and destructive comparison.

Dimensional inspection

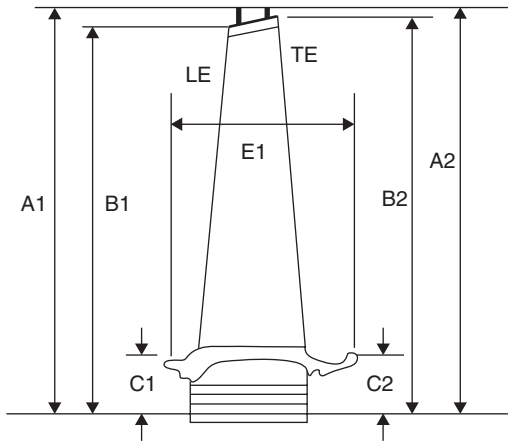
Critical dimensions must be closely controlled to ensure proper fit and function (Fig. 13.12). In general, these are surfaces that mate with, have a close tolerance with, or seal against other turbine surfaces, such as diameters, axial and radial locations with respect to reference machined surfaces, angles, blade tip height and seal surfaces, vane throat openings, etc. Measurement techniques commonly used are conventional instruments (micrometers, callipers, swing gages, dial indicators, etc.), coordinate measuring machines (CMM), checking fixtures (IN or OUT of Tolerance), mock-ups of mating/supporting parts (vanes and combustion parts), etc. Reference dimensions are difficult to obtain; some information is available in instruction manuals or OEM inspection sheets. Customized fixturing is required for each component to ensure a proper fit of a set of components.

Metallurgical evaluation

NDE can provide information on the effect of service on component integrity. However, many life-limiting material characteristics cannot be assessed by such techniques. Destructive analysis is often the only reliable and accurate means to obtain details from critical features beneath the surface that restrict component performance. Destructive investigations therefore play a central role in assessing the component set integrity.

Destructive analyses obtain fundamental information to determine the necessary repair work-scope. Selecting the appropriate rejuvenation programme

© Woodhead Publishing Limited, 2013



13.12 Overall dimensions on a shrouded blade.

optimizes component life extension and gas turbine efficiency. Furthermore the information gathered during a destructive analysis can be studied together with the gas turbine running conditions to identify the critical operating parameters. The main benefits of destructive analysis[18] are that it:

- Establishes possible sources of contamination from chemical characterization of corrosion products.
- Determines the most effective repair work-scope by characterizing the internal cooling-hole microstructure, which often differs from the behaviour of the external material.
- Correlates component service temperature from both gamma prime coarsening and diffusion zone growth.
- Prevents blending of sound base material by establishing crack location, frequency and penetration.
- Minimizes cost associated with non-value added work by identifying irreparable components early in the rejuvenation programme.

The test-piece is usually analysed for three main reasons: to determine and define the material and the coating composition, and to assess the condition of the microstructure of base material. There are a variety of materials investigation techniques that applies for the lifetime assessments. Material investigation can include one or more of the following:

- Replica of structure.
- Hardness test.
- Mechanical properties.
- Chemical composition.

© Woodhead Publishing Limited, 2013

- Metallographic inspection.
- Material sampling.

Replication method

A surface replica is an impression of the surface. There are many process variables for replication. The degree of etching is an important parameter. Other important variables are the material of the primary replica and the method of observation transmission electron microscopy (TEM) or scanning electron microscopy (SEM). Single-stage replication is a relatively simple technique, very suited for the non-destructive microstructural investigation of service exposed gas turbine blades.[19]

Hardness test

The hardness of any material reduces as it undergoes different degradation modes caused by creep-fatigue as a result of high-temperature exposure for a long period of time and high stress condition during start-ups and shutdowns. The hardness of materials changes with ageing time, temperature and stress, and as a result hardness decreases with exposure to creep.

Mechanical properties

In some cases a piece of material is extracted from the turbine component to check mechanical properties such as yield strength, ultimate tensile strength, elongation, fracture toughness, etc. This data helps in estimating the remaining life of the component/material.

Stress-rupture tests are high temperature, constant load tensile tests used to quantify creep strength. The rupture life of a material provides comparative information on the extent of material degradation it has undergone.

Chemical composition

Material information is key for a lifetime assessment. If not available, a different method is needed, for example the non-destructive (XRF) and the destructive method.

Material sampling (SPT)

If structural integrity of the component is really important and a real specimen is necessary, sometime a thin layer of material (scoop) is removed to perform the assessment in the laboratory environment.

The small punch test (SPT) method is an innovative technique that has the potential for residual life assessment of components in service. The main tasks of the technique are to derive standard material properties with

© Woodhead Publishing Limited, 2013

limited amount of materials, including strength/toughness, creep and fatigue behaviour.

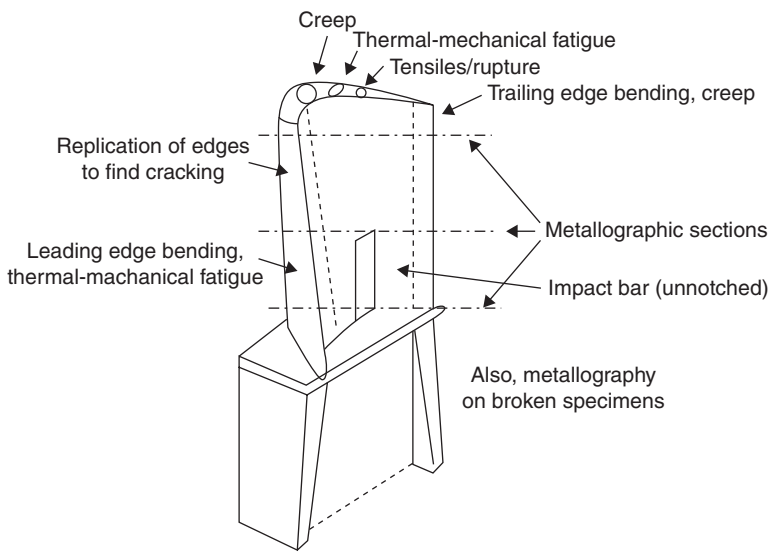
Metallographic inspections

Material degradation can be quantified through microscopic examination and mechanical testing. Optical microscopy and SEM are used to evaluate the morphology of the material microstructure.

Light microscopes are extensively used to assess the nature of the microstructure and its condition, with two objectives. The first is to determine the relationship between the microstructure and the nature of corrosion or wear damage. The second is to determine whether processing or service conditions have produced undesirable microstructural conditions that have contributed to the failure, such as abnormalities due to material quality, fabrication, heat treatment and service conditions.

Detailed observation of the fracture surface is best accomplished by use of SEM, or by examination of replicas with TEM. SEM is one of the most versatile methods for investigating the microstructure of metallic materials. Compared to the optical (light) microscope, it expands the resolution range by more than one order of magnitude to approximately 10 nm (l00 Å) in routine instruments, with ultimate values below 3 nm (30 Å).[20]

Metallographic inspection requires location selection and sample preparation for the optical microscope inspection. The most critical areas are the root, blade tip and trailing and leading edges. Platform is also becoming critical. Figure 13.13 shows different locations at:



13.13 Selection of blade areas for metallographic examination.[11]

© Woodhead Publishing Limited, 2013

- Airfoil locations with extensive damage, including cooling passage oxidation.
- Blade root, much cooler – microstructure is 'like new' used as a reference.

Computational methods

Engineering analysis is performed on major components subject to high temperatures and stresses to estimate remaining life. Steady and non-steady state turbine operational data are used for lifetime analysis. Creep acts in steady state, while thermal cyclic stresses result from transient operations. These combined stresses, responsible for low-cycle fatigue, are the principal degradation mechanisms that can lead to crack initiation and growth. The critical factors for a meaningful component analysis are the basic design data and appropriate boundary conditions like thermal convection and radiation, mechanical restrains or contacts during operation.

Thus finite element analysis (FEA) can be applied to obtain solutions to a variety of problems, steady state, transient, linear or non-linear problems in thermomechanics of solids, stress analysis, heat transfer, fluid flow, lubrication, vibration analysis, etc.

13.4.6 Repair process

The repair process can start after a component is cleaned/stripped, solution heat treated, and inspected. The sequence, or order, in which the repair process takes place is as important as the individual steps. The sequence is component specific, and any coating or specialized finishing operations must be taken into account.[21]

During service the microstructure of the hot section components deteriorates as was discussed in previous sections. Heat treatment and HIP play critical roles in restoring alloy microstructure, preparing base alloy prior to welding (annealing), promoting coating diffusion, removing or reducing residual stress, and in developing maximum strength.

Welding process

Welding is used to repair cracks but filler materials have their own limits (welding repair limits) based on the mechanical stresses (centrifugal stresses and gas flow stream load) to withstand. There are different types of welding:

- Gas tungsten arc welding (GTAW) or tungsten inert gas (TIG) welding.
- Plasma and microplasma transferred arc welding (PTAW).
- Laser welding (LBW) (LPW) (LFW).
- Electron-beam welding (EBW).

© Woodhead Publishing Limited, 2013

Superalloy weldability

This section addresses the general welding characteristics common to both solid-solution-strengthened and precipitation-hardened nickel and cobalt alloys:

- Solid-solution-strengthened, for vanes and combustion parts based on cobalt and nickel superalloys.
- Precipitation (gamma prime), strengthened for blades and vanes based on nickel superalloys.

The former category is not appreciably strengthened by heat treatment, whereas the latter category is typically used in the age-hardened or heat-treated condition. It is important to distinguish between these two classes of alloys when considering post-weld heat treatment. In general, alloys that contain significant amounts of age-hardening elements, such as aluminium, titanium, and niobium, are heat treatable. Table 13.7 is a reasonably inclusive list of the alloys that have found application as high-temperature materials and that have demonstrated some degree of weldability.

All are difficult to weld. Weld repair of these alloys is one of the most difficult technical challenges in the industry. All of the precipitation (γ') strengthened alloys are in 'Limited' or 'Difficult' (Fig. 13.14).

Gas tungsten arc welding (GTAW)

GTAW, also known as TIG, has been and remains the most used process for blade repair. The melting temperature needed to weld materials with GTAW is obtained by maintaining an arc between a tungsten alloy electrode and the workpiece (Fig. 13.15). Weld pool temperatures can approach 2500°C (4530°F). An inert gas sustains the arc and protects the molten metal from atmospheric contamination. The inert gas is normally argon, helium, or a mixture of helium and argon.[22] Weaker, solid-solution-strengthened filler materials are used to restore missing or worn areas, including IN 625 (the most popular filler), as well as IN 617 and Haynes 230 (generally accepted alternatives for industrial blades), and others (e.g., Hastelloy X and IN 600).

TIG welding equipment is readily available and affordable. Manual welding is the dominant method. However, some OEMs and independent repair shops have automated processes to handle the repair of tip rubs on production runs of the more commonly repaired designs.

Plasma and microplasma transferred arc processes (PTAW)

PTAW is often characterized as a modified form of GTAW. Both processes produce heat by ionizing an inert gas, both use tungsten electrodes and, in

© Woodhead Publishing Limited, 2013

Table 13.7 Nominal composition of high-temperature alloys[22]

Alloy	Composition										
	Ni	Cr	Co	Fe	Mo	Ti	W	Nb	Al	C	Other
Solid-solution nickel-base alloy											
Hastelloy N	72.0	7.0	...	5.0 MAX	16.0	0.5 MAX	...	...	...	0.06	...
Hastelloy S	67.0	15.5	...	1.0	15.5	...	...	...	0.2	0.02 MAX	0.02 LA
Hastelloy X	49.0	22.0	1.5 MAX	18.5	9.0	...	0.6	...	2.0	0.15	...
HAYNES 230	BAL	22	0–5	0–3	2	...	14	...	0.3	0.1	0.5 MN, 0.4 SI, 0.02 LA, 0.005 B
INCONEL 600	76.0	15.5	...	8.0	...	...	...	...	...	0.08	0.25 CU MAX
INCONEL 601	60.5	23.0	...	14.1	...	...	...	...	1.35	0.05	0.5 CU MAX
INCONEL 617	55.0	22.0	12.5	...	9.0	...	...	...	1.0	0.07	...
INCONEL 625	61.0	21.5	...	2.5	9.0	0.2	...	3.6	0.2	0.05	...
Precipitation-hardenable nickel-base alloys											
GMR-235	63.0	15.5	...	10.0	5.25	2.0	...	...	3.0	0.15	0.06B
INCONEL 702	79.5	15.5	...	0.4	...	0.7	...	...	3.4	0.04	...
INCONEL 706	41.5	16.0	...	37.5	...	1.75	...	2.9	0.2	0.03	...
IN-713C	74.0	12.5	...	...	4.2	0.8	...	2.0	6.0	0.12	0.012 B, 0.10 ZR
INCONEL 718	52.5	19.0	...	18.5	3.0	0.9	...	5.0	0.5	0.08 MAX	0.15 CU MAX
INCONEL 722	75.0	15.5	...	7.0	...	2.5	...	...	0.7	0.04	...
INCONEL X-750	73.0	15.5	...	7.0	...	2.5	...	1.0	0.7	0.04	0.25 CU MAX
INCOLOY 901	42.5	12.5	...	36.2	6.0	2.7	...	...	...	0.10 MAX	...
M-252	56.5	19.0	10.0	<0.75	10.0	2.6	...	...	1.0	0.15	0.005B
RENÉ	55.0	19.0	11.0	<0.3	10.0	3.1	...	...	1.5	0.09	0.01B
UDIMET 700	53.0	15.0	18.5	<1.0	5.0	3.4	...	...	4.3	0.07	0.03B
WASPALOY	57.0	19.5	13.5	2.0 MAX	4.3	3.0	...	...	1.4	0.07	0.006B, 0.09 ZR

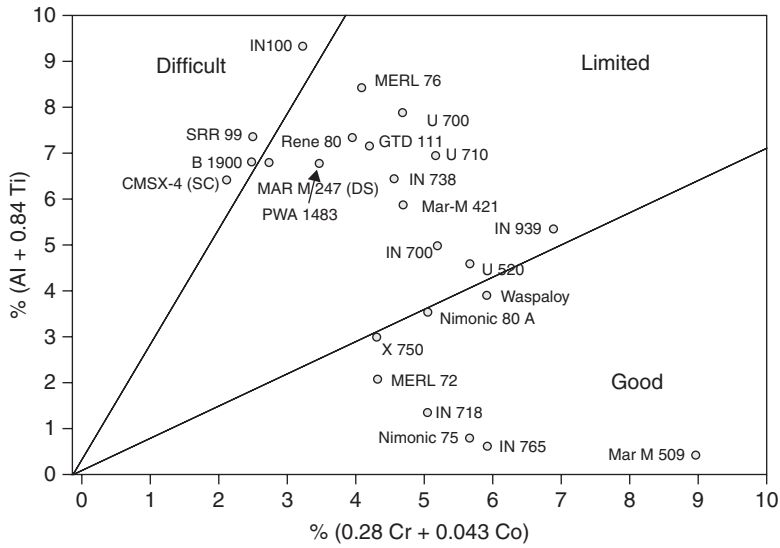
(*Continued*)

© Woodhead Publishing Limited, 2013

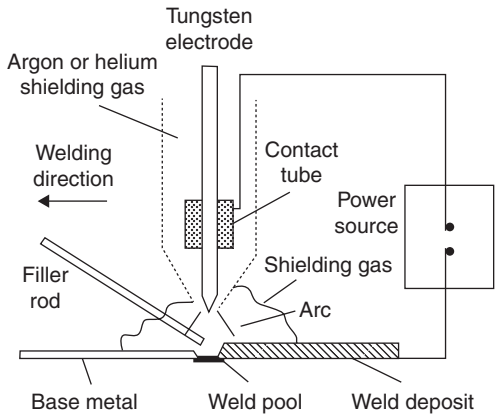
Table 13.7 Continued

Alloy	Composition										
	Ni	Cr	Co	Fe	Mo	Ti	W	Nb	Al	C	Other
Solid-solution cobalt-base alloys											
HAYNES 25 (-605)	10.0	20.0	50.0	3.0	...	...	15.0	...	...	0.10	1.5 MN
HAYNES 188	22.0	22.0	37.0	3.0 MAX	...	...	14.5	...	...	0.10	0.04 LA
S-816	20.0	20.0	42.0	4.0	4.0	...	4.0	4.0	...	0.38	...
STELLITE 6B	1.0	30.0	61.5	1.0	...	...	4.5	...	...	1.0	...
UMC0–50	...	28.0	49.0	21.0	...	...	...	...	...	0.12 MAX	...
Precipitation-hardenable cobalt-base alloys											
AR-213	0.5 MAX	19.0	65.0	0.5 MAX	...	...	4.5	...	3.5	0.17	6.5 TA, 0.15 ZR, 0.1 Y
MP-35N	35.0	20.0	35.0	...	10.0	...	...	...	...	...	...
MP-159	25.0	19.0	36.0	9.0	7.0	3.0	...	0.6	0.2	...	...

© Woodhead Publishing Limited, 2013



13.14 Superalloy weldability.[17]

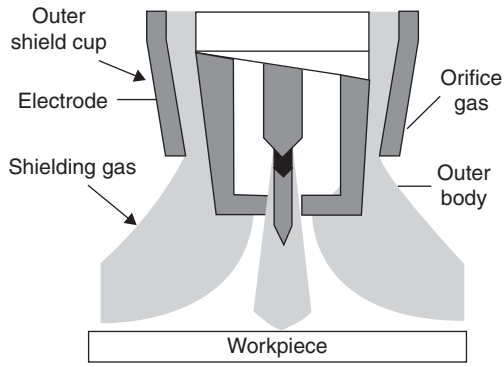


13.15 GTAW.[22]

most industrial applications, PTAW is specified as an acceptable alternative for GTAW. The fundamental difference is that PTAW involves constriction of the arc by an orifice assembly surrounding the electrode (see Fig. 13.16). This constriction increases the amount of ionization (or plasma) created, producing a more concentrated heat pattern and higher arc temperatures.

PTAW has disadvantages compared to GTAW. The cost of PTAW equipment is two to five times higher than comparably sized GTAW equipment. PTAW requires more welder knowledge. The highly concentrated plasma

© Woodhead Publishing Limited, 2013



13.16 Plasma transferred arc processes.[22]

stream can produce unwanted results quickly when heat-related problems arise.

Laser welding

The strongest motive for using these alloys is their good weldability. Due to the lower creep resistance of the filler metals, the repair of a component is limited to positions that endure low stresses, e.g. the upper part of the airfoil. In this way, the local creep strength required does not exceed the creep strength of the filler metal.

When using filler metals with identical composition and thus comparable mechanical properties, the repair limits can be extended. Predominantly due to the strengthening mechanisms taking place during solidification after welding and subsequent ageing heat treatments, microfissuring is almost inevitable when conventional room temperature TIG welding is applied. A way to overcome these limitations is to reduce the heat input. This can be achieved by, for example, laser welding.

Laser technology is promising. High-energy concentrations allow low heat input and produce small heat affected zones, limited distortions, and good dimensional control of the welding seam. Laser welding systems are highly flexible and are relatively easy to automate.[15]

LBW's main advantages are:

- Heating and melting are very localized. The total energy input to the weld joint is low, resulting in narrow weld widths and small heat affected zones.
- Because of the high-energy density in LBW, welds can be performed with more precision and at significantly faster rates than with arc welding.
- LBW is a non-contact process requiring only a line of sight to the weld joint.

© Woodhead Publishing Limited, 2013

- Easy to automate – basically mirror manipulation and adjusting speeds and feeds.
- Very fast and accurate – less finish grinding.

The disadvantages are high initial, maintenance and operating costs. LBW requires skilled and trained operators.

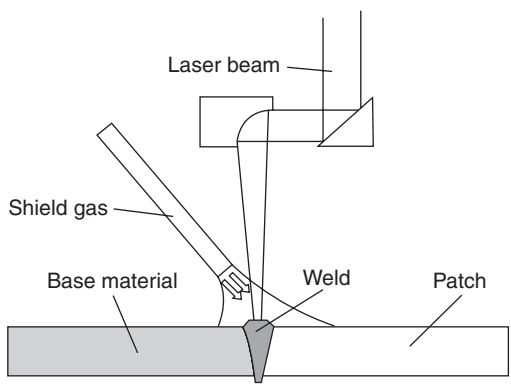
Laser fusion welding (LFW)

LFW offers many advantages, in particular allowing the replacement of a component piece by a patch, low distortions of the component, no filler metal is required, and high welding velocity. The type of patch material can vary, and the choice of material depends on the desired mechanical properties and/or oxidation and corrosion resistance. No filler metal is required during LFW. Due to the low heat input, hardly any deformation of the component takes place (Fig. 13.17).

A narrow welding seam is formed with a homogeneous texture. The overall heat input of the work piece is very low, due to a small, narrowly limited heat source with high energy. Then, less heat input is needed when using LFW. The weld is narrow compared to conventional TIG welding. In addition, with laser welding less deformation of the material is obtained.

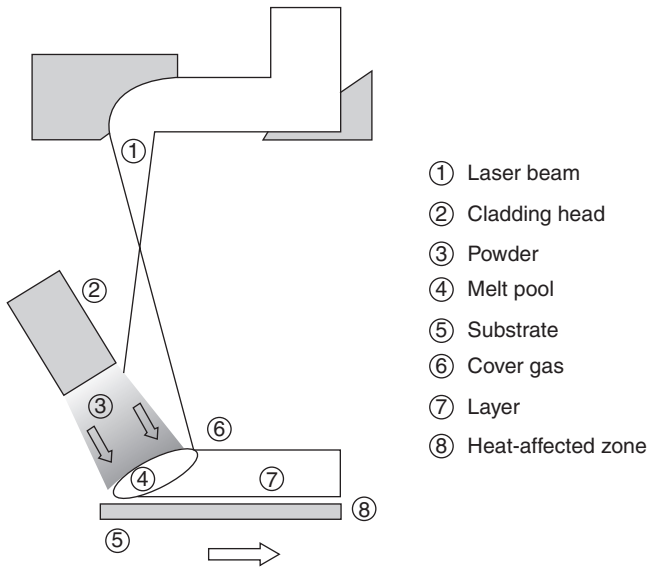
Laser powder welding (LPW)

LPW allows obtaining a near net shape weld of the original geometry using metal powder as filler metal, thin layers and less weld clean-up. The metal powder composition depends on the required mechanical properties. Low degree of deformation due to low heat input. This welding process is able to continue the crystallographic orientation and is applied to blade tip repair



13.17 Schematic representation of the LFW process.[15]

© Woodhead Publishing Limited, 2013



13.18 Schematic representation of laser powder welding.[23]

and build-up, seal replacement and build-up, knife edge seals and unlimited alloys.

This process offers defect-free build-up with filler metals that have a higher creep strength as compared to the ductile filler metals used during conventional TIG welding. Due to the low heat input during laser powder welding, less deformation occurs as compared to TIG welding.[15] The restored area is rebuilt near net shape, which reduces work during the next steps in the repair sequence. However, advanced programming is required for the near net shape build-up components (Fig. 13.18).

In the case of DS and SX repair, it is most important to continue the crystallographic orientation. This implies the formation of columnar dendrites, which from a solidification point of view is dictated by the thermal gradient and the velocity of the solidification front.

Electron-beam welding (EBW)

EBW is a high-energy density fusion process that is accomplished by bombarding the joint to be welded with an intense (strongly focused) beam of electrons that have been accelerated up to velocities 0.3–0.7 times the speed of light. The instantaneous conversion of the kinetic energy of these electrons into thermal energy as they impact and penetrate into the work piece on which they are impinging causes the weld-seam interface surfaces to melt and produces the weld-joint coalescence desired. EBW is used to weld

© Woodhead Publishing Limited, 2013

any metal that can be arc welded; weld quality in most metals is equal to or superior to that produced by GTAW.[22] The main advantages are:

- It can make deeper and more narrow welds than any other process.
- High speeds and high production rates.
- Good energy conversion efficiency ~65%. For production applications is cheaper to operate than LBW.

However the first cost is high. Because of the small beam, joints and tooling must be precise.

Brazing process

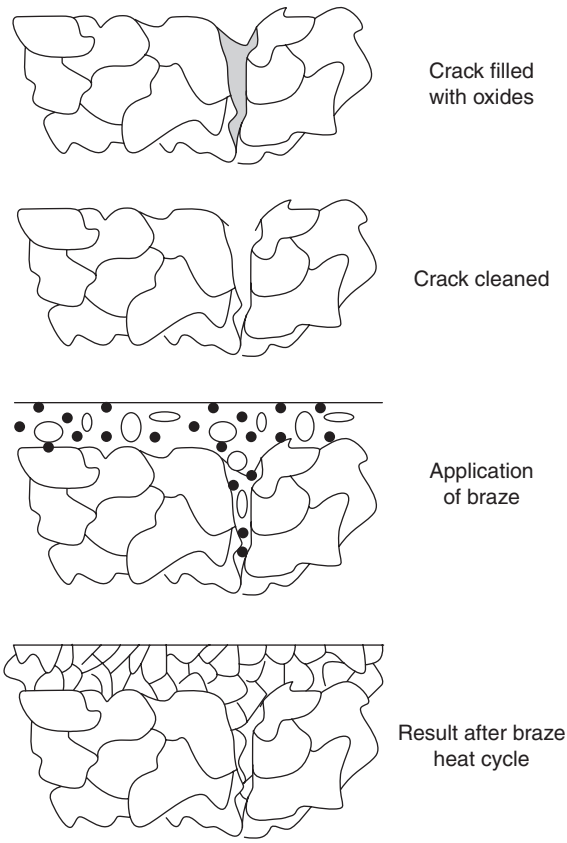
Brazing is a process for joining solid metals in close proximity by introducing a liquid metal that melts above 450°C (840°F). A sound brazed joint generally results when an appropriate filler alloy is selected, the parent metal surfaces are clean and remain clean during heating to the flow temperature of the brazing alloy, and a suitable joint design is used.[22] The braze should melt at a temperature below the melting point of the base metal (Table 13.8). It is also undesirable if the braze starts melting at operating temperatures. These upper and lower limits determine the temperature range of the braze, its use and composition. Nickel-based superalloys contain aluminium and titanium. While these elements give the material its unique characteristics, they are also very reactive with oxygen. If the process is performed in air oxide inclusions a poor joint will result. So brazing is performed in a vacuum furnace in temperatures well above 1100°C.

Brazing is usually applied to built-up wall thickness and pitting and it is the best alternative for specific applications, such as alloys that are difficult to weld, either the alloy itself or in areas where the restraint is high, and repairs over large areas (Fig 13.19). A key advantage of brazing over welding is that the entire part is heated, so there are no temperature differentials.

Table 13.8 Braze compound composition examples[22]

No	Commercial name	Composition	Liquidus temperature (°C)
1	DF3	Ni-20Cr-20Co-3Ta-3B-0.05La	1122
2	DF4B	Ni-14Cr-10Co-2.5Ta-3,5Al-2.7B-.02Y	1122
3	DF5	Ni-13Cr-3Ta-4Al-2.7B-.02Y	1157
4	DF6	Ni-20Cr-3Ta-2.8B-.04Y	1057
5	BRB	Ni-14Cr-9.5Co-4Al-2.5B	1066
6	775	Ni-15Cr-3.5B	1052
7	S57B	Co-10Ni-21Cr-5Ta-2.5Al-3B-3Si-.02Y	1128

© Woodhead Publishing Limited, 2013



13.19 Schematic representation of high temperature brazing.[22]

Welding involves localized heating and associated temperature differentials and strains. Brazing can be employed for the repair of nickel, as well as cobalt-based alloys.

The disadvantages are that the microstructure of the braze joint can be very unpredictable. Since brazing is a process controlled by diffusion, each alloy will react differently with a certain braze composition. During the brazing process boron forms borides. These borides can occur as needle-shaped phases. These phases are very brittle and can have a detrimental impact on the mechanical properties of the joint. The key is the control of the distribution and morphology of these borides. Two different approaches to brazing can be distinguished: overlay brazing to rebuild large surface areas (e.g. areas with oxidation or corrosion attack) and narrow gap brazing of fine thermal fatigue cracks, where the liquid braze is transported by capillary force into the crack.

© Woodhead Publishing Limited, 2013

Overlay brazing

The use of overlay brazing in order to perform a surface restoration is supported by a variety of brazing supplements like pastes, tapes or pre-sintered preforms.

Narrow gap brazing

Narrow gap brazing is typically used to repair thermal fatigue cracking in turbine vanes. The quality of the braze repair depends greatly on the cleanliness of the surfaces to be brazed. Cracks in land-based turbine components are generally deeper and more heavily oxidized due to the longer duty cycles at high temperatures. Typically, fluoride ion cleaning is employed to achieve acceptable cleaning of the cracks. The narrow gap brazing process itself is performed similarly to the overlay brazing process. While in the latter a sluggish braze–base material mixture is preferred, the narrow gap brazing process relies on the presence of a liquid mixture that gives the opportunity for the capillary forces to fill the cavity.

Coupon repair

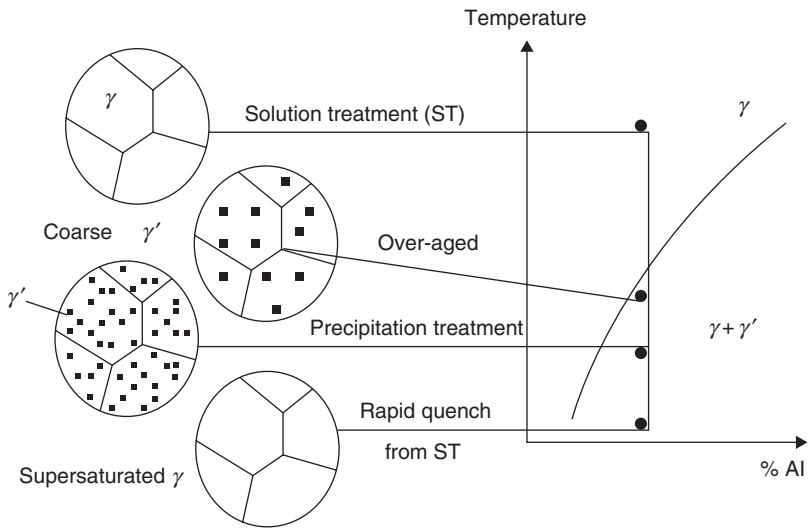
When damage to the parts is so extensive that regular repair by welding and/or brazing is not sufficient, special repairs are applied, such as coupon repairs, a very attractive option for non-rotating parts. This is to physically remove the damaged section and replace it with a pre-manufactured identical leading edge section, referred to as a 'coupon'. Coupon replacement is a common practice, and the leading and trailing edges are the sections most often repaired this way.

The restoration of vane airfoils reduces the need for replacement parts. Coupons are cast with a similar-sized material grain structure to the base nozzle material. The coupon becomes a valuable and robust process to service shops when the intricate cooling-hole geometry is already machined into the coupon itself. The holes are made using an electro-discharge machining (EDM) process, which creates a highly accurate hole geometry.

Heat treating and HIP ping

During service the size and shape of the gamma prime precipitates changes and a brittle layer of carbides is formed along the grain boundaries. This leads to a decrease of toughness and creep strength, two aspects necessary for operating a gas turbine. As the gamma prime was formed during manufacturing by a specific heat treatment, these precipitates can return into solution by raising the temperature above the gamma prime solution temperature (solution heat treatment) (Fig. 13.20). By quenching the

© Woodhead Publishing Limited, 2013



13.20 Heat-treatment diagram for precipitation strengthening in nickel-based.[26]

components, the gamma prime formation is inhibited. In this stage, all the mechanical work and brazing or welding is carried out. Later on, after application of the coating, an ageing heat-treatment cycle is carried out to form the gamma prime precipitates again at the original size and shape. Sometimes the solution heat treatment is combined with isostatic pressing (HIP consists of a pressure vessel that can be pressurized and heated simultaneously, to produce an environment that can collapse internal cavities and sinter or bond surface or powders together). Depending upon the results of the metallurgical evaluations, the material and the coating repair requirements, different heat treatments are applicable.

These methods include pre- and post-weld heat treatments. Cast nickel alloys can be joined by welding processes. For optimum results, casting should be solution-annealed before welding to relieve some of the casting stresses and provide some homogenization of the cast structure. Solution annealing should be conducted after welding the age-hardenable alloys when highly restrained joints are involved.

Important variables in the heat-treatment process include time at temperature, furnace atmosphere, and heating/cooling rates. Generally, heat treating cast superalloys involves homogenization, solution heat treatments or ageing heat treatments. Three basic heat-treatment steps used are: solution, stabilization and ageing. Solution heat treatment is employed to dissolve the phases in the as-cast microstructure, ideally returning the alloy microstructure to a single-phase γ (fcc) solid solution, and to homogenize

© Woodhead Publishing Limited, 2013

the segregated as-cast microstructure. The solution treatment is performed at a temperature above or near the γ' solvus temperature.[25]

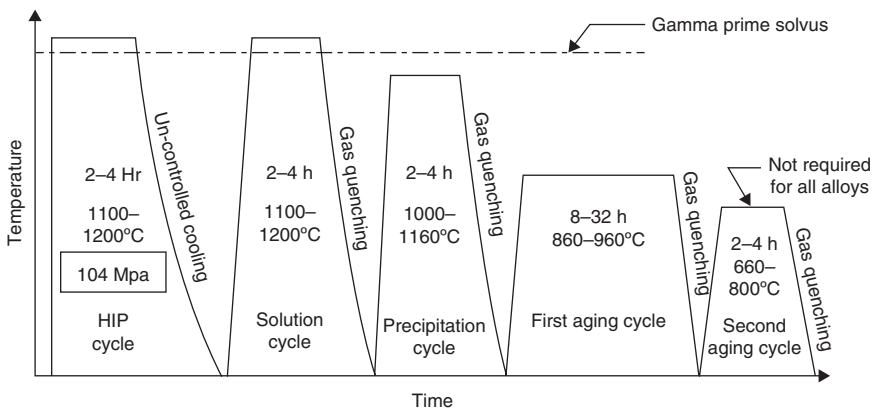
In nickel-based superalloys, growth of the fine γ' precipitate phase is very rapid at a few hundred degrees Fahrenheit below the high temperature involved in solution heat treatment. Therefore, it is necessary to cool the casting rapidly, to prevent coarsening of the γ' during the cooling cycle, which can degrade the properties of the casting.

A temperature between the solution and ageing temperature is used. The purpose of this heat treatment is to optimize the γ' size and morphology and to assist decomposition of the coarse, as-cast MC carbides into fine, grain-boundary carbides. With nickel-base alloys used for turbine airfoils, the stabilization heat treatment is often combined with the heat treatment used to bond or diffuse a coating onto the alloy substrate. The stabilization heat treatment is carried out in a protective atmosphere, such as argon, helium, hydrogen, or in a vacuum, to prevent excessive oxidation of the casting. Cooling rates equivalent to air cooling or faster are normally used.[25]

Stress-relief heat treatments are performed following welding or other processing on the casting that increases residual stress. They are usually carried out between the stabilization and ageing temperatures in a protective atmosphere. The ageing heat treatment is employed to precipitate additional γ' as very fine precipitates. This is important to achieve tensile and lower-temperature creep-rupture properties.

A two-step ageing treatment is commonly used to control the size distribution of γ' and γ'' precipitates. The main reason is, in addition to γ' or γ'' control, to precipitate or control grain-boundary carbide morphology.

The combination of HIP plus heat treatment has also greatly enhanced properties (Fig. 13.21).



13.21 Different heat and HIP treating during the repair process.[17]

© Woodhead Publishing Limited, 2013

13.4.7 Coating processes

Once the material adding operations have been completed, the components are NDT inspected to make sure that they are free of cracks. This is especially critical for items that cannot be inspected or corrected later in the repair process because of heat treatment, coating, or assembly issues. During the repair process the cooling holes may have been blocked by braze or weld. Due to the high strength of the nickel- and cobalt-based superalloys, cooling holes have to be opened up by EDM. The repair cycle is completed by adding a coating to the base material. This coating can be of two types:

1. Metallic coatings (diffusion coating, overlay coating).
2. TBC.

After the coating application, a final heat treatment is performed separately, since the cooling rate is critical for the size, morphology and distribution of the microstructural elements that determine material properties.

As discussed in section operating condition the most important applications for hot section gas turbine parts are:

- Oxidation and corrosion resistant coatings. The high turbine inlet temperatures require improved resistance for oxidation. Mostly aluminides, produced by chemical vapour deposition (CVD) type processes (e.g. pack), MCrAlY type of coatings, produced by thermal spray processes, or combined techniques are used.
- TBCs, based on zirconia are produced by thermal spray techniques or electron-beam physical vapour deposition.
- Erosion resistant coatings are made from hard carbides, where at high temperatures chromium carbide is the best choice (WC, Cr_3C_2). They are mainly applied by thermal spray processes.

In modern gas turbines, a combination of different coating processes are used to get the optimal application of the coating mentioned.

The selection of coating process depends on component design and application. For example, coatings required for protection against hot corrosion may not be optimum for oxidation protection. Some common coating processes are:

Diffusion coatings:

- Pack process.
- Above-the-pack process.
- CVD.

© Woodhead Publishing Limited, 2013

Overlay coatings:

- Overlay coating deposited by spray process:
  - Cold spray.
  - Thermal spray:
    - Detonation of combustion gases (detonation gun).
    - Flame created by combustion of gases (flame spray, high-velocity oxygen fuel (HVOF)).
    - Sustained plasma created by electrical discharge (plasma spray).
    - Electric arc (electric arc spray, electro-spark deposition (ESD)).
- PVD process:
  - Ion beam processes.
  - Ion plating.
  - EB-PVD.

TBCs:

- Plasma spray:
  - Solution precursor plasma spray (SPPS).
- EB-PVD:
  - Directed vapour EB-PVD.

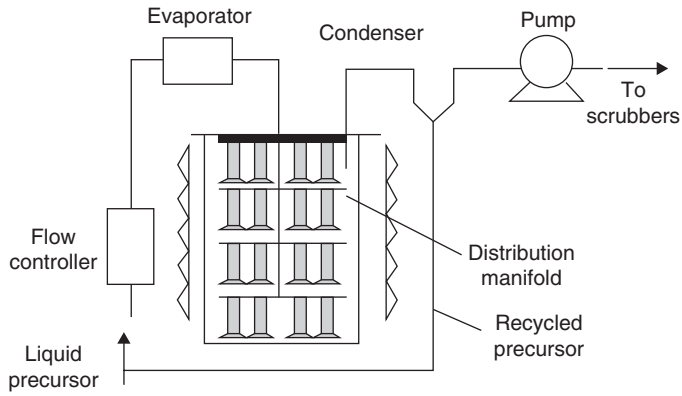
To produce a quality coating it is necessary to have adequate control of the coating process, the material used, and the support services such as abrasive grit blasting, degreasing, masking, stripping, heat treating and inspection. It is essential that all stages of a given process are optimized and documented in detail to standardize the procedure and to assure reproducibility. Checks to monitor quality and repeatability should be conducted, these include:

- Verify coating thickness using eddy current, weight-gain, or physical measurement methods.
- Take bond-strength and metallurgical samples to confirm use of specified procedures.
- Perform a destructive metallurgical evaluation of an actual part to evaluate coating quality.

Diffusion coatings

Diffusion coatings[29,30] consist of a substrate alloy surface layer enriched with the oxide scale formers Al, Cr, Si, or their combination to a depth of 10–100 μm. These elements combine with the primary constituents of the substrate alloy to form intermetallics with significant levels of the oxide scale formers.[28]

© Woodhead Publishing Limited, 2013



13.22 Schematic of the CVD coating process.[9]

The basic process consists of the following steps: generation of Al-, Cr-, or Si-containing vapours; transport of the vapours to the component surface; reaction of the vapours with the substrate alloy; associated diffusion processes within the alloy; and additional heat treatments as necessary to achieve desired coating composition and coating as well as substrate properties.

Diffusion coatings can be produced by one of the three major processes, that is, the pack, above-the-pack, and CVD (Fig. 13.22).

Chemical vapour deposition (CVD)

CVD is a process in which a coating is formed by a chemical reaction between a gaseous phase and a heated substrate. The process can be used to apply metallic, intermetallic and refractory coating of almost any composition. The benefit of CVD is that it can deposit coatings of a large variety of compositions at or near theoretical density and chemistry. It can also coat complex shapes and small internal openings.

Overlay coating

Diffusion coating behaviour is strongly dependent on the composition of the substrate alloy, because the alloy participates in the coating formation. So, these coatings do not offer wide flexibility for incorporation of minor elements. In order to address this limitation, 'overlay' coatings have been developed with minimal direct contribution of the substrate alloy. Overlay coating consists of a thin layer of a discrete alloy composition applied to the metal surface. The coating alloy can be chosen for maximum corrosion resistance, since it does not depend on the substrate composition to develop corrosion resistance. The overlay coatings have a typical composition represented by MCrAlX, where M stands for Ni, Co, and occasionally Fe, and X

© Woodhead Publishing Limited, 2013

represents oxygen-reactive elements such as Zr, Hf, Si, and Y.[28] The overlay coatings are usually deposited either by EB-PVD or by spray processes.

Plasma spray

Plasma spray is a thermal spraying process, in which a powder of the coating material is heated to near or above its melting point, and accelerated toward the part being coated by a plasma gas stream. Plasma spraying can either be performed in air at atmospheric pressure, or by air plasma spraying (APS), or in a vacuum, where it is referred to as vacuum plasma spraying (VPS), or by low pressure plasma spraying (LPPS).

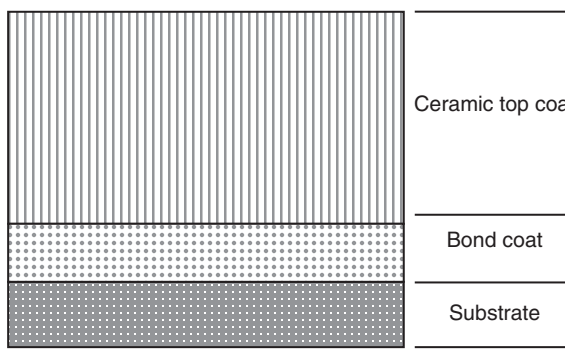
With APS, the sprayed particles impact and deform, but perfect bonding is not achieved due to the presence of surface oxide films that cause oxide stringers to be present; consequently, they are characterized by their relatively low bond strengths and appreciable porosity.

The LPPS or VPS processes circumvent some of these difficulties, because clean coatings are produced with virtually no oxide inclusions. The oxidation resistance of metallic NiCoCrAlY coatings deposited by the LPPS process is about twice that of an equivalent coating composition deposited by APS.

Thermal barrier coating (TBC)

The function of TBCs is to reduce component temperatures and thereby increase life by reducing the severity of thermal transients and lower the substrate temperature, enhancing the thermal fatigue and creep capabilities of coated components. In addition, although TBCs do not provide significant reduction in oxygen transport to the substrate, the lower temperature can lead to a reduction in oxidation and hot corrosion. TBCs are able to decrease metal part surface temperature by about 180°F (100°C).

TBCs are generally a combination of multiple layers of coatings (Fig. 13.23). The topmost layer provides thermal insulation and consists of



13.23 TBC structure.

© Woodhead Publishing Limited, 2013

a ceramic, with low thermal conductivity, typically ZrO_2, known as zirconia. This ceramic insulating layer is deposited on the substrate alloy with an intervening oxidation resistant metallic layer called the 'bond coat'. The metallic coating is either a diffusion aluminide, such as platinum aluminide, or an overlay coating of general composition NiCoCrAlY, conforming somewhat to the substrate alloy composition.[28]

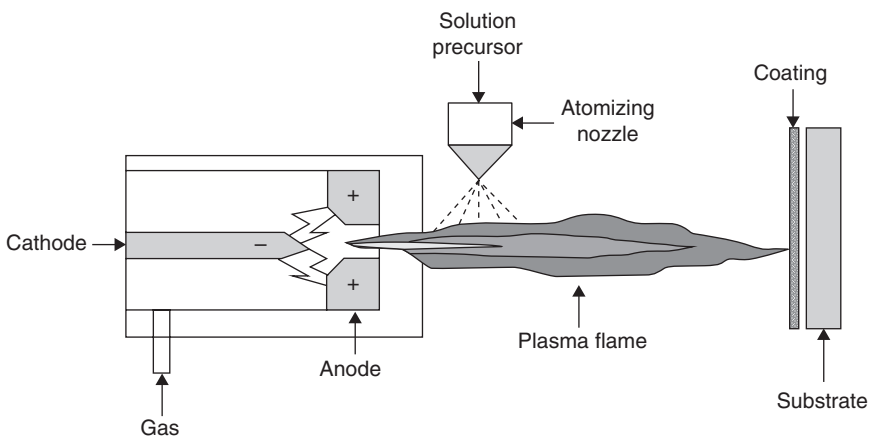
Different OEMs have different specifications concerning the microstructure characteristics and properties. Key differences are in bond coat chemistry, porosity levels and microstructure, coating thickness requirements on the TBC top coat, and surface finish requirements.

Plasma sprayed TBCs

Coatings based on zirconia can only be deposited by processes capable of adding enough energy to the raw materials to melt, evaporate, or chemically fragment to dimensions that can be deposited with adequate cohesive and adhesive strength. One of the processes that can deliver high energy is based on the phenomenon of plasma.

In this process,[38] a plasma jet melts the coating raw material in the form of powder. The plasma is created in a plasma gun. It is called the APS process because it is conducted in air. Several APS designs are available.[28]

A variant of the plasma spray process is the SPPS process (Fig. 13.24),[39,40] in which the raw material injected into the plasma is not in the form of powder but is a liquid, preferably an aqueous precursor, which undergoes physical and chemical changes of pyrolysis and sintering during flight through the plasma jet prior to deposition as 7YSZ coating. The microstructure of TBC deposited through the SPPS process is characterized by transverse



13.24 Solution precursor spray process.[42]

© Woodhead Publishing Limited, 2013

microcracks and a splat structure of a finer scale than with conventional plasma sprayed TBC. The microstructural features improve durability of SPPS-derived TBC and provide tolerance to increased thickness compared with the traditional APS-deposited TBC.[41]

Electron-beam physical vapour deposition (EB-PVD) TBCs

The basic principle of the EB-PVD process consists of creating a melt pool of the raw material in an evacuated chamber by heating 7YSZ with the focused high-energy electron beam. The pool generates vapour. The part to be coated is held over the pool. The coating on the surface of the part forms by the deposition of the molecules in the vapour, as opposed to the deposition of large molten particles formed in the plasma spray process. The complete process is conducted inside an EB-PVD coating chamber. Parts to be coated are fixtured on a part manipulator attached to a rotating shaft called the sting.

EB-PVD coating is characterized by a columnar microstructure. Neighbouring columns have weak intercolumnar bonds. This allows the structure to provide strain tolerance during use. Several geometrical, as well as thermally induced, processes influence the formation of the microstructure. These include the adsorption of the vapour molecule (or atom), desorption of some of the molecules during deposition, the vapour impingement angle on the substrate, shadowing of the incoming molecules by the existing deposits, surface diffusion, and volume diffusion.

13.4.8 Quality control and final inspection

After repair completion, several on-line inspections follow, including flow testing, dimensional verification and testing of operational properties, such as frequency analysis to determine the natural frequencies of rotating blades, moment-weight charting for balancing of rotating blades, harmonic check of nozzles to avoid flow induced vibration, verification of unrestricted internal cooling passages, and visual inspection. The quality process has to include different verifications, which assure the quality standard for the whole process, such as, flow test, final inspection, documents, protocols, customer report, ISO 9001 and 14001, process, audits, etc.

After coating and inspection are complete, component reassembly can proceed. During reassembly, dimensional checks are necessary to ensure proper installation of core plugs, wear strips, etc.

The repair process can be considered complete after the repair vendor´s final report is received and accepted. It should include all certifications, inspections, and engineering recommendations. This information is important if problems arise. Also, it provides valuable input to the repair specification development for the next overhaul.

© Woodhead Publishing Limited, 2013

Flow testing

As part of the repair process, a work-scope flow test must be incorporated. This is particularly important for the following components of gas turbine, such as liners, fuel nozzles, air-cooled vanes and blades.

Combustion liner

A critical inspection for louvered combustion liners is airflow testing. Flow testing checks that each liner in the set is flowing the same amount of air, minimizing temperature variances. In the refurbishment process, there are ways in which the liner airflow distribution can be disrupted if quality control is poor. When a liner has the TBC stripped and re-applied to its inner surface, the flow area through the numerous film-cooling holes in the liner may change. Therefore, it is recommended that liners are flow tested in the as-found and refurbished condition. The flow test should specifically measure the total film-cooling flow area before and after the repair.

Fuel nozzle

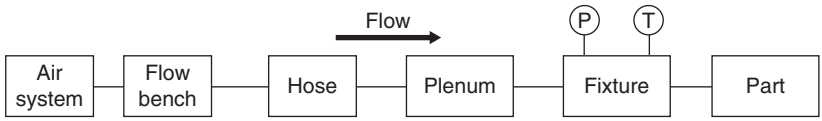
Flow testing of fuel nozzle tips and passageways is of critical importance, especially for multinozzle systems and DLN operation. Equalized fuel flow minimizes temperature spreads and can-to-can pressure differences between the combustors. The flow-test units use a computer-controlled system that calculates the variation of each tip to that of the set tips. Bodies or covers are tested and then matched to fuel tips to completely optimize the system. The final assembly is typically limited to a variance of less than 2% between assemblies. A lean combustor can be responsible for just about any type of DLN combustion problem: high emissions, lean blow out, mode transfer failure, reduced load turndown, flashback into the premixing zone, and high dynamics.[18]

Air-cooled vane

Vane flow testing has to be performed at incoming inspection and after completion of vane repair and recoating. All testing is to be performed with vane segments fully assembled (all core plugs and cover plates installed). This is a quantitative test where cooling flow rates are measured and recorded. The purpose of this test is to determine if the vane cooling system has been affected by the repair and recoating processes. It is conducted by connecting a pressurized air supply to a vane/mounting fixture and measuring the total air flow through each vane.

There are numerous airflow test stand configurations (Fig. 13.25) that are acceptable for use in conducting this testing. Some test stands measure and display flow directly in engineering units (kg/s, lb/s, SCFM, etc.). Others, such

© Woodhead Publishing Limited, 2013



13.25 Airflow test stand configuration.

as those that use a critical flow nozzle, measure and display system pressures which, as long as the nozzle is maintained at choke flow, are directly proportional to flow.

Air-cooled blade

Testing cooling passage flows has to be performed prior to and after repair of air-cooled gas turbine blades. There are two types of procedures. The qualitative pressurized water test is a qualitative test procedure, in that specific cooling passage flow rates are not measured/recorded. The purpose of this test is to determine by visual inspection that all blade cooling passages and exit holes/slots are unobstructed. The quantitative pressurized airflow test is a quantitative test procedure, in that cooling flow rates or test stand pressures that are directly proportional to flow are measured and recorded. The purpose of this test is to determine if the blade cooling system has been affected by the repair and recoating processes.

Moment-weight charting

The purpose of weight balancing or weight charting is to minimize the corrections needed in the dynamic balancing procedure by statically balancing all the components as much as possible. Weight balancing requires the measurement/calculation of the moment weight of all blades. In the next step all data are entered into a computer and the assembly order that gives the lowest possible residual unbalance is determined. Although the weight balancing procedure applies basically to all rotating parts, the blades account for a significant contribution to imbalance.[15]

Frequency analysis

During operation, the turbine components are exposed to a number of vibrational excitations, due to mechanical sources and/or aerodynamic sources. Each blade has a specific response to an excitation. The magnitude of this response depends on the excitation frequency, energy, and the physical properties of the blade. The response of turbine parts to a given excitation can be predicted with a complicated FEM calculation. In this respect the turbine blades are the most critical parts and need special attention.

© Woodhead Publishing Limited, 2013

If the excitation frequency coincides with the natural frequency of the blade, the vibrational level can easily soar unacceptably, and the risk of blade failure can be encountered. There are two possibilities to reduce the vibration level in a turbine – by reducing the vibration sources, and reducing the response of the turbine parts.

After a repair, the natural frequency of a blade can change by changing mass distribution. The impact of the material additions, such as welding and brazing, is relatively small, but there can be a more substantial impact if a coating system is changed from a diffusion coating to an overlay coating. This change in frequency has to be considered.

Dimensional verification and final visual inspection

Dimensional verification of critical measurements, including roundness, clearances, height, thickness, throat openings, etc., provided by the repair facility is strongly recommended. The validity of these measurements depends in large measure on the dimensional accuracy of fixtures used as part of the repair process. True verification of dimensional accuracy comes when components are reassembled into the gas turbine. Feedback from this work should be incorporated into the final report and factored into future decisions regarding vendor selection.

Before the components are loaded for shipment, it is recommended to conduct a final visual inspection to ensure that the parts are clean and not susceptible to handling damage. This is especially important for the fragile coating edges. Also, it is important to keep in mind that the coating and the last grit cleaning operation can close up cooling holes. They should be inspected using wire, light, water, and/or air methods.

Quality records

The quality management system should meet the requirements of international quality system standards. All subcontracted activities shall also be subject to the same quality standard. The final step of any final-inspection verification should be a review of all quality records for conformance to specifications and quality control protocol for repaired parts. That is[5]:

- The quality plan should provide the sequence and list of activities throughout the repair – of the components and assessment of the condition from the start until its delivery to the customer.
- The subcontractors qualified for the established quality standards should be identified.
- Before starting work, the vendor should document the programme to monitor quality, inspections and testing of the repair process and/or manufacturing of the components to be supplied. This should include

© Woodhead Publishing Limited, 2013

the methods established, procedures, material specifications, approval of processes, follow-up sheets, etc.

- All records should be signed by the appropriate technician, inspector, or engineer, and dated. Documentation should include certificates for materials and specifics of all subcontracted processes.
- Limits of acceptance criteria for inspections, acceptance of defects, etc. should be recorded.
- Quality control/inspections/tests are required at each stage of the process and inspection frequency for each component. These should include:
  - Verifying the traceability of materials (including weld filler and braze) to their certificates.
  - Confirming proper heat treatment based on recorded temperatures, time on temperature, heating and cooling rates, and quality of atmosphere.
  - Checking coating certifications, including metallurgical evaluations, and inspection documents (NDE, non-destructive examination), dimensional, flow, frequency, area, and harmonics, as well as moment-weight and sequence charts.

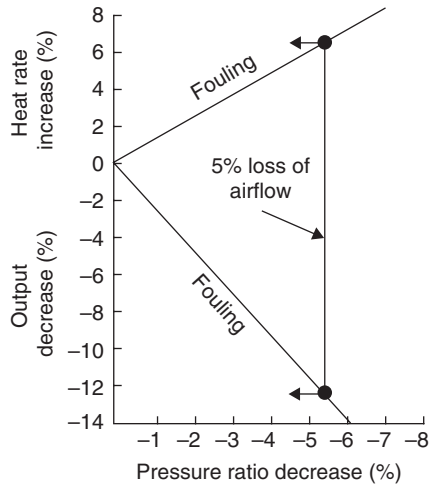
13.5 Compressor cleaning

Often airborne contaminants adhere to compressor blade surfaces. These contaminants can be airborne salt, industrial pollution, exhausts emissions, exhausts and oil vapours., and mineral deposits such as limestone, coal, dust, and cement dust, insects, dirty water or vapour from various sources, agricultural particulates and others. Combinations of fouling agents, such as oil leakage, with other contaminants may cause severe loss of performance (Fig.13.26).

It has been estimated that in fouling environments the accumulation of deposits during engine operation may cause as much as 70–80% of the performance degradation[46] of a gas turbine. The performance loss arises from the adherence of particulates on blades and surfaces of the first few compressor stages, building up a new material layer around them. This will increase surface roughness, causing a thicker boundary layer and a smaller effective flow area. These flow changes will cause a reduced airflow capacity, lower efficiency and a lower surge line. The reader is referred to Chapter 16 for a more detailed description of gas turbine degradation. To overcome the consequences of fouling, firing temperatures are often increased to keep a constant power output. This will result in an increase in emissions and a lower hot section creep life.[45] Frequently used techniques to prevent the consequences of fouling are[47]:

- Manual cleaning.
- Abrasive cleaning.

© Woodhead Publishing Limited, 2013



13.26 Fouling effects on heat rate, power output and pressure ratio.[45]

- Off-line washing.
- On-line washing.

13.5.1 Manual cleaning

This consists of the manual use of brushes and detergent. The engine needs to be left to cool after shut-down. It is then partially disassembled *in situ* and cleaning follows. This is a good method used in some older engines. The cleaning personnel could also inspect the blades for other defects, such as erosion, corrosion effects or some material cracks.[48] This procedure is time consuming but offers very good power recovery. It can be used during overhaul.

13.5.2 Abrasive method

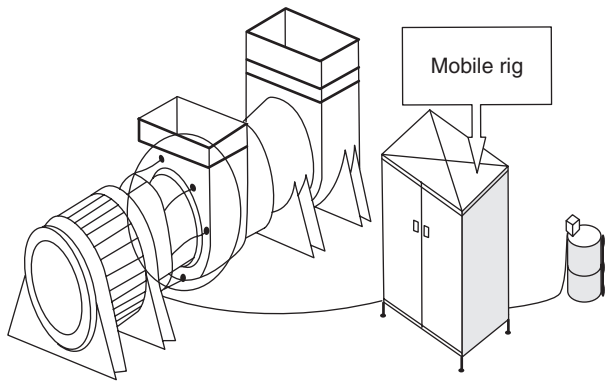
An early, invasive, method for cleaning compressor blades consisted of the injection of abrasive organic materials, such as rice, charcoal and nut shells. This was done with the gas turbine running at normal speed, so the particles injected could achieve high speeds to remove the deposits by hitting the compressor blades. Particles sizes must be suited for the cleaning agents to remain airborne. The main advantage of this method is the low cost and its ability to be applied without a shut-down and loss of revenue, where this is important. There is a risk of erosion and compressor coating damage associated with this technique. This risk is higher in modern engines with their high speeds and sharper blade profiles.

© Woodhead Publishing Limited, 2013

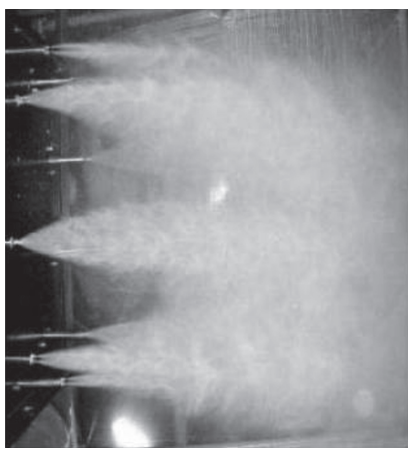
13.5.3 Off-line washing

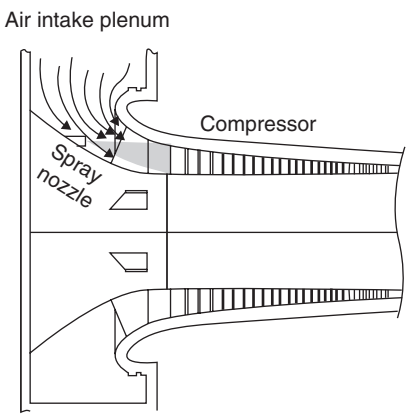
In the early 1980s off-line compressor washing using water or detergent was introduced. The operation was conducted with the gas turbine rotating at crank speed (20–30% of the nominal value) (Fig. 13.27).

Cleaning fluid is injected when the gas turbine is stopped. After a short soaking period the rotor is accelerated to crank speed. Then the nozzles of the washing system inject water wash solvent. The injection of the washing fluid is through the use of spray nozzles, which are fitted at the inlet (Fig. 13.28). The last step of the operation is the rinse cycle with demineralised, deionised water. The whole process can be repeated several times depending on severity.



13.27 Off-line washing system.[49]





13.28 Off-line process.[50]

© Woodhead Publishing Limited, 2013

Off-line washing is carried out at the sub-idle regime, with no power production. In this regime most blow-off valves are open and fluid may spill if appropriate care is not taken. The type of cleaning fluid is dependent on the nature of the fouling. The simplest option is to use water. When the deposits are oily or greasy the washing fluid must be more effective, for example solvent based.

Dirty and effluent water are left after the end of the wash. Draining is needed. This requires the insulation of critical areas to ensure effluent water does not enter. So to avoid the possibility of water runoff, the drain points in critical areas such as combustor chamber and compressor casing must be positioned carefully.

Off-line washing is very effective and not expensive. However, given the need to shut down the plant and let it cool, it is executed every few months in continuous-duty applications.

13.5.4 On-line washing

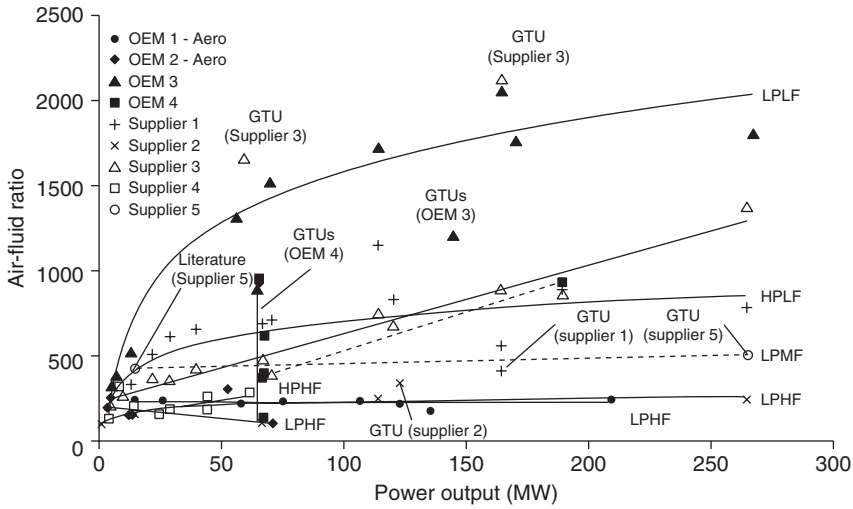
When gas turbines are used in continuous duty a shut-down for an off-line wash is very expensive in terms of lost production. So there is an interest in on-line compressor washing (Fig. 13.29). This permits compressor cleaning while the engine is running at high power, with no loss of production. Given its low cost, it can be applied very frequently, often as a preventive maintenance approach. In this context, it is possible to include inhibiting agents in the wash fluid to reduce the rate of adhesion of fouling agents.

Demineralised water, with or without cleaning detergents, is injected through tailor-made nozzles. These nozzles and the associated equipment may be purpose built or supplied with the plant by the OEM (Fig. 13.30).



13.29 Nozzles location for on-line washing system.[51]

© Woodhead Publishing Limited, 2013



13.30 Air–fluid ratio vs engine power for state of the art washing systems.[53] LPLF – low pressure low flow, HPLF – high pressure low flow, LPMF – low pressure medium flow, HPHF – high pressure high flow, LPHF – low pressure high flow.

Some users have implemented retrofits supplied by specialists. One or more rinse on-line washing following the cleaning fluid injection is less effective than off-line wash, but it can be carried out very frequently. On-line and off-line washing can be used in a complementary manner.[48,50,52]

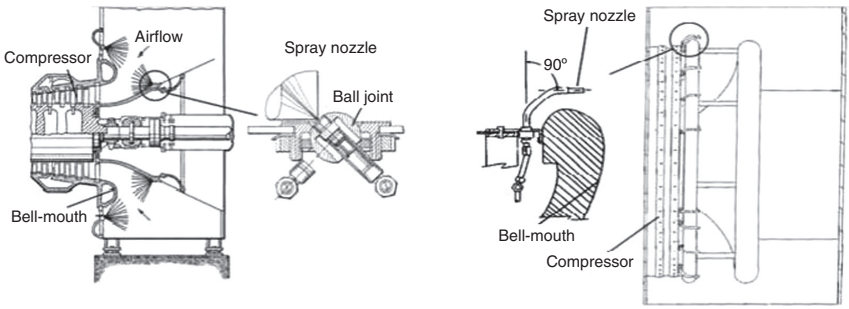
Droplet size is an issue. Big droplets have a better mechanical cleaning effect but there may be a risk of erosion. Smaller droplets are less prone to centrifuging by the rotating blades and can be accelerated more quickly by the airflow; however, they will evaporate more quickly. Droplet size is typically within the range of 50–250 μm.[48] Droplet size is dependent on fluid pressure and nozzle design. To gain a wider coverage, fan spray nozzles are often used.[53]

The nozzles are normally pointing toward the compressor inlet in an axial direction to give the droplets axial momentum. Nozzles can be angled differentially to take into account the airflow pattern induced by the design of the inlet[53] (Fig. 13.31).

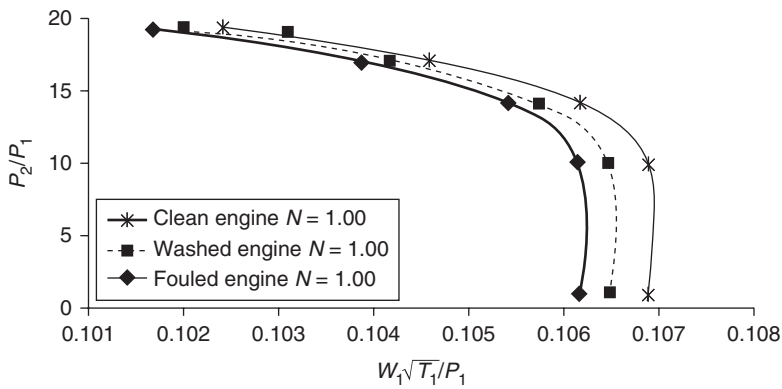
13.5.5 Compressor cleaning economics

The use of combined on-line and off-line compressor washing presents many attractions in fouling environments. Using on-line washes enhances performance retention and postpones the need for off-line washes and the required shut-down. This can be extended a step further in looking at the combination of filtering and washing as a performance retention technique.

© Woodhead Publishing Limited, 2013



13.31 On-line wash nozzle location.[52]



13.32 Fouling and washing effects on a gas turbine at its design rotational speed $N = 1$.[54]

Much research in this area has been carried out at Cranfield University in the UK. This work has been based on computations and a fouling rig.[55,56] Figure 13.32 shows the result of washing on compressor performance. In a recent study[47] it was shown that in some circumstances it may be beneficial to implement less efficient filters, coupled with compressor on-line wash and accept a slightly higher maintenance cost. The additional revenue associated with a lower pressure loss at the compressor inlet compensated for the additional costs and produced a better economic result in some cases. This trend is likely to strengthen with continuously increasing fuel costs.

13.6 Future trends

The modem gas turbine engine is a highly sophisticated device. It is very difficult to predict the exact conditions that gas turbine parts will be subjected to in the operational environment. These comprise a wide range

© Woodhead Publishing Limited, 2013

of atmospheric temperature and pressure conditions, load settings, sand, dust, corrosive environments and transient load rates with a variety of fuels. Internal engine conditions change as a function of these variables. The designer is faced with hundreds of combinations of possible operating conditions and a variety of failure modes. The repair/rework designer must make the best decision using past experience, design and analytical methods, computer simulations and extensive coupon, rig and engine testing. Gas turbine blades experience dimensional and metallurgical degradation during engine operation. Dimensional degradation derives from wear, nicks, dents, hot corrosion and, in the case of coated blades, stripping and recoating as in repair. Metallurgical degradation mainly derives from material ageing, fatigue and high-temperature creep.

The high replacement cost of gas turbine blades and vanes has created a fast-growing, highly-specialized segment of the hot gas path component repair industry. Repair procedures and limits are established by engine manufacturer (OEM) and are interpreted and applied by engine operators and/or repair facilities. Every repair/rework/design change, while fixing a type of degradation, has the potential of introducing a new fault or defect. It leads to the need for a qualification methodology to assure a safe and cost-effective repair. Moreover, it would allow the opening of the 'gas turbine aftermarket', promoting on the one hand the entry of new players and, on the other hand, end users to be more confident of these new alternatives.

The qualification of hot gas path components has not been common outside the OEM domain in the past. Design proprietary information, full scale test facility development and operational costs, and the costs of qualifying these repairs have precluded operator instigated repair process development.

The qualification methodology includes how to design and certify a repair as being worthy and safety for the next replacement/repair cycle following a systematic and responsible procedure. To do so, the methodology must address such issues as repair design, life analysis, verification testing, and personnel qualification requirements. The qualification methodology for gas turbine repair/rework usually comprises the following components, (a) failure mode, effects and criticality analysis (FMECA) methodology, (b) coupon level testing methodology, (c) component rig testing methodology engine testing, and (d) design change approval (depending upon the criticality of the component and repair/rework, (c) and (d) can be eliminated).[57]

The future of hot gas path component repair will be determined by replacement part pricing, 'break-out' sales activity, advanced repair available, labour costs (labour-intensive activity), and the development of a certification and qualification methodology of repair. The advent and diffusion of 'power by the hour', 'long-term service agreements', 'total care packages', etc. are changing the economics of the aftermarket.

© Woodhead Publishing Limited, 2013

Maintenance costs, downtime costs, fuel costs, and equipment costs are constituents of total operating costs, which will change with operating regime. Gas turbines are used more and more in part-load mode, accruing more cycles than originally planned. Fuel prices are increasing. This is exacerbated by the introduction of CO_2 taxes and/or trading. In these changing conditions, operators need to be very aware of the changing techno-economic environment to achieve good outcomes.

13.7 Acknowledgement

The authors thank Mr P. Giannakakis for his help with this chapter.

13.8 Bibliography

Active Thermography for Dimensional Measurements on Gas Turbine Components. Matthias Goldammer, Siemens AG, Munich Germany. Werner Heinrich, Siemens AG, Berlin, Germany. ECNDT 2006.

Dedicated Electron Beam Reactive Physical Vapor Deposition (R.P.V.D.) Apparatus For The Production Of Ceramic Thermal Barrier Coatings. Project Final Report Dec. 1981. E. Demaray.

Development of Electron Beam Physical Vapor Deposition of Ceramic Coatings Fairbanks et al. editors; May 1982 Demaray et al.

Effects of Hot Isostatic Pressing on the Microstructure of Ni-base Superalloy. Choul Jun Choi, Hyun Yong Choi, Dong Jo Yang, Jane Yeol Kim. *Advanced Material Research* Vols. 123–125 (2010) pp 467–470.

Fluoride Ion Cleaning (FIC) at Sub-atmospheric pressure. ASME TURBOEXPO 2000, May 8–11, 2000, Munich Germany. Warren Miglietti and Tom Cullen.

Gas Turbine Hot Section life assessment and extension: Status & Issues. M I Wood, ERA Technology Ltd.

Hot Isostatic Pressing Rejuvenation Technology. John E Radavich School of Materials Engineering and Pramod D. Desai MIAC/CINDAS. June 1994.

Innovative IGT Repair Solutions to Enhance Power Plant Profitability. Kevin Davis, President of Frarendi, Inc.

Laser Powder Fusion Welding. David Kaser. Huffman Corporation.

Manufacturing Engineering and Technology. Edited by Prentice Hall 2001. Serope Kalpakjian and Steven Schmid.

NDE and material evaluation for lifetime assessment of Power Plant components. Waheed Abbasi, Ph D. Sazzadur Rahman, Ph.D. and Michael J. Metala. Siemens Energy, Inc.

Nickel-based Superalloy Welding Practices for Industrial Gas Turbine Apllications. M.B. Henderson, D. Arrell, M. Heobel, R. Larsson and G. Marchant. ALSTOM Power.

Physical Vapor Deposition of Ceramic Coatings for Gas Turbine Engine Components; *ASME* 1982. R. E. Demaray, J. W. Fairbanks and D. H. Boone.

Thermal Barrier Coatings for Turbine Airfoils. Apr. 1984 T. E. Strangman.

Thermo-Mechanical Fatigue Life Prediction: A critical Review. W.Z. Zhuang and N.S. Swansson. Airframe and Engine Division Aeronautical and Maritime Research Laboratory.

© Woodhead Publishing Limited, 2013

Towards durable TBC with novel microstructure deposited by solution-precursor plasma spray. N.P. Padture et al. *Acta Materialia*, July 17, 2001, vol **49**, pp 2251–2257.

Turnaround Shutdown and Outage Management. Second Edition Tom Lenahan. Fairbanks et al. editors; December 2005. ISBN: 0750667877. Publisher: Elsevier Science & Technology Books.

Welding metallurgy and weldability of nickel-base. John N. DuPont, John C. Lippold, and Samuel D. Kiser. Published by John Wiley & Sons, Inc., Hoboken, New Jersey.

Welding Metallurgy. Second Edition. Sindo Kou. Winley – Interscience a John Wiley & Sons Inc., Publication 2003.

13.9 References

1. Álvarez Tejedor, T. (2011). 'Gas turbine materials selection, life management and performance improvement'. *Power Plant Life Management and Performance Improvement*. Edited by J. E. Oakey, Cranfield University, UK, Woodhead Publishing Series in Energy No. 23.
2. Singh, R. (1999). 'Managing gas turbine availability, performance and life usage via advanced diagnostics'. Keynote, *44th Gas Turbine Users Association Annual Conference*, 9–14 May, Dubai, United Arab Emirates.
3. Magerat, F. and Singh. R. (1997). 'A method of evaluating the life cycle costs of combined cycle power plants'. Advances in Turbine Materials, Design and Manufacturing, *Proceedings of the Fourth International Charles Parsons Turbine Conference*, 4–6 November, Newcastle upon Tyne, UK.
4. Balebic, D., Burger, R., Forry, D. (2004). *Heavy-Duty Gas Turbine Operating and Maintenance Considerations*. General Electric.
5. Six steps to successful repair of GT components. Selecting the appropriate vendor to refurbish parts for your turbines. Shops verify as-received condition of components with an 'incoming' inspection. Verifying repairs, final inspection results. By Hans van Esch, TEServices. Ron Natole. Global Gas Turbine News May/June 1995. *Combined Cycle Journal*, Second Quarter 2005.
6. *Surface Engineering*. Volume 5 of ASM Handbook. ASM International Handbook Committee. (1994).
7. K. Schneider, *et al*. (1985). 'Experience with repair of stationary gas-turbine blades-view of a turbine manufacturer'. *Materials Science and Technology*, August, **1**, 613–619.
8. Sohr, J. M. and Thorpe, M. L. (1993). 'Coating removal with high-pressure waterjets'. *Aerospace Engineering*, **13**(3), 19–23.
9. Liburdi, J. (1998). *Enabling Technologies for Turbine Component Life Extension.* Liburdi Engineering Limited.
10. Haynes, R. H., Miller, M. O., and Thomson, W. R. (2009). *Remove Coatings from Turbine Components without Damaging Them and Lower Costs*. Power Engineering.
11. *Failure Analysis and Prevention. Volume 11 of ASM Handbook.* ASM International Handbook Committee. (2002).
12. Natole, R. (1995). 'Gas turbine components – repair or replace?'. *Global Gas Turbine News*, May/June.

© Woodhead Publishing Limited, 2013

13. *Heat-Resistant Materials. ASM Specialty Handbook.* ASM International (1997).
14. Liburdi, J., Lowden, P., Nagy, D., De Priamus, T. R. and Shaw, S. (2009). 'Practical experience with the development of superalloy rejuvenation'. Paper No. GT2009-59444, *ASME Turbo Expo 2009, Gas Turbine Technical Congress & Exposition*, June 8–12, Orlando, Florida, USA.
15. *The Repair and Manufacture of Advanced Gas Turbine Components*. Sulzer Turbo Services (2005).
16. *Nondestructive Evaluation and Quality Control.* Volume 17 of ASM Handbook. International Handbook Committee. (1989).
17. *Repair Technology for Gas Turbine Hot Section Components*. Frame 9FA Work Shop Madrid, Spain, EPRI. (July 2010).
18. Pallos, K. J. *Gas Turbine Repair Technology*. GE Power System. GER-3957B. General Electric Company.
19. Kolkman, H. J. and Kool, G. A. *Non Destructive Investigation of the Condition of Gas Turbine Blades.* National Aerospace Laboratory NLR. Amsterdam, The Netherlands.
20. Van der Voort, G. (2004). *ASM Handbook Volume 9: Metallography and Microstructures*. ASM International.
21. *The Gas Turbine Handbook.* US Department of Energy 2006. Office of Fossil Energy. National Energy Technology Laboratory.
22. *Welding, Brazing an*d Soldering. Volume 6 of ASM Handbook. International Handbook Committee. Published in 1993.
23. Krause, S. *Laser Powder Build-up Welding*. Sulzer Turbomachinery Services. Sulzer Technical Review 4/2001.
24. McGraw, J., Anton, R., Van Deventer, G. and Burns, A. (2006). 'Advancements in gas turbine vane repair'. *Proceedings of PWR2006: ASME Power*, May 2–4, Atlanta, Georgia.
25. *Heat Treatment. Volume 4 of ASM Handbook.* ASM International Handbook Committee. Published in 1991.
26. Meetham, G. W. and Van de Voorde, M. H. (2000). *Superalloys.*
27. Liburdi, J. (1979). 'Rejuvenation of used turbine blades by hot isostatic pressing'. ASME. *International Gas Turbine Conference*, March 11–15, San Diego, California USA.
28. Bose, S. (2007). *High Temperature Coatings.* Butterworth-Heinemann 2007. ISBN:13: 978–0–7506–8252–7; ISBN 10: 0–7506–8252–3.
29. Goward, G. W., Seigle, L. L., Bennett, L. K. and Bayer, G. T. (1994). *Diffusion Coatings*. ASM International, Member/Customer Service Center, Materials Park, OH 44073–0002, USA, pp. 611–620.
30. Goward, G. W. (1998). Progress in coatings for gas turbine airfoils. *Surface Coating Technology*, **108–109**, 73–79.
31. *Coating for High-Temperature Structural Materials: Trends and Opportunities.* National Materials Advisory Board. Academy Press, Washington D.C. (1996).
32. Kadyrov, E. and Kadyrov, V. (1995). 'Gas dynamical parameters of detonation powder spraying'. *Journal of Thermal Spray Technology*, **4**, 280–286.
33. Sturgeon, A. J., Harvey, M. D. F., Blunt, F. J. and Dunkerton, S. B. (1995). *Conference Proceedings: Thermal Spraying--Current Status and Future Trends*, Ed. A. Ohmori, High Temperature Society of Japan, Osaka, pp. 101–106,

© Woodhead Publishing Limited, 2013

34. Reed, R. C. (2008). *The Superalloy. Fundamentals and Applications*. Cambridge University Press.
35. Muehlberger, E. (1998). 'Method of forming uniform thin coatings on large substrates'. US Patent 5.853.815.
36. Scott, H. G. (1975). 'Phase relationships in the zirconia-yttria system'. *Journal of Materials* Science., **10**[Y], 1527–1535.
37. Stecura, S. (1985). *Optimization of NiCrAl-Y/ZrO2-Y2O3 thermal barrier system*. NASA Tech. Memo. 86905, NASA, Cleveland, OH.
38. Herman, H. (1988). 'Plasma spray deposition process'. *MRS Bulletin,* December,**47,** 60–67.
39. Gell, M., Xie, L., Jordan, E. H. and Padture, N. (2004). 'Mechanisms of spallation of solution precursor plasma spray thermal barrier coatings'. *Surface Coating Technology*, **188–189**, 101–106.
40. Bhatia, T., Ozturk, A., Xie, L., Jordan, E., Cetegen, B. M., Gell, M., Ma, X. and Padture, N. P. (2002). 'Mechanisms of ceramic coating deposition in solution-precursor plasma spray.' *Journal of Materials Research*,, **17**(9), 2363–2372.
41. Gell, M., Jordan, E. H., Teicholz, M., Cetegen, B. M., Padture, N. P., Xie, L., Chen, D., Ma, X. and Roth, J. (2008). 'Thermal barrier coatings made by the solution precursor plasma spray process'. *Journal of Thermal Spray Technology*, **17**(1).
42. *Superior Thermal Barrier Coating for Industrial Gas-Turbine Engines Using a Novel Solution-Precursor Plasma-Spray Process.* University of Connecticut: Prof. Eric H. Jordan. The Ohio State University: Prof. Nitin P. Padture. SCIS Project 03–01-SR107. DOE Cooperative Agreement DE-FC26–02NT41431.
43. Groves, J. F. (1998). 'Directed vapor deposition'. Ph.D. Dissertation, University of Virginia.
44. Groves, J. F., Mattausch, G., Morgner, H., Haas, D. D. and Wadley, H. N. G. (2000). 'Technology update-directed vapor deposition'. *Surface Engineering*, **16**(6), 461–464.
45. RL. Loud, A. A. S. (1991), 'Gas turbine inlet air treatment'. *General Elect. Company – Schenectady, US.*
46. Bromley, A. F. and Meher, C. B. (2004). 'Gain a competitive edge with a better understanding of GT compressor fouling, washing'. *Combined Cycle Journal*, Fourth Quarter, 37.
47. Sugliano, R. (2010). 'Technoeconomic analysis of different filter systems in combination with compressor cleaning'. MSc Thesis, Cranfield University.
48. Mund, F. C. and Pilidis, P. (2006). 'Gas turbine compressor washing: historical developments, trends and main design parameters for online systems'. *Journal of Engineering for Gas Turbines and Power*, **128**, 2, 344–353.
49. Arebi, A. W. A., Ramsden, K. W. and Cranfield University. School of Engineering (2005), *Benefit of compressor cleaning on power output for oil and gas field applications*. – find original reference
50. Lambart, P. and Gordon, R. RMC limited – private communication.
51. Lambart, P. and Gordon, R. RMC limited – private communication.
52. Mund, F. C. and Pilidis, P. (2005). 'Online compressor washing: a numerical survey of influencing parameters'. *Proceedings of the Institution of Mechanical Engineers, Part A: Journal of Power and Energy*, **219**, 1, 13–23.
53. Mund, F. C. (2006) 'Coordinated application of CFD and gas turbine performance methods'. Ph.D. thesis, Cranfield University,

© Woodhead Publishing Limited, 2013

54. Igie, U., Pilidis, P., Fouflias, D. and Ramsden, K. and Lambart, P. (2011). 'On-line compressor cascade washing for gas turbine performance investigation'. *Proceedings of ASME Turbo Expo,* GT2011–46210, June 6–10, Vancouver, Canada.
55. Nikolaidis, T. (2009). 'Water ingestion effects on gas turbine engine performance'. Ph.D. thesis, Cranfield University, School of Engineering, UK.
56. Mustafa, Z. (2005). 'Aerodynamic investigation of fluid injection in an axial compressor'. Unpublished Ph.D. thesis. Cranfield University, School of Engineering, UK.
57. Patnaik, P. C. and Thamburaj, R. (1998). *'Development of a Qualification Methodology for Advanced Gas Turbine Engine Repair/Reworks'.* Advanced Material and Energy System (AMES). Orenda Aerospace Corporation. *RTO AVT Workshop on Qualification of Life Extension Schemes for Engine Components*, Greece.

© Woodhead Publishing Limited, 2013

14

Fuel flexibility in gas turbine systems: impact on burner design and performance

M. HUTH and A. HEILOS, Siemens AG Energy, Germany

DOI: 10.1533/9780857096067.3.635

Abstract: This chapter discusses fuel flexibility in terms of running heavy duty gas turbines (GTs) with various feedstocks. In the beginning an overview about the most important gaseous and liquids fuels which can be burned directly as primary fuels in a heavy duty GT combustor and their origin is given. Next, integrated gasification combined cycle (IGCC) technology is discussed briefly: this technology is also producing coal and similar solid fuels applicable after conversion to syngas to gas turbine (GT) technology. In the subsequent section, important combustion features such as emission, flashback, blow-off, combustion dynamics which are potentially affected by changing the fuel are discussed. An overview about parameters for describing the combustion behavior of fuels and technologies in order to extend the range of fuel flexibility follows. At the end an outlook on future trends is given.

Key words: fuel flexibility, liquefied natural gas, hydrogen, syngas, diesel, naphtha, heavy fuel oil, Wobbe index, flame speed, autoignition.

14.1 Introduction

This chapter is divided into five main parts:

1. Sections 14.2 and 14.3 give an overview of the most important gaseous and liquid fuels which can be burned directly as primary fuels in a heavy duty gas turbine (GT) combustor, including their origin.
2. Section 14.4 briefly discusses integrated gasification combined cycle (IGCC) technology which is producing coal and similar fuels as secondary fuels after syngas conversion that are applicable to gas turbine (GT) technology.
3. Sections 14.5 and 14.6 give an overview of parameters to describe the combustion behavior of gaseous fuel and technologies to extend the range of fuel flexibility.
4. Section 14.7 briefly discusses parameters to describe liquid fuels.
5. Section 14.8 gives an outlook on future trends.

© Woodhead Publishing Limited, 2013

This section primarily deals with fuels, and fuel flexibility, with respect to heavy duty gas turbines. For a discussion of aero engines, the reader should look to other literature.

14.2 Primary fuel characterization

In general, fuels may be characterized by their state of aggregation, as solid, liquid and gaseous. Examples are given below:

Solid fuels

- Coal.
- Brown coal/lignite.
- Wood (biomass).
- Domestic waste/sewage sludge.

Gaseous fuels

- Natural gas/liquefied natural gas (LNG).
- Liquefied petroleum gas (LPG).
- Low-LHV natural gases.
- Syngas.
- Hydrogen.
- Blast furnace gas/Corex gas/coke oven gas.

Liquid fuels

- Diesel/fuel oil.
- Marine diesel/heavy fuel oil.
- Crude oil.
- Naphtha and condensates.

Solid fuels contain significant amounts of ash-forming content, which in consequence leads to a harsh environment for the hot gas path parts of a gas turbine. This has so far prohibited the direct use of those fuels in commercial gas turbine engines, although the low specific costs, availability in many countries, and the comparatively large worldwide resources of solid fuels would be an attractive reason for their application. However, in order to enable the use of such fuels in gas turbines, they need to be processed by gasification or conversion to liquid fuel and raw gas cleaning before use. The conversion of those fuels into clean gaseous fuels would give an opportunity to apply these lower cost, lower quality fuels in highly efficient combined cycle technology. However, the conversion process consumes the efficiency, and significantly increases the required investment. Finally, the overall plant

© Woodhead Publishing Limited, 2013

configuration has to compete with conventional boiler technology for solid fuel application.

The standard fuel for stationary gas turbines is natural gas, whose main component is methane and which consequently behaves very similarly to methane. Since high quality natural gas is not easily available in all regions, but only lower quality gases with significant amounts of inert components, such low-LHV natural gases provide an interesting alternative. For lower heating value natural gases, the requirement for larger fuel mass flows, as well as the reduced chemical reactivity, has to be taken into account.

Furthermore, a large number of individual gases associated with industrial processes are potential fuels for stationary gas turbines (e.g. blast furnace gas (BFG), coke oven gas (COG), Corex gas, and syngas). Those fuels are characterized by a low content, or absence, of methane, while the main contributors for the stored chemical energy in the fuel are hydrogen and carbon monoxide. In addition, they contain a certain fraction of inert gases (mainly nitrogen and carbon dioxide) and are typically characterized by a lower heating value compared to standard natural gas. Consequently those gases behave significantly differently from natural gas. For application of those gases in stationary gas turbines, the required high fuel mass flows, as well as the different chemical reactivity compared to natural gas, has to be considered. This finally leads to certain adjustments at gas turbines, additional to applications with standard natural gases.

Liquid fuels, in comparison to gaseous fuels (except the liquefied LNG and LPG), provide the possibility for relatively easy on-site storage, which provides independence from permanent supply. While for aero engine application this is a requirement, in many cases for stationary gas turbines liquid fuels are only used as a backup or secondary fuel. This allows operation independently from the supply of the main (gaseous) fuel, having in mind that the typical specific costs of high quality liquid fuel (diesel) are above those of natural gas. Liquid fuels can be applied directly, or after external vaporization. Direct use and atomization/vaporization inside the combustor is the established technology. Heavy oil requires heating in order to achieve appropriate viscosity and atomization capability, and care has to be taken concerning typically contained trace elements (especially vanadium). Liquid fuels with low flash point temperature, such as gasoline, kerosene, naphtha or condensates, require special care along the fuel line with respect to tightness and explosion and fire protection.

14.3 Fuels directly introduced into gas turbine burners

In the following section a characterization of fuels which can be directly burned in gas turbines is given.

© Woodhead Publishing Limited, 2013

14.3.1 Gaseous fuels: types and characteristics

An overview of the typical composition bandwidth of the most important gaseous fuels is given in Table 14.1, discussed in more detail in the subsequent sections.

(a) Natural gas

Natural gas is the standard fuel for stationary gas turbines. Since this gas is a natural product, it is a mixture of several gaseous components, and does not have a unique composition of individual components, but is found within a typical bandwidth.

In certain regions without direct pipeline access to natural gas resources, LNG is applied. As a consequence of the liquefaction process by cooling down to below –161°C, LNG is typically to some extent enriched with higher hydrocarbons.

Based on the typical requirements of domestic and industrial gas heating devices, a classification into certain groups is defined in the standards. For example, in the EN437 (European Committee for Standardization EN437, 2009) H-gas, L-gas and E-gas are defined based on Wobbe index (see Section 14.5.2; Table 14.2).

(b) LPG

LPG is a by-product of the refinery process. It consists mainly of propane (C_3H_8) and butane (C_4H_{10}) but may in addition contain some of the unsaturated components propene (C_3H_6) and butene (C_4H_8). The composition of LPG from its individual components is not fixed. LPG might consist almost entirely of propane but could also contain more than 50% butane. In some regions there is also a shift of the composition between summer and winter season (more propane in winter, more butane in summer), which helps to keep the storage pressure more independent from the season (ambient conditions). At typical ambient temperatures, LPG is liquid at about 8 bar. At the higher end of typical ambient temperatures, the pressure still remains moderate (the vapor pressure of propane at 55°C is about 20 bar), which enables economic storage. Compared to air, LPG has a higher density. Consequently, in the case of leaks, LPG generates a layer upon the ground and does not easily escape as do lighter gases (natural gas, hydrogen, etc.). This characteristic promotes the formation of ignitable mixtures near to the ground in the case of leaks in the fuel system, and consequently, for explosion protection, special attention is required to avoid leakages.

While LPG is only in few cases used as a main fuel, it is used as a start-up/ignition fuel to support subsequent liquid fuels operation or as a secondary fuel alternative for fuel oil. However, storage of fuel oil is less complex and typically is more attractive than LPG as secondary fuel. In comparison to

© Woodhead Publishing Limited, 2013

© Woodhead Publishing Limited, 2013

Table 14.1 Composition bandwidth of the most important gaseous fuels

		Natural gas		LNG		LPG		Undiluted syngas		Undiluted CSS H_2		BFG		COG	
		Min.	Max.	Min.	Max.	Min.	Max.	Min.	Max.	Min.	Max.	Min.	Max.	Min.	Max.
Methane (CH_4)	[vol%]	80	100	80	99	–	–	0	6	–	–	–	–	20	30
Ethane (C_2H_6)	[vol%]	0	15	1	17	–	–	–	–	–	–	–	–	1	3
Propane (C_3H_8)	[vol%]	0	5	0.1	5	0	100	–	–	–	–	–	–	0	1
Butane (C_4H_{10})	[vol%]	0	0.5	0.1	2	100	0	–	–	–	–	–	–	0	0.5
Hydrogen (H_2)	[vol%]	–	–	–	–	–	–	25	50	80	90	2	6	50	60
Carbon monoxide (CO)	[vol%]	–	–	–	–	–	–	35	65	0	5	20	30	4	6
Nitrogen (N_2)	[vol%]	0	15	0	1	–	–	1	10	5	10	45	60	10	12
Carbon dioxide (CO_2)	[vol%]	0	6	–	–	–	–	2	20	0	1	20	25	1	2

Table 14.2 Wobbe index range according to European standard EN437

Gas-group	Min. Wobbe index [MJ/m³]	Max. Wobbe index [MJ/m³]
H	45.7	54.7
L	39.1	44.8
E	40.9	54.7

Source: European Committee for Standardization EN437, 2009.

natural gas, LPG has a somewhat higher adiabatic flame temperature, which has impact on NO_x emissions. Furthermore, it has a lower autoignition temperature, which is of relevance concerning flashback in premix combustion systems.

(c) Low-LHV gas

Low-LHV gas refers to gaseous fuels with typical LHV below about 35 MJ/kg. There are two main categories of low-LHV gases:

1. high inert components (N_2, CO_2) containing natural gases (CH_4 based);
2. product or by-product gas from an industrial process that typically contains carbon monoxide, hydrogen, inert components and, in some cases, some hydrocarbons (see syngas, blast furnace gas).

The low heating value leads to an increased fuel mass flow to achieve the required thermal input. Consequently, the fuel auxiliaries, as well as the gas injection design at the burners, have to be considered accordingly. The reactivity of the fuel depends on the composition. In case of the low-LHV natural gases (CH_4 based, larger amounts of inert components) the reactivity is reduced. This requires special attention concerning the stability against lean-flame blow-off. Since premix combustion systems are typically more sensitive to lean-flame blow-off stability, it might be required to apply a generically more stable diffusion-type combustion system. The increased content of inert components leads to a reduced adiabatic flame temperature, which is of advantage in terms of NO_x formation. Because of this, for low-LHV natural gas the NO_x emissions of diffusion-type combustion systems, compared to premix combustion systems, do not increase to the extent as standard natural gas.

(d) Syngas

Gasification of 'low quality' (cheap) primary fuels, biomass or even waste (e.g. refinery residues), and in some cases also the reforming of 'high quality' fuel, natural gas is used for generation of so-called syngas. Syngas from

© Woodhead Publishing Limited, 2013

gasification (after cleaning) contains about 25–50% hydrogen (H_2) and 35–65% carbon monoxide (CO) as the combustible components. In the case of fluidized bed gasification, there is also up to about 6% methane (CH_4). Furthermore, a certain fraction of inert components, such as nitrogen (N_2) from about 1% to 10%, carbon dioxide (CO_2) from about 2% to 20%, and a low content of water vapor (H_2O) and argon (Ar), are typically contained as main fractions. It has to be considered that syngases in general are liable to contain in addition special contaminants, relevant for corrosive effects (e.g. H_2S, COS, etc.) or deposition formation (e.g. dust, metal carbonyls, etc.). The heating value of raw syngases from oxygen-blown gasifiers is typically in the range of about 10–15 MJ/kg. The composition, as well as the contamination, depends on the feedstock, the gasification process, and gasification conditions while contamination in addition strongly depends on the efficiency of the gas cleaning process. Because syngas contains CO, it is very poisonous.

The name syngas is related to the initial typical use for chemical synthesis of basic chemicals (methanol, ammonia, etc.) as well as synthetic liquid fuels (Fischer-Tropsch). Besides the reforming of natural gas, which is only applied for chemical synthesis, syngas is typically generated in gasifiers by partial oxidation of carbon containing solid or liquid feedstocks. In order to reduce the gasifier size and the typical requirement of a pressurized syngas, the gasification is done under elevated pressures. Typical pressure levels are about 20–80 bar, depending on the process type and feedstock. Since the initial target application of gasifiers historically was the generation of H_2/CO mixtures for chemical synthesis, the gasification process by several plant vendors has been evolutionarily developed with the application of oxygen as oxidizer.

Although the heating value is significantly lower compared to natural gas, the hydrogen content leads to a chemical reactivity (burning velocity) significantly above that for natural gas. As consequence of the high reactivity of this hydrogen containing fuel, and the special characteristic of maximal reactivity under fuel rich conditions (see Section 14.3.2), the application of premix combustion systems for syngas is connected with generically increased risk of flashback into the mixing section. Due to this, state-of-the-art syngas combustion systems in commercial heavy duty gas turbines apply robust diffusion-type combustion systems. In order to achieve the required emissions comparable to state-of-the-art natural gas application in gas turbines, the raw syngas from the gasifier is typically diluted by nitrogen or water vapor (reduction of adiabatic flame temperature). In addition, dilution enables adjustment of specific burner requirements concerning Wobbe index and heating value. Due to the high reactivity of the contained hydrogen, there is the possibility to adjust the diluted mixtures to a similar reactivity and adiabatic flame temperature significantly below those of natural gas. This provides sufficiently low NO_x emissions and stable operation

© Woodhead Publishing Limited, 2013

with applications of diffusion-type combustion systems. Since for gasification with oxygen-blown gasifiers, oxygen has to be separated from air, the remaining 'waste nitrogen' of the air-separation unit can be used as diluent at the release pressure level of the air-separation unit. Additional dilution or adjustment of required conditions is possible by saturation at specific conditions (temperature, pressure) with water vapor and subsequent superheating (avoidance of fog, droplets in the fuel) since the reduction of reactivity and adiabatic flame temperature is more efficient with water vapor than nitrogen.

As described, it is typically required that the raw syngas from an oxygen-blown gasification process has to be diluted. Consequently, the necessity for oxygen generation can be avoided by using air-blown gasification, which directly delivers a lower reactivity, lower adiabatic flame temperature syngas. The final selection of air-blown or oxygen-blown gasification, and the balance between both options, has to consider all project boundaries as well as existing experience with the individual options.

As for low-LHV gases in general, the lower heating value requires increased fuel mass flows and a larger-sized fuel system. Due to the content of poisonous CO and the wide ignition window, as well as high reactivity associated with increased explosion affinity, special care has to be taken concerning fuel system tightness and the detection of potential leakages (=> welded seals, evacuation systems, continuous CO detection, etc.). In order to avoid uncontrolled reactions due to air penetration from the combustor into the fuel system, comprehensive purge procedures before and after syngas operation are recommended.

Furthermore, potential corrosive contents as well as deposition-forming components have to be taken into account for the fuel system as well as for the burner hardware.

(e) Hydrogen

The application of hydrogen offers the opportunity for CO_2-free gas turbine operation since hydrogen does not contain the CO_2-forming carbon. Hydrogen has a significantly increased reactivity (high burning velocity, wide ignition window) compared to natural gas. Furthermore, it has a higher mass specific heating value, a larger adiabatic flame temperature, but a volumetric heating value, as well as Wobbe index, below those of natural gas (see Table 14.4). These properties lead to similar requirements compared to the application of syngas (see (f)). Especially, the extremely high reactivity typically requires dilution in order to enable safe operation with state-of-the-art gas turbine combustion systems. The higher adiabatic flame temperature of hydrogen compared to natural gas is a driver for an increase of NO_x emissions from syngas flames. However, this can be compensated by

© Woodhead Publishing Limited, 2013

dilution with inert gases. Due to the high reactivity, dilution is a suitable method for adjusting the properties to the requirements of the combustion hardware without compromising lean-flame blow-off stability. The technically produced hydrogen based on gasification, water gas shift reaction and final CO_2 scrubbing (carbon capture and storage (CCS)) is targeted to contain typically about 80–90% hydrogen (H_2), about 5–10% nitrogen (N_2), up to 5% carbon monoxide (CO), and some minor content of residual carbon dioxide (CO_2) and argon (Ar).

(f) Blast Furnace Gas (BFG), Corex Gas, Coke Oven Gas (COG)

These gases are residuals of processes connected with steel generation and are to some extent similar to syngases.

BFG is a by-product of the chemical reduction of iron ore in blast furnaces. It typically contains about 20–30% carbon monoxide (CO) and about 2–6% hydrogen (H_2) as combustible components, and a significant amount of inert gases with about 45–60% nitrogen (N_2), and 20–25% carbon dioxide (CO_2) (see Table 14.1). Due to the high inert gas content and the already relatively low heating value of the main combustible component CO, it has a low heating value in the range of 3–4 MJ/m^3. As a consequence of the low heating value and the low reactivity of the main combustible component CO, the reactivity of BFG is very low and special care has to be taken that lean-flame blow-off stability and burn out are sufficiently achieved by the combustion system.

Corex gas is a by-product of the upcoming cost-efficient and environmentally friendly Corex iron-generation process, which is based on a 'smelting reduction' process without requiring coke but directly applying coal. The residual gas of this process, called Corex export gas, typically contains about 42–47% carbon monoxide (CO), about 20% hydrogen (H_2) and about 2% methane (CH_4) as combustible components, and about 30% carbon dioxide (CO_2). The heating value is about 8 MJ/m^3. Composition and heating value are nearer to typical 'raw syngases' in comparison to BFG. Consequently, similar requirements are valid as for syngas application.

Coke oven gas is the by-product of the pyrolysis of coal, which is the basic process for coke production for the blast furnace process. It typically contains about 5% carbon monoxide (CO), about 55% hydrogen (H_2), about 25% methane (CH_4) and about 3% higher hydrocarbons as combustible components. Furthermore, it contains about 10–12% nitrogen (N_2) and about 2% carbon dioxide (CO_2) as well as contaminants (H_2S, HCN, CS_2, HG, Cd, etc.). Due to its relatively high hydrogen (H_2) and methane (CH_4) content, it has a higher heating value and Wobbe index compared to BFG and Corex gas, but below the level of standard natural gases (E, H or L). The reactivity is in the range of typical syngases and above the reactivity

© Woodhead Publishing Limited, 2013

of natural gas. Depending on the combustion system specifics it potentially requires dilution.

Again, as for other low-LHV gases in general, and also for BFG, Corex gas and COG, the reduced heating value compared to standard fuels leads to increased fuel mass flows and the requirement for a larger fuel system. Due to the poisonous CO content, special care has to be taken concerning fuel system tightness and detection of potential leakages (see Section 14.3.1 (d) Syngas).

14.3.2 Liquid fuels: types and characteristics

Since liquid fuels have to be transferred into a gaseous state of aggregation prior to combustion, atomization and evaporation are required, in addition compared to the combustion of gaseous fuels. Concerning the atomization quality as well as the compliance with pump specification, viscosity is an important parameter. Since the viscosity is temperature dependent, an adjustment to the requirements is possible by selection and control of the fuel temperature between the acceptable limits. The density has an impact concerning the required fuel injection-hole diameters. Further important parameters are the flash point (lower temperature limit for formation of ignitable mixtures of the liquid fuel in air) of concern for storage and handling safety, and the pour point (lower temperature limit for flowing capability of the fuel) which is relevant for the capability to feed the fuel into the combustor.

Table 14.3 gives an overview about important liquid fuel properties and liquid fuel types, discussed in more detail in the subsequent sections.

(a) Diesel or fuel oil

Diesel, or fuel oil, is the standard liquid fuel for stationary gas turbines, due to the good storage and combustion properties. It is a product from crude oil in the distillation window between 200°C and 350°C. It consists of approximately 75% aliphatic hydrocarbons ($C_{10}H_{20}$–$C_{15}H_{28}$) and about 25% aromatic hydrocarbons (e.g. benzene, styrene). The typical atomic mass concentrations are about 86% C, 14% H and a minor fraction of sulfur depending on crude oil source and cleaning quality. The heating value is about 42.6 MJ/kg, and the density from 0.82 to 0.86 kg/L. The kinematic viscosity at 40°C is in the range of 2–5 mm^2/s. The flash point is > 55°C. The definition for this type of fuel is specified in the following standards ISO 4261 (1993), ASTM D975 (2011) and ASTM D2880 (2010).

Beyond the integration of the liquid fuel system and a burner, suitable for atomization and combustion of fuel oil, gas turbines are typically capable for this fuel without significant further modifications. However, care has to

© Woodhead Publishing Limited, 2013

Table 14.3 Characteristics of selected liquid GT fuels

Fuel property	Units	Impact on fuel system	Impact on combustion/ turbine/HRSG	Diesel oil	Heavy fuel oil/marine diesel	Crude oil	Naphtha	Condensates
Distillation range	°C	Explosion protection Cavitation	Ignition delay time	200–350	350–500	45–500	30–200	30–350 (450)
Density	kg/L	Atomization pressure	Droplet size Flame length	0.82–0.86	0.85–0.97	~.87	0.69–0.79	0.72–0.79
Lower heating value	MJ/kg	Pump capacity		42.6	39.5–40.9	~42	43.4–45	43.4 (–48)
Kinematic viscosity	mm^2/s (=cSt)	Pump pressure lubrication Atomization pressure	Droplet size Flame length Ignition	2–5 at 40°C	>30 at 40°C	high	>0.5 at 20°C	>0.5 at 20°C
Flash point temperature	°C	Explosion protection		>55	>60	<0	<0	<0
Pour point temperature	°C	Pumping		<–15	<30	<0		
Nitrogen content	Mass ppm		NO_x emission	<150	5400	~3500	<10	<100
Hydrogen content	Mass %		Soot emission	12–14	var	var	14–16	14–16
Metallic contaminants	Mass ppm		High temperature corrosion Deposits on turbine blading	<0.2	100	>20	<2	<3
Sulfur content	Mass %		SO_x emission HRSG efficiency	<0.2	~2.8	>2	<0.05	<0.1
Carbon residue	Mass %		Coking of burner nozzles	<0.15	>0.1–10	var	<0.01	<0.07–2

Source: Waldinger *et al.*, 2010; Moliere, 2002.

© Woodhead Publishing Limited, 2013

be taken during the design process concerning emissions and the thermal loading of hot gas path parts.

(b) Heavy fuel oil or marine diesel

Marine diesel or heavy fuel oil are toxic residuals from the distillation of crude oil with a boiling temperature between about 350°C and 500°C and a significantly increased viscosity compared to diesel. There more than just one specific fuel called marine diesel or heavy fuel oil. The typical heating value is about 40.9 MJ/kg and the flash point is typically >60°C. In order to be suitable for pumping and to achieve sufficient atomization, heavy fuel oil is typically heated up to a level with sufficient margin against the flash point. Directly prior to injection it is typically further heated to levels of about 140°C to achieve good atomization. In comparison to diesel, heavy fuel oil has a higher content of sulfur as well as of other critical contaminants for gas turbine operation (e.g. vanadium). In order to prevent hot gas corrosion of combustor and turbine parts, which is promoted by vanadium, it might be necessary to add chemical inhibitors. In general, the application of heavy fuel oil requires a robust technology in the hot gas path section of gas turbines, which typically prohibits the use of latest GT technology (e.g. application of 'film cooling'), required for the highest efficiency levels. The higher amount of sulfur and other contaminants, as well as the more difficult atomization and evaporation, introduce further difficulties in achieving low emissions and long parts lifetimes. However, the lower cost of heavy fuel oil compared to diesel makes the application attractive.

(c) Crude oil

Crude oil is a non-treated toxic liquid, directly received from the oil well. It is a mixture of a large number of individual chemical components, with a wide range of boiling temperatures. Due to this, crude oil combines the requirements concerning tightness and explosion safety necessary for the low boiling components, with the difficulties associated with application of heavy fuel oil. The composition depends on the oil field. Typical atomic weight composition is 83–87% C, 10–14% H up to 2% N and O, up to 6% S and a minor content of metals. Since crude oil is untreated, it does not require the efforts connected with the refinery process, and is potentially attractive from the cost point of view. However, in terms of the engine suitability and emissions, the same is valid as mentioned for heavy fuel oil. In addition, the safety requirements for the fuel system are increased. Care has to be taken to control the properties of the crude oil during operation, since this is not a standardized fuel and may change from time to time.

© Woodhead Publishing Limited, 2013

(d) Naphtha and condensates

Naphtha is a toxic kind of raw petrol or gasoline distilled from crude oil and a raw material for the chemical industry. It contains the fractions from crude oil, with a boiling temperature from 30°C to 200°C (below the temperature window of diesel) and may have a significant share of aromatic compounds. The detailed composition depends on the specific crude oil source. For gas turbines so-called 'heavy naphtha' (boiling temperature from about 100°C to 200°C) is a niche application. While naphtha is characterized by high heating values and low content of mineral contaminants, similar to diesel, it has lower density and viscosity. Naphtha has high vapor pressure at atmospheric conditions and a low flash point, similar to gasoline. Consequently, the safety requirements for handling are similar to those for petrol or gasoline. Due to the lower viscosity, compared to diesel, lubrication behavior has to be considered in order to avoid fuel pump failures. Condensates are liquid fractions of natural gas from some natural gas wells, containing hydrocarbon fractions above C3. They have similar properties to naphtha (e.g. density, viscosity, heating value, vapor pressure and flash point).

14.4 Integrated gasification combined cycle (IGCC) technology options with and without air-side integration and carbon capture and storage (CCS)

In an IGCC power plant a combined cycle power island is connected with a chemical plant, which produces a synthetic fuel for direct consumption in the power plant, typically without storage or long transport distances. The core of the gas production unit is an oxygen or air-blown gasifier, operating under elevated pressure. The raw gas from gasification has to be treated (cleaned, cooled and diluted) before it can be burned in the gas turbine. The main components of an IGCC power plant are:

- Gasification unit.
- Systems for utilization of the raw gas heat.
- Gas cleaning section including sulfur recovery.
- Air-separation unit (in case of oxygen-blown gasification).
- Gas turbine package.
- Heat recovery steam generator.
- Steam turbine.

In the case of CCS the following units are required in addition:

- Water gas shift reactor.
- Carbon dioxide removal.
- Carbon dioxide compression.

© Woodhead Publishing Limited, 2013

Since the fuel properties of syngases and CCS-based hydrogen fuels are distinctly different from those of natural gas or fuel oil, the combustion system has to be adjusted accordingly:

- In order to allow for the high fuel mass flows due to lower LHV, the fuel nozzles require adjustment.
- The typically high reactivity, wide flammability range, high burning velocity and low ignition delay time require a design which is robust against flash back or flame stabilization directly at the gas injectors (risk of overheating). Consequently, so far, robust diffusion-type combustion systems have been applied in IGCC gas turbine combustors.

NO_x emissions of diffusion-type combustors are very sensitive to adiabatic flame temperatures. Since the undiluted syngases have in any case a very high reactivity, dilution with inert gases (reduction of flame temperature) is a powerful method in order to reduce NO_x emissions down to levels typically achieved with the premixed combustion of natural gas. Due to the high reactivity, stable combustion can still be maintained. Since in oxygen-blown gasification plants 'waste N_2' is available as the residual of the air separation, this N_2 is typically directly available as diluent. If N_2 is not available, or if further dilution is required, H_2O can be added. Application of a saturator system is an effective method of dilution with H_2O. Liquid water can be compressed efficiently to the required pressure level, and low temperature heat is sufficient for evaporation. After saturation, heating up to the design fuel temperatures is necessary. Care has to be taken that sufficient margin to the dew point is achieved, in order to avoid the impact of fog and droplets. Such a saturation system has exergetic advantages compared to steam injection, because in most cases low temperature energy is available and can be reintroduced into the high temperature gas turbine cycle in this way.

Finally, the required amount of dilution depends on the specific syngas composition, as delivered from the gasification unit, the combustion system design, and the NO_x emission target.

As a consequence of the typically low fuel heating value and the connected high fuel mass flow, the application of gasification products in gas turbines, which are developed for operation with natural gas or fuel oil, leads to a mismatch between compressor and turbine mass flow. Due to the high fuel mass flow, the turbine mass flow is significantly increased. This may lead to:

- Exceeding the turbine mass flow capabilities.
- High pressure ratios, which might be above the design limit of the engine.

© Woodhead Publishing Limited, 2013

Consequently it might be necessary to avoid or reduce this mismatch, which could be achieved by the following options:

1. Extraction of air (e.g. feed to air-separation unit) from the compressor exit without adjusting the compressor inlet mass flow or turbine design.
2. Reduction of the compressor inlet mass flow and adjustment of the rear compressor section to achieve the required surge margin.
3. Opening of the turbine flow path for reduction of the pressure ratio and adjustment of turbine blade profiles to enable increased mass flows.

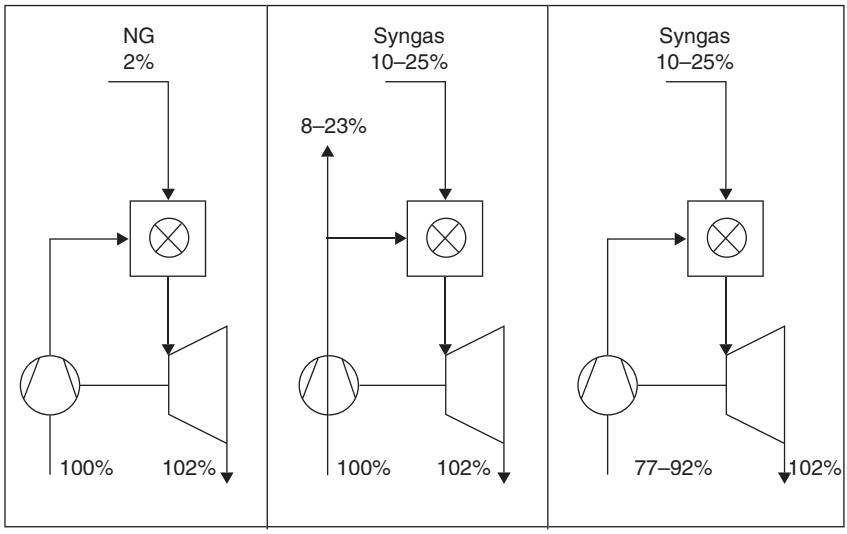
The first option makes sense if the air can be used for the air-separation unit and leads to a so-called air-side integrated plant arrangement. This arrangement has the advantage that potentially required gas turbine compressor modifications can be avoided, the investment cost for air compression to the air-separation unit can be reduced, and the overall plant efficiency can be improved. On the other, hand the air-side integration has the disadvantage of a more complex interaction between gas turbine and gasification operation. Partial air-side integration is a potential compromise offering the most advantages and least disadvantages from both options.

The second or third, or a combination of the second and third, option can be used if air extraction is not possible or not wanted. In this case, the air compression for the air-separation unit, or directly for an air-blown gasifier, is done by a separate external compressor. If there is a requirement for full performance operation with high heating value (secondary) fuel, modifications at the compressor and optionally at the turbine have to be made, not only to adjust the operation points but to enlarge the operational window. Since the design and modification efforts at the turbine are larger compared to compressor modifications, adjustments at the compressor are the more attractive choice compared to turbine modifications.

Figure 14.1 gives a simplified description of the potential air extraction or compressor adjustment requirements at the gas turbine for syngases with 4–10 MJ/kg compared to about 50 MJ/kg for natural gas. As a first guess the fuel mass flows are directly related to the heating value, and a mass flow balance is done to keep the turbine mass flow constant. For a more detailed analysis a full thermodynamic process analysis is required, but typical boundaries give results in the same range.

For the optional compressor adjustment, it is necessary to enable a compressor inlet mass flow reduction for the whole operation range. The pressure ratio, however, is similar to that of the engine without adjustment in operation with a standard high heating value fuel. The lower compressor inlet mass flow leads to a reduced stage pressure ratio at the compressor front stages, but an increased loading of the compressor rear stages. Consequently, overloading of the rear stages has to be avoided by reducing

© Woodhead Publishing Limited, 2013



14.1 Potential air extraction or compressor adjustment requirements at the gas turbine for syngases with 4–10 MJ/kg compared to 50 MJ/kg for natural gas.

the load from the rear stages and adding one or more stages at the compressor rear section. By these measures, a compressor with increased operation range and increased surge capability can be achieved.

As a consequence of such a compressor modification, the axial pressure distribution through the compressor is modified, which might introduce the additional requirement for an adjustment of the extraction positions of the secondary air system to achieve sufficient supply pressure for turbine cooling.

The advantages of the IGCC technology are:

- Potential for increased plant efficiencies compared to conventional steam power plants if using highest efficiency gas turbines.
- Low emissions.
- Possibility for integration with pre-combustion CCS.

Current main disadvantage of this technology is:

- Higher investment costs compared to conventional steam power plants.

14.5 Characterizing fuel gases

Changes in fuel composition always imply potential effects on the combustion behavior. There are basically four combustor operability issues that may be affected:

© Woodhead Publishing Limited, 2013

1. Emissions.
2. Combustion oscillation.
3. Overheating by flashback or autoignition.
4. Blow-out.

Two combustion techniques are applied in current GT combustors associated with different ways in NO_x control: lean premixed combustion (dry low NO_x (DLN) control) and diffusion combustion (wet NO_x control). Lean premix combustion is currently mainly used for different types of NG, whereas diffusion combustion is usually chosen for high reactivity gases, such as gases with high H_2 or elevated content of higher hydrocarbons.

The four combustor operability issues listed above affect both combustion techniques, but premix combustion is far more susceptible to fuel composition changes. Furthermore, premix combustion is currently the predominant technique used for heavy duty GT combustor for NG like fuels, due to its effectiveness in controlling NO_x without using water or downstream selective catalytic reduction (SCR) modules.

Therefore, in the following paragraphs fuel flexibility will be discussed in affecting premixed combustion (DLN) if not explicitly stated different.

14.5.1 Parameters affecting combustion

(*a*) *Parameters for characterizing fuel gases*

The typical composition of the most important gaseous fuels discussed in Section 14.3.1 and their properties is shown in Table 14.4.

Table 14.4 1is divided vertically into three main sections titled in the first column:

1. Typical composition of fuel gases.
2. Typical thermodynamic properties.
3. Typical kinetic properties.[1]

All data are valid for typical 'F-class' related boundary conditions: pressure = 18 bar, air temperature = 420°C, fuel temperature = 200°C.

Characterizing fuel gases targets ultimately the definition of lumped parameters. These parameters should capture fuel quality such that fuel

1 Kinetic properties are calculated with the Chemkin kinetic software package. The GRI3.0 chemical reaction mechanism (Smith *et al.*) is used. The GRI3.0 is optimized and validated for NG including certain fractions of higher hydrocarbons. Application for syngases and gases with high H_2 and CO content is outside its validated range. Consequently, the kinetic data calculated for these gases is connected with larger uncertainties

© Woodhead Publishing Limited, 2013

Table 14.4 Typical composition of most important gaseous fuels and their properties at 18 bar – fuel–air mixtures calculated with 420°C air temperature and 200°C fuel temperature

				Pure gases		
	Description	Symbol	Unit	CH_4	H_2	CO
Typical Composition	CH_4		[vol%]	100	–	–
	C_2H_6		[vol%]	–	–	–
	C_3H_8		[vol%]	–	–	–
	C_4H_{10}		[vol%]	–	–	–
	Content of higher hydrocarbons	C2+	[vol%]	–	–	–
	H_2		[vol%]	–	100	–
	CO		[vol%]	–	–	100
	CO_2		[vol%]	–	–	–
	N_2		[vol%]	–	–	–
	H_2O		[vol%]	–	–	–
Typical thermodynamic properties	Density, standard (273.15K, 10135 Pa)	ρ_{FG}^{Θ}	[kg/mN³]	0.718	0.090	1.251
	Lower heating value – Mass	LHV_M	[MJ/kg]	50.06	119.97	10.1
	Lower heating value – Volumetric	LHV_V^{Θ}	[MJ/mN³]	35.91	10.78	12.63
	Wobbe index	Wo	[MJ/mN³]	48.21	40.9	12.85
	Stoichiometric air demand	l_{min}	[kg/kg]	17.35	34.53	2.49
	Flame temperature (for mixture with max temperature)	T_{FI} (max)	[°C]	2206	2376	2370
Kinetic properties	Laminar flame speed (max)	S_L (max)	[cm/s]	54	770	2.7
	Laminar flame speed (at λ = 2)	S_L (λ = 2)	[cm/s]	12	43	0.8
	Chemical reaction time (min)	τ_c (min)	[s]	2E–05	2E–07	6E–03
	Chemical reaction time (at λ = 2)	τ_c (λ = 2)	[s]	4E–04	4E–05	8E–02
	Auto ignition time at 1000°C mixture temperature (min)	τ_{ai} (min)	[s]	1E–03	2E–05	4E–02

© Woodhead Publishing Limited, 2013

Natural gas 'like' gases				Syngases					
NG H	NG L	LNG	LPG	Undiluted	Diluted	Undiluted	Diluted	Undiluted	Diluted
				Coal (Buggenum)		Tar (ISAB)		CSS	
98.4	81.8	87.0	–	–	–	–	–	–	0.0
0.5	2.8	9.4	-	–	–	–	–	–	–
0.2	0.4	2.3	50.0	–	–	–	–	–	–
0.1	0.2	0.6	50.0	–	–	–	–	–	–
0.8	3.4	12.3	100.0	–	–	–	–	–	–
–	–	–	–	30.0	12.0	48.0	31.0	88.2	41.4
–	–	–	–	64.0	25.0	46.0	30.0	5.0	2.3
–	0.8	–	–	2.0	1.0	5.0	3.0	0.5	0.2
0.8	14.0	0.7	–	3.0	43.0	1.0	1.0	6.3	40.1
–	–	–	–	1.0	19.0	–	35.0	–	16.0
0.729	0.830	0.822	2.356	0.913	1.048	0.729	0.772	0.231	0.709
49.3	38.29	48.83	45.99	12.41	4.2975	15.076	9.44	43.974	6.774
35.96	31.77	40.12	108.35	11.33	4.503	10.991	7.283	10.143	4.802
47.88	39.663	50.33	80.27	13.48	5.002	14.637	9.429	24.015	6.486
17.09	13.26	16.87	15.66	3.2	1.109	4.006	2.507	12.54	1.932
2206	2189	2214	2253	2330	1782	2318	2052	2339	1853
55	53	62	89	225	30	318	81	589	80
12	12	14	20	31	6	33	13	42	8
2E–05	2E–05	1E–05	5E–06	1E–06	5E–05	7E–07	9E–06	3E–07	1E–04
4E–04	4E–04	3E–04	1E–04	6E–05	1E–03	6E–05	4E–04	3E–05	9E–04
8E–04	5E–04	3E–04	3E–04	1E–05	6E–05	1E–05	5E–05	2E–05	6E–05

© Woodhead Publishing Limited, 2013

gases in the same parameter range behave similarly in terms of their combustor operability, especially for the four issues listed in the introduction.

Table 14.5 gives an overview of commonly used parameters (for the fuel or the fuel–air mixture) and the mainly affected operability issues:

The definition of the different parameters and their relevance for fuel characterization are discussed below.

Wobbe index

Most of the current premixing combustors inject the fuel via hundreds of small holes into the air (see Siemens – Hermsmeyer *et al*., 2009; General Electric – Feigl *et al*., 2006; Alstom – Döbbeling *et al*., 2008; Mitsubishi – Tsukagoshi *et al*., 2010; Figs 14.2–14.5). The basic principle of this 'showerhead premixer design' is to bring the fuel gas through channels near to every stream line of the combustion air and inject this fuel into this air stream line. If every air stream line gets the same amount of fuel a homogeneous fuel–air mixture is produced. The basic subsystem for this fuel injection technique is a '(fuel) jet in (air) cross-flow' type of system. The source of these fuel jets maybe air swirler vanes (e.g. called 'swirler fuel injection' at Siemens or 'swozzle design' at GE, used also in the most recent G-class MHI burner designs), the hub of the air swirlers (as e.g. in older F-class MHI or Siemens can-annular designs) or the rim of the slots that introduce air into the burner cone ('EV burner' of Alstom).

The common feature of all these 'shower head – jet in cross-flow systems' is that the mixing pattern and mixing quality are strongly affected by the penetration depth h of the fuel jet into the air (see Fig. 14.6).

The jet penetration depth h at a given thermal heat input Q is dependent on the Wobbe index respectively the Gas index as shown subsequently.

The penetration depth increases with the square root of the momentum flux density ratio of fuel and air and the nozzle diameter d:

$$\frac{h}{d} = \text{const} \times \sqrt{\frac{\rho_{FG} \times c_{FG}^2}{\rho_{Air} \times c_{Air}^2}} \qquad [14.1]$$

where

h: penetration depth of the fuel gas jet
d: nozzle diameter
ρ_{FG}: density of the fuel gas
c_{FG}: velocity of the fuel gas
ρ_{Air}: density of air
c_{Air}: velocity of air

The proportionality coefficient is dependent on the velocity profile of the fuel jet at the nozzle outlet and is of the order of 2 (Karp *et al*., 1970).

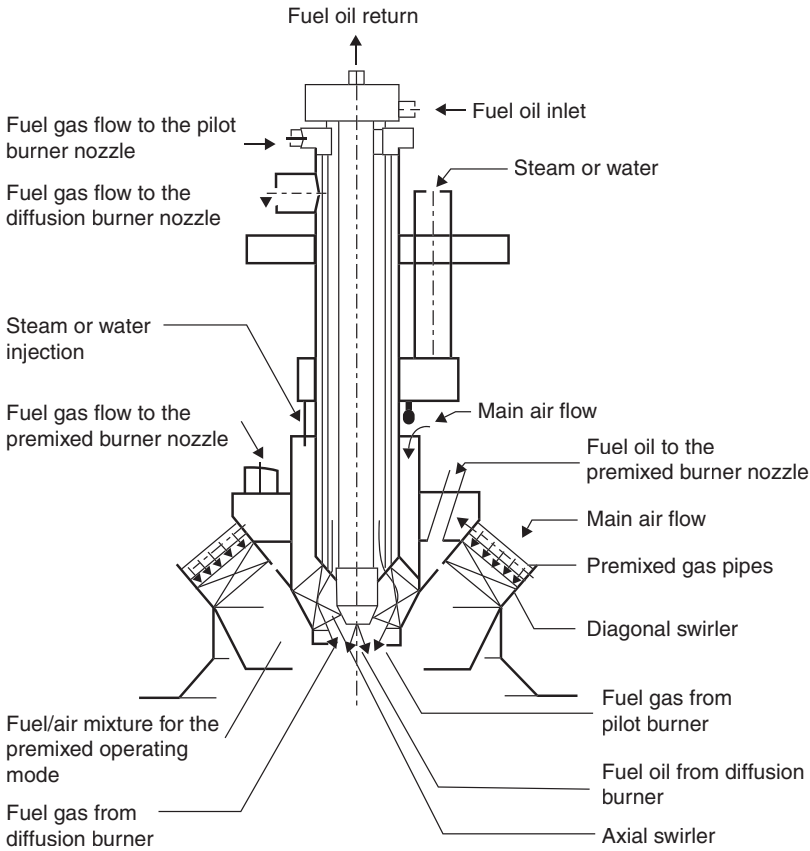
© Woodhead Publishing Limited, 2013

Table 14.5 Commonly used fuel parameters and the mainly affected operability issues

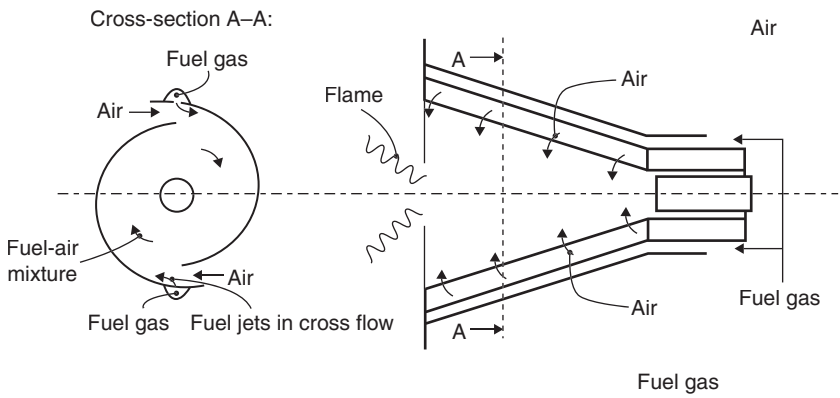
	Parameter	Symbol	Emissions	Combustion oscillation	Overheating by flashback or autoignition	Blow-out
Typical composition	Content of higher hydrocarbons	C2+	x	xx	xx	
	Liquid hydrocarbons	C-li			xx	
Typical thermodynamic properties	Lower Heating value – Mass	LHV_M	xx	xx		
	Lower Heating value – Volumetric	$LHV_V^{\ominus}$	xx	xx		
	Wobbe index	Wo	xx	xx		
	GI	GI	xx	xx		
	Flame temperature	T_{FI}	x		x	x
Kinetic properties	Laminar flame speed	S_L	xx	xx	xx	xx
	Chemical reaction time	τ_c		x	x	xx
	Damköhler number	Da		x	x	xx
	Auto ignition time	τ_{ai}	x		xx	xx

Note: xx: strong impact, x: moderate impact, blank: very weak or no impact.

© Woodhead Publishing Limited, 2013

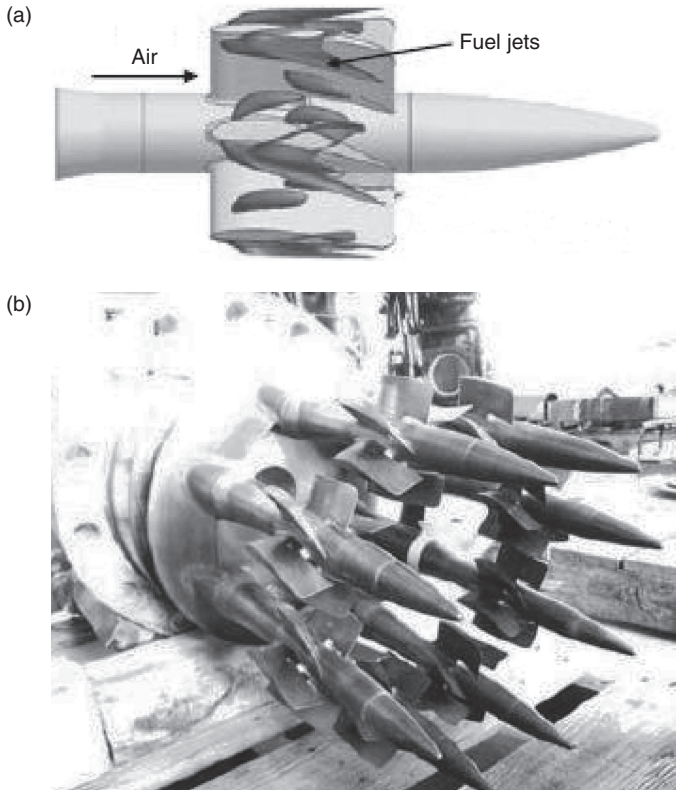


14.2 Standard Siemens Energy Hybrid burner for annular combustion chambers (see also Hermsmeyer *et al.*, 2009).

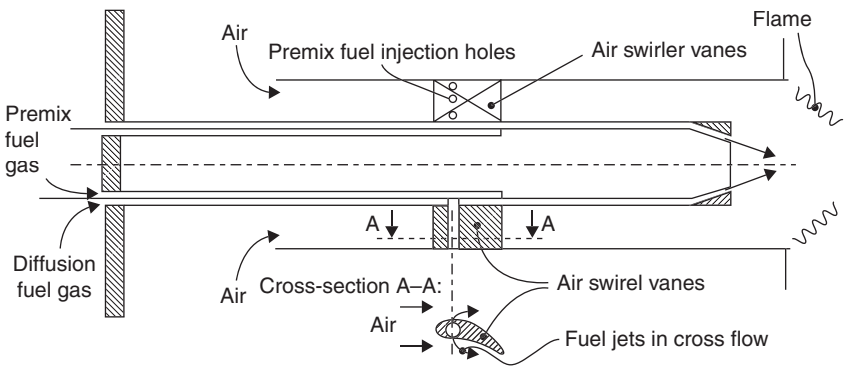


14.3 Sketch of the Alstom EV premix burner (based on Döbbeling *et al.*, 2008, Fig. 7).

© Woodhead Publishing Limited, 2013

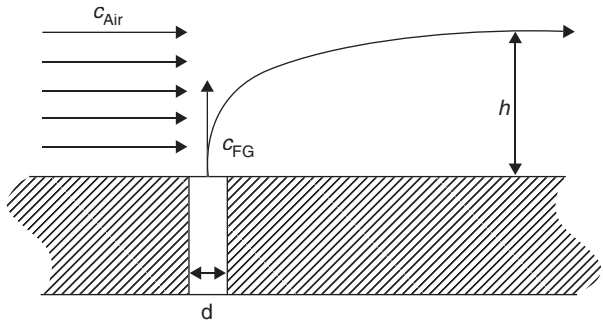


14.4 Fuel and air mixing at swirler of MHI combustor for G class engine. (*Source*: From Tsukagoshi *et al.*, 2010.) (a) One main swirler: details; (b) main swirler assembly.



14.5 Schematic, simplified sketch of GE DLN2.5H Gas Nozzle (based on Feigl *et al.*, 2006, Fig. 3).

© Woodhead Publishing Limited, 2013



14.6 Jet in cross-flow geometry.

The momentum flux density of the fuel gas can be rephrased in terms of thermal heat input Q of the gas turbine and the lower volumetric heating value LHV_V:

$$\rho_{FG} \times c_{FG}^2 = \left(\frac{\dot{V}_{FG}}{A_{FG}}\right)^2 \cdot \rho_{FG} = \left(\frac{1}{A_{FG}}\right)^2 \cdot \left(\frac{Q}{LHV_V \cdot \frac{\rho_{FG}}{\rho_{FG}^{\Theta}}}\right)^2 \cdot \rho_{FG}$$
$$= \left(\frac{1}{A_{FG}}\right)^2 \cdot Q^2 \cdot \frac{\rho_{FG}^{\Theta}}{LHV_V{}^2} \cdot \frac{\rho_{FG}^{\Theta}}{\rho_{FG}} \qquad [14.2]$$

with

Q: thermal heat input into the gas turbine [MJ]
A_{FG}: cross-section area of fuel gas nozzle [m²]
LHV_V: lower volumetric heating value of the fuel gas at reference temperature and pressure [MJ/m³]; Reference conditions are 273 K and 1013.25 kPa
ρ_{FG}: density of the fuel gas at gas turbine pressure and temperature
ρ_{FG}^{θ}: density of the fuel gas at reference temperature and pressure
V_{FG}: volumetric flow rate of the fuel gas

Obviously, fuel composition affects only the term $LHV_v/(\rho_{FG}{}^{\Theta})^{0.5}$ which is proportional to the Wobbe index:

$$Wo = \frac{LHV_V}{\sqrt{\rho_{FG}^{\Theta}/\rho_{Air}^{\Theta}}} \qquad [14.3]$$

with

ρ_{Air}^{Θ}: density of the air at reference temperature and pressure.

© Woodhead Publishing Limited, 2013

It is common to introduce air as reference density and thus make the fuel density dimensionless. As a consequence Wo and LHV_V have the same dimension: MJ/m³.

With these definitions the penetration depth h can be written as:

$$\frac{h}{d} = \text{const} \times \frac{Q}{A_{FG}} \times \frac{1}{\text{Wo}} \times \sqrt{\frac{\rho_{FG}^{\Theta}}{\rho_{FG}}} \sqrt{\frac{\rho_{Air}^{\Theta}}{\rho_{Air} \times c_{Air}^2}} \qquad [14.4]$$

Very often the fuel gas behaves approximately as an ideal gas, and the fuel gas density ratio can be rewritten as $\rho_{FG}^{\Theta}/\rho_{FG} = T_{FG}/T_{FG}^{\Theta} \times p^{\Theta}/p$ (p^{Θ}: reference pressure (10 135Pa)); note that the pressure is related to the pressure at the nozzle outlet, which can be assumed to be equal to the combustion air pressure at the injection location. Furthermore, very often pressure and air flow conditions are unchanged if only fuel quality and/or fuel temperature changes. In these cases, the penetration depth at a given thermal load Q is only dependent on the Wobbe index and fuel gas temperature ratio:

$$\frac{h}{d} = \text{const} \times \frac{Q}{A_{FG}} \times \frac{1}{\text{Wo} \times \sqrt{T_{FG}^{\Theta} / T_{FG}}} \times \sqrt{\frac{p^{\Theta}}{p}} \sqrt{\frac{\rho_{Air}^{\Theta}}{\rho_{Air} \times c_{Air}^2}} \qquad [14.5]$$

where

Wo: Wobbe index [MJ/mN³]
T_{FG}^{Θ}: reference temperature (273.15 K) [K]
T_{FG}: real fuel temperature in [K]
p^{Θ}: reference pressure (10 135Pa) [Pa]
p: fuel pressure at fuel nozzle outlet (approximately equal to air pressure at nozzle outlet) in [Pa].

The two square roots at the end of the equation are only dependent on the operation conditions of the gas turbine and not on the fuel gas quality or temperature.

In some cases, a temperature-corrected form of the Wobbe index, referred to here as the 'Gas index' (GI), is used to evaluate the fuel. The GI is defined as the temperature-corrected product of the Wobbe index and the square root of the reference temperature divided by fuel temperature at operation conditions:

$$\text{GI} = \text{Wo} \times \sqrt{\frac{T_{FG}^{\Theta}}{T_{FG}}} \qquad [14.6]$$

© Woodhead Publishing Limited, 2013

Compared to the Wobbe index, the GI is the preferable number to be applied for fuel characterization from aerodynamic and combustion perspective, because it better describes the interaction between air and fuel for different fuel preheating temperatures:

$$\frac{h}{d} \propto \frac{Q}{A_{FG}} \times \frac{1}{GI} \qquad [14.7]$$

Note that the formula describes also how the fuel nozzle diameter d affects the penetration depth h: $h \sim 1/d$ (because $A_{FG} \sim d^2$). This means that h stays constant if $d \times GI = d \times Wo \times T_{FG}^{\ominus}/T_{FG}$ stays constant. A smaller Wo can therefore be compensated by a proportional increase of d or a proportional decrease in T_{FG}.

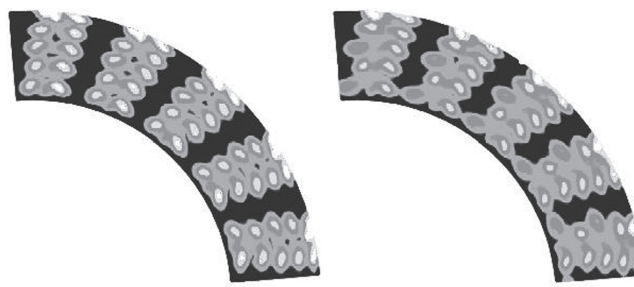
An example for the compensation of a decrease Wo index by an increase of fuel nozzle diameter d to get constant penetration depth h is given in Fig. 14.7: Here, the mixing pattern at the trailing edge of the swirler vanes of a Siemens Hybrid burner for H-gas and standard nozzle size is compared with an increased nozzle size for low BTU gas application at base load conditions. Although the fuel mass flow is approximately doubled from left to right, the mixing pattern could almost be kept unchanged (Hermsmeyer *et al.*, 2009).

The Wobbe index respectively the Gas index has another feature: for fuel gases with the same GI the pressure drop across the fuel nozzle stays constant. This can be derived by remembering that the momentum flux density of the fuel gas is also proportional to the pressure drop across the fuel nozzle for orifice type of nozzles (this is basically an application of the Bernoulli Equation):

$$\rho_{FG} \times c_{FG}^2 = \text{const} \times \Delta p_{FG} \qquad [14.8]$$

with:

Δp_{FG}: pressure drop across the fuel gas orifice



14.7 Fuel–air mixing profile at the trailing edge of the swirler vanes for H-gas. Left picture – with standard nozzle and low BTU gas; right picture – with adapted nozzle size. White/light grey is representing high fuel concentration, black/dark grey is representing low fuel concentration. (*Source*: From Hermsmeyer *et al.*, 2009.)

© Woodhead Publishing Limited, 2013

Combining this relationship with Equation [14.2] and rearrangement gives:

$$Q = \text{const} \cdot A_{FG} \cdot \frac{\text{Wo}}{\sqrt{T_{FG}/T_{FG}^{\Theta}}} \cdot \sqrt{\frac{p}{p^{\Theta}}} \cdot \sqrt{\Delta p_{FG}} \qquad [14.9]$$

or

$$Q \propto A_{FG} \cdot \text{GI} \cdot \sqrt{\Delta p_{FG}} \qquad [14.10]$$

The fuel pressure drop for a given thermal load Q is dependent on the GI and the injection geometry.

Compensation of penetration depth due to a decrease in Wo respectively LHV_V can be done in two ways:

1. By lowering fuel gas preheat temperature at a constant injection geometry (fuel nozzle diameter and number). In this case the pressure drop is also constant. Or more generally: if penetration depth is constant, the pressure drop is also constant for a given burner.
2. By increasing the fuel nozzle diameter d at a constant fuel gas preheat temperature. In this case the pressure drop decreases.

Flame temperature

Generally CH_4 and other hydrocarbons have about 150°C lower maximal adiabatic flame temperature than CO and H_2. This difference is also valid for natural gases in comparison to (undiluted) syngases (see Table 14.4). To get to the same flame temperature, syngases need therefore to be diluted with a higher amount of inert gases than natural gas. For burning syngases in diffusion mode, this means they need a higher dilution ratio than natural gases or LPG to achieve the same NO_x level.

Note also another difference between the two types of fuels: the maximal adiabatic flame temperature for 'natural gas like' fuels is approximately at stoichiometric air–fuel ratios λ of 1; for H_2, CO and for syngases it occurs at rich conditions at approximately $\lambda \approx 0.9$.

Laminar and turbulent flame speed

Laminar flame speed S_L is the propagation velocity of a laminar flame front into the unburned premixed gas. It depends on the fuel type, air–fuel ratio, temperature and pressure. It can be calculated with good approximation by kinetic mechanisms for various fuels (see Table 14.4, here GRI3.0 chemical reaction mechanism is used (Smith *et al.*)). The laminar flame speed is maximal near stoichiometric conditions for hydrocarbon fuels: CH_4 shows maximal reactivity (fastest burning velocity) near to stoichiometric condition (see Fig. 14.8). For CO, and even more pronounced for H_2, the maximum is

© Woodhead Publishing Limited, 2013

shifted into the fuel rich region: maximum at stoichiometric air fuel ratio λ of 0.6–0.8 (see Fig. 14.8).

Between H_2, CH_4 and CO there is about one order of magnitude difference in the laminar burning velocity, with H2 the fastest, and CO the slowest burning fuel gas. Figures 14.8 and 14.9 show curves 18 bar and 420°C air temperature, which is typical for 'F-class' conditions. At these conditions, maximal laminar speed for H_2 is 7.7 m/s, for CH_4 it is 0.55 m/s, and for CO it is 0.03 m/s.

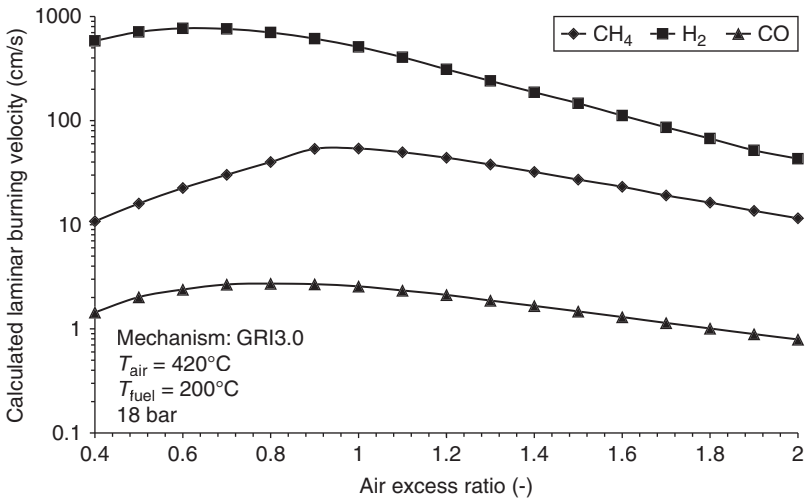
Ethane, C_2H_6, and propane, C_3H_8, have slightly higher maximal laminar flame speeds than CH_4 of about 0.7–0.9 m/s (18 bar and 420°C) (see Fig. 14.9); saturated hydrocarbons with more C atoms (up to C7) have approximately similar maximal laminar flame speeds to propane.

Compared to CH_4, H- and L-type natural gases show very similar kinetic properties. The LNG example shows some increase in reactivity, visible in larger laminar burning velocities as a result of the larger content of higher hydrocarbons. This increased reactivity, compared to CH_4, is even more pronounced for propane.

The laminar flame speed increases with the unburned mixture temperature and decreases with pressure for most of the lower hydrocarbons, and can be approximately described by the following equation (Poinsot, 2005, p. 55; Günther, 1984, pp. 78–81):

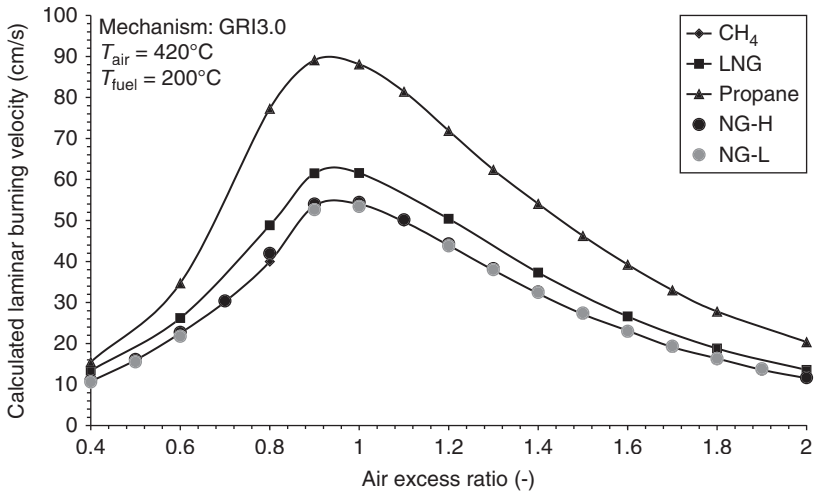
$$S_L \sim \frac{1}{p^n} \cdot T^m \qquad [14.11]$$

where p and T are the pressure and the temperature respectively in the unburned mixture. The exponents n and m are dependent mainly on the fuel



14.8 Laminar burning velocity for CH_4, H_2 and CO (pressure = 18 bar, air temperature = 420°C, fuel temperature = 200°C).

© Woodhead Publishing Limited, 2013



14.9 Laminar burning velocity for a typical H- and L-type natural gas, a typical LNG and propane compared to CH_4 (pressure = 18 bar, air temperature = 420°C, fuel temperature = 200°C).

type and somewhat on the stoichiometry. For methane $n \approx 0.5$ and $m \approx 2$; for propane $n \approx 0.2$ and $m \approx 2$ (Poinsot, 2005, p. 55).

The unburned mixture temperature is mainly impacted for 'natural gas like fuels' by the air temperature, because of the high stoichiometric air demand of hydrocarbons.

During loading of the gas turbine, air pressure and air temperature increase, which affects laminar flame speed in the opposite direction. However, the maximum laminar flame speed increases on loading a GT, because typically the effect of an increase of compressor end temperature overcompensates the effect of an increase of pressure. This means that e.g. flashback risk is increases with load and blow-off stability improves with load.

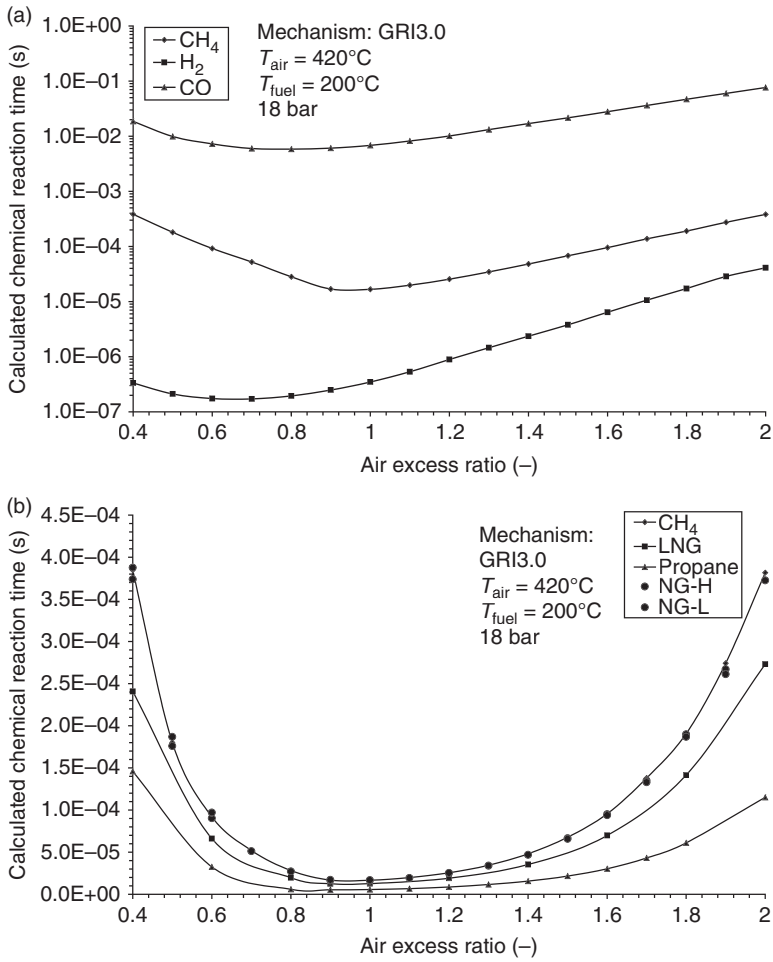
Another way to measure the reactivity of a propagating flame is the chemical time τ_C:

$$\tau_C = \frac{a}{S_L^2} \qquad [14.12]$$

where:

a: thermal conductivity [m²/s]
S_L: laminar flame speed of the fuel–air mixture [m/s]
τ_C: is basically a measure for the residence time in the laminar flame sheet (more specifically, the residence time in the preheat zone), thus for the time needed to complete the combustion reaction under consideration of the heat conduction from the burned gas into the unburned gas (Warnatz *et al.*, 2006, Chapter 8).

© Woodhead Publishing Limited, 2013



14.10 Chemical reaction time: (a) for CH_4, H_2 and CO; (b) for a typical H- and L-type natural gas, a typical LNG and propane compared to CH_4 (pressure = 18 bar, air temperature = 420°C, fuel temperature = 200°C).

The chemical reaction time may be compared directly to typical residence time in the burner, and is therefore useful to describe blow-off and flash-back phenomena.

Figure 14.10 shows the chemical reaction times of the gases discussed above.

Turbulence promotes flame propagation, giving a turbulent flame speed which is considerably higher than the laminar one. The turbulent flame speed is often described as

$$\frac{S_T}{S_L} = f\left(u', L_{\text{turb}}, \text{fuel–air mixture}\right)$$

© Woodhead Publishing Limited, 2013

u': turbulent velocity fluctuation
L_{turb}: turbulent length scale
Turbulent flame speeds in GTs are about 10–20 m/s.

The enhancement factor due to turbulence $f(u', L_{turb}$, fuel–air mixture) is unfortunately also dependent on the fuel and the stoichiometry. The impact of fuel is often explained by the impact of thermal and molecular fuel diffusivity on the evolution of corrugated flamelets that can be captured by the Lewis number (ratio of thermal diffusivity and molecular diffusivity). Especially hydrogen shows a higher increase of S_T/S_L with u' than normal hydrocarbons, such as methane or propane (see Lieuwen *et al.*, 2006; Kido *et al.*, 2002). This is usually explained by the lower Le number of hydrogen in comparison to the Le number of hydrocarbons.

For typical gas turbine burners, the flow regime is turbulent and the turbulent flame speed basically should be used to describe blow-off and flashback for a given burner. Unfortunately, the turbulent flame speed is much more difficult to estimate than the laminar flame speed, because it is impacted in addition by turbulence parameters. Therefore, in the literature the laminar flame speed is usually used for assessing flashback/blow-off.

Autoignition time and temperature

Autoignition refers to a homogeneous ignition of the fuel–air mixture. Homogeneous means there is no external ignition source (e.g. a spark) needed. Autoignition can happen everywhere after fuel and air have been mixed in the premixer. But autoignition upstream of the combustion chamber inside the premixer is the most important operational issue for the subsequent discussion flashback.

The autoignition temperature is defined as the limit temperature above which a fuel/air mixture ignites if given enough time. Table 14.6 gives an overview showing often used values of autoignition temperature for long ignition times.

However, these temperature values only making sense if the related ignition delay time (=autoignition time) is explicitly defined. Temperature and time form a pair of values which are mutually dependent (Warnatz *et al.*, Chapter 10, 2006).

The autoignition time is much more relevant, because it can be directly compared to the residence time in the premixing section of gas turbine combustors.

The autoignition time decreases exponentially with increasing unburned mixture temperature, and approximately linearly with increasing pressure (see, e.g. Li and Williams, 2000).

$$\tau_{ai} \propto 1/p \cdot \exp(-E/R \times T) \qquad [14.13]$$

© Woodhead Publishing Limited, 2013

Table 14.6 Autoignition temperatures: for stoichiometric mixture and at 1 bar

Component	Autoignition temperature [°C]
Carbon monoxide	605
Hydrogen	560
Methane	610
Ethane	525
Propane	470
n-Pentane	285
n-Octane	210
Benzene	555

Source: Günther, 1984, p. 64.

The autoignition time decreases with increasing size of the hydrocarbon molecule. This is due to quicker build-up of radicals during the break of the longer hydrocarbon chain in the combustion zone.

Values for autoignition times are shown in Table 14.4 and Fig. 14.11. Calculation results are based on the GRI3.0 mechanism, which is reasonable for the high temperature range for >1000°C but overestimates the values for the low temperature range considerably. For this reason only GRI3.0 calculation results above 1000°C are shown. The temperature dependency of autoignition time is shown in Fig. 14.11, based on measurement and calculations (Spadaccini, 1980, 1994).

At typical compressor outlet conditions, with temperature of ~500°C and pressure of ~18 bar, methane has autoignition times of the order of 200 ms. Adding C_2H_6 or C_3H_8 to CH_4 reduces the autoignition time (Beerer *et al.*, 2010): a mixture with 40% C_3H_8 and 60% CH_4 has about a factor of three lower autoignition time (Riccius *et al.*, 2005). Still higher hydrocarbons are liquid, such gas oil or kerosene. For gas oil or kerosene at ~500°C/20 bar autoignition time may come down to 1–10 ms (see Fig. 14.11; Spadaccini, 1980; Sattelmayr, 2010).

Adding hydrogen at low temperature (~500°C/15 bar) only weakly decreases the autoignition time of methane (Lieuwen *et al.*, 2006). Only at high temperatures (>700°C) a more pronounced reduction is found.

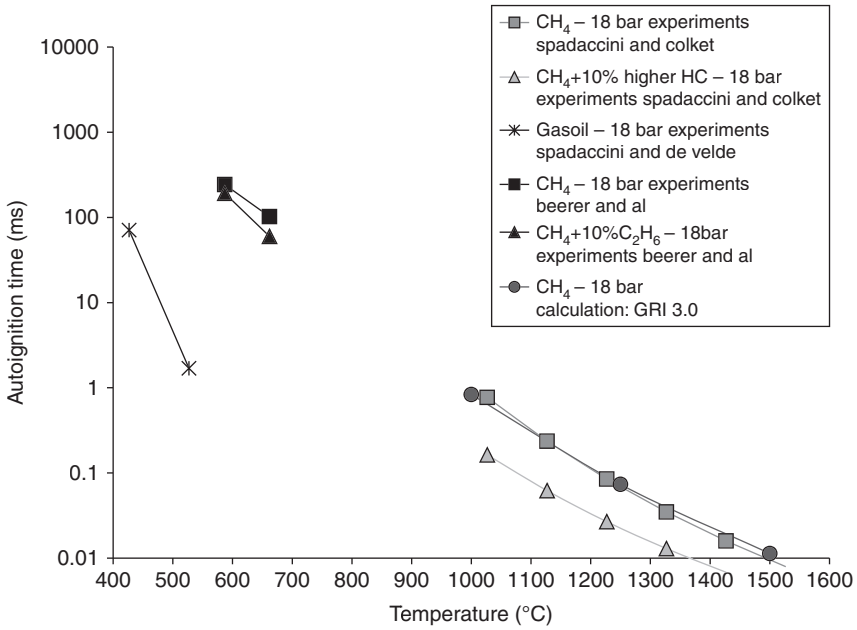
Pure CO has higher autoignition times than H_2 or CH_4. Adding a small amount of H_2 decreases the autoignition time to similar values as H_2.

(*b*) *Impact on combustion performance*

Emissions

In lean premixed combustion fuel quality affects NO_x emissions at a given GT-load mainly by the following parameters:

© Woodhead Publishing Limited, 2013



14.11 Autoignition time for various fuels at 18 bar and a stoichiometric air–fuel ratio of 2 (see also Sattelmayr, 2010); CH_4 calculations for >1000°C uses GRI3.0 (Smith *et al.*)

- the premixing quality,
- the fuel splits (e.g. % of diffusion pilot) applied,
- the adiabatic flame temperature.

Poor premixing introduces temperature peaks in and downstream of the combustion zone. As NO_x production increases exponentially with the combustion temperature, the NO_x produced by these high temperature streaks cannot be compensated by low temperature streaks. All the impact parameters listed above contribute to the strength of the temperature non-uniformity: premixing quality directly, unfavorable fuel splits by disturbing fuel premixing uniformity, and adiabatic flame temperature by increasing the level of the peak temperatures.

The premixing quality is dependent on the uniformity of the mixing of the fuel with the air, and on the position of the flame downstream of the premixing device.

Most of the current premixing combustors are using '(fuel) jet in (air) cross-flow' type of systems. For these systems, an increase of penetration depth of the fuel jet into the air cross-flow very often increases (but not

© Woodhead Publishing Limited, 2013

always) the premixing quality. The penetration depth is directly related to the Wobbe index, as discussed in the preceding sections.

The position of the flame is mostly affected by the laminar flame speed and for some types of combustors (such as the Alstom GT24/26 SEV reheat combustor (Riccius *et al.*, 2005)) by the autoignition time. The $C2^+$ or hydrogen content increases the laminar flame speed and decreases the autoignition time. Higher laminar flame speed or lower autoignition time moves the flame closer to the burner, reduces the premixing length downstream of the premixer but upstream of the flame zone in the combustion chamber, and increases in this way the NO_x emissions. If a change in fuel quality affects the turbulence level, then this effect may also contribute to a change in mixing quality and flame length. However for 'natural gas like fuels' the effect on turbulence is often small, because usually the amount of fuel mass flow/momentum flux is only a small percentage of the air flow/momentum flux.

Increasing adiabatic flame temperature increases the level of temperature peaks for a given mixture field.

The choice of fuel splits is very often restricted by the level of combustion oscillations. Therefore, all effects by which the fuel quality may affect combustion oscillations are also prone to affect NO_x, via changed fuel splits.

Combustion oscillations

Combustion oscillations in the intermediate frequency range (IF: ~50 to ~500 Hz) are often influenced by the location of the heat release zone relative to the combustor outlet and inlet. The acoustic pressure amplitude distribution (especially the location of pressure antinodes) is determined by the combustor length. The essential physical condition for combustion oscillations is that the combustion heat release oscillation amplitude and pressure oscillation amplitude are in phase (Rayleigh criterion). If the heat release zone shifts relative to the pressure antinode, combustion oscillations may be affected. The heat release zone location is determined by similar parameters to the premixing length inside the combustor impacting emissions: flame speed and autoignition time.

In many combustors also the fuel mixing profile, influenced via the penetration depth of the fuel jets by the Wobbe index, has an impact on the flame zone location.

Furthermore, an increasing Wobbe index increases the pressure drop across the fuel injection nozzles. Increasing pressure drop decreases the impact of potential fuel system resonances (which is usually described by the acoustic impedance of the fuel nozzles) on the mixing and on air–fuel ratio oscillations. This may affect combustion oscillations in either way: enhancing or damping.

Therefore, changes in the Wobbe index may also impact combustion oscillations.

© Woodhead Publishing Limited, 2013

Overheating by autoignition and flashback

Typically, combustors of heavy duty GT have a residence time between premixer and flame zone of <5 ms. As discussed above, typical autoignition times for fuel gas air mixtures are from 100 to 1000 ms; this holds for LNG, LPG and syngases.

It can therefore be concluded that autoignition as source of overheating in well-designed fuel gas premix combustors is of minor importance (the exception is the reheat combustion chamber, see above). The only ignition risk comes from condensate droplets if the fuel gas is cooled below the hydrocarbon dew point (see Section 14.5.3). These droplets may provide a heterogeneous ignition source associated with much shorter autoignition times than for the homogeneous gas mixture. All gas turbine manufacturers require therefore that fuel gas temperatures are 15–30°C above the hydrocarbon dew point before entering the combustor (see Section 14.5.2 for further discussion).

Premixing of liquid fuels deserves a more careful design effort. Flashback occurs when the flame travels back upstream in the direction of the premixers, in the worst case into the premixers. This occurs when the local turbulent flame speed exceeds the local flow velocity. It happens especially in the boundary layer, where the flow velocity decreases towards the wall (Lieuwen *et al*., 2006; Sangl *et al*., 2010). The layer in which the upstream travel of the flame front may happen is limited by the extinction thickness. Turbulent flame velocity increases with the laminar flame speed S_L (for further discussion see the section 'Laminar and turbulent flame speed'). Therefore, increasing content of H_2 or higher hydrocarbons increases the risk of flashback.

Blow-out

If premixed flames are operated at very lean conditions, the flame is blown out from the burner mouth and may get extinguished. Very lean conditions are characterized by a high stoichiometric air–fuel ratio λ and a very low equivalence ratio Φ ($\lambda = 1/\Phi$). Often combustion oscillation at low frequencies (LF) occurs when the blow-out limit is approached. There are many studies in which blow-out correlations based on empirical or physical correlations (e.g. well-stirred reactor or turbulent flame speed approaches) have been developed (Lieuwen *et al*., 2006; Hoffmann, 1994; Günther, 1984). Practically all of them can be transferred into a comparison between chemical time scale τ_C and a characteristic residence time τ_R. According to these correlations, blow-out occurs if $\tau_C > \tau_R$; this means the flame propagation takes more time than the available residence time for mixing and for reaction. This can be rephrased into a Damköhler number Da:

$$\mathrm{Da} = \frac{\tau_R}{\tau_C} \qquad [14.14]$$

© Woodhead Publishing Limited, 2013

The chemical time τ_C was introduced in the section 'Laminar and turbulent flame speed' in Equation [14.12].

The residence time τ_R is defined as the ratio of a characteristic burner length scale D (e.g. diameter of the burner mouth or recirculation zone length) and a characteristic burner flow velocity u (e.g. bulk velocity in the combustor):

$$\tau_R = \frac{D}{u} \qquad [14.15]$$

Blow-out occurs:

- when the velocity in the burner increases above a burner characteristic limit (for constant fuel and stoichiometric fuel air ratio);
- when the burning velocity decreases or the chemical time increases by running the combustor at leaner conditions or changing to fuels with reduced reactivity in terms of flame propagation (for constant velocity).

Both effects decrease the Damköhler number of the burner. The empirical respectively physical correlations suggest that blow-out occurs below a Damköhler number $\mathrm{Da}_{\mathrm{Bo}}$, which is characteristic for the given combustor:

$$\mathrm{Da} < \mathrm{Da}_{\mathrm{Bo}} \text{ (Blow-out limit)} \qquad [14.16]$$

The Da criterion gives then:

$$\mathrm{Da} = \frac{D \times S_L^2}{u \times a} < \mathrm{Da}_{\mathrm{Bo}}$$

$$u > \frac{S_L^2}{a} \cdot \frac{D}{\mathrm{Da}_{\mathrm{Bo}}} \qquad [14.17]$$

The factor $D/\mathrm{Da}_{\mathrm{Bo}}$ is characteristic for the burner and is dependent on the choice of burner dimension D. For a given burner the blow-out velocity decreases with increasing chemical time scale τ_C. Highly reactive gases such as hydrogen have therefore a relatively high blow-out velocity. Note that [Equation 14.17] give also some forecast of temperature and pressure dependency of the blow-out velocity via the pressure and temperature dependency of the thermal conductivity a and of the laminar flame speed S_L.

14.5.2 Parameters affecting operation of the gas turbine

All gas turbine manufacturers require a certain fuel gas temperature, to avoid the condensation of water or hydrocarbons in the fuel gas system and

© Woodhead Publishing Limited, 2013

the burner, and set limits for maximum levels of contaminants, such as Na and others. Violation of these requirements will negatively affect plant components, mainly outside the combustor, such as the auxiliary system for the fuel supply or the hot gas path through the turbine up to the stack: these are described in this chapter as operation affecting parameters, and are discussed subsequently.

Water dew point

A temperature difference in the range of about 15–30°C (Siemens 15°C; GE 18°C) between the fuel preheat temperature and water dew point is normally required for gas turbine operation. Condensation of water can result in corrosion and erosion in the auxiliary systems and the fuel nozzles. Furthermore, the sudden release of condensed water accumulated in the fuel gas system may lead to fuel gas fluctuation and thus to power extrusions.

Hydrocarbon dew point

As for the water dew point, a temperature difference in the range approximately of 15–30°C between the fuel preheat temperature and the hydrocarbon dew point is normally required for gas turbine operation. Condensation of higher hydrocarbons may produce droplets of these high hydrocarbons that are blown into the combustion chamber. For premixing systems for natural gas, these droplets may lower the autoignition time in the premix zone considerably. Typical liquid or waxy hydrocarbons with seven or more C atoms have autoignition times of 1–10 ms (see Fig. 14.11). This time may be lower than the residence time in the premixing zone and is therefore very often considered as potential source for overheating/flashback into the burner via autoignition.

Another serious issue is if the condensate collects over long periods of time, resulting in liquid slugging e.g. in fuel supply pipe. When gas flow rates are increased after a period of reduced power operation, the sudden convection of the condensates into the combustor can lead to uncontrolled heat release.

The hydrocarbon dew point is best determined via measurements (e.g. using chilled mirror devices (Deuker, 2010 and DIN51871, 1985)). Alternatively, a gas chromatographic analysis may be applied. In the latter case, it is very important that the components are analyzed up to hydrocarbons with 14 C atoms or more. Neglecting even small amounts of these high hydrocarbons may result in dew point changes of 20°C and more.

Contaminants – trace metals

The following trace metal contaminants are usually limited by heavy duty gas turbine suppliers: lead (Pb), vanadium (V), calcium (Ca), magnesium (Mg),

© Woodhead Publishing Limited, 2013

sodium (Na) and potassium (K). Sodium is normally the only trace metal contaminant found in natural gas. The source of sodium in natural gas is salt water. Other fuel gases, e.g. syngases, may also contain other metals.

During the passage through the hot gas path of the combustion chamber and the turbine, Na and K can combine with sulfur and/or vanadium to form highly corrosive compounds. Ca can lead to hard and tenacious deposits, such as CaO or $CaSO_4$ anhydrite, which neither spall off when the gas turbine is shut down, nor are readily removable by water washing of the turbine. These deposits on turbine blades and vanes will degrade performance, and may also abrade turbine coatings.

Usually the concentration of these contaminants is limited to levels of the order of 1 ppmw (ppmw: parts per million by weight) depending on the turbine technology applied. Coated blades and vanes and low turbine inlet temperatures allow higher concentration limits.

Contaminants – sulfur and hydrogen sulfides

Sulfur in the fuel may lead to the following issues:

1. formation of deposits in the fuel gas system,
2. corrosion in the fuel gas system,
3. hot gas path corrosion,
4. deposits and corrosion in heat recovery steam generator (HRSG) and SCR units.

In the fuel gas system elemental sulfur may form deposits. The formation of sulfur particles and coating is promoted by retrograde condensation during reducing pressures in valves and other components (issue #1). This condensation is avoided by preheating the fuel gas in the case of increased sulfur content. Sulfides in the form of H_2S or other components may lead to the formation of FeS again building up deposits in the fuel gas system. If O_2 comes into contact with sulfidic layers, oxidation (rust formation) is promoted strongly. If oxygen comes into contact with FeS particles on fuel gas filters, very high temperatures may occur. H_2S itself promotes stress corrosion in the fuel system (issue #2). During combustion, sulfur and hydrogen sulfidie are oxidized, mainly to SO_2 and, to about 2–3%, SO_3. In the downstream sections of the combustor in the turbine and the exhaust gas duct SO_2 to SO_3 conversion continues, such that typically 10% of the sulfur is emitted as SO_3. SO_3 forms corrosive salts with the trace metals discussed above. However, the concentration of these corrosive components is normally limited by the low level of trace metals, so that the issue #3 is not really limiting the sulfur content. Sulfur levels should also be considered when addressing HRSG corrosion (by sulfurous acid) and the performance of SCR modules (ammonium sulfate formation and deposits).

© Woodhead Publishing Limited, 2013

Usually the concentration of sulfur is limited by GT suppliers to levels of the order of 0.2–1%w.

14.6 Measures for extending operation range for fuel gases

This section gives an overview about technologies to extend the range of fuel flexibility and discusses some specific examples.

14.6.1 Overview

From 2005 to 2010 in the US market, the increased application of LNG drove the discussion about the band width of fuel gas quality applicable for natural gas combustion equipment including gas turbines. What parameters can capture the fuel quality, and what are the allowed ranges, was an important part of the discussion.

The result of the discussion were the so-called NGC+ interim guidelines, issued by the National Gas Council, which describe the interchangeability of future gases in terms of the Wobbe index bandwidth (±4% from historic Wo and a maximum Wo of 52.2 MJ/Nm^3), maximal contents of higher hydrocarbons (Butanes+ <1.5 mol%), and maximum of total inerts (<4 mol%).

This demonstrates that throughout the natural gas using industry the Wobbe index and some limiting values for higher hydrocarbons/inerts are currently the most common used interchangeability parameters.

This is also applicable to gas turbine manufacturers, who usually specify the allowable fuel gas bandwidth in terms of these parameters. Table 14.7 gives an overview.

The values shown depend:

- on the GT supplier, and thus on the combustor design,
- on the GT class: high turbine inlet temperature engines (such as F-, G-, H- and J-class engines or GT24/26 engines) have usually more narrow ranges than low turbine inlet temperature engines (such as D- and E-class engines),
- on the level of NO_x and CO emission targets: low NO_x values and high turndown ratio with low CO emissions call for narrower ranges.

Table 14.7 Typical parameter range for NG like fuels specified by gas turbine suppliers: Wo – Index range is given in percentage of the Wo Index design point around the design point

Wo – Index range		Wo – Index change rate	C2+	C3+
Without hardware change	With hardware change		mol%	mol%
5% ... 10%	... 15%	2%/min ... 4%/min	...16%	2%... 10%

© Woodhead Publishing Limited, 2013

- on special control system features, which are widening the allowable range: see below.

Some values stated in the table can be found in fuel gas specifications of the manufacturers or in Hermsmeyer *et al*. (2009), Boon (2010), Laughlin (2008) and in Popovic *et al*. (2010).

The allowable Wo index range without hardware change is often even narrower if no active tuning is allowed to react on fuel gas quality changes. Ranges down to ±2% can be found in specifications of manufacturers.

14.6.2 Approaches of different manufacturers

Improvements in the control system

All premix combustion systems use a certain number of independently metered and controlled fuel supply stages to adapt the combustion system to changes in load, ambient conditions (e.g. ambient temperature) and, last but not least, fuel quality. The simplest configuration is a main premix stage and a pilot stage. A pilot stage can be characterized as using only a small amount (usually up to 10%) of the fuel, which is burned as diffusion flame or as a premix flame richer in fuel than the main flame. More sophisticated systems use more than one pilot stage or split up the main stages into subgroups. Furthermore, the burners can be divided into subgroups. Currently. up to five stages can be found in the combustion hardware of different manufacturers. Tuning is the process of establishing a certain distribution of fuel between the existing stages, with the target to keep emissions and combustion dynamics low. Let us consider, as an example, the above mentioned simple system with two fuel stages: pilot stage and main stage. At low load with lean conditions, the pilot fuel may be increased to high levels to damp combustion dynamics near to the lean blow-off limit but accepting relatively high NO_x levels. At high load, with comparatively rich conditions, the pilot may be decreased to a low level in keeping combustion dynamics still low but minimizing NO_x emission. Historically, changes in fuel splits were used to operate the engine from ignition over idling up to baseload covering a wide span of stoichiometric conditions (at idling, stoichiometric air–fuel ratio is about 10; at base load, the air–fuel ratio is about 2).

The same strategy of changing fuel splits to optimize emissions and combustion dynamics is also applied to respond to changes in fuel quality.

Table 14.8 shows different levels of complexity of controlling fuel splits in response to changes of fuel quality.

Subsequently, two examples are discussed in more detail.

© Woodhead Publishing Limited, 2013

Table 14.8 Control system adaptations to improve fuel flexibility

Level of control complexity	Level of adapt-ability	Additional equip-ment	Disturbance variable	Adapted variable	Feedback variable for closed loop control	Control strategy	Engine affected	Application example	Reference literature	Reference in text
Low	Low	None	T-amb, Wo, C2+	Fuel splits	None	Tune manually	All	All GT with premix combustors		1
Med	Med	None	T-amb	Internal Pilot stage	None	Open loop control of fuel splits in depen-dence of T-amb	E-class	Siemens 50Hz (E-class engines)	Hermsmeyer *et al.*, 2009	2
Med	Med	Med	C2+	SEV / EV fuel split	None	Open loop control to minimize flashback	F-class	Alstom: (GT24/26)	Riccius *et al.*, 2005	3
Med	High	High	Wo	Fuel tempe-rature	GI	Closed loop control of T-fuel in order to keep GI constant	E-class	General Electric (E-class engines)	Forte *et al.*, 2008	4
Med	High	Low	T-amb, Wo, C2+	External Pilot stage	Combustion Dyna-mics	Automatic Tuning: control fuel splits in closed loop to minimize emissions	E-class	Alstom (GT13E2)	Döbbeling *et al.*, 2008	5

(*Continued*)

© Woodhead Publishing Limited, 2013

Table 14.8 Continued

Level of control complexity	Level of adaptability	Additional equipment	Disturbance variable	Adapted variable	Feedback variable for closed loop control	Control strategy	Engine affected	Application example	Reference literature	Reference in text
High	High	Med	T-amb, Wo	Fuel splits	NO_x	Model based closed loop control	E, F-class	General Electric Opflex	Popovic *et al.*, 2010	6
High	High	Med	T-amb, Wo, C2+	Internal Pilot-stages (1…2)	Combustion Dynamics, NO_x	Automatic tuning: control fuel splits in closed loop to minimize emissions	E, F, H, G	Siemens (IFGC), Mitsubishi (Advanced combustion pressure fluctuation monitoring)	Laughlin, 2008; Huth *et al.*, 2008; Engel *et al.*, 2007	7

© Woodhead Publishing Limited, 2013

Example 1: Closed loop control of fuel temperature in order to keep GI constant (Forte et al., 2008; Line 4 in Table 14.8)

This system is used on General Electric E-class engines. The burners are designed for the Wo index at the lower limit of the Wo index band to be covered and are running on cold fuel gas for this gas quality.

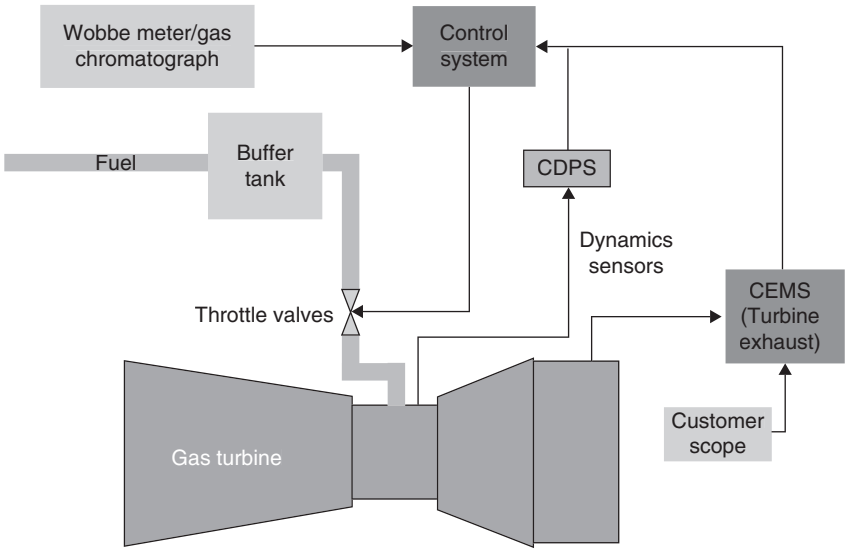
If a gas with a higher Wo needs to be used, it is heated, in order to achieve a target GI. The Wo index can be increased to an upper limit, which is defined by the maximum fuel preheat temperature (GI should stay constant independently of Wo). The maximum fuel preheat temperature is not reported in Forte *et al.* (2008) but is usually about 200°C. As explained in the section 'Laminar and turbulent flame speed' (dealing with the Wobbe index) holding the GI constant means that the fuel pressure drop and the penetration depth do not change. In Forte *et al.* (2008) engine test results for two fuel gases with a difference of about 16% in Wo index are presented. NO_x is equal for the two gases at base load, but is lower at part load for the high Wo index gas with heated fuel. CO and combustion dynamics level are nearly identical over the entire load range.

The system is based on a closed loop control on the GI (called the modified Wobbe index by General Electric) of the fuel. Two gas chromatographs, located upstream of the combustor inlet, measure the gas characteristics (LHV, specific gravity and temperature) and calculate the GI. If it is different from the target, it is corrected by modifying the temperature set point of a heat exchanger. The hardware uses one more gas chromatograph, called the plant gas chromatograph, located upstream the heat exchanger. The plant gas chromatograph evaluates the change rate of the Wo index before it gets to the burner. If it changes faster than a predefined limit change rate, it induces a switch-over of the burners from premix to diffusion combustion mode. For standard operation, diffusion mode is only used up to 50% GT-load. Usually, diffusion mode can also be used at higher loads and allows safe operation with low combustion dynamics up to base load but violates low NO_x emission limits.

Example 2: Automatic Tuning: closed loop control of fuel splits in order to minimize emissions (Engel et al., 2007; Line 7 in Table 14.8)

The system is used on Siemens F-class engines and is called the integrated fuel gas characterization (IFGC) system (Fig. 14.12). This IFGC system utilizes a rapid response Wobbe meter with a redundant gas chromatograph. This IFGC meter is installed upstream of the Econopac and its signal is fed into the engine control system. A fuel gas buffer tank is used to create a delay to accommodate for the response time of the IFGC meter. Depending on the changes in the Wobbe index of the incoming fuel, the control system is designed to adjust the engine tuning settings to compensate for this change feed-forward control. These feed-forward control changes are optimized

© Woodhead Publishing Limited, 2013



14.12 IFGC system.

subsequently by the combustion dynamics protection system (CDPS) in closed loop control mode. The CDPS is an active control dynamics monitoring and control system. It receives signals from the sensors measuring the pressure oscillations in the combustion chambers and from a continuous emissions monitoring system (CEMS) at the turbine exhaust. It compares this with the unit-specific emissions permit. Depending on the variation between the two, it adjusts the control settings in closed loop control to bring the unit to within the permitted emissions limits while maintaining acceptable levels of combustion dynamics.

The IFGC system also addresses the possibility of poor light-off scenarios associated with fuel quality. The IFGC system with its feed-forward control can accommodate this fuel quality variation and ensure adequate fuel flows for light-off.

14.7 Characterizing liquid fuels

This section gives a brief overview about parameters characterizing liquid fuel used in heavy duty gas turbines.

14.7.1 Introduction

Liquid fuels are the primary feed stock for aero engines. Liquid fuel flexibility is therefore of high importance for these engines and is discussed in detail in the aero engine literature.

© Woodhead Publishing Limited, 2013

For stationary heavy duty gas turbines liquid fuels are mainly used in two application scenarios:

- As backup for gaseous fuel in case its supply is interrupted (eventually in Europe) or not possible (e.g. during hurricanes in Florida).
- As primary fuel relying on a distinct feedstock, such as naphtha in India or crude oil in Saudi Arabia.

In both scenarios the fuel quality changes of the feedstock for a given gas turbine plant are limited. Fuel flexibility is more related to the ability of the GT to burn both liquid and gaseous fuel.

14.7.2 Parameters affecting combustion of liquid fuels

Table 14.9 is giving an overview about of the features of the most common liquid fuels discussed in Section 14.3.2, it is an excerpt of Table 14.3. The impact of their most important properties on the fuel system design, on the combustion behavior and on their impact on the turbine and downstream components (mainly HRSG) operation is shown.

As for the gaseous fuels, liquid fuels are burned in diffusion or premixed mode in stationary gas turbines. Premixed mode is often called lean premixed prevaporized (LPP) combustion.

Diesel oil – the most common liquid GT fuel – is very often burned in an LPP mode. Condensates and naphtha are sometimes burned in premix mode. The other fuel types are typically burned as diffusion flame.

For the premix combustion the most important parameters impacting combustion behavior are density, kinematic viscosity and distillation range. Density and viscosity impact the injection velocity and/or characteristic film thickness at the fuel oil nozzle. These parameters directly affect the atomization quality and the droplet sizes. Droplet sizes impact the flame length and by this have influence on combustion dynamics and NO_x emissions by similar effects as were discussed for premix combustion of gaseous fuels (see Section 14.5.1b). However, for premix fuel oil combustion, often water is added for NO_x reduction and a water/oil emulsion is prepared. The water content of this emulsion usually affects the combustion behavior more strongly than the properties of the pure fuel.

Kinematic viscosity is especially important if ignition has to be performed with the liquid fuel. At ignition a good atomization is needed to prepare effectively an oil–vapor–air mixture. Therefore, some preheating of the liquid fuel is used in order to lower the viscosity to get smaller droplet diameters and quicker vaporization.

The distillation range (see Table 14.9) may have a certain effect on the content of components with low autoignition time delay (usually heavier

© Woodhead Publishing Limited, 2013

Table 14.9 Important properties of liquid fuels and their impact on the fuel and combustion system performance of heavy duty gas turbines (excerpt of Table 14.3)

Fuel property	Units	Impact on fuel system	Impact on combustion/ turbine/HRSG
Distillation range	°C	Explosion protection Cavitation	Ignition delay time
Density	kg/L	Atomization pressure	Droplet size Flame length
Lower heating value	MJ/kg	Pump capacity	
Kinematic viscosity	mm^2/s (=cSt)	Pump pressure Lubrication Atomization pressure	Droplet size Flame length Ignition
Flash point temperature	°C	Explosion protection	
Pour point temperature	°C	Pumping	
Nitrogen content	Mass ppm		NO_x emission
Hydrogen content	Mass %		Soot emission
Metallic contaminants	Mass ppm		High temperature corrosion Deposits on turbine blading
Sulfur content	Mass %		SO_x emission HRSG efficiency
Carbon residue	Mass %		Coking of burner nozzles

hydrocarbons with longer chain length) and therefore affect the flashback behavior of the combustion system.

A fuel flexible combustor is important if with the same burner different fuel types listed in Table 14.3 are applied. In this case the fuel–water split may be used to accommodate different fuel qualities (see e.g. Prade *et al.*, 2002).

If only one fuel type from Table 14.3 is used, combustion behavior is less variable than for fuel gas combustion because the change of fuel properties within one fuel type is usually limited.

14.8 Future trends

Natural gas like fuels

Trends are different for different regions of the world. For certain regions an increased trend to LNG may happen, either because NG resources delivered

© Woodhead Publishing Limited, 2013

by pipelines decrease or to diversify the NG supply in order to become less dependent on single supply countries. This means that delivery by ships will gain more and more importance. Investigation about consequences of introduction of LNG on a larger scale was carried out for example in the US from 2005 to 2010, mainly because of a fear of declining national NG resources. Diversification of NG resources plays a role in Europe.

Furthermore, for locally constrained application, biogas and H_2 admixing may become important. H_2 production may rise because of the increasing electricity production by regenerative energy and its need for storage of the energy produced by wind and sun.

For the combustion system this means that the trend to a wider Wobbe index range to be burned with one combustion system will continue. Therefore, more sophisticated feedback loop systems with the ability to auto-tune the premix combustion system without the interference of a human operator will gain importance. Also, more complex strategies, including self-adaptive learning systems, may become commercially available.

For the GT engine, the trend to more usage of regenerative energy calls for power flexible engines, with the ability to quickly change load level in a wide load range with low emission and high part load efficiency.

Syngases

The future role of syngases is difficult to assess. Syngases are closely tied to the IGCC technology. In the last 15 years several prototype plants were built but the commercial break through did not happen, probably mainly due to the high investment cost for an IGCC plant. The reliability and availability issues of the early prototype plants have probably also contributed to their limited commercial success.

If the CO_2 economy becomes important, IGCC plants may be more often applied. The IGCC technology allows for a separation of CO_2 on the fuel feed side before the fuel is burned. This means that the massflow of gas to be cleaned up is smaller than for technologies for carbon capture from the exhaust. In connection with CCS, IGCC technology may gain importance.

A disadvantage of IGCC in the light of the recent trend towards regenerative energy production is that these plants are up to now not very power flexible. The reason is that IGCC plant components, such as the gasifier or the air-separation unit, often call for slow load changes.

Liquid fuels

As for natural gas, there is a trend for enforced application of biofuels, for example, biodiesel produced in Argentina or Brasilia.

An interesting alternative to LNG is the chemical conversion of CH_4 to methanol or dimethyl ester (DME). This conversion makes the transport by ship easier, because no low storage temperature is needed anymore. This

© Woodhead Publishing Limited, 2013

low temperature is needed to keep the NG liquid and is associated with losses by evaporation during the transport.

From point of view of combustion technology, a trend towards DLN combustion is visible.

14.9 References

ASTM International D2880-03 (2010), 'ASTM D2880 - 03(2010) Standard Specification for Gas Turbine Fuel Oils', ASTM International, West Conshohocken, PA, DOI: 10.1520/D2880-03R10, www.astm.org.

ASTM International D975 (2012), 'ASTM D975-12 Standard Specification for Diesel Fuel Oils', ASTM International, West Conshohocken, PA, DOI: 10.1520/D0975-12, www.astm.org.

Beerer B, McDonell V, Samuelsen S and Angello L (2010), *An Experimental Ignition Delay Study of Alkane Mixtures on Turbulent Flows ot Elevated Pressure ond Intermediate Temperatures*, Paper GT2010–22865, ASME Turbo Expo 2010, 18–18 June, Glasgow, UK.

Boon G (2010), *Overview: New Generation of Gas Turbines*, Paper B9, VGB congress, Power Plants 2010, 22–24 September 2010, Essen, Germany.

Deuker E, Hellat J and Kroll W (2010), 'Brennstoff, Brennstoffsystem und Fahrkonzept', in Lechner C and Seume J (eds.), *Stationäre Gasturbinen*, Berlin Heidelberg, Springer Verlag, p. 494, Chapter 11.

DIN51871: Prüfung von gasförmigen Brennstoffen und sonstigen Technischen Gasen; Bestimmung des Wasserdampf-Taupunktes; Verfahren mit gekühltem Spiegel (1985).

Döbbeling K, Meeuwissen T, Zajadatz M and Flohr P (2008), *Fuel Flexibility of the Alstom Gt13e2 Medium Sized Gas Turbine*, Paper GT2008–50950, Proceedings of ASME Turbo Expo 2008, 9–13 June, Berlin, Germany.

Engel J, Nag P, Abou-Joude K, Wu J and LaGrow M (2007), *Liquified Natural Gas (LNG) Flexibility Solutions for Large-Scale Gas Turbines,* POWER-GEN International 2007 – New Orleans, LA, USA, 11–13 December 2007.

European Committee for Standardization EN437 (2009), 'EN 437:2009 Test gases – Test pressures – Appliance categories', ISBN: 0580218805, DIN Deutsches Institut für Normung (Berlin), Verlag Beuth Berlin, Germany.

Feigl M, Myers G, Thomas S R and Smith R (2006), *7H™ Combustion System Performance with Fuel Moisturization*, Paper GT2006–90281, Proceedings of ASME Turbo Expo 2006, 8–11 May, Barcelona, Spain.

Forte Asti A, Bei S, Betti M and D'Ercole M (2008), *A Gas Turbine Innovative System for Managing Fuel with different and variable-over-time Wobbe Indexes*, Paper GT2008–51189, Proceedings of ASME Turbo Expo 2008, 9–13 June, Berlin, Germany.

Günther R (1984), *Verbrennung und Feuerungen*, Berlin Heidelberg New York, Springer Verlag.

Hermsmeyer H, Prade B, Berenbrink P and Köstlin B (2009), *Siemens Gas Turbines with High Fuel Flexibility on Natural Gases*, POWER-GEN Asia 2009 – Bangkok, Thailand, 7–8 October 2009.

Hoffmann S (1994), *Untersuchungen des Stabilisierungsverhaltens und der Stabilisierungsgrenzen von Drallflammen mit innerer Rückströmzone*, Dissertation, Universität Karlsruhe (TH), Kapitel 2.4.

© Woodhead Publishing Limited, 2013

Huth M, Gruschka U, Janus B, Meisl J and Wasif S (2008), *ULN System for the New Sgt5–8000h Gas Turbine: Design and High Pressure Rig Test Results*, Paper GT2008–51208, ASME Turbo Expo 2008, 9–13 June, Berlin, Germany.

International Organization for Standards ISO 4261 (1993), 'ISO 4261:1993 Petroleum products – Fuels (class F) – Specifications of gas turbine fuels for industrial and marine applications'.

Karp I N, Kaminskaya O W and Marzewoj E P (1970), ‚Untersuchung von Gasmischern mit der Schlierenmethode', *Verfahrenstechnik* **4**, Nr.5, 213–214.

Kido H, Nakahara M, Nakashima K and Hashimoto J (2002), 'Influence of local flame displacement velocity on turbulent burning velocity', *Proc. Comb. Inst.*, **29**, 1855–1861.

Laughlin J (2008), *Meeting Gas Quality Changes*, Engineering world wide, Volume **112**, Issue 5, May 1, 2008, Pennwell.

Li S C and Williams F A (2000), *Reaction Mechanisms for Methane Ignition*, Paper GT2006–90281, Proceedings of ASME Turbo Expo 2000, 8–11 May, Munich, Germany.

Lieuwen T, McDonell V, Petersen E and Santavicca D (2006), *Fuel Flexibility Influences on Premixed Combustor Blowout, Flashback, Autoignition and Stability*, Paper GT2006–90770, Proceedings of ASME Turbo Expo 2006, 8–11 May, Barcelona, Spain.

Moliere M (2002), *Benefiting from the Wide Fuel Capability of Gas Turbines: A Review of Application Opportunities*, Paper GT-2002–30017, Proceedings of ASME Turbo Expo 2002, 3–6 June, Amsterdam, The Netherlands.

Poinsot T and Veynante D (2005), *Theoretical and Numerical Combustion*, 2nd edition, USA, Edwards.

Popovic P, Myers G, Symonds R and Campbell A (2010), *Fuel Flexibility with Low Emissions in Heavy Duty Industrial Gas Turbines*, Paper GT2010–22267, Proceedings of ASME Turbo Expo 2010, 14–18 June, Glasgow, UK.

Prade B, Meisl J, Berenbrink P and Hoffmann S (2002), *Further development of low-emissions oil combustion in the Vx4.3A Hybrid burner*, VGB Power Tech 8/2002, pp. 51–55.

Riccius O, Smith R, Güthe F and Flohr P (2005), *The GT24/26 Combustion Technology and High Hydrocarbon ('C2+') Fuels*, Paper GT2005–68799, Proceedings of ASME Turbo Expo 2005, 6–9 June, Reno-Tahoe, Nevada, USA.

Sangl J, Mayer C and Sattelmayr T (2010), *Dynamic Adaptation of Aerodynamic Stabilization of a Premix Swirl Burner to Fuel Reactivity Using Fuel Momentum*, Paper GT2010–22340, Proceedings of ASME Turbo Expo 2010; 14–18 June, Glasgow, UK.

Sattelmayr T (2010), 'Grundlagen der Verbrennung in stationären Gasturbinen', in Lechner C and Seume J (eds.), *Stationäre Gasturbinen*, Berlin Heidelberg, Springer Verlag, pp. 442, 443, Chapter 9.

Smith G P, Golden D M, Frenklach M, Moriarty N W, Eiteneer B, Goldenberg M, Bowman C T, Hanson R K, Song S, Gardiner W C, Lissianski V V and Qin Z, *GRI-Mech 3.0*, Available from: http://www.me.berkeley.edu/gri-mech/

Spadaccini L J and TeVelde J A (1980), *Autoignition Characteristics of Aircraft-Type Fuels*, Nasa Contractor Report, Nasa CR-159886.

Spadaccini L J and Colket M B (1994), 'Ignition Delay Characteristics of Methane Fuels', *Prog. Energy Comb. Sci.*, **20**, 431–460.

© Woodhead Publishing Limited, 2013

Tsukagoshi K, Arimura K, Katsunori T, Nishida K, Konishi T, Akamatsu S, Kishida H and Sato K (2010), *Development of Air Cooled Combustor for Mitsubishi G Class Gas Turbine*, Paper GT2010–22864, Proceedings of ASME Turbo Expo 2010, 14–18 June, Glasgow, UK.

Waldinger R and Hellat J (2010), 'Besonderheiten des Betriebs mit Schweröl, Naphta und Kondensaten', in Lechner C and Seume J (eds.), *Stationäre Gasturbinen*, Berlin Heidelberg, Springer Verlag, p. 541, Chapter 13.

Warnatz J, Maas U and Dibble R W (2006), *Combustion*, 4th edition, Berlin Heidelberg New York, Springer Verlag.

© Woodhead Publishing Limited, 2013

15

Carbon dioxide (CO_2) capture and storage for gas turbine systems

C. D. SOOTHILL, M. T. BIALKOWSKI, G. L. GUIDATI and A. ZAGORSKIY,
Alstom (Schweiz) AG, Switzerland

DOI: 10.1533/9780857096067.3.685

Abstract: Power generation is a major contributor to the worldwide CO_2 emissions. Carbon capture and storage (CCS) is a means to reduce CO_2 emissions from gas turbines. This chapter describes the three different routes that are considered, namely pre-combustion capture, oxy-fuel combustion, and post-combustion capture. The impact of CCS on today's natural gas combined cycle (NGCC) plants is discussed. Future trends for second generation CCS are outlined. All concepts lead to a notable loss in efficiency compared to a standard NGCC plants.

Key words: carbon capture and storage (CCS), pre-combustion capture, oxy-fuel combustion, post-combustion capture.

15.1 Introduction

The role of fossil fuels in climate change was established by the Intergovernmental Panel on Climate Change (IPCC) (Pachauri and Reisinger, 2007). The anthropogenic emissions of CO_2, including the combustion of biomass and long-cycle fossil fuels, was shown to be a substantial contributor to the increase in CO_2 concentration in the atmosphere. This causes climatic changes, such as increase in atmospheric temperature, and a rise of the sea-level. The power generation industry is responsible for a substantial amount of CO_2 emission, and hence there is intense and growing pressure and economic investment to find new and adaptive technologies for power generation with substantially reduced CO_2 and other greenhouse gas emissions.

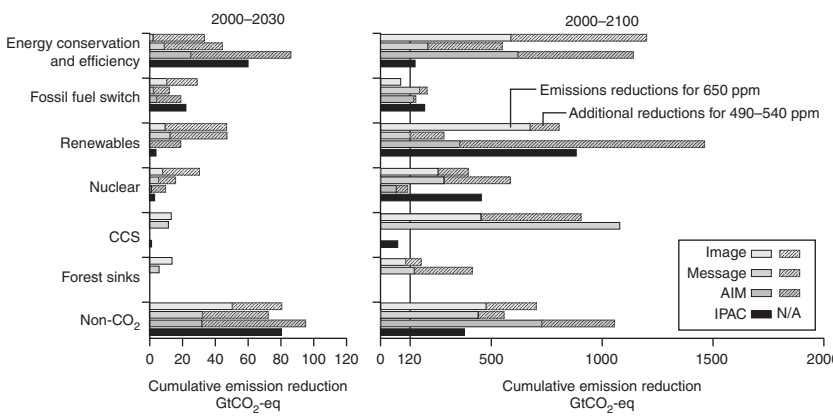
The IPCC reports that 57% of all greenhouse gas (GHG) emissions are related to the use of fossil fuels (e.g. electricity production, transport, industry). Other contributors are methane and nitrous oxides from agriculture, and CO_2 from deforestation. Twenty-six per cent of GHG emissions can be related to the energy sector, mostly the generation of electricity in fossil

Published by Woodhead Publishing Limited, 2013

fuel power generation plants (coal, oil and gas). Although from a global perspective coal continues to increase in its use for electricity generation, in Western Europe and North America natural gas has and will continue to strongly increase its share. Typical CO_2 emissions from a modern coal plant are 800–1000 g/kWh (based on 40–50% gross efficiency). Emissions from a modern NGCC plant are less than half, at approximately 350–400 g/kWh (based on 50–60% gross efficiency). An aspect that must be considered is the life cycle CO_2 emissions from fossil fuels, since both coal mining and natural gas extraction release substantial quantities of CO_2 and other greenhouse gases to the atmosphere.

The growth of renewables in the electricity generation mix is a result of the environmental concerns. It brings substantial costs to the overall electricity generation and transmission system, and also increases the need for flexibility in operation of fossil plants to support fluctuating energy production. NGCC plants already offer startup and load change rates twice as rapidly as modern coal-fired plants. This functionality will be increasingly important. Due to the variable and, to a great extent, unpredictable nature of renewable energy sources, such as wind and solar, an increase of their share will necessitate a stronger support to the grid from power plants capable of fast and controllable load variations, first of all gas and hydro. The development of CO_2 capture from NGCC plants must take this in to account.

The analysis of possible scenarios for stabilizing the CO_2 emissions has resulted in a set of mitigation options, which are schematically represented in Fig. 15.1 (Pachauri and Reisinger, 2007). Stabilization until 2100 requires a mix of equally important measures, among which energy conservation and efficiency, renewables and CCS are dominant.



15.1 Schematic representation of the options for mitigating CO_2 emissions.

CCS technologies have been in development over many years in laboratories. Some of them have found industrial application, e.g. the injection of CO_2 into oil and gas wells for enhanced recovery. These processes include elements such as CO_2 compression and pipeline transport and can be applied to CCS from fossil fuel power generation. However, so far the overall system demonstration for large-scale applications is in the development stage.

Since the specific emissions of CO_2 are twice as high for coal, the focus for CCS development has been on coal plants. With a shift towards NGCC plants, particularly in the USA and Europe, their share of CO_2 emissions will rise. Therefore, as part of the overall plan to mitigate climate change, a solution to remove the CO_2 emitted by NGCC is required.

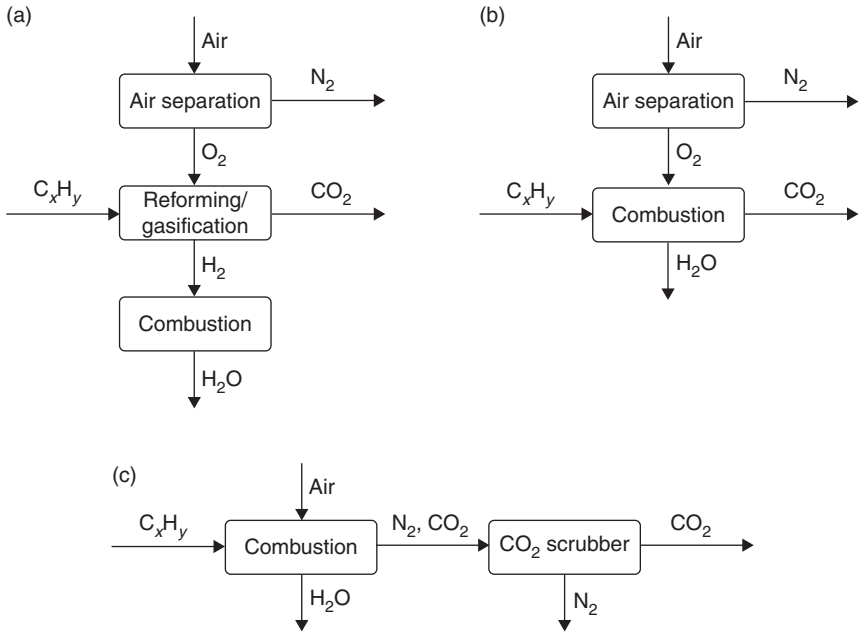
The structure of this chapter is as follows. Section 15.2 introduces the three main routes that are followed for CO_2 capture from gas turbine power plants. Section 15.3 addresses the main impact on today's gas turbine technology, highlighting the challenges, opportunities and fields of development required for the different routes. Section 15.4 addresses future trends, which may become reality for the next generation of gas based power plants with CCS. Section 15.5 describes some aspects relevant for the actual implementation of CO_2 capture for gas turbines, while Section 15.6 summarizes the outcome of this chapter.

15.2 CO_2 capture technologies

When a carbon-containing fuel (coal, oil, gas) is combusted with a quantity of air larger than the stoichiometric value, the resulting exhaust gas stream will contain a mixture of nitrogen and its oxides, carbon dioxide, water and some residual oxygen. Water can be easily removed by condensation. The challenge is the separation of CO_2 from the other non-condensable gases.

There are three distinct approaches to this problem, which target (1) the upstream processing of the fuel, (2) the combustion itself and (3) the resulting flue gas (Foy and Yantovski, 2006). Pre-combustion capture (Fig. 15.2a) utilizes the fact that the separation of oxygen from nitrogen in an air separation unit (ASU) is a well-established technology. Oxygen is used in a fuel reforming/gasification step to create a stream of CO_2 and hydrogen. The separation of these two gases is also well established, e.g. as the Rectisol process (Hochgesand, 1970). Hydrogen can then be combusted without further CO_2 emission. Oxy-fuel processes (Fig. 15.2b) again use the ASU technology (or modern variants of it, such as membranes or chemical looping, which utilizes an oxygen carrier) to combust the fuel in the absence of nitrogen. The resulting exhaust gas consists mainly of water and CO_2, which can be easily separated from each other. Finally the post-combustion processes

Published by Woodhead Publishing Limited, 2013



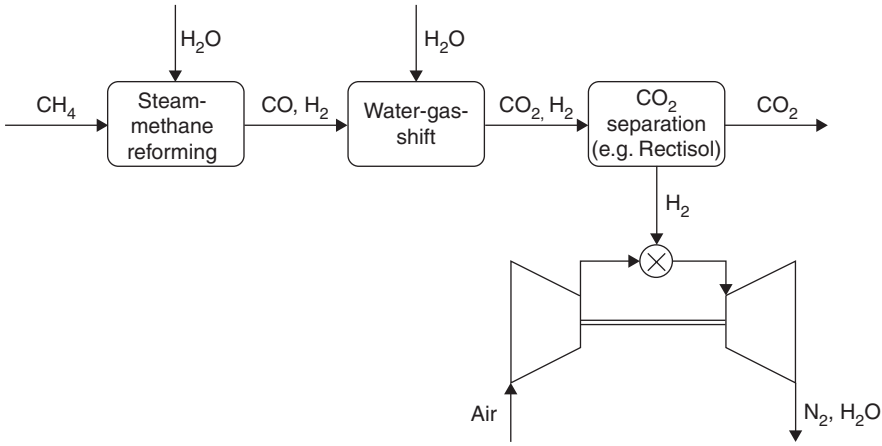
15.2 CO_2 capture technologies. (a) Pre-combustion capture, (b) oxy-fuel processes and (c) post-combustion processes.

(Fig. 15.2c) tackle the problem of separating nitrogen and CO_2 in a dedicated CO_2 scrubber.

15.2.1 Pre-combustion capture

The first option for reducing or avoiding CO_2 emissions from gas turbines addresses the fuel side rather than combustion products. It is therefore commonly labelled pre-combustion capture. Any hydrocarbon fuel has a typical elementary composition of the main constituents, namely carbon (C) and hydrogen (H). While methane has the most favorable molar ratio of H/C = 4, this value drops to approximately 2 for liquid fuels and to 0–1 for coal. Reducing CO_2 emissions requires an increase of the H/C ratio. Complete avoidance can only be achieved by converting the fuel into hydrogen (H/C = ∞) and by pre-separating all carbon in the form of CO_2. Pre-combustion capture has been studied in a number of EU-funded projects with the participation of industry and academia (Decarbit, 2008; EnCap, 2004).

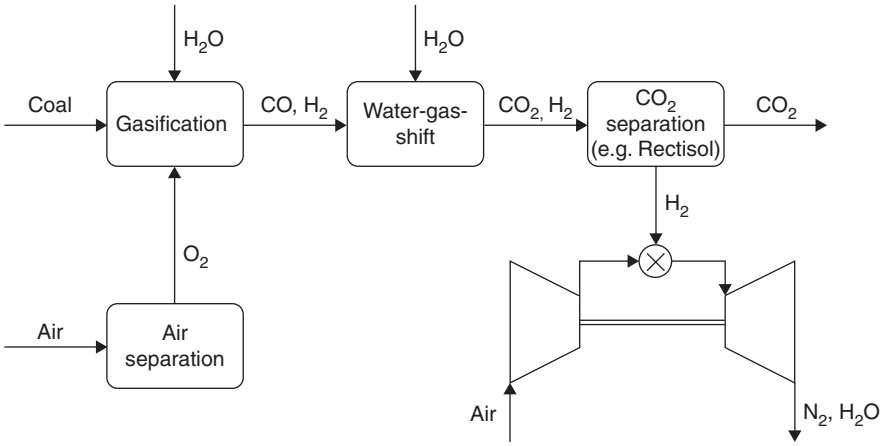
Depending on the input fuel, different technological routes are followed. For methane, the standard process is called steam methane reforming



15.3 An IRCC consists of a combination of steam methane reforming and a gas turbine.

(Higman and van der Burgt, 2003). Methane and steam react at high temperatures (700–1000°C) under the presence of a nickel catalyst to carbon monoxide (CO) and hydrogen. The hydrogen yield can be increased by letting CO react with steam to form CO_2 and hydrogen. This process is called the water-gas shift (WGS) reaction. This leads to a resulting stream, which is dominated by CO_2 and hydrogen. CO_2 can be separated using a standard process, such as Rectisol (Hochgesand, 1970). Steam methane reforming is the main technological route for the production of hydrogen (e.g. for feeding hydrocrackers in oil refineries or for ammonia synthesis). Integrated Reforming Combined Cycle (IRCC), see Fig. 15.3 is a combination of steam methane reforming and a gas turbine.

If coal is chosen as the primary fuel, there are a large variety of gasification processes (Higman and van der Burgt, 2003). They all follow the same principle, namely, to let carbon react with water and oxygen in order to form a syngas that consists of carbon monoxide, hydrogen and some fraction of CO_2. Pure oxygen is required to maintain the desired conversion rate of coal, and to avoid introducing nitrogen. The molar ratio of H_2 to CO depends on the feedstock and on the process, and is typically between 0.3 and 0.8. CO can again be converted into CO_2 by the WGS reaction. The resulting gas consists mainly of H_2 and CO_2, where the latter is separated by a standard process. The combination of coal gasification and a gas turbine is commonly termed Integrated Gasification Combined Cycle (IGCC), see Fig. 15.4. It should be noted that the motivation for developing IGCC was not originally to avoid CO_2 emissions, but to turn coal into a gaseous fuel that could be burned in a gas turbine. In this case there is no need for the WGS reaction, and the syngas can be used directly. Currently, most of the



15.4 An IGCC consists of a combination of coal gasification and a gas turbine.

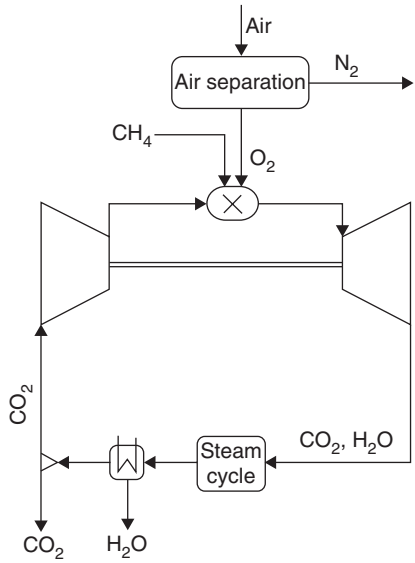
gasification applications are aimed at producing chemical feedstock and fertilizer via ammonia/urea.

Methane and coal are only the two extremes in terms of H/C ratio. Any hydrocarbon material with intermediate values (oil residues, waste, biomass, etc.) can be converted into hydrogen and CO_2, with the latter being ready for disposal. Therefore, pre-combustion capture has the additional benefit of making a large range of fuels accessible for application in gas turbine combustion. Pre-combustion CO_2 capture options involve high capital investment for preparation of the hydrogen fuel associated with the ASU, the gasifiers and the further processing equipment. Energy losses are related to the requirements of the ASU and to the different chemical transformation steps (mainly the WGS reaction). In addition, the high hydrogen content in the fuel can raise the combustion temperature; therefore, some combination of fuel dilution and gas turbine firing temperature derating is necessary.

15.2.2 Oxy-fuel combustion

The second option for avoiding CO_2 emissions from gas turbines addresses the combustion itself. A hydrocarbon fuel is burned in the presence of pure oxygen. Therefore, this option is commonly labelled oxy-firing. In order to avoid the mixing with nitrogen, no atmospheric air is introduced; instead, a portion of the flue gas is re-cycled to the compressor inlet. In order to close the mass balance, CO_2 and water have to be continuously removed from the cycle. The obvious advantage is that almost pure CO_2 can be extracted without the energy-intensive separation from nitrogen (see next section). The drawback is that oxygen has to be separated from nitrogen.

Published by Woodhead Publishing Limited, 2013



15.5 The semi-closed oxy-fuel combustion combined cycle (SCOC-CC, ENCAP 2004) is the simplest oxy-fuel gas turbine cycle.

Depending on the oxygen supply, gas turbine types used in oxy-fuel power cycles can be divided into two groups: the power cycles with external oxygen separation, and the power cycles with an internal oxygen separation (see Section 15.4). Figure 15.5 shows the most simple oxy-fuel gas turbine cycle, labelled the semi-closed oxy-fuel combustion combined cycle (SCOC-CC) (ENCAP, 2004). It uses a standard bottoming steam cycle to utilize the turbine exhaust heat. A very large variety of further cycles have been developed. Since the working medium is a mixture of CO_2 and water, this approach to CO_2 capture has the largest impact on the gas turbine design and operation (see Section 15.4).

For all variants of oxy-fuel cycles, capital investments for the process mostly consist of the costs for the ASU and the CO_2 compression train. Energy losses are also related to these main components.

15.2.3 Post-combustion capture

The third option for avoiding CO_2 emission from gas turbines addresses the flue gas exiting the gas turbine. Since a hydrocarbon fuel is burned in the presence of air, this approach necessitates the separation of CO_2 from the rest of the flue gas constituents. This option is commonly labelled post-combustion capture. The clear advantage is that this technology is retrofittable

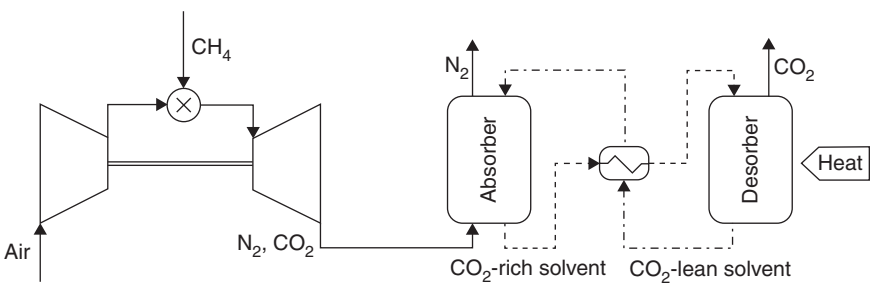
to the installed base of coal and gas plants, provided some basic requirements are met such as additional space and the possibility to extract steam for the CO_2 desorber. Such a plant is often called 'capture ready'.

Since the flue gas will usually be at near atmospheric pressure, the low partial pressure of CO_2 drastically restricts the range of physical and chemical principles that can be effectively applied at an industrial scale. At the moment, the focus is on the development of chemical CO_2 extraction processes.

There are several technologies which are close to full-scale implementation at power plants, the basic principles being similar (Fig. 15.6). The flue gas is put in direct contact with a solvent inside an absorber unit. The CO_2-depleted flue gas leaves the top of the column towards the stack. The CO_2-lean solvent is introduced at the top of the absorber unit and is retrieved at its bottom as a CO_2-rich solvent. Since the absorption occurs at lower temperature than desorption, the rich solvent is heated by the lean solvent that exits the CO_2 desorber through a heat exchanger network. The rich solvent is further heated up in the desorber and releases the CO_2, which is processed (cleaned, compressed) before being fed to the pipeline. The now lean solvent is fed back to the absorber. An actual realization of a CO_2 scrubber will have several additional elements, such as further purification of the CO_2-lean flue gas from the solvent, in order to minimize solvent leakage to the atmosphere.

The solvent binds CO_2 by a reversible chemical reaction, which is usually exothermic. The energy requirement of the capture process results from the fact that the desorption, i.e. the chemical separation of CO_2 from the solvent, is endothermic and occurs at higher temperature than the absorption. The heat of the reaction has to be supplied, usually through extraction of steam from the inlet of the low pressure turbine, which in turn cannot do work anymore.

A major line of development is, therefore, a reduction of the heat of reaction, which would reduce the steam requirement and losses in power plant



15.6 The principles of post-combustion CO_2 capture.

output. Other key features of a solvent are reactive capacity (the amount of CO_2 that can be absorbed per unit of solvent), stability against impurities in the flue gas (e.g. sulphur, mercury), volatility and toxicity.

Two types of solvent families are considered: one is based on monoethanolamine (MEA) and its variants (generally termed amine solvents). The other is ammonia.

Improved amine-based systems are pursued by a number of process developers; a few of these are Mitsubishi Heavy Industries (MHI), Fluor and Cansolv Technologies. Fluor's Econamine FG Plus is a proprietary acid gas removal system, which has demonstrated greater than 95% availability with NGCC plants, specifically on a 350 ton/day CO_2 capture plant in Bellingham, MA. MHI has developed an absorption process, referred to as KS-1. A key factor in this development is the utilization of an amine-type solvent for the capture of CO_2 from flue gas (BP, 2005).

The advanced amine process is based on the chemistry of the amine CO_2–H_2O system, and the ability of the amine solution to absorb CO_2 at low temperatures and release it at moderately elevated temperatures. CO_2 and water produce carbonic acid, which reacts with the amine solution in the absorption column. Alstom collaborates with The Dow Chemical Company (Dow) to jointly develop an advanced amine process technology that utilizes Ucarsol 3000 from Dow in combination with Alstom flow schemes, to provide cost-effective post-combustion carbon capture technology (Pontbriand *et al.*, 2009).

The chilled ammonia process (CAP) uses the ammonium-carbonate/ammonium-bicarbonate absorption chemistry and absorbs the CO_2 at low temperature. The low temperature is required to decrease the ammonia slip in the absorber and to decrease the flue gas volume. The CO_2-rich stream is pumped to a heat exchanger, where its temperature increases, and is then sent to the desorber. CAP has the potential for improved energy efficiency over amine-based systems and can avoid some of the amine degradation products. CAP technology has been applied to coal plants by Alstom: a 5 MW pilot test at We Energies Pleasant Prairie Power Plant, and a 30 MW (thermal) product validation plant, with up to 100 000 tons of CO_2 being captured per year, at AEP's 1300-MW Mountaineer Plant in New Haven, WV. The Technology Center Mongstad in Norway has contracted to test Alstom's CAP for CO_2 capture from the natural gas combined heat and power plant in a 40 MW (thermal) facility.

A proprietary post-combustion carbon capture process based on amino acid salts is another example of CO_2 capture technology offering several significant environmental and energy efficiency advantages compared to first generation technologies, e.g. the MEA process (Jockenhoevel, 2008). This technology is designed for both new fossil-fired power plants and for retrofitting existing plants. The process has been developed and

Published by Woodhead Publishing Limited, 2013

optimized by Siemens at E.ON's Staudinger coal-fired power plant in Germany.

For all of these promising post-combustion technologies, capital investment for the process mostly consist of the costs of absorber, desorber, the CO_2 compression train and ancillary devices (blowers, pumps, etc.). Losses in power plant output are related mainly to the solvent regeneration process, which consumes heat (Fig. 15.6), and the CO_2 compression to pipeline pressure (approximately 100 bar).

The principles of post-combustion capture of CO_2 from the flue gas of NGCC plants are similar to those from a coal plant. The main technical issue is the lower CO_2 concentration of 3–4% vs 10–14% for coal plants. This reduces the achievable loading of the solvent, with subsequent impact on the equipment design. Reheat gas turbines, such as Alstoms GT24/GT26, have a higher CO_2 concentration in the exhaust gas and, thus, are better suited for CO_2 capture than non-reheat ones. Partial recirculation of the flue gas can increase the CO_2 concentration (see Section 15.3). Another important difference to CCS from coal plants is the cleaner flue gas, which reduces the effort for pre-cleaning.

15.3 Impact of carbon capture and storage (CCS) on current gas turbines

The previous section introduced the three options for CO_2 capture from gas turbines that are currently studied. This section highlights the impact of CO_2 capture on NGCC power plants of today. Focus is on pre- and post-combustion capture because (i) the impact is limited, and (ii) both technologies have reached a level of technological maturity that allows for realizing demonstration projects within the next few years. Oxy-fuel combustion will lead to completely new gas power plant concepts, which are treated in the following section on future trends.

The impact of pre-combustion capture is mainly related to the combustion of hydrogen. Post-combustion capture can have a minimal influence on a NGCC plant; however, it was found that partial recirculation the flue gas can improve the economy of the capture system.

15.3.1 Hydrogen combustion

Pre-combustion CO_2 capture necessitates the complete conversion of the syngas into hydrogen. Diffusion burners are presently used for combusting H_2-rich fuels (Ewers, 2006). This allows for a stable combustion; however, the high flame temperatures lead to high NO_x emissions, which can only be controlled by large amounts of dilution (N_2 and/or steam, typically

>50 vol. %). Dilution in this case has the effect of lowering the flame temperature. An alternative approach is the reduction of firing temperature, but this has a negative impact on the overall cycle efficiency (Shilling and Jones, 2003).

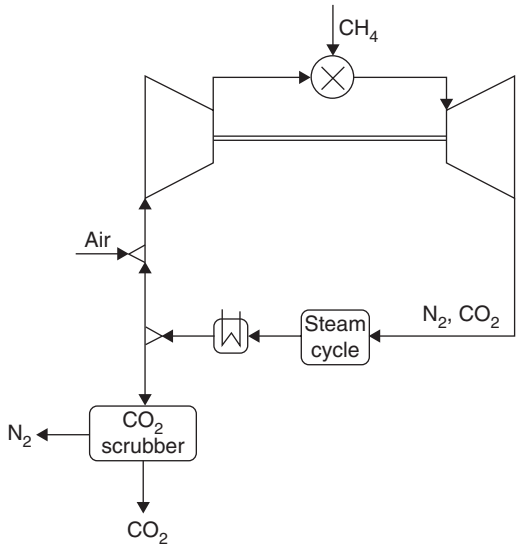
A further reduction of emissions can only be achieved with lean-premixed combustion. Hydrogen distinguishes itself from methane in that its flame speed is an order of magnitude higher, its ignition time an order of magnitude lower, and its density an order of magnitude smaller. A safe gas turbine burner operation implies protection against pre-ignition and flashback. Substantial research work was undertaken within the ENCAP project (ENCAP, 2004) and the solution found was again dilution with nitrogen (approximately 40–50 vol. %). In this case the dilution has the effect to lower the flame propagation speed, which allows for a stable premix operation.

15.3.2 Flue gas recirculation

A major difference from a classical open gas turbine cycle is the partial or full recirculation of flue gas to the inlet of the compressor. Limited amounts of recirculation will increase the CO_2 and decrease the oxygen content of the gas entering the compressor. Above a certain recirculation rate (40–60%) there is not enough oxygen present to sustain stable combustion and to burn the fuel completely. When oxygen is supplied, e.g. by an ASU, the recirculation rate can be effectively increased to 100%. At this limit of oxy-fuel combustion, no atmospheric air is used within the cycle. Since CO_2 and water have to be continuously removed from the system, the full recirculation case is more correctly labelled a semi-closed cycle (see Section 15.4). Figure 15.7 shows a simplified scheme of partial flue gas recirculation. Since the exhaust temperature behind the heat recovery steam generator of a bottoming steam cycle is usually in the order of 80–120°C, a cooler is required both for the CO_2 scrubber and for the compressor inlet.

There is a natural limit to the amount of gas which can be recirculated (FGR ratio). This is determined by the amount of oxygen in the air and the gas turbine cycle parameters. For non-reheat gas turbines, this limit and the maximum CO_2 concentration is achieved at a FGR ratio of 60–65%, whereas for the modern reheat gas turbine cycle this happens at about 50%. Typical dependencies of the O_2 and CO_2 concentrations at the exhaust of a reheat gas turbine and the corresponding inlet O_2 concentration as a function of the FGR ratio are depicted in Fig. 15.8 (Burdet *et al.*, 2010).

The benefit of FGR is an increase of CO_2 concentration in the flue gas, which enables a more efficient absorption process. At the same time the

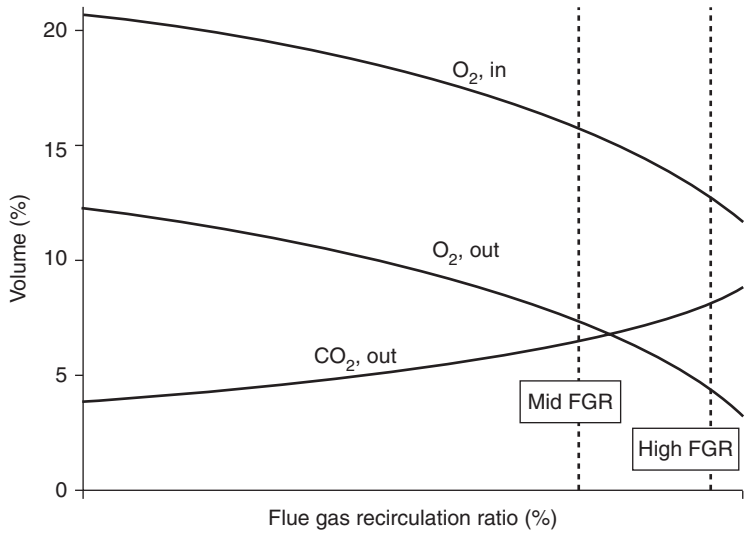


15.7 A simplified scheme of partial flue gas recirculation.

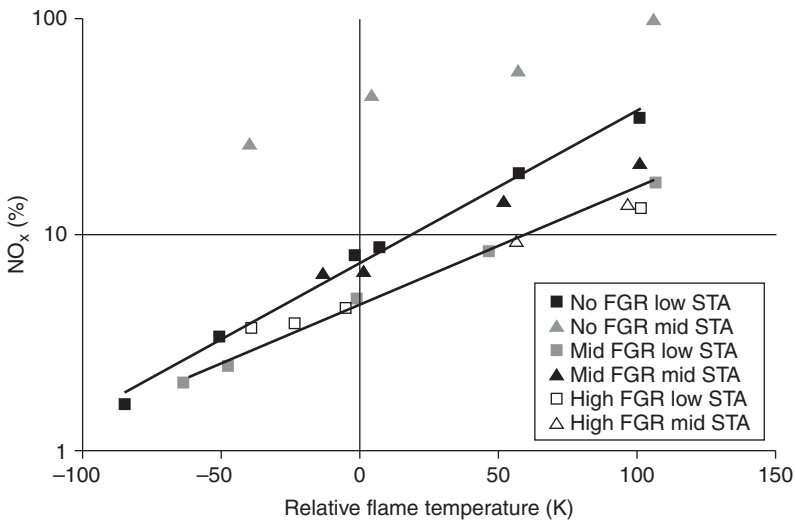
volume of the flue gas to be treated is reduced proportionally to the recirculation ratio, and so is the flow area of the absorption column and the blowing power. Furthermore, the reduction of the O_2 concentration and the corresponding changes in combustion kinetics lead to the reduction of the NO_x emissions, as is shown in Fig. 15.9 (Burdet *et al.*, 2010; Daniele *et al.*, 2008; Müller *et al.*, 2008).

There exist also technical challenges related to FGR implementation, namely an increased plant complexity as new elements of the flue gas path (blower, cooler, ducts, gas mixer, dampers, instrumentation, etc.) are introduced and significant modifications of the gas turbine control system are made. A special gas mixing device will be required, which assures uniform velocity, temperature and gas composition fields at the inlet of compressor. Above a certain recirculation level, a notable increase in CO content in the exhaust gas can be expected (Fig. 15.10). This limits the technically achievable FGR ratio (Botero *et al.*, 2009; Burdet *et al.*, 2010).

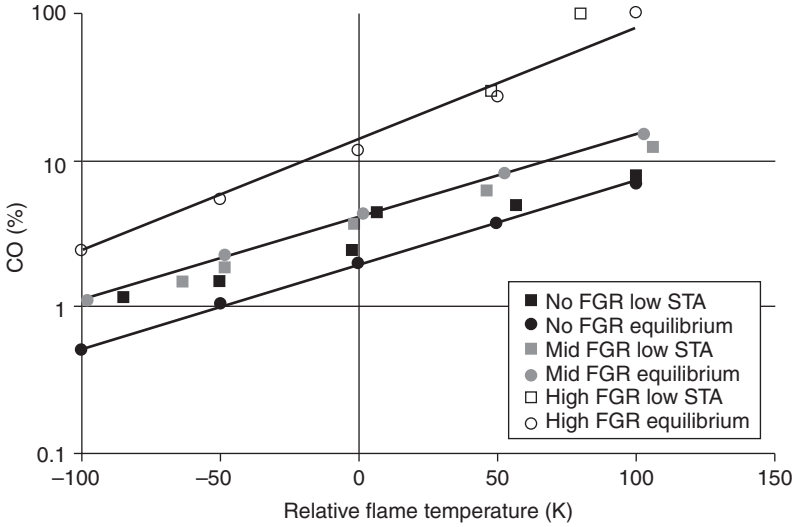
Areas of current research are the impact of the FGR on the combustion process. A number of projects have been undertaken by gas turbine OEMs in order to establish the principles of FGR gas turbine combustion and/or to develop FGR-specific combustion technologies (Botero *et al.*, 2009; ElKady *et al.*, 2008; Guethe *et al.*, 2009, 2011; Ito *et al.*, 2007; Kobayashi *et al.*, 2007; Winkler *et al.*, 2009). Those projects did confirm the ability of an existing low-NO_x combustion system to operate stably up to an FGR ratio of at least



15.8 Typical dependencies of the O_2 and CO_2 concentrations at the exhaust of a reheat gas turbine and the corresponding inlet O_2 concentration as a function of the FGR ratio (Burdet *et al.*, 2010).



15.9 The reduction of the O_2 concentration and the corresponding changes in combustion kinetics lead to the reduction of the NO_x emissions (Burdet *et al.*, 2010; Daniele *et al.*, 2008; Müller *et al.*, 2008).



15.10 Above a certain recirculation level, a notable increase in CO content in the exhaust gas may be expected.

30–35%. In summary, FGR is considered an effective means to improve the operation and economy of CO_2 capture in an NGCC plant (Botero *et al.*, 2009; Chinn *et al.*, 2004; Griffin *et al.*, 2008; Ito *et al.*, 2007).

15.3.3 Compressor and turbine

Compressors and turbines in a gas turbine arrangement are impacted by all CO_2 capture options. Pre-combustion capture has a minor effect, resulting from changes of the combustion gas composition. Post-combustion capture without flue gas recirculation has negligible impact. Adding recirculation increases the CO_2 concentration, which leads to a modified adiabatic exponent of the working fluid. As a consequence, the proportion of pressure and temperature ratio changes. Furthermore, the speed of sound changes, and so do the Mach numbers on the blades. For recirculation ratios, which can be achieved without the addition of oxygen, this effect is visible but does not require a redesign of the turbomachinery; even so, some adaptation may still be required.

Another aspect to be considered is the choice of materials. The presence of CO_2 at the compressor inlet may incur a risk of CO_2-associated corrosion of steel. In addition, the reduction of O_2 content in the combustion gases may affect the oxidation/corrosion behavior of hot gas path materials, which is strongly dependent on the kinetics of surface oxide formation. The aforementioned change in adiabatic exponent of the working medium

results in an increased hot gas temperature downstream of the first turbine stage, which may necessitate design changes. The impact of contaminants entrained from the fuel on turbo machinery material are concerns that should not be neglected.

15.3.4 Operation and control

As mentioned in Section 15.1, the feature that makes gas turbines attractive is their flexibility for rapid load changes. This becomes even more important in a world that sees an increasing share of fluctuating and unpredictable renewable sources. Besides being technically capable of such flexibility, the economy of gas turbines is driven by fuel costs and, to a lesser, extent by capital costs. This allows operation of gas turbines economical at much lower capacity factors than capital driven plants, such as coal or nuclear.

Operational flexibility constitutes one of the major competitive advantages of the NGCC plant compared to the coal-fired one. An NGCC plant may be operated with a more aggressive and rapid startup/shutdown cycle, or alternate the load according to rapid electricity demand changes of their customers. This would need to be either followed, or at least tolerated, by the CO_2 capture equipment. It may be also expected that the transients reduce the CO_2-capturing efficiency and/or impose additional hardware margins and energy consumption in order to maintain it.

Each option for CO_2 capture involves the coupling of a gas turbine with additional elements, such as gasification equipment (pre-combustion), ASUs (pre-combustion and oxy-fuel combustion) and CO_2 scrubbers (post-combustion). The most notable features of these elements are a much lower flexibility of fast load changes or even frequent start/stops, and a high capital investment. The combination of gas turbines with CO_2 capture units will therefore lead to a system which is strongly driven towards continuous operation, both by the inflexibility of the CO_2 capture equipment and by the larger capital investment.

For pre-combustion capture, a decoupling of the fuel preparation and the power production in a gas turbine is at least thinkable. Possible means are local storage of fuel (pressurized containments, underground caverns), connection to a pipeline network, and an alternative use of the fuel (polygeneration). Since a full capture of CO_2 leads to hydrogen as the main fuel constituent, such alternatives call for a hydrogen infrastructure that is currently not available at the conventional power plant. Some variants of IRCC or IGCC foresee a further integration of the gas turbine cycle and the fuel preparation, e.g. feeding the ASU using compressor air, or the usage of N_2 for dilution in H_2 combustion. Again, such integrations limit the flexibility of gas turbines.

Published by Woodhead Publishing Limited, 2013

Post-combustion CO_2 capture will significantly affect the power island. For solvent regeneration either an additional steam extraction from the steam cycle (normally from its low pressure part) with the corresponding impact on the steam turbine or installation of the auxiliary boiler will be required. The operational and protection concepts of the gas and steam turbine are to be aligned with those of the CO_2 capture unit. This is related to the fact that its startup, shutdown and transition times are expected to be notably longer than those of the NGCC plant. At least some of the protection events which may be generated within the CO_2 capture unit (e.g. trip, steam rejection, blower failure, etc.) will require corresponding reactions of the gas/steam turbine control systems.

An NGCC plant is much more sensitive to variations of ambient conditions than a coal-fired plant. Within an air temperature range of −30°C to +30°C, the mass flow through a gas turbine may change by more than 50%. The exhaust temperature behind a heat recovery steam generator also varies significantly. Thus, whatever reference point is selected, additional design margins would be required to assure the proper operation of a gas turbine with a CO_2 capture unit at off-design conditions.

15.4 Novel approaches

Pre- and post-combustion capture will constitute the first generation of CO_2 capture on NGCC power plants. As shown in the previous section, this is mainly due to the limited impact on today's technology. This section gives an overview of novel approaches, which depart significantly from the classical air-breathing NGCC (see ENCAP, 2004; GAS-ZEP, 2003; IEA, 2006). Some of these cycles have been systematically compared to more conventional pre- and post-combustion approaches within the ENCAP project (ENCAP, 2004). Efficiency figures, including CO_2 separation and compression, are given in Section 15.5. Note that absolute figures evolve with time as the technology improves. Therefore, Fig. 15.18 shows the efficiency drop in absolute percentage points with reference to a standard NGCC plant without CO_2 capture. The efficiency of the baseline plant in ENCAP was 56.6%. Other comprehensive studies of various novel cycles have been undertaken by Kvamsdal *et al*. (2004) and Rezvani *et al*. (2009).

Several variants of oxy-firing cycles are introduced. Although they may seem very different, they have some common features. Combustion of a hydrocarbon fuel in an oxygen environment will create a gas that consists of water and CO_2. The working medium of the cycle will be composed of the same two gases. CO_2 can be easily extracted from this mixture through condensation of water. The main differentiator is the way oxygen is provided to the cycle: some use an external oxygen supply (ASU), others an internal air separation, such as membranes, oxygen carriers as in chemical looping,

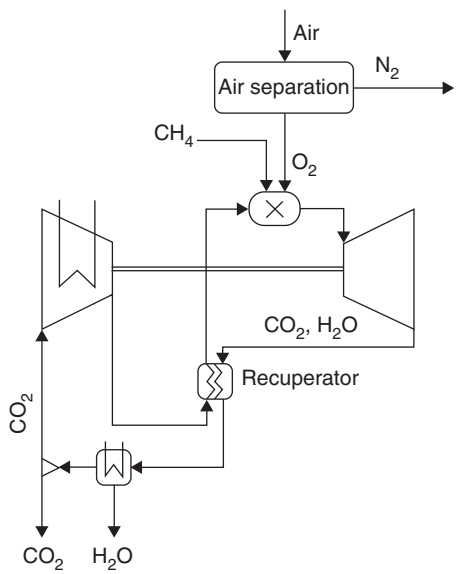
Published by Woodhead Publishing Limited, 2013

or even fuel cells. All cycles involve the development of new turbomachinery components capable of operating with mixtures of water and CO_2 as the principle working fluid. Since nitrogen is excluded from the combustion process, the generation of nitrous oxides is effectively avoided.

15.4.1 Semi-closed cycles with external oxygen supply

As mentioned before, the combustion of hydrocarbons with oxygen from an ASU will lead to water and CO_2 as combustion products. Since for stoichiometric conditions the firing temperature will be too high, part of this combustion gas is recirculated. Among this class of cycles, the main differentiator is the composition of the working fluid.

A typical cycle, which works mainly with CO_2, has been shown already in Fig. 15.5. This SCOC-CC cycle was studied in the ENCAP project (ENCAP, 2004) and has a standard bottoming steam cycle. There is an alternative way to utilize the turbine exhaust heat, namely a recuperator (Fig. 15.11). This variant is called an E-Matient cycle (Mathieu, 2003). A similar cycle was proposed by Enge *et al*. (2006). Water is condensed after the expansion turbine. CO_2 is recirculated to the combustion chamber via an intercooled compressor and a recuperator. The CO_2, which is newly created through combustion, is removed from the cycle, either at the lower or at the higher

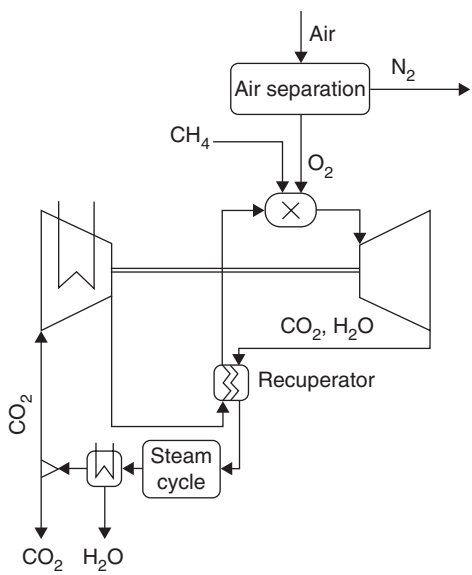


15.11 In an E-Matient cycle, a recuperator enables the utilization of turbine exhaust heat.

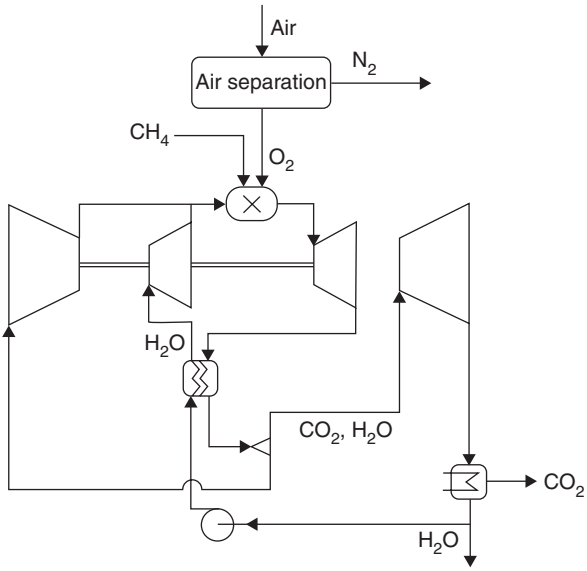
pressure level. As this cycle works independently of atmospheric air, the compressor inlet pressure can be freely chosen. This opens up two interesting opportunities: an overall elevated cycle pressure can reduce the size and costs of turbomachinery; and, the power can be regulated by inventory control, i.e. by changing the amount of working fluid (and therefore the density and pressure) inside the cycle.

Two other variants of Matient cycles exist. The original Matient concept foresees a peak cycle pressure of 300 bar, the advantage being that CO_2 can partly be pumped, which requires less work than compression. The technological challenges are substantial, e.g. expansion turbines with 300 bar inlet pressure and recuperators which see peak temperatures around 1200 K (Hochenauer *et al.*, 2004). Another variant is called the CC-Matient cycle (Mathieu, 2003). This uses a bottoming steam cycle in addition to the recuperator (Fig. 15.12). The SCOC-CC cycle (Fig. 15.5) was studied within the ENCAP project and the efficiency drop was estimated to be 9% absolute, compared to an NGCC plant without CO_2 capture (see Fig. 15.18).

A cycle that works with a mixture of water and CO_2 is the Graz cycle. It constitutes a hybrid between a steam and a gas turbine cycle (see Fig. 15.13 for the S-Graz variant). The pressure of water is increased through pumping in the liquid state and, after a heat recovery steam generator (HRSG),



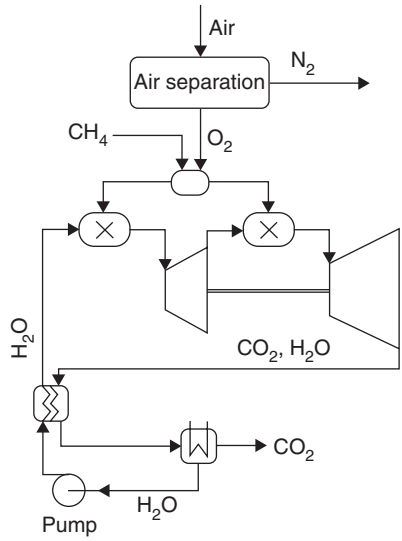
15.12 A CC-Matient cycle uses a bottoming steam cycle in addition to the recuperator.



15.13 The S-Graz variant of the Graz cycle, which works with a mixture of water and CO_2.

the expansion partially takes place in a steam turbine. The steam is mixed with compressed CO_2 and enters a combustion chamber. After combustion the exhaust gas is again expanded in a turbine. The steam content is much higher than can be handled by present gas turbines. After part of the gas is directed to the compressor, the final expansion down to condenser pressure takes place. CO_2 is extracted at this point. The cycle combines the advantages of high temperature gas turbine Brayton cycle and low temperature steam Rankine cycle (Heitmer and Jericha, 2003; Hochenauer *et al.*, 2004; Jericha *et al.*, 2004; Sanz *et al.*, 2005). Within the ENCAP project the efficiency loss for the S-Graz cycle was estimated to be 8% absolute compared to a NGCC plant without CO_2 capture (see Fig. 15.18).

The other extreme in terms of working medium is the water cycle (Bolland *et al.*, 2001). It is in principle a Brayton cycle (Fig. 15.14). In the first chamber of a specially designed combustor the temperature is lowered by water injection to control the flame temperature created by the combustion of natural gas with high-purity oxygen. The resulting high temperature gas is used in an expander. After a second combustion and expansion, water is condensed and recirculated. CO_2 can be captured for further processing. It was concluded that the water cycle offered no efficiency advantages over a conventional combined cycle with post-combustion capture (Bolland *et al.*, 2001; Kvamsdal, 2004). Within the ENCAP project the efficiency loss of the



15.14 The water cycle is based on the principles of the Brayton cycle.

water cycle was estimated to be 14% absolute, compared to a NGCC plant without CO_2 capture (see Fig. 15.18).

There exist several principal technology issues which have to be addressed while designing a CO_2/water-based cycle. Significant efforts in the area of materials are to be made, both at the hot part of the cycles, where the turbine materials including base alloys and coatings would face a completely different environment than in the conventional air turbines, and at the cold end of the cycle, where the steels have to withstand the wet CO_2 environment. The cleaning of recirculated gas has to be considered, as unburned hydrocarbons and oxide particles can accumulate and cause plugging of cooling systems or fouling of aerodynamic surfaces. Modern gas turbine designs do rely heavily on thermal barrier coatings, whose applicability to the closed-loop CO_2/water cycle is questionable. This may require new blade-cooling concepts to be developed. The reduction of the gas turbine size, due to high cycle pressure, even though having positive impact on the costs of turbine itself, may necessitate an increase in rotational speed and, therefore, use of gearboxes, which may limit the output power.

Considering the need for recirculation and the transient regime, where combustion starts with air and moves slowly to oxygen with recirculation, a new control system should be developed especially for starting-up and shutting down the gas turbine. If the unit had to be started up on CO_2, this would require a CO_2 storage tank at the plant site. An evaluation of components for various cycles was done by Franco *et al*. (2006).

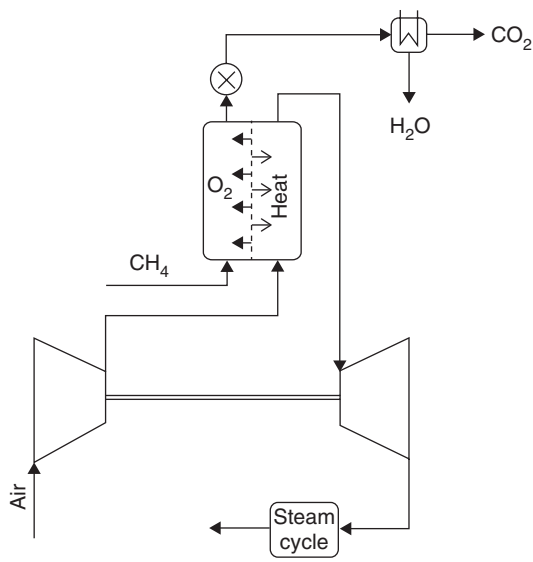
Published by Woodhead Publishing Limited, 2013

15.4.2 Oxygen supply via membranes

Another type of gas turbine-based oxy-fuel power cycle is the Advanced Zero Emission Power Plant (AZEP). It represents a cycle with internal oxygen separation by a membrane (see Fig. 15.15). The AZEP concept was jointly developed by Alstom and Norsk Hydro. Its main features are a low efficiency penalty, 100% capture of CO_2, and no NO_x emissions (Bill *et al.*, 2001; Bücker *et al.*, 2004; Eklund *et al.*, 2003; Sundkvist *et al.*, 2001).

The combustor in an ordinary gas turbine is replaced by a mixed-conducting membrane (MCM) reactor, which includes a combustor, an air separation membrane, and a high temperature heat exchanger (Griffin *et al.*, 2003, 2005). Combustion of natural gas occurs in a nitrogen free environment, and the heat of combustion is transferred to the oxygen-depleted air by a high temperature heat exchanger. In order to improve the efficiency, the residual heat of the CO_2 stream is also passed to the steam cycle (not shown in Fig. 15.15). The efficiency losses of the AZEP process (90% CO_2 capture) were estimated to be 5% absolute compared to an NGCC cycle without CO_2 capture (see Fig. 15.18, ENCAP, 2004), provided that its ceramic membrane reactor can be operated at temperatures approaching today's gas turbine combustors (Griffin *et al.*, 2003).

A potential benefit of AZEP compared to other oxy-fuel concepts is the fact that the turbomachines and their auxiliary systems can be based

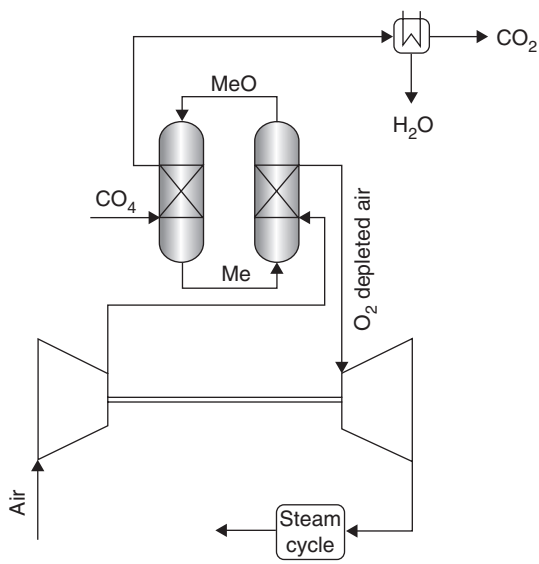


15.15 AZEP represents a cycle with internal oxygen separation by a membrane.

on slightly modified standard, air-based equipment (Griffin *et al.*, 2003). This limits the development effort and reduces the technical and commercial risks. Higher efficiencies can be achieved with auxiliary firing within a sequential combustor, which is also called the AEP 85% case (Möller *et al.*, 2006). This, however, leads to CO_2 emissions from the process. The greatest weakness of AZEP is its dependence on ceramic components, which have not yet been validated. Finally, due to the size of the AZEP membrane reactors and the necessary design modifications of the gas turbine, this technology cannot be considered as retrofittable.

15.4.3 Chemical looping

An alternative oxy-fuel combustion approach, which needs neither an ASU nor a membrane, is chemical looping combustion (CLC). A sketch of the concept is shown in Fig. 15.16. Atmospheric air is compressed and introduced to the oxidation reactor (oxidizer). Oxygen reacts with the oxygen carrier, heating up the air before expansion in the turbine. The oxidized carrier is separated from the air and fed to the reduction (fuel) reactor (reducer). Here the carrier is reduced by releasing oxygen to the fuel. Since the oxidization of the fuel occurs in absence of nitrogen, only water and CO_2 leave the fuel reactor. In order to increase the efficiency, the process includes an expansion of the CO_2 stream and a preheating of the fuel, which are not shown in Fig. 15.16.

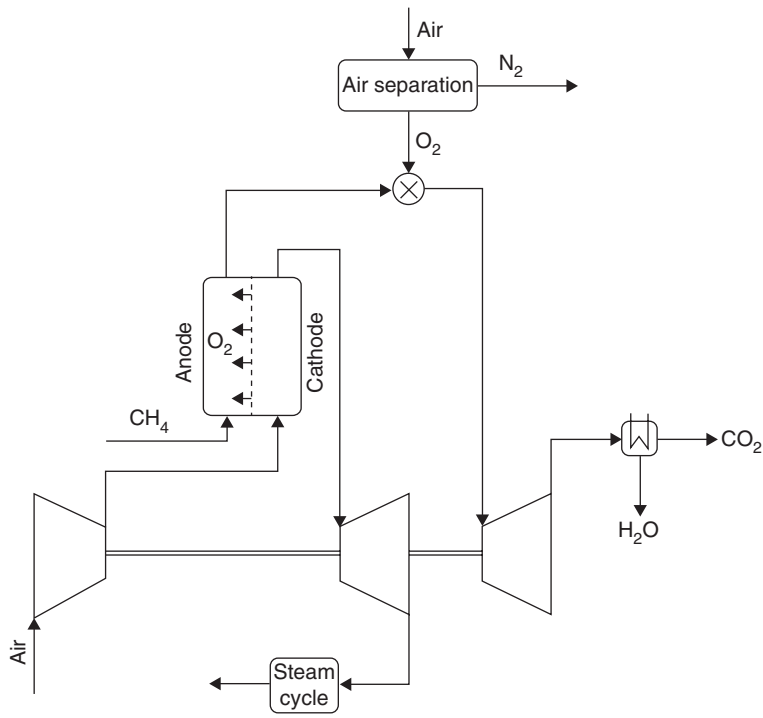


15.16 CLC is an alternative oxy-fuel combustion approach.

Different options for CLC were studied with ENCAP (ENCAP, 2004). ALSTOM continues CLC development with two oxygen carrier: limestone and metal oxide (Mattisson *et al.*, 2008). Efficiency losses were found to range between 4% and 14% absolute compared to a standard NGCC plant without CO_2 capture (see also Naqvi, 2004).

15.4.4 Fuel cells

Another option for realizing an oxy-fuel combustion cycle is based on high temperature fuel cells such as solid oxide fuel cells (SOFC) or molten carbonate fuel cells (MCFC). Generally, such fuel cells can be coupled with elements of gas turbine power cycles. Integrating CO_2 capture is a natural further step, since a fuel cell, by its nature, is an oxygen separation device. Figure 15.17 shows a sketch of a possible realization. Air is compressed and fed to the cathode side. Oxygen passes through the electrolyte and oxidizes the fuel on the anode side. The oxygen-depleted air is expanded in a turbine and the exhaust heat is utilized in a bottoming steam cycle (variants with recuperators are also possible).



15.17 Fuel cells are another option for realizing an oxy-fuel combustion cycle.

The key to CO_2 capture is keeping the cathode and anode streams separate. The latter contains some fraction of unburned fuel. This has to be further combusted in a normal combustion chamber, which requires oxygen from a standard ASU. However, this can be smaller than for an oxy-fired cycle with external oxygen supply, since roughly two-thirds of the power conversion takes place in the fuel cell. The anode stream that consists of water and CO_2 is expanded, and CO_2 is captured through condensation of water. Again it must be noted that Fig. 15.17 is a sketch that omits certain important features, such as a partial flue gas recirculation on both the anode and cathode side.

Fuel cell systems were not studied within ENCAP. According to Damen *et al.* (2006), efficiencies of up to 69% can be expected for 90% CO_2 capture firing natural gas fuel (including CO_2 compression to pipeline pressure).

15.4.5 Carbon-neutral fuels

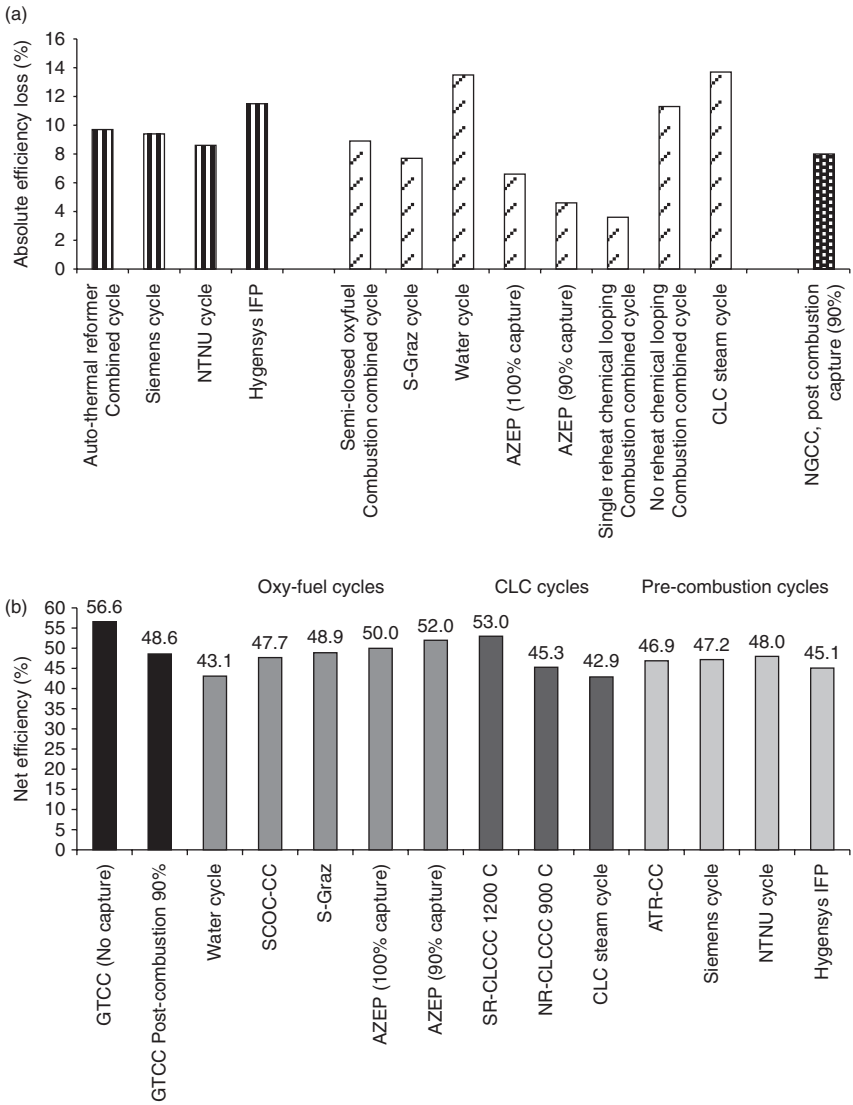
An active field of research is the production of synthetic natural gas (SNG) from various biomass sources (Gassner and Marechal, 2009; Specht *et al.*, 2009). SNG-fired gas turbines could potentially be CO_2 neutral even without capture. However, as with all biofuels, consideration has to be given to the (possibly fossil) energy that is required for harvesting, transportation and processing. In the future, some fraction of renewable electricity may have to be converted into a permanent chemical form that can compensate for seasonal variations in primary energy production (wind, solar). Such synthetic fuels may still be based on hydrocarbons, the carbon coming either from biomass or directly from the atmosphere. A combination of these sustainable, synthetic fuels with CO_2 capture would actually constitute a negative CO_2 emission.

15.5 Implementation of carbon capture and storage (CCS) for gas turbines

This section highlights some of the drivers that impact a possible market introduction of CO_2 capture for gas turbines.

15.5.1 Efficiency of CO_2 capture cycles

The previous sections have shown that there are a variety of options for CO_2 capture from gas turbines, which can be grouped according to pre-/post-combustion and oxy-fuel, with many sub-variants. A comprehensive analysis of several options was undertaken within the EU-funded project ENCAP (ENCAP, 2004). Figure 15.18 gives an overview. A large scatter is visible with efficiency losses ranging between 4% and 13% (absolute) compared to a standard NGCC plant.



15.18 An overview of the efficiency of CO_2 capture cycles. (a) Absolute efficiency loss and (b) net efficiency.

15.5.2 Capital investments and operational costs

Capturing CO_2 from gas turbines would have a significant impact on capital and O&M costs. As shown in Section 15.2, each of the three main options requires additional elements, the main ones being gasification equipment (pre-combustion), ASUs (pre-combustion and oxy-firing), and CO_2 scrubbers (post-combustion). These elements impact the investment costs of the

power plant and introduce additional maintenance cost. Additional operational costs are mainly related to the energy consumed by the associated gas treatment processes. Precise quantitative statements cannot be made at this stage.

The large-scale market introduction of the CO_2 capture will be driven by the political pressure and social responsibility, either directly or through their legal realizations (environmental standards, legislation) and economy instruments (carbon taxes, CO_2 certificates, etc.).

15.5.3 Market introduction

The three main CO_2 capture options have completely different characteristics, which largely impact their chances for a market introduction. As long as natural gas in the form of methane remains readily available at a competitive price, it will be the fuel of choice for NGCCs. Only if synthetic gases from coal gasification were to become significantly cheaper than natural gas would the combustion of hydrogen gases in combined cycled plants become the preferred choice.

Oxy-fuel cycles deviate most from today's air-breathing gas turbine combined cycles. Although the membrane-based AZEP cycles appear to be the most promising in terms of efficiency, there will be a considerable hesitation in the power market to enter a totally new route.

With no strong differentiation between the three main groups, the simplest solution will prevail, and therefore post-combustion capture technologies have the best chance for a fast market introduction. Since this option has actually the least impact on the gas turbine itself, it can be considered to be retrofittable, having the advantage of being applicable to a much wider market. It can also be introduced more quickly, thereby having a larger impact on CO_2 emission reduction.

Three steps in the market introduction of the post-combustion CO_2 capture at gas turbine combined cycles can be envisaged:

1. CCS solutions with minimum or no effect on key components, which would be fully retrofittable into existing NGCC plants if the required space and infrastructure are available. This would be a low-risk solution, which seems promising for demonstration plants.
2. Concepts with a significant level of CCS integration into the NGCC plant (FGR, solvent stripping in the boiler, steam turbine tailored also for CCS needs, etc.) being optimized for the CO_2-capturing operation, but still able to work with the capture unit disengaged when required. These concepts might be still retrofittable into the 'capture-ready' plants.
3. Fully integrated NGCC-CCS concepts, which would be designed for CO_2 capturing. At this phase, implementation of new principles may become possible. A possible combination of FGR with the pressurized capture

Published by Woodhead Publishing Limited, 2013

after an intercooled gas turbine compressor (Finkenrath *et al.*, 2007) is an example.

15.5.4 Demonstration

Pre-combustion, oxy-fuel and post-combustion technologies have all been developed for application to coal plants, and are expected to become commercial within this decade. Many demonstration projects are in planning and preparation, and at this stage they require substantial government support for the development cost, the capital cost and the operation cost. The main reason for this is that at present the CO_2 price in the EU Emissions Trading System is not sufficient to fund the full cost of the CCS plants.

The Technology Center Mongstad in Norway has contracted to test Alstom's CAP for CO_2 capture from the natural gas combined heat and power plant in a 40 MW (thermal) facility.

The early demonstration plants incur additional costs in the form of first-of-kind costs due to increased redundancy in the plant equipment, increased supply chain costs, reduced operation time, and special instrumentation and control. For the transport and storage, until a network of CO_2 pipelines is established, each individual plant will incur disproportionately high costs for transport of CO_2 to the storage well.

15.6 Conclusion

The power generation industry must play its part in the shift to sustainability. Therefore, in the long term the move to non-fossil energy sources is to be expected. NGCCs with CO_2 capture, capable of rapid startup, shutdown and flexible operation, are the perfect partners for fluctuating renewable energy sources and will have a place in the portfolio over that period.

The power industry sees a shift towards NGCC plants, due to their inherently lower CO_2 emissions. However, in order to meet CO_2 emission targets, fuel substitution on its own will not be sufficient. CCS must be deployed on a range of fossil fuel power plants as broadly as possible. CCS on NGCCs is technically feasible but requires development and demonstration with a target for commercial operation within this decade.

Many workers are active in the field of CCS from power generation. One source of further information is the European Technology platform zero emissions fossil fuel power generation plant (ZEP).

15.7 Acknowledgements

The authors gratefully acknowledge the valuable contribution of Dieter Winkler (University of Applied Sciences and Arts, Northwestern Switzerland) to this chapter.

15.8 References

01NT41145. National Energy Technology Laboratory.

Bill A, Span R, Griffin T, Kelsall G and Sundkvist S G (2001), *Technology options for 'Zero Emissions' gas turbine power generation*, International Conference Power Generation and Sustainable Development, Liège, Belgium.

Bolland O, Kvamsdal H M and Boden J C (2001), *A thermodynamic comparison of the oxy-fuel power cycles: Water Cycle, Graz Cycle, and Matiant Cycle*, The Proceedings of the International Conference Power Generation and Sustainable Development, Liège, Belgium.

Botero C, Finkenrath M, Bartlett M, Chu R, Choi G and Chinn D (2009), Redesign, optimization, and economic evaluation of a natural gas combined cycle with the best integrated technology CO_2 capture, *Energy Procedia*, **1**, 3835–3842.

BP America (2005). CO_2 Capture Project Technical Report DEFC26-

Bücker D, Holmberg D and Griffin T (2004), Technoeconomic evaluation of a power plant using Mixed Conducting Membranes, to appear in the monograph, CCP Technical Summary Volume.

Burdet A, Lachaux Th, de la Cruz García M and Winkler D (2010), *Combustion under flue gas recirculation conditions in a gas turbine lean premix burner*, GT2010–23396, Proceedings of ASME Turbo Expo 2010: Power for Land, Sea and Air GT2010, Glasgow, Scotland, UK.

Chinn, D, Choi, N G, Chu R and Degen B (2004), *Cost efficient amine plant design for post combustion CO_2 capture from powerplant flue gas*, Proceedings of 7th International Conference on Greenhouse Gas Control Technologies, Toronto, Canada.

Damen K, van Troost M, Faaji A and Turkenburg W (2006), A comparison of electricity and hydrogen production systems with CO_2 capture and storage. Part A: review and selection of promising conversion and capture technologies, *Progress in Energy and Combustion Science*, **32**, 215.

Daniele S, Jansohn P, Boulouchos K (2008), *Lean premixed combustion of undiluted syngas at gas turbine relevant conditions: NO_x emissions and lean operational limits*, GT-2008–50265, ASME Turbo Expo 2008, Berlin

Decarbit Public Reports (2008), www.decarbit.com.

Eklund H, Sundkvist S G, Wilhelmsen K, Aasen K and Griffin T (2003), *Development of a membrane-based CO_2 emission-free gas turbine system*, Proceedings of 7th International Conference on Technologies and Combustion for a Clean Environment, Lisbon.

ElKady A, Evulet A, Brand A, Ursin T P and Lynghjem A (2008) *Exhaust Gas Recirculation in DLN F-class Gas Turbines for Post-combustion CO_2 Capture*, Proceedings of GT2008, Paper number DRAFT GT2008- 51152.

ENCAP Public Report (2004), SES6-CT-2004–502666.

Enge Y O, Wirsum M, Wettstein H E (2006), *The potential of recuperated semi-closed CO_2 cycles*, Proceedings of the ASME Turbo Expo 2006, GT2006–90888.

Ewers J *et al.* (2006), *Hydrogen-rich syngas combustion: prerequisite for CO_2-free IGCC power stations*, PowerGen 2006, Milan.

Foy K and Yantovski E (2006), History and state-of-the-art of fuel fired zero emission power cycles, *International Journal of Thermodynamics*, **9** (2), 37–63.

Franco, F, Mina, T, Woolatt, G, Rost, M and Bolland, O (2006), *Characteristics of cycle components for CO_2 capture*, Proceedings of GHGT-8, Trondheim, Norway.

Gassner, M, Marechal, F (2009), Thermo-economic process model for thermochemical production of Synthetic Natural Gas (SNG) from lignocellulosic biomass, *Biomass and Bioenergy*, **33**, 1587–1604.

Griffin T, Bücker D and Pfeffer A (2008), Technology options for gas turbine power generation with reduced CO_2 emission, *Journal of Engineering for Gas Turbines and Power*, **130** / 041801–1.

Griffin T, Buecker D and Pfeffer A (2005), *Technology options for gas turbine power generation with reduced CO_2 emission*, Proceedings of GT2005 ASME Turbo Expo.

Griffin T, Sundkvist S G, Aasen K and Bruun T (2003), *AZEP: Advanced Zero Emissions Power Plant*, ASME GT Expo, GT-2003–38426.

Griffin T, Sundkvist S G, Åsen K and Bruun T (2003), *Advanced zero emissions gas turbine power plant*, GT2003–38426, Proceedings of ASME Turbo Expo 2003.

Guethe F, de la Cruz García M and Burdet A (2009), *Flue gas recirculation in gas turbine: investigation of combustion reactivity and NO_x emission*, GT2009–59221, Proceedings of ASME Turbo Expo 2009: Power for Land, Sea and Air. Orlando, Florida, USA.

Guethe F, Stankovic D, Genin F, Syed K and Winkler D (2011), *Flue gas recirculation of the Alstom sequential gas turbine combustor tested at high pressure*, GT2011–45379, Proceedings of ASME Turbo Expo 2011: Power for Land, Sea and Air, Vancouver, Canada.

Heitmer F and Jericha H (2003), *Graz cycle – an optimised power plant concept for CO_2 retention,* First International Conference on Industrial GT Technologies, RTD Framework Programme of the European Union, Brussel.

Higman C and van der Burgt M (2003), *Gasification*, Amsterdam, Gulf Professional Publishing.

Hochenauer C, Hohenwarter U, Sanz W and Schlamadinger, B (2004), *Bio-energy cogeneration systems with CO2 separation and storage*, ASME Turboexpo 2004, Vienna, Austria, Paper No GT2004–54224.

Hochgesand G (1970), Rectisol and Purisol, *Industrial and Engineering Chemistry*, **62**(7), 37–43.

IEA Greenhouse Gas R&D Programme (IEA GHG) (2006), Near zero emission technology for CO_2 capture from power plant, Report 2006/13.

Ito E, Okada I, Tsukagoshi K, Muyama A and Masada J (2007), *Development of key technologies for the next generation gas turbine*, Proceedings of GT2007, Paper number GT2007–28211.

Jericha H, Göttlich E, Sanz W and Heitmeir F (2004), Design optimization of the Graz Cycle prototype plant, *Journal of Engineering for Gas Turbines and Power*, 126.

Jockenhovel T, (2008), *Development of and Economic Post-Combustion Carbon Capture Process*, GHGT-9 Conference, Washington D.C., USA

Kobayashi H, Hagiwara H, Kaneko H and Ogami Y (2007), Effects of CO_2 dilution on turbulent premixed flames at high pressure and high temperature, *Proceedings of the Combustion Institute*, **31**, 1451–1458.

Kvamsdal H M, Maurstad O, Jordal K and Bolland O (2004), *Benchmarking of Gas-Turbine Cycles with CO_2 Capture*, GHGT-7, Vancouver.

M. Finkenrath *et al.* (2007), *Performance and cost analysis of a novel gas turbine cycle with CO_2 capture*, Proceedings of ASME Turbo Expo 2007, Paper GT2007–27764.

Mathieu P (2003), Mitigation of CO_2 emissions using low and near zero CO_2 emission power plant, *International Journal on Energy for a Clean Environment*, **4**, 1–16.

Mattisson T, Adanez J, Proell T, Kuusik R, Beal C, Assinkf J, Snijkers F and Lyngfelt A, (2008) Chemical-looping combustion CO_2 ready gas power, *Energy Procedia*, **1**(1), Greenhouse Gas Control Technologies 9, Proceedings of the 9th International Conference on Greenhouse Gas Control Technologies (GHGT-9).

Möller B, Torisson T, Assadi M, Sundkvist S G, Sjödin M, Klang Å, Åsen K I and Wilhelmsen K (2006), AZEP gas turbine combined cycle power plants – thermo-economic analysis, *International Journal of Thermodynamics*, **9**(1), 21–28.

Müller P, Winkler D, Griffin T, Jansohn P and Daniele S (2008), *Combustion of syngases: fundamental combustion studies at gas turbine conditions*, IGTC08_P43, The Future of Gas Turbine Technology, 4th International Conference, Brussels, Belgium.

Naqvi R, Bolland O, Brandvoll Ø and Helle K (2004), *Chemical looping combustion analysis of natural gas fired power cycle with inherent CO_2-capture*, Proceedings of ASME Turbo EXPO 2004.

Natural Gas Fired Zero Emission Plant (GAS-ZEP)- Revised Specification for GAS-ZEP Optimum Concept OXY1 (2003), ALSTOM Power Technology Centre Report No U21625/009.

Pachauri R K and Reisinger A (2007), *Contribution of Working Groups I, II and III to the Fourth Assessment Report of the Intergovernmental Panel on Climate Change*, Geneva, Available from: http://www.ipcc.ch/publications_and_data/publications_and_data_reports.shtml#1.

Pontbriand M, Czarnecki L, Kozak F and Muraskin, D (2009), Post-combustion capture: aiming to be commercial by 2015, *Modern Power Systems*, San Francisco, CA, **29**(12), 10–13.

Rezvani S, Bolland O, Franco F, Huang Y, Span R, Keyser J, Sander F, McIlveen-Wright D. and Hewitt N. (2009), Natural gas oxy-fuel cycles – Part 3: Economic evaluation, *Energy Procedia*, **1**, 565–572.

Sanz W, Jericha H, Moser M and Heitmeir F (2005), Thermodynamic and economic investigation of an improved Graz Cycle power plant for CO_2 Capture, *Journal of Engineering for Gas Turbines and Power,* **127**, 765.

Shilling N and Jones R (2003), *The response of gas turbines to a CO_2 constrained environment*, Gasification Technology Conference.

Specht M, Baumgart F, Feigl B, Frick V, Stürmer B, Zuberbühler U, Sterner M, Hahn, B and Waldstein G (2009), *New routes for the production of substitute natural gas (SNG) from renewable energy*, Kraftstoffe der Zukunft, Berlin.

Sundkvist S G, Griffin T and Thorshaug (2001), *AZEP-development of an integrated air separation membrane –gas turbine,* Second Nordic Minisymposium in Carbon Dioxide Capture and Storage, Göteborg.

Winkler D, Müller P, Reimer S, Griffin T, Burdet A, Mantzaras J and Ghermay Y (2009), *Improvement of gas turbine combustion reactivity under flue gas recirculation condition with in-situ hydrogen addition*, GT2009–59182, Proceedings of ASME Turbo Expo 2009: Power for Land, Sea and Air GT2009, Orlando, Florida, USA.

16

Ultra-low nitrogen oxides (NO_x) emissions combustion in gas turbine systems

G. E. ANDREWS, University of Leeds, UK

DOI: 10.1533/9780857096067.3.715

Abstract: The historical development of gas turbine low NO_x combustion from the pioneering NASA work in the early 1970s to the present generation of ultra-low NO_x industrial gas turbine combustors is reviewed. The principles of operation of single digit ultra-low NO_x gas turbine combustion for industrial applications are outlined. The review shows the potential has been demonstrated by several investigators using different flame stabilizers for NO_x to be reduced to 1 ppm at 1700 K, 2 ppm at 1800 K and 3–4 ppm at 1900 K with no influence of operating pressure and with a practical operating flame stability margin. Under these conditions it is shown that no thermal NO_x should occur and all the NO_x is formed by the prompt NO_x mechanisms. The elimination of thermal NO_x makes the NO_x emissions independent of residence time or reference velocity and independent of pressure. Also there is no influence of air inlet temperature for the same flame temperature. Where legislation requires emissions to be as low as can be achieved, emissions below 4 ppm in production engines are current technology and this review shows the potential to get even lower than this in the future.

Key words: gas turbine combustion, ultra-low NO_x, swirlers, weak extinction.

16.1 Introduction

16.1.1 Environmental problems from NO_x emissions

Nitrogen oxides emissions, or NO_x (NO + NO_2), are of major importance in the generation of ozone through photochemical reactions with reactive hydrocarbons. Ozone is the principle contributor to photochemical smog and is toxic to humans. Ozone decreases lung function and this triggers asthma attacks. The associated reduction in oxygen supply to the blood leads to heart-related problems, through increased work by the heart. NO_2 emissions are also directly harmful to humans, causing a decrease in lung function and related cardiac problems. Ozone is also a powerful greenhouse gas (×2000 for CO_2 equivalence in ppmv), which makes NO_x a secondary greenhouse

© Woodhead Publishing Limited, 2013

gas. NO_x reacts in the atmosphere to form nitric acid and thus contributes to acid rain damage to the ecosystem. Finally, NO_x plays a role in the depletion of stratospheric ozone. Hence, NO_x emissions play a role in all the current environmental air-quality control problems and are thus subject to strict emissions control by air-quality regulators around the world.

As a result of these environmental and health concerns, strict NO_x emissions regulations for all combustion sources have been introduced. For the power generation sector, gas turbine NO_x emissions have been more strictly limited than for coal-fired power generation. This was because the combustion technology reviewed in this chapter enabled NO_x to be controlled for gas turbines and equivalent technology was not available for coal-fired power stations without using very expensive ammonia-based SCR exhaust catalysts. The power generation NO_x emissions legislation is not in terms of $g/MWh_{electric}$, which would be sensible, but in terms of volume concentration corrected to a reference oxygen level, which is 15% for gas turbines based on typical oxygen levels in industrial gas turbine exhausts in the 1970s when the legislation was first initiated. This is an illogical unit, as no benefit is given for improved thermal efficiency. In countries such as Canada (Klein, 1999) mass based power generation emissions regulations do exist.

Aero-gas turbines have not been as severely restricted in NO_x, due to safety concerns over the problem of flame stability at low powers for well-mixed combustion, as well as the greater range of operating powers. However, aero-gas turbine emissions regulation are in sensible units of g_{NO_x}/kg_{fuel} or Emission Index at each power condition and g/cycle thrust for the test cycle weighted emissions. This gives credit for reduced fuel consumption or improved thermal efficiency. Road transport emissions are in sensible units of g/km for passenger cars, or g/kWh for truck engines, which benefits those vehicles with an improved thermal efficiency or specific fuel consumption.

Industrial gas turbines emit very low levels of hydrocarbons, but there are plenty of other sources of hydrocarbons in the atmosphere. Thus the contribution of industrial gas turbines to ozone formation is mainly through NO_x emissions. The ability to design industrial gas turbines with ultra-low NO_x emissions has led to some of the most stringent regulations being passed in the power generation sector. NO_x emissions below 25 ppm or 50 mg/m^3 at 15% oxygen are required in most countries in the world. The European Industrial Emissions Directive, due to come into force in 2016, requires 50 mg/m^3 (~25 ppm). In many countries, NO_x below 10 ppm is required. For example, Italy (Bonzani *et al.*, 2010), which has a significant ozone problem, has regulated for sub-10 ppm NO_x from 2008. In California, sub-2.5 ppm is required and, when converted into the same units, this is the same NO_x emissions as for SULEV emissions control for passenger cars. For large diesel truck engines the 2010 CARB requirements convert to below 11 ppm

© Woodhead Publishing Limited, 2013

NO_x at 15% oxygen (Chen *et al.*, 2010). In ozone non-attainment areas in the USA, no additional NO_x can be emitted by a new gas turbine power station, which leads to the requirement for the lowest possible NO_x emissions from gas turbines for power generation. This chapter describes the combustor design principles that can achieve ultra-low NO_x emissions (<10 ppm) that the NO_x regulations require.

16.1.2 Gas turbine thermal efficiency and turbine entry temperatures

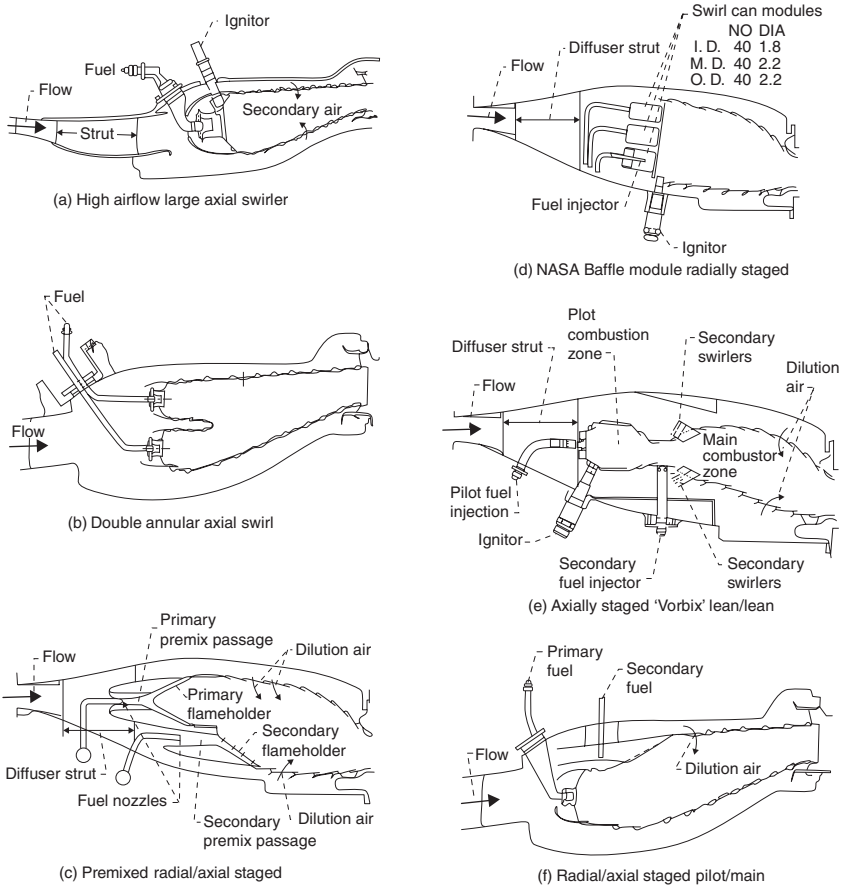
Gas turbine thermal efficiency in simple cycles is limited by the turbine entry temperature and the history of the development of aero and industrial gas turbines can be traced by the year by year increase in turbine entry temperature. This is limited by turbine blade materials and cooling technology, and developments in both of these areas have led to advances in turbine entry temperatures. Today the highest turbine entry temperature is about 1750 K for the G and H class industrial gas turbine with 60% thermal efficiency in combined cycle mode (Ai *et al.*, 2009), although 1950 K is under development with potentially 65% thermal efficiency (Ito *et al.*, 2009). However, all industrial and aero-gas turbines, including these future developments, have turbine entry temperatures well below the maximum near-stoichiometric flame temperature. For example at 700 K inlet temperature the maximum adiabatic flame temperature is 2450 K, so there is major development work ahead in the next 40 years or so, as the industry moves towards the most efficient near-stoichiometric gas turbine cycles. 1950 K occurs at $\Phi = 0.6$ with 1750 K at $\Phi = 0.47$ for 700 K compressor outlet temperature. In older D and F class industrial gas turbines the turbine entry temperature is 1400–1600 K or $\Phi = 0.28$–0.33 and this is the region of overall Φ where most work on ultra-low NO_x gas turbines has taken place.

The combustion in gas turbines has always been very lean, and will remain very lean at $\Phi = 0.6$ for at least the next decade or more of gas turbine developments. This is why lean well-mixed combustion is the solution to low NO_x in gas turbines. Gas turbine combustion also occurs in near adiabatic conditions, as the aim is not to extract heat from the combustion system. Heat transfer to the wall is transferred to the cooling air, which is added to the turbine entry flow so that overall the combustion is adiabatic. The only system heat loss is by convection from the outer engine casing, and this is very low at <1% of the heat input. Thus, gas turbine combustion can be treated as adiabatic, and this makes computation of the NO_x formed easier than in boilers and furnaces. Heat transfer to the walls is the aim for water heating and steam generation so that the furnace temperatures are not adiabatic.

© Woodhead Publishing Limited, 2013

16.2 The NASA clean combustor programme

Low NO_x gas turbine combustor design technology dates back to the NASA aero engine 'clean combustor programme' in the 1970s, which investigated the systems shown in Fig. 16.1 (Jones, 1973; Niedzweiki and Jones, 1976; Mularz, 1976; Rudey, 1976). This programme was accompanied by classic work on grid-plate flame stabilizer premixed flames by Anderson (1973, 1975), who was the first to demonstrate that lean well-mixed combustion could achieve ultra-low NO_x emissions, which was confirmed by the grid-plate premixed work of Spadaccini and Szetela (1975). Anderson demonstrated 6 ppm NO_x at 1800 K combustor exit temperature, using a 61 hole grid plate operated at 5.5 bar with 590 and 800 K air temperature and a reference velocity (mean isothermal velocity based on the combustor cross-sectional area) of 25 m/s



16.1 (a–f) NASA clean low NO_x combustor designs (Jones, 1973; Mularz, 1976; Niedzweiki and Jones, 1976; Rudley, 1976).

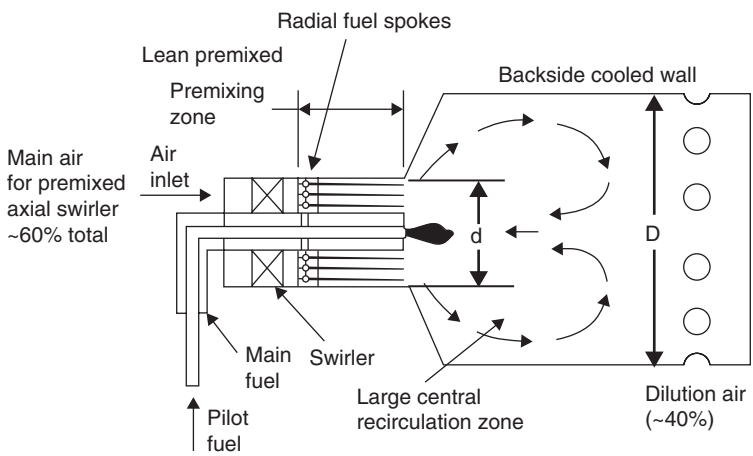
© Woodhead Publishing Limited, 2013

(reference Mach number M_{ref} ~ 0.05). As no industrial gas turbine currently operates above 1800 K turbine entry temperature (the H class is close to this at ~1750 K), this early work showed that single digit NO_x was possible in advanced gas turbines. For combustor exit temperatures lower than this, less than 6 ppm must be possible. Thirty years after Anderson's work, industrial gas turbines with single digit NO_x were in production. The development of the NASA low NO_x concepts into practical industrial low NO_x gas turbines is discussed in the following sections.

16.2.1 Large high airflow axial swirlers

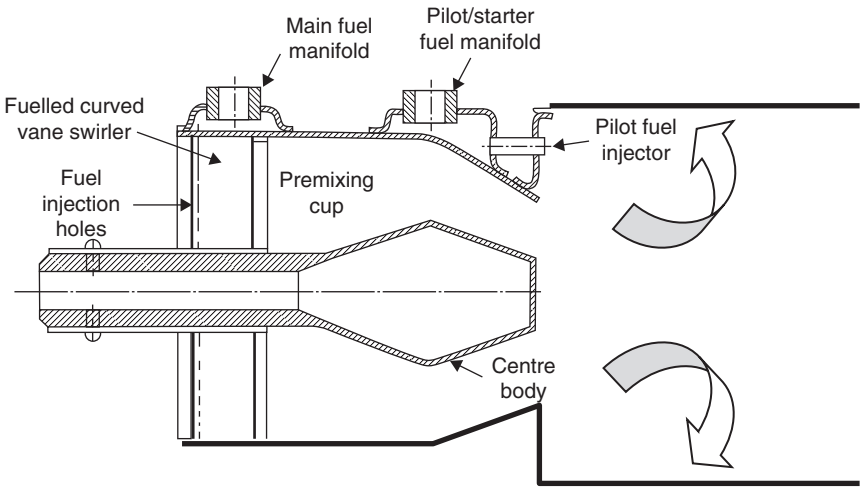
The various designs from the NASA work in Fig. 16.1 each have a current industrial low NO_x gas turbine based on them. The high air flow swirler in Fig. 16.1a is used to allow large proportions of air to enter the primary zone to achieve lean combustion and Figs 16.2–16.4 show three current industrial gas turbine low NO_x applications of this concept. The first of these is the classic cylindrical combustor configuration of the SoLoNO$_x$ design shown in Fig. 16.2 (Rohrbacher, 1996; Fahm and Smith, 1999). This has a large airflow capacity axial swirler, downstream radial spoke multihole fuel injector and then a short mixing length nozzle of diameter d that exits to a dump expansion into the combustor of diameter D. A central pilot is used, which is located in the swirler hub (diameter d_h) with an exit at the premixing passage exit plane.

Razdan *et al*. (1994) also used a large swirler in a cylindrical combustor and mixed the fuel using hollow axial swirl blades with fuel injection along the blade surface, as shown in Fig. 16.3. They were the first to introduce this

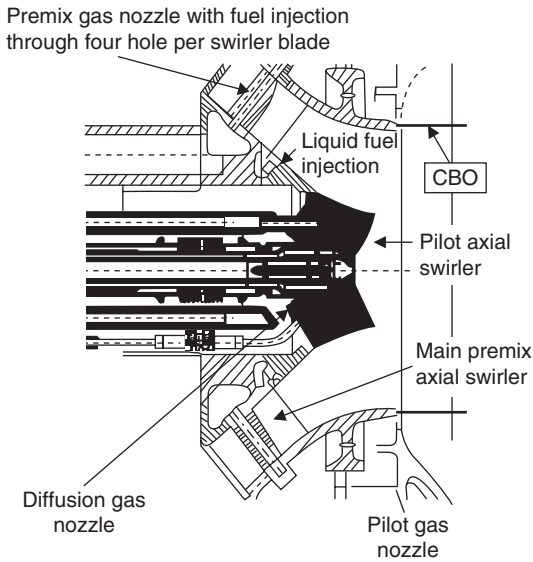


16.2 Conventional axial swirler, radial premixing fuel spokes downstream of the swirler, mixing length, dump flow expansion – SoLoNO$_x$ (Rohrbacher, 1996; Fahme and Smith, 1999).

© Woodhead Publishing Limited, 2013



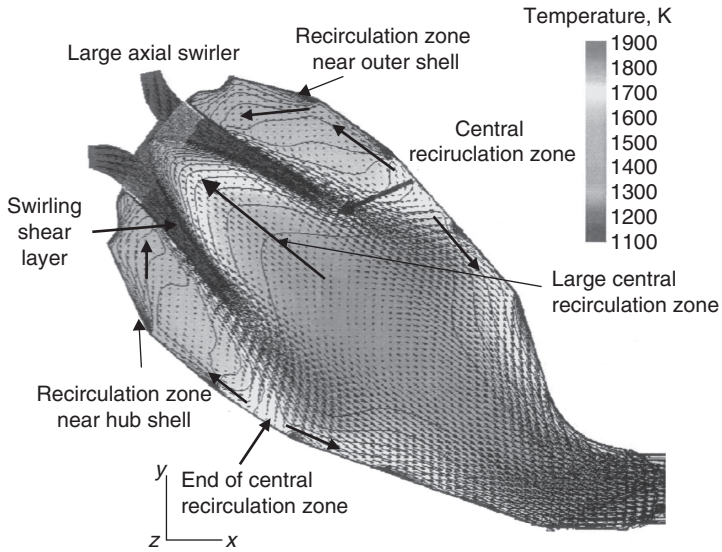
16.3 Large axial swirler with fuel injection through the swirl-blade surface, with a contracted mixing duct outlet (Razdan *et al.*, 1994).



16.4 Hybrid burner with large axial swirler and central pilot swirler with an outlet nozzle, CBO – cylindrical burner outlet. (Prade *et al.*, 2002).

axial swirler method of fuel injection and today most users of axial swirlers in industrial gas turbines mix the fuel-and-air in this way. The swirler in Fig. 16.3 has an outlet restrictor to prevent flashback and a central hub that is not used to locate a pilot fuel. Instead, the outer dump expansion plane is used to pilot the flame in the outer recirculation zone.

© Woodhead Publishing Limited, 2013



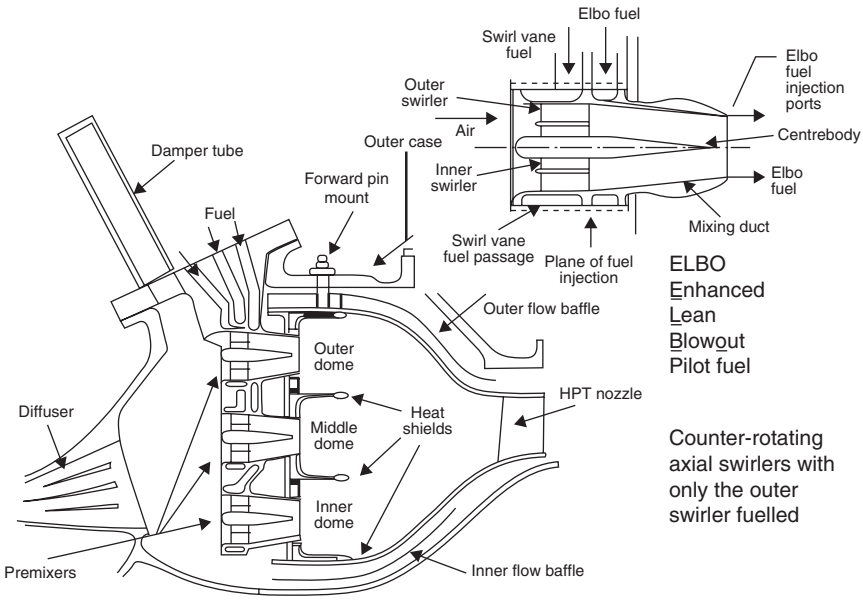
16.5 CFD predictions of flame temperature contours in the Hybrid burner HR-3 with CBO (swirler short outlet nozzle), consisting of a large axial swirler with fuel injection through the swirl-blade surface (Streb, 2010).

Figure 16.4 shows a large industrial gas turbine using an annular combustor with a series of axial swirlers with central pilots (with separate axial swirled pilot air) that occupy a large proportion of the depth of the large annular combustor (Prade *et al*., 2002). Figure 16.5 shows the predicted flame temperature development in this combustor. This shows the long flame development length of lean low NO_x combustion. Figure 16.5 also shows the hot central recirculation zone that helps to stabilize the lean flames.

16.2.2 Double and triple annular swirl combustors

The double annular axial swirler design in Fig. 16.1b is the basis today of one class of aero-derivative industrial low NO_x gas turbines, as shown in Fig. 16.6 (Joshi *et al*., 1998). This is available as double annular and triple annular (Fig. 16.6) depending on the engine size. A series of counter-rotating axial swirlers is used, and only the outer swirler is fuelled. A pilot fuel flow, as shown in Fig. 16.6, is used to aid lean stability. Engine-power reduction is achieved using fuel staging between the three banks of swirlers. The cooled wall divider between the rows of swirlers is to prevent unfuelled swirlers from mixing with the fuelled swirlers during fuel staging, as this would deteriorate the combustion efficiency and flame stability.

© Woodhead Publishing Limited, 2013



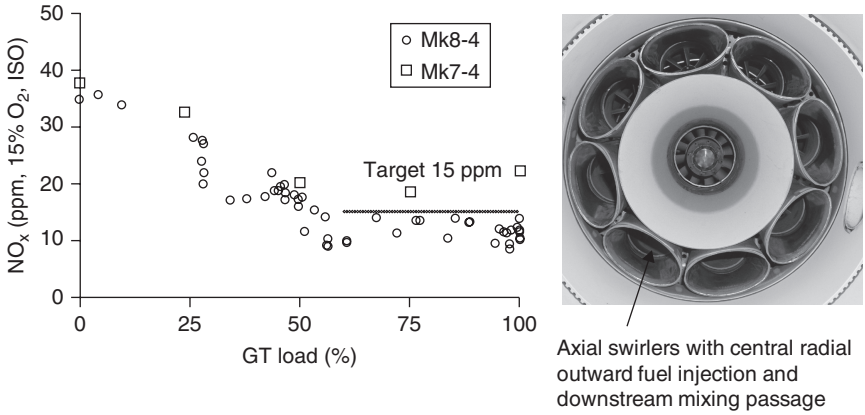
16.6 LM6000 44 MW Industrial gas turbine with three parallel axial counter-rotating swirlers for fuel staging at low power (Joshi *et al.*, 1998).

16.2.3 Arrays of axial swirlers in a combustor

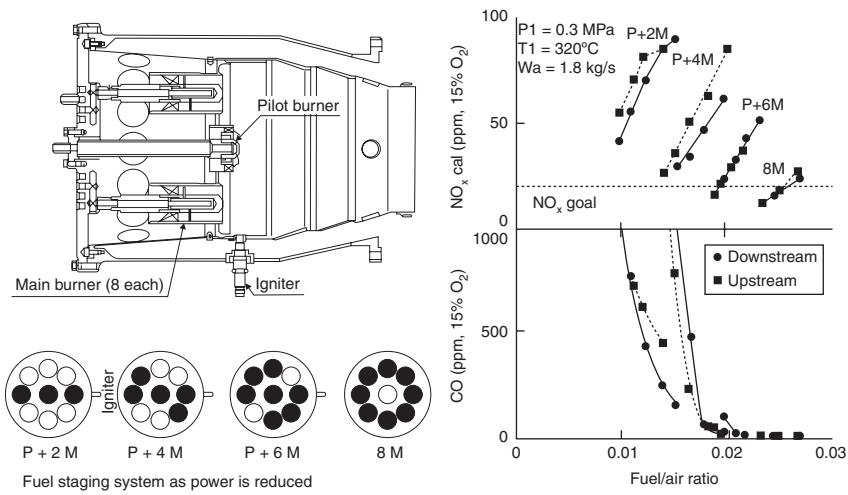
In contrast to the double or triple annular staged combustor, Fig. 16.1d shows the NASA swirl can module design. This has an array of axial swirlers in a flat axial plane with no cooled walls between the swirlers. This principle of a planar array of axial swirlers in a cylindrical combustor has been developed by a number of gas turbine manufacturers over a wide range of engine sizes. Figure 16.7 shows an eight-axial-swirler array around a central baffle with a central axial swirler, which is used in the largest F-H class gas turbines. Figure 16.7 also shows that this is one of the designs that can maintain sub-15 ppm over the 50–100% power range.

A very similar eight axial swirler with a central pilot axial swirler is shown in Fig. 16.8 for a small gas turbine application (Kitajima *et al.*, 1995). Figure 16.9 shows the axial swirler design that is used in a five-axial-swirler array in a cylindrical combustor for large heavy duty F-H class engines (Myers *et al.*, 2003). This is a good example of a design that has sufficient flame stability in the well-mixed mode to sustain <10 ppm NO_x to 43% of maximum power. The unique feature of this design is that there are three stages of main fuel injection, two through the hollow swirl blades and one through premixed fuel injection well upstream of the swirler (F Class). Power is increased from 50% on this premixed air, with the fuelling to 50%

© Woodhead Publishing Limited, 2013



16.7 Eight axial swirlers with a short downstream mixing passage around a central baffle and central pilot axial swirler (Rodriguez *et al.*, 2008).



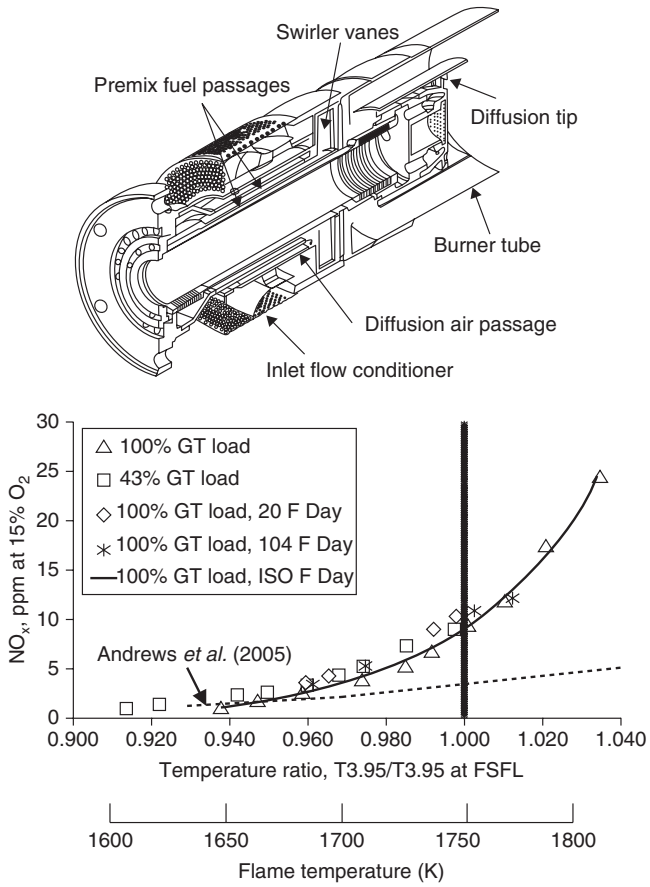
16.8 Axial swirler fuel stage combustor with no separation between the swirlers (Kitajima *et al.*, 1995).

on the swirler-vane fuel flow. The axial staging of the fuel, which introduces two fuel supply-time constants, also helps to resist acoustic resonance.

16.2.4 Grid-plate type flame stabilizers

The grid-plate type flame stabilizers introduced by Anderson (1973, 1975) have led to gas turbine flame stabilizers that use grid or conical grid flame stabilizers in production industrial gas turbines. The multicluster

© Woodhead Publishing Limited, 2013



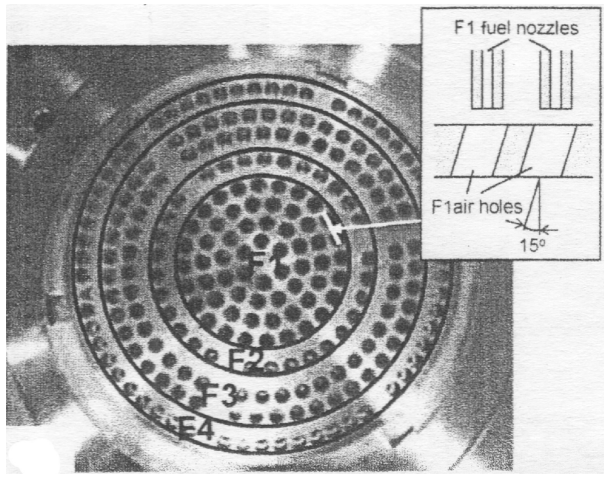
16.9 Axial swirler in a cylindrical combustor with two stages of premixed fuelling (Myers *et al.*, 2003); comparison with axial swirler results of Andrews *et al.* (2005) at 740 K and 1 bar.

flame stabilizer (Koganezawa, 2007) is shown in Fig. 16.10 and is used in a 4 MW gas turbine. It consists of a grid plate formed by a series of tubes, into which there is a main fuel injector on the centreline of each tube, as shown in Fig. 16.10. Another grid-plate type design is shown in Fig. 16.11; this uses a conical flame stabilizer with slotted rectangular grid holes. This was developed by Sasao *et al.* (2007) for use in a 27 MW industrial gas turbine.

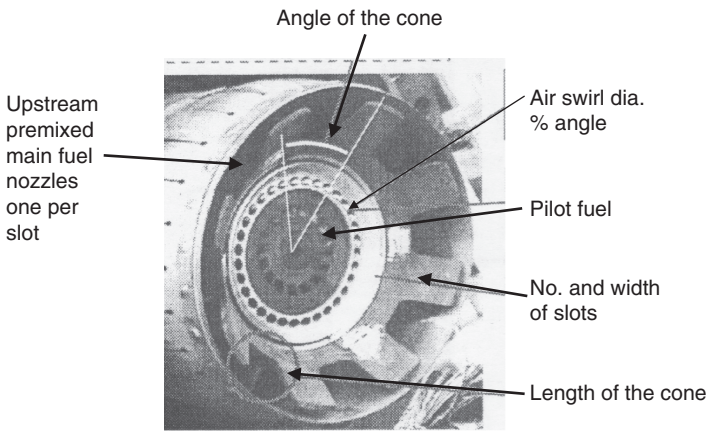
16.2.5 Conical two slot grid stabilizer – the EV, AEV and TE burners

Another form of conical baffle stabilizer is the EV burner (Fig. 16.12) developed by Sattlemeyer *et al.* (1990). In this, a conical stabilizer is split in half and then offset to form two tangential air-entry slots along the length of the

© Woodhead Publishing Limited, 2013



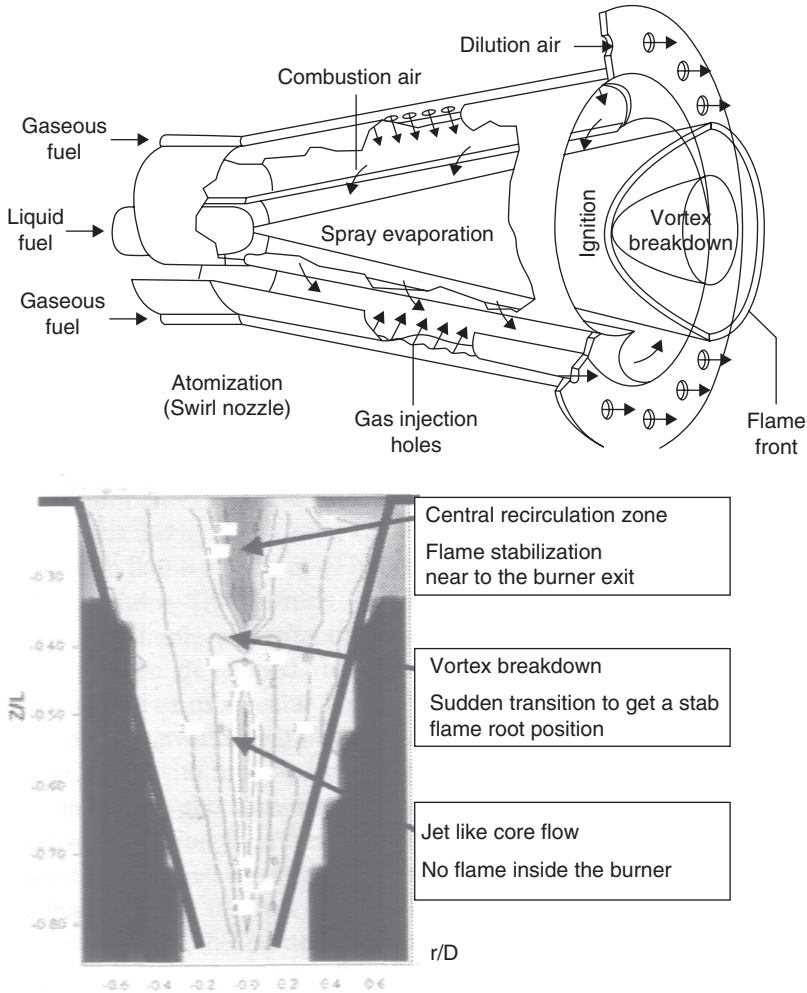
16.10 Grid-plate type flame stabilizer with separate fuelling of each hole, with the Multicluster burner used in a 4 MW gas turbine (Koganezawa *et al.*, 2007).



16.11 Conical grid-plate well-mixed flame stabilizer with the important design variables as used in a 27 MW gas turbine (Sasao *et al.*, 2007).

cone on opposite sides of the cone. A fuel injection tube is mounted at the entry to this slot with fuel injection holes uniformly along the length of the slot. This is used in the E-H class gas turbines, with the number of EV burners increasing as the engine size increases. A similar flame stabilizer, termed the TE burner (Bhargava *et al.*, 2000a), has been developed to operate in aero-derivative industrial gas turbines. One version of the TE burner is shown in Fig. 16.13, and has an outer cylindrical shape with two air-entry

© Woodhead Publishing Limited, 2013

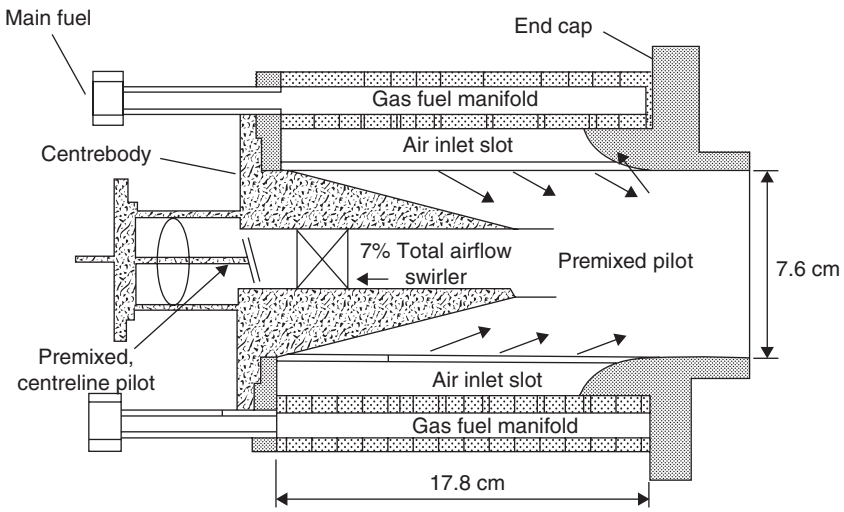


16.12 The EV burner – a conical 2 slot radial swirler with fuel injected along the length of the slot. Liquid fuel or gaseous pilot fuel can be injected at the base of the cone (Sattlemeyer *et al.,* 1990).

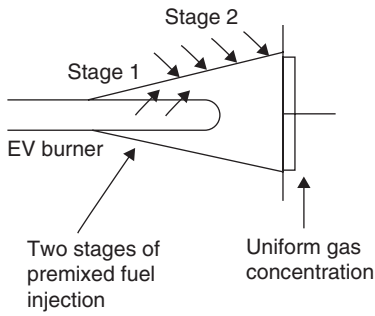
slots, which were fuelled in the same way as the EV burner, and an inner conical blockage. The result was a stabilizer outlet flow area that increased in the direction of the outflow in the same way as in the EV burner.

Both of these designs found it difficult to achieve perfect mixing at the burner outlet, and the EV burner has been developed, as shown in Fig. 16.14, with staged central and air-slot fuel injection to give better mixing and lower NO_x (Kokanovic *et al*., 2006). An earlier method of improving the mixing in the EV burner was the use of four tangential slots along the cone, with

© Woodhead Publishing Limited, 2013



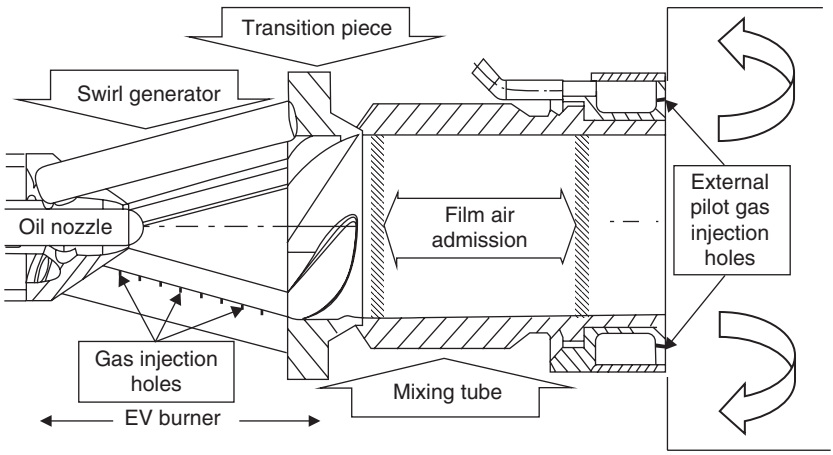
16.13 The TE burner with two main air and fuel inlet slots generating a radial swirler with two inlet vanes of great depth (Bhargava *et al.*, 2000a).



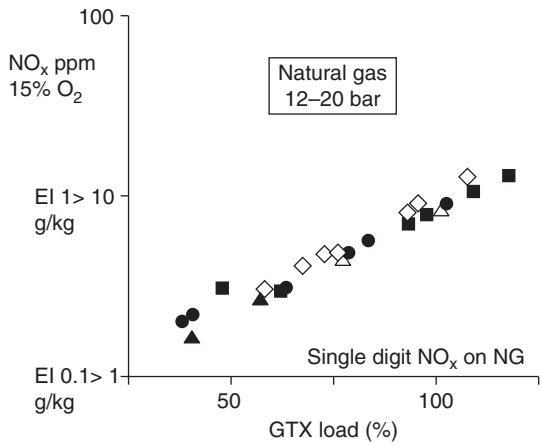
16.14 The improved EV burner with better premixing and lower NO_x (Hiddemann and Marx, 2010).

a simple cylindrical mixing length addition at the end of the EV burner, as shown in Fig. 16.15, which was termed the advanced EV (AEV) burner. This four-slot conical flame stabilizer is similar to the radial swirler designs discussed below. The improved fuel-and-air mixing in the AEV burner gave very good NO_x emissions and $NO_x < 10$ ppm for engine powers from 100% to 40%, as shown in Fig. 16.16. This AEV design was piloted in a different way from the EV burner in Fig. 16.12, where a pilot injector at the base of the cone was used. With the addition of the cylindrical mixing zone the pilot fuel would also be mixed so it did not act as a pilot. The AEV design used the outer dump expansion region as a pilot, as shown in Fig. 16.15. A development of the AEV burner is in current use (Lorstad *et al.*, 2009).

© Woodhead Publishing Limited, 2013



16.15 The advanced EV burner (AEV) with mixing tube added and a new pilot fuel location in the corner recirculation zone (Jansohn, 1997; Kokanovic *et al.*, 2006).

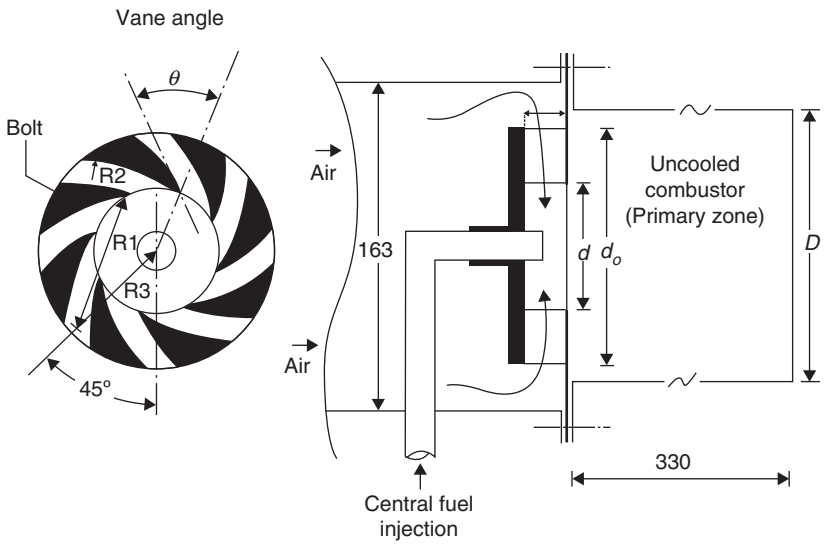


16.16 NO_x emissions as a function of engine power for AEV burners (Jansohn *et al.*, 1997).

16.2.6 Radial swirlers

One type of low NO_x flame stabilizer, which was not in the design options investigated in the NASA programmes in the 1970s, is the radial swirler. Radial swirlers are suitable for reverse-flow gas turbine combustors, which are the common configuration in industrial gas turbines, but rarely used in axial flow aero-gas turbines where NASA's main interest lay. Radial swirlers with radial vane passage fuel injection, as shown in Fig. 16.17, were first

© Woodhead Publishing Limited, 2013

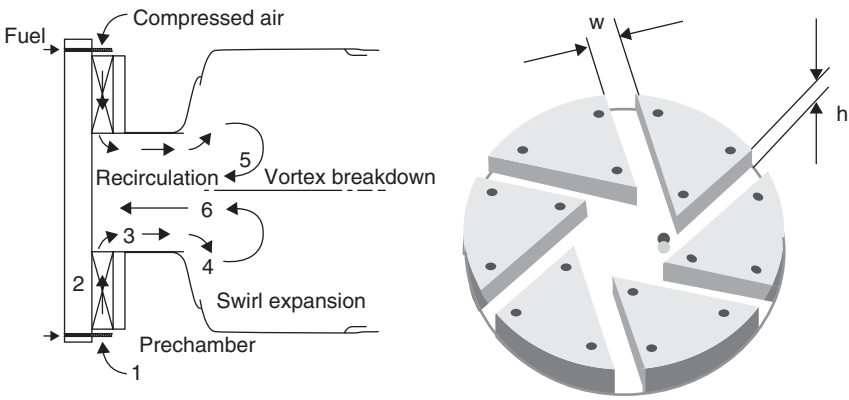


16.17 Radial swirler with vane passage fuel injection for the well-mixed mode and central injection for pilot fuel, with no downstream mixing throat: $D/d = 140/76 = 1.84$ (Alkabie and Andrews, 1988, 1989a).

shown by Alkabie and Andrews (1988, 1989a) to have extremely low NO_x characteristics without the need for any downstream mixing passage. They used relatively low-depth radial passages with a relatively low air flow capacity. Escott *et al*. (1993) showed that the radial swirler design could be scaled up for larger flow capacity by increasing the vane depth of the swirler without changing the outlet diameter. The curved blade passage was not crucial to the function of the fuel-and-air mixing, and Andrews *et al*. (2008) investigated four-radial swirler-vane passage designs in the configuration of Fig. 16.17, with a greater vane depth. The passage shape in Fig. 16.17 was compared with an aerodynamic radial vane of the type used by Willis *et al*. (1993) in their counter-rotating radial swirler. It was also compared with a rectangular constant-area vane passage and a circular radial vane passage. The results showed that the vane passage shape only had a small effect on the NO_x emissions with vane passage fuel injection. All current industrial applications of this design use a rectangular constant-area passage shape, as shown in Fig. 16.18 for one manufacturer (Lee *et al*., 2011).

Alkabie *et al*. (1989a, 1989b, 1989c, 1990, 1991b, 1991c) have investigated the influence of fuel injection location on the emissions for radial swirlers. Four fuel injection positions were investigated, as shown in Fig. 16.19, and vane passage and swirler outlet throat wall fuel injection both gave near premixed performance, and the central injection and dump expansion corner recirculation fuel injection were suitable for pilot fuel locations. The

© Woodhead Publishing Limited, 2013



16.18 Radial swirler as used in a 250 kW gas turbine with rectangular vane passages and a downstream exit throat and dump flow expansion (Lee *et al.*, 2011).

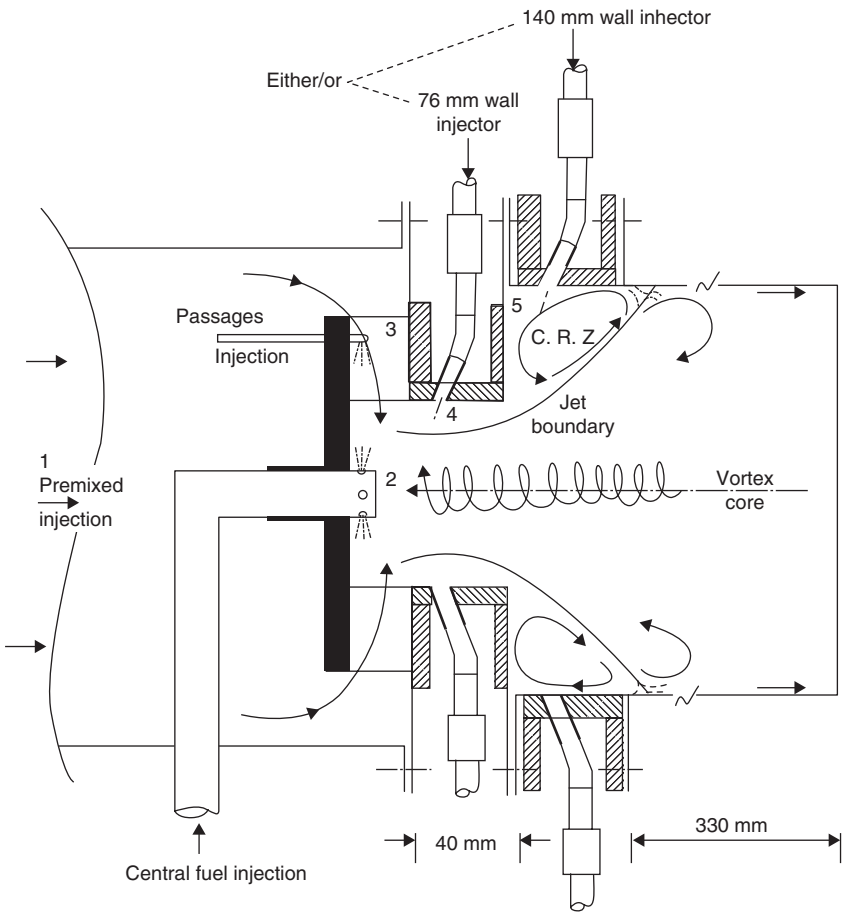
latter pilot location was essentially the same as that used in the AEV burner, as shown in Fig. 16.15. The use of swirler outlet throat wall fuel injection was investigated, as no flashback could occur and, for liquid fuels, no autoignition could occur. However, the method required an outlet throat to be added to the radial swirler exit. Every industrial application of the radial swirler design has used an outlet mixing throat but without the wall fuel injection, as all use vane passage fuel injection.

One of the earliest applications of radial swirlers with rectangular constant-area vane passages and fuel injection into the vane passages is shown in Fig. 16.20 (Hornsby and Norster, 1997). A range of different-sized radial swirler low NO_x combustors of this type were designed for different gas turbine sizes (Boyns and Pater, 1997; Gallimore *et al.*, 1997; Kowkabi *et al.*, 1997; Scholz and Depitro, 1997). Another radial swirler design with vane passage fuel injection is shown in Fig. 16.21; this design is termed the radial swirler premixing nozzle (RSPN), and has a radial swirler, outlet mixing length and a flashback outlet area reduction. The main difference between this and the radial swirlers in Figs 16.17–16.20 is the greater radial swirler depth of passage, shorter passage length and the use of a higher number of radial swirler passages. Counter-rotating radial swirlers with vane passage fuel injection have also been investigated by Andrews *et al.* (2005) and Escott *et al.* (2005), and applied in the primary zone of an axially fuel staged low NO_x combustor (Willis *et al.*, 1993).

16.3 Acoustic resonance and catalytic combustion

A problem of lean, well-mixed, low NO_x gas turbines is that of acoustic resonance. This is driven by a coupling between heat release in a relatively thin reaction with a characteristic chemical time constant with an acoustic time

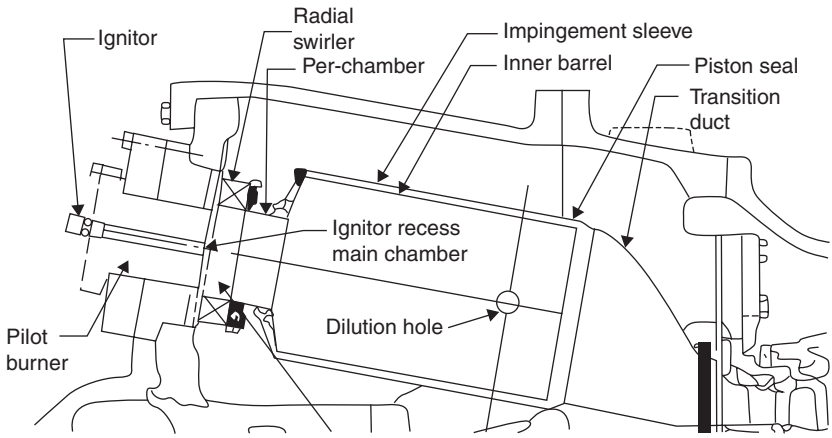
© Woodhead Publishing Limited, 2013



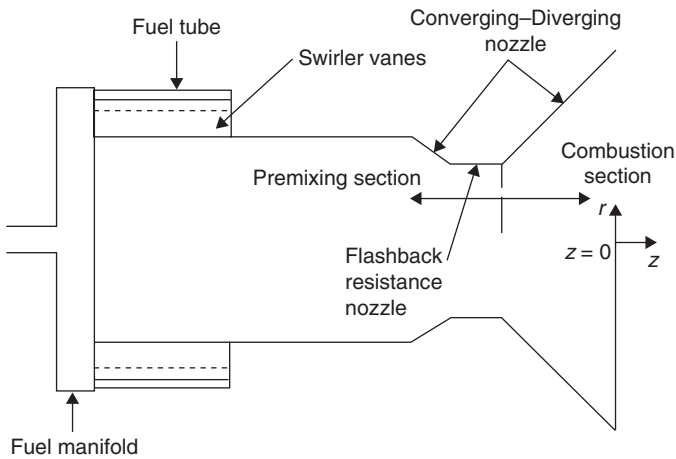
16.19 Radial swirler with outlet throat 76 mm wall fuel injection, compared with the downstream aerodynamics and the alternative vane passage fuel injection and two locations for pilot fuel – central and 140 mm wall (Alkabie *et al.*, 1991b).

constant, such that the acoustic wave is amplified on each passage through the reaction zone, leading to destructive pressure oscillations. This phenomenon has been reviewed in Chapter 13 and will not be discussed in detail in this chapter. However, in many practical cases, including most of the designs reviewed here, the critical equivalence ratio for the onset of resonance was at a higher primary zone temperature than would be operated in a low NO_x combustor at any current or future operating turbine entry temperature up to at least 1950 K. However, if the primary zone operates with inadequate air flow, so that its equivalence ratio is in the critical range for acoustic resonance, even though the overall equivalence ratio is not, then not only will the NO_x be too high but acoustic resonance problems may be encountered.

© Woodhead Publishing Limited, 2013



16.20 Radial swirler low NO_x combustor with rectangular radial vane passage shape and downstream mixing throat as used in several industrial gas turbine applications (Hornsby and Norster, 1997).



16.21 RSPN with downstream mixing throat with flashback resistant outlet convergence (Puri *et al.*, 1995).

Acoustic pressure oscillations are a common low NO_x gas turbine combustion problem and many manufacturers of low NO_x gas turbines have had to redesign the combustor geometry and air flow splits to move out of the acoustic resonance region. However, acoustic resonance is not a problem that inevitably occurs in low NO_x combustors, as some manufacturers have

© Woodhead Publishing Limited, 2013

developed low NO_x combustors with no acoustic problems (McLeroy *et al.*, 1995; Ogata *et al.*, 1999; Baker *et al.*, 2000; Toh *et al.*, 2001; Austrem *et al.*, 2002; Saitou *et al.*, 2005). Many ultra-low NO_x gas turbine combustors have had to solve the problem of acoustic instability, and this normally involves making a change in the flame stabilizer design, so that a combustion or mixing time constant is changed. The alternative is to alter the combustor or plenum-chamber length or volume to change the acoustic constant, and this is normally much too costly. Some examples of successful design changes that remove acoustic resonance are an exit throat extension (Prade *et al.*, 2002) on a large axial swirler low NO_x burner, changing the area of the premixing tube part way along its length (Steele, 1999), staging the fuel in the premixer (Myers *et al.*, 2003; Kokanovic *et al.*, 2006) and staging the air admission to a premixing duct (Scarinci *et al.*, 2004). Many manufacturers also use a pilot fuel that helps to stabilize the premixed flame better; the proportion of pilot fuel is then an important control parameter to move out of acoustic resonance or to extend the flame lean stability limit (Kowkabi *et al.*, 1997; Alkabie, 1998; Farber *et al.*, 2009; Levy *et al.*, 2010). Unfortunately, the use of diffusion type pilots usually increases NO_x emissions.

16.3.1 Catalytic combustion

Catalytic combustion will not be reviewed in detail here, as there are no production gas turbines using catalytic combustion. This is mainly because, in spite of the vast amount of work carried out, a NO_x performance better than can be achieved in lean well-mixed combustion has not been demonstrated. To achieve <3 ppm NO_x, a catalytic combustor has to have an upstream fuel-and-air mixer that is as good as that used in lean well-mixed combustion; it also has to have an air temperature above about 700 K, as the catalyst is not active at lower temperatures. If the compressor exit temperature is lower than this, then a pre-burner is required, and the NO_x generated by this would compromise the overall NO_x (Dalla Betta *et al.*, 1996). Power turndown is even more problematic than in lean premixed combustion, without resorting to the use of pilot combustion at low powers. There are some advantages in using a premixed catalytic pilot combustor in conjunction with premixed main combustion (Fujii *et al.*, 1996), but similar results can be obtained with a premixed flame-stabilized pilot upstream of a premixed main combustor, known as the lean/lean-fuel staged approach. A thorough discussion of this approach is outside the scope of this chapter; however, as lean premixed combustors are currently achieving NO_x in the region of 3–4 ppm (Benoit *et al.*, 2010; Zito *et al.*, 2010) and all demonstrations of <3 ppm NO_x using catalytic combustion are for turbine entry temperatures <1750 K, it is not likely that catalytic combustion will have a major impact on future gas turbines.

© Woodhead Publishing Limited, 2013

16.4 Thermal NO_x formation

16.4.1 Thermal, prompt and FBN NO_x formation routes

There are three sources of NO_x emissions in combustion: thermal, prompt, and fuel bound nitrogen (FBN). Prompt NO_x is the NO_x that remains after thermal and FBN NO_x have been eliminated and, in lean well-mixed combustion, is usually <5 ppm. Prompt NO_x is important, as it is the cause of the residual NO_x that prevents zero NO_x from being achieved. However, the reduction of thermal NO_x to near zero is a prerequisite to the achievement of ultra-low NO_x emissions, and this is the main topic of this review.

FBN occurs when the fuel contains organic nitrogen compounds, such as pyridine and, when they burn in lean well-mixed combustion, the organic nitrogen is oxidized to NO. These fuels are thus incompatible with lean well-mixed gas turbine combustor designs. Fuels with high FBN are coal or coal-derived liquids and heavy fuel oil, and these are not practical industrial gas turbine fuels today. Consequently, FBN will not be discussed in detail. However, the solution to the FBN problem is to first burn the fuel in a rich zone, where the organic nitrogen compounds are reduced to N_2, and then to add air to produce a well-mixed lean zone. This technique also reduces thermal NO_x but not to ultra-low NO_x levels, and rich/lean combustion will not be discussed further in this work. Rich/lean combustion is also the burner design method that is used to reduce NO_x from near-stoichiometric operation in process burners and steam turbine boilers.

Natural gas is the main fuel used in low NO_x industrial gas turbines for power generation, and this has no FBN. Fuel oil or diesel has low levels of FBN, typically of the order of 100 ppm and, at this level, FBN will account for about 5 ppm NO_x at 15% oxygen. Clearly, if FBN approaches 500 ppm in the fuel, a lean well-mixed combustor will convert all of this to NO. 25 ppm NO_x emissions regulations will be generated by the FBN alone, and no thermal or prompt NO_x would then be possible if a 25 ppm NO_x limit was to be met. As this is unrealistic, the effective maximum FBN is about 400 ppm, as this would allow a 25 ppm limit to be just met if the thermal and prompt NO_x were no more than 5 ppm. For liquid fuels, the level of FBN is normally of some significance in the NO_x emissions, and is one of the reasons why single digit NO_x is very difficult to achieve with fuel oil. Typical FBN in fuel oil is from 50 to 200 ppm, which yields about 2–10 ppm NO_x at 15% oxygen.

16.4.2 Thermal NO_x formation kinetics

Thermal NO_x occurs at high flame temperatures and involves the following three reactions:

© Woodhead Publishing Limited, 2013

$$N_2 + O <> NO + N \quad [16.1]$$

$$N + O_2 <> NO + O \quad [16.2]$$

$$N + OH <> NO + H \quad [16.3]$$

The first two reactions were first determined by Zeldovich (1946) and the third reaction was added (Lavoie *et al.*, 1970) to account for thermal NO_x formation in rich mixtures where atomic oxygen levels are low. Thermal NO_x and extended Zeldovich NO_x are used in the literature to refer to NO_x formation by the above three reactions. However, for well-mixed lean gas turbine combustion with a low residence time, the first reaction is rate limiting, as the second reaction relies on N produced by the first reaction, there being no significant dissociation of gaseous nitrogen at hydrocarbon/air flame temperatures. Thus, NO_x production is limited by the production of atomic oxygen by dissociation at high flame temperatures and by the rate constant of [16.1]. Hence, for lean premixed fuel-and-air combustion in gas turbines, the generation of thermal NO_x can reliably be predicted by [16.4]:

$$\frac{d[NO]}{dt} = K[O][N_2] \quad [16.4]$$

where K is the forward rate constant, typically $7.6 \times 10^{13} \exp[-38\,000/T]$ cm^3/mol·s.

16.4.3 NO conversion to NO_2 in lean low NO_x combustion

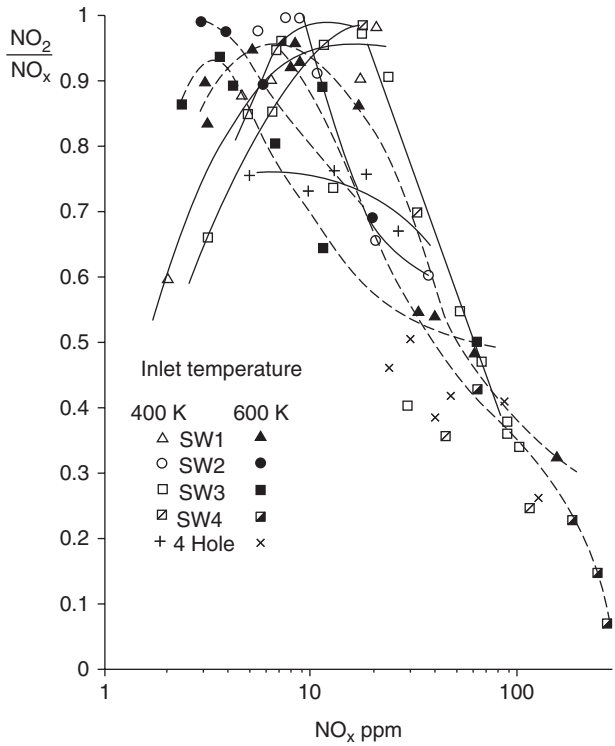
NO_x ($NO + NO_2$) is first formed as NO, mainly by the above thermal mechanism, but some can be subsequently converted to NO_2 in the combustor. The key reaction (Kyne *et al.*, 2003) in this conversion is Equation [16.5]:

$$HO_2 + NO = NO_2 + OH \quad [16.5]$$

This is a fast reaction at low temperatures, and leads to high proportions of NO_2 in conventional gas turbine combustors at idle. As ultra-low NO_x combustors operate at low overall primary zone temperatures, NO_2 is a high proportion of the total NO_x due to the significance of Equation [16.5] in low temperature low NO_x gas turbine combustion. An example of this is shown in Fig. 16.22 for premixed axial swirlers, where the total NO_x is almost all NO_2 in some cases for low overall NO_x.

NO_2 at concentrations above about 13 ppm in stack gases is visible as a light brown plume, which normally is not allowed by local environmental

© Woodhead Publishing Limited, 2013



16.22 NO_2/NO ratios for four axial swirlers for premixed propane/air $M = 0.05$ and 400 and 600 K air inlet temperatures (Ahmad and Andrews, 1983).

regulations on stack gas visibility. However, this would only be a problem in low NO_x gas turbines if the total NO_x were just below 25 ppm with 50% of this converted to NO_2. Most production low NO_x gas turbines have NO_x around 15 ppm or lower and there is generally no visible NO_2 problem. This is occasionally a problem in gas turbines with auxiliary heaters (duct burners) prior to the combined cycle steam generators, as these very effectively convert NO into NO_2, in the same way that reheat burners convert NO into NO_2 in military aero-gas turbines (Kyne *et al.*, 2003).

16.4.4 Pressure dependence of thermal NO_x

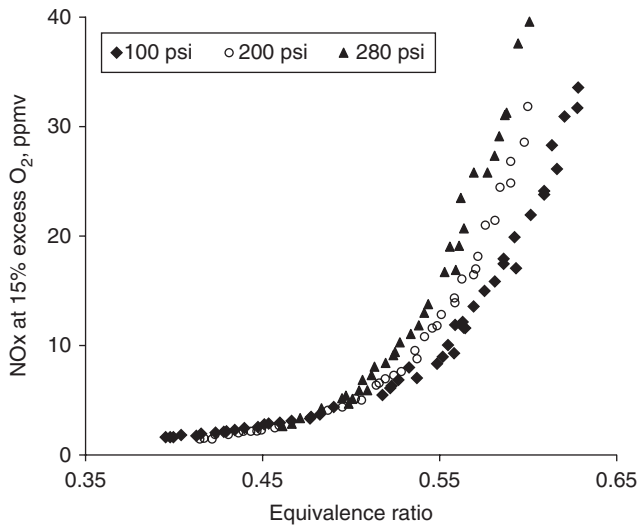
The [O] concentration in Equation [16.4] is proportional to $[O_2]^{0.5}$ and this leads to a square root dependence of NO_x formation on pressure for the same flame temperature. For conventional diffusion flame gas turbine combustors, there is ample evidence for the thermal NO_x to vary with the square

© Woodhead Publishing Limited, 2013

root of pressure (Sawyer, 1973), and this pressure relationship is embedded in the CAEP NO_x regulations for aero-gas turbines.

A key feature of ultra-low NO_x gas turbines that have eliminated thermal NO_x formation through operating lean and well-mixed is that there is no pressure dependence of the NO_x emissions. An illustration of this is shown for the cylindrical fuel injector shown in Fig. 16.13. This had two tangential injection slots with fuel spokes along the slots and a conical central insert (Bhargava *et al.*, 2000a), and is a form of radial swirler with two radial vanes of great depth. The experimental results for this low NO_x burner for the influence of pressure are shown in Fig. 16.23. This shows that for $\emptyset < 0.51$ there was no influence of pressure on NO_x, and this condition corresponds to a flame temperature of 1820 K at the 700 K air inlet temperature of this work. Considerable work was undertaken on this device to improve the fuel-and-air mixing, and this relatively low critical temperature for the onset of thermal NO_x was due to inadequate main fuel-and-air mixing quality.

The critical flame temperature at which NO_x emissions have no significant thermal NO_x is also the temperature at which there is no measurable influence of pressure, and this depends on the quality of the fuel-and-air mixing. Altermark and Knauber (1987) found, for premixed combustion, that NO_x was independent of pressure for $\emptyset < 0.6$, which for a 600 K inlet temperature is a critical temperature for the onset of thermal NO_x of 1920 K. For a premixed grid plate Leonard and Correa (1990) found no



16.23 The influence of pressure on NO_x as a function of Ø (Bhargava *et al.*, 2000a).

© Woodhead Publishing Limited, 2013

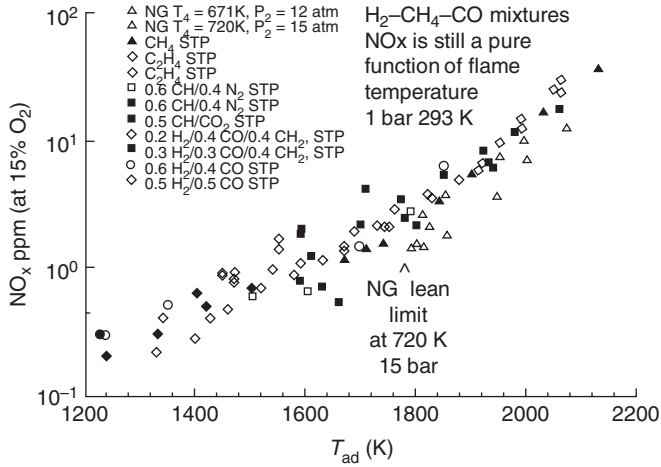
influence of pressure (3–10 bar) on NO_x up to Ø = 0.7 at 600 K and this corresponds to a flame temperature of 2050 K, where the NO_x was 4 ppm. Leonard and Stagmaier (1994) found no influence of pressure on NO_x for premixed combustion over the flame temperature range investigated of 1700–1920 K, where the NO_x was 2–8 ppm. Other investigators have found no pressure effect below 1900 K (Marutani *et al.*, 2003) and 2000 K (Cheng *et al.*, 2006) where NO_x was <10 ppm up to 2000 K. The above work on the pressure effect indicates that the critical temperature for the onset of thermal NO_x is in the region of 1900 K, but could be as high as 2000 K for very well-mixed combustion. A reasonable maximum critical temperature would be 1950 K, and this is supported by the thermal NO_x kinetic predictions discussed below.

The lack of influence of pressure on NO_x emissions, once thermal NO_x has been eliminated, allows ultra-low NO_x combustors to be developed at atmospheric pressure, where all the work on fuel-and-air mixing development can take place. Only once <10 ppm has been achieved at atmospheric pressure would a full engine pressure test be warranted. Most industrial gas turbine manufacturers have taken this atmospheric pressure low NO_x combustor route in their low NO_x engine development. All the work of the author, presented as part of this review, was undertaken at atmospheric pressure with electrical air preheat up to 900 K.

16.4.5 Fuel effects on flame temperature and NO_x

The importance of the flame temperature on thermal NO_x means that any fuel that has a higher stoichiometric flame temperature than that of common hydrocarbon fuels will have higher NO_x. The influence of fuel composition on NO_x will not be reviewed here as all the main gas turbine fuels such as natural gas, LPG, kerosene and fuel oil, all have very similar temperatures, with natural gas being slightly lower than the others. However, hydrogen has a much higher maximum flame temperature, so that any fuel with hydrogen added will have a higher maximum temperature and hence a greater sensitivity to unmixedness in the flame. All these fuels can be burned with low NO_x if the fuel-and-air mixing is controlled and the above primary zone temperature conditions are adhered to. The addition of hydrogen to natural gas has received a lot of attention recently, and this has the added advantage of increased flame stability and hence a better power turndown capability in gas turbines. This is illustrated in Fig. 16.24 (Littlejohn *et al.*, 2008) where a well-mixed axial swirler with central non-swirling air (LSI) has been operated with natural gas and hydrogen. The results show that hydrogen allows the premixed flame to be stable to 1200 K, whereas with natural gas the stability was 1700 K at

© Woodhead Publishing Limited, 2013



16.24 Axial swirler with central air injection (LSI) operated on natural gas and natural gas with hydrogen added (Littlejohn *et al.*, 2008).

atmospheric pressure and 1780 K at pressure. These results show that NO_x below 1 ppm occurs in the 1200–1600 K region. Figure 16.24 also shows very good agreement between the high pressure results at 15 bar and the atmospheric pressure results for the same flame temperature, again illustrating that NO_x is not pressure-sensitive once thermal NO_x has been eliminated. This is valid in Fig. 16.24 up to the limit of the temperatures investigated of 2100 K, where the high pressure NO_x was below the atmospheric pressure results.

The manufacture of 'green' hydrogen is problematic, as all current sources are derived from fossil fuels, usually natural gas or coal and these processes release CO_2, so that benefits in overall CO_2 emissions are not achieved. The flame stability, and the achievement of power turndown without flame stability problems, is a big advantage of hydrogen, which can lead to significant part-load thermal efficiency improvements, as it can make air blowoff or the use of NGVs at part-power unnecessary. Andrews *et al.* (2007) have shown that the use of hydrogen as pilot fuel has many advantages in flame stability for power turndown, and requires less hydrogen for a given stability improvement, compared with premixed natural gas and hydrogen. The disadvantage is a greater increase in NO_x with the use of pilot flame stabilization compared with a natural gas pilot. For premixed hydrogen and natural gas there is no NO_x disadvantage of hydrogen for the same flame temperature, as shown in Fig. 16.24. This is because there is no hydrogen diffusion burning, so there can be no local zones burning at the higher peak flame temperature of hydrogen in air mixtures.

© Woodhead Publishing Limited, 2013

16.5 Prompt NO_x

16.5.1 Prompt NO_x kinetics

Experimental results, such as those in Figs 16.23 and 16.24, show that when thermal NO_x has been eliminated (~1950 K), the residual NO_x is not zero. This residual NO_x is known as prompt NO_x, and when NO_x is plotted on a linear scale against equivalence ratio or flame temperature, as in Fig. 16.23, thermal NO_x gives a strong increase in NO_x with flame temperature and the prompt NO_x is the deviation from this near-linear trend for very lean mixtures. This occurs at temperatures below 1950 K where NO_x is <10 ppm.

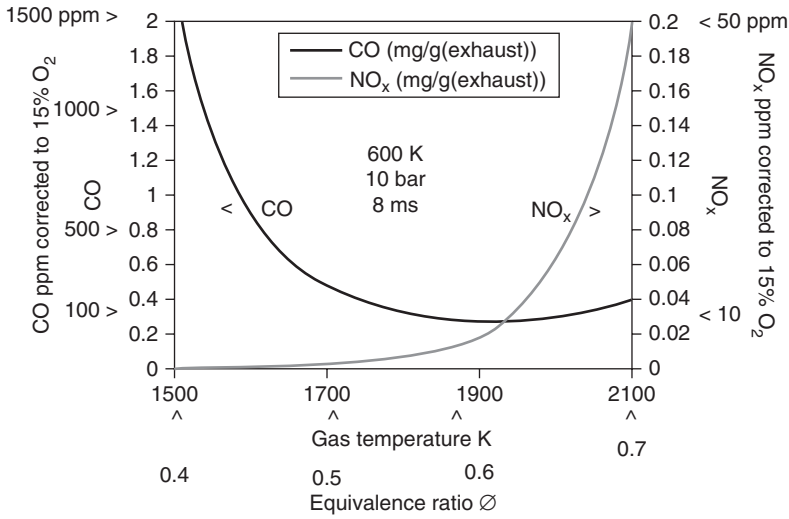
Prompt NO_x was first measured by Fenimore (1971) by traversing inside flames and showing that close to the burner the NO_x was not zero. Thermal NO_x should increase linearly with axial distance in a flame due to increased residence time. Experimental flame data show that the thermal NO_x production was preceded by a rapid NO_x formation zone located in the initial flame development region. Fenimore (1971) termed this prompt NO_x and gave the first kinetic explanation for its origin, which involved the reaction between hydrocarbon generated CH and N_2 as in Equation [16.6]:

$$N_2 + CH = HCN + N \qquad [16.6]$$

N goes on to form NO_x by Equation [16.2] of the thermal mechanism, and HCN oxidizes under lean conditions to NO by a sequence of reactions involving HCN > CN> NCO > NO (Lefebvre, 1995). This form of prompt NO_x is sensitive to the level of hydrocarbons in the flame front, which is related to the reaction zone thickness. Reaction zone thickness is dependent on the flame stabilizer design, and this is the reason for premixed combustion NO_x to be highly dependent on the flame stabilizer design, as discussed later.

Nicol *et al*. (1992) showed that another route to prompt NO was through N_2O formed by the reaction of N_2 and O, which then went on to form NO through the reaction of N_2O and O. Finally, Bozzelli *et al*. (1995) showed that the reaction between N_2 and H to form NNH was also a significant route to the formation of prompt NO. All these kinetic routes to the formation of NO_x in addition to the thermal route are normally referred to as full kinetic NO_x predictions, and the complete NO_x mechanisms are included in the GRI NO_x kinetics scheme and in Chemkin flame kinetics models. An example of the application of full kinetics NO_x modelling is shown in Fig. 16.25 for 10 bar 600 K with 10 ms residence time (Rokke *et al*., 2003). This shows that for temperatures below 1950 K NO_x is predicted to be <10 ppm and most of the NO_x is then by the prompt mechanism. At higher temperatures the NO_x increases sharply due to the thermal mechanism. This supports the above conclusions that for well-mixed combustion, thermal NO_x is small for temperatures below 1950 K.

© Woodhead Publishing Limited, 2013



16.25 Chemkin predictions with GRI kinetics of CO and NO_x emissions for 600 K inlet temperature at 10 bar with 8 ms residence time (Rokke *et al.*, 2003).

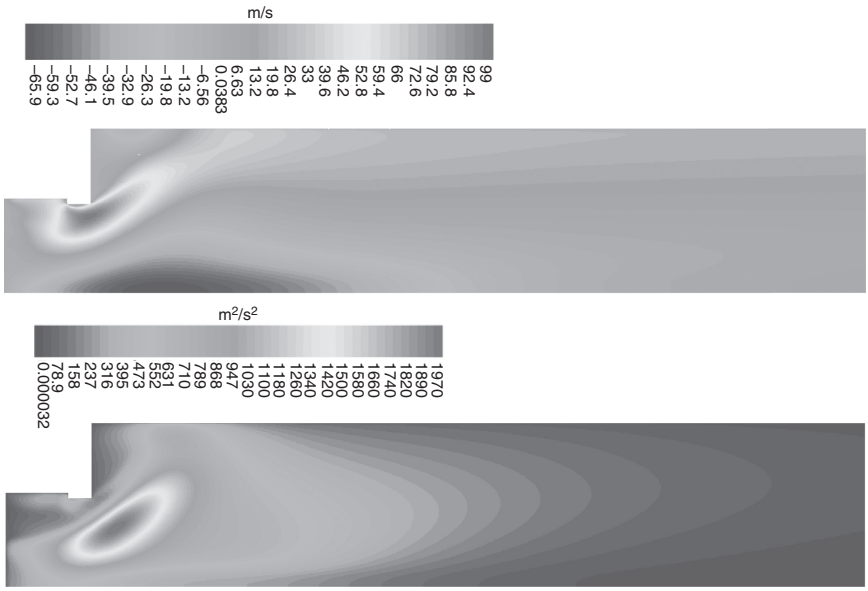
16.5.2 Pressure dependence of prompt NO_x

Herberling (1976) has shown that prompt NO_x has no pressure dependence over the range 1–18 bar. There is theoretical and experimental evidence that the N_2O kinetic route for prompt NO_x has a negative pressure dependence (Steele *et al.*, 1995; Bhargava *et al.*, 2000a; Malte and Rutar, 2001) in the region where NO is <3 ppm. These results indicate that once thermal NO_x has been eliminated by operating the primary zone well mixed at a flame temperature below 1950 K then it is reasonable to assume no significant increase in NO_x with pressure will occur. Furthermore, a decrease in NO_x with pressure is most likely in this ultra-low NO_x region where <3 ppm NO_x occurs. This means that demonstration of <3 ppm NO_x technology at atmospheric pressure (with the engine compressor exit air temperature) should be a prerequisite to any full engine pressure tests if ultra-low NO_x performance is desired.

16.5.3 Prompt NO_x dependence on flame stabilizer design

Prompt NO_x kinetics are responsible for much of the variation in NO_x emissions between different stabilizers for the same primary zone temperature. The problem is the large distance over which heat release occurs in the very lean, highly turbulent combustion in low NO_x gas turbine combustion. This was shown by the internal gas composition traverses and

© Woodhead Publishing Limited, 2013



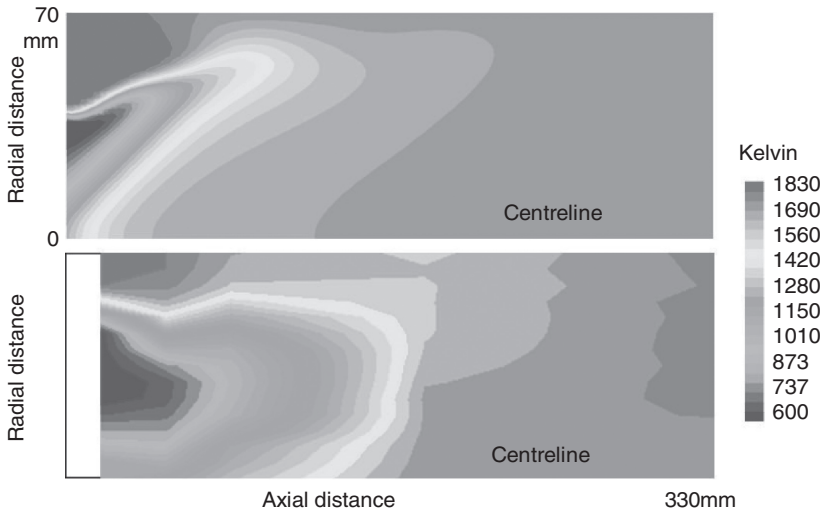
16.26 Radial swirler with vane passage fuel injection, 76 mm outlet diameter and dump expansion into a 140 mm diameter combustor. K-ε CFD predictions of the axial velocity (top) and kinetic energy of turbulence (bottom). *Source*: King *et al.* (2008).

flamelet CFD predictions with full NO_x chemistry of King *et al.* (2008, 2009), for the radial swirler configuration shown in Fig. 16.17, with vane passage fuel injection. Figure 16.26 shows the predicted aerodynamics of dump flow expansion from radial swirlers (King *et al.*, 2008, 2009; Alkabie and Andrews, 1991a, 1991d). There was a strong shear layer generated in the expanding swirl flow and the turbulence was concentrated there. A very strong central recirculation zone was generated that extended about half the length of the combustor. These aerodynamics are very similar to those for axial swirlers of the same outer diameter and same dump flow expansion (Andrews *et al.*, 2005). Many practical low NO_x industrial gas turbines use similar combustor aerodynamics with either radial or axial swirlers.

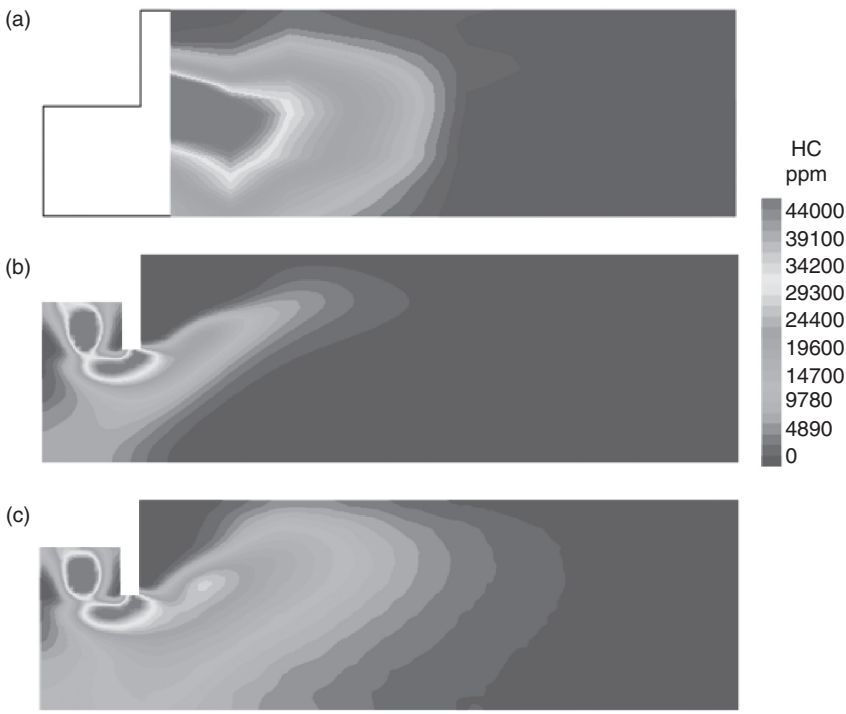
16.5.4 Flame structure in the prompt NO_x premixed combustion region

The flame structure of this type of combustion is shown in the temperature profiles in Fig. 16.27, which shows the slow development of the flame temperature. Figure 16.28 shows the large distance over which hydrocarbons are significant, which is not predicted using flamelet modelling (King *et al.*,

© Woodhead Publishing Limited, 2013

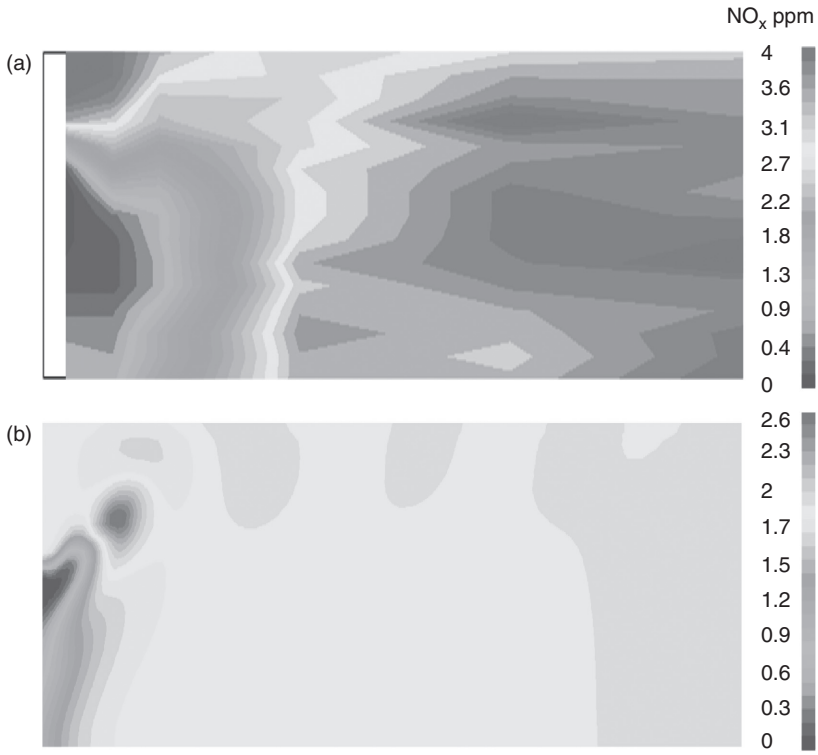


16.27 CFD Prediction of temperature (top) using flamelet model with 54-species detailed chemistry; comparison with experimental results (bottom) (King *et al.*, 2008).



16.28 Comparison of hydrocarbon distributions for (a) experiment, (b) flamelet model, and (c) pdf transport model (King *et al.*, 2008).

© Woodhead Publishing Limited, 2013

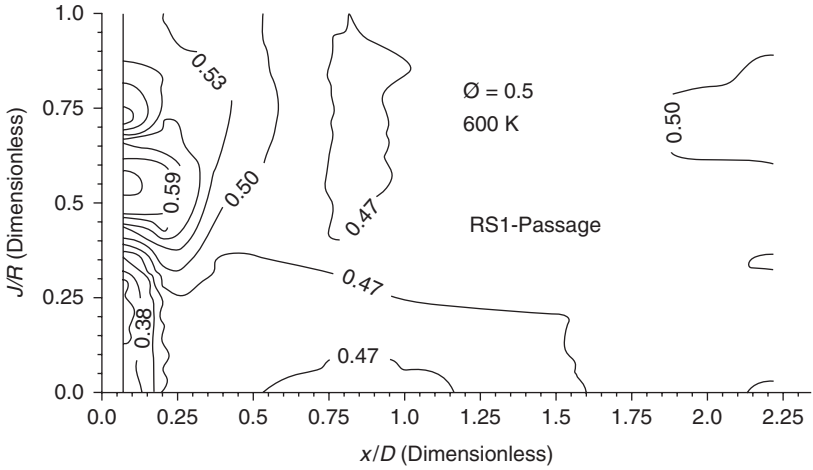


16.29 Distribution of NO as measured (a) and predicted (b) by the NO_x model (King *et al.*, 2009).

2008, 2009). Figure 16.29 shows the NO_x distribution for a condition with 600 K inlet temperature and Ø = 0.5, where the mean adiabatic flame temperature is 1800 K. Figure 16.9 shows that 1800 K is not reached until the last third of the combustor length. The NO_x predictions in Fig. 16.29 show an exit NO_x of about 3.5 ppm, but most of this NO_x is formed in the first half of the flame development, where the temperatures are low and the hydrocarbons are high, which leads to prompt NO from the hydrocarbon prompt NO_x mechanism. The underprediction of these hydrocarbons by the full NO_x chemistry flamelet model leads to an underprediction of the prompt NO. Yuen and Gulder (2010) have shown that a flamelet approach to the modelling of lean low NO_x gas turbine flames with very low laminar burning velocities and significant laminar flame thicknesses is inappropriate.

The temperature and NO_x profiles were not influenced by fuel-and-air mixing as this was uniform for most of the combustion. Figure 16.30 shows the equivalence ratio distribution by carbon balance for vane passage fuel

© Woodhead Publishing Limited, 2013



16.30 Equivalence ratio contours derived by carbon balance from the radial gas composition traverses. Radial swirler-vane passage fuel injection (King *et al.*, 2008).

injection in 76 mm outlet diameter radial swirlers with a dump expansion into a 140 mm diameter combustion. This shows that at the dump expansion plane there was a local rich zone of Ø = 0.6 for an overall Ø of 0.5, but there was no combustion occurring at this location as shown in Figs 16.27 and 16.28. Once the flame started to develop, the unmixedness was <5% across the combustor radius at all axial positions from 35 mm from the dump expansion plane. The flame development structure is dependent on the type of flame stabilizer and the downstream aerodynamics that are generated.

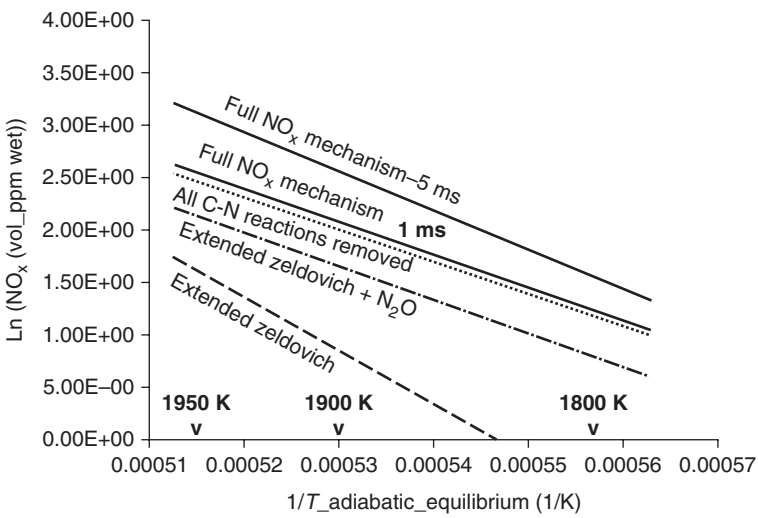
CFD predictions for a commercial low NO_x combustor, the hybrid burner shown in Fig. 16.4, are shown in Fig. 16.5 to predict a long flame development (Streb, 2010). The hybrid burner has a large axial premixed swirl burner with fuel injection through the swirl-blade surface coupled with a central pilot axial swirler that can be operated in diffusion or premixed mode. This has a ceramic-tiled wall with back-side cooling that flows into the combustor as film cooling air. This is part of the reason for the lower wall temperatures and hotter central recirculation region, which does not exceed the threshold for thermal NO_x formation. Figure 16.5 shows that the 1800 K primary zone temperature does not develop until some distance from the swirler outlet. Figure 16.5 also shows that the main premixed swirling jets penetrate about a third of the combustor length before flame development occurs. This shows why perfect mixing at the swirler outlet plane is not necessary, as mixing can continue in the expanding swirling jet before the flame develops in the jet shear layer.

© Woodhead Publishing Limited, 2013

16.5.5 Kinetic predictions of the relative contributions of thermal and prompt NO_x

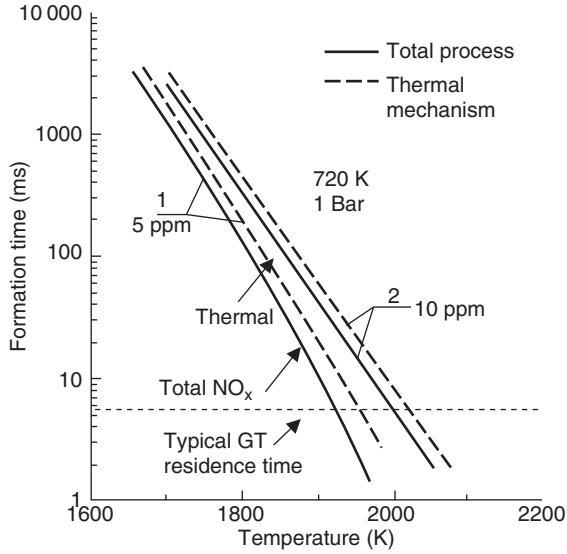
Figure 16.31 shows the GRI full kinetic computations of Syed and Buchannan (2005) for stirred reactor conditions at 1 and 5 ms residence time. At 1900 K and 1 ms residence time the thermal NO_x was 1 ppm but the total NO_x was 2.2 ppm and this only increased to 2.7 ppm with 5 ms residence time. At 1800 K with 1ms residence time, thermal NO_x was negligible and total NO_x was 1.2 ppm, increasing to 1.5 ppm at 5 ms. At 1950 K with 5 ms residence time the full kinetics total NO_x was predicted to be 3.2 ppm, confirming that low NO_x should be achievable up to 1950 K, as concluded earlier.

Similar conclusions regarding the importance of prompt NO_x at conditions where thermal NO_x was small were also made using stirred reactor analysis by Corr *et al*. (1991). They found that at 1521 K with 2.9 ms residence time the total NO_x was 5 and 4.1 ppm of this came from the hydrocarbon prompt route and 0.75 ppm from the N_2O prompt route with thermal NO_x at 0.15 ppm. Similar computations have been made for practical low NO_x gas turbine combustors for syngas fuels (Anandi *et al*., 2005), where at 1800 K thermal NO_x was computed at 1 ppm and prompt NO_x at 4.5 ppm giving a total NO_x of 5.5 ppm. At 1900 K thermal and prompt NO_x was 7 ppm, giving a total NO_x of 14 ppm.



16.31 GRI 3.0 NO_x mechanism predictions of NO_x from the different kinetic routes using a PSR computation. Predictions for 1 and 5 ms reactor residence time at 14 bar and 673 K inlet (Syed and Buchannan, 2005).

© Woodhead Publishing Limited, 2013



16.32 Influence of residence time on NO_x production for thermal and total NO_x formation kinetics (Vedeshkin *et al.*, 2007).

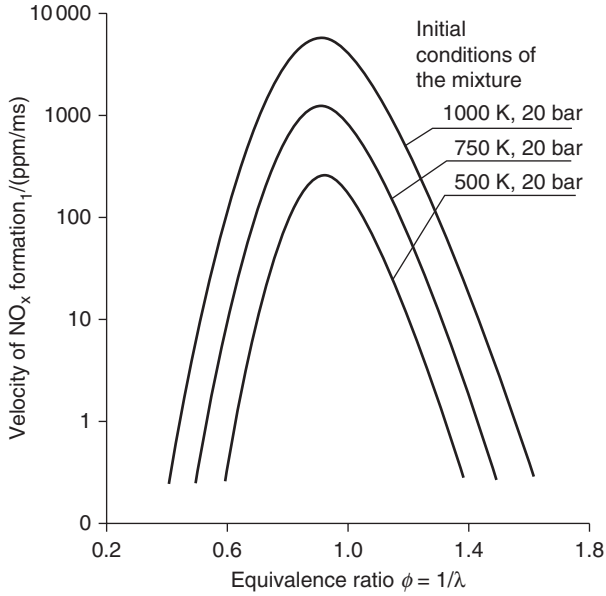
Vedeshkin *et al*. (2007) computed the thermal NO_x and total NO_x contributions to total NO_x of 5 and 10 ppm, as shown in Fig. 16.32. For a 5 ms residence time this required 1960 K flame temperature for 5 ppm to be all due to thermal NO_x and 1910 K if prompt NO_x sources were included as well. If the residence time was 10 ms then the two temperatures for 5 ppm NO_x were 1990 and 1970 K for total NO_x kinetics and for thermal NO_x only respectively. Figure 16.32 shows that at 1800 K it would take a residence time of 200 ms to generate 5 ppm NO_x from the thermal mechanism and 100 ms from the thermal plus prompt mechanisms. At 2000 K 5 ppm NO_x would be generated in 2 ms by the thermal mechanism and in 0.8 ms by the thermal plus prompt mechanisms. All of these computations indicate that $NO_x < 10$ ppm can be achieved for flame temperatures <1950 K including the thermal and prompt kinetic routes to NO formation, provided the residence time is not too high.

16.6 Predictions of thermal NO_x

16.6.1 Premixed combustion thermal NO_x

The above computations for full kinetic schemes for NO_x production show that if thermal NO_x is eliminated in lean well-mixed combustion then the residual NO_x is low. Predicting the conditions under which thermal NO_x is

© Woodhead Publishing Limited, 2013



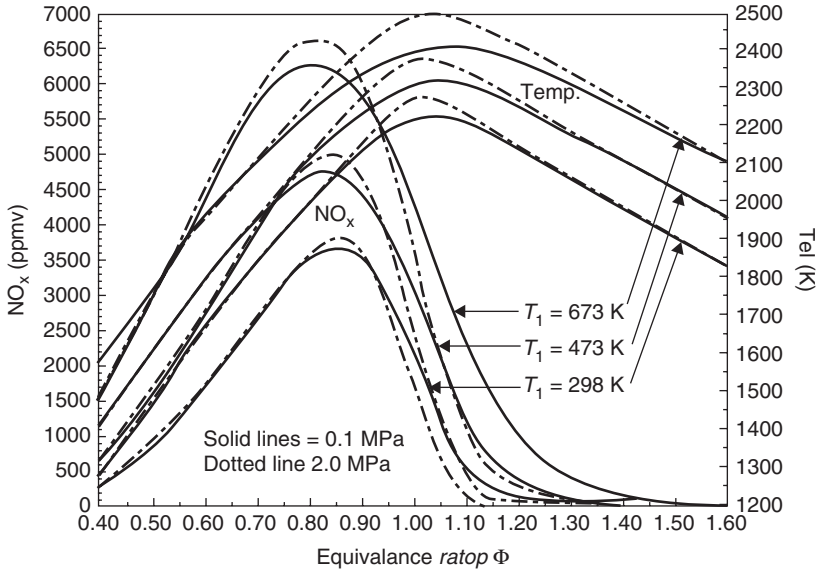
16.33 Thermal NO_x predictions for the rate of formation of NO_x at 20 bar for 500, 750 and 1000 K inlet temperatures (Saul and Altemark, 1992).

small and the design factors that influence this, leads to the design principles for low NO_x gas turbine combustion. This is the objective of the rest of this chapter.

Figure 16.33 shows the results of the computations of thermal NO_x from Equation [16.1] by Saul and Altemark (1992) for natural gas combustion at 20 bar for a range of combustion air inlet temperatures of 500, 750 and 1000 K. Figure 16.33 shows that peak NO_x formation occurs at Ø = ~0.85–0.9, where gas fired furnaces and boilers operate. This makes well-mixed combustion the worst NO_x production design for furnace burner applications. Figure 16.34 shows the equilibrium NO_x predictions of Rokke *et al*. (1993) together with the adiabatic flame temperature, and this shows the significant difference in equivalence ratio for peak temperature at Ø ~ 1.05 and peak equilibrium NO_x at Ø ~ 0.85, the same as for the thermal NO_x peaks in Fig. 16.33. Thermal NO_x formation requires high flame temperatures but also requires oxygen so that peak NO_x formation does not occur at the same condition as peak flame temperature.

Figure 16.34 shows that at 673 K air temperature and 1922 K flame temperature (Ø = 0.6) the equilibrium NO_x was predicted to be 4300 ppm. Wade *et al*. (1973) showed that for thermal NO_x alone it would take >1000 ms

© Woodhead Publishing Limited, 2013



16.34 Equilibrium NO_x and adiabatic temperature predictions as a function of Ø for 1 and 20 bar at 298, 473 and 673 K (Rokke *et al.*, 1993).

to reach equilibrium NO for 1922 K for 811 K air inlet temperature at 3 bar and Ø = 0.5. Gas turbine combustors have much smaller residence times than this and a 1 m long combustor with a 25 m/s reference velocity at 700 K has a residence time at 1800 K of 15 ms, and normally combustors are shorter than this so residence times are usually <10 ms, as discussed in more detail later. Figure 16.32 shows that with 12 ms residence time at 1922 K the thermal NO_x was predicted to be 5 ppm, but for total NO_x kinetics this NO_x was reached after 5 ms. The predictions in Fig. 16.31 show that at 1922 K a residence time of 5 ms was predicted to give a total NO_x of 3 ppm for 673 K air inlet temperature and 14 bar pressure. The predictions in Fig. 16.33 for 1922 K at 750 K air temperature (Ø = 0.53) give a thermal NO_x production rate of 0.6 ppm/ms and for 5 ms residence time this give 3 ppm thermal NO_x. Wade *et al.* (1973) predicted that at 1922 K (811 K air inlet temperature and 3 bar) thermal NO_x would generate 4 ppm NO_x after 5 ms. All these predictions indicate that total $NO_x < 10$ ppm should be achievable up to 1950 K at the typical 5 ms residence time of industrial gas turbine combustors. The predictions indicate that the thermal NO_x will be <5 ppm at 1950 K. However, NO_x emissions will be sensitive to residence time through the thermal NO_x mechanism, and this is discussed in more detail later.

© Woodhead Publishing Limited, 2013

16.6.2 Application of thermal NO_x predictions to engine operating conditions

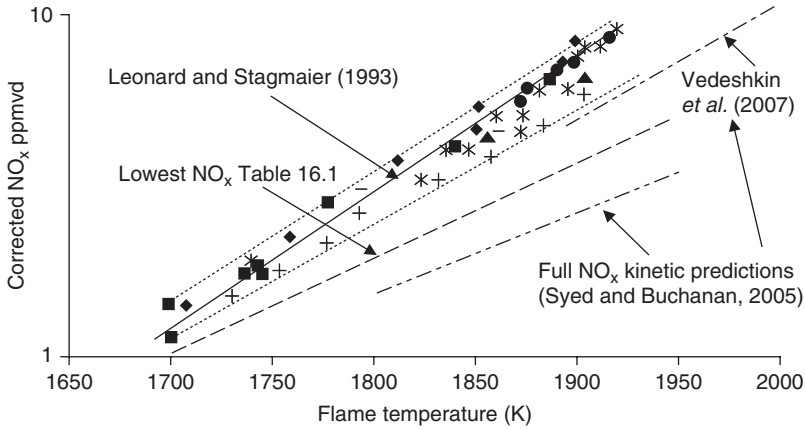
All gas turbines with firing temperatures below 1750 K (H Class) have Ø < 0.47 at 700 K air inlet temperature and Fig. 16.33 shows that this is a thermal NO_x production rate of 0.2 ppm/ms. Thermal NO_x of <1 ppm would then be expected at 1750 K and most of the NO_x at this condition would be prompt NO_x. 1950 K can be taken as the critical flame temperature for significant (>3 ppm) thermal NO_x formation, and this is in agreement with the onset of a pressure dependence of NO_x, discussed above. Also, this is the primary zone temperature that some low NO_x gas turbines use at maximum power (Willis, 1993). The prompt NO_x kinetic computations discussed above also support the achievement of total NO_x below 10 ppm at 1950 K.

All current and future planned gas turbines operate at <1950 K turbine entry temperature, so all current and future industrial gas turbines should be capable of operating at <10 ppm NO_x if the fuel-and-air mixing is sufficiently uniform. For future industrial gas turbines at 1950 K for 700 K air inlet temperature the overall Ø is 0.57. These flame temperature considerations also apply to primary zone operating conditions if the overall turbine entry temperature is ~1950 K, then thermal NO_x will be <10 ppm if the primary zone is 1950 and dilution air is used to achieve the desired turbine entry temperature.

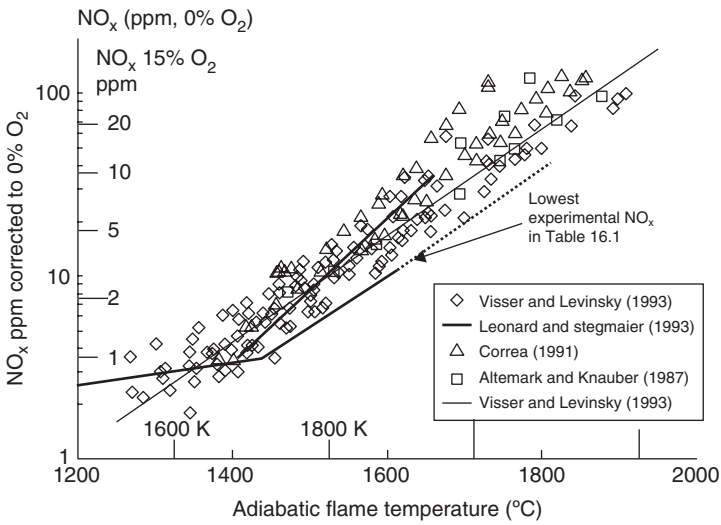
16.6.3 Experimental support for ultra-low NO_x emissions at the conditions where thermal NO_x has been eliminated

The kinetic NO_x predictions are supported by experimental measurements in well-mixed combustion designs at gas turbine combustion operating conditions, as shown in Fig. 16.35. Leonard and Stagmaier (1993) measured NO_x corrected to 15% oxygen for premixed combustion, and their results are shown in Fig. 16.35 as a function of the adiabatic flame temperature. They investigated various flame stabilizers at operating pressures from 1 to 30 bar and air temperatures from 300 to 800 K with residence times from 2 to 100 ms. There is some variation in the results, indicating an influence of the flame stabilizer design, which at 1900 K is 5–8 ppm. The full NO_x kinetics predictions of Syed and Buchanan (2005) are shown to predict NO_x emissions lower than the lowest range of the Leonard and Stagmaier results (1993) and the full kinetic predictions of Vedeshkin *et al*. (2007) lie above the upper range of the Leonard and Stagmaier (1993) results. Some of the other kinetic predictions reviewed above give even higher NO_x predictions.

© Woodhead Publishing Limited, 2013



16.35 NO_x corrected to 15% oxygen as a function of flame temperature for various flame stabilizers, pressures from 1 to 30 bar, air temperatures from 300 to 800 K and residence times from 2 to 100 ms . Comparison with kinetic predictions and other experiments in Table 16.1.



16.36 NO_x emissions as a function of adiabatic flame temperature for several investigators (based on Visser and Bahlmann, 1994).

A further data set for premixed combustion NO_x emissions for a range of unspecified flame stabilizers with premixed combustion was provided by Visser and Bahlmann (1994) and this is shown in Fig. 16.36. This includes data sets from Visser and Levinsky (1993), Altemark and Knauber (1987) and Correa (1991) as well as the Leonard and Stagmaier (1993) NO_x line.

© Woodhead Publishing Limited, 2013

16.6.4 Survey of ultra-low NO_x emissions experimental data

A much wider variation of flame stabilizer designs than those of Leonard and Stagmaier (1993) and Visser and Bahlmann (1994) have been investigated in the literature, and Table 16.1 presents a review of the literature where ultra-low NO_x has been demonstrated. In the table results for natural gas are selected on the basis that <8 ppm is demonstrated at 1900 K, <5 ppm at 1800 K, <2 ppm at 1700 K and <1 ppm at 1600 K. There are 41 published low NO_x designs in Table 16.1 that meet this criterion, and 17 of these are from the author's research group. Most of these demonstrations of low NO_x are not for premixed combustion. Many published premixed results do not exhibit low NO_x or the capability to operate below 1800 K. However, as some premixed results do exhibit low NO_x, as shown in Table 16.1, it is clear that the stabilizer design is the most important feature in achieving low NO_x, once rapid fuel-and-air mixing has been achieved.

Table 16.1 shows that many of the results are in the data range in the measurements of Leonard and Stagmaier (1993). However, many of the results are substantially below their data range. There is support from several investigators for NO_x emissions of ~0.8 ppm at 1600 K (12 investigators), ~1 ppm at 1700 K (15 investigators), ~2 ppm at 1800 K (16 investigators) and ~3.5 ppm at 1900 K (13 investigators) and this line is shown in Fig. 16.35 to be significantly below the data range in Leonard and Stagmaier's work. About half of these ultra-low NO_x flame stabilizer designs are from the author's research group, which pioneered the use of direct fuel injection with rapid fuel-and-air mixing and no conventional premixing passage.

Leonard and Stagmaier (1993) primarily investigated grid plate, baffle and axial swirler flame stabilizers, whereas a much wider range of designs are included in Table 16.1. Some of the designs in Table 16.1 are the basis of production low NO_x gas turbines. Radial swirlers are in used by at least five manufacturers and the use of several axial swirlers in a can is common; one of these production designs is that of Colibab-Evulet *et al*. (2004), where the NO_x results are below the line in Fig. 16.35. Lacarelle *et al*. (2010) have also demonstrated the capability of the production AEV burner to achieve NO_x at close to the minimum NO_x line in Fig. 16.35.

Figure 16.36 shows that the lowest data in Table 16.1 lie at the bottom of the data range of Visser and Bahlmann (1994) and hence this new line should be taken as the lowest NO_x that is achievable in well-mixed combustion systems. The extrapolation of this line in Fig. 16.36 is supported by the minima of the data in Fig. 16.36, and this extrapolation indicates that for the best flame stabilizer designs $NO_x < 10$ ppm could be achieved for adiabatic flame temperature up to 2050 K. However, the higher the flame temperature the greater the range of measured NO_x as shown in Fig. 16.36,

© Woodhead Publishing Limited, 2013

Table 16.1 Experimental measurements of ultra-low NO_x emissions (NO_x < 8 ppm at 1900 K). All results are for natural gas (NG) unless it is stated to be propane (P)

Author	Year	Stabilizer	Fuel injection	P bar T°K	1500 K NO_x ppm 15% O_2	1600 K NO_x ppm 15%O_2	1700 K NO_x ppm 15%O_2	1800 K NO_x ppm 15%O_2	1900 K NO_x ppm 15%O_2
Anderson	1973 1975	61 hole grid	Premixed propane	5.5 bar 590–800	No flame	No flame	2	3	9
Al-Dabbagh and Andrews	1981	4 hole grid 16 hole grid	Premixed propane	1 bar 400–650 K	No flame	1 No flame	1.5 3	3 4.5	6 8
Andrews *et al.*	1983	Jet mix	Premixed propane	1 bar 650 K	No flame	No flame	3	4	7
Ahmad and Andrews	1983	Axial swirler	Premixed propane	1 bar 600 K	1.5	1.5	2.0	2.5	5.5
Ali and Andrews	1985	Conical grid 90 holes 4 holes	Premixed propane	1 bar 600 K	No flame No flame	1.0 1.2	2.0 1.5	3.0 2.0	5 3
Alkabie and Andrews	1989a, 1989b, 1989c	Radial swirler	Premixed propane	1 bar 600 K	No flame	1.2	1.5	2.5	4
Alkabie and Andrews	1989	Radial swirler	Vane passage fuel Inj.	1 P NG 600 K	1.5 No flame	2.5 1.2	4 1.2	7 1.3	10 2
Alkabie and Andrews	1990 1991b, 1991c	Radial swirler	Outlet throat wall fuel Inj.	1 P NG 600 K	0.9 No flame	1.2 0.8	2.5 0.8	4 0.8	7 1.0
Leonard and Correa	1990	Grid	Premixed	3–10.7 615 K	No flame	No flame	1.5	3	7

(*Continued*)

© Woodhead Publishing Limited, 2013

Table 16.1 Continued

Author	Year	Stabilizer	Fuel injection	P bar T°K	1500 K NO_x ppm 15% O_2	1600 K NO_x ppm 15%O_2	1700 K NO_x ppm 15%O_2	1800 K NO_x ppm 15%O_2	1900 K NO_x ppm 15%O_2
Al-Shaikley *et al.*	1992	Grid mix	Direct Inj. per hole	1 bar P 600 K	1.3	1.5	2.5	4	7
Lovett and Abuaf	1992	Axial swirler	Premixed	10.5 bar 615 K	No flame	No flame	1	2.5	5.5
Leonard and Stagmaier	1993	Various	Premixed	1–30 300–800	No flame	No flame	1.2	3	7
Kim *et al.*	1993	40 mm diameter radial swirler	Vane passage	1 bar NG 900 K	1.0	1.5	3	5	8
Kajita *et al.*	1993	Axial swirler	Upstream fuel spoke no mixing duct	1 300 K	No flame	1	2.5	3.5	5
Escott *et al.*	1993	Radial swirler 26.5 mm vane	Vane passage	1 bar 740 K	No flame	0.9	2.0	3.5	6
Andrews and Ahmad	1994	Grid mix Four triangular holes	Direct NG Fuel Inj. D 76 mm	1 bar 600 K	No flame	1	1.5	2	3
Polifke *et al.*	1995	2 slot cone (EV)	Direct slot	1 bar 630 K	No flame	0.6	0.9	2.5	
Lovett and Mick	1995	Axial swirler	Radial spoke	10.3 bar 620 K	No flame	No flame	1	2	6

© Woodhead Publishing Limited, 2013

Kinoshita *et al.*	1997	Cylindrical	Radial tube	20 bar	2	3	5	10	20
Kitajima *et al.*	1997	tube swirler	passage	600 K					
Bhargava *et al.*	2000b	TE burner	Radial slot	7 bar	No flame	No flame	1.5	2.5	6
		Half size	direct	733 K					
		No pilot	Fig. 16.48						
Miyasto *et al.*	2000	Axial swirl	Direct P	1 bar	0.5	0.8	1.2	2	3.5
			Central radial and wall	700 K					
Andrews and Mkpadi	2001	Counter radial swirl	Lean/lean	1 bar	2	1	2	3	6
			Central pilot, main vane passage	600 K					
Andrews and Kim	2001	Radial swirl	Vane passage	1 bar	No flame	1	2	3.2	5.5
		26.5 mm vane depth		740					
Yamamota *et al.*	2003	Conical slot	Pilot and premixed	3 bar	–	–	1	2	–
				700 K					
Wheatley *et al.*	2003	Surface	535–590 K	10.1 bar	No flame	No flame	No flame	1.3	3
Arellano *et al.*	2004	nanoSTAR	640 K	12.4 bar		No flame	No flame	2.0	4
		Premixed	650 K	16 bar			1.5	3.5	4.5
			650 K	1 bar			1.5	2.0	4
			475–700 K	5–12 bar			1.5	3.0	6
Aida *et al.*	2003	Lean/lean	Axial staged premixed	1 bar	2	2	2	3	5
				500 K					
Colibab-Evulet *et al.*	2004	Four axial swirlers	Well mixed	175 kW Micro GT	No flame	No flame	No flame	1.5	3.2
Andrews *et al.*	2005	Axial swirler	Outlet throat wall	1 bar	No flame	1.5	2	3	6
				740 K					

(*Continued*)

© Woodhead Publishing Limited, 2013

Table 16.1 Continued

Author	Year	Stabilizer	Fuel injection	P bar T°K	1500 K NO_x ppm 15% O_2	1600 K NO_x ppm 15%O_2	1700 K NO_x ppm 15%O_2	1800 K NO_x ppm 15%O_2	1900 K NO_x ppm 15%O_2
Sidwell *et al.*	2005	Axial swirler	Premixed 550 K	4.3–6.3 bar	No flame	No flame	1.3	2.5	5.5
Yamada *et al.*	2005	Radial swirler	Lean/lean premixed	1 bar 473 K	2	2.	2	2	3.5
Cheng *et al.*	2006	Axial swirl Low swirl LSI	Premixed	6–15 bar 700 K	No flame	No flame	No flame	2	4
Edmonds *et al.*	2006	Trapped vortex	Premixed low pilot	10 bar 600 K	No flame	No flame	No flame	2.5	4.5
Brueckner-Kalb *et al.*	2007	2 tube Radial swirler CPMCP	Premixed	1 bar 780 K	0.5	0.8	1.8	3.5	–
Boschek *et al.*	2007	Dump expansion no swirl	Premixed	5 and 10 bar 673 K	No flame	No flame	0.5	1.3	–
Hiramatsu *et al.*	2007a 2007b	Lean/lean Three stage premixed	Swirling Radial injection	1 bar 700 K	2	2	2	2.5	4
Andrews *et al.*	2008	Radial swirler RS5 RS6	Vane passage	1 bar 740 K	0.8	0.8	1.1	1.7	2.2
Andrews *et al.*	2008	Radial swirler RS2 Aero vanes	Exit throat wall fuel injection	1 bar 740 K	No flame	0.7	1.1	3	–

© Woodhead Publishing Limited, 2013

Andrews and Ahmad	2008	16 slot hole grid $D = 140$ mm	Each hole direct fuel	1 bar 600 K	1.2	1.8	3	4	6
Giglio *et al.*	2009	Axial swirl 1.5D mixing throat	Effusion fuel in blade	12 bar 293 K	1.0	1.2	2.5	3.5	4.5
Lammel *et al.*	2010	FLOX 12 slot holes	Direct centre jets	7 bar 673 K	No flame	No flame	No flame	No flame	3
Lacarelle *et al.*	2010	EV 2 slot radial swirl	Direct along air slot no pilot	1 bar 423 K	No flame	No flame	1.5	2	4
Levy *et al.*	2010	Conical jet with dump expansion	Central main fuel and conical wall pilot fuel	600 K 1 bar	–	1.3 1650 K 0.8 with 2% pilot	–	–	–
Andrews and Ahmad	2011	Axial swirler SW3	Premixed Propane	1 bar 600 K	1.5	1.5	1.8	2.5	4.5
ElKady *et al.*	2011	Grid plate	Premixed methane	7–17 bar 633 K	No flame	No flame	1.5	4	7.5
Lee *et al.*	2011	Radial swirler	Vane passage	1 bar 673 K	No flame	No flame	0.3	0.65	–
Luckerath *et al.*	2011	8 Axial swirlers with central pilot swirler	Swirler blade surface	4 bar 704 K	–	–	–	1850 K 2.8	–
Andrews and Ahmad	2012	Axial swirler *SW6S3*	Premixed propane	1 bar 600 K	2.2	2.8	3.5	4	5

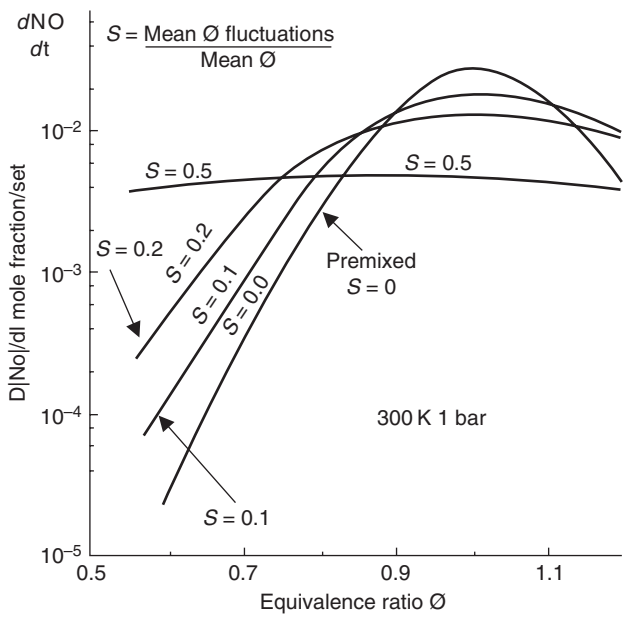
© Woodhead Publishing Limited, 2013

where NO_x as high as 30 ppm occur at conditions where the best systems have 10 ppm. Figure 16.36 shows that the design of the flame stabilizer has a crucial impact on the NO_x emissions. Not all the low NO_x designs in Table 16.1 are for premixed combustion and this chapter will discuss why premixed combustion often does not achieve low NO_x emissions. Some of the designs in Table 16.1 involve combined pilot and main fuelling with axial staging between the fuel injection locations. Some of the design use very high internal EGR (Lammel *et al.*, 2010).

16.7 Influence of mixing on thermal NO_x

16.7.1 The *S* parameter of mixing and its influence on NO_x

The influence of mixing imperfections on the rate of formation of thermal NO_x at atmospheric conditions is illustrated in Fig. 16.37 for application to process burners. The influence of mixing was shown by imposing a sinusoidal variation of Ø around the mean Ø and then using thermal NO_x kinetics only to predict the consequences for NO_x formation. The *S* parameter of

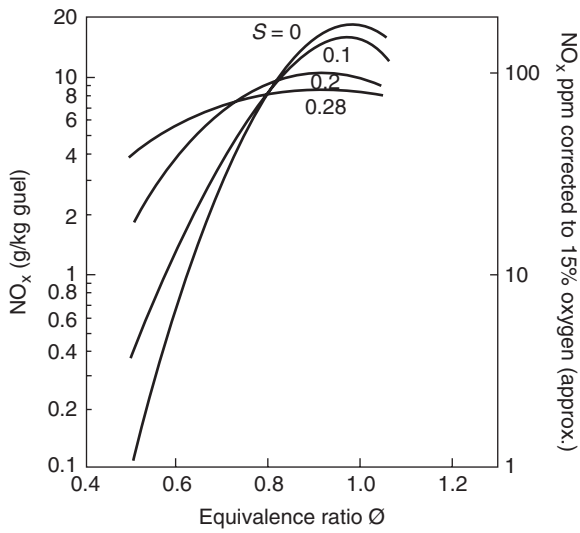


16.37 Rate of formation of NO_x as a function of equivalence ratio with influence of the mixing parameter *S* at 0.1, 0.2 and 0.5 (Fletcher and Heywood, 1971; Appleton and Heywood, 1973).

© Woodhead Publishing Limited, 2013

mixing is the ratio of the amplitude of the fluctuations in Ø to the mean Ø. The premixed results are for $S = 0$ and the influence of mixing imperfections, or increased S, is to reduce the NO_x formation in the near-stoichiometric region. This is because fluctuations on the rich and lean sides are both lower NO_x than stoichiometric, so the worse the mixing is the lower the NO_x. This is important in the design of process burners, where perfect mixing is not the design choice for low NO_x.

In the equivalence ratio region of relevance to gas turbine combustion, leaner than Ø = 0.6, Fig. 16.37 shows that mixing imperfections increase NO_x. This is because fluctuations richer than the mean have much higher local temperatures and rates of NO_x formation. Figure 16.37 indicates that for Ø = 0.5 S should be <0.1 if the increase in NO_x from that for premixed combustion is to be ×3. Figure 16.38 shows the results of similar calculations at gas turbine conditions of 30 bar, 800 K air temperature and 5 ms residence time. These are in terms of NO_x emissions index, g_{NOx}/kg_{fuel} (EI), and roughly an EI of 1 is 10 ppm NO_x corrected to 15% oxygen. The results in Fig. 16.38 show that at Ø = 0.5 (1900 K) the thermal NO_x for premixed combustion would be about 1 ppm at 15% oxygen and this would increase to about 4 ppm for $S = 0.1$ and 20 ppm for $S = 0.2$. It is clear that for fuel-and-air mixing to be considered well mixed, the value of S at the position in the flame where the heat release is near completion S should be <0.1.



16.38 Influence of S on NO_x as a function of Ø for 30 bar, 800 K and 5 ms residence time (Lyons, 1981).

© Woodhead Publishing Limited, 2013

16.7.2 Mixing prior to the completion of combustion in a flame

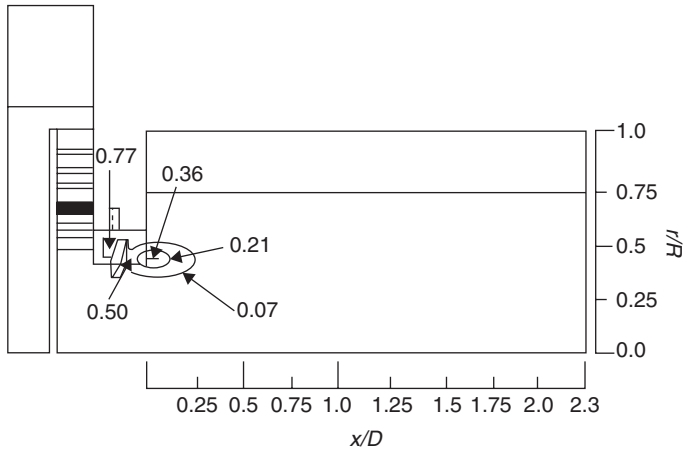
It is important to note that $S < 0.1$ is not a requirement at the burner or premixing duct outlet, as the flame does not develop there. Mixing continues in the expanding shear layer as the flow expands from the minimum flow area and highest local velocities in the flame stabilizer to the mean velocity in the combustor. The high turbulence in the shear layers, such as those for radial swirlers shown in Fig. 16.26, occurs before the temperature is high enough to be significant for thermal NO_x generation, as shown in Fig. 16.27. This shows that the temperature at which unmixedness would give rise to thermal NO_x implications is halfway along the combustor and mixing must be complete well before this point, but it does not need to be complete at the flame stabilizer outlet.

Mixing of fuel-and-air is completed in the high turbulence region in the shear layer downstream of the flame stabilizer before the main heat release of the flame. The fuel must be injected at a position which enables the fuel to reach the high turbulence region. The location of the fuel injection is as important as the aerodynamics of the flame stabilizer in achieving good mixing and low NO_x emissions. It is possible to achieve good mixing and low NO_x without any premixing, and this is most clearly demonstrated in the work of Alkabie and Andrews (1990) in Table 16.1, where the fuel was injected downstream of the radial swirler-vane passages using eight equispaced fuel injection holes around the radial swirler outlet throat.

16.7.3 Example of good mixing for radial swirlers with vane passage fuel injection and no downstream premixing passage

Figure 16.39 shows the CFD predictions of S for a radial swirler with fuel injection through the wall of the outlet throat. This shows $S < 0.05$ within 0.25 D of the dump expansion plane. This configuration has been traversed using a single point gas sample probe and the resultant flame structure for Ø, flame temperature and NO_x are shown in Fig. 16.40. This shows extremely rapid fuel-and-air mixing in the turbulent shear layer, as predicted in Fig. 16.39. The flame development was very slow, similar to that shown in Fig. 16.27 for radial vane passage fuel injection. The peak temperature of 1750 K was not reached until near the 330 mm position at the combustor wall, but much sooner in the central recirculation zone. The NO_x emissions were all <7 ppm and mainly formed in the regions below 1650 K where prompt NO_x would be the dominant route to NO_x formation.

© Woodhead Publishing Limited, 2013



16.39 CFD predictions of *S* for a radial swirler with a 40 mm outlet throat and 76 mm wall fuel injection.

16.7.4 Measurement of scalar mixing in the development of ultra-low NO_x burners

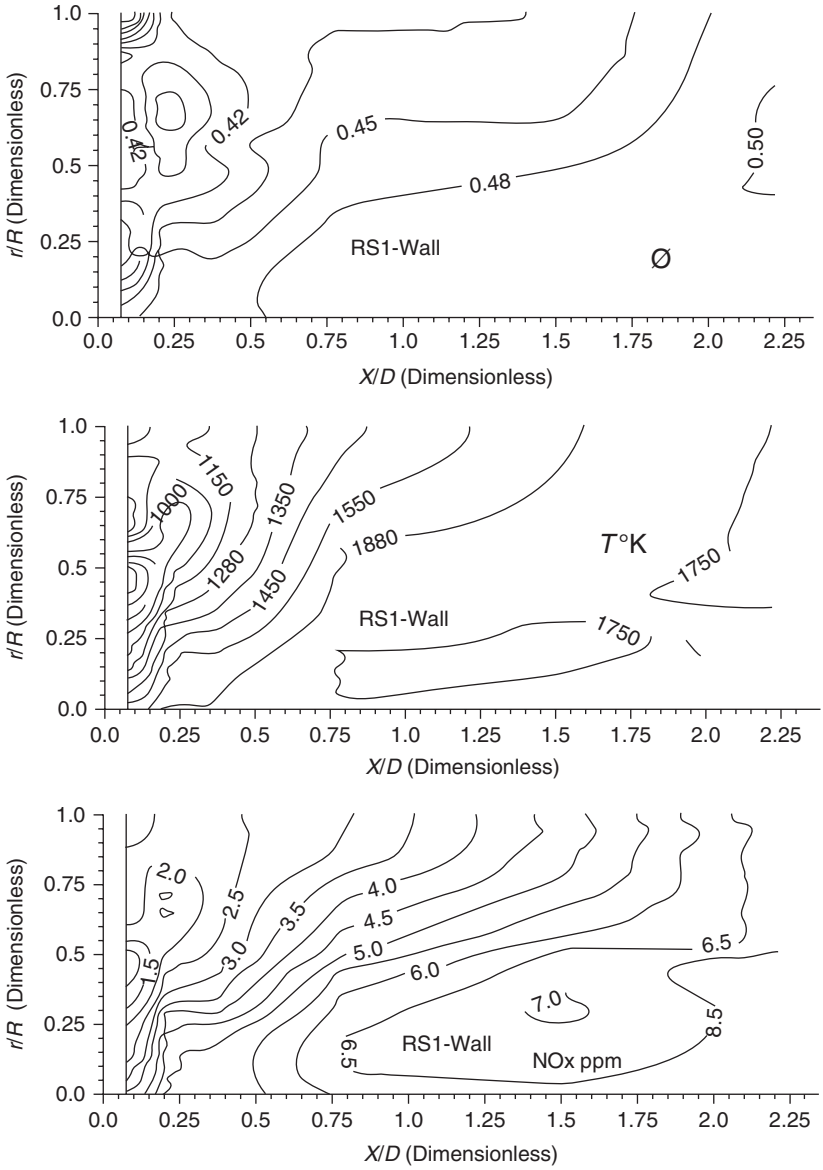
Many manufacturers have all used scalar mixing studies in the development of low NO_x combustors, generally on an atmospheric cold flow test rig with a tracer gas to represent the fuel. Fast response extractive probes have been used with a hydrocarbon tracer gas and laser-diode infra-red absorption (Girard *et al.*, 2001). Water flow visualization test rigs have also been used with fluorescent dye or salt solution as the 'fuel' with conductivity fluctuations giving the scalar turbulent mixing parameter (Andrews and Abdul Hussain, 1992). Many manufacturers have demonstrated $S < 0.1$ for the flame stabilizers prior to combustion tests.

Dodds and Ekstedt (1985) evaluated 15 baffle type flame stabilizer and fuel injector design on a purely isothermal mixing basis at 14 bar and 800 K, using gas samples of the unburned mixture in the mixing duct and burning the gas sample to determine Ø from the CO_2 and O_2. They correlated their data for *S* by Equation [16.7] with experimental data for *S* ranging from 0.03 to 2.5. However, they did not include axial or radial swirlers in their study and Equation [16.7] may not apply to swirlers.

$$S = 0.18L^{-0.74}\left(\frac{N}{A_t}\right)^{-0.60}\left(\frac{\Delta P}{P}\right)^{-2.12} \qquad [16.7]$$

where L is the mixing duct length, N is the number of fuel injection points, A_t is the duct area at the fuel injection plane (A_2 in this publication), $\Delta P/P$ is the flame stabilizer and mixing duct pressure loss.

© Woodhead Publishing Limited, 2013



16.40 Flame structure at 600 K and Ø = 0.52 of a radial swirler with fuel injection through the wall of a 76 mm diameter outlet throat. Dump flow expansion into a 140 mm diameter combustion, 330 mm long (Alkabie and Andrews, 1991b, 1991d).

© Woodhead Publishing Limited, 2013

Equation [16.7] shows the key features that make S small: a high pressure loss and hence high turbulence, a large number of fuel injection locations N and a long duct, L. A_t and the pressure loss are interrelated as discussed later; a small A_t directly reduces S but it also increases the pressure loss for the same flow rate. The dominant term in Equation [16.7] is the pressure loss; doubling the pressure loss reduces S by a factor of 4.3 and much larger changes in the other parameters have to be made to achieve the same reduction in S. As pressure loss energy produces the turbulence in the flame stabilizer flow, it is clear that mixing is controlled by the turbulence generated by the flame stabilizer, as shown above for radial swirlers.

16.8 Impact of fuel-and-air mixing quality on thermal NO_x emissions

16.8.1 Upstream fuel injection for premixed combustion

In Table 16.1 where 'premixed' is referred to as the method of fuel injection, then this means fuel injection well upstream of the flame stabilizer, typically with a 2 m long mixing pipe after an X configuration multihole fuel injection spoke. Maughan *et al*. (1992) investigated how far upstream the fuel needed to be for premixed NO_x results to be achieved for V-gutter flame stabilizers. The natural gas was injected through 12 1 mm diameter fuel holes on two spokes. These could be moved upstream of the flame stabilizer and the experiments showed that at 6 bar and 672 K with V_{ref} = 24.4 m/s the NO_x results were not independent of the upstream mixing length until this was 0.5 m upstream of the stabilizers. At 1800 K this then achieved 2 ppm NO_x, which is as good as the best system in Table 16.1. This is not a practical mixing distance to use in an engine.

16.8.2 Advantage of mixing imperfections on flame stability

In practice, all lean well-mixed designs can tolerate some unmixedness close to the stabilizer outlet, for the reasons discussed above. The advantage of this unmixedness is improved flame weak extinction. Table 16.1 shows that 16 of the low NO_x flame stabilizers, whether premixed or rapidly mixed, cannot maintain a flame at 1600 K and hence have little power turndown capability in the low NO_x mode. Many of the designs with very good flame stability to <1600 K are of the rapid mixing type without conventional premixing. The stability of these is aided by the unmixedness at the base of the stabilizing shear layers.

© Woodhead Publishing Limited, 2013

Five of the low NO_x stabilizers in Table 16.1 cannot maintain a flame at 1700 K and one cannot maintain a flame at 1800 K. Good flame stability is crucial to the operation of a low NO_x gas turbine combustor, as this determines the power turndown range that can be achieved in the well-mixed low NO_x mode. The ideal flame stabilizer can maintain a stable flame all the way to the fundamental flammability limit at around 1500 K (Andrews *et al*., 2009). If low (<10 ppm) NO_x can be achieved at 1900 K or 1950 K, and the flame is stable to 1500 K, then 50% or more of the power turndown can be in the well-mixed low NO_x mode. An example of a design that can achieve this is shown in Fig. 16.9 (Myers *et al*., 2003).

A good premixed or rapidly mixed design will be stable down to close to the fundamental lean flammability limit, as shown by Andrews *et al*. (2009). Many low NO_x flame stabilizers are not sufficiently stable to operate close to the lean flammability limit flame temperature of ~1500 K, as shown in Table 16.2 (Andrews *et al*., 2009). The ability to operate in the sub-10 ppm region over an adequate engine-power range is fundamental to the operation of low NO_x combustor designs. Table 16.1 shows several excellent designs in terms of low NO_x at 1800 and 1900 K but an inability to operate at 1600 or 1700 K (Wheatley *et al*., 2003; Calibab-Evalet *et al*., 2004; Cheng *et al*., 2005; Edmunds *et al*., 2006; Lammel *et al*., 2010). It is possible to cope with a poor lean flame stability if the NO_x in the 1800–1900 K temperature region is very low and the Calibab-Evalet *et al*. (2004) four axial swirler design is an example of a production engine that has to cope with the poor flame stability in the low NO_x mode by operating with a primary zone air proportion suitable to achieve the require primary zone temperatures for flame stability and then to have pilot or air/fuel scheduling procedures to keep the flame stable as the power is reduced. However, it is preferable to have a low NO_x design with a stable flame and low NO_x from >1900 K+ to <1500 K.

Table 16.2 Summary of the weak extinction data in terms of critical weak extinction flame temperature and laminar burning velocity

Flame temperature (K)	Data points	%	U_L (m/s)
1400–1500	21	16	0.05–0.075
1500–1600	68	53	0.075–0.13
1600–1700	20	16	0.13–0.16
1700–1800	10	8	0.16–0.18
1800–2000	9	7	0.18–0.26

Source:Andrews *et al*. (2009).

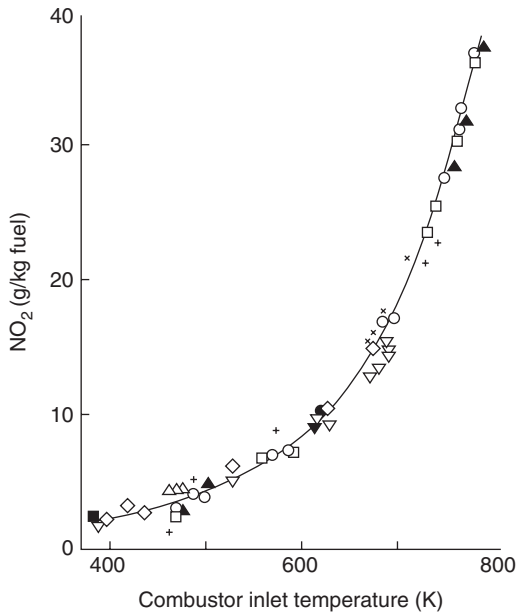
© Woodhead Publishing Limited, 2013

16.8.3 Pilot flame for premixed flame stability enhancement

Diffusion type pilot flames are often added to improve the flame stability and allow the main premixed combustion to operate leaner. Diffusion type pilot flames are undesirable as they create local hot zones and impair the NO_x performance. Current ultra-low NO_x flames in large gas turbines do not use pilot flames (Myers *et al.*, 2003) and well-designed premixed flames should be sufficiently stable to operate without a pilot at full load conditions. If a pilot is used then it should be a premixed pilot with separate air and fuel metering. These have minimum NO_x emissions and can even reduce the NO_x from the main burner operation alone, as discussed later. These are in essence a form of lean/lean staged premixed system.

16.9 Influence of air inlet temperature

For diffusion flame combustion the effect of the air inlet temperature is to increase the temperature of the local stoichiometric zones, and hence to increase NO_x. The classic work of Lipfert (1972) is shown in Fig. 16.41, where NO_x appears to increase with inlet temperature. However, in this case inlet



16.41 NO_x emissions as a function of inlet temperature for aero engine diffusion combustors of c.1970 design (Lipfert, 1972).

© Woodhead Publishing Limited, 2013

temperature is increased by increasing the engine power, so air pressure, air temperature and Ø are all increasing. This gives an apparently very large effect of inlet temperature on NO_x, which is not the same as varying inlet temperature with the other parameters constant.

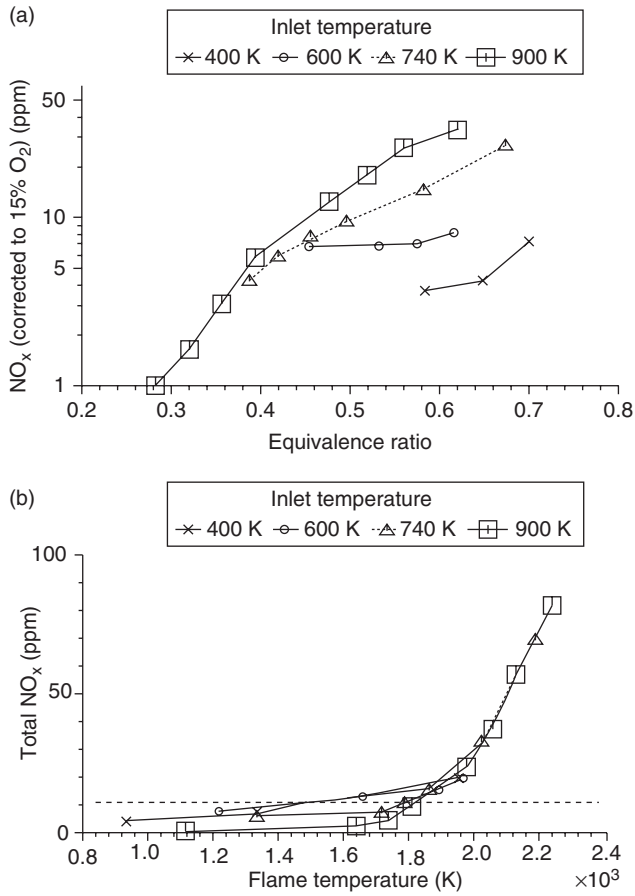
Thermal NO_x is controlled by the flame temperature, but for a fixed equivalence ratio the thermal NO_x increases with the air inlet temperature due to the increase in flame temperature. An example of these trends is shown in Fig. 16.41a (Kim *et al*., 1993) for a 40 mm outlet radial swirler in a 76 mm diameter combustor with radial vane passage fuel injection, where the fuel-and-air mixing was not perfect. Figure 16.41a shows that at Ø = 0.6 NO_x increases from 4 to 30 ppm for an increase in air inlet temperature from 400 to 900 K air temperature.

The NO_x emissions in Fig. 16.41a are shown as a function of the adiabatic flame temperature in Fig. 16.41b. This shows that the same NO_x was achieved for the same flame temperature in the thermal NO_x region for $NO_x > 10$ ppm (Kim *et al*., 1993). Figure 16.41b shows that NO_x was <10 ppm for flame temperatures below 1800 K with air inlet temperatures from 400 to 900 K as shown in Fig. 16.42 (Kim *et al*., 1993). When corrected to 15% oxygen this 10 ppm raw NO_x at 1800 K was 6 ppm at 900 K, 7.5 ppm at 740 K, 6.5 ppm at 600 K and 4.5 ppm at 400 K. The difference in corrected oxygen was due to the different equivalence ratios that generated 10 ppm NO_x at the same flame temperature. Comparison with well-mixed systems in Table 16.1 shows that many had lower NO_x at around 2–3 ppm at 1800 *K*. For 40 mm outlet radial swirlers the vane depths were large in order to get sufficient flow to achieve the desired lean equivalence ratio. With one fuel injection point per vane duct, the mixing in the duct was relatively poor due to the aspect ratio of the duct. This resulted in higher NO_x than for many designs in Table 16.1, including radial swirlers with larger diameter and smaller vane depth.

If NO_x is compared at constant flame temperature for different inlet temperatures then no effect of inlet temperature on thermal NO_x should occur, as shown in Fig. 16.41b. The primary zone of the combustor has to operate leaner as the inlet temperature increases if the same flame temperature is to be achieved. This leaner operation is possible as the weak extinction becomes leaner as the inlet temperature increases (Andrews *et al*., 2009). Below 10 ppm NO_x the NO_x in Fig. 16.41b was lower for higher air temperatures. This was due to the leaner mixtures used and their lower hydrocarbons, which lowers prompt NO_x formation.

Alkabie and Andrews (1989) also found for larger (76 mm outlet) radial swirlers that vane passage fuel injection did not give the lowest NO_x, with lower NO_x achieved with outlet throat wall fuel injection, as shown in Table 16.1. Escott *et al*. (1993) showed that the same swirlers with a greater vane passage depth and higher flow capacity had lower NO_x for vane passage fuel injection, as shown in Table 16.1. However, Andrews *et al*. (2006) have shown that this work on curved passage radial

© Woodhead Publishing Limited, 2013

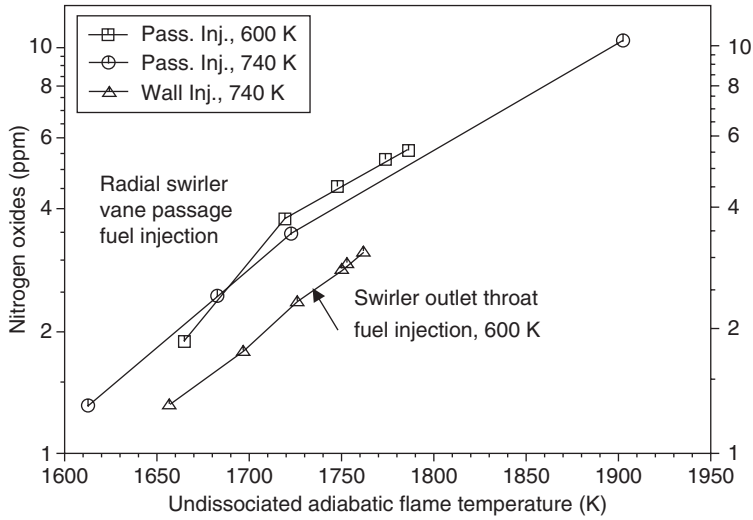


16.42 NO_x as a function of Ø (a) and flame temperature (b) for inlet temperatures of 400, 600, 740 and 900 K for 40 mm outlet radial swirlers with vane passage natural gas fuel injection (Kim *et al.*, 1993).

swirlers could be improved using parallel passage vane swirlers with vane passage fuel injection. This design achieved better fuel-and-air mixing with 2–3 ppm NO_x at 15% oxygen at 1800 K for 600 K inlet temperature, as shown in Table 16.1. Parallel passage radial swirlers are in production for at least two industrial gas turbine manufacturers (Boyns and Patel, 1997; Lee *et al.*, 2011).

Figure 16.43 shows the NO_x results as a function of flame temperature for an aerodynamic vane radial swirler (RS2) at 600 and 740 K (Andrews *et al.*, 2008). With vane passage fuel injection the same NO_x was achieved at the same flame temperature, indicating that thermal NO_x had been eliminated. Figure 16.43 also shows that this swirler achieved lower NO_x for

© Woodhead Publishing Limited, 2013



16.43 Large 76 mm outlet diameter radial swirlers with aerodynamic vanes (RS2) (Andrews *et al.,* 2008).

swirler outlet throat wall fuel injection at 740 K air inlet temperature. This fuel injection location has no premixing as it is close to the exit of the outlet throat of the radial swirler.

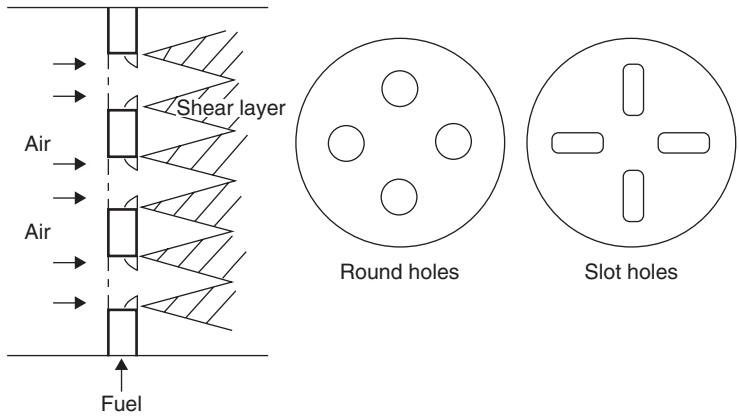
A further demonstration of the lack of inlet air temperature effect on NO_x at the same flame temperature is shown for the Grid Mix flame stabilizer shown in Fig. 16.44. This had four slot holes and each air hole was fuelled by eight radial inward jets (Andrews and Ahmad, 1994). The results in Fig. 16.45 show <10 ppm NO_x below 1980 K and operation at 1–2 ppm NO_x corrected to 15% oxygen was possible below 1800 K with no CO emissions problems.

16.10 Influence of residence time in premixed combustion: reference velocity and reference Mach number

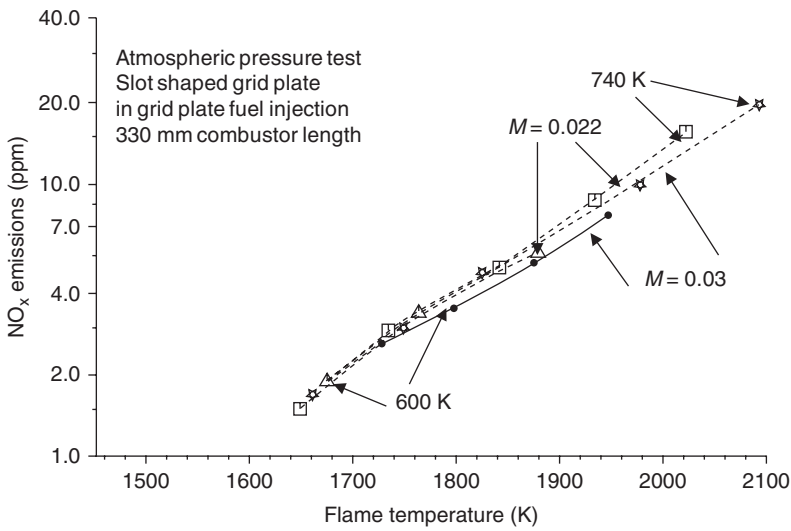
16.10.1 Influence of mean residence time on NO_x

Equation [16.4] and Fig. 16.32 show that thermal NO_x is dependent on the residence time at the adiabatic flame temperature. Prompt NO_x is not dependent on the residence time post completion of combustion. However, it may nevertheless have a residence time dependence through the dependence of the flame thickness on reference Mach number and hence on residence time. Prompt NO_x occurs in the flame development zone and if this is extended,

© Woodhead Publishing Limited, 2013



16.44 The grid mix flame stabilizer with eight fuel holes injecting into each air hole in the grid-plate stabilizer, and a four-hole design used in a 76 mm diameter combustor (Al-Dabbagh *et al.*, 1984; Andrews and Ahmad, 1994).



16.45 Four hole slot shaped grid-plate flame stabilizer with Grid Mix fuel injection radially into each air hole using eight radial jets per hole. Influence of air inlet temperature and reference Mach number (Andrews and Ahmad, 1994).

at high reference Mach number or low residence time, then this can lead to an increase in prompt NO_x. The extended flame zone and the dominance of prompt NO_x in the final NO_x is shown in Figs 16.5, 16.27, 16.29 and 16.40.

© Woodhead Publishing Limited, 2013

The thermal NO_x produced at a particular flame temperature is the product of the rate of formation of NO_x and the residence time. The mean residence time depends on the combustor length or primary zone length at the peak temperature and on the primary zone reference velocity, which depends on the proportion of the total combustor air flow that passes through the primary zone. The mean residence time is important in low NO_x combustor designs and this is the subject of this section.

The minimization of the overall residence time in conventional aero-gas turbine combustors has been one of the ways that NO_x has been reduced. Lewis (1999) showed that reducing the total volume of the combustor by 30% reduced the NO_x by 30% through the increase in mean velocity and associated reduction in residence time and hence in thermal NO_x production. Effectively, this is the same as increasing the heat release per volume, which is discussed later. For well-mixed lean combustion, changing the mean residence time is another way of showing whether thermal NO_x has been eliminated. Reducing isothermal mean velocity or reference velocity increases the residence time, and no effect on NO_x would be expected for temperatures below 1950 K where well-mixed systems thermal NO_x should be low.

16.10.2 Pressure loss and reference Mach number influences on NO_x

Increasing the combustor area and hence volume for the same total flow rate reduces the mean reference velocity. It also changes the mean upstream unburned air velocity and this changes the pressure loss across the flame stabilizer. The pressure loss in a flame stabilizer controls the energy dissipated for fuel-and-air mixing and for turbulent flame propagation. This is controlled by the air mass flow through the flame stabilizer and the stabilizer open flow area A_2 as shown in Equations [16.8] and [16.9].

$$\frac{\mathrm{d}m}{\mathrm{d}t} = C_D A_2 \left[2\rho\Delta P\right]^{0.5} \qquad [16.8]$$

$$\frac{\Delta P}{P} = 0.5\left(\frac{\gamma}{C_D{}^2}\right) M_1{}^2 \left(\frac{A_1}{A_2}\right)^2 = 0.5\left(\frac{\gamma}{C_D{}^2}\right) M_2{}^2 \qquad [16.9]$$

where A_1 is the maximum cross-sectional area of the combustor, m^2, A_2 is the open flow area of the flame stabilizer, m^2, C_D is the flame stabilizer discharge coefficient, A_2 is the effective flow area of the stabilizer, m^2, M_1 is the reference Mach number based on A_1 and the air inlet temperature, T.

© Woodhead Publishing Limited, 2013

$$M_1 = \frac{U_1}{(\gamma RT)^{0.5}} \quad [16.10]$$

where

$$U_1 = \frac{m_a}{\rho A_1} \quad [16.11]$$

$$M_2 = \frac{U_2}{(\gamma RT)^{0.5}} \quad [16.12]$$

where

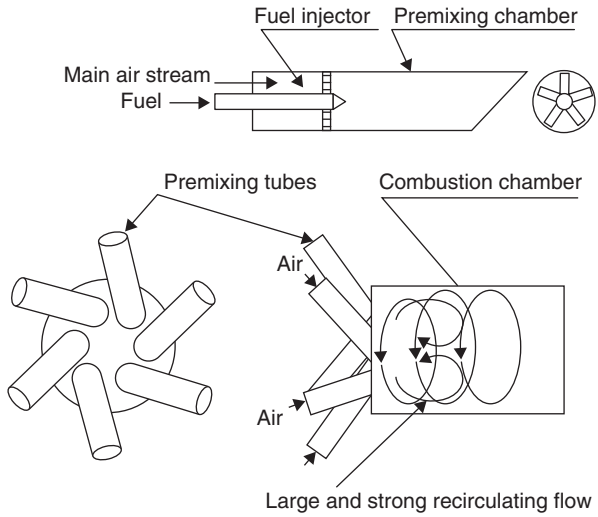
$$U_2 = \frac{m_a}{\rho A_2} \quad [16.13]$$

where m_a = air mass flow rate, kg/s, U_1 = mean velocity in A_1, the reference velocity, M_1 = Mach number in A_1, the reference Mach number, U_2 = mean velocity over the flame stabilizer open flow area A_2, M_2 = Mach number in A_2, ρ = air density upstream of the combustor, kg/m^3 [=P/RT where R = 287 J/kgK for air].

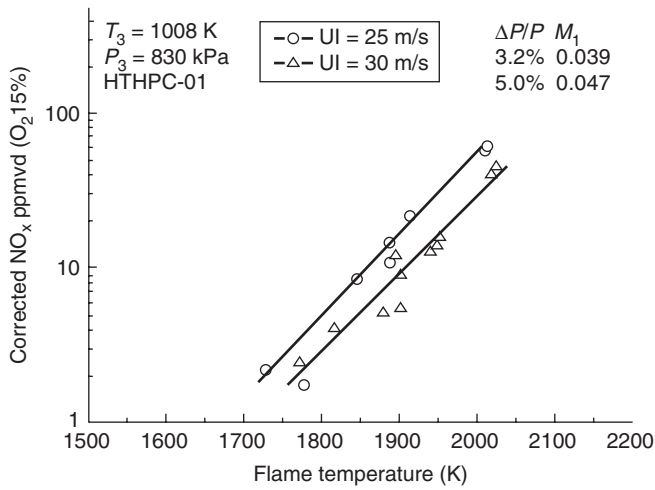
Equation [16.9] shows that if a fixed flow area flame stabilizer is used and M_1 is varied, then there is an associated change in the stabilizer pressure loss and hence in the turbulence levels in the flame front. NO_x results for different M_{ref} or V_{ref} often show higher NO_x at the lower M_1 and higher residence time. An example of this was found for a circular tube radial swirler, as shown in Fig. 16.46 (Kinoshita *et al.*, 1999), with the NO_x results at two reference velocities shown as a function of flame temperature in Fig. 16.47 (Kitajima *et al.*, 1997).

For direct fuel injection rapid mixing flame stabilizers, changes in pressure loss can also influence the turbulent fuel-and-air mixing parameter, S, in the flame and this can also result in lower NO_x at the higher M_1 for the same flame temperature and increasing M_1 at constant A_2 increased the pressure loss. Figure 16.45 shows NO_x results for a direct injection Grid Mix design (Fig. 16.44) with slot shaped holes, with a comparison of NO_x at two M_1. This shows little difference in the NO_x until the thermal NO_x region of >1950 K occurs. This indicates not only that there was no thermal NO_x increase due to the change in mean residence time, but also that the mixing was complete at the lower M_1 as there was no reduction at the higher pressure loss of the higher M_1 tests.

© Woodhead Publishing Limited, 2013



16.46 Circular mixing tube radial swirler (Kinoshita *et al.*, 1999).

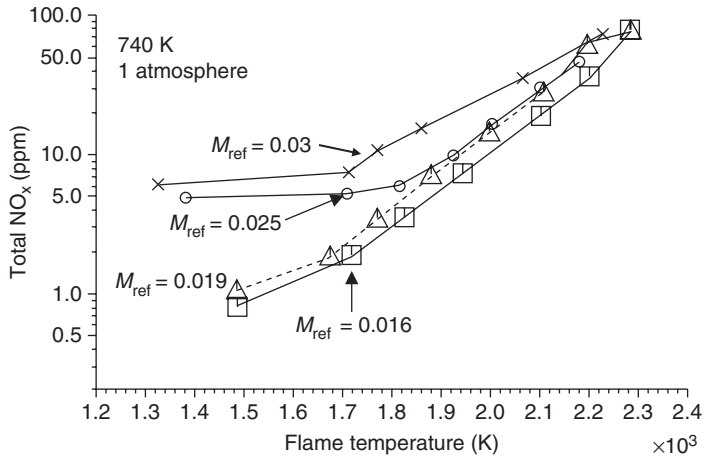


16.47 The influence of mean residence time on NO_x emissions through increasing the reference velocity to decrease the residence time (Kitajima *et al.*, 1997).

16.10.3 The influence of residence time at constant flame stabilizer pressure loss

For a more realistic comparison of the influence of residence time, a new flame stabilizer should be designed for each reference velocity condition so

© Woodhead Publishing Limited, 2013



16.48 Influence of reference Mach number on NO_x for a 40 mm outlet radial swirler in a 76 mm combustor at constant pressure loss of 2.7%, using a larger radial swirler as M_{ref} is increased (Kim *et al.*, 1993).

that the pressure loss is the same. This has been done by Kim *et al.* (1993) and the results are shown in Fig. 16.48. Small radial swirlers with 40 mm outlet diameter were used, intended for use as premixed pilot combustion with a downstream larger radial swirler (Kim *et al.*, 1993). For each M_1 a separate stabilizer was manufactured with reduced open area and this enabled M_1 to be varied without changing the pressure loss, which was constant at 2.7%. Figure 16.48 shows that NO_x was reduced as M_1 was reduced and this is the opposite effect that would be predicted if thermal NO_x was the source of the NO_x. The reason for the lower NO_x was due to lower prompt NO_x through the HC mechanism. This was due to the reduced HC at the higher residence time at the lower M_1.

16.10.4 Residence time and reference Mach number changes with the primary/dilution air flow split

The primary zone of a low NO_x gas turbine, which operates at full power turbine entry temperatures below 1950 K, does not need all the combustion air to pass through the flame stabilizer, although this is a design option if the lowest NO_x is desired. If reduced primary zone air flow is used then the primary zone reference Mach number is decreased and the surplus air is used for wall film cooling and/or dilution air. This can be simulated in flame stabilizer tests by operating the primary zone with the well-mixed low NO_x stabilizer at a reduced M_1. For example if the primary zone was operated at 1950 K and the turbine entry temperature

© Woodhead Publishing Limited, 2013

Table 16.3 Primary zone reference velocities (m/s) as a function of the primary zone air flow as a % of total combustor air flow

Primary air (%)	40%	60%	80%	100%
M_1	0.02	0.03	0.04	0.05
400 K	8 m/s	12 m/s	16 m/s	20 m/s
600 K	10 m/s	15 m/s	20 m/s	25 m/s
800 K	11 m/s	17 m/s	23 m/s	28 m/s
1000 K	13 m/s	19 m/s	25 m/s	32 m/s

was 1500 K for 700 K inlet temperature only about 64% of the air flow needs to pass through the low NO_x flame stabilizer, which gives a primary zone M_1 of 0.032. This is a typical design condition for the first generation of DLN gas turbine combustion.

Table 16.3 shows the reduction in mean primary zone velocity as M_1 is reduced for various proportions of the total combustor air flow used in the low NO_x primary zone and for various air inlet temperatures. The length of the primary zone divided by the velocity in Table 16.3 gives the isothermal flow residence time. Clearly, reducing the proportion of the air used in the primary zone will increase the residence time and this may increase the NO_x, if there is any residual unmixedness that gives thermal NO_x in the primary zone.

Table 16.4 shows the proportion of primary zone air that is required to achieve 1700 K primary zone temperature at 600 K inlet air temperature for 1300–1700 K turbine entry temperatures. This is approximately G Class gas turbine conditions if all the air enters the primary zone so that the turbine entry temperature is 1700 K. As the turbine entry temperature increases a larger proportion of the combustor airflow has to pass through the primary zone and the primary zone reference Mach number increases and the residence time decreases. Tables 16.5 and 16.6 tabulate equivalent data for 700 K air inlet temperature and 1800 and 1950 K primary zone temperatures. These are approximately G and J class gas turbine operating conditions if all the air enters the primary zone.

For the highest turbine entry temperatures today, at 1800 K, a low NO_x gas turbine would have to have nearly 100% of the combustion air passing through the low NO_x flame stabilizer with the primary zone reference Mach number at $M = 0.05$. Unfortunately there are few data, apart from the early work undertaken in the NASA Clean Combustor Programme (Jones, 1973; Mularz, 1976; Niedzweiki and Jones, 1976; Rudey, 1976), for low NO_x flame stabilizers operated at such high mean flow velocities. For the lowest NO_x the maximum primary zone M_1 should be used and all the air should flow through the stabilizer. This gives the highest flow velocities in the flame

© Woodhead Publishing Limited, 2013

Table 16.4 Primary zone conditions for different proportions of combustion air for 1700 K turbine entry temperature at maximum power for 600 K inlet temperature (~G Class)

Primary zone temperature (K)	Primary (Ø)	Primary air (%)	Primary (M_{ref})	Combustion intensity (MW/m²bar)
1300	0.28	58	0.029	6.5
1400	0.33	69	0.035	9.2
1500	0.38	79	0.04	12.2
1600	0.43	90	0.045	15.5
1700	0.48	100	0.05	19.2

Table 16.5 Primary zone conditions for different proportions of combustion air for 1800 K turbine entry temperature at maximum power for 700 K inlet temperature (~H Class)

Primary zone temperature (K)	Primary (Ø)	Primary air (%)	Primary (M_{ref})	Combustion intensity (MW/m²bar)
1400	0.30	60	0.03	7.2
1500	0.35	70	0.035	9.8
1600	0.40	80	0.04	12.8
1700	0.45	90	0.045	16.2
1800	0.50	100	0.05	20

Table 16.6 Primary zone conditions for different proportions of combustion air for 1950 K turbine entry temperature at maximum power for 700 K inlet temperature (~J Class)

Primary zone temperature (K)	Primary (Ø)	Primary air (%)	Primary (M_{ref})	Combustion intensity (MW/m²bar)
1500	0.35	61	0.031	8.7
1600	0.40	70	0.035	11.2
1700	0.45	79	0.040	14.4
1800	0.50	88	0.044	17.6
1950	0.57	100	0.05	22.8

stabilizer and can lead to difficulties in flame stability, so that the very lean combustion required for low NO_x conditions cannot be sustained with all the combustion air flowing through the flame stabilizer. This is the main reason that most combustors with turbine entry temperatures below 1950 K do not pass all the combustion air through the flame stabilizer. Also many of the low NO_x investigations in Table 16.1 were demonstrated at quite low Mach numbers and the achievement of low NO_x at Mach numbers approaching 0.05 is rare.

© Woodhead Publishing Limited, 2013

16.10.5 Combustor residence times and the choice of reference Mach number, M_1

The choice of the reference Mach number, M_1, or reference velocity, U_1, is controlled by the choice of the combustor cross-sectional flow area, A_1. From aero-gas turbine combustor practice the reference Mach number is typically 0.05 for subsonic aircraft and 0.07 for supersonic aircraft. The reference Mach number is based on all the combustion air flow passing through the cross-sectional area of the combustor. Clearly, if the reference combustor area A_1 is made larger the residence times at all power operating conditions will be longer and thermal NO_x is likely to be higher. The reference Mach number is another way of expressing combustion loading or heat release per combustor volume, and this is shown in 16.10.6 Some large industrial gas turbines use a lower M_1 than is common in aero-gas turbine practice and they generally do not have the lowest NO_x achievable.

If M_1 is too low or A_1 too large, there is also a significant influence on the flame stabilizer aerodynamics in terms of the size of the outer and inner recirculation zone in swirl flow and the distance between air jet holes in non-swirling flow. For swirl-based flame stabilization there is another area that is important, and that is the area of the combustor occupied by the flame stabilizer, A_3. For axial swirlers this is the area based on the outer diameter of the axial swirl blades (d), for radial swirlers it is the outlet area from the radial passages of diameter d in a combustor of diameter D. A_3 is normally $>A_2$, especially for swirl-based flame stabilizers. For grid-plate flame stabilizers A_2 and A_3 can be the same.

The aerodynamics downstream of the swirl-based flame stabilizers depend on the ratio of D/d (this is $A_1/A_3^{0.5}$) for swirlers in cylindrical combustors, and on $(A_1/A_3)^{0.5}$ if it is a swirler in an annular combustor. Many developers of low NO_x designs use single burner tests in a cylindrical combustor and the D/d ratio is the important parameter that controls the downstream aerodynamics. This is influenced by the presence of a hub in the centre of a swirler, which may carry a pilot burner. If A_1 is too large or M_1 too low, which means D/d is too high, then unrealistically large recirculation zones are generated and this can make the NO_x unrealistically high. The importance of the D/d ratio on the combustor aerodynamics was shown by Cai *et al.* (2005) for a counter-rotating radial swirler of outlet diameter d. The combustor diameter D was varied to achieve a D/d range from 2.9 to 5.9 at a swirler pressure loss of 4%. This was done by increasing the combustor diameter for a fixed counter-rotating swirler design. The downstream aerodynamics and turbulence levels showed a major dependence on D/d with the size of the central recirculation zone and the radial

© Woodhead Publishing Limited, 2013

Table 16.7 Can type combustor design parameters for a central flame stabilizer of outlet diameter *d* with a dump flow expansion into a combustor of diameter *D*

Primary flow (%)	40	60	60	80	100
M_1 Primary	0.02	0.03	0.03	0.04	0.05
Cd	0.7	0.7	0.5	0.5	0.5
$\Delta P/P$ %	3	3	4	4	4
A_2/A_1	0.138	0.207	0.251	0.335	0.418
Blockage %	86.2	79.3	74.9	66.5	58.2
$D/d = (A_1/A_2)^{0.5}$	2.7	2.2	2.0	1.73	1.55
$D/dt = (A_1/A_2)^{0.5}(A_2/A_3)^{0.5}$ for $A_3/A_2 = 1.5$	2.2	1.8	1.6	1.4	1.26

position of peak turbulence being significantly different at $D/d = 2.9$ than at higher D/d.

The use of inappropriately large values of D/d has been a common problem in research for low NO_x gas turbines, as reviewed by King *et al.* (2008). Table 16.7 shows for a swirler in a cylindrical combustor that if sensible values of M_1 are to be achieved and a high air flow passed through the flame stabilizer at pressure losses of 3% or 4%, then D/d cannot be greater than 2.2 if 60% of the combustion air flow is to pass through the swirler and if 100% of the combustion air is to pass through the stabilizer then the D/d will be around 1.5. However, this calculation assumes that there is a direct expansion from the flame stabilizer flow area A_2 to the combustor area A_1. This only occurs for grid-plate flame stabilizers, such as in the multicluster burner of Saitos *et al.* (2005). For radial or axial swirlers the swirler outlet diameter, d_t, with area A_3 is always greater than the open flow area A_2 of the stabilizer, especially if there is a downstream throat after the swirler of area A_3. The combustor aerodynamics are then an expansion of the flow from A_3 to A_1. Table 16.7 shows the impact of this on the D/d_t ratio for $A_3/A_2 = 1.5$ is to reduce D/d by 0.816. The practical range of D/d_t is now 1.26–2.2. This means that the swirler is very large relative to the combustor flame tube area.

Unfortunately little of the research on low NO_x swirlers for gas turbine applications has been carried out at such low values of D/d_t and more work is required in this area. Andrews and Ahmad (2011) have investigated axial swirlers with D/d from 1.1 to 1.6 at $M_1 = 0.05$ and have shown that the premixed NO_x is significantly higher for the same flame temperature if D/d_t is very low. This shows that the development of the expanding shear layer, as well as the generation of central recirculation, is important. A large internal recirculation zone, created by the presence of a large central hub, without outer recirculation was also shown to increase NO_x emissions.

© Woodhead Publishing Limited, 2013

16.10.6 Heat release per cross-sectional area related to the M_1

It may be shown using Equations [16.9] and [16.10] that the reference Mach number, M_1, is related to the heat release (MW) per cross-sectional area, A_1, per bar by Equation [16.14]:

$$\frac{\text{MW}}{PA_1} = \left[\left(\frac{\varnothing}{S}\right) M_1 \text{CV} \left(\frac{\gamma}{RT}\right)^{0.5}\right] \text{MW/bar m}^2 \qquad [16.14]$$

where S is the stoichiometric A/F by mass, CV is the calorific value of the fuel, MJ/kg.

Equation [16.14] shows that the heat release rate is linearly related to M_1, CV and to the combustor equivalence ratio, Ø. For CV = 50 MJ/kg, S = 16.5 (typical for natural gas), γ = 1.4 and R = 287 for air Equation [16.14] reduces to:

At 600 K $\text{MW/PA}_1 = 864\ \text{Ø}\ M_1$
At 700 K $\text{MW/PA}_1 = 800\ \text{Ø}\ M_1$

Values of heat release per combustor cross-sectional flow area are given in Table 16.4 for a range of primary zone low NO_x combustor operating conditions. The range of primary zone heat release per combustor area per bar is from 6.6 to 22.8, with the higher values more appropriate where all the combustion air passes through the primary zone.

An example of the inappropriate choice of low reference velocities and the penalty of the increased residence times is given in the development of the FLOX burner for gas turbine applications (Lammel *et al.*, 2010). They give a typical minimum value for gas turbine combustion of the above heat release parameter as 10 MW/m^{2}bar, which Table 16.4 shows to be appropriate for primary zones with a low proportion of the total air flow. Table 16.1 shows that the NO_x results at this heat release were very low at 1900 K, but there were flame stability problems and results at lower temperatures were not reported. In earlier work (Luckerath *et al.*, 2006) on the FLOX burner a heat release of a 2.5 MW/m^{2}bar was used and much higher NO_x were generated. This was due to the creation of a large recirculation zone in the large diameter combustor. As a consequence, there was a high residence time and when the cross-sectional area of the combustor was reduced to give a more realistic heat release rate or reference Mach number, then lower NO_x emissions were achieved, with no compromise on the CO emissions, as shown in Table 16.1. They also improved the mixing in the air and fuel jets using a rectangular cross-sectional area jet, as had first been demonstrated by Andrews and Ahmad (1994) and shown in Figs 16.44 and 16.45.

© Woodhead Publishing Limited, 2013

Table 16.8 Flame residence time for M_{ref} = 0.03 and 0.05 for three primary zone temperatures, two combustor lengths and two inlet temperatures

Primary temperature (K)	0.33 m M = 0.03	0.33 m M = 0.03	1 m M = 0.03	1 m M = 0.03	0.33 m M = 0.05	0.33 m M = 0.05
	400 K	1000 K	400 K	1000 K	400 K	1000 K
1600 K	6.9 ms	10.9 ms	20.7 ms	32.7 ms	4.1 ms	6.5 ms
1800 K	6.1 ms	9.6 ms	18.3 ms	28.9 ms	3.7 ms	5.8 ms
2200 K	5.0 ms	7.9 ms	15.0 ms	23.7 ms	3.0 ms	4.7 ms

16.10.7 Influence of combustor length and post flame residence time

The other factor that directly influences the residence time is the combustor length. This has often been made long in industrial gas turbines so as to achieve low CO emissions. However, the limiting temperature for low CO and HC emissions in lean premixed primary zones is about 1680 K (Escott *et al*., 1993) and there is no incompatibility in achieving low NO_x and low CO in lean well-mixed primary zones. In general, if extra combustor length is added to reduce CO emissions there is a detrimental influence on NO_x. One industrial GT manufacturer, using the lean/lean approach, has found that reducing the combustor length produced significantly lower NO_x with no CO penalty (Moran, 2010).

The residence times discussed above all refer to the isothermal flow residence times. However, for thermal NO_x generation it is the residence time at the adiabatic flame temperature that matters, and this depends on the flame development distance. The worst case hot gas residence times are shown in Table 16.8, and these calculations assume that combustion is complete at the adiabatic temperature immediately downstream of the flame stabilizer. Table 16.8 shows that for 1800 K combustion temperature, the maximum possible residence time is 6–10 ms for M = 0.03 for a 0.33 m long combustor, which reduces to 4–6 ms for M_1 = 0.05. This increases to 18–29 ms for a 1 m long combustor with M_1 = 0.03.

Combustion does not develop instantaneously downstream of the flame stabilizer, and lean low NO_x flames take a considerable distance to develop the final flame temperature. This is shown in Figs 16.5 and 16.27, and for a given combustor length the actual hot gas residence time should be based on a shorter distance than the combustor length to take into account the flame development length. This flame development distance depends on the type of flame stabilizer used. However, for illustration purposes it will be assumed that the flame development length is 0.2 m. If the combustor length was 0.33 m then the hot gas residence times are reduced by 60% to 2.5–4 ms at M = 0.03, but only by 20% for a 1m long

© Woodhead Publishing Limited, 2013

combustor. Thus, if a combustor is longer than it needs to be for complete heat release, then there is likely to be a bigger NO_x penalty than simply the ratio of the two lengths. This will be without compensating gains in CO emissions, as the CO should be very low if the combustion is lean and well mixed, to avoid significant thermal NO_x generation. This then leaves the question of how long a combustor needs to be for complete heat release and this depends on the flame stabilizer geometry and on the size of the gas turbine and the decision on the number of flame stabilizers or fuel injectors that are used.

16.11 Conclusions

1. The lowest achievable NO_x at turbine entry temperatures or primary zone temperatures of 1700, 1800 and 1900 K is 1, 2 and 3.5 ppm respectively. This is supported by a wide range of experimental results using different flame stabilizers. Several experimental results support NO_x emissions of 2, 3 and 5 ppm for the same three flame temperatures in agreement with the work of Leonard and Stagmaier (1993). All of these designs have eliminated thermal NO_x and the residual NO_x is due to the prompt NO_x mechanism. Thus, lean well-mixed combustion should be able to achieve low single digit NO_x for current and future turbine entry temperatures.
2. Gas turbine combustion with good fuel-and-air mixing that is operating with a lean primary zone below the critical thermal NO_x formation temperature show no dependence of NO_x on pressure, as prompt NO_x is not pressure dependent. Low NO_x combustors can thus be developed at atmospheric pressure and only need testing at pressure once the desired NO_x has been demonstrated at atmospheric pressure.
3. Low NO_x flame stabilizers that have eliminated thermal NO_x show no dependence on the air inlet temperature for the same adiabatic flame temperature.
4. To achieve these ultra-low NO_x levels the flame stabilizers must be stable down to the laminar flame flammability limit, with a critical flame temperature at weak extinction of 1500 K. This allows primary zone operation down to at least 1600 K, or 1550 K in some cases, and these designs have the greatest power turndown capability in the premixed mode. Not all the designs that demonstrate low NO_x can demonstrate acceptable weak extinction and one without the other is not acceptable for engine applications. Table 16.1 shows that some low NO_x designs have no measured NO_x at 1600 and 1700 K, as the flame has already extinguished before this.
6. To achieve a high proportion of the combustion air through the flame stabilizer so as to operate the primary zone lean enough to achieve primary

© Woodhead Publishing Limited, 2013

zone temperatures <1950 K, the flame stabilizer must be large relative to the combustion. The interaction between the flame stabilizer and combustor dominates the primary zone aerodynamics and for can combustors the practical range of the combustor to stabilizer outlet diameter is 1.2–1.6 for >60% of the combustion air in the primary zone. Many investigations of low NO_x combustors have used swirl flame stabilizers in a can that is too large and the resultant combustion aerodynamics are not those of ultra-low NO_x combustors.

16.12 Acknowledgements

Many thanks to the fourteen research students and many MSc project students who have worked under my supervision on ultra-low NO_x gas turbine combustion. Thanks also to the UK EPSRC who provided the experimental equipment through several research contracts over the period 1980–2000. Thanks to the industrial lecturers from Siemens, Alstom, GE and Rolls Royce on the CPD course on Ultra-Low NO_x Combustion and to the many industrial delegates over 20 years who keep my research on low NO_x research focussed on practical issues.

16.13 References

Ahmad, N.T. and Andrews, G.E., 'Emissions from enclosed swirl stabilised premixed flames'. ASME Paper 83-GT-192, 1983. Also in *Int. J. Turbo Jet Engines*, Vol. **3**, pp. 147–158 (1986).

Ai, T., Koeneke, C., Arimura, H. and Hyakutake, Y., 'Development of an air cooled G class turbine (the M501GAC)'. ASME Paper GT2009–60321 (2009).

Aida, N., Nishijima, T., Yamada, H., Hayashi, S. and Kawakami, T., 'Injection of lean mixtures into hot burned gas for maintaining low-Nox emissions ove an extended range of fuel-air ratios in prevaporized combustion'. *Proc. Int. Gas Turbine Congress*, Tokyo, IGTC2003Tokyo TS-142 (2003).

Al-Dabbagh, N.A. and Andrews, G.E., 'Influence of flame stabiliser geometry on premixed combustion flame stability and emissions'. ASME Paper 81-GT- Trans. of ASME, *J. Eng. Power*, Vol. **103**, pp. 749–758 (1981).

Ali, A.F. and Andrews, G.E., 'Conical grid plate flame stabilisers for gas turbine primary zones'. ASME Paper 85-GT-53, 1985. Also in *Int. J. Turbo Jet Engines*, Vol. **3**, pp. 171–180 (1986).

Alkabie, H.S., Andrews, G.E. and Ahmad, N.T., 'Lean low NO_x primary zones using radial swirlers'. ASME Paper 88-GT-245 (1988).

Alkabie, H.S. and Andrews, G.E., 'Ultra-low NO_x emissions for gas and liquid fuels using radial swirlers'. ASME Paper 89-GT-322 (1989a).

Alkabie, H.S. and Andrews, G.E., 'The influence of fuel placement on NO_x emissions from flames stabilized by radial swirlers at gas turbine primary zone conditions'. presented at the IMechE Seminar on Gas Turbines – Technology and Development (1989b).

© Woodhead Publishing Limited, 2013

Alkabie, H.S. and Andrews, G.E., 'The influence of fuel placement on NO_x emissions from flames stabilized by radial swirlers'. *Proceedings of the Joint Meeting of the British and French Sections of the Combustion Institute*, pp. 33–36 (1989c).

Alkabie, H.S. and Andrews, G.E., 'Radial swirlers with peripheral fuel injection for ultra-low NO_x emissions'. ASME Paper 90-GT-102 (1990).

Alkabie, H.S. and Andrews, G.E., 'The aerodynamics of radial swirlers in lean gas turbine primary zones'. IMechE Conference Proceedings C430/070, pp. 81–90 (1991a).

Alkabie, H.S. and Andrews, G.E., 'The influence of fuel placement on NO_x emissions from flames stabilized by radial swirlers'. Proceedings of the Tenth International Symposium on Air Breathing Engines (10th ISABE), AIAA, vol. 1, pp. 411–420, ISBN 1–56347–006–3 (1991b).

Alkabie, H.S. and Andrews, G.E., 'The influence of fuel placement on NO_x emissions from flames stabilized by radial swirlers at gas turbine primary zone conditions'. 1991 Yokohama Japanese International Gas Turbine Congress (1991c).

Alkabie, H.S. and Andrews, G.E., 'The aerodynamics of radial swirlers in lean gas turbine primary zones'. Proceedings of the Second IMechE International Conference on 'Computers in Engine Technology'. C430, pp. 91–100 (1991d).

Alkabie, H.S., 'Design methods of alstom gas turbine DLE combustion system'. IMechE Seminar S601, Turbulent Combustion of Gases and Liquids, Lincoln, 15–16 December 1998.

Al-Shaikhly, A.F., Andrews, G.E. and Aniagolu, C.O., 'Jet shear layer turbulent diffusion flames for ultra-low NO_x emissions'. Transactions of the ASME, *J. Eng. Gas Turbines Power*, Vol. **114**, pp. 55–62 (1992).

Altemark, D. and Knauber, R., 'Ergebnisse von Untersuchungen an einem Vormischbrenner unter Druck mit extrem niedriger NO_x-emission'. VDI Berichte No. 645, pp. 299–311 (1987).

Anandi, A., Haynes, J., May, P. and Iyev, V., 'Evaluation of emission performance of existing combustion technology for syngas combustion'. ASME Paper 2005–68513 (2005).

Anderson, D.N., 'Effects of premixing on nitric oxide emissions'. NASA TM-X-68220 (1973).

Anderson, D.N., 'Effects of equivalence ratio and dwell time on exhaust emissions from and experimental premixing prevaporising burner'. NASA TM-X-71592 (1975).

Andrews, G.E. and Abdul Hussain, U.S., 'Concentration fluctuations in turbulent cross jet mixing'. Proceedings of the ASME IGTI International Gas Turbine Congress, Cologne, ASME Paper 92-GT-346 (1992).

Andrews, G.E., Abdul-Aziz, M.M. and Al-Dabbagh, N.A., 'Mixing and fuel atomisation effects on premixed combustion performance'. ASME Paper 83-GT-55 (1983).

Andrews, G.E. and Ahmad, S.A.R., 'Noncircular jet shear layer turbulent diffusion flames for ultra low NO_x gas turbine primary zones'. ASME Cogen-Turbo, Portland, pp. 411–417 (1994).

Andrews, G.E., Escott, N.H., Al-Shailkly, A.F. and Alkabie, H.S., 'Counter rotating radial swirlers from low NO_x emissions with passage fuel injection'. 12th International Symposium on Air Breathing Engines (ISABE), ed. F.S. Billig. Vol. II, pp. 1235–1248, Melbourne, Published by ISABE and AIAA (1995).

© Woodhead Publishing Limited, 2013

Andrews, G.E. and Mkpadi, M.C., 'High turndown ratio, low NO_x gas turbine combustion'. ASME Paper 2001-GT-59 (2001).

Andrews, G.E., Matt Lazim, T.B.M. and Mkpadi, M.C., 'Low NO_x axial swirler with fuel injection into the downstream dump expansion shear layer'. *J. Energy Institute*, Vol. **78**, No. 4, pp. 172–184 (2005).

Andrews, G.E., Delgadillo, E.Z., Mkpadi, M.C. and Hayes, G., 'Hydrogen as a pilot gas to improve power turndown in simulated ultra low NO_x gas turbine combustion'. ASME Paper GT2007–27414 (2007b).

Andrews, G.E., Escott, N. and Mkpadi, M.C., 'Radial swirler designs for ultra-low NO_x gas turbine combustion'. ASME Paper GT2008–50406 (2008).

Andrews, G.E. and Ahmad, S.A.R., 'Jet shear layer size and number influences on grid plate direct fuel injection shear layer mixing low NO_x gas turbine combustion with fuel staging for power turn down'. ASME paper GT2008–50408 (2008).

Andrews, G.E., Ahmad, N.T., Phylaktou, H.N. and King, P., 'Weak extinction in low NO_x gas turbine combustion'. ASME Paper GT2009–59830 (2009).

Andrews, G.E. and Ahmad, N.T., 'Axial swirler design influences on NO_x emissions for premixed combustion in gas turbine combustors with all the combustor air flow passing through the swirlers'. ASME Paper GT2011–45418 (2011).

Andrews, G.E. and Ahmad, N.T., 'Axial swirler outlet shroud influences on premixed combustion NO_x emissions for all the combustion air passing through the swirler'. Proc. ASME Turbo Expo, Copenhagen. ASME Paper GT2012–68642 (2012).

Appleton, J.P. and Heywood, J.B., 'The effects of imperfect fuel-air mixing in a burner on NO formation from nitrogen in the air and the fuel'. Fourteenth Symposium (International) on Combustion, The Combustion Institute, Pittsburgh, pp. 777–786 (1973).

Arellano, L.O., McDongald, N.K. and Greenberg, S.J., 'Full scale demonstration of surface stabilised fuel injectors for sub three ppm NO_x emissions'. ASME Paper 2004GT-53629 (2004).

Austrem, I., Mowill, J.A. and Klein, S.A., 'The development of an ultra low emissions liquid fuel combustor for the OPRA OP16 gas turbine'. ASME Paper GT-2002–30107.

Baker, D., Taylor, P. and McMillan, R., 'Duel fuel DLE typhoon commercial operating experience and improvement upgrades'. ASME Paper 2000-GT-112 (2000).

Benoit, J.A., Ellis, C. and Cook, J., 'Ultra low emissions combustion and control systems installation into mature power plant gas turbines'. ASME Paper GT2010–22261 (2010).

Bhargava, A., Kendrick, D.W., Castleton, K.H., Colket, M.B. and Sowa, W.A., 'Pressure effect on NO_x and CO emissions in industrial gas turbines'. ASME Paper 2000-GT-97 (2000a).

Bhargava, A., Kendrick, D.W., Castleton, K.H., Colket, M.B. and Sowa, W.A., ' NO_x scaling characteristics for industrial gas turbine fuel injection'. ASME Paper 2000-GT-98 (2000b).

Bonzani, F., Piano, C. and Zito, D., 'VeLoNO_x combustion system operating experience on heavy duty gas turbine'. Proceedings of ASME Turbo Expo 2007: Power for Land Sea and Air, ASME Paper GT2010–22254 (2010).

Boschek, E., Griebel, P. and Jonsohn, P., 'Fuel variability effects on turbulent lean premixed flames at high pressure'. Proceedings of ASME Turbo Expo 2007: Power for Land Sea and Air, ASME Paper GT2007–27496 (2007).

© Woodhead Publishing Limited, 2013

Boyns, M.B. and Patel, R., 'The application of DLN Technology to the Tornado and tempest industrial gas turbines'. ASME Paper 97-GT-59 (1997).

Bozzelli, J.W. and Antony, M., 'NNH: Possible new route for NO_x formation in flames'. *J. Chem. Kinetics*, Vol. **27**, Issue 11, pp. 1097–1109 (1995).

Brueckner-Kalb, J.R., Napravnik, C., Hirsch, C. and Sattlemayer, T., 'Development of a fuel-air premixer for a sub-ppm NO_x burner'. ASME Paper GT2007–27779 (2007).

Cai, J., Jeng, C.M., Fu, Y. and Mongia, H., 'Confinement effects on the swirling flow of a counter-rotating swirl cup'. ASME Paper GT2005–68622 (2005).

Chen, J., Mitchell, M.G. and Nourse, J.G., 'Development of ultr-low emission diesel fuel-fired microturbine engines for vehicular heavy duty applications: Combustion modifications'. ASME Paper GT2010–23181 (2010).

Cheng, R.K., Littlejohn, D., Nazeer, W.A. and Smith K.O., 'Laboratory studies of the flow field characteristics of low-swirl injectors for adaptation to fuel-flexible turbines'. Proc. ASME Turbo Expo 2006: Power for Land Sea and Air, ASME Paper GT2006–90878 (2006).

Colibaba-Evulet, A., Brand, A.R. and Bowman, M.J., 'Design and evaluation of the AIMS combustor'. ASME Paper GT2004–53150 (2004).

Corr, R.A., Malte, P.C. and Morinar, N.M., 'Evaluation of NO_x mechanisms for lean premixed combustion'. ASME Paper 91-GT-257 (1997).

Correa, S.M., 'Lean-premixed combustion for gas turbines: Review and required research'. ASME Fossil Fuel Combustion, PD-Vol. 33, pp. 1–9 (1991).

Cramb, D.J. and McMillan, R., 'Tempest dual fuel DLE development and commercial operating experience and ultra low NO_x gas operation'. ASME Paper 2001-GT-76 (2001).

Davis, L.B., 'Dy low NO_x combustion systems for GE heavy-duty gas turbines'. Proceedings of the 1995 Yokohama International Gas Turbine Congress, Vol. 1, pp. 237–246, 95-Yokohama-IGTC-139 (1995).

Davis, L.B., 'Dry low NO_x combustion systems for GE heavy-duty gas turbines'. Proc. Int. Gas Turbine and Aeroengine Congress, ASME Paper 96-GT-27 (1996).

Della Betta, R.A., Schlatter, J.C., Nickolas, S.G., Cutrone, M.B., Beebe, K.W., Furuse, Y. and Tsuchiya, T., 'Development of a catalytic combustor for a heavy duty utility gas turbine'. ASME Paper 96-GT-485 (1996).

Dodds, W.J. and Ekstedt, E.E., 'Evaluation of fuel preparation systems for lean premixing –prevaporizing combustors'. Proc. ASME IGTI Int. Gas Turbine Congress. ASME Paper 85-GT-137 (1985).

Eggels, R., 'Modelling of NO_x formation of a premixed DLE gas turbine combustor'. Proc. Int. ASME IGTI Gas Turbine Congress, ASME Paper 2001-GT-69 (2001).

ElKady, A.M., Kalitan, D., Akula, R.K., Herbon, J., Karim, H., Hadley, M. and Leonard, G., 'Gas turbine emission characteristics in perfectly premixed combustion'. Proc. ASME Turbo Expo, 2011 Vancouver. ASME paper GT2011–46470 (2011).

Escott, N.H., Andrews, G.E., Alkabie, H.S., Al-Shaikhly, A.F. and George, B., 'Large airflow capacity radial swirlers for ultra low NO_x at high inlet temperatures'. Proceedings of IGTI Seventh Congress and Exposition on Gas Turbines in Co-generation, Utility, Industrial and Independent Power Generation, Vol. 8, ASME COGEN TURBO '93, pp. 241–243 (1993).

© Woodhead Publishing Limited, 2013

Escott, N.H., Andrews, G.E., Al-Shaikhly, A.F. and Al-Kabie, H.S., 'Counter-rotating radial swirlers for low NO_x emissions with air staging'. Proceedings of the 1995 Yokohama International Gas Turbine Congress, Vol. II, pp. 333–334 (1995).

Farber, J., Koch, R., Bauer, H-J, Hase, M. and Krebs, W. 'Effects of pilot fuel and liner cooling on the flame structure in a full scale swirl-stabilised combustion setup'. Proc. ASME Turbo Expo 2009. ASME Paper GT2009–59345 (2009).

Fenimore, C.P., 'Formation of nitric oxide in premixed hydrocarbon flames'. Thirtheenth Symposium (Int.) on Combustion, The Combustion Institute, pp. 373–380 (1971).

Fetescu, M., 'High efficiency coal and gas (HE-C&G), an advanced hybrid power plant concept with sequential combustion gas turbine GT24/GT26'. ASME Paper 97-GT-361 (1997).

Fletcher, R.S. and Heywood, J.B., 'A model for nitric oxide emissions from aircraft gas turbine engines'. AIAA Paper No. 71–123 (1971).

Fujii, T., Ozawa, Y., Kikumoto, S., Sato, M., Yuasa, Y. and Inoue, H., 'High pressure test results of a catalytic combustor for gas turbine'. ASME Paper 96-GT-382 (1996).

Gallimore, S., Vickers, R.M. and Boyns, M.B., 'The design modifications of the EGT Tornado industrial gas turbine to incorporate a dry low emissions combustion system'. ASME Paper 97-GT-159 (1997).

Girard, J.W., Dibble, R.W., Arellano, L.O. and Smith, K.O., 'Use of an extractive laser probe for time-resolved mixture fraction measurements in a 9 atm gas turbine fuel injector'. ASME Paper 2001-GT-372 (2001).

Herberling, P.V., 'Prompt NO measurements at high pressures'. Sixteenth Symp. (Int.) on Combustion, The Combustion Institute, pp. 159–168 (1976).

Hilt, M.B. and Waslo, J., 'Evolution of NO_x abatement techniques through combustor design for heavy duty gas turbines'. Proc. ASME IGTI Int Gas Turbine Congress, 1984, ASME Paper 84-GT-48 (1984).

Hiramatsu, M., Nakashima, Y., Koneko, S., Yamasaki, Y. and Adachi, S., 'Combustion characteristics of small size gas turbine combustor fuelled by biomass gas employing flameless combustion'. ASME Paper GT2007–27636 (2007a).

Hiramatsu, M., Y., Nakashima, Y., Kaneko, S. and Hayashi, S., 'Design of small size gas turbine combustor fueled by low-calorific gas based on analyis of flameless combustion'. Proc, 9th International Congress on Gas Turbines, IGTC 2007 Tokyo, Paper IGTC2007 Tokyo TS-146, (2007b).

Hornsby, C. and Norster, E.R., 'Application of CFD to DLN combustion'. ASME Paper 97-GT-371 (1997).

Ito, E., Pkada, I., Tsukagoshi, K., Muyama, A. and Masada, J., 'Development of Key Technologies for the Next Generation 1700C-Class Gas Turbine'. ASME Paper GT2009–59783 (2009).

Jansohn, P., Ruck, T., Steinbach, C., Knцpfel, H.P. and Sattelmayer, T., 'Development of the Advanced EV (AEV) Burner for the ABB GTX100 Gas Turbine'. ASME Turbo Asia 1997, No. 97-AA-139, Singapore (1997).

Jones, R.E., 'Advanced Technology for Reducing Aircraft Engine Pollution'. ASME Paper 73-WA/Aero-2 (1973).

Kajita, S., Ohga, J. and Kitajima, T., 'Development of a Dry Low Nox Combustor for 1.5MW Gas Turbine'. ASME Paper 93-GT-393 (1993).

© Woodhead Publishing Limited, 2013

Kim, S., Andrews, G.E. and Alkabie, H.S. 'An Ultra-low NO_x Pilot Combustor for Staged Low NO_x Designs'. Eleventh International Symposium on Air Breathing Engines, Tokyo, XI ISABE, AIAA (1993).

King, P.T., Escott, N.H., Andrews, G.E., Pourkashanian, M. and McIntosh, A.C., 'CFD predictions of low NO_x radial swirlers with vane passage fuel injection with comparison with internal gas analysis flame composition'. ASME Paper GT2008–51138 (2008).

King, P.T., Andrews, G.E., Pourkashanian, M. and McIntosh, A.C., 'CFD prediction and design of low NO_x radial swirler systems'. ASME Paper GT2009–60107 (2009).

Kinoshita, Y., Oda, T. and Kitajima, J., 'Research on a low NO_x combustor for a Mach 3 supersonic transporter turbojet engine'. Proc. of the Inter. Gas Turbine Congress 1999, Kobe. IGTC99Kobe OS-502. Vol. 1 p.185–192 (1999).

Kitajima, J., Oda, T. and Kinoshita, Y., 'Low NO_x combustor research for a Mach 3 turbojet concept validation'. ASME Paper 97-GT-153 (1997).

Klein, M., 'The need for standards to promote low emission, high efficiency gas turbine facilities'. ASME Paper 99-GT-405 (1999).

Koganezawa, T., Abe, K., Miura, K., Saito, T. and Inoue, H., 'Performance of a cluster nozzle burner for the advanced humid air turbine'. Proc. Int. Gas Turbine Congress 2007 Toyko, IGTC2007 Tokyo TS-134 (2007).

Kokanovic, S., Guidati, G., Torchalla, S. and Schuermans, B., 'Active combustion control system for reduction of NO_x and pulsation levels in gas turbines'. Proc. ASME Turbo Expo 2006: Power for Land, Sea and Air, ASME Paper GT2006–90895 (2006).

Kowkabi, M., Noden, R. and DePietro, S. 'The development of a dry low NO_x combustion system for the EGT typhoon'. ASME Paper 97-GT-60 (1997).

Kyne, A.G., Williams, A., Wilson, C.W. and Pourkashanian, M., 'Modelling NO-NO_2 conversion in counter-flow diffusion flames'. ASME Paper 2003–38017 (2003).

Lammel, O., Schutz, H., Schmidt, G., Luckerath, R., Stohr, M., Noil, B., Aigner, M., Hase, M. and Krebs, W., 'FLOX combustion at high power density and high flame temperatures'. ASME Paper GT2010–23385 (2010).

Lavoie, G.A., Heywood, J.B. and Keck, J.C., 'Experimental and theoretical study of nitric oxide formation in internal combustion engines'. *Comb. Sci. Tech*. **1**, 313–326 (1970).

Lee, G.J., Armstrong, J.P. and Santavicca, D.A., 'Experiments on lean blowout and NO_x emissions of a premixed trapped vortex combustor with high G-loading'. Proc. ASME Turbo Expo 2011, ASME Paper GT2011–46396 (2011).

Lefebvre, A.H., 'The role of fuel preparation in iow emissions combustion'. ASME Paper 95-GT-465 (1995).

Leonard, G. and Correa, S.M., Second ASME Power Division Fossil Fuel Comb. Symp., Vol. 30, S.N. Singh, S.N. Ed. P.69–74 (1990).

Leonard, G. and Stegmaier, J., 'Development of an aeroderivative gas turbine dry low emissions combustion system'. Proc. Int. Gas Turbine and Aeroengine Congress, 1993. ASME Paper 93-GT-288, 1993. Also in Trans. of ASME, J. Eng. Gas Turbine Power, p. 542 (1994).

Levy, Y., Gany, A., Goldman, Y., Erenburg, V., Sherbaum, V., Ovcharenko, V. and Rosentsvit, L., 'Increasing operational stability in low NO_x GT combustion by a pilot flame'. Proc. ASME Turbo Expo 2010: ASME GT2010–22785 (2010).

© Woodhead Publishing Limited, 2013

Lewis, G., NATO RTO-MP-14, Paper K. (1999).
Littlejohn, D., Cheng, R.K., Noble, D.R. and Lieuwen, T., 'Laboratory investigations of low-swirl injectors operating with syngas'. ASME Paper GT2008–51298 (2008).
Lorstad, D., Pettersson, J. and Lindholm, A., 'Emissions reduction and cooling improvements due to the introduction of passive acoustic damping in an existing SGT-800 combustor'. Proc. ASME Turbo Expo 2009, Orlando. ASME Paper GT2009–59313 (2009).
Lovett, J.A. and Abuaf, N., 'Emissions and stability characteristics of flame holders for lean premixed combustion'. ASME Paper 92-GT-120 (1992).
Lovett, J.A. and Mick, W.J., 'Development of a swirl and bluff-body stabilizer burner for low-NO_x, lean-premixed combustor'. ASME Paper 95-GT-166 (1995).
Luckerath, R., Meier, W. and Aigner, M., 'FLOX combustion at high pressure with different fuel compositions'. ASME GT2007–27337. Also: J. Eng. for Gas Turbines and Power, 130[1], p. 01150505–1–7 (2007).
Luckerath, R., Lammel, O., Stohr, M., Boxx, I., Stopper, U., Meier, W., Janus, B. and Wegner, B. 'Experimental investigations of flame stabilization of a gas turbine combustor'. Proc. ASME Turbo Expo 2011, Vancouver. ASME Paper GT2011–45790 (2011).
Lyons, V.J., 'Fuel/air nonuniformity – effect of nitric oxide emissions'. 19th AIAA Aerospace Sciences Meeting, St. Louis, 1981. AIAA Paper 810327 (1981).
Malte, P.C. and Rutar, T., 'NO_x formation in high pressure jet stirred reactors with significance to lean-premixed combustion turbines'. ASME Paper 2001-GT-67 (2001).
Marutani, Y., Fujimori, T., Riechelmann, D., Mizutani, T. and Mikami, M., 'Study on pre-vaporized and premixed gas turbine combustion technology for high carbon ratio fuel (HFRF)'. Oric. Int. Gas Turbine Congress 2003 Tokyo, Paper IGTC2003Tokyo TS-152 (2003).
Maughan, J.R., Warren, R.E., Tolpadi, A.K. and Roloff, T.P., 'Effect of initial fuel distribution and subsequent mixing on emissions from lean, premixed flames'. ASME Paper 92-GT-121 (1992).
McLerory, J.T., Smith, D.A. and Razdan, M.K., 'Development and engine testing of a dry low emissions combustor for allison 501-K industrial gas turbine engines'. ASME Paper 95-GT-335 (1995).
Miyasto, M.M., Flores, R.M., Samuelson, S.G. and McDonell, V.G., 'Response of a model GT combustor to variations in gaseous fuel composition'. ASME Paper 2000-GT-141 (2000).
Mkpadi, M.C., Andrews, G.E., Khan, I., Mohd Jaafar, M.N., Pourkashanian, M. and Yang, Y., 'Lean/lean staged low NO_x combustion for near stoichiometric gas turbine primary zone conditions'. ASME Paper 2001-GT-82 (2001).
Mularz, E.J., 'Results of the pollution reduction technology program for turbo-prop engineers'. NASA-TM-X-71911 (1976).
Myers, G., Couture, B., Tegel, D., Fitts, D., Setzer, F., Fiegl, M., Tuthill, R. and Bechtel, W. 'Dry low emission for the H heavy duty industrial gas turbine: Full scale combustion system rig test'. ASME Paper GT 2003–38193.
Nicol, D.G., Malte, P.C., Lai, J., Marinov, N.N. and Pratt, D.T., 'NO_x sensitivities for gas turbine engines operated on lean premixed combustion and conventional diffusion flames'. ASME Paper 92-GT-115 (1992).
Niedzwiecki, R.W. and Jones, R.E., 'The experimental clean combustor program description and status'. NASA TM-X-71547 (1976).

© Woodhead Publishing Limited, 2013

Ogata, M., Kajita, S., Kimura, T., Okuto, A., Doura, Y., Hihinuma, M., Fakatani, N. and Asano, Y., 'Development of a dry low NO_x combustor for a 650kW-class gas turbine'. Proc. Of the Int. Gas Turbine Congress 1999 Kobe, IGTC 99 Kobe TS-69. Vol. 2 p.767–773 (1999).

Okuto, A., Kitajima, J., Ogata, M., Ohga, S. and Kimura, T., 'An advanced development of second generation dry low NO_x combustor for 1.5MW gas turbine'. ASME Paper 96-GT-49 (1996).

Polifke, W., Dobberling, K., Sattlemeyer, T., Nicol, D. and Malte, P.C., 'A NO_x prediction scheme for lean premixed gas turbine combustion based on detailed chemical kinetics'. ASME Paper 95-GT-108 (1995).

Prade, B., Hermsmeye, H., Hoffman, S., Schmidt, U. and Krebs, W., 'V64.3A gas turbine natural gas burner development'. ASME Paper GT-2002–30106 (2002).

Puri, R., Stansel, D., Smith, D.A. and Razdan, M.K., 'Dry ultra low NO_x 'green thumb' combustor for allison's 501-K series industrial engines'. ASME Paper 95-GT-406 (1995).

Roberts, R., Peduzzi, A. and Vitti, G.E., 'Experimental clean combustor program-phase II, final report'. NASA CR-134969 (1976).

Rodriguez, J., Tanimura, S., Nose, M., Takiguchi, S. and Ishizaka, K., 'Advanced dry low NO_x combustor for mitsubishi G class gas turbines'. ASME Paper GT2008–50819 (2008).

Rohrbacher, B.J., 'Refurbishment of a solar centaur compresser set to meet european environment regulations'. ASME Paper 96-GT-276 (1996).

Rokke, N.A., Hustad, J.E. and Berg, S., 'Pollutant emissions from gas fired turbine engines in offshore practical measurements', ASME Paper 93-GT-170 (1993).

Rokke, P.E., Hustad, J.E., Rokke, N.A. and Svendsgaard, O.B., 'Technology update on gas turbine dual fuel, dry low emissions combustion systems'. ASME Paper GT2003–38112 (2003).

Rudey, R.A., 'Status review of NASA programs for reducing aircraft gas turbine engine emissions'. NASA-TM-X-71861 (1976).

Saitou, T., Inoui, H., Miura, K., Kobayashi, N. and Suzuki. S., 'Performance demonstration of the full size multi-cluster combustor for DME under real engine conditions'. ASME Paper GT2005–68647 (2005).

Sasao, T., Takehara, I., Hayashi, A. and Inage, S., 'Development of the new duel fuel type low NO_x combustor and the results of tis performance test'. Proc. Int. Gas Turbine Congress 2007 Tokyo, IGTC2007 Toyo TS-130 (2007).

Sattlemeyer, T., Felchlin, M.P, Haumann, J., Hellat, J. and Styner, D. (1990). Second generation low emission combustor for ABB gas turbines: Burner development and tests at atmospheric pressure. Proc. ASME Gas Turbine and Aeroengine Congress (1990), Brussels. ASME Paper 90-GT-162 and also in Trans. ASME, J. Gas Turbines and Power, Vol. 114, pp.118–124 (1992).

Saul and Altemark, D., European Gas Research Association, Gas '92 (1992).

Sawyer, R.F., AGARD CPP 125, 22:1–13 (1973).

Scarinci, T., Freeman, C. and Day, I., 'Passive control of combustion instabilities in a low emission aeroderivative gas turbine'. ASME Paper GT2004–53767.

Scholz, M.H.H. and Depietro, S.M., Field experience on DLN typhoon industrial gas turbine. ASME Paper 97-GT-61 (1997).

© Woodhead Publishing Limited, 2013

Sidwell, T., Casleton, K., Straub, D., Maloney, D., Richards, G., Strakey, P., Ferguson, D. and Beer, S., 'Development and operation of a pressurized optically-accessible research combustor for simulation validation and fuel variability studies'. Proc. of GT2005, ASME Turbo Expo 2005: Power for Land, Sea and Air. ASME Paper GT2005–68752 (2005).

Smith, D.A., Razdan, M.K. and Frey, S.F., 'Low emission combustion system for the allison ATS engine'. ASME Paper 97-GT-311 (1997).

Steele, R.C., Jorett, A. and Nicol, D., 'Variables affecting NO_x formation in lean premixed combustion'. ASME Paper 95-GT-107 (1995).

Steele, R.C., 'Passive control of combustion instability in lean premixed combustion'. ASME Paper 99-GT-052 (1999).

Spadaccini, L.J. and Szetela, E.J., 'Approaches to the prevaporiszed-premixed combustor concept for gas turbines'. ASME Paper 75-GT-85 (1975).

Streb, H., 'Development of the hybrid burner for gas turbines with an annular combustor'. Leeds University CPD Course on ultra low NO_x gas turbine combustion (2010).

Syed, K.J. and Buchanan, E., 'The nature of NO_x formation within an industrial gas turbine dry low emissions combustor', ASME Paper GT2005–68070 (2005).

Toh, H., Murayama, M. and Ikezaki, T., 'The performance of the low NO_x aero gas turbine combustor under high pressure'. ASME Paper 2001-GT-84 (2001).

Vedeshkin, G., Sverdlov, E., Goltsev, V., Doubovitsky, A. and Usenko, D., 'Low emission combustor developed for industrial gas turbine with NO_x/CO level <5ppm'. Proc. Int. Gas Turbine Congress 2007 Tokyo, IGTC2007 Tokyo TS-132 (2007).

Visser, B.M. and Levinsky, H.B., 'Premixed combustion in gas fired equipment', VDI Berichte 1090 (1993).

Visser, B.M. and Bahlmann, F.C., 'Variations in the NO_x emissions of gas turbines: Effects of air temperature, air humidity and natural gas composition'. ASME Paper 94-GT-261 (1994).

Wade, W.R., Shen, P.I., Owen, C.W. and Mclean, A.F., 'Low emission combustion for the regenerative gas turbine Pt.1 – theoretical and design considerations'. ASME Paper 73-GT-11 (1973).

Wheatley, C.K., Arellano, L.O., McDougald, N.K., Kendall, R.M. and Greenberg, S.J., 'Surface stabilized fuel injectors with sub 3ppm NO_x emissions for a 5.5MW gas turbine engine'. ASME Paper GT2003–38489 (2003).

Willis, J.D., Toon, I.J., Schweiger, T. and Owen, D.A., 'Industrial RB211 Dry Low Emission Combustor'. ASME Paper 93-GT-391 (1993).

Yamada, H, Takagi, H. and Hayeshi, S., 'Low NO_x emissions over an enlarged range of overall equivalence ratios by staging lean premixed tubular flame combustion'. Proc. of GT2005, ASME Turbo Expo 2005: Power for Land, Sea and Air. ASME Paper GT2005–68849 (2005).

Yamamoto, T., Kurosawa, Y., Tachibana, S., Yoshida, S., Shimodaira, K. and Suzuki, K., 'Conical flameholder with pilot burner for lean premixed combustion'. Proc. Int. Gas Turbine Congress 2003 Tokyo 2003, IGTC2003 TS-141 (2003).

Yuen, F.T.C. and Gulder, O.L., 'Lean premixed turbulent flame front structure and implications for modeling'. ASME Paper GT2010–23214 (2010).

© Woodhead Publishing Limited, 2013

Zeldovich, Ya B., 'The oxidation of nitrogen in combustion explosions'. *ACTA Physiochimica*, XXI, No. 6 (1946).

Zito, D., Bonzani, F., Piana, C. and Chiationi, A. 'Design validation on pressurized test rig of upgraded VeloNO_x combustion system for F-class engine'. ASME Paper GT2010–22256 (2010).

© Woodhead Publishing Limited, 2013

Index

abrasive blast cleaning, 584
acid cleaning, 583
acoustic forcing, 410
acoustic resonance, 730–3
Actionable Information, 533
adiabatic expansion process, 54, 57
adiabatic-isentropic process, 48, 60
adiabatic reversible process, 53
advanced component repair technology, 573, 579–623
  coating processes, 614–19
    CVD coating process schematic, 616
    diffusion coatings, 615–16
    overlay coating, 616–17
    TBC structure, 617
    thermal barrier coating (TBC), 617–19
  condition and remaining life assessment, 586–601
    computational methods, 601
    degradation mechanisms schematic, 592
    determination of reparablity, 587–92
    long-term creep prediction using the Larson-Miller time-temperature parameter, 588
    superalloy rejuvenation, 591
  incoming inspection, 582–4
    chemical cleaning processes, 583
    cleaning and degreasing, 582–3
    mechanical cleaning and surface preparation, 583–4
  metallurgical evaluation, 597–601
    chemical composition, 599
    hardness test, 599
    material sampling, 599
    mechanical properties, 599
    metallographic inspections, 600–1
    overall dimensions on shrouded blade, 598
    replication method, 599
    selection of blade areas for metallographic examination, 600
  non-destructive evaluation (NDE), 592–7
    dimensional inspection, 597
    eddy current inspection, 593–4
    eddy current inspection illustration, 594
    liquid penetrant inspection, 593
    methods, 593
    radiographic inspection, 595–6
    radiographic inspection illustration, 596
    thermography inspection, 596–7
    ultrasonic inspection, 594–5
    ultrasonic inspection illustration, 595
    visual inspection, 592
    visual inspection illustration, 594
  on-site assessment and inspection, 579–81
    checking dimensions and damage mapping, 579
    condition-based maintenance (CBM), 579–81
  preparation for repair, 584–6
    ceramic coatings removal, 585
    metallic coatings removal, 585
    stripping process schematic, 585
    verification of coating removal, 586
  quality control and final inspection, 619–23
    airflow test stand configuration, 621
    dimensional verification and final visual inspection, 622

© Woodhead Publishing Limited, 2013

advanced component repair technology (*cont.*)
flow testing, 620
frequency analysis, 621–2
moment-weight charting, 621
quality records, 622–3
repair process, 580, 601–13
braze compound composition examples, 609
brazing process, 609–11
coupon repair, 611
different heat and HIP treating during the repair process, 613
Gas Tungsten Arc Welding (GTAW), 602–9
Gas Tungsten Arc Welding (GTAW) illustration, 605
heat treating and HIPping, 611–13
heat-treatment diagram for precipitation strengthening in nickel-based, 612
high temperature brazing, 610
laser powder welding schematic representation, 608
LFW process schematic representation, 607
nominal composition of high-temperature alloys, 603–4
plasma transferred arc processes, 606
superalloy weldability, 605
welding process, 601–2
repair specification and vendor qualification, 581–2
advanced EV (AEV) burner, 727
Advanced Pulsation Control Logic (APCL), 165
Advanced Zero Emission Power Plant (AZEP), 705–6
schematic diagram, 705
Advisory Council for Aviation Research and Innovation in Europe (ACARE), 6, 20
aero-derivative, 31
gas turbines, 191
aero-engines, 28–31
turbofan engine, 30
turboshaft engine, 29
types, 28
aero-gas turbines, 716
aerodynamic/reduced speed, 104
aerodynamic speedlines, 105
aerodynamics, 193–202, 218–20
axial solidity of vanes and blades in F- G- and H-class turbines, 200
different shapes of blade tip winglets, 219
diffuser arrangement 1966 and modern GT, 202
diffuser pressure loss as function of turbine exit Mach number, 201
diffuser pressure recovery *vs.* area ratio, 202
last stage blade velocity triangles, 198
mean blade speed, 195
optimum axial solidity with typical angles for first stage vane, 199
Smith chart, 194
Smith chart location, 196
stage efficiency improvement due to profiled end walls, 219
turbine exit Mach number, 201
velocity triangles, 197
aeroengines, 241–2
air-cooled generators
higher ratings, 319–21
cooling approach using intercoolers, 321
cost savings, 321
inner stator frame, 320
steps in the development of large air-cooled turbogenerators, 319
air-cooled turbogenerators, 253
air excess ratio, 385
air/fuel ratio, 58–9
air plasma spaying (APS), 617
air separation unit (ASU), 687
air-side integration, 649
aircraft engines, 475

© Woodhead Publishing Limited, 2013

aircraft propulsion, 475
alkaline cleaning, 583
ALSTOM's reheat systems, 392
ammonia, 693
Ampere's law, 258, 261
Arrhenius temperature term, 400
Asset Management Cockpit, 532–3
ASTM D975 (2011), 644
ASTM D2880 (2010), 644
auto ignition, 393–4
autoignition temperature, 387, 665–6
  impact on combustion performance, 666–70
  stoichiometric mixture, 666
autoignition temperature (AIT), 394
autoignition time, 665–6
  various fuel and stoichiometric air-fuel ratio, 667
automatic voltage regulator (AVR), 249, 310–12
  electrical output monitoring, 311
aviation, 5–7
  efficiency developments since 6, 1960

Benedict Web Ruben equation, 441
Biot–Savart's law, 258–9
blade cooling, 83–4
blade weight reduction, 145–6
  application of composite material for compressor blading, 146
blading pressure ratio, 104
Blast Furnace Gas (BFG), 643–4
blasting, 584
blisk technology, 146–7
  application, 147
blow-out, 669–70
bolted rotor, 99
Brayton cycle, 427, 703–4
brazing process, 609–11
  braze compound composition examples, 609
  high temperature brazing, 610
  narrow gap brazing, 611
  overlay brazing, 611
brush-gear cubicle, 252
burner time lag, 412
bus ducts, 249
bushing, 248
bypass ratio (BPR), 480

Capstone, 27
carbon capture and storage (CCS), 18, 39, 511
  IGCC technology options, 647–50
carbon dioxide (CO_2) capture and storage
  capture technologies, 687–94
    pre-combustion, oxy-fuel and post-combustion processes, 688
  gas turbine systems, 685–711
    impact on current gas turbines, 694–700
    schematic diagram of CO_2 emissions, 686
  impact on current gas turbines, 694–700
    compressor and turbine, 698–9
    flue gas recirculation, 695–8
    hydrogen combustion, 694–5
    operation and control, 699–700
  implementation, 708–11
    absolute efficiency loss and net efficiency, 709
    capital investments and operational costs, 709–10
    demonstration, 711
    efficiency of CO_2 capture cycles, 708
    market introduction, 710–11
  novel approaches, 700–8
    carbon-neutral fuels, 708
    chemical looping, 706–7
    fuel cells, 707–8
    oxygen supply via membranes, 705–6
    semi-closed cycles with external oxygen supply, 701–4
carbon monoxide, 403–6, 511
carbon-neutral fuels, 708
Carnot cycle efficiency, 429
catalytic combustion, 733
CC-Matient cycle, 702

© Woodhead Publishing Limited, 2013

centre for remote monitoring and diagnostics (CMD), 533–59
combined cycle power plants, 547–59
actionable information, 548
condition monitoring and diagnostic system, 553
data fusion for CCPP, 551–3
data sources for data fusion, 552
electrical equipment condition analysis, 555
fluid condition analysis, 555
functional diagram of RM&D, 550
illustration of remaining-life-assessment procedure, 557
logic diagram for blade disposition, 558
mechanic and rotor dynamic condition analysis, 554–5
mechanical integrity and remaining-life assessment, 555–8
power plant monitoring and diagnosis vs control system, 549
RAM metrics, 558–9
thermodynamic condition analysis, 553–4
design process, 535–47
analysis of data and diagnosis inference in plant, 545–6
monitoring and diagnostic centre, 546
telecommunication system, 546
gas turbine system FMECA, 538–43
integration process for the key factor of power generation management, 534
chemical looping combustion (CLC), 706–7
schematic diagram, 706
chemical vapour deposition (CVD), 616
coating process schematic, 616
Chemkin flame kinetics model, 740
kinetics of CO and NO_x emissions, 741
chilled ammonia process (CAP), 693
CO_2 emission
reduction, 4–5, 10
reduction efficiency improvement, 10–11
sources of worldwide emissions, 5
Coke oven gas, 643–4
cold loss, 450
cold tones, 386
combined-cycle gas turbine (CCGT) plant, 10
combined cycle power plant (CCPP), 288, 384, 534
combined gas-steam cycles, 79–83
configurations of HRSG for combined cycles, 82
schematic diagram, 80
temperature-heat transferred diagram for single pressure HRSG, 81
combustion
dynamics, 407–15
change in time lag resulting from burner design with CBO, 412
feedback loop for thermo-acoustical pressure fluctuations in a combustor, 410
flame shape and strong temperature gradient, Plate XIV
pressure fluctuation signal, 409
parameters affecting, 651–70
fuel gases characteristics, 651–66
impact on combustion performance, 666–70
combustion dynamics protection system (CDPS), 678
combustion efficiency, 450
combustion oscillations, 668
combustor, 446–51
design principles, 153–62
can combustor layout with the Alstom LEC-III, 161
components making up the sub-5 ppm NO_x LEC-III combustion system, 161
cooling, 160–2
design, 156–60
EV and SEV single-row annular combustors in GT26 configuration, 158
EV double-row combustor in GT13E2 configuration, 159

© Woodhead Publishing Limited, 2013

main components of the GT24/GT26 EV combustor, Plate V
main components of the GT24/GT26 SEV combustor, 160
premix burner, 153–6
transition from a single-burner combustor via a multi-burner silo, 158
first gas turbine for power generation, 152
fuel flexibility, 179–84
future trends, 184–6
emission reduction, 184–5
engine firing temperature increase, 185
flue-gas recirculation concept, 185
fuel flexibility, 185–6
operational flexibility, 186
gas turbines, 151–86
operation, 162–79
GT13E2 APCL, 165
GT13E2 operation concept, 164
low load operation concept, 178–9
reheat combustion, 172–8
staged premix combustion, 165–72
combustor frequency, 412
combustor outlet temperature (COT), 83
combustor parts
materials and coatings development, 341–2
base materials, 342
coated parts in HGP, 341
combustor loading, 341
combustor materials, 342
combustor pressure drop, 193
compressibility factor, 48–9
compression, 427
compressor, 444–6, 698–9
characteristic parameters, 103–16
blading considerations, 106–16
general considerations, 103–6
map for a stationary gas turbine, 105
thermodynamic interfaces, 103
thermodynamic simulation by cycle performance tool, 106
design process, 135–41
concept phase, 137
design system, 141
manufacturing support process of discipline mechanical design, 141
mechanical design steps, 140–1
mechanical integrity steps, 138–40
model and drawing generation process of discipline mechanical design, 140
overall aerodynamic compressor blading design process, 139
overall blading design process, 138
overall mechanical integrity compressor blading design process, 139
possible design system setup to support development, 142
schematic diagram, 136
steps, 136–8
gas turbines system, 89–150
operational requirements, 116–35
additional requirements, 127–35
behaviour along quasi operating lines, 118
behaviour and requirements under load conditions, 116–20
dependencies of the aerodynamic speed in absolute terms, 118
gas turbine interaction with changed ambient conditions, 119
internal compressor load shift, 120
operating range requirements, 120–1
start-up requirements, 122–7
role, 89–90
stationary gas turbine compressor elements, 96, 98–103
technological trends and special features, 141–8
aerodynamically driven, 143–5
flow field along a straight and a bowed vane, Plate II
mechanical integrity and manufacturing, 145–8
profile boundary layer flow suction, Plate III
types, 90–6
basic, 90–1

© Woodhead Publishing Limited, 2013

compressor (*cont.*)
compressor types to suit mass flow and pressure ratio requirements, 90
drivers, 91
typical stationary gas turbine compressor data, 96
typical stationary gas turbine compressor systems, 91–5
compressor ageing, 129–30
pitting corrosion and consequential damage of a compressor blade, 130
compressor blading, 106–16
aerodynamics, 109–12
angle definitions, 110
detailed assessment, Plate I
mach number distributions, 112
aerodynamics of compressor stages, 106–8
aerodynamic stage parameter, 108
thermodynamic blade/vane loading balance parameter, 108
thermodynamic stage parameter, 107
geometry
parameter, 109
manufacturing, 115–16
CAM models for fast and reliable milling processes, 116
manufacturing process, 147–8
preforged and a milled compressor blade, 148
mechanical design, 114–15
complete compressor blading row, 115
mechanical integrity, 112–14
assessment, 113
assessment including dynamical forces/Haigh diagram, 114
compressor cleaning, 128–9, 623–8
abrasive method, 624
air-fluid ratio vs engine power for state of the art washing systems, 627
economics, 627–8
fouling and washing effects on gas turbine, 628
fouling effects on heat rate, 624
manual cleaning, 624
nozzles location for on-line washing system, 626
off-line process, 625
off-line washing, 625
off-line washing system, 625
on-line washing, 626–7
online wash nozzle location, 628
compressor damage, 130–1
compressor efficiency, 61
compressor fouling, 128–9
compressor icing, 127
compressor performance degradation, 131–2
vs. equivalent operating hours, 132
compressor power, 96
compressor surge, 132–5
aerodynamic flow limits for a typical compressor blading section, 133
aerodynamic flow structure during rotating stall of compressor blade, 134
underfrequency/surge protection scheme, 135
compressor variable stators (VSV), 508
Computational Added Manufacturing (CAM), 115
computational fluid dynamics (CFD), 239
concentrated solar power (CSP), 16
condensates, 647
condition assessment, 586
condition-based maintenance (CBM), 579–81
condition monitoring, 527
constructed blade, 340
continuous emissions monitoring system (CEMS), 678
control system, 674–8
adaptations to improve fuel flexibility, 675–6
controlled diffusion airfoil (CDA), 111, 142
convective cooling, 203, 213
cooling, 160–2, 202–7, 220
aero-engine cooling effectiveness over heat load parameter, 205

© Woodhead Publishing Limited, 2013

aero-engine cooling technology, 203
aero-engine evolution of material surface temperature, 204
calculated temperatures and thermal paint results from a liner segment, Plate VI
casted-metal liner segments, 162
cyclic thermal loading pattern in sector tests, 163
five stage turbine layout and cooling systems, 208
high pressure rig for liner segments, 163
sealing geometry for liner segments, 164
cooling effectiveness, 206
cooling efficiency, 206
cooling gas circuit, 305–7
Corex gas, 643–4
cracks, 588
creep, 207, 453
critical turn down ratio, 406
criticality, 537
crude oil, 646

damage severity, 588–9
Damkohler number, 669–70
Data Acquisition System (DAS), 547
data fusion, 526
data mining tools, 526
data processing and validation, 525
de Haller number, 111
density, 679
design-point modelling, 424–6
first law of thermodynamics, 425
second law of thermodynamics, 425–6
deviation angle, 110
diesel, 644, 646, 679
diffusion coatings, 615–16
diffusion combustion, 651
dimensional inspection, 597
disc rotor, 102
distillation range, 679–80
distributed control system (DCS), 547
Dry Low Emission (DLE) combustion system, 505
dry low NO_x (DLN), 17

e-maintenance, 560–1
E-Matient cycle, 701
Econamine FG Plus, 693
economy-of-scale, 36
eddy current
inspection, 593–4
losses, 260
efficiency, 274–6
contributions of the various losses, 276
efficiency improvement, 143
efficient production index (EPI), 553
electric systems, 40
electrical generator protection, 310–12
electrical output monitoring, 311
electrical output, 310
electricity generation, 248–51
electrical energy generation, 248
single-shaft combined-cycle sets, 250
electro-slag remelting (ESR), 372
electromagnetic loading, 272–4
electron-beam physical vapour deposition (EB-PVD) TBC, 619
electron-beam welding (EBW), 608–9
emission, 666–8
Emission Index, 716, 759
EN437, 638
ENCAP project, 695, 700
Enet, 498
engine firing temperature, 185
enthalpy, 46
entropy, 426
EnVironmental (EV) burner, 154–5, 724–7
EnVironmental (EV) combustor, 157, 159–60
equation of state, 46
equivalence ratio (EQR), 384
equivalent operating hours (EOH), 525
Ericsson cycle, 474
esentropic efficiency, 432
European Industrial Emissions Directive, 716
event tree analysis (ETA), 536
excitation current, 251–2
exciter, 303
exhaust systems, 457–61
exit Mach numbers, 196, 200

© Woodhead Publishing Limited, 2013

factored starts, 567, 568
failure modes, effects and criticality analysis (FMECA), 536
failure modes and effects analysis (FMEA), 536
fan pressure ratios (FPR), 480
fault tree analysis (FTA), 536
Fenimore mechanism, 398
field winding, 249, 251
film cooling, 205, 646
film cooling effectiveness, 206
Finite Element Analysis (FEA), 411, 601
'first generation' single crystal superalloys, 337
first-order ordinary differential equations, 500
Fischer-Tropsch, 641
flame speed, 387
flame stabilisation, 387–97, 764
  auto ignition delay time, 395
  combustor inlet temperature, 394–5
  combustor pressure, 395
  flame propagation, 387–93
    challenges involved in stabilising a flame, 390
    characteristic engine operation points ignition, FSNL and base load, 388
  fuel/air stoichiometry, 396
  fuel composition, 395–6
  self- or autoignition, 393–4
flame temperature, 661
flamelet modelling, 742, 744
FlameSheet, 156, 160, 168
flashback, 669
flow compatibility equation, 503
flow factor, 107
flow testing, 620–1
  air-cooled blade, 621
  air-cooled vane, 620–1
  combustion liner, 620
  fuel nozzle, 620
flow turning, 109
FLOX burner, 778
flue gas, 692
  recirculation, 695–8
    increase in CO content, 698
    O_2 and CO_2 at exhaust of a reheat gas turbine, 697
    reduction of O_2 concentration and NO_x emissions, 697
    schematic of gas recirculation, 696
fluid flow analysis, 238–40
Fnet, 497
free power turbine, 486
Froude efficiency, 477
fuel
  gases characteristics, 650–73
    composition of gaseous fuels and their properties, 652–3
    fuel parameters and affected operability issues, 655
    parameters affecting combustion, 651–70
    parameters affecting gas turbine operation, 670–3
  primary, characterisation, 636–7
fuel-air ratio, 448
fuel bound nitrogen (FBN), 734
fuel cells, 707–8
  schematic diagram, 707
fuel flexibility, 179–84, 185–6
  gas turbine system, 635–82
    fuel gases characteristics, 650–73
    fuels directly introduced in gas turbine burners, 637–47
    future trends, 680–2
    integrated gasification combined cycle (IGCC) technology and carbon capture and storage (CCS), 647–50
    liquid fuel characteristics, 678–80
    primary fuel characterisation, 636–7
  operation range for fuel gases, 673–8
    approaches of different manufacturers, 674–8
    overview, 673–4
    typical parameter range for NG-like fuels, 673
fuel oil, 183, 644, 646
fuel reheating, 228
fuel spectrum, 39
furnace cycling test (FCT), 360

© Woodhead Publishing Limited, 2013

gamma prime formers, 329
gas compression, 486
gas-cooled turbogenerators
  higher ratings, 321–2
    losed air cooling (TEWAC), 322
gas cooling casting (GCC), 339
gas index, 659–60, 677
Gas Tungsten Arc Welding (GTAW), 602–9
gas turbine, 3–20
  adaptive model-based control, 504–9
    control strategy for DLE combustion using single combustion stage requiring the use of blow-off, 507
    control strategy for DLE combustion using single combustion stage without the use of blow-off, 509
    effect of decreasing the power turbine area on the GG pressure ratio, 507
    running line on the compressor characteristic for two-shaft gas turbine, 506
  asset and performance management, 515–61
    centre for remote monitoring and diagnostics (CMD), 533–59
    e-maintenance and future trends, 559–61
    gas turbine in projected power generation, 517
    gas turbine system FMECA, 538–43
    hot gas path management, 523–33
    hot gas path section, 517
    new competitive arena for power generation, 516
    pathways to achieve advanced thermal power plants, 559
  combustors, 151–86
    design principles, 153–62
    first gas turbine for power generation, 152
    fuel flexibility, 179–84
    future trends, 184–6
    operation, 162–79
  component characteristics, 483–6
    axial compressor showing first and last stages, 484
    compressor characteristic, 485
    flow turbine characteristic when NGVs are choked, 485
    turbine efficiency characteristic, 486
compressors system, 89–150
  characteristic parameters, 103–16
  design process, 135–41
  optional requirements, 116–35
  role, 89–90
  stationary gas turbine compressor elements, 96, 98–103
  technological trends and special features, 141–8
  types, 90–6
degradation, 518–23
  effect on a single-shaft engine operating line, 521
  effect on map, 521
  effect on single-shaft engine, 521, 522
  effect on two-shaft engine operating line, 522
  single-shaft engine operating line, 520
  two-shaft engine operating line, 519
design-point performance modelling, analysis and performance optimisation, 464–74
  intercooled, reheat and regenerative cycle, 472–4
  intercooled cycle, 467–9
  performance as carpet plot for regenerative gas turbine cycle, 467
  performance of practical simple gas turbine cycle, 465
  regenerative cycle, 466–7
  reheat cycle, 469–72
  schematic representation of intercooled, reheat and regenerative cycle, 473
  schematic representation of intercooled gas turbine, 469
  schematic representation of regenerative gas turbine cycle, 466

© Woodhead Publishing Limited, 2013

gas turbine (*cont.*)
schematic representation of reheat gas turbine, 471
simple cycle, 464–6
temperature-entropy diagram for ideal, reheat gas turbine cycle, 471
temperature-entropy diagram of ideal, intercooled gas turbine, 468
variation of thermal efficiency with specific work for practical intercooled, reheat and regenerative cycle, 474
variation of thermal efficiency with specific work when optimised for maximum specific work, 473
variation of thermal efficiency with specific work when optimised for maximum thermal efficiency, 472
design-point performance modelling of are gas turbines, analysis and optimisation, 474–83
schematic representation of turbo-fan, 479
schematic representation of turbo-jet, 475
schematic representation of turbo-propeller engine or turbo-prop, 483
turbo-fan, 479–82
turbo-jet engine, 475–9
turbo-props or propeller turbine engines, 482–3
variation of SFC with fan pressure ratio for an unmixed and mixed turbo-fan, 480
variation of SFC with specific thrust of turbo-jet, 478
variation of specific thrust with fan pressure ratio for an unmixed and mixed turbo-fan, 481
determining component performance using specific heats, 463–4
efficiency improvement, 11–16
hybrid cycles, 16
technology and system efficiency, 13–16
total life cycle costs, 11–13
emissions variations, 397–407
averaged energy of activation for the CO oxidation, 404
carbon monoxide, 403–6
CO emission of perfectly premixed flame, 405
fundamental limitation for lean premixed combustion systems, 407
low NO and CO_x and CO emission (turndown operation range), 406
nitrogen oxides, 397–403
NO_x emission, 400
progress of temperature, CH_4 as educt, CO as intermediate species and CO_2 as product of CH_4(temp)/air reaction, 403
engine configurations, 486–91
schematic representation of three-shaft gas turbine, 488
schematic representation of two-shaft gas turbine, 488
three-shaft free turbine gas turbine, 487
triple spool high bypass turbo-fan engine, 490
twin spool high bypass turbo-fan engine, 489
twin spool low bypass mixed turbo-fan engine, 490
two-shaft gas turbine operating with free power turbine, 487
two-shaft turbo-prop operating with free power turbine, 490
heat exchangers and recovery processes, 224–46
applications, 241–2
cycle efficiency *vs.* cycle pressure ratio and load performance for turbine cycles, 226
future trends, 242–3
heat exchange processes, 225–8
heat transfer equipment, 228–39
recuperated simple gas turbine cycle, 225
ideal simple gas turbine cycle, 427–31
effect of pressure ratio on temperature-entropy diagram, 430

© Woodhead Publishing Limited, 2013

gas turbine cycle on temperature-entropy diagram, 428
PV diagram, 428
schematic representation, 428
variation of thermal efficiency and specific work with compressor pressure ratio, 431
importance for aviation sector, 5–7
efficiency developments since 6, 1960
importance for CO_2 reduction, 4–5
sources of worldwide emissions, 5
importance for power generation sector, 7–11
electricity production by fuel type (2010 and 2035), 7
maintenance and repair of components, 565–630
advanced component repair technology, 573, 579–623
compressor cleaning, 623–8
future trends, 628–30
outage cycle, 569–73, 574–8
outage quality scorecard, 574–8
maintenance factors, 566–9
failure modes for HGP components, 567
life-limiting factors for HGP components, 566
maintenance interval for hot gas path inspection, 568
market trends, 19
materials and coatings development, 327–80
ceramics for hot gas path parts, 370–2
coatings for hot gas path parts, 342–70
combustor parts, 341–2
nomenclature, 379–80
rotor parts, 372–4
turbine parts, 327–41
off-design performance behaviour, 500–4
characteristics of turbines operating in series, 503
running line on the compressor characteristic for a two-shaft gas turbine, 504
series of running lines due to power and ambient temperatures, 502
off-design performance prediction, 491–6
operation and combustion performance issues, 383–420
catalytic combustion, 417–20
efficiency increase, 417
flame stabilisation mechanisms, 387–97
future trends, 415–20
NO_x emissions calculated from a kinetical model of combustor, 419
parameters that highlight the operational challenges of gas turbine combustion systems, 386
simplified sketch of an EGR cycle, 416
wide range of operational conditions required for gas turbine combustors, 385
performance modelling, analysis and optimisation, 423–512
design-point modelling of gas turbine cycles, 424–6
future trends, 510–12
steady flow energy equation, 426
reversibility and efficiency, 431–41
compressor and turbine irreversibility and efficiency, 431–6
effect of irreversibilities during compression and expansion on thermal efficiency, 436–40
effect of pressure losses during heat addition and heat rejection, 440–1
gas turbine cycle on temperature-entropy diagram when irreversibilities are present, 437
polytropic process of multistage compressor, 433
temperature-entropy diagram for practical simple gas turbine, 440
variation of isentropic efficiency with pressure ration for a polytropic efficiency of 0.87, 436

© Woodhead Publishing Limited, 2013

gas turbine (*cont.*)
variation of thermal efficiency with pressure ratio of simple cycle gas turbine, 438
technology trends, 16–19
fuel and operational flexibility, 17–18
NO_x reduction, 17
reliability and availability, 18–19
thermodynamic modelling of components applicable for practical gas turbine cycles, 444–63
combustor, 446–51
compressor, 444–6
fuel gas composition made up of hydrocarbons and inert components, 448
heat exchangers and coolers, 461–3
turbines, 451–61
thermophysical properties of air and combustion products, 441–4
coefficient for calculation the specific air and products of combustion, 442
composition of dry air on gravimetric basis, 443
transient performance modelling, 496–500
boundary conditions, 499–500
diving flow or blow-off element, 497
elemental representation of single shaft gas turbine, 497
turbogenerators, 247–325
component design, 251–76
design concept, 294–312
development, 312–18
development history, 276–94
future trends, 322–5
overview, 247–51
recent developments, 318–22
turbogenerators developed for, 284–90
60 MVA generators, 286
4 MW prototype, 284
ABB air-cooled generator, 291
air-cooled turbogenerator range, 287
ALSTOM air-cooled generator, 290
BBC air-cooled series, 287
compact overhung exciter in an ALSTOM air-cooled generator, 291
development steps of the small air-cooled range, 290
dual-shaft sequential-combustion gas turbine plant, 285
French designs, 288–9
overall design, 287–8
static starting system, 288
Swedish designs, 289
transportation and installation, 288
transportation by flatbed cars, 289
transversal arrangement of the coolers, 288
types and applications, 21–40
advantages and limitations, 36–8
aero-engines, 28–31
application *vs.* power output, 22
future trends, 38–40
global production, 22
industrial turbines, 31–5
large combined cycle power plant, 37
microturbines, 35–6
power generation, 23–7
variation of thermal efficiency with specific work for practical intercooled gas turbine
when LP compressor pressure ration is optimised for maximum specific work, 470
when optimised for maximum thermal efficiency, 470
with intercooled compressor, 72–5
schematic diagram, 72
T-s diagram intercooled compression, 73
T-s diagram of an intercooled compression ideal cycle, 74
T-s diagram of an intercooled compression real cycle, 75
T-s diagram of cycle II of an intercooled compression real cycle, 75

© Woodhead Publishing Limited, 2013

with reheat, 75–7
schematic diagram, 76
T-s diagram of cycle II of reheated real cycle, 77
T-s diagram of the reheat real cycle, 76
gas turbine cycles, 40
blade cooling, 83–4
combined gas-steam cycles, 79–83
fundamentals, 44–85
future trends, 84–5
improvements, 64, 66–79
gas turbine with intercooled compressor, 72–5
gas turbine with reheat, 75–7
recuperated gas turbine, 67–72
wet cycles, 77–9
Joule–Brayton cycle, 50–64
thermodynamic properties, 46–50
gas turbine efficiency, 81
gas turbine life cycle cost, 565
gas turbine performance, 565
gas turbine system
carbon dioxide capture and storage, 685–711
capture technologies, 687–94
impact on current gas turbines, 694–700
implementation, 708–11
novel approaches, 700–8
fuel flexibility, 635–82
fuel gases characteristics, 650–73
fuels directly introduced in gas turbine burners, 637–47
future trends, 680–2
integrated gasification combined cycle (IGCC) technology and carbon capture and storage (CCS), 647–50
liquid fuel characteristics, 678–80
operation range for fuel gases, 673–8
primary fuel characterisation, 636–7
ultra-low NO_x emissions, 715–81
acoustic resonance and catalytic combustion, 730–3
impact of fuel-and-air mixing quality on thermal NO_x, 763–5
influence of air inlet temperature, 765–8
influence of mixing on thermal NO_x, 758–63
NASA Clean Combustor Programme, 718–30
predictions of thermal NO_x, 747–58
prompt NO_x, 740–7
reference velocity and Mach number, 768–80
thermal NO_x formation, 734–9
gas unit, 310
gaseous fuel, 636
types and characteristics, 638–44
composition bandwidth of gaseous fuel, 639
gearbox, 483
generator active power output, 310
generator speed, 295
generator terminals, 248
global vacuum pressure impregnation, 255–6
GR13 reaction mechanism, 401
grain boundary strengtheners, 329
Graz cycle, 702–3
greenhouse gas (GHG) emissions, 685–6
GRI NO_x kinetics scheme, 740, 746
grid stabilisation, 39–40
grid voltage, 249
GT24/26, 27

hazard and operability studies (HAZOP), 536
heat exchange, 225–8
fuel reheating, 228
heat recovery steam generator (HRSG), 227–8
inlet cooling, 225–7
intercooling, 227
recuperators, 227
reheat, 227
heat exchanger
applications, 241–2
coolers, 461–3
performance curve of typical coun-

© Woodhead Publishing Limited, 2013

heat exchanger (*cont.*)
ter flow heat exchanger, 463
schematic representation of heat exchanger, 461
future trends, 242–3
gas turbines, 224–46
heat exchange processes, 225–8
heat transfer equipment, 228–39
heat exchanger sizing, 240
heat load parameter, 206
heat recovery
applications, 241–2
future trends, 242–3
gas turbines, 224–46
heat transfer equipment, 228–39
heat recovery steam generator (HRSG), 79–3, 227–8, 384
heat release zone, 26–7
heat transfer
equipment, 228–39
intercoolers, 233–40
recuperators, 228–32
recuperators vs. regenerators, 233
rotary generators, 233
numerical methods, 238–40
heat transfer coefficient (HTC), 213
heavy fuel oil ; *see* marine diesel
high cycle fatigue, 209, 211
high fogging application, 89, 93–5
actual demonstration, 95
gas turbine power gain, 95
process chart, 95
high temperature brazing, 610
hot corrosion, 589
hot gas path, 565
BM/LPPS BC/APS TBC and BM/APS BC and APS TBC, 344
ceramics for parts, 370–2
coated parts, 342–3
coatings for parts, 342–70
engine experience, 365
CMAS deposit on TBC, 370
coating parameters of parts from different turbine stages, 369
coating parameters of parts from same turbine stage, 368
hot corrosion attack of BC/TBC, 369
stiffness and temperature at TBC surface, 368
strain-to-failure of 4-point-bend samples, 367
MCrAlY as protective coating, 343–51
coating consumption, 345–7
comparison of experimental results with prediction, 350
consumption of coating due to oxidation and interdiffusion, 346
consumption of coating due to oxidation in lab furnace, 347
future coatings for superalloys, 348–51
reactive elements effect on oxidation of beta phase containing NiCoCrAlY coatings, 350
thermo-mechanical behaviour, 347–8
thermo-mechanical loading of coated turbine blade, 348
TMF of 200μm thick MCrAlY coating, 349
TMF test samples, 349
TMF test samples with same MCrAlY coating, 349
validation of coating consumption based on assessment of blades, 347
TBC coated substrate, 351–65
coating system after operation, 355
cross section of coating system after operation, 354
effect of TBC coated substrate, 365
effect of TBC on material temperature and heat flux, 352
FCT results for samples machined from ‘engine ready’ turbine blades, 361
influence of BC thickness and BC roughness on TBC lifetime, 363
influence of BC thickness and TBC thickness on TBC lifetime, 363
lifetime prediction, 359–62
optimised BC/TBC system for blading, 362–5
role and limitation of the BC, 354–8
role and limitation of the TBC,

© Woodhead Publishing Limited, 2013

358–9
TBC material and microstructure, 359
TBC thickness influence on time to TBC spallation, 364
TBC thickness range, 364, 366
temperature dependence of FCT results for samples, 361
temperature dependence of residual stress of the TGO and thermal expansion of MCrAlY, 356
temperature profile through the wall of cooled GT part, 351
TGO and BC depletion zone thickness of spalled TBC samples, 362
TGO thickness on rough MCrAlY coating, 355
thermal strain of relaxed BM/BC/TBC, 353
ternary equivalent composition blading base material and coating, 345
hot gas path management, 523–33
data fusion architecture, 527
data fusion system with interconnections via WAN, 528
level 1: sensor level, 523–4
level 2: control and supervision level, 525–7
level 3: condition monitoring, 527–9
level 4: performance and health assessment, 530
level 5: prognostics, 531
level 6: decision support, 531–2
level 7: Asset Management Cockpit, 532–3
power generation asset and performance management, 523
hot isostatic pressure treatment (HIP), 340
hot tones, 386
humid air cycles (HAT cycles), 79
hybrid cars, 40
hybrid cycles, 16
efficiency improvement of gas fired CC and coal-fired IGCC and combination with fuel cells, 16
hydrocarbon dew point, 671
hydrogen, 511, 642–3, 739
hydrogen /water-cooled turbogenerators, 306
hydrogen combustion, 694–5
hydrogen-cooled generators, 305, 308
hydrogen-cooled units, 296–7
schematic diagram, 297
hydrogen management, 308–10
drain oil flow, 309
gas unit, 310
generator housing, 308
single-circuit seal, 309
hydrogen sulphides, 672–3
hydrogen/water-cooled units, 298

idle operating line, 105
ignition delay time, 394
incidence angle, 110
indirect-cooled windings, 299–300
industrial gas turbines, 31–5, 188–220, 241
aerodynamics, 193–202
combined heat and power, 34–5
schematic diagram, 35
cooling, 202–7
durability and damage, 207–12
Campbell diagram for uncoupled and coupled blades, 212
creep strain relation, 208
failure mechanism and sensitivity, 210
future trends, 218–20
aerodynamics, 218–20
cooling and manufacturing, 220
GT Pressure ratio, 189
interfaces and integration, 192–3
combustor, 192–3
secondary air systems (SAF), 192
mechanical drives, 33–4
schematic diagram, 34
parts and interfaces, 212–17
aero-engine (Rolls-Royce) evolution, 215
aero-engine (Rolls-Royce) front stage rotating blade cooling scheme, 215
aero-engine (Rolls-Royce) front stage vane cooling scheme, 216
General Electric front stage heat

© Woodhead Publishing Limited, 2013

industrial gas turbines (*cont.*)
shield, 217
GT26 LPT front stage vane, Plate XII
internal cooling feature, 214
Siemens first stage unshrouded blade and Alstom front stage blade, 216
schematic diagram, 31
surface transport, 32–3
marine propulsion systems, 32
turbine exhaust temperature, 190
turbine inlet temperature, 189
infrared thermography, 240
inlet cooling, 225–7
inlet fogging application, 89, 93–5
actual demonstration, 95
gas turbine power gain, 95
process chart, 95
inlet guide vane (IGV), 102, 106, 384
inlet Mach number, 110
intake systems, 454–7
integrated fuel gas characterisation (IFGC) system, 677–8
schematic diagram, 678
integrated gasification combined cycle (IGCC), 416, 511, 689
plant, 9, 19
technology, 647–50
potential air extraction or compressor adjustment requirements, 650
integrated reforming combined cycle (IRCC), 689
intercooled compressor, 72–5
intercoolers, 233–40
heat exchanger sizing procedure, 240
thermal-hydraulic characteristics, 236–7
primary surface cross wavy corrugated plates, 237
types, 234–6
tube-fin heat exchanger layout, 234
intercooling, 14, 227
application, 93
actual demonstration, 94
process chart, 94
internal microstructural damage, 588
isentropic efficiency, 458
isentropic index, 502
isentropic pressure ratio, 445
isentropic stagnation enthalpy, 456
ISO 4261 (1993), 644
ISO Turbine inlet temperature (TIT_{ISO}), 83

JMatPro modelled phase, 331
Joule–Brayton cycle, 50–64
closed gas turbine cycle, 51
ideal cycle, 53–6
different pressure ratios, 55
ideal efficiency *vs.* pressure ratio, 57
specific work *vs.* pressure ratio, 55
open gas turbine cycle, 51
real cycle, 56–64
evolution of TIT with cooling techniques, 65
ideal and real efficiency of gas turbines, 63
improvements of gas turbine nozzles and blades material temperature, 64
increase of compressor pressure ratio, 65
minimum compressor efficiency vs. pressure ratio, 62
pressure ratio for maximum power output *vs.* TIT, 66
T-s diagram, 58
T-s diagram, 51
Joules cycle, 427

KA plants, 288
kinematic viscosity, 679
KS-1, 693

laminar flame speed, 661–5
burning velocity for CH_4, H_2 and CO, 662
burning velocity for H- and L-type natural gas, LNG and propane *vs* CH_4, 663
chemical reaction times, 664
large air-cooled generators, 305
cooling principles, 306
large air-cooled units, 296
schematic diagram, 297
large eddy simulation (LES), 411

© Woodhead Publishing Limited, 2013

Larson-Miller parameter, 587
laser fusion welding (LFW), 607
laser powder welding (LPW), 607–8
laser welding, 606–7
Laves phases, 331
lean blow-out, 26
lean/lean-fuel staged approach, 733
lean premixed combustion, 651
lean premixed prevaporised combustion, 679
lean prevaporised premixed mode, 396
LEC-III, 160, 168
Lenz's law, 258
L'Hôpital's rule, 435
life-cycle costs (LCC), 561
linear cumulative damage, 468
linear damage summation model, 568
linear life fraction, 568
liquid crystal thermography (LCT), 240
liquid fuel, 636, 637, 681–2
  characteristics, 678–80
    impact on fuel and combustion system performance, 680
    parameters affecting combustion, 679–80
    properties and impact on combustion system performance, 680
  types and characteristics, 644–7
    characteristics of selected liquid GT fuels, 645
liquid metal cooling (LMC), 339
liquid penetrant inspection, 593
LNG, 638
loading operating line, 105–6
low calorific gases, 183–4
  EV burner for combustion of syngas fuels, 183
  single burner design, Plate XI
low-LHV gas, 640
low load operation concept, 178–9
  FlameSheet and conventional 501FD2 emissions, 179
  GT24/GT26 engi, 178
low pressure plasma spraying (LPPS), 617
lower heating value, 449
LP compressor pressure ratio, 480
LPG, 638, 640
Mach number, 459
  combustor residence times and choice of reference Mach number, 776–7
    combustor design parameters for central flame stabiliser, 777
  heat release per cross-sectional area, 778–9
  influence of combustor length and post flame residence time, 779–80
    flame residence time, 779
  pressure loss and, 770–2
    influence of mean residence time on NO_x emissions, 772
  residence time and, changes with primary dilution air flow split, 773–5
    primary zone conditions for different proportions of combustion air, 775
    primary zone conditions of combustion air for 1700K turbine entry temperature, 775
    primary zone conditions of combustion air for 1800K turbine entry temperature, 775
    primary zone conditions of combustion air for 1950K turbine entry temperature, 775
    Primary Zone Reference Velocities, 774
marine diesel, 646
Markov analysis (MA), 536
mass flow function, 206
mass flow variation range, 91
material degradation, 590
maximum cycle temperature, 59
Maxwell's equations, 257
mechanical drives, 486
mechanical shaft speed, 91
methane, 688–90
microturbines, 35–6, 241
  schematic diagram, 36
mild combustion systems, 418
Monkmon-Grant parameter, 587
monoethanolamine (MEA), 693
multi-pass blade, 216–17

© Woodhead Publishing Limited, 2013

multi-pass cooling, 213
multi-shaft application, 92–3
  actual demonstration, 93
  process chart, 93

naphtha, 647
narrow gap brazing, 611
NASA Clean Combustor Programme, 718–30
  axial swirlers in a combustor, 722–3
    axial swirler fuel stage combustor, 723
    axial swirler in a cylindrical combustor, 724
    axial swirlers with a short downstream mixing passage, 723
  conical two slot grid stabiliser, 724–8
    advanced EV burner (AEV), 728
    EV burner, 726
    improved EV burner with better premixing and lower NO_x, 727
    NO_x emissions as a function of engine power for AEV burners, 728
    TE burner, 727
  double and triple annular swirl combustors, 721
    LM6000 44MW Industrial gas turbine with axial counter-rotating swirlers, 722
  grid-plate type flame stabilisers, 723–4
    conical grid-plate well-mixed flame stabiliser, 725
    stabiliser with Multicluster burner, 725
  large high airflow axial swirlers, 719–21
    CFD predictions of flame temperature contours, 721
    conventional axial swirler, 719
    fuel injection through the swirl-blade surface, 720
    hybrid burner with large axial and central pilot swirler, 720
  NO_x combustor designs, 718
  radial swirlers, 728–30
    radial swirler premixing nozzle (RSPN) with downstream mixing throat, 732
    swirler low NO_x combustor, 732
    swirler with outlet throat 76 mm wall fuel injection, 731
    swirler with vane passage fuel injection, 729
    used in a 250 kw gas turbine, 730
natural gas, 180–2, 637, 638, 680–1, 734
  C2+ operation concept for reheat engines, 181
  FlameSheet full-scale high pressure rig results operations, 182
  GT26 fleet C2+ concentrations and Wobbe index variations, Plate X
  Wobbe index range according to European standard EN437, 640
Newton Raphsons, 494
Newton's method of approximation, 494
Newton's second law of motion, 500
Ni-base superalloys, 328–35
nitrogen oxides, 397–403
noise reduction, 145
  by leaned vanes, Plate IV
non-destructive evaluation (NDE), 592–7
normal base-load start, 567
normalised aerodynamic/reduced speed, 104
normalised blading pressure ratio, 104
normalised polytropic blading efficiency, 105
normalised reduced inlet mass flow, 104
NO_x emission, 648
  environmental problems, 715–17
  gas turbine thermal efficiency and turbine entry temperatures, 717
  influence of air inlet temperature, 765–8
    400, 600, 740 and 900 K for 40 mm outlet radial swirlers, 767
    grid mix flame stabiliser, 769
    large 76 mm outlet diameter radial swirlers, 768
    NO_x emissions as a function of inlet temperature, 764
  influence of residence time in premixed combustion, 768–80
    circular mixing tube radial swirler,

© Woodhead Publishing Limited, 2013

772
combustor residence times and choice of reference Mach number, 776–7
four hole slot shaped grid-plate flame stabiliser, 769
heat release per cross-sectional area related to the M_1, 778–9
influence of residence time at constant flame stabiliser pressure loss, 772–3
Mach number influence on NO_x, 773
mean residence time influence on NO_x, 768–70
pressure loss and Mach number influences, 770–2
residence time and, changes with primary dilution air flow split, 773–5
prompt NO_x, 740–7
reduction control, 17
thermal NO_x formation, 734–9
fuel effects on flame temperature and NO_x, 738–9
NO conversion to NO_2, 735–6
pressure dependence, 736–8
thermal, prompt and FBN NO_x formation routes, 734
thermal NO_x formation kinetics, 734–5
ultra-low, gas turbine systems, 715–81
acoustic resonance and catalytic combustion, 730–3
impact of fuel-and-air mixing quality on thermal NO_x, 763–5
influence of air inlet temperature, 765–8
influence of mixing on thermal NO_x, 758–63
NASA Clean Combustor Programme, 718–30
predictions of thermal NO_x, 747–58
nozzle guide vanes (NGV), 506
nozzle velocity coefficient, 460
number of transfer units (NTU), 462
off-line cleaning, 128–9
on-line cleaning, 128
on-line data acquisition, 525
operating line, 117
operating range, 120–1
compressor surge line, 121
requested underfrequency, 121
outage cycle, 569–73, 574–8
execution, 571–2
fishbone analysis, 573
kick-off meeting, 571
operational and maintenance data, 572
outage quality scorecard, 574–8
planning and initiation, 570
post-outage review, 572–3
process, 570
recording operational and maintenance data, 571
scheduling and preparation, 570–1
outer flow channel, 100
outlet guide vane, 106
overall pressure ratio (OPR), 14
overheating, 669
overlay brazing, 611
overlay coating, 616–17
oxidation, 209
oxy-firing, 690
oxy-fuel combustion, 690–1
semi-closed oxy-fuel combustion combined cycle (SCOC-CC), 691
oxygen, 705–6
ozone, 715

part load behaviour extension, 143–4
partial air-side integration, 649
partially premixed mode, 396
partially recuperated cycle, 70
particle image velocimetry (PIV), 240
Peng Robinson equation, 441
Petri net analysis, 536
PHACOMP, 331
Pilling-Bedworth ratio (PBR), 356
piloting, 391
plant gas chromatograph, 677
plasma and microplasma transferred arc processes (PTAW), 602, 605–6

© Woodhead Publishing Limited, 2013

plasma spray, 617
TBC, 618–19
plasma transferred arc processes, 606
plate-fin recuperator, 229
plate-like topologically closed packed (TCP) phases, 331
plate type heat exchangers, 230–1
polytropic blading efficiency, 105
polytropic efficiency, 433
post-combustion capture, 691–4
principles, 692
power chart, 250–1
interaction between active and reactive power, 251
power generation, 7–11, 23–7
CO_2 emission reduction, 10
conversion processes, 8–10
commercial availability and efficiency improvements of coal conversion technologies, 10
electricity production (2035), 9
efficiency improvement for CO_2 emission reduction, 10–11
electricity production by fuel type (2010 and 2035), 7
gas turbine product incorporating an advanced cycle feature, 27
global
worldwide CO_2 emissions (relative shares) per sector (2008 and 2035), 8
large heavy duty gas turbine model, 24
NO_x emission trend for gas turbine combustors, 26
operating parameters variation depending on gas turbine size, 24
scaling criteria for 50 Hz *vs* 60 Hz designs, 25
power system stabiliser (PSS), 251
pre-combustion capture, 688–90
IGCC of a combination of coal gasification and a gas turbine, 690
IRCC of steam methane reforming and a gas turbine, 689
premix burner, 153–6
EV burner principle, 155
evolution of the EV burner, 156
flow design of the FlameSheet system, 156
milestones in the burner and combustor development, 154
premix combustion, 193
primary surface recuperator (PSR), 229
prompt NO_x, 740–7, 768–9
dependence on flame stabiliser design, 741–2
radial swirler with vane passage fuel injection, 742
flame structure in premixed combustion region, 742–5
CFD Prediction of temperature, 743
distribution of NO, 744
hydrocarbon distributions, 743
kinetic predictions of relative contributions, 746–7
GRI3.0 NO_x mechanism predictions of NO_x from different kinetic routes, 746
influence of residence time on NO_x production, 747
kinetics, 740–1
pressure dependence, 741
prop-fan engines, 512
propeller turbine engines, 482–3
Proportional Integral Derivative (PID), 505
propulsive efficiency, 477
pulsations, 407

quality assurance programme (QAP), 571

radial swirler premixing nozzle (RSPN), 730
radiographic inspection, 595–6
Rayleigh criterion, 411, 668
reconditioning scope, 586
Rectisol process, 687
recuperated gas turbine, 67–72
cycle, 67
efficiency *vs.* pressure ratio, 69, 71
T-s diagram of ideal cycle, 68
T-s diagram of the recuperated cycle, 70
recuperation ratio, 69
recuperators, 227, 228–32

© Woodhead Publishing Limited, 2013

design, 229
materials issues, 232
primary surface geometries, 229–30
Honeywell recuperator, 231
RSAB recuperator, 230
recent investigation, 231–2
vs. regenerators, 233
reduced inlet mass flow, 104
reduced properties, 49
regenerative cycle, 466–7
reheat, 75–7, 227
reheat combustion, 172–8
combustor design, 173–6
operation principle of the SEV burner, 175
upstream view from the combustor into SEV burner, 175
concept, 173
reheat cycle principle, 174
sequential combustion gas turbine, 174
emissions, 177–8
engine operation, 176–7
operation concept of the GT24/GT26 engines, 176
reheat cycle, 469–72
rejuvenation, 581
process, 590
relative bulk velocity, 390
reliability, availability, maintainability, durability (RAM-D), 558–9
reliability block diagram analysis (RBD), 536
remote monitoring and diagnostic (RM&D) system, 534
renewable energy sources (RES), 516
residence time, 779
combustor, and choice of reference Mach number, 776–7
influence on NO_x, 768–70
Mach number and, changes with primary dilution air flow split, 773–5
post flame, influence of combustor length and, 779–80
resin rich (RR), 256–7
risk priority number (RPN), 530
rotary generators, 233
rotating electrical machines, 247–8
steam power plant, 248
rotating excitation, 304–5
schematic diagram, 304
rotating magnetic field, 253
rotating stall, 132–5
aerodynamic flow limits for a typical compressor blading section, 133
aerodynamic flow structure during rotating stall of compressor blade, 134
underfrequency/surge protection scheme, 135
rotor, 301–3
end windings for small generators, 303
main components, 302
rotor body, 301
rotor current, 251–2
rotor parts, 372–4
chemical composition of materials, 373
Ni-base alloys, 374
rotor steels, 373–4
rotor winding, 251, 301
rounds per minute (RPM), 25
run-up time, 391

seal oil auxiliary, 308
seal oil system, 308–10
secondary air systems (SAF)
modern SAF turbine systems, 192
semi-closed oxy-fuel combustion combined cycle (SCOC-CC), 701–4
CC-Matient cycle, 702
E-Matient cycle, 701
S-Graz variant of the Graz cycle, 703
water cycle based on principles of the Brayton cycle, 704
sequential EV (SEV) combustor, 157, 159–60
service damage, 590
shot peening, 584
simple cycle, 464–6
single-circuit seal, 308
single crystal alloys, 337–8
single-shaft application
actual demonstration, 92
process chart, 92
single-shaft combined-cycle, 249

© Woodhead Publishing Limited, 2013

small air-cooled generators, 305
small air-cooled units, 295
  schematic diagram, 296
Small Punch Test (SPT), 599
Smith chart, 195
solid fuel, 636–7
solid rotor, 99, 102–3
solid solution elements, 329
solution precursor spray process, 618
staged premix combustion, 165–72
  emission characteristics, 171–2
    LEC-III emissions characteristic, 173
    NO_x emissions of the staged and standard EV burners, 172
  flame stability, 170–1
    NO_x emissions and pulsations against adiabatic flame temperature, 171
    NO_x emissions and pulsations against stage 1 ratio, 171
  mixing properties, 168–70
    comparison of fuel streamlines for premixed and staged fuel gas injection, Plate VII
    comparison of mixing fields between different staged EV variants, Plate VIII
    comparison of mixing fields of the staged and standard EV burners, Plate IX
    experimental burner development process, 169
    unmixedness of mixing field and NO_x emissions correlation, 170
  staging concept, 166–8
    operation modes of the staged EV burner, 167
    operation modes of the standard EV burner, 166
stagnation-to-static temperature, 459
start-up phase, 122–7
  compressor blow-off concept, 122
  compressor loading, 123
  gas turbine start-up graph, 125
  gas turbine start-up power contributors, 124
  thermal growth of structural parts during transients., 126
start-up Power Balance, 123–4
static excitation, 303
  schematic diagram, 304
static frequency converter (SFC), 288
stationary gas turbine compressor
  data, 96
    schematic diagram, 97
  elements, 96, 98–103
    blow-off system application, 101
    compressor blading views/types, 102
    inlet and compressor components, 98
    intake system, 99
    single-shaft bolted and a solid gas turbine rotor, 100
    solid compressor rotor and a compressor casing, 100
  systems, 91–5
    inlet or high fogging application, 93–5
    intercooling application, 93
    multi-shaft application, 92–3
    single-shaft application, 92
stator, 298–301
  stacked silicon-steel lam, 299
stator concave/convex wedging system, 299
  schematic diagram, 300
stator core, 252
stator end winding, 299
  schematic diagram, 301
stator outlet temperature, 453
stator winding, 248, 252, 299
  schematic diagram, 300
steady flow energy equation, 426
steam injected cycles, 78
steam methane reforming, 688–9
steam turbines, 511
  turbogenerators developed for, 277–83
    bottleneck stator winding, 278
    cooled stator windings, 281
    DC excited machine, 282
    DC exciter machines, 280
    direct copper cooling, 282
    direct water cooling of the stator winding, 283
    direct water cooling of the stator winding through corrosion, 283

© Woodhead Publishing Limited, 2013

full-speed rating, 279
rotor body consists of a cylindrically shaped steel forging, 278
steam engines, 277
stress assisted grain boundary oxidation (SABGO), 374
stress-relief heat treatments, 613
stress-rupture test, 590
sulphur, 672–3
superalloy, 203
weldability, 602, 605
surge line, 105
surge margin extension, 144–5
casing treatment concept to extend compressor surge margin, 144
syngas, 640–2, 681
system efficiency, 13–16
improvement, 14–16
cycle options for aero-derivative-based GTCC plants, 15
potential pathways to improve heavy duty GTCC plant, 15

tangential velocity, 106
TE burner, 725–6
thermal barrier coating (TBC), 617–19
electron-beam physical vapour deposition (EB-PVD) TBC, 619
plasma sprayed, 618–19
structure, 617
thermal barrier coatings, 205
thermal capacity ratio, 462
thermal efficiency, 425
gas turbine, 717
thermal-mechanical fatigue (TMF), 566
thermal NO_x, 770
formation, 734–9
axial swirler with central air injection, 739
fuel effects on flame temperature and NO_x, 738–9
influence of pressure on NO_x, 737
NO_2 /NO ratios for four axial swirlers, 736
NO conversion to NO_2, 735–6
pressure dependence, 736–8
thermal, prompt and FBN NO_x formation routes, 734
thermal NO_x formation kinetics, 734–5
impact of fuel-and-air mixing quality, 763–5
advantage of mixing imperfections on flame stability, 763–5
pilot flame for premixed flame stability enhancement, 765
upstream fuel injection for premixed combustion, 763
Weak Extinction Data, 765
influence of mixing, 758–63
CFD predictions of S for a radial swirler, 761
example of good mixing for radial swirlers, 760–1
flame structure, temperature and NO_x, 762
influence of S on NO_x, 759
measurement of scalar mixing in ultra-low NO_x burner development, 761–3
mixing prior to completion of combustion in a flame, 760
rate of formation of NO_x at atmospheric conditions, 758
S parameter of mixing, 758–9
predictions, 747–58
applications to engine operating conditions, 750
computations of thermal NO_x for natural gas combustion, 748
equilibrium NO_x and adiabatic temperature predictions, 749
experimental measurements of ultra-low NO_x emissions, 753–7
experimental support for ultra-low NO_x emissions, 750–1
NO_x corrected to 15% oxygen, 751
NO_x emissions as a function of adiabatic flame temperature, 751
premixed combustion thermal NO_x, 747–9
survey of experimental data, 752–8
thermal ratio, 461
thermo-mechanical fatigue (TMF), 336
thermodynamic closed cycles, 52

© Woodhead Publishing Limited, 2013

thermodynamic properties, 46–50
compressibility factor *vs.* reduced pressure, 49
T-s diagram for an ideal gas, 47
thermography inspection, 596–7
three-body reactions, 399
time lag modelling, 411
total life cycle costs, 11–13
efficiency improvement of gas turbines since, 12
influencing factors for various power generation systems, 12
trace metals, 671–2
transient liquid phase (TLP) brazing, 340
tubular heat exchangers, 230
turbine entry temperature (TET), 478, 717
turbine exit temperature, 462
turbine inlet temperature (TIT), 13–14, 83, 84, 328
combined-cycle plant efficiency, 14
turbine parts
alloys for turbine blading, 328–41
Bridgman, LMC and Gas Cooling casting processes, 338
chemical composition of IGT superalloys, 330
cubical and rafted morphology of ⊠' phase in highly alloyed superalloy, 333
directionally solidified and single crystal technology, 335–7
IGT blades with conventional, DS and single crystal grain structure, 336
Kikuchi crystal orientation map of SX brazed joint and Laser clad-ded SX coating, Plate XIII
Ni-base superalloys, 328–35
oxide formation ternary diagram using Ni-, Cr- and Al- equivalents, 334
phase structure vs temperature for alloy IN939, 331
phase structure vs temperature for alloy MarM247LC, 332
progress in aero- and IGT blade material, 335
reconditioning of single crystals, 340
single crystal alloys, 337–8
single crystal brazing for manufacturing and repair, 340–1
single crystal/directional solidification casting process, 338–40
materials and coatings development, 327–41
turbine loading, 328
hot gas path of Alstom's GT24/GT26, 328
turbine temperature ratio, 502
turbines, 451–61, 698–9
convergent and convergent-divergent propelling nozzles, 458
enthalpy-entropy diagram of subsonic intake system, 456
entry temperature and stator outlet temperature, 452–3
exhaust systems, 457–61
intake systems, 454–7
schematic representation of industrial gas turbine inlet system, 455
turbo-fan, 479–82
turbo-propeller turbines, 512
turbo-props, 482–3
turbofan, 28–9
turbogenerators
component design, 251–76
calculations, 259–64
conductors equipped with channels, 255
cooling media air *vs.* hydrogen, 272
d-/q-axis modelling, 267
efficiency, 274–6
fundamental rules, 270–4
magnetic field pattern, 260

© Woodhead Publishing Limited, 2013

main generator components, 252
operation parameters, 264–70
phasor diagrams, 266
physical laws, 257–9
principle design of a Roebel bar, 259
relationship between the field current and stator voltage, 268
rotating magnetic field, 253
rotor winding current heat loss, 254
rotor with p pairs of north and south poles, 265
simplified analysis of a single strand, 262
single bar of insulated twisted strands, 261
stator bars are commonly designed as Roebel bars, 256
stator slot contains two winding bars, 256
sudden short-circuit test, 270
total flux minimisation, 263
design concept, 294–312
automatic voltage regulator and electrical generator protection, 310–12
component design, 298–305
cooling gas circuit, 305–7
hydrogen management and seal oil system, 308–10
layout, 295–8
water-cooled stator bars, 307–8
development, 312–18
capability chart, 313
measured armature voltage, 317
measured generator voltage, 318
methods and validation, 315–18
running test results of a 400 MVA air-cooled generator, 317
running test results of a 530 MVA indirect hydrogen-cooled generator, 318
standards, 314–15
development history, 276–94
air-cooled 9A4 generator, 292
closed frame design of General Electric's 7FH2 generator, 293
7FH2 generator, 293
gas turbines, 284–90
German Siemens type SGen-100A-2P (TLRI), 294
international developments, 290–4
steam turbines, 277–83
future trends, 322–5
refining stator wirings, 324
rotor coils incorporating high-temperature superconductors, 324
gas turbine systems, 247–325
overview, 247–51
electricity generation, 248–51
rotating electrical machines, 247–8
recent developments, 318–22
turbojet, 28–9
engine, 475–9
TURBOMATCH, 520
turboprop, 28–9
turboshaft, 28–9
turbulent flame speed, 661–5

ultrasonic inspection, 594–5
unducted fan engine, 512
uninterrupted power supply (UPS), 35

vacuum arc remelting (VAR), 372
vacuum degasation processes, 372
vacuum plasma spraying (VPS), 617
vacuum pressure impregnation (VPI), 255
variable vanes, 91
velocity coefficient (cv), 460
viscosity, 679
visual inspection, 592
volume flow, 89

water-cooled stator bars, 307–8
equipped large generators, 307
water dew point, 671

© Woodhead Publishing Limited, 2013

welding process, 601–2
wet cycles, 77–9
  steam injected gas turbine., 78
Wobbe index, 654, 656–61
  Alstom EV premix burner, 656
  fuel-air mixing profile, 660
  Jet in cross-flow geometry, 658
  MHI combustor, 657
  schematic diagram of GE DLN2.5H Gas Nozzle, 657
  Standard Siemens Energy Hybrid burner, 656
work factor, 107
WR-21, 27

Zeldovich mechanism, 399
Zeldovich NO_x, 735

© Woodhead Publishing Limited, 2013